JPL Publication **06-2**

Chemical Kinetics and Photochemical Data for Use in Atmospheric Studies

Evaluation Number 15

NASA Panel for Data Evaluation:

S. P. Sander
R. R. Friedl
NASA/Jet Propulsion Laboratory
Pasadena, California

A. R. Ravishankara
NOAA Earth System Research Laboratory
Boulder, Colorado

D. M. Golden
Stanford University
Stanford, California

C. E. Kolb
Aerodyne Research, Inc.
Billerica, Massachusetts

M. J. Kurylo
NASA Headquarters
Washington, D.C.

M. J. Molina
University of California, San Diego
La Jolla, California

G. K. Moortgat
H. Keller-Rudek
Max-Planck Institute for Chemistry
Mainz, Germany

B. J.Finlayson-Pitts
University of California, Irvine
Irvine, California

P. H. Wine
Georgia Institute of Technology
Atlanta, Georgia

R. E. Huie
V. L. Orkin
National Institute of Standards and Technology
Gaithersburg, Maryland

National Aeronautics and Space Administration

Jet Propulsion Laboratory
California Institute of Technology
Pasadena, California

July 10, 2006

The research described in this publication was carried out by the Jet Propulsion Laboratory, California Institute of Technology, under a contract with the National Aeronautics and Space Administration.

Reference herein to any specific commercial product, process, or service by trade name, trademark, manufacturer, or otherwise, does not constitute or imply its endorsement by the United States Government or the Jet Propulsion Laboratory, California Institute of Technology

ABSTRACT

This is the fifteenth in a series of evaluated sets of rate constants and photochemical cross sections compiled by the NASA Panel for Data Evaluation.

The data are used primarily to model stratospheric and upper tropospheric processes, with particular emphasis on the ozone layer and its possible perturbation by anthropogenic and natural phenomena.

Copies of this evaluation are available in electronic form and may be printed from the following Internet URL:

http://jpldataeval.jpl.nasa.gov/

TABLE OF CONTENTS

INTRODUCTION xv
1.1 Basis of the Recommendations xvii
1.2 Scope of the Evaluation xvii
1.3 Format of the Evaluation xviii
1.4 Computer Access xviii
1.5 Data Formats xviii
1.6 Units xviii
1.7 Noteworthy Changes in this Evaluation xviii
1.8 Acknowledgements xxi
1.9 References xxi

SECTION 1. BIOMOLECULAR REACTIONS 1-1
1.1 Introduction 1-1
1.2 Uncertainty Estimates 1-2
1.3 Notes to Table 1 1-33
1.4 References 1-119

SECTION 2. TERMOLECULAR REACTIONS 2-1
2.1 Introduction 2-1
2.2 Low-Pressure-Limiting Rate Constant $k^x_o(T)$ 2-2
2.3 Temperature Dependence of Low-Pressure Limiting Rate Constants: T^n 2-2
2.4 High-Pressure-Limit Rate Constants, $k_\infty(T)$ 2-3
2.5 Temperature Dependence of High-Pressure Limiting Rate Constants: T^m 2-3
2.6 Uncertainty Estimates 2-6
2.7 Notes to Table 2 2-8
2.8 References 2-19

SECTION 3. EQUILIBRIUM CONSTANTS 3-1
3.1 Format 3-1
3.2 Definitions 3-1
3.3 Notes to Table 3 3-3
3.4 References 3-6

SECTION 4. PHOTOCHEMICAL DATA 4-1
4.1 Format and Error Estimates 4-4
4.2 Halocarbon Absorption Cross Sections and Quantum Yields 4-5
4.3 Web Access to Recommended Data in Text and Graphical Formats 4-5
4.4 References 4-211

SECTION 5. HETEROGENEOUS CHEMISTRY 5-1
5.1 Introduction 5-1
5.2 Surface Types—Acid/Water, Liquids and Solids 5-2
5.3 Surface Types—Soot and Alumina 5-2
5.4 Surface Types—Solid Alkali Halide Salts and Aqueous Salt Solutions 5-3
5.5 Surface Composition and Morphology 5-4
5.6 Surface Porosity 5-6
5.7 Temperature Dependences of Parameters 5-5
5.8 Solubility Limitations 5-5
5.9 Data Organization 5-5
5.10 Parameter Definitions 5-5
5.11 Mass Accommodation Coefficients for Surfaces Other Than Soot 5-9
5.12 Notes to Table 5-1 5-12
5.13 Gas/Surface Reaction Probabilities for Surfaces Other Than Soot 5-21
5.14 Notes to Table 5-2 5-26
5.15 Soot Surface Uptake Coefficients 5-50
5.16 Notes to Table 5-3 5-50

5.17 Henry's Law Constants for Pure Water 5-53
5.18 Notes to Table 5-4 5-56
5.19 Ion-Specific Schumpe Parameters 5-61
5.20 Henry's Law Constants for Acids 5-62
5.21 Notes to Table 5-6 5-63
5.22 References 5-66

APPENDIX A. GAS-PHASE ENTROPY AND ENTHALPY VALUES
FOR SELECTED SPECIES AT 298.15 K AND 100 KPA A-1

TABLES

Table 1-1. Rate Constants for Second-Order Reactions 1-5

Table 2-1. Rate Constants for Termolecular Reactions 2-4

Table 3-1. Equilibrium Constants 3-2

Table 4-1. Photochemical Reactions 4-6
Table 4-2. Combined Uncertainties for Cross Sections and Quantum Yields 4-9
Table 4-3. Absorption Cross Sections of O_2 Between 205 and 240 nm 4-10
Table 4-4. Summary of O_3 Cross Section Measurements 4-11
Table 4-5. Absorption Cross Sections of O_3 at 218 and 293-298 K 4-15
Table 4-6. Parameters for the Calculation of $O(^1D)$ Quantum Yields 4-17
Table 4-7. Absorption Cross Sections of HO_2 4-18
Table 4-8. Absorption Cross Sections of H_2O Vapor 4-18
Table 4-9. Absorption Cross Sections of H_2O_2 Vapor 4-19
Table 4-10. Mathematical Expression for Absorption Cross Sections of H_2O_2 as a Function of Temperature 4-19
Table 4-11. Summary of NO_2 Cross Section Measurements 4-20
Table 4-12. Absorption Cross Sections of NO_2 at 220 and 294 K 4-23
Table 4-13. Quantum Yields for NO_2 Photolysis 4-24
Table 4-14. Summary of NO_3 Cross Section Measurements 4-25
Table 4-15. Absorption Cross Sections of NO_3 at 298 K 4-28
Table 4-16. Quantum Yields (multiplied by 1000) for the Product Channels $NO + O_2$ and $NO_2 + O(^3P)$ in the Photolysis of NO_3 at 298, 230 and 190 K 4-30
Table 4-17. Summary of N_2O Cross Section Measurements 4-31
Table 4-18. Absorption Cross Sections of N_2O at 298 K 4-32
Table 4-19. Mathematical Expression for Absorption Cross Sections of N_2O as a Function of Temperature 4-32
Table 4-20. Absorption Cross Sections of N_2O_4 at 220 K 4-33
Table 4-21. Absorption Cross Sections N_2O_5 at 195-300 K and Temperature Coefficients 4-35
Table 4-22. Quantum Yields from Photolysis of N_2O_5 4-36
Table 4-23. Summary of HONO Cross Section Measurements 4-36
Table 4-24. Absorption Cross Sections of HONO at 298 K 4-38
Table 4-25. Absorption Cross Sections at 298 K and Temperature Coefficients of HNO_3 Vapor 4-40
Table 4-26. Absorption Cross Sections at HO_2NO_2 at 296-298 K 4-41
Table 4-27. Quantum Yields of HO_2NO_2 4-42
Table 4-28. Photodissociation Band Strengths and Quantum Yields for Several Overtone and Combination Bands of HO_2NO_2 4-42
Table 4-29. Summary of CH_2O Cross Section Measurements 4-42
Table 4-30. Absorption Cross Sections of CH_2O at 298 K and Temperature Coefficients Averaged over 1-nm Intervals 4-45
Table 4-31. Absorption Cross Sections of CH_2O at 298 K and Temperature Coefficients Averaged over Intervals Used in Atmospheric Modeling 4-46
Table 4-32. Quantum Yields for Photolysis of CH_2O at 296-300 K 4-47
Table 4-33. Absorption Cross Sections of CH_3CHO at 298-300 K 4-49
Table 4-34. Recommended Quantum Yields for the Photolysis of CH_3CHO at 1 bar Total Pressure 4-50
Table 4-35. Absorption Cross Sections of C_2H_5CHO at 298-300K 4-51
Table 4-36. Absorption Cross Sections of CH_3O_2, $C_2H_5O_2$, and $CH_3C(O)O_2$ 4-52
Table 4-37. Absorption Cross Sections of CH_3OOH 4-53

Table 4-38. Absorption Cross Sections of $HOCH_2OOH$ 4-54
Table 4-39. Absorption Cross Sections of $CH_3C(O)O_2NO_2$ at 298 K, Temperature Coefficients B 4-55
Table 4-40. Absorption Cross Sections of $C_2H_5C(O)O_2NO_2$ at 296 K and Temperature Coefficients B 4-56
Table 4-41. Absorption Cross Sections of CH_2=CHCHO at 298 K 4-57
Table 4-42. Absorption Cross Sections of CH_2=C(CH_3)CHO at 298 K 4-58
Table 4-43. Absorption Cross Sections of CH_3(O)CH=CH_2 at 298 K 4-60
Table 4-44. Absorption Cross Sections of $HOCH_2CHO$ at 298 K 4-61
Table 4-45. Absorption Cross Sections of $CH_3C(O)CH_3$ at 298 K and Temperature Coefficients 4-64
Table 4-46. Quantum Yields for the Photolysis of Acetone 4-66
Table 4-47. Absorption Cross Sections of $CH_3C(O)CH_2OH$ at 298 K 4-67
Table 4-48. Absorption Cross Sections of CHOCHO at 296 K 4-69
Table 4-49. Absolute Quantum Yields in the Photolysis of CHOCHO 4-70
Table 4-50. Absorption Cross Sections of $CH_3COC(O)H$ at 295-298 K 4-71
Table 4-51. Absorption Cross Sections of HC(O)OH and $(HC(O)OH)_2$ at 302 K 4-74
Table 4-52. Absorption Cross Sections of $CH_3C(O)OH$ and $(CH_3C(O)OH)_2$ at 298 K 4-75
Table 4-53. Absorption Cross Sections of $CH_3C(O)OOH$ at 298 K 4-76
Table 4-54. Absorption Cross Sections of $CH_3C(O)C(O)OH$ at 298 K 4-77
Table 4-55. Absorption Cross Sections of $HC(O)OCH_3$ at 297-298 K 4-78
Table 4-56 Absorption Cross Sections of $HC(O)OC_2H_5$ at 297 K 4-78
Table 4-57. Absorption Cross Sections of FO_2 at 295 K 4-79
Table 4-58. Absorption Cross Sections of F_2O at 273 K 4-79
Table 4-59. Absorption Cross Sections of F_2O_2 at 193-195 and 273 K 4-80
Table 4-60. Absorption Cross Sections of FNO at 298 K 4-81
Table 4-61. Absorption Cross Sections of COF_2 at 298 K 4-82
Table 4-62. Absorption Cross Sections of COHF at 298 K 4-82
Table 4-63. Absorption Cross Sections of CF_3OOCF_3 at 298 K 4-83
Table 4-64. Absorption Cross Sections of $CF_3O_3CF_3$ at 298 K 4-84
Table 4-65. Absorption Cross Sections of CF_3CHO at 298 K 4-85
Table 4-66. Absorption Cross Sections of $CF_3C(O)F$ at 298 K 4-86
Table 4-67. Absorption Cross Sections of $CF_3C(O)Cl$ at 296-298 K 4-86
Table 4-68. Absorption Cross Sections of $CF_3(O)O_2NO_2$ at 298 K 4-87
Table 4-69. Absorption Cross Sections of CF_3CH_2CHO at 298 K 4-88
Table 4-70. Absorption Cross Sections of $CF_3C(O)OH$ at 296 K 4-89
Table 4-71. Absorption Cross Sections of $CH_3C(O)F$ at 296 K 4-89
Table 4-72. Absorption Cross Sections of CH_2=$CHCF_3$ at 295 K 4-90
Table 4-73. Absorption Cross Sections of CH_2=$CFCF_3$ at 295 K 4-90
Table 4-74. Absorption Cross Sections of CF_2=CF_2 at 295-298 K 4-91
Table 4-75. Absorption Cross Sections of CF_2=$CFCF_3$ at 295-298 K 4-92
Table 4-76. Absorption Cross Sections of Cl_2 at 298 K 4-93
Table 4-77. Absorption Cross Sections of ClO at 298 K 4-94
Table 4-78. Absorption Cross Sections of ClO at the band heads of the v′, v″ = 1,0 to 21,0 bands 4-95
Table 4-79. Absorption Cross Sections of ClOO 4-95
Table 4-80. Summary of Previous Measurements of OClO Cross Sections 4-96
Table 4-81. Absorption Cross Sections of OClO at 204 K (averages over 1-nm intervals) 4-97
Table 4-82. Absorption Cross Sections of OClO at the a(21) to a(3) Band Peaks at 213-293 K 4-98
Table 4-83. Absorption Cross Sections of OClO at the Band Peaks (after Wahner et al. [830]) 4-99
Table 4-84. Absorption Cross Sections of Cl_2O 4-101
Table 4-85. Absorption Cross Sections of ClOOCl at 195-265 K 4-102
Table 4-86. Absorption Cross Sections of Cl_2O_3 at 220-260 K 4-103
Table 4-87. Absorption Cross Sections of Cl_2O_4 at 298 K 4-104
Table 4-88. Absorption Cross Sections of Cl_2O_6 at 298 K 4-105
Table 4-89. Absorption Cross Sections of Cl_2O_7 at 298 K 4-105
Table 4-90. Absorption Cross Sections of $ClClO_2$ at 298 K 4-106
Table 4-91. Absorption Cross Sections of HCl and DCl at 298 K 4-107
Table 4-92. Absorption Cross Sections of HOCl 4-108
Table 4-93. Absorption Cross Sections of ClNO 4-109
Table 4-94. Absorption Cross Sections of $ClNO_2$ at 298 K 4-110
Table 4-95. Absorption Cross Sections of ClONO at 231 K 4-110
Table 4-96. Absorption Cross Sections and Temperature Coefficients of $ClONO_2$ 4-111
Table 4-97. Absorption Cross Sections of CCl_4 at 295-298 K 4-114

Table 4-98. Absorption Cross Sections of CH_3OCl 4-114
Table 4-99. Absorption Cross Sections of $CHCl_3$ at 295-298 K 4-115
Table 4-100. Absorption Cross Sections of CH_2Cl_2 at 295-298 K 4-116
Table 4-101. Absorption Cross Sections of CH_3Cl at 295-298 K 4-117
Table 4-102. Absorption Cross Sections of CH_3CCl_3 at 295-298 K 4-118
Table 4-103. Absorption Cross Sections of CH_3CH_2Cl at 298 K 4-118
Table 4-104. Absorption Cross Sections of $CH_3CHClCH_3$ at 295 K 4-118
Table 4-105. Absorption Cross Sections of $COCl_2$ at 294-298 K 4-120
Table 4-106. Absorption Cross Sections of COHCl at 298 K 4-121
Table 4-107. Absorption Cross Sections of COFCl at 296-298 K 4-123
Table 4-108. Absorption Cross Sections of $CFCl_3$ at 295-298 K 4-124
Table 4-109. Absorption Cross Sections of CF_2Cl_2 at 295-298 K 4-125
Table 4-110. Absorption Cross Sections of CF_3Cl at 295 K 4-125
Table 4-111. Absorption Cross Sections of $CF_2ClCFCl_2$ at 295-298 K 4-126
Table 4-112. Absorption Cross Sections of CF_2ClCF_2Cl at 295 K 4-127
Table 4-113. Absorption Cross Sections of CF_3CF_2Cl at 295-298 K 4-129
Table 4-114. Absorption Cross Sections of $CHFCl_2$ at 295-298 K 4-130
Table 4-115. Absorption Cross Sections of CHF_2Cl at 295-298 K 4-131
Table 4-116. Absorption Cross Sections of CH_2FCl at 298 K 4-131
Table 4-117. Absorption Cross Sections of CF_3CHCl_2 at 295 K 4-133
Table 4-118. Absorption Cross Sections of CF_3CHFCl at 295 K 4-134
Table 4-119. Absorption Cross Sections of CF_3CH_2Cl at 298 K 4-134
Table 4-120. Absorption Cross Sections of CH_3CFCl_2 at 295-298 K 4-135
Table 4-121. Absorption Cross Sections of CH_3CF_2Cl at 295-298 K 4-136
Table 4-122. Absorption Cross Sections of CH_2ClCHO at 298 K 4-137
Table 4-123. Absorption Cross Sections of $CHCl_2CHO$ at 298 K 4-138
Table 4-124. Absorption Cross Sections of CF_2ClCHO at 298 K and Temperature Coefficients 4-139
Table 4-125. Absorption Cross Sections of $CFCl_2CHO$ at 298 K and Temperature Coefficients 4-139
Table 4-126. Absorption Cross Sections of CCl_3CHO at 298 K and Temperature Coefficients 4-140
Table 4-127. Absorption Cross Sections of $CH_3C(O)Cl$ at 295-298 K 4-141
Table 4-128. Absorption Cross Sections of $CH_2ClC(O)Cl$ at 298 K 4-142
Table 4-129. Absorption Cross Sections of $CHCl_2C(O)Cl$ at 298 K 4-142
Table 4-130. Absorption Cross Sections of $CCl_3C(O)Cl$ at 295 K 4-143
Table 4-131. Absorption Cross Sections of $CF_3CF_2CHCl_2$ and CF_2ClCF_2CFCl at 298 K 4-144
Table 4-132. Absorption Cross Sections of $CH_3C(O)CH_2Cl$ at 296 K 4-145
Table 4-133. Summary of Cross Section Measurements of Br_2 4-146
Table 4-134. Absorption Cross Sections of Br_2 at 298 K 4-147
Table 4-135. Summary of Cross Section Measurements of HBr 4-147
Table 4-136. Absorption Cross Sections of HBr at 296-298 K 4-148
Table 4-137. Summary of Cross Section Measurements of BrO 4-148
Table 4-138. Absorption Cross Sections at the Vibrational Band Peaks in the A ← X Spectrum of BrO (0.4 nm resolution) 4-149
Table 4-139. Absorption Cross Sections of BrO at 298 K 4-150
Table 4-140. Peak Absorption Cross Sections of OBrO at 298 K 4-152
Table 4-141. Absorption Cross Sections of OBrO at 298 K 4-153
Table 4-142. Absorption Cross Sections of Br_2O at 298 K 4-154
Table 4-143. Absorption Cross Sections of HOBr 4-155
Table 4-144. Absorption Cross Sections of BrNO at 298 K 4-157
Table 4-145. Absorption Cross Sections of BrONO at 253 K 4-157
Table 4-146. Absorption Cross Sections of $BrONO_2$ at 296 K and Temperature Coefficients 4-159
Table 4-147. Absorption Cross Sections of BrCl at 298 K 4-161
Table 4-148. Absorption Cross Sections of BrOCl at 298 K 4-161
Table 4-149. Absorption Cross Sections of CH_3Br at 295-296 K 4-162
Table 4-150. Absorption Cross Sections of CH_2Br_2 at 295-298 K 4-164
Table 4-151. Absorption Cross Sections of $CHBr_3$ at 295-296 K 4-165
Table 4-152. Absorption Cross Sections of CH_2BrCH_2Br at 295 K 4-166
Table 4-153. Absorption Cross Sections of C_2H_5Br at 295 K 4-166
Table 4-154. Absorption Cross Sections of $COBr_2$ at 298 K 4-167
Table 4-155. Absorption Cross Sections of COHBr at 298 K 4-168
Table 4-156. Absorption Cross Sections of CH_2ClBr at 295 K 4-169

Table 4-157. Absorption Cross Sections of $CHClBr_2$ at 296 K 4-170
Table 4-158. Absorption Cross Sections of $CHCl_2Br$ at 298 K 4-171
Table 4-159. Absorption Cross Sections of CCl_3Br at 298 K 4-171
Table 4-160. Absorption Cross Sections of CHF_2Br at 298 K 4-172
Table 4-161. Absorption Cross Sections of CF_2Br_2 at 295-296 K 4-174
Table 4-162. Absorption Cross Sections of CF_2ClBr_2 at 295-298 K 4-177
Table 4-163. Absorption Cross Sections of CF_3Br at 295-298 K 4-179
Table 4-164. Absorption Cross Sections of CH_2=CHBr at 295 K 4-179
Table 4-165. Absorption Cross Sections of CHBr=CF_2 at 295 K 4-180
Table 4-166. Absorption Cross Sections of CFBr=CF_2 at 295 K 4-180
Table 4-167. Absorption Cross Sections of CH_2=$CBrCF_3$ at 295 K 4-181
Table 4-168. Absorption Cross Sections of CF_3CH_2Br at 295 K 4-181
Table 4-169. Absorption Cross Sections of $CF_3CHClBr$ at 295-298 K 4-182
Table 4-170. Absorption Cross Sections of CF_3CHFBr at 295 K 4-183
Table 4-171. Absorption Cross Sections of CF_2BrCF_2Br at 296 K 4-184
Table 4-172. Absorption Cross Sections of CF_3CF_2Br at 298 K 4-185
Table 4-173. Absorption Cross Sections of $CH_3CH_2CH_2Br$ and $CH_3CHBrCH_3$ at 295 K 4-185
Table 4-174. Absorption Cross Sections of $CH_3C(O)CH_2Br$ at 296 K 4-186
Table 4-175. Absorption Cross Sections of I_2 at 295 K 4-188
Table 4-176. Cross Sections at the Maxima and Minima of I_2 at 295 K 4-189
Table 4-177. Summary of Cross Section Measurements of IO 4-190
Table 4-178. Absorption Cross Sections of IO at 298 K 4-191
Table 4-179. Absorption Cross Sections of OIO at 295 K 4-193
Table 4-180. Absorption Cross Sections of HI at 298 K 4-195
Table 4-181. Absorption Cross Sections of HOI at 295-298 K 4-196
Table 4-182. Absorption Cross Sections of ICI at 298 K 4-197
Table 4-183. Absorption Cross Sections of IBr at 298 K 4-198
Table 4-184. Absorption Cross Sections of INO at 298 K 4-198
Table 4-185. Absorption Cross Sections of IONO at 298 K 4-199
Table 4-186. Absorption Cross Sections of $IONO_2$ at 298 K 4-199
Table 4-187. Absorption Cross Sections of CH_3I at 296-298 K and Temperature Coefficients 4-201
Table 4-188. Absorption Cross Sections of CH_2I_2 at 298 K 4-202
Table 4-189. Absorption Cross Sections of C_2H_5I at 298 K and Temperature Coefficients 4-203
Table 4-190. Absorption Cross Sections of CH_3CHI_2 at 298 K 4-203
Table 4-191. Absorption Cross Sections of C_3H_7I at 298 K and Temperature Coefficients 4-205
Table 4-192. Absorption Cross Sections of $(CH_3)_3CI$ at 298 K 4-206
Table 4-193. Absorption Cross Sections of CF_3I at 295-300 K 4-208
Table 4-194. Absorption Cross Sections of CF_2I_2 at 294 K 4-210
Table 4-195. Absorption Cross Sections of C_2F_5I at 323 K 4-210
Table 4-196. Absorption Cross Sections of 1-C_3F_7I at 295-298 K 4-211
Table 4-197. Absorption Cross Sections of CH_2ICI at 298 K and Temperature Coefficients 4-212
Table 4-198. Absorption Cross Sections of CH_2BrI at 298 K and Temperature Coefficients 4-212

Table 5-1. Mass Accommodation Coefficients (α)for Surfaces Other Than Soot 5-9
Table 5-2. Gas/Surface Reaction Probabilities (γ) for Surfaces Other Than Soot 5-21
Table 5-3. Soot Surface Uptake Coefficients 5-50
Table 5-4. Henry's Law Constants for Pure Water 5-53
Table 5-5. Ion-Specific Schumpe Parameters 5-61
Table 5-6. Henry's Law Constants for Acids 5-62

FIGURES

Figure 4-1. Absorption Spectrum of NO_3 4-31
Figure 4-2. Absorption Spectrum of ClO 4-94
Figure 4-3. Absorption Spectrum of OClO at 204 K (after Wahner et al. [830]) 4-99
Figure 4-4. Absorption Spectrum of BrO (after Wahher et al. [829]) 4-151
Figure 4-5. Absorption Spectrum of OBrO (after Knight et al. [413]) 4-154

Figure 5-1. Recommended Reactive Uptake Coefficients as a Function of Temperature for Key Stratospheric Heterogeneous Processes on Sulfuric Acid Aerosols 5-9

INTRODUCTION

This compilation of kinetic and photochemical data is an update to the 14th evaluation prepared by the NASA Panel for Data Evaluation. The Panel was established in 1977 by the NASA Upper Atmosphere Research Program Office for the purpose of providing a critical tabulation of the latest kinetic and photochemical data for use by modelers in computer simulations of atmospheric chemistry. Table I-1 lists this publication's editions:

Table I-1: Editions of this Publication

	Edition	Reference
1	NASA RP 1010, Chapter 1	Hudson et al. [1]
2	JPL Publication 79-27	DeMore et al. [12]
3	NASA RP 1049, Chapter 1	Hudson and Reed [2]
4	JPL Publication 81-3	DeMore et al. [10]
5	JPL Publication 82-57	DeMore et al. [8]
6	JPL Publication 83-62	DeMore et al. [9]
7	JPL Publication 85-37	DeMore et al. [3]
8	JPL Publication 87-41	DeMore et al. [4]
9	JPL Publication 90-1	DeMore et al. [5]
10	JPL Publication 92-20	DeMore et al. [6]
11	JPL Publication 94-26	DeMore et al. [7]
12	JPL Publication 97-4	DeMore et al. [11]
13	JPL Publication 00-3	Sander et al. [19]
14	JPL Publication 02-25	Sander et al. [18]
15	JPL Publication 06-2	Sander et al. [17]

In addition to the current edition, several previous editions are available for download from the website.

Panel members, and their major responsibilities for the current evaluation are listed in Table I-2.

Table I-2: Panel Members and their Major Responsibilities for the Current Evaluation

Panel Members	Responsibility
S. P. Sander, Chairman	Editorial Review, publication, website, ClO_x/BrO_x reactions, photochemistry
V. L. Orkin M. J. Kurylo	Cl reactions with halocarbons
D. M. Golden	Three-body reactions, equilibrium constants, editorial review
R. E. Huie	Aqueous chemistry, thermodynamics
C. E. Kolb B. J. Finlayson-Pitts M. J. Molina	Heterogeneous chemistry, Na chemistry
R. R. Friedl	HO_x reactions, OH + C_3 hydrocarbon reactions, photochemistry
A. R. Ravishankara	$O(^1D)$, $O_2(^1\Sigma)$, OH + hydrocarbon reactions, photochemistry
G. K. Moortgat H. Keller-Rudek	Photochemistry (O_3, HO_x, NO_x, carbonyls, FO_x, ClO_x, BrO_x, IO_x)
P. H. Wine	Sulfur chemistry

As shown above, each Panel member concentrates his efforts on a given area or type of data. Nevertheless, the Panel's final recommendations represent a consensus of the entire Panel. Each member reviews the basis for all recommendations, and is cognizant of the final decision in every case.

Address communications regarding particular reactions to the appropriate panel member:

S. P. Sander
R. R. Friedl
NASA/Jet Propulsion Laboratory
M/S 183-901
4800 Oak Grove Drive
Pasadena, CA 91109
Stanley.Sander@jpl.nasa.gov
randall.friedl@jpl.nasa.gov

D. M. Golden
Department of Mechanical Engineering
Stanford University
Bldg 520
Stanford, CA 94305
david.golden@stanford.edu

M. J. Kurylo
Earth Science Division
Mail Suite 3F71
NASA Headquarters
Washington, D.C. 20546
Michael.J.Kurylo@nasa.gov

A. R. Ravishankara
Earth System Research Laboratory
Chemical Sciences Division
National Oceanic and Atmospheric Administration
Boulder CO 80305
A.R.Ravishankara@noaa.gov

C. E. Kolb
Aerodyne Research Inc.
45 Manning Rd.
Billerica, MA 01821
kolb@aerodyne.com

M. J. Molina
University of California, San Diego
9500 Gilman Drive, MC 0356
La Jolla, CA 92093-0356
mjmolina@ucsd.edu

G. K. Moortgat
H. Keller-Rudek
Max-Planck-Institut für Chemie
Atmospheric Chemistry Division
Postfach 3060
55020 Mainz
Germany
moo@mpch-mainz.mpg.de
keller@mpch-mainz.mpg.de

B. J. Finlayson-Pitts
Department of Chemistry
University of California, Irvine
516 Rowland Hall
Irvine, CA 92697-2025
bjfinlay@uci.edu

P. H. Wine
Department of Chemistry and Biochemistry
Georgia Institute of Technology
770 State St.
Atlanta, GA 30332-0400
paul.wine@chemistry.gatech.edu

V. L. Orkin
R. E. Huie
National Institute of Standards and Technology
Physical and Chemical Properties Division
Gaithersburg, MD 20899
vladimir.orkin@nist.gov
robert.huie@nist.gov

I.1 Basis of the Recommendations

The recommended rate data and cross sections are based on laboratory measurements. In order to provide recommendations that are as up-to-date as possible, preprints and written private communications are accepted, but only when it is expected that they will appear as published journal articles. Under no circumstances are rate constants adjusted to fit observations of atmospheric concentrations. The Panel considers the question of consistency of data with expectations based on the theory of reaction kinetics, and when a discrepancy appears to exist this fact is pointed out in the accompanying note. The major use of theoretical extrapolation of data is in connection with three-body reactions, in which the required pressure or temperature dependence is sometimes unavailable from laboratory measurements, and can be estimated by use of appropriate theoretical treatment. In the case of important rate constants for which no experimental data are available, the panel may provide estimates of rate constant parameters based on analogy to similar reactions for which data are available.

I.2 Scope of the Evaluation

In the past (releases 1-12 of this evaluation) it has been the practice of the Panel to reevaluate the entire set of reactions with individual Panel members taking responsibility for specific chemical families or processes. In recent years, the upper troposphere and lower stratosphere (UT/LS) have become the primary areas of focus for model calculations and atmospheric measurements related to studies of ozone depletion and climate change. Because the UT/LS is a region of relatively high chemical and dynamical complexity, a different approach has been adopted for future releases of the evaluation. Specifically, the entire reaction set of the data evaluation will no longer be re-evaluated for each release. Instead, specific subsets will be chosen for re-evaluation, with several Panel members working to develop recommendations for a given area. This approach will make it possible to treat each subset in greater depth, and to expand the scope of the evaluation to new areas. It is the aim of the Panel to consider the entire set of kinetics, photochemical and thermodynamic parameters every three review cycles. Each release of the evaluation will contain not only the new evaluations, but also recommendations for every process that has been considered in the past. In this way, the tables for each release will constitute a complete set of recommendations.

It is recognized that important new laboratory data may be published that lie outside the specific subset chosen for re-evaluation. In order to ensure that these important data receive prompt consideration, each evaluation will also have a “special topics” category. Feedback from the atmospheric modeling community is solicited in the selection of reactions for this category.

For the current evaluation, the specific subsets include the following:

- Hydrocarbon chemistry of the upper troposphere (C_3 hydrocarbons and below).
- Reactions of Cl with halocarbon species.
- Reactions of sulfur compounds.
- Photochemistry of O_3, NOx, carbonyl compounds, FOx, ClOx, BrOx and IOx
- Heterogeneous processes on liquid water, water ice, alumina and solid alkali halide salts
- Gas-liquid solubility (Henry’s Law Constants and Schumpe Parameters)
- Thermodynamic parameters (entropy and enthalpy of formation)
- The special topics category includes several important reactions in atmospheric chemistry such as O+ClO, HO_2+HO_2, HO_2+BrO.

I.3 Format of the Evaluation

Changes or additions to the data tables are indicated by shading. A new entry is completely shaded, whereas a changed entry is shaded only where it has changed. In some cases only the note has been changed, in which case the corresponding note number in the table is shaded.

I.4 Computer Access

This document is available online in the form of individual chapters and as a complete document in Adobe PDF (Portable Data File) format. Files may be downloaded from http://jpldataeval.jpl.nasa.gov/. This document is not available in printed form from JPL.

The tables of recommended cross sections from this evaluation can be downloaded from the spectral atlas of the Max-Planck Institute for Chemistry at:
http://www.atmosphere.mpg.de/enid/2295

To receive email notification concerning releases of new publications and errata, a mailing list is available. To subscribe, send a blank message to join-jpl-dataeval@list.jpl.nasa.gov with "Subscribe" (without quotes) in the subject line.

For more information, contact Stanley Sander (Stanley.Sander@jpl.nasa.gov).

I.5 Data Formats

In Table 1 (Rate Constants for Bimolecular Reactions) the reactions are grouped into the classes O_x, HO_x, NO_x, Organic Compounds, FOx, ClOx, BrOx, IOx, SOx and Metal Reactions. The data in Table 2 (Rate Constants for Association Reactions) are presented in the same order as the bimolecular reactions. The presentation of photochemical cross section data follows the same sequence.

I.6 Units

Rate constants are given in units of concentration expressed as molecules per cubic centimeter and time in seconds. That is, for first-, second-, and third-order reactions, units of k are s^{-1}, cm^3 $molecule^{-1}$ s^{-1}, and cm^6 $molecule^{-2}$ s^{-1}, respectively. Cross sections are expressed as cm^2 $molecule^{-1}$, base e.

I.7 Noteworthy Changes in this Evaluation

I.7.1 Bimolecular Reactions (Section 1)

The rate constants for the reactions of O(1D) with N_2, O_2, and H_2O have been revised and the uncertainties in their values greatly reduced in this evaluation. These reactions (in competition) exert a significant influence on the production of HO_x throughout most of the lower and middle atmosphere. There have been previous suggestions that the reaction of $O_2(1\Sigma)$ with H_2 could be a source of HO_x. The overall rate coefficient for this reaction along with the branching ratio for the production of the reaction to produce 2 OH has been evaluated; this reaction is unlikely to be a significant source of HO_x anywhere in the troposphere and the stratosphere.

The reaction of $O_2(1\Sigma)$ with N_2O, a suggested route for the formation of NO_x in the atmosphere, has been evaluated. As in the case of $O_2(1\Sigma)$ reaction with H_2, this reaction to produce NO_x is small and negligible.

The reaction of OH with aldehydes has been updated and expanded. The new recommendation for the OH + acetone reaction indicates that the reaction products are almost exclusively $CH_3C(O)CH_2$ and H_2O. (Since the evaluation was completed, there is a suggestion based on calculations that the reaction of HO_2 with acetone at low temperatures could be an important loss process for acetone in the upper troposphere and thus alter the production of HO_x from acetone. This process has not been evaluated here.)

A comprehensive review of the reactions of hydrogen, methane, ethane, propane, and industrial and naturally occurring halogenated hydrocarbons with chlorine atoms was conducted for this evaluation. In doing so, attempts were made to understand and reconcile apparent differences between the results of absolute and relative rate measurements for some of the reactions. Relative rate constants were "renormalized" using the revised recommendations for the reference reactions. Thus, the re-evaluation procedure was an iterative one, since relative rate studies themselves were often included as the basis for the rate constant recommendations of these very reference reactions. The recommendations were then checked for self-consistency by seeing if ratios of the recommended rate constants were in agreement with published relative rate measurements. In some cases, disparities may seem to exist. However, it should be recognized that the focus of this re-evaluation was generating recommended rate constants over the temperature range of atmospheric importance (i.e., below 300 K). Finally, uncertainty factors (f and g) were carefully reviewed in an attempt to reasonably narrow the rate constant uncertainties for modeling purposes. Previous uncertainty limits were overly conservative in some cases.

A number of reactions in the inorganic reactions in the ClO_x and BrO_x families were reviewed with particular attention to reactions of stratospheric interest (e.g. O + ClO, BrO + HO_2, Br + HO_2, BrO + BrO, OH + HBr). For the most part, changes to the database for these reactions have not influenced the recommended values. However, the uncertainties have been reduced in many cases, particularly at low temperatures.

The section on SO_x reactions has been updated for the first time in nearly a decade. All literature published before the end of 2004 and selected more recent publications have been examined. Recommendations for approximately 30 reactions that appeared in Table 1 of Evaluation 14 have been revised. Reactions of dimethyl sulfoxide ($CH_3S(O)CH_3$) and methane sulfinic acid ($CH_3S(O)OH$) are included in Table 1 for the first time, as are bimolecular reactions of the weakly bound adducts SCS−OH, $(CH_3)2S$−OH, SCS−Cl, $(CH_3)2S$−Cl, and $(CH_3)2(O)S$−Cl. Also included in Table 1 for the first time are recommendations for the reactions BrO + CH_3SSCH_3, $CH_3SCH_2O_2$ + $CH_3SCH_2O_2$, and SH + N_2O.

Reactions involving atomic sodium and its oxide, hydroxide, carbonate, bicarbonate, and chloride molecules are updated in Section 1, Bimolecular Reactions, and Section 4, Photochemical Data, of this report. Although there is some evidence that volcanic action can deposit sodium species in the stratosphere, the main source of upper atmospheric sodium species is believed to be ablation from meteorites in the upper mesosphere and lower thermosphere. Meteorite ablation also deposits gaseous K, Li, Ca, Mg, Al and Fe species at these altitudes, but the observed concentrations of Na and Fe and the computed concentrations of their gaseous compounds significantly exceed concentrations of other mesospheric metals. Atmospheric models of meteor metal ablation and subsequent atmospheric chemistry have recently been reviewed by McNeil et al. [14] and laboratory and ab initio studies of their chemical kinetics and photochemistry have been reviewed by Plane [15, 16]. Since the available laboratory data for kinetic and photochemical processes involving sodium and its compounds significantly exceed those for other meteor metals and since Na is believed to have the most vigorous and complex atmospheric chemistry, we have restricted our evaluation of meteor metal chemical kinetics to Na species. Those interested in the chemical kinetics of meteor metals other than Na should see Plane [15, 16]. The major deficiency in current models of atmospheric Na chemistry and other meteor metals is the lack of quantitative data to model the sink for gaseous compounds, which is believed to be condensation on ultrafine oxide particulates of meteor "smoke" present in the mesosphere and upper stratosphere [13, 16].

I.7.2 Termolecular Reactions and Equilibrium Constants (Sections 2 and 3)

A specific entry has been written for the reaction OH + NO_2 + M → HOONO + M. This pathway was called out in the note in the last evaluation, but is now explicitly entered in the table.

The reaction OH + CO has been moved from Table 1 to Table 2. It is shown with two entries, one each for the association reaction to form HOCO and one for the chemical activation process to form H+CO_2. It is important to note that the chemical activation process is calculated using the expression for these types of reactions that is delineated in the Introduction to Table 2.

In addition to the changes to which attention is called by the shading convention, it should be noted that several reactions of species containing sulfur have been added to the table.

The equilibrium constant for the process forming HOONO from OH and NO_2 has been added, as have some sulfur reactions.

I.7.3 Photochemical Data (Section 4)

The section dealing with photochemical data has been greatly expanded and revised for all the chemical families (with the exception of HO_x). In all, 78 new species were added. The evaluations for many other species were revised and expanded. Most of the new species are organics and halogen-substituted organics including carbonyl compounds (aldehydes and ketones, both saturated and unsaturated). We have also included a number of new inorganic halogens that are important in the troposphere and stratosphere including Br_2, OBrO, I_2, IO, OIO, HOI and $IONO_2$.

I.7.4 Heterogeneous Chemistry (Section 5)

New and/or updated heterogeneous kinetics evaluations in this document have focused on processes on liquid water, on water ice, on alumina, and on solid alkali halide salts and and their aqueous solutions. Uptake studies of volatile organic species (VOCs) on water ice surfaces have not been included in his evaluation. A few important uptake processes occurring on liquid sulfuric acid surfaces have also been added or updated. The compilation of Henrys law parameters for pure water has been extended and a procedure for estimating the effective Henrys law parameters for aqueous salt solutions has been added.

I.7.5 Thermodynamic Parameters (Appendix A)

The table in Appendix A contains selected entropy and enthalpy of formation values at 298 K for a number of atmospheric species. As much as possible, the values were taken from primary evaluations, that is, evaluations that develop a recommended value from the original studies. Otherwise, the values were selected from the original literature, which is referenced in the table. Often, the enthalpy of formation and the entropy values are taken from different sources, usually due to a more recent value for the enthalpy of formation. The cited error limits are from the original references and therefore reflect widely varying criteria. Some enthalpy values were corrected slightly to reflect the value of a reference compound selected for this table; these are indicated. Values that are calculated or estimated are also indicated in the table.

I.8 Acknowledgements

The Panel wishes to acknowledge the contributions of the following persons for their assistance in the preparation and review of this report: Kyle Bayes (JPL), Jim Burkholder (NOAA), Carissa Howard (Georgia Tech), Rachna Kamath (Georgia Tech) and Ranajit Talukdar (NOAA). We also gratefully acknowledge the expert typing and editing skills of Rose Kendall (CSC), Xuan Sabounchi (JPL), Kathy Thompson (CSC) and Tom Wilson (JPL). Financial support from the NASA Upper Atmosphere Research and Tropospheric Chemistry Programs is gratefully acknowledged.

SPS wishes to acknowledge Joan and Steven Sander, whose love and support made this report possible.

I.9 References

1. Chlorofluoromethanes and the Stratosphere. In *NASA Reference Publication 1010*; R. D. Hudson, Ed.; NASA: Washington, D.C, 1977.
2. The Stratosphere: Present and Future. In *NASA Reference Publication 1049*; R. D. Hudson and E. I. Reed, Eds.; NASA: Washington, D.C, 1979.
3. DeMore, W. B., D. M. Golden, R. F. Hampson, C. J. Howard, M. J. Kurylo, J. J. Margitan, M. J. Molina, A. R. Ravishankara and R. T. Watson "Chemical Kinetics and Photochemical Data for Use in Stratospheric Modeling, Evaluation Number 7," JPL Publication 85-37, Jet Propulsion Laboratory, California Institute of Technology, Pasadena CA, 1985.
4. DeMore, W. B., D. M. Golden, R. F. Hampson, C. J. Howard, M. J. Kurylo, M. J. Molina, A. R. Ravishankara and S. P. Sander "Chemical Kinetics and Photochemical Data for Use in Stratospheric Modeling, Evaluation Number 8," JPL Publication 87-41, Jet Propulsion Laboratory, California Institute of Technology, Pasadena CA, 1987.
5. DeMore, W. B., D. M. Golden, R. F. Hampson, C. J. Howard, M. J. Kurylo, M. J. Molina, A. R. Ravishankara and S. P. Sander "Chemical Kinetics and Photochemical Data for Use in Stratospheric Modeling, Evaluation Number 9," JPL Publication 90-1, Jet Propulsion Laboratory, California Institute of Technology, Pasadena CA, 1990.
6. DeMore, W. B., D. M. Golden, R. F. Hampson, C. J. Howard, M. J. Kurylo, M. J. Molina, A. R. Ravishankara and S. P. Sander "Chemical Kinetics and Photochemical Data for Use in Stratospheric Modeling, Evaluation Number 10," JPL Publication 92-20, Jet Propulsion Laboratory, California Institute of Technology, Pasadena, CA, 1992.
7. DeMore, W. B., D. M. Golden, R. F. Hampson, C. J. Howard, M. J. Kurylo, M. J. Molina, A. R. Ravishankara and S. P. Sander "Chemical Kinetics and Photochemical Data for Use in Stratospheric Modeling, Evaluation Number 11," JPL Publication 94-26, Jet Propulsion Laboratory, California Institute of Technology, Pasadena, CA, 1994.
8. DeMore, W. B., D. M. Golden, R. F. Hampson, C. J. Howard, M. J. Kurylo, M. J. Molina, A. R. Ravishankara and R. T. Watson "Chemical Kinetics and Photochemical Data for Use in Stratospheric Modeling, Evaluation Number 5," JPL Publication 82-57, Jet Propulsion Laboratory, California Institute of Technology, Pasadena CA, 1982.
9. DeMore, W. B., D. M. Golden, R. F. Hampson, C. J. Howard, M. J. Kurylo, M. J. Molina, A. R. Ravishankara and R. T. Watson "Chemical Kinetics and Photochemical Data for Use in Stratospheric Modeling, Evaluation Number 6," JPL Publication 83-62, Jet Propulsion Laboratory, California Institute of Technology, Pasadena CA, 1983.
10. DeMore, W. B., D. M. Golden, R. F. Hampson, M. J. Kurylo, J. J. Margitan, M. J. Molina, L. J. Stief and R. T. Watson "Chemical Kinetics and Photochemical Data for Use in Stratospheric Modeling, Evaluation Number 4," JPL Publication 81-3, Jet Propulsion Laboratory, California Institute of Technology, Pasadena CA, 1981.
11. DeMore, W. B., S. P. Sander, D. M. Golden, R. F. Hampson, M. J. Kurylo, C. J. Howard, A. R. Ravishankara, C. E. Kolb and M. J. Molina "Chemical Kinetics and Photochemical Data for Use in Stratospheric Modeling, Evaluation Number 12," JPL Publication 97-4, Jet Propulsion Laboratory, California Institute of Technology, Pasadena, CA, 1997.
12. DeMore, W. B., L. J. Stief, F. Kaufman, D. M. Golden, R. F. Hampson, M. J. Kurylo, J. J. Margitan, M. J. Molina and R. T. Watson "Chemical Kinetics and Photochemical Data for Use in Stratospheric Modeling, Evaluation Number 2," JPL Publication 79-27, Jet Propulsion Laboratory, California Institute of Technology, Pasadena, CA, 1979.
13. Hunten, D. M., R. P. Turco and O. B. Toon, 1980, J. Atmos. Sci., **37**, 1342-1357.

14. McNeil, W. J., E. Murad and J.M.C. Plane. Models of Meteoric Metals in the Atmosphere In Meteors in the Earth's Atmosphere; Cambridge University Press, Cambridge, U.K., 2002; pp 265-287.
15. Plane, J. M. C. Laboratory Studies of Meteoric Metal Chemistry, In Meteors in the Earth's Atmosphere; Cambridge University Press, Cambridge, U.K., 2002; pp 289-309.
16. Plane, J. M. C., 2003, Chem. Rev., **103**, 4963-4984.
17. Sander, S. P., B. J. Finlayson-Pitts, R. R. Friedl, D. M. Golden, R. E. Huie, H. Keller-Rudek, C. E. Kolb, M. J. Kurylo, M. J. Molina, G. K. Moortgat, V. L. Orkin, A. R. Ravishankara and P. H. Wine "Chemical Kinetics and Photochemical Data for Use in Atmospheric Studies, Evaluation Number 15," JPL Publication 06-2, Jet Propulsion Laboratory, Pasadena, 2006.
18. Sander, S. P., B. J. Finlayson-Pitts, R. R. Friedl, D. M. Golden, R. E. Huie, C. E. Kolb, M. J. Kurylo, M. J. Molina, G. K. Moortgat, V. L. Orkin and A. R. Ravishankara "Chemical Kinetics and Photochemical Data for Use in Atmospheric Studies, Evaluation Number 14," JPL Publication 02-25, Jet Propulsion Laboratory, Pasadena, 2002.
19. Sander, S. P., R. R. Friedl, W. B. DeMore, D. M. Golden, M. J. Kurylo, R. F. Hampson, R. E. Huie, G. K. Moortgat, A. R. Ravishankara, C. E. Kolb and M. J. Molina "Chemical Kinetics and Photochemical Data for Use in Stratospheric Modeling, Evaluation Number 13," JPL Publication 00-3, Jet Propulsion Laboratory, California Institute of Technology, Pasadena, CA, 2000.

SECTION 1. BIMOLECULAR REACTIONS

Table of Contents

SECTION 1. BIMOLECULAR REACTIONS 1-1
1.1 Introduction 1-1
1.2 Uncertainty Estimates 1-2
1.3 Notes to Table 1 1-33
1.4 References 1-119

Tables

Table 1-1. Rate Constants for Second-Order Reactions 1-5

Figures

Figure 1. Symmetric and Asymmetric Error Limits 1-3

1.1 Introduction

In Table 1 (Rate Constants for Second-Order Reactions) the reactions are grouped into the classes O_x, $O(^1D)$, Singlet O_2, HO_x, NO_x, Organic Compounds, FO_x, ClO_x, BrO_x, IO_x, SO_x and Metals. Some of the reactions in Table 1 are actually more complex than simple two-body reactions. To explain the pressure and temperature dependences occasionally seen in reactions of this type, it is necessary to consider the bimolecular class of reactions in terms of two subcategories, direct (concerted) and indirect (nonconcerted) reactions.

A direct or concerted bimolecular reaction is one in which the reactants A and B proceed to products C and D without the intermediate formation of an AB adduct that has appreciable bonding, i.e., there is no bound intermediate; only the transition state $(AB)^{\neq}$ lies between reactants and products.

$$A + B \rightarrow (AB)^{\neq} \rightarrow C + D$$

The reaction of OH with CH_4 forming $H_2O + CH_3$ is an example of a reaction of this class.

Very useful correlations between the expected structure of the transition state $[AB]^{\neq}$ and the A-Factor of the reaction rate constant can be made, especially in reactions that are constrained to follow a well-defined approach of the two reactants in order to minimize energy requirements in the making and breaking of bonds. The rate constants for these reactions are well represented by the Arrhenius expression $k = A \exp(-E/RT)$ in the 200–300 K temperature range. These rate constants are not pressure dependent.

The indirect or nonconcerted class of bimolecular reactions is characterized by a more complex reaction path involving a potential well between reactants and products, leading to a bound adduct (or reaction complex) formed between the reactants A and B:

$$A + B \leftrightarrow [AB]^* \rightarrow C + D$$

The intermediate $[AB]^*$ is different from the transition state $[AB]^{\neq}$, in that it is a bound molecule which can, in principle, be isolated. (Of course, transition states are involved in all of the above reactions, both forward and backward, but are not explicitly shown.) An example of this reaction type is ClO + NO, which normally produces $Cl + NO_2$. Reactions of the nonconcerted type can have a more complex temperature dependence and can exhibit a pressure dependence if the lifetime of $[AB]^*$ is comparable to the rate of collisional deactivation of $[AB]^*$. This arises because the relative rate at which $[AB]^*$ goes to products C + D vs. reactants A + B is a sensitive function of its excitation energy. Thus, in reactions of this type, the distinction between the bimolecular and termolecular classification becomes less meaningful, and it is especially necessary to study such reactions under the temperature and pressure conditions in which they are to be used in model calculation, or, alternatively, to develop a reliable theoretical basis for extrapolation of data.

The rate constant tabulation for second-order reactions (Table 1) is given in Arrhenius form:

$$k(T)=A\bullet\exp\left(-\frac{E/R}{T}\right)$$

and contains the following information:

1. Reaction stoichiometry and products (if known). The pressure dependences are included, where appropriate.
2. Arrhenius A-factor: **A**
3. Temperature dependence ("activation temperature"): **E/R**
4. Rate constant at 298 K: **k(298 K)**
5. Rate constant uncertainty factor at 298 K: **f(298 K)** (see below)
6. A parameter used to calculate the rate constant uncertainty at temperatures other than 298 K: **g** (see below)
7. Index number for a detailed note containing references to the literature, the basis of recommendation and in several cases, alternative methods to calculate the rate constant.

For a few reactions, the A-factor, E/R and k(298 K) are italicized. These represent estimates by the Panel in cases where there are no literature data or where the existing data are judged to be of insufficient quality to base a recommendation.

1.2 Uncertainty Estimates

For bimolecular rate constants in Table 1, an estimate of the uncertainty at any given temperature, f(T), may be obtained from the following expression:

$$f(T)=f(298\text{ K})\exp\left|g\left(\frac{1}{T}-\frac{1}{298}\right)\right|$$

Note that the exponent is an absolute value. An upper or lower bound (corresponding approximately to one standard deviation) of the rate constant at any temperature T can be obtained by multiplying or dividing the recommended value of the rate constant at that temperature by the factor f(T). The quantity f(298 K) is the uncertainty in the rate constant at T = 298 K. The quantity g has been defined in this evaluation for use with f(298 K) in the above expression to obtain the rate constant uncertainty at different temperatures. It should not be interpreted as the uncertainty in the Arrhenius activation temperature (E/R). Both uncertainty factors, f(298 K) and g, do not necessarily result from a rigorous statistical analysis of the available data. Rather, they are chosen by the evaluators to construct the appropriate uncertainty factor, f(T), shown above.

This approach is based on the fact that rate constants are almost always known with minimum uncertainty at room temperature. The overall uncertainty normally increases at other temperatures, because there are usually fewer data at other temperatures. In addition, data obtained at temperatures far distant from 298 K may be less accurate than at room temperature due to various experimental difficulties.

The uncertainty represented by f(T) is normally symmetric; i.e., the rate constant may be greater than or less than the recommended value, k(T), by the factor f(T). In a few cases in Table 1 asymmetric uncertainties are given in the temperature coefficient. For these cases, the factors by which a rate constant is to be multiplied or divided to obtain, respectively, the upper and lower limits are not equal, except at 298 K where the factor is simply f(298 K). Explicit equations are given below for the case where g is given as (+a, –b):

For T > 298 K, multiply by the factor

$$f(298)e^{\left[a\left(\frac{1}{298}-\frac{1}{T}\right)\right]}$$

and divide by the factor

$$f(298)e^{\left[b\left(\frac{1}{298}-\frac{1}{T}\right)\right]}$$

For T < 298 K, multiply by the factor

$$f(298)e^{\left[b\left(\frac{1}{T}-\frac{1}{298}\right)\right]}$$

and divide by the factor

$$f(298)e^{\left[a\left(\frac{1}{T}-\frac{1}{298}\right)\right]}$$

Examples of symmetric and asymmetric error limits are shown in Figure 1.

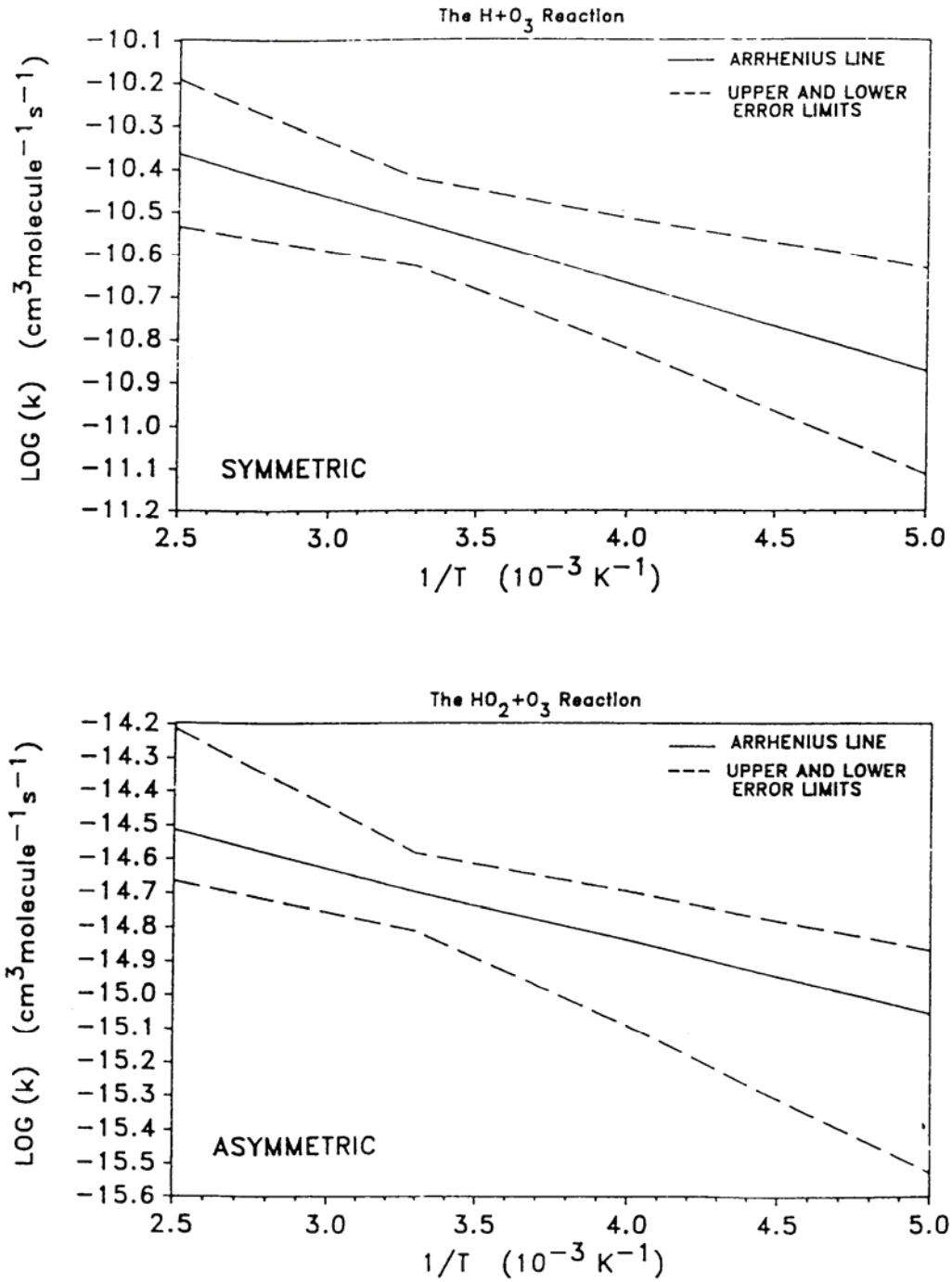

Figure 1. Symmetric and Asymmetric Error Limits

The assigned uncertainties represent the subjective judgment of the Panel. They are not determined by a rigorous, statistical analysis of the database, which generally is too limited to permit such an analysis. Rather, the

uncertainties are based on knowledge of the techniques, the difficulties of the experiments, and the potential for systematic errors.

There is obviously no way to quantify these “unknown” errors. The spread in results among different techniques for a given reaction may provide some basis for an uncertainty, but the possibility of the same, or compensating, systematic errors in all the studies must be recognized.

Furthermore, the probability distribution may not follow the normal Gaussian form. For measurements subject to large systematic errors, the true rate constant may be much further from the recommended value than would be expected based on a Gaussian distribution with the stated uncertainty. As an example, in the past the recommended rate constants for the reactions HO_2 + NO and Cl + $ClONO_2$ changed by factors of 30–50. These changes could not have been allowed for with any reasonable values of σ in a Gaussian distribution.

Table 1-1. Rate Constants for Second-Order Reactions

Reaction	A-Factor[a]	E/R	k(298 K)[a]	f(298 K)[b]	g	Notes
O_x Reactions						
$O + O_2 \xrightarrow{M} O_3$	(See Table 2)					
$O + O_3 \rightarrow O_2 + O_2$	8.0×10^{-12}	2060	8.0×10^{-15}	1.15	250	A1
$O(^1D)$ Reactions						A2, A19
$O(^1D) + O_2 \rightarrow O + O_2$	3.3×10^{-11}	–55	3.95×10^{-11}	1.1	20	A2, A3
$O(^1D) + O_3 \rightarrow O_2 + O_2$	1.2×10^{-10}	0	1.2×10^{-10}	1.2	50	A2, A4
$\rightarrow O_2 + O + O$	1.2×10^{-10}	0	1.2×10^{-10}	1.2	50	A2, A4
$O(^1D) + H_2 \rightarrow OH + H$	1.1×10^{-10}	0	1.1×10^{-10}	1.1	100	A2, A5
$O(^1D) + H_2O \rightarrow OH + OH$	1.63×10^{-10}	-60	2.0×10^{-10}	1.15	45	A2, A6
$O(^1D) + N_2 \rightarrow O + N_2$	2.15×10^{-11}	–110	3.1×10^{-11}	1.10	30	A2, A7
$O(^1D) + N_2 \xrightarrow{M} N_2O$	(See Table 2-1)					
$O(^1D) + N_2O \rightarrow N_2 + O_2$ (a)	4.7×10^{-11}	-20	5.0×10^{-11}	1.15	50	A2, A8
$\rightarrow NO + NO$ (b)	6.7×10^{-11}	-20	6.7×10^{-11}	1.15	50	A2, A8
$O(^1D) + NH_3 \rightarrow OH + NH_2$	2.5×10^{-10}	0	2.5×10^{-10}	1.3	100	A2, A9
$O(^1D) + CO_2 \rightarrow O + CO_2$	7.5×10^{-11}	–115	1.1×10^{-10}	1.15	40	A2, A10
$O(^1D) + CH_4 \rightarrow$ products	1.5×10^{-10}	0	1.5×10^{-10}	1.2	100	A2, A11
$O(^1D) + HCl \rightarrow$ products	1.5×10^{-10}	0	1.5×10^{-10}	1.15	50	A2, A12
$O(^1D) + HF \rightarrow$ products	5.0×10^{-11}	0	5.0×10^{-11}	2.0	100	A2, A13
$O(^1D) + NF_3 \rightarrow$ products	2.0×10^{-11}	-25	2.2×10^{-11}	2	25	A2, A14
$O(^1D) + HBr \rightarrow$ products	1.5×10^{-10}	0	1.5×10^{-10}	2.0	100	A2, A15
$O(^1D) + Cl_2 \rightarrow$ products	2.7×10^{-10}	0	2.7×10^{-10}	1.15	50	A2, A16
$O(^1D) + CCl_2O \rightarrow$ products	2.2×10^{-10}	-30	2.4×10^{-10}	1.15	50	A2, A17
$O(^1D) + CClFO \rightarrow$ products	1.9×10^{-10}	0	1.9×10^{-10}	2.0	100	A2, A18
$O(^1D) + CF_2O \rightarrow$ products	7.4×10^{-11}	0	7.4×10^{-11}	2.0	100	A2, A18

Reaction	A-Factor[a]	E/R	k(298 K)[a]	f(298 K)[b]	g	Notes
$O(^1D) + CCl_4 \rightarrow$ products (CFC-10)	3.3×10^{-10}	0	3.3×10^{-10}	1.2	100	A19
$O(^1D) + CH_3Br \rightarrow$ products	1.8×10^{-10}	0	1.8×10^{-10}	1.3	100	A19 , A20
$O(^1D) + CH_2Br_2 \rightarrow$ products	2.7×10^{-10}	0	2.7×10^{-10}	1.3	100	A19, A21
$O(^1D) + CHBr_3 \rightarrow$ products	6.6×10^{-10}	0	6.6×10^{-10}	1.5	100	A19, A22
$O(^1D) + CH_3F \rightarrow$ products (HFC-41)	1.5×10^{-10}	0	1.5×10^{-10}	1.2	100	A19, A23
$O(^1D) + CH_2F_2 \rightarrow$ products (HFC-32)	5.1×10^{-11}	0	5.1×10^{-11}	1.3	100	A19, A24
$O(^1D) + CHF_3 \rightarrow$ products (HFC-23)	9.1×10^{-12}	0	9.1×10^{-12}	1.2	100	A19, A25
$O(^1D) + CHCl_2F \rightarrow$ products (HCFC-21)	1.9×10^{-10}	0	1.9×10^{-10}	1.3	100	A19, A26
$O(^1D) + CHClF_2 \rightarrow$ products (HCFC-22)	1.0×10^{-10}	0	1.0×10^{-10}	1.2	100	A19, A27
$O(^1D) + CHF_2Br \rightarrow$ products	1.75×10^{-10}	-70	2.2×10^{-10}	1.2	40	A19, A28
$O(^1D) + CCl_3F \rightarrow$ products (CFC-11)	2.3×10^{-10}	0	2.3×10^{-10}	1.2	100	A19
$O(^1D) + CCl_2F_2 \rightarrow$ products (CFC-12)	1.4×10^{-10}	0	1.4×10^{-10}	1.3	100	A19
$O(^1D) + CClF_3 \rightarrow$ products (CFC-13)	8.7×10^{-11}	0	8.7×10^{-11}	1.3	100	A19, A29
$O(^1D) + CClBrF_2 \rightarrow$ products (Halon-1211)	1.5×10^{-10}	0	1.5×10^{-10}	1.3	100	A19, A30
$O(^1D) + CBr_2F_2 \rightarrow$ products (Halon-1202)	2.2×10^{-10}	0	2.2×10^{-10}	1.3	100	A19, A31
$O(^1D) + CBrF_3 \rightarrow$ products (Halon-1301)	1.0×10^{-10}	0	1.0×10^{-10}	1.3	100	A19, A32
$O(^1D) + CF_4 \rightarrow CF_4 + O$ (CFC-14)			2.0×10^{-14}	1.5		A19, A33
$O(^1D) + CH_3CH_2F \rightarrow$ products (HFC-161)	2.6×10^{-10}	0	2.6×10^{-10}	1.3	100	A19, A34
$O(^1D) + CH_3CHF_2 \rightarrow$ products (HFC-152a)	2.0×10^{-10}	0	2.0×10^{-10}	1.3	100	A19, A35
$O(^1D) + CH_3CCl_2F \rightarrow$ products (HCFC-141b)	2.6×10^{-10}	0	2.6×10^{-10}	1.3	100	A19, A36
$O(^1D) + CH_3CClF_2 \rightarrow$ products (HCFC-142b)	2.2×10^{-10}	0	2.2×10^{-10}	1.3	100	A19, A37
$O(^1D) + CH_3CF_3 \rightarrow$ products (HFC-143a)	1.0×10^{-10}	0	1.0×10^{-10}	3.0	100	A19, A38
$O(^1D) + CH_2ClCClF_2 \rightarrow$ products (HCFC-132b)	1.6×10^{-10}	0	1.6×10^{-10}	2.0	100	A19, A39
$O(^1D) + CH_2ClCF_3 \rightarrow$ products (HCFC-133a)	1.2×10^{-10}	0	1.2×10^{-10}	1.3	100	A19, A40
$O(^1D) + CH_2FCF_3 \rightarrow$ products (HFC-134a)	4.9×10^{-11}	0	4.9×10^{-11}	1.3	100	A19, A41

Reaction	A-Factor[a]	E/R	k(298 K)[a]	f(298 K)[b]	g	Notes
$O(^1D) + CHCl_2CF_3 \rightarrow$ products (HCFC-123)	2.0×10^{-10}	0	2.0×10^{-10}	1.3	100	A19, A42
$O(^1D) + CHClFCF_3 \rightarrow$ products (HCFC-124)	8.6×10^{-11}	0	8.6×10^{-11}	1.3	100	A19, A43
$O(^1D) + CHF_2CF_3 \rightarrow$ products (HFC-125)	1.2×10^{-10}	0	1.2×10^{-10}	2.0	100	A19, A44
$O(^1D) + CCl_3CF_3 \rightarrow$ products (CFC-113a)	2×10^{-10}	0	2×10^{-10}	2.0	100	A19, A45
$O(^1D) + CCl_2FCClF_2 \rightarrow$ products (CFC-113)	2×10^{-10}	0	2×10^{-10}	2.0	100	A19, A46
$O(^1D) + CCl_2FCF_3 \rightarrow$ products (CFC-114a)	1×10^{-10}	0	1×10^{-10}	2.0	100	A19, A47
$O(^1D) + CClF_2CClF_2 \rightarrow$ products (CFC-114)	1.3×10^{-10}	0	1.3×10^{-10}	1.3	100	A19, A48
$O(^1D) + CClF_2CF_3 \rightarrow$ products (CFC-115)	5×10^{-11}	0	5×10^{-11}	1.3	100	A19, A49
$O(^1D) + CBrF_2CBrF_2 \rightarrow$ products (Halon-2402)	1.6×10^{-10}	0	1.6×10^{-10}	1.3	100	A19, A50
$O(^1D) + CF_3CF_3 \rightarrow$ products (CFC-116)			1.5×10^{-13}	1.5		A19, A51
$O(^1D) + CHF_2CF_2CF_2CHF_2 \rightarrow$ products (HFC-338pcc)	1.8×10^{-11}	0	1.8×10^{-11}	1.5	100	A19, A52
$O(^1D) + c\text{-}C_4F_8 \rightarrow$ products			8×10^{-13}	1.3		A19, A53
$O(^1D) + CF_3CHFCHFCF_2CF_3 \rightarrow$ products (HFC-43-10mee)	2.1×10^{-10}	0	2.1×10^{-10}	4	100	A19, A54
$O(^1D) + C_5F_{12} \rightarrow$ products (CFC-41-12)			3.9×10^{-13}	2		A19, A55
$O(^1D) + C_6F_{14} \rightarrow$ products (CFC-51-14)			1×10^{-12}	2		A19, A56
$O(^1D) + 1,2\text{-}(CF_3)_2c\text{-}C_4F_6 \rightarrow$ products			2.8×10^{-13}	2		A19, A57
$O(^1D) + SF_6 \rightarrow$ products			1.8×10^{-14}	1.5		A58
Singlet O_2 Reactions						
$O_2(^1\Delta) + O \rightarrow$ products			$<2\times10^{-16}$			A59
$O_2(^1\Delta) + O_2 \rightarrow$ products	3.6×10^{-18}	220	1.7×10^{-18}	1.2	100	A60
$O_2(^1\Delta) + O_3 \rightarrow O + 2O_2$	5.2×10^{-11}	2840	3.8×10^{-15}	1.2	500	A61
$O_2(^1\Delta) + H_2O \rightarrow$ products			4.8×10^{-18}	1.5		A62
$O_2(^1\Delta) + N \rightarrow NO + O$			$<9\times10^{-17}$			A63
$O_2(^1\Delta) + N_2 \rightarrow$ products			$<10^{-20}$			A64
$O_2(^1\Delta) + CO_2 \rightarrow$ products			$<2\times10^{-20}$			A65

Reaction	A-Factor[a]	E/R	k(298 K)[a]	f(298 K)[b]	g	Notes
$O_2(^1\Sigma) + O \rightarrow$ products			8×10^{-14}	5.0		A66
$O_2(^1\Sigma) + O_2 \rightarrow$ products			3.9×10^{-17}	1.5		A67
$O_2(^1\Sigma) + O_3 \rightarrow$ products	3.5×10^{-11}	135	2.2×10^{-11}	1.15	50	A68
$O_2(^1\Sigma) + H_2 \rightarrow$ products $O_2(^1\Sigma) + H_2 \rightarrow 2\ OH$	6.4×10^{-12}	600	8.5×10^{-13} $<4\times10^{-17}$ (see note)	1.15	100	A69
$O_2(^1\Sigma) + H_2O \rightarrow O_2 + H_2O$	3.9×10^{-12}	-125	5.9×10^{-12}	1.3	100	A70
$O_2(^1\Sigma) + N \rightarrow$ products			$<10^{-13}$			A71
$O_2(^1\Sigma) + N_2 \rightarrow$ products	1.8×10^{-15}	-45	2.1×10^{-15}	1.1	100	A72
$O_2(^1\Sigma) + N_2O \rightarrow$ products $O_2(^1\Sigma) + N_2O \rightarrow NO + NO_2$	7.0×10^{-14}	-75	9.0×10^{-14} $< 2\times10^{-17}$ (see Note)	1.3	50	A73
$O_2(^1\Sigma) + CO_2 \rightarrow$ products	4.2×10^{-13}	0	4.2×10^{-13}	1.2	200	A74
HO_x Reactions						
$O + OH \rightarrow O_2 + H$	2.2×10^{-11}	–120	3.3×10^{-11}	1.15	50	B1
$O + HO_2 \rightarrow OH + O_2$	3.0×10^{-11}	–200	5.9×10^{-11}	1.05	50	B2
$O + H_2O_2 \rightarrow OH + HO_2$	1.4×10^{-12}	2000	1.7×10^{-15}	1.3	200	B3
$H + O_2 \xrightarrow{M} HO_2$	(See Table 2-1)					
$H + O_3 \rightarrow OH + O_2$	1.4×10^{-10}	470	2.9×10^{-11}	1.1	70	B4
$H + HO_2 \rightarrow 2\ OH$	7.2×10^{-11}	0	7.2×10^{-11}	1.3	100	B5
$\rightarrow O + H_2O$	1.6×10^{-12}	0	1.6×10^{-12}	1.5	100	B5
$\rightarrow H_2 + O_2$	6.9×10^{-12}	0	6.9×10^{-12}	1.4	100	B5
$OH + O_3 \rightarrow HO_2 + O_2$	1.7×10^{-12}	940	7.3×10^{-14}	1.2	80	B6
$OH + H_2 \rightarrow H_2O + H$	2.8×10^{-12}	1800	6.7×10^{-15}	1.05	100	B7
$OH + HD \rightarrow$ products	5.0×10^{-12}	2130	4.0×10^{-15}	1.2	100	B8
$OH + OH \rightarrow H_2O + O$	1.8×10^{-12}	0	1.8×10^{-12}	1.3	100	B9
$\xrightarrow{M} H_2O_2$	(See Table 2-1)					
$OH + HO_2 \rightarrow H_2O + O_2$	4.8×10^{-11}	–250	1.1×10^{-10}	1.25	80	B10

Reaction	A-Factor[a]	E/R	k(298 K)[a]	f(298 K)[b]	g	Notes
$OH + H_2O_2 \rightarrow H_2O + HO_2$	See Note					B11
$HO_2 + O_3 \rightarrow OH + 2O_2$	1.0×10^{-14}	490	1.9×10^{-15}	1.15	+160 –80	B12
$HO_2 + HO_2 \rightarrow H_2O_2 + O_2$	3.5×10^{-13}	–430	1.5×10^{-12}	1.2	200	B13
$+ M \rightarrow H_2O_2 + O_2$	1.7×10^{-33} [M]	–1000	4.9×10^{-32} [M]	1.2	200	B13
NO_x Reactions						
$O + NO \xrightarrow{M} NO_2$	(See Table 2-1)					
$O + NO_2 \rightarrow NO + O_2$	5.1×10^{-12}	-210	1.04×10^{-11}	1.1	20	C 1
$O + NO_2 \xrightarrow{M} NO_3$	(See Table 2-1)					
$O + NO_3 \rightarrow O_2 + NO_2$	1.0×10^{-11}	0	1.0×10^{-11}	1.5	150	C 2
$O + N_2O_5 \rightarrow$ products			$<3.0\times10^{-16}$			C 3
$O + HNO_3 \rightarrow OH + NO_3$			$<3.0\times10^{-17}$			C 4
$O + HO_2NO_2 \rightarrow$ products	7.8×10^{-11}	3400	8.6×10^{-16}	3.0	750	C 5
$H + NO_2 \rightarrow OH + NO$	4.0×10^{-10}	340	1.3×10^{-10}	1.3	300	C 6
$OH + NO \xrightarrow{M} HONO$	(See Table 2-1)					
$OH + NO_2 \xrightarrow{M} HNO_3$	(See Table 2-1)					
$OH + NO_3 \rightarrow$ products			2.2×10^{-11}	1.5		C 7
$OH + HONO \rightarrow H_2O + NO_2$	1.8×10^{-11}	390	4.5×10^{-12}	1.5	+200 –500	C 8
$OH + HNO_3 \rightarrow H_2O + NO_3$	(See Note)			1.2		C 9
$OH + HO_2NO_2 \rightarrow$ products	1.3×10^{-12}	–380	4.6×10^{-12}	1.3	+270 –500	C10
$OH + NH_3 \rightarrow H_2O + NH_2$	1.7×10^{-12}	710	1.6×10^{-13}	1.2	200	C11
$HO_2 + NO \rightarrow NO_2 + OH$	3.5×10^{-12}	–250	8.1×10^{-12}	1.15	50	C12
$HO_2 + NO_2 \xrightarrow{M} HO_2NO_2$	(See Table 2-1)					
$HO_2 + NO_2 \rightarrow HONO + O_2$	(See Note)					C13
$HO_2 + NO_3 \rightarrow$ products			3.5×10^{-12}	1.5		C14
$HO_2 + NH_2 \rightarrow$ products			3.4×10^{-11}	2.0		C15

Reaction	A-Factor[a]	E/R	k(298 K)[a]	f(298 K)[b]	g	Notes
$N + O_2 \rightarrow NO + O$	1.5×10^{-11}	3600	8.5×10^{-17}	1.25	400	C16
$N + O_3 \rightarrow NO + O_2$			$<2.0\times10^{-16}$			C17
$N + NO \rightarrow N_2 + O$	2.1×10^{-11}	–100	3.0×10^{-11}	1.3	100	C18
$N + NO_2 \rightarrow N_2O + O$	5.8×10^{-12}	–220	1.2×10^{-11}	1.5	100	C19
$NO + O_3 \rightarrow NO_2 + O_2$	3.0×10^{-12}	1500	1.9×10^{-14}	1.1	200	C20
$NO + NO_3 \rightarrow 2NO_2$	1.5×10^{-11}	–170	2.6×10^{-11}	1.3	100	C21
$NO_2 + O_3 \rightarrow NO_3 + O_2$	1.2×10^{-13}	2450	3.2×10^{-17}	1.15	150	C22
$NO_2 + NO_3 \rightarrow NO + NO_2 + O_2$ $NO_2 + NO_3 \xrightarrow{M} N_2O_5$	(See Note) (See Table 2-1)					C23
$NO_3 + NO_3 \rightarrow 2NO_2 + O_2$	8.5×10^{-13}	2450	2.3×10^{-16}	1.5	500	C24
$NH_2 + O_2 \rightarrow$ products			$<6.0\times10^{-21}$			C25
$NH_2 + O_3 \rightarrow$ products	4.3×10^{-12}	930	1.9×10^{-13}	3.0	500	C26
$NH_2 + NO \rightarrow$ products	4.0×10^{-12}	–450	1.8×10^{-11}	1.3	150	C27
$NH_2 + NO_2 \rightarrow$ products	2.1×10^{-12}	–650	1.9×10^{-11}	3.0	250	C28
$NH + NO \rightarrow$ products	4.9×10^{-11}	0	4.9×10^{-11}	1.5	300	C29
$NH + NO_2 \rightarrow$ products	3.5×10^{-13}	–1140	1.6×10^{-11}	2.0	500	C30
$O_3 + HNO_2 \rightarrow O_2 + HNO_3$			$<5.0\times10^{-19}$			C31
$N_2O_5 + H_2O \rightarrow 2HNO_3$			$<2.0\times10^{-21}$			C32
$N_2(A,v) + O_2 \rightarrow$ products			2.5×10^{-12}, v=0	1.5		C33
$N_2(A,v) + O_3 \rightarrow$ products			4.1×10^{-11}, v=0	2.0		C34
Reactions of Organic Compounds						
$O + CH_3 \rightarrow$ products	1.1×10^{-10}	0	1.1×10^{-10}	1.3	250	D 1
$O + HCN \rightarrow$ products	1.0×10^{-11}	4000	1.5×10^{-17}	10	1000	D 2
$O + C_2H_2 \rightarrow$ products	3.0×10^{-11}	1600	1.4×10^{-13}	1.3	250	D 3
$O + H_2CO \rightarrow$ products	3.4×10^{-11}	1600	1.6×10^{-13}	1.25	250	D 4

Reaction	A-Factor[a]	E/R	k(298 K)[a]	f(298 K)[b]	g	Notes
$O_2 + HOCO \rightarrow HO_2 + CO_2$			$2x10^{-12}$ (See Note)	2		D 5
$O + CH_3CHO \rightarrow CH_3CO + OH$	1.8×10^{-11}	1100	4.5×10^{-13}	1.25	200	D 6
$O_3 + C_2H_2 \rightarrow$ products	1.0×10^{-14}	4100	1.0×10^{-20}	3	500	D 7
$O_3 + C_2H_4 \rightarrow$ products	1.2×10^{-14}	2630	1.7×10^{-18}	1.25	100	D 8
$O_3 + C_3H_6 \rightarrow$ products	6.5×10^{-15}	1900	1.1×10^{-17}	1.15	200	D 9
$OH + CO \rightarrow$ Products	(See Table 2-1)					D10
$OH + CH_4 \rightarrow CH_3 + H_2O$	2.45×10^{-12}	1775	6.3×10^{-15}	1.1	100	D11
$OH + {}^{13}CH_4 \rightarrow {}^{13}CH_3 + H_2O$	(See Note)					D12
$OH + CH_3D \rightarrow$ products	3.5×10^{-12}	1950	5.0×10^{-15}	1.15	200	D13
$OH + H_2CO \rightarrow H_2O + HCO$	5.5×10^{-12}	-125	8.5×10^{-12}	1.15	50	D14
$OH + CH_3OH \rightarrow$ products	2.9×10^{-12}	345	9.1×10^{-13}	1.10	60	D15
$OH + CH_3OOH \rightarrow$ products	3.8×10^{-12}	–200	7.4×10^{-12}	1.4	150	D16
$OH + HC(O)OH \rightarrow$ products	4.0×10^{-13}	0	4.0×10^{-13}	1.2	100	D17
$OH + HC(O)C(O)H \rightarrow$ products	1.15×10^{-11}	0	$1.15x10^{-11}$	1.5	200	D18
$OH + HOCH_2CHO \rightarrow$ products	1.1×10^{-11}	0	$1.1x10^{-11}$	1.2	200	D19
$OH + HCN \rightarrow$ products	1.2×10^{-13}	400	3.1×10^{-14}	3	150	D20
$OH + C_2H_2 \xrightarrow{M}$ products	(See Table 2)					
$OH + C_2H_4 \xrightarrow{M}$ products	(See Table 2)					
$OH + C_2H_6 \rightarrow H_2O + C_2H_5$	8.7×10^{-12}	1070	2.4×10^{-13}	1.1	100	D21
$OH + C_3H_8 \rightarrow$ products	8.7×10^{-12}	615	$1.1x10^{-12}$	1.05	50	D22
$OH + C_2H_5CHO \rightarrow C_2H_5CO + H_2O$	4.9×10^{-12}	–405	1.9×10^{-11}	1.05	80	D23
$OH + 1\text{–}C_3H_7OH \rightarrow$ products	4.4×10^{-12}	–70	5.6×10^{-12}	1.05	80	D24
$OH + 2\text{–}C_3H_7OH \rightarrow$ products	3.0×10^{-12}	–180	5.5×10^{-12}	1.05	80	D25
$OH + C_2H_5C(O)OH \rightarrow$ products	1.2×10^{-12}	0	1.2×10^{-12}	1.1	200	D26

Reaction	A-Factor[a]	E/R	k(298 K)[a]	f(298 K)[b]	g	Notes
$OH + CH_3C(O)CH_3 \rightarrow H_2O + CH_3C(O)CH_2$ $\rightarrow CH_3 + CH_3C(O)OH$	See Note		< 2% of k			D27
$OH + CH_3CN \rightarrow$ products	7.8×10^{-13}	1050	2.3×10^{-14}	1.5	200	D28
$OH + CH_3ONO_2 \rightarrow$ products	8.0×10^{-13}	1000	2.8×10^{-14}	1.7	200	D29
$OH + CH_3C(O)O_2NO_2$ (PAN) $\rightarrow$ products			$<4 \times 10^{-14}$			D30
$OH + C_2H_5ONO_2 \rightarrow$ products	1.0×10^{-12}	490	2.0×10^{-13}	1.4	150	D31
$OH + 1\text{–}C_3H_7ONO_2 \rightarrow$ products	7.1×10^{-13}	0	7.1×10^{-13}	1.5	200	D32
$OH + 2\text{–}C_3H_7ONO_2 \rightarrow$ products	1.2×10^{-12}	320	4.1×10^{-13}	1.5	200	D33
$HO_2 + CH_2O \rightarrow$ adduct	6.7×10^{-15}	–600	5.0×10^{-14}	5	600	D34
$HO_2 + CH_3O_2 \rightarrow CH_3OOH + O_2$	4.1×10^{-13}	–750	5.2×10^{-12}	1.3	150	D35
$HO_2 + C_2H_5O_2 \rightarrow C_2H_5OOH + O_2$	7.5×10^{-13}	–700	8.0×10^{-12}	1.5	250	D36
$HO_2 + CH_3C(O)O_2 \rightarrow$ products	4.3×10^{-13}	–1040	1.4×10^{-11}	2	500	D37
$HO_2 + CH_3C(O)CH_2O_2 \rightarrow$ products	8.6×10^{-13}	–700	9.0×10^{-12}	2	300	D38
$NO_3 + CO \rightarrow$ products			$<4.0\times10^{-19}$			D39
$NO_3 + CH_2O \rightarrow$ products			5.8×10^{-16}	1.3		D40
$NO_3 + CH_3CHO \rightarrow$ products	1.4×10^{-12}	1900	2.4×10^{-15}	1.3	300	D41
$CH_3 + O_2 \rightarrow$ products			$<3.0\times10^{-16}$			D42
$CH_3 + O_2 \xrightarrow{M} CH_3O_2$	(See Table 2-1)					
$CH_3 + O_3 \rightarrow$ products	5.4×10^{-12}	220	2.6×10^{-12}	2	150	D43
$HCO + O_2 \rightarrow CO + HO_2$	5.2×10^{-12}	0	5.2×10^{-12}	1.4	100	D44
$CH_2OH + O_2 \rightarrow CH_2O + HO_2$	9.1×10^{-12}	0	9.1×10^{-12}	1.3	200	D45
$CH_3O + O_2 \rightarrow CH_2O + HO_2$	3.9×10^{-14}	900	1.9×10^{-15}	1.5	300	D46
$CH_3O + NO \rightarrow CH_2O + HNO$ $CH_3O + NO \xrightarrow{M} CH_3ONO$	(See Note) (See Table 2-1)					D47
$CH_3O + NO_2 \rightarrow CH_2O + HONO$	1.1×10^{-11}	1200	2.0×10^{-13}	5	600	D48

Reaction	A-Factor[a]	E/R	k(298 K)[a]	f(298 K)[b]	g	Notes
$CH_3O + NO_2 \xrightarrow{M} CH_3ONO_2$	(See Table 2-1)					
$CH_3O_2 + O_3 \rightarrow$ products	2.9×10^{-16}	1000	1.0×10^{-17}	3	500	D49
$CH_3O_2 + CH_3O_2 \rightarrow$ products	9.5×10^{-14}	–390	3.5×10^{-13}	1.2	100	D50
$CH_3O_2 + NO \rightarrow CH_3O + NO_2$	2.8×10^{-12}	–300	7.7×10^{-12}	1.15	100	D51
$CH_3O_2 + NO_2 \xrightarrow{M} CH_3O_2NO_2$	(See Table 2-1)					
$CH_3O_2 + CH_3C(O)O_2 \rightarrow$ products	2.0×10^{-12}	–500	1.1×10^{-11}	1.5	250	D52
$CH_3O_2 + CH_3C(O)CH_2O_2 \rightarrow$ products	7.5×10^{-13}	–500	4.0×10^{-12}	2	300	D53
$C_2H_5 + O_2 \rightarrow C_2H_4 + HO_2$ $C_2H_5 + O_2 \xrightarrow{M} C_2H_5O_2$	(See Table 2-1)		$<2.0\times10^{-14}$			D54
$C_2H_5O + O_2 \rightarrow CH_3CHO + HO_2$	6.3×10^{-14}	550	1.0×10^{-14}	1.5	200	D55
$C_2H_5O + NO \xrightarrow{M}$ products	(See Table 2-1)					
$C_2H_5O + NO_2 \xrightarrow{M}$ products	(See Table 2-1)					
$C_2H_5O_2 + C_2H_5O_2 \rightarrow$ products	6.8×10^{-14}	0	6.8×10^{-14}	2	300	D56
$C_2H_5O_2 + NO \rightarrow$ products	2.6×10^{-12}	–365	8.7×10^{-12}	1.2	150	D57
$CH_3C(O)O_2 + CH_3C(O)O_2 \rightarrow$ products	2.9×10^{-12}	–500	1.5×10^{-11}	1.5	150	D58
$CH_3C(O)O_2 + NO \rightarrow$ products	8.1×10^{-12}	–270	2.0×10^{-11}	1.5	100	D59
$CH_3C(O)O_2 + NO_2 \xrightarrow{M}$ products	(See Table 2-1)					
$CH_3C(O)CH_2O_2 + NO \rightarrow$ products	2.9×10^{-12}	–300	8.0×10^{-12}	1.5	300	D60
FO_x Reactions						
$O + FO \rightarrow F + O_2$	2.7×10^{-11}	0	2.7×10^{-11}	3.0	250	E 1
$O + FO_2 \rightarrow FO + O_2$	5.0×10^{-11}	0	5.0×10^{-11}	5.0	250	E 2
$OH + CH_3F \rightarrow CH_2F + H_2O$ (HFC–41)	2.5×10^{-12}	1430	2.1×10^{-14}	1.15	150	E 3
$OH + CH_2F_2 \rightarrow CHF_2 + H_2O$ (HFC-32)	1.7×10^{-12}	1500	1.1×10^{-14}	1.15	150	E 4
$OH + CHF_3 \rightarrow CF_3 + H_2O$ (HFC-23)	6.3×10^{-13}	2300	2.8×10^{-16}	1.2	200	E 5
$OH + CH_3CH_2F \rightarrow$ products (HFC-161)	2.5×10^{-12}	730	2.2×10^{-13}	1.15	150	E 6

Reaction	A-Factor[a]	E/R	k(298 K)[a]	f(298 K)[b]	g	Notes
OH + CH_3CHF_2 → products (HFC-152a)	9.4×10^{-13}	990	3.4×10^{-14}	1.1	100	E 7
OH + CH_2FCH_2F → $CHFCH_2F$ + H_2O (HFC-152)	1.1×10^{-12}	730	9.7×10^{-14}	1.1	150	E 8
OH + CH_3CF_3 → CH_2CF_3 + H_2O (HFC-143a)	1.1×10^{-12}	2010	1.3×10^{-15}	1.1	100	E 9
OH + CH_2FCHF_2 → products (HFC-143)	3.9×10^{-12}	1620	1.7×10^{-14}	1.2	200	E10
OH + CH_2FCF_3 → $CHFCF_3$ + H_2O (HFC-134a)	1.05×10^{-12}	1630	4.4×10^{-15}	1.1	200	E11
OH + CHF_2CHF_2 → CF_2CHF_2 + H_2O (HFC-134)	1.6×10^{-12}	1660	6.1×10^{-15}	1.2	200	E12
OH + CHF_2CF_3 → CF_2CF_3 + H_2O (HFC-125)	6.0×10^{-13}	1700	2.0×10^{-15}	1.2	150	E13
OH + CH_3CHFCH_3 → products (HFC-281ea)	3.0×10^{-12}	490	5.8×10^{-13}	1.2	100	E14
OH + $CF_3CH_2CH_3$ → products (HFC-263fb)	–	–	4.2×10^{-14}	1.5	–	E15
OH + $CH_2FCF_2CHF_2$ → products (HFC-245ca)	2.1×10^{-12}	1620	9.2×10^{-15}	1.2	150	E16
OH + $CHF_2CHFCHF_2$ → products (HFC-245ea)	–	–	1.6×10^{-14}	2.0	–	E17
OH + CF_3CHFCH_2F → products (HFC-245eb)	–	–	1.5×10^{-14}	2.0	–	E18
OH + $CHF_2CH_2CF_3$ → products (HFC-245fa)	6.1×10^{-13}	1330	7.0×10^{-15}	1.2	150	E19
OH + $CF_3CF_2CH_2F$ → CF_3CF_2CHF + H_2O (HFC-236cb)	*1.3×10^{-12}*	*1700*	*4.4×10^{-15}*	2.0	*200*	E20
OH + $CF_3CHFCHF_2$ → products (HFC-236ea)	9.4×10^{-13}	1550	5.2×10^{-15}	1.2	200	E21
OH + $CF_3CH_2CF_3$ → CF_3CHCF_3 + H_2O (HFC–236fa)	1.45×10^{-12}	2500	3.3×10^{-16}	1.15	150	E22
OH + CF_3CHFCF_3 → CF_3CFCF_3+H_2O (HFC-227ea)	4.3×10^{-13}	1650	1.7×10^{-15}	1.1	150	E23
OH + $CF_3CH_2CF_2CH_3$ → products (HFC-365mfc)	1.8×10^{-12}	1660	6.9×10^{-15}	1.3	150	E24
OH + $CF_3CH_2CH_2CF_3$ → products (HFC-356mff)	3.4×10^{-12}	1820	7.6×10^{-15}	1.2	300	E25
OH + $CF_3CF_2CH_2CH_2F$ → products (HFC-356mcf)	1.7×10^{-12}	1100	4.2×10^{-14}	1.3	150	E26
OH + $CHF_2CF_2CF_2CF_2H$ → products (HFC-338pcc)	7.7×10^{-13}	1540	4.4×10^{-15}	1.2	150	E27
OH + $CF_3CH_2CF_2CH_2CF_3$ → products (HFC-458mfcf)	1.1×10^{-12}	1800	2.6×10^{-15}	1.5	200	E28
OH + $CF_3CHFCHFCF_2CF_3$ → products (HFC-43-10mee)	5.2×10^{-13}	1500	3.4×10^{-15}	1.2	150	E29
OH + $CF_3CF_2CH_2CH_2CF_2CF_3$ → products (HFC–55-10-mcff)	*3.5×10^{-12}*	*1800*	8.3×10^{-15}	1.5	*300*	E30
OH + CH_2=CHF → products	1.5×10^{-12}	–390	5.5×10^{-12}	1.3	150	E31

Reaction	A-Factor[a]	E/R	k(298 K)[a]	f(298 K)[b]	g	Notes
$OH + CH_2{=}CF_2 \rightarrow$ products	*6.2×10^{-13}*	*–350*	2.0×10^{-12}	1.5	*150*	E32
$OH + CF_2{=}CF_2 \rightarrow$ products	3.4×10^{-12}	–320	1.0×10^{-11}	1.15	100	E33
$OH + CF_3OH \rightarrow CF_3O + H_2O$			$<2\times10^{-17}$			E34
$OH + CH_2(OH)CF_3 \rightarrow$ products	1.6×10^{-12}	830	9.8×10^{-14}	1.15	200	E35
$OH + CH_2(OH)CF_2CF_3 \rightarrow$ products	1.15×10^{-12}	730	1.0×10^{-13}	1.2	200	E36
$OH + CF_3CH(OH)CF_3 \rightarrow$ products	5.1×10^{-13}	900	2.5×10^{-14}	1.3	200	E37
$OH + CH_3OCHF_2 \rightarrow$ products (HFOC-152a)	6.0×10^{-12}	1530	3.5×10^{-14}	1.3	200	E38
$OH + CF_3OCH_3 \rightarrow CF_3OCH_2 + H_2O$ (HFOC-143a)	1.5×10^{-12}	1450	1.2×10^{-14}	1.1	150	E39
$OH + CF_2HOCF_2H \rightarrow CF_2OCF_2H + H_2O$ (HFOC-134)	1.1×10^{-12}	1830	2.4×10^{-15}	1.15	150	E40
$OH + CF_3OCHF_2 \rightarrow CF_3OCF_2 + H_2O$ (HFOC-125)	4.6×10^{-13}	2040	4.9×10^{-16}	1.2	200	E41
$OH + CHF_2OCH_2CF_3 \rightarrow$ products (HFOC-245fa)	3.1×10^{-12}	1660	1.2×10^{-14}	1.2	200	E42
$OH + CH_3OCF_2CHF_2 \rightarrow$ products	1.7×10^{-12}	1300	2.2×10^{-14}	1.3	200	E43
$OH + CH_3OCF_2CF_3 \rightarrow$ products	1.1×10^{-12}	1370	1.1×10^{-14}	1.2	150	E44
$OH + CH_3OCF_2CF_2CF_3 \rightarrow$ products	1.4×10^{-12}	1440	1.1×10^{-14}	1.15	150	E45
$OH + CH_3OCF(CF_3)_2 \rightarrow$ products	1.3×10^{-12}	1330	1.5×10^{-14}	1.3	200	E46
$OH + CHF_2OCH_2CF_2CHF_2 \rightarrow$ products	1.8×10^{-12}	1410	1.6×10^{-14}	1.3	200	E47
$OH + CHF_2OCH_2CF_2CF_3 \rightarrow$ products	1.6×10^{-12}	1510	1.0×10^{-14}	1.3	200	E48
$F + O_2 \xrightarrow{M} FO_2$	(See Table 2-1)					
$F + O_3 \rightarrow FO + O_2$	2.2×10^{-11}	230	1.0×10^{-11}	1.5	200	E49
$F + H_2 \rightarrow HF + H$	1.4×10^{-10}	500	2.6×10^{-11}	1.2	200	E50
$F + H_2O \rightarrow HF + OH$	1.4×10^{-11}	0	1.4×10^{-11}	1.3	200	E51
$F + NO \xrightarrow{M} FNO$	(See Table 2-1)					
$F + NO_2 \xrightarrow{M} FNO_2$	(See Table 2-1)					
$F + HNO_3 \rightarrow HF + NO_3$	6.0×10^{-12}	–400	2.3×10^{-11}	1.3	200	E52
$F + CH_4 \rightarrow HF + CH_3$	1.6×10^{-10}	260	6.7×10^{-11}	1.4	200	E53

Reaction	A-Factor[a]	E/R	k(298 K)[a]	f(298 K)[b]	g	Notes
$FO + O_3 \rightarrow$ products			$<1 \times 10^{-14}$			E54
$FO + NO \rightarrow NO_2 + F$	8.2×10^{-12}	–300	2.2×10^{-11}	1.5	200	E55
$FO + NO_2 \xrightarrow{M} FONO_2$	(See Table 2-1)					
$FO + FO \rightarrow 2F + O_2$	1.0×10^{-11}	0	1.0×10^{-11}	1.5	250	E56
$FO_2 + O_3 \rightarrow$ products			$<3.4\times10^{-16}$			E57
$FO_2 + NO \rightarrow FNO + O_2$	7.5×10^{-12}	690	7.5×10^{-13}	2.0	400	E58
$FO_2 + NO_2 \rightarrow$ products	3.8×10^{-11}	2040	4.0×10^{-14}	2.0	500	E59
$FO_2 + CO \rightarrow$ products			$<5.1\times10^{-16}$			E60
$FO_2 + CH_4 \rightarrow$ products			$<2\times10^{-16}$			E61
$CF_3 + O_2 \xrightarrow{M} CF_3O_2$	(See Table 2-1)					
$CF_3O + M \rightarrow F + CF_2O + M$	(See Table 2-1)					
$CF_3O + O_2 \rightarrow FO_2 + CF_2O$	$<3 \times 10^{-11}$	5000	$<1.5 \times 10^{-18}$	1.3	–	E62
$CF_3O + O_3 \rightarrow CF_3O_2 + O_2$	2×10^{-12}	1400	1.8×10^{-14}		600	E63
$CF_3O + H_2O \rightarrow OH + CF_3OH$	3×10^{-12}	>3600	$<2 \times 10^{-17}$	1.2	–	E64
$CF_3O + NO \rightarrow CF_2O + FNO$	3.7×10^{-11}	–110	5.4×10^{-11}		70	E65
$CF_3O + NO_2 \rightarrow$ products $\xrightarrow{M} CF_3ONO_2$	(See Note) (See Table 2-1)					E66
$CF_3O + CO \rightarrow$ products $\xrightarrow{M} CF_3OCO$	(See Table 2-1)		$<2 \times 10^{-15}$			E67
$CF_3O + CH_4 \rightarrow CH_3 + CF_3OH$	2.6×10^{-12}	1420	2.2×10^{-14}	1.1	200	E68
$CF_3O + C_2H_6 \rightarrow C_2H_5 + CF_3OH$	4.9×10^{-12}	400	1.3×10^{-12}	1.2	100	E69
$CF_3O_2 + O_3 \rightarrow CF_3O + 2O_2$			$<3 \times 10^{-15}$			E70
$CF_3O_2 + CO \rightarrow CF_3O + CO_2$			$<5 \times 10^{-16}$			E71
$CF_3O_2 + NO \rightarrow CF_3O + NO_2$	5.4×10^{-12}	–320	1.6×10^{-11}	1.1	150	E72
$CF_3O_2 + NO_2 \xrightarrow{M} CF_3O_2NO_2$	(See Table 2-1)					

Reaction	A-Factor[a]	E/R	k(298 K)[a]	f(298 K)[b]	g	Notes
ClO_x Reactions						
$O + ClO \rightarrow Cl + O_2$	2.8×10^{-11}	-85	3.7×10^{-11}	1.10	50	F 1
$O + OClO \rightarrow ClO + O_2$	2.4×10^{-12}	960	1.0×10^{-13}	2.0	300	F 2
$O + OClO \xrightarrow{M} ClO_3$	(See Table 2-1)					
$O + Cl_2O \rightarrow ClO + ClO$	2.7×10^{-11}	530	4.5×10^{-12}	1.3	150	F 3
$O + HCl \rightarrow OH + Cl$	1.0×10^{-11}	3300	1.5×10^{-16}	2.0	350	F 4
$O + HOCl \rightarrow OH + ClO$	1.7×10^{-13}	0	1.7×10^{-13}	3.0	300	F 5
$O + ClONO_2 \rightarrow$ products	2.9×10^{-12}	800	2.0×10^{-13}	1.5	200	F 6
$O_3 + OClO \rightarrow$ products	2.1×10^{-12}	4700	3.0×10^{-19}	2.5	1000	F 7
$O_3 + Cl_2O_2 \rightarrow$ products			$<1.0\times10^{-19}$			F 8
$OH + Cl_2 \rightarrow HOCl + Cl$	1.4×10^{-12}	900	6.7×10^{-14}	1.2	400	F 9
$OH + ClO \rightarrow Cl + HO_2$ $\rightarrow HCl + O_2$	7.4×10^{-12} 6.0×10^{-13}	–270 –230	1.8×10^{-11} 1.3×10^{-12}	1.4 3.0	100 150	F10
$OH + OClO \rightarrow HOCl + O_2$	4.5×10^{-13}	–800	6.8×10^{-12}	2.0	200	F11
$OH + HCl \rightarrow H_2O + Cl$	2.6×10^{-12}	350	8.0×10^{-13}	1.1	100	F12
$OH + HOCl \rightarrow H_2O + ClO$	3.0×10^{-12}	500	5.0×10^{-13}	3.0	500	F13
$OH + ClNO_2 \rightarrow HOCl + NO_2$	2.4×10^{-12}	1250	3.6×10^{-14}	2.0	300	F14
$OH + ClONO_2 \rightarrow$ products	1.2×10^{-12}	330	3.9×10^{-13}	1.5	200	F15
$OH + CH_3Cl \rightarrow CH_2Cl + H_2O$	2.4×10^{-12}	1250	3.6×10^{-14}	1.15	100	F16
$OH + CH_2Cl_2 \rightarrow CHCl_2 + H_2O$	1.9×10^{-12}	870	1.0×10^{-13}	1.15	100	F17
$OH + CHCl_3 \rightarrow CCl_3 + H_2O$	2.2×10^{-12}	920	1.0×10^{-13}	1.15	150	F18
$OH + CCl_4 \rightarrow$ products	*~1.0×10^{-12}*	*>2300*	$<5.0\times10^{-16}$	–	–	F19
$OH + CH_2FCl \rightarrow CHClF + H_2O$ (HCFC-31)	2.4×10^{-12}	1210	4.1×10^{-14}	1.15	200	F20
$OH + CHFCl_2 \rightarrow CFCl_2 + H_2O$ (HCFC-21)	1.2×10^{-12}	1100	3.0×10^{-14}	1.2	150	F21
$OH + CHF_2Cl \rightarrow CF_2Cl + H_2O$ (HCFC-22)	1.05×10^{-12}	1600	4.8×10^{-15}	1.1	150	F22
$OH + CFCl_3 \rightarrow$ products (CFC-11)	*~1.0×10^{-12}*	*>3700*	$<5.0\times10^{-18}$			F23

Reaction	A-Factor[a]	E/R	k(298 K)[a]	f(298 K)[b]	g	Notes
OH + CF_2Cl_2 → products (CFC-12)	*~1.0×10^{-12}*	*>3600*	<6.0×10^{-18}			F24
OH + CH_2ClCH_3 → products	5.4×10^{-12}	800	3.7×10^{-13}	1.2	100	F25
OH + CH_3CCl_3 → CH_2CCl_3 + H_2O	1.64×10^{-12}	1520	1.0×10^{-14}	1.15	100	F26
OH + CH_3CFCl_2 → CH_2CFCl_2 + H_2O (HCFC-141b)	1.25×10^{-12}	1600	5.8×10^{-15}	1.15	150	F27
OH + CH_3CF_2Cl → CH_2CF_2Cl + H_2O (HCFC-142b)	1.3×10^{-12}	1770	3.4×10^{-15}	1.2	150	F28
OH + CH_2ClCF_2Cl → $CHClCF_2Cl$ +H_2O (HCFC-132b)	3.6×10^{-12}	1600	1.7×10^{-14}	1.5	200	F29
OH + CH_2ClCF_3 → $CHClCF_3$ + H_2O (HCFC-133a)	5.6×10^{-13}	1100	1.4×10^{-14}	1.3	200	F30
OH + $CHCl_2CF_2Cl$ → CCl_2CF_2Cl (HCFC-122) + H_2O	7.7×10^{-13}	810	5.1×10^{-14}	1.2	150	F31
OH + $CHFClCFCl_2$ → $CFClCFCl_2$ (HCFC-122a) + H_2O	7.1×10^{-13}	1140	1.6×10^{-14}	1.3	150	F32
OH + $CHCl_2CF_3$ → CCl_2CF_3 + H_2O (HCFC-123)	6.3×10^{-13}	850	3.6×10^{-14}	1.2	100	F33
OH + $CHFClCF_2Cl$ → $CFClCF_2Cl$ +H_2O (HCFC-123a)	8.6×10^{-13}	1250	1.3×10^{-14}	1.3	200	F34
OH + $CHFClCF_3$ → $CFClCF_3$ + H_2O (HCFC-124)	7.1×10^{-13}	1300	9.0×10^{-15}	1.15	100	F35
OH + $CH_3CF_2CFCl_2$ → products (HCFC-243cc)	7.7×10^{-13}	1720	2.4×10^{-15}	1.3	200	F36
OH + $CHCl_2CF_2CF_3$ → products (HCFC-225ca)	6.3×10^{-13}	960	2.5×10^{-14}	1.2	200	F37
OH + $CHFClCF_2CF_2Cl$ → products (HCFC-225cb)	5.5×10^{-13}	1230	8.9×10^{-15}	1.2	150	F38
OH + CH_2=CHCl → products	1.3×10^{-12}	–500	6.9×10^{-12}	1.2	100	F39
OH + CH_2=CCl_2 → products	1.9×10^{-12}	–530	1.1×10^{-11}	1.15	150	F40
OH + CHCl=CCl_2 → products	8.0×10^{-13}	–300	2.2×10^{-12}	1.2	100	F41
OH + CCl_2=CCl_2 → products	4.7×10^{-12}	990	1.7×10^{-13}	1.2	200	F42
OH + CH_3OCl → products	2.5×10^{-12}	370	7.1×10^{-13}	2.0	150	F43
OH + CCl_3CHO → H_2O + CCl_3CO	9.1×10^{-12}	580	1.3×10^{-12}	1.3	200	F44
HO_2 + Cl → HCl + O_2	1.8×10^{-11}	–170	3.2×10^{-11}	1.5	200	F45
→ OH + ClO	4.1×10^{-11}	450	9.1×10^{-12}	2.0	200	F45
HO_2 + ClO → HOCl + O_2	2.7×10^{-12}	–220	5.6×10^{-12}	1.3	200	F46
H_2O + $ClONO_2$ → products			<2.0×10^{-21}			F47

Reaction	A-Factor[a]	E/R	k(298 K)[a]	f(298 K)[b]	g	Notes
$NO + OClO \rightarrow NO_2 + ClO$	2.5×10^{-12}	600	3.4×10^{-13}	2.0	300	F48
$NO + Cl_2O_2 \rightarrow$ products			$<2.0\times10^{-14}$			F49
$NO_3 + OClO \xrightarrow{M} O_2ClONO_2$	(See Table 2-1)					
$NO_3 + HCl \rightarrow HNO_3 + Cl$			$<5.0\times10^{-17}$			F50
$HO_2NO_2 + HCl \rightarrow$ products			$<1.0\times10^{-21}$			F51
$Cl + O_2 \xrightarrow{M} ClOO$	(See Table 2-1)					
$Cl + O_3 \rightarrow ClO + O_2$	2.3×10^{-11}	200	1.2×10^{-11}	1.15	50	F52
$Cl + H_2 \rightarrow HCl + H$	3.05×10^{-11}	2270	1.5×10^{-14}	1.1	100	F53
$Cl + H_2O_2 \rightarrow HCl + HO_2$	1.1×10^{-11}	980	4.1×10^{-13}	1.3	300	F54
$Cl + NO \xrightarrow{M} NOCl$	(See Table 2-1)					
$Cl + NO_2 \xrightarrow{M} ClONO\ (ClNO_2)$	(See Table 2-1)					
$Cl + NO_3 \rightarrow ClO + NO_2$	2.4×10^{-11}	0	2.4×10^{-11}	1.5	400	F55
$Cl + N_2O \rightarrow ClO + N_2$	(See Note)					F56
$Cl + HNO_3 \rightarrow$ products			$<2.0\times10^{-16}$			F57
$Cl + HO_2NO_2 \rightarrow$ products			$<1\times10^{-13}$			F58
$Cl + CO \xrightarrow{M} ClCO$	(See Table 2-1)					
$Cl + CH_4 \rightarrow HCl + CH_3$	7.3×10^{-12}	1280	1.0×10^{-13}	1.05	50	F59
$Cl + CH_3D \rightarrow$ products	7.0×10^{-12}	1380	6.8×10^{-14}	1.07	50	F60
$Cl + H_2CO \rightarrow HCl + HCO$	8.1×10^{-11}	30	7.3×10^{-11}	1.15	100	F61
$Cl + HC(O)OH \rightarrow$ products			2.0×10^{-13}	1.5		F62
$Cl + CH_3O_2 \rightarrow$ products			1.6×10^{-10}	1.5		F63
$Cl + CH_3OH \rightarrow CH_2OH + HCl$	5.5×10^{-11}	0	5.5×10^{-11}	1.2	100	F64
$Cl + CH_3OOH \rightarrow$ products			5.7×10^{-11}	2.0		F65
$Cl + CH_3ONO_2 \rightarrow$ products	*1.3×10^{-11}*	*1200*	2.3×10^{-13}	1.5	*300*	F66
$Cl + C_2H_2 \xrightarrow{M} ClC_2H_2$	(See Table 2-1)					

Reaction	A-Factor[a]	E/R	k(298 K)[a]	f(298 K)[b]	g	Notes
$Cl + C_2H_4 \xrightarrow{M} ClC_2H_4$	(See Table 2-1)					
$Cl + C_2H_6 \rightarrow HCl + C_2H_5$	7.2×10^{-11}	70	5.7×10^{-11}	1.07	20	F67
$Cl + C_2H_5O_2 \rightarrow ClO + C_2H_5O$			7.4×10^{-11}	2.0		F68
$\rightarrow HCl + C_2H_4O_2$			7.7×10^{-11}	2.0		F68
$Cl + CH_3CH_2OH \rightarrow$ products	9.6×10^{-11}	0	9.6×10^{-11}	1.2	100	F69
$Cl + CH_3C(O)OH \rightarrow$ products			2.8×10^{-14}	2.0		F70
$Cl + CH_3CN \rightarrow$ products	1.6×10^{-11}	2140	1.2×10^{-14}	2.0	300	F71
$Cl + C_2H_5ONO_2 \rightarrow$ products	*1.5×10^{-11}*	*400*	3.9×10^{-12}	1.5	*200*	F72
$Cl + CH_3CO_3NO_2 \rightarrow$ products			$<1\times10^{-14}$			F73
$Cl + C_3H_8 \rightarrow HCl + CH_3CHCH_3$	6.54×10^{-11}		8.0×10^{-11}	1.1	20	F74
$\rightarrow HCl + CH_2CH_2CH_3$	7.85×10^{-11}	80	6.0×10^{-11}	1.05	20	F74
$Cl + CH_3C(O)CH_3 \rightarrow CH_3C(O)CH_2 + HCl$	7.7×10^{-11}	1000	2.7×10^{-12}	1.3	500	F75
$Cl + C_2H_5CO_3NO_2 \rightarrow$ products			1.1×10^{-12}	2.0		F76
$Cl + 1\text{-}C_3H_7ONO_2 \rightarrow$ products	*4.5×10^{-11}*	*200*	2.3×10^{-11}	1.5	*200*	F77
$Cl + 2\text{-}C_3H_7ONO_2 \rightarrow$ products	*2.3×10^{-11}*	*400*	6.0×10^{-12}	2.0	*200*	F78
$Cl + OClO \rightarrow ClO + ClO$	3.4×10^{-11}	–160	5.8×10^{-11}	1.25	200	F79
$Cl + ClOO \rightarrow Cl_2 + O_2$	2.3×10^{-10}	0	2.3×10^{-10}	3.0	250	F80
$\rightarrow ClO + ClO$	1.2×10^{-11}	0	1.2×10^{-11}	3.0	250	F80
$Cl + Cl_2O \rightarrow Cl_2 + ClO$	6.2×10^{-11}	–130	9.6×10^{-11}	1.2	130	F81
$Cl + Cl_2O_2 \rightarrow$ products			1.0×10^{-10}	2.0		F82
$Cl + HOCl \rightarrow$ products	2.5×10^{-12}	130	1.6×10^{-12}	1.5	250	F83
$Cl + ClNO \rightarrow NO + Cl_2$	5.8×10^{-11}	–100	8.1×10^{-11}	1.5	200	F84
$Cl + ClONO_2 \rightarrow$ products	6.5×10^{-12}	–135	1.0×10^{-11}	1.2	50	F85
$Cl + CH_3Cl \rightarrow CH_2Cl + HCl$	2.17×10^{-11}	1130	4.9×10^{-13}	1.07	50	F86
$Cl + CH_2Cl_2 \rightarrow HCl + CHCl_2$	7.4×10^{-12}	910	3.5×10^{-13}	1.07	100	F87

Reaction	A-Factor[a]	E/R	k(298 K)[a]	f(298 K)[b]	g	Notes
$Cl + CHCl_3 \rightarrow HCl + CCl_3$	3.310^{-12}	990	$1.2x10^{-13}$	1.15	100	F88
$Cl + CH_3F \rightarrow HCl + CH_2F$ (HFC-41)	$1.96x10^{-11}$	1200	$3.5x10^{-13}$	1.15	150	F89
$Cl + CH_2F_2 \rightarrow HCl + CHF_2$ (HFC-32)	*$4.9x10^{-12}$*	*1500*	$3.2x10^{-14}$	1.5	200	F90
$Cl + CHF_3 \rightarrow HCl + CF_3$ (HFC-23)			$<5.0x10^{-16}$			F91
$Cl + CH_2FCl \rightarrow HCl + CHFCl$ (HCFC-31)	*$5.9x10^{-12}$*	*1200*	$1.05x10^{-13}$	1.1	200	F92
$Cl + CHFCl_2 \rightarrow HCl + CFCl_2$ (HCFC-21)	$6.0x10^{-12}$	1700	$2.0x10^{-14}$	1.2	200	F93
$Cl + CHF_2Cl \rightarrow HCl + CF_2Cl$ (HCFC-22)	$5.6x10^{-12}$	2430	$1.6x10^{-15}$	1.15	200	F94
$Cl + CH_3CCl_3 \rightarrow CH_2CCl_3 + HCl$	$3.23x10^{-12}$	1770	$8.5x10^{-15}$	1.2	200	F95
$Cl + CH_3CH_2F \rightarrow HCl + CH_3CHF$ (HFC-161)	$1.82x10^{-11}$	330	$6.0x10^{-12}$	1.1	100	F96
$\rightarrow HCl + CH_2CH_2F$	$1.4x10^{-11}$	940	$6.0x10^{-13}$	1.15	100	F96
$Cl + CH_3CHF_2 \rightarrow HCl + CH_3CF_2$ (HFC-152a)	$5.8x10^{-12}$	950	$2.4x10^{-13}$	1.1	100	F97
$\rightarrow HCl + CH_2CHF_2$	$6.25x10^{-12}$	2320	$2.6x10^{-15}$	1.15	200	F97
$Cl + CH_2FCH_2F \rightarrow HCl + CHFCH_2F$ (HFC-152)	$2.27x10^{-11}$	1050	$6.7x10^{-13}$	1.15	200	F98
$Cl + CH_3CFCl_2 \rightarrow HCl + CH_2CFCl_2$ (HCFC-141b)	$3.4x10^{-12}$	2200	$2.1x10^{-15}$	1.15	200	F99
$Cl + CH_3CF_2Cl \rightarrow HCl + CH_2CF_2Cl$ (HCFC-142b)	$1.35x10^{-12}$	2400	$4.3x10^{-16}$	1.15	200	F100
$Cl + CH_3CF_3 \rightarrow HCl + CH_2CF_3$ (HFC-143a)	$1.44x10^{-11}$	3940	$2.6x10^{-17}$	3.0	300	F101
$Cl + CH_2FCHF_2 \rightarrow HCl + CH_2FCF_2$ (HFC-143)	$6.8x10^{-12}$	1670	$2.5x10^{-14}$	1.3	200	F102
$\rightarrow HCl + CHFCHF_2$	$9.1x10^{-12}$	1770	$2.4x10^{-14}$	1.3	200	F102
$Cl + CH_2ClCF_3 \rightarrow HCl + CHClCF_3$ (HCFC-133a)	$1.83x10^{-12}$	1680	$6.5x10^{-15}$	1.2	200	F103
$Cl + CH_2FCF_3 \rightarrow HCl + CHFCF_3$ (HFC-134a)	$2.4x10^{-12}$	2200	$1.5x10^{-15}$	1.1	200	F104
$Cl + CHF_2CHF_2 \rightarrow HCl + CF_2CHF_2$ (HCF-134)	$7.0x10^{-12}$	2430	$2.0x10^{-15}$	1.2	200	F105
$Cl + CHCl_2CF_3 \rightarrow HCl + CCl_2CF_3$ (HCFC-123)	$5.0x10^{-12}$	1800	$1.2x10^{-14}$	1.15	200	F106
$Cl + CHFClCF_3 \rightarrow HCl + CFClCF_3$ (HCFC-124)	$1.13x10^{-12}$	1800	$2.7x10^{-15}$	1.2	200	F107
$Cl + CHF_2CF_3 \rightarrow HCl + CF_2CF_3$ (HFC-125)	*$1.8x10^{-12}$*	*2600*	$3.0x10^{-16}$	1.5	300	F108
$Cl + C_2Cl_4 \xrightarrow{M} C_2Cl_5$	(See Table 2-1)					

Reaction	A-Factor[a]	E/R	k(298 K)[a]	f(298 K)[b]	g	Notes
$ClO + O_3 \rightarrow ClOO + O_2$			$<1.4\times10^{-17}$			F109
$\rightarrow OClO + O_2$	*1.0×10^{-12}*	*>4000*	$<1.0\times10^{-18}$			F109
$ClO + H_2 \rightarrow$ products	*~1.0×10^{-12}*	*>4800*	$<1.0\times10^{-19}$			F110
$ClO + NO \rightarrow NO_2 + Cl$	6.4×10^{-12}	–290	1.7×10^{-11}	1.15	100	F111
$ClO + NO_2 \xrightarrow{M} ClONO_2$	(See Table 2-1)					
$ClO + NO_3 \rightarrow ClOO + NO_2$	4.7×10^{-13}	0	4.7×10^{-13}	1.5	400	F112
$ClO + N_2O \rightarrow$ products	~1.0×10^{-12}	>4300	$<6.0\times10^{-19}$			F113
$ClO + CO \rightarrow$ products	~1.0×10^{-12}	>3700	$<4.0\times10^{-18}$			F114
$ClO + CH_4 \rightarrow$ products	~1.0×10^{-12}	>3700	$<4.0\times10^{-18}$			F115
$ClO + H_2CO \rightarrow$ products	~1.0×10^{-12}	>2100	$<1.0\times10^{-15}$			F116
$ClO + CH_3O_2 \rightarrow$ products	3.3×10^{-12}	115	2.2×10^{-12}	1.5	115	F117
$ClO + ClO \rightarrow Cl_2 + O_2$	1.0×10^{-12}	1590	4.8×10^{-15}	1.5	300	F118
$\rightarrow ClOO + Cl$	3.0×10^{-11}	2450	8.0×10^{-15}	1.5	500	F118
$\rightarrow OClO + Cl$	3.5×10^{-13}	1370	3.5×10^{-15}	1.5	300	F118
$ClO + ClO \xrightarrow{M} Cl_2O_2$	(See Table 2-1)					
$ClO + OClO \xrightarrow{M} Cl_2O_3$	(See Table 2-1)					
$HCl + ClONO_2 \rightarrow$ products			$<1.0\times10^{-20}$			F119
$CH_2Cl + O_2 \xrightarrow{M} CH_2ClO_2$	(See Table 2-1)					
$CHCl_2 + O_2 \xrightarrow{M} CHCl_2O_2$	(See Table 2-1)					
$CCl_3 + O_2 \xrightarrow{M} CCl_3O_2$	(See Table 2-1)					
$CFCl_2 + O_2 \xrightarrow{M} CFCl_2O_2$	(See Table 2-1)					
$CF_2Cl + O_2 \xrightarrow{M} CF_2ClO_2$	(See Table 2-1)					
$CCl_3O_2 + NO_2 \xrightarrow{M} CCl_3O_2NO_2$	(See Table 2-1)					
$CFCl_2O_2 + NO_2 \xrightarrow{M} CFCl_2O_2NO_2$	(See Table 2-1)					
$CF_2ClO_2 + NO_2 \xrightarrow{M} CF_2ClO_2NO_2$	(See Table 2-1)					

Reaction	A-Factor[a]	E/R	k(298 K)[a]	f(298 K)[b]	g	Notes
$CH_2ClO + O_2 \rightarrow CHClO + HO_2$			6×10^{-14}	5		F120
$CH_2ClO_2 + HO_2 \rightarrow CH_2ClO_2H + O_2$	3.3×10^{-13}	–820	5.2×10^{-12}	1.5	200	F121
$CH_2ClO_2 + NO \rightarrow CH_2ClO + NO_2$	7×10^{-12}	–300	1.9×10^{-11}	1.5	200	F122
$CCl_3O_2 + NO \rightarrow CCl_2O + NO_2 + Cl$	7.3×10^{-12}	–270	1.8×10^{-11}	1.3	200	F123
$CCl_2FO_2 + NO \rightarrow CClFO + NO_2 + Cl$	4.5×10^{-12}	–350	1.5×10^{-11}	1.3	200	F124
$CClF_2O_2 + NO \rightarrow CF_2O + NO_2 + Cl$	3.8×10^{-12}	–400	1.5×10^{-11}	1.2	200	F125
BrO_x Reactions						
$O + BrO \rightarrow Br + O_2$	1.9×10^{-11}	–230	4.1×10^{-11}	1.5	150	G 1
$O + HBr \rightarrow OH + Br$	5.8×10^{-12}	1500	3.8×10^{-14}	1.3	200	G 2
$O + HOBr \rightarrow OH + BrO$	1.2×10^{-10}	430	2.8×10^{-11}	3.0	300	G 3
$O + BrONO_2 \rightarrow NO_3 + BrO$	$1.9\text{x}10^{-11}$	-215	$3.9\text{x}10^{-11}$	1.25	40	G 4
$OH + Br_2 \rightarrow HOBr + Br$	2.1×10^{-11}	-240	4.6×10^{-11}	1.1	50	G 5
$OH + BrO \rightarrow$ products	$1.7\text{x}10^{-11}$	-250	3.9×10^{-11}	1.4	100	G 6
$OH + HBr \rightarrow H_2O + Br$	$5.5\text{x}10^{-12}$	-200	1.1×10^{-11}	1.1	100	G 7
$OH + CH_3Br \rightarrow CH_2Br + H_2O$	2.35×10^{-12}	1300	3.0×10^{-14}	1.1	100	G 8
$OH + CH_2Br_2 \rightarrow CHBr_2 + H_2O$	2.0×10^{-12}	840	1.2×10^{-13}	1.15	150	G 9
$OH + CHBr_3 \rightarrow CBr_3 + H_2O$	1.35×10^{-12}	600	1.8×10^{-13}	1.5	100	G10
$OH + CHF_2Br \rightarrow CF_2Br + H_2O$	1.0×10^{-12}	1380	1.0×10^{-14}	1.1	100	G11
$OH + CH_2ClBr \rightarrow CHClBr + H_2O$	2.4×10^{-12}	920	1.1×10^{-13}	1.1	100	G12
$OH + CF_2ClBr \rightarrow$ products (Halon-1211)	*~1×10⁻¹²*	*>2600*	$<1.5\times10^{-16}$			G13
$OH + CF_2Br_2 \rightarrow$ products (Halon-1202)	*~1×10⁻¹²*	*>2200*	$<5.0\times10^{-16}$			G14
$OH + CF_3Br \rightarrow$ products (Halon-1301)	*~1×10⁻¹²*	*>3600*	*<6.0×10⁻¹⁸*			G15
$OH + CH_2BrCH_3 \rightarrow$ products	2.9×10^{-12}	640	3.4×10^{-13}	1.2	150	G16
$OH + CH_2BrCF_3 \rightarrow CHBrCF_3 + H_2O$	1.4×10^{-12}	1340	1.6×10^{-14}	1.2	150	G17
$OH + CHFBrCF_3 \rightarrow CFBrCF_3 + H_2O$	7.3×10^{-13}	1120	1.7×10^{-14}	1.2	100	G18

Reaction	A-Factor[a]	E/R	k(298 K)[a]	f(298 K)[b]	g	Notes
$OH + CHClBrCF_3 \rightarrow CClBrCF_3 + H_2O$	1.1×10^{-12}	940	4.7×10^{-14}	1.2	150	G19
$OH + CHFClCF_2Br \rightarrow CFClCF_2Br + H_2O$	8.4×10^{-13}	1220	1.4×10^{-14}	1.3	200	G20
$OH + CF_2BrCF_2Br \rightarrow$ products (Halon-2402)	*~1×10⁻¹²*	*>3600*	*<6×10⁻¹⁸*			G21
$OH + CH_2BrCH_2CH_3 \rightarrow$ products	3.0×10^{-12}	330	1.0×10^{-12}	1.1	50	G22
$OH + CH_3CHBrCH_3 \rightarrow$ products	1.85×10^{-12}	270	7.5×10^{-13}	1.15	50	G23
$HO_2 + Br \rightarrow HBr + O_2$	4.8×10^{-12}	310	1.7×10^{-12}	1.3	150	G24
$HO_2 + BrO \rightarrow$ products	4.5×10^{-12}	–460	2.1×10^{-11}	1.15	100	G25
$NO_3 + HBr \rightarrow HNO_3 + Br$			$<1.0\times10^{-16}$			G26
$Cl + CH_2ClBr \rightarrow HCl + CHClBr$	*6.8×10^{-12}*	*870*	3.7×10^{-13}	1.2	100	G27
$Cl + CH_3Br \rightarrow HCl + CH_2Br$	1.4×10^{-11}	1030	4.4×10^{-13}	1.05	50	G28
$Cl + CH_2Br_2 \rightarrow HCl + CHBr_2$	6.3×10^{-12}	800	4.3×10^{-13}	1.1	50	G29
$Cl + CHBr_3 \rightarrow CBr_3 + HCl$	4.85×10^{-12}	850	2.8×10^{-13}	1.3	200	G30
$Br + O_3 \rightarrow BrO + O_2$	1.7×10^{-11}	800	1.2×10^{-12}	1.2	200	G31
$Br + H_2O_2 \rightarrow HBr + HO_2$	1.0×10^{-11}	>3000	$<5.0\times10^{-16}$			G32
$Br + NO_2 \xrightarrow{M} BrNO_2$	(See Table 2-1)					
$Br + NO_3 \rightarrow BrO + NO_2$			1.6×10^{-11}	2.0		G33
$Br + H_2CO \rightarrow HBr + HCO$	1.7×10^{-11}	800	1.1×10^{-12}	1.3	200	G34
$Br + OClO \rightarrow BrO + ClO$	2.6×10^{-11}	1300	3.4×10^{-13}	2.0	300	G35
$Br + Cl_2O \rightarrow BrCl + ClO$	2.1×10^{-11}	470	4.3×10^{-12}	1.3	150	G36
$Br + Cl_2O_2 \rightarrow$ products			3.0×10^{-12}	2.0		G37
$BrO + O_3 \rightarrow$ products	$\sim1.0\times10^{-12}$	>3200	$<2.0\times10^{-17}$			G38
$BrO + NO \rightarrow NO_2 + Br$	8.8×10^{-12}	–260	2.1×10^{-11}	1.15	130	G39
$BrO + NO_2 \xrightarrow{M} BrONO_2$	(See Table 2-1)					
$BrO + NO_3 \rightarrow$ products			1.0×10^{-12}	3.0		G40
$BrO + ClO \rightarrow Br + OClO$	9.5×10^{-13}	–550	6.0×10^{-12}	1.25	150	G41

Reaction	A-Factor[a]	E/R	k(298 K)[a]	f(298 K)[b]	g	Notes
$\rightarrow Br + ClOO$	2.3×10^{-12}	–260	5.5×10^{-12}	1.25	150	G41
$\rightarrow BrCl + O_2$	4.1×10^{-13}	–290	1.1×10^{-12}	1.25	150	G41
$BrO + BrO \rightarrow$ products	1.5×10^{-12}	–230	3.2×10^{-12}	1.15	150	G42
$CH_2BrO_2 + NO \rightarrow CH_2O + NO_2 + Br$	4×10^{-12}	–300	1.1×10^{-11}	1.5	200	G43
IO_x Reactions						
$O + I_2 \rightarrow IO + I$	1.4×10^{-10}	0	1.4×10^{-10}	1.4	250	H 1
$O + IO \rightarrow O_2 + I$			1.2×10^{-10}	2.0		H 2
$OH + I_2 \rightarrow HOI + I$			1.8×10^{-10}	2.0		H 3
$OH + HI \rightarrow H_2O + I$			3.0×10^{-11}	2.0		H 4
$OH + CH_3I \rightarrow H_2O + CH_2I$	2.9×10^{-12}	1100	7.2×10^{-14}	1.5	300	H 5
$OH + CF_3I \rightarrow HOI + CF_3$	2.5×10^{-11}	2070	2.4×10^{-14}	1.3	200	H 6
$HO_2 + I \rightarrow HI + O_2$	1.5×10^{-11}	1090	3.8×10^{-13}	2.0	500	H 7
$HO_2 + IO \rightarrow HOI + O_2$			8.4×10^{-11}	1.5		H 8
$NO_3 + HI \rightarrow HNO_3 + I$	(See Note)					H 9
$Cl + CH_3I \rightarrow CH_2I + HCl$	2.9×10^{-11}	1000	1.0×10^{-12}	1.5	250	H10
$I + O_3 \rightarrow IO + O_2$	2.3×10^{-11}	870	1.2×10^{-12}	1.2	200	H11
$I + NO \xrightarrow{M} INO$	(See Table 2-1)					
$I + NO_2 \xrightarrow{M} INO_2$	(See Table 2-1)					
$I + BrO \rightarrow IO + Br$			1.2×10^{-11}	2.0		H12
$IO + NO \rightarrow I + NO_2$	9.1×10^{-12}	–240	2.0×10^{-11}	1.2	150	H13
$IO + NO_2 \xrightarrow{M} IONO_2$	(See Table 2-1)					
$IO + ClO \rightarrow$ products	5.1×10^{-12}	–280	1.3×10^{-11}	2.0	200	H14
$IO + BrO \rightarrow$ products			6.9×10^{-11}	1.5		H15
$IO + IO \rightarrow$ products	1.5×10^{-11}	–500	8.0×10^{-11}	1.5	500	H16
$INO + INO \rightarrow I_2 + 2NO$	8.4×10^{-11}	2620	1.3×10^{-14}	2.5	600	H17

Reaction	A-Factor[a]	E/R	k(298 K)[a]	f(298 K)[b]	g	Notes
$INO_2 + INO_2 \rightarrow I_2 + 2NO_2$	2.9×10^{-11}	2600	4.7×10^{-15}	3.0	1000	H18
SO_x Reactions						
$O + SH \rightarrow SO + H$			1.6×10^{-10}	5.0		I 1
$O + CS \rightarrow CO + S$	2.7×10^{-10}	760	2.1×10^{-11}	1.1	250	I 2
$O + H_2S \rightarrow OH + SH$	9.2×10^{-12}	1800	2.2×10^{-14}	1.7	550	I 3
$O + OCS \rightarrow CO + SO$	2.1×10^{-11}	2200	1.3×10^{-14}	1.15	150	I 4
$O + CS_2 \rightarrow CS + SO$	3.2×10^{-11}	650	3.6×10^{-12}	1.2	150	I 5
$O + SO_2 \xrightarrow{M} SO_3$	(See Table 2-1)					
$O + CH_3SCH_3 \rightarrow CH_3SO + CH_3$	1.3×10^{-11}	–410	5.0×10^{-11}	1.1	100	I 6
$O + CH_3SSCH_3 \rightarrow CH_3SO + CH_3S$	3.9×10^{-11}	–290	1.03×10^{-10}	1.1	100	I 7
$O + CH_3S(O)CH_3 \rightarrow$ products	2.0×10^{-12}	–440	8.8×10^{-12}	1.2	200	I 8
$O_3 + H_2S \rightarrow$ products			$<2.0\times10^{-20}$			I 9
$O_3 + CH_3SCH_3 \rightarrow$ products			$<1.0\times10^{-18}$			I10
$O_3 + SO_2 \rightarrow SO_3 + O_2$	3.0×10^{-12}	>7000	$<2.0\times10^{-22}$			I11
$OH + H_2S \rightarrow SH + H_2O$	6.1×10^{-12}	75	4.7×10^{-12}	1.1	75	I12
$OH + OCS \rightarrow$ products	1.1×10^{-13}	1200	1.9×10^{-15}	2.0	500	I13
$OH + CS_2 \rightarrow SH + OCS$			$<2.0\times10^{-15}$			I14
$OH + CS_2 \rightarrow CS_2OH \xrightarrow{O_2}$ products	(See Note)	(See Note)	1.2×10^{-12} at $P_{air} = 1$ atm	1.25		I15
$CS_2OH + O_2 \rightarrow$ products	2.8×10^{-14}	0	2.8×10^{-14}	1.2	100	I16
$OH + CH_3SH \rightarrow CH_3S + H_2O$	9.9×10^{-12}	–360	3.3×10^{-11}	1.07	75	I17
$OH + CH_3SCH_3 \rightarrow H_2O + CH_2SCH_3$	1.1×10^{-11}	240	4.9×10^{-12}	1.1	100	I18
$OH + CH_3SCH_3 \xrightarrow{O_2} (CH_3)_2SOH \xrightarrow{O_2}$ products	(See Note)	(See Note)	1.6×10^{-12} at $P_{air} = 1$ atm	1.2		I19
$(CH_3)_2SOH + O_2 \rightarrow$ products	9.6×10^{-13}	0	9.6×10^{-13}	1.3	0	I20
$OH + CH_3SSCH_3 \rightarrow$ products	6.0×10^{-11}	–400	2.3×10^{-10}	1.2	200	I21
$OH + CH_3S(O)CH_3 \rightarrow$ products	6.1×10^{-12}	–800	8.9×10^{-11}	1.2	500	I22

Reaction	A-Factor[a]	E/R	k(298 K)[a]	f(298 K)[b]	g	Notes
$OH + CH_3S(O)OH \rightarrow$ products			9.0×10^{-11}	1.4		I23
$OH + S \rightarrow H + SO$			6.6×10^{-11}	3.0		I24
$OH + SO \rightarrow H + SO_2$	2.7×10^{-11}	–335	8.3×10^{-11}	1.2	150	I25
$OH + SO_2 \xrightarrow{M} HOSO_2$	(See Table 2-1)					
$HO_2 + H_2S \rightarrow$ products			$<3.0\times10^{-15}$			I26
$HO_2 + CH_3SH \rightarrow$ products			$<4.0\times10^{-15}$			I26
$HO_2 + CH_3SCH_3 \rightarrow$ products			$<5.0\times10^{-15}$			I26
$HO_2 + SO_2 \rightarrow$ products			$<1.0\times10^{-18}$			I27
$NO_2 + SO_2 \rightarrow$ products			$<2.0\times10^{-26}$			I28
$NO_3 + H_2S \rightarrow$ products			$<8.0\times10^{-16}$			I29
$NO_3 + OCS \rightarrow$ products			$<1.0\times10^{-16}$			I30
$NO_3 + CS_2 \rightarrow$ products			$<4.0\times10^{-16}$			I31
$NO_3 + CH_3SH \rightarrow$ products		–210	8.9×10^{-13}	1.25	210	I32
$NO_3 + CH_3SCH_3 \rightarrow CH_3SCH_2 + HNO_3$		–500	1.0×10^{-12}	1.15	200	I33
$NO_3 + CH_3SSCH_3 \rightarrow$ products		270	5.3×10^{-13}	1.4	270	I34
$NO_3 + CH_3S(O)CH_3 \rightarrow$ products			2.9×10^{-13}	1.6		I35
$NO_3 + SO_2 \rightarrow$ products			$<7.0\times10^{-21}$			I36
$N_2O_5 + CH_3SCH_3 \rightarrow$ products			$<1.0\times10^{-17}$			I37
$CH_3O_2 + SO_2 \rightarrow$ products			$<5.0\times10^{-17}$			I38
$F + CH_3SCH_3 \rightarrow$ products			$2.4.\times10^{-10}$	2.0		I39
$Cl + H_2S \rightarrow HCl + SH$	3.7×10^{-11}	–210	7.4×10^{-11}	1.2	100	I40
$Cl + OCS \rightarrow$ products			$<1.0\times10^{-16}$			I41
$Cl + CS_2 \rightarrow$ products	(See Table 2-1)					
$CS_2Cl + O_2 \rightarrow$ products			$<2.5\times10^{-16}$			I42
$Cl + CH_3SH \rightarrow CH_3S + HCl$	1.2×10^{-10}	–150	2.0×10^{-10}	1.1	100	I43

Reaction	A-Factor[a]	E/R	k(298 K)[a]	f(298 K)[b]	g	Notes
$Cl + CH_3SCH_3 \rightarrow CH_3SCH_2 + HCl$	1.6×10^{-10}	0	1.6×10^{-10}	1.6	350	I44
$Cl + CH_3SCH_3 \xrightarrow{M} (CH_3)_2SCl$	(See Table 2-1)					
$(CH_3)_2SCl + O_2 \rightarrow$ products			$<4.0\times10^{-18}$			I45
$(CH_3)_2SCl + NO \rightarrow$ products			1.2×10^{-11}	1.25		I45
$(CH_3)_2SCl + NO_2 \rightarrow$ products			2.7×10^{-11}	1.25		I45
$Cl + CH_3S(O)CH_3 \rightarrow CH_3S(O)CH_2 + HCl$			1.7×10^{-11}	1.25		I46
$Cl + CH_3S(O)CH_3 \xrightarrow{M} CH_3(Cl)S(O)CH_3$	(See Table 2-1)					
$CH_3(Cl)S(O)CH_3 + O_2 \rightarrow$ products			$<1.0\times10^{-17}$			I47
$CH_3(Cl)S(O)CH_3 + NO \rightarrow$ products			1.6×10^{-11}	1.5		I47
$CH_3(Cl)S(O)CH_3 + NO_2 \rightarrow$ products			2.0×10^{-11}	1.5		I47
$ClO + OCS \rightarrow$ products			$<2.0\times10^{-16}$			I48
$ClO + CH_3SCH_3 \rightarrow$ products	2.1×10^{-15}	–340	6.6×10^{-15}	1.5	300	I49
$ClO + CH_3S(O)CH_3 \rightarrow$ products			$<2.0\times10^{-14}$			I50
$ClO + SO \rightarrow Cl + SO_2$	2.8×10^{-11}	0	2.8×10^{-11}	1.3	50	I51
$ClO + SO_2 \rightarrow Cl + SO_3$			$<4.0\times10^{-18}$			I48
$Br + H_2S \rightarrow HBr + SH$	1.4×10^{-11}	2750	1.4×10^{-15}	2.0	300	I52
$Br + CH_3SH \rightarrow CH_3S + HBr$	9.2×10^{-12}	390	2.5×10^{-12}	2.0	100	I52
$Br + CH_3SCH_3 \rightarrow CH_3SCH_2 + HBr$	9.0×10^{-11}	2390	3.0×10^{-14}	1.4	150	I53
$Br + CH_3SCH_3 \xrightarrow{M} (CH_3)_2SBr$	(See Table 2-1)					
$Br + CH_3S(O)CH_3 \rightarrow$ products			1.2×10^{-14}	1.5		I54
$BrO + CH_3SCH_3 \rightarrow$ products	1.4×10^{-14}	–950	3.4×10^{-13}	1.25	200	I55
$BrO + CH_3SSCH_3 \rightarrow$ products			1.5×10^{-14}	2.0		I56
$BrO + CH_3S(O)CH_3 \rightarrow$ products			1.0×10^{-14}	2.0		I57
$BrO + SO \rightarrow Br + SO_2$			5.7×10^{-11}	1.4		I58
$IO + CH_3SH \rightarrow$ products			6.6×10^{-16}	2.0		I59

Reaction	A-Factor[a]	E/R	k(298 K)[a]	f(298 K)[b]	g	Notes
$IO + CH_3SCH_3 \rightarrow$ products			1.2×10^{-14}	1.3		I60
$S + O_2 \rightarrow SO + O$	2.3×10^{-12}	0	2.3×10^{-12}	1.2	200	I61
$S + O_3 \rightarrow SO + O_2$			1.2×10^{-11}	2.0		I62
$SO + O_2 \rightarrow SO_2 + O$	1.25×10^{-13}	2190	8.0×10^{-17}	1.3	350	I63
$SO + O_3 \rightarrow SO_2 + O_2$	3.4×10^{-12}	1100	8.4×10^{-14}	1.1	150	I64
$SO + NO_2 \rightarrow SO_2 + NO$	1.4×10^{-11}	0	1.4×10^{-11}	1.2	50	I65
$SO + OClO \rightarrow SO_2 + ClO$			1.9×10^{-12}	3.0		I66
$SO_3 + 2\ H_2O \rightarrow$ products	(See Note)	(See Note)	(See Note)	1.2	200	I67
$SO_3 + NH_3 \rightarrow$ products	(See Table 2-1)					
$SO_3 + NO_2 \rightarrow$ products			1.0×10^{-19}	10.0		I68
$SH + O_2 \rightarrow OH + SO$			$<4.0\times10^{-19}$			I69
$SH + O_3 \rightarrow HSO + O_2$	9.0×10^{-12}	280	3.5×10^{-12}	1.2	200	I70
$SH + H_2O_2 \rightarrow$ products			$<5.0\times10^{-15}$			I71
$SH + NO \xrightarrow{M} HSNO$	(See Table 2-1)					
$SH + NO_2 \rightarrow HSO + NO$	2.9×10^{-11}	–240	6.5×10^{-11}	1.2	50	I72
$SH + N_2O \rightarrow HSO + N_2$			$<5.0\times10^{-16}$			I73
$SH + Cl_2 \rightarrow ClSH + Cl$	1.4×10^{-11}	690	1.4×10^{-12}	1.15	200	I74
$SH + BrCl \rightarrow$ products	2.3×10^{-11}	–350	7.4×10^{-11}	2.0	200	I75
$SH + Br_2 \rightarrow BrSH + Br$	6.0×10^{-11}	–160	1.0×10^{-10}	2.0	160	I75
$SH + F_2 \rightarrow FSH + F$	4.3×10^{-11}	1390	4.0×10^{-13}	2.0	200	I75
$HSO + O_2 \rightarrow$ products			$<2.0\times10^{-17}$			I76
$HSO + O_3 \rightarrow$ products			1.0×10^{-13}	1.3		I77
$HSO + NO \rightarrow$ products			$<1.0\times10^{-15}$			I78
$HSO + NO_2 \rightarrow HSO_2 + NO$			9.6×10^{-12}	2.0		I78
$HSO_2 + O_2 \rightarrow HO_2 + SO_2$			3.0×10^{-13}	3.0		I79

Reaction	A-Factor[a]	E/R	k(298 K)[a]	f(298 K)[b]	g	Notes
$HOSO_2 + O_2 \rightarrow HO_2 + SO_3$	1.3×10^{-12}	330	4.3×10^{-13}	1.15	200	I80
$CS + O_2 \rightarrow OCS + O$			2.9×10^{-19}	2.0		I81
$CS + O_3 \rightarrow OCS + O_2$			3.0×10^{-16}	3.0		I82
$CS + NO_2 \rightarrow OCS + NO$			7.6×10^{-17}	3.0		I82
$CH_3S + O_2 \rightarrow$ products			$<3.0\times10^{-18}$			I83
$CH_3S + O_3 \rightarrow$ products	1.5×10^{-12}	–360	5.0×10^{-12}	1.15	100	I84
$CH_3S + NO \rightarrow$ products			$<1.0\times10^{-13}$			I85
$CH_3S + NO \xrightarrow{M}$ products	(See Table 2-1)					
$CH_3S + NO_2 \rightarrow CH_3SO + NO$	3.0×10^{-11}	–240	6.7×10^{-11}	1.2	150	I86
$CH_2SH + O_2 \rightarrow$ products			6.5×10^{-12}	2.0		I87
$CH_2SH + O_3 \rightarrow$ products			3.5×10^{-11}	2.0		I88
$CH_2SH + NO \rightarrow$ products			1.9×10^{-11}	2.0		I89
$CH_2SH + NO_2 \rightarrow$ products			5.2×10^{-11}	2.0		I90
$CH_3SO + O_3 \rightarrow$ products			4.0×10^{-13}	1.5		I91
$CH_3SO + NO_2 \rightarrow CH_3SO_2 + NO$			1.2×10^{-11}	1.2		I92
$CH_3SOO + O_3 \rightarrow$ products			$<8.0\times10^{-13}$			I93
$CH_3SOO + NO \rightarrow$ products	1.1×10^{-11}	0	1.1×10^{-11}	2.0	100	I93
$CH_3SO_2 + NO_2 \rightarrow$ products	2.2×10^{-11}	0	2.2×10^{-11}	2.0	100	I94
$CH_3SCH_2 + O_2 \xrightarrow{M} CH_3SCH_2O_2$	(See Table 2-1)					
$CH_3SCH_2 + NO_3 \rightarrow$ products			3.0×10^{-10}	2.0		I95
$CH_3SCH_2O_2 + NO \rightarrow CH_3S + CH_2O + NO_2$	4.9×10^{-12}	–260	1.2×10^{-11}	1.3	200	I96
$CH_3SCH_2O_2 + CH_3SCH_2O_2 \rightarrow$ products			1.0×10^{-11}	1.25		I97
$CH_3SS + O_3 \rightarrow$ products			4.6×10^{-13}	2.0		I98
$CH_3SS + NO_2 \rightarrow$ products			1.8×10^{-11}	2.0		I99
$CH_3SSO + NO_2 \rightarrow$ products			4.5×10^{-12}	2.0		I99

Reaction	A-Factor[a]	E/R	k(298 K)[a]	f(298 K)[b]	g	Notes
Sodium Reactions						
$Na + O_2 \xrightarrow{M} NaO_2$	(See Table 2-1)					
$Na + O_3 \rightarrow NaO + O_2$	1.0×10^{-9}	95	7.3×10^{-10}	1.2	50	J 1
$\rightarrow NaO_2 + O$			$<4.0\times10^{-11}$			J 1
$Na + N_2O \rightarrow NaO + N_2$	2.8×10^{-10}	1600	1.3×10^{-12}	1.2	400	J 2
$Na + Cl_2 \rightarrow NaCl + Cl$	7.3×10^{-10}	0	7.3×10^{-10}	1.3	200	J 3
$NaO + O \rightarrow Na + O_2$	4.4×10^{-10}	0	4.4×10^{-10}	1.5	200	J 4
$NaO + O_2 \xrightarrow{M} NaO_3$	(See Table 2-1)					
$NaO + O_3 \rightarrow NaO_2 + O_2$	1.1×10^{-9}	570	1.6×10^{-10}	1.5	300	J 5
$\rightarrow Na + 2O_2$	6.0×10^{-11}	0	6.0×10^{-11}	3.0	800	J 5
$NaO + H_2 \rightarrow NaOH + H$	2.6×10^{-11}	0	2.6×10^{-11}	2.0	600	J 6
$NaO + H_2O \rightarrow NaOH + OH$	4.3×10^{-10}	500	8.0×10^{-11}	1.5	200	J 7
$NaO + NO \rightarrow Na + NO_2$	1.5×10^{-10}	0	1.5×10^{-10}	4.0	400	J 8
$NaO + CO_2 \xrightarrow{M} NaCO_3$	(See Table 2-1)					
$NaO + HCl \rightarrow$ products	2.8×10^{-10}	0	2.8×10^{-10}	3.0	400	J 9
$NaO_2 + O \rightarrow NaO + O_2$	2.2×10^{-11}	0	2.2×10^{-11}	5.0	600	J10
$NaO_2 + NO \rightarrow NaO + NO_2$			$<10^{-14}$			J11
$NaO_2 + HCl \rightarrow$ products	2.3×10^{-10}	0	2.3×10^{-10}	3.0	400	J12
$NaOH + HCl \rightarrow NaCl + H_2O$	2.8×10^{-10}	0	2.8×10^{-10}	3.0	400	J13
$NaHCO_3 + H \rightarrow Na + H_2O + CO_2$	1.4×10^{-11}	1000	5×10^{-13}	2.0	100	J14
$NaOH + CO_2 \xrightarrow{M} NaHCO_3$	(See Table 2-1)					

Shaded areas indicate changes or additions since JPL 97-4/JPL 00-3. Italicized entries denote estimates.

[a] Units are cm^3 $molecule^{-1}$ s^{-1}.

[b] f(298 K) is the uncertainty factor at 298 K. To calculate the uncertainty at other temperatures, use the expression:

$$f(T) = f(298)\exp\left|g\left(\frac{1}{T} - \frac{1}{298}\right)\right|$$

Note that the exponent is absolute value.

1.3 Notes to Table 1

JPL Publication numbers for the most recent revision of the table entry and note are given at the end of each note.

A1. $O + O_3$. The recommended rate expression is from Wine et al. [1468] and is a linear least squares fit of all data (unweighted) from Davis et al. [360], McCrumb and Kaufman [891], West et al. [1442], Arnold and Comes [32], and Wine et al. [1468]. (Table: 83-62, Note: 83-62) Back to Table

A2. $O(^1D)$ Reactions. In general, the rate constants given in the table are for the disappearance of $O(^1D)$, which includes physical quenching or deactivation and chemical reaction. Where information is available, the rate coefficient for a specific channel is also given. The details of deriving a recommended rate coefficient are given in the note for that reaction. In deriving recommended values direct measurements are used whenever they are available. However, the rate coefficients measured via relative rate techniques have also been considered for checking consistency in measured elementary reaction rate coefficients.

The rate constant recommendations are based on the absolute rate constants reported by Streit et al. [1249], Davidson et al. [353] and Davidson et al. [352] for N_2O, H_2O, CH_4, H_2, N_2, O_2, O_3, CCl_4, $CFCl_3$, CF_2Cl_2, NH_3, and CO_2; by Amimoto et al. [21], Amimoto et al. [20], and Force and Wiesenfeld [467, 468] for N_2O, H_2O, CH_4, N_2, H_2, O_2, O_3, CO_2, CCl_4, $CFCl_3$, CF_2Cl_2, and CF_4; by Wine and Ravishankara [1469-1471] for N_2O, H_2O, N_2, H_2, O_3, CO_2, and CF_2O; by Lee and Slanger [791, 792] for H_2O and O_2; by Gericke and Comes [491] for H_2O; and by Shi and Barker [1180] for N_2 and CO_2, by Talukdar and Ravishankara [1289] for H_2, by Dunlea and Ravishankara [419] or N_2, O_2, O_3, CO_2, N_2O, and H_2O; by Strekowski et al. [1253] for N_2 and O_2, and by Blitz et al. for N_2, O_2, N_2O, CH_4, H_2, and CO_2 [153]. Measurements for other reactions are specifically cited in the notes for those reactions. The weight of the evidence from the studies noted above indicates that the results of Heidner and Husain [565], Heidner et al. [564] and Fletcher and Husain [461, 462] contain a systematic error. (Note: 06-2) Back to Table

A3. $O(^1D) + O_2$. The 298 K recommended rate coefficient is derived from the studies of Blitz et al., Amimoto et al., Lee and Slanger, Davidson et al., Dunlea and Ravishankara, Streit et al., and Strekowski et al. (See above for references) The temperature dependence was computed by normalizing the results of Strekowski et al., Dunlea and Ravishankara, and Streit et al. at 298 K to the value recommended here. The deactivation of $O(^1D)$ by O_2 leads to the production of $O_2(^1\Sigma)$ with an efficiency of 80±20%. (Noxon [1003], Biedenkapp and Bair [137], Snelling [1220], and Lee and Slanger [791]). The $O_2(^1\Sigma)$ is produced in the v=0, 1, and 2 vibrational levels in the amounts 60%, 40%, and <3%, respectively (Gauthier and Snelling [487] and Lee and Slanger [791]). The fractional deactivation of $O(^1D)$ that leads to the excitation of $O_2(^3\Sigma)$ to $O_2(^1\Delta)$ is expected to be ~20%. (Table: 06-2, Note: 06-2) Back to Table

A4. $O(^1D) + O_3$. k(298 K) was derived from results of Davidson et al., Streit et al., Amimoto et al., Wine and Ravishankara, Talukdar et al. and Dunlea and Ravishankara. The rate coefficients measured for this reaction by Husain's group (Gilpin et al., and Heidner and Husain) are not expected to be influenced by the possible systematic error(s) that affect their other rate coefficient determinations. Their results are consistent with the recommended values. The reaction of $O(^1D)$ with O_3 gives O_2 + O_2 or O_2 + O + O. Davenport et al. [347] and Amimoto et al. [21] reported that, on average, one ground state O is produced per $O(^1D)$ reacting with O_3. Very recent results from Dunlea et al. [422] also show that the yield of $O(^3P)$ in this reaction is close to, but not exactly, unity. Also, Dunlea et al. suggest a small but significant temperature dependence to this yield. Further studies on this yield would be useful. A unity yield of $O(^3P)$ is recommended. (Table: 06-2, Note: 06-2) Back to Table

A5. $O(^1D) + H_2$. The recommended rate coefficient is based on the references noted in Note A2. Wine and Ravishankara [1470] have determined that the yield of $O(^3P)$ is less than 4.9%. The major products are H + OH. Koppe et al. [737] report a 2.7 times larger rate coefficient at a collisional energy of 0.12eV. This does not agree with the observations of Davidson et al. [353], who reported that k is independent of temperature (200–350 K) and Matsumi et al. [886] who report no change in k when translationally hot $O(^1D)$ is moderated with Ar. (Table: 97-4, Note: 97-4) Back to Table

A6. $O(^1D) + H_2O$. The recommended k(298 K) is based on the results of Davidson et al., Amimoto et al., Wine and Ravishankara, Gericke and Comes, and Dunlea and Ravishankara, [420] but is weighted towards the study of Dunlea and Ravishankara because the latter study used several different methods to quantify the water vapor concentration. The results of Lee and Slanger are consistent with the recommended value. The temperature dependence of this rate coefficient is derived from the data of Streit et al. and of Dunlea and Ravishankara, after normalizing the results from the two studies to k(298 K) recommended here. The $O_2 + H_2$ product yield was measured by Zellner et al. [1516] to be (1 +0.5 or –1)% and by Glinski and Birks [512] to be (0.6 +0.7 or –0.6)%. The yield of $O(^3P)$ from $O(^1D) + H_2O$ is reported to be less than (4.9±3.2)% by Wine and Ravishankara [1470] and (2±1)% by Takahashi et al. [1276]. Therefore, we recommend the yield of OH in this reaction to be 2.0.

To calculate the rates of OH production via $O(^1D)$ reactions in the atmosphere, the quantities of interest are the ratios of the rate coefficients for the reaction of $O(^1D)$ with H_2O to those with N_2 and with O_2. The ratios of the rate coefficients for $O(^1D)$ reactions measured using the same method (and often the same apparatus) are more accurate (and precise) than the individual rate constants that are quoted in Table 1. Ratio data are given in the original references for this reaction. (Table: 06-2, Note: 06-2) Back to Table

A7. $O(^1D) + N_2$. The rate coefficient for this reaction is taken from the paper of Ravishankara et al., [1092] which includes results from three different groups (Strekowski et al., Blitz et al., and Dunlea and Ravishankara) (See Note A2). Strekowski et al., have reported the rate coefficient for $O(^1D)$ removal by air and their results are in excellent agreement with the value derived using the current recommendation for $O(^1D)$ removal by N_2 and O_2. (Table: 06-2, Note: 06-2) Back to Table

A8. $O(^1D) + N_2O$. This reaction has two channels, one producing 2NO and the other producing $N_2 + O_2$. For atmospheric calculations of NO_x production, the rate coefficient for the channel that produces NO is critical, while the overall rate coefficient is important for deriving the loss rate of N_2O. The procedure employed to derive the rate coefficients recommended here was as follows: (1) the overall rate coefficient at 298 K and as a function of temperature for the removal of $O(^1D)$ in the interaction with N_2O was evaluated; (2) the branching ratio for the two possible channels shown in the table was evaluated for 298 K, the only temperature at which such data are available; (3) the overall rate coefficient from step 1 was divided into the two channels derived in step 2 to obtain the k(298 K) for the two channels listed in the table at 298 K; (4) the individual rate coefficients for the two channels as a function of temperature was derived by assuming that the branching ratio for the two channels is invariant with temperature.

The branching ratio for the reaction of $O(^1D)$ with N_2O to give $N_2 + O_2$ or NO + NO is an average of the values reported by Davidson et al. [350]; Volltrauer et al. [1381]; Marx et al. [885] and Lam et al. [763], with a spread in R=k(NO + NO)/k(Total) = 0.52 – 0.62. Cantrell et al. [229] reported a measurement of R=0.57 and an analysis of all measurements from 1957–1994 led them to recommend a value of R=0.61±0.06, where the uncertainty indicates their 95% confidence interval. The recommended branching ratio agrees well with earlier measurements of the quantum yield from N_2O photolysis (Calvert and Pitts [220]). Dependencies on $O(^1D)$ translational energy and temperature are not clearly resolved. Wine and Ravishankara [1470] have determined that the yield of $O(^3P)$ from $O(^1D) + N_2O$ is less than 4.0%. The uncertainty for this reaction includes factors for both the overall rate coefficient and the branching ratio. A direct measurement by Greenblatt and Ravishankara [524] of the NO yield from the $O(^1D) + N_2O$ reaction in synthetic air and a reanalysis of this data by Dunlea and Ravishankara [419] agrees very well with the value predicted using the recommended $O(^1D)$ rate constants for N_2, O_2, and N_2O and the $O(^1D) + N_2O$ product branching ratio to give NO + NO.

The overall rate coefficient for the removal of $O(^1D)$ by N_2O was derived from the results of Davidson et al., Amimoto et al., Wine and Ravishankara, Blitz et al., and Dunlea and Ravishankara. The temperature dependence of this rate coefficient was derived from the results of Davidson et al. and Dunlea and Ravishankara, after normalizing both data sets to the k(298 K) recommended here for the overall rate coefficient, i.e., the sum of the two channels. The ratios of the rate coefficients for $O(^1D)$ reactions measured using the same method (and often the same apparatus) may be more accurate and precise than the individual rate constants that are quoted in Table 1. The values of f

and g listed in Table 1 were derived from all the available information. Better branching ratio measurements at the stratospheric temperatures and/or measurements of NO yield in this reaction as a function of temperature below 298 K would be useful for stratospheric modeling. (Table: 06-2, Note: 06-2) Back to Table

A9. $O(^1D) + NH_3$. Sanders et al. [1141] have detected the products $NH(a^1\Delta)$ and OH formed in the reaction. They report that the yield of $NH(a^1\Delta)$ is in the range 3–15% of the amount of OH detected. (Table: 82-57, Note: 82-57) Back to Table

A10. $O(^1D) + CO_2$. k(298 K) was derived from the studies of Davidson et al., Streit et al., Amimoto et al., Blitz et al., Dunlea and Ravishankara, and Shi and Barker, Blitz et al. Temperature dependence was computed after normalizing the results of Dunlea and Ravishankara and Streit et al. (only the data in the range of 200 to 354 K) to the value of k(298 K) recommended here. The rate coefficient at 195 K reported by Blitz et al. is consistent with the recommendation.

This reaction produces $O(^3P)$ and CO_2, and is expected to proceed through the formation of a CO_3 complex (see for example DeMore and Dede, [378]). This complex formation leads to isotopic scrambling (See for example Perri et al. [1046]). There appears to be a small, but non-negligible, channel for $O(^1D)$ quenching. A reactive channel to give CO and O_2 has been reported ([1167]), but needs better quantification. (Table: 06-2, Note: 06-2) Back to Table

A11. $O(^1D) + CH_4$. The reaction products are (a) CH_3 + OH, (b) CH_3O or CH_2OH + H and (c) CH_2O + H_2. Lin and DeMore [830] analyzed the final products of N_2O/CH_4 photolysis mixtures and concluded that (a) accounted for about 90% and that CH_2O and H_2 (c) accounted for about 9%. Addison et al. [9] reported an OH yield of 80%. Casavecchia et al. [233] used a molecular beam experiment to observe H and CH_3O (or CH_2OH) products. They reported that the yield of H_2 was less than 25% of the yield of H from (b). Satyapal et al. [1147] observed the production of H atoms in a pulsed laser experiment and reported a yield of H of (25±8)%. Matsumi et al. [886] measured the yields of H and $O(^3P)$ in low pressure gas mixtures and reported that the yield of H was (15±3)% and the yield of $O(^3P)$ was <5%. Wine and Ravishankara [1470] reported that the yield of $O(^3P)$ was less than 4.3%. Takahashi et al. [1276] reported that the $O(^3P)$ yield is less than 1%. We recommend the following branching ratios: (a) (75±15)%, (b) (20±7)%, (c) (5±5)%. (Table: 94-26, Note: 97-4) Back to Table

A12. $O(^1D)$ + HCl. The recommendation is based on the measurements by Davidson et al. [353], Wine et al. [1476]and Chichinin [262]. The temperature dependence is based on Davidson et al. Product studies by Wine et al. indicate: $O(^3P)$ + HCl (9±5)%; H + ClO (24±5)%; and OH + Cl (67±10)%. Takahashi et al. [1276] report that the $O(^3P)$ yield is (15±4)%. (Table: 06-2, Note: 06-2) Back to Table

A13. $O(^1D)$ + HF. The recommended value of k(298 K) is based on the one reported value of Sorokin et al. [1223]. It is assumed that the rate coefficient is independent of temperature. The possible products of this reaction are: HF + $O(^3P)$ and F + OH. The channel to give H + FO is endothermic and, hence, considered to be unimportant. (Table: 06-2, Note: 06-2) Back to Table

A14. $O(^1D) + NF_3$. The recommended value of k(298 K) is based on the results of Sorokin et al. [1223] and Barone et al. [85]. The temperature dependence of the rate coefficient is based on Barone et al., the only temperature dependence study. Sorokin et al. and Barone et al., respectively, report that 70 and 80% of the $O(^1D)$-NF_3 collisions lead to removal of NF_3, i.e., products other than $O(^3P) + NF_3$. The identities of the products are not known. Therefore, the rate coefficient for the removal of NF_3 by reaction with $O(^1D)$ is greater than 70% of the overall rate coefficient for $O(^1D)$ removal by NF_3. NEW ENTRY Back to Table

A15. $O(^1D)$ + HBr. Rate coefficient and product yields at 298 K was reported by Wine et al. [1476]. There are no reports on the temperature dependence of this rate coefficient. Because it is close to a collisional rate coefficient, the rate coefficient is assumed to be temperature independent. Product yields: HBr + $O(^3P)$ (20±7)%, H + BrO <4.5%, and OH + Br (80±12)%. (Table: 87-41, Note: 87-41) Back to Table

A16. $O(^1D) + Cl_2$. The recommended k(298 K) is based on the reports of Wine et al. [1466], and Sorokin et al. [1223]. There are no reports on the temperature dependence of this rate coefficient. The rate

coefficient is assumed to be temperature independent because k(298 K) is close to a collisional rate coefficient. Both Sorokin et al. and Wine et al. report that the branching ratio to produce ClO + Cl is 0.75, based on their measured $O(^3P)$ yield. This value is in excellent agreement with the directly measured ClO yield of (74±15)%, by Takahashi et al. [1276]. An indirect study by Freudenstein and Biedenkapp [471] is in reasonable agreement on the yield of ClO. Though energetically allowed, the formation of Cl_2O is expected to be negligible under atmospheric conditions of pressure and temperature. (Table: 06-2, Note: 06-2) Back to Table

A17. $O(^1D) + COCl_2$. The recommended value of k(298 K) is derived from the values reported by Chichinin [262] and Strekowski et al. [1251]. The value of Fletcher and Husain, reduced by a factor of 2 to account for the systematic errors in their measurement method, is in reasonable agreement with the recommended value. The relative rate study of Jayanty et al. [654] is also consistent with the recommended value. The temperature dependence is taken from Strekowski et al. There are three possible reactive channels: CO + ClO + Cl; CO_2 + 2 Cl; $CO_2 + Cl_2$. In the stratosphere, all these processes will lead to CO_2 and ClO. Chichinin reports that the above 3 reactions account for 80% of $O(^1D)$ loss with 20% leading to $O(^3P)$. The rate coefficient for the loss of $COCl_2$ via reaction with $O(^1D)$ is expected to be more than 80% for the overall rate coefficient recommended here. (Table: 06-2, Note: 06-2) Back to Table

A18. $O(^1D)$ + COClF and COF_2. For the reactions of $O(^1D)$ with COClF the recommended rate constants are derived from data of Fletcher and Husain [463]. For consistency, the recommended values for these rate constants were derived using a scaling factor (0.5) that corrects for the difference between rate constants from the Husain laboratory and the recommendations for other $O(^1D)$ rate constants in this table. The recommendation for COF_2 is from the data of Wine and Ravishankara [1471]. Their result is preferred over the value of Fletcher and Husain [463] because it appears to follow the pattern of decreased reactivity with increased fluorine substitution observed for other halocarbons. These reactions have been studied only at 298 K. Based on consideration of similar $O(^1D)$ reactions, it is assumed that E/R equals zero, and therefore the value shown for the A-factor has been set equal to k(298 K). (Table: 82-57, Note: 97-4) Back to Table

A19. $O(^1D)$ + Halocarbons. The halocarbon rate constants are for the total disappearance of $O(^1D)$ and probably include physical quenching. Products of the reactive channels may include $CX_3O + X$, $CX_2O + X_2$ (or 2X), and CX_3 + XO, where X = H, F, Cl, or Br in various combinations. Bromine, chlorine and hydrogen are more easily displaced than fluorine from halocarbons. Some values have been reported for the fractions of the total rate of disappearance of $O(^1D)$ proceeding through physical quenching and reactive channels. For CCl_4: quenching = (14±6)% and reaction = (86±6)% (Force and Wiesenfeld [468]), ClO yield = (90±19)% (Takahashi et al. [1276]); for $CFCl_3$: quenching = (25±10)%, ClO formation = (60±15)% (Donovan, private communication, 1980), ClO yield = (88±18)% (Takahashi et al.); for CF_2Cl_2: quenching = (14±7)% and reaction = (86±14)% (Force and Wiesenfeld [468]), quenching = (20±10)%, ClO formation = (55±15)% (Donovan), quenching = (19±5)% and ClO formation = (87±18%) (Takahashi et al.). (Table: 82-57, Note: 97-4) Back to Table

A20. $O(^1D) + CH_3Br$. The recommendation is based on data from Thompson and Ravishankara [1298]. They report that the yield of $O(^3P)$ from physical quenching is 0±7%. (Table: 94-26, Note: 94-26) Back to Table

A21. $O(^1D) + CH_2Br_2$. The recommendation is based on data from Thompson and Ravishankara [1298]. They report that the yield of $O(^3P)$ from physical quenching is (5±7)%. (Table: 94-26, Note: 94-26) Back to Table

A22. $O(^1D) + CHBr_3$. The recommendation is based on data from Thompson and Ravishankara [1298]. The rate coefficient is somewhat large compared to analogous compounds. They report that the yield of $O(^3P)$ from physical quenching is (32±8)%. (Table: 94-26, Note: 94-26) Back to Table

A23. $O(^1D) + CH_3F$ (HFC-41). The recommendation is the average of measurements of Force and Wiesenfeld [468] and Schmoltner et al. [1159]. The $O(^3P)$ product yield was reported to be (25±3)% by Force and Wiesenfeld, (11±5)% by Schmoltner et al., and (19±5)% by Takahashi et al. [1276]. Burks and Lin [202] reported observing vibrationally excited HF as a product. Park and Wiesenfeld [1035] observed OH. (Table: 94-26, Note: 97-4) Back to Table

A24. $O(^1D) + CH_2F_2$ (HFC-32). The recommendation is based upon the measurement of Schmoltner et al. [1159], who reported that the yield of $O(^3P)$ is (70±11)%. Green and Wayne [522] measured the loss of CH_2F_2 relative to the loss of N_2O. Their value when combined with our recommendation for $O(^1D) + N_2O$ yields a rate coefficient for reactive loss of CH_2F_2 that is about three times the result of Schmoltner et al., Burks and Lin [202] reported observing vibrationally excited HF as a product. (Table: 94-26, Note: 94-26) Back to Table

A25. $O(^1D) + CHF_3$ (HFC-23). The recommendation is the average of measurements of Force and Wiesenfeld [468] and Schmoltner et al. [1159]. The $O(^3P)$ product yield was reported to be (77±15)% by Force and Wiesenfeld and (102±3)% by Schmoltner et al. Although physical quenching is the dominant process, detectable yields of vibrationally excited HF have been reported by Burks and Lin [202] and Aker et al. [17], which indicate the formation of HF + CF_2O products. (Table: 94-26, Note: 94-26) Back to Table

A26. $O(^1D) + CHCl_2F$ (HCFC-21). The recommendation is based upon the measurement by Davidson et al. [352] of the total rate coefficient (physical quenching and reaction). Takahashi et al. [1276] report that the yield of ClO is (74±15)%. (Table: 90-1, Note: 94-26) Back to Table

A27. $O(^1D) + CHClF_2$ (HCFC-22). The recommendation is based upon the measurements by Davidson et al. [352] and Warren et al. [1426] of the total rate coefficient. A measurement of the rate of reaction (halocarbon removal) relative to the rate of reaction with N_2O by Green and Wayne [522] agrees very well with this value when the $O(^1D) + N_2O$ recommendation is used to obtain an absolute value. A relative measurement by Atkinson et al. [46] gives a rate coefficient about a factor of two higher. Addison et al. [9] reported the following product yields: ClO (55±10)%, CF_2 (45±10)%, $O(^3P)$ (28 +10 or –15)%, and OH 5%, where the $O(^3P)$ comes from a branch yielding CF_2 and HCl. Warren et al. [1426] also report a yield of $O(^3P)$ of (28±6)%, which they interpret as the product of physical quenching. (Table: 92-20, Note: 92-20) Back to Table

A28. $O(^1D) + CHF_2Br$. The recommended k(298 K) and the temperature dependence are based on the study of Strekowski et al., [1252] which is the only available investigation of this reaction. They report a branching ratio for $O(^3P)$ production of ~40%, independent of temperature and a branching ratio for H atom production of ~2% at 298 K. Therefore, 60% of the reaction is expected to lead to destruction of CHF_2Br. NEW ENTRY Back to Table

A29. $O(^1D) + CClF_3$ (CFC-13). The recommendation is based on the measurement by Ravishankara et al.[1097] who report (31±10)% physical quenching. Takahashi et al. [1276] report the yields of $O(^3P)$ (16±5)% and ClO (85±18)%. (Table: 92-20, Note: 97-4) Back to Table

A30. $O(^1D) + CClBrF_2$ (Halon 1211). The recommendation is based on data from Thompson and Ravishankara [1298]. They report that the yield of $O(^3P)$ from physical quenching is (36±4)%. (Table: 94-26, Note: 94-26) Back to Table

A31. $O(^1D) + CBr_2F_2$ (Halon 1202). The recommendation is based on data from Thompson and Ravishankara [1298]. They report that the yield of $O(^3P)$ from physical quenching is (54±6)%. (Table: 94-26, Note: 94-26) Back to Table

A32. $O(^1D) + CBrF_3$ (Halon 1301). The recommendation is based on data from Thompson and Ravishankara [1298]. They report that the yield of $O(^3P)$ from physical quenching is (59±8)%. Lorenzen-Schmidt et al. [844] measured the Halon removal rate relative to the N_2O removal rate and report that the rate coefficient for the Halon destruction path is $(4.0\pm0.4) \times 10^{-11}$, which is in excellent agreement with Thompson and Ravishankara. (Table: 94-26, Note: 97-4) Back to Table

A33. $O(^1D) + CF_4$ (CFC-14). The recommendation is based upon the measurement by Ravishankara et al. [1097], who report (92±8)% physical quenching. Force and Wiesenfeld [468] measured a quenching rate coefficient about 10 times larger. Shi and Barker [1180] report an upper limit that is consistent with the recommendation. The small rate coefficient for this reaction makes it vulnerable to interference from reactant impurities. For this reason the recommendation should probably be considered an upper limit. (Table: 92-20, Note: 92-20) Back to Table

A34. $O(^1D) + CH_3CH_2F$ (HFC 161). The recommendation is based on data from Schmoltner et al. [1159]. They report that the yield of $O(^3P)$ from physical quenching is (18±5)%. (Table: 94-26, Note: 94-26) Back to Table

A35. $O(^1D) + CH_3CHF_2$ (HFC-152a). The recommendation is based on the measurements of Warren et al. [1426], who report (54±7)% physical quenching. (Table: 92-20, Note: 92-20) Back to Table

A36. $O(^1D) + CH_3CCl_2F$ (HCFC-141b). The recommendation is based upon the measurement of Warren et al. [1426], who report (31±5)% physical quenching. (Table: 92-20, Note: 92-20) Back to Table

A37. $O(^1D) + CH_3CClF_2$ (HCFC-142b). The recommendation is based upon the measurement of Warren et al. [1426], who report (26±5)% physical quenching. This agrees very well with Green and Wayne [522], who measured the loss of CH_3CF_2Cl relative to the loss of N_2O, when the recommendation for N_2O is used. (Table: 92-20, Note: 92-20) Back to Table

A38. $O(^1D) + CH_3CF_3$ (HFC-143a). The recommendation is based upon the relative rate measurement of Green and Wayne [522], who measured the loss of CH_3CF_3 relative to the loss of N_2O. The recommendation for N_2O is used to obtain the value given. It is assumed that there is no physical quenching, although the reported physical quenching by CH_2FCF_3 and CH_3CHF_2 suggests some quenching is possible. (Table: 90-1, Note: 90-1) Back to Table

A39. $O(^1D) + CH_2ClCClF_2$ (HCFC-132b). The recommendation is based upon the relative rate measurement of Green and Wayne [522], who measured the loss of CH_2ClCF_2Cl relative to the loss of N_2O. The recommendation for N_2O is used to obtain the value given. It is assumed that there is no physical quenching. (Table: 90-1, Note: 90-1) Back to Table

A40. $O(^1D) + CH_2ClCF_3$ (HCFC-133a). The recommendation is based upon the measurement of Warren et al. [1426], who report (20±5)% physical quenching. This agrees with Green and Wayne [522] who measured the loss of CH_2ClCF_3 relative to the loss of N_2O, when the recommendation for N_2O is used. (Table: 92-20, Note; 92-20) Back to Table

A41. $O(^1D) + CH_2FCF_3$ (HFC-134a). The recommendation is based on the measurement of Warren et al. [1426] who report (94+6/–1)% physical quenching. The predominance of physical quenching is surprising, considering the presence of C–H bonds, which are usually reactive toward $O(^1D)$. (Table: 92-20, Note: 92-20) Back to Table

A42. $O(^1D) + CHCl_2CF_3$ (HCFC-123). The recommendation is based upon measurements by Warren et al. [1426]. The relative rate measurement of Green and Wayne [522], who measured the loss of $CHCl_2CF_3$ relative to the loss of N_2O, agrees well with the recommendation when the recommendation for N_2O is used. Warren et al. report (21 ± 8)% physical quenching. (Table: 92-20, Note: 92-20) Back to Table

A43. $O(^1D) + CHClFCF_3$ (HCFC-124). The recommendation is based upon the measurement of Warren et al. [1426], who report (31 ± 10)% physical quenching. (Table: 92-20, Note: 92-20) Back to Table

A44. $O(^1D) + CHF_2CF_3$ (HFC-125). The recommendation is based upon the measurement of Warren et al. [1426], who report (85+15/–22)% physical quenching. Green and Wayne [522] measured the loss of CHF_2CF_3 relative to the loss of N_2O and report a loss corresponding to about 40% of the recommended rate coefficient. This reaction is much faster than one would predict by analogy to similar compounds, such as CH_2FCF_3. (Table: 92-20, Note: 92-20) Back to Table

A45. $O(^1D) + CCl_3CF_3$ (CFC-113a). The recommendation is an estimate based on analogy to similar compounds. (Table: 92-20, Note: 92-20) Back to Table

A46. $O(^1D) + CCl_2FCClF_2$ (CFC-113). The recommendation is an estimate based on analogy to similar compounds. (Table: 92-20, Note: 92-20) Back to Table

A47. $O(^1D) + CCl_2FCF_3$ (CFC-114a). The recommendation is an estimate based on analogy to similar compounds. (Table: 92-20, Note: 92-20) Back to Table

A48. $O(^1D) + CClF_2CClF_2$ (CFC-114). The recommendation is based on the measurement by Ravishankara et al. [1097], who report (25 ± 9)% physical quenching. (Table: 92-20, Note: 92-20) Back to Table

A49. $O(^1D) + CClF_2CF_3$ (CFC-115). The recommendation is based on the measurement by Ravishankara et al.[1097], who report (70 ± 7)% physical quenching. (Table: 92-20, Note: 92-20) Back to Table

A50. $O(^1D) + CBrF_2CBrF_2$ (Halon 2402). The recommendation is based on data from Thompson and Ravishankara [1298]. They report that the yield of $O(^3P)$ from physical quenching is (25±7)%. Lorenzen-Schmidt et al. [844] measured the Halon removal rate relative to the N_2O removal rate and report that the rate coefficient for the Halon destruction path is $(8.8 \pm 1.2) \times 10^{-11,}$ in fair agreement with the result of Thompson and Ravishankara. (Table: 94-26, Note: 97-4) Back to Table

A51. $O(^1D) + C_2F_6$ (CFC-116). The recommendation is based on a measurement by Ravishankara et al. [1097], who report (85 ± 15)% physical quenching. The small rate coefficient for this reaction makes it vulnerable to interference from reactant impurities. For this reason the recommendation should probably be considered an upper limit. (Table: 94-26, Note: 94-26) Back to Table

A52. $O(^1D) + CHF_2CF_2CF_2CHF_2$ (HFC 338 pcc). The recommendation is based on data from Schmoltner et al. [1159]. They report that the yield of $O(^3P)$ from physical quenching is (97 ± 9)%. (Table: 94-26, Note: 94-26) Back to Table

A53. $O(^1D) + c\text{-}C_4F_8$. The recommendation for perfluorocyclobutane is based upon the measurement by Ravishankara et al. [1097], who report (100 +0 /–15)% physical quenching. The small rate coefficient for this reaction makes it vulnerable to interference from reactant impurities. For this reason the recommendation should probably be considered an upper limit. (Table: 92-20, Note: 92-20) Back to Table

A54. $O(^1D) + CF_3CHFCHFCF_2CF_3$ (HFC 43-10 mee). The recommendation is based on data from Schmoltner et al. [1159]. The rate coefficients for this compound and CHF_2CF_3 do not follow the reactivity trend of other HFCs. Schmoltner et al. report that the yield of $O(^3P)$ from physical quenching is (91±4)%. (Table: 94-26, Note: 94-26) Back to Table

A55. $O(^1D) + C_5F_{12}$ (CFC 41-12). The recommendation is based on data from Ravishankara et al. [1097]. They report that the yield of $O(^3P)$ from physical quenching is (79±12)%. (Table: 94-26, Note: 94-26) Back to Table

A56. $O(^1D) + C_6F_{14}$ (CFC 51-14). The recommendation is based on data from Ravishankara et al. [1097]. They report that the yield of $O(^3P)$ from physical quenching is (75±9)%. (Table: 94-26, Note: 94-26) Back to Table

A57. $O(^1D) + 1,2\text{-}(CF_3)_2c\text{-}C_4F_6$. The recommendation is based on data from Ravishankara et al. [1097]. They report that the yield of $O(^3P)$ from physical quenching is (84±16)%. (Table: 94-26, Note: 94-26) Back to Table

A58. $O(^1D) + SF_6$. The recommendation is based upon measurements by Ravishankara et al. [1097] who report (32±10)% physical quenching. The small rate coefficient for this reaction makes it vulnerable to interference from reactant impurities. For this reason the recommendation should probably be considered an upper limit. (Table: 92-20, Note: 92-20) Back to Table

A59. $O_2(^1\Delta) + O$. The recommendation is based on the upper limit reported by Clark and Wayne [269]. (Table: 92-20, Note: 92-20) Back to Table

A60. $O_2(^1\Delta) + O_2$. The recommendation is the average of eight room temperature measurements: Steer et al. [1235], Findlay and Snelling [454], Borrell et al. [163], Leiss et al. [796], Tachibana and Phelps [1270], Billington and Borrell [145], Raja et al. [1087], and Wildt et al. [1455]. The temperature dependence is derived from the data of Findlay and Snelling, and Billington and Borrell. Several other less direct measurements of the rate coefficient agree with the recommendation, including Clark and Wayne [270], Findlay et al. [453], and McLaren et al. [894]. Wildt et al. [1456] report observations of weak emissions in the near IR due to collision-induced radiation. Wildt et al. [1457] give rate coefficients for this process. (Table: 92-20, Note: 94-26) Back to Table

A61. $O_2(^1\Delta) + O_3$. The recommendation is the average of the room temperature measurements of Clark et al. [268], Findlay and Snelling [455], Becker et al. [107], and Collins et al. [305]. Several less direct measurements agree well with the recommendation (McNeal and Cook [895], Wayne and Pitts [1438], and Arnold and Comes [33]). The temperature dependence is from Findlay and Snelling and Becker et al., who agree very well, although both covered a relatively small temperature range. An earlier study by Clark et al. covered a much larger range, and found a much smaller temperature coefficient. The reason for this discrepancy is not clear. The yield of $O + 2O_2$ products appears to

be close to unity, based on many studies of the quantum yield of O_3 destruction near the peak of the Hartley band. For example, measurements of the number of O_3 molecules destroyed per photon absorbed: Von Ellenrieder et al. [1382], Ravishankara et al. [1103], Lissi and Heicklen [836], and references cited therein and measurements of O_3 loss and O atom temporal profiles in pulsed experiments Klais et al. [720] and Arnold and Comes [33]. Anderson et al. [29] report that the rate coefficient for atom exchange between $O_2(^1\Delta)$ and O_3 is $< 5\times10^{-16}$ at 300 K. (Table: 92-20, Note: 94-26) Back to Table

A62. $O_2(^1\Delta) + H_2O$. The recommendation is the average of the measurements reported by Becker et al. [106] and Findlay and Snelling [454]. An earlier study by Clark and Wayne [270] reported a value about three times larger. (Table: 92-20, Note: 92-20) Back to Table

A63. $O_2(^1\Delta) + N$. The recommendation is an upper limit based upon the measurement reported by Westenberg et al. [1450], who used ESR to detect $O_2(X^3\Sigma$ and $a^1\Delta)$, $O(^3P)$ and $N(^4S)$ with a discharge flow reactor. They used an excess of $O_2(^1\Delta)$ and measured the decay of N and the appearance of O at 195 and 300 K. They observed that the reaction of N with $O_2(^1\Delta)$ is somewhat slower than its reaction with $O_2(^3\Sigma)$. The recommended rate constant value for the latter provides the basis for the recommendation. Clark and Wayne [269, 271] and Schmidt and Schiff [1156] reported observations of an $O_2(^1\Delta)$ reaction with N that is about 30 times faster than the recommended limit. Schmidt and Schiff attribute the observed loss of $O_2(^1\Delta)$ in excess N to a rapid energy exchange with some constituent in discharged nitrogen, other than N. (Table: 92-20, Note: 92-20) Back to Table

A64. $O_2(^1\Delta) + N_2$. The recommendation is based upon the measurements by Findlay et al. [453] and Becker et al. [106]. Other studies obtained higher values for an upper limit: Clark and Wayne [270] and Steer et al. [1235]. (Table: 92-20, Note: 92-20) Back to Table

A65. $O_2(^1\Delta) + CO_2$. The recommendation is based on the measurements reported by Findlay and Snelling [454] and Leiss et al. [796]. Upper limit rate coefficients reported by Becker et al. [106], McLaren et al. [894], and Singh et al. [1197] are consistent with the recommendation. (Table: 92-20, Note: 92-20) Back to Table

A66. $O_2(^1\Sigma) + O$. The recommendation is based on the measurement reported by Slanger and Black [1211]. (Table: 92-20, Note: 92-20) Back to Table

A67. $O_2(^1\Sigma) + O_2$. The recommendation is the average of values reported by Martin et al. [881], Lawton et al. [775], and Lawton and Phelps [776], who are in excellent agreement. Measurements by Thomas and Thrush [1297], Chatha et al. [247], and Knickelbein et al. [726] are in reasonable agreement with the recommendation. Knickelbein et al. report an yield of $O_2(^1\Delta)$ product to be approximately unity. (Table: 92-20, Note: 92-20) Back to Table

A68. $O_2(^1\Sigma) + O_3$. The recommendation is based upon the room temperature measurements of Gilpin et al. [506], Gauthier and Snelling [488], Slanger and Black [1211], Choo and Leu [264], Shi and Barker [1180], Turnipseed et al. [1342], and Dunlea et al [423]. Measurements by Snelling [1220], Amimoto and Wiesenfeld [22], and Ogren et al. [1005] are in agreement with the recommendation. The value from the study of Biedenkapp and Baer [136] is lower than the recommended value. The temperature dependence is taken from the results of Dunlea et al., who measured the rate coefficient between 210 and 370 K. The results of Choo and Leu, which encompassed 295-362 K, are consistent with the recommended value. This reaction has multiple product channels. The yield of $O + 2O_2$ products is reported to be (70±20)% by Slanger and Black and Amimoto and Wiesenfeld. The remaining ~30% of the reaction is expected to lead to quenching to $O_2(^1\Delta$ or $^3\Sigma)$ while leaving ozone intact; the electronic state of O_2 that is produced in all these channels are not known. (Table: 06-2, Note: 06-2) Back to Table

A69. $O_2(^1\Sigma) + H_2$. The rate coefficient for this reaction at, or around 298 K, has been measured by Kohse-Hoinghaus and Stuhl [734], Braithwaite et al., [174], Choo and Leu, [264], Singh and Setser, [1197], Wildt et al., [1455], Michelangeli et al., [922], Borrell and Richards, [164], Hohmann et al. [594], and Talukdar et al. [1283]. k(298K) was derived from the results of all, but two, of the above studies.

Results of Singh and Setser and Borrell and Richards, which are clearly outside of the range of values obtained by others, were not used.

The temperature dependence of the rate coefficient was computed using the results of Braithwaite et al., Hohmann et al., and Talukdar et al. The results of Kohse-Hoinghaus and Stuhl were not included because it is assumed to be superseded by those of Hohmann et al. from the same group. It is suspected that the Kohse-Hoinghaus and Stuhl study was hampered by impurities in their system, as discussed in Talukdar et al.

The rate coefficient for the reaction to produce 2 OH radicals is listed separately as an upper limit at 298 K and is based on the results of Talukdar et al. The same upper limit is shown to be valid even at 209 K. Therefore, this upper limit is recommended for all atmospheric calculations.

This reaction could also produce $O(^3P) + H_2O$. However, there is no evidence for the formation of $O(^3P)$ (Dunlea et al.[418]). Therefore, it is assumed that $O_2(^1\Sigma)$ is removed exclusively via quenching. The electronic state of O_2 that is produced is not known. NEW ENTRY Back to Table

A70. $O_2(^1\Sigma) + H_2O$. The recommendation is the average of room temperature measurements reported by Stuhl and Niki [1256], Aviles et al., [57] Shi and Barker [1180], and Dunlea et al. [421]. Measurements reported by O'Brien and Myers [1004] are lower likely due to an interference from $O_2(^1\Sigma)$ regeneration.. The results of Derwent and Thrush [385], and Thomas and Thrush [1297] are in agreement with the recommendation. The value reported by Gauthier and Snelling [488] has a very large uncertainty and hence overlaps with the recommendation. It is not clear why the results of Filseth et al. are lower than all the other reported values; perhaps, they had an error in measuring water vapor concentration. The temperature dependence of the reaction is taken from the only reported value of Dunlea et al. Wildt et al. [1455] report that the yield of $O_2(^1\Delta)$ greater than 90%. There are no thermodynamically allowed reactive channels for this reaction. Therefore, the reaction products are written as $O_2 + H_2O$ [421].(Table: 06-2, Note: 06-2) Back to Table

A71. $O_2(^1\Sigma) + N$. The recommendation is based on the limit reported by Slanger and Black [1211]. (Table: 92-20, Note: 92-20) Back to Table

A72. $O_2(^1\Sigma) + N_2$. The recommendation is the average of measurements reported by Izod and Wayne [646], Stuhl and Welge [1259], Filseth et al. [452], Martin et al. [881], Kohse-Höinghaus and Stuhl [734], Choo and Leu [264], Wildt et al. [1455], Shi and Barker [1180], and Dunlea et al.[421]. Less direct measurements reported by Noxon [1003], Myers and O'Brien [940], and Chatha et al. [247] are consistent with the recommendation. The temperature dependence of the rate coefficient is derived from the results of Kohse-Höinghaus and Stuhl between 203 and 349 K and of Dunlea et al. between 210 and 370 K.

There are no exothermic reaction channels. The channel to produce 2 NO molecules is endothermic by 5.6 kcal mol^{-1} at 298 K. (Table: 06-2, Note: 06-2) Back to Table

A73. $O_2(^1\Sigma) + N_2O$. The rate coefficient for the removal of $O_2(^1\Sigma)$ by N_2O at 298 K is derived from the studies of Filseth et al., [452, 1297] Borrell et al., [162] and Dunlea et al. [424]. The results of Gauthier and Snelling has a very large error bar and overlaps with the recommended value within their quoted error bars. The temperature dependence of this rate coefficient is taken from Dunlea et al., who are the only ones to report this value.

There are many possible reactive channels for this reaction:

$$O_2(^1\Sigma_g^+) + N_2O \rightarrow NO + NO_2; \qquad \Delta_{rxn}H_{298} = -27.6 \text{ kcal/mol} \qquad (a)$$

$$\rightarrow N_2 + O_3; \qquad \Delta_{rxn}H_{298} = -23.0 \text{ kcal/mol} \qquad (b)$$

$$\xrightarrow{M} N_2O_3; \qquad \Delta_{rxn}H_{298} = -37.3 \text{ kcal/mol} \qquad (c)$$

$$\rightarrow O_2(^3\Sigma_g^-) + N_2O; \qquad \Delta_{rxn}H_{298} = -37.5 \text{ kcal/mol} \qquad (d)$$

$\rightarrow O_2(^1\Delta_g) + N_2O$; $\Delta_{rxn}H_{298}$ = - 15.0 kcal/mol (e)

Dunlea et al. have placed upper limits of $<2 \times 10^{-4}$, $<1 \times 10^{-3}$, and $<3 \times 10^{-3}$ for channel (a+c), channel (c), and overall N_2O loss from this reaction at 298 K. Based on these results, we recommend the upper limit for the NO_x production process in the table. The upper limit for NO_x production from this reaction noted in the table is assumed to be valid for all atmospheric temperatures. NEW ENTRY Back to Table

A74. $O_2(^1\Sigma) + CO_2$. The recommendation is the average of measurements reported by Filseth et al. [452], Davidson et al. [351], Avilés et al. [57], Muller and Houston [937], Choo and Leu [264], Wildt et al. [1455], Hohmann et al. [594], Dunlea and Ravishankara, and Shi and Barker [1180] at room temperature. The temperature dependence is from the work of Choo and Leu. Muller and Houston, and Singh and Setser [1197] give evidence that $O_2(^1\Delta)$ is a product. Wildt et al. report that the yield of $O_2(^1\Delta) \geq 90\%$. (Table: 92-20, Note: 06-2) Back to Table

B1. O + OH. The rate constant for O + OH is a fit to three temperature dependence studies: Westenberg et al. [1448], Lewis and Watson [817], and Howard and Smith [609]. This recommendation is consistent with earlier work near room temperature as reviewed by Lewis and Watson [817] and with the measurements of Brune et al. [185], Smith and Stewart [1215] and Robertson and Smith [1121]. The ratio $k(O + HO_2)/k(O + OH)$ measured by Keyser [708] agrees with the rate constants recommended here. (Table: 06-2, Note: 06-2) Back to Table

B2. $O + HO_2$. The recommended values are based on the results of studies over a range of temperatures by Keyser [707] and Nicovich and Wine [971] and the room temperature studies of Sridharan et al.[1226], Ravishankara et al. [1103], and Brune et al. [185]. Earlier studies by Hack et al. [536] and Burrows et al. [203, 206] are not considered, because the $OH + H_2O_2$ reaction was important in these studies and the value used for its rate constant in their analyses has been shown to be in error. A study by Lii et al. [825] is also not considered because of the insensitivity of the observed to decays to $O + HO_2$. Data from Ravishankara et al. [1103] at 298 K show no dependence on pressure between 10 and 500 torr N_2. The ratio $k(O + HO_2)/k(O + OH)$ measured by Keyser [708] agrees with the rate constants recommended here. Sridharan et al. [1224] showed that the reaction products correspond to abstraction of an oxygen atom from HO_2 by the O reactant. Keyser et al. [712] reported <1% O_2 $(^1\Delta)$ yield. (Table: 06-2, Note: 06-2) Back to Table

B3. $O + H_2O_2$. There are two direct studies of the $O + H_2O_2$ reaction: Davis et al. [361] and Wine et al. [1468]. The recommended value is a fit to the combined data. An indirect measurement of the E/R by Roscoe [1124] is consistent with the recommendation. The A-factor for both data sets is quite low compared to similar atom-molecule reactions. A somewhat higher activation barrier reported by Albers et al. [18] over the temperature range 370-800 K is suggestive of a non-linear temperature dependence. (Table: 06-2, Note: 06-2) Back to Table

B4. $H + O_3$. The recommendation is an average of the results of Lee et al. [783] and Keyser [703], which are in excellent agreement over the 200–400 K range. Results by Finlayson-Pitts, Seeley [1168] and Kleindienst [459] agree well with the present recommendations. An earlier study by Clyne and Monkhouse [290] is in very good agreement on the T dependence in the range 300–560 K but lies about 60% below the recommended values. Although we have no reason not to believe the Clyne and Monkhouse values, we prefer the two studies that are in excellent agreement, especially since they were carried out over the T range of interest. Reports of a channel forming $HO_2 + O$ (Finlayson-Pitts and Kleindienst [459]: ~25%, and Force and Wiesenfeld [467]: ~40%) have been contradicted by other studies (Howard and Finlayson-Pitts [608]: <3%; Washida et al.[1429]: <6%; Finlayson-Pitts et al. [460]: <2%; and Dodonov et al. [403]: <0.3%). Secondary chemistry is believed to be responsible for the observed O-atoms in this system. Washida et al. [1430] measured a low limit (<0.1%) for the production of singlet molecular oxygen in the reaction $H + O_3$. (Table: 06-2, Note: 06-2) Back to Table

B5. $H + HO_2$. There are five studies of this reaction: Hack et al. [540], Hack et al. [538], Thrush and Wilkinson [1304], Sridharan et al. [1226] and Keyser [710]. Related early work and combustion studies are referenced in the Sridharan et al. paper. All five studies used discharge flow systems. It is difficult to obtain a direct measurement of the rate constant for this reaction because both reactants

are radicals and the products OH and O are very reactive toward the HO_2 reactant. The recommendation is based on the kinetics and product data of Sridharan et al. and Keyser because their measurements were the most direct and required the fewest corrections. Keyser found the rate coefficient and product yields to be independent of temperature for 245 < T < 300 K. The other measurements, $(5.0\pm1.3) \times 10^{-11}$ cm^3 $molecule^{-1}$ s^{-1} by Thrush and Wilkinson [1304] and $(4.65\pm1) \times 10^{-11}$ by Hack et al. [538] are in reasonable agreement with the recommended value. Hislop and Wayne [585], Keyser et al. [712], and Michelangeli et al. [922] reported on the yield of O_2 ($b^1\Sigma$) formed in the $H_2 + O_2$ channel as $(2.8\pm1.3) \times 10^{-4}$, $<8 \times 10^{-3}$, and $<2.1 \times 10^{-2}$, respectively as a fraction of the overall reaction. (Table: 06-2, Note: 06-2) Back to Table

B6. OH + O_3. Recommended values are based on the results of studies over a range of temperatures by Anderson and Kaufman [26], Ravishankara et al. [1102], Smith et al. [1214] and Nizkorodov et al. [999] and the room temperature measurements of Kurylo [749], Zahniser and Howard [1508], and Kulcke et al. [744]. The recommended E/R and k(298 K) values are based on averages of the individual E/R and k(298 K) values obtained in the above-mentioned studies. The values reported by Kulcke et al. [744] and Nizkorodov et al. [1000] have been corrected for a minor contribution from k(HO_2 + O_3). (Table: 02-25, Note: 02-25) Back to Table

B7. OH + H_2. The OH + H_2 reaction has been the subject of numerous studies. The recommendation is fixed to the average of eleven studies at 298 K: Greiner [525], Stuhl and Niki [1258], Westenberg and de Haas [1446], Smith and Zellner [1217], Atkinson et al. [48], Overend et al. [1028], Tully and Ravishankara [1332], Zellner and Steinert [1515], Ravishankara et al. [1095], Talukdar et al. [1284] and Orkin et al. [1019]. Temperature dependent studies of Orkin et al. Talukdar et al. and Ravishankara et al. find that the reaction does not follow a simple Arrehenius expression over a large range of temperature. The recommended temperature dependence is based on the average of E/R's determined in the above-mentioned studies for temperatures below 300 K. Accordingly, the recommended Arrehenius expression is only valid between 200 – 300 K. Even over this range the simple Arrhenius expression likely overestimates, near 250 K, and underestimates, near 200 K, the data by approximately 10%. (Table: 06-2, Note: 06-2) Back to Table

B8. OH + HD. The recommendation is based on direct measurements made by Talukdar et al. [1284] using pulsed photolysis-laser induced fluorescence over the temperature range 248–418 K. The recommendation is in excellent agreement with the ratio k(OH + H_2)/k(OH + HD) = 1.65±0.05 at 298 K reported by Ehhalt et al. [433] when combined with the recommended k(OH + H_2). (Table: 06-2, Note: 06-2) Back to Table

B9. OH + OH. The recommendation for the OH + OH reaction is the average of seven measurements near 298 K: Westenberg and de Haas [1445], McKenzie et al. [893], Clyne and Down [279], Trainor and von Rosenberg [1319], Farquharson and Smith [446], Wagner and Zellner [1384], and Bedjanian et al. [110]. The rate constants for these studies all fall between (1.4 and 2.3) $\times 10^{-12}$ cm^3 $molecule^{-1}$ s^{-1}. Temperature studies by Wagner and Zellner, which show a slight positive T-dependence, are in contrast with those of Bedjanian et al. which show a small negative T-dependence. The earlier work might have been complicated by an increased contribution of the OH + H reaction due to an underestimate of its reaction rate. However, theoretical calculations by Harding and Wagner [551] suggest that the reaction rate is substantially influenced by tunneling. In taking account of the tunneling contribution the rate constant is found to reach a minimum value near room temperature. In view of this predicted behavior and given that the experimental data are consistent with each other, within their stated uncertainties, we recommend a temperature independent value for the rate constant over the 200 – 300 K range. (Table: 06-2, Note: 06-2) Back to Table

B10. OH + HO_2. A study by Keyser [711] appears to resolve a discrepancy among low-pressure discharge flow experiments that all gave rate coefficients near 7×10^{-11} cm^3 $molecule^{-1}$ s^{-1}: Keyser [706], Thrush and Wilkinson [1305], Sridharan et al. [1225], [1227], Temps and Wagner [1292], and Rozenshtein et al. [1128], and atmospheric pressure studies that gave rate coefficients near 11×10^{-11}: Lii et al. [824], Hochanadel et al. [592], DeMore [370], Cox et al. [317], Burrows et al. [205], and Kurylo et al. [755]. Laboratory measurements using a discharge flow experiment and a chemical model analysis of the results by Keyser [711] demonstrate that the previous discharge flow measurements were probably subject to interference from small amounts of O and H. In the presence

of excess HO_2 these atoms generate OH and result in a rate coefficient measurement that falls below the true value. The temperature dependence is from Keyser [711], who covered the range 254 to 382 K. A flow tube study by Schwab et al. [1164] reported k = (8.0 +3/–4) × 10^{-11}. These workers measured the concentrations of HO_2, OH, O, and H and used a computer model of the relevant reactions to test for interference. A flow tube study by Dransfeld and Wagner [413] employing an isotope labeled ^{18}OH reactant obtained k = (11±2) × 10^{-11} in good agreement with the recommendation. They attributed about half of the reactive events to isotope scrambling because control experiments with ^{16}OH gave k = 6 × 10^{-11}. It should be noted that their control experiments were subject to the errors described by Keyser [711] due to the presence of small amounts of H and O, whereas their ^{18}OH measurements were not. Kurylo et al. [755] found no evidence of significant scrambling in isotope studies of the OH and HO_2 reaction. An additional careful study of the reaction temperature dependence would be useful. Hippler and Troe [583] have analysed data for this reaction at temperatures up to 1250 K. In summary, this has historically been a difficult reaction to study. Earlier problems appear to have been resolved, as discussed above, and results now tend to converge on a central value, but the recommended value is still subject to a large uncertainty. (Table: 06-2, Note: 06-2) Back to Table

B11. OH + H_2O_2. Data from a number of studies are in relatively good agreement between 300 and 500 K after revising some of the data to account for the H_2O_2 UV absorption cross section recommendations in this evaluation. Taken together the studies of Keyser [704], Sridharan et al. [1228], Wine et al. [1472], Kurylo et al. [759], Lamb et al. [764], and Vaghjiani et al. [1364] show that the reaction displays a small (~160 kcal/mole) positive temperature dependence over the 300 – 500 K range. Measurements at room temperature by Marinelli and Johnston [873], Turnipseed et al. [1342] and Vakhtin et al. [1365] agree well with the other studies. A value of 1.8 × 10^{-12} cm^3 $molecule^{-1}s^{-1}$ is obtained by averaging all of the room temperature data. Below room temperature measurements by Lamb et al. and Vaghjiani diverge from the other studies, finding k to increase slightly with decreasing temperature. Vakhtin et al. have used a pulsed Laval nozzle technique to study the reaction at very low temperatures (165 K - 96 K). They measure a significant increase in k with decreasing temperature and suggest that the reaction mechanism includes formation of a hydrogen-bonded complex. Given the propensity of H_2O_2 for heterogeneous wall interactions at low temperatures, more studies are needed for this reaction, especially at low temperature and high pressures. Hippler and Troe [583] have analysed data for this reaction at temperatures up to 1250 K. At this time, we recommend a temperature independent value of 1.8 × 10^{-12} over the temperature range of 200 – 300 K. (Table: 06-2, Note: 06-2) Back to Table

B12. HO_2 + O_3. The recommended values are based on results of studies over a range of temperatures by DeMore [368] at 231 to 334 K, Zahniser and Howard [1508] at 245 to 365 K, Manzanares et al. [864] at 298 K, Sinha et al. [1206] at 243 to 413 K, Wang et al. [1424] at 233 to 400 K and Herndon et al. [574] at 200 to 298 K. The data of Simonaitis and Heicklen [1192] and DeMore and Tschuikow-Roux [381] were not considered. The temperature dependence studies show varying degrees of curvature in the Arrhenius plots, with the E/R decreasing at lower temperature. This is especially evident in the low temperature data of Herndon et al. where a number of measures were taken to control potential kinetic complications. The recommended E/R and k(298 K) values are based on averages of the individual E/R and k(298 K) values. Furthermore, only data at temperatures less than 298 K were used for the E/R determination, accordingly the recommendation is not valid for T>298 K. Additional temperature dependence data are needed for this reaction over a larger range to more fully characterize the non-linear behavior of the rate constant. The mechanism of the reaction has been studied using ^{18}O labeled HO_2 by Sinha et al. [1206], who reported that the reaction occurs 75±10% via H atom transfer at 297 K and by Nelson and Zahniser [951], who reported branching ratios for H transfer vs O transfer over the range 226–355 K. They report that the H atom transfer decreases from 94±5% at 226±11 K to 88±5% at 355±8 K. (Table: 00-3, Note: 00-3) Back to Table

B13. HO_2 + HO_2. Two separate expressions are given for the rate constant for the HO_2 + HO_2 reaction. The effective rate constant is given by the sum of these two equations. This reaction has been shown to have a pressure-independent bimolecular component and a pressure-dependent termolecular component. Both components appear to have negative temperature coefficients. However, Christensen et al. [266] found that all of the previous temperature studies, which used CH_3OH as a

precursor, are complicated below 298 K by a reaction between CH_3OH and HO_2. The bimolecular expression is obtained by fitting low pressure data of Cox and Burrows [316], Thrush and Tyndall [1301, 1302], Kircher and Sander [714], Takacs and Howard [1274, 1275], Sander [1134] and Kurylo et al. [761] above 298K so as to avoid possible complications due to CH_3OH chemistry. Data of Rozenshtein et al. [1128] are consistent with the low pressure recommendation, but they report no change in k with pressure up to 1 atm. Results of Thrush and Wilkinson [1303] and Dobis and Benson [401] are inconsistent with the recommendation. The termolecular expression is obtained from data of Sander et al. [1138], Simonaitis and Heicklen [1194], and Kurylo et al. [761] at room temperature and from Christensen [266] and Kircher and Sander [714] (only data above 298 K) for the temperature dependence. The recommended equation applies to M = air. The $HO_2 + HO_2$ reaction also exhibits a dependence on water vapor (Hamilton [544], Hochanadel et al. [591], Hamilton and Lii [545], Cox and Burrows [316], DeMore [368], Lii et al. [826], Sander et al. [1138], and Andersson et al. [30]) and H/D isotopic substitution (Hamilton and Lii [476] and Sander et al. [1138]). For systems containing water vapor, the multiplicative factor given by Lii et al. [826] and Kircher and Sander [714] can be used: $1 + 1.4 \times 10^{-21}$ $[H_2O]$ exp(2200/T). The major reaction products at 300 K have been identified as $H_2O_2 + O_2$ by Su et al. [1260], Niki et al. [988], Sander et al. [1138], and Simonaitis and Heicklen [1194]. Sahetchian et al. [1132, 1133] give evidence for the formation of a small amount of H_2 (~10%) at temperatures near 500 K, but Baldwin et al. [67] and Ingold [640] give evidence that the yield must be much less. Glinski and Birks [512] report an upper limit of 1% H_2 yield at a total pressure of about 50 torr and 298 K, but their experiment may have interference from wall reactions. A smaller limit to H_2 production (0.01%) was later determined in the same laboratory (Stephens et al. [1238]). The mechanism of the reaction has been studied using ^{18}O labelled HO_2 by Sinha et al. [1206], who reported that the reaction occurs 75±10% via H atom transfer at 297 K and by Nelson and Zahniser [951], who reported branching ratios for H transfer vs O transfer over the range 226–355 K. They report that the H atom transfer decreases from 94±5% at 226±11 K to 88±5% at 355±8 K Lightfoot et al. [822] reported atmospheric pressure measurements over the temperature range 298–777 K that are in agreement with the recommended value at room temperature but indicate an upward curvature in the Arrhenius plot at temperatures above 500 K. A high temperature study by Hippler et al. [584] confirms the strong curvature, where a number of measures were taken to control potential kinetic complications. Because of this complex reaction behavior, the recommended rate expressions are only valid for temperatures below 500 K. Additional temperature dependence data are needed for this reaction over a larger range to more fully characterize the non-linear behavior of the rate constant. (Table: 06-2, Note: 06-2) Back to Table

C1. $O + NO_2$. The recommended values are based on the results of studies over a range of temperatures by Estupiñán et al. [440], Gierczak et al. [492], Ongstad and Birks [1012], Slanger et al. [1212] and Geers-Muller and Stuhl [489] and the room temperature study of Paulson et al. [1040]. In the most recent studies of Estupiñán et al. [440] and Gierczak et al. [492], special emphasis was placed on accurate measurement of the NO_2 concentration and on measurements at low temperatures. The results of earlier studies by Davis et al. [356] and Bemand et al. [127] were not used in deriving the recommended values either because of possible complications from decomposition of NO_2 at higher temperatures or lack of direct NO_2 detection. (Table: 06-2, Note: 06-2) Back to Table

C2. $O + NO_3$. The recommendation is based on the study of Graham and Johnston [520] at 298 K and 329 K. While limited in temperature range, the data indicate no temperature dependence. Furthermore, by analogy with the reaction of O with NO_2, it is assumed that this rate constant is independent of temperature. Clearly, temperature-dependence studies are needed. (Table: 82-57, Note: 82-57) Back to Table

C3. $O + N_2O_5$. The recommendation is based on the study by Kaiser and Japar [686]. (Table: 82-57, Note: 82-57) Back to Table

C4. $O + HNO_3$. The upper limit reported by Chapman and Wayne [245] is accepted. (Table: 82-57, Note: 82-57) Back to Table

C5. $O + HO_2NO_2$. The recommended value is based on the study of Chang et al. [243]. The large uncertainty in E/R and k at 298 K are due to the fact that the recommendation is based on a single study. (Table: 82-57, Note: 82-57) Back to Table

C6. H + NO_2. The recommended value of k_{298} is derived from the studies of Wagner et al. [1386], Bemand and Clyne [125], Clyne and Monkhouse [290], Michael et al. [917] and Ko and Fontijn [732]. The temperature dependence is from the studies of Wagner et al. and Ko and Fontijn. The data from Wategaonkar and Setser [1433] and Agrawalla et al. [16] were not considered. (Table: 92-20, Note: 92-20) Back to Table

C7. OH + NO_3. The recommendation is derived from an average of the results of Boodaghians et al. [158], Mellouki et al. [904], Becker et al. [103] and Mellouki et al. [907]. There are no temperature dependence data. The reaction products are probably HO_2 + NO_2. (Table: 94-26, Note: 94-26) Back to Table

C8. OH + HONO. The recommended rate expression is derived from the work of Jenkin and Cox [660], which supersedes the earlier room temperature study of Cox et al. [323]. Results from the Burkholder et al. [200] suggest that the reaction may have a small negative temperature dependence. (Table: 92-20, Note: 92-20) Back to Table

C9. OH + HNO_3. The recent study of Brown et al. [184] furnishes the most comprehensive set of rate measurements for N_2 as the bath gas over a significant range of temperature (200–350 K) and pressure (20–500 torr). They analyzed their results in terms of the mechanism proposed by Smith et al. [1214], involving the formation of a bound, relatively long-lived $HO{\cdot}HNO_3$ complex, as well as the direct reaction channel. Studies of the effects of isotopic substitution on the reactions $OD+DNO_3$, $OH+DNO_3$, $OD+HNO_3$ and $^{18}OH+HNO_3$ by Brown et al. [183] support this mechanism and suggest that the structure of the intermediate consists of a H-bonded six-membered ring. Thus, the P dependence can be represented by combining a low pressure (bimolecular) limit, k_0, with a Lindemann-Hinshelwood expression for the p-dependence:

$$k([M],T)=k_o+\frac{k_3[M]}{1+\frac{k_3[M]}{k_2}} \qquad \left\{\begin{array}{l} k_o = 2.4x10^{-14}\exp(460/T) \\ k_2 = 2.7x10^{-17}\exp(2199/T) \\ k_3 = 6.5x10^{-34}\exp(1335/T) \end{array}\right\}$$

The coefficients k_3 and k_2 are the termolecular and high pressure limits for the "association" channel. The value of k at high pressures is the sum $k_0 + k_2$.

This expression for k([M],T) and the values of the Arrhenius parameters for k_0, k_2, and k_3 derived by Brown et al. [184] for N_2 as the bath gas constitute the recommended values for this rate coefficient. These recommended values are derived from a fit to the data of Brown et al. [184], Stachnik et al. [1230], Devolder et al. [386] and Margitan and Watson [868].

The reaction yield of NO_3 (per OH removed) is assumed to be unity at all temperatures for either reaction channel. These assumptions are supported by the isotopic studies of Brown et al. [183] and the theoretical calculations of Xia and Lin [1490]. (Table: 00-3, Note: 02-25) Back to Table

C10. OH + HO_2NO_2. The recommendation for both k at 298 K and the Arrhenius expression is based upon the data of Trevor et al. [1321], Barnes et al. [73], C. A. Smith et al. [1214] and Barnes et al. [75]. Trevor et al. studied this reaction over the temperature range 246–324 K and reported a temperature invariant value of 4.0×10^{-12} cm^3 $molecule^{-1}$ s^{-1}, although a weighted least squares fit to their data yields an Arrhenius expression with an E/R value of (193±193) K. In contrast, Smith et al. studied the reaction over the temperature range 240–300 K and observed a negative temperature dependence with an E/R value of –(650±30) K. The early Barnes et al. study [73] was carried out only at room temperature and 1 torr total pressure while their later study was performed in the pressure range 1–300 torr N_2 and temperature range 268–295 K with no rate constant variation being observed. In addition, k_{298} derived in Barnes et al. [73] was revised upward in the later study from 4.1×10^{-12} to 5.0×10^{-12} due to a change in the rate constant for the reference reaction. The values of k at 298 K from the four studies are in excellent agreement. An unweighted least squares fit to the data from the above-mentioned studies yields the recommended Arrhenius expression. The less precise value for k at 298 K reported by Littlejohn and Johnston [837] is in fair agreement with the recommended value. The error limits on the recommended E/R are sufficient to encompass the results of both Trevor et al. and Smith et al. It should be noted that the values of k at 220 K deduced

from the two studies differ by a factor of 2. Clearly, additional studies of k as a function of temperature and the identification of the reaction products are needed. (Table 02-25, Note: 02-25) Back to Table

C11. OH + NH_3. The recommended value at 298 K is the average of the values reported by Stuhl [1254], Smith and Zellner [1218], Perry et al. [1048], Silver and Kolb [1184], Stephens [1237] and Diau et al. [388]. The values reported by Pagsberg et al. [1030] and Cox et al. [322] were not considered because these studies involved the analysis of a complex mechanism and the results are well outside the error limits implied by the above six direct studies. The results of Kurylo [749] and Hack et al. [534] were not considered because of their large discrepancies with the other direct studies (factors of 3.9 and 1.6 at room temperature, respectively). Because the Arrhenius plot displays considerable curvature, the temperature dependence is based only on the data below 300 K, i.e., the studies of Smith and Zellner [1218] and Diau et al. [388], and the A-factor has been selected to fit the recommended room temperature value. (Table: 92-20, Note: 92-20) Back to Table

C12. HO_2 +NO. The recommendation for HO_2 + NO is based on the average of eight measurements of the rate constant at room temperature and below: Howard and Evenson [607], Leu [812], Howard [604], Glaschick-Schimpf et al. [507], Hack et al. [537], Thrush and Wilkinson [1305] and Jemi-Alade Thrush [657], and Seeley et al. [1170]. All of these are in quite good agreement. The results of Imamura and Washida [638] were not considered due to the relatively large uncertainty limits reported in this study. An earlier study, Burrows et al. [203] has been disregarded because of an error in the reference rate constant, k(OH + H_2O_2). The room temperature study of Rozenshtein et al. [1128] has also been disregarded due to an inadequate treatment of possible secondary reactions. The recommended Arrhenius parameters are obtained from a fit to all the data. The recommended value of k(298 K) is obtained from the Arrhenius line. (Table: 97-4, Note: 97-4) Back to Table

C13. HO_2 + NO_2. Tyndall et al. [1348] obtained an upper limit to the rate coefficient of 5×10^{-16} cm^3 $molecule^{-1}$ s^{-1} based on static photolysis experiments with FTIR analysis at 296 K and 760 torr of N_2. (Table: 97-4, Note: 97-4) Back to Table

C14. HO_2 + NO_3. The recommendation for k_{298} is based on a weighted average of the data of Hall et al. [542], Mellouki et al. [904], Becker et al. [103] and Mellouki et al. [907]. There are insufficient data on which to base the temperature dependence of the rate coefficient. The measured branching ratios for the OH + NO_2 + O_2 channel range from 0.57 to 1.0. The most direct measurement is derived from the study of Mellouki et al. [907], which obtained a value of 1.0 +0.0/–0.3 at 298 K**.** (Table: 94-26, Note: 94-26) Back to Table

C15. HO_2 + NH_2. There is a fairly good agreement on the value of k at 298 K between the direct study of Kurasawa and Lesclaux [748] and the relative studies of Cheskis and Sarkisov [260] and Pagsberg et al. [1030]. The recommended value is the average of the values reported in these three studies. The identity of the products is not known; however, Kurasawa and Lesclaux suggest that the most probable reaction channels give either NH_3 + O_2 or HNO + H_2O as products. (Table: 83-62, Note: 83-62) Back to Table

C16. N + O_2. The recommended expression is derived from a least squares fit to the data of Kistiakowsky and Volpi [716], Wilson [1461], Becker et al. [105], Westenberg et al. [1450], Clark and Wayne [271], Winkler et al. [1479] and Barnett et al. [84]. k(298 K) is derived from the Arrhenius expression and is in excellent agreement with the average of all of the room temperature determinations. (Table: 90-1, Note: 90-1) Back to Table

C17. N + O_3. The recommendation is based on the results of Barnett et al. [84]. The value of $(1.0\pm0.2) \times 10^{-16}$ cm^3 $molecule^{-1}$ s^{-1} reported by Barnett et al. should probably be considered an upper limit rather than a determination. The low values reported by Barnett et al., Stief et al. [1247] and Garvin and Broida [486] cast doubt on the much faster rates reported by Phillips and Schiff [1055], and Chen and Taylor [256]. (Table: 90-1, Note: 90-1) Back to Table

C18. N + NO. The recommended temperature dependence is based on the discharge flow-resonance fluorescence studies of Wennberg and Anderson [1441], and the discharge flow-resonance fluorescence and flash photolysis-resonance fluorescence studies of Lee et al. [785]. There is relatively poor agreement between these studies and the results of Clyne and McDermid [287],

Kistiakowsky and Volpi [717], Herron [575], Phillips and Schiff [1055], Lin et al. [828], Ishikawa et al. [643], Sugawara et al. [1264], Cheah and Clyne [248], Husain and Slater [626], Clyne and Ono [294], Brunning and Clyne [186] and Jeoung et al. [670]. (Table: 94-26, Note: 94-26) Back to Table

C19. $N + NO_2$. The recommendation for k_{298} is from the discharge flow-resonance fluorescence study of Wennberg and Anderson [1441]. The latter study had significantly better sensitivity for $N(^4S)$ than the discharge flow-resonance fluorescence study of Clyne and Ono [294], which obtained a value about four times smaller. The results of Husain and Slater [626] and Clyne and McDermid [287] are not considered. The temperature dependence is obtained from the study of Wennberg and Anderson. In the latter study, atomic oxygen was shown to be the principal reaction product, in agreement with Clyne and McDermid. A recent study by Iwata et al. [644] suggested an upper limit of 3.3×10^{-13} cm^3 $molecule^{-1}$ s^{-1} for the corresponding reaction involving $N(^2D)$ and $N(^2P)$ atoms (sum of all reaction channels). (Table: 94-26, Note: 94-26) Back to Table

C20. $NO + O_3$. The recommended values are based on the results of studies over a range of temperatures by Birks et al. [147], Lippmann et al. [833], Ray and Watson [1109], Michael et al. [912], Borders and Birks [160] and Moonen et al. [931] and the room temperature studies of Stedman and Niki [1233] and Bemand et al. [127]. The six temperature-dependent studies were given equal weighting in the recommendation by averaging over the E/R's from each individual data set. Following the Moonen et al. recommendation, the 200-K data point from their study has been excluded from the fit. All of the temperature dependence studies show some curvature in the Arrhenius plot at temperatures below 298 K. Increasing scatter between the data sets is evident at the lower temperatures. Clough and Thrush [275], Birks et al., Schurath et al. [1163], and Michael et al. have reported individual Arrhenius parameters for the two primary reaction channels producing ground and excited molecular oxygen. (Table: 00-3, Note: 00-3) Back to Table

C21. $NO + NO_3$. The recommendation is based on the studies of Hammer et al. [546], Sander and Kircher [1137] and Tyndall et al. [1349], which are in excellent agreement. (Table: 92-20, Note: 92-20) Back to Table

C22. $NO_2 + O_3$. The recommended expression is derived from a least squares fit to the data of Davis et al. [359], Graham and Johnston [519], Huie and Herron [620], and Cox and Coker [318]. The data of Verhees and Adema [1373] and Stedman and Niki [1233] were not considered because of systematic discrepancies with the other studies. (Table: 90-1, Note: 90-1) Back to Table

C23. $NO_2 + NO_3$. The existence of the reaction channel forming $NO + NO_2 + O_2$ has not been firmly established. However, studies of N_2O_5 thermal decomposition that monitor NO_2 (Daniels and Johnston [345]; Johnston and Tao [675]; Cantrell et al. [227]) and NO (Hjorth et al. [587], and Cantrell et al. [230]) require reaction(s) that decompose NO_3 into $NO + O_2$. The rate constant from the first three studies is obtained from the product kK_{eq}, where K_{eq} is the equilibrium constant for $NO_2 + NO_3 \rightarrow N_2O_5$, while for the latter two studies the rate constant is obtained from the ratio $k/k(NO + NO_3)$, where $k(NO + NO_3)$ is the rate constant for the reaction $NO + NO_3 \rightarrow 2NO_2$. Using K_{eq} and $k(NO + NO_3)$ from this evaluation, the rate expression that best fits the data from all five studies is $4.5 \times 10^{-14} \exp(-1260/T)$ cm^3 $molecule^{-1}$ s^{-1} with an overall uncertainty factor of 2. (Table: 92-20, Note: 92-20) Back to Table

C24. $NO_3 + NO_3$. The recommendation for k(298 K) is from the studies of Graham and Johnston [520] and Biggs et al. [141]. The temperature dependence is from Graham and Johnston. (Table: 94-26, Note: 94-26) Back to Table

C25. $NH_2 + O_2$. This reaction has several product channels which are energetically possible, including $NO + H_2O$ and $HNO + OH$. With the exception of the studies of Hack et al. [533] and Jayanty et al. [653] and several studies at high temperature, there is no evidence for a reaction. The following upper limits have been measured (cm^3 $molecule^{-1}$ s^{-1}): 3×10^{-18} (Lesclaux and Demissy [798]), 8×10^{-15} (Pagsberg et al. [1030]), 1.5×10^{-17} (Cheskis and Sarkisov [260]), 3×10^{-18} (Lozovsky et al. [852]), 1×10^{-17} (Patrick and Golden [1039]) and 7.7×10^{-18} (Michael et al. [913]) and 6×10^{-21} (Tyndall et al. [1351]). The recommendation is based on the study of Tyndall et al., which was sensitive to reaction paths leading to the products NO, NO_2 and N_2O. The reaction forming NH_2O_2

cannot be ruled out, but is apparently not important in the atmosphere. (Table: 92-20, Note: 92-20) Back to Table

C26. $NH_2 + O_3$. There is poor agreement among the recent studies of Cheskis et al. [259], k(298) = 1.5 × 10^{-13} cm^3 s^{-1}, Patrick and Golden [1039], k(298 K) = 3.25 × 10^{-13} cm^3 s^{-1}, Hack et al. [532], 1.84 × 10^{-13} cm^3 s^{-1}, Bulatov et al. [193], 1.2 × 10^{-13} cm^3 s^{-1}, and Kurasawa and Lesclaux [747], 0.63 × 10^{-13} cm^3 s^{-1}. The very low value of Kurasawa and Lesclaux may be due to regeneration of NH_2 from secondary reactions (see Patrick and Golden), and it is disregarded here. The discharge flow value of Hack et al. is nearly a factor of two less than the recent Patrick and Golden flash photolysis value. The large discrepancy between Bulatov et al. and Patrick and Golden eludes explanation. The recommendation is the k(298 K) average of these four studies, and E/R is an average of Patrick and Golden (1151 K) with Hack et al. (710 K). (Table: 90-1, Note: 90-1) Back to Table

C27. $NH_2 + NO$. The recommended value for k at 298 K is the average of the values reported by Lesclaux et al. [800], Hancock et al. [547], Sarkisov et al. [1145], Stief et al. [1245], Andresen et al. [31], Whyte and Phillips [1451], Dreier and Wolfrum [415], Atakan et al. [37], Wolf et al. [1480], Diau et al. [389] and Imamura and Washida [638]. The results of Gordon et al. [516], Gehring et al. [490], Hack et al. [539] and Silver and Kolb [1185] were not considered because they lie at least 2 standard deviations from the average of the previous group. The results tend to separate into two groups. The flash photolysis results average 1.8 × 10^{-11} cm^3 $molecule^{-1}$ s^{-1} (except for the pulse radiolysis study of Gordon et al.), while those obtained using the discharge flow technique average 0.9 × 10^{-11} cm^3 $molecule^{-1}$ s^{-1}. The apparent discrepancy cannot be due simply to a pressure effect as the pressure ranges of the flash photolysis and discharge flow studies overlapped and none of the studies observed a pressure dependence for k. Whyte and Phillips have suggested that the difference may be due to decomposition of the adduct NH_2NO, which occurs on the timescale of the flow experiments, but not the flash experiments. There have been many studies of the temperature dependence but most have investigated the regime of interest to combustion and only two have gone below room temperature (Hack et al. from 209–505 K and Stief et al. from 216–480 K. Each study reported k to decrease with increasing temperature. The recommended temperature dependence is taken from a fit to the Stief et al. data at room temperature and below. The reaction proceeds along a complex potential energy surface, which results in product branching ratios that are strongly dependent on temperature. *Ab initio* calculations by Walch [1389] show the existence of four saddle points in the potential surface leading to $N_2 + H_2O$ without a reaction barrier. Elimination to form $OH + HN_2$ can occur at any point along the surface. While results from early studies on the branching ratio for OH formation differ significantly, the most recent studies (Hall et al., Dolson [405], Silver and Kolb [1188], Atakan et al., Stephens et al. [1236], Park and Lin [1036]) agree on a value around 0.1 at 300 K, with N_2+H_2O making up the balance. (Table: 97-4, Note: 97-4) Back to Table

C28. $NH_2 + NO_2$. There have been four studies of this reaction (Hack et al. [539]; Kurasawa and Lesclaux [746]; Whyte and Phillips [1451]; and Xiang et al. [1491]). There is very poor agreement among these studies both for k at 298 K (factor of 2.3) and for the temperature dependence of k ($T^{-3.0}$ and $T^{-1.3}$). The recommended values of k at 298 K and the temperature dependence of k are averages of the results reported in these four studies. Hack et al. have shown that the predominant reaction channel (>95%) produces $N_2O + H_2O$. Just as for the $NH_2 + NO$ reaction, the data for this reaction seem to indicate a factor of two discrepancy between flow and flash techniques, although the data base is much smaller. (Table: 85-37, Note: 87-41) Back to Table

C29. NH + NO. The recommendation is derived from the room temperature results of Hansen et al. [550], Cox et al. [313] and Harrison et al. [553]. The temperature dependence is from Harrison et al. (Table: 92-20, Note: 92-20) Back to Table

C30. $NH + NO_2$. The recommendation is derived from the temperature-dependence study of Harrison et al. [553]. (Table: 92-20, Note: 92-20) Back to Table

C31. $O_3 + HNO_2$. Based on Kaiser and Japar [685] and Streit et al. [1250]. (Table: 82-57, Note: 82-57) Back to Table

C32. $N_2O_5 + H_2O$. The recommended value at 298 K is based on the studies of Tuazon et al. [1327], Atkinson et al. [54] and Hjorth et al. [588]. Sverdrup et al. [1266] obtained an upper limit that is a factor of four smaller than that obtained in the other studies, but the higher upper limit is

recommended because of the difficulty of distinguishing between homogeneous and heterogeneous processes in the experiment. See the heterogeneous chemistry section of this evaluation for additional rate data for this reaction. (Table: 85-37, Note: 90-1) Back to Table

C33. $N_2(A,v) + O_2$. Rate constants for the overall reaction for the v=0, 1 and 2 vibrational levels of $N_2(A)$ have been made by Dreyer et al. [416], Zipf [1530], Piper et al. [1059], Iannuzzi and Kaufman [636], Thomas and Kaufman [1296] and De Sousa et al. [365]. The results of these studies are in relatively good agreement. The recommended values are (2.5±0.4), (4.0±0.6) and (4.5±0.6) ($\times 10^{-12}$ cm^3 $molecule^{-1}$ s^{-1}), from the work of De Sousa et al. The only temperature dependence data are from De Sousa et al., who obtained $k(T,v)=k(v,298K)(T/300)^{0.55}$ for v=0,1,2. The observation of high N_2O production initially reported by Zipf [1530] has not been reproduced by other groups, and the branching ratio for this channel is probably less than 0.02 (Iannuzzi et al. [635], Black et al. [150], De Sousa et al. [365], Fraser and Piper [469]). The branching ratios for the other channels are poorly established, although there is strong evidence for the formation of both $O(^3P)$ and $O_2(B^3\Sigma_u^-)$. (Table: 94-26, Note: 94-26) Back to Table

C34. $N_2(A,v) + O_3$. The only study is that of Bohmer and Hack [156], who obtained 298 K rate constants of 4.1±1.0, 4.1±1.2, 8.0±2.3, and 10±3.0 ($\times 10^{-11}$ cm^3 $molecule^{-1}$ s^{-1}) for the v=0–3 vibrational levels of $N_2(A)$, respectively. This study determined that the NO channel accounts for about 20% of the reaction products. (Table: 94-26, Note: 94-26) Back to Table

D1. $O + CH_3$. The recommended k(298 K) is the weighted average of three measurements by Washida and Bayes [1431], Washida [1428], and Plumb and Ryan [1065]. The E/R value is based on the results of Washida and Bayes [1431], who found k to be independent of temperature between 259 and 341 K. (Table 83-62, Note: 83-62) Back to Table

D2. O + HCN. Because it is a very slow reaction, there are no studies of this reaction below 450 K. Davies and Thrush [354] studied this reaction between 469 and 574 K while Perry and Melius [1051] studied it between 540 and 900 K. Results of Perry and Melius are in agreement with those of Davies and Thrush. Our recommendation is based on these two studies. The higher-temperature (T>1000 K) combustion-related studies of Roth et al. [1125], Szekely et al. [1267], and Louge and Hanson [845] have not been considered. This reaction has two reaction pathways: $O + HCN \rightarrow H + NCO$, $\Delta H = -2$ kcal/mol (k_a); and $O + HCN \rightarrow CO + NH$ (k_b), $\Delta H = -36$ kcal/mol. The branching ratio k_a/k_b for these two channels has been measured to be ~2 at T = 860 K. The branching ratio at lower temperatures, which is likely to vary significantly with temperature, is unknown. (Table 87-41, Note: 92-20) Back to Table

D3. $O + C_2H_2$. The value at 298 K is an average of ten measurements (Arrington et al. [34], Sullivan and Warneck [1265], Brown and Thrush [181], Hoyermann et al. [610, 611], Westenberg and deHaas [1443], James and Glass [649], Stuhl and Niki [1257], Westenberg and deHaas [1447], and Aleksandrov et al. [19]). There is reasonably good agreement among these studies. Arrington et al. [34] did not observe a temperature dependence, an observation that was later shown to be erroneous by Westenberg and deHaas [1443]. Westenberg and deHaas [1443], Hoyermann et al. [611] and Aleksandrov et al. [19] are the only authors, who have measured the temperature dependence below 500 K. Westenberg and deHaas observed a curved Arrhenius plot at temperatures higher than 450 K. In the range 194–450 K, Arrhenius behavior provides an adequate description and the E/R obtained by a fit of the data from these three groups in this temperature range is recommended. The A-factor was calculated to reproduce k(298 K). This reaction can have two sets of products, i.e., $C_2HO + H$ or $CH_2 + CO$. Under molecular beam conditions C_2HO has been shown to be the major product. The study by Aleksandrov et al. using a discharge flow-resonance fluorescence method (under undefined pressure conditions) indicates that the $C_2HO + H$ channel contributes no more than 7% to the net reaction at 298 K, while a similar study by Vinckier et al. [1379] suggests that both CH_2 and C_2HO are formed. (Table: 82-57, Note: 82-57) Back to Table

D4. $O + H_2CO$. The recommended values for A, E/R and k(298 K) are the averages of those determined by Klemm [722] (250 to 498 K) using flash photolysis-resonance fluorescence, by Klemm et al. [723] (298 to 748 K) using discharge flow-resonance fluorescence, and Chang and Barker [240] (296 to 436 K) using discharge flow-mass spectrometry techniques. All three studies are in good agreement. The k(298 K) value is also consistent with the results of Niki et al. [984], Herron and

Penzhorn [577], and Mack and Thrush [854]. Although the mechanism for O + H_2CO has been considered to be the abstraction reaction yielding OH + HCO, Chang and Barker suggest that an additional channel yielding H + HCO_2 may be occurring to the extent of 30% of the total reaction. This conclusion is based on an observation of CO_2 as a product of the reaction under conditions where reactions such as O + HCO → H + CO_2 and O + HCO → OH + CO apparently do not occur. This interesting suggestion needs independent confirmation. (Table: 82-57, Note: 82-57) Back to Table

D5. O_2 + HOCO. HOCO is produced by the association of OH with CO (See Table 2). The rate coefficient for the reaction of O_2 with HOCO has been measured by Petty et al. [1053] and Nolte et al. [1001] and the recommendation is based on these measurements. There are no reports on the temperature dependence of this reaction; however, the value at 298 K would be appropriate for all atmospheric conditions. The products of this reaction are HO_2, as shown by Nolte et al., and CO_2, as seen in numerous previous studies where it has been known to be the product of the reaction of OH with CO in air. NEW ENTRY Back to Table

D6. O + CH_3CHO. The recommended k(298 K) is the average of three measurements by Cadle and Powers [215], Mack and Thrush [855], and Singleton et al. [1200], which are in good agreement. Cadle and Powers and Singleton et al. studied this reaction as a function of temperature between 298 and 475 K and obtained very similar Arrhenius parameters. The recommended E/R value was obtained by considering both sets of data. This reaction is known to proceed via H-atom abstraction (Mack and Thrush [855], Avery and Cvetanovic [56], and Singleton et al. [1200]). (Table 87-41, Note: 87-41) Back to Table

D7. O_3 + C_2H_2. The database for this reaction is not well established. Room temperature measurements (Cadle and Schadt [216]; DeMore [366]; DeMore [367]; Stedman and Niki [1232]; Pate et al. [1038]; and Atkinson and Aschmann [39]) disagree by as much as an order of magnitude. It is probable that secondary reactions involving destruction of ozone by radical products resulted in erroneously high values for the rate constants in several of the previous measurements. The present recommendation for k(298 K) is based on the room temperature value of Atkinson and Aschmann [39], which is the lowest value obtained and therefore perhaps the most accurate. The temperature dependence is estimated, based on an assumed A-factor of 10^{-14} cm^3 s^{-1} similar to that for the O_3 + C_2H_4 reaction and corresponding to the expected five-membered ring structure for the transition state (DeMore [366, 367]). Further studies, particularly of the temperature dependence, are needed. Major products in the gas phase reaction are CO, CO_2, and HCOOH, and chemically-activated formic anhydride has been proposed as an intermediate of the reaction (DeMore [367], and DeMore and Lin [379]). The anhydride intermediates in several alkyne ozonations have been isolated in low temperature solvent experiments (DeMore and Lin [379]). (Table: 90-1, Note: 90-1) Back to Table

D8. O_3 + C_2H_4. The rate constant of this reaction is well established over a large temperature range, 178 to 360 K. The present recommendation is based on the data of DeMore [366], Stedman et al. [1234], Herron and Huie [576], Japar et al. [650, 651], Toby et al. [1310], Su et al. [1262], Adeniji et al. [10], Kan et al. [692], Atkinson et al. [44], and Bahta et al. [64]. (Table: 90-1, Note: 90-1) Back to Table

D9. O_3 + C_3H_6. The rate constant of this reaction is well established over the temperature range 185 to 360 K. The present recommendation is based largely on the data of Herron and Huie [576], in the temperature range 235–362 K. (Note that a typographical error in Table 2 of that paper improperly lists the lowest temperature as 250 K, rather than the correct value, 235 K.) The recommended Arrhenius expression agrees within 25% with the low temperature (185–195 K) data of DeMore [366], and is consistent with, but slightly higher (about 10%) than Treacy et al. [1320] and slightly lower (about 40%) than the data of Adeniji et al. [10] in the temperature range 260–294 K. Room temperature measurements of Cox and Penkett [328], Stedman et al. [1234], Japar et al. [650, 651], and Atkinson et al. [44] and Neeb and Moorgat [948] are in good agreement (10% or better) with the recommendation. (Table: 06-2, Note: 06-2) Back to Table

D10. OH + CO. The recommendation allows for an increase in k with pressure. The zero pressure value was derived by averaging direct low pressure determinations (those listed in Baulch et al. [100]) and the values reported by Dreier and Wolfrum [414], Husain et al. [624], Ravishankara and Thompson

[1098], Paraskevopoulos and Irwin [1033], Hofzumahaus and Stuhl [593]. The results of Jonah et al. [677] are too high and were not included. An increase in k with pressure has been observed by a large number of investigators (Overend and Paraskevopoulos [1027], Perry et al. [1050], Chan et al. [239], Biermann et al. [139], Cox et al. [323], Butler et al. [214], Paraskevopoulos and Irwin [1032, 1033], DeMore [371], Hofzumahaus and Stuhl [593], Hynes et al. [633]). In addition, Niki et al. [992] have measured k relative to OH + C_2H_4 in one atmosphere of air by following CO_2 production using FTIR. The recommended 298 K value was obtained by using a weighted nonlinear least squares analysis of all pressure-dependent data in N_2 (Paraskevopoulos and Irwin [1033], DeMore [371], Hofzumahaus and Stuhl [593], and Hynes et al. [633]) as well as those in air (Niki et al. [994], Hynes et al. [633]), to the form k = (A+BP)/(C+DP), where P is pressure in atmospheres. The data were best fit with D = 0 and therefore a linear form is recommended. Previous controversy regarding the effect of small amounts of O_2 (Biermann et al. [139]) has been resolved and is attributed to secondary reactions (DeMore [371], Hofzumahaus and Stuhl [593]). The results of Butler et al. [214] have to be re-evaluated in the light of refinements in the rate coefficient for the OH + H_2O_2 reaction. The corrected rate coefficient is in approximate agreement with the recommended value. Currently, there are no indications to suggest that the presence of O_2 has any effect on the rate coefficient other than as a third body. The E/R value in the pressure range 50–760 torr has been shown to be essentially zero between 220 and 298 K by Hynes et al. [633]. Further substantiation of the temperature independence of k at 1 atm. may be worthwhile. Beno et al. [128] observe an enhancement of k with water vapor, which is in conflict with the flash photolysis studies; e.g., Ravishankara and Thompson [1098], Paraskevopoulos and Irwin [1033], and Hynes et al. [633]. The uncertainty factor is for 1 atm. of air.

The bimolecular channel yields H + CO_2 while the addition leads to HOCO. In the presence of O_2, the HOCO intermediate is converted to HO_2 + CO_2 (DeMore [371], Miyoshi et al. [924]). Miyoshi et al. report a rate constant for the reaction of HOCO with O_2 of ~1.5×10^{-12} cm^3 $molecule^{-1}$ s^{-1} at 298 K). Therefore, for atmospheric purposes, the products can be taken to be HO_2 and CO_2. (Table: 06-2, Note: 06-2) Back to Table

D11. OH + CH_4. This reaction has been extensively studied. The most recent data are from Vaghjiani and Ravishankara [1363], Saunders et al. [1149], Finlayson-Pitts et al. [458], Dunlop and Tully [426], Mellouki et al. [910], and Gierczak et al. [498], who measured the absolute rate coefficients for this reaction using discharge flow and pulsed photolysis techniques. Sharkey and Smith [1179] have reported a high value (7.7×10^{-15} cm^3 $molecule^{-1}$ s^{-1}) for k(298 K), and this value has not been considered here. The current recommendation for k(298 K) was derived from the results of Vaghjiani and Ravishankara, Dunlop and Tully, Saunders et al., Mellouki et al., Finlayson-Pitts et al., and Gierczak et al. The temperature dependence of this rate coefficient has been measured by Vaghjiani and Ravishankara (223–420 K), Dunlop and Tully (above 298 K), Finlayson-Pitts et al. (278–378 K), and Mellouki et al. (233–343 K). Gierczak et al. have extended the measurements of k to 195 K, and it appears that the rate coefficient does not strictly follow an Arrhenius expression. The recommended E/R was obtained from these results using data below 300 K. A more accurate representation of the rate constant as a function of temperature is obtained by using the three-parameter expression: $k = 2.80\times10^{-14} T^{0.667} \exp(-1575/T)$. This three-parameter fit may be preferred for lower stratosphere and upper troposphere calculations. A very recent report on this rate coefficient by Bonard et al. [157] agrees extremely with the value recommended here. (Table: 97-4, Note: 06-2) Back to Table

D12. OH + $^{13}CH_4$. This reaction has been studied relative to the OH + CH_4 reaction, since the ratio of the rate coefficients is the quantity needed for quantifying methane sources. Rust and Stevens [1129], Davidson et al. [349], and Cantrell et al. [231] have measured k_{12}/k_{13} at 298 K to be 1.003, 1.010, and 1.0055, respectively. Cantrell et al.'s data supersede the results of Davidson et al. The recommended value of 1.005 ± 0.002 is based on the results of Rust and Stevens and Cantrell et al. Cantrell et al. find k_{12}/k_{13} to be independent of temperature between 273 and 353 K. (Table: 92-20, Note: 92-20) Back to Table

D13. OH + CH_3D. The rate coefficient for this reaction has been measured between 249 and 422 K using a pulsed laser photolysis-laser induced fluorescence system by Gierczak et al. [497]. The recommended values of k (298 K) and E/R are from this study. The recommendation agrees within

about 10% at 298 K with the rate constant measured by DeMore [375] in a relative rate study over the temperature range 298–360 K. The difference, while small in an absolute sense, is nevertheless significant for the isotopic fractionation of atmospheric CH_3D and CH_4 by OH. An earlier result of Gordon and Mulac at 416 K [517] is in good agreement with the extrapolated data of both of these determinations. However, that measurement has not been explicitly included in this recommendation because the experiments were carried out at higher temperatures and therefore are less applicable to the atmosphere. The rate coefficients for the reactions of OH with other deuterated methanes have also been measured (Dunlop and Tully [426], Gierczak et al. [1284], Gordon and Mulac [517]). (Table: 94-26, Note: 94-26) Back to Table

D14. OH + H_2CO. The value for k(298 K) is the average of those determined by Niki et al. [993], Atkinson and Pitts [51], Stief et al. [1246], Yetter et al. [1498], Temps and Wagner [1293], and Sivakumaran et al. [1207]. The value reported by Morris and Niki [934] is expected to be superseded by the later report of Niki et al. [993]; but, it agrees within the stated uncertainty. There are two relative values that are not in agreement with the recommendations. The value of Niki et al. [986] relative to the OH + C_2H_4 reaction is higher, while the value of Smith [1219] relative to the OH + OH reaction is lower. The later report of Niki et al. [993] is assumed to supersede the earlier rate constant. The rate coefficient reported by Zabarnick et al. [1503] at and above 298 K are consistently higher than those recommended here, but overlap within the combined uncertainty. The temperature dependence was calculated from the data of Stief et al. obtained below 298 K and from the data of Sivakumaran et al. below 330 K after normalizing the results of both studies to k(298 K) recommended here. There is a clear indication that the Arrhenius plot of this rate coefficient is curved with a positive activation energy at temperatures above ~330 K. It is therefore important that the recommended rate coefficients be used only in the 200-300K temperature range. The abstraction reaction shown in the table is the major channel (Temps and Wagner [1293], Niki et al. [992]); other channels may contribute to a small extent (Horowitz et al. [601]). There is no indication that this rate coefficient is pressure dependent under atmospheric pressures and temperatures. (Table: 06-2, Note: 06-2) Back to Table

D15. OH + CH_3OH. The recommended value for k(298 K) is the average of direct studies by Overend and Paraskevopoulos [1026], Ravishankara and Davis [1090], Hagele et al. [541], Meier et al. [897], McCaulley et al. [890], Wallington and Kurylo [1410], Hess and Tully [579], Jimenez et al. [673], and Dillon et al. [392]. When these measurements were not at exactly 298 K, their values were recalculated for 298 K by using the E/R recommended here. Indirect measurements by Campbell et al. [221], Barnes et al. [74], Tuazon et al. [1328], Picquet et al. [1056], and Klopffer et al. [725] are in good agreement with the recommended value. The temperature dependence of k has been measured by Hagele et al., Meier et al., Greenhill and O'Grady, Wallington and Kurylo, Hess and Tully, Jimenez et al., and Crowley et al. The recommended value of E/R was calculated using the results obtained at temperature below 330 K by Wallington and Kurylo, Meier et al., Hess and Tully, Jimenez et al., and Crowley et al. The results of Greenhill and O'Grady is in reasonable agreement with the recommendation at and above 298 K, but it is clearly lower than the recommendation below 298 K. Hess and Tully report a curved Arrhenius plot over the temperature range 298 – 1000 K, while Meier et al. do not observe such a curvature. This reaction has two pathways: abstraction of the H-atom from the methyl group to give CH_2OH + H_2O or from the OH group to give CH_3O + H_2O. The results of Hagele et al., Meier et al., and Hess and Tully suggest that H abstraction from the methyl group to give CH_2OH + H_2O is the dominant channel below room temperature. At 298 K, for example, the branching ratio for the formation of CH_2OH is about 0.85 and increases as the temperature decreases. In the Earth's atmosphere, the eventual products of OH + CH_3OH reaction are the same: CH_2O and HO_2. (Table: 06-2, Note: 06-2) Back to Table

D16. OH + CH_3OOH. The recommended value for k(298 K) is the average of the rate coefficients measured by Niki et al. [991] and Vaghjiani and Ravishankara [1362], which differ by nearly a factor of two. Niki et al. measured the rate coefficient relative to that for OH with C_2H_4 (= 8.0×10^{-12} cm^3 $molecule^{-1}$ s^{-1}) by monitoring CH_3OOH disappearance using an FTIR system. Vaghjiani and Ravishankara monitored the disappearance of OH, OD, and ^{18}OH in excess CH_3OOH in a pulsed photolysis-LIF system. They measured k between 203 and 423 K and report a negative activation energy with E/R = –190 K; the recommended E/R is based on their results. The reaction of OH with CH_3OOH occurs via abstraction of H from the oxygen end to produce the CH_3OO radical and from

the CH_3 group to produce the CH_2OOH radical, as originally proposed by Niki et al. and confirmed by Vaghjiani and Ravishankara. CH_2OOH is unstable and falls apart to CH_2O and OH within a few microseconds. The possible reaction of CH_2OOH with O_2 is unimportant under atmospheric conditions (Vaghjiani and Ravishankara). The recommended branching ratios are,

$$OH + CH_3OOH \rightarrow CH_3O_2 + H_2O \qquad \text{(a) } 70\%$$

$$OH + CH_3OOH \rightarrow CH_2OOH + H_2O \qquad \text{(b) } 30\%,$$

(from Vaghjiani and Ravishankara) and are nearly independent of temperature. (Table: 02-25, Note: 02-25) Back to Table

D17. OH + HC(O)OH. The recommended value of k(298 K) is the average of those measured by Zetzsch and Stuhl [1518], Wine et al. [1462], Jolly et al. [676], Dagaut et al. [344], and Singleton et al. [1205]. The temperature dependence of k has been studied by Wine et al. and by Singleton et al., who observed k to be essentially independent of T.

Wine et al. found the rate coefficient for the OH + HC(O)OH reaction to be the same as that for OH + DC(O)OH reaction. Jolly et al. found the formic acid dimer to be unreactive toward OH, i.e., abstraction of the H atom attached to C was not the major pathway for the reaction. A comprehensive study of Singleton et al. showed that reactivity of HC(O)OH is essentially the same as that of DC(O)OH, but DC(O)OD reacts much slower than HC(O)OH and DC(O)OH. These observations show that the reaction proceeds via abstraction of the acidic H atom. Wine et al. and Jolly et al. also found that H atoms are produced in the reaction, which is consistent with the formation of HC(O)O, which would rapidly fall apart to CO_2 and H. End product studies are also consistent with the formation of CO_2 and H_2O in this reaction (Singleton et al. [1205]). The products of this reaction would be mostly HC(O)O and H_2O. The fate of HC(O)O in the atmosphere will be to give HO_2 either directly via reaction with O_2 or via thermal decomposition to H atom, which adds to O_2.

Wine et al. have suggested that, in the atmosphere, the formic acid could be hydrogen bonded to a water molecule and its reactivity with OH could be lowered because the hydrogen bonded water would obstruct the abstraction of the H atom. This suggestion needs to be checked. (Table: 02-25, Note: 02-25) Back to Table

D18. OH + HC(O)C(O)H. The only available data are from the 298 K relative rate study of Plum et al. [1064] and the results are recommended here. Because the rate coefficient is so large, it is unlikely to have a substantial temperature dependence and an E/R of zero is recommended. This reaction is expected to proceed via H-abstraction to yield H_2O, CO and HCO. NEW ENTRY Back to Table

D19. OH + $HOCH_2CHO$. The available data are from relative rate studies at 298 K(Bacher et al. [61], Niki et al. [995], and Mellouki et al. [900]). The recommendation is based on all these studies, which are in good agreement. Because the rate coefficient is very large, it is unlikely to have a substantial temperature dependence. Therefore, we recommend an E/R of zero. There are three possible sites for H-abstraction: the alcohol group, the CH_2 group and the carbonyl group. Of these, the likely pathways for abstraction are from the latter two sites:

$$OH + HOCH_2CHO \rightarrow H_2O + HOC(H)CHO \qquad (a)$$

$$OH + HOCH_2CHO \rightarrow H_2O + HOCH_2CO \qquad (b)$$

Niki et al. have shown that the branching ratio for channel (b) is 0.8 and for channel (a) is 0.2. It is unlikely that the branching ratio changes significantly with temperature. NEW ENTRY Back to Table

D20. OH + HCN. This reaction is pressure dependent. The recommended value is the high pressure limit measured by Fritz et al. [476] using a laser photolysis-resonance fluorescence apparatus. Phillips [1054] studied this reaction using a discharge flow apparatus at low pressures and found the rate coefficient to have reached the high pressure limit at ~10 torr at 298 K. Fritz et al.'s results contradict this finding. They agree with Phillip's measured value, within a factor of two, at 7 torr, but they find k to increase further with pressure. The products of the reaction are unknown. (Table 83-62, Note: 83-62) Back to Table

D21. OH + C_2H_6. There are nineteen studies of this reaction at 298 K (Greiner [526], Howard and Evenson [605], Overend et al. [1028], Lee and Tang [787], Leu [812], Tully et al. [1333], Jeong et al. [667], Tully et al. [1331], Nielsen et al. [979], Zabarnick et al. [1503], Wallington et al. [1412], Smith et al. [1214], Baulch et al. [99], Bourmada et al. [168], Abbatt et al. [2], Schiffman et al. [1152], Talukdar et al. [1287], Sharkey and Smith [1179] and Anderson and Stephens [27]). The recommended value is obtained by averaging the results of the recent investigations by Tully et al., Wallington et al., Abbatt et al., Schiffman et al., Talukdar et al. and Anderson and Stephens. The results of Sharkey and Smith are approximately 20% higher than those recommended here. When the measurements were not carried out at exactly 298 K, we have recalculated k using an E/R of 1070 K. The temperature dependence of the rate coefficient below 298 K has been measured only by Jeong et al., Wallington et al., Talukdar et al. and Anderson and Stephens. The last three studies are in good agreement. The recommended E/R is obtained from an analysis of the data of these three studies. The ratio of the rate coefficients for OH reactions with C_2H_6 and C_3H_8 has been measured by Finlayson-Pitts [458]. Our recommendations are in reasonable agreement with this ratio. Crowley et al. [335] have measured k at 247, 294, and 303 K, and the results are in agreement with the recommendations. (Table: 92-20, Note: 94-26) Back to Table

D22. OH + C_3H_8. There are many measurements of the rate coefficients at 298 K. In this evaluation we have considered only the direct measurements (Greiner [526], Tully et al. [1333], Droege and Tully [417], Schmidt et al. [1157], Baulch et al. [99], Bradley et al. [171], Abbatt et al. [2], Schiffman et al. [1152], Talukdar et al. [1287], Mellouki et al. [910], Donahue et al. [410], Clarke et al. [273] and Kozlov et al. [738]). The 298 K value is the average of these thirteen studies. Greiner, Tully et al. [1330], Droege and Tully, Talukdar et al., Mellouki et al., Donahue et al., Clarke et al. and Kozlov et al. [738] have measured the temperature dependence of this reaction. Donahue and Clark [411] have shown that there is outstanding agreement between all of the data sets after correcting some of them for small offsets due to systematic calibration errors. Due to the significant curvature in the Arrhenius behavior over the studied temperature range, the recommended Arrhenius expression is only valid between 190 – 300 K. The recommended E/R is obtained from a composite fit to the four data sets (Kozlov et al., Clarke et al., Talukdar et al, and Mellouki et al.) at temperature below 300 K. Each data set was normalized to the recommended k(298). This reaction has two possible channels, i.e., abstraction of the primary and the secondary H-atom. Observations of both channels by Tully et al. and Droege and Tully indicate that the reaction exhibits non-Arrhenius behavior over a wide temperature range. The branching ratios were estimated from the latter study:

$$k_{primary} = 6.3 \times 10^{-12} \exp(-1050/T)\ cm^3\ molecule^{-1}\ s^{-1}$$

$$k_{secondary} = 6.3 \times 10^{-12} \exp(-580/T)\ cm^3\ molecule^{-1}\ s^{-1}$$

These numbers are in reasonable agreement with the older data of Greiner. The ratio of the rate coefficients for OH reactions with C_2H_6 and C_3H_8 has been measured by Finlayson-Pitts et al. [458] and DeMore and Bayes [377]. Our recommendations are in reasonable agreement with their ratios. (Table: 06-2, Note: 06-2) Back to Table

D23. OH + C_2H_5CHO. The recommended value at 298 K is an average of the results from Niki et al., Niki et al. [986], Audley et al. [55], Kerr and Sheppard [700], Semmes et al. [1177], Papagni [1031], Thevenet [1295], and D'Anna [339]. The temperature dependence has been measured by Thevenet. The E/R is taken from Thevenet and the A-factor is adjusted to reproduce k(298 K). Vandenberk and Peeters [1367] measured unity yields of H_2O from the reaction and conclude that the reaction proceeds exclusively by H-abstraction of the aldehydic H-atom. NEW ENTRY Back to Table

D24. OH + 1-C_3H_7OH. There have been a number of room temperature measurements that are in excellent agreement. The recommended value is an average of the results from absolute kinetics studies by Overend and Paraskevopoulos [1026], Wallington and Kurylo [1410], Nelson et al. [955], and Yujing and Mellouki [1501]. Relative rate studies of Nelson et al., Oh and Andino [1007], Wu et al. [1488], and Cheema et al. [249] are in excellent agreement with the recommended value. The indirect study of Campbell [221] is consistent with but 30% lower than the recommended value. The reaction is observed to be nearly temperature independent; Yujing and Mellouki find a slight positive temperature dependence while Cheema et al. find a small negative temperature dependence. The recommended E/R value is based on the direct study of Yujing and Mellouki. End product

studies carried out by Azad and Andino [60] support predictions based on the structure-activity relationship that identify the primary reaction channels as hydrogen abstraction by the OH radical from the α (~75%) and β(~20) carbons. NEW ENTRY Back to Table

D25. OH + 2-C_3H_7OH. The recommended value at 298 K is an average of the absolute measurements by Overend and [1026], Wallington and Kurylo [1410], Nelson et al. [955], Dunlop and Tully [425], and Yujing and Mellouki [1501]. A relative rate study by Lloyd et al. [840] is, within its wide error limits, consistent with the recommendation. The temperature dependence is observed to vary little with temperature below 400 K. Measurements over the range 293-745 K by Dunlop and Tully revealed a "bowl" shaped temperature dependence, with a minimum in the rate coefficient observed at 378 K. The recommended E/R is based on the measurements of Yujing and Mellouki and, on account of the complex reaction behavior, is valid only for temperatures below 400 K. Temperature dependent data of Dunlop and Tully and Wallington and Kurylo are, within the experimental uncertainties, consistent with the recommendation. By using isotopic substitution, Dunlop and Tully determined that the primary reaction channel below 400K involves H atom abstraction by OH from the α-site. This result is in agreement with estimates based on the structure-activity relationship (Yujing and Mellouki). NEW ENTRY Back to Table

D26. OH + $C_2H_5C(O)OH$. Studies of this reaction have been confined to 298 K and above on account of the tendency of propionic acid to dimerize at lower temperatures and higher concentrations. Kinetic isotope effects measured by Singleton et al. [1204] are consistent with a two channel mechanism proposed previously for OH reaction with acetic acid. In the propionic acid case, the channel involving direct abstraction of an alkyl hydrogen is predominant, thus accounting for the observed temperature independence of the rate constant. The recommended temperature independent rate constant, is based on an average of the results of Singleton et al. and Dagout et al. [344] taken at a variety of temperatures between 298 K and 446 K. An earlier study room temperature measurement by Zetsch and Stuhl [1518] is ~30% higher, but consistent with the recommendation. Further studies below 298 K would be desirable in order to investigate possible non-Arrhenius behavior. NEW ENTRY Back to Table

D27. OH + $CH_3C(O)CH_3$. The rate coefficient for this reaction has been measured at temperatures close to 298 K by Cox et al. [325], Zetzsch [1517], Chiorboli et al. [263], Kerr and Stocker [701], Wallington and Kurylo [1411], LeCalve et al. [780], Wollenhaupt et al. [1481], Gierczak et al. [493] and Yamada et al. [1496]. Cox reported only an upper limit of $<5 \times 10^{-13}$ cm^3 $molecule^{-1}s^{-1}$, which is consistent with this recommendation. The primary aim of Chiorboli et al. was to examine the atmospheric degradation of styrene, which produces acetone. They employed a relative rate measurement and reported a value of k(298 K) that is almost three times faster than the recommended value. Because of possible complications in their system, we have not included their results in arriving at the recommended value. Wallington and Kurylo, LeCalve et al., Wollenhaupt et al., Gierczak et al., and Yamada et al. have reported k as a function of temperature; all these studies directly measured the rate constant using the pulsed photolysis method where the temporal profile of OH was measured using resonance fluorescence or laser induced fluorescence. The extensive data of Wollenhaupt et al. and Gierczak et al. seem to show that this rate coefficient does not follow an Arrhenius expression. The results of LeCalve et al. and Wallington et al. are in general agreement with the results of Wollenhaupt et al. and Gierczak et al. The non-Arrhenius behavior was not evident in the results of Wallington et al. and LeCalve et al. because they measured the rate constant at a few temperatures and did not explore temperature below 240 K, where the curvature becomes increasingly evident. Yamada et al. measured k only above room temperature and their values are consistently lower than those of all the others noted above. As they noted in their paper, Yamada et al. did not measure the acetone concentration in the reactor and, thus, could have overestimated its concentration leading to consistently lower values of k. We have not included data of Yamada et al. (2003) in deriving the fit because of this possible systematic error and because they did not report k under atmospheric temperatures. The following recommendation reproduces all reported data, except that of Chiorboli et al. within the recommended uncertainty of 25% at all temperatures:

$$k(T) = 1.33 \times 10^{-13} + 3.82 \times 10^{-11}\exp(-2000/T)$$

This reaction can proceed via the abstraction of an H atom or via the formation of a complex that decomposes to give many different products, which include CH_3 + $CH_3C(O)OH$, CH_3OH + $CH_3C(O)$, CH_4 + CH_3CO_2, H_2O + $CH_3C(O)CH_2$. The branching ratios for the formation of different sets of products could vary with temperature. Wollenhaupt and Crowley (2000) have deduced that CH_3 radicals are produced with a yield of ~50% at 298 K and ~30% at 233 K. A similar branching ratio has also been reported by Vasvari et al. [1372]. The results of Gierczak et al. on OH + $CD_3C(O)CD_3$ reaction, whose rate coefficient nearly obeys an Arrhenius expression between 240 and 400 K and is nearly an order of magnitude smaller than the non-deuterated analog at 250 K, suggests that H abstraction may be the dominant channel. Vandenberk et al. [1369], Tyndall et al. [1344], and Talukdar et al. [1285], clearly show that $CH_3C(O)OH$ is a minor, if not negligible, product of this reaction and that the reaction proceeds to abstract an H atom. The results of Yamada et al. are consistent with this finding. Theoretical calculations of Henon et al. [571], and Vandenberk et al. [1368]also suggest that formation of acetic acid is negligible**.** We recommend that the products of this reaction be taken as H_2O and $CH_3C(O)CH_2$. (Table: 06-2, Note: 06-2) Back to Table

D28. OH + CH_3CN. This rate coefficient has been measured as a function of temperature by Harris et al. [552] between 298 and 424 K, Kurylo and Knable [756] between 250 and 363 K, Rhasa [1116] between 295 and 520 K, and Hynes and Wine [630] between 256 and 388 K. In addition, the 298 K value has been measured by Poulet et al. [1071]. The 298 K results of Harris et al. are in disagreement with all other measurements and therefore have not been included. The recommended 298 K value is a weighted average of all other studies. The temperature dependence was computed using the results of Kurylo and Knable, the lower temperature values (i.e., 295–391 K) of Rhasa, and the data of Hynes and Wine. Three points are worth noting: (a) Rhasa observed a curved Arrhenius plot even in the temperature range of 295 to 520 K, and therefore extrapolation of the recommended expression could lead to large errors; (b) Hynes and Wine observed a pressure dependent increase of k(298 K) that levels off at about 1 atmosphere, and this observation is contradictory to the results of other investigations; (c) Hynes and Wine have carried out extensive pressure, temperature, O_2 concentration, and isotope variations in this reaction. Hynes and Wine postulate that the reaction proceeds via addition as well as abstraction pathways. They observe OH regeneration in the presence of O_2. The recommended k(298 K) and E/R are applicable for only lower tropospheric conditions. Because of the unresolved questions of pressure dependence and reaction mechanism, the recommended value may not be applicable under upper tropospheric and stratospheric conditions. (Table: 92-20, Note: 92-20) Back to Table

D29. OH + CH_3ONO_2. The rate coefficient for this reaction at 298 K has been measured by Kerr and Stocker [701], Nielsen et al. [981], Gaffney et al. [479], Talukdar et al. [479], Kakesu et al. [690] and Shallcross et al. [1178]. The results of Kerr and Stocker and of Nielsen et al. are a factor of ten higher than those reported by the other groups. There are no obvious reasons for the reported differences but the lower values are preferred for a number of reasons. Firstly, Talukdar et al. have carried out a large number of checks which ruled out possible effects in their system due to the regeneration of OH via secondary reactions, to bath gas pressure, and to formation of an adduct that could undergo further reaction in the presence of oxygen. Secondly, the lower values are more consistent with reactivity predictions of Atkinson and Aschmann [42], who assumed that the series of nitrate reactions proceed by H-atom abstraction pathways. Kinetic measurements of Talukdar et al. performed with isotopically substituted hydroxyl radical (OH, ^{18}OH, and OD) and methyl nitrate (CH_3ONO_2 and CD_3ONO_2) are consistent with this reaction proceeding via an H-atom abstraction pathway. Accordingly, the recommended value of k(298 K) is based on an average of the values given by Gaffney et al, Talukdar et al., Kakesu et al. and Shallcross et al. Further verification of the reaction mechanism by identification of the products of the reaction is needed. The temperature dependence of the rate coefficient has been measured by Nielsen et al., Talukdar et al., and Shallcross et al. While Nielsen et al. report a negative activation energy, Talukdar et al. and Shallcross et al. report positive values. For the reasons given above, the temperature dependence recommended here is based on an average of Talukdar et al. and Shallcross et al. (Table: 06-2, Note: 06-2) Back to Table

D30. OH + $CH_3C(O)O_2NO_2$ (PAN). This reaction has been studied by four groups, Winer et al. [1477], Wallington et al. [1393], Tsalkani et al. [1322], and Talukdar et al. [1282]. Winer et al. obtained only

an upper limit for the rate coefficient. Tsalkani et al. noted that their system was very ill-behaved and obtained a value of k(298 K) that is a factor of ~2 lower than that obtained by Wallington et al. The pulsed photolysis study of Wallington et al. yielded consistent results, but PAN was not directly measured and photodissociation of H_2O in the vacuum UV, where PAN absorbs strongly, was used as the OH source. The recent study of Talukdar et al. [1282] yielded much lower rate coefficients. These investigators measured the PAN concentration directly in their system, minimized secondary reactions due to the photodissociation of PAN, and carried out extensive tests for decomposition of PAN, impurities, and secondary reactions. The recommended upper limit is a factor of two higher than the highest value measured by Talukdar et al. at 298 K and at 272 K. The quoted upper limit is expected to be valid at all atmospheric temperatures. The products of the reaction are not known. Further measurements of the rate coefficients and information on the reaction pathways are needed. (Table: 94-26, Note: 94-26) Back to Table

D31. OH + $C_2H_5ONO_2$. The rate constant for this reaction at 298 K has been measured by Kerr and Stocker [701], Nielsen et al. [981], Talukdar et al. [1286], Kakesu et al. [690], and Shallcross et al. [1178]. As in the case of the reaction of OH with CH_3ONO_2, the results of Kerr and Stocker and of Nielsen et al. are larger (by a factor of 3) than those of the more recent studies. The reasons for the differences are not clear. Because of the exhaustive tests carried out (see the note for the OH + CH_3ONO_2 reaction), the values of Talukdar et al., Kakesu et al., and Shallcross et al. are recommended. Nielsen et al., Talukdar et al., and Shallcross et al. have measured the rate constant as a function of temperature. As with the OH + CH_3ONO_2 reaction, Nielsen et al. report a negative activation energy while Talukdar et al. and Shallcross et al. have observed a small positive activation energy. Talukdar et al. note that the rate coefficient for this reaction does not strictly follow Arrhenius behavior, consistent with the abstraction of both the primary and the secondary H atoms. Above 298 K, E/R values measured by Shallcross et al. and Talukdar et al. are in excellent agreement. Only Talukdar et al. have kinetics data below 298 K and the recommended E/R value was obtained by fitting the rate coefficients measured by Talukdar et al. at or below 298 K. The large uncertainty encompasses the results of Kerr and Stocker and Nielsen et al. (Table: 06-2, Note: 06-2) Back to Table

D32. OH + 1-$C_3H_7ONO_2$. The reaction has been studied by Kerr and Stocker [701] and Atkinson and Aschmann [42] at room temperature and by Nielsen et al. [981] between 298 and 368 K. The results of the three studies are in good agreement at room temperature. Nielsen et al. find that the reaction is temperature independent within the measurement uncertainty over the range studied. However as discussed above, the Nielson et al. results for the analogous reactions of OH with CH_3ONO_2 and $C_2H_5ONO_2$, yield negative activation energies that disagree with the positive activation energies obtained by others. Judging from the E/R's for the analogous reactions, one might expect the E/R for this reaction to be on the order of 300 kcal/mole. Accordingly, we place a large uncertainty on the recommended temperature dependence. A thorough investigation of the temperature dependence of this reaction is needed. (Table: 02-25, Note: 02-25) Back to Table

D33. OH + 2-$C_3H_7ONO_2$. The reaction has been studied by Atkinson and Aschmann [42], Atkinson et al. [43] and Becker and Wirtz [109] at room temperature and by Talukdar et al. [1286] over the range 233 and 395 K. The results of Atkinson and Aschmann supersede those of Atkinson et al. There is fair agreement between the results of the three studies at room temperature, with roughly a factor of two spread in the values. The recommendation is based on an average of the room temperature values and the E/R measured by Talukdar et al. (Table: 02-25, Note: 02-25) Back to Table

D34. HO_2 + CH_2O. There is sufficient evidence to suggest that HO_2 adds to CH_2O (Su et al. [1261, 1263], Veyret et al. [1376], Zabel et al. [1504], Barnes et al. [80], and Veyret et al. [1375]). The recommended k(298 K) is the average of values obtained by Su et al. [1261], Veyret et al. [1376], and Veyret et al. [1375]. The temperature dependence observed by Veyret et al. [1375] is recommended. The value reported by Barnes et al. at 273 K is consistent with this recommendation. The adduct HO_2•CH_2O seems to isomerize to $HOCH_2OO$ reasonably rapidly and reversibly. There significant discrepancies between measured values of the equilibrium constants for this reaction. (Table: 90-1, Note: 90-1) Back to Table

D35. HO_2 + CH_3O_2. This recommendation is taken from the evaluated review of Tyndall et al. [1346]. The kinetics of this reaction has been studied by using UV absorption following pulsed photolytic

production of the radicals. These authors first analyzed the available data for the products of the reaction and concluded that the major products are CH_3OOH and O_2. They used this product yield information with their evaluated UV absorption cross sections for HO_2 and CH_3O_2 to reanalyze the UV absorption profiles measured in kinetics experiments by Dagaut et al. [343] and by Lightfoot et al. [823], the two groups that carried out the most extensive studies. They found that rate coefficients reported by these two groups need to be increased by ~20%. The recommended value is based on the average of the corrected data from these two groups. The temperature dependence was evaluated by Tyndall et al. by assuming that the absorption cross sections of CH_3O_2 and HO_2 are independent of temperature at the wavelengths used for the kinetics studies. The products of this reaction are shown as $CH_3OOH + O_2$ in the table. However, Elrod et al. [436] have determined that the reaction also yields $CH_2O + H_2O + O_2$ with yields that range from 0.1 at 298 K and 0.3 at 220 K. In anticipation of further work, the recommended product yield for the CH_2O channel is zero..(Table: 02-25, Note: 06-2) Back to Table

D36. $HO_2 + C_2H_5O_2$. The recommended value is the weighted average of those measured by Cattell et al. [237], Dagaut et al. [342], Fenter et al. [451], and Maricq and Szente [870]. In all experiments the rate coefficient was obtained by modeling the reaction system. Also, the calculated rate coefficients depended on the UV absorption cross sections of both $C_2H_5O_2$ and HO_2. The absorption cross section of $C_2H_5O_2$ is not well-defined. The value reported by Dagaut et al. would be ~30% higher if the cross sections used by Maricq and Szente were used. The recommended E/R is derived from the measurements of Dagaut et al., Fenter et al., and Maricq and Szente. Wallington and Japar [1409] have shown that $C_2H_5O_2H$ and O_2 are the only products of this reaction. (Table: 94-26, Note: 94-26) Back to Table

D37. $HO_2 + CH_3C(O)O_2$. This recommendation is taken from the evaluated review of Tyndall et al. [1346]. This reaction has two sets of products:

$$CH_3C(O)O_2 + HO_2 \xrightarrow{k_a} CH_3C(O)O_2H + O_2 \text{ (a)}$$

$$CH_3C(O)O_2 + HO_2 \xrightarrow{k_b} CH_3C(O)OH + O_3 \text{ (b)}$$

The majority of the reaction proceeds via channel (a), but there is clear evidence for channel (b). Tyndall et al. reevaluated the available data on end products of this reaction, particularly those of Crawford et al. [333], Moortgat et al. [932], and Horie and Moortgat [598], and concluded that channel (a) contributes ~80% while channel (b) contributes ~20% at 298 K. They also concluded that $k_a/k_b = 37 \times \exp(-660/T)$ with a large uncertainty in this value. They derived the overall rate coefficient for this reaction, which has been measured only by following the radical concentrations via UV absorption. They based their recommendation mostly on the results of Moortgat et al. [932] and Tomas et al. [1314]. (Table: 02-25, Note: 02-25) Back to Table

D38. $HO_2 + CH_3C(O)CH_2O_2$. This recommendation is from Tyndall et al. [1346]. This reaction has been studied by only Bridier et al. [177] and Tyndall et al. based their recommendation on this one study. (Table: 02-25, Note: 02-25) Back to Table

D39. $NO_3 + CO$. The upper limit is based on the results of Hjorth et al. [589], who monitored isotopically labeled CO loss in the presence of NO_3 by FTIR. Burrows et al. [207] obtained an upper limit of 4×10^{-16} cm^3 molecule^{-1} s^{-1}, which is consistent with the Hjorth et al. study. Products are expected to be $NO_2 + CO_2$, if the reaction occurs. (Table 87-41, Note: 92-20) Back to Table

D40. $NO_3 + CH_2O$. There are three measurements of this rate coefficient at 298 K: Atkinson et al. [53], Cantrell et al. [232], and Hjorth et al. [590]. The value reported by Atkinson et al. [53], $k = (3.23 \pm 0.26) \times 10^{-16}$ cm^3 molecule^{-1} s^{-1}, is corrected to 5.8×10^{-16} cm^3 molecule^{-1} s^{-1} to account for the different value of the equilibrium constant for the $NO_3 + NO_2 \rightarrow N_2O_5$ reaction that was measured subsequent to this study by the same group using the same apparatus. This correction is in accordance with their suggestion (Tuazon et al. [1329]). The values reported by Cantrell et al. and Hjorth et al., $k = 6.3 \times 10^{-16}$ cm^3 molecule^{-1} s^{-1} and $(5.4\pm1.1) \times 10^{-16}$ cm^3 molecule^{-1} s^{-1}, respectively, are in good agreement with the corrected value of Atkinson et al. The recommended value is the average of these three studies. Cantrell et al. have good evidence to suggest that HNO_3 and CHO are the products of this reaction. The temperature dependence of this rate coefficient is

unknown, but comparison with the analogous NO_3 + CH_3CHO reaction suggests a large E/R. (Table: 90-1, Note: 90-1) Back to Table

D41. NO_3 + CH_3CHO. There are four measurements of this rate constant: Morris and Niki [935], Atkinson et al. [53], Cantrell et al. [226], and Dlugokencky and Howard [394]. The value reported by Atkinson et al. [53], k = (1.34±0.28) × 10^{-15} cm^3 $molecule^{-1}$ s^{-1}, is corrected to 2.4 × 10^{-15} cm^3 $molecule^{-1}$ s^{-1} as discussed for the NO_3 + H_2CO reaction above and as suggested by Tuazon et al. [1329]. The recommended value is the average of the values obtained by Atkinson et al., Cantrell et al., and Dlugokencky and Howard. The results of Morris and Niki agree with the recommended value when their original data is re-analyzed using a more recent value for the equilibrium constant for the reaction NO_2 + NO_3 ↔ N_2O_5 as shown by Dlugokencky and Howard. Dlugokencky and Howard have studied the temperature dependence of this reaction. Their measured value of E/R is recommended. The A-factor has been calculated to yield the k(298 K) recommended here. Morris and Niki, and Cantrell et al. observed the formation of HNO_3 and PAN in their studies, which strongly suggests that HNO_3 and CH_3CO are the products of this reaction. (Table 87-41, Note: 87-41) Back to Table

D42. CH_3 + O_2. This bimolecular reaction is not expected to be important, based on the results of Baldwin and Golden [66], who found k < 5 × 10^{-17} cm^3 $molecule^{-1}$ s^{-1} for temperatures up to 1200 K. Klais et al. [719] failed to detect OH (via CH_3 + O_2 → CH_2O + OH) at 368 K and placed an upper limit of 3 × 10^{-16} cm^3 $molecule^{-1}$ s^{-1} for this rate coefficient. Bhaskaran et al. [133] measured k = 1×10^{-11} exp (–12,900/T) cm^3 $molecule^{-1}$ s^{-1} for 1800 < T < 2200 K. The latter two studies thus support the results of Baldwin and Golden. Studies by Selzer and Bayes [1176] and Plumb and Ryan [1065] confirm the low value for this rate coefficient. Previous studies of Washida and Bayes [1431] are superseded by those of Selzer and Bayes. Plumb and Ryan have placed an upper limit of 3 × 10^{-16} cm^3 $molecule^{-1}$ s^{-1} based on their inability to find HCHO in their experiments. A study by Zellner and Ewig [1514] suggests that this reaction is important at combustion temperature but is unimportant for the atmosphere. (Table 83-62, Note: 83-62) Back to Table

D43. CH_3 + O_3. The recommended A-factor and E/R are those obtained from the results of Ogryzlo et al. [1006]. The results of Simonaitis and Heicklen [1193], based on an analysis of a complex system, are not used. Washida et al. [1430] used O + C_2H_4 as the source of CH_3. Studies on the O + C_2H_4 reaction (Schmoltner et al. [1158], Kleinermanns and Luntz [721], Hunziker et al. [621], and Inoue and Akimoto [641]) have shown this reaction to be a poor source of CH_3. Therefore, the results of Washida et al. are also not used. (Table 83-62, Note: 83-62) Back to Table

D44. HCO + O_2. The value of k(298 K) is the average of the determinations by Washida et al. [1432], Shibuya et al. [1182], Veyret and Lesclaux [1374], Langford and Moore [769], Nesbitt et al. [959], Temps et al. [1293], and Ninomiya et al. [996]. There are three measurements of k where HCO was monitored via the intracavity dye laser absorption technique (Reilly et al. [1110], Nadtochenko et al. [941], and Gill et al. [499]). Even though these studies agree with the recent measurements of Nesbitt et al., the only recent measurement to obtain a low value, they have not been included in deriving the recommended value of k(298 K). However, the uncertainty has been increased to overlap with those measurements. The main reason for not including them in the average is the possible depletion of O_2 in those static systems (as suggested by Veyret and Lesclaux). Also, these experiments were designed more for the study of photochemistry than kinetics. The temperature dependence of this rate coefficient has been measured by Veyret and Lesclaux, Timonen et al. [1309], and Nesbitt et al. While Timonen et al. obtain a slightly positive activation energy, Veyret and Lesclaux, and Nesbitt et al. measure slightly negative activation energy. It is very likely that the Arrhenius expression is curved. We recommend an E/R value of zero, with an uncertainty of 100 K. Veyret and Lesclaux preferred a T^n form (k = 5.5 × 10^{-11} $T^{-(0.4\pm0.3)}$ cm^3 $molecule^{-1}$ s^{-1}). Hsu et al.[612] suggest that this reaction proceeds via addition at low temperature and abstraction at higher temperatures. (Table: 02-25, Note: 02-25) Back to Table

D45. CH_2OH + O_2. The rate coefficient was first measured directly by Radford [1083] by detecting the HO_2 product in a laser magnetic resonance spectrometer. The wall loss of CH_2OH could have introduced a large error in this measurement. Radford also showed that the previous measurement of Avramenko and Kolesnikova [58] was in error. Wang et al. [1422] measured a value of 1.4 × 10^{-12} cm^3 $molecule^{-1}$ s^{-1} by detecting the HO_2 product. Recently, Dobe et al. [397], Grotheer et al. [529],

Payne et al. [1042], Grotheer et al. [530] and Nesbitt et al. [962] have measured k(298 K) to be close to 1.0×10^{-11} cm^3 $molecule^{-1}$ s^{-1} under conditions where wall losses are small. This reaction appears to exhibit a very complex temperature dependence. Based on the recent data of Grotheer et al. [530], and Nesbitt et al. [962], k appears to increase from 200 K to approximately 250 K in an Arrhenius fashion, levels off at approximately 300 K, decreases from 300 to 500 K, and finally increases as temperature is increased. This complex temperature dependence is believed to be due to the formation of a $CH_2(OH)\bullet O_2$ adduct which can isomerize to $CH_2O\bullet HO_2$ or decompose to reactants. The $CH_2O\bullet HO_2$ isomer can also decompose to CH_2O and HO_2 or reform the original adduct. At temperatures less than 250 K, the data of Nesbitt et al. suggests an E/R value of ~1700 K. For atmospheric purposes, the value E/R = 0 is appropriate. (Table: 90-1, Note: 90-1) Back to Table

D46. $CH_3O + O_2$. The recommended value for k(298 K) is the average of those reported by Lorenz et al. [843] and Wantuck et al. [1425]. The recommended E/R was obtained using the results of Gutman et al. [531] (413 to 608 K), Lorenz et al. [843] (298 to 450 K), and Wantuck et al. [1425] (298 to 498 K). These investigators have measured k directly under pseudo–first order conditions by following CH_3O via laser induced fluorescence. Wantuck et al. measured k up to 973 K and found the Arrhenius plot to be curved; only their lower temperature data are used in the fit to obtain E/R. The A factor has been adjusted to reproduce the recommended k(298 K). The previous high temperature measurements (Barker et al. [71] and Batt and Robinson [96]) are in reasonable agreement with the derived expression. This value is consistent with the 298 K results of Cox et al. [324], obtained from an end product analysis study, and with the upper limit measured by Sanders et al. [1142]. The A-factor appears low for a hydrogen atom transfer reaction. The reaction may be more complicated than a simple abstraction. At 298 K, the products of this reaction are HO_2 and CH_2O, as shown by Niki et al. [989]. (Table 87-41, Note: 87-41) Back to Table

D47. $CH_3O + NO$. The reaction of CH_3O with NO proceeds mainly via addition to form CH_3ONO (Batt et al. [95], Wiebe and Heicklen [1454], Frost and Smith [477], and Ohmori et al. [1008]). However, a fraction of the energized CH_3ONO adducts decompose to $CH_2O + HNO$, and appear to be a bimolecular channel. This reaction has been investigated recently by direct detection of CH_3O via laser-induced fluorescence (Zellner [1512]; Frost and Smith [477]; Ohmori et al. [1008]). The previous end-product studies (Batt et al. [95], Wiebe and Heicklen [1454]) are generally consistent with this conclusion. Since the fraction of the CH_3ONO adduct that falls apart to $CH_2O + HNO$ decreases with increases in pressure and decreases in temperature, it is not possible to derive a "bimolecular" rate coefficient. A value of $k < 8\times10^{-12}$ cm^3 $molecule^{-1}$ s^{-1} can be deduced from the work of Frost and Smith [477] and Ohmori et al.[1008] for lower atmospheric conditions. (Table: 97-4, Note: 97-4) Back to Table

D48. $CH_3O + NO_2$. The reaction of CH_3O with NO_2 proceeds mainly via the formation of CH_3ONO_2. However, a fraction of the energized adducts fall apart to yield $CH_2O + HNO_2$. The bimolecular rate coefficient reported here is for the fraction of the reaction that yields CH_2O and HNO_2. It is not meant to represent a bimolecular metathesis reaction. The recommended value was derived from the study of McCaulley et al. [890] and is discussed in the section on association reactions. (Table: 97-4, Note: 97-4) Back to Table

D49. $CH_3O_2 + O_3$. This recommendation is from Tyndall et al. [1346]. Their recommendation is based mostly on the recent study by Tyndall et al. [1357]. The temperature dependence is based on the assumption that the only possible reaction which can occur is the O atom transfer from the CH_3O_2 radical and that the activation energy of ~2 kcal mol^{-1} for this O-atom transfer is similar to that in the $HO_2 + O_3$ reaction. (Table: 02-25, Note: 02-25) Back to Table

D50. $CH_3O_2 + CH_3O_2$. This recommendation is from Tyndall et al. [1346]. There are two confirmed sets of products for this reaction.

$$CH_3O_2 + CH_3O_2 \xrightarrow{k_a} CH_3O + CH_3O + O_2 \text{ (a)}$$

$$CH_3O_2 + CH_3O_2 \xrightarrow{k_b} CH_3OH + HCHO + O_2 \text{ (b)}$$

The relative product yield, k_a/k_b, was evaluated by Tyndall et al. to be $(26.2 \pm 6.6) \times \exp((-1130 \pm 240)/T)$. They concluded that there was no evidence for the formation of the CH_3OOCH_3. The

kinetics of this reaction has been studied by using UV absorption following pulsed photolytic production of the radicals. Tyndall et al. used the values of k/σ measured by a large number of groups along with the σ values from their evaluation to calculate k. (σ is the absorption cross section of the radical at the wavelength at which it was monitored.) They only used the kinetics data obtained at wavelengths larger than 240 nm, since the absorption by HO_2 radicals that are unavoidably produced in these measurements can significantly contribute to the measure UV profiles at shorter wavelengths. They noted that the values of k/σ measured by various groups were much more accurate than the values of σ measured by the same groups. The value of k obtained by this method was then corrected using the above branching ratio for the production of CH_3O that leads to the unavoidable occurrence of the $CH_3O_2 + HO_2$ side reaction; this side reaction consumes another CH_3O_2 radical. (Table: 02-25, Note: 02-25) Back to Table

D51. $CH_3O_2 + NO$. This recommendation is from Tyndall et al. [1346]. They evaluated the available information to deduce that the main set of products under atmospheric conditions is $CH_3O + NO_2$. They noted, however, that a very small yield, <0.5%, of CH_3ONO_2 is also possible. The rate coefficient for the reaction at 298 K and its temperature dependence is based on numerous direct studies of this reaction that have been reported. (Table: 02-25, Note: 02-25) Back to Table

D52. $CH_3O_2 + CH_3C(O)O_2$. This recommendation is from Tyndall et al. [1346]. This reaction has two sets of products:

$$CH_3C(O)O_2 + CH_3O_2 \xrightarrow{k_a} CH_3 + CO_2 + CH_3O + O_2 \text{ (a)}$$

$$CH_3C(O)O_2 + CH_3O_2 \xrightarrow{k_b} CH_3C(O)OH + HCHO + O_2 \text{ (b)}$$

Tyndall et al. reanalyzed the previously available data on the branching ratios for this reaction and concluded that the branching ratio for channel (a) was $k_a/k = 0.9\pm0.1$ and $k_b/k = 0.1\pm0.1$ at 298 K. They also concluded that branching ratios could not be derived for other temperatures from the existing data and therefore did not make a recommendation for the temperature dependence. The recommendation from Tyndall et al. is based on the work of Roehl et al. [1123] and Villenave et al. [1377]. Their recommended temperature dependence for the overall rate coefficient is based on analogy with other RO_2 reactions. (Table: 02-25, Note: 02-25) Back to Table

D53. $CH_3O_2 + CH_3C(O)CH_2O_2$. This recommendation is from Tyndall et al. [1346]. This reaction has three possible sets of products:

$$CH_3C(O)CH_2O_2 + CH_3O_2 \xrightarrow{k_a} CH_3C(O) + HCHO + CH_3O + O_2 \text{ (a)}$$

$$CH_3C(O)CH_2O_2 + CH_3O_2 \xrightarrow{k_b} CH_3C(O)CH_2OH + HCHO + O_2 \text{ (b)}$$

$$CH_3C(O)CH_2O_2 + CH_3O_2 \xrightarrow{k_c} CH_3C(O)CHO + CH_3OH + O_2 \text{ (c)}$$

The branching ratios for these channels, $k_a/k = 0.3\pm0.1$, $k_b/k = 0.2\pm0.1$, and $k_c/k = 0.5\pm0.1$, are based on the work of Bridier et al. [177] and Jenkin et al. [661]. The overall rate coefficient for this reaction has been studied only at 298 K by Bridier et al. and the recommendation is based on this value. The recommended values of E/R and g are based on analogy with other RO_2 reactions. (Table: 02-25, Note: 02-25) Back to Table

D54. $C_2H_5 + O_2$. This is a complex reaction that involves the formation of an $C_2H_5O_2$ adduct, which can either be stabilized by collisions or fall apart to HO_2 and C_2H_4 (Wagner et al. [1383], Bozzelli and Dean [170], and Kaiser et al. [687]). The fraction of the energized adducts that fall apart to give HO_2 and C_2H_4 will decrease with increasing pressure and decreasing temperature, i.e., as the $C_2H_5O_2$ formation increases. The C_2H_4-formation channel cannot be separated from the addition reaction. We recommend a conservative upper limit as a guide to the extent of this reaction. This upper limit is applicable only for lower atmospheric pressure and temperature conditions. (Table: 94-26, Note: 94-26) Back to Table

D55. $C_2H_5O + O_2$. The recommendation is based on the pulsed laser photolysis studies of Gutman et al. [531] and Hartmann et al. [554]. In both these studies, removal of C_2H_5O in an excess of O_2 was

directly monitored via laser induced fluorescence. Gutman et al. measured k at only two temperatures, while Hartmann et al. measured k at 5 temperatures between 295 and 411 K. The E/R is from Hartmann et al. The 298 K value deduced from an indirect study by Zabarnick and Heicklen [1502] is in reasonable agreement with the recommended value. (Table: 92-20, Note: 92-20) Back to Table

D56. $C_2H_5O_2 + C_2H_5O_2$. k(298 K) has been studied by Adachi et al. [7], Anastasi et al. [25], Munk et al. [938], Cattell et al. [237], Anastasi et al. [24], Wallington et al. [1399], Bauer et al. [98], and Fenter et al. [451]. All the above determinations used only UV absorption to monitor $C_2H_5O_2$ and hence measured k/σ, where σ is the absorption cross section of $C_2H_5O_2$ at the monitoring wavelength. These investigators also measured the σ that was used in evaluating the rate coefficient. There are large discrepancies in the measured values of σ. For this evaluation, we have used the cross sections recommended here and recalculated the values of k from each investigation. The recommended k is based on the results of Cattell et al., Wallington et al., Bauer et al., and Fenter et al. In all these experiments the observed rate coefficient is higher than the true rate coefficient because of secondary reactions involving HO_2. HO_2 is formed by the reaction of CH_3CH_2O with O_2 and it reacts with $C_2H_5O_2$ to enhance the observed rate coefficient (see Wallington et al. [1401] or Lightfoot et al. [821] for further discussion). Based on product branching ratios discussed below, which determine the magnitude of the necessary correction, the recommended rate coefficient is 0.6 times the average observed rate coefficient. The recommended value of E/R was obtained from the results of Anastasi et al., Wallington et al., Cattell et al., Bauer et al., and Fenter et al. The observed products (Niki et al. [990]), suggest that at 298 K the channel to yield 2 $C_2H_5O + O_2$ accounts for about 60% of the reaction; the channel to yield $CH_3CHO + C_2H_5OH + O_2$ accounts for about 40% of the reaction; and the channel to yield $C_2H_5O_2C_2H_5 + O_2$ accounts for less than 5% of the reaction. These branching ratios were used above to obtain the true rate coefficient from the observed rate coefficient. (Table: 94-26, Note: 94-26) Back to Table

D57. $C_2H_5O_2 + NO$. The recommended k(298 K) is obtained from the results of Plumb et al. [1067], Sehested et al. [1174], Daele et al. [341], Eberhard and Howard [427], and Maricq and Szente [871]. The value reported by Adachi and Basco [6], which is a factor of three lower than the recommended value, was not used. The rate coefficient for the $CH_3O_2 + NO$ reaction measured by Basco and co-workers (Adachi et al. [7]), using the same apparatus, is also much lower than the value recommended here. The recommended temperature dependence is derived from Eberhardt and Howard, and Maricq and Szente, which are in good agreement. (Table: 97-4, Note: 97-4) Back to Table

D58. $CH_3C(O)O_2 + CH_3C(O)O_2$. This reaction has been studied by Addison et al. [8], Basco and Parmar [94], Moortgat et al. [932], Maricq and Szente [871], and Roehl et al. [1123], using UV absorption techniques. The recommended value is obtained from the data of Moortgat et al., Maricq and Szente, and Roehl et al. As pointed out by Moortgat et al., the six times lower value of k obtained by Addison et al. is likely due to the use of incorrect UV absorption cross sections for the peroxy radical. The k obtained by Basco and Parmar is ~2 times lower than the recommended value. This discrepancy is possibly due to neglecting the UV absorption of CH_3O_2 and other stable products in their data analysis (Moortgat et al., Maricq and Szente). The recommended temperature dependence was calculated from the data of Moortgat et al. and Maricq and Szente. Addison et al. reported the formation of O_3, which was attributed to the reaction channel which produces $CH_3C(O)OCH_3C(O) + O_3$. Moortgat et al. place an upper limit of 2% for this channel. The main products of this reaction appear to be $CH_3C(O)O + O_2$. The $CH_3C(O)O$ radicals rapidly decompose to give CH_3 and CO_2. (Table: 97-4, Note: 97-4) Back to Table

D59. $CH_3C(O)O_2 + NO$. This recommendation is from Tyndall et al. [1346]. These authors have argued that the only set of products of importance in the atmosphere is the production of $CH_3 + CO_2 + NO_2$. This is because the alkoxy radical produced upon O abstraction from the peroxy radical by NO will be unstable towards decomposition to give CH_3 and CO_2. The rate coefficient for the reaction was deduced primarily from direct studies, but was found to be consistent with the relative rate studies. In the relative rate studies, this rate coefficient was measured relative to the rate coefficient for the reaction of $CH_3C(O)O_2$ with NO_2. The temperature dependence of this rate coefficient was derived

from a set of direct measurement and kept consistent with the observed temperature dependence of the rate coefficient for the $CH_3C(O)O_2 + NO_2$ reaction. (Table: 02-25, Note: 02-25) Back to Table

D60. $CH_3C(O)CH_2O_2 + NO$. This recommendation is from Tyndall et al. [1346]. They deduced, based on the results of Sehested et al. [1171], Jenkin et al. [661], and Orlando et al. [1023], that the products of this reaction are $CH_3C(O)CH_2O + NO_2$. The $CH_3C(O)CH_2O$ radical decomposes rapidly to give $CH_3C(O) + CH_2O$. The only kinetics study of this reaction by Sehested et al. forms the basis for the rate coefficient at 298 K. This value is uncertain because of the corrections that had to be made in the study of Sehested et al. to account for the production of NO_2, the monitored species, via the reaction of peroxy radicals (such as $CH_3C(O)O_2$ and CH_3O_2) with NO. The temperature dependence of the reaction is derived based on analogy with other peroxy radical reactions. (Table: 02-25, Note: 02-25) Back to Table

E1. O + FO. The recommended value is based on results of the room temperature study of Bedzhanyan et al. [123]. The temperature dependence of the rate constant is expected to be small, as it is for the analogous ClO reaction. (Table: 94-26, Note: 94-26) Back to Table

E2. $O + FO_2$. No experimental data. The rate constant for such a radical-atom process is expected to approach the gas collision frequency, and is not expected to exhibit a strong temperature dependence. (Table: 82-57, Note: 82-57) Back to Table

E3. $OH + CH_3F$ (HFC-41). The recommended values for k(298 K) and E/R are averages of these parameters derived from fits to the data of Schmoltner et al. [1159], Nip et al [998], Hsu and DeMore [615], and DeMore [376] (with the relative rate constants from the last two studies recalculated based on the current recommendations for the rate constants for the $OH + CH_3CHF_2$ and $OH + CH_3Cl$ reference reactions respectively.) The A factor was then calculated. The renormalization procedure for relative rate measurements referenced to the $OH + CH_3CHF_2$ reaction is discussed in the note for that reaction. The results of Howard and Evenson [606], Jeong and Kaufman [669], and Wallington and Hurley [1405] appear to be systematically lower than those of the other studies over the temperature region of interest and were not used to derive the recommended parameters. (Table: 02-25, Note: 02-25) Back to Table

E4. $OH + CH_2F_2$ (HFC-32). The recommended value of k(298 K) is an average from the studies of Nip et al. [998], Jeong and Kaufman [669], Talukdar et al. [1281], Hsu and DeMore [615] (recalculated based on the current recommendation for the rate constant for the $OH + CH_3CHF_2$ reference reaction, as described in the note for that reaction), and Szilagyi et al. [1268]. The recommended value for E/R is derived from an Arrhenius fit to the data from these same five studies below 400 K. The results of Howard and Evenson [606], Clyne and Holt [282], and Bera and Hanrahan [130] were not used in deriving the recommended parameters. (Table: 02-25, Note: 02-25) Back to Table

E5. $OH + CHF_3$ (HFC-23). The recommended values for k(298 K) and E/R are averages of the values Schmoltner et al. [1159], and Hsu and DeMore [615] (recalculated based on the current recommendation for the rate constant for the $OH + CHF_2CF_3$ reference reaction). The results of Jeong and Kaufman [669], and Medhurst et al. [896], being predominantly above room temperature, were not used in deriving the recommended parameters. The results from Clyne and Holt [282] and Bera and Hanrahan [130] were also not used due to their inconsistency with the other studies. The room temperature values of Howard and Evenson [606] and Nip et al. [998] are encompassed within the 2σ confidence limits. (Table: 02-25, Note: 02-25) Back to Table

E6. $OH + CH_3CH_2F$ (HFC-161). The recommended value for k(298 K) is an average of the values from Nip et al. [998], Schmoltner et al. [1159], and Kozlov et al. [738]. The value of E/R is based on a fit to the data from these three studies from room temperature and below. The relative rate study by Hsu and DeMore [615] reports a temperature dependence that is markedly different from those of Schmoltner et al. [1159] and Kozlov et al. [738], which are in excellent agreement. This difference is due to significantly lower rate constant values being obtained in the Hsu and DeMore study in the region near room temperature. Given the most recent results for the reaction of $OH + CH_3CHF_2$ (HFC-152a), it seems likely that the HFC-161 reaction also has two channels with different activation energies and that the temperature dependence below room temperature should be less than that recommended for HFC-152a, consistent with the present recommendation. Curvature in the Arrhenius plot is evident from the study by Kozlov et al. [738], which was conducted over an

extended temperature range above and below room temperature. Singleton et al. [1202] determined that 85 ± 3% of the abstraction by OH is from the fluorine substituted methyl group at room temperature. Hence this curvature is quite possibly due to the increasing importance of hydrogen abstraction from the unsubstituted methyl group with increasing temperature. Due to such occurrence, the recommended parameters should not be used for calculating rate constants above room temperature. (Table: 02-25, Note: 02-25) Back to Table

E7. OH + CH_3CHF_2 (HFC-152a). The recommended value for k(298 K) is an average of the values from Howard and Evenson [605], Handwerk and Zellner [549], Nip et al. [998], Gierczak et al. [495] (two different absolute determinations), Hsu and DeMore [615] (two relative rate determinations which have been recalculated based on the current recommendations for the rate constants of the OH + CH_4 and OH + CH_3CCl_3 reference reactions), and Kozlov et al [738]. There are systematic differences in the temperature dependencies determined in the absolute studies (particularly below room temperature) and relative studies (conducted at room temperature and above). Curvature in the Arrhenius plot (as suggested by the data of Gierczak et al. [495]) has been more clearly demonstrated by the study of Kozlov et al. [738] and seems to explain the earlier cited differences between the relative and absolute rate data. This curvature is likely due to the presence of two hydrogen-abstraction reaction channels. Hence, care must be taken in deriving a recommended rate expression suitable for atmospheric modeling (in the temperature region below room temperature).

In spite of the noticeable Arrhenius curvature over the temperature range from 480 K to 210 K, the data below 300 K can be well represented by a two-parameter Arrhenius expression. Thus, the recommended value for E/R is derived from a fit to the data (T ≤ 300 K) of Gierczak et al. and Kozlov et al. The results from Clyne and Holt [282], Brown et al. [179], Nielsen [975], and Liu et al. [839] (superceded by the study of Kozlov et al.) were not used in deriving the recommended parameters.

Clearly, in light of the observed Arrhenius curvature, the above procedure for deriving our recommendation for E/R below 300 K does not yield a parameter suitable for use in recalculating rate constants from relative rate studies in which the OH + CH_3CHF_2 reaction was the reference and which were conducted at temperatures above 300 K. Use of the below-room-temperature value for E/R for such purposes results in rate constant values that are systematically different from those determined relative to other reactions or determined by absolute techniques. For such renormalization purposes, one should use an Arrhenius expression derived from data over the appropriate temperature range. A fit to the absolute rate data of Gierczak et al. [495] and Kozlov et al. [738] between room temperature and 400 K yields the Arrhenius expression

$$k_{abs} = 2.36 \times 10^{-12} \exp\{-1255/T\}$$

This is in good agreement with the expression derived from the relative rate data of Hsu and DeMore [615]

$$k_{rel} = 2.1 \times 10^{-12} \exp\{-1265/T\}$$

The small difference in the pre-exponential factors results from a slight systematic difference in the actual rate constants determined in these three studies that is probably within the combined uncertainties of the determinations. Thus, the following expression derived from the above room temperature E/R value and the recommended k(298 K) has been used for renormalization purposes in this evaluation.

$$k_{T\geq 300K} = 2.33 \times 10^{-12} \exp\{-1260/T\}$$

However, this expression should not be used below 298 K, as erroneous values for OH + CH_3CHF_2 reaction rate constants would be obtained. (Table: 02-25, Note: 02-25) Back to Table

E8. OH + CH_2FCH_2F (HFC-152). The recommended value for k(298 K) is an average of the values from Martin and Paraskevopoulos [880], Kozlov et al. [738], and DeMore et al. [384] (three relative rate studies using HFC-152a, cyclopropane, and ethane as reference reactants). The value for E/R is from a fit to the data of Kozlov et al. [738] at room temperature and below. The A factor was then calculated to yield the recommended value for k(298 K). The data above room temperature from Kozlov et al. [738] are in excellent agreement with the three relative rate data sets of DeMore et al.

[384]. Together, they show a pronounced curvature in the Arrhenius plot, which may indicate the existence of different conformers for HFC-152, each with differing temperature populations and reactivities. (Table: 02-25, Note: 02-25) Back to Table

E9. OH + CH_3CF_3 (HFC-143a). The recommended value for k(298 K) is an average of the values from Martin and Paraskevopoulos [880], Orkin et al. [1013], Talukdar et al. [1281] (two different determinations), and Hsu and DeMore [615] (two relative rate determinations which have been recalculated based on the current recommendations for the rate constants of the OH + CH_4 and OH + CHF_2CF_3 reference reactions). The value for E/R is an average of the E/R values from the last three of these studies which are in excellent agreement (Martin and Paraskevopoulos having made measurements only at room temperature). The data of Clyne and Holt [282] were not used due to their inconsistency with the other studies. (Table: 02-25, Note: 02-25) Back to Table

E10. OH + CH_2FCHF_2 (HFC-143). The recommended temperature dependence is based on results of the relative rate study of Barry et al. [90] normalized to the value of the rate constant for the reference reaction (OH + CH_3CCl_3) recommended in this evaluation. The value for k(298 K) is an average of the room temperature values of Martin and Paraskevopoulos [880] and Barry et al. The significantly higher values reported by Clyne and Holt [282] were not used in the derivation of the recommended parameters. (Table: 02-25, Note: 02-25) Back to Table

E11. OH + CH_2FCF_3 (HFC-134a). The recommended value for k(298 K) is an average of the values from Martin and Paraskevopoulos [880], Bednarek et al. [118], Orkin and Khamaganov [1015], Leu and Lee [801], Gierczak et al. [495] (two different determinations), Liu et al. [839], and DeMore [374] (three determinations which have been recalculated based on the current recommendations for the rate constants for the reference reactions OH + CH_4, OH + CH_3CCl_3, and OH + CHF_2CF_3). The value for E/R is an average of the E/R values from the last five of these investigations (the studies by Martin and Paraskevopoulos and by Bednarek et al. being conducted only at room temperature). The 270 K result of Zhang et al. [1521] is in excellent agreement with the recommendation. The data of Jeong et al. [667], Brown et al. [179], and Clyne and Holt [282] were not used in deriving the recommended parameters. (Table: 02-25, Note: 02-25) Back to Table

E12. OH + CHF_2CHF_2 (HFC-134). The preferred rate expression is based on results of the three relative rate measurements by DeMore [374] (which have been recalculated based on the current rate constant recommendations for the OH + CH_3CCl_3, OH + CH_2FCF_3, and OH + CHF_2CF_3 reference reactions). The room temperature value of Clyne and Holt [282] agrees within the 2σ confidence limits. (Table: 02-25, Note: 02-25) Back to Table

E13. OH + CHF_2CF_3 (HFC-125). The recommended rate expression is derived from a combined fit to the temperature dependence data of Talukdar et al. [1281] and DeMore [374] and the room temperature data of Martin and Paraskevopoulos [880]. The data of Brown et al. [179] and Clyne and Holt [282] were not used in deriving the recommended parameters. (Table: 02-25, Note: 02-25) Back to Table

E14. OH + CH_3CHFCH_3 (HFC-281ea). The recommended parameters were derived from a fit to the data of DeMore and Wilson [383] who conducted five independent relative rate determinations. Using infrared detection, these investigators based their determinations on the reference reactions of OH with C_2H_6, C_3H_8, and C_2H_5Cl. Using gas chromatographic detection, they based their determinations on the reference reactions of OH with C_2H_6 and C_3H_8. All of the data were recalculated based on the current recommendations for the reference rate constants. (Table: 02-25, Note: 02-25) Back to Table

E15. OH + $CH_3CH_2CF_3$ (HFC-263fb). Based on room temperature measurement of Nelson et al. [953]. (Table: 97-4, Note: 97-4) Back to Table

E16. OH + $CH_2FCF_2CHF_2$ (HFC-245ca). The absolute rate constant results of Zhang et al. [1524] differ from the relative rate data (Hsu and DeMore [615]) by approximately 30 to 40% over the temperature region of measurement overlap. Both studies, however, derive nearly identical T-dependencies. The recommended rate expression, hence, averages both the k(298 K) and E/R values from these studies (with the results of Hsu and DeMore [615] recalculated using the current recommendation for the rate constant of the OH + CH_4 reference reaction). (Table: 02-25, Note: 02-25) Back to Table

E17. OH + $CHF_2CHFCHF_2$ (HFC-245ea). Based on room temperature measurement of Nelson et al. [953]. (Table: 02-25, Note: 02-25) Back to Table

E18. OH + $CH_2FCHFCF_3$ (HFC-245eb). Based on room temperature measurement of Nelson et al. [953]. (Table: 02-25, Note: 02-25) Back to Table

E19. OH + $CHF_2CH_2CF_3$ (HFC-245fa). The recommended room temperature value is the mean of the values reported by Orkin et al. [1013] and Nelson et al. [953], which are in good agreement. The temperature dependence is from Orkin et al. The A-factor has been calculated to fit the recommended room temperature value. (Table: 02-25, Note: 02-25) Back to Table

E20. OH + $CH_2FCF_2CF_3$ (HFC-236cb). The recommended rate expression is estimated as being the same as that for the reaction of OH with CH_2FCF_3 (HFC-134a), since these reactions are expected to have very similar Arrhenius parameters. This estimate is preferred over the results reported by Garland et al. [483], the only published experimental study. The A-factor reported in that study is much lower than expected and the value reported for E/R (1107 K) is lower than that reported for any similar halocarbon reaction. (Table: 02-25, Note: 02-25) Back to Table

E21. OH + CHF_2CHFCF_3 (HFC-236ea). The recommended value for k(298 K) averages the values reported by Hsu and DeMore [615] by a relative rate method (recalculated based on the current recommendation for the rate constant of the OH + CH_4 reference reaction) and by Nelson et al. [953] by an absolute technique. The temperature dependence is from Hsu and DeMore [615], with the A-factor adjusted to fit the recommended room temperature value. The higher and somewhat more scattered values of Garland et al. [483] and Zhang et al. [1524] were not used in deriving the recommended expression. (Table: 02-25, Note: 02-25) Back to Table

E22. OH + $CF_3CH_2CF_3$ (HFC-236fa). The recommended rate expression is derived from a combined fit to the data from the relative rate study of Hsu and DeMore [615] (recalculated based on the current recommendation for the rate constant for the reference reaction OH + CHF_2CF_3) and the absolute rate study of Gierczak et al. [496]. The higher results of Nelson et al. [953] and of Garland and Nelson [484], which superseded the earlier results of Garland et al. [484], were not used. A relative rate determination at room temperature by Barry et al. [88] yields a rate constant in excellent agreement with the recommended value. However, the extremely small rate constant ratio measured (relative to OH + $CH_3CF_2CH_2CF_3$) resulted in fairly large uncertainties. Hence this determination was not directly used in the evaluation. (Table: 02-25, Note: 02-25) Back to Table

E23. OH + CF_3CHFCF_3 (HFC-227ea). The recommended rate expression is derived from a combined fit to the data (below 400 K) from the absolute studies of Nelson et al. [949], Zellner et al. [1513], and Zhang et al. [1524] and the relative rate studies of Hsu and DeMore [615] (two determinations which have been recalculated based on the current recommendations for the rate constants for the reference reactions OH + CH_4 and OH + CHF_2CF_3). (Table: 02-25, Note: 02-25) Back to Table

E24. OH + $CH_3CF_2CH_2CF_3$ (HFC-365mfc). The recommended value of k(298 K) is an average of the values obtained from the individual rate expressions by Mellouki et al. [911] and Barry et al. [88] (renormalized to the current recommendation for the rate constant for the reference reaction OH + CH_3CCl_3). The value for E/R is an average of the values for this parameter from the same two studies. (Table: 02-25, Note: 02-25) Back to Table

E25. OH + $CF_3CH_2CH_2CF_3$ (HFC-356mff). The recommended value of k(298 K) is an average of the values from Nelson et al.[953] and Zhang et al. [1524]. The temperature dependence is from a fit to the data of Zhang et al. excluding the lowest temperature points (at 260 K), which are somewhat higher than an extrapolation from their other data would indicate. The A-factor has been calculated to fit the recommended room temperature value. (Table: 02-25, Note: 02-25) Back to Table

E26. OH + $CH_2FCH_2CF_2CF_3$ (HFC-356mcf). The recommended parameters are based on a fit to the data of Nelson et al. [953]. (Table: 02-25, Note: 02-25) Back to Table

E27. OH + $CHF_2CF_2CF_2CHF_2$ (HFC-338pcc). The recommended values for both k(298 K) and E/R are averages of these values taken from the individual fits to the data of Schmoltner et al. [1159] and Zhang et al. [1527]. (Table: 02-25, Note: 02-25) Back to Table

E28. OH + $CF_3CH_2CF_2CH_2CF_3$ (HFC-458mfcf). The recommended values for both k(298 K) and E/R are from a fit to the data of Nelson et al. [953]. (Table: 02-25, Note: 02-25) Back to Table

E29. OH + $CF_3CHFCHFCF_2CF_3$. (HFC-43-10mee). The recommended rate expression is derived from a combined fit to the data from Schmoltner et al. [1159] and Zhang et al. [1527]. (Table: 02-25, Note: 02-25) Back to Table

E30. OH + $CF_3CF_2CH_2CH_2CF_2CF_3$ (HFC-55-10mcff). The recommended value for k(298 K) is based on Nelson et al. [953]. As expected, the rate constant is similar to that for $CF_3CH_2CH_2CF_3$. Hence the recommendation for E/R is estimated as being approximately the same as for this reaction, with the A-factor calculated to yield k(298 K). (Table: 02-25, Note: 02-25) Back to Table

E31. OH + CH_2=CHF. The recommended parameters were derived from a fit to the data of Perry et al. [1047]. (Table: 02-25, Note: 02-25) Back to Table

E32. OH + CH_2=CF_2. The recommended value for k(298 K) is from Howard [603]. The value of E/R was estimated as being similar to that for the reactions of OH with CH_2=CHF and with CF_2=CF_2, and the value for A was then calculated. (Table: 02-25, Note: 02-25) Back to Table

E33. OH + CF_2=CF_2. The recommended value for k(298 K) is an average of the values determined in the studies of Acerboni et al. [5] (two relative rate determinations referenced to the rate constants for the reactions of OH with propene and cyclohexane) and the absolute rate studies of Orkin et al. [1014], and Orkin et al. [1020]. The value for E/R is from a fit to the data of Orkin et al. [1020], with the value for A calculated to yield the recommended value for k(298 K). (Table: 02-25, Note: 02-25) Back to Table

E34. OH + CF_3OH. There are no measurements of the rate coefficient of this reaction. The recommendation is based on the recommended limit for the reverse reaction rate coefficient and an estimated equilibrium constant. The thermochemistry of CF_3O and CF_3OH are taken from *ab initio* calculations (Montgomery et al. [930] and Schneider and Wallington [1160]) and laboratory measurements (Huey et al. [619]) to estimate $\Delta G°_{298}$(OH + $CF_3OH \rightarrow CF_3O + H_2O$) to be about (2±4) kcal mol^{-1}. In considering the large uncertainty in the free energy change, the estimated rate coefficient limit is based on the assumption that the reaction is approximately thermoneutral. (Table: 97-4, Note: 97-4) Back to Table

E35. OH + $CH_2(OH)CF_3$. The recommended value for k(298 K) is an average of the values reported by Wallington et al. [1400], Inoue et al. [642], and Tokuhashi et al. [1311] (two independent studies). The recommended value for E/R is derived from the data of Tokuhashi et al. [1311]. The A factor was calculated to agree with the recommended value for k(298 K). (Table: 02-25, Note: 02-25) Back to Table

E36. OH + $CH_2(OH)CF_2CF_3$. The recommended parameters were derived from a combined fit to the data of Tokuhashi et al. [1311] (two independent absolute measurement studies) and the relative rate study of Chen et al. [255] (recalculated based on the current recommendation for the rate constant for the OH + CH_2Cl_2 reference reaction). (Table: 02-25, Note: 02-25) Back to Table

E37. OH + $CF_3CH(OH)CF_3$. The recommended parameters were derived from a fit to the data (below 400 K) of Tokuhashi et al. [1311] (two independent absolute measurement studies). (Table: 02-25, Note: 02-25) Back to Table

E38. OH + CH_3OCHF_2 (HFOC-152a). The recommended rate expression is derived from a fit to the data of Orkin et al. [1017] below 400 K. (Table: 02-25, Note: 02-25) Back to Table

E39. OH + CH_3OCF_3 (HFOC-143a). The preferred rate expression is derived from a combined fit to the data of Orkin et al. [1017] and Hsu and DeMore [616] (two relative rate determinations which have been recalculated based on the current recommendations for the rate constants of the OH + CH_3CHF_2 and OH + CH_2F_2 reference reactions). The renormalization procedure for relative rate measurements referenced to the OH + CH_3CHF_2 reaction is discussed in the note for that reaction. The room temperature result of Zhang et al. [1526] was not used in the derivation since it is significantly higher than the values of the other studies and may be influenced by the presence of reactive impurities. (Table: 97-4, Note: 02-25) Back to Table

E40. OH + CHF_2OCHF_2 (HFOC-134). The recommended values of k(298 K) and E/R were derived from a combined fit to the data of Hsu and DeMore [616] (a relative rate study whose results have been recalculated using the current recommendation for the rate constant of the OH + CH_3CCl_3 reference reaction), Orkin et al. [1021], and Wilson et al. [1460]. The more scattered measurements of Garland et al. [483] were not used in derivation of the preferred value. (Table: 02-25, Note: 02-25) Back to Table

E41. OH + CHF_2OCF_3 (HFOC-125). The recommended rate expression is based on results of the relative rate study of Hsu and DeMore [616] (recalculated using the rate constant for the CHF_3 reference reaction given in this evaluation). Additional measurements by Hsu and DeMore [616] relative to CHF_2CF_3 and CH_4 are encompassed well within the 2σ limits, but were not used for assigning the recommended rate expression due to the large differences in reactivity between these two species and the target molecule. The room temperature result of Zhang et al. [1526] lies significantly higher than the recommended value, possibly due to the presence of reactive impurities in the sample. (Table: 02-25, Note: 02-25) Back to Table

E42. OH + $CHF_2OCH_2CF_3$ (HFOC-245fa). The recommended rate expression is derived from a fit to the data of Orkin et al. [1017] below 400 K. (Table: 02-25, Note: 02-25) Back to Table

E43. OH + $CH_3OCF_2CHF_2$. The recommended parameters were derived from a fit to the data (below 400 K) of Tokuhashi et al. [1313] (two independent absolute measurement studies). A room temperature measurement by Heathfield et al. [561] is nearly an order of magnitude higher than recommended and may be affected by reactive impurities. (Table: 02-25, Note: 02-25) Back to Table

E44. OH + $CH_3OCF_2CF_3$. The recommended parameters were derived from a fit to the data (below 400 K) of Tokuhashi et al. [1312] (two independent absolute measurement studies). The expression, as expected, is similar to those for the OH + CH_3OCF_3 and OH + $CH_3OCF_2CF_2CF_3$ reactions. (Table: 02-25, Note: 02-25) Back to Table

E45. OH + $CH_3OCF_2CF_2CF_3$. The recommended value for k(298 K) is an average of the values reported by Tokuhashi et al. [1312] (two independent absolute measurement studies) and Nonomiya et al. [996] (two relative rate determinations which have been recalculated based on the current recommendations for the rate constants of the OH + CH_4 and OH + CH_3Cl reference reactions). The value for E/R was determined from a fit to the data (below 400 K) of Tokuhashi et al. and the A factor calculated to agree with the value for k(298 K). The expression, as expected, is similar to those for the OH + CH_3OCF_3 and OH + $CH_3OCF_2CF_3$ reactions. (Table: 02-25, Note: 02-25) Back to Table

E46. OH + $CH_3OCF(CF_3)_2$. The recommended parameters were derived from a fit to the data (below 400 K) of Tokuhashi et al. [1312] (two independent absolute measurement studies). The rate constants from this study are surprisingly somewhat larger than those for the similar OH + CH_3OCF_3 and OH + $CH_3OCF_2CF_3$ reactions. (Table: 02-25, Note: 02-25) Back to Table

E47. OH + $CHF_2OCH_2CF_2CHF_2$. The recommended parameters were derived from a fit to the data (below 400 K) of Tokuhashi et al. [1313] (two independent absolute measurement studies). (Table: 02-25, Note: 02-25) Back to Table

E48. OH + $CHF_2OCH_2CF_2CF_3$. The recommended parameters were derived from a fit to the data (below 400 K) of Tokuhashi et al. [1313] (two independent absolute measurement studies). (Table: 02-25, Note: 02-25) Back to Table

E49. F + O_3. The recommended value is based on results of the room temperature study of Bedzhanyan et al. [120] and the temperature-dependent study of Wagner et al. [1387]. The value appears to be quite reasonable in view of the well-known reactivity of atomic chlorine with O_3. (Table: 94-26, Note: 94-26) Back to Table

E50. F + H_2. The value of k at 298 K seems to be well established with the results reported by Zhitneva and Pshezhetskii [1529], Heidner et al. [562, 563], Wurzberg and Houston [1489], Dodonov et al. [402], Clyne et al. [288], Bozzelli [169], Igoshin et al. [637], Clyne and Hodgson [281] and Stevens et al. [1241] being in excellent agreement (range of k being 2.3–3.0 × 10^{-11} cm^3 $molecule^{-1}$ s^{-1}). The preferred value at 298 K is taken to be the mean of the values reported in these references. Values of

E/R range from 433–595 K (Heidner et al.; Wurzberg and Houston; Igoshin et al.; and Stevens et al.). The preferred value of E/R is derived from a fit to the data in these studies. The A-factor was chosen to fit the recommended room temperature value. (Table: 90-1, Note: 90-1) Back to Table

E51. F + H_2O. The recommended temperature-independent value is based on results reported in the study by Stevens et al. [1241] over the temperature range 240–373 K using a discharge flow system with chemical conversion of fluorine atoms to deuterium atoms and detection of the latter by resonanace fluorescence. This value is in excellent agreement with the room temperature results of Frost et al. [478] and Walther and Wagner [1414]. The latter authors in a limited temperature-dependent study reported an E/R value of 400 K. Although these data have not been included in the derivation of the preferred value, with the exception of the one low temperature data point, they are encompassed within the indicated uncertainty limits. (Table: 90-1, Note: 90-1) Back to Table

E52. F + HNO_3. The recommendation is based on results of the temperature-dependent study of Wine et al. [1475] and the room temperature results of Mellouki et al. [903], Rahman et al. [1085] and Becker et al. [102]. The values at room temperature are in good agreement. The study of Wine et al. [1475] was over the temperature range 260–373 K. Below 320 K the data were fitted with the Arrhenius expression recommended here, whereas at higher temperatures a temperature-independent value was found, suggesting the occurrence of different mechanisms in the two temperature regimes. (Table: 90-1, Note: 90-1) Back to Table

E53. F + CH_4. The recommended room temperature value is the mean of the results of Wagner et al. [1385], Clyne et al. [288], Kompa and Wanner [736], Foon and Reid [466], Fasano and Nogar [448], and Persky et al. [1052]. The temperature dependence is that reported by Persky et al. in a competitive study using the reaction F + D_2 as the reference reaction. These results are preferred over the temperature dependences reported in the earlier studies of Wagner et al. and Foon and Reid. (Table: 97-4, Note: 97-4) Back to Table

E54. FO + O_3. Recommended upper limit is based on the results of Li et al. [819] in a study using a discharge flow-mass spectrometric technique. FO was produced in the reaction of F atoms with excess O_3. No appreciable decay of FO, and only a small increase in FO_2, was detected, allowing an upper limit to the rate constant of 10^{-14} cm^3 $molecule^{-1}s^{-1}$ to be derived. A two orders of magnitude higher upper limit was derived by Sehested et al. [1175]. A lower value of the upper limit was derived by Colussi and Grela [307] from a re-analysis of data on the quantum yields for ozone destruction in F_2/O_3 mixtures reported by Starrico et al. [1231]. The results of the recent, more direct, study of Li et al. [819] are preferred over the earlier results of Starrico et al. There are two possible pathways which are exothermic, resulting in the production of F + $2O_2$ or FO_2 + O_2. (Table: 97-4, Note: 97-4) Back to Table

E55. FO + NO. The recommended value is based on results of the temperature-dependent study of Bedzhanyan et al. [121] and the value reported by Ray and Watson [1108] for k at 298 K using the discharge flow-mass spectrometric technique. (Table: 94-26, Note: 94-26) Back to Table

E56. FO + FO. The recommended value is based on the results of Bedzhanyan et al. [122] and Clyne and Watson [299]. Wagner et al. [1387], in a less direct study, report a higher value. The results of Bedzhanyan et al. indicate the predominant reaction channel is that to produce 2F + O_2. (Table: 94-26, Note: 94-26) Back to Table

E57. FO_2 + O_3. Recommended value is based on results of Sehested et al. [1175]. A higher upper limit has been reported by Li et al. [819]. (Table: 94-26, Note: 97-4) Back to Table

E58. FO_2 + NO. Recommended values are based on results of Li et al. [819], the only temperature-dependent study. The room temperature value is nearly a factor of 2 less than the previous recommendation, which was based on the results of Sehested et al. [1175]. (Table: 97-4, Note: 97-4) Back to Table

E59. FO_2 + NO_2. Recommended values are based on results of Li et al. [819], the only temperature-dependent study. The room temperature value is a factor of 2.5 less than the previous recommendation, which was based on the results of Sehested et al. [1175]. This discrepancy might be attributable to a small NO impurity in the NO_2 sample used in the Sehested et al. study. (Table: 97-4, Note: 97-4) Back to Table

E60. FO_2 + CO. Recommended value is based on results of Sehested et al. [1175], the only published study of this reaction. (Table: 94-26, Note: 94-26) Back to Table

E61. FO_2 + CH_4. Recommended value is based on results of Li et al. [819]. This upper limit is a factor of 20 less than the previously recommended upper limit, which was based on the results of Sehested et al. [1175]. (Table: 97-4, Note: 97-4) Back to Table

E62. CF_3O + O_2. The recommendation is based upon the results of Turnipseed et al. [1336] who reported k(373 K) $\leq 4 \times 10^{-17}$. Assuming an E/R of 5000 K, which is equal to the reaction endothermicity, yields the recommended A and k(298 K) limits. By comparison to other reactions involving abstraction by O_2 the A- factor is likely to be much smaller. (Table: 94-26, Note: 94-26) Back to Table

E63. CF_3O + O_3. The recommendation is based on the average of room temperature measurements reported by Turnipseed et al. [1336], Wallington and Ball [1396] , and Bourbon et al. [165]. Turnipseed et al. and Bourbon et al. made direct measurements using LIF detection of CF_3O with pulsed photolysis and flow tube reactors, respectively. Wallington and Ball used a competetive reaction scheme with IR absorption detection and CF_3O + CH_4 as the reference reaction. The recommended A factor is estimated by comparison to other CF_3O reactions, and the E/R is calculated to give the recommended k(298 K). Upper limits reported by Maricq and Szente [869], Nielsen and Sehested [980], and Wallington et al. [1406] are consistent with the k(298 K) recommendation. Measurements reported by Fockenberg et al. [464] and Meller and Moortgat [898] gave rate coefficients about an order of magnitude less than the recommended value. Although the reason for this discrepancy is not known, both studies appear to have the possibility of significant secondary chemistry. The reaction products have not been observed. (Table: 97-4, Note: 97-4) Back to Table

E64. CF_3O + H_2O. The recommendation is based upon the measurement k(381) $\leq 2 \times 10^{-16}$ reported by Turnipseed et al. [1334]. The A factor is estimated and the E/R is calculated to fit k(381). The limits k = (0.2–40) $\times 10^{-17}$ at 296 ± 2 K given by Wallington et al. [1407] are consistent with the recommendation. (Table: 94-26, Note: 94-26) Back to Table

E65. CF_3O + NO. The recommendation is based upon the room temperature rate coefficients reported by Sehested and Nielsen [1173], Turnipseed et al. [1336], and Jensen et al. [664] which are in very good agreement. An earlier low value given by Bevilacqua et al. [132] is superseded by Jensen et al. The temperature-dependence is derived from measurements by Turnipseed (233–360 K) and Jensen et al. (231–393 K). Room temperature results from Bourbon et al. [166] and Bhatnagar and Carr [134] and a temperature dependence study by Dibble et al. [391] are in good agreement with the recommendation. The reaction products have been reported by Chen et al. [252] Bevilacqua et al. [132], Bhatnagar and Carr and Dibble et al. (Table: 94-26, Note: 97-4) Back to Table

E66. CF_3O + NO_2. There are no published measurements of the rate coefficient for this reaction. The reaction products have been reported by Chen et al. [251] who used photolysis of CF_3NO to prepare CF_3O_2 and subsequently CF_3O in 700 torr of air at 297±2 K. They considered two product channels: (a) CF_3ONO_2 obtained via three-body recombination and (b) CF_2O + FNO_2 obtained via fluorine transfer. Products from both channels were observed and found to be thermally stable in their reactor. They report $k_a/(k_a + k_b) \geq 90\%$ and $k_b/(k_a + k_b) \leq 10\%$, thus the formation of CF_3ONO_2 is the dominant channel at 700 torr and 297 K. (Table: 94-26, Note: 94-26) Back to Table

E67. CF_3O + CO. The kinetics of this reaction were studied by Turnipseed et al. [1334], who used pulsed laser photolysis with pulsed laser-induced fluorescence detection and a flow tube reactor with chemical ionization detection to obtain data at temperatures from 233 to 332 K and at pressures from 0.8 to about 300 torr in He and at about 300 torr in SF_6. The reaction was found to be predominantly a three-body recombination, presumably producing CF_3OCO as described in Table 2. The bimolecular reaction has at least two product channels: (a) CF_2O + CFO and (b) CF_3 + CO_2. The recommended bimolecular rate coefficient limit is derived from the low pressure results of Turnipseed et al., where the reaction was in the fall-off region. Their low pressure data indicate that $k_b < 4 \times 10^{-16}$ cm^3 molecule^{-1} s^{-1} at 298 K. The fate of the CF_3OCO adduct is uncertain, and it may lead to the regeneration of CF_3 or CF_3O radicals in the atmosphere. Wallington and Ball [1397]

report a yield of 96±8% CO_2 at one atmosphere and 296±2 K. (Table: 94-26, Note: 97-4) Back to Table

E68. $CF_3O + CH_4$. The absolute rate coefficients reported by Saathoff and Zellner [1131], Barone et al. [86], Jensen et al. [664], Bourbon et al. [167], and Bednarek et al. [119] at room temperature are in excellent agreement. Kelly et al. [697] used a relative method with FTIR detection to determine the ratio $k(CF_3O + CH_4)/k(CF_3O + C_2H_6) = R = 0.01\pm0.001$ at 298±2 K. This does not agree with the ratio of our recommended values, which is 0.017. A relative rate measurement reported by Chen et al. [253] using FTIR methods also gives a low result for the rate coefficient. A relative rate measurement reported by Wallington and Ball [1397], R = 0.0152±0.0023 at 296 K, is in good agreement with the recommended rate coefficients. The temperature dependence is from the data of Barone et al. (247–360 K), Jensen et al. (231–385 K), and Bednarek et al. (235–401 K), who agree very well. Measurements at higher temperatures by Bourbon et al. (296–573 K) gave a higher E/R (1606 K). The k(298 K) is the average of the three absolute studies. The CF_3OH product was observed by Jensen et al. and Bevilacqua et al. [132]. (Table: 97-4, Note: 97-4) Back to Table

E69. $CF_3O + C_2H_6$. The room temperature recommendation is based on results reported by Saathoff and Zellner [1131], Barone et al. [86], and Bourbon et al. [167]. These studies are in excellent agreement. Chen et al. [253] measured the rate coefficient relative to that for the $CF_3O + NO$ reaction in 700 torr of air at 297 K. Their ratio is in good agreement with the values recommended in this evaluation. Kelly et al. [697] used a relative method with FTIR detection to determine the ratio $k(CF_3O + CH_4)/k(CF_3O + C_2H_6) = 0.01\pm0.001$ at 298±2 K. This does not agree with the ratio of our recommended values, which is 0.017. A relative rate measurement reported by Wallington and Ball [1397], R = 0.0152±0.0023 at 296 K is in good agreement with the recommended rate coefficients. The temperature dependence is from the work of Barone et al., who studied the reaction over the temperature range from 233 to 360 K. Measurements by Bourbon et al. (295–573 K) gave a higher E/R (642 K). The products are inferred by analogy to other reactions of CF_3O with organic compounds. (Table: 97-4, Note: 97-4) Back to Table

E70. $CF_3O_2 + O_3$. The recommended upper limit is given by the measurements reported by Ravishankara et al. [1099] who used chemical ionization detection of CF_3O_2 with a flow tube reactor. No measurable reaction was observed in their study. The less direct studies of Nielsen and Sehested [980], Maricq and Szente [869] and Turnipseed et al. [1336] report somewhat larger upper limits to the rate coefficient. An observable reaction was reported in an indirect measurement by Meller and Moortgat [898]. Their result for the $CF_3O + O_3$ reaction is not consistent with the value recommended above. Their study may have interference from unknown reactions. The products are assumed to be $CF_3O + 2O_2$. (Table: 94-26, Note: 94-26) Back to Table

E71. $CF_3O_2 + CO$. The recommended upper limit is reported by Turnipseed et al. [1334] who used chemical ionization mass spectrometric detection of CF_3OO with a flow tube reactor at 296 K. This result is at odds with an earlier study by Czarnowski and Schumacher [338], who deduced a "fast reaction" when they observed the thermal decomposition of CF_3OOOCF_3 to accelerate in the presence of CO at 315–343K. It is possible that the reaction of CF_3O with CO could account for their observations. (Table: 94-26, Note: 94-26) Back to Table

E72. $CF_3O_2 + NO$. The recommendation is an average of the room temperature rate coefficients reported by Plumb and Ryan [1066], Dognon et al. [404], Peeters et al. [1044], Bevilacqua et al. [132], Sehested and Nielsen [1173], Turnipseed et al. [1336], Bourbon et al. [166], and Bhatnagar and Carr [134], all of whom are in excellent agreement. The temperature dependence is derived from the results of Dognon et al. Several studies have confirmed the identity of the products. (Table: 97-4, Note: 97-4) Back to Table

F1. O + ClO. There have been five studies of this rate constant over an extended temperature range using a variety of techniques: Leu [815]; Margitan [866]; Schwab et al. [1165]; Ongstad and Birks [1012]; Nicovich et al. [973] and Goldfarb et al. [513]. The recommended value is based on a least squares fit to the data reported in these studies and in the earlier studies of Zahniser and Kaufman [1509] and Ongstad and Birks [1011]. Values reported in the early studies of Bemand et al. [126] and Clyne and Nip [292] are significantly higher and were not used in deriving the recommended value. Leu and Yung [810] were unable to detect $O_2(^1\Delta)$ or $O_2(^1\Sigma)$ and set upper limits to the

branching ratios for their production of 4.4×10^{-4} and 2.5×10^{-2} respectively. (Table: 06-2, Note: 06-2) Back to Table

F2. O + OClO. The recommended value is based on results of the DF-RF study of Gleason et al. [510]. Over the temperature range from 400 K down to 240 K their data are well fitted by this Arrhenius expression, but at lower temperatures down to 200 K their data show an abrupt change to a negative temperature dependence. At 200 K the value measured is a factor of 3 higher than that calculated from the Arrhenius expression. Similar results were obtained in a recent study (Toohey, Avallone, and Anderson, private communication). Over the temperature range 413–273 K their data showed a temperature dependence very similar to that reported by Gleason et al. over the same temperature range. Moreover, as the temperature was lowered further their rate constant values also levelled off and then increased at the lowest temperature. Their rate constant values were nearly 50% lower than the values of Gleason et al. from 400 K down to 273 K and 30% lower at 253 K. Colussi [306], using a laser-flash photolysis–resonance fluorescence technique over an extended pressure range, reported a value of the bimolecular rate coefficient at room temperature 50% higher than the recommended value. Colussi et al. [308] extended these measurements down to 248 K; in contrast to the positive temperature dependence over this temperature range reported by Gleason et al., these authors report a negative temperature dependence. The bimolecular rate constants reported by Colussi et al. are not directly measured but are derived quantities which are consistent with fall-off curves fitted to the experimental data over the pressure range 20–600 torr. It appears that the experiments of Bemand et al. [126], were complicated by secondary chemistry. The results of Colussi and Colussi et al. over an extended pressure range demonstrate the importance of the termolecular reaction O + OClO + M $\rightarrow$ ClO_3 + M (see entry for this reaction in Table 2). It should be noted that the termolecular rate constants derived by Gleason et al. on the basis of their low temperature data are not consistent with the termolecular rate constant expression recommended in this evaluation (factor of 3 difference). The recommended expression is based on the results of Colussi [306] and Colussi et al. [308]. (Table: 94-26, Note: 94-26) Back to Table

F3. O + Cl_2O. Recommended value is based on the results of Stevens and Anderson [1240] and Miziolek and Molina [925], which are in good agreement. The significantly lower values of Wecker et al. [1439] are not included, nor are earlier results by Basco and Dogra [92] and Freeman and Phillips [470] due to data analysis difficulties in both studies. (Table: 94-26, Note: 94-26) Back to Table

F4. O + HCl. Fair agreement exists between the results of Brown and Smith [182], Wong and Belles [1482], Ravishankara et al. [1096], Hack et al. [535] and Singleton and Cvetanovic [1199] at 300 K (some of the values for k(300 K) were obtained by extrapolation of the experimentally determined Arrhenius expressions), but these are a factor of ~7 lower than that of Balakhnin et al. [65]. Unfortunately, the values reported for E/R are in complete disagreement, ranging from 2260–3755 K. The preferred value was based on the results reported by Brown and Smith, Wong and Belles, Ravishankara et al., Hack et al. and Singleton and Cvetanovic, but not on those reported by Balakhnin et al. (Table: 82-57, Note: 82-57) Back to Table

F5. O + HOCl. Recommended value is based on results of Schindler et al. [1154]. In this study the rate constant was found to be practically independent of temperature in the range 213–298 K. Product analysis indicated that Cl atom abstraction is the predominant primary reaction channel. (Table: 97-4, Note: 97-4) Back to Table

F6. O + $ClONO_2$. The results reported by Molina et al. [928] and Kurylo [750] are in good agreement, and these data have been used to derive the preferred Arrhenius expression. The value reported by Ravishankara et al. [1091] at 245 K is a factor of 2 greater than those from the other studies, and this may possibly be attributed to (a) secondary kinetic complications, (b) the presence of NO_2 as a reactive impurity in the $ClONO_2$, or (c) formation of reactive photolytic products. None of the studies reported identification of the reaction products. The room temperature result of Adler-Golden and Wiesenfeld [11] is in good agreement with the recommended value. (Table: 82-57, Note: 82-57) Back to Table

F7. O_3 + OClO. The recommended value is based on results over the temperature range 262–296 K reported by Wongdontri-Stuper et al. [1483]. Within the indicated uncertainty limits it also

encompasses the somewhat lower room temperature result of Birks et al. [146]. (Table: 90-1, Note: 90-1) Back to Table

F8. $O_3 + Cl_2O_2$. The recommended upper limit is taken from the study of DeMore and Tschuikow-Roux [382] measured at 195 K. (Table: 90-1, Note: 90-1) Back to Table

F9. $OH + Cl_2$. The recommended room temperature value is the average of the results reported by Boodaghians et al. [159], Loewenstein and Anderson [841], Ravishankara et al. [1093], and Leu and Lin [806]. The temperature dependence is from Boodaghians et al. Loewenstein and Anderson determined that the exclusive products are Cl + HOCl. (Table 87-41, Note: 87-41) Back to Table

F10. OH + ClO. The reaction has two known product channels under atmospheric conditions: $OH + ClO \rightarrow Cl + HO_2$ and $OH + ClO \rightarrow HCl + O_2$. Most studies measure the rate coefficients for the overall reaction ($OH + ClO \rightarrow$ products) that is presumably the sum of the two channels. The recommendation for the $Cl + HO_2$ channel is obtained from the difference between a critical assessment of the measurements of the overall reaction and the recommendation for the $HCl + O_2$ channel as discussed below. The assessment of the overall reaction ($OH + ClO \rightarrow$ products) is based on a fit to the 219–373 K data of Hills and Howard [582], the 208–298 K data of Lipson et al. [835], the 234–356 K data of Kegley-Owen et al. [696] and the 298 K data of Poulet et al. [1075]. Data reported in the studies of Burrows et al. [208], Ravishankara et al. [1093], and Leu and Lin [806] were not used in deriving the recommended value because ClO was not measured directly in these studies and the concentration of ClO was determined by an indirect method. Recent measurements of the overall rate constant by Wang and Keyser (218–298 K) [1416], Bedjanian et al. (230–360 K) [113] and Tyndall et al. (298 K) [1347] are consistent with the recommendation.

The minor reaction channel forming HCl poses significant experimental difficulties due to the complications associated with the measurement of the HCl reaction product. Early studies inferred the HCl branching ratio without measuring HCl. These included the 298 K measurements of Leu and Lin [806] (>0.65); Burrows et al. [208] (0.85±0.2) and Hills and Howard [582] (0.86±0.14). Poulet et al. [1075] measured the HCl product yield to be 0.98±0.12 using mass spectroscopy but their HCl sensitivity was marginal. These studies were not considered in the evaluation. Later studies using mass spectroscopy [834] and diode laser spectroscopy [1417] improved the precision of the HCl product channel measurements. Lipson et al. measured rate constants for the HCl channel over the temperature range 207–298 K while Wang and Keyser [1417] measured the HCl yield between 218–298 K, obtaining (9.0±4.8) %, independent of temperature. The recommendation for the HCl channel is based on an average of the results of Lipson et al. and the rate expression obtained from the product of the HCl yield of Wang and Keyser and the evaluated overall rate constant as discussed above. Recent measurements by Tyndall et al. [1347] and Bedjanian et al. [113] are noted but are not considered in this evaluation. (Table 00-3, Note: 00-3) Back to Table

F11. OH + OClO. The recommended value is that reported by Poulet et al. [1079], the only reported study of this rate constant, using a discharge flow system in which OH decay was measured by LIF or EPR over the temperature range 293–473 K. Product HOCl was detected by modulated molecular beam mass spectrometry. The branching ratio for the channel to produce $HOCl + O_2$ was determined to be close to unity, but experimental uncertainty would allow it to be as low as 0.80. (Table: 90-1, Note: 90-1) Back to Table

F12. OH + HCl. The recommended value is based on a least squares fit to the data over the temperature range 240–300 K reported in the studies by Molina et al. [929], Keyser [709], Ravishankara et al. [1105] and Battin-Leclerc et al. [97]. In these studies particular attention was paid to the determination of the absolute concentration of HCl by UV and IR spectrophotometry. Earlier studies by Takacs and Glass [1271], Zahniser et al. [1510], Smith and Zellner [1217], Ravishankara et al. [1096], Hack et al. [535], Husain et al. [624], Cannon et al. [222], Husain et al. [625], and Smith and Williams [1216] had reported somewhat lower room temperature values. The data of Sharkey and Smith [1179] over the temperature range 138–216 K and Battin-Leclerc et al. [97] below 240 K depart from normal Arrhenius behavior. It is unknown whether this is due to an effect such as tunneling at low temperature or a systematic experimental error. Additional work at low temperature is needed. (Table 00-3, Note: 00-3) Back to Table

F13. OH + HOCl. In the only reported study of this system Ennis and Birks [439] reported the value of this rate constant at room temperature to lie in the range (1.7 – 9.5) × 10^{-13} cm^3 $molecule^{-1}$ s^{-1}. A temperature-dependent expression has been estimated by choosing a pre-exponential factor by analogy with the OH + H_2O_2 reaction and selecting the midpoint of the experimental range for the room temperature rate constant. The large uncertainty factor is needed to encompass the entire range. (Table 87-41, Note: 87-41) Back to Table

F14. OH + $ClNO_2$. The recommended value is based on results of the direct study of Ganske et al. [480, 481] using the discharge flow-resonance fluorescence technique. Mass spectrometric studies showed HOCl to be the major chlorine-containing product, with no evidence for a channel to produce $HONO_2$ + Cl. (Table: 94-26, Note: 94-26) Back to Table

F15. OH + $ClONO_2$. The results reported by Zahniser et al. [1507] and Ravishankara et al. [1091] are in good agreement at ~245 K (within 25%), considering the difficulties associated with handling $ClONO_2$. The preferred value is that of Zahniser et al. Neither study reported any data on the reaction products. (Table: 82-57, Note: 82-57) Back to Table

F16. OH + CH_3Cl. The recommended rate expression is derived from a combined fit (for T ≤ 400 K) to the data from the relative rate study by Hsu and DeMore [614] (recalculated based on the current recommendation for the rate constant for the OH + CH_3CHF_2 reference reaction, as described in the note for that reaction) and the absolute rate studies of Orkin et al. [1017] and Herndon et al. [573]. Data from the earlier studies of Howard and Evenson [606], Perry et al. [1049], Davis et al. [358], Paraskevopoulos et al. [1034], Taylor et al. [1290], and Jeong and Kaufman [669] are reasonably well encompassed within the 2σ limits. The room temperature value from Taylor et al. [1290] is inconsistent with the higher temperature results in the same study and with the other investigations and lies outside of the 2σ band, as do the higher room temperature values of Cox et al. [320] and Brown et al. [180]. (Table: 02-25, Note: 02-25) Back to Table

F17. OH + CH_2Cl_2. The recommended values for k(298 K) and E/R are averages of the values from the absolute rate studies of Villenave et al. [1378] and Herndon et al. [573] and the relative rate study of Hsu and DeMore [614] (two determinations which have been recalculated based on the current recommendations for the rate constants of the OH + CH_3CHF_2 and OH + CH_3CH_2F reference reactions). The renormalization procedure for relative rate measurements referenced to the OH + CH_3CHF_2 reaction is discussed in the note for that reaction. The rate constant determined relative to the rate constant of the OH + CH_3CH_2F was recalculated using a rate constant of the reference reaction obtained from the data of Schmoltner et al. [1159] and Kozlov et al. [738] above room temperature. The results of Cox et al. [320] and Davis et al. [358] support this recommendation. The results from Taylor et al. [1291], Jeong and Kaufman [669], Perry et al. [1049] and Howard and Evenson [606] lie considerably higher and were not used in deriving the recommended parameters. (Table: 02-25, Note: 02-25) Back to Table

F18. OH + $CHCl_3$. The recommended value for k(298 K) is an average of the values from the relative rate study of Hsu and DeMore [614] (which has been recalculated based on the current recommendation for the rate constant of the OH + CH_3CHF_2 reference reaction, as described in the note for that reaction) and the absolute rate studies of Taylor et al. [1291] (which superseded Taylor et al. [1290]), Jeong and Kaufman [669], Davis et al. [358], and Howard and Evenson [606]. The recommended value of E/R is an average of values for this parameter derived in the first four of the above studies. (Table: 02-25, Note: 02-25) Back to Table

F19. OH + CCl_4. The recommended upper limit at 298 K is based on the upper limit reported in the competitive study by Cox et al. [320]. The value given there has been increased by a factor of four to allow for uncertainties in the number of NO molecules oxidized. The recommendation is compatible with the less sensitive upper limits reported by Howard and Evenson [606] and Clyne and Holt [283]. None of these investigators reported any evidence for reaction between these species. The A-factor was estimated and a lower limit for E/R was derived. (Table: 90-1, Note: 90-1) Back to Table

F20. OH + CH_2FCl (HCFC-31). The recommended value for k(298 K) is an average of the values from the relative rate study of DeMore [376] (which has been recalculated based on the current recommendation for the rate constant of the OH + CH_2Cl_2 reference reaction) and the absolute rate

studies of Howard and Evenson [606], Paraskevopoulos et al. [1034], Watson et al. [1434], Handwerk and Zellner [549] and Jeong and Kaufman [669]. The recommended value for E/R is an average of the values for this parameter determined by DeMore and by Watson et al., Handwerk and Zellner, and Jeong and Kaufman below 400 K. (Table: 02-25, Note: 02-25) Back to Table

F21. OH + $CHFCl_2$ (HCFC-21). The recommended rate expression is derived from a combined fit to the data of Howard and Evenson [606], Perry et al. [1049], Watson et al. [1434], Chang and Kaufman [241], Paraskevopoulos et al. [1034], Jeong and Kaufman [669], and Fang et al. [444]. The rate constants reported by Clyne and Holt [282] are significantly higher than those from the other seven studies and were not used in deriving the recommended parameters. (Table: 02-25, Note: 02-25) Back to Table

F22. OH + CHF_2Cl (HCFC-22). Results for this compound show very good agreement among both absolute and relative rate constant measurements. The recommended rate expression is derived from a combined fit to the relative rate data of Hsu and DeMore [615] (which has been recalculated based on the current recommendation for the rate constant of the OH + CH_4 reference reaction), and the absolute rate studies of Orkin and Khamaganov [1015], Fang et al. [444], Atkinson et al. [48], Watson et al. [1434], Chang and Kaufman [241], Paraskevopoulos et al. [1034] and Jeong and Kaufman [669]. The more scattered results of Handwerk and Zellner [549] are in general agreement. The results from the studies of Howard and Evenson [606] and Clyne and Holt [282] are significantly different from those of the other studies and were not used in the derivation. (Table: 02-25, Note: 02-25) Back to Table

F23. OH + $CFCl_3$ (CFC-11). The A-factor was estimated, and a lower limit for E/R was derived by using the upper limit for the rate constant reported by Chang and Kaufman [242] at about 480 K. This expression is compatible with the upper limits reported by Atkinson et al. [48], Howard and Evenson [606], Cox et al. [320] and Clyne and Holt [283]. None of the investigators reported any evidence for reaction. (Table: 02-25, Note: 02-25) Back to Table

F24. OH + CF_2Cl_2 (CFC-12). The A-factor was estimated, and a lower limit for E/R was derived by using the upper limit for the rate constant reported by Chang and Kaufman [242] at about 480 K. This expression is compatible with the upper limits reported by Atkinson et al. [48], Howard and Evenson [606], Cox et al. [320], and Clyne and Holt [283]. None of the investigators reported any evidence for reaction. (Table: 02-25, Note: 02-25) Back to Table

F25. OH + CH_2ClCH_3. The recommended value for k(298 K) is an average of the values reported by Howard and Evenson [605], Paraskevopoulos et al. [1034], Kasner et al. [694], and Herndon et al. [573]. The recommended value for E/R is an average of the values for this parameter determined by Kasner et al. and Herndon et al. with the value for A calculated to yield the recommended value for k(298 K). Data from the study by Markert and Nielsen [874] were not used to derive the recommended parameters, as they are somewhat more scattered. (Table: 02-25, Note: 02-25) Back to Table

F26. OH + CH_3CCl_3. The recommended value for k(298 K) is an average of the values from the absolute rate studies of Talukdar et al. [1288] and Finlayson-Pitts et al. [457], and a relative rate study of DeMore [373] (recalculated based on the current recommendation for the rate constant of the OH + CH_4 reference reaction). The temperature dependence is a fit to the data between 243 K and 379 K of Talukdar et al. [1288]. These studies indicate both a lower k(298 K) and E/R than was reported in earlier studies: Nelson et al. [956], Jeong and Kaufman [668], and Kurylo et al. [753]. More recent measurements by Jiang et al. [671] and Lancar et al. [766] yield rate constants that are slightly higher at 298 K than this recommendation. (Table: 06-2, Note: 06-2) Back to Table

F27. OH + CH_3CFCl_2 (HCFC-141b). Both absolute and relative rate measurements are in excellent agreement for this compound, and the data are linear over a wide temperature range. The recommended rate expression is derived from a combined fit to the data of Huder and DeMore [618] (two relative rate determinations which have been recalculated based on the current recommendations for the rate constants for the reference reactions OH + CH_4 and OH + CH_3CCl_3), Lancar et al. [766], Zhang et al. [1521] (together with the data at 330 K and above from Liu et al. [839], Talukdar et al. [1281] above 253 K (two studies), and Mors et al.[936]. The temperature-dependence data of Brown et al. [179] were not considered because the relatively large rate constants

and Arrhenius curvature are suggestive of sample impurities. (Table: 02-25, Note: 02-25) Back to Table

F28. OH + CH_3CF_2Cl (HCFC-142b). The recommended value for k(298 K) is an average of the values from Howard and Evenson [605], Cox et al. [320], Paraskevopoulos et al. [1034], Mors et al. [936], Watson et al. [1434], Handwerk and Zellner [549], Liu et al. [839], Gierczak et al. [495], and Fang et al. [445]. The recommended value of E/R is an average of values for this parameter derived in the last five of these studies. The data from Brown et al. [179] and Clyne and Holt [282] were not used to derive the recommended parameters. The 270 K data of Zhang et al. [1521] are in reasonable agreement with the recommendation. (Table: 02-25, Note: 02-25) Back to Table

F29. OH + CH_2ClCF_2Cl (HCFC-132b). The recommended rate expression was derived from the data of Watson et al. [1436], which were corrected by these authors for the presence of alkene impurities. The data of Jeong et al. [667], indicating faster rate constants, may have been affected by such impurities; hence they were not included in deriving the recommendation. (Table: 02-25, Note: 02-25) Back to Table

F30. OH + CH_2ClCF_3 (HCFC-133a). The recommended value of k_{298} is the average of the values of Howard and Evenson [605] and Handwerk and Zellner [549] adjusted to 298 K. The recommended temperature dependence was derived from the data of Handwerk and Zellner [549]. The data of Clyne and Holt [282] were not used in deriving the recommended parameters but (below 400 K) are encompassed within the 2σ limits. (Table: 02-25, Note: 02-25) Back to Table

F31. OH + $CHCl_2CF_2Cl$ (HCFC-122). The recommended rate expression is derived from a combined fit to the data of Orkin and Khamaganov [1015] (below 400 K) and DeMore [376] (two determinations which have been recalculated based on the current recommendations for the rate constants of the OH + CH_2Cl_2 and OH + $CHCl_2CF_3$ reference reactions). (Table: 02-25, Note: 02-25) Back to Table

F32. OH + $CHFClCFCl_2$ (HCFC-122a). The recommended rate expression was derived from the relative rate data of Hsu and DeMore [615] (recalculated based on the current recommendation for the rate constant for the OH + CH_3CHF_2 reference reaction, as discussed in the note for that reaction). (Table: 02-25, Note: 02-25) Back to Table

F33. OH + $CHCl_2CF_3$ (HCFC-123). The recommended value of k_{298} is the average of the values from the absolute studies of Gierczak et al. [495] (two determinations) Liu et al. [839], and Yamada et al. [1494], and from the relative rate study by Hsu and DeMore [615] (recalculated based on the current recommendation for the rate constant for the OH + CH_3CHF_2 reference reaction, as discussed in the note for that reaction). The recommendation for the temperature dependence is derived from a fit to the data of these same five investigations. The temperature dependence data of Nielsen [975], Watson et al. [1436], Clyne and Holt [282], and Brown et al. [179] and the room temperature data of Howard and Evenson [605] were not used in the derivations. (Table: 02-25, Note: 02-25) Back to Table

F34. OH + $CHFClCF_2Cl$ (HCFC-123a). The recommended rate expression is based on the data of Orkin and Khamaganov [1015]. (Table: 02-25, Note: 02-25) Back to Table

F35. OH + $CHFClCF_3$ (HCFC-124). The recommended value for k(298 K) is an average of the values from the studies of Watson et al. [1436], Gierczak et al. [495] (2 studies), Yamada et al. [1494], and Hsu and DeMore [615] (two relative rate determinations which have been recalculated based on the current recommendations for the rate constants of the OH + CH_4 and OH + CHF_2CHF_2 reference reactions). The room temperature rate constant of Howard and Evenson [605] is considerably higher than these other values and was not included in the average. The recommended temperature dependence is an average of the dependencies derived from these same studies (but using only data below 400 K from Gierczak et al. [495] and Yamada et al. [1494]. (Table: 02-25, Note: 02-25) Back to Table

F36. OH + $CH_3CF_2CFCl_2$ (HCFC-243cc). The recommended rate expression is derived from the temperature-dependence data of Nelson et al. [952]. Although there is only a single study of this reaction, the uncertainties have been assigned to reflect our belief that the rate constant for this reaction should be less than that for OH + CH_3CF_2Cl. (Table: 02-25, Note: 02-25) Back to Table

F37. OH + $CHCl_2CF_3CF_2$ (HCFC-225ca). The recommended value for k(298 K) is an average of the values from Nelson et al. [952] and Zhang et al. [1522]. The recommendation for E/R is taken from Nelson et al. [952]. The temperature-dependence data of Brown et al. [178] were not considered because the relatively large rate constants at and below room temperature and the Arrhenius curvature are suggestive of sample impurities. The temperature dependence results of Zhang et al. [1522] are in reasonable agreement with those of Nelson et al. [952] over the temperature range of measurement overlap. However, the complete Zhang et al. [1522] data set yields a value for E/R much larger than currently recommended for the OH + $CHCl_2CF_3$ (HFC-123) reaction, for which the activation energy should be similar. (Table: 02-25, Note: 02-25) Back to Table

F38. OH + CF_2ClCF_2CHFCl (HCFC-225cb). The recommended rate expression is derived from a combined fit to the temperature-dependence data of Nelson et al. [952] and Zhang et al. [1522], which are in excellent agreement. (Table: 02-25, Note: 02-25) Back to Table

F39. OH + CH_2=CHCl. The recommended value for k(298 K) is an average of the values reported by Howard [603], Perry et al. [1047], Liu et al. [838] and [1495]. The recommended value for E/R is an average of the values for this parameter derived from fits to the data of Perry et al., Liu et al. and Yamada et al. at temperatures below about 400 K. In the 400–500 K region the rate constant levels off before increasing at higher temperatures, suggesting the stronger importance of an abstraction mechanism at the higher temperatures. (Table: 02-25, Note: 02-25) Back to Table

F40. OH + CH_2=CCl_2. The recommended value for k(298 K) is an average of the values reported by Edney et al. [431], Tuazon et al. [1325], Abbatt and Anderson [1], Zhang et al. [1523], Canosa-Mas et al. [224], and [1493]. The recommended value for E/R comes from a combined fit to the data of Abbatt and Anderson, Zhang et al., and Yamada et al. The data of Kirchner et al. [715] were not used in deriving the recommended parameters since they were obtained at very low pressure and the much stronger temperature dependence obtained may be indicative of a pressure dependence above room temperature. (Table: 02-25, Note: 02-25) Back to Table

F41. OH + CHCl=CCl_2. The recommended value for k(298 K) is the mean of the values reported by Howard [603], Chang and Kaufman [241], Kirchner et al. [715], Klopffer et al. [725], Edney et al. [431] and Tichenor et al. [1306]. The recommended value of E/R is an average of values for this parameter derived by Chang and Kaufman [241], Kirchner et al. [715], and Tichenor et al. [1306]. The value for k(298 K) derived from a relative rate study by Winer et al. [1478] is a factor of ~2 greater than the other values and is not considered in deriving the preferred value. An absolute study by Jiang et al. [672] yielding a significantly higher value for k(298 K) as well as a considerably stronger temperature dependence (E/R = –970 K) is assumed to be superseded by Tichenor et al. [1306]. (Table: 02-25, Note: 02-25) Back to Table

F42. OH + CCl_2=CCl_2. The recommended value for k(298 K) is the mean of the values reported by Howard [603], Chang and Kaufman [241], and Kirchner et al. [715]. The room temperature value reported by Winer et al. [1478] is more than a factor of 10 greater and was not used in deriving the recommendation. The recommended value for E/R is an average of values for this parameter derived by Chang and Kaufman [241] and Kirchner et al. [715]. A study by Tichenor et al. [1307] yields a value for k(298 K) slightly lower than these other studies, but a temperature dependence less than half of that recommended. While these latest results were not used in deriving the recommendations, they are encompassed within the 95% confidence limits. (Table: 02-25, Note: 02-25) Back to Table

F43. OH + CH_3OCl. The recommended rate expression is derived from a fit to the data of Crowley et al. [335], the only reported study of this reaction. (Table: 02-25, Note: 02-25) Back to Table

F44. OH + CCl_3CHO. The recommended value for k(298 K) is an average of the values reported by Barry et al. [89] (using three independent techniques), Dobe et al. [395], Nelson et al. [956], Ballestra-Garcia et al. [68], and Scollard et al. [1166]. The temperature dependence is derived from a fit to the data of Dobe et al. [395]. The A factor was then calculated to agree with the recommended value for k(298 K). (Table: 02-25, Note: 02-25) Back to Table

F45. HO_2 + Cl. The recommendations for the two reaction channels are based upon the results by Lee and Howard [793] using a discharge flow system with laser magnetic resonance detection of HO_2,

OH, and ClO. The total rate constant is temperature independent with a value of $(4.2\pm0.7) \times 10^{-11}$ cm^3 $molecule^{-1}$ s^{-1} over the temperature range 250–420 K. This value for the total rate constant is in agreement with the results of indirect studies relative to Cl + H_2O_2 (Leu and DeMore [802], Poulet et al. [1077], Burrows et al. [203] or to Cl + H_2 (Cox [314]). The contribution of the reaction channel producing OH + ClO (21% at room temperature) is much higher than the upper limit reported by Burrows et al. (1% of total reaction). Cattell and Cox [238], using a molecular modulation-UV absorption technique over the pressure range 50–760 torr, report results in good agreement with those of Lee and Howard both for the overall rate constant and for the relative contribution of the two reaction channels. A study by Dobis and Benson [400] reports a total rate constant in good agreement with this recommendation but a much lower contribution (5±3%) of the channel producing OH + ClO. The rate constant for the channel producing ClO + OH can be combined with that for the reaction ClO + OH > Cl + HO_2 to give an equilibrium constant from which a value of the heat of formation of HO_2 at 298 K of 3.0 kcal/mol can be derived. (Table: 82-57, Note: 94-26) Back to Table

F46. HO_2 + ClO. Three new studies by Nickolaisen et al [965], Knight et al. [727], and Laszlo et al. [771] have been added to the previous five studies of this rate constant (Reimann and Kaufman, [1111]; Stimpfle et al. [1248]; Leck et al. [781]; Burrows and Cox [204]; Cattell and Cox [238]). The studies span a wide variety of pressure conditions and detection techniques. The studies of Cattell and Cox and Nickolaisen et al. were performed over extended pressure ranges and indicate that the reaction is pressure independent. However, the room temperature rate constant obtained by averaging the five low pressure (< 10 torr) studies is slightly lower (5.1±1.5 vs. 6.5±1.2 in units of 10^{-12} cm^3 $molecule^{-1}$ s^{-1}) than that obtained by averaging the higher pressure measurements (> 50 torr). Although within the combined uncertainty, this offset may suggest possible systematic experimental complications (e.g. unknown secondary reactions) in the low or high pressure experiments. The recommended value for k(298 K) is the mean of the eight studies. Temperature-dependence data has been obtained by Stimpfle et al., Nickolaisen et al., Knight et al., and Laszlo et al. The earliest study (Stimpfle et al.) observed nonlinear Arrhenius behavior. The data were best described by a four parameter equation of the form $k=A\exp(-B/T)+CT^n$, possibly suggesting that two different mechanisms may be occurring. The more recent studies find the T-dependence to display linear Arrhenius behavior over the entire temperature range. Moreover, they derive much smaller E/R values (17 to 312) than that obtained by Stimpfle (E/R ≈ 700 for T<300 K). The recommended value for E/R is based on an average of the four studies over their entire temperature ranges. The two most probable pairs of reaction products are, (1) HOCl + O_2 and (2) HCl + O_3. Leu [814], Leck et al., Knight et al., and Laszlo et al. used mass spectrometric detection of ozone to place upper limits on channel 2 of 1.5%, 2%, 1%, and 2%, respectively at 298 K. In addition, Leck et al. and Laszlo set upper limits of 3.0% (248 K); and 5.0% (243 K), respectively, on k_2/k. Burrows and Cox report an upper limit of 0.3% for k_2/k at 300 K. Finkbeiner et al. [456], using matrix-isolation/FTIR spectroscopy, studied product formation between 210 and 300 K at 700 torr. HOCl was observed as the dominant product (> 95% at all temperatures). The branching ratio values for k_2/k were determined to be <1% at 300 K and 270 K, 2±1% at 240 K, and 5±2% at 210 K. No evidence for any other product channel was found. Theoretical calculations by Nickolaisen et al. suggest that the reaction to channel (1) proceeds mainly through the ClO-HO_2 complex on the triplet potential surface. However, these calculations also suggest that collisionally stabilized HOOOCl formed on the singlet surface will possess an appreciable lifetime. Further studies on possible formation of HOOOCl are warranted. (Table: 02-25, Note: 02-25) Back to Table

F47. H_2O + $ClONO_2$. This recommendation is based on the upper limits to the homogeneous bimolecular rate constant reported by Atkinson et al. [54], and by Hatakeyama and Leu [558, 559]. Atkinson et al. observed by FTIR analysis the decay of $ClONO_2$ in the presence of H_2O in large-volume (2500 and 5800 liters) Teflon or Teflon-coated chambers. Their observed decay rate gives an upper limit to the homogeneous gas phase rate constant, and they conclude that the decay observed is due to heterogeneous processes. Hatakeyama and Leu, using a static photolysis system with FTIR analysis, derive a similar upper limit. Rowland et al. [1126] concluded that the decay they observed resulted from rapid heterogeneous processes. The homogeneous reaction is too slow to have any significant effect on atmospheric chemistry. (Table 87-41, Note: 87-41) Back to Table

F48. NO + OClO. The Arrhenius expression was estimated based on 298 K data reported by Bemand, Clyne and Watson [126]. (Table: 82-57, Note: 82-57) Back to Table

F49. NO + Cl_2O_2. The recommended upper limit is that determined by Friedl (private communication) in a study using a DF-MS technique. (Table: 90-1, Note: 90-1) Back to Table

F50. NO_3 + HCl. The recommended upper limit is that reported by Mellouki et al. [905] in a study using DF-EPR techniques. This upper limit shows that this reaction is of negligible importance in stratospheric chemistry. Somewhat lower upper limits have been reported by Cantrell et al. [228] and Canosa-Mas et al. [225]; the latter study also reports Arrhenius parameters at higher temperatures (333–473 K). (Table: 90-1, Note: 90-1) Back to Table

F51. HO_2NO_2 + HCl. This upper limit is based on results of static photolysis-FTIR experiments reported by Leu et al. [805]. (Table: 90-1, Note: 90-1) Back to Table

F52. Cl + O_3. The results reported for k(298 K) by Watson et al. [1435], Zahniser et al. [1511], Kurylo and Braun [754], Clyne and Nip [293], Nicovich et al. [968], Seeley et al. [1169] and Beach et al. [101] are in good agreement, and have been used to determine the preferred value at this temperature. The values reported by Leu and DeMore [802] (due to the wide error limits) and Clyne and Watson [298] (the value is inexplicably high) are not considered. The six Arrhenius expressions are in fair agreement within the temperature range 205–300 K. In this temperature range, the rate constants at any particular temperature agree to within 30–40%. Although the values of the activation energy obtained by Watson et al. and Kurylo and Braun are in excellent agreement, the value of k in the study of Kurylo and Braun is consistently (~17%) lower than that of Watson et al. This may suggest a systematic underestimate of the rate constant, as the values from the other three agree so well at 298 K. Two recent studies (Nicovich et al. and Seeley et al.) obtained significantly smaller temperature dependences than those observed in the earlier studies. There is no reason to prefer any one set of data to any other; therefore, the preferred Arrhenius expression shown above was obtained by computing the mean of the six results between 205 and 298 K. DeMore [372] directly determined the ratio k(Cl + O_3)/k(Cl + CH_4) at 197–217 K to be within 15% of that calculated from the absolute rate constant values recommended here.

Vanderzanden and Birks [1370] have interpreted their observation of oxygen atoms in this system as evidence for some production (0.1–0.5%) of O_2 ($^1\Sigma_g^+$) in this reaction. The possible production of singlet molecular oxygen in this reaction has also been discussed by DeMore [369], in connection with the Cl_2 photosensitized decomposition of ozone. However Choo and Leu [265] were unable to detect $O_2(^1\Sigma)$ or $O_2(^1\Delta)$ in the Cl + O_3 system and set upper limits to the branching ratios for their production of 5×10^{-4} and 2.5×10^{-2}, respectively. They suggested two possible mechanisms for the observed production of oxygen atoms, involving reactions of vibrationally excited ClO radicals with O_3 or with Cl atoms, respectively. Burkholder et al. [199], in a study of infrared line intensities of the ClO radical, present evidence in support of the second mechanism. In their experiments with excess Cl atoms, the vibrationally excited ClO radicals produced in the Cl + O_3 reaction can react with Cl atoms to give Cl_2 and oxygen atoms, which can then remove additional ClO radicals. These authors point out the possibility for systematic error from assuming a 1:1 stoichiometry for [Cl]:$[O_3]_o$ when using the Cl + O_3 reaction as a quantitative source of ClO radicals for kinetic and spectroscopic studies. (Table: 06-2, Note: 06-2) Back to Table

F53. Cl + H_2. The recommended value for k(298 K) is an average of the values measured by Westenberg and De Haas [1449], Lee et al. [784], Miller and Gordon [923], and Kita and Stedman [718]. The value of k(298 K) derived in the flash photolysis resonance fluorescence study of Davis et al. [355] agrees with these studies but was probably overestimated by ~10% (the authors assumed that the fluorescence signal, I_f was proportional to $[Cl]^{0.9}$, whereas a linear relationship between I_f and [Cl] probably held under their experimental conditions). Room temperature determinations by Kumaran et al. [745] (focused primarily on high temperature measurements) and Eberhard et al. [428] (focused on obtaining yields of HCl product in different vibrational levels) are both in reasonable agreement with the recommendation as are the results from the relative rate studies by Su et al. [1260] and by Rodebush and Klingelhoefer [1122]. The value for E/R is derived from a fit to the data at temperatures below 300 K reported by Westenberg and De Haas [1449], Lee et al. [784], and

Miller and Gordon [923]. The value is in good agreement with that determined by Adusei and Fontijn [12], although these data lie systematically lower than the results from other studies. The Arrhenius A-factor was calculated from k(298 K) and E/R. Extrapolation above room temperature using the recommended Arrhenius parameters is in reasonable agreement with the data of Benson et al. [129] and Kita and Stedman [718]. For a discussion of the large body of rate data at high temperatures, see the review by Baulch et al. [100]. Miller and Gordon [923] and Kita and Stedman [718] also measured the rate of the reverse reaction, and found the ratio to be in good agreement with equilibrium constant data. (Table: 06-2, Note: 06-2) Back to Table

F54. Cl + H_2O_2. The absolute rate coefficients determined at ~298 K by Watson et al. [1435], Leu and DeMore [802], Michael et al. [921], Poulet et al. [1077] and Keyser [705] range in value from (3.6–6.2) × 10^{-13}. The studies of Michael et al., Keyser, and Poulet et al. are presently considered to be the most reliable. The preferred value for the Arrhenius expression is taken to be that reported by Keyser. The A-factor reported by Michael et al. is considerably lower than that expected from theoretical considerations and may possibly be attributed to decomposition of H_2O_2 at temperatures above 300 K. The data of Michael et al. at and below 300 K are in good agreement with the Arrhenius expression reported by Keyser. More data are required before the Arrhenius parameters can be considered to be well-established. Heneghan and Benson [569], using mass spectrometry, confirmed that this reaction proceeds only by the abstraction mechanism giving HCl and HO_2 as products. (Table: 02-25, Note: 02-25) Back to Table

F55. Cl + NO_3. The recommended value at room temperature is based on the discharge flow-EPR study of Mellouki et al. [903] and the discharge flow-mass spectrometric study of Becker et al. [104]. The results of these direct absolute rate studies are preferred over results of the earlier relative rate studies of Cox et al. [315], Burrows et al. [207], and Cox et al. [326], in all of which NO_3 was monitored in the photolysis of Cl_2-$ClONO_2$-N_2 mixtures. Complications in the chemistry of the earlier systems probably contributed to the spread in reported values. This radical-radical reaction is expected to have negligible temperature dependence, which is consistent with the results from the study of Cox et al. [326] in which the complications must have been temperature independent. (Table: 94-26, Note: 94-26) Back to Table

F56. Cl + N_2O. This rate coefficient has been determined in a study of the halogen-catalyzed decomposition of nitrous oxide at about 1000 K by Kaufman et al. [695]. The largest value reported was 10^{-17} cm^3 $molecule^{-1}$ s^{-1}, with an activation energy of 34 kcal/mol. Extrapolation of these results to low temperature shows that this reaction cannot be of any significance in atmospheric chemistry. (Table 87-41, Note: 87-41) Back to Table

F57. Cl + HNO_3. The recommended upper limit at room temperature is that reported in the study of Wine et al. [1475], in which long-path laser absorption spectroscopy was used to look for the appearance of NO_3 following the pulsed laser photolysis of Cl_2-HNO_3 mixtures with no evidence for NO_3 production was observed. In the same study a less sensitive upper limit was derived from monitoring Cl atom decay by resonance fluorescence. A less sensitive upper limit was also found in the discharge flow-EPR study of Zagogianni et al. [1505]. Higher values obtained in earlier studies (Leu and DeMore [802], Kurylo et al. [760], and Clark et al. [272]) as well as the higher temperature results of Poulet et al. [1077] are not used. (Table: 90-1, Note: 90-1) Back to Table

F58. Cl + HO_2NO_2. The only study of this reaction is by Simonaitis and Leu [1195] using the low pressure discharge flow technique coupled with resonance fluorescence detection of Cl and mass spectrometric detection of HO_2NO_2 ion fragments. Consistent results were obtained monitoring either Cl or HO_2NO_2 decays and retrieved rate constants were less than 1 × 10^{-13} cm^3 $molecule^{-1}$ s^{-1} for all conditions. Impurities in the HO_2NO_2 sample (especially H_2O_2) complicated the measurements. A limited temperature study over the 298–399 K range suggests that E/R is in the range of 500 – 1500. Given the experimental difficulties, only an upper limit is recommended for the reaction rate. (Table: 02-25, Note: 02-25) Back to Table

F59. Cl + CH_4. The recommended value for k(298 K) is based on the values reported in the absolute rate constant studies of Manning and Kurylo [862], Whytock et al. [1452], Michael and Lee [914], Lin et al. [831], Zahniser et al. [1506], Keyser [702], Baghal-Vayjooee et al. [63], Ravishankara and Wine [1100], Heneghan et al. [570], Dobis and Benson [398], Sawerysyn et al. [1150], Lazarou et al.

[777], Beichert et al. [124], Seeley et al. [1169], Pilgrim et al. [1058], Mellouki et al. [899], Wang and Keyser [1415], and Bryukov et al. [189], all of which fall in the range (0.9 – 1.13) × 10^{-13}. Other absolute studies by Davis et al. [355], Clyne and Walker [297], Poulet et al. [1076], Leu and DeMore [802], Watson et al. [1435], and Schlyer et al. [1155] give rate constant values slightly higher than those of the aforementioned studies. In some cases, this may be due to uncertainties in correcting the data for OH loss via reaction with trace levels of ethane and propane in the methane samples used. Nevertheless, these results were not used in deriving the recommended value for k(298 K). The values derived for k at 298 K from the competitive chlorination studies of Pritchard et al. [1080], Pritchard et al. [1081], Knox [729], Knox and Nelson [731], Lee and Rowland [782], and Lin et al. [831] range from (0.8–1.6) × 10^{-13} when the original data are referenced to the presently recommended rate constant values for the reference reactions of Cl with H_2 and C_2H_6. The recommended value k(298 K) = 1.0 × 10^{-13} is derived as an unweighted average of the rate constants from the thirteen preferred absolute studies and the most recent and comprehensive relative rate study of Lin et al. [831].

There have been nine absolute studies of the temperature dependence of k in which the measurements extend below 300 K (Watson et al. [1435], Manning and Kurylo [862], Whytock et al. [1452], Lin et al. [831], Zahniser et al. [1506], Keyser [702], Ravishankara and Wine [1100], Heneghan et al. [570], and Seeley et al. [1169]). In general, the agreement among most of these studies is quite good. However, systematic differences in activation energies are apparent when calculated using data obtained below 300 K versus data from above 300 K. Three resonance fluorescence studies have been performed over the temperature region between 200 and 500 K (Whytock et al. [1452], Zahniser et al. [1506] and Keyser [702]), and in each case a non-linear Arrhenius behavior was observed. Ravishankara and Wine [1100] also noted nonlinear Arrhenius behavior over a more limited temperature range. This behavior tends to partially explain the variance in the values of E/R reported between those investigators who mainly studied this reaction below 300 K (Watson et al. [1435], Manning and Kurylo [862], and Seeley et al. [1169]) and those who only studied it above 300 K (Clyne and Walker [297], Poulet et al. [1076], and Lin et al. [831]). The agreement between all studies below 300 K is reasonably good, with values of E/R ranging from 1060 K to 1320 K. There have not been any absolute studies at stratospheric temperatures other than those that utilized the resonance fluorescence technique. Ravishankara and Wine [1100] have suggested that the results obtained using the discharge flow and competitive chlorination techniques may be in error at the lower temperatures (<240 K) due to a non-equilibration of the $^2P_{1/2}$ and $^2P_{3/2}$ states of atomic chlorine. They observed that at temperatures below 240 K the apparent bimolecular rate constant was dependent upon the chemical composition of the reaction mixture; i.e., if the mixture did not contain an efficient spin equilibrator, e.g., Ar or CCl_4, the bimolecular rate constant decreased at high CH_4 concentrations. The chemical composition in each of the flash photolysis studies contained an efficient spin equilibrator, whereas this was not the case in the discharge flow studies. However, the reactor walls in the discharge flow studies could have been expected to have acted as an efficient spin equilibrator. Consequently, until the hypothesis of Ravishankara and Wine is proven, it is assumed that the discharge flow and competitive chlorination results are reliable. A composite unweighted Arrhenius fit to all of the temperature dependent absolute studies with data in the temperature region ≤300 K (with the exception of the data of Watson et al. [1435], which appear to be systematically high due to reactive impurities) yields E/R = 1280 K and k(298 K) = 1.0 × 10^{-13}. The Arrhenius A-factor was calculated from recommended k(298 K) and E/R. (Table: 06-2, Note: 06-2) Back to Table

F60. Cl + CH_3D. The recommended value for k(298 K) is an average of the relative rate determinations by Saueressig et al. [1148] (two independent measurements) and by Tyler et al. [1343]. It agrees with the value determined by Wallington and Hurley [1404] after the latter is corrected as per a personal communication from the authors. The value for E/R is an average of the values determined by Saueressig et al. and Tyler et al. (Table: 06-2, Note: 06-2) Back to Table

F61. Cl + H_2CO. The results from five of the six published studies (Michael et al. [918], Anderson and Kurylo [28], Niki et al. [985], Fasano and Nogar [447] and Poulet et al. [1072]) are in good agreement at ~298 K, but are ~50% greater than the value reported by Foon et al. [465]. The preferred value at 298 K was obtained by combining the absolute values reported by Michael et al.,

Anderson and Kurylo, and Fasano and Nogar, with the values obtained by combining the ratio of $k(Cl + H_2CO)/k(Cl + C_2H_6)$ reported by Niki et al. (1.3±0.1) and by Poulet et al. (1.16±0.12) with the preferred value of 5.7×10^{-11} for $k(Cl + C_2H_6)$ at 298 K. The preferred value of E/R was obtained from a least squares fit to all the data reported in Michael et al. and in Anderson and Kurylo. The A-factor was adjusted to yield the preferred value at 298 K. (Table: 82-57, Note: 82-57) Back to Table

F62. Cl + HC(O)OH. The room temperature kinetics of this reaction have been studied by Wallington et al. [1390] and Li et al. [818]. Wallington et al. used a relative rate technique at atmospheric pressure while Li et al. employed flash photolysis and operated at 10 torr. The results of the two studies are in excellent agreement and have been averaged together to derive the recommended value. Reaction products have been investigated by Tyndall et al. [1358] at room temperature and 700 torr pressure. They measured the CO_2 yield to be 96 ± 5% and suggested that the HOCO complex reacted with either O_2 or Cl_2 in their experiment to give the observed product. (Table: 02-25, Note: 02-25) Back to Table

F63. Cl + CH_3O_2. Recommended value is based on results of Maricq et al. [872], Jungkamp et al. [683], and Daele and Poulet [340]. All three studies agree that this overall reaction is very fast. However, there is a discrepancy in the reported values of the branching ratios for the two pathways producing ClO + CH_3O (a) and HCl + CH_2O_2 (b). The branching ratio for the reaction channels producing HCl + CH_2O_2 (b) has been reported to be 50% by both Maricq et al. [872] and Jungkamp et al., but has been reported to be 90% by Daele and Poulet. Because of this large discrepancy no branching ratios are recommended. (Table: 97-4, Note: 97-4) Back to Table

F64. Cl + CH_3OH. This recommendation at 298 K) is based on results of the absolute rate studies of Michael et al. [919], Payne et al. [1042], Dobe et al. [396], Pagsberg et al. [1029] and Tyndall et al. [1350], and results obtained in the competitive chlorination studies of Wallington et al. [1413], Lightfoot et al. [823], Nelson et al. [955] and Tyndall et al. The temperature independence of the rate constant was reported by Michael et al. in a direct study. This is consistent with the indirect results of Lightfoot et al. who deduced the rate coefficient for this reaction relative to that for methane as a function of temperature. This reaction can have two sets of products: CH_2OH + HCl, channel (a) and CH_3O + HCl, channel (b). Product analysis and isotopic substitution have established that the reaction proceeds via channel (a) rather than via channel (b). See Radford [1083], Radford et al. [1084], Meier et al. [897], and Payne et al. [1042]. This reaction has been used in the laboratory as a source of CH_2OH and as a source of HO_2 by the reaction of CH_2OH with O_2. (Table: 02-25, Note: 02-25) Back to Table

F65. Cl + CH_3OOH. The only study of this reaction was by Wallington et al. [1390], who measured the rate relative to Cl + C_2H_6 at 295 K and atmospheric pressure. (Table: 02-25, Note: 02-25) Back to Table

F66. Cl + CH_3ONO_2. This reaction has been studied at 298 K by Nielsen et al [981] using a relative rate technique. The reference compound was ethane. The recommended value is adjusted from that given by Nielsen et al. using the currently recommended value for k (Cl + C_2H_6). The temperature dependence is estimated by assuming an A-factor equal to approximately 20 times that of OH + CH_3ONO_2. This is consistent with observed OH/Cl A-factor ratios for primary H-abstraction from alkanes. (Table: 02-25, Note: 02-25) Back to Table

F67. Cl + C_2H_6. The recommended value for k(298 K) is an average of the absolute rate coefficients reported in the studies of Manning and Kurylo [862], Lewis et al. [816], Dobis and Benson [399], Beichert et al. [124], Pilgrim et al. [1058], Tyndall et al. [1352], Hitsuda et al. [586], Bryukov et al. [190], and Hickson and Keyser [580], all of which fall in the range $(5.3 - 6.1) \times 10^{-11}$. The value derived by Ray et al. [1107] in a study whose primary focus was not the determination of the rate constant for the target reaction, lies in the same range. A somewhat higher value reported by Davis et al. [355], was probably overestimated by ~10% (the authors assumed that the fluorescence signal, I_f was proportional to $[Cl]^{0.9}$, whereas a linear relationship between I_f and [Cl] probably held under their experimental conditions). The rate constant reported by Schlyer et al. [1155] lies significantly lower than those from all other absolute studies while the values from Mellouki et al. [899] and from Kaiser et al. [688] lie slightly higher. Room temperature rate constants derived from the relative rate

experiments of Pritchard et al. [1081], Knox and Nelson [731], Atkinson and Aschmann [40], Atkinson and Ashmann [41], Tschuikow-Roux et al. [1323], Wallington et al. [1413], Beichert et al. [124], Hooshiyar and Niki [597], and Lin et al. [831] exhibit considerably more scatter even when recalculated based on the same current recommendation for the rate constant of the reference reactions. Nevertheless, most are encompassed within the 95% uncertainty limits recommended for the value of k(298 K). The relative rate results of Kelly et al. [698] and Lee and Rowland [782] are significantly lower than other room temperature measurements. The recommended value for E/R is taken from a combined fit to the data of Manning and Kurylo [862], Dobis and Benson [399], and Hickson and Keyser [580] after normalizing all three data sets to the recommended value of k(298 K). The data from Lewis et al. [816] and Lin et al. [831] below 300 K are encompassed by the 95% uncertainty bands. The temperature dependent studies by Pilgrim et al. [1058] and Bryukov et al. did not extend below room temperature. An extrapolation of the recommended Arrhenius parameters and the 95% uncertainty bands above room temperature encompasses the data of Pilgrim et al. but not those of Bryukov et al., which are characterized by a much stronger temperature dependence. The Arrhenius A-factor was calculated from recommended k(298 K) and E/R. (Table: 06-2, Note: 06-2) Back to Table

F68. Cl + $C_2H_5O_2$. Recommended value is based on results of Maricq et al. [872]. (Table: 94-26, Note: 94-26) Back to Table

F69. Cl + CH_3CH_2OH. The rate coefficient for this reaction has been studied at 298 K by four groups using a relative rate technique: Nelson et al. [955] (relative to Cl + cyclohexane), Wallington et al. [1413] (relative to Cl + C_2H_6), Edelbuttel-Einhaus et al. [429] (relative to Cl + C_2H_6), and Taatjes et al. [1269]. Nelson et al measured this rate constant relative to the Cl + cyclohexane while the others used the Cl + C_2H_6 reaction. Taatjes et al. also measured this rate coefficient by measuring the temporal profile of the HCl product. The agreement between these five measurements is quite good, yielding an average value that is recommended. The temperature dependence of this rate coefficient is based on the results of Taatjes et al., who studied this reaction above 298 K and found it to be essentially independent of temperature. We recommend the same independence of temperature at atmospheric temperatures.

This reaction can have three sets of products: CH_2CH_2OH + HCl, channel (a); CH_3CHOH, channel (b); and CH_3CH_2O channel (c). Taatjes et al. have deduced that channel (c) is negligible and that channel (a) is about 8% at 298 K. Therefore, the majority of reaction is expected to occur via channel (b). It is very unlikely that these branching ratios will change significantly at lower atmospheric temperatures. (Table: 02-25, Note: 02-25) Back to Table

F70. Cl + $CH_3C(O)OH$. Koch and Moortgat [733] have studied this reaction at room temperature using the relative rate technique. Deuterium substitution of the methyl hydrogens decreased the observed rate by a factor of 3.75. In addition, CO and CO_2 reaction products were observed in a stoichiometric ratio of 1:1. These observations were interpreted in terms of methyl hydrogen abstraction from acetic acid to form the $CH_2C(O)OH$ radical followed by reaction with O_2 to form a peroxy radical. Thermal decomposition of the peroxy radical produces HCHO, CO_2, and atomic H. In the laboratory system, the HCHO reacts with atomic chlorine to yield CO. (Table: 02-25, Note: 02-25) Back to Table

F71. Cl + CH_3CN. The recommendation is based on results of the study of Tyndall et al. [1353]. The results of this study, using both relative and absolute methods and measured over a wide range of experimental conditions are preferred over the results of earlier studies of Kurylo and Knable [756], Poulet et al. [1071], and Olbregts et al. [1009]. Product studies reported by Tyndall et al. show that reaction proceeds predominantly by hydrogen atom abstraction. (Table: 97-4, Note: 97-4) Back to Table

F72. Cl + $C_2H_5ONO_2$. Wallington et al. [1403] and Nielsen et al [981] have measured the rate of this reaction at room temperature relative to atomic chlorine reactions with ethyl chloride and ethane, respectively. The two studies are in excellent agreement and the recommended value is based on an average of the two. The values given in Wallington et al and Nielsen et al. were adjusted based on the currently accepted values of the reference rate constants. The temperature dependence is estimated by assuming an A-factor equal to approximately 20 times that of OH + CH_3ONO_2. This is

consistent with observed OH/Cl A-factor ratios for primary H-abstraction from alkanes. (Table: 02-25, Note: 02-25) Back to Table

F73. Cl + $CH_3CO_3NO_2$ (PAN). The recommended value is based on results of the relative rate study of Wallington et al. [1390]. In this study no reaction of PAN was observed in the presence of Cl atoms. These results are preferred over the results of the direct study of Tsalkani et al. [1322] using a discharge flow system with EPR detection of Cl atom decay (in which study the authors reported a rate constant of $(3.7\pm1.7) \times 10^{-13}$ cm^3 $molecule^{-1}$ s^{-1}). In both studies the major impurity in the PAN samples would be the alkane solvent. The presence of 0.1% tridecane in the PAN sample used by Tsalkani et al. could account for the observed Cl atom decay; however, solvent impurities in the PAN sample would be of no consequence in the relative rate study of Wallington et al. (Table: 92-20, Note: 92-20) Back to Table

F74. Cl + C_3H_8. The recommended value for k(298 K) is the mean of results of the competitive chlorination studies of Pritchard et al. [1081], Knox and Nelson [731], Kelly et al. [698], Tschuikow-Roux et al. [1324], Atkinson and Aschmann [40], Wallington et al. [1413], Beichert et al. [124], Hooshiyar and Niki [597], Tyndall et al. [1352] (two determinations), and Sarzynski and Sztuba [1146] and the absolute rate studies of Lewis et al. [816], Beichert et al. [124], Pilgrim et al. [1058]), Mellouki [899], and Hitsuda et al. [586]. The recommended E/R = 0 is based on the data obtained between 300 K and 400 K in the most recent and comprehensive study of Sarzynski and Sztuba.

The recommended k(298 K) values for both reaction channels are the means of the results from the competitive chlorination studies by Knox and Nelson [731], Kelly et al. [698], Tschuikow-Roux et al. [1324], Tyndall et al. [1352], and Sarzynski and Sztuba [1146]. The recommended E/R values are based on the data of Sarzynski and Sztuba Sztuba obtained between 300 K and 400 K. The Arrhenius A-factors were calculated from recommended k(298 K) and E/R. A sum of the recommended rate constant expressions for the two channels gives the same values as the rate constant expression recommended for the total reaction (A-factor: 1.45×10^{-10}, E/R: 0, k(298 K): 1.4×10^{-10},f(298 K): 1.07 g: 20). (Table: 06-2, Note: 06-2) Back to Table

F75. Cl + $CH_3C(O)CH_3$. The rate coefficient for this reaction has only been reported at 298 K. Wallington et al. [1413] and Olsson et al. [1010] report values of 2.37×10^{-12} and 1.69×10^{-12} cm^3 $molecule^{-1}$ s^{-1} at 298 K measured via relative rate methods. The only direct measurement of this rate constant is by Notario et al. [1002] who report a value of $(3.06 \pm 0.38) \times 10^{-12}$ cm^3 $molecule^{-1}$ s^{-1} at 298 K. Because of the reasons noted by Wallington et al. [1413], the value reported by Olsson et al. is suspect and is not considered here. The average of the results from Wallington et al. and Notario et al. is recommended for k(298 K). In the absence of temperature dependent measurements, based on analogy with other Cl atom reactions with halogenated hydrocarbons whose rate coefficients at 298 K are close to that for Cl + $CH_3C(O)CH_3$, we recommend an E/R value of 1000 K with a g value of 500 K. Such a temperature dependence is consistent with this reaction proceeding via H atom abstraction. This E/R and k(298 K) lead to an A factor of 7.7×10^{-11} cm^3 $molecule^{-1}$ s^{-1} . This A factor is the same as that for the reaction of Cl atom with ethane, which also contains six primary C–H bonds. End product studies clearly show that the products of this reaction are $CH_3C(O)CH_2$ and HCl. (Table: 02-25, Note: 02-25) Back to Table

F76. Cl + $C_2H_5CO_3NO_2$. Wallington et al. [1390] have measured this rate constant relative to Cl + CH_3Cl. The recommended value is adjusted from that given by Wallington et al. using the currently recommended value for the reference reaction rate constant. (Table: 02-25, Note: 02-25) Back to Table

F77. Cl + 1-$C_3H_7ONO_2$. Wallington et al. [1403] and Nielsen et al [981] have measured the rate of this reaction at room temperature relative to atomic chlorine reactions with ethyl chloride and ethane, respectively. The two studies are in excellent agreement and the recommended value is based on an average of the two. The values given in Wallington et al. and Nielsen et al. were adjusted based on the currently accepted values of the reference rates. The temperature dependence is estimated by assuming an A-factor equal to approximately 20 times that of OH + CH_3ONO_2. This is consistent with observed OH/Cl A-factor ratios for primary H-abstraction from alkanes. (Table: 02-25, Note: 02-25) Back to Table

F78. Cl + 2-$C_3H_7ONO_2$. This reaction has been measured by Wallington et al [1403] at 295 K relative to Cl + C_2H_5Cl. The reported ratio of 0.46 ± 0.03 has been converted to an absolute rate using the currently recommended value for the ethyl chloride reaction rate. The temperature dependence is estimated by assuming an A-factor equal to approximately 20 times that of OH + CH_3ONO_2. This is consistent with observed OH/Cl A-factor ratios for primary H-abstraction from alkanes. (Table: 02-25, Note: 02-25) Back to Table

F79. Cl + OClO. The data of Toohey [1315] are in good agreement with the results of Bemand et al. [126] at room temperature, and the recommended value at room temperature is the mean of the values reported in these two studies. The slight negative temperature dependence reported by Toohey [1315] is accepted but with error limits that encompass the temperature independence reported in the earlier study. (Table: 90-1, Note: 90-1) Back to Table

F80. Cl + ClOO. The recommended value is based on the results of studies by Mauldin et al. [887] and Baer et al. [62], in which ClOO was formed by the pulsed photolysis of Cl_2/O_2 mixtures and its overall loss rate was monitored by UV absorption. In both studies k was found to be independent of temperature. These results are preferred over the results of the earlier, indirect studies of Johnston et al. [674], Cox et al. [321], and Ashford et al. [36]. The earlier studies did show that the predominant reaction pathway is that yielding Cl_2 + O_2 as products. From the branching ratio data of Cox et al., Ashford et al., and Nicholas and Norrish [963], it can be estimated that this reaction channel constitutes 95% of the overall reaction with ClO + ClO the products of the minor (5%) reaction channel. (Table: 92-20, Note: 92-20) Back to Table

F81. Cl + Cl_2O. The preferred value was determined from results of the temperature-dependent study of Stevens and Anderson [1240] and the results of two independent absolute rate coefficient studies reported by Ray et al. [1107], which used the discharge flow-resonance fluorescence and discharge flow-mass spectrometric techniques. This value has been confirmed by Burrows and Cox [204], who determined the ratio
$k(Cl + Cl_2O)/k(Cl + H_2) = 6900$ in modulated photolysis experiments. The earlier value reported by Basco and Dogra [93] has been rejected. (Table: 94-26, Note: 94-26) Back to Table

F82. Cl + Cl_2O_2. The recommended value is that determined by Friedl (private communication) in a study using a DF-MS technique. It is in agreement with the value reported by Cox and Hayman [327] in a study using a static photolysis technique with photodiode array UV spectroscopy. (Table: 90-1, Note: 90-1) Back to Table

F83. Cl + HOCl. This recommendation is based on results over the temperature range 243–365 K reported by Cook et al. [309] and the room temperature result of Vogt and Schindler [1380]. There is a significant discrepancy in the reported values of the product branching ratios. Ennis and Birks [438] reported that the major reaction channel is that to give the products Cl_2 + OH with a yield of 91±6%, whereas Vogt and Schindler report this yield to be 24±11%, with the major reaction channel giving HCl + ClO as products. (Table: 94-26, Note: 94-26) Back to Table

F84. Cl + ClNO. The discharge flow-resonance fluorescence study of Abbatt et al. [4] provides the first reliable data on the temperature dependence. The laser photolysis-LMR study of Chasovnikov et al. [246] provides rate data for each Cl atom spin state, and they attribute the low value reported by Nelson and Johnston [954] in a laser flash photolysis-resonance fluorescence study to reaction of the Cl $^2P_{1/2}$ state. Adsorption and decomposition of ClNO on the walls of their static system may account for the very low value of Grimley and Houston [528]. The results of Clyne and Cruse [278] in a discharge flow-resonance fluorescence study are significantly lower than all recent results. The recommended value at room temperature is the mean of the values reported by Abbatt et al. [4], Chasovnikov et al. [246], Nesbitt et al. [961], and Kita and Stedman [718]. The recommended temperature dependence is from the study of Abbatt et al. [4]. (Table: 90-1, Note: 90-1) Back to Table

F85. Cl + $ClONO_2$. Recommended value is based on the results of Yokelson et al. [1499] and those of Margitan [865]. These results are in excellent agreement; the slightly higher values of Kurylo et al. [757] are encompassed within the stated uncertainties. Yokelson et al. report that at 298 K, more than 95% of this reaction proceeds by the reaction channel giving Cl_2 + NO_3 as products. (Table: 97-4, Note: 97-4) Back to Table

F86. Cl + CH_3Cl. The recommended value for k(298 K) is the mean of results of the absolute rate study of Manning and Kurylo [862] and the relative rate studies of Wallington et al. [1390], Beichert et al. [124], and Orlando [1022] (two independent determinations). The recommended temperature dependence is derived from a fit to the data from Manning and Kurylo [862] and from the two relative rate studies of Orlando [1022]. The Arrhenius A-factor was calculated from k(298 K) and E/R. While the 298 K results reported by Clyne and Walker [297] are in good agreement, the value of the activation energy derived by these researchers is significantly higher than that recommended, similar to the situation encountered for the Cl + CH_4 reaction. Hence, it is assumed that the discharge flow-mass spectrometric studies of these authors were subject to a systematic error. Both the room temperature measurements and E/R obtained between 300 K and 400 K by Bryukov et al. [190], from a study primarily focused at higher temperatures, are in good agreement with the recommendations. The early relative rate studies by Pritchard et al. [1081], Goldfinger et al. [514], Knox [729], and Tschuikow-Roux et al. [1323], were not used to derive the recommended parameters since they were performed at temperatures above 298 K and, with the exception of Pritchard et al., yield somewhat higher values for E/R. (Table: 06-2, Note: 06-2) Back to Table

F87. Cl + CH_2Cl_2. The recommended value for k(298 K) is an average of the values measured in the relative rate studies of Niki et al. [987], Beichert et al. [124], Catoire et al. [236], and Orlando [1022] (two independent determinations) and in the absolute rate study of Bryukov et al [190]. For this evaluation all of the relative rate measurements were recalculated based on the current recommendations for the rate constant of the reference reactions. The recommended value for E/R is taken from a fit to the data of Orlando and agrees with a fit to the data of Bryukov et al. (obtained at room temperature and above) up to 400 K. Above 400K, these latter data increase more rapidly with temperature. The relative rate studies of Goldfinger et al. [514], Knox [730], Tschuikow-Roux et al. [1323] were performed at temperatures above 298 K and yield significantly higher values for E/R, with the exception of one of the Knox et al. determinations (relative to CH_4), which gives a value of E/R in good agreement with that recommended. The results of Clyne and Walker [297] are higher than those from any other study and were not used in deriving the recommended parameters. (Table: 06-2, Note: 06-2) Back to Table

F88. Cl + $CHCl_3$. The recommended k(298 K) is an average of the values measured in the relative rate studies of Beichert et al. [124], Brahan et al. [172] (two independent determinations), Catoire et al. [236], and Orlando [1022] (two independent determinations). The recommended temperature dependence is derived from a fit to the two determinations by Orlando and agrees with a fit to the absolute rate data of Bryukov et al. [190] (obtained at room temperature and above) up to 400 K. Above 400 K, these latter data increase more rapidly with temperature. The room temperature value determined in the relative rate study by Yu and Wijnen [1500] is a factor of 50 greater than recommended and was not considered in the recommendation. The results of the absolute investigation of Clyne and Walker [297] are also higher and more scattered than those from most other studies and were not used, nor was the room temperature value derived from the study by Jeoung et al. [670], which is more than a factor of two lower than recommended. The relative rate study by Goldfinger et al. [514] performed near 500 K also resulted in values higher than those in more recent investigations. The relative rate study of Knox [730] yields a similiar temperature dependence to that recommended but with rate constant values systematically lower than other studies. The absolute study by Talhaoui et al. [1278] yielded a 298 K rate constant somewhat lower than recommended and a temperature dependence somewhat higher. For this evaluation all of the relative rate measurements were recalculated based on the current recommendations for the rate constant of the reference reactions. The Arrhenius A-factor has been derived from the recommended parameters. (Table: 06-2, Note: 06-2) Back to Table

F89. Cl + CH_3F (HFC-41). The recommended value for k(298 K) is an average of the values from the absolute rate study of Manning and Kurylo [862] and Hitsuda et al. [586] and the relative rate studies of Tschuikow-Roux et al. [1323], Tuazon et al. [1326], and Wallington et al. [1398]. The recommended value for E/R is based on the study of Tschuikow-Roux et al. conducted at room temperature and above. However, in formulating this recommendation, their reported value for the temperature dependence was reduced slightly (by approximately 100 K) to account for what appears to be a small systematic difference between the activation energies obtained in their similar

investigations of the Cl + CH_3Cl and Cl + CH_3Br reactions above room temperature and the recommendations that are based on data at 300 K and below. The temperature dependence reported by Manning and Kurylo is significantly lower, seemingly due to a shift in their data below 250 K. This lower value of E/R is not consistent with the recommended values of E/R for Cl + CH_3Cl and Cl + CH_3Br when compared with those for OH + CH_3F, OH + CH_3Cl, and OH + CH_3Br. Hence, it appears that the Manning and Kurylo data may have been influenced by some systematic error at the lower temperatures. (Table: 06-2, Note: 06-2) Back to Table

F90. Cl + CH_2F_2 (HFC-32). The recommended value for k(298 K) is from the relative rate study of Nielsen et al. [976], calculated using the rate constant for the reference reaction (Cl + CH_4) recommended in this evaluation. The room temperature value from the relative rate study of Tschuikow-Roux et al. [1324] is encompassed within the recommended 95% uncertainty limits. The temperature dependence is estimated from a comparison among the Cl and OH reactions with CH_2F_2, CH_2Cl_2, and CH_2FCl. The recommended value of E/R (identical to that for the OH + CH_2F_2 reaction) is slightly lower than that determined by Tschuikow-Roux et al. from data at room temperature and above. However, as discussed for other Cl + halomethane reactions, there appears to be a small systematic overestimation in the temperature dependencies determined by these authors. The A-factor has been calculated from the recommended parameters. (Table: 06-2, Note: 06-2) Back to Table

F91. Cl + CF_3H (HFC-23). The recommended upper limit for k(298 K) is based on results from the absolute rate study by Jourdain et al. [682] and from the relative rate study by Coomber and Whittle [310], which gives a room temperature value a factor of 50 smaller. (Table: 06-2, Note: 06-2) Back to Table

F92. Cl + CH_2FCl (HCFC-31). The recommended value for k(298 K) is an average of the room temperature results from the absolute rate study by Jourdain et al. [682] and the relative rate studies by Tuazon et al. [1326] and Wallington et al. [1408]. The temperature dependence is estimated from a comparison among the Cl and OH reactions with CH_2F_2, CH_2Cl_2, and CH_2FCl. The recommended value of E/R (essentially the same as that for the OH + CH_2FCl reaction) is slightly lower than that determined by Tschuikow-Roux et al. [1323], recalculated based on the current recommendation for the rate constant of the reference reaction (Cl + CH_4). However, as discussed for other Cl + halomethane reactions, there appears to be a small systematic overestimation in the temperature dependences determined by these authors. The A-factor has been calculated from the recommended parameters. (Table: 06-2, Note: 06-2) Back to Table

F93. Cl + $CHFCl_2$ (HCFC-21). The recommended value for k(298 K) is the average of the results from the relative rate study of Tuazon et al. [1326] and the absolute rate study of Talhaoui et al. [1278]. These results are preferred over the earlier room temperature results of Glavas and Heicklen [508]. The room temperature value of Jourdain et al. [682] is approximately 50% higher than the recommendation. The recommended value for E/R was obtained from a fit to the data of Talhaoui et al. The A-factor has been calculated from the recommended k(298 K) and E/R. (Table: 06-2, Note: 06-2) Back to Table

F94. Cl + CHF_2Cl (HCFC-22). The recommended value for k(298 K) is the mean of the values derived in the relative rate study by Tuazon et al. [1326] and in the absolute rate studies of Jourdain et al. [682] and Talhaoui et al. [1278] (which is assumed to supercede the earlier study by Sawerysyn et al. [1151]). The temperature dependence is from Talhaoui et al. The A-factor from that study has been adjusted to fit the recommended room temperature value. (Table: 06-2, Note: 06-2) Back to Table

F95. Cl + CH_3CCl_3. The recommended value for k(298 K) is an average of the results from the absolute rate study by Talhaoui et al. [1279] and the relative rate study by Platz et al. [1063]. The recommended value for E/R is derived from a fit to the data of Talhaoui et al. It is reasonably consistent with the value derived by Cillien et al. [267] in a relative rate study conducted over a very narrow temperature range above room temperature, but is somewhat smaller than the value derived in the relative rate study of Tschuikow-Roux et al. [1324]. (Table: 06-2, Note: 06-2) Back to Table

F96. Cl + CH_3CH_2F (HFC-161). The recommended values for both k(298 K) and E/R for each of the two reaction channels are averages of the individual values derived in the relative rate studies of Cadman et al. [217], Martens et al. [875], and Tschuikow-Roux et al. [1324], with each recalculated based on

the current recommendation for the rate constant of the reference reaction. The value for k(298 K) of the total reaction obtained from a sum of the two channels is in excellent agreement with the value obtained in the absolute rate study by Hitsuda et al. [586]. The parameters for the total reaction are: A-factor: 2.28×10^{-11}, E/R: 370, k(298 K): 6.6×10^{-12}, f(298 K): 1.1, g: 100. (Table: 06-2, Note: 06-2) Back to Table

F97. Cl + CH_3CHF_2 (HFC-152a). The recommended values for both k(298 K) and E/R for each of the two reaction channels are averages of the individual values derived in the relative rate studies of Cadman et al. [217], Martens et al. [875], and Yano and Tschuikow-Roux [1497], with each recalculated based on the current recommendation for the rate constant of the appropriate reference reaction. The value for k(298 K) for the overall reaction obtained by summing the values from the two channels is in excellent agreement with results of the room temperature relative rate studies of Wallington and Hurley [1404], and Tuazon et al. [1326]. The parameters for the overall reaction (Cl + $CH_3CHF_2 \rightarrow$ products) are: A-Factor: 6.0×10^{-12}, E/R: 960, k(298 K): 2.4×10^{-13}, f(298 K): 1.1, g: 100) (Table: 06-2, Note: 06-2) Back to Table

F98. Cl + CH_2FCH_2F (HFC-152). The recommended value for k(298 K) is an average of the values derived in the relative rate studies of Yano and Tschuikow-Roux [1497] and Wallington et al. [1408] (two determinations), after recalculating each one based on the current recommendation for the rate constant of the appropriate reference reaction. The recommended temperature dependence was determined from a fit to the data of Yano and Tschuikow-Roux, which were obtained at room temperature and above. The temperature dependence may exhibit curvature below room temperature, similar to that for OH + CH_2FCH_2F. Such curvature is most probably encompassed by the assigned uncertainty parameters. (Table: 06-2, Note: 06-2) Back to Table

F99. Cl + CH_3CFCl_2 (HCFC-141b). The recommended value for k(298 K) is an average of the values derived in the absolute rate studies of Talhaoui et al. [1279] by the discharge flow - mass spectrometric and the relative rate studies of Wallington and Hurley [1404] and Tuazon et al. [1326]. The room temperature results of Talhaoui et al. are assumed to supercede those of Sawerysyn et al. [1151]. The recommended E/R was obtained from a fit to the data of Talhaoui et al. The data of Warren and Ravishankara [1427] at room temperature agree with the recommendation. However, at higher temperatures the data exhibit considerable scatter apparently due to Cl atom regeneration from decomposition of the radical product (CH_2-$CFCl_2$). Hence, this study was not used in deriving the recommended parameters. (Table: 06-2, Note: 06-2) Back to Table

F100. Cl + CH_3CF_2Cl (HCFC-142b). The recommended value for k(298 K) is an average of the results of the relative rate studies of Wallington and Hurley [1404], and Tuazon et al. [1326], and the absolute rate studies of Jourdain et al. [682] and Talhaoui et al. [1279], which is assumed to supercede the earlier study by Sawerysyn et al. [1151]. The recommended temperature dependence is a fit to the data of Talhaoui et al. The A-factor from that study has been adjusted to fit the recommended room temperature value. (Table: 06-2, Note: 06-2) Back to Table

F101. Cl + CH_3CF_3 (HFC-143a). The recommended values for k(298 K) and E/R are based on results of the relative rate study of Tschuikow-Roux et al. [1324], recalculated based on the current recommendation for the rate constant of the reference reaction (Cl + CH_4). An upper limit for k(298 K) more than two orders of magnitude larger than the recommended value was derived by Hitsuda et al. [586]. (Table: 06-2, Note: 06-2) Back to Table

F102. Cl + CH_2FCHF_2 (HFC-143). The recommended values for k(298 K) and E/R for each of the two reaction channels are based on results of the relative rate study of Tschuikow-Roux et al. [1324] recalculated based on the current recommendation for the rate constant of the reference reaction (Cl + CH_4). The recommended parameters for the total reaction are derived from the sum of the recommended rate expressions for the two reaction channels. The parameters for the total reaction are: A-factor: 1.57×10^{-11}, E/R: 1720, k(298 K): 4.9×10^{-14}, f(298 K): 1.3, g: 200. (Table: 06-2, Note: 06-2) Back to Table

F103. Cl + CH_2ClCF_3 (HCFC-133a). The recommended value for k(298 K) is an average of the results from the absolute rate study of Jourdain et al. [679] and the relative rate study of Mogelberg et al. [926] (two determinations). The recommended value for E/R is a fit to the data of Jourdain et al. (Table: 06-2, Note: 06-2) Back to Table

F104. Cl + CH_2FCF_3 (HFC-134a). The recommended value for k(298 K) is an average of the results from the relative rate studies of Wallington and Hurley [1404], Tuazon et al. [1326], and Kaiser [684] and from the absolute rate study of Louis et al. [846], which is assumed to supercede the earlier study by Sawerysyn et al. [1151]. The recommended value for E/R is an average of the values determined by Kaiser et al. and Louis et al. (Table: 06-2, Note: 06-2) Back to Table

F105. Cl + CHF_2CHF_2 (HFC-134). The recommended value for k(298 K) is an average of the results from the relative rate studies of Nielsen et al. [977] and Yano and Tschuikow-Roux [1497], each recalculated based on the current recommendation for the rate constant of the appropriate reference reaction. The recommended value of E/R is determined from a fit to the data of Yano and Tschuikow-Roux. (Table: 06-2, Note: 06-2) Back to Table

F106. Cl + $CHCl_2CF_3$ (HCFC-123). The recommended value for k(298 K) is an average of the results from the absolute rate study of Warren and Ravishankara [1427] and the relative rate studies of Wallington and Hurley [1404] and Tuazon et al. [1326] each recalculated based on the current recommendation for the rate constant of the appropriate reference reaction. The recommended value of E/R is derived from a fit to the data of Warren and Ravishankara. (Table: 06-2, Note: 06-2) Back to Table

F107. Cl + $CHFClCF_3$ (HCFC-124). The recommended value for k(298 K) is an average of the results from the absolute rate study by Warren and Ravishankara [1427] and the relative rate study by Tuazon et al. [1326]. The recommended value for E/R is based on a fit to the data of Warren and Ravishankara. (Table: 06-2, Note: 06-2) Back to Table

F108. Cl + CHF_2CF_3 (HFC-125). The recommended value for k(298 K) is an average of the results from the relative rate studies of Tuazon et al. [1326], Sehested et al. [1172], and Edney and Driscoll [430], all conducted only at room temperature. The temperature dependence is estimated from a comparison among the Cl and OH reactions with CH_2FCF_3, CHF_2CHF_2, and CHF_2CF_3. The relative rate study by Coomber and Whittle [310] conducted between 303 K and 399 K corresponds to a value for k(298 K) a factor of 2.5 greater than that recommended. However, the value for E/R derived by these authors is only slightly lower than that estimated. (Table: 06-2, Note: 06-2) Back to Table

F109. ClO + O_3. There are two possible channels for this reaction: ClO + $O_3 \rightarrow$ ClOO + O_2 (k_1); and ClO + $O_3 \rightarrow$ OClO + O_2 (k_2). The recommended upper limit for k_1 at 298 K is based on results of the recent study by Stevens and Anderson [1239]. These authors also report that $k_1 = (4\pm2) \times 10^{-16}$ cm^3 $molecule^{-1}$ s^{-1} at 413 K. These data can be combined to derive the Arrhenius parameters $A = 2 \times 10^{-12}$ cm^3 $molecule^{-1}$ s^{-1} and E/R > 3600 K. The upper limit for k_2 is based on results reported by DeMore et al. [380] and Wongdontri-Stuper et al. [1483], the Arrhenius parameters for k_2 were estimated. (Table: 92-20, Note: 92-20) Back to Table

F110. ClO + H_2. The Arrhenius expression was estimated based on the ~600 K data of Walker (reported in Clyne and Watson [298]). (Table: 82-57, Note: 82-57) Back to Table

F111. ClO + NO. The absolute rate coefficients determined in the four discharge flow-mass spectrometric studies (Clyne and Watson [298], Leu and DeMore [804], Ray and Watson [1108] and Clyne and MacRobert [284]) and the discharge flow laser magnetic resonance study of Lee et al. [794] are in excellent agreement at 298 K, and are averaged to yield the preferred value. The value reported by Zahniser and Kaufman [1509] from a competitive study is not used in the derivation of the preferred value as it is about 33% higher. The magnitudes of the temperature dependences reported by Leu and DeMore [804] and Lee et al. are in excellent agreement. Although the E/R value reported by Zahniser and Kaufman [1509] is in fair agreement with the other values, it is not considered as it is dependent upon the E/R value assumed for the Cl + O_3 reaction. The Arrhenius expression was derived from a least squares fit to the data reported by Clyne and Watson, Leu and DeMore, Ray and Watson, Clyne and MacRobert, and Lee et al. (Table: 82-57, Note: 82-57) Back to Table

F112. ClO + NO_3. The recommended value is based on results reported by Cox et al. [315], Cox et al. [326] Biggs et al. [142], and Kukui et al. [741]. Biggs et al. report the rate constant to be independent of temperature, consistent with the results of Cox et al. [326]. This recent study of Kukui et al. supersedes the earlier study of Becker et al. [104] from the same laboratory, which had

indicated the major products to be OClO + NO_2. There is now agreement among all studies that the major reaction channel forms ClOO + NO_2 (see Biggs et al. [142] Cox et al. [326], and Kukui et al. From a study of the OClO/NO_3 system Friedl et al. [475] conclude that at 220 K the formation of ClOO + NO_2 is favored. (Table: 82-57, Note: 82-57) Back to Table

F113. ClO + N_2O. The Arrhenius expression was estimated based on the ~600 K data of Walker (reported in Clyne and Watson [298]). (Table: 82-57, Note: 82-57) Back to Table

F114. ClO + CO. The Arrhenius expression was estimated based on the ~600 K data of Walker (reported in Clyne and Watson [298]). (Table: 82-57, Note: 82-57) Back to Table

F115. ClO + CH_4. The Arrhenius expression was estimated based on the ~600 K data of Walker (reported in Clyne and Watson [298]). (Table: 82-57, Note: 82-57) Back to Table

F116. ClO + H_2CO. Poulet et al. [1078] have reported an upper limit of 10^{-15} cm^3 $molecule^{-1}$ s^{-1} for k at 298 K using the discharge flow-EPR technique. (Table: 81-3, Note: 81-3) Back to Table

F117. ClO + CH_3O_2. The recommended expressions for the overall rate constant is based on the results of Helleis et al. [566]. It is consistent with the room temperature measurements of Simon et al. [1190] and Kenner et al. [699]. The results of Kukui et al. [743] for the overall reaction are in agreement with the recommendation at room temperature, but these values show a slight negative temperature dependence in contrast with the slight positive temperature dependence recommended here. There is general agreement that the only important reaction channels are the two channels resulting in the production of ClOO + CH_3O (a) and CH_3OCl + O_2 (b). However, there is severe disagreement on their relative importance; at room temperature reaction channel (a) is reported to be the major channel by Helleis et al. [566], Simon et al. [1190], Kukui et al. and Helleis et al. [567] but it is reported to be the minor channel by Biggs et al. [140] and Daele and Poulet [340]. Because of this large discrepancy, no branching ratios are recommended. The branching ratio studies that go down to low temperatures (Helleis et al. [566], Kukui et al. , and Helleis et al. [567]) report that reaction channels (a) and (b) are both significant down to lower polar stratospheric temperatures. (Table: 97-4, Note: 97-4) Back to Table

F118. ClO + ClO. There are three bimolecular channels for this reaction: ClO + ClO $\rightarrow$ Cl_2 + O_2 (k_1); ClO + ClO $\rightarrow$ ClOO + Cl (k_2); and ClO + ClO $\rightarrow$ OClO + Cl (k_3). The recommended values for the individual reaction channels are from the study of Nickolaisen et al. [964]. This study, using a flash photolysis/long path ultraviolet absorption technique, is the most comprehensive study of this system, covering a wide range of temperature and pressure. These results are preferred over the results of earlier studies of the total bimolecular rate coefficient at low pressures by Clyne and Coxon [276], Clyne and White [302], and Clyne et al. [289], and those of other studies reported by Hayman et al. [560], Cox and Derwent [319], Simon et al. [1191], Horowitz et al. [599], and Horowitz et al. [600]. The room temperature branching ratio are k_1:k_2:k_3 = 0.29:0.50:0.21. The reaction exhibits both bimolecular and termolecular reaction channels (see entry in Table 2). The termolecular reaction dominates at pressures higher than about 10 torr. The equilibrium constant for formation of the Cl_2O_2 dimer is given in Table 3. (Table: 94-26, Note: 97-4) Back to Table

F119. HCl + $ClONO_2$. Results of four studies of the kinetics of this system have been published, in which the following upper limits to the homogeneous bimolecular rate constant were reported: 10^{-19} cm^3 $molecule^{-1}$ s^{-1} by a static wall-less long-path UV absorption technique and a steady-state flow FTIR technique (Molina et al. [927]); 5×10^{-18} using a flow reactor with FTIR analysis (Friedl et al. [473]); and 8.4×10^{-21} using a static photolysis system with FTIR analysis (Hatakeyama and Leu [558] and Leu et al. [805]), and 1.5×10^{-19} by FTIR analysis of the decay of $ClONO_2$ in the presence of HCl in large-volume (2500 and 5800 liters) Teflon or Teflon-coated chambers (Atkinson et al. [41]). Earlier, Birks et al. [146] had reported a higher upper limit. All studies found this reaction to be catalyzed by surfaces. The differences in the reported upper limits can be accounted for in terms of the very different reactor characteristics and detection sensitivities of the various studies. The homogeneous reaction is too slow to have any significant effect on atmospheric chemistry. (Table 87-41, Note: 87-41) Back to Table

F120. CH_2ClO + O_2. The CH_2ClO radical is reported to be resistant to unimolecular dissociation into Cl + CH_2O products, according to chain reaction/product analysis studies by Sanhueza and Heicklen

[1143] and Niki et al. [987] and kinetics studies by Catoire et al. [235]. The recommendation is based on the work of Kaiser and Wallington [689] who studied the competition between reaction with O_2 and HCl elimination in a complex photochemical reaction system using FTIR detection of stable products. The recommendation is a factor of 5 higher than estimated using the empirical relationship given by Atkinson and Carter [47]. The fate of CH_2ClO in the atmosphere is this reaction with O_2. (Table: 94-26, Note: 94-26) Back to Table

F121. CH_2ClO_2 + HO_2. The recommendation is based on the measurement reported by Catoire et al. [235], who used pulsed photolysis with UV absorption detection at 1 atm pressure and 251–588 K. (Table: 94-26, Note: 94-26) Back to Table

F122. CH_2ClO_2 + NO. The recommendation is based on the value reported by Sehested et al. [1174], who used pulsed radiolysis and UV absorption detection of NO_2 to measure the rate coefficient. The temperature dependence is estimated by analogy to similar RO_2 + NO reactions. (Table: 94-26, Note: 94-26) Back to Table

F123. CCl_3O_2 + NO. The recommendation is based upon the measurements of Ryan and Plumb [1130] and Dognon et al. [404], who agree well at room temperature. The temperature dependence is derived from the data of Dognon et al., who covered the temperature range 228–413 K. The CCl_3O primary product of the reaction of CCl_3O_2 with NO decomposes rapidly to eliminate Cl, according to Lesclaux et al. [799]. (Table: 94-26, Note: 94-26) Back to Table

F124. CCl_2FO_2 + NO. The recommendation is based on the measurements made by Dognon et al. [404] using pulsed photolysis with mass spectrometry detection at 1–10 torr and 228–413 K. These results supersede the earlier study of Lesclaux and Caralp [797]. The CCl_2FO radical primary product of the CCl_2FO_2 + NO reaction is reported by Lesclaux et al. [799] and Wu and Carr [1487] to rapidly decompose to eliminate Cl and to give the products indicated. (Table: 94-26, Note: 94-26) Back to Table

F125. $CClF_2O_2$ + NO. The recommendation is based on the measurements made by Dognon et al. [404], who used pulsed photolysis with mass spectrometry detection at 1–10 torr and 228–413 K, and Sehested et al. [1174], who used pulsed radiolysis with UV absorption detection of the NO_2 product at one atm and 298 K. Wu and Carr [1487] observed the $CClF_2O$ radical primary product to rapidly dissociate to CF_2O and Cl. (Table: 94-26, Note: 94-26) Back to Table

G1. O + BrO. The preferred value is based on the value reported by Thorn et al. [1300] using a dual laser flash photolysis/long path absorption/resonance fluorescence technique. Clyne et al. [291] reported a value approximately 40% lower. (Table: 97-4, Note: 97-4) Back to Table

G2. O + HBr. Results of the flash photolysis-resonance fluorescence study of Nava et al. [945] for 221–455 K and the laser flash photolysis-resonance fluorescence study of Nicovich and Wine [972] for 250–402 K provide the only data at stratospheric temperatures. Results reported include those of Singleton and Cvetanovic [1198] for 298–554 K by a phase-shift technique, and discharge flow results of Brown and Smith [182] for 267–430 K and Takacs and Glass [1272] at 298 K. The preferred value is based on the results of Nava et al., as well as those of Nicovich and Wine and those of Singleton and Cvetanovic over the same temperature range, since these results are less subject to complications due to secondary chemistry than are the results using discharge flow techniques. The uncertainty at 298 K has been set to encompass these latter results. (Table: 90-1, Note: 90-1) Back to Table

G3. O + HOBr. Recommended room temperature value is the mean of results of Monks et al. [1300] and Kukui et al. [742]. The temperature dependence is from Nesbitt et al. [960]. The A-factor from that study has been adjusted to fit the recommended room temperature value. Kukui et al. determined that the Br atom abstraction channel is the only pathway at room temperature. (Table: 97-4, Note: 97-4) Back to Table

G4. O + $BrONO_2$. The recommendation is based on the study of Soller et al. [1221] that employed the laser flash photolysis – res onance fluorescence technique and covered the temperature range 227 – 339 K. The recommended uncertainty parameters are larger than those reported by Soller et al. pending independent confirmation of their results. Burkholder [198] has coupled laser flash

photolysis with detection of NO_3 by long path absorption spectroscopy to show that the NO_3 yield is >0.85 at 298 K. NEW ENTRY. Back to Table

G5. OH + Br_2. The recommended room temperature value is the average of the values reported by, Poulet et al. [1073], Loewenstein and Anderson [841], Gilles et al. [501] and Bedjanian et al. [111]. The temperature dependence is from an average of the E/R values of Gilles et al. and Bedjanian et al. The results of Boodaghians et al. [159] were not considered. Loewenstein and Anderson determined that the exclusive products are Br + HOBr. (Table: 06-2, Note: 06-2) Back to Table

G6. OH + BrO. The preferred value of k_{298} is from an average of the results of Gilles et al. [502] and Bedjanian et al. [116]. The only temperature dependence study is from Bedjanian et al. The recommendation is based on their results. The likely products of this reaction are Br + HO_2. Bedjanian et al. attempted to measure the branching ratio for HBr formation but there were significant problems from secondary chemistry. An upper limit of 3% was reported for the HBr yield. (Table: 06-2, Note: 06-2) Back to Table

G7. OH + HBr. The preferred value at room temperature is the average of the values reported by Ravishankara et al. [1101] using FP-RF, by Jourdain et al. [681] using DF-EPR, by Cannon et al. [222] using FP-LIF, by Ravishankara et al. [1104] using LFP-RF and LFP-LIF and Bedjanian et al. [114]. Values reported by Takacs and Glass [1273] and by Husain et al. [624] as well as the preliminary value of Smith and Zellner [1217] are a factor of 2 lower and were not included in the derivation of the preferred value. The recommendation for the temperature dependence is derived from the data of Bedjanian et al. [114]. This study obtained a small negative temperature dependence which is in qualitative agreement with the Laval nozzle studies of Sims et al. [1196], Atkinson et al. [38] and Jaramillo et al. [652] over the 200-300 K temperature range. The data of Ravishankara et al. [1101] show no dependence on temperature over the range 249–416 K. (Table: 06-2, Note: 06-2) Back to Table

G8. OH + CH_3Br. The recommended rate expression is derived from a combined fit to the data from the relative rate study of Hsu and DeMore [614] (recalculated based on the current recommendation for the rate constant for the OH + CH_3CHF_2 reference reaction, as discussed in the note for that reaction) and the absolute determinations by Chichinin et al. [261], Mellouki et al. [909] and Zhang et al. [1525]. The results of these extensive studies are in excellent agreement and are preferred over the higher values reported in the earlier studies of Davis et al. [358] and Howard and Evenson [606]. (Table: 02-25, Note: 02-25) Back to Table

G9. OH + CH_2Br_2. The recommended value for k(298 K) is an average of the values from the absolute studies of Mellouki et al. [909] and Zhang et al. [1519] and from the relative rate measurements of DeMore [376] (recalculated based on the current recommendation for the rate constant for the OH + CH_2Cl_2 reference reaction) and Orlando et al. [1025] (recalculated based on the current recommendation for the rate constant for the OH + $CH_3(CO)CH_3$ reference reaction). The recommended value of E/R is from the study of Mellouki et al. [909]. (Table: 02-25, Note: 02-25) Back to Table

G10. OH + $CHBr_3$. The recommended rate expression is derived from a fit to the data from the relative rate study of DeMore [376] (recalculated based on the current recommendation for the rate constant for the OH + CH_2Cl_2 reference reaction). The results of Orkin et al. [1017] are higher by a factor of 2 but have the same temperature dependence. They are encompassed within the 2σ confidence limits. (Table: 02-25, Note: 02-25) Back to Table

G11. OH + CHF_2Br. The recommended values for k(298 K) and E/R are derived from a fit to the data of Talukdar et al. [1280] (two studies), Orkin and Khamaganov [1016], and Hsu and DeMore [615] (a relative rate measurement recalculated using the current recommendation for the rate constant for the OH + CH_4 reference reaction). These data are preferred over the consistently higher results reported by Brown et al. [178]. (Table: 02-25, Note: 02-25) Back to Table

G12. OH + CH_2ClBr. The recommended value for k(298 K) is an average of the values from two relative rate studies by DeMore [376] (recalculated based on the current recommendation for the rate constant for the OH + CH_2Cl_2 reference reaction) and Bilde et al. [144] (recalculated using the current recommendation for the rate constant for the OH + CH_2Br_2 reference reaction) and two

absolute determinations by Orkin et al. [1018], all of which are in good agreement. The recommended E/R is obtained from a fit to the data of DeMore and Orkin et al. The A factor was then calculated. (Table: 02-25, Note: 02-25) Back to Table

G13. OH + CF_2ClBr. The A-factor was estimated, and a lower limit for E/R was derived using the upper limit for the rate constant at 298 K reported by Burkholder et al. [201] in a study using pulsed photolysis-LIF and DF-LMR techniques. A less sensitive upper limit was reported by Clyne and Holt [283]. (Table: 02-25, Note: 02-25) Back to Table

G14. OH + CF_2Br_2. The A-factor was estimated, and a lower limit for E/R was derived by using the upper limit for the rate constant at 298 K reported by Burkholder et al. [201] in a study using pulsed photolysis-LIF and DF-LMR techniques. (Table: 02-25, Note: 02-25) Back to Table

G15. OH + CF_3Br. The A-factor was estimated and a lower limit for E/R was derived by using the upper limit for the rate constant at 460 K reported by Orkin and Khamaganov [1016]. These parameters were then used to calculate an upper limit for k(298 K). The upper limit for k(298 K) determined by Burkholder et al. [201] in a study using pulsed photolysis-LIF and DF-LMR techniques at room temperature is understandably higher. A less sensitive upper limit was also reported by Le Bras and Combourieu [778]. (Table: 02-25, Note: 02-25) Back to Table

G16. OH + CH_2BrCH_3. The recommended values for k(298 K) and E/R are derived from a fit to the data ($T \leq 300$ K) of Herndon et al. [573]. These data suggest a curvature of the Arrhenius plot similar to that found for the OH reaction with CH_3CH_2F. The data of Qiu et al. [1082] (which include earlier data reported by the same research group in Xing et al. [1492]) were not used because they were obtained mainly at above room temperature and exhibit a very steep temperature dependence resulting in a value for E/R that is larger than the E/R value obtained from data at $T > 298$ K for the OH reaction with CH_3CH_2F. The k(300 K) value reported by Donaghy et al. [409] seems too low for this reaction when compared with the recommendation for presumably slower (and better studied) OH reaction with CH_3CH_2F. (Table: 02-25, Note: 02-25) Back to Table

G17. OH + CH_2BrCF_3. The recommended values for k(298 K) and E/R are from a combined fit to the data of Nelson et al. [949] and Orkin and Khamaganov [1016]. (Table: 02-25, Note: 02-25) Back to Table

G18. OH + $CHFBrCF_3$. The recommended rate expression is derived from a combined fit to the data (below 400°K) of Orkin and Khamaganov [1016] and Brown et al. [178]. (Table: 02-25, Note: 02-25) Back to Table

G19. OH + $CHClBrCF_3$. The recommended rate expression is derived from a fit to the data of Orkin and Khamaganov [1016] (for $T \leq 400$ K). The room temperature value measured by Brown et al. [179] lies somewhat higher than this recommendation but is encompassed within the 2σ confidence limits. (Table: 02-25, Note: 02-25) Back to Table

G20. OH + $CHFClCF_2Br$. The recommended rate expression is derived from a fit to the data from the relative rate study of DeMore [376] (recalculated based on the current recommendation for the rate constant for the OH + CH_3CCl_3 reference reaction). (Table: 02-25, Note: 02-25) Back to Table

G21. OH + CF_2BrCF_2Br. The A-factor was estimated and a lower limit for E/R was derived by using the upper limit for the rate constant at 460 K reported by Orkin and Khamaganov [1016]. These parameters were then used to calculate an upper limit for k(298 K). The upper limit for k(298 K) determined by Burkholder et al. [201] in a study using pulsed photolysis-LIF and DF-LMR techniques at room temperature is understandably higher. (Table: 02-25, Note: 02-25) Back to Table

G22. OH + $CH_2BrCH_2CH_3$. The recommended values for k(298 K) and E/R are derived from a fit to the data ($T \leq 300$ K) from Donaghy et al. [409], Teton et al. [1294], Nelson et al. [950], Herndon et al. [573], Gilles et al. [500], and Kozlov et al. [738]. Significant curvature in the Arrhenius plot has been observed over the 480 to 210 K temperature range, due to the three different hydrogen-abstraction reaction channels that occur. These channels have been quantified in the study of Gilles et al. In spite of the noticeable Arrhenius curvature, the data below 300 K can be well represented by a two-parameter Arrhenius fit. (Table: 02-25, Note: 02-25) Back to Table

G23. OH + $CH_3CHBrCH_3$. The recommended values for k(298 K) and E/R are averages of the parameters derived from a fit to the data (T ≤ 300 K) of Herndon et al. [573] and Kozlov et al. [738] which are in excellent agreement. The A factor was then calculated. The room temperature relative rate determination by Donaghy et al. [409] and the absolute temperature dependent data of Teton et al. [1294] lie systematically higher than those from these two more recent studies. Significant curvature in the Arrhenius plot has been observed over the 480 K to 210 K temperature range by Kozlov et al., presumably due to the two different hydrogen-abstraction reaction channels that occur. In spite of the noticeable Arrhenius curvature, the data below 300 K can be well represented by a two-parameter Arrhenius fit. (Table: 02-25, Note: 02-25) Back to Table

G24. HO_2 + Br. The room temperature rate constant is obtained from an average of the results of Laverdet et al. [774], Toohey et al. [1317] and Bedjanian et al. [115]. The results of Posey et al. [1069] were not considered because of problems with the experimental method. The results of Poulet et al. [1074] were not considered because of complications associated with secondary reactions. The recommendation for the temperature dependence is based on the results of Bedjanian et al. [115]. (Table: 06-2, Note: 06-2) Back to Table

G25. HO_2 + BrO. The recommendation is based on results of the temperature-dependent studies of Elrod et al. [435], Li et al. [820] and Bedjanian et al. [117]. It is assumed that the Bedjanian et al. results superce those of Larichev et al. [770] since the same experimental technique was used, and the same research group was involved in both studies. The recommended room temperature value is the mean of the values reported in these studies, as well as those of Cronkhite et al. [334] and Bloss et al. [155]. The room temperature value of Bridier et al. [176], which was not obtained under pseudo–first-order decay conditions, was not included in derivation of the recommendation. Bedjanian et al. have determined an upper limit of 0.4% for production of HBr and O_3 at 298 K. From a study of the reverse reaction above room temperature, Mellouki et al. [908] determined by extrapolation that the yield of HBr + O_3 is an insignificant fraction (<0.01%) of the total reaction down to 200 K. (Table: 06-2, Note: 06-2) Back to Table

G26. NO_3 + HBr. The recommended upper limit is the upper limit reported by Mellouki et al. [905] in a study using DF-EPR techniques. This upper limit shows that this reaction is of negligible importance in stratospheric chemistry. Canosa-Mas et al. [225] reported a value that is consistent, within experimental error, with the upper limit of Mellouki et al. (Table: 90-1, Note: 92-20) Back to Table

G27. Cl + CH_2ClBr. The recommended value for k(298 K) is an average of two relative rate determinations by Bilde et al. [144] (recalculated based on the current recommendation for the rate constants of the reference). The temperature dependence is estimated from a comparison with the reactions of Cl with CH_2Cl_2 and CH_2Br_2. The relative rate investigation by Tschuikow-Roux et al. [1323] gives a value for k(298 K) only slightly larger than recommended, but a temperature dependence that is significantly stronger and inconsistent with the that recommended for the Cl + CH_2Cl_2 and Cl + CH_2Br_2 reactions. (Table: 06-2, Note: 06-2) Back to Table

G28. Cl + CH_3Br. The recommended value for k(298 K) is an average of the results from the absolute rate studies of Gierczak et al. [494], Kambanis et al. [691] and Piety et al. [1057] and from the relative rate study of Orlando et al. [1025]. The recommended value for E/R is based on a combined fit to these same four studies restricted to temperatures of 300 K and below. Results of the relative rate study Tschuikow-Roux et al. [1323] were not used in derivation of the recommended values since they appear to be systematically higher than the results of the other investigations. The products of this reaction are expected to primarily CH_2Br and HCl. The possible production of CH_3Cl + Br is very small in the atmosphere [515]. (Table: 06-2, Note: 06-2) Back to Table

G29. Cl + CH_2Br_2. The recommended value for k(298 K) is an average of the results from the absolute rate studies of Gierczak et al. [494] and Kambanis et al. [691] and from the three relative rate experiments of Orlando et al. [1025]. The recommended value for E/R is based on a combined fit to the data (T < 300 K) from these same studies after normalizing each one to the recommended value for k(298 K). Results of the relative rate study of Tschuikow-Roux et al. [1323] were not used in derivation of the recommended parameters since they are significantly greater at 298 K and

correspond to a temperature dependence substantially stronger than derived from the data of other investigations. (Table: 06-2, Note: 06-2) Back to Table

G30. Cl + $CHBr_3$. The recommended parameters are based on the only reported study of this reaction by Kambanis et al. [691], who employed a very low pressure reactor and monitored reactants and products using mass spectrometry. (Table: 06-2, Note: 06-2) Back to Table

G31. Br + O_3. The results reported for k(298 K) by Clyne and Watson [300], Leu and DeMore [803], Michael et al. [915], Michael and Payne [920], and Toohey et al. [1318] are in excellent agreement. The preferred value at 298 K is derived by taking a simple mean of these five values. The temperature dependences reported for k by Leu and DeMore and by Toohey et al. are in good agreement, but they can only be considered to be in fair agreement with those reported by Michael et al. and Michael and Payne. The preferred value was synthesized to best fit all the data reported from these five studies. The results of Nicovich et al. [968] are in excellent agreement with this recommendation. (Table 87-41, Note: 90-1) Back to Table

G32. Br + H_2O_2. The recommended upper limit to the value of the rate constant at room temperature is based on results reported in the study by Toohey et al. [1317] using a discharge flow-resonance fluorescence/laser magnetic resonance technique. Their upper limit determined over the temperature range 298–378 K is consistent with less sensitive upper limits determined by Leu [813] and Posey et al. [1069] using the discharge flow-mass spectrometric technique. The much higher value reported by Heneghan and Benson [569] may result from the presence of excited Br atoms in the very low pressure reactor. The pre-exponential factor was chosen to be consistent with that for the Cl + H_2O_2 rate constant, and the E/R value was fitted to the upper limit at 298 K. Mellouki et al. [908] have measured the rate of the reverse reaction. (Table 87-41, Note: 94-26) Back to Table

G33. Br + NO_3. The recommended value is that reported by Mellouki et al. [905] in a study using DF-DPR techniques. (Table: 90-1, Note: 92-20) Back to Table

G34. Br + H_2CO. There have been two studies of this rate constant as a function of temperature: Nava et al. [947], using the flash photolysis–resonance fluorescence technique, and Poulet et al. [1072], using the discharge flow-mass spectrometric technique. These results are in reasonably good agreement. The Arrhenius expression was derived from a least squares fit to the data reported in these two studies. The higher room temperature value of Le Bras et al. [779], using the discharge flow–EPR technique, has been shown to be in error due to secondary chemistry (Poulet et al.). (Table: 82-57, Note: 82-57) Back to Table

G35. Br + OClO. The recommended value at room temperature is the mean of the values reported by Clyne and Watson [301] and Toohey [1315]. In the study of Clyne and Watson, correction for the effect of the rapid reverse reaction was required. The temperature dependence reported by Toohey [1315] is accepted but with increased error limits. (Table: 90-1, Note: 90-1) Back to Table

G36. Br + Cl_2O. The recommended value is based on results reported by Stevens and Anderson [1240] and by Sander and Friedl [1136], which are in good agreement. (Table: 94-26, Note: 94-26) Back to Table

G37. Br + Cl_2O_2. The recommended value is that determined by Friedl (private communication) in a study using a DF-MS technique. (Table: 90-1, Note: 90-1) Back to Table

G38. BrO + O_3. There have been two recent studies of this reaction. Rattigan et al. [1088] report an overall rate constant of ~10^{-17} cm^3 $molecule^{-1}s^{-1}$ over the temperature range 318–343 K. Rowley et al. [1127] report a room temperature upper limit of 2×10^{-17} cm^3 $molecule^{-1}s^{-1}$. Both papers report a value of ~2×10^{-18} cm^3 $molecule^{-1}$ s^{-1} for the channel to produce OBrO + O_2. The recommended upper limit of 2×10^{-17} cm^3 $molecule^{-1}s^{-1}$ is a factor of 2.5 less than the previously recommended upper limit of 5×10^{-17}, which was based on Mauldin et al. [888]. The pre-exponential factor was estimated, and E/R was calculated. (Table: 97-4, Note: 97-4) Back to Table

G39. BrO + NO. The results of the three low pressure mass spectrometric studies (Clyne and Watson [300]; Ray and Watson [1108]; Leu [811]) and the high pressure UV absorption study (Watson et al. [1437]), which all used pseudo–first-order conditions, are in excellent agreement at 298 K and are thought to be much more reliable than the earlier low pressure UV absorption study (Clyne and Cruse [277]). The results of the two temperature-dependence studies are in good agreement and

both show a small negative temperature dependence. The preferred Arrhenius expression was derived from a least squares fit to all the data reported in the four recent studies. By combining the data reported by Watson et al. with those from the three mass spectrometric studies, it can be shown that this reaction does not exhibit any observable pressure dependence between 1 and 700 torr total pressure. The temperature dependences of k for the analogous ClO and HO_2 reactions are also negative and are similar in magnitude. (Table: 82-57, Note: 82-57) Back to Table

G40. BrO + NO_3. The recommended value is the geometric mean of the lower and upper limits reported by Mellouki et al. [905] in a study using DF-DPR techniques. These reported limits are encompassed within the indicated uncertainty limits. (Table: 90-1, Note: 92-20) Back to Table

G41. BrO + ClO. Friedl and Sander [474], using DF/MS techniques, measured the overall rate constant over the temperature range 220–400 K and also over this temperature range determined directly branching ratios for the reaction channels producing BrCl and OClO. The same authors in a separate study using flash photolysis–ultraviolet absorption techniques (Sander and Friedl [1136]) determined the overall rate constant over the temperature range 220–400 K and pressure range 50–750 torr and also determined at 220 K and 298 K the branching ratio for OClO production. The results by these two independent techniques are in excellent agreement, with the overall rate constant showing a negative temperature dependence. Toohey and Anderson [1316], using DF/RF/LMR techniques, reported room temperature values of the overall rate constant and the branching ratio for OClO production. They also found evidence for the direct production of BrCl in a vibrationally excited Π state. Poulet et al. [1070], using DF/MS techniques, reported room temperature values of the overall rate constant and branching ratios for OClO and BrCl production. Overall room temperature rate constant values reported also include those from the DF/MS study of Clyne and Watson [301] and the very low value derived in the flash photolysis study of Basco and Dogra [91] using a different interpretation of the reaction mechanism. The recommended Arrhenius expressions for the individual reaction channels are taken from the study of Friedl and Sander [474] and Turnipseed et al. [1339]. These studies contain the most comprehensive sets of rate constant and branching ratio data. The overall rate constants reported in these two studies are in good agreement (20%) at room temperature and in excellent agreement at stratospheric temperatures. Both studies report that OClO production by channel (1) accounts for 60% of the overall reaction at 200 K. Both studies report a BrCl yield by channel (3) of about 8%, relatively independent of temperature. The recommended expressions are consistent with the body of data from all studies except those of Hills et al. [581] and Basco and Dogra [91]. (Table 00-3, Note: 00-3) Back to Table

G42. BrO + BrO. Measurements of the overall rate constant can be divided into categories—those in which BrO was monitored by UV absorption and those in which BrO was monitored by mass spectrometer. Gilles et al. [504] have re-analyzed the results of the UV absorption studies and scaled the reported values of the rate constant to the UV absorption cross sections reported in their paper. When scaled in this manner, the room temperature rate constant values reported in the UV absorption studies (Sander and Watson [1139], Mauldin et al. [888], Bridier et al. [176], Rowley et al. [1127], Laszlo et al. [772], and Gilles et al.) come into very good agreement among themselves and also with results of the mass spectrometric studies of Clyne and Watson [300] and Lancar et al. [765]. This provides the basis for the recommended room temperature value. The temperature dependence is based on results of Sander and Watson, Turnipseed et al. [1338] and Gilles et al. The results of Harwood et al. [556] are in good agreement with the recommendation.

There are two possible bimolecular channels for this reaction: BrO + BrO $\rightarrow$ 2Br + O_2 (k_1) and BrO + BrO $\rightarrow$ Br_2 + O_2 (k_2). The partitioning of the total rate constant into its two components, k_1 and k_2, has been measured at room temperature by Sander and Watson [1139], Turnipseed et al. [1338] and Lancar et al. [765], by Jaffe and Mainquist [648] from 258 to 333 K, by Cox et al. [330] from 278 to 348 K and by Mauldin et al. [888] from 220 to 298 K. All are in agreement that k_1/k = 0.85±0.03 at 298 K. From the values of k_1/k = 0.85 at 298 K (all studies) and 0.68 at 220 K (Mauldin et al. and Cox et al. extrapolated), one can derive the temperature-dependent expression $k_1/k = 1.60 \exp(-190/T)$. From the recommended Arrhenius expression for the overall rate constant $k = k_1 + k_2$ and the expression for the branching ratio k_1/k, one can derive the following Arrhenius expressions for the individual reaction channels: $k_1 = 2.4 \times 10^{-12} \exp(40/T)$ cm^3 molecule^{-1}s^{-1} and $k_2 = 2.8 \times 10^{-14} \exp(860/T)$ cm^3 molecule^{-1}s^{-1}. (Table: 97-4, Note: 97-4) Back to Table

G43. CH_2BrO_2 + NO. The recommendation is based on the 298 K measurement of Sehested et al. [1174], who used pulsed radiolysis with UV absorption detection of the NO_2 product formation rate. The temperature dependence is estimated based on analogy to similar RO_2 + NO reactions. The CH_2BrO product has been shown to undergo rapid unimolecular decomposition to yield CH_2O + Br by Chen et al. [250] and Orlando et al. [1024]. The domination of this channel over the reaction of CH_2BrO with O_2 is consistent with the fate of other alkoxy radicals (Chen et al. and Orlando et al.), but contradicts the earlier result of Nielson et al. [978]. Back to Table

H1. O + I_2. Based on the room temperature data of Ray and Watson [1108] and Laszlo et al. [773]. The molecular beam study of Parrish and Herschbach [1037] suggests a zero activation energy, consistent with the near gas kinetic value of k at 298 K. (Table: 97-4, Note: 97-4) Back to Table

H2. O + IO. Based on results of Laszlo et al. [773], the only reported study of this rate constant. This value was derived from modeling a system in which the concentrations of I_2 and IO were monitored simultaneously. This rate constant is a factor of 4 greater than the values for the corresponding reactions of O with ClO and BrO. (Table: 97-4, Note: 97-4) Back to Table

H3. OH + I_2. Based on the data of Loewenstein and Anderson [842] and Jenkin et al. [658]. (Table: 94-26, Note: 94-26) Back to Table

H4. OH + HI. Based on the data of Lancar et al. [767] and MacLeod et al. [857]. (Table: 94-26, Note: 94-26) Back to Table

H5. OH + CH_3I. The recommended rate expression is derived from a fit to the data of Brown et al. [180], the only reported study of this reaction. (Table: 02-25, Note: 02-25) Back to Table

H6. OH + CF_3I. The recommended rate expression is derived from a fit to the data of Gilles et al. [503]. The results from the studies by Garraway and Donovan [485] and Berry et al. [131] were not used in deriving the recommendation as the results were possibly influenced by reactant photolysis. The room temperature value from the discharge flow/resonance fluorescence study of Brown et al. [180] agrees within the 2σ limits. (Table: 02-25, Note: 02-25) Back to Table

H7. HO_2 + I. Based on the data of Jenkin et al. [663], the only reported study of this reaction. (Table: 94-26, Note: 94-26) Back to Table

H8. HO_2 + IO. The recommended value is the average of the values reported by Jenkin et al. [662] and Maguin et al. [860]. (Table: 94-26, Note: 94-26) Back to Table

H9. NO_3 + HI. No recommendation is given, based on the potential for severe complications resulting from secondary chemistry in the only reported study of the reaction (Lancar et al. [767]). (Table: 94-26, Note: 94-26) Back to Table

H10. Cl + CH_3I. This reaction, thought to be a simple H abstraction reaction, has been shown by Ayhens et al. [59] to be quite complex. At low temperatures, Cl atom reversibly adds to CH_3I to form CH_3ICl. Thus, there are at least two channels for this reaction,

$$Cl + CH_3I \rightarrow CH_2I + HCl \qquad (a)$$

$$Cl + CH_3I \leftrightarrow CH_3ICl \qquad (b)$$

The rate coefficient for channel (a) has been measured by Ayhens et al. above 364 K, Kambanis et al. [691] between 273 and 363 K, Bilde and Wallington [143] at 298 K, and Cotter et al. [312] at 298 K. The recommendation is based on these studies.

Under atmospheric conditions reaction (b) to form the adduct is about two orders of magnitude faster than reaction (a). However, the fate of the CH_3ICl adduct in the atmosphere is unclear. Its lifetime, based on the studies of Ayhens et al., can be as long as a few seconds at 200 K and a few hundred Torr pressure. Therefore, it is possible that it could react with O_2 or be photolyzed. At 298 K, in one atmosphere of O_2, it appears that the overall fate of the CH_3ClI is to decompose back to the reactants, based on the work of Bilde and Wallington [143]. Therefore, if O_2 were to react with CH_3ICl, this rate coefficient has to be less than about 10^{-17} cm^3 $molecule^{-1}$ s^{-1}, using the rate coefficient for its decomposition measured by Ayhens et al. If the rate coefficient for CH_3ICl + O_2 were to remain approximately the same, i.e., 10^{-17} cm^3 $molecule^{-1}$ s^{-1}, at lower temperatures, the

possible loss of CH_3ICl via reaction with O_2 cannot be ignored. Further, the possible atmospheric photolysis of CH_3ICl may be important if it has a J-value greater than 0.1 s^{-1}.

There is a third possible product channel for this reaction to yield CH_3Cl + I (Goliff and Rowland [515]). Based on the results of Bilde and Wallington and Goliff and Rowland, we recommend that the rate coefficient for the Cl + $CH_3I \rightarrow CH_3Cl$ + I reaction to be less than $0.2k_a$ at 298 K. Since such a reaction is likely to have a significant barrier in the gas phase, even though it is exothermic by ~14 kcal mol^{-1} at 298 K, the branching ratio for the production of CH_3Cl and I in the atmosphere will be likely less than that at 298 K. (Table: 02-25, Note: 02-25) Back to Table

H11. I + O_3. Based on the room temperature data of Jenkin and Cox [659] and Sander [1135], and the temperature dependent data of Buben et al. [191] and Turnipseed et al. [1340]. (Table: 97-4, Note: 97-4) Back to Table

H12. I + BrO. Based on results of Laszlo et al. [772], the only reported study of this rate constant. This value was derived from modeling the simultaneous decay of BrO and IO in a $Br_2/I_2/N_2O$ system. (Table: 97-4, Note: 97-4) Back to Table

H13. IO + NO. Based on the data of Ray and Watson [1108], Daykin and Wine [364], Buben et al. [192], and Turnipseed et al. [1340]. (Table: 94-26, Note: 94-26) Back to Table

H14. IO + ClO. Based on results of Turnipseed et al. [1341], the only reported study of this reaction. These authors also reported the product yield for channel(s) yielding an I atom to be 0.8 ± 0.2. (Table: 97-4, Note: 97-4) Back to Table

H15. IO + BrO. Based primarily on results of Laszlo et al. [772]. Gilles et al. [505] reported the following Arrhenius expression for non-iodine atom producing channels: $2.5 \times 10^{-11} \exp(260/T)$ cm^3 $molecule^{-1}s^{-1}$. They also reported a branching ratio of <0.35 for channels producing I atoms. From their data they could constrain the value of the overall rate constant to be: $6 \times 10^{-11} < k < 10 \times 10^{-11}$ cm^3 $molecule^{-1}s^{-1}$, the range of which is consistent with the results of Laszlo et al. (Table: 97-4, Note: 97-4) Back to Table

H16. IO + IO. Changed from the previous recommendation, which was based on the results of Sander [1135]. In that study, over the temperature range 250–373 K, a negative temperature dependence was reported for the overall rate constant and for the absorption cross section at 427.2 nm. In the recent study of Harwood et al. [555], the overall rate constant and the absorption cross section were found to be independent of temperature from 253 to 320 K. The recommended room temperature value is the average of the values reported by Sander, Harwood et al., and Laszlo et al. [773]. The recommended temperaure dependence is the average of the values reported by Sander and by Harwood et al., with an uncertainty sufficient to encompass the two reported values. The A-factor has been fitted to the recommended room temperature rate constant and the recommended temperature dependence. The overall rate constant for the decay of IO in the absence of ozone has been found to be independent of pressure by Sander, Laszlo et al., and Harwood et al. A comparison of the overall rate observed in excess ozone to that in the absence of ozone was interpreted by Sander and by Harwood et al. to imply that formation of the dimer I_2O_2 is the dominant reaction channel in the IO self-reaction. (Table: 97-4, Note: 97-4) Back to Table

H17. INO + INO. Based on the data of Van den Bergh and Troe [1366]. (Table: 94-26, Note: 94-26) Back to Table

H18. INO_2 + INO_2. Based on the data of Van den Bergh and Troe [1366]. (Table: 94-26, Note: 94-26) Back to Table

I1. O + SH. This recommendation accepts the results of Cupitt and Glass [336]. The large uncertainty reflects the absence of any confirming investigation. (Table: 82-57, Note: 82-57) Back to Table

I2. O + CS. The room temperature recommendation is an average of the rate constants determined by Slagle et al. [1210], Bida et al. [135], Lilenfeld and Richardson [827], and Hancock and Smith [548]. The temperature dependence is that of Lilenfeld and Richardson, with the A-factor adjusted to yield the recommended value of k(298 K). (Table: 94-26, Note: 94-26) Back to Table

I3. O + H_2S. This recommendation is derived from an unweighted least squares fit of the data of Singleton et al. [1201] and Whytock et al. [1453]. The results of Slagle et al. [1208] show very good

agreement for E/R in the temperature region of overlap (300 – 500 K) but lie systematically higher at every temperature. The uncertainty factor at 298 K has been chosen to encompass the room temperature rate constant values of Slagle et al. [1208] and Hollinden et al. [595]. Other than the 263 K data point of Whytock et al. and the 281 K point of Slagle et al., the main body of rate constant data below 298 K comes from the study of Hollinden et al., which indicates a dramatic change in E/R in this temperature region. Thus, the parameter g was set to account for these observations. Such a nonlinearity in the Arrhenius plot might indicate a change in the reaction mechanism from abstraction (as written) to addition. An addition channel (resulting in H atom displacement) has been proposed by Slagle et al. [1208], Singleton et al. [1201], and Singleton et al. [1203]. In the latter two studies, an upper limit of 20% was placed on the displacement channel. Direct observations of product HSO were made in the reactive scattering experiments of Clemo et al. [274] and Davidson et al. [348]. A threshold energy of 3.3 kcal/mole was observed (similar to the activation energy measured in earlier studies), suggesting the importance of this direct displacement channel. Addition products from this reaction have been seen in a matrix by Smardzewski and Lin [1213]. Further kinetic studies in the 200–300-K temperature range, as well as quantitative direct mechanistic information, could clarify these issues. However, this reaction is thought to be of limited importance in atmospheric chemistry. (Table: 82-57, Note: 82-57) Back to Table

I4. O + OCS. The value of k(298 K) is the average of the determinations by Westenberg and de Haas [1444], Klemm and Stief [724], Wei and Timmons [1440], Manning et al. [863], and Breckenridge and Miller [175]. The recommended value of E/R is the average value taken from the first three listed studies. Hsu et al. [613] report that this reaction proceeds exclusively by a stripping mechanism. The vibrational and rotational state distributions in the SO and CO products have been reported by Chen et al. [257] and Nickolaisen et al. [966] respectively. (Table: 06-2, Note: 06-2) Back to Table

I5. O + CS_2. The value of k(298 K) is an average of the rate constants determined by Wei and Timmons [1440], Westenberg and de Haas [1444], Slagle et al. [1209], Callear and Smith [219], Callear and Hedges [218], Homann et al. [596], Borissenko et al. [161] and Graham and Gutman [518]. The E/R value is an average of the determinations by Wei and Timmons and Graham and Gutman. The g value has been set to encompass the limited temperature-dependent data of Westenberg and de Haas. The principal reaction products are thought to be CS + SO. However, Hsu et al. [613] report that 1.4% of the reaction at 298 K proceeds through a channel yielding CO + S_2 and calculate a rate constant for the overall process in agreement with that recommended. Graham and Gutman [518] have found that 9.6% of the reaction proceeds to yield OCS + S at room temperature. Using time-resolved diode laser spectroscopy, Cooper and Hershberger [311] determined the branching ratios for the CO- and OCS-producing channels to be (3.0±1.0)% and (8.5±1.0)% respectively. (Table: 82-57, Note: 82-57) Back to Table

I6. O + CH_3SCH_3. This recommendation is based on a fit of the data from Nip et al. [997], Lee et al. [790], and Lee et al. [789]. Product studies by Cvetanovic et al. [337] indicate that the reaction proceeds almost entirely by addition followed by rapid fragmentation to the products as written. Pavanaja et al. [1041] examined the pressure and reactant ratio dependencies of OH($A^2\Sigma^+$) and SO_2(^3B, ^1B) emissions in this reaction system. Their observations are consistent with initial product formation as written, followed by secondary generation of both OH and SO_2. (Table: 94-26, Note: 97-4) Back to Table

I7. O + CH_3SSCH_3. This recommendation averages the 298 K rate constants of Nip et al. [997] and Borissenko et al. [161], which are in good agreement with each other, but are about a factor of 2 slower than the value reported by Lee et al. [786]. The recommendation for E/R has been obtained from an unweighted Arrhenius fit that employs all available data, but scales the data of Lee et al. downward by a factor of 2.04 to bring their data into agreement with the other data at room temperature. Product studies by Cvetanovic et al. [337] indicate that the reaction proceeds mainly by addition followed by rapid fragmentation to the products as written. Pavanaja et al. [1041] examined the pressure and reactant ratio dependencies of OH($A^2\Sigma^+$) and SO_2(^3B, ^1B) emissions in this reaction system. Their observations are consistent with initial product formation as written, followed by secondary generation of both OH and SO_2. (Table: 06-2, Note: 06-2) Back to Table

I8. O + $CH_3S(O)CH_3$. The recommended 298 K rate constant is the average of values reported from a laser flash photolysis – resonance fluorescence study by Pope et al. [1068], and from a discharge flow − mass spectrometry study by Riffault et al. [1119]. A rate constant reported by Barnes et al. [76] (with no details about how the rate constant was obtained) is somewhat faster than the recommendation, but in agreement to within the recommended uncertainty factor. The recommended value for E/R is from Pope et al. The recommended value for the parameter g is larger than the value reported by Pope et al. to reflect the fact that only a single temperature dependence study has been reported. In their study at one Torr total pressure, Riffault et al. found that the products SO_2 + 2 CH_3 are produced with near unit yield. NEW ENTRY Back to Table

I9. O_3 + H_2S. This upper limit was determined by Becker et al. [108] from measurements of the rates of SO_2 production and O_3 consumption. The heterogeneous reaction between H_2S and O_3 is far more efficient in most laboratory systems. (Table: 92-20, Note: 92-20) Back to Table

I10. O_3 + CH_3SCH_3. This rate constant upper limit is based on the measurements of Martinez and Herron [884], which represent the only reported study of this reaction. (Table: 94-26, Note: 94-26) Back to Table

I11. O_3 + SO_2. This recommendation is based on the limited data of Davis et al. [359] at 300 K and 360 K in a stopped flow investigation using mass spectrometric and UV spectroscopic detection. (Table: 85-37, Note: 85-37) Back to Table

I12. OH + H_2S. The values of k(298 K) and E/R are derived from a composite unweighted least squares fit to the individual data points of Perry et al. [1048], Cox and Sheppard [329], Wine et al. [1464], Leu and Smith [808], Michael et al. [916], Lin [829], Lin et al. [832], Wang and Lee [1419], Barnes et al. [72], and Lafage et al. [762]. The studies of Leu and Smith [808], Lin et al. [832], Lin [829], and Lafage et al. [762] show a slight parabolic temperature dependence of k with a minimum occurring near room temperature. However, with the error limits stated in this evaluation, all data are fit reasonably well by an Arrhenius expression. Lafage et al. and Michael et al. discuss the results in terms of a two-channel reaction scheme involving direct H atom abstraction and complex (adduct) formation. Lafage et al. analyzed their results above room temperature to yield an apparent E/R = 400 K for the abstraction channel, in good agreement with the E/R value determined above room temperature by Westenberg and de Haas [1445]. The results of these latter workers lie systematically higher (by about 70%), presumably due to secondary reactions. The room temperature value measured by Stuhl [1255] lies just outside the 2σ error limit set for k(298 K). Butkovskaya and Setser [211] have observed infrared emission from vibrationally excited levels of the expected reaction product H_2O. (Table: 06-2, Note: 06-2) Back to Table

I13. OH + OCS. The value of k(298 K) is an average of the determinations by Wahner and Ravishankara [1388] and Cheng and Lee [258]. The room temperature rate constants from these studies are a factor of 3 higher than the earlier determination by Leu and Smith [807]. As discussed in the later studies, this difference may be due to an overcorrection of the Leu and Smith data to account for OH reaction with H_2S impurities and also to possible regeneration of OH. Nevertheless, the uncertainty factor at 298 K has been set to encompass the earlier study within 2σ. The work by Wahner and Ravishankara [1388] supersedes the study of Ravishankara et al. [1094], which minimized complications due to secondary and/or excited state reactions that presumably were interfering with the experiments of Atkinson et al. [50] and of Kurylo [751]. The upper limit for k(298 K) reported by Cox and Sheppard [329] is too insensitive to permit comparison with the more recent studies. The room temperature measurements of Wahner and Ravishankara demonstrate the lack of an effect of total pressure (or O_2 partial pressure) on the rate constant and are supported by the more limited pressure- and O_2-dependent studies of Cheng and Lee. The recommendation for E/R is based on the study of Cheng and Lee who determined a value considerably lower than reported by Leu and Smith, although this difference may be due in part to the earlier mentioned overcorrection of the data by the latter authors.

Product observations by Leu and Smith indicate that SH is a primary product of this reaction and tentatively confirm the suggestion of Kurylo and Laufer [758] that the predominant reaction pathway is to produce SH + CO_2 through a complex (adduct) mechanism similar to that observed for the OH

+ CS_2 reaction. However, the absence of an O_2/pressure effect for OH + OCS is in marked contrast with the strong dependence seen in studies of OH + CS_2 (see note for the latter reaction).

Experiments by Greenblatt and Howard [523] have shown that oxygen atom exchange in the reaction of ^{18}OH with OCS is relatively unimportant, leading to an upper limit of 10^{-15} being set on the rate constant of the exchange reaction. (Table 87-41, Note: 92-20) Back to Table

I14. OH + CS_2 → SH + OCS. There is a consensus of experimental evidence that this reaction proceeds very slowly as a direct bimolecular process. Wine et al. [1473] set an upper limit on k(298 K) of 1.5 × 10^{-15} $cm^3molec^{-1}s^{-1}$. A consistent upper limit is also reported by Iyer and Rowland [645] for the rate of direct production of OCS, suggesting that OCS and SH are primary products of the bimolecular process. This mechanistic interpretation is further supported by the studies of Leu and Smith [809] and Biermann et al. [138], which set somewhat higher upper limits on k(298 K). The more rapid reaction rates measured by Atkinson et al. [50], Kurylo [751], and Cox and Sheppard [329] may be attributable to severe complications arising from excited state and secondary chemistry in their photolytic systems. The Cox and Sheppard study in particular may have been affected by the reaction of electronically excited CS_2 (produced via the 350 nm photolysis) with O_2 (in the 1-atm synthetic air mixture) as well as by the accelerating effect of O_2 on the OH + CS_2 reaction itself, which has been observed by other workers as summarized below. The possible importance of electronically excited CS_2 reactions in the tropospheric oxidation of CS_2 to OCS has been discussed by Wine et al. [1463]. (Table: 06-2, Note: 06-2) Back to Table

I15. OH + CS_2 → $CS_2OH \xrightarrow{O_2}$ products. An accelerating effect of O_2 on the OH + CS_2 reaction rate has been observed by Jones et al. [678], Barnes et al. [79], and Hynes et al. [632], along with a near unity product yield for SO_2 and OCS. In the latter two studies the effective bimolecular rate constant was found to be a function of total pressure (O_2 + N_2), and exhibited an appreciably negative temperature dependence. These observations are consistent with the formation of a long-lived adduct as postulated by Kurylo [751] and Kurylo and Laufer [758] followed by its reaction with O_2:

$$OH + CS_2 + M \underset{k_b}{\overset{k_a}{\rightleftharpoons}} CS_2OH + M$$

$$CS_2OH + O_2 \xrightarrow{k_c} \text{Products}$$

The effective second order rate constant for CS_2 or OH removal in the above reaction scheme can be expressed as

$$1/k_{eff} = (k_b/k_ak_c)(1/P_{O2}) + (1/k_a)(1/P_M)$$

where P_{O_2} is the partial pressure of O_2 and P_M equals $P_{O_2} + P_{N_2}$. The validity of this expression requires that k_a and k_b are invariant with the P_{O_2}/P_{N_2} ratio. A 1/k vs $1/P_{O_2}$ plot of the data of Jones et al. [678] taken at atmospheric pressure exhibits marked curvature, suggesting a more complex mechanistic involvement of O_2, whereas the data of Barnes et al. [79] and Hynes et al. [632] are more satisfactorily represented by this analytical expression. Nevertheless, while the qualitative features of the data from all three laboratories agree, there are some quantitative inconsistencies. First, under similar conditions of O_2 and N_2 pressures, the Barnes et al. rate constants lie approximately 60% higher than those of Jones et al. and up to a factor of 2 higher than those derived by Hynes et al. Secondly, two fits each of both the Barnes et al. and Hynes et al. data can be made: one at fixed P_M and varying P_{O_2}, and the other at fixed P_{O_2} and varying P_M (i.e., varying added N_2). Within each data set, rate constants calculated from both fits agree reasonably well for mole fractions of O_2 near 0.2 (equivalent to air) but disagree by more than a factor of 2 for measurements in a pure O_2 system. Finally, the temperature dependence (from 264–293 K) of the k_{eff} values from Barnes et al. varies systematically from an E/R of –1300 K for experiments in pure O_2 (at 700 torr total pressure) to –2900 K for experiments in a 50 torr O_2 plus 650 torr N_2 mixture. An Arrhenius fit of the Hynes et al. data (from 251–348 K) recorded in synthetic air at 690 torr yields an E/R = –3300 K, although the data show marked curvature over the temperature range of study. These observations suggest that k_a and k_b may not be independent of the identity of M. For this reason, we limit our recommendation to air mixtures (i.e., P_{O_2}/P_{N_2} = 0.25) at atmospheric pressure. Since most

CS_2 is oxidized within the atmospheric boundary layer, such restriction does not limit the applicability of this recommendation in atmospheric modeling.

The present recommendation accepts the measurements of Hynes et al. [632], which appear to be the most sensitive of the three investigations. Thus, k(298 K) is derived from the Arrhenius fit of the data near room temperature.

$$k(298\ K) = 1.2 \times 10^{-12}\ cm^3molec^{-1}s^{-1}$$

To compute values of k below 298 K, we have accepted the analysis of Hynes et al.:

$$k(T) = \{1.25 \times 10^{-16} \exp(4550/T)\}/\{T + 1.81 \times 10^{-3} \exp(3400/T)\}\ cm^3molec^{-1}s^{-1}.$$

This recommendation is only valid for one atmosphere pressure of air. It is interesting to note that measurements by Hynes et al. [632] at approximately 250 K and 700 Torr total pressure result in k_{eff} values that are independent of the amount of O_2 for partial pressures between 145 and 680 Torr. This suggests that the adduct is quite stable with respect to dissociation into the reactants (OH + CS_2) at this low temperature and that the effective rate constant for reactant removal approaches the elementary rate constant for adduct formation. NEW ENTRY Back to Table

I16. $CS_2OH + O_2$. Three groups have obtained kinetic information about this reaction by observing either the perturbation of OH/CS_2OH equilibration kinetics upon addition of O_2, or by modeling the dependence of the observed rate constant for OH loss on [O_2]. Hynes et al. [632], Murrells et al. [939], and Diau and Lee [387] agree quite well on the value of k, with an average value of 2.8 x 10^{-14} $cm^3molec^{-1}s^{-1}$ independent of temperature and pressure being recommended. Diau and Lee also report rate constants for the reactions of the adduct (CS_2OH) with NO and NO_2 to be 7.3×10^{-13} and 4.2×10^{-11} $cm^3molec^{-1}s^{-1}$, respectively.

From a mechanistic viewpoint, the primary products of this reaction determine the products of CS_2 oxidation in air. Lovejoy et al. [849] have shown that the yields of HO_2 and SO_2 are equal and near unity. Further insight is provided by the mechanistic study of Stickel et al. [1242], who observe OCS and CO product yields of (0.83±0.08) and (0.16±0.03), respectively. The results from this study are interpreted to imply that OCS and CO are formed either as primary products of the $CS_2OH + O_2$ reaction or as products of a secondary reaction between a primary product and O_2. These same authors report an SO_2 yield of (1.15±0.10), with the results suggesting that only about 75% of the SO_2 is formed as a prompt product, with the remainder generated via a slow reaction of SO (generated as a prompt product of the $CS_2OH + O_2$ reaction) with O_2. Insight into the specific reaction pathways can be gleaned from the study of Lovejoy et al. [848] in which the rate constant for the reaction of $CS_2OD + O_2$ was found to be the same as that for $CS_2OH + O_2$, indicating that simple H atom abstraction is not the likely process. Rather, HO_2 production most likely involves complex formation followed by HO_2 elimination. Lovejoy et al. [850] found that the ^{18}O atom in the ^{18}OH reactant is transferred predominantly (90 ± 20)% to the SO_2 product. These findings are consistent with an S–O-bonded CS_2–OH adduct and preservation of the S–O bond in the steps leading to SO_2 formation.

Theoretical studies by Zhang and Qin [1520] and by McKee and Wine [892] have provided further insight into the reaction mechanism. The initial step is, indeed, formation of SCS−OH followed by addition of O_2 to the carbon atom. A key subsequent step appears to be an O atom transfer to the sulfur bearing the hydroxyl group which leads directly to HOSO + OCS. The reaction HOSO + O_2 → HO_2 + SO_2 is expected to occur rapidly under atmospheric conditions. One remaining problem is identification of the pathway for generation of CO, which is observed as a minor product. NEW ENTRY Back to Table

I17. OH + CH_3SH. This recommendation is based on a composite fit to the data of Atkinson et al. [49], Wine et al. [1464], Wine et al. [1474], and Hynes and Wine [629], which are in excellent agreement. The results from the relative rate study of Barnes et al. [72] are in agreement with this recommendation and indicate that the higher value of Cox and Sheppard [329] is due to complications resulting from the presence of O_2 and NO in their reaction system. MacLeod et al. [858, 859] and Lee and Tang [788] obtained rate constants at 298 K approximately 50% lower than recommended here. These authors also obtained lower values for the ethanethiol reaction in comparison with results from studies upon which the methanethiol recommendation is made. Wine

et al. [1474] present evidence that this reaction proceeds via adduct formation to produce a species that is thermally stable over the temperature range and time scales of the kinetic measurements. Tyndall and Ravishankara [1355] have determined the yield of CH_3S (via laser–induced fluorescence) to be unity, indicating that any adduct must be short lived (less than 100 µs). Longer lifetimes would have led to anomalies in the OH decay kinetics used for the rate constant determinations. Butkovskaya and Setser [213], based on observations of IR emissions from the products of the reactions of OH and OD with CH_3SH and CH_3SD, conclude that H-abstraction from the methyl group occurs with a yield of 24±8% for the OH reactions and 11±4% for the OD reactions. Hynes and Wine [629] observed that the rate constant is independent of O_2 partial pressure. (Table: 06-2, Note: 06-2) Back to Table

I18. $OH + CH_3SCH_3 \rightarrow H_2O + CH_2SCH_3$. The $OH + CH_3SCH_3$ reaction is complex, proceeding by both H-abstraction and reversible addition pathways. In the presence of atmospheric levels of O_2, adduct reaction with O_2 makes the addition pathway partially irreversible. Only kinetic data obtained in the absence of O_2 and at low enough CH_3SCH_3 concentrations for the adduct to be a negligible reservoir for OH are considered in evaluation of the H-abstraction rate constant. This recommendation is based on the results of Hynes et al. [634], Wine et al. [1464], Hsu et al. [617], Abbatt et al. [3], Barone et al. [87], Turnipseed et al. [1337], and Williams et al. [1458]. The earlier higher rate constant values of Atkinson et al. [50] and Kurylo [752] are presumably due to reactive impurities, while those of MacLeod et al. [859] were most likely overestimated because of heterogeneous reactions. Absolute determinations lower than those recommended were obtained by Martin et al. [878], Wallington et al. [1392], and Nielsen et al. [983]. The reasons for these differences are not readily apparent. Confirmation that H-abstraction is the dominant pathway under the experimental conditions specified above comes from the studies of Stickel et al. [1244] and Turnipseed et al. [1337]. Stickel et al. used tunable diode laser spectroscopy to measure an HDO product yield of 0.84±0.15 for the $OD + CH_3SCH_3$ reaction in 10-30 Torr N_2, while Turnipseed et al. used laser induced fluorescence observations of CH_3S production from $OH + CH_3SCH_3$ to show that the branching ratio for the CH_3S elimination channel is <0.04 and the direct H-abstraction yield is 0.84±0.26. Further support for the dominance of the H-abstraction pathway comes from the work of Zhao et al. [1528], who obtained an upper limit yield of 0.07 for the methyl elimination channel in the $OD + CH_3SCH_3$ reaction. Barnes et al. [82, 83], Turnipseed et al., and Urbanski et al. [1360] all report that the abstraction product CH_3SCH_2 is converted predominantly to CH_3S under atmospheric conditions. Barnes et al. [82] measure a 0.7% yield of OCS under low NO_x conditions, which they attribute to further oxidation of CH_3S. (Table: 06-2, Note: 06-2) Back to Table

I19. $OH + CH_3SCH_3 \rightarrow (CH_3)_2SOH \xrightarrow{O_2}$ products. The $OH + CH_3SCH_3$ reaction is complex, proceeding by both direct H-abstraction and reversible addition pathways. Much of the kinetic data available for evaluating this reaction were obtained for $OH + CD_3SCD_3$. Since the methyl hydrogens are not directly involved in the reaction, the rate constant is virtually the same for CH_3SCH_3 as for CD_3SCD_3; hence, data for both reactants are used in the evaluation. The recommended expression (units are $cm^3molec^{-1}s^{-1}$),

$$k(T,[O_2]) = 1.0 \times 10^{-39} [O_2] \exp(+5820/T) / \{1 + 5.0 \times 10^{-30} [O_2] \exp(+6280/T)\}$$

is the best representation of the data of Hynes et al. [634] and Williams et al. [1458], and represents the rate constant for irreversible addition of OH to CH_3SCH_3 as a function of temperature and $[O_2]$. Both studies employed the laser flash photolysis − pulsed laser induced fluorescence technique, and obtained kinetic information by monitoring the decay of OH. The recommended expression is applicable at pressures near 1 atm over the temperature range 240 − 320 K, and can be used over the pressure range 0.1 − 1 atm at T = 298 K. Since the kinetic data of Hynes et al. and Williams et al. were obtained by monitoring OH loss, the overall rate constant for removal of CH_3SCH_3 would be underestimated if the adduct + O_2 reaction generated OH + dimethylsulfone ($CH_3(O)S(O)CH_3$) with a significant yield; the available data cannot rule out a small but significant branching ratio for this channel. Recommended rate constants for the elementary steps leading to OH loss and product formation (adduct formation, adduct dissociation, and adduct + O_2 reaction) are also provided in this document. NEW ENTRY Back to Table

I20. $(CH_3)_2SOH + O_2$. All available kinetic data for this reaction were obtained by measuring k_{obs} for the $OH + CH_3SCH_3$ reaction as a function of O_2 partial pressure ($k_{obs} \equiv$ the sum of the rate constants for H-abstraction and irreversible addition). Most of the available data were obtained for OH + CD_3SCD_3. Since the methyl hydrogens are not directly involved in the reaction, the rate constant is expected to be virtually the same for CH_3SCH_3 as for CD_3SCD_3; hence, data for both reactants are used in the evaluation. The recommendation is based on the data of Hynes et al. [628] and Barone et al. [87]. The Hynes et al. study supercedes an earlier report of a considerably faster rate constant [634]. Over the range of experimental conditions where data are available (222 – 267 K and 30 – 200 Torr), the rate constant is essentially independent of temperature and pressure. By monitoring the regeneration of OH in the presence of NO, Hynes et al. [627] and Turnipseed et al. [1337] have determined the yield for the $HO_2 + CH_3S(O)CH_3$ (DMSO) channel to be ~0.5. NEW ENTRY Back to Table

I21. $OH + CH_3SSCH_3$. This recommendation is based on the temperature–dependent studies of Wine et al. [1464] and Abbatt et al. [3] and the room temperature relative rate study of Cox and Sheppard [329]. Domine and Ravishankara [407] have observed both CH_3S (via laser–induced fluorescence) and CH_3SOH (via photo-ionization mass spectrometry) as products of this reaction. At 298 K, the yield of CH_3S alone was quantified at approximately 30%. An FTIR product study of the photooxidation of dimethyl disulfide by Barnes et al. [81] presents evidence that oxidation of the CH_3SOH product is the principal source of the methane sulfonic acid observed. Butkovskaya and Setser [212] have observed that HDO and D_2O are produced from $OD + CH_3SSCH_3$ in the same proportion and with the same vibrational state distributions as the products observed by the same investigators in a similar study of the $OD + CH_3SD$ reaction [213], leading these authors to suggest that the major product channel for $OD + CH_3SSCH_3$ is $CH_3SD + CH_3SO$. (Table: 94-26, Note: 94-26) Back to Table

I22. $OH + CH_3S(O)CH_3$. The recommended 298 K rate constant is the average of the direct studies of Hynes and Wine [631], Urbanski et al. [1359], and Kukui et al. [739], which employed three different experimental approaches and are in excellent agreement. Competitive kinetics studies by Barnes et al. [76] and Falbe-Hanson et al. [443] in 1 atm. of air report rate constants about a factor of 1.5 slower than those obtained in the direct studies. The recommended value for E/R is based on the only study of the temperature dependence [631], where a significant negative activation energy was observed. The large uncertainty in E/R reflects the availability of very limited data (none below room temperature). The experimental studies of Urbanski et al., Kukui et al. and Arsene et al. [35], as well as the theoretical study of Wang and Zhang [1418], provide strong evidence that the dominant reaction channel is production of $CH_3 + CH_3S(O)OH$ (MSIA, methanesulfinic acid). Arsene et al. attribute the failure to observe MSIA production in the chamber study of Sorensen et al. [1222] to loss via secondary gas phase and condensed phase oxidation before sampling. NEW ENTRY Back to Table

I23. $OH + CH_3S(O)OH$. The recommendation is based on a turbulent flow reactor − chemical ionization mass spectrometry study by Kukui et al. [739], which was carried out with OH in excess over $CH_3S(O)OH$ at total pressures of 200−400 Torr N_2. The large uncertainty factor results from the facts that (1) only a single room temperature study is reported in the literature and (2) $CH_3S(O)OH$ is a difficult species to study in the gas phase because of it low vapor pressure. Kukui et al. found that SO_2 was produced as a reaction product with near unit yield, suggesting that the dominant reaction channel (at least in the absence of O_2) is production of $CH_3 + SO_2 + H_2O$. NEW ENTRY Back to Table

I24. OH + S. This recommendation is based on the study by Jourdain et al. [680]. Their measured value for k(298 K) compares favorably with the recommended value of k(O + OH) when one considers the slightly greater exothermicity of the present reaction. (Table: 82-57, Note: 82-57) Back to Table

I25. OH + SO. The value recommended for k(298 K) is an average of the determinations by Fair and Thrush [441], Jourdain et al. [680], and Blitz et al. [154]. The result reported by Fair and Thrush is corrected using the present recommendation for the O + OH reaction. The recommended value for E/R is taken from the temperature dependent data of Blitz et al. over the range 295−453 K. Higher temperature data of Blitz et al. are not used because significant curvature in the Arrhenius plot is

observed at T > 500 K. The recommended value for g is conservative because only one temperature dependence study has been reported. (Table: 06-2, Note: 06-2) Back to Table

I26. $HO_2 + H_2S$, $HO_2 + CH_3SH$, $HO_2 + CH_3SCH_3$. These upper limits are taken from the discharge flow laser magnetic resonance study of Mellouki and Ravishankara [906]. The H_2S value disagrees with the rate constant reported by Bulatov et al. [197] by approximately three orders of magnitude. The reason for this difference is not readily apparent. However, the recommended upper limit is consistent with the values for CH_3SH and CH_3SCH_3, which respectively agree with upper limits from the work of Barnes et al. [72] and Niki (reported as a private communication in the Mellouki and Ravishankara paper). (Table: 94-26, Note: 94-26) Back to Table

I27. $HO_2 + SO_2$. This upper limit is based on the atmospheric pressure study of Graham et al. [521]. A low pressure laser magnetic resonance study by Burrows et al. [203] places a somewhat higher upper limit on k(298 K) of 4×10^{-17} $cm^3molec^{-1}s^{-1}$ (determined relative to $OH + H_2O_2$). Their limit is based on the assumption that the products are OH and SO_3. The weight of evidence from both studies suggests an error in the earlier determination by Payne et al. [1043]. (Table: 82-57, Note: 82-57) Back to Table

I28. $NO_2 + SO_2$. This recommendation is based on the study of Penzhorn and Canosa [1045] using second derivative UV spectroscopy. While these authors actually report a measured value for k(298 K), their observations of strong heterogeneous and water vapor catalyzed effects prompt us to accept their measurement as an upper limit. This value is approximately two orders of magnitude lower than that for a dark reaction observed by Jaffe and Klein [647], much of which may have been due to heterogeneous processes. Penzhorn and Canosa suggest that the products of this reaction are NO + SO_3. (Table: 85-37, Note: 85-37) Back to Table

I29. $NO_3 + H_2S$. This recommendation accepts the upper limit set by Dlugokencky and Howard [393] based on experiments in which NO_3 loss was followed in the presence of large concentrations of H_2S. Less sensitive upper limits for the rate constant have been reported by Wallington et al. [1394] and Cantrell et al. [228]. (Table: 90-1, Note: 90-1) Back to Table

I30. NO_3 + OCS. This upper limit is based on the relative rate data of MacLeod et al. [856]. (Table: 90-1, Note: 90-1) Back to Table

I31. $NO_3 + CS_2$. This upper limit is based on the study of Burrows et al. [207]. A somewhat higher upper limit was derived in the relative rate study of MacLeod et al. [856]. (Table: 90-1, Note: 90-1) Back to Table

I32. $NO_3 + CH_3SH$. The recommended values are derived from a composite fit to the data of Wallington et al. [1394], Rahman et al. [1085], and Dlugokencky and Howard [393]. The room temperature rate constant derived in the relative rate experiments of MacLeod et al. [856] is in good agreement with the recommended value. The suite of investigations shows the rate constant to be pressure independent over the range1–700 torr. Dlugokencky and Howard place an upper limit of 5% on the production of NO_2 via this reaction at low pressure. Based on the product distribution observed in their investigation, Jensen et al. [666] propose a reaction mechanism initiated by abstraction of the hydrogen atom from the SH group, possibly after formation of an initial adduct as suggested by Wallington et al. and Dlugokencky and Howard. (Table: 90-1, Note: 94-26) Back to Table

I33. $NO_3 + CH_3SCH_3$. The recommended values are derived from a composite fit to the data of Wallington et al. [1394], Tyndall et al. [1345], and Dlugokencky and Howard [393]. The relative rate study of Atkinson et al. [52] yields a rate constant at room temperature in good agreement with that recommended. The experimental data from all investigations demonstrate the pressure independence of the rate constant over the range 1–740 torr. Room temperature investigations by Daykin and Wine [362] and Wallington et al. [1395] are also in agreement with the recommended value. Jensen et al. [665] propose a mechanism that involves hydrogen abstraction as the first step to explain their observed product distribution. In a later study, Jensen et al. [666] measured a kinetic isotope effect for the rate constant for CH_3SCH_3 vs. that for CD_3SCD_3 of $k_H/k_D = (3.8\pm0.6)$, in agreement with the kinetic isotope effect reported by Daykin and Wine; this provides further confirmation of the H-abstraction mechanism. Butkovskaya and Le Bras [209] utilized chemical titration of the primary radical produced from $NO_3 + CH_3SCH_3$ in a discharge flow − mass

spectrometry system to show that the reaction produces predominantly CH_3SCH_2 + HNO_3. An upper limit of 2% was placed on the reaction channel yielding CH_3 + CH_3SONO_2. (Table: 06-2, Note: 06-2) Back to Table

I34. NO_3 + CH_3SSCH_3. The recommended values were derived from a composite fit to the data of Wallington et al. [1394] and Dlugokencky and Howard [393]. The investigation by Atkinson et al. [45] indicates that the relative rate technique cannot be considered as yielding reliable rate data for this reaction due to chemical complexities. Thus, the much lower room temperature results from the study of MacLeod et al. [856] can be considered to be erroneous. Based on their observations of intermediate and end products, Jensen et al. [666] proposed a reaction mechanism in which the initial addition of NO_3 to one of the sulfur atoms results in formation of CH_3S + CH_3SO + NO_2. (Table: 90-1, Note: 94-26) Back to Table

I35. NO_3 + $CH_3S(O)CH_3$. The recommendation is the geometric mean of the rate constants reported by Barnes et al. [76] and Falbe-Hansen et al. [443] from similar competitive kinetics studies; the reported rate constants and associated 2σ uncertainties in units of 10^{-13} $cm^3molec^{-1}s^{-1}$ are 1.7±0.6 (Barnes et al.) and 5.0±3.8 (Falbe-Hansen et al.). In both studies, the only observed sulfur−containing end product was dimethylsulfone ($CH_3(O)S(O)CH_3$). Barnes et al. suggest that reaction proceeds via formation of an adduct that rapidly decomposes to NO_2 + $CH_3(O)S(O)CH_3$. NEW ENTRY Back to Table

I36. NO_3 + SO_2. This recommended upper limit for k(298 K) is based on the study by Daubendiek and Calvert [346]. Considerably higher upper limits have been derived by Burrows et al. [207], Wallington et al. [1394], Canosa–Mas et al. [223], and Dlugokencky and Howard [393]. (Table 87-41, Note: 90-1) Back to Table

I37. N_2O_5 + CH_3SCH_3. This recommendation is based on the value estimated by Tyndall and Ravishankara [1356] from the study by Atkinson et al. [52]. (Table: 92-20, Note: 92-20) Back to Table

I38. CH_3O_2 + SO_2. This recommendation accepts the results from the study of Sander and Watson [1140]. These authors conducted experiments using much lower CH_3O_2 concentrations than employed in the earlier investigations of Sanhueza et al. [1144] and Kan et al. [693], both of which resulted in k(298 K) values approximately 100 times greater. A later report by Kan et al. [692] postulates that these differences are due to the reactive removal of the $CH_3O_2SO_2$ adduct at high CH_3O_2 concentrations prior to its reversible decomposition into CH_3O_2 and SO_2. They suggest that such behavior of $CH_3O_2SO_2$ or its equilibrated adduct with O_2 ($CH_3O_2SO_2O_2$) would be expected in the studies yielding high k values, while decomposition of $CH_3O_2SO_2$ into reactants would dominate in the Sander and Watson experiments. It does not appear likely that such secondary reactions involving CH_3O_2, NO, or other radical species would be rapid enough, if they occur under normal atmospheric conditions to compete with the adduct decomposition. This interpretation, unfortunately, does not explain the high rate constant derived by Cocks et al. [304] under conditions of low [CH_3O_2]. (Table: 81-3, Note: 81-3) Back to Table

I39. F + CH_3SCH_3. This recommendation is based on the discharge flow mass spectrometric study by Butkovskaya et al. [210]. The uncertainty placed on this recommendation has been increased over that estimated by the authors to reflect the lack of any confirming investigations. Titration of the primary organic radical products indicated that the reaction proceeds via two channels to produce HF + CH_3SCH_2 and CH_3 + CH_3SF with a branching ratio of approximately 0.8/0.2 respectively. (Table: 97-4, Note: 97-4) Back to Table

I40. Cl + H_2S. This recommendation is based on the study by Nicovich et al. [970], who conducted an elaborate study with attention to sources of possible systematic error. The rate constant at 298 K is in good agreement with that determined by Nesbitt and Leone [957], who refined the data of Braithwaite and Leone [173], but is significantly greater than the values reported by Clyne and Ono [295], Clyne et al. [286], Nava et al. [946], and Chen et al. [254]. The small, but clearly observed, negative activation energy determined by Nicovich et al. contrasts with the lack of a temperature dependence observed by Nava et al. In fact, at the lowest temperature of overlap, the results from these two studies differ by 50%. Nevertheless, the Nicovich et al. study yields consistent results for both H_2S and CH_3SH as well as for D_2S and CD_3SD. In addition, Hossenlopp et al. [602] report a

room temperature rate constant for Cl + D_2S that is in excellent agreement with the value reported by Nicovich et al. While the reason for these differences remains to be determined, the full range of reported values is encompassed within the 2σ error limits recommended. Lu et al. [853] also measured a temperature–independent rate constant but report a value at 298 K that is about 40% greater than that of Nicovich et al. However, the presence of 4000 Torr of CF_3Cl bath gas in the Lu et al. study may suggest a slight pressure dependence of the reaction, although Nicovich et al. observed no pressure dependence for pressures ranging up to 600 Torr N_2. A theoretical study by Wilson and Hirst [1459] suggests the dominance of an addition-elimination pathway with a small but significant fraction of reactive events occurring via a direct hydrogen abstraction mechanism. (Table: 06-2, Note: 06-2) Back to Table

I41. Cl + OCS. This upper limit is based on the minimum detectable decrease in atomic chlorine measured by Eibling and Kaufman [434]. Based on the observation of product SCl, these authors set a lower limit on k(298 K) of 10^{-18} $cm^3molec^{-1}s^{-1}$ for the SCl + CO reaction channel. Considerably higher upper limits on k(298 K) were determined in the studies of Clyne et al. [286] and Nava et al. [946]. (Table 83-62, Note: 87-41) Back to Table

I42. $CS_2Cl + O_2$. This recommendation is based on the study of Nicovich et al. [969] who employed a laser flash photolysis − resonance fluorescence technique to observe the effect of added O_2 on the kinetics of the Cl + $CS_2 \leftrightarrow CS_2Cl$ equilibration reactions. Martin et al. [876] report competitive kinetics results which they interpret as suggesting a fast $CS_2Cl + O_2$ reaction, but Wallington et al. [1391] have suggested that secondary production of OH in the photochemical system employed by Martin et al. is responsible for the observed dependence of the CS_2 loss rate on [O_2]. Back to Table

I43. Cl + CH_3SH. This recommendation is based on the results of Nicovich et al. [970], who used laser photolysis with resonance fluorescence detection to study the reactions of Cl with H_2S, D_2S, CH_3SH, and CD_3SD. The room temperature determination by Nesbitt and Leone [957] is in good agreement with the recommended value. The k(298 K) value from the study of Mellouki et al. [902] is nearly a factor of 2 lower. However, the low sensitivity of EPR detection of Cl atoms did not permit these latter authors to conduct a precise determination of k under pseudo first–order conditions, and a more complex analysis of experiments conducted under second–order conditions was required. Nesbitt and Leone [958] report that 2±1% of the reaction occurs via abstraction of an H atom from the CH_3 group. A theoretical study by Wilson and Hirst [1459] predicts a Cl−S adduct bond strength (298 K) of 13.6 kcal mol^{-1}, but is unable to deduce the relative importance of addition-elimination vs. direct hydrogen abstraction pathways. (Table: 06-2, Note: 06-2) Back to Table

I44. Cl + CH_3SCH_3. Stickel et al. [1243] have used laser photolysis − resonance fluorescence to measure the rate constant between 240 and 421 K, over the pressure range 3–700 Torr. The rate constant is near collisional but increases with increasing pressure from a low pressure limit of 1.8×10^{-10} to a value of 3.3×10^{-10} $cm^3molec^{-1}s^{-1}$ at 700 Torr. The yield of HCl at 297 K, measured by diode laser spectroscopy, decreased from near unity at low pressure to a value of approximately 0.5 at 203 Torr, suggesting that stabilization of a $(CH_3)_2SCl$ adduct becomes competitive with hydrogen atom abstraction with increasing pressure. These investigators also observed a negative temperature dependence for the reaction. Butkovskaya et al. [210] conducted a discharge flow − mass spectrometry study at 298 K, in which they determined that the reaction proceeds to form HCl + CH_3SCH_2 almost exclusively at 1 Torr total pressure. The sum of all other possible channels was estimated at less than 3%. Zhao et al. [1528] used laser photolysis coupled with CH_3 detection by time–resolved tunable diode laser absorption spectroscopy to determine an upper limit yield of 0.02 for CH_3 elimination at 298 K and pressures in the range 10–30 Torr. Langer et al. [768] coupled cw photolysis with gas chromatographic detection of products to show that the yield of CH_3Cl is (1.34 ± 0.07) x 10^{-3}. Theoretical studies by Wilson and Hirst [1459], Resende and De Almeida [1114] and Thompson et al. [1299] support the experimentally-observed dominance of the H-abstraction pathway at low pressure. Diaz-de-Mera et al. [390] have employed a discharge flow − mass spectrometry technique to measure rate constants at pressures of 0.5 − 1.0 Torr He over the temperature range 259 − 364 K. The 298 K rate constant reported by Diaz-de-Mera et al. is nearly a factor of 3 slower than the low-temperature limit value reported by Stickel et al. Furthermore, Diaz-de-Mera et al. report a small positive activation energy whereas Stickel et al. report a small negative activation energy. The present recommendation for the H-abstraction pathway is based on an

extrapolated low pressure limit rate constant obtained from the data of Stickel et al., with the uncertainty adjusted to encompass the result of Diaz-de-Mera et al. Until additional temperature dependence data become available, a temperature-independent rate constant is recommended. The data of Stickel et al. suggest that a high pressure limit is reached at P ~ 150 Torr. Urbanski and Wine [1361] have observed the UV-visible absorption spectrum of $(CH_3)_2SCl$ in 155 Torr O_2 and used absorbance rise−time data to derive a rate constant that agrees well with those measured by Stickel et al. at pressures of 150−750 Torr N_2. Enami et al. [437] have observed the kinetics of adduct formation using cavity ring down spectroscopy, and derived rate constants over the temperature and pressure ranges 278−318 K and 20−300 Torr N_2 that also agree well with those reported by Stickel et al. Room temperature competitive kinetics measurements by Nielsen et al. [982] at 740 Torr and Kinnison et al. [713] at 760 Torr agree quite well with the results of Stickel et al., Urbanski and Wine, and Enami et al. Kinnison et al. also observed the rate constant to increase from 3.6×10^{-10} to 4.2×10^{-10} $cm^3molec^{-1}s^{-1}$ when the bath gas was changed from pure N_2 to synthetic air, suggesting that the $(CH_3)_2SCl$ adduct reacts with O_2; however, the results of Urbanski and Wine, and Enami et al. argue against the occurrence of such a reaction. Based on available data, a temperature-independent rate constant of $3.5x10^{-10}$ $cm^3molec^{-1}s^{-1}$ in air at P > 150 Torr is recommended. NEW ENTRY Back to Table

I45. $(CH_3)_2SCl + O_2$, NO, NO_2. The recommendations are based on the study of Urbanski and Wine [1361] which combined laser flash photolytic production of $(CH_3)_2SCl$ with kinetic observations by time-resolved absorption spectroscopy. The recommended uncertainties for the NO and NO_2 reactions are larger than those reported by Urbanski and Wine pending independent confirmation of their results. As in the Urbanski and Wine study, Enami et al. [437] report no observable reaction between $(CH_3)_2SCl$ and O_2. NEW ENTRY Back to Table

I46. $Cl + CH_3S(O)CH_3 \rightarrow CH_3S(O)CH_2 + HCl$. The recommended value of k(298 K) for H-abstraction is based on the low pressure discharge flow − mass spectrometry studies of Martinez et al. [883] and Riffault et al. [1118]. Riffault et al. measured a yield of 91% for HCl production in 1.0 Torr of helium bath gas. The total rate constants reported by Martinez et al. at helium pressures of 0.5 − 3.0 Torr are scaled downward by 5−20% to account for the estimated contribution of an addition channel to the observed reactivity. The temperature dependence studies of Martinez et al. [883] (273-335 K) and Wine et al. (438-603 K) [1465] suggest the possibility of curvature in the Arrhenius plot. No recommendation is made for E/R pending the availability of additional data. Vandresen and Resende [1371] report a theoretical rate coefficient of 1.2×10^{-10} $cm^3molec^{-1}s^{-1}$, i.e., a factor of seven faster than the value suggested by experimental results. NEW ENTRY Back to Table

I47. $CH_3(Cl)S(O)CH_3 + O_2$, NO, NO_2. The recommendations are based on the study of Wine et al. [1465] which combined laser flash photolytic production of $CH_3(Cl)S(O)CH_3$ with kinetic observations by time-resolved absorption spectroscopy. The recommended uncertainties for the NO and NO_2 reactions are larger than those reported by Wine et al. pending independent confirmation of their results. NEW ENTRY Back to Table

I48. ClO + OCS; ClO + SO_2. These recommendations are based on the discharge flow mass spectrometric data of Eibling and Kaufman [434]. The upper limit on k(298 K) for ClO + OCS was set from the minimum detectable decrease in ClO. No products were observed. The upper limit on k(298 K) for ClO + SO_2 is based on the authors' estimate of their SO_3 detection limit. The upper limit for this same reaction based on the minimum detectable decrease in ClO was not used due to the potential problem of ClO reformation from the Cl + O_3 source reaction. (Table 83-62, Note: 83-62) Back to Table

I49. ClO + CH_3SCH_3. The 298 K recommendation is the average of the values reported in discharge flow – mass spectrometry studies by Barnes et al. [77] and Diaz-de-Mera et al. [390]. Barnes et al. prefer their more recent rate constant to one a factor of 4 higher that they determined in an earlier version of their apparatus. The recommendation for E/R is based on the temperature dependence observed by Diaz-de-Mera et al. over the range 259 – 335 K. The uncertainty factors reflect the fact that the two reported values for k(298 K) differ by more than a factor of two and that the activation energy is defined by data from a single study over a moderately narrow temperature range. (Table: 06-2, Note: 06-2) Back to Table

I50. ClO + $CH_3S(O)CH_3$. The recommendation is based on the results of a low-pressure discharge flow − mass spectrometry study by Riffault et al. [1118]. These investigators were also able to establish an even lower upper limit of 2 x 10^{-15} $cm^3molec^{-1}s^{-1}$ for the channel that produces Cl atoms. NEW ENTRY Back to Table

I51. ClO + SO. The value of k(298 K) is an average of the determinations by Clyne and MacRobert [285] and Brunning and Stief [187]. The temperature independence is taken from the latter study with the A–factor recalculated to fit the k(298 K) recommendation. (Table 87-41, Note: 87-41) Back to Table

I52. Br + H_2S, Br + CH_3SH. These recommendations are based on the study by Nicovich et al. [967] who measured both the forward and reverse reactions by time–resolved resonance fluorescence detection of Br atoms. The uncertainties placed on these recommendations have been increased over those estimated by the authors to reflect the absence of any confirming investigations. (Table: 94-26, Note: 94-26) Back to Table

I53. Br + CH_3SCH_3. It is well-established based on studies by Wine et al. [1467], Ingham et al. [639], and Nakano et al. [944] that, under atmospheric conditions, attack of Br on CH_3SCH_3 occurs predominantly by addition to the sulfur atom. Above 375K, adduct decomposition is so rapid that the addition channel is effectively negligible. Jefferson et al. [656] report high temperature experiments where the individual hydrogen transfer reactions Br + CH_3SCH_3 → CH_3SCH_2 + HBr (forward reaction) and CH_3SCH_2 + HBr → Br + CH_3SCH_3 (reverse reaction) were isolated in a laser flash photolysis − resonance fluorescence system, and their kinetics were separately studied over the temperature range 386 − 604 K. These investigators determined Arrhenius expressions for the forward and reverse reactions to be 9.0 x 10^{-11} exp(-2386/T) and 8.6 x 10^{-13} exp(+836/T) $cm^3molec^{-1}s^{-1}$, respectively. Analysis of the equilibrium data also permitted determination of the heat of formation of CH_3SCH_2 (see Appendix 1). Extrapolation of the Jefferson et al. Arrhenius expression to 298 K gives a rate constant for the non-adduct-forming part of the Br + CH_3SCH_3 reaction (presumably direct hydrogen abstraction) of 3.0 x 10^{-14} $cm^3molec^{-1}s^{-1}$. This estimated rate constant agrees quite well with the value of (4.9 ± 2.0) x 10^{-14} $cm^3molec^{-1}s^{-1}$ obtained in a competitive kinetics study at atmospheric pressure in air by Ballesteros et al. [70], and is consistent with an upper limit of 1 x 10^{-13} $cm^3molec^{-1}s^{-1}$ reported in a similar study by Maurer et al. [889]. Direct comparison of the Jefferson et al. and Ballesteros et al. kinetic data is warranted only if essentially all adduct formation is reversible in the Ballesteros et al. experiment, which is possible based on the apparent absence of an adduct + O_2 pathway [889], [944], but is not yet well-established. The recommendation for the pressure-independent bimolecular reaction is based on extrapolation of the Arrhenius expression of Jefferson et al. to the atmospheric temperature regime. The large uncertainty reflects the need for a rather long extrapolation. (Table: 06-2, Note: 06-2) Back to Table

I54. Br + $CH_3S(O)CH_3$. The recommendation is based on the results of a low-pressure discharge flow − mass spectrometry study by Riffault et al. [1118]. These authors obtained an upper limit for the total rate constant of 1.5 x 10^{-14} $cm^3molec^{-1}s^{-1}$, and also report channel−specific rate constants in units of 10^{-15} $cm^3molec^{-1}s^{-1}$ of 11±3 for the H−abstraction channel and 1.2±0.3 for the methyl elimination channel. A competitive kinetics study in 740 Torr air by Ballesteros et al. [70] reports a less sensitive upper limit rate constant of 6 x 10^{-14} $cm^3molec^{-1}s^{-1}$. NEW ENTRY Back to Table

I55. BrO + CH_3SCH_3. This recommendation is an average of results obtained in the discharge flow studies of Barnes et al. [77] and Bedjanian et al. [112], and the flash photolysis studies of Ingham et al. [639] and Nakano et al. [944]. The flash photolysis studies were carried out at pressures of 60–200 Torr and give rate constants that are almost a factor of two faster than those obtained in the discharge flow studies at P ~ 1 Torr. The error limits in the present evaluation are adjusted to include all available data. A new study to investigate the pressure dependence of the rate constant is needed. Both Bedjanian et al. and Ingham et al. have shown that DMSO ($CH_3S(O)CH_3$) is produced with near unit yield. Ballesteros et al. [70] report that the rate constants for BrO + CH_3SCH_3 and BrO + CD_3SCD_3 are identical, a result that is consistent with reaction proceeding via formation of a short-lived adduct that rapidly decomposes to Br + DMSO. (Table: 06-2, Note: 06-2) Back to Table

I56. BrO + CH_3SSCH_3. The recommendation is based on a competitive kinetics study in 740 Torr air by Ballesteros et al. [70]. The large uncertainty factor results from the fact that the reported rate constant is measured relative to an assumed value of 3.2 x 10^{-13} $cm^3molec^{-1}s^{-1}$ for the BrO + CH_3SCH_3 rate constant, which has an uncertain pressure dependence (see above), and from the fact that there is only a single study upon which to base a recommendation. NEW ENTRY Back to Table

I57. BrO + $CH_3S(O)CH_3$. The recommendation is based on a competitive kinetics study in 740 Torr air by Ballesteros et al. [70]. A low-pressure discharge flow − mass spectrometry study by Riffault et al. [1118], gives an upper limit that is consistent with the recommendation. The large uncertainty factor results primarily from the fact that the reported rate constant is obtained from a series of competitive kinetics experiments that are referenced to an assumed value of 3.2 x 10^{-13} $cm^3molec^{-1}s^{-1}$ for the BrO + CH_3SCH_3 rate constant, which has an uncertain pressure dependence (see above). NEW ENTRY Back to Table

I58. BrO + SO. This recommendation is based on the measurements of Brunning and Stief [188] performed under both excess BrO and excess SO conditions. The rate constant is supported by the lower limit assigned by Clyne and MacRobert [285] from measurements of SO_2 production. (Table 87-41, Note: 87-41) Back to Table

I59. IO + CH_3SH. The value of k(298 K) comes from the study by Maguin et al. [861] using discharge flow mass spectrometry. The investigators establish a branching ratio near unity for the production of HOI. The uncertainty factor reflects the absence of any confirming investigations. (Table: 94-26, Note: 94-26) Back to Table

I60. IO + CH_3SCH_3. This recommendation comes from the studies by Daykin and Wine [363] using laser photolysis − absorption spectroscopy and the studies of Maguin et al. [861], Barnes et al. [77], and Knight et al. [728] using discharge flow − mass spectrometry. These groups obtained rate constants of $\leq 3.5 \times 10^{-14}$, 1.5×10^{-14}, 8.8×10^{-15}, and 1.6×10^{-14} $cm^3molec^{-1}s^{-1}$, respectively. The studies of Maguin et al. and Barnes et al. supersede earlier, less direct measurements by the same groups, which resulted in rate constants of 1.5×10^{-11} (Martin et al. [877]) and 3.0×10^{-11} $cm^3molec^{-1}s^{-1}$ (Barnes et al. [78]). Nakano et al. [943] have employed a laser flash photolysis – cavity ring down spectroscopy technique to investigate the temperature and pressure dependence of the rate constant. These investigators report that the 298 K rate constant increases from 1 to 25 x 10^{-14} $cm^3molec^{-1}s^{-1}$ as pressure increases from 5 to 100 Torr N_2, then levels off at higher pressure. Nakano et al. also investigated the temperature dependence of the rate constant at P = 100 Torr and observed a very strong negative temperature dependence, i.e., E/R = –2230 ± 460. The pressure dependence reported by Nakano et al. appears to be in conflict with the results of Daykin and Wine, who found k < 3.5 x 10^{-14} $cm^3molec^{-1}s^{-1}$ at all pressures in the range 40 – 300 Torr. The results of Nakano et al. are not used in the current recommendation pending independent verification. (Table: 06-2, Note: 06-2) Back to Table

I61. S + O_2. This recommendation is based primarily on the study of Davis et al. [357]. Modest agreement at 298 K is found in the studies of Fair and Thrush [441], Fair et al. [442], Donovan and Little [412], and Clyne and Townsend [296]. The study by Clyne and Whitefield [303], which indicates a slightly negative E/R between 300 and 400 K, is encompassed by the assigned uncertainty limits. (Table: 82-57, Note: 82-57) Back to Table

I62. S + O_3. This recommendation accepts the only available experimental data of Clyne and Townsend [296]. In this study the authors measure a value of the rate constant for S + O_2 in reasonable agreement with that recommended above. (Table: 82-57, Note: 82-57) Back to Table

I63. SO + O_2. This recommendation is based on the low temperature measurements of Black et al. [151, 152] and Schurath and Goede [1162]. The room temperature rate constant reported by Black et al. supercedes an earlier value [151] as recommended by the authors. The recommended values for k(T) lie significantly higher than an extrapolation of the higher temperature data of Homann et al. [596], but are consistent with the more recent high temperature study of Garland [482]. A room temperature upper limit on k set by Breckenridge and Miller [175] is consistent with the recommendation. (Table: 06-2, Note: 06-2) Back to Table

I64. $SO + O_3$. The value of k(298 K) is an average of the determinations by Halstead and Thrush [543], Robertshaw and Smith [1120], Schurath and Goede [1162] and Black et al. [151, 152]. The value of E/R is an average of the values reported by Halstead and Thrush, Schurath and Goede, and Black et al. [151], with the A-factor recalculated to fit the recommendation for k(298 K). (Table: 06-2, Note: 06-2) Back to Table

I65. $SO + NO_2$. The value of k(298 K) is an average of the determinations by Clyne and MacRobert [284], Black et al. [152], and Brunning and Stief [187], which agree quite well with the rate constant calculated from the relative rate measurements of Clyne et al. [280]. The Arrhenius parameters are taken from Brunning and Stief. (Table: 82-57, Note: 82-57) Back to Table

I66. SO + OClO. This recommendation is based on the room temperature study by Clyne and MacRobert [285]. The uncertainty reflects the absence of any confirming investigation. (Table: 82-57, Note: 82-57) Back to Table

I67. $SO_3 + 2\ H_2O$. Several research groups have attempted to quantify the rate of sulfuric acid formation via this reaction in the gas phase. Reiner and Arnold [1112] placed an upper limit of 2.4×10^{-15} $cm^3molec^{-1}s^{-1}$ on the rate constant, slightly lower than that determined by Wang et al. [1423]. The inability to cite the results as other than an upper limit is due to the difficulty in excluding all heterogeneous effects from the experiments. The higher rate constant reported earlier by Castleman et al. [234] may have resulted from an underestimation of the effects of such heterogeneous reactions. Subsequently, Reiner and Arnold [1113] sought to improve their rate constant determination by more detailed quantification of heterogeneous contributions. They derived a value of 1.2×10^{-15} $cm^3molec^{-1}s^{-1}$, independent of pressure (from 31–260 mbar of synthetic air). Evidence was also obtained that H_2SO_4 was, indeed, the product of the reaction.

Kolb et al. [735] attempted to measure the gas phase rate constant using a turbulent flow reactor designed to minimize wall effects. Their results, when analyzed as representing a bimolecular reaction, support a rate constant in the range $(1 – 7) \times 10^{-15}$ $cm^3molec^{-1}s^{-1}$. However, a more detailed analysis of the data indicated that the gas phase reaction was second order in water vapor. The reaction rate was also observed to increase as the temperature was lowered from 333 K to 243 K. These observations, together with calculations by Morokuma and Mugurama [933], led the latter authors to suggest that SO_3 consumption likely involved its reaction with the water dimer or the reaction $SO_3–H_2O + H_2O$, leading to the formation of sulfuric acid.

A laminar flow reactor study by Lovejoy et al. [847] over the temperature range 250 to 360 K also revealed SO_3 loss to be second order in water concentration and independent of pressure (from 20 to 80 Torr of N_2 at 300 K). These latter authors measured a strong negative temperature dependence for the rate constant and a significant kinetic isotope effect ($k_{H2O} \approx 2k_{D2O}$), leading them to describe the reaction as proceeding via the rapid association between SO_3 and H_2O followed by a slower reaction between the adduct and water to form sulfuric acid. Lovejoy at al.'s measurement of a –13 kcal mol^{-1} "activation" energy was viewed as energetically inconsistent with a SO_3 + water dimer reaction mechanism since it would require a large negative activation energy for the $SO_3 + (H_2O)_2$ step. Jayne et al. [655] have carried out a turbulent flow reactor study over the temperature range 283 to 370 K and the pressure range 100 to 760 Torr N_2. Their results provide further support for a mechanism involving formation of an $SO_3–H_2O$ adduct that reacts with a second H_2O to form H_2SO_4, and the rate constants they report agree quite well with those reported by Lovejoy et al. The recommended expression for first order loss of SO_3,

$$k^I = 8.5 \times 10^{-41} \exp(+6540/T)\ [H_2O]^2\ s^{-1} \quad ([H_2O] \text{ in molec cm}^{-3})$$

is the best fit of the combined data of Lovejoy et al. and Jayne et al. to an Arrhenius form. NEW ENTRY Back to Table

I68. $SO_3 + NO_2$. This recommendation is based on the study of Penzhorn and Canosa [1045] using second derivative UV spectroscopy. These authors observe the production of a white aerosol, which they interpret to be the adduct NSO_5. This claim is supported by ESCA spectra. (Table: 85-37, Note: 85-37) Back to Table

I69. $SH + O_2$. This upper limit for k(298 K) is based on the study by Stachnik and Molina [1229] utilizing experiments sensitive to the production of OH. Somewhat higher upper limits of $1.0 \times 10^{-}$

^{17} and 1.5×10^{-17} were assigned by Friedl et al. [472] and Wang et al. [1421] respectively from the detection sensitivities for OH detection and SH decay respectively. An even higher upper limit by Black [148], based on the lack of SH decay, may have been complicated by SH regeneration. Much less sensitive upper limits have been calculated by Tiee et al. [1308], Nielsen [974], and Cupitt and Glass [336]. Stachnik and Molina [1229] also report a somewhat higher upper limit ($< 1.0 \times 10^{-18}$) for the rate constant for the sum of the two SH + O_2 reaction channels (producing OH + SO and H + SO_2). (Table: 85-37, Note: 85-37) Back to Table

I70. SH + O_3. The value for k(298 K) is an average of the determinations by Friedl et al. [472] (laser–induced fluorescence detection of SH), Schonle et al. [1161] (mass spectrometric detection of reactant SH and product HSO) as revised by Schindler and Benter [1153], and Wang and Howard [1420] (laser magnetic resonance detection of SH). The temperature dependence is from Wang and Howard with the A–factor calculated to agree with the recommended value for k(298 K). The recommendation for g reflects the fact that the temperature dependence comes from measurements above room temperature and, thus, extrapolation to lower temperatures may be subject to additional uncertainties. Wang and Howard report observing a minor reaction channel that produces H + SO + O_2. A theoretical study by Resende and Ornellas [1115] concludes that if reaction occurs on the ground state potential energy surface, the rate constant should be several orders of magnitude slower than the experimental value. (Table: 06-2, Note: 06-2) Back to Table

I71. SH + H_2O_2. This recommended upper limit for k(298 K) is based on the study of Friedl et al. [472]. Their value is calculated from the lack of SH decay (measured by laser–induced fluorescence) and the lack of OH production (measured by resonance fluorescence). The three possible product channels are H_2S + HO_2, HSOH + OH, and HSO + H_2O. (Table: 85-37, Note: 85-37) Back to Table

I72. SH + NO_2. This recommendation is based on the measurements of Wang et al. [1421]. These authors suggest that the lower values of k(298 K) reported by Black [148], Friedl et al. [472], and Bulatov et al. [194] are due to SH regeneration from the H_2S source compound. In the study by Stachnik and Molina [1229], attempts were made at minimizing such regeneration, and the reported value of k(298 K) was significantly higher than that from the earlier studies, but still 30% lower than that measured by Wang et al., who used two independent SH source reactions. A slightly higher rate constant measured by Schonle et al. [1161], as revised by Schindler and Benter [1153], has not been recommended due to the somewhat more limited database for their determination. The reaction as written represents the most exothermic channel. In fact, HSO has been detected as a product by Leu and Smith [808], Bulatov et al. [194], Schonle et al. [1161], and Wang et al. [1421]. The absence of a primary deuterium isotope effect, as observed by Wang et al. [1421], coupled with the large magnitude of the rate constant suggests that the (four–center intermediate) channels producing SO + HNO and OH + SNO are of minor importance. No evidence for a three–body combination reaction was found by either Black [148] or Friedl et al. [472]. Based on a pressure independence of the rate constant between 30 and 300 torr, Black set an upper limit of 7.0×10^{-31} for the termolecular rate constant. Similarly, Stachnik and Molina [1229] observed no change in decay rate between 100 and 730 torr with O_2 (although these O_2 experiments were designed primarily to limit SH regeneration). The recommendation given here is supported by the discharge flow laser–induced fluorescence study of the SD + NO_2 reaction by Fenter and Anderson [450]. These investigators report a rate constant at 298 K of 6.8×10^{-11} cm^3 molec^{-1} s^{-1}, which compares favorably with the value of 7.1×10^{-11} cm^3 molecule^{-1} s^{-1} determined in the Wang et al. study of the same reaction. Fenter and Anderson also obtained an E/R value of –210 K, very similar to the –237 K value derived by Wang et al. for the SH reaction. (Table: 97-4, Note: 97-4) Back to Table

I73. SH + N_2O. The recommendation is the upper limit rate constant reported by Herndon et al. [572]. As discussed by Herndon et al., the much faster (four orders of magnitude) rate constant reported by Ravichandran et al. [1089] appears to result from mis−interpretation of the source of electronically excited HSO, chemiluminescence from which was employed by Ravichandran et al. to follow the reaction kinetics. NEW ENTRY Back to Table

I74. SH + Cl_2. The recommended 298 K rate constant is based on the work of Nesbitt and Leone [957], who studied the kinetics of the Cl + H_2S → SH + HCl, SH + Cl_2 → ClSH + Cl chain reaction. Fenter and Anderson [449] employed a discharge flow − laser induced fluorescence technique to study the SD + Cl_2 reaction over the temperature range 273−373 K. The 298 K rate constant

reported by Fenter and Anderson is about 20% faster than the one reported by Nesbitt and Leone, which is consistent with the expected secondary kinetic isotope effect. The recommended value of E/R is taken from the work of Fenter and Anderson; the recommended value for the parameter g reflects the absence of any confirming studies and uncertainty in the isotope effect on E/R. (Table: 06-2, Note: 06-2) Back to Table

I75. SH + BrCl; SH + Br_2; SH + F_2. The recommendations for these reactions are derived from the data of Fenter and Anderson [449] for the SD radical. The uncertainties have been increased over those estimated by the investigators to reflect the absence of any confirming investigations and the influence of the secondary isotope effect. For the BrCl reaction, the channel producing ClSD + Br was found to be described by the rate expression $k = 2.3 \times 10^{-11} \exp(100/T)$ cm^3 $molecule^{-1}$ s^{-1}. (Table: 92-20, Note: 06-2) Back to Table

I76. HSO + O_2. This recommendation is based on the study by Lovejoy et al. [851], who employed laser magnetic resonance monitoring of HSO in a discharge flow system. The upper limit thus derived for k(298 K) is nearly two orders of magnitude lower than measured by Bulatov et al. [196]. (Table 87-41, Note: (Table: 92-20, Note: 92-20)) Back to Table

I77. HSO + O_3. This recommendation is based on the determinations by Friedl et al. [472] and Wang and Howard [1420]. In the first study, performed at higher O_3 concentrations, greater quantities of HSO were produced in the flow tube and SH approached a steady state due to its generation via HSO + O_3. The rate constant for this reaction was thus determined relative to SH + O_3 from measurements of the steady state SH concentration as a function of the initial SH concentration. In the second study, the rate constant and its branching ratio were measured at two temperatures. At room temperature, the overall rate constant is in excellent agreement with that of Friedl et al. More recently, Lee et al. [795] determined a room temperature rate constant of 4.7×10^{-14} $cm^3molec^{-1}s^{-1}$ for the sum of all reaction channels not producing HS. This value is approximately 30% greater than that measured by Wang and Howard for the same channels. Lee et al. derive an Arrhenius activation energy of 1120 K for these channels from data between 273and 423 K, in agreement with the more limited temperature-dependent data of Wang and Howard.

The lack of an isotope effect when SD was employed in the Friedl et al. study suggests that the products of the HSO + O_3 reaction are SH + $2O_2$ (analogous to those for HO_2 + O_3). However, Wang and Howard found that only 70% of the reaction leads to HS formation. In addition, their observations of HO_2 production in the presence of O_2 suggests the existence of a reaction channel producing HSO_2 + O_2 followed by $HSO_2 + O_2 \rightarrow HO_2 + SO_2$. At the present time, no recommendation is given for the product channels. Further mechanistic work is suggested, since it is important to understand whether this reaction in the atmosphere leads to HS regeneration or to oxidation of the sulfur. (Table: 92-20, Note: 94-26) Back to Table

I78. HSO + NO; HSO + NO_2. The recommendations for these reactions are based on the study by Lovejoy et al. [851] in which laser magnetic resonance was used to monitor HSO in a discharge flow system. Their upper limit for the NO reaction is a factor of 25 lower than the rate constant measured by Bulatov et al. [195] using intracavity laser absorption at pressures between 10 and 100 torr. Since it is unlikely that this reaction rate undergoes a factor of 25 increase between 1 torr (the pressure of the Lovejoy et al. work) and 10 torr, the higher rate constant may be due to secondary chemistry associated with the HSO production methods employed.

The recommendation for the NO_2 reaction is a factor of 2 higher than the rate constant reported by Bulatov et al. [194]. Lovejoy et al. have attributed this difference to HSO regeneration under the experimental conditions used by Bulatov et al. [194]. The product assignment for this reaction is discussed in the note for the HSO_2 + O_2 reaction. (Table 87-41, Note: 87-41) Back to Table

I79. HSO_2 + O_2. This recommendation is based on the rate of HO_2 formation measured by Lovejoy et al. [851] upon addition of O_2 to the HSO + NO_2 reaction system. While HSO_2 was not observed directly, a consideration of the mechanistic possibilities for HSO + NO_2, coupled with measurements of the HO_2 production rate at various O_2 pressures, led these authors to suggest that HSO_2 is both a major product of the HSO + NO_2 reaction and a precursor for HO_2 via reaction with O_2. (Table 87-41, Note: 87-41) Back to Table

I80. $HOSO_2 + O_2$. This recommendation is based on the studies of Gleason et al. [511] and Gleason and Howard [509] in which the $HOSO_2$ reactant was monitored using a chemical ionization mass spectrometric technique. Gleason and Howard conducted their measurements over the 297–423 K temperature range in the only temperature dependence investigation. Thus, the parameter g has been increased from their quoted limits to account for the potential uncertainties in extrapolating their data to sub–ambient temperatures. The value of k(298 K) derives further support from the studies of Margitan [867] and Martin et al. [879], both of whom used modeling fits of OH radical decays in the $OH + SO_2 + M$ reaction system in the presence of O_2 and NO. In this latter analysis, the $HOSO_2$ reacts with O_2, yielding HO_2, which subsequently regenerates OH through its reaction with NO. The infrared spectrum of $HOSO_2$ has been recorded in low temperature matrix isolation experiments by Hashimoto et al. [557] and Nagase et al. [942]. Mass spectrometric detection of $HOSO_2$ in the gas phase has also been reported by Egsgaard et al. [432]. (Table: 06-2, Note: 06-2) Back to Table

I81. $CS + O_2$. The recommendation given for k(298 K) is based on the work of Black et al. [150] using laser–induced fluorescence to monitor CS. This value agrees with the somewhat less precise determination by Richardson [1117] using OCS formation rates. The latter author presents evidence that this reaction channel dominates over the one producing SO + CO by more than a factor of 10. Measurements by Richardson at 293 K and 495 K yield an E/R of 1860 K. However, use of this activation energy with the recommended value of k(298 K) results in an unusually low Arrhenius A-factor of 1.5×10^{-16} $cm^3molec^{-1}s^{-1}$. In view of this, no recommendation is given for the temperature dependence. (Table: 85-37, Note: 85-37) Back to Table

I82. $CS + O_3$; $CS + NO_2$. The k(298 K) recommendations for both reactions accept the results of Black et al. [150], who used laser–induced fluorescence to monitor the CS reactant in a room temperature experiment. The uncertainty factors reflect the absence of any confirming measurements. (Table: 85-37, Note: 85-37) Back to Table

I83. $CH_3S + O_2$. This upper limit is based on the study by Tyndall and Ravishankara [1354]. Somewhat higher upper limits were derived in the earlier studies of Balla et al. [69] and Black and Jusinski [149]. (Table: 90-1, Note: 90-1) Back to Table

I84. $CH_3S + O_3$. The recommendation for k(298 K) is the average of room temperature rate constants reported by Tyndall and Ravishankara [1355], Domine et al. [408], Turnipseed et al. [1335], and Martinez et al. [882]. The recommendation for E/R is the average of values obtained from least squares fits of the temperature-dependent data of Turnipseed et al. and Martinez et al. using only rate constants at temperatures below 345 K. A failure to observe significant reaction in the study by Black and Jusinski [149] is interpreted as due to rapid regeneration of CH_3S in their system. Tyndall and Ravishankara [1355] corrected their measured 298 K rate constant downward by ~20% to account for CH_3S regeneration via the $CH_3SO + O_3$ reaction, but the magnitude of the correction is now highly uncertain in light of the results of Domine et al. and Turnipseed et al. Domine et al. measured the yield of CH_3SO to be 15%. (Table: 06-2, Note: 06-2) Back to Table

I85. $CH_3S + NO$. The upper limit for the bimolecular reaction between CH_3S and NO is based on estimates by Balla et al. [69], who conducted a temperature dependence study of the termolecular reaction. (Table: 92-20, Note: 92-20) Back to Table

I86. $CH_3S + NO_2$. The recommendation for k(298 K) is the average of room temperature rate constants reported by Tyndall and Ravishankara [1354], Domine et al. [406], Turnipseed et al. [1335], Martinez et al. [882], and Chang et al. [244]. The recommendation for E/R is the average of values reported by Turnipseed et al., Martinez et al., and Chang et al. An earlier study by Balla et al. [69] appears to have been affected by secondary reactions resulting from high radical concentrations. Tyndall and Ravishankara determined the NO yield to be (80 ± 20)%. Together with the unity yield of CH_3SO obtained by Domine et al., this implies that the primary reaction channel is as written. (Table: 06-2, Note: 06-2) Back to Table

I87. $CH_2SH + O_2$. This recommendation is the average of the rate constant obtained by Rahman et al. [1086] in a fast flow mass spectrometer system and that from Anastasi et al. [23] using a pulse radiolysis − kinetic absorption apparatus. The value of Anastasi et al. is nearly twice that of Rahman et al. It is difficult at present to indicate a preference for the results of one study over the other, and the value of f(298 K) has been chosen to reflect this uncertainty. Since this is a fast bimolecular

reaction, one would expect the products to be HO_2 + CH_2S, by analogy with the reaction between CH_2OH and O_2. (Table: 94-26, Note: 94-26) Back to Table

I88. CH_2SH + O_3. The value of k(298 K) comes from the study by Rahman et al. [1086] using fast flow − mass spectrometry. The uncertainty factor reflects the absence of any confirming investigations. (Table: 94-26, Note: 94-26) Back to Table

I89. CH_2SH + NO. The value of k(298 K) comes from the study by Anastasi et al. [23] using a pulse radiolysis − kinetic absorption apparatus. The uncertainty factor reflects the absence of any confirming investigations. (Table: 94-26, Note: 94-26) Back to Table

I90. CH_2SH + NO_2. This recommendation averages the rate constant obtained by Rahman et al. [1086] in a fast flow − mass spectrometry system with that from Anastasi et al. [23], using a pulse radiolysis kinetic absorption apparatus. The value of Rahman et al. is nearly twice that of Anastasi et al. It is difficult at present to indicate a preference for the results of one study over the other, and the value of f(298 K) has been chosen to reflect this uncertainty. (Table: 94-26, Note: 94-26) Back to Table

I91. CH_3SO + O_3. This recommendation is the average of values reported by Domine et al. [408] and Borissenko et al. [161]. It is supported by the study of Tyndall and Ravishankara [1355], in which the rate constant was derived from a complex analysis of the CH_3S + O_3 reaction system. Borissenko et al. measured the rate constant relative to the rate constant for the CH_3SO + NO_2 reaction; they report that CH_3SO + NO_2 is faster by a factor of 47. Domine et al. place the direct yield of CH_2SO at approximately 10% and that of CH_3S at 13% at low pressure. Borissenko et al. report that the SO_2 yield is near unity in 100−600 Torr N_2. (Table: 06-2, Note: 06-2) Back to Table

I92. CH_3SO + NO_2. This recommendation is based on the direct measurements of Domine et al. [406]. The results are supported by somewhat less direct measurements of Tyndall and Ravishankara [1354], Mellouki et al. [901], and Kukui et al. [740]. The results of Kukui et al. suggest a small negative activation energy, but their data set is not extensive enough to warrant a recommendation for E/R without independent confirmation. Borissenko et al. [161] report that the SO_2 yield drops from ~0.4 in 100 Torr N_2 to ~0.25 in 660 Torr N_2. (Table: 06-2, Note: 06-2) Back to Table

I93. CH_3SOO + O_3, CH_3SOO + NO, CH_3SOO + NO_2. These recommendations are based on the experiments of Turnipseed et al. [1335] in which CH_3S was monitored by LIF in equilibrium with CH_3SOO. The upper limit for the O_3 reaction was determined from experiments at 227 K. The results for the NO and NO_2 reactions were independent of temperature over the ranges 227–256 K and 227–246 K, respectively. The uncertainties placed on these recommendations have been increased over those estimated by the authors to reflect the absence of any confirming investigations. (Table: 94-26, Note: 94-26) Back to Table

I94. CH_3SO_2 + NO_2. This recommendation is based on the study by Ray et al. [1106] using a discharge flow reactor equipped with laser–induced fluorescence and mass spectrometric detection. The CH_3SO_2 was produced by the sequential oxidation of CH_3S and CH_3SO by NO_2 and is to be differentiated from the weakly bound adduct, CH_3SOO, formed by the reaction of CH_3S with O_2 at low temperature (Turnipseed et al. [1335]). The uncertainty limit on the rate constant has been increased over that given by the authors to reflect the absence of any confirming investigation. However, some additional support for this recommendation does come from the study of the CH_3S + NO_2 reaction by Tyndall and Ravishankara [1354]. These authors observed fluorescence from a product species tentatively identified as CH_3SO_2, produced by the reaction of CH_3SO with NO_2. Computer simulation of the rise and fall of the fluorescence signal yielded an approximate rate constant value for the reaction CH_3SO_2 + NO_2 of 7.0×10^{-12} cm^3 $molec^{-1}$ s^{-1}. However, an unambiguous differentiation between the production and disappearance rate constants was not possible. (Table: 97-4, Note: 97-4) Back to Table

I95. CH_3SCH_2 + NO_3. This recommendation is based on the experiments of Butkovskaya and Le Bras [209]. The uncertainty factor reflects the absence of any confirming investigation. (Table: 94-26, Note: 94-26) Back to Table

I96. $CH_3SCH_2O_2$ + NO. The recommended 298 K rate constant is based on the experiments of Urbanski et al. [1360], which are less impacted by secondary chemistry complications than the experiments of Wallington et al. [1402] or Turnipseed et al. [1337]; the error limits are chosen to encompass the rate

constants reported in all three studies. The E/R value is taken from Urbanski et al., who report the only available temperature dependence data. The recommended value for the parameter g is larger than reported by Urbanski et al. pending independent confirmation of their result. (Table: 06-2, Note: 06-2) Back to Table

I97. $CH_3SCH_2O_2 + CH_3SCH_2O_2$. The recommended 298 K rate constant is the average of values reported by Wallington et al. [1402] using a pulse radiolysis − UV absorption technique and Urbanski et al. [1360] using a laser flash photolysis − tunable diode laser absorption technique. Urbanski et al. observed that the reaction produces formaldehyde with unit yield, suggesting that the dominant reaction pathway is $2\ CH_3SCH_2O_2 \rightarrow 2\ CH_3SCH_2O + O_2$ (CH_3SCH_2O rapidly decomposes to $CH_3S + H_2CO$). NEW ENTRY Back to Table

I98. $CH_3SS + O_3$. This recommendation is based on the discharge flow-photoionization mass spectroscopy study by Domine et al. [408]. The uncertainty factor reflects the absence of any confirming investigations. The rate constant ratio for the reactions of CH_3SS with O_3 and NO_2 is consistent with the rate constant ratio for the corresponding CH_3S reactions. (Table: 92-20, Note: 92-20) Back to Table

I99. $CH_3SS + NO_2$; $CH_3SSO + NO_2$. These recommendations are based on the discharge flow − photoionization mass spectrometry study by Domine et al. [406]. The rate constant ratio for these two reactions agrees with that observed for other RS/RSO radicals with NO_2. The assigned uncertainties reflect this agreement but acknowledge the absence of any confirming investigation. In the Domine et al. study, CH_3SSO was produced by reacting away all CH_3SS with high NO_2 concentrations. Thus, as expected, O atom transfer may be the primary channel in the CH_3SS reaction. (Table: 92-20, Note: 92-20) Back to Table

J1. $Na + O_3$. The recommendation is based on the measurements of Ager et al. [15], Worsnop et al. [1484] as corrected in Worsnop et al. [1485], and Plane et al. [1061]. The data of Worsnop et al. supersede earlier work from that laboratory (Silver and Kolb [1187]). Measurements made by Husain et al. [623] at 500 K are somewhat lower, probably because they did not recognize that secondary chemistry, $NaO + O_3 \rightarrow Na + 2O_2$, interferes with the rate coefficient measurement. The temperature dependence is from results of Worsnop et al. [1485] (214–294 K) and Plane et al. [1061] (208–377K). Ager et al. [15] estimate that the $NaO_2 + O$ product channel is $\leq 5\%$. Evidence that the NaO product is in the $^2\Sigma^+$ excited electronic state was reported by Shi et al. [1181] and Wright et al. [1486]. (Table: 94-26, Note: 94-26) Back to Table

J2. $Na + N_2O$. The recommendation incorporates the data of Husain and Marshall [622], Ager et al. [15], Plane and Rajasekhar [1062], and Worsnop et al. [1485]. Silver and Kolb [1187] measured a rate coefficient at 295 K that is lower and is superseded by Worsnop et al. [1485]. Helmer and Plane [568] report a measurement at 300 K in excellent agreement with the recommendation. Earlier, less direct studies are discussed by Ager et al. [15]. The NaO product does not react significantly with N_2O at room temperature [k (for $Na + N_2 + O_2$ products) $\leq 10^{-16}$ and k (for $NaO_2 + N_2$ products) $\leq 2 \times 10^{-15}$ (Ager et al.). Wright et al. [Wright, 1993 #1863] used UV photoelectron spectroscopy to determine the product NaO is formed predominantly in the excited $^2\Sigma^+$ state. (Table: 92-20, Note: 94-26) Back to Table

J3. $Na + Cl_2$. Two measurements of the rate coefficient for this reaction are in excellent agreement: Silver [1183] and Talcott et al. [1277]. The recommended value is the average of these room temperature results. (Table 87-41, Note: 87-41) Back to Table

J4. NaO + O. The recommendation is based on measurements by Plane and Husain [1060] and Griffin et al. [527]. The $Na + O_3$ reaction produces NaO predominately in the low laying A $^2\Sigma^+$ state which can radiatively and collisionally decay slowly to the X $^2\Pi$ gound state. The Plane and Husain [1060] experiment was configured so the the predominant reactant was NaO X $^2\Pi$ while the Griffin et al. [527] experiment was designed to maximize NaO A $^2\Sigma^+$ concentrations. While the two states may not have identical reaction rate constants, their energy difference is small compared to reaction exothermicity and both states show reaction rate constants near the collisional limit. Since this reaction in the atmosphere will probably proceed through a mixture of the two lowest NaO electronic states and data are available at only one temperature for each state, the recommended rate

constant is an average of the two measurements. Plane and Husain [1060] reported that ~0.01 of the Na product is in the 3^2P excited state, while Griffin et al. [527] report a Na 3^2P product branching ratio of 0.14±0.04. This difference is consistent with the orbital correlation predictions of products for reaction of each NaO state as presented by Herschbach et al. [578]. (Table: 06-2, Note: 06-2) Back to Table

J5. NaO + O_3. This reaction was studied by Silver and Kolb [1187], Ager et al. [15], and Plane et al. [1061], who agree on the rate coefficient and branching ratio. This agreement may be fortuitous because Silver and Kolb used an indirect method and an analysis based on their rate coefficient for the Na + O_3 reaction, which is about 1/2 of the recommended value. Ager et al. employed a somewhat more direct measurement, but the study is complicated by a chain reaction mechanism in the Na/O_3 system. Plane et al. reported rate coefficient measurements for the NaO_2 + O_2 product channel over the temperature range 207–377 K using pulsed photolysis LIF methods. The recommendation for that channel is based on all three studies, and the recommendation for the Na + $2O_2$ channel is based upon the results of Silver and Kolb and Ager et al. The latter reaction channel may also have a significant temperature dependence. (Table: 94-26, Note: 94-26) Back to Table

J6. NaO + H_2. The recommendation is based on a measurement by Ager and Howard [14]. They also reported a significant Na + H_2O product channel and that a small fraction of the Na from this channel is in the 3^2P excited state. (Table 87-41, Note: 87-41) Back to Table

J7. NaO + H_2O. The recommendation is based on a room temperature measurement by Ager and Howard [14] and a temperature dependent measurement by Cox and Plane [331] with the more extensive temperature dependent data favored. (Table: 06-2, Note: 06-2) Back to Table

J8. NaO + NO. The recommendation is based on an indirect measurement reported by Ager et al. [15]. (Table 87-41, Note: 87-41) Back to Table

J9. NaO + HCl. There is only one indirect measurement of the rate coefficient for this reaction, that from the study by Silver et al. [1189]. They indicate that the products are NaCl and OH, although some NaOH and Cl production is not ruled out. (Table: 85-37, Note: 85-37) Back to Table

J10. NaO_2 + O. The recommendation is based on a flow tube study at 300 K by Helmer and Plane [568]. (Table: 94-26, Note: 94-26) Back to Table

J11. NaO_2 + NO. This reaction is endothermic. The upper limit recommended is from an experimental study by Ager et al. [15]. (Table 87-41, Note: 87-41) Back to Table

J12. NaO_2 + HCl. The recommendation is based on a measurement reported by Silver and Kolb [1186]. They indicated that the products are NaCl + HO_2, but NaOOH + Cl may be possible products. (Table 87-41, Note: 87-41) Back to Table

J13. NaOH + HCl. The recommendation is based on the study by Silver et al. [1189], which is the only published study of this reaction. (Table: 85-37, Note: 85-37) Back to Table

J14. $NaHCO_3$ + H. The recommendation is based on measurements at 307 and 227 K by Cox et al. [332]. It is consistent with an upper limit reported by Ager and Howard [13]. NEW ENTRY Back to Table

1.4 References

1. Abbatt, J. P. D. and J. G. Anderson, 1991, J. Phys. Chem. B, **95**, 2382-2390.
2. Abbatt, J. P. D., K. L. Demerjian and J. G. Anderson, 1990, J. Phys. Chem., **94**, 4566-4575.
3. Abbatt, J. P. D., F. F. Fentner and J. G. Anderson, 1992, J. Phys. Chem., **96**, 1780-1785.
4. Abbatt, J. P. D., D. W. Toohey, F. F. Fenter, P. S. Stevens, W. H. Brune and J. G. Anderson, 1989, J. Phys. Chem., **93**, 1022-1029.
5. Acerboni, G., N. R. Jensen, B. Rindone and J. JHjorth, 1999, Chem. Phys. Lett., **309**, 364-368.
6. Adachi, H. and N. Basco, 1979, Chem. Phys. Lett., **63**, 490.
7. Adachi, H., N. Basco and D. G. L. James, 1979, Int. J. Chem. Kinet., **11**, 1211-1229.
8. Addison, M. C., J. P. Burrows, R. A. Cox and R. Patrick, 1980, Chem. Phys. Lett., **73**, 283-287.
9. Addison, M. C., R. J. Donovan and J. Garraway, 1979, J. Chem. Soc. Faraday Disc., **67**, 286-296.
10. Adeniji, S. A., J. A. Kerr and M. R. Williams, 1981, Int. J. Chem. Kinet., **13**, 209.
11. Adler-Golden, S. M. and J. R. Wiesenfeld, 1981, Chem. Phys. Lett., **82**, 281-284.
12. Adusei, G. Y. and A. Fontijn. "Experimental studies of Cl-atom reactions at high temperatures: Cl + H_2 = HCl + H from 291 to 1283 K"; Int. Symp. on Combust., 1994.
13. Ager, J. W., III and C. J. Howard, 1987, J. Geophys. Res., **92**, 6675-6678.
14. Ager, J. W., III and C. J. Howard, 1987, J. Chem. Phys., **87**, 921-925.
15. Ager, J. W., III, C. L. Talcott and C. J. Howard, 1986, J. Chem. Phys., **85**, 5584-5592.
16. Agrawalla, B. S., A. S. Manocha and D. W. Setser, 1981, J. Phys. Chem., **85**, 2873-2877.
17. Aker, P. M., B. I. Niefer, J. J. Sloan and H. Heydtmann, 1987, J. Chem. Phys., **87**, 203-209.
18. Albers, E. A., K. Hoyermann, H. G. Wagner and J. Wolfram. "Symp. Int. Combustion Proc.," 1971.
19. Aleksandrov, E. N., V. S. Arutyunov and S. N. Kozlov, 1981, Kinetics and Catalysis, **22**, 391-394.
20. Amimoto, S. T., A. P. Force, R. G. Gulotty, Jr. and J. R. Wiesenfeld, 1979, J. Chem. Phys., **71**, 3640-3647.
21. Amimoto, S. T., A. P. Force and J. R. Wiesenfeld, 1978, Chem. Phys. Lett., **60**, 40-43.
22. Amimoto, S. T. and J. R. Wiesenfeld, 1980, J. Chem. Phys., **72**, 3899-3903.
23. Anastasi, C., M. Broomfield, O. J. Nielsen and P. Pagsberg, 1992, J. Phys. Chem., **96**, 696-701.
24. Anastasi, C., M. J. Brown, D. B. Smith and D. J. Waddington. Joint French and Italian sections of the Combustion Institute, 1987, Amalfi, Italy.
25. Anastasi, C., D. J. Waddington and A. Woolley, 1983, J. Chem. Soc. Faraday Trans., **79**, 505-516.
26. Anderson, J. G. and F. Kaufman, 1973, Chem. Phys. Lett., **19**, 483-486.
27. Anderson, L. G. and R. D. Stephens.
28. Anderson, P. C. and M. J. Kurylo, 1979, J. Phys. Chem., **83**, 2055.
29. Anderson, S. M., J. Morton, K. Mauersberger, Y. L. Yung and W. B. DeMore, 1992, Chem. Phys. Lett., **189**, 581-585.
30. Andersson, B. Y., R. A. Cox and M. E. Jenkin, 1988, Int. J. Chem. Kinetics, **20**, 283-295.
31. Andresen, P., A. Jacobs, C. Kleinermanns and J. Wolfrum. In *19th Symp. (Intl.) Combustion*, 1982; pp 11.
32. Arnold, I. and F. J. Comes, 1979, Chem. Phys., **42**, 231.
33. Arnold, I. and F. J. Comes, 1980, Chem. Phys., **47**, 125-130.
34. Arrington, C. A., W. Brennen, G. P. Glass, J. V. Michael and H. Niki, 1965, J. Chem. Phys., **43**, 525.
35. Arsene, C., I. Barnes, K. H. Becker, W. F. Schneider, T. J. Wallington, N. Mihalopoulos and J. V. Patroescu-Klotz, 2002, Environ. Sci. Technol., **36**, 5155 - 5163.
36. Ashford, R. D., N. Basco and J. E. Hunt, 1978, Int. J. Chem. Kinet., **10**, 1233-1244.
37. Atakan, B. A. Jacobs, M. Wahl, R. Weller and J. Wolfrum, 1989, Chem. Phys. Lett., **155**, 609-613.
38. Atkinson, D. B., V. I. Jaramillo and M. A. Smith, 1997, J. Phys. Chem A, **101**, 3356-3359.
39. Atkinson, R. and S. M. Aschmann, 1984, Int. J. Chem. Kinet., **16**, 259.
40. Atkinson, R. and S. M. Aschmann, 1985, Int. J. Chem. Kinet., **17**, 33-41.
41. Atkinson, R. and S. M. Aschmann, 1987, Int. J. Chem. Kinet., **19**, 1097-1105.
42. Atkinson, R. and S. M. Aschmann, 1989, Int. J. Chem. Kinet., **21**, 1123-1129.
43. Atkinson, R., S. M. Aschmann, W. P. L. Carter and A. M. Winer, 1982, International Journal of Chemical Kinetics, **14**, 919-926.

44. Atkinson, R., S. M. Aschmann, D. R. Fitz, A. M. Winer and J. N. Pitts, Jr., 1982, Int. J. Chem. Kinet., **14**, 13.
45. Atkinson, R., S. M. Aschmann and J. N. Pitts, Jr., 1988, J. Geophys. Res., **93**, 7125-7126.
46. Atkinson, R., G. M. Breuer and J. N. Pitts Jr., 1976, J. Geophys. Res., **81**, 5765-5770.
47. Atkinson, R. and W. P. L. Carter, 1991, J. Atmos. Chem., **13**, 195-210.
48. Atkinson, R., D. A. Hansen and J. N. Pitts, Jr., 1975, J. Chem. Phys., **63**, 1703-1706.
49. Atkinson, R., R. A. Perry and J. N. Pitts, Jr., 1977, J. Chem. Phys., **66**, 1578.
50. Atkinson, R., R. A. Perry and J. N. Pitts Jr., 1978, Chem. Phys. Lett., **54**, 14.
51. Atkinson, R. and J. N. Pitts, Jr., 1978, J. Chem. Phys., **68**, 3581.
52. Atkinson, R., J. N. Pitts, Jr. and S. M. Aschmann, 1984, J. Phys. Chem., **88**, 1584.
53. Atkinson, R., C. N. Plum, W. P. L. Carter, A. M. Winer and J. N. Pitts, Jr., 1984, J. Phys. Chem., **88**, 1210-1215.
54. Atkinson, R., R. C. Tuazon, H. Macleod, S. M. Aschmann and A. M. Winer, 1986, Geophys. Res. Lett., **13**, 117-120.
55. Audley, G. J., D. L. Baulch and I. M. Campbell, 1981, Int. J. Chem. Kinet., **77**, 2541.
56. Avery, H. E. and R. J. Cvetanovic, 1965, J. Chem. Phys., **43**, 3727-3733.
57. Aviles, R. G., D. F. Muller and P. L. Houston, 1980, Appl. Phys. Lett., **37**, 358-360.
58. Avramenko, L. I. and R. V. Kolesnikova, 1961, Bull. Acad. Sci. USSR, Div. Chem. Sci., 545.
59. Ayhens, Y. V., J. M. Nicovich, M. L. McKee and P. H. Wine, 1997, J. Phys. Chem. A, **101**, 9382-9390.
60. Azad, K. and J. M. Andino, 1999, Int. J. Chem. Kinet., **31**, 810-818.
61. Bacher, C., G. S. Tyndall and J. J. Orlando, 2001, J. Atmos. Chem., **39**, 171-189.
62. Baer, S., H. Hippler, R. Rahn, M. Siefke, N. Seitzinger and J. Troe, 1991, J. Chem. Phys., **95**, 6463-6470.
63. Baghal-Vayjooee, M. H., A. J. Colussi and S. W. Benson, 1978, J. Am. Chem. Soc., **100**, 3214-3215.
64. Bahta, A., R. Simonaitis and J. Heicklen, 1984, Int. J. Chem. Kinet. , **16**, 1227.
65. Balakhnin, V. P., V. I. Egorov and E. I. Intezarova, 1971, Kinetics and Catalysis **12**, 299.
66. Baldwin, A. C. and D. M. Golden, 1978, Chem. Phys. Lett., **55**, 350.
67. Baldwin, R. R., C. E. Dean, M. R. Honeyman and R. W. Walker, 1984, J. Chem. Soc. Faraday Trans. 1, **80**, 3187-3194.
68. Balestra-Garcia, C., G. Le Bras and H. MacLeod, 1992, J. Phys. Chem., **96**, 3312-3316.
69. Balla, R. J., H. H. Nelson and J. R. McDonald, 1986, Chem. Phys., **109**, 101.
70. Ballesteros, B., N. R. Jensen, and J. Hjorth, 2002, J. Atmos. Chem., **43**, 135-150.
71. Barker, J. R., S. W. Benson and D. M. Golden, 1977, Int. J. Chem. Kinet., **9**, 31.
72. Barnes, I., V. Bastian, K. H. Becker, E. H. Fink and W. Nelsen, 1986, J. Atmos. Chem., **4**, 445-466.
73. Barnes, I., V. Bastian, K. H. Becker, E. H. Fink and F. Zabel, 1981, Chem. Phys. Lett. , **83**, 459-464.
74. Barnes, I., V. Bastian, K. H. Becker, E. H. Fink and F. Zabel, 1982, Atmos. Environ., **16**, 545.
75. Barnes, I., V. Bastian, K. H. Becker, E. H. Fink and F. Zabel, 1986, Chem. Phys. Lett., **123**, 28-32.
76. Barnes, I., V. Bastian, K. H. Becker and D. Martin, 1989, Biogenic Sulfur in the Environment, **393**, 476 - 488.
77. Barnes, I., V. Bastian, K. H. Becker and R. D. Overath, 1991, Int. J. Chem. Kinet., **23**, 579-591.
78. Barnes, I., K. H. Becker, P. Carlier and G. Mouvier, 1987, Int. J. Chem. Kinet., **19**, 489-501.
79. Barnes, I., K. H. Becker, E. H. Fink, A. Reimer, F. Zabel and H. Niki, 1983, Int. J. Chem. Kinet., **15**, 631-645.
80. Barnes, I., K. H. Becker, E. H. Fink, A. Reimer, F. Zabel and H. Niki, 1985, Chem. Phys. Lett. , **115**, 1.
81. Barnes, I., K. H. Becker and N. Mihalopoulas, 1994, J. Atmos. Chem., **18**, 267-289.
82. Barnes, I., K. H. Becker and I. Patroescu, 1994, Geophys. Res. Lett., **21**, 2389-2392.
83. Barnes, I., K. H. Becker and I. Patroescu, 1996, Atmos. Environ., **30**, 1805-1814.
84. Barnett, A. J., G. Marston and R. P. Wayne, 1987, J. Chem. Soc. Faraday Trans. 2, **83**, 1453-1463.
85. Barone, S. B., C. M. Bensen, E. J. Dunlea, R. K. Talukdar, R. Portmann and A. R. Ravishankara, 2004, Phys. Chem. Chem. Phys., To be submitted.
86. Barone, S. B., A. A. Turnipseed and A. R. Ravishankara, 1994, J. Phys. Chem., **98**, 4602-4608.

87. Barone, S. B., A. A. Turnipseed and A. R. Ravishankara, 1996, J. Phys. Chem., **100**, 14694-14702.
88. Barry, J., G. Locke, D. Scollard, H. Sidebottom, J. Treacy, C. Clerbaux, R. Colin and J. Franklin, 1997, Int. J. Chem. Kinet., **29**, 607-617.
89. Barry, J., D. J. Scollard, J. J. Treacy, H. W. Sidebottom, G. Le Bras, G. Poulet, S. Teton, A. Chichinin, C. E. Canosa-Mas, D. J. Kinnison, R. P. Wayne and O. J. Nielsen, 1994, Chem. Phys. Lett., **221**, 353-358.
90. Barry, J., H. Sidebottom, J. Treacy and J. Franklin, 1995, Int. J. Chem. Kinet., **27**, 27-36.
91. Basco, N. and S. K. Dogra, 1971, Proc. Roy. Soc. A., **323**, 417-429.
92. Basco, N. and S. K. Dogra, 1971, Proc. Roy. Soc. A., **323**, 29-68.
93. Basco, N. and S. K. Dogra, 1971, Proc. Roy. Soc. A., **323**, 401.
94. Basco, N. and S. S. Parmar, 1985, Int. J. Chem. Kinet., **17**, 891-900.
95. Batt, L., R. T. Milne and R. D. McCulloch, 1977, Int. J. Chem. Kinet., **9**, 567-587.
96. Batt, L. and G. N. Robinson, 1979, Int. J. Chem. Kinet., **11**, 1045.
97. Battin-Leclerc, F., I. K. Kim, R. K. Talukdar, R. W. Portmann, A. R. Ravishankara, R. Steckler and D. Brown, 1999, J. Phys. Chem. A, **103**, 3237-3244.
98. Bauer, D., J. N. Crowley and G. K. Moortgat, 1992, J. Photochem and Photobiol., **A65**, 329-344.
99. Baulch, D. L., I. M. Campbell and S. M. Saunders, 1985, J. Chem. Soc. Faraday Trans. 1, **81**, 259-263.
100. Baulch, D. L., R. A. Cox, R. F. Hampson, Jr., J. A. Kerr, J. Troe and R. T. Watson, 1980, J. Phys. Chem. Ref. Data, **9**, 295-471.
101. Beach, S. D., I. W. M. Smith and R. P. Tuckett, 2001, Int. J. Chem. Kin., **34**, 104-109.
102. Becker, E., T. Benter, R. Kampf, R. N. Schindler and U. Wille, 1991, Ber. Bunsenges. Phys. Chem., **95**, 1168-1173.
103. Becker, E., M. M. Rahman and R. N. Schindler, 1992, Ber. Bunsenges. Phys. Chem., **96**, 776-783.
104. Becker, E., U. Wille, M. M. Rahman and R. H. Schindler, 1991, Ber. Bunsenges. Phys. Chem., **95**, 1173-1179.
105. Becker, K. H., W. Groth and D. Kley, 1969, Z. Naturforsch, **A24**, 1280.
106. Becker, K. H., W. Groth and U. Schurath, 1971, Chem. Phys. Lett., **8**, 259-262.
107. Becker, K. H., W. Groth and U. Schurath, 1972, Chem. Phys. Lett. , **14**, 489-492.
108. Becker, K. H., M. A. Inocencio and U. Schurath, 1975, Int. J. Chem. Kinet., **Symp. No. 1**, 205-220.
109. Becker, K. H. and K. Wirtz, 1989, Journal of Atmospheric Chemistry, **9**, 419-433.
110. Bedjanian, Y., G. Le Bras and G. Poulet, 1999, J. Phys. Chem.,, **103**, 7017-7025.
111. Bedjanian, Y., G. Le Bras and G. Poulet, 1999, Int. J. Chem. Kin., **31**, 698-704.
112. Bedjanian, Y., G. Poulet and G. Le Bras, 1996, Int. J. Chem. Kinet, **28**, 383-389.
113. Bedjanian, Y., V. Riffault and G. Le Bras, 2001, Int. J. Chem. Kin., **33**, 587-599.
114. Bedjanian, Y., V. Riffault, G. Le Bras and G. Poulet, 1999, J. Photochem. Photobiol. A, **128**, 15-25.
115. Bedjanian, Y., V. Riffault, G. Le Bras and G. Poulet, 2001, J. Phys. Chem A, **105**, 573-578.
116. Bedjanian, Y., V. Riffault, G. Le Bras and G. Poulet, 2001, J. Phys. Chem A, **105**, 6154-6166.
117. Bedjanian, Y., V. Riffault and G. Poulet, 2001, J. Phys. Chem A, **105**, 3167-3175.
118. Bednarek, G., M. Breil, A. Hoffman, J. P. Kohlman, V. Mors and R. Zellner, 1996, Ber. Bunsenges. Phys. Chem., **100**, 528-539.
119. Bednarek, G., J. P. Kohlmann, H. Saathoff and R. Zellner, 1995, Z, Phys. Chem., **188**, 1-15.
120. Bedzhanyan, Y. R., E. M. Markin and Y. M. Gershenzon, 1993, Kinetics and Catalysis, **33**, 594-601.
121. Bedzhanyan, Y. R., E. M. Markin and Y. M. Gershenzon, 1993, Kinetics and Catalysis, **34**, 1-3.
122. Bedzhanyan, Y. R., E. M. Markin and Y. M. Gershenzon, 1993, Kinetics and Catalysis, **33**, 601-606.
123. Bedzhanyan, Y. R., E. M. Markin, G. G. Politenkova and Y. M. Gershenzon, 1993, Kinetics and Catalysis, **33**, 797-801.
124. Beichert, P., L. Wingen, J. Lee, R. Vogt, M. J. Ezell, M. Ragains, R. Neavyn and B. J. Finlayson-Pitts, 1995, J. Phys. Chem., **99**, 13156-13162.
125. Bemand, P. P. and M. A. A. Clyne, 1977, J. Chem. Soc. Faraday Trans. 2, **73**, 394.

126. Bemand, P. P., M. A. A. Clyne and R. T. Watson, 1973, J. Chem. Soc. Faraday Trans. 1, **69**, 1356-1374.
127. Bemand, P. P., M. A. A. Clyne and R. T. Watson, 1974, J. Chem. Soc. Faraday Trans. 2, **70**, 564-576.
128. Beno, M. F., C. D. Jonah and W. A. Mulac, 1985, Int. J. Chem. Kinet., **17**, 1091-1101.
129. Benson, S. W., F. R. Cruickshank and R. Shaw, 1969, Int. J. Chem. Kinet., **1**, 29.
130. Bera, R. K. and R. J. Hanrahan, 1988, Radiation Physics and Chemistry, **32**, 579-584.
131. Berry, R., J. Yuan, A. Misra and P. Marshall, 1998, J. Phys. Chem. A, **102**, 5182-5188.
132. Bevilacqua, T. J., D. R. Hanson and C. J. Howard, 1993, J. Phys. Chem., **97**, 3750-3757.
133. Bhaskaran, K. A., P. Frank and T. Just. In *12th International Shock Tube Symposium* Jerusalem., 1979.
134. Bhatnagar, A. and R. W. Carr, 1994, Chem. Phys. Lett., **231**, 454-459.
135. Bida, G. T., W. H. Breckenridge and W. S. Kolln, 1976, J. Chem. Phys., **64**, 3296.
136. Biedenkapp, D. and E. J. Bair, 1969, J.Chem. Soc., **52**, 6119.
137. Biedenkapp, D. and E. J. Bair, 1970, J. Chem. Phys., **52**, 6119-6125.
138. Biermann, H. W., G. W. Harris and J. N. Pitts, Jr., 1982, J. Phys. Chem., **86**, 2958-2964.
139. Biermann, H. W., C. Zetzsch and F. Stuhl, 1978, Ber. Bunsenges Phys. Chem., **82**, 633.
140. Biggs, P., C. E. Canosa-Mas, J.-M. Fracheboud, D. E. Shallcross and R. P. Wayne, 1995, Geophys. Res. Lett., **22**, 1221-1224.
141. Biggs, P., C. E. Canosa-Mas, P. S. Monks, R. P. Wayne, T. Benter and R. N. Schindler, 1993, Int. J. Chem. Kinet., **25**, 805-817.
142. Biggs, P., M. H. Harwood, A. D. Parr and R. P. Wayne, 1991, J. Phys. Chem., **97**, 7746-7751.
143. Bilde, M. and T. J. Wallington, 1998, J. Phys. Chem., **102**, 1550-1555.
144. Bilde, M., T. J. Wallington, G. Ferronato, J. J. Orlando, G. S. Tyndall, E. Estupinan and S. Haberkorn, 1998, J. Phys.Chem. A, **102**, 1976-1986.
145. Billington, A. P. and P. Borrell, 1986, J. Chem. Soc. Faraday Trans. 2, **82**, 963-970.
146. Birks, J. W., B. Shoemaker, T. J. Leck, R. A. Borders and L. J. Hart, 1977, J. Chem. Phys., **66**, 4591-4599.
147. Birks, J. W., B. Shoemaker, T. J. Leck and D. M. Hinton, 1976, J. Chem. Phys., **65**, 5181-5185.
148. Black, G., 1984, J. Chem. Phys., **80**, 1103-1107.
149. Black, G. and L. E. Jusinski, 1986, J. Chem. Soc. Faraday Trans. 2, **86**, 2143.
150. Black, G., L. E. Jusinski and T. G. Slanger, 1983, Chem. Phys. Lett., **102**, 64-68.
151. Black, G., R. L. Sharpless and T. G. Slanger, 1982, Chem. Phys. Lett., **93**, 598-602.
152. Black, G., R. L. Sharpless and T. G. Slanger, 1982, Chem. Phys. Lett., **90**, 55-58.
153. Blitz, M. A., T. J. Dillon, D. E. Heard, M. J. Pilling and I. D. Trought, 2004, Phys. Chem. Chem. Phys., **6**, 2162-2171.
154. Blitz, M. A., K. W. McKee and M. J. Pilling, 2000, Proceedings of the Combustion Institute, **28**, 2491 - 2497.
155. Bloss, W. J., D. M. Rowley, R. A. Cox and R. L. Jones, 2002, Phys. Chem. Chem. Phys., **4**, 3639-3647.
156. Bohmer, E. and W. Hack, 1991, Ber. Bunsenges. Phys. Chem., **95**, 1688-1690.
157. Bonard, A., V. Daele, J.-L. Delfau and C. Vovelle, 2002, J. Phys. Chem. A, **106**, 4348-4389.
158. Boodaghians, R. B., C. E. Canosa-Mas, P. J. Carpenter and R. P. Wayne, 1988, J. Chem. Soc. Faraday Trans. 2, **84**, 931-948.
159. Boodaghians, R. B., I. W. Hall and R. P. Wayne, 1987, J. Chem. Soc. Faraday Trans. 2, **83**, 529-538.
160. Borders, R. A. and J. W. Birks, 1982, J. Phys. Chem., **86**, 3295-3302.
161. Borissenko, D., A. Kukui, G. Laverdet and G. Le Bras, 2003, J. Phys. Chem. A, **107**, 1155 - 1161.
162. Borrell, P., P. Borrell and K. R. Grant, 1983, J. Chem. Phys., **78**, 748.
163. Borrell, P., P. M. Borrell and M. D. Pedley, 1977, Chem. Phys. Lett., **51**, 300-302.
164. Borrell, P. and D. Richards, 1989, J. Chem. Soc., **85**, 1401.
165. Bourbon, C., M. Brioukov and P. Devolder, 1996, C.A. Acad. Sci. Paris, **322**, 181-188.
166. Bourbon, C., M. Brioukov, B. Hanoune, J. P. Sawerysyn and P. Devolder, 1996, Chem. Phys. Lett., **254**, 203-212.
167. Bourbon, C., C. Fittschen, J. P. Sawerysyn and P. Devolder, 1995, J. Phys. Chem., **99**, 15102-15107.

168. Bourmada, N., C. Lafage and P. Devolder, 1987, Chem. Phys. Lett., **136**, 209-214.
169. Bozzelli, J. W. *Ph.D. Thesis*; Dept. of Chemistry, Princeton University, (Diss. Abstr. Int. B 34(2) 608), 1973.
170. Bozzelli, J. W. and A. M. Dean, 1990, J. Phys. Chem., **94**, 3313-3317.
171. Bradley, J. N., W. Hack, K. Hoyermann and H. G. Wagner, 1973, J. Chem. Soc. Faraday Trans. 1, **69**, 1889.
172. Brahan, K. M., A. D. Hewitt, G. D. Boone and S. A. Hewitt, 1996, Int. J. Chem. Kinet., **28**, 397-404.
173. Braithwaite, M. and S. R. Leone, 1978, J. Chem. Phys., **69**, 839-845.
174. Braithwaite, M., E. A. Ogryzlo, J. A. Davidson and H. I. Schiff, 1976, J. Chem. Phys., **2772**, 2075.
175. Breckenridge, W. H. and T. A. Miller, 1972, J. Chem. Phys., **56**, 465.
176. Bridier, I., B. Veyret and R. Lesclaux, 1993, Chem. Phys. Lett., **201**, 563-568.
177. Bridier, I., B. Veyret, R. Lesclaux and M. E. Jenkin, 1993, J. Chem. Soc. Faraday Trans., **89**, 2993-2997.
178. Brown, A. C., C. E. Canosa-Mas, A. D. Parr, K. Rothwell and R. P. Wayne, 1990, Nature, **347**, 541-543.
179. Brown, A. C., C. E. Canosa-Mas, A. D. Parr and R. P. Wayne, 1990, Atmos. Environ., **24A**, 2499-2511.
180. Brown, A. C., C. E. Canosa-Mas and R. P. Wayne, 1990, Atmos. Environ., **24A**, 361-367.
181. Brown, A. C. and B. A. Thrush, 1967, Trans. Faraday Soc., **63**, 630.
182. Brown, R. D. and I. W. M. Smith, 1975, Int. J. Chem. Kinet. , **7**, 301.
183. Brown, S. S., J. B. Burkholder, R. K. Talukdar and A. R. Ravishankara, 2001, Journal of Physical Chemistry A, **105**, 1605-1614.
184. Brown, S. S., R. K. Talukdar and A. R. Ravishankara, 1999, J. Phys. Chem. A, **103**, 3031-3037.
185. Brune, W. H., J. J. Schwab and J. G. Anderson, 1983, J. Phys. Chem., **87**, 4503-4514.
186. Brunning, J. and M. A. A. Clyne, 1984, J. Chem. Soc. Faraday Trans 2, **80**, 1001-1014.
187. Brunning, J. and L. J. Stief, 1986, J. Chem. Phys., **84**, 4371-4377.
188. Brunning, J. and L. J. Stief, 1986, J. Chem. Phys., **85**, 2591.
189. Bryukov, M. G., I. R. Slagle and V. D. Knyazev, 2002, J. Phys. Chem. A, **106**, 10532-10542.
190. Bryukov, M. G., I. R. Slagle and V. D. Knyazev, 2003, J. Phys. Chem. A, **107**, 6565-6573.
191. Buben, S. N., I. K. Larin, N. A. Messineva and E. M. Trofimova, 1990, Khim. Fiz., **9**, 116-126.
192. Buben, S. N., I. K. Larin, N. A. Messineva and E. M. Trofimova, 1991.
193. Bulatov, V. P., A. A. Buloyan, S. G. Cheskis, M. Z. Kozliner, O. M. Sarkisov and A. I. Trostin, 1980, Chem. Phys. Lett., **74**, 288.
194. Bulatov, V. P., M. Z. Kozliner and O. M. Sarkisov, 1984, Khim. Fiz., **3**, 1300-1305.
195. Bulatov, V. P., M. Z. Kozliner and O. M. Sarkisov, 1985, Khimi Fiz. , **4**, 1353.
196. Bulatov, V. P., O. M. Sarkisov, M. Z. Kozliner and V. G. Ergorov, 1986, Khim. Fiz., **5**, 1031.
197. Bulatov, V. P., S. I. Vereschchuk, F. N. Dzegilenko, O. M. Sarkisov and V. N. Khabarov, 1990, Khim. Fiz., **9**, 1214.
198. Burkholder, J. B., 2000, J. Phys. Chem. A, **104**, 6733-6737.
199. Burkholder, J. B., P. D. Hammer, C. J. Howard and A. Goldman, 1989, J. Geophys. Res., **94**, 2225-2234.
200. Burkholder, J. B., A. Mellouki, R. Talukdar and A. R. Ravishankara, 1994, Int. J. Chem. Kinet., **24**, 711-725.
201. Burkholder, J. B., R. R. Wilson, T. Gierczak, R. Talukdar, S. A. McKeen, J. J. Orlando, G. L. Vaghjiani and A. R. Ravishankara, 1991, J. Geophys. Res., **96**, 5025-5043.
202. Burks, T. L. and M. C. Lin, 1981, Int. J. Chem. Kinet., **13**, 13977-13999.
203. Burrows, J. P., D. I. Cliff, G. W. Harris, B. A. Thrush and J. P. T. Wilkinson, 1979, Proc. Roy. Soc. (London), **A368**, 463-481.
204. Burrows, J. P. and R. A. Cox, 1981, J. Chem. Soc. Faraday Trans. 1, **77**, 2465.
205. Burrows, J. P., R. A. Cox and R. G. Derwent, 1981, J. Photochem., **16**, 147-168.
206. Burrows, J. P., G. W. Harris and B. A. Thrush, 1977, Nature, **267**, 233-234.
207. Burrows, J. P., G. S. Tyndall and G. K. Moortgat, 1985, J. Phys. Chem., **89**, 4848-4856.
208. Burrows, J. P., T. J. Wallington and R. P. Wayne, 1984, J. Chem. Soc. Faraday Trans. 2, **80**, 957-971.
209. Butkovskaya, N. I. and G. Le Bras, 1994, J. Phys. Chem., **98**, 2582-2591.

210. Butkovskaya, N. I., G. Poulet and G. Le Bras, 1995, J. Phys. Chem., **99**, 4536-4543.
211. Butkovskaya, N. I. and D. W. Setser, 1998, J. Phys. Chem. A, **102**, 6395-6405.
212. Butkovskaya, N. I. and D. W. Setser, 1999, Chem. Phys. Lett., **312**, 37-44.
213. Butkovskaya, N. I. and D. W. Setser, 1999, J. Phys. Chem. A, **103**, 6921-6929.
214. Butler, R., I. J. Solomon and A. Snelson, 1978, Chem. Phys. Lett., **54**, 19.
215. Cadle, R. D. and J. W. Powers, 1967, J. Phys. Chem., **71**, 1702-1706.
216. Cadle, R. D. and C. Schadt, 1953, J. Phys. Chem., **21**, 163.
217. Cadman, P., A. W. Kirk and A. F. Trotman-Dickenson, 1976, J. Chem. Soc. Chem. Commun., **72**, 1027-1032.
218. Callear, A. B. and R. E. M. Hedges, 1970, Trans. Faraday Soc., **66**, 605.
219. Callear, A. B. and I. W. M. Smith, 1967, Nature, **213**, 382.
220. Calvert, J. G. and J. N. Pitts *Photochemistry*; John Wiley & Sons, Inc.: New York, 1966.
221. Campbell, I. M., D. F. McLaughlin and B. J. Handy, 1976, Chem. Phys. Lett., **38**, 362-364.
222. Cannon, B. D., J. S. Robertshaw, I. W. M. Smith and M. D. Williams, 1984, Chem. Phys. Lett., **105**, 380-385.
223. Canosa-Mas, C., S. J. Smith, S. Toby and R. P. Wayne, 1988, J. Chem. Soc. Faraday Trans. 2, **84**, 247-262.
224. Canosa-Mas, C. E., R. J. Dillon, H. Sidebotom, K. C. Thompson and R. P. Wayne, 2001, Phys. Chem. Chem. Phys., **3**, 542-550.
225. Canosa-Mas, C. E., S. J. Smith, S. Toby and R. P. Wayne, 1989, J. Chem. Soc. Faraday Trans. 2, **85**, 709-725.
226. Cantrell, C. A., J. A. Davidson, K. L. Busarow and J. G. Calvert, 1986, J. Geophys. Res., **91**, 5347-5353.
227. Cantrell, C. A., J. A. Davidson, A. H. McDaniel, R. E. Shetter and J. G. Calvert, 1988, J. Chem. Phys., **88**, 4997-5006.
228. Cantrell, C. A., J. A. Davidson, R. E. Shetter, B. A. Anderson and J. G. Calvert, 1987, J. Phys. Chem., **91**, 6017-6021.
229. Cantrell, C. A., R. E. Shetter and J. G. Calvert, 1994, J. Geophys. Res., **99**, 3739-3743.
230. Cantrell, C. A., R. E. Shetter, A. H. McDaniel and J. G. Calvert, 1990, J. Geophys. Res., **95**, 20531-20537.
231. Cantrell, C. A., R. E. Shetter, A. J. McDaniel, J. G. Calvert, J. A. Davidson, D. C. Lowe, S. C. Tyler, R. J. Cicerone and J. P. Greenberg, 1990, J. Geophys. Res., **95**, 22455-22462.
232. Cantrell, C. A., W. R. Stockwell, L. G. Anderson, K. L. Busarow, D. Perner, A. Schmeltekopf, J. G. Calvert and H. S. Johnston, 1985, J. Phys. Chem., **89**, 139-146.
233. Casavecchia, P., R. J. Buss, S. J. Sibener and Y. T. Lee, 1980, J. Chem. Phys., **73**, 6351-6352.
234. Castleman, A. W., R. E. Davis, H. R. Munkelwitz, I. N. Tang and W. P. Wood, 1975, Int. J. Chem. Kinet., **Symp. 1**, 629.
235. Catoire, V., R. Lesclaux, P. D. Lightfoot and M.-T. Rayez, 1994, J. Phys. Chem., **98**, 2889-2898.
236. Catoire, V., R. Lesclaux, W. F. Schneider and T. J. Wallington, 1996, J. Phys. Chem., **100**, 14356-14371.
237. Cattell, F. C., J. Cavanagh, R. A. Cox and M. E. Jenkin, 1986, J. Chem. Soc. Faraday Trans. 2, **82**, 1999-2018.
238. Cattell, F. C. and R. A. Cox, 1986, J. Chem. Soc. Faraday Trans. 2, **82**, 1413-1426.
239. Chan, W. H., W. M. Uselman, J. G. Calvert and J. H. Shaw, 1977, Chem. Phys. Lett., **45**, 240.
240. Chang, J. S. and J. R. Barker, 1979, J. Phys. Chem., **83**, 3059.
241. Chang, J. S. and F. Kaufman, 1977, J. Chem. Phys., **66**, 4989.
242. Chang, J. S. and F. Kaufman, 1977, Geophys. Res. Lett., **4**, 192-194.
243. Chang, J. S., P. L. Trevor and J. R. Barker, 1981, Int. J. Chem. Kinet., **13**, 1151-1161.
244. Chang, P.-F., T. T. Wang, S. W. Niann, Y.-L. Hwang and Y.-P. Lee, 2000, J. Phys. Chem. A, **104**, 52525 - 5529.
245. Chapman, C. J. and R. P. Wayne, 1974, Int. J. Chem. Kinet., **6**, 617-630.
246. Chasovnikov, S. A., A. I. Chichinin and L. N. Krasnoperov, 1987, Chem. Phys., **116**, 91-99.
247. Chatha, J. P. S., P. K. Arora, N. Raja, P. B. Kulkarni and K. G. Vohra, 1979, Int. J. Chem. Kinetics, **11**, 175-185.
248. Cheah, C. T. and M. A. A. Clyne, 1980, J. Chem. Soc. Faraday Trans., **76**, 1543.

249. Cheema, S. A., K. A. Holbrook, G. A. Oldershaw and R. W. Walker, 2002, Int. J. Chem. Kinet., **34**, 110-121.
250. Chen, J., V. Catoire and H. Niki, 1995, Chem. Phys. Lett, **245**, 519-528.
251. Chen, J., V. Young, T. Zhu and H. Niki, 1993, J. Phys. Chem., **97**, 11696-11698.
252. Chen, J., T. Zhu and H. Niki, 1992, J. Phys. Chem., **96**, 6115-6117.
253. Chen, J., T. Zhu, H. Niki and G. J. Mains, 1992, Geophys. Res. Lett., **19**, 2215-2218.
254. Chen, K. S., S. S. Cheng and Y. P. Lee, 2003, J. Chem. Phys., **119**, 4229-4236.
255. Chen, L., F. Fukuda, N. Takenaka, H. Bandow and Y. Maeda, 2000, Int. J. Chem. Kinet., **25**, 73-78.
256. Chen, M. C. and H. A. Taylor, 1961, J. Chem. Phys., **34**, 1344-1347.
257. Chen, X., F. Wu and B. R. Weiner, 1995, Chem. Phys. Lett., **247**, 313-320.
258. Cheng, B.-M. and Y.-P. Lee, 1986, Int. J. Chem. Kinet., **18**, 1303-1314.
259. Cheskis, S. G., A. A. Iogansen, O. M. Sarkisov and A. A. Titov, 1985, Chem. Phys. Lett., **120**, 45-49.
260. Cheskis, S. G. and O. M. Sarkisov, 1979, Chem. Phys. Lett., **62**, 72.
261. Chichinin, A., S. Teton, G. Le Bras and G. Poulet, 1994, J. Atmos. Chem, **18**, 239-245.
262. Chichinin, A. I., 1997, J. Chem. Phys., **106**, 1057.
263. Chiorboli, C., C. A. Bignozzi, A. Maldotti, P. F. Giardini, A. Rossi and V. Carassiti, 1983, Int. J. Chem. Kinet., **15**, 579-586.
264. Choo, K. Y. and M.-T. Leu, 1985, Int. J. Chem. Kinetics, **17**, 1155-1167.
265. Choo, K. Y. and M. T. Leu, 1985, J. Phys. Chem., **89**, 4832-4837.
266. Christensen, L. E., M. Okumura, S. P. Sander, R. J. Salawitch, G. C. Toon, B. Sen, J.-F. Blavier and K. W. Jucks, 2002, Geophys. Res. Let., **29**, 1029/2001GL014525.
267. Cillien, C., P. Goldfinger, G. Huybrechts and G. Martens, 1967, Trans. Faraday Soc., **63**, 1631-1635.
268. Clark, I. D., I. T. N. Jones and R. P. Wayne, 1970, Proc. Roy. Soc. Lond. A., **317**, 407-416.
269. Clark, I. D. and R. P. Wayne, 1969, Chem. Phys. Lett., **3**, 405-407.
270. Clark, I. D. and R. P. Wayne, 1969, Proc. Roy. Soc. Lond. A., **314**, 111-127.
271. Clark, I. D. and R. P. Wayne, 1970, Proc. Roy. Soc. London. A., **316**, 539-550.
272. Clark, R. H., D. Husain and J. Y. Jezequel, 1982, J. Photochem., **18**, 39-46.
273. Clarke, J. S., J. H. Kroll, N. M. Donahue and J. G. Anderson, 1998, J. Phys. Chem. A,, **102**, 9847-9857.
274. Clemo, A. R., F. E. Davidson, G. L. Duncan and R. Grice, 1981, Chem. Phys. Lett., **84**, 509-511.
275. Clough, P. N. and B. A. Thrush, 1967, Trans. Faraday Soc., **63**, 915-925.
276. Clyne, M. A. A. and J. A. Coxon, 1968, Proc. Roy. Soc. A, **303**, 207-231.
277. Clyne, M. A. A. and H. W. Cruse, 1970, Trans. Faraday Soc., **66**, 2227.
278. Clyne, M. A. A. and H. W. Cruse, 1972, J. Chem. Soc. Faraday Trans. 2, **68**, 1281.
279. Clyne, M. A. A. and S. Down, 1974, J. Chem. Soc. Faraday Trans. 2, **70**, 253-266.
280. Clyne, M. A. A., C. J. Halstead and B. A. Thrush, 1966, Proc. Soc. London Ser. A., **295**, 355.
281. Clyne, M. A. A. and A. Hodgson, 1985, J. Chem. Soc. Faraday Trans. 2, **81**, 443-455.
282. Clyne, M. A. A. and P. M. Holt, 1979, J. Chem. Soc. Faraday Trans. 2, **75**, 582-591.
283. Clyne, M. A. A. and P. M. Holt, 1979, J. Chem. Soc. Faraday Trans. 2, **75**, 569-581.
284. Clyne, M. A. A. and A. J. MacRobert, 1980, Int. J. Chem. Kinet., **12**, 79-96.
285. Clyne, M. A. A. and A. J. MacRobert, 1981, Int. J. Chem. Kinet., **13**, 187-197.
286. Clyne, M. A. A., A. J. MacRobert, T. P. Murrells and L. J. Stief, 1984, J. Chem. Soc. Faraday Trans. 2, **80**, 877-886.
287. Clyne, M. A. A. and I. S. McDermid, 1975, J. Chem. Soc. Faraday Trans. 1, **71**, 2189.
288. Clyne, M. A. A., D. J. McKenney and R. F. Walker, 1973, Can. J. Chem., **51**, 3596.
289. Clyne, M. A. A., D. J. McKenney and R. T. Watson, 1975, Chem. Soc. Faraday Trans. 1, **71**, 322-335.
290. Clyne, M. A. A. and P. Monkhouse, 1977, J. Chem. Soc. Faraday Trans. 2, **73**, 298-309.
291. Clyne, M. A. A., P. B. Monkhouse and L. W. Townsend, 1976, Int. J. Chem. Kinet., **8**, 425.
292. Clyne, M. A. A. and W. S. Nip, 1976, J. Chem. Soc. Faraday Trans. 1, **72**, 2211-2217.
293. Clyne, M. A. A. and W. S. Nip, 1976, J. Chem. Soc. Faraday Trans. 2, **72**, 838-847.
294. Clyne, M. A. A. and Y. Ono, 1982, Chem. Phys., **69**, 381-388.
295. Clyne, M. A. A. and Y. Ono, 1983, Chem. Phys. Lett., **94**, 597-602.

296. Clyne, M. A. A. and L. W. Townsend, 1975, Int. J. Chem. Kinet., **Symp. 1**, 73-84.
297. Clyne, M. A. A. and R. F. Walker, 1973, J. Chem. Soc. Faraday Trans. 1, **69**, 1547-1567.
298. Clyne, M. A. A. and R. T. Watson, 1974, J. Chem. Soc. Faraday Trans. 1, **70**, 2250-2259.
299. Clyne, M. A. A. and R. T. Watson, 1974, J. Chem. Soc. Faraday Trans. 1, **70**, 1109.
300. Clyne, M. A. A. and R. T. Watson, 1975, J. Chem. Soc. Faraday Trans. 1, **71**, 336.
301. Clyne, M. A. A. and R. T. Watson, 1977, J. Chem. Soc. Faraday Trans. 1, **73**, 1169-1187.
302. Clyne, M. A. A. and I. F. White, 1971, Trans. Faraday Soc., **67**, 2068-2076.
303. Clyne, M. A. A. and P. D. Whitefield, 1979, J. Chem. Soc. Faraday Trans. 2, **75**, 1327.
304. Cocks, A. T., R. P. Fernanado and I. S. Fletcher, 1986, Atmos. Environ., **20**, 2359-2366.
305. Collins, R. J., D. Husain and R. J. Donovan, 1973, J. Chem. Soc. Faraday Trans. 2, **69**, 145-157.
306. Colussi, A. J., 1990, J. Phys. Chem., **94**, 8922-8926.
307. Colussi, A. J. and M. A. Grela, 1994, Chem. Phys. Lett., **229**, 134-138.
308. Colussi, A. J., S. P. Sander and R. R. Friedl, 1992, J. Phys.Chem., **96**, 4442-4445.
309. Cook, J. L., C. A. Ennis, T. J. Leck and J. W. Birks, 1981, J. Chem. Phys., **74**, 545.
310. Coomber, J. W. and E. Whittle, 1966, Trans. Faraday Soc., **62**, 2183-2190.
311. Cooper, W. F. and J. F. Hershberger, 1992, J. Phys. Chem., **96**, 5405-5410.
312. Cotter, E. S. N., N. J. Booth, C. E. Canosa-Mas, D. J. Gray, D. E. Shallcross and R. P. Wayne, 2001, Chem. Phys. Phys. Chem, **3**, 402-408.
313. Cox, J. W., H. H. Nelson and J. R. McDonald, 1985, Chem. Phys., **96**, 175.
314. Cox, R. A., 1980, Int. J. Chem. Kinet., **12**, 649.
315. Cox, R. A., R. A. Barton, E. Ljungstrum and D. W. Stocker, 1984, Chem. Phys. Lett., **108**, 228-232.
316. Cox, R. A. and J. P. Burrows, 1979, J. Phys. Chem., **83**, 2560-2568.
317. Cox, R. A., J. P. Burrows and T. J. Wallington, 1981, Chem. Phys. Lett., **84**, 217-221.
318. Cox, R. A. and G. B. Coker, 1983, J. Atmos. Chem., **1**, 53.
319. Cox, R. A. and R. G. Derwent, 1979, J. Chem. Soc. Far. Trans. 1, **75**, 1635-1647.
320. Cox, R. A., R. G. Derwent, A. E. J. Egg1eton and J. E. Lovelock, 1976, Atmos. Environ., **10**, 305.
321. Cox, R. A., R. G. Derwent, A. E. J. Eggleton and H. J. Read, 1979, J. Chem. Soc. Faraday Trans. I, **75**, 1648-1666.
322. Cox, R. A., R. G. Derwent and P. M. Holt, 1975, Chemosphere, **4**, 201.
323. Cox, R. A., R. G. Derwent and P. M. Holt, 1976, J. Chem. Soc. Faraday Trans. 1, **72**, 2031.
324. Cox, R. A., R. G. Derwent, S. V. Kearsey, L. Batt and K. G. Patrick, 1980, J. Photochem., **13**, 149.
325. Cox, R. A., R. G. Derwent and M. R. Williams, 1980, Environ. Sci. and Technol., **14**, 57-61.
326. Cox, R. A., M. Fowles, D. Moulton and R. P. Wayne, 1987, J. Phys. Chem., **91**, 3361-3365.
327. Cox, R. A. and G. D. Hayman, 1988, Nature, **332**, 796-800.
328. Cox, R. A. and S. A. Penkett, 1972, J. Chem. Soc., Faraday Trans. 1, **68**, 1735.
329. Cox, R. A. and D. Sheppard, 1980, Nature, **284**, 330-331.
330. Cox, R. A., D. W. Sheppard and M. P. Stevens, 1982, J. Photochem., **19**, 189-207.
331. Cox, R. M. and J. M. C. Plane, 1999, Phys. Chem, Chem. Phys., **1**, 4713-4720.
332. Cox, R. M., D. E. Self and J. M. C. Plane, 2001, J. Geophys. Res., **106**, 1733-1739.
333. Crawford, M. A., T. J. Wallington, J. J. Szente, M. M. Maricq and J. S. Francisco, 1999, J. Phys. Chem. A, **103**, 365-378.
334. Cronkhite, J. M., R. E. Stickel, J. M. Nicovich and P. H. Wine, 1998, J. Phys. Chem A, **102**, 6651-6658.
335. Crowley, J. N., P. Campuzano-Jost and G. K. Moortgat, 1996, J. Phys. Chem., **100**, 3601-3606.
336. Cupitt, L. T. and G. P. Glass, 1975, Int. J. Chem. Kinet., **Symp. 1**, 39-50.
337. Cvetanovic, R. J., D. L. Singleton and R. S. Irwin, 1981, J. Am. Chem. Soc., **103**, 3530.
338. Czarnowski, J. and H. J. Schumacher, 1981, Int. J. Chem. Kinet., **13**, 639-649.
339. D'Anna, B., O. Andresen, Z. Gefen, C. J. Nielsen, K. Brudnik and J. T. Jodkowski, 2001, Phys. Chem. Chem. Phys., **3**, 3057-3063.
340. Daele, V. and G. Poulet, 1996, J. Chim. Phys., **93**, 1081-1099.
341. Daele, V., A. Ray, I. Vassali, G. Poulet and G. Le Bras, 1995, Int. J. Chem. Kinet., **27**, 1121-1133.
342. Dagaut, P., T. J. Wallington and M. J. Kurylo, 1988, J. Phys. Chem., **92**, 3836-3839.
343. Dagaut, P., T. J. Wallington and M. J. Kurylo, 1988, J. Phys. Chem., **92**, 3833-3836.
344. Dagaut, P., T. J. Wallington, R. Liu and M. J. Kurylo, 1988, Int. J. Chem. Kinet., **20**, 331-338.
345. Daniels, F. and E. H. Johnston, 1921, J. Am. Chem. Soc., **43**, 53.

346. Daubendiek, R. L. and J. G. Calvert, 1975, Environ. Lett., **8**, 103.
347. Davenport, J. E., B. Ridley, H. I. Schiff and K. H. Welge, 1972, J. Chem. Soc. Faraday Discussion, **53**, 230-231.
348. Davidson, F. E., A. R. Clemo, G. L. Duncan, R. J. Browett, J. H. Hobson and R. Grice, 1982, Molec. Phys., **46**, 33-40.
349. Davidson, J. A., C. A. Cantrell, S. C. Tyler, R. E. Shetter, R. J. Cicerone and J. G. Calvert, 1987, J. Geophys. Res., **92**, 2195-2199.
350. Davidson, J. A., C. J. Howard, H. I. Schiff and F. C. Fehsenfeld, 1979, J. Chem. Phys., **70**, 1697-1704.
351. Davidson, J. A., K. E. Kear and E. W. Abrahamson, 1972/1973, J. Photochem., **1**, 307-316.
352. Davidson, J. A., H. I. Schiff, T. J. Brown and C. J. Howard, 1978, J. Chem. Phys., **69**, 4277-4279.
353. Davidson, J. A., H. I. Schiff, G. E. Streit, J. R. McAfee, A. L. Schmeltekopf and C. J. Howard, 1977, J. Chem. Phys., **67**, 5021-5025.
354. Davies, P. B. and B. A. Thrush, 1968, Trans. Far. Soc., **64**, 1836.
355. Davis, D. D., W. Braun and A. M. Bass, 1970, Int. J. Chem. Kinet., **2**, 101.
356. Davis, D. D., J. T. Herron and R. E. Huie, 1973, J. Chem. Phys., **58**, 530-535.
357. Davis, D. D., R. B. Klemm and M. Pilling, 1972, Int. J. Chem. Kinet., **4**, 367-382.
358. Davis, D. D., G. Machado, B. Conaway, Y. Oh and R. T. Watson, 1976, J. Chem. Phys., **65**, 1268.
359. Davis, D. D., J. Prusazcyk, M. Dwyer and P. Kim, 1974, J. Phys. Chem., **78**, 1775-1779.
360. Davis, D. D., W. Wong and J. Lephardt, 1973, Chem. Phys. Lett., **22**, 273-278.
361. Davis, D. D., W. Wong and R. Schiff, 1974, J. Phys. Chem., **78**, 463-464.
362. Daykin, E. P. and P. H. Wine, 1990, Int. J. Chem. Kinet., **22**, 1083-1094.
363. Daykin, E. P. and P. H. Wine, 1990, J. Geophys. Res., **95**, 18547-18553.
364. Daykin, E. P. and P. H. Wine, 1990, J. Phys. Chem. , **94**, 4528-4535.
365. De Sousa, A. R., M. Touzeau and M. Petitdidier, 1985, Chem. Phys. Lett., **121**, 423-428.
366. DeMore, W. B., 1969, Int. J. Chem. Kinet., **1**, 209-220.
367. DeMore, W. B., 1971, Int. J. Chem. Kinet., **3**, 161-173.
368. DeMore, W. B., 1979, J. Phys. Chem., **83**, 1113-1118.
369. DeMore, W. B. 182nd National Meeting of the American Chemical Society, 1981, New York.
370. DeMore, W. B., 1982, J. Phys. Chem, **86**, 121-126.
371. DeMore, W. B., 1984, Int. J. Chem. Kinet., **16**, 1187-1200.
372. DeMore, W. B., 1991, J. Geophys. Res., **96**, 4995-5000.
373. DeMore, W. B., 1992, Geophys. Res. Lett., **19**, 1367-1370.
374. DeMore, W. B., 1993, Geophys. Res. Lett., **20**, 1359-1362.
375. DeMore, W. B., 1993, J. Phys. Chem., **97**, 8564-8566.
376. DeMore, W. B., 1996, J. Phys. Chem., **100**, 5813-5820.
377. DeMore, W. B. and K. D. Bayes, 1999, J. Phys. Chem. A, **103**, 2649-2654.
378. DeMore, W. B. and C. Dede, 1970, J. Phys. Chem., **74**, 2621-2625.
379. DeMore, W. B. and C. L. Lin, 1973, J. Org. Chem., **38**, 985-989.
380. DeMore, W. B., C. L. Lin and S. Jaffe. 12th Informal Conference on Photochemistry, 1976.
381. DeMore, W. B. and E. Tschuikow-Roux, 1974, J. Phys. Chem., **78**, 1447-1451.
382. DeMore, W. B. and E. Tschuikow-Roux, 1990, J. Phys. Chem., **94**, 5856-5860.
383. DeMore, W. B. and E. W. Wilson Jr., 1999, J. Phys. Chem. A, **103**, 573-576.
384. DeMore, W. B., E. W. Wilson Jr., A. Jacoby, S. Kutka and A. S. Gilbert. 223rd American Chemical Society Meeting, 2002, Orlando.
385. Derwent, R. G. and B. A. Thrush, 1971, Trans. Faraday Soc., **67**, 2036-2043.
386. Devolder, P., M. Carlier, J. F. Pauwels and L. R. Sochet, 1984, Chem. Phys. Lett., **111**, 94-99.
387. Diau, E. W.-G. and Y.-P. Lee, 1991, J. Phys. Chem., **95**, 7726-7732.
388. Diau, E. W.-G., T.-L. Tso and Y.-P. Lee, 1990, J. Phys. Chem., **94**, 5261-5265.
389. Diau, E. W., T. Yu, M. A. G. Wagner and M. C. Lin, 1994, J. Phys. Chem., **98**, 4034-4042.
390. Diaz-de-Mera, Y., A. Aranda, D. Rodriguez, R. López, B. Cabañas and E. Martinez, 2002, J. Phys. Chem. A, **106**, 8627-8633.
391. Dibble, T. S., M. M. Maricq, J. J. Szente and J. S. Francisco, 1995, J. Phys. Chem., **99**, 17394-17402.
392. Dillon, T. J., D. Hölscher, V. Sivakumaran, A. Horowitz and J. N. Crowley, 2004, Phys. Chem. Chem. Phys., Submitted.

393. Dlugokencky, E. J. and C. J. Howard, 1988, J. Phys. Chem., **92**, 1188-1193.
394. Dlugokencky, E. J. and C. J. Howard, 1989, J. Phys. Chem., **93**, 1091-1096.
395. Dobe, S., L. A. Khachatryan and T. Berces, 1989, Ber. Bunsenges. Phys. Chem., **93**, 847-852.
396. Dobe, S., M. Otting, F. Temps, H. G. Wagner and H. Ziemer, 1993, Ber. Bunsenges. Phys. Chem., **97**, 877-884.
397. Dobe, S., F. Temps, T. Bohland and H. G. Wagner, 1985, Z. Naturforsch., **40a**, 1289-1298.
398. Dobis, O. and S. W. Benson, 1987, Int. J. Chem. Kinet., **19**, 691-708.
399. Dobis, O. and S. W. Benson, 1991, J. Am. Chem. Soc., **113**, 6377-6386.
400. Dobis, O. and S. W. Benson, 1993, J. Am. Chem. Soc., **115**, 8798-8809.
401. Dobis, O. and S. W. Benson, 1993, J. Am. Chem. Soc., **115**, 8798-8809.
402. Dodonov, A. F., G. K. Lavrovskaya, I. I. Morozov and V. L. Tal'rose, 1971, Dokl. Adak. Nauk USSR, 1971, Vol. 198, 622: Dokl. Phys. Chem. (Engl. Trans.), **198**, 440-442.
403. Dodonov, A. F., V. V. Zelenov, A. S. Kukui and E. A. P. V. L. Tal'Rose, 1985, Khim. Fiz., **4**, 1335-1343.
404. Dognon, A. M., F. Caralp and R. Lesclaux, 1985, J. Chim. Phys. Phys.-Chim. Biol., **82**, 349-352.
405. Dolson, D. A., 1986, J. Phys. Chem., **90**, 6714-6718.
406. Domine, F., T. P. Murrells and C. J. Howard, 1990, J. Phys. Chem., **94**, 5839-5847.
407. Domine, F. and A. R. Ravishankara, 1992, Int. J. Chem. Kinet., **24**, 943-951.
408. Domine, F., A. R. Ravishankara and C. J. Howard, 1992, J. Phys. Chem., **96**, 2171-2178.
409. Donaghy, T., I. Shanahan, M. Hande and S. Fitzpatrick, 1993, Int. J. Chem. Kinet., **25**, 273-284.
410. Donahue, N. M., J. G. Anderson and K. L. Demerjian, 1998, J. Phys. Chem. A, **102**, 3121-3126.
411. Donahue, N. M. and J. S. Clarke, 2004, Int. J. Chem. Kinet., **36**, 259-272.
412. Donovan, R. J. and D. J. Little, 1972, Chem. Phys. Lett., **13**, 488.
413. Dransfeld, P. and H. G. Wagner, 1987, Z. Naturforsch., **42a**, 471-476.
414. Dreier, T. and J. Wolfrum. In *18th International Symposium on Combustion*; The Combustion Institute, 1980; pp 801-809.
415. Dreier, T. and J. Wolfrum. 20th International Symposium on Combustion, 1984.
416. Dreyer, J. W., D. Perner and C. R. Roy, 1974, J. Chem. Phys., **61**, 3164.
417. Droege, A. T. and F. P. Tully, 1986, J. Phys. Chem., **90**, 1949-1954.
418. Dunlea, E. J. Atmospheric reactions of electronically excited atomic and molecular oxygen, Ph. D., University of Colorado, Boulder, 2002.
419. Dunlea, E. J. and A. R. Ravishankara, 2004, Phys. Chem. Chem. Phys., **6**, 2152-2161.
420. Dunlea, E. J. and A. R. Ravishankara, 2004, Phys. Chem. Chem. Phys., **6**, 3333-3340.
421. Dunlea, E. J. and A. R. Ravishankara, 2005, Phys. Chem. Chem. Phys., to be submitted.
422. Dunlea, E. J., A. R. Ravishankara, R. S. Strekowski, J. M. Nicovich and P. H. Wine, 2004, Phys. Chem. Chem. Phys., in press.
423. Dunlea, E. J., R. K. Talukdar and A. R. Ravishankara, 2005, J. Phys. Chem. A, **109**, 3912-3920.
424. Dunlea, E. J., R. K. Talukdar and A. R. Ravishankara, 2006, to be submitted.
425. Dunlop, J. R. and F. P. Tully, 1993, J. Phys. Chem., **97**, 6457-6464.
426. Dunlop, J. R. and F. P. Tully, 1993, J. Phys. Chem., **97**, 11148-11150.
427. Eberhard, J. and C. J. Howard, 1996, Int. J. Chem. Kinet., **28**, 731-740.
428. Eberhard, J., P.-S. Yeh and Y.-P. Lee, 1997, J. Chem. Phys., **107**, 6499-6502.
429. Edelbuttel-Einhaus, J., K.-H. Hoyermann, G. Rohde and J. Seeba, 1992, Proc. Symp. (Int.) Combustion, **24**, 661+.
430. Edney, E. O. and D. J. Driscoll, 1992, Int. J. Chem. Kinet., **24**, 1067-1081.
431. Edney, E. O., T. E. Kleindienst and E. W. Corse, 1986, Int. J. Chem. Kinet., **18**, 1355-1371.
432. Egsgaard, H., L. Carlson, H. Florencio, T. Drewello and H. Schwarz, 1988, Chem. Phys. Lett., **148**, 537-540.
433. Ehhalt, D. H., J. A. Davidson, C. A. Cantrell, I. Friedman and S. Tyler, 1989, J. Geophys. Res., **94**, 9831-9836.
434. Eibling, R. E. and M. Kaufman, 1983, Atmos. Environ., **17**, 429-431.
435. Elrod, M. J., R. F. Meads, J. B. Lipson, J. V. Seeley and M. J. Molina, 1996, J. Phys. Chem., **100**, 5808-5812.
436. Elrod, M. J., D. L. Ranschaert and N. J. Schneider, 2001, Int. J. Chem. Kinet., **33**, 363-376.
437. Enami, S., Y. Nakano, S. Hashimoto, M. Kawasaki, S. Aloisio and J. S. Francisco, 2004, J. Phys. Chem. A, **108**.

438. Ennis, C. A. and J. W. Birks, 1985, J. Phys. Chem., **89**, 186-191.
439. Ennis, C. A. and J. W. Birks, 1988, J. Phys. Chem., **93**, 1119-1126.
440. Estupiñán, E. G., J. M. Nicovich and P.H. Wine, 2001, J. Phys. Chem. A, **105**, 9697-9703.
441. Fair, R. W. and B. A. Thrush, 1969, Trans. Faraday Soc., **65**, 1557.
442. Fair, R. W., A. van Roodaelaar and O. P. Strausz, 1971, Can. J. Chem., **49**, 1659.
443. Falbe-Hansen, H., S. Sorensen, N. R. Jensen, T. Pedersen and J. Hjorth, 2000, Atmos. Environ., **34**, 1543-1551.
444. Fang, T. D., P. H. Taylor and B. Dellinger, 1996, J. Phys. Chem., **100**, 4048-4054.
445. Fang, T. D., P. H. Taylor, B. Dellinger, C. J. Ehlers and R. J. Berry, 1997, J. Phys. Chem. A, **101**, 5758-5764.
446. Farquharson, G. K. and R. H. Smith, 1980, Aust. J. Chem., **33**, 1425-1435.
447. Fasano, D. M. and N. S. Nogar, 1981, Int. J. Chem. Kinet., **13**, 325.
448. Fasano, D. M. and N. S. Nogar, 1982, Chem. Phys. Lett., **92**, 411-414.
449. Fenter, F. F. and J. G. Anderson, 1991, J. Phys. Chem., **95**, 3172-3180.
450. Fenter, F. F. and J. G. Anderson, 1994, Int. J. Chem. Kinet., **26**, 801-812.
451. Fenter, F. F., V. Catoire, R. Lesclaux and P. D. Lightfoot, 1993, J. Phys. Chem., **97**, 3530-3538.
452. Filseth, S. V., A. Zia and K. H. Welge, 1970, J. Chem. Phys., **52**, 5502-5510.
453. Findlay, F. D., C. J. Fortin and D. R. Snelling, 1969, Chem. Phys. Lett., **3**, 204-206.
454. Findlay, F. D. and D. R. Snelling, 1971, J. Chem. Phys., **55**, 545-551.
455. Findlay, F. D. and D. R. Snelling, 1971, J. Chem. Phys., **54**, 2750-2755.
456. Finkbeiner, M., J. N. Crowley, O. Horie, R. Muller, G. K. Moortgat and P. J. Crutzen, 1995, J. Phys. Chem., **99**, 16264-16275.
457. Finlayson-Pitts, B. J., M. J. Ezell, T. M. Jayaweera, H. N. Berko and C. C. Lai, 1992, Geophys. Res. Lett., **19**, 1371-1374.
458. Finlayson-Pitts, B. J., S. K. Hernandez and H. N. Berko, 1993, J. Phys. Chem., **97**, 1172-1177.
459. Finlayson-Pitts, B. J. and T. E. Kleindienst, 1979, J. Chem. Phys., **70**, 4804-4806.
460. Finlayson-Pitts, B. J., T. E. Kleindienst, J. J. Ezell and D. W. Toohey, 1981, J. Chem. Phys., **74**, 4533-4543.
461. Fletcher, I. S. and D. Husain, 1976, J. Phys. Chem., **80**, 1837-1840.
462. Fletcher, I. S. and D. Husain, 1976, Can. J. Chem., **54**, 1765-1770.
463. Fletcher, I. S. and D. Husain, 1978, J. Photochem., **8**, 355-361.
464. Fockenberg, C., H. Saathoff and R. Zellner, 1994, Chem. Phys. Lett., **218**, 21-28.
465. Foon, R., G. Le Bras and J. Combourieu, 1979, C.R. Acad. Sci. Paris, **Series C 288**, 241.
466. Foon, R. and G. P. Reid, 1971, Trans. Faraday Soc., **67**, 3513.
467. Force, A. P. and J. R. Wiesenfeld, 1981, J. Chem. Phys., **74**, 1718-1723.
468. Force, A. P. and J. R. Wiesenfeld, 1981, J. Phys. Chem., **85**, 782-785.
469. Fraser, M. E. and L. G. Piper, 1989, J. Phys. Chem., **93**, 1107-1111.
470. Freeman, C. G. and L. F. Phillips, 1968, J. Phys. Chem., **72**, 3025.
471. Freudenstein, K. and D. Biedenkapp, 1976, Ber. Bunsenges. Phys. Chem., **80**, 42-48.
472. Friedl, R. R., W. H. Brune and J. G. Anderson, 1985, J. Phys. Chem., **89**, 5505-5510.
473. Friedl, R. R., J. H. Goble and S. P. Sander, 1986, Geophys. Res. Lett., **13**, 1351-1354.
474. Friedl, R. R. and S. P. Sander, 1989, J. Phys. Chem., **93**, 4756-4764.
475. Friedl, R. R., S. P. Sander and Y. L. Yung, 1992, J. Phys. Chem., **96**, 7490-7493.
476. Fritz, B., K. Lorenz, W. Steinert and R. Zellner, 1984, Oxidation Communications, **6**, 363-370.
477. Frost, M. J. and I. W. M. Smith, 1990, J. Chem. Soc. Farad. Trans., **86**, 1757-1762.
478. Frost, R. J., D. S. Green, M. K. Osborn and I. W. M. Smith, 1986, Int. J. Chem. Kinet., **18**, 885-898.
479. Gaffney, J. S., R. Fajer, G. I. Senum and J. H. Lee, 1986, Int. J. Chem. Kinet., **18**, 399-407.
480. Ganske, J. A., H. N. Berko, M. J. Ezell and B. J. Finlayson-Pitts, 1992, J. Phys. Chem., **96**, 2568-2572.
481. Ganske, J. A., M. J. Ezell, H. N. Berko and B. J. Finlayson-Pitts, 1991, Chem. Phys. Lett., **179**, 204-210.
482. Garland, N. L., 1998, Chem. Phys. Lett., **290**, 385 - 390.
483. Garland, N. L., L. J. Medhurst and H. H. Nelson, 1993, J. Geophys. Res. D., **98**, 23107-23111.
484. Garland, N. L. and H. H. Nelson, 1996, Chem. Phys. Lett., **248**, 296-300.
485. Garraway, J. and R. J. Donovan, 1979, J. Chem. Soc. Chem. Commun., 1108.

486. Garvin, D. and H. P. Broida. 9th Symposium on Combustion, 1963.
487. Gauthier, M. J. E. and D. R. Snelling, 1974, Can. J. Chem., **52**, 4007-4015.
488. Gauthier, M. J. E. and D. R. Snelling, 1974, J. Photochem., **4**, 27-50.
489. Geers-Muller, R. and F. Stuhl, 1987, Chem. Phys. Lett., **135**, 263-268.
490. Gehring, M., K. Hoyermann, H. Sahaeke and J. Wolfrum. 14th Int. Symposium on Combustion, 1973.
491. Gericke, K.-H. and F. J. Comes, 1981, Chem. Phys. Lett., **81**, 218-222.
492. Gierczak, T., J. B. Burkholder and A. R. Ravishankara, 1999, J. Phys. Chem. A, **103**, 877-883.
493. Gierczak, T., M. K. Gilles and A. R. Ravishankara, 2002, J. Phys. Chem., submitted.
494. Gierczak, T., L. Goldfarb, D. Sueper and A. R. Ravishankara, 1994, Int. J. Chem. Kinet., **26**, 719-728.
495. Gierczak, T., R. Talukdar, G. L. Vaghjiani, E. R. Lovejoy and A. R. Ravishankara, 1991, J. Geophys. Res., **96**, 5001-5011.
496. Gierczak, T., R. K. Talukdar, J. B. Burkholder, R. W. Portmann, J. S. Daniel, S. Solomon and A. R. Ravishankara, 1996, J. Geophys. Res., **101**, 12905-12911.
497. Gierczak, T., R. K. Talukdar and A. R. Ravishankara, 1997, J. Phys. Chem., in press.
498. Gierczak, T., S. Talukdar, S. Herndon, G. L. Vaghjiani and A. R. Ravishankara, 1997, J. Phys. Chem. A, **101**, 3125-3134.
499. Gill, R. J., W. D. Johnson and G. H. Atkinson, 1981, Chem. Phys., **58**, 29.
500. Gilles, M. K., J. B. Burkholder, T. Gierczak, P. Marshall and A. R. Ravishankara, 2002, J. Phys.Chem. A, **104**, 8945-8950.
501. Gilles, M. K., J. B. Burkholder and A. R. Ravishankara, 1999, Int. J. Chem. Kin., **31**, 417-424.
502. Gilles, M. K., D. C. McCabe, J. B. Burkholder and A. R. Ravishankara, 2001, J. Phys. Chem A, **105**, 5849-5853.
503. Gilles, M. K., R. K. Talukdar and A. R. Ravishankara, 2000, J. Phys. Chem. A, **104**, 8945-8950.
504. Gilles, M. K., A. A. Turnipseed, J. B. Burkholder and A. R. Ravishankara, 1997, J. Phys. Chem. A, **101**, 5526-5534.
505. Gilles, M. K., A. A. Turnipseed, J. B. Burkholder, A. R. Ravishankara and S. Solomon, 1996, manuscript.
506. Gilpin, R., H. I. Schiff and K. H. Welge, 1971, J. Chem. Phys., **55**, 1087-1093.
507. Glaschick-Schimpf, I., A. Leiss, P. B. Monkhouse, U. Schurath, K. H. Becker and E. H. Fink, 1979, Chem. Phys. Lett., **67**, 318-323.
508. Glavas, S. and J. Heicklen, 1985, J. Photochem., **31**, 21-28.
509. Gleason, J. F. and C. J. Howard, 1988, J. Phys. Chem. , **92**, 3414-3417.
510. Gleason, J. F., F. L. Nesbitt and L. J. Stief, 1994, J. Phys. Chem., **98**, 126-131.
511. Gleason, J. F., A. Sinha and C. J. Howard, 1987, J. Phys. Chem., **91**, 719-724.
512. Glinski, R. J. and J. W. Birks, 1985, J. Phys. Chem., **89**, 3449-3453.
513. Goldfarb, L., J. B. Burkholder and A. R. Ravishankara, 2001, J. Phys. Chem A, **105**, 5402-5409.
514. Goldfinger, P., G. Huybrechts and G. Martens, 1961, Trans. Faraday Soc., **57**, 2210-2219.
515. Goliff, W. S. and F. S. Rowland, 1997, Geophys. Res. Lett., **23**, 3029-3032.
516. Gordon, S., W. Mulac and P. Nangia, 1971, J. Phys. Chem., **75** 2087.
517. Gordon, S. and W. A. Mulac, 1975, Int. J. Chem. Kinet., **Symp. 1**, 289-299.
518. Graham, R. A. and D. J. Gutman, 1977, J. Phys. Chem., **81**, 207.
519. Graham, R. A. and H. S. Johnston, 1974, J. Chem. Phys., **60**, 4628.
520. Graham, R. A. and H. S. Johnston, 1978, J. Phys. Chem., **82**, 254-268.
521. Graham, R. A., A. M. Winer, R. Atkinson and J. N. Pitts, Jr., 1979, J. Phys. Chem., **83**, 1563.
522. Green, R. G. and R. P. Wayne, 1976/77, J. Photochem., **6**, 371-374.
523. Greenblatt, G. D. and C. J. Howard, 1989, J. Phys. Chem., **93**, 1035-1042.
524. Greenblatt, G. D. and A. R. Ravishankara, 1990, J. Geophys. Res., **95**, 3539-3547.
525. Greiner, N. R., 1969, J. Chem. Phys., **51**, 5049-5051.
526. Greiner, N. R., 1970, J. Chem. Phys., **53**, 1284-1285.
527. Griffin, J., D.R. Worsnop, R.C. Brown, C.E. Kolb and D.R. Herschbach, 2001, J. Phys. Chem A, **105**, 1643-1648.
528. Grimley, A. J. and P. L. Houston, 1980, J. Chem. Phys., **72**, 1471-1475.
529. Grotheer, H. H., G. Riekert, U. Meier and T. Just, 1985, Ber. Bunsenges. Phys. Chem., **89**, 187-191.

530. Grotheer, H. H., G. Riekert, D. Walter and T. Just, 1988, J. Phys. Chem., **92**, 4028.
531. Gutman, D., N. Sanders and J. E. Butler, 1982, J. Phys. Chem., **86**, 66.
532. Hack, W., O. Horie and H. G. Wagner, 1981, Ber. Bunsenges. Phys. Chem., **85**, 72.
533. Hack, W., O. Horie and H. G. Wagner, 1982, J. Phys. Chem. , **86**, 765.
534. Hack, W., K. Hoyermann and H. G. Wagner, 1974, Ber. Bunsenges. Phys. Chem., **78**, 386.
535. Hack, W., G. Mex and H. G. Wagner, 1977, Ber. Bunsenges. Phys. Chem., **81**, 677-684.
536. Hack, W., A. W. Preuss, F. Temps and H. G. Wagner, 1979, Ber. Bunsenges. Phys. Chem., **83**, 1275-1279.
537. Hack, W., A. W. Preuss, F. Temps, H. G. Wagner and K. Hoyermann, 1980, Int. J. Chem. Kinet., **12**, 851-860.
538. Hack, W., A. W. Preuss, H. G. Wagner and K. Hoyermann, 1979, Ber. Bunsenges. Phys. Chem., **83**, 212-217.
539. Hack, W., H. Schacke, M. Schroter and H. G. Wagner. 17th International Symposium on Combustion, 1979.
540. Hack, W., H. G. Wagner and K. Hoyermann, 1978, Ber. Bunsenges. Phys. Chem., **82**, 713-719.
541. Hagele, J., K. Lorenz, D. Rhasa and R. Zellner, 1983, Ber. Bunsenges. Phys. Chem., **87**, 1023-1026.
542. Hall, I. W., R. P. Wayne, R. A. Cox, M. E. Jenkin and G. D. Hayman, 1988, J. Phys. Chem., **92**, 5049-5054.
543. Halstead, C. J. and B. A. Thrush, 1966, Proc. Roy. Soc. London, **Ser. A 295**, 380
544. Hamilton, E. J., Jr., 1975, J. Chem. Phys., **63**, 3682-3683.
545. Hamilton, E. J., Jr. and R.-R. Lii, 1977, Int. J. Chem. Kinet., **9**, 875-885.
546. Hammer, P. D., E. J. Dlugokencky and C. J. Howard, 1986, J. Phys. Chem., **90**, 2491-2496.
547. Hancock, G., W. Lange, M. Lenzi and K. H. Welge, 1975, Chem. Phys. Lett., **33**, 168.
548. Hancock, G. and I. W. M. Smith, 1971, Trans. Faraday Soc., **67**, 2586.
549. Handwerk, V. and R. Zellner, 1978, Ber. Bunsenges. Phys. Chem., **82**, 1161-1166.
550. Hansen, I., K. Hoinghaus, C. Zetzsch and F. Stuhl, 1976, Chem. Phys. Lett., **42**, 370-372.
551. Harding, L. B. and A. F. Wagner. 22nd International Symposium on Combustion, 1988, Pittsburgh.
552. Harris, G. W., T. E. Kleindienst and J. N. Pitts, Jr., 1981, Chem. Phys. Lett., **80**, 479-483.
553. Harrison, J. A., A. R. Whyte and L. F. Phillips, 1986, Chem. Phys. Lett., **129**, 346-352.
554. Hartmann, D., J. Karthauser, J. P. Sawerysyn and R. Zellner, 1990, Ber. Bunsenges. Phys. Chem., **94**, 639-645.
555. Harwood, M. H., J. B. Burkholder, M. Hunter, R. W. Fox and A. R. Ravishankara, 1997, J. Phys. Chem. A, **101**, 853-863.
556. Harwood, M. H., D. M. Rowley, R. A. Cox and R. L. Jones, 1998, J. Phys. Chem A, **102**, 1790-1802.
557. Hashimoto, S., G. Inoue and H. Akimoto, 1984, Chem. Phys. Lett., **107**, 198-202.
558. Hatakeyama, S. and M. T. Leu, 1986, Geophys. Res. Lett., **13**, 1343-1346.
559. Hatakeyama, S. and M. T. Leu, 1989, J. Phys. Chem., **93**, 5784-5789.
560. Hayman, G. D., J. M. Davies and R. A. Cox, 1986, Geophys. Res. Lett., **13**, 1347-1350.
561. Heathfield, A. E., C. Anastasi, P. Pagsberg and A. McCulloch, 1998, Atmos. Environ., **32**, 711-717.
562. Heidner, R. F., J. F. Bott, C. E. Gardner and J. E. Melzer, 1979, J. Chem. Phys., **70**, 4509.
563. Heidner, R. F., J. F. Bott, C. E. Gardner and J. E. Melzer, 1980, J. Chem. Phys., **72**, 4815.
564. Heidner, R. F., III , D. Husain and J. R. Weisenfeld, 1973, J. Chem. Soc. Faraday Trans. 2, **69**, 927-938.
565. Heidner, R. F., III and D. Husain, 1973, Int. J. Chem. Kinet., **5**, 819-831.
566. Helleis, F., J. N. Crowley and G. K. Moortgat, 1993, J. Phys. Chem., **97**, 11464-11473.
567. Helleis, F., J. N. Crowley and G. K. Moortgat, 1994, Geophys. Res. Lett., **21**, 1795-1798.
568. Helmer, M. and J. M. C. Plane, 1993, J. Geophys. Res., **98**, 23207-23222.
569. Heneghan, S. P. and S. W. Benson, 1983, Int. J. Chem. Kinet., **15**, 1311-1319.
570. Heneghan, S. P., P. A. Knoot and S. W. Benson, 1981, Int. J. Chem. Kinet., **13**, 677-691.
571. Henon, E., S. Canneaux, F. Bohr and S. Dobe, 2003, Phys. Chem. Chem. Phys., **5**, 333-341.
572. Herndon, S. C., K. D. Froyd, E. R. Lovejoy and A. R. Ravishankara, 1999, J. Phys. Chem. A, **103**, 6778 - 6785.

573. Herndon, S. C., Gierczak, R. K. Talukdar and A. R. Ravishankara, 2001, Phys. Chem. Chem. Phys., **3**, 4529-4535.
574. Herndon, S. C., P. W. Villalta, D. D. Nelson, J. T. Jayne and M. S. Zahniser, 2001, J. Phys. Chem. A, **105**, 1583-1591.
575. Herron, J. T., 1961, J. Chem. Phys., **35**, 1138.
576. Herron, J. T. and R. E. Huie, 1974, J. Phys. Chem., **78**, 2085
577. Herron, J. T. and R. D. Penzhorn, 1969, J. Phys. Chem., **73**, 191.
578. Herschbach, D. R., C.E. Kolb, D.R. Worsnop and X. Shi, 1992, Nature, **356**, 414-416.
579. Hess, W. P. and F. P. Tully, 1989, J. Phys. Chem., **93**, 1944-1947.
580. Hickson, K. M. and L. F. Keyser, 2004, Journal of Physical Chemistry A, **108**, 1150-1159.
581. Hills, A. J., R. J. Cicerone, J. G. Calvert and J. W. Birks, 1988, J. Phys. Chem., **92**, 1853-1858.
582. Hills, A. J. and C. J. Howard, 1984, J. Chem. Phys., **81**, 4458-4465.
583. Hippler, H. and J. Troe, 1992, Chem. Phys. Lett., **192**, 333-337.
584. Hippler, H., J. Troe and J. Willner, 1990, J. Chem. Phys., **93**, 1755-1760.
585. Hislop, J. R. and R. P. Wayne, 1977, J. Chem. Soc. Faraday Trans. 2, **73**, 506-516.
586. Hitsuda, K., K. Takahashi, Y. Matsumi and T. J. Wallington, 2001, J. Phys. Chem. A, **105**, 5131-5136.
587. Hjorth, J., F. Cappellani, C. J. Nielsen and G. Restelli, 1989, J. Phys. Chem., **93**, 5458-5461.
588. Hjorth, J., G. Ottobrini, F. Cappellani and G. Restelli, 1987, J. Phys. Chem., **91**, 1565-1568.
589. Hjorth, J., G. Ottobrini and G. Restelli, 1986, Int. J. Chem. Kinet., **18**, 819-828.
590. Hjorth, J., G. Ottobrini and G. Restelli, 1988, J. Phys. Chem., **92**, 2669.
591. Hochanadel, C. J., J. A. Ghormley and P. J. Ogren, 1972, J. Chem. Phys., **56**, 4426-4432.
592. Hochanadel, C. J., T. J. Sworski and P. J. Ogren, 1980, J. Phys. Chem., **84**, 3274-3277.
593. Hofzumahaus, A. and F. Stuhl, 1984, Ber. Bunsenges Phys. Chem., **88**, 557-561.
594. Hohmann, J., G. Muller, G. Schonnenbeck and F. Stuhl, 1994, Chem. Phys. Lett., **217**, 577.
595. Hollinden, G. A., M. J. Kurylo and R. B. Timmons, 1970, J. Phys. Chem., **74**, 988-991.
596. Homann, K. H., G. Krome and H. G. Wagner, 1968, Ber. Bunsenges. Phys. Chem., **72**, 998.
597. Hooshiyar, P. A. and H. Niki, 1995, Int. J. Chem. Kinet., **27**, 1197-1206.
598. Horie, O. and G. K. Moortgat, 1992, J. Chem. Soc. Faraday Trans., **88**, 3305-3312.
599. Horowitz, A., D. Bauer, J. N. Crowley and G. K. Moortgat, 1993, Geophys. Res. Lett., **20**, 1423-1426.
600. Horowitz, A., J. N. Crowley and G. K. Moortgat, 1994, J. Phys. Chem., **98**, 11924-11930.
601. Horowitz, A., F. Su and J. G. Calvert, 1978, Int. J. Chem. Kinet., **10**, 1099.
602. Hossenlopp, J. M., J. F. Hershberger and G. W. Flynn, 1990, J. Phys. Chem., **94**, 1346 - 1351.
603. Howard, C. J., 1976, J. Chem. Phys., **65**, 4771.
604. Howard, C. J., 1979, J. Chem. Phys., **71**, 2352-2359.
605. Howard, C. J. and K. M. Evenson, 1976, J. Chem. Phys., **64**, 4303.
606. Howard, C. J. and K. M. Evenson, 1976, J. Chem. Phys., **64**, 197.
607. Howard, C. J. and K. M. Evenson, 1977, Geophys. Res. Lett., **4**, 437-440.
608. Howard, C. J. and B. J. Finlayson-Pitts, 1980, J. Chem. Phys., **72**, 3842-3843.
609. Howard, M. J. and I. W. M. Smith, 1981, J. Chem. Soc. Faraday Trans. 2, **77**, 997-1008.
610. Hoyermann, K., H. G. Wagner and J. Wolfrum, 1967, Z. Phys. Chem., **55**, 72.
611. Hoyermann, K., H. G. Wagner and J. Wolfrum, 1969, Z. Phys. Chem., **63**, 193.
612. Hsu, C.-C., A. M. Mebel and M. C. Lin, 1996, J. Chem. Phys., **105**, 2346.
613. Hsu, D. S. Y., W. M. Shaub, T. L. Burks and M. C. Lin, 1979, Chem Phys., **44**, 143-150.
614. Hsu, K. J. and W. B. DeMore, 1994, Geophys. Res. Lett., **21**, 805-808.
615. Hsu, K. J. and W. B. DeMore, 1995, J. Phys. Chem., **99**, 1235-1244.
616. Hsu, K. J. and W. B. DeMore, 1995, J. Phys. Chem., **99**, 11141-11930.
617. Hsu, Y.-C., D.-S. Chen and Y.-P. Lee, 1987, Int. J. Chem. Kinet., **19** 1073-1082.
618. Huder, K. J. and W. B. DeMore, 1993, Geophys. Res. Lett., **20**, 1575-1577.
619. Huey, L. G., E. J. Dunlea and C. J. Howard, 1996, J. Phys. Chem, **100**, 6504-6508.
620. Huie, R. E. and J. T. Herron, 1974, Chem. Phys. Lett., **27**, 411.
621. Hunziker, H. E., H. Kneppe and H. R. Wendt, 1981, J. Photochem., **17**, 377.
622. Husain, D. and P. Marshall, 1985, Combust. and Flame, **60**, 81-87.
623. Husain, D., P. Marshall and J. M. C. Plane, 1985, J. Chem. Soc. Chem. Comm., 1216-1218.

624. Husain, D., J. M. C. Plane and N. K. H. Slater, 1981, J. Chem. Soc. Faraday Trans. 2, **77**, 1949-1962.
625. Husain, D., J. M. C. Plane and C. C. Xiang, 1984, J. Chem. Soc. Faraday Trans. 2, **80**, 713-728.
626. Husain, D. and N. K. H. Slater, 1980, J. Chem. Soc. Faraday Trans. 2, **76**, 606-619.
627. Hynes, A. J., R. E. Stickel, A. J. Pounds, Z. Zhao, T. McKay, J. D. Bradshaw and P. H. Wine, 1993, Dimethylsulfide: Oceans, Atmosphere, and Climate, ed. by G. Restelli and G. Angletti, Kluwer Academic Publishers, Brusse;Science, 211 - 221.
628. Hynes, A. J., R. B. Stocker, A. J. Pounds, T. Mckay, J. D. Bradshaw, J. M. Nicovich and P. H. Wine, 1995, J. Phys. Chem., **99**, 16967-16975.
629. Hynes, A. J. and P. H. Wine, 1987, J. Phys. Chem., **91**, 3672.
630. Hynes, A. J. and P. H. Wine, 1991, J. Phys. Chem., **95**, 1232-1240.
631. Hynes, A. J. and P. H. Wine, 1996, J. Atmos. Chem., **24**, 23 - 37.
632. Hynes, A. J., P. H. Wine and J. M. Nicovich, 1988, J. Phys. Chem., **92**, 3846-3852.
633. Hynes, A. J., P. H. Wine and A. R. Ravishankara, 1986, J. Geophys. Res., **91**, 815-820.
634. Hynes, A. J., P. H. Wine and D. H. Semmes, 1986, J. Phys. Chem., **90**, 4148-4156.
635. Iannuzzi, M. P., J. B. Jeffries and F. Kaufman, 1982, Chem. Phys. Lett., **87**, 570-574.
636. Iannuzzi, M. P. and F. Kaufman, 1981, J. Phys. Chem., **85**, 2163
637. Igoshin, V. I., L. V. Kulakov and A. I. Nikitin, 1974, Sov. J. Quant. Electron., **3**, 306.
638. Imamura, T. and N. Washida, 1995, Laser Chem., **16**, 43-51.
639. Ingham, T., D. Bauer, R. Sander, P. J. Crutzen and J. N. Crowley, 1999, J. Phys. Chem. A, **103**, 7199-7209.
640. Ingold, K. U., 1988, J. Phys. Chem., **92**, 4568-4569.
641. Inoue, G. and H. Akimoto, 1981, J. Chem. Phys., **84**, 425-433.
642. Inoue, G., K. Izumi and V. A. Lozovsky, 1993, presented at the Third International Conference on Chemical Kinetics, Gaithersburg, MD.
643. Ishikawa, Y., K. Sugawara and S. Sato *Abstracts of Papers*; ACS/CSJ Chemical Congress, 1979; Vol. 1.
644. Iwata, R., R. A. Ferrieri and A. P. Wolf, 1986, J. Phys. Chem., **90**, 6722-6726.
645. Iyer, R. S. and F. S. Rowland, 1980, Geophys. Res. Lett., **7**, 797-800.
646. Izod, T. P. J. and R. P. Wayne, 1968 Proc. Roy. Soc. A, **308**, 81-94.
647. Jaffe, S. and F. S. Klein, 1966, Trans. Faraday Soc., **62**, 2150-2157.
648. Jaffe, S. and W. K. Mainquist, 1980, J. Phys. Chem, **84**, 3277.
649. James, G. S. and G. P. Glass, 1970, J . Chem . Phys . **50**, 2268
650. Japar, S. M., C. H. Wu and H. Niki, 1974, J. Phys. Chem., **78**, 2318.
651. Japar, S. M., C. H. Wu and H. Niki, 1976, J. Phys. Chem., **80**, 2057.
652. Jaramillo, V. I., S. Gougeon, S. Le Picard, A. Canosa, M. Smith and B. Rowe, 2002, Int. J. Chem. Kinet., **34**, 339-344.
653. Jayanty, R. K. M., R. Simonaitis and J. Heicklen, 1976, J. Phys. Chem., **80**, 443.
654. Jayanty, R. K. M., R. Simonaitis and J. Heicklen, 1976, J. Photochem., **5**, 217.
655. Jayne, J. T., U. Poschl, Y. Chen, D. Dai, L. T. Molina, D. R. Worsnop, C. E. Kolb and M. J. Molina, 1997, J. Phys. Chem. A, **101**, 10,000-10,011.
656. Jefferson, A., J. M. Nicovich and P. H. Wine, 1994, J. Phys. Chem., **98**, 7128-7135.
657. Jemi-Alade, A. A. and B. A. Thrush, 1990, J. Chem. Soc. Faraday Trans. 2, **86**, 3355-3363.
658. Jenkin, M. E., K. C. Clemitshaw and R. A. Cox, 1984, J. Chem. Soc. Faraday Trans. 2, **80**, 1633-1641.
659. Jenkin, M. E. and R. A. Cox, 1985, J. Phys. Chem., **89**, 192-199.
660. Jenkin, M. E. and R. A. Cox, 1987, Chem. Phys. Lett., **137**, 548-552.
661. Jenkin, M. E., R. A. Cox, M. Emrich and G. K. Moortgat, 1993, J. Chem. Soc. Faraday Trans., **89**, 2983-2991.
662. Jenkin, M. E., R. A. Cox and G. D. Hayman, 1991, Chem. Phys. Lett., **177**, 272-278.
663. Jenkin, M. E., R. A. Cox, A. Mellouki, G. Le Bras and G. Poulet, 1990, J. Phys. Chem., **94**, 2927-2934.
664. Jensen, N. R., D. R. Hanson and C. J. Howard, 1994, J. Phys. Chem., **98**, 8574-8579.
665. Jensen, N. R., J. Hjorth, C. Lohse, H. Skov and G. Restelli, 1991, Atmos. Environ., **24A**, 1897-1904.
666. Jensen, N. R., J. Hjorth, C. Lohse, H. Skov and G. Restelli, 1992, J. Atmos. Chem., **14**, 95-108.

667. Jeong, K. M., K. J. Hsu, J. B. Jeffries and F. Kaufman, 1984, J. Phys. Chem., **88**, 1222-1226.
668. Jeong, K. M. and F. Kaufman, 1979, Geophys. Res. Lett., **6**, 757-759.
669. Jeong, K. M. and F. Kaufman, 1982, J. Phys. Chem., **86**, 1808-1815.
670. Jeoung, S. C., K. Y. Choo and S. W. Benson, 1991, J. Phys. Chem., **95**, 7282-7290.
671. Jiang, Z., P. H. Taylor and B. Dellinger, 1992, J. Phys. Chem., **96**, 8961-8964.
672. Jiang, Z., P. H. Taylor and B. Dellinger, 1993, J. Phys. Chem., **97**, 5050-5053.
673. Jimenez, E., M. K. Gilles and A. R. Ravishankara, 2003, J. Photochem. Photobiol. A: Chem., **157**, 237-245.
674. Johnston, H. S., E. D. Morris, Jr. and J. Van den Bogaerde, 1969, J. Am. Chem. Soc., **91**, 7712-7727.
675. Johnston, H. S. and Y.-S. Tao, 1951, J. Am. Chem Soc., **73**, 2948.
676. Jolly, G. S., D. J. McKenney, D. L. Singleton, G. Paraskevopoulos and A. R. Bossard, 1986, J. Phys. Chem., **90**, 6557-6562.
677. Jonah, C. D., W. A. Mulac and P. Zeglinski, 1984, J. Phys. Chem., **88**, 4100-4104.
678. Jones, B. M. R., J. P. Burrows, R. A. Cox and S. A. Penkett, 1982, Chem. Phys. Lett., **88**, 372-376.
679. Jourdain, J. L., G. Le Bras and J. Combourieu, 1978, J. Chim. Phys., **75**, 318-323.
680. Jourdain, J. L., G. Le Bras and J. Combourieu, 1979, Int. J. Chem. Kinet., **11**, 569-577.
681. Jourdain, J. L., G. Le Bras and J. Combourieu, 1981, Chem. Phys. Lett., **78**, 483.
682. Jourdain, J. L., G. Poulet, J. Barassin, G. Le Bras and J. Combourieu, 1977, Pollut. Atmos., **75**, 256-259.
683. Jungkamp, T. P., A. Kukui and R. N. Schindler, 1995, Ber. Bunsenges. Phys. Chem., **99**, 1057-1066.
684. Kaiser, E. W., 1993, Int. J. Chem. Kinet., **25**, 667-680.
685. Kaiser, E. W. and S. M. Japar, 1977, Chem. Phys . Lett., **52**, 121.
686. Kaiser, E. W. and S. M. Japar, 1978, Chem. Phys. Lett., **54**, 265.
687. Kaiser, E. W., I. M. Lorkovic and T. J. Wallington, 1990, J. Phys. Chem., **94**, 3352-3354.
688. Kaiser, E. W., L. Rimai, E. Schwab and E. C. Lim, 1992, J. Phys. Chem., **96**, 303-306.
689. Kaiser, E. W. and T. J. Wallington, 1994, J. Phys. Chem., **98**, 5679-5685.
690. Kakesu, M., H. Bandow, N. Takenaka, Y. Maeda and N. Washida, 1997, International Journal of Chemical Kinetics, **29**, 933-941.
691. Kambanis, K. G., Y. G. Lazarou and P. J. Papagiannakopoulos, 1997, J. Phys. Chem., **101**, 8496.
692. Kan, C. S., J. G. Calvert and J. H. Shaw, 1981, J. Phys. Chem., **85**, 1126-1132.
693. Kan, C. S., R. D. McQuigg, M. R. Whitbeck and J. G. Calvert, 1979, Int. J. Chem. Kinet., **11**, 921-933.
694. Kasner, J. H., P. H. Taylor and B. Dellinger, 1990, J. Phys.Chem., **94**, 3250-3253.
695. Kaufman, F., N. J. Gerri and D. A. Pascale, 1956, J. Chem. Phys., **24**, 32-34.
696. Kegley-Owen, C. S., M. K. Gilles, J. B. Burkholder and A. R. Ravishankara, 1999, J. Phys. Chem. A, **103**, 5040-5048.
697. Kelly, C., J. Treacy, H. W. Sidebottom and O. J. Nielsen, 1993, Chem. Phys. Lett., **207**, 498-503.
698. Kelly, C. C., W. H. S. Yu and M. H. J. Wijnen, 1970, Can. J. Chem., **48**, 603-606.
699. Kenner, R. D., K. R. Ryan and I. C. Plumb, 1993, Geophys. Res. Lett., **20**, 1571-1574.
700. Kerr, J. A. and D. W. Sheppard, 1981, Environ. Sci. and Technol., **15**, 960.
701. Kerr, J. A. and D. W. Stocker, 1986, J. Atmos. Chem., **4**, 253-262.
702. Keyser, L. F., 1978, J. Chem. Phys., **69**, 214-218.
703. Keyser, L. F., 1979, J. Phys. Chem., **83**, 645-648.
704. Keyser, L. F., 1980, J. Phys. Chem., **84** 1659-1663.
705. Keyser, L. F., 1980, J. Phys. Chem., **84**, 11-14.
706. Keyser, L. F., 1981, J. Phys. Chem., **85**, 3667-3673.
707. Keyser, L. F., 1982, J. Phys. Chem., **86**, 3439-3446.
708. Keyser, L. F., 1983, J. Phys. Chem., **87**, 837-841.
709. Keyser, L. F., 1984, J. Phys. Chem., **88**, 4750-4758.
710. Keyser, L. F., 1986, J. Phys. Chem., **90**, 2994-3003.
711. Keyser, L. F., 1988, J. Phys. Chem., **92**, 1193-1200.
712. Keyser, L. F., K. Y. Choo and M. T. Leu, 1985, Int. J. Chem. Kinet., **17**, 1169-1185.
713. Kinnison, D. J., W. Mengon and J. A. Kerr, 1996, J. Chem. Soc. Faraday Trans., **92**, 369-372.

714. Kircher, C. C. and S. P. Sander, 1984, J. Phys. Chem., **88**, 2082-91.
715. Kirchner, K., D. Helf, P. Ott and S. Vogt, 1990, Ber. Bunsenges. Phys. Chem., **94**, 77-83.
716. Kistiakowsky, G. B. and G. G. Volpi, 1957, J. Chem. Phys., **27**, 1141-1149.
717. Kistiakowsky, G. B. and G. G. Volpi, 1958, J. Chem. Phys., **28**, 665.
718. Kita, D. and D. H. Stedman, 1982, J. Chem. Soc. Faraday Trans. 2, **78**, 1249-1259.
719. Klais, O., P. C. Anderson, A. H. Laufer and M. J. Kurylo, 1979, Chem. Phys. Lett., **66**, 598.
720. Klais, O., A. H. Laufer and M. J. Kurylo, 1980, J. Chem. Phys., **73**, 2696-2699.
721. Kleinermanns, K. and A. C. Luntz, 1981, J. Phys. Chem., **85**, 1966.
722. Klemm, R. B., 1979, J. Chem. Phys. , **71**, 1987.
723. Klemm, R. B., E. G. Skolnik and J. V. Michael, 1980, J. Chem. Phys., **72**, 1256.
724. Klemm, R. B. and L. J. Stief, 1974, J. Chem. Phys., **61**, 4900.
725. Klopffer, W., R. Frank, E. G. Kohl and F. Haag, 1986, Chemiker-Zeitung, **110**, 57-61.
726. Knickelbein, M. B., K. L. Marsh, O. E. Ulrich and G. E. Busch, 1987, J. Chem. Phys., **87**, 2392-2393.
727. Knight, G. P., T. Beiderhase, F. Helleis, G. K. Moortgat and J. N. Crowley, 2000, Journal of Physical Chemistry A, **104**, 1674-1685.
728. Knight, G. P. and J. N. Crowley, 2001, Phys. Chem. Chem. Phys., **3**.
729. Knox, J. H., 1955, Chemistry and Industry, 1631-1632.
730. Knox, J. H., 1962, Trans. Faraday Soc., **58**, 275.
731. Knox, J. H. and R. L. Nelson, 1959, Trans. Far. Soc., **55**, 937-946.
732. Ko, T. and A. Fontijn, 1991, J. Phys. Chem. , **95**, 3984-3987.
733. Koch, S. and G. K. Moortgat, 1990, Chem. Phys. Lett., **173**, 531-536.
734. Kohse-HÖinghaus, K. and F. Stuhl, 1980, J. Chem. Phys., **72**, 3720-3726.
735. Kolb, C. E., J. T. Jayne, D. R. Worsnop, M. J. Molina, R. F. Meads and A. A. Viggiano, 1994, J. Am. Chem. Soc., **116**, 10314-10315.
736. Kompa, K. L. and J. Wanner, 1972, Chem. Phys. Lett., **12**, 560.
737. Koppe, S., T. Laurent, P. D. Naik, H.-R. Volpp, J. Wolfrum, T. Arusi-Parpar, I. Bar and S. Rosenwaks, 1993, Chem. Phys. Lett., **214**, 546-552.
738. Kozlov, S. N., V. L. Orkin, R. E. Huie and M. J. Kurylo, 2003, J. Phys. Chem. A, **107**, 1333-1338.
739. Kukui, A., D. Borrisenko, G. Laverdet and G. Le Bras, 2003, J. Phys. Chem. A, **107**, 5732-5742.
740. Kukui, A., V. Bossoutrot, G. Laverdet and G. Le Bras, 2000, J. Phys. Chem. A, **104**, 935 - 946.
741. Kukui, A., T. P. W. Jungkamp and R. N. Schindler, 1994, Ber. Bunsenges. Phys. Chem., **98**, 1619-1621.
742. Kukui, A., U. Kirchner, T. Benter and R. N. Schindler, 1996, Ber. Bunsenges. Phys. Chem., **100**, 455-461.
743. Kukui, A. S., T. P. W. Jungkamp and R. N. Schindler, 1994, Ber. Bunsenges. Phys. Chem., **98**, 1298-1302.
744. Kulcke, A., B. Blackman, W. B. Chapman, I. K. Kim and D. J. Nesbitt, 1998, J. Phys. Chem. A, **102**, 1965-1972.
745. Kumaran, S. S., K. P. Lim and J. V. Michael, 1994, J. Chem. Phys., **101**, 9487-9498.
746. Kurasawa, H. and R. Lesclaux, 1979, Chem. Phys. Lett., **66**, 602.
747. Kurasawa, H. and R. Lesclaux, 1980, Chem. Phys. Lett., **72**, 437.
748. Kurasawa, H. and R. Lesclaux. 14th Informal Photochemistry Conference, 1980, Newport Beach, CA.
749. Kurylo, M. J., 1973, Chem. Phys. Lett., **23**, 467-471.
750. Kurylo, M. J., 1977, Chem. Phys. Lett., **49**, 467.
751. Kurylo, M. J., 1978, Chem. Phys. Lett., **58**, 238-242.
752. Kurylo, M. J., 1978, Chem. Phys. Lett., **58**, 233.
753. Kurylo, M. J., P. C. Anderson and O. Klais, 1979, Geophys. Res. Lett., **6**, 760-762.
754. Kurylo, M. J. and W. Braun, 1976, Chem. Phys. Lett., **37**, 232-235.
755. Kurylo, M. J., O. Klais and A. H. Laufer, 1981, J. Phys. Chem., **85**, 3674-3678.
756. Kurylo, M. J. and G. L. Knable, 1984, J. Phys. Chem., **88**, 3305-3308.
757. Kurylo, M. J., G. L. Knable and J. L. Murphy, 1983, Chem. Phys. Lett., **95**, 9-12.
758. Kurylo, M. J. and A. H. Laufer, 1979, J. Chem. Phys., **70**, 2032-2033.

759. Kurylo, M. J., J. L. Murphy, G. S. Haller and K. D. Cornett, 1982, Int. J. Chem. Kinet, **14**, 1149-1161.
760. Kurylo, M. J., J. L. Murphy and G. L. Knable, 1983, Chem. Phys. Lett., **94**, 281-284.
761. Kurylo, M. J., P. A. Ouellette and A. H. Laufer, 1986, J. Phys. Chem., **90**, 437-440.
762. Lafage, C., J.-F. Pauwels, M. Carlier and P. Devolder, 1987, J. Chem. Soc. Faraday Trans. 2, **83**, 731-739.
763. Lam, L., D. R. Hastie, B. A. Ridley and H. I. Schiff, 1981, J. Photochem., **15**, 119-130.
764. Lamb, J. J., L. T. Molina, C. A. Smith and M. J. Molina, 1983, J. Phys. Chem., **87**, 4467-4470.
765. Lancar, I., G. Laverdet, G. Le Bras and G. Poulet, 1991, Int. J. Chem. Kinet., **23**, 37-45.
766. Lancar, I., G. Le Bras and G. Poulet, 1993, J. Chim. Physique, **90**, 1897-1908.
767. Lancar, I., A. Mellouki and G. Poulet, 1991, Chem. Phys. Lett., **177**, 554-558.
768. Langer, S., B. T. McGovney, B. J. Finlayson-Pitts and R. M. Moore, 1996, Geophys. Res. Lett., **23**, 1661-1664.
769. Langford, A. O. and C. B. Moore, 1984, J. Chem. Phys., **80**, 4211-4221.
770. Larichev, M., F. Maguin, G. Le Bras and G. Poulet, 1995, J. Phys. Chem., **99**, 15911-15918.
771. Laszlo, B., R. R. Friedl and S. P. Sander, J. Phys. Chem. A, to be submitted.
772. Laszlo, B., R. E. Huie, M. J. Kurylo and A. W. Miziolek, 1997, J. Geophys. Res., **102**, 1523-1532.
773. Laszlo, B., M. J. Kurylo and R. E. Huie, 1995, J. Phys. Chem., **99**, 11701-11707.
774. Laverdet, G., G. Le Bras, A. Mellouki and G. Poulet, 1990, Chem. Phys. Lett., **172**, 430-434.
775. Lawton, S. A., S. E. Novick, H. P. Broida and A. V. Phelps, 1977, J. Chem. Phys., **66**, 1381-1382.
776. Lawton, S. A. and A. V. Phelps, 1978, J. Chem. Phys., **69**, 1055-1068.
777. Lazarou, Y. G., C. Michael and P. Papagiannakopoulos, 1992, J. Phys. Chem., **96**, 1705-1708.
778. Le Bras, G. and J. Combourieu, 1978, Int. J. Chem. Kinet., **10**, 1205-1213.
779. Le Bras, G., R. Foon and J. Combourieu, 1980, Chem. Phys. Lett., **73**, 357.
780. Le Calve, S., D. Hitier, G. Le Bras and A. Mellouki, 1998, J. Phys. Chem. A, **102**, 4579-4584.
781. Leck, T. J., J. E. Cook and J. W. Birks, 1980, J. Chem. Phys., **72**, 2364-2373.
782. Lee, F. S. C. and F. S. Rowland, 1977, J. Phys. Chem., **81**, 86-87.
783. Lee, J. H., J. V. Michael, W. A. Payne, Jr. and L. J. Stief, 1978, J. Chem. Phys., **69**, 350-353.
784. Lee, J. H., J. V. Michael, W. A. Payne, Jr. and L. J. Stief, 1977, J. Chem. Soc. Faraday Trans. 1, **73**, 1530-1536.
785. Lee, J. H., J. V. Michael, W. A. Payne, Jr. and L. J. Stief, 1978, J. Chem. Phys., **69**, 3069-3076.
786. Lee, J. H. and I. N. Tang, 1980, J. Chem. Phys., **72**, 5718-5720.
787. Lee, J. H. and I. N. Tang, 1982, J. Chem. Phys., **77**, 4459-63.
788. Lee, J. H. and I. N. Tang, 1983, J. Chem. Phys., **78**, 6646.
789. Lee, J. H., I. N. Tang and R. B. Klemm, 1980, J. Chem. Phys., **72**, 1793-1796.
790. Lee, J. H., R. B. Timmons and L. J. Stief, 1976, J. Chem. Phys., **64**, 300-305.
791. Lee, L. C. and T. G. Slanger, 1978, J. Chem. Phys., **69**, 4053-4060.
792. Lee, L. C. and T. G. Slanger, 1979, Geophys. Res. Lett., **6**, 165-166.
793. Lee, Y.-P. and C. J. Howard, 1982, J. Chem. Phys., **77** 756-763.
794. Lee, Y.-P., R. M. Stimpfle, R. A. Perry, J. A. Mucha, K. M. Evenson, D. A. Jennings and C. J. Howard, 1982, Int. J. Chem. Kinet., **14**, 711-732.
795. Lee, Y.-Y., Y.-P. Lee and N. S. Wang, 1994, J. Chem. Phys., **100**, 387-392.
796. Leiss, A., U. Schurath, K. H. Becker and E. H. Fink, 1978, J. Photochem., **8**, 211-214.
797. Lesclaux, R. and F. Caralp, 1984, Int. J. Chem. Kinet., **16**, 1117-1128.
798. Lesclaux, R. and M. Demissy, 1977, Nouv. J. Chim., **1**, 443.
799. Lesclaux, R., A. M. Dognon and F. Caralp, 1987, J. Photochem. and Photobiol., **A41**, 1-11.
800. Lesclaux, R., P. V. Khe, P. Dezauzier and J. C. Soulignac, 1975, Chem. Phys. Lett., **35**, 493.
801. Leu, G.-H. and Y.-P. Lee, 1994, J. Chin. Chem. Soc., **41**, 645-649.
802. Leu, M.-T. and W. B. DeMore, 1976, Chem. Phys. Lett. , **41**, 121-124.
803. Leu, M.-T. and W. B. DeMore, 1977, Chem. Phys. Lett., **48**, 317.
804. Leu, M.-T. and W. B. DeMore, 1978, J. Phys. Chem., **82**, 2049.
805. Leu, M.-T., S. Hatkeyama and K. J. Hsu, 1989, J. Phys. Chem., **93**, 5778-5784.
806. Leu, M.-T. and C. L. Lin, 1979, Geophys. Res. Lett., **6**, 425-428.
807. Leu, M.-T. and R. H. Smith, 1981, J. Phys. Chem., **85**, 2570-2575.
808. Leu, M.-T. and R. H. Smith, 1982, J. Phys. Chem., **86**, 73-81.
809. Leu, M.-T. and R. H. Smith, 1982, J. Phys. Chem., **86**, 958-961.

810. Leu, M.-T. and Y. L. Yung, 1987, Geophys. Res. Lett., **14**, 949-952.
811. Leu, M. T., 1979, Chem. Phys. Lett., **61**, 275-279.
812. Leu, M. T., 1979, J. Chem. Phys., **70**, 1662-1666.
813. Leu, M. T., 1980, Chem. Phys. Lett., **69**, 37-39.
814. Leu, M. T., 1980, Geophys. Res. Lett., **7**, 173-175.
815. Leu, M. T., 1984, J. Phys. Chem., **88**, 1394-1398.
816. Lewis, R. S., S. P. Sander, S. Wagner and R. T. Watson, 1980, J. Phys. Chem., **84**, 2009-2015.
817. Lewis, R. S. and R. T. Watson, 1980, J. Phys. Chem., **84**, 3495-3503.
818. Li, Q., M. C. Osborne and I. W. M. Smith, 2000, Int. J. Chem. Kin., **32**, 85-91.
819. Li, Z., R. R. Friedl and S. P. Sander, 1995, J. Phys. Chem., **99**, 13445-13451.
820. Li, Z., R. R. Friedl and S. P. Sander, 1997, J. Chem. Soc. Farad. Trans., submitted.
821. Lightfoot, P. D., R. A. Cox, J. N. Crowley, M. Destriau, G. D. Hayman, M. E. Jenkin, G. K. Moortgat and F. Zabel, 1992, Atmos. Environ., **26A**, 1805-1961.
822. Lightfoot, P. D., B. Veyret and R. Lesclaux, 1988, Chem. Phys. Lett., **150**, 120-126.
823. Lightfoot, P. D., B. Veyret and R. Lesclaux, 1990, J. Phys. Chem., **94**, 708-714.
824. Lii, R.-R., R. A. Gorse, Jr., M. C. Sauer, Jr. and S. Gordon, 1980, J. Phys. Chem., **84**, 819-821.
825. Lii, R.-R., M. C. Sauer and S. Gordon, 1980, J. Phys. Chem.,, **84**, 817-.
826. Lii, R.-R., M. C. Sauer, Jr. and S. Gordon, 1981, J. Phys. Chem., **85**, 2833-2834.
827. Lilenfeld, H. V. and R. J. Richardson, 1977, J. Chem. Phys., **67**, 3991.
828. Lin, C.-L., D. A. Parkes and F. Kaufman, 1970, J. Chem. Phys., **53**, 3896-3900.
829. Lin, C. L., 1982, Int. J. Chem. Kinet., **14**, 593-598.
830. Lin, C. L. and W. B. DeMore, 1973, J. Phys. Chem., **77** 863-869.
831. Lin, C. L., M. T. Leu and W. B. DeMore, 1978, J. Phys. Chem., **82**, 1772-1777.
832. Lin, Y.-L., N.-S. Wang and Y.-P. Lee, 1985, Int. J. Chem. Kinet., **17**, 1201-1214.
833. Lippmann, H. H., B. Jesser and U. Schurath, 1980, Int. J. Chem. Kinet., **12**, 547-554.
834. Lipson, J. B., T. W. Beiderhase, L. T. Molina, M. J. Molina and M. Olzmann, 1999, J. Phys. Chem. A, **103**, 6540-6551.
835. Lipson, J. B., M. J. Elrod, T. W. Beiderhase, L. T. Molina and M. J. Molina, 1997, J. Chem. Soc. Faraday Trans., **93**, 2665-2673.
836. Lissi, E. and J. Heicklen, 1972, J. Photochem., **1**, 39-68.
837. Littlejohn, D. and H. S. Johnston, 1980, EOS, **61**, 966.
838. Liu, A., W. A. Mulac and C. D. Jonah, 1989, J. Phys. Chem., **93**, 4092-4094.
839. Liu, R., R. E. Huie and M. J. Kurylo, 1990, J. Phys. Chem., **94**, 3247-3249.
840. Lloyd, A. C., K. R. Darnall, A. M. Winer and J. N. Pitts Jr., 1976, Chem. Phys. Lett., **42**, 205-208.
841. Loewenstein, L. M. and J. G. Anderson, 1984, J. Phys. Chem., **88**, 6277-6286.
842. Loewenstein, L. M. and J. G. Anderson, 1985, J. Phys. Chem., **89**, 5371-5379.
843. Lorenz, K., D. Rhasa, R. Zellner and B. Fritz, 1985, Ber. Bunsenges. Phys. Chem., **89**, 341-342.
844. Lorenzen-Schmidt, H., R. Weller and O. Schrems, 1994, Ber. Bunsenges. Phys. Chem., **98**, 1622-1629.
845. Louge, M. Y. and R. K. Hanson, 1984, Twentieth Symposium (International) on Combustion, 665-672.
846. Louis, F., A. Talhaoui, J.-P. Sawerysyn, M.-T. Rayez and J.-C. Rayez, 1997, J. Phys. Chem. A, **101**, 8503-8507.
847. Lovejoy, E. R., D. R. Hanson and L. G. Huey, 1996, J. Phys. Chem., **100**, 19911-19916.
848. Lovejoy, E. R., K. S. Kroeger and A. R. Ravishankara, 1990, Chem. Phys. Lett., **167**, 183-187.
849. Lovejoy, E. R., T. P. Murrells, A. R. Ravishankara and C. J. Howard, 1990, J. Phys. Chem., **94**, 2386-2393.
850. Lovejoy, E. R., A. R. Ravishankara and C. J. Howard, 1994, Int. J. Chem. Kinet., **26**, 551-560.
851. Lovejoy, E. R., N. S. Wang and C. J. Howard, 1987, J. Phys. Chem., **91**, 5749-5755.
852. Lozovsky, V. A., M. A. Ioffe and O. M. Sarkisov, 1984, Chem. Phys. Lett., **110**, 651-654.
853. Lu, E. C. C., R. S. Iyer and F. S. Rowland, 1986, J. Phys. Chem., **90**, 1988-1990.
854. Mack, G. P. R. and B. Thrush, 1973, J. Chem. Soc. Faraday Trans. 1, **69**, 208.
855. Mack, G. P. R. and B. Thrush, 1974, J. Chem. Soc. Faraday Trans. 1, **70**, 173-186.
856. MacLeod, H., S. M. Aschmann, R. Atkinson, E. C. Tuazon, J. A. Sweetman, A. M. Winer and J. N. Pitts, Jr., 1986, J. Geophys. Res., **91**, 5338.

857. MacLeod, H., C. Balestra, J. L. Jourdain, G. Laverdet and G. Le Bras, 1990, Int. J. Chem. Kinet., **22**, 1167-1176.
858. MacLeod, H., J. L. Jourdain, G. Poulet and G. Le Bras, 1984, Atmos. Environ., **18**, 2621.
859. MacLeod, H., G. Poulet and G. Le Bras, 1983, J. Chim. Phys., **80**, 287.
860. Maguin, F., G. Laverdet, G. Le Bras and G. Poulet, 1992, J. Phys. Chem., **96**, 1775-1780.
861. Maguin, F., A. Mellouki, G. Laverdet, G. Poulet and G. Le Bras, 1991, Int. J. Chem. Kinet., **23**, 237-245.
862. Manning, R. and M. J. Kurylo, 1977, J. Phys. Chem., **81**, 291-296.
863. Manning, R. G., W. Braun and M. J. Kurylo, 1976, J. Chem. Phys., **65**, 2609.
864. Manzanares, E. R., M. Suto, L. C. Lee and D. Coffey, 1986, J. Chem. Phys., **85**, 5027-5034.
865. Margitan, J. J., 1983, J. Phys. Chem., **87**, 674-679.
866. Margitan, J. J., 1984, J. Phys. Chem., **88**, 3638-3643.
867. Margitan, J. J., 1984, J. Phys. Chem., **88**, 3314-3318.
868. Margitan, J. J. and R. T. Watson, 1982, J. Phys. Chem., **86**, 3819-3824.
869. Maricq, M. M. and J. J. Szente, 1993, Chem. Phys. Lett., **213**, 449-456.
870. Maricq, M. M. and J. J. Szente, 1994, J. Phys. Chem., **98**, 2078-2082.
871. Maricq, M. M. and J. J. Szente, 1996, J. Phys. Chem., **100**, 12374.
872. Maricq, M. M., J. J. Szente, E. W. Kaiser and J. Shi, 1994, J. Phys. Chem., **98**, 2083-2089.
873. Marinelli, W. J. and H. S. Johnston, 1982, J. Chem. Phys., **77**, 1225-1234.
874. Markert, F. and O. J. Nielsen, 1992, Chem. Phys. Lett., **194**, 123-127.
875. Martens, G. J., M. Godfroid, J. Delvaux and J. Verbeyst, 1976, Int. J. Chem. Kinet., **8**, 153-158.
876. Martin, D., I. Barnes and K. H. Becker, 1987, Chem. Phys. Lett., **140**, 195.
877. Martin, D., J. L. Jourdain, G. Laverdet and G. Le Bras, 1987, Int. J. Chem. Kinet., **19**, 503-512.
878. Martin, D., J. L. Jourdain and G. Le Bras, 1985, Int. J. Chem. Kinet., **17**, 1247.
879. Martin, D., J. L. Jourdain and G. Le Bras, 1986, J. Phys. Chem., **90**, 4143-4147.
880. Martin, J.-P. and G. Paraskevopoulos, 1983, Can. J. Chem., **61**, 861-865.
881. Martin, L. R., R. B. Cohen and J. F. Schatz, 1976, Chem. Phys. Lett., **41**, 394-396.
882. Martinez, E., A. Albaladejo, E. Jiminez, A. Notario and A. Aranda, 1999, **308**, 37-44.
883. Martinez, E., A. Aranda, Y. Diaz-de-Mera, D. Rodriguez, M. Reyes Lopez and J. Albaladejo, 2002, Environ. Sci. Technol., **36**, 1226-1230.
884. Martinez, R. I. and J. T. Herron, 1978, Int. J. Chem. Kinet., **10**, 433.
885. Marx, W., F. Bahe and U. Schurath, 1979, Ber. Bunsenges. Phys. Chem., **83**, 225-230.
886. Matsumi, Y., K. Tonokura, Y. Inagaki and M. Kawasaki, 1993, J. Phys. Chem., **97**, 6816-6821.
887. Mauldin, R. L., III, J. B. Burkholder and A. R. Ravishankara, 1992, J. Phys. Chem., **96**, 2582-2588.
888. Mauldin, R. L., III, A. Wahner and A. R. Ravishankara, 1993, J. Phys. Chem., **97**, 7585-7596.
889. Maurer, T., I. Barnes, and K. H. Becker, 1999, Int. J. Chem. Kinet., **31**, 883-893.
890. McCaulley, J. A., S. M. Anderson, J. B. Jeffries and F. Kaufman, 1985, Chem Phys. Lett., **115**, 180.
891. McCrumb, J. L. and F. Kaufman, 1972, J. Chem. Phys., **57**, 1270-1276.
892. McKee, M. L. and P. H. Wine, 2001, J. Am. Chem. Soc., **123**, 2344-2353.
893. McKenzie, A., M. F. R. Mulcahy and J. R. Steven, 1973, J. Chem. Phys. , **59**, 3244-3254.
894. McLaren, I. A., N. W. Morris and R. P. Wayne, 1981, J. Photochem., **16**, 311-319.
895. McNeal, R. J. and G. R. Cook, 1967, J. Chem. Phys., **47**, 5385-5389.
896. Medhurst, L. J., J. Fleming and H. H. Nelson, 1977, Chem. Phys. Lett., **266**, 607-611.
897. Meier, U., H. H. Grotheer and T. Just, 1984, Chem. Phys. Lett., **106**, 97-101.
898. Meller, R. and G. K. Moortgat, 1995, J. Photochem. Photobio. A: Chem., **86**, 15-25.
899. Mellouki, A., 1998, J. Chim. Phys., **95**, 513-522.
900. Mellouki, A., 2005, To be submitted.
901. Mellouki, A., J. L. Jourdain and G. Le Bras, 1988, Chem. Phys. Lett., **148**, 231-236.
902. Mellouki, A., G. Laverdet, L. Jourdain and G. Poulet, 1989, Int. J. Chem. Kinet., **21**, 1161-1172.
903. Mellouki, A., G. Le Bras and G. Poulet, 1987, J. Phys. Chem., **91**, 5760-5764.
904. Mellouki, A., G. Le Bras and G. Poulet, 1988, J. Phys. Chem., **92**, 2229-2234.
905. Mellouki, A., G. Poulet, G. Le Bras, R. Singer, J. P. Burrows and G. K. Moortgat, 1989, J. Phys. Chem., **93**, 8017-8021.
906. Mellouki, A. and A. R. Ravishankara, 1994, Int. J. Chem. Kinet., **26**, 355-365.

907. Mellouki, A., R. K. Talukdar, A. M. R. P. Bopegedera and C. J. Howard, 1993, Int. J. Chem. Kinet., **25**, 25-39.
908. Mellouki, A., R. K. Talukdar and C. J. Howard, 1994, J. Geophys. Res., **99**, 22949-22954.
909. Mellouki, A., R. K. Talukdar, A.-M. Schmoltner, T. Gierczak, M. J. Mills, S. Soloman and A. R. Ravishankara, 1992, Geophys. Res. Lett., **19**, 2059-2062.
910. Mellouki, A., S. Teton, G. Laverdet, A. Quilgars and G. Le Bras, 1994, J. Chem. Physique, **91**, 473-487.
911. Mellouki, A., S. Teton and G. Le Bras, 1995, Geophys. Res. Lett., **22**, 389-392.
912. Michael, J. V., J. E. Allen, Jr. and W. D. Brobst, 1981, J. Phys. Chem., **85**, 4109-4117.
913. Michael, J. V., R. B. Klemm, W. D. Brobst, S. R. Bosco and D. F. Nava, 1985, J. Phys. Chem., **89**, 3335-3337.
914. Michael, J. V. and J. H. Lee, 1977, Chem. Phys. Lett., **51**, 303-306.
915. Michael, J. V., J. H. Lee, W. A. Payne and L. J. Stief, 1978, J. Chem. Phys., **68**, 4093.
916. Michael, J. V., D. F. Nava, W. Brobst, R. P. Borkowski and L. J. Stief, 1982, J. Phys. Chem., **86**, 81-84.
917. Michael, J. V., D. F. Nava, W. A. Payne, J. H. Lee and L. J. Stief, 1979, J. Phys. Chem., **83**, 2818.
918. Michael, J. V., D. F. Nava, W. A. Payne and L. J. Stief, 1979, J. Chem. Phys., **70**, 1147.
919. Michael, J. V., D. F. Nava, W. A. Payne and L. J. Stief, 1979, J. Chem. Phys., **70**, 3652.
920. Michael, J. V. and W. A. Payne, 1979, Int. J. Chem. Kinet., **11**, 799.
921. Michael, J. V., D. A. Whytock, J. H. Lee, W. A. Payne and L. J. Stief, 1977, J. Chem. Phys., **67**, 3533.
922. Michelangeli, D. V., K.-Y. Choo and M. T. Leu, 1988, Int. J. Chem. Kinet., **20**, 915-938.
923. Miller, J. C. and R. J. Gordon, 1981, J. Chem. Phys., **75**, 5305.
924. Miyoshi, A., H. Matsui and N. Washida, 1994, J. Chem. Phys., **100**, 3532-3539.
925. Miziolek, A. W. and M. J. Molina, 1978, J. Phys. Chem., **82**, 1769.
926. Mogelberg, T. E., O. J. Nielsen, J. Sehested and T. J. Wallington, 1995, J. Phys. Chem., **99**, 13437-13444.
927. Molina, L. T., M. J. Molina, R. A. Stachnik and R. D. Tom, 1985, J. Phys. Chem., **89**, 3779-3781.
928. Molina, L. T., J. E. Spencer and M. J. Molina, 1977, Chem. Phys. Lett., **45**, 158-162.
929. Molina, M. J., L. T. Molina and C. A. Smith, 1984, Int. J. Chem. Kinet., **16**, 1151-1160.
930. Montgomery, J. A., H. H. Michels and J. S. Francisco, 1994, Chem. Phys. Lett., **220**, 391-396.
931. Moonen, P. C., J. N. Cape, R. L. Storeton-West and R. McColm, 1998, J. Atmos. Chem., **29**, 299-314.
932. Moortgat, G. K., B. Veyret and R. Lesclaux, 1989, J. Phys. Chem., **93**, 2362-2368.
933. Morokuma, K. and C. Mugurama, 1994, J. Am. Chem. Soc., **116**, 10316-10317.
934. Morris, E. D., Jr. and H. Niki, 1971, J. Chem. Phys., **55**, 1991-1992.
935. Morris, E. D. and H. Niki, 1974, J. Phys. Chem., **78**, 1337-1338.
936. Mors, V., A. Hoffman, W. Malms and R. Zellner, 1996, Ber. Bunsenges, Phys. Chem., **100**, 540-552.
937. Muller, D. F. and P. L. Houston, 1981, J. Phys. Chem., **85**, 3563-3565.
938. Munk, J., P. Pagsberg, E. Ratajczak and A. Sillesen, 1986, J. Phys. Chem. , **90**, 2752-2757.
939. Murrells, T. P., E. R. Lovejoy and A. R. Ravishankara, 1990, J. Phys. Chem., **94**, 2381-2386.
940. Myers, G. H. and R. J. O'Brien, Jr., 1970, Ann. N.Y. Acad. Sci., **171**, 224-225.
941. Nadtochenko, V. A., O. M. Sarkisov and V. I. Vedeneev, 1979, Doklady Akademii Nauk SSSR, **244**, 152.
942. Nagase, S., S. Hashimoto and H. Akimoto, 1988, J. Phys. Chem., **92**, 641-644.
943. Nakano, Y., S. Enami, S. Nakamichi, S. Aloisio, S. Hashimoto and M. Kawasaki, 2003, J. Phys. Chem., **107**, 6381 - 6387.
944. Nakano, Y., M. Goto, S. Hashimoto, M. Kawasaki, and T. J. Wallington, 2001, J. Phys. Chem. A, **105**, 11045-11050.
945. Nava, D. F., S. R. Bosco and L. J. Stief, 1983, J. Chem. Phys., **78**, 2443-2448.
946. Nava, D. F., W. D. Brobst and L. J. Stief, 1985, J. Phys. Chem., **89**, 4703-4707.
947. Nava, D. F., J. V. Michael and L. J. Stief, 1981, J. Phys. Chem., **85**, 1896.
948. Neeb, P. and G. K. Moorgat, 1999, J. Phys. Chem. A., **103**, 9003-9012.
949. Nelson, D. D., Jr. , M. S. Zahniser and C. E. Kolb, 1993, Geophys. Res. Lett., **20**, 197-200.

950. Nelson, D. D., Jr., J. C. Wormhoudt, M. S. Zahniser, C. E. Kolb, M. K. W. Ko and D. K. Weisenstein, 1997, J. Phys. Chem. A, **101**, 4987-4990.
951. Nelson, D. D., Jr. and M. S. Zahniser, 1994, J. Phys. Chem., **98**, 2101-2104.
952. Nelson, D. D., Jr., M. S. Zahniser and C. E. Kolb, 1992, J. Phys. Chem., **96**, 249-253.
953. Nelson, D. D., M. S. Zahniser, C. E. Kolb and H. Magid, 1995, J. Phys. Chem., **99**, 16301-16306.
954. Nelson, H. H. and H. S. Johnston, 1981, J. Phys. Chem., **85**, 3891-3896.
955. Nelson, L., O. Rattigan, R. Neavyn, H. Sidebottom, J. Treacy and O. J. Nielsen, 1990, Int. J. Chem. Kinet., **22**, 1111-1126.
956. Nelson, L., I. Shanahan, H. W. Sidebottom, J. Treacy and O. J. Nielsen, 1990, Int. J. Chem. Kinet., **22**, 577-590.
957. Nesbitt, D. J. and S. R. Leone, 1980, J. Chem. Phys., **72**, 1722-1732.
958. Nesbitt, D. J. and S. R. Leone, 1981, J. Chem. Phys., **75**, 4949.
959. Nesbitt, F. L., J. F. Gleason and L. J. Stief, 1999, J. Phys. Chem. A, **103**, 3038-3043.
960. Nesbitt, F. L., P. S. Monks, W. A. Payne, L. J. Stief and R. Toumi, 1995, Geophys. Res. Lett., **22**, 827-830.
961. Nesbitt, F. L., D. F. Nava, W. A. Payne and L. J. Stief, 1987, J. Phys. Chem., **91**, 5337-5340.
962. Nesbitt, F. L., W. A. Payne and L. J. Stief, 1988, J. Phys. Chem., **92**, 4030-4032.
963. Nicholas, J. E. and R. G. W. Norrish, 1968, Proc. Roy. Soc. A, **307**, 391.
964. Nickolaisen, S. L., R. R. Friedl and S. P. Sander, 1994, J. Phys. Chem., **98**, 155-169.
965. Nickolaisen, S. L., C. M. Roehl, L. K. Blakeley, R. R. Friedl, J. S. Francisco, R. F. Liu and S. P. Sander, 2000, J. Phys. Chem. A, **104**, 308-319.
966. Nickolaisen, S. L., D. W. Veney and H. E. Cartland, 1994, J. Chem. Phys., **100**, 4925-4931.
967. Nicovich, J. M., K. D. Kreutter, C. A. van Dijk and P. H. Wine, 1992, J. Phys. Chem., **96**, 2518-2528.
968. Nicovich, J. M., K. D. Kreutter and P. H. Wine, 1990, Int. J Chem. Kinet., **22**, 399-414.
969. Nicovich, J. M., C. J. Shackelford and P. H. Wine, 1990, J. Phys. Chem., **94**, 2896-2903.
970. Nicovich, J. M., S. Wang and P. H. Wine, 1995, Int. J. Chem. Kinet., **27**, 359-368.
971. Nicovich, J. M. and P. H. Wine, 1987, J. Phys. Chem., **91**, 5118-5123.
972. Nicovich, J. M. and P. H. Wine, 1990, Int. J. Chem. Kinet., **22**, 379-397.
973. Nicovich, J. M., P. H. Wine and A. R. Ravishankara, 1988, J. Chem. Phys., **89**, 5670-5679.
974. Nielsen, O. J. "Chemical Kinetics in the Gas Phase Pulse Radiolysis of Hydrogen Sulfide Systems," Riso-M-2216, Riso National Laboratory 1979.
975. Nielsen, O. J., 1991, Chem. Phys. Lett., **187**, 286-290.
976. Nielsen, O. J., T. Ellermann, E. Bartkiewicz, T. J. Wallington and M. D. Hurley, 1992, Chem. Phys. Lett., **192**, 82-88.
977. Nielsen, O. J., T. Ellermann, J. Sehested and T. J. Wallington, 1992, J. Phys. Chem., **96**, 10875-10879.
978. Nielsen, O. J., J. Munk, G. Locke and T. J. Wallington, 1991, J. Phys. Chem., **95**, 8714-8719.
979. Nielsen, O. J., J. Munk, P. Pagsberg and A. Sillesen, 1986, Chem. Phys. Lett., **128**, 168-171.
980. Nielsen, O. J. and J. Sehested, 1993, Chem. Phys. Lett., **213**, 433-441.
981. Nielsen, O. J., H. W. Sidebottom, M. Donlon and J. Treacy, 1991, Chem. Phys. Lett., **178**, 163-170.
982. Nielsen, O. J., H. W. Sidebottom, L. Nelson, O. Rattigan, J. J. Treacy and D. J. O'Farrell, 1990, Int. J. Chem. Kinet., **22**, 603-612.
983. Nielsen, O. J., H. W. Sidebottom, L. Nelson, J. J. Treacy and D. J. O'Farrell, 1989, Int. J. Chem. Kinet., **21**, 1101-1112.
984. Niki, H., E. E. Daby and B. Weinstock. In *Twelfth Symposium (International) on Combustion*; The Combustion Institute, 1969; pp 277.
985. Niki, H., P. D. Maker, L. P. Breitenbach and C. M. Savage, 1978, Chem. Phys. Lett., **57**, 596.
986. Niki, H., P. D. Maker, C. M. Savage and L. P. Breitenbach, 1978, J. Phys. Chem., **82**, 132.
987. Niki, H., P. D. Maker, C. M. Savage and L. P. Breitenbach, 1980, Int. J. Chem. Kinet., **12**, 1001-1012.
988. Niki, H., P. D. Maker, C. M. Savage and L. P. Breitenbach, 1980, Chem. Phys. Lett., **73**, 43-46.
989. Niki, H., P. D. Maker, C. M. Savage and L. P. Breitenbach, 1981, J. Phys. Chem., **85**, 877.
990. Niki, H., P. D. Maker, C. M. Savage and L. P. Breitenbach, 1982, J. Phys. Chem., **86**, 3825.
991. Niki, H., P. D. Maker, C. M. Savage and L. P. Breitenbach, 1983, J. Phys. Chem., **87**, 2190-2193.

992. Niki, H., P. D. Maker, C. M. Savage and L. P. Breitenbach, 1984, J. Phys. Chem., **88**, 2116-2119.
993. Niki, H., P. D. Maker, C. M. Savage and L. P. Breitenbach, 1984, J. Phys. Chem., **88**, 5342-5344.
994. Niki, H., P. D. Maker, C. M. Savage and L. P. Breitenbach, 1985, J. Phys. Chem., **89**, 588.
995. Niki, H., P. D. Maker, C. M. Savage and M. D. Hurley, 1987, J. Phys.Chem., **91**, 2174-2178.
996. Ninomiya, Y., M. Kawasaki, A. Guschin, L. T. Molina, M. J. Molina and T. J. Wallington, 2000, Environ. Sci. Technol., **34**, 2973-2978.
997. Nip, W. S., D. L. Singleton and R. J. Cvetanovic, 1981, J. Am. Chem. Soc., **103**, 3526.
998. Nip, W. S., D. L. Singleton, R. Overend and G. Paraskevopoulos, 1979, J. Phys. Chem., **83**, 2440-2443.
999. Nizkorodov, S. A., W. W. Harper, B. W. Blackmon and D. J. Nesbitt, 2000, J. Phys. Chem. A, **104**, 3964-3973.
1000. Nizkorodov, S. A. and P. O. Wennberg, 2002, J. Phys. Chem. A, in press.
1001. Nolte, J., J. Grussdorf, F. Temps and H. Wagner, 1993, Zeit. fur Naturforschung Sec A-1. J. of Physical Sciences, **48**, 1234-1238.
1002. Notario, A., A. Mellouki and G. Le Bras, 2000, Int. J. Chem. Kinet., **32**, 62-66.
1003. Noxon, J. F., 1970, J. Chem. Phys. , **52**, 1852-1873.
1004. O'Brien, R. J., Jr. and G. H. Myers, 1970, J. Chem. Phys., **53**, 3832-3835.
1005. Ogren, P. J., T. J. Sworski, C. J. Hochanadel and J. M. Cassel, 1982, J. Phys. Chem., **86**, 238-242.
1006. Ogryzlo, E. A., R. Paltenghi and K. D. Bayes, 1981, Int. J. Chem. Kinet., **13**, 667-675.
1007. Oh, S. and J. Andino, 2000, Atmos. Environ., **34**, 2901-2908.
1008. Ohmori, K., K. Yamasaki and H. Matsui, 1993, Bull. Chem. Soc. Jpn., **66**, 51-56.
1009. Olbregts, J., G. Brasseur and E. J. Arijs, 1984, J. Photochem., **24**, 315-322.
1010. Olsson, B., M. Hallquist, E. Ljungstrom and J. Davidsson, 1997, Int. J. Chem. Kinet., **29**, 195.
1011. Ongstad, A. P. and J. W. Birks, 1984, J. Chem. Phys., **81**, 3922-3930.
1012. Ongstad, A. P. and J. W. Birks, 1986, J. Chem. Phys., **85**, 3359-3368.
1013. Orkin, V. L., R. E. Huie and M. J. Kurylo, 1996, J. Phys. Chem., **100**, 8907-8912.
1014. Orkin, V. L., R. E. Huie and M. J. Kurylo, 1997, J. Phys. Chem. A, **101**, 9118-9124.
1015. Orkin, V. L. and V. G. Khamaganov, 1993, J. Atmos. Chem., **16**, 157-167.
1016. Orkin, V. L. and V. G. Khamaganov, 1993, J. Atmos. Chem., **16**, 169-178.
1017. Orkin, V. L., V. G. Khamaganov, A. G. Guschin, R. E. Huie and M. J. Kurylo. International Symposium on Gas Kinetics, 1994, Dublin.
1018. Orkin, V. L., V. G. Khamaganov, A. G. Guschin, R. E. Huie and M. J. Kurylo, 1997, J. Phys. Chem. A, **101**, 174-178.
1019. Orkin, V. L., S. N. Kozlov, G. A. Poskrebyshev, R. E. Huie and M. J. Kurylo, 2006, J. Phys. Chem. A, **110**, 6978-6985.
1020. Orkin, V. L., F. Louis, R. E. Huie and M. J. Kurylo, 2002, J. Phys. Chem. A, **106**, 10195-10199.
1021. Orkin, V. L., E. Villenave, R. E. Huie and M. J. Kurylo, 1999, Journal of Physical Chemistry A, **103**, 9770-9779.
1022. Orlando, J. J., 1999, Int. J. Chem. Kinet., **31**, 515-524.
1023. Orlando, J. J., G. S. Tyndall, L. Vereecken and J. Peeters, 2000, J. Phys. Chem. A, **104**, 11578-11588.
1024. Orlando, J. J., G. S. Tyndall and T. J. Wallington, 1996, J. Phys. Chem., **100**, 7026-7033.
1025. Orlando, J. J., G. S. Tyndall, T. J. Wallington and M. Dill, 1996, Int. J. Chem. Kinet., **28**, 433-442.
1026. Overend, R. and G. Paraskevopoulos, 1978, J. Phys. Chem., **82**, 1329-1333.
1027. Overend, R. P. and G. Paraskevopoulos, 1977, Chem. Phys. Lett., **49**, 109.
1028. Overend, R. P., G. Paraskevopoulos and R. J. Cvetanovic, 1975, Canad. J. Chem., **53**, 3374-3382.
1029. Pagsberg, P., J. Munk, A. Sillesen and C. Anastasi, 1988, Chem. Phys. Lett., **146**, 375-381.
1030. Pagsberg, P. B., J. Erikson and H. C. Christensen, 1979, J. Phys. Chem., **83**, 582.
1031. Papagni, C., J. Arey and R. Atkinson, 2000, Int. J. Chem. Kinet., **32**, 79-.
1032. Paraskevopoulos, G. and R. S. Irwin. XV Informal Conference on Photochemistry, 1982, Stanford, CA.
1033. Paraskevopoulos, G. and R. S. Irwin, 1984, J. Chem. Phys., **80**, 259-266.
1034. Paraskevopoulos, G., D. L. Singleton and R. S. Irwin, 1981, J. Phys. Chem., **85**, 561.
1035. Park, C. R. and J. R. Wiesenfeld, 1991, Chem. Phys. Lett., **186**, 170-176.
1036. Park, J. and M. C. Lin, 1996, J. Phys. Chem., **100**, 3317-3319.
1037. Parrish, D. D. and D. R. Herschbach, 1973, J. Am. Chem. Soc., **95**, 6133.

1038. Pate, C. T., R. Atkinson and J. N. Pitts, Jr., 1976, J. Environ. Sci. Health, **A11**, 1.
1039. Patrick, R. and D. M. Golden, 1984, J. Phys. Chem., **88**, 491-495.
1040. Paulson, S. E., J. J. Orlando, G. S. Tyndall and J. G. Calvert, 1995, Int. J. Chem. Kinet., **27**, 997-1008.
1041. Pavanaja, U. B., H. P. Upadhyaya, A. V. Sapre, K. V. S. R. Rao and J. P. Mittal, 1994, J. Chem. Soc. Faraday. Trans., **90**, 825-829.
1042. Payne, W. A., J. Brunning, M. B. Mitchell and L. J. Stief, 1988, Int. J. Chem. Kinet., **20**, 63-74.
1043. Payne, W. A., L. J. Stief and D. D. Davis, 1973, J. Am. Chem. Soc., **95**, 7614.
1044. Peeters, J., J. Vertommen and I. Langhans, 1992, Ber. Bunsenges. Phys. Chem., **96**, 431-436.
1045. Penzhorn, R. D. and C. E. Canosa, 1983, Ber. Bunsenges. Phys. Chem., **87**, 648-654.
1046. Perri, M. J., A. L. Van Wyngarden, K. A. Boering, J. J. Lin and Y. T. Lee, 2003, J. Chem. Phys., **119**, 8213-8216.
1047. Perry, R. A., R. Atkinson and J. N. Pitts, 1977, J. Chem. Phys., **67**, 458-462.
1048. Perry, R. A., R. Atkinson and J. N. Pitts, Jr., 1976, J. Chem. Phys., **64**, 3237.
1049. Perry, R. A., R. Atkinson and J. N. Pitts, Jr., 1976, J. Chem. Phys., **64**, 1618.
1050. Perry, R. A., R. Atkinson and J. N. Pitts, Jr., 1977, J. Chem. Phys., **67**, 5577.
1051. Perry, R. A. and C. F. Melius. In *Twentieth Symposium (International) on Combustion*; The Combustion Institute, 1984; pp 639-646.
1052. Persky, A., 1996, J. Phys. Chem., **100**, 689-693.
1053. Petty, J. T., J. A. Harrison and C. B. Moore, 1993, J. Phys. Chem., **97**, 11194-11198.
1054. Phillips, L. F., 1978, Chem. Phys. Lett., **57**, 538-539.
1055. Phillips, L. F. and H. I. Schiff, 1962, J. Chem. Phys., **36**, 1509-1517.
1056. Picquet, B., S. Heroux, A. Chebbi, J. Doussin, R. Durand-Jolibois, A. Monod, H. Loirat and P. Carlier, 1998, Int. J. Chem. Kinet., **30**, 839.
1057. Piety, C. A., R. Soller, J. M. Nicovich, M. L. McKee and P. H. Wine, 1998, Chem. Phys., **231**, 155-169.
1058. Pilgrim, J. S., A. McIlroy and C. A. Taatjes, 1997, J. Phys. Chem. A, **101**, 1873-1880.
1059. Piper, L. G., G. E. Caledonia and J. P. Konnealy, 1981, J. Chem. Phys., **74**, 2888.
1060. Plane, J. M. C. and D. Husain, 1986, J. Chem. Soc. Faraday 2, **82**, 2047-2052.
1061. Plane, J. M. C., C.-F. Nien, M. R. Allen and M. Helmer, 1993, J. Phys. Chem., **97**, 4459-4467.
1062. Plane, J. M. C. and B. Rajasekhar, 1989, J. Phys. Chem., **93**, 3135-3140.
1063. Platz, J., O. J. Nielson, J. Sehested and T. J. Wallington, 1995, J. Phys. Chem., **99**, 6570-6579.
1064. Plum, C. N., E. Sanhueza, R. Atkinson, W. P. L. Carter and J. N. J. Pitts, 1983, Environ. Sci. Technol., **17**, 479-484.
1065. Plumb, I. C. and K. R. Ryan, 1982, Int. J. Chem. Kinet., **14**, 861-874.
1066. Plumb, I. C. and K. R. Ryan, 1982 Chem. Phys. Lett., **92**, 236-238.
1067. Plumb, I. C., K. R. Ryan, J. R. Steven and M. F. R. Mulcahy, 1982, Int. J. Chem. Kinet., **14**, 183.
1068. Pope, F. D., J. M. Nicovich and P. H. Wine, 2002, Int. J. Chem. Kinet., **34**, 156-161.
1069. Posey, J., J. Sherwell and M. Kaufman, 1981, Chem. Phys. Lett., **77**, 476-479.
1070. Poulet, G., I. T. Lancar, G. Laverdet and G. Le Bras, 1990, J. Phys. Chem., **94**, 278-284.
1071. Poulet, G., G. Laverdet, J. L. Jourdain and G. Le Bras, 1984, J. Phys. Chem., **88**, 6259-6263.
1072. Poulet, G., G. Laverdet and G. Le Bras, 1981, J. Phys. Chem., **85**, 1892.
1073. Poulet, G., G. Laverdet and G. Le Bras, 1983, Chem. Phys. Lett., **94**, 129-132.
1074. Poulet, G., G. Laverdet and G. Le Bras, 1984, J. Chem. Phys., **80**, 1922-1928.
1075. Poulet, G., G. Laverdet and G. Le Bras, 1986, J. Phys. Chem., **90**, 159-165.
1076. Poulet, G., G. Le Bras and J. Combourieu, 1974, J. Chim. Physique, **71**, 101-106.
1077. Poulet, G., G. Le Bras and J. Combourieu, 1978, J. Chem. Phys., **69**, 767.
1078. Poulet, G., G. Le Bras and J. Combourieu, 1980, Geophys. Res. Lett., **7**, 413-414.
1079. Poulet, G., H. Zagogianni and G. Le Bras, 1986, Int. J. Chem. Kinet., **18**, 847-859.
1080. Pritchard, H. O., J. B. Pyke and A. F. Trotman-Dickenson, 1954, J. Amer. Chem. Soc., **76**, 1201-1202.
1081. Pritchard, H. O., J. B. Pyke and A. F. Trotman-Dickenson, 1955, J. Amer. Chem. Soc., **77**, 2629-2633.
1082. Qiu, L. X., S.-H. Shi, S. B. Xing and X. G. Chen, 1992, J. Phys.Chem., **96**, 685-689.
1083. Radford, H. E., 1980, Chem. Phys. Lett., **71**, 195.
1084. Radford, H. E., K. M. Evenson and D. A. Jennings, 1981, Chem. Phys. Lett., **78**, 589.

1085. Rahman, M. M., E. Becker, T. Benter and R. N. Schindler, 1988, Ber. Bunsenges. Phys. Chem., **92**, 91-100.
1086. Rahman, M. M., E. Becker, U. Wille and R. N. Schindler, 1992, Ber. Bunsenges. Phys. Chem., **96**, 783-787.
1087. Raja, N., P. K. Arora and J. P. S. Chatha, 1986, Int. J. Chem. Kinetics, **18**, 505-512.
1088. Rattigan, O. V., R. A. Cox and R. L. Jones, 1995, J. Chem. Soc. Faraday Soc. Trans., **91**, 4189-4197.
1089. Ravichandran, K., R. Williams and T. R. Fletcher, 1994, Chem. Phys. Lett., **217**, 375-380.
1090. Ravishankara, A. R. and D. D. Davis, 1978, J. Phys. Chem., **82**, 2852-2853.
1091. Ravishankara, A. R., D. D. Davis, G. Smith, G. Tesi and J. Spencer, 1977, Geophys. Res. Lett., **4**, 7.
1092. Ravishankara, A. R., E. J. Dunlea, M. A. Blitz, T. J. Dillon, D. E. Heard, M. J. Pilling, R. S. Strekowski, J. M. Nicovich and P. H. Wine, 2002, Geophys. Res. Lett., **29**, 35.
1093. Ravishankara, A. R., F. L. Eisele and P. H. Wine, 1983, J. Chem. Phys., **78**, 1140-1144.
1094. Ravishankara, A. R., N. M. Kreutter, R. C. Shah and P. H. Wine, 1980, Geophys. Res. Lett., **7**, 861-864.
1095. Ravishankara, A. R., J. M. Nicovich, R. L. Thompson and F. P. Tully, 1981, J. Phys. Chem., **85**, 2498-2503.
1096. Ravishankara, A. R., G. Smith, R. T. Watson and D. D. Davis, 1977, J. Phys. Chem., **81**, 2220-2225.
1097. Ravishankara, A. R., S. Solomon, A. A. Turnipseed and R. F. Warren, 1993, Science, **259**, 194-199.
1098. Ravishankara, A. R. and R. L. Thompson, 1983, Chem. Phys. Lett., **99**, 377.
1099. Ravishankara, A. R., A. A. Turnipseed, N. R. Jensen, S. Barone, M. Mills, C. J. Howard and S. Solomon, 1994, Science, **263**, 71-75.
1100. Ravishankara, A. R. and P. H. Wine, 1980, J. Chem. Phys., **72**, 25-30.
1101. Ravishankara, A. R., P. H. Wine and A. O. Langford, 1979, Chem. Phys. Lett., **63**, 479-484.
1102. Ravishankara, A. R., P. H. Wine and A. O. Langford, 1979, J. Chem. Phys., **70**, 984-989.
1103. Ravishankara, A. R., P. H. Wine and J. M. Nicovich, 1983, J. Chem. Phys., **78**, 6629-6639.
1104. Ravishankara, A. R., P. H. Wine and J. R. Wells, 1985, J. Chem. Phys., **83**, 447-448.
1105. Ravishankara, A. R., P. H. Wine, J. R. Wells and R. L. Thompson, 1985, Int. J. Chem. Kinet., **17**, 1281-1297.
1106. Ray, A., I. Vassalli, G. Laverdet and G. Le Bras, 1996, J. Phys. Chem., **100**, 8895-8900.
1107. Ray, G. W., L. F. Keyser and R. T. Watson, 1980, J. Phys. Chem., **84**, 1674-1681.
1108. Ray, G. W. and R. T. Watson, 1981, J. Phys. Chem., **85**, 2955-2960.
1109. Ray, G. W. and R. T. Watson, 1981, J. Phys. Chem., **85** 1673-1676.
1110. Reilly, J. D., J. H. Clark, C. B. Moore and G. C. Pimentel, 1978, J. Chem. Phys., **69**, 4381.
1111. Reimann, B. and F. Kaufman, 1978, J. Chem. Phys., **69**, 2925
1112. Reiner, T. and F. Arnold, 1993, Geophys. Res. Lett., **20**, 2659-2662.
1113. Reiner, T. and F. Arnold, 1994, J. Chem. Phys., **101**, 7399-7407.
1114. Resende, S. M. and W. B. D. Almeida, 1997, J. Phys. Chem. A, **101**, 9738-9744.
1115. Resende, S. M. and R. Ornellas, 2001, Chem. Phys. Lett., **349**, 123 - 130.
1116. Rhasa, D. In *Diplomarbeit* Univ. of Gottingen FRG, 1983.
1117. Richardson, R. J., 1975, J. Phys. Chem., **79**, 1153-1158.
1118. Riffault, V., Y. Bedjanian and G. Le Bras, 2003, Phys. Chem. Chem. Phys., **5**, 2828-2835.
1119. Riffault, V., Y. Bedjanian and G. Le Bras, 2003, J. Phys. Chem. A, **107**, 5404 - 5411.
1120. Robertshaw, J. S. and I. W. M. Smith, 1980, Int . J . Chem. Kinet . **12**, 729
1121. Robertson, R. G. and G. P. Smith, 2002, Chem. Phys. Lett., **358**, 157-162.
1122. Rodebush, W. H. and W. C. Klingelhoefer, Jr., 1933, J. Am. Chem. Soc., **55**, 130.
1123. Roehl, C. M., D. Bauer and G. K. Moortgat, 1996, J. Phys. Chem., **100**, 4038-4047.
1124. Roscoe, J. M., 1982, Int. J. Chem. Kinet., **14**, 471-478.
1125. Roth, P., R. Lohr and H. D. Hermanns, 1980, Ber. Bunsenges. Phys. Chem., **84**, 835-840.
1126. Rowland, F. S., H. Sato, H. Khwaja and S. M. Elliott, 1986, J. Phys. Chem., **90**, 1985 -1988.
1127. Rowley, D. M., M. H. Harwood, R. A. Freshwater and R. L. Jones, 1996, J. Phys. Chem., **100**, 3020-3029.

1128. Rozenshtein, V. B., Y. M. Gershenzon, S. O. Il'in and O. P. Kishkovitch, 1984, Chem. Phys. Lett., **112**, 473-478.
1129. Rust, F. and C. M. Stevens, 1980, Int. J. Chem. Kinet., **12**, 371-377.
1130. Ryan, K. R. and I. C. Plumb, 1984, Int. J. Chem. Kinet., **16**, 591-602.
1131. Saathoff, H. and R. Zellner, 1993, Chem. Phys. Lett., **206**, 349-354.
1132. Sahetchian, K. A., A. Heiss and R. Rigny, 1982, Can. J. Chem., **60**, 2896-2902.
1133. Sahetchian, K. A., A. Heiss and R. Rigny, 1987, J. Phys. Chem., **91**, 2382-2386.
1134. Sander, S. P., 1984, J. Phys. Chem., **88**, 6018-6021.
1135. Sander, S. P., 1986, J. Phys. Chem., **90**, 2194-2199.
1136. Sander, S. P. and R. R. Friedl, 1989, J. Phys. Chem., **93**, 4764-4771.
1137. Sander, S. P. and C. C. Kircher, 1986, Chem. Phys. Lett., **126**, 149-152.
1138. Sander, S. P., M. Peterson, R. T. Watson and R. Patrick, 1982, J. Phys. Chem., **86**, 1236-1240.
1139. Sander, S. P. and R. T. Watson, 1981, J. Phys. Chem., **85**, 4000.
1140. Sander, S. P. and R. T. Watson, 1981, Chem. Phys. Lett., **77**, 473-475.
1141. Sanders, N. D., J. E. Butler and J. R. McDonald, 1980, J. Chem. Phys., **73**, 5381-5383.
1142. Sanders, N. D., J. E. Butler, L. R. Pasternack and J. R. McDonald, 1980, Chem. Phys., **48**, 203.
1143. Sanhueza, E. and J. Heicklen, 1975, J. Phys. Chem., **79**, 7-11.
1144. Sanhueza, E., R. Simonaitis and J. Heicklen, 1979, Int. J. Chem. Kinet., **11**, 907.
1145. Sarkisov, O. M., S. G. Cheskis and E. A. Sviridenkov, 1978, Bull. Acad. Sci. USSR Chem., **Ser. 27**, 2336.
1146. Sarzynski, D. and S. Sztuba, 2002, Int. J. Chem. Kinet., 34, No.12, 651-658 (2002), **34**, 651-658.
1147. Satyapal, S., J. Park, R. Bersohn and B. Katz, 1989, J. Chem. Phys., **91**, 6873-6879.
1148. Saueressig, G., P. Bergamaschi, J. N. Crowley, H. Fischer and G. W. Harris, 1996, Geophys. Res. Lett., **23**, 3619-3622.
1149. Saunders, S. M., K. J. Hughes, M. J. Pilling, D. L. Baulch and P. I. Smurthwaite. "Reactions of hydroxyl radicals with selected hydrocarbons of importance in atmospheric chemistry"; Optical Methods in Atmospheric Chemistry, 1992, Berlin.
1150. Sawerysyn, J.-P., C. Lafage, B. Meriaux and A. Tighezza, 1987, J. Chim. Phys., **84**, 1187-1193.
1151. Sawerysyn, J. P., A. Talhaoui, B. Meriaux and P. Devolder, 1992, Chem. Phys. Lett., **198**, 197-199.
1152. Schiffman, A., D. D. Nelson, M. S. Robinson and D. J. Nesbitt, 1991, J. Phys. Chem., **95**, 2629-2636.
1153. Schindler, R. N. and T. Benter, 1988, Ber. Bunsenges. Phys. Chem., **92**, 558.
1154. Schindler, R. N., J. Dethlefs and M. Schmidt, 1996, Ber. Bunsenges. Phys. Chem., **100**, 1242-1249.
1155. Schlyer, D. F., A. P. Wolf and P. P. Gaspar, 1978, J. Phys. Chem., **82**, 2633-2637.
1156. Schmidt, C. and H. I. Schiff, 1973, Chem. Phys. Lett., **23**, 339-342.
1157. Schmidt, V., G. Y. Zhu, K. H. Becker and E. H. Fink, 1985, Ber. Bunsenges. Phys. Chem., **89**, 321.
1158. Schmoltner, A.-M., P. M. Chu, R. J. Brudzynski and Y. T. Lee, 1989, J. Chem. Phys., **91**, 6926-6936.
1159. Schmoltner, A.-M., R. K. Talukdar, R. F. Warren, A. Mellouki, L. Goldfarb, T. Gierczak, S. A. McKeen and A. R. Ravishankara, 1993, J. Phys. Chem., **97**, 8976-8982.
1160. Schneider, W. F. and T. J. Wallington, 1994, J. Phys. Chem., **98**, 7448-7451.
1161. Schonle, G., M. M. Rahman and R. N. Schindler, 1987, Ber. Bunsenges. Phys. Chem., **91**, 66-75.
1162. Schurath, U. and H.-J. Goede, 1984, Physico-Chemical Behaviour of Atmospheric Pollutants, Proc. 3rd European Symposium, Varese, Italy, 227 - 239.
1163. Schurath, U., H. H. Lippmann and B. Jesser, 1981, Ber. Bunsenges. Phys. Chem., **85**, 807-813.
1164. Schwab, J. J., W. H. Brune and J. G. Anderson, 1989, J. Phys. Chem., **93**, 1030-1035.
1165. Schwab, J. J., D. W. Toohey, W. H. Brune and J. G. Anderson, 1984, J. Geophys. Res., **89**, 9581-9587.
1166. Scollard, D. J., J. J. Treacy, H. W. Sidebottom, C. Balestra-Garacia, G. Laverdet, G. Le Bras, H. MacLeod and S. Teton, 1993, J. Phys. Chem., **97**, 4683-4688.
1167. Sedlacek, A. J., D. R. Harding, J. Weston, R.E. , T. G. Kreutz and G. W. Flynn, 1989, J. Chem. Phys., **91**, 7550-7555.
1168. Seeley, J. V., J. T. Jayne and M. J. Molina, 1993, Int. J. Chem. Kinet.,, **25**, 571-594.

1169. Seeley, J. V., J. T. Jayne and M. J. Molina, 1996, J. Phys. Chem., **100**, 4019-4025.
1170. Seeley, J. V., R. F. Meads, M. J. Elrod and M. J. Molina, 1996, J. Phys. Chem., **100**, 4026-4031.
1171. Sehested, J., L. K. Christensen, O. J. Nielsen, M. Bilde, T. J. Wallington, J. J. Schneider, J. J. Orlando and G. S. Tyndall, 1998, Int. J. Chem. Kinet., **30**, 475-489.
1172. Sehested, J., T. Ellermann, O. J. Nielsen, T. J. Wallington and M. D. Hurley, 1993, Int. J. Chem. Kinet., **25**, 701-717.
1173. Sehested, J. and O. J. Nielsen, 1993, Chem. Phys. Lett., **206**, 369-375.
1174. Sehested, J., O. J. Nielsen and T. J. Wallington, 1993, Chem. Phys. Lett., **213**, 457-464.
1175. Sehested, J., K. Sehested, O. J. Nielsen and T. J. Wallington, 1994, J. Phys. Chem., **98**, 6731-6739.
1176. Selzer, E. A. and K. D. Bayes, 1983, J. Phys. Chem., **87**, 392-394.
1177. Semmes, D. H., A. R. Ravishankara, C. A. Gump-Perkins and P. H. Wine, 1985, Int. J. Chem. Kinet., **17**, 303-313.
1178. Shallcross, D. E., P. Biggs, C. E. CanosaMas, K. C. Clemitshaw, M. G. Harrison, M. R. L. Alanon, J. A. Pyle, A. Vipond and R. P. Wayne, 1997, Journal of the Chemical Society-Faraday Transactions, **93**, 2807-2811.
1179. Sharkey, P. and I. W. M. Smith, 1993, J. Chem. Soc. Faraday Trans., **89**, 631-638.
1180. Shi, J. and J. R. Barker, 1990, Int. J. Chem. Kinetics, **20**, 1283-1301.
1181. Shi, X., D. R. Herschbach, D. R. Worsnop and C. E. Kolb, 1993, J. Phys. Chem., **97**, 2113-2122.
1182. Shibuya, K., T. Ebatu, K. Obi and I. Tanaka, 1977, J. Phys. Chem., **81**, 2292.
1183. Silver, J. A., 1986, J. Chem. Phys., **84**, 4718-4720.
1184. Silver, J. A. and C. E. Kolb, 1980, Chem. Phys. Lett., **75**, 191.
1185. Silver, J. A. and C. E. Kolb, 1982, J. Phys. Chem., **86**, 3240-3246.
1186. Silver, J. A. and C. E. Kolb, 1986, J. Phys. Chem., **90**, 3267-3269.
1187. Silver, J. A. and C. E. Kolb, 1986, J. Phys. Chem., **90**, 3263-3266.
1188. Silver, J. A. and C. E. Kolb, 1987, J. Phys. Chem., **91**, 3713-3714.
1189. Silver, J. A., A. D. Stanton, M. S. Zahniser and C. E. Kolb, 1984, J. Phys. Chem., **88**, 3123-3129.
1190. Simon, F. G., J. P. Burrows, W. Schneider, G. K. Moortgat and P. J. Crutzen, 1989, J. Phys. Chem., **93**, 7807-7813.
1191. Simon, F. G., W. Schneider, G. K. Moortgat and J. P. Burrows, 1990, J. Photochem. Photobiol., **A55**, 1-23.
1192. Simonaitis, R. and J. Heicklen, 1973, J. Phys. Chem, **77**, 1932-1935.
1193. Simonaitis, R. and J. Heicklen, 1975, J. Phys. Chem., **79**, 298.
1194. Simonaitis, R. and J. Heicklen, 1982, J. Phys. Chem., **86**, 3416-3418.
1195. Simonaitis, R. and M. T. Leu, 1985, Int. J. Chem. Kinet., **17**, 293-301.
1196. Sims, I. R., I. W. M. Smith, D. C. Clary, P. Bocherel and B. R. Rowe, 1994, J. Chem. Phys., **101**, 1748-1751.
1197. Singh, J. P. and D. W. Setser, 1985, J. Phys. Chem., **89**, 5353-5358.
1198. Singleton, D. L. and R. J. Cvetanovic, 1978, Can. J. Chem., **56**, 2934.
1199. Singleton, D. L. and R. J. Cvetanovic, 1981, Int. J. Chem. Kinet., **13**, 945.
1200. Singleton, D. L., R. S. Irwin and R. J. Cvetanovic, 1977, Can. J. Chem., **55**, 3321-3327.
1201. Singleton, D. L., R. S. Irwin, W. S. Nip and R. J. Cvetanovic, 1979, J. Phys. Chem., **83**, 2195-2200.
1202. Singleton, D. L., G. Paraskevopoulos and R. S. Irwin, 1980, J. Phys. Chem., **84** 2339-2343.
1203. Singleton, D. L., G. Paraskevopoulos and R. S. Irwin, 1982, J. Phys. Chem., **86**, 2605-2609.
1204. Singleton, D. L., G. Paraskevopoulos and R. S. Irwin, 1989, J. Am. Chem. Soc., **111**, 5248-5251.
1205. Singleton, D. L., G. Paraskevopoulos, R. S. Irwin, G. S. Jolly and D. J. McKenney, 1988, J. Am. Chem. Soc., **110**, 7786-7790.
1206. Sinha, A., E. R. Lovejoy and C. J. Howard, 1987, J. Chem. Phys., **87**, 2122-2128.
1207. Sivakumaran, V., D. Holscher, T. J. Dillon and J. Crowley, 2003, Phys. Chem. Chem. Phys., **5**, 4821.
1208. Slagle, I. R., F. Baiocchi and D. Gutman, 1978, J. Phys. Chem., **82** 1333.
1209. Slagle, I. R., J. R. Gilbert and D. Gutman, 1974, J. Chem. Phys., **61**, 704.
1210. Slagle, I. R., R. E. Graham, J. R. Gilbert and D. Gutman, 1975, Chem. Phys. Lett., **32**, 184.
1211. Slanger, T. G. and G. Black, 1979, J. Chem. Phys., **70**, 3434-3438.
1212. Slanger, T. G., B. J. Wood and G. Black, 1973, Int. J. Chem. Kinet., **5**, 615-620.

1213. Smardzewski, R. R. and M. C. Lin, 1977, J. Chem. Phys., **66**, 3197-3204.
1214. Smith, C. A., L. T. Molina, J. J. Lamb and M. J. Molina, 1984, Int. J. Chem. Kinet., **16**, 41-55.
1215. Smith, I. W. M. and D. W. A. Stewart, 1994, J. Chem. Soc. Faraday Trans.,, **90**, 3221-3227.
1216. Smith, I. W. M. and M. D. Williams, 1986, J. Chem. Soc. Faraday Trans. 2, **82**, 1043-1055.
1217. Smith, I. W. M. and R. Zellner, 1974, J. Chem. Soc.. Faraday Trans. 2, **70**, 1045-1056.
1218. Smith, I. W. M. and R. Zellner, 1975, Int. J. Chem. Kinet., **Symp. 1**, 341.
1219. Smith, R. H., 1978, Int. J. Chem. Kinet., **10**, 519.
1220. Snelling, D. R., 1974, Can. J. Chem., **52**, 257-270.
1221. Soller, R. J., J. M. Nicovich and P. H. Wine, 2001, J. Phys. Chem. A, **105**, 1416-1422.
1222. Sorensen, S., H. Falbe-Hansen, M. Mangoni, J. Hjorth and N. R. Jensen, 1996, J. Atmos. Chem., **24**, 299-315.
1223. Sorokin, V. I., N. P. Gristan and A. I. Chichinin, 1998, J. Chem. Phys., **108**, 8995-9003.
1224. Sridharan, U. C., F. S. Klein and F. Kaufman, 1985, J. Chem. Phys., **82**, 592-593.
1225. Sridharan, U. C., L. X. Qiu and F. Kaufman, 1981, J. Phys. Chem., **85**, 3361-3363.
1226. Sridharan, U. C., L. X. Qiu and F. Kaufman, 1982, J. Phys. Chem., **86**, 4569-4574.
1227. Sridharan, U. C., L. X. Qiu and F. Kaufman, 1984, J. Phys. Chem., **88**, 1281-1282.
1228. Sridharan, U. C., B. Reimann and F. Kaufman, 1980, J. Chem. Phys., **73** 1286-1293.
1229. Stachnik, R. A. and M. J. Molina, 1987, J. Phys. Chem., **91**, 4603
1230. Stachnik, R. A., M. J. Molina and L. T. Molina, 1986, J. Phys. Chem., **90**, 2777-2780.
1231. Staricco, E. H., S. E. Sicre and H. J. Schumacher, 1962, Z. Phys . Chem. N.F., **31**, 385.
1232. Stedman, D. H. and H. Niki, 1973, Environ. Lett., **4**, 303.
1233. Stedman, D. H. and H. Niki, 1973, J. Phys. Chem., **77**, 2604-2609.
1234. Stedman, D. H., C. H. Wu and H. Niki, 1973, J. Phys. Chem., **77**, 2511.
1235. Steer, R. P., R. A. Ackerman and J. N. Pitts, Jr., 1969, J. Chem. Phys., **51**, 843-844.
1236. Stephens, J. W., C. L. Morter, S. K. Farhat, G. P. Glass and R. F. Curl, 1993, J. Phys. Chem., **97**, 8944-8951.
1237. Stephens, R. D., 1984, J. Phys. Chem. , **88**, 3308-3313.
1238. Stephens, S. L., J. W. Birks and R. J. Glinski, 1989, J. Phys. Chem., **93**, 8384-8385.
1239. Stevens, P. S. and J. G. Anderson, 1990, Geophys. Res. Lett., **17**, 1287-1290.
1240. Stevens, P. S. and J. G. Anderson, 1992, J. Phys. Chem., **96**, 1708-1718.
1241. Stevens, P. S., W. H. Brune and J. G. Anderson, 1989, J. Phys. Chem., **93**, 4068-4079.
1242. Stickel, R. E., M. Chin, E. P. Daykin, A. J. Hynes, P. H. Wine and T. J. Wallington, 1993, J. Phys. Chem., **97**, 13653-13661.
1243. Stickel, R. E., J. M. Nicovich, S. Wang, Z. Zhao and P. H. Wine, 1992, J. Phys. Chem., **96**, 9875-9883.
1244. Stickel, R. E., Z. Zhao and P. H. Wine, 1993, Chem. Phys. Lett., **212**, 312-318.
1245. Stief, L. J., W. D. Brobst, D. F. Nava, R. P. Borkowski and J. V. Michael, 1982, J. Chem. Soc. Faraday Trans. 2, **78**, 1391-1401.
1246. Stief, L. J., D. F. Nava, W. A. Payne and J. V. Michael, 1980, J. Chem. Phys., **73**, 2254-2258.
1247. Stief, L. J., W. A. Payne, J. H. Lee and J. V. Michael, 1979, J. Chem. Phys., **70**, 5241-5243.
1248. Stimpfle, R., R. Perry and C. J. Howard, 1979, J. Chem. Phys., **71**, 5183-5190.
1249. Streit, G. E., C. J. Howard, A. L. Schmeltekopf, J. A. Davidson and H. I. Schiff, 1976, J. Chem. Phys., **65**, 4761-4764.
1250. Streit, G. E., J. S. Wells, F. C. Fehsenfeld and C. J. Howard, 1979, J. Chem. Phys., **70**, 3439-3443.
1251. Strekowski, R. S., J. M. Nicovich and P. H. Wine, 2000, Chem. Phys. Lett., **330**, 354-360.
1252. Strekowski, R. S., J. M. Nicovich and P. H. Wine, 2001, Int. J. Chem. Kin., **33**, 262-270.
1253. Strekowski, R. S., J. M. Nicovich and P. H. Wine, 2004, Phys. Chem. Chem. Phys., **6**, 2145-2151.
1254. Stuhl, F., 1973, J. Chem. Phys., **59**, 635.
1255. Stuhl, F., 1974, Ber. Bunsenges. Phys. Chem., **78**, 230.
1256. Stuhl, F. and H. Niki, 1970, Chem. Phys. Lett., **7**, 473-474.
1257. Stuhl, F. and H. Niki, 1971, J. Chem. Phys., **55**, 3954-3957.
1258. Stuhl, F. and H. Niki, 1972, J. Chem. Phys., **57**, 3671-3677.
1259. Stuhl, F. and K. H. Welge, 1969, Can. J. Chem., **47**, 1870-1871.
1260. Su, F., J. G. Calvert, C. R. Lindley, W. M. Uselman and J. H. Shaw, 1979, J. Phys. Chem., **83**, 912-920.
1261. Su, F., J. G. Calvert and J. H. Shaw, 1979, J. Phys. Chem., **83**, 3185-3191.

1262. Su, F., J. G. Calvert and J. H. Shaw, 1980, J. Phys. Chem., **84**, 239.
1263. Su, F., J. G. Calvert, J. H. Shaw, H. Niki, P. D. Maker, C. M. Savage and L. D. Breitenbach, 1979, Chem. Phys. Lett., **65**, 221-225.
1264. Sugawara, K., Y. Ishikawa and S. Sato, 1980, Bull. Chem. Soc. Japan, **53**, 3159.
1265. Sullivan, J. O. and P. Warneck, 1965, J. Phys. Chem., **69**, 1749.
1266. Sverdrup, G. M., C. W. Spicer and G. F. Ward, 1987, Int. J. Chem. Kinet., **19**, 191-205.
1267. Szekely, A., R. K. Hanson and C. Bowman. In *Twentieth Symposium (International) on Combustion*; The Combustion Institute, 1984; pp 647-654.
1268. Szilagyi, I., S. Dobe and T. Berces, 2000, Reaction Kinetics and Catalysis Letters, **70**, 319-324.
1269. Taatjes, C. A., L. K. Christensen, M. D. Hurley and T. J. Wallington, 1999, J. Phys.Chem. A, **103**, 9805.
1270. Tachibana, K. and A. V. Phelps, 1981, J. Chem. Phys., **75**, 3315-3320.
1271. Takacs, G. A. and G. P. Glass, 1973, J. Phys. Chem., **77**, 1948-1951.
1272. Takacs, G. A. and G. P. Glass, 1973, J. Phys. Chem., **77**, 1182.
1273. Takacs, G. A. and G. P. Glass, 1973, J. Phys. Chem., **77**, 1060.
1274. Takacs, G. A. and C. J. Howard, 1984, J. Phys. Chem. , **88**, 2110.
1275. Takacs, G. A. and C. J. Howard, 1986, J. Phys. Chem., **90**, 687-690.
1276. Takahashi, K., R. Wada, Y. Matsumi and M. Kawasaki, 1996, J. Phys. Chem., **100**, 10145-10149.
1277. Talcott, C. L., J. W. Ager, III and C. J. Howard, 1986, J. Chem. Phys., **84**, 6161-6169.
1278. Talhaoui, A., B. Louis, B. Meriaux, P. Devolder and J. P. Sawerysyn, 1996, J. Phys. Chem., **100**, 2107-2113.
1279. Talhaoui, A., F. Louis, P. Devolder, B. Meriaux, J. P. Sawerysyn, M. T. Rayez and J. C. Rayez, 1996, J. Phys. Chem., **100**, 13531-13538.
1280. Talukdar, R., A. Mellouki, T. Gierczak, J. B. Burkholder, S. A. McKeen and A. R. Ravishankara, 1991, Science, **252**, 693-695.
1281. Talukdar, R., A. Mellouki, T. Gierczak, J. B. Burkholder, S. A. McKeen and A. R. Ravishankara, 1991, J. Phys. Chem., **95**, 5815-5821.
1282. Talukdar, R. K., J. B. Burkholder, A.-M. Schmoltner, J. M. Roberts, R. Wilson and A. R. Ravishankara, 1995, J. Geophys. Res., **100**, 14163-14173.
1283. Talukdar, R. K., E. J. Dunlea, S. S. Brown, J. S. Daniel and A. R. Ravishankara, 2002, J. .Phys. Chem. A, **106**, 8461.
1284. Talukdar, R. K., T. Gierczak, L. Goldfarb, Y. Rudich, B. S. Madhava Rao and A. R. Ravishankara, 1996, J. Phys. Chem., **100**, 3037-3043.
1285. Talukdar, R. K., T. Gierczak, D. C. McCabe and A. R. Ravishankara, 2003, J. Phys. Chem. A, **107**, 5021-5032.
1286. Talukdar, R. K., S. C. Herndon, J. B. Burkholder, J. M. Roberts and A. R. Ravishankara, 1997, Journal of the Chemical Society-Faraday Transactions, **93**, 2787-2796.
1287. Talukdar, R. K., A. Mellouki, T. Gierczak, S. Barone, S.-Y. Chiang and A. R. Ravishankara, 1994, Int. J. Chem. Kinet., **26**, 973-990.
1288. Talukdar, R. K., A. Mellouki, A.-M. Schmoltner, T. Watson, S. Montzka and A. R. Ravishankara, 1992, Science, **257**, 227-230.
1289. Talukdar, R. K. and A. R. Ravishankara, 1996, Chem. Phys. Lett., **253**, 177-183.
1290. Taylor, P. H., J. A. D'Angelo, M. C. Martin, J. H. Kasner and B. Dellinger, 1989, Int. J. Chem. Kinet., **21**, 829-846.
1291. Taylor, P. H., Z. Jiang and B. Dellinger, 1993, Int. J. Chem. Kinet., **25**, 9-23.
1292. Temps, F. and H. G. Wagner, 1982, Ber. Bunsenges. Phys. Chem., **86**, 119-125.
1293. Temps, F. and H. G. Wagner, 1984, Ber. Bunsenges Phys. Chem., **88**, 415.
1294. Teton, S., A. El-Boudali and A. Mellouki, 1996, J. Chim. Phys., **93**, 274-282.
1295. Thevenet, R., A. Mellouki and G. LeBras, 2000, Int. J. Chem. Kinet., **32**, 676-685.
1296. Thomas, J. W. and F. Kaufman, 1985, J. Chem. Phys., **83**, 2900-2903.
1297. Thomas, R. G. O. and B. A. Thrush, 1975, J. Chem. Soc. Faraday Trans. 2, **71**, 664-667.
1298. Thompson, J. E. and A. R. Ravishankara, 1993, Int. J. Chem. Kinet., **25**, 479-487.
1299. Thompson, K. C., C. E. Canosa-Mas and R. P. Wayne, 2002, Phys. Chem. Chem. Phys., **4**, 4133 - 4139.
1300. Thorn, R. P., J. M. Conkhite, J. M. Nicovich and P. H. Wine, 1995, J. Chem. Phys., **102**, 4131-4142.

1301. Thrush, B. A. and G. S. Tyndall, 1982, Chem. Phys. Lett., **92**, 232-235.
1302. Thrush, B. A. and G. S. Tyndall, 1982, J. Chem. Soc. Faraday 2, **78**, 1469-1475.
1303. Thrush, B. A. and J. P. T. Wilkinson, 1979, Chem. Phys. Lett., **66**, 441-443.
1304. Thrush, B. A. and J. P. T. Wilkinson, 1981, Chem. Phys. Lett., **84**, 17-19.
1305. Thrush, B. A. and J. P. T. Wilkinson, 1981, Chem. Phys. Lett., **81**, 1-3.
1306. Tichenor, L. B., A. El-Sinawi, T. Yamada, P. H. Taylor, J. P. Peng, X. Hu and P. Marshall, 2001, Chemosphere, **42**, 571-577.
1307. Tichenor, L. B., J. L. Graham, T. Yamada, P. H. Taylor, J. P. Peng, X. H. Hu and P. Marshall, 2000, Journal of Physical Chemistry A, **104**, 1700-1707.
1308. Tiee, J. J., F. B. Wampler, R. C. Oldenborg and W. W. Rice, 1981, Chem. Phys. Lett., **82**, 80-84.
1309. Timonen, R. S., E. Ratajczak and D. Gutman, 1988, J. Phys. Chem., **92**, 651-655.
1310. Toby, F. S., S. Toby and H. E. O'Neal, 1976, Int. J. Chem. Kinet., **8**, 25.
1311. Tokuhashi, K., H. Nagai, A. Takahashi, M. Kaise, S. Kondo, A. Sekiya, M. Takahashi, Y. Gotoh and A. Suga, 1999, J. Phys. Chem. A, **103**, 2664-2672.
1312. Tokuhashi, K., A. Takahashi, M. Kaise, S. Kondo, A. Sekiya, S. Yamashita and H. Ito, 1999, Int. J. Chem. Kinet., **31**, 846-853.
1313. Tokuhashi, K., A. Takahashi, M. Kaise, S. Kondo, A. Sekiya, S. Yamashita and H. Ito, 2000, J. Phys. Chem., A, **104**, 1165-1170.
1314. Tomas, A. E., E. Villenave and R. Lesclaux, 2001, J. Phys. Chem. A, **105**, 3505-3514.
1315. Toohey, D. W. Kinetic and Mechanistic Studies of Reactions of Bromine and Chlorine Species Important in the Earth's Stratosphere, Ph. D. Thesis, Harvard University, 1988.
1316. Toohey, D. W. and J. G. Anderson, 1988, J. Phys. Chem., **92**, 1705-1708.
1317. Toohey, D. W., W. H. Brune and J. G. Anderson, 1987, J. Phys. Chem. , **91**, 1215-1222.
1318. Toohey, D. W., W. H. Brune and J. G. Anderson, 1988, Int. J. Chem. Kinet., **20**, 131-144.
1319. Trainor, D. W. and C. W. von Rosenberg, Jr., 1974, J. Chem. Phys., **61**, 1010-1015.
1320. Treacy, J., M. E. Hag, D. O'Farrell and H. Sidebotto, 1992, Ber. Bunsenges. Phys. Chem., **96**, 422-427.
1321. Trevor, P. L., G. Black and J. R. Barker, 1982, J. Phys. Chem., **86**, 1661.
1322. Tsalkani, N., A. Mellouki, G. Poulet, G. Toupance and G. Le Bras, 1988, J. Atmos. Chem., **7**, 409-419.
1323. Tschuikow-Roux, E., F. Faraji, S. Paddison, J. Niedzielski and K. Miyokawa, 1988, J. Phys. Chem., **92**, 1488-1495.
1324. Tschuikow-Roux, E., T. Yano and J. Niedzielski, 1985, J. Chem. Phys., **82** 65-74.
1325. Tuazon, E. C., R. Atkinson, S. M. Aschmann, M. A. Goodman and A. M. Winer, 1988, Int. J. Chem. Kinet., **20**, 241-265.
1326. Tuazon, E. C., R. Atkinson and S. B. Corchnoy, 1992, Int. J. Chem. Kinet., **24**, 639-648.
1327. Tuazon, E. C., R. Atkinson, C. N. Plum, A. M. Winer and J. N. Pitts, 1983, Geophys. Res. Lett., **10**, 953-956.
1328. Tuazon, E. C., W. P. L. Carter, R. Atkinson and J. N. Pitts, Jr., 1983, Int. J. Chem. Kinet., **15**, 619-629.
1329. Tuazon, E. C., E. Sanhueza, R. Atkinson, W. P. L. Carter, A. M. Winer and J. N. Pitts, Jr., 1984, J. Phys. Chem., **88**, 3095-3098.
1330. Tully, F. P., 1983, Chem. Phys. Lett., **96**, 148-153.
1331. Tully, F. P., A. T. Droege, M. L. Koszykowski and C. F. Melius, 1986, J. Phys. Chem., **90**, 691-698.
1332. Tully, F. P. and A. R. Ravishankara, 1980, J. Phys. Chem., **84**, 3126-3130.
1333. Tully, F. P., A. R. Ravishankara and K. Carr, 1983, Inter. J. Chem. Kinet., **15**, 1111-1118.
1334. Turnipseed, A. A., S. B. Barone, N. R. Jensen, D. R. Hanson, C. J. Howard and A. R. Ravishankara, 1995, J. Phys. Chem., **99**, 6000-6009.
1335. Turnipseed, A. A., S. B. Barone and A. R. Ravishankara, 1993, J. Phys. Chem., **97**, 5926-5934.
1336. Turnipseed, A. A., S. B. Barone and A. R. Ravishankara, 1994, J. Phys. Chem., **98**, 4594-4601.
1337. Turnipseed, A. A., S. B. Barone and A. R. Ravishankara, 1996, J. Phys. Chem., **100**, 14703-14713.
1338. Turnipseed, A. A., J. W. Birks and J. G. Calvert, 1990, J. Phys. Chem., **94**, 7477-7482.
1339. Turnipseed, A. A., J. W. Birks and J. G. Calvert, 1991, J. Phys. Chem., **95**, 4356-4364.

1340. Turnipseed, A. A., M. K. Gilles, J. B. Burkholder and A. R. Ravishankara, 1995, Chem. Phys. Lett., **242**, 427-434.
1341. Turnipseed, A. A., M. K. Gilles, J. B. Burkholder and A. R. Ravishankara, 1997, J. Phys. Chem., A., **101**, 5517-5525.
1342. Turnipseed, A. A., G. L. Vaghjiani, T. Gierczak, J. E. Thompson and A. R. Ravishankara, 1991, J. Chem. Phys., **95**, 3244-3251.
1343. Tyler, S. C., H. O. Ajie, A. L. Rice and R. J. Cicerone, 2000, Geophys. Res. Letters, **27**, 1715-1718.
1344. Tyndall, G. R. S., J. J. Orlando, T. J. Wallington, M. D. Hurley, M. Goto and M. Kawasaki, 2002, Phys. Chem. Chem. Phys., **4**, 2189-2193.
1345. Tyndall, G. S., J. P. Burrows, W. Schneider and G. K. Moortgat, 1986, Chem. Phys. Lett., **130**, 463-466.
1346. Tyndall, G. S., R. A. Cox, C. Granier, R. Lesclaux, G. K. Moortgat, M. J. Pilling, A. R. Ravishankara and T. J. Wallington, 2001, J. Geophys. Res., **106**, 12157-12182.
1347. Tyndall, G. S., C. S. Kegley-Owen, G. S. Orlando and A. Fried, 2002, J. Phys.Chem. A, **106**, 1567-1575.
1348. Tyndall, G. S., J. J. Orlando and J. G. Calvert, 1995, Environ. Sci. Technol., **29**, 202-206.
1349. Tyndall, G. S., J. J. Orlando, C. A. Cantrell, R. E. Shetter and J. G. Calvert, 1991, J. Phys. Chem., **95**, 4381-4386.
1350. Tyndall, G. S., J. J. Orlando, C. S. Kegley-Owen, T. J. Wallington and M. D. Hurley, 1999, Int. J. Chem. Kinet., **31**, 776-784.
1351. Tyndall, G. S., J. J. Orlando, K. E. Nickerson, C. A. Cantrell and J. G. Calvert, 1991, J. Geophys. Res., **96**, 20761-20768.
1352. Tyndall, G. S., J. J. Orlando, T. J. Wallington, M. Dill and E. W. Kaiser, 1997, Int. J. Chem. Kinet., **29**, 43-55.
1353. Tyndall, G. S., J. J. Orlando, T. J. Wallington, J. Sehested and O. J. Nielsen, 1996, J. Phys. Chem., **100**, 660-668.
1354. Tyndall, G. S. and A. R. Ravishankara, 1989, J. Phys. Chem., **93**, 2426-2435.
1355. Tyndall, G. S. and A. R. Ravishankara, 1989, J. Phys. Chem., **93**, 4707-4710.
1356. Tyndall, G. S. and A. R. Ravishankara, 1991, Int. J. Chem. Kinet., **23**, 483-527.
1357. Tyndall, G. S., T. J. Wallington and J. C. Ball, 1998, J. Phys. Chem. A, **102**, 2547-2554.
1358. Tyndall, G. S., T. J. Wallington and A. R. Potts, 1991, Chemical Physics Letters, **186**, 149-153.
1359. Urbanski, R. E. Stickel and P. H. Wine, 1998, J. Phys. Chem. A, **102**, 10522-10529.
1360. Urbanski, S. P., R. E. Stickel, Z. Zhao and P. H. Wine, 1997, J. Chem. Soc. Farad. Trans., **93**, 2813 - 2819.
1361. Urbanski, S. P. and P. H. Wine, 1999, J. Phys. Chem. A, **103**, 10935-10944.
1362. Vaghjiani, G. L. and A. R. Ravishankara, 1989, J. Phys. Chem., **93**, 1948.
1363. Vaghjiani, G. L. and A. R. Ravishankara, 1991, Nature, **350**, 406-409.
1364. Vaghjiani, G. L., A. R. Ravishankara and N. Cohen, 1989, J. Phys. Chem., **93**, 7833-7837.
1365. Vakhtin, A. B., D. C. McCabe, A. R. Ravishankara and S. R. Leone, 2003, J. Phys. Chem., A, **17**, 10642-10647.
1366. Van den Bergh, H. and J. Troe, 1976, J. Chem. Phys., **64**, 736-742.
1367. Vandenberk, S. and J. Peeters, 2003, J. Photochem. Photobiol. A, **157**, 269-274.
1368. Vandenberk, S., L. Vereecken and J. Peeters, 2002, Phys. Chem. Chem. Phys., **4**, 461-466.
1369. Vandenberk, S., L. Vereecken and J. Peeters, 2002, Phys. Chem. Chem. Phys., **4**, 461-466.
1370. Vanderzanden, J. W. and J. W. Birks, 1982, Chem. Phys. Lett., **88**, 109-114.
1371. Vandresen, S. and S. M. Resende, 2004, J. Phys. Chem. A, **108**, 2284-2289.
1372. Vasvari, G., I. Szilagyi, A. Bencsura, S. Dobe, T. Berces, E. Heron, S. Canneaux and F. Bohr, 2001, Phys. Chem. Chem. Phys., **3**, 551-555.
1373. Verhees, P. W. C. and E. H. Adema, 1985, J. Atmos. Chem., **2**, 387.
1374. Veyret, B. and R. Lesclaux, 1981, J. Phys. Chem., **85**, 1918.
1375. Veyret, B., R. Lesclaux, M.-T. Rayez, J.-C. Rayez, R. A. Cox and G. K. Moortgat, 1989, J. Phys. Chem. , **93**, 2368-2374.
1376. Veyret, B., J. C. Rayez and R. Lesclaux, 1982, J. Phys. Chem., **86**, 3424-3430.
1377. Villenave, E. and R. Lesclaux, 1996, J. Phys. Chem., **100**, 14372-14382.
1378. Villenave, E., V. L. Orkin, R. E. Huie and M. J. Kurylo, 1997, J. Phys. Chem. A, **101**, 8513-8517.

1379. Vinckier, C., M. Schaekers and J. Peeters, 1985, J. Phys. Chem., **89**, 508-512.
1380. Vogt, R. and R. N. Schindler, 1993, Ber. Bunsenges. Phys. Chem., **97**, 819-829.
1381. Volltrauer, H. N., W. Felder, R. J. Pirkle and A. Fontijn, 1979, J. Photochem., **11**, 173-181.
1382. Von Ellenrieder, G., E. Castellano and H. J. Schumacher, 1971, Chem. Phys. Lett., **9**, 152-156.
1383. Wagner, A. F., I. R. Slagle, D. Sarzynski and D. Gutman, 1990, J. Phys. Chem., **94**, 1853-1864.
1384. Wagner, G. and R. Zellner, 1981, Ber. Bunsenges. Phys. Chem., **85**, 1122-1128.
1385. Wagner, H. G., J. Warnatz and C. Zetzsch, 1971, Anales Assoc. Quim. Argentina, **59**, 169-177.
1386. Wagner, H. G., U. Welzbacher and R. Zellner, 1976, Ber Bunsenges. Phys. Chem., **80**, 1023-1027.
1387. Wagner, H. G., C. Zetzsch and J. Warnatz, 1972, Ber. Bunsenges. Phys. Chem., **76**, 526.
1388. Wahner, A. and A. R. Ravishankara, 1987, J. Geophys. Res. , **92**, 2189-2194.
1389. Walch, S. P., 1993, J. Chem. Phys., **99**, 5295-5300.
1390. Wallington, T. J., J. M. Andino, J. C. Ball and S. M. Japar, 1990, J. Atmos. Chem., **10**, 301-313.
1391. Wallington, T. J., J. M. Andino, A. R. Potts and P. H. Wine, 1991, Chem. Phys. Lett., **176**, 103-108.
1392. Wallington, T. J., R. Atkinson, E. C. Tuazon and S. M. Aschmann, 1986, Int. J. Chem. Kinet., **18**, 837-846.
1393. Wallington, T. J., R. Atkinson and A. M. Winer, 1984, Geophys. Res. Lett., **11**, 861-864.
1394. Wallington, T. J., R. Atkinson, A. M. Winer and J. N. Pitts, Jr., 1986, J. Phys. Chem., **90**, 5393-5396.
1395. Wallington, T. J., R. Atkinson, A. M. Winer and J. N. Pitts Jr., 1986, J. Phys. Chem., **90**, 4640-4644.
1396. Wallington, T. J. and J. C. Ball, 1995, Chem. Phys. Lett., **234**, 187-194.
1397. Wallington, T. J. and J. C. Ball, 1995, J. Phys. Chem., **99**, 3201-3205.
1398. Wallington, T. J., J. C. Ball, O. J. Nielsen and E. Bartkiewicz, 1992, J. Phys. Chem. , **96**, 1241-1246.
1399. Wallington, T. J., P. Dagaut and M. J. Kurylo, 1988, J. Photochem. Photobiol. A: Chemistry, **42**, 173-185.
1400. Wallington, T. J., P. Dagaut and M. J. Kurylo, 1988, J. Phys. Chem., **92**, 5024-5028.
1401. Wallington, T. J., P. Dagaut and M. J. Kurylo, 1992, Chem. Rev., **92**, 667-710.
1402. Wallington, T. J., T. Ellermann and O. J. Nielsen, 1993, J. Phys. Chem., **97**, 8442-8449.
1403. Wallington, T. J., M. M. Hinman, J. M. Andino, W. O. Siegl and S. M. Japar, 1990, International Journal of Chemical Kinetics, **22**, 665-671.
1404. Wallington, T. J. and M. D. Hurley, 1992, Chem. Phys. Lett., **189**, 437-442.
1405. Wallington, T. J. and M. D. Hurley, 1993, Environ. Sci. Technol., **27**, 1448-1452.
1406. Wallington, T. J., M. D. Hurley and W. F. Schneider, 1993, Chem. Phys. Lett., **213**, 442-448.
1407. Wallington, T. J., M. D. Hurley, W. F. Schneider, J. Sehested and O. J. Nielsen, 1993, J. Phys. Chem., **97**, 7606-7611.
1408. Wallington, T. J., M. D. Hurley, W. F. Schneider, J. Sehested and O. J. Nielsen, 1994, Chem. Phys. Lett., **218**, 34-42.
1409. Wallington, T. J. and S. M. Japar, 1990, Chem. Phys. Lett., **166**, 495-499.
1410. Wallington, T. J. and M. J. Kurylo, 1987, Int. J. Chem. Kinet., **19**, 1015-1023.
1411. Wallington, T. J. and M. J. Kurylo, 1987, J. Phys. Chem., **91**, 5050-5054.
1412. Wallington, T. J., D. M. Neuman and M. J. Kurylo, 1987, Int. J. Chem. Kinet., **19**, 725-739.
1413. Wallington, T. J., L. M. Skewes, W. O. Siegl, C. H. Wu and S. M. Japar, 1988, Int. J. Chem. Kinet., **20**, 867-875.
1414. Walther, C.-D. and H. G. Wagner, 1983, Ber. Bunsenges. Phys. Chem., **87**, 403-409.
1415. Wang, J. J. and L. F. Keyser, 1999, Journal of Physical Chemistry A, **103**, 7460-7469.
1416. Wang, J. J. and L. F. Keyser, 2001, J. Phys.Chem. A, **105**, 10544-10552.
1417. Wang, J. J. and L. F. Keyser, 2001, J. Phys.Chem. A, **105**, 6479-6489.
1418. Wang, L. and J. Zhang, 2002, Chem. Phys. Lett., **356**, 490-496.
1419. Wang, N.-S. and Y.-P. Lee, 1985, Proc. Nat. Sci. Council(Taiwan), **9**, 87 - 94.
1420. Wang, N. S. and C. J. Howard, 1990, J. Phys. Chem., **94**, 8787-8794.
1421. Wang, N. S., E. R. Lovejoy and C. J. Howard, 1987, J. Phys. Chem., **91**, 5743-5749.
1422. Wang, W. C., M. Suto and L. C. Lee, 1984, J. Chem. Phys., **81**, 3122-3126.
1423. Wang, X., Y. G. Jin, M. Suto and L. C. Lee, 1988, J. Chem. Phys., **89**, 4853-4860.
1424. Wang, X., M. Suto and L. C. Lee, 1988, J. Chem. Phys., **88** 896-899.

1425. Wantuck, P. J., R. C. Oldenberg, S. L. Baughcum and K. R. Winn, 1987, J. Phys. Chem., **91**, 4653.
1426. Warren, R., T. Gierczak and A. R. Ravishankara, 1991, Chem. Phys. Lett., **183**, 403-409.
1427. Warren, R. F. and A. R. Ravishankara, 1993, Int. J. Chem. Kinet., **25**, 833-844.
1428. Washida, N., 1980, J. Chem. Phys., **73**, 1665.
1429. Washida, N., H. Akimoto and M. Okuda, 1980, J. Chem. Phys., **72**, 5781-5783.
1430. Washida, N., H. Akimoto and M. Okuda, 1980, Bull. Chem. Soc. Japan, **53**, 3496-3503.
1431. Washida, N. and K. D. Bayes, 1976, Int. J. Chem. Kinet., **8**, 777
1432. Washida, N., R. J. Martinez and K. D. Bayes, 1974, Z. Naturforsch., **29A**, 251.
1433. Wategaonkar, S. J. and D. W. Setser, 1989, J. Chem. Phys., **90**, 251-264.
1434. Watson, R. T., G. Machado, B. C. Conaway, S. Wagner and D. D. Davis, 1977, J. Phys. Chem. , **81**, 256.
1435. Watson, R. T., G. Machado, S. Fischer and D. D. Davis, 1976, J. Chem. Phys., **65**, 2126-2138.
1436. Watson, R. T., A. R. Ravishankara, G. Machado, S. Wagner and D. D. Davis, 1979, Int. J. Chem. Kinet., **11**, 187-197.
1437. Watson, R. T., S. P. Sander and Y. L. Yung, 1979, J. Phys. Chem., **83**, 2936.
1438. Wayne, R. P. and J. N. Pitts, Jr., 1969, J. Chem. Phys., **50**, 3644-3645.
1439. Wecker, D., R. Johanssen and R. N. Schindler, 1982, Ber. Bunsenges. Phys. Chem., **86**, 532-538.
1440. Wei, C. N. and R. B. Timmons, 1975, J. Chem. Phys., **62**, 3240.
1441. Wennberg, P. O., J. G. Anderson and D. K. Weisenstein, 1994, J. Geophys. Res., **99**, 18839-18846.
1442. West, G. A., R. E. Weston, Jr. and G. W. Flynn, 1978, Chem. Phys. Lett., **56**, 429.
1443. Westenberg, A. A. and N. de Haas, 1969, J. Phys. Chem., **73**, 1181.
1444. Westenberg, A. A. and N. de Haas, 1969, J. Chem. Phys., **50**, 707-709.
1445. Westenberg, A. A. and N. de Haas, 1973, J. Chem. Phys., **58**, 4066-4071.
1446. Westenberg, A. A. and N. de Haas, 1973, J. Chem. Phys., **58**, 4061-4065.
1447. Westenberg, A. A. and N. de Haas, 1977, J. Chem. Phys., **66**, 4900.
1448. Westenberg, A. A., N. de Haas and J. M. Roscoe, 1970, J. Phys. Chem., **74**, 3431.
1449. Westenberg, A. A. and N. DeHaas, 1968, J. Chem. Phys., **48**, 4405.
1450. Westenberg, A. A., J. M. Roscoe and N. de Haas, 1970, Chem. Phys. Lett., **7**, 597-599.
1451. Whyte, A. R. and L. F. Phillips, 1983, Chem. Phys. Lett., **102**, 451-454.
1452. Whytock, D. A., J. H. Lee, J. V. Michael, W. A. Payne and L. J. Stief, 1977, J. Chem. Phys., **66**, 2690-2695.
1453. Whytock, D. A., R. B. Timmons, J. H. Lee, J. V. Michael, W. A. Payne and L. J. Stief, 1976, J. Chem. Phys., **65**, 2052-2055.
1454. Wiebe, H. A. and J. Heicklen, 1973, J. Am. Chem. Soc., **95**, 1-7.
1455. Wildt, J., G. Bednarek, E. H. Fink and R. P. Wayne, 1988, Chem. Phys., **122**, 463-470.
1456. Wildt, J., E. H. Fink, P. Biggs and R. P. Wayne, 1989, Chem. Phys., **139**, 401-407.
1457. Wildt, J., E. H. Fink, P. Biggs, R. P. Wayne and A. F. Vilesov, 1992, Chem. Phys., **159**, 127-140.
1458. Williams, M. B., P. Campuzano-Jost, D. Bauer and A. J. Hynes, 2001, Chem. Phys. Lett., **344**, 61 - 67.
1459. Wilson, C. and D. M. Hirst, 1997, J. Chem. Soc. Farad. Trans., **93**, 2831 - 2837.
1460. Wilson, E. W., A. A. Sawyer and H. A. Sawyer, 2001, J. Phys. Chem. A, **105**, 1445-1448.
1461. Wilson, W. E., 1967, J. Chem. Phys., **46**, 2017-2018.
1462. Wine, P. H., R. J. Astalos and R. L. Mauldin, III, 1985, J. Phys. Chem., **89**, 2620-2624.
1463. Wine, P. H., W. L. Chameides and A. R. Ravishankara, 1981, Geophys. Res. Lett., **8** 543-546.
1464. Wine, P. H., N. M. Kreutter, C. A. Gump and A. R. Ravishankara, 1981, J. Phys. Chem., **85**, 2660-2665.
1465. Wine, P. H., J. M. Nicovich, M. L. McKee, K. M. Kleissas, S. Parthasarathy, F. D. Pope, A. T. Pegus and . "Kinetics, Spectroscopy, and Thermochemistry of the Cl-DMSO Adduct"; 18th International Symposium on Gas Kinetics, 2004, Bristol, UK.
1466. Wine, P. H., J. M. Nicovich and A. R. Ravishankara, 1985, J. Phys. Chem., **89**, 3914-3918.
1467. Wine, P. H., J. M. Nicovich, R. E. Stickel, Z. Zhao, C. J. Shackelford, K. D. Kreutter, E. P. Daykin and S. Wang *The Tropospheric Chemistry of Ozone in the Polar Regions*; Springer-Verlag: Berlin, 1993; Vol. 17.

1468. Wine, P. H., J. M. Nicovich, R. J. Thompson and A. R. Ravishankara, 1983, J. Phys. Chem., **87**, 3948-3954.
1469. Wine, P. H. and A. R. Ravishankara, 1981, Chem. Phys. Lett., **77**, 103-109.
1470. Wine, P. H. and A. R. Ravishankara, 1982, Chem. Phys., **69**, 365-373.
1471. Wine, P. H. and A. R. Ravishankara, 1983, Chem. Phys. Lett., **96**, 129-132.
1472. Wine, P. H., D. H. Semmes and A. R. Ravishankara, 1981, J. Chem. Phys., **75**, 4390-4395.
1473. Wine, P. H., R. C. Shah and A. R. Ravishankara, 1980, J. Phys. Chem., **84**, 2499-2503.
1474. Wine, P. H., R. J. Thompson and D. H. Semmes, 1984, Int. J. Chem. Kinet., **16**, 1623.
1475. Wine, P. H., J. R. Wells and J. M. Nicovich, 1988, J. Phys. Chem., **92**, 2223-2228.
1476. Wine, P. H., J. R. Wells and A. R. Ravishankara, 1986, J. Chem. Phys., **84**, 1349-1354.
1477. Winer, A. M., A. C. Lloyd, K. R. Darnall, R. Atkinson and J. N. Pitts, Jr., 1977, Chem. Phys. Lett., **51**, 221-226.
1478. Winer, A. M., A. C. Lloyd, K. R. Darnall and J. N. Pitts, Jr., 1976, J. Phys. Chem., **80**, 1635.
1479. Winkler, I. C., R. A. Stachnik, J. I. Steinfeld and S. M. Miller, 1986, J. Chem. Phys., **85**, 890.
1480. Wolf, M., D. L. Yang and J. L. Durant, 1994, J. Photochem. Photobiol. A: Chem., **80**, 85-93.
1481. Wollenhaupt, M., S. A. Carl, A. Horowitz and J. N. Crowley, 2000, J. Phys. Chem., A, **104**, 2695-2705.
1482. Wong, E. L. and F. R. Belles; NASA TN D-6495 NASA Washington, D. C., 1971.
1483. Wongdontri-Stuper, W., R. K. M. Jayanty, R. Simonaitis and J. Heicklen, 1979, J. Photochem., **10**, 163.
1484. Worsnop, D. R., M. S. Zahniser and C. E. Kolb, 1991, J. Phys. Chem., **95**, 3960-3964.
1485. Worsnop, D. R., M. S. Zahniser and C. E. Kolb, 1992, J. Phys. Chem., **96**, 9088.
1486. Wright, T. G., A. M. Ellis and J. M. Dyke, 1993, J. Chem. Phys., **98**, 2891-2907.
1487. Wu, F. and R. W. Carr, 1992, J. Phys. Chem., **96**, 1743-1748.
1488. Wu, H., Y. Mu, X. Xhang and G. Jiang, 2003, Int. J. Chem. Kinet., **35**, 81-87.
1489. Wurzburg, E. and P. L. Houston, 1980, J. Chem. Phys., **72**, 4811.
1490. Xia, W. S. and M. C. Lin, 2001, Journal of Chemical Physics, **114**, 4522-4532.
1491. Xiang, T., M. L. Torres and W. A. Guillory, 1985, J. Chem. Phys., **83**, 1623-1629.
1492. Xing, S. B., S.-H. Shi and L. X. Qiu, 1992, Int. J. Chem. Kinet., **24**, 1-10.
1493. Yamada, T., A. El-Sinawi, M. Siraj, P. H. Taylor, J. Peng, X. Hu and P. Marshall, 2001, J. Phys.Chem. A, **105**, 7588-7597.
1494. Yamada, T., T. D. Fang, P. H. Taylor and R. J. Berry, 2000, J. Phys. Chem. A, **104**, 5013-5022.
1495. Yamada, T., M. Siraj, P. H. Taylor, J. Peng, X. Hu and P. Marshall, 2001, J. Phys.Chem. A, **105**, 9436-9444.
1496. Yamada, T., P. H. Taylor, A. Goumri and P. Marshall, 2003, J. Chem. Phys., **119**, 10600-10606.
1497. Yano, T. and E. Tschuikow-Roux, 1986, J. Photochem., **32**, 25-37.
1498. Yetter, R. A., H. Rabitz, F. L. Dryer, R. G. Maki and R. B. Klemm, 1989, J. Chem. Phys., **91**, 4088-4097.
1499. Yokelson, R. J., J. B. Burkholder, L. Goldfarb, R. W. Fox, M. K. Gilles and A. R. Ravishankara, 1995, J. Phys. Chem., **99**, 13976-13983.
1500. Yu, W. H. S. and M. H. J. Wijnen, 1970, J. Chem. Phys., **52**, 2736-2739.
1501. Yujing, M. and A. Mellouki, 2001, Chem. Phys. Lett., **333**, 63-68.
1502. Zabarnick, S. and J. Heicklen, 1985, Int. J. Chem. Kinet., **17**, 455-476.
1503. Zabarnick, S., J. W, Fleming and M. C. Lin, 1988, Int. J. Chem. Kinet., **20**, 117-129.
1504. Zabel, F., K. A. Sahetchian and C. Chachaty, 1987, Chem. Phys. Lett., **134**, 433.
1505. Zagogianni, H., A. Mellouki and G. Poulet, 1987, C. R. Acad. Sci. Paris, **Series II 304**, 573-578.
1506. Zahniser, M. S., B. M. Berquist and F. Kaufman, 1978, Int. J. Chem. Kinet., **10**, 15-29.
1507. Zahniser, M. S., J. Chang and F. Kaufman, 1977, J. Chem. Phys., **67**, 997-1003.
1508. Zahniser, M. S. and C. J. Howard, 1980, J. Chem. Phys., **73**, 1620-1626.
1509. Zahniser, M. S. and F. Kaufman, 1977, J. Chem. Phys., **66**, 3673-3681.
1510. Zahniser, M. S., F. Kaufman and J. G. Anderson, 1974, Chem. Phys. Lett., **27**, 507-510.
1511. Zahniser, M. S., F. Kaufman and J. G. Anderson, 1976, Chem. Phys. Lett., **37**, 226-231.
1512. Zellner, R., 1987, J. Chem. Phys., **84**, 403.
1513. Zellner, R., G. Bednarek, A. Hoffmann, J. P. Kohlmann, V. Mors and H. Saathoff, 1994, Ber. Bunsenges. Phys. Chem., **98**, 141-146.
1514. Zellner, R. and F. Ewig, 1988, J. Phys Chem., **92**, 2971.

1515. Zellner, R. and W. Steinert, 1981, Chem. Phys. Lett., **81**, 568-572.
1516. Zellner, R., G. Wagner and B. Himme, 1980, J. Phys. Chem., **84**, 3196-3198.
1517. Zetzsch, C. "Rate constants for the reactions of OH with acetone and methylethylketone in the gas phase"; 7th International Symposium on Gas Kinetics, 1982, Goettingen, Germany.
1518. Zetzsch, C. and F. Stuhl. In *Proceedings of the 2nd European Symposium on the Physico-Chemical Behaviour of Atmospheric Pollutants*; D. Reidel Publishing Co.: Dordrecht, Holland, 1982; pp 129-137.
1519. Zhang, D. Q., J. X. Zhong and L. X. Qiu, 1997, J. Atmos. Chem., **27**, 209-215.
1520. Zhang, L. and Q.-Z. Qin, 2000, J. Mol. Structure (Theochem), **531**, 375 - 379.
1521. Zhang, Z., R. E. Huie and M. J. Kurylo, 1992, J. Phys. Chem., **96**, 1533-1535.
1522. Zhang, Z., R. Liu, R. E. Huie and M. J. Kurylo, 1991, Geophys. Res. Lett., **18**, 5-7.
1523. Zhang, Z., R. F. Liu, R. E. Huie and M. J. Kurylo, 1991, J. Phys. Chem., **95**, 194-196.
1524. Zhang, Z., S. Padmaja, R. D. Saini, R. E. Huie and M. J. Kurylo, 1994, J. Phys. Chem., **98**, 4312-4315.
1525. Zhang, Z., R. D. Saini, M. J. Kurylo and R. E. Huie, 1992, Geophys. Res. Lett., **19**, 2413-2416.
1526. Zhang, Z., R. D. Saini, M. J. Kurylo and R. E. Huie, 1992, J. Phys. Chem., **96**, 9301-9304.
1527. Zhang, Z., R. D. Saini, M. J. Kurylo and R. E. Huie, 1992, Chem. Phys. Lett., **200**, 230-234.
1528. Zhao, Z., R. E. Stickel and P. H. Wine, 1996, Chem. Phys. Lett., **251**, 59-66.
1529. Zhitneva, G. P. and S. Y. Pshezhetskii, 1978, Kinetika i Kataliz, **19**, 296.
1530. Zipf, E. C., 1980, Nature (London), **287**, 523-525.

SECTION 2. TERMOLECULAR REACTIONS

Table of Contents

SECTION 2. TERMOLECULAR REACTIONS 2-1
2.1 Introduction 2-1
2.2 Low-Pressure-Limiting Rate Constant, $k^x_o(T)$ 2-2
2.3 Temperature Dependence of Low–Pressure Limiting Rate Constants: T^n 2-2
2.4 High-Pressure-Limit Rate Constants, $k_\infty(T)$ 2-3
2.5 Temperature Dependence of High-Pressure-Limiting Rate Constants: T^m 2-3
2.6 Uncertainty Estimates 2-3
2.7 Notes to Table 2 2-8
2.8 References 2-19

Tables

Table 2-1. Rate Constants for Termolecular Reactions 2-2-4

2.1 Introduction

Rate constants for association reactions (Table 2) of the type A + B ↔ [AB]* $\xrightarrow{M}$ AB can be pressure dependent. The low-pressure-limiting rate constants are given in the form:

$$k_o(T) = k_o^{300}\left(\frac{T}{300}\right)^{-n} \text{ cm}^6 \text{ molecule}^{-2} \text{ s}^{-1},$$

(where k_o^{300} has been adjusted for air as the third body). The limiting high-pressure rate constant is given in a similar form:

$$k_\infty(T) = k_\infty^{300}\left(\frac{T}{300}\right)^{-m} \text{ cm}^3 \text{ molecule}^{-1} \text{ s}^{-1}.$$

To obtain the effective second-order rate constant for a given condition of temperature and pressure (altitude), the following formula is used:

$$k_f([M],T) = \left(\frac{k_o(T)[M]}{1+\frac{k_o(T)[M]}{k_\infty(T)}}\right) 0.6^{\left\{1+\left[\log_{10}\left(\frac{k_o(T)[M]}{k_\infty(T)}\right)\right]^2\right\}^{-1}}$$

The fixed value 0.6 that appears in this formula fits the data for all listed reactions adequately, although in principle this quantity may be different for each reaction, and also temperature dependent.

Some reactions that appear to be simple bimolecular processes proceed via bound intermediates. The reaction between HO and CO to yield H + CO_2 takes place on a potential energy surface that contains the radical HOCO. The yield of H and CO_2 is diminished as the pressure rises. The loss of reactants is thus the sum of two processes, an association to yield HOCO and the chemical activation process yielding H and CO_2. The total rate constant for loss of reactants is fit by the equation above for the association added to the chemical activation rate constant which can be represented by a similar looking equation:

$$k_f^{ca}([M],T)=\left(\frac{k_o(T)}{1+\frac{k_o(T)}{k_\infty(T)/[M]}}\right)0.6^{\left\{1+\left[\log_{10}\left(\frac{k_o(T)}{k_\infty(T)/[M]}\right)\right]^2\right\}^{-1}}$$

Thus, a compilation of rate constants requires the stipulation of the four parameters, $k_o(300)$, n, $k_\infty(300)$, and m. These can be found in Table 2. The discussion that follows outlines the general methods we have used in establishing this table, and the notes to the table discuss specific data sources. Recent advances in theory have allowed direct calculation of rate constants for some reactions using RRKM/Master Equation methods.

When sufficient and precise data exist for a given reaction, we have fit the data to the four parameter expression above. We have used theory as a guide whenever possible.

2.2 Low-Pressure-Limiting Rate Constant, $k^x_o(T)$

Troe [324] has described a simple method for obtaining low-pressure-limiting rate constants. In essence this method depends on the definition:

$$k_o^x(T) \equiv \beta_x k_{o,sc}^x$$

Here sc signifies "strong" collisions, x denotes the bath gas, and β_x is an efficiency parameter ($0 < \beta_x < 1$), which provides a measure of energy transfer. The strong collision rate constant can be calculated with some accuracy from knowledge of molecular parameters available from experiment and more and more from theory.

The coefficient β_x is related to the average energy transferred in a collision with gas x, $\langle\Delta E\rangle_x$, via:

$$\frac{\beta_x}{\left(1-\sqrt{\beta_x}\right)} = \frac{\langle\Delta E\rangle_x}{F_E kT}$$

Notice that $\langle\Delta E\rangle$ is quite sensitive to β. F_E is the correction factor of the energy dependence of the density of states (a quantity of the order of 1.1 for most species of stratospheric interest).

For some of the reactions of possible stratospheric interest reviewed here, there exist data in the low-pressure limit (or very close thereto), and we have chosen to evaluate and unify this data by calculating $k_o^x(T)$ for the appropriate bath gas x and computing the value of β_x corresponding to the experimental value [324]. A compilation [265] gives details for many of the reactions considered here.

From the β_x values (most of which are for N_2, i.e., β_{N_2}), we compute $\langle\Delta E\rangle_X$ according to the above equation. Values of $\langle\Delta E\rangle_{N_2}$ of approximately 0.3–1 kcal mole^{-1} are generally expected. If multiple data exist, we average the values of $\langle\Delta E\rangle_{N_2}$ and recommend a rate constant corresponding to the β_{N_2} computed in the equation above.

Master equation calculations allow direct calculation of low pressure rate constants and of β_x.

Where no data exist we have sometimes estimated the low-pressure rate constant by taking β_{N_2} = 0.3 at T = 300 K, a value based on those cases where data exist.

2.3 Temperature Dependence of Low–Pressure Limiting Rate Constants: T^n

The value of n recommended here comes from measurements or, in some cases, a calculation of $\langle\Delta E\rangle_{N_2}$ from the data at 300 K, and a computation of β_{N_2} (200 K) assuming that $\langle\Delta E\rangle_{N_2}$ is independent of temperature in this range. This β_{N_2} (200 K) value is combined with the computed value of k_o^{sc} (200 K) to give the expected value of the actual rate constant at 200 K. This latter, in combination with the value at 300 K, yields the value of n.

This procedure can be directly compared with measured values of k_o (200 K) when those exist. Unfortunately, very few values at 200 K are available. There are often temperature-dependent studies, but some

ambiguity exists when one attempts to extrapolate these down to 200 K. If data are to be extrapolated beyond the measured temperature range, a choice must be made as to the functional form of the temperature dependence.

There are two general ways of expressing the temperature dependence of rate constants. Either the Arrhenius expression

$$k_o(T) = A \exp(-E/RT)$$

or the form

$$k_o(T) = A' T^{-n}$$

is employed. Neither of these extrapolation techniques is soundly based, and since they often yield values that differ substantially, we have used the method above as the basis of our recommendations.

2.4 High-Pressure-Limit Rate Constants, $k_\infty(T)$

High-pressure rate constants can often be obtained experimentally, but those for the relatively small species of atmospheric importance usually reach the high-pressure limit at inaccessibly high pressures. This leaves two sources of these numbers, the first being estimates based upon theory, and the second being extrapolation of fall-off data up to higher pressures.

Stratospheric conditions generally render reactions of interest much closer to the low-pressure limit and thus are fairly insensitive to the high-pressure value. This means that while the extrapolation is long, and the value of $k_\infty(T)$ is often not very accurate, a "reasonable guess" of $k_\infty(T)$ will then suffice. In a few cases we have declined to guess since the low-pressure limit is effective over the entire range of stratospheric conditions.

2.5 Temperature Dependence of High-Pressure-Limiting Rate Constants: T^m

There are very few data upon which to base a recommendation for values of m. Values in Table 2 are often estimated, based on models for the transition state of bond-association reactions and whatever data are available. In general the temperature dependence of these rate constants is expected to be small.

2.6 Uncertainty Estimates

For three-body reactions (Table 2) uncertainties are assigned using a procedure that is analogous to that employed for bimolecular reactions in Table 1. Values of f(298 K) are given for these rate constants at room temperature and assumed to be valid at all pressures. The additional uncertainty arising from the temperature extrapolation has in previous evaluations been expressed as an uncertainty in the temperature coefficients n and m. In this evaluation, the reactions have been re-evaluated and uncertainties expressed with a g-factor as in Table 1. Given that uncertainties for an expression with four parameters is expressed with only two parameters, a certain amount of arbitrariness is involved in their choice. In general we have tried to have the "two sigma" range incorporate most of the data.

Table 2-1. Rate Constants for Termolecular Reactions

Reaction	Low-Pressure Limit[a] $k_o(T) = k_o^{300}(T/300)^{-n}$		High-Pressure Limit[b] $k_\infty(T) = k_\infty^{300}(T/300)^{-m}$		f	g	Notes
	k_o^{300}	n	k_∞^{300}	m			
O_x Reactions							
$O + O_2 \xrightarrow{M} O_3$	(6.0) (–34)	2.4	–	–	1.1	50	A1
$O(^1D)$ Reactions							
$O(^1D) + N_2 \xrightarrow{M} N_2O$	(2.8) (–36)	0.9	–	–	1.3	75	A2
HO_x Reactions							
$H + O_2 \xrightarrow{M} HO_2$	(4.4) (–32)	1.3	(4.7) (–11)	0.2	1.3	50	B1
$OH + OH \xrightarrow{M} H_2O_2$	(6.9) (–31)	1.0	(2.6) (–11)	0	1.5	100	B2
NO_x Reactions							
$O + NO \xrightarrow{M} NO_2$	(9.0) (–32)	1.5	(3.0) (–11)	0.0	1.2	100	C1
$O + NO_2 \xrightarrow{M} NO_3$	(2.5) (–31)	1.8	(2.2) (–11)	0.7	1.3	100	C2
$OH + NO \xrightarrow{M} HONO$	(7.0) (–31)	2.6	(3.6) (–11)	0.1	1.2	50	C3
$OH + NO_2 \xrightarrow{M} HONO_2$	(1.8) (–30)	3.0	(2.8) (–11)	0	1.3	100	C4
$OH + NO_2 \xrightarrow{M} HOONO$	(9.1) (–32)	3.9	(4.2) (–11)	0.5	1.5	200	C4
$HO_2 + NO_2 \xrightarrow{M} HO_2NO_2$	(2.0) (–31)	3.4	(2.9) (–12)	1.1	1.1	50	C5
$NO_2 + NO_3 \xrightarrow{M} N_2O_5$	(2.0) (–30)	4.4	(1.4) (–12)	0.7	1.2	100	C6
$NO_3 \xrightarrow{M} NO + O_2$	See Note						C7
Hydrocarbon Reactions							
$OH + CO \xrightarrow{M} HOCO$ $OH + CO \xrightarrow{M} H + CO_2$ [See Note]	(5.9) (–33) (1.5) (–13)	1.4 -0.6	(1.1) (–12) (2.1) (9)	-1.3 -6.1	1.1	100	D1
$CH_3 + O_2 \xrightarrow{M} CH_3O_2$	(4.0) (–31)	3.6	(1.2) (–12)	-1.1	1.1	50	D2
$C_2H_5 + O_2 \xrightarrow{M} C_2H_5O_2$	(1.5) (–28)	3.0	(8.0) (–12)	0	1.2	50	D3
$OH + C_2H_2 \xrightarrow{M} HOCHCH$	(5.5) (–30)	0.0	(8.3) (–13)	–2	1.1	50	D4
$OH + C_2H_4 \xrightarrow{M} HOCH_2CH_2$	(1.0) (–28)	4.5	(8.8) (–12)	.85	1.2	50	D5
$CH_3O + NO \xrightarrow{M} CH_3ONO$	(2.3) (–29)	2.8	(3.8) (–11)	0.6	1.3	100	D6

Reaction	Low-Pressure Limit[a] $k_o(T) = k_o^{300}(T/300)^{-n}$		High-Pressure Limit[b] $k_\infty(T) = k_\infty^{300}(T/300)^{-m}$		f	g	Notes
	k_o^{300}	n	k_∞^{300}	m			
$CH_3O + NO_2 \xrightarrow{M} CH_3ONO_2$	(5.3) (–29)	4.4	(1.9) (–11)	1.8	1.1	0	D7
$C_2H_5O + NO \xrightarrow{M} C_2H_5ONO$	(2.8) (–27)	4.0	(5.0) (–11)	0.2	1.2	50	D8
$C_2H_5O + NO_2 \xrightarrow{M} C_2H_5ONO_2$	(2.0) (–27)	4.0	(2.8) (–11)	1.0	1.1	100	D9
$CH_3O_2 + NO_2 \xrightarrow{M} CH_3O_2NO_2$	(1.0) (–30)	4.8	(7.2) (–12)	2.1	1.5	100	D10
$C_2H_5O_2 + NO_2 \xrightarrow{M} C_2H_5O_2NO_2$	(1.2)(–29)	4.0	(9.0)(–12)	0.0	1.3	50	D11
$CH_3C(O)O_2 + NO_2 \xrightarrow{M} CH_3C(O)O_2NO_2$	(9.7) (–29)	5.6	(9.3)(–12)	1.5	1.2	50	D12
$CH_3CH_2C(O)O_2 + NO_2 \xrightarrow{M} CH_3CH_2C(O)O_2NO_2$	(9.0) (–28)	8.9	(7.7) (–12)	0.2	2.0	100	D13
$CH_3C(O)CH_2 + O_2 \xrightarrow{M} CH_3C(O)CH_2O_2$	See Note						D14
FO_x Reactions							
$F + O_2 \xrightarrow{M} FO_2$	(5.8) (–33)	1.7	(1)(-10)	0	1.3	100	E1
$F + NO \xrightarrow{M} FNO$	(1.2) (–31)	0.5	(2.8) (–10)	0	1.4	200	E2
$F + NO_2 \xrightarrow{M} FNO_2$	(1.5) (–30)	2.0	(1.0) (–11)	0.0	1.3	100	E3
$FO + NO_2 \xrightarrow{M} FONO_2$	(2.6) (–31)	1.3	(2.0) (–11)	1.5	3	200	E4
$CF_3 + O_2 \xrightarrow{M} CF_3O_2$	(3.0) (–29)	4.0	(3.0) (–12)	1.0	1.2	100	E5
$CF_3O + NO_2 \xrightarrow{M} CF_3ONO_2$	1.7(–28)	6.9	1.1(–11)	1	1.1	50	E6
$CF_3O_2 + NO_2 \xrightarrow{M} CF_3O_2NO_2$	(1.5) (–29)	2.2	(9.6) (–12)	1	1.1	50	E7
$CF_3O + CO \xrightarrow{M} CF_3OCO$	(2.5) (–31)	2	(6.8) (–14)	–1.2	1.2	500	E8
$CF_3O \xrightarrow{M} CF_2O + F$	See Note						E9
ClO_x Reactions							
$Cl + O_2 \xrightarrow{M} ClOO$	(2.2) (–33)	3.1	(1.8)(-10)	0	1.1	50	F1
$Cl + NO \xrightarrow{M} ClNO$	(7.6) (–32)	1.8	–	–	1.2	50	F2
$Cl + NO_2 \xrightarrow{M} ClONO$	(1.3) (–30)	2	(1) (–10)	1	1.2	100	F3
$\xrightarrow{M} ClNO_2$	(1.8) (–31)	2	(1) (–10)	1	1.3	100	
$Cl + CO \xrightarrow{M} ClCO$	(1.3) (–33)	3.8	–	–	1.1	50	F4
$Cl + C_2H_2 \xrightarrow{M} ClC_2H_2$	(5.2) (–30)	2.4	(2.2) (–10)	0.7	1.1	50	F5
$Cl + C_2H_4 \xrightarrow{M} ClC_2H_4$	(1.6) (–29)	3.3	(3.1) (–10)	1.0	1.5	50	F6

Reaction	Low-Pressure Limit[a] $k_o(T) = k_o^{300}(T/300)^{-n}$		High-Pressure Limit[b] $k_\infty(T) = k_\infty^{300}(T/300)^{-m}$		f	g	Notes
	k_o^{300}	n	k_∞^{300}	m			
$Cl + C_2Cl_4 \xrightarrow{M} C_2Cl_5$	(1.4) (–28)	8.5	(4.0) (–11)	1.2	1.2	50	F7
$ClO + NO_2 \xrightarrow{M} ClONO_2$	(1.8) (–31)	3.4	(1.5) (–11)	1.9	1.3	50	F8
$OClO + NO_3 \xrightarrow{M} O_2ClONO_2$	See Note						F9
$ClO + ClO \xrightarrow{M} Cl_2O_2$	(1.6) (–32)	4.5	(2.0) (–12)	2.4	1.1	25	F10
$ClO + OClO \xrightarrow{M} Cl_2O_3$	(6.2) (–32)	4.7	(2.4) (–11)	0	1.1	25	F11
$OClO + O \xrightarrow{M} ClO_3$	(2.9) (–31)	3.1	(8.3) (–12)	0	1.1	100	F12
$CH_2Cl + O_2 \xrightarrow{M} CH_2ClO_2$	(1.9) (–30)	3.2	(2.9) (–12)	1.2	1.1	125	F13
$CHCl_2 + O_2 \xrightarrow{M} CHCl_2O_2$	(1.3) (–30)	4.0	(2.8) (–12)	1.4	1.1	125	F14
$CCl_3 + O_2 \xrightarrow{M} CCl_3O_2$	(8) (–31)	6	(3.5) (–12)	1	1.2	50	F15
$CFCl_2 + O_2 \xrightarrow{M} CFCl_2O_2$	(5.0) (–30)	4.0	(6.0) (–12)	1.0	1.3	200	F16
$CF_2Cl + O_2 \xrightarrow{M} CF_2ClO_2$	(1.0) (–29)	4.0	(6) (–12)	1.0	2	300	F17
$CCl_3O_2 + NO_2 \xrightarrow{M} CCl_3O_2NO_2$	(2.9) (–29)	6.8	(1.3) (–11)	1	1.1	50	F18
$CFCl_2O_2 + NO_2 \xrightarrow{M} CFCl_2O_2NO_2$	(2.2) (–29)	5.8	(1.0) (–11)	1	1.1	50	F19
$CF_2ClO_2 + NO_2 \xrightarrow{M} CF_2ClO_2NO_2$	(1.1) (–29)	4.6	(1.7) (–11)	1.2	2	300	F20
BrO_x Reactions							
$Br + NO_2 \xrightarrow{M}$ t- BrONO	(4.2) (–31)	2.4	(2.7) (–11)	0	1.1	50	G1
$BrO + NO_2 \xrightarrow{M} BrONO_2$	(5.2) (–31)	3.2	(6.9 (–12)	2.9	1.2	400	G2
IO_x Reactions							
$I + NO \xrightarrow{M} INO$	(1.8) (–32)	1.0	(1.7) (–11)	0	1.3	150	H1
$I + NO_2 \xrightarrow{M} INO_2$	(3.0) (–31)	1.0	(6.6) (–11)	0	1.5	300	H2
$IO + NO_2 \xrightarrow{M} IONO_2$	(6.5) (–31)	3.5	(7.6) (–12)	1.5	1.3	50	H3
SO_x Reactions							
$HS + NO \xrightarrow{M} HSNO$	(2.4) (–31)	2.5	(2.7) (–11)	0	1.2	100	I1
$CH_3S + NO \xrightarrow{M} CH_3SNO$	(3.2) (–29)	4.0	(3.5) (–11)	1.8	1.2	100	I2
$O + SO_2 \xrightarrow{M} SO_3$	(1.8)(–33)	–2	4.2(-14)	-1.8	2	100	I3
$OH + SO_2 \xrightarrow{M} HOSO_2$	(3.3) (–31)	4.3	(1.6) (–12)		1.1	100	I4

Reaction	Low-Pressure Limit[a] $k_o(T) = k_o^{300}(T/300)^{-n}$		High-Pressure Limit[b] $k_\infty(T) = k_\infty^{300}(T/300)^{-m}$		f	g	Notes
	k_o^{300}	n	k_∞^{300}	m			
$CH_3SCH_2 + O_2 \xrightarrow{M} CH_3SCH_2O_2$	See Note						I5
$SO_3 + NH_3 \xrightarrow{M} H_3NSO_3$	(3.6) (–30)	6.1	(4.3) (–11)	0	1.2	200	I6
$HO + CS_2 \xrightarrow{M} HO\text{---}CS_2$	(4.9) (–31)	3.5	(1.4) (–11)	1	1.5	100	I7
$Cl + CS_2 \xrightarrow{M} Cl\text{---}CS_2$	(5.9) (–31)	3.6	(4.6) (–10)	0	1.1	50	I8
$Cl + (CH_3)_2S \xrightarrow{M} Cl\text{---}(CH_3)_2S$	(4) (–28)	7	(2) (–10)	1	1.1	50	I9
$Br + (CH_3)_2S \xrightarrow{M} Br\text{---}(CH_3)_2S$	(3.7) (–29)	5.3	(1.5) (–10)	2	1.1	100	I10
Metal Reactions							
$Na + O_2 \xrightarrow{M} NaO_2$	(3.2) (–30)	1.4	(6.0) (–10)	0	1.3	200	J1
$NaO + O_2 \xrightarrow{M} NaO_3$	(3.5) (–30)	2.0	(5.7) (–10)	0	1.3	200	J2
$NaO + CO_2 \xrightarrow{M} NaCO_3$	(8.7) (–28)	2.0	(6.5) (–10)	0	1.3	200	J3
$NaOH + CO_2 \xrightarrow{M} NaHCO_3$	(1.3) (–28)	2.0	(6.8) (–10)	0	1.3	200	J4

Shaded areas indicate changes or additions since JPL 02-25.
The values quoted are suitable for air as the third body, M.
a Units are cm^6/molecule^2-s.
b Units are cm^3/molecule-s.
f(298 K) is the uncertainty factor at 298 K. To calculate the uncertainty at other temperatures, use the expression:

$$f(T) = f(298)\exp\left|g\left(\frac{1}{T} - \frac{1}{298}\right)\right|$$

Note that the exponent is absolute value

2.7 Notes to Table 2

JPL Publication numbers for the most recent revision of the table entry and note are given at the end of each note.

A1. $O + O_2$. Low pressure limit and T dependence are an average of Klais et al. [180], Huie et al. [156] and Lin and Leu [205]. These studies in N_2 and Ar are in the temperature range (200<T/K<268). The result is in agreement with the study of Hippler et al. [146] and the extrapolated recommendation fits their lower pressure N_2 data down to 100 K. High pressure studies by Croce de Cobos and Troe [84] are in agreement with this recommendation. Rawlins et al. [280] estimate values in Ar between 80 and 150 K from nascent vibrational distributions that are a factor of two higher than the recommendation extrapolated to 80 K. The temperature dependence of the rate constant determined from the experimental data is in excellent agreement with the value of n=2.36 determined from the calculations of Patrick and Golden [265].

Kaye [174] has calculated isotope effects for this reaction, using methods similar to those discussed in the Introduction of this document (see Troe [324] and Patrick and Golden [265].) Isotope effects have been reported by Anderson et al. [9] and Gross and Billing [137]. Measurements of isotopic fractionation by Mauersberger and colleagues [360] and Thiemens and co–workers [294] reveal distinctly non–statistical effects. Various attempts at theoretical explanations exist [141], but the detailed knowledge of the potential energy surface required is unavailable. (Table: 02-25, Note: 02-25) Back to table

A2. $O(^1D) + N_2$. Recommended parameters (including f and g) from Estupiñán et al. [109] whose detection capabilities were more advanced than those employed in earlier studies. Kajimoto and Cvetanovic [173] report a value at 296K of 6.5×10^{-37} $cm^6 s^{-1}$. Maric and Burrows [213] extract $(8.8\pm3.3)\times10^{-37}$ $cm^6 s^{-1}$ from a study of the photolysis of synthetic air. Gaedtke et al. [128] report an approximate value of 10^{12} in molar units, which translates to 2.8×10^{-36} in molecular units. The rate constant is extremely low in this special system due to electronic curve crossing. (Table: 06-2, Note: 06-2) Back to table

B1. $H + O_2$. Studies by Kurylo [186], Wong and Davis [362], Hsu et al. [155], Hsu et al. [154], Cobos et al. [70], Pirraglia et al. [271], Carleton et al. [60], Troe [325], Bates et al. [25] and Michael et al. [223] have been considered. All are in good agreement. The parameters in [25] are the basis for the recommendation. Several studies, [25, 223] have pointed out the large effect of water vapor as the collider gas. (Table: 06-2, Note: 06-2) Back to table

B2. OH + OH. Recommended values are from fits of measurements by Zellner et al. [369] in N_2, by Forster et al. [118] and Fulle et al. [126] in 1–150 bar He scaled to N_2. A study by Fagerstrom et al. [110] in 85–1000 mbar SF_6 gives slightly different values. A pressure independent bimolecular channel to $H_2O + O$ with a rate 4.2×10^{-12} exp(–240/T) is observed (see Table 1). Zellner et al. used somewhat different values for this rate constant to make substantial corrections to their measured values. Changing to the accepted value will make large changes in the Zellner et al. values and it is unclear how to evaluate this. Trainor and von Rosenberg [323] report a value at 300 K that is lower than recommended by a factor of 2.7. (Table: 02-25, Note: 02-25) Back to table

C1. O + NO. Low pressure limit and n from direct measurements of Schieferstein et al. [295] and their re–analysis of the data of Whytock et al. [355]. Error limits encompass other studies. High pressure limit and m from fitting the data of Hippler et al. [147], who report higher values for the high pressure limiting rate constant, to the format used in this compilation. Shock tube measurements by Yarwood et al. [365] in argon from 300–1300 K are consistent with the values in Table 2. (Table: 06-2, Note: 06-2) Back to table

C2. $O + NO_2$. Values of rate constants and temperature dependences from a combination of the study by Burkholder and Ravishankara [50] and that of Hahn et al. [138]. At 300 K these studies almost overlap at the highest pressure of Burkholder and Ravishankara and the lowest pressure studied by Hahn et al. The former values are larger by a factor of 2.2 under these conditions. This recommendation is in reasonable agreement with the evaluation of Baulch et al. [27], which fits the Hahn et al. values very well. (Table: 02-25, Note: 02-25) Back to table

C3. OH + NO. The low pressure limit rate constant has been reported by Anderson and Kaufman [7], Stuhl and Niki [319], Morley and Smith [230], Westenberg and de Haas [354], Anderson et al. [8], Howard and Evenson [153], Harris and Wayne [140], Atkinson et al.[17], Overend et al. [252], Anastasi and Smith [6], Burrows et al. [52] and Atkinson and Smith [12]. The general agreement is good, and the recommended values of both the rate constant and the temperature dependence are weighted averages. Studies by Sharkey et al. [304] and Donahue et al. [103] in the transition regime between low and high pressure limits are in agreement and serve to reduce the uncertainty. These latter studies yield a value for the high pressure limiting rate constant in agreement with the results of Forster et al. [118], whose study reached pressures of 100 bar in He. The temperature dependence of the high pressure limiting rate constant is from the data of Anastasi and Smith [6]

and Sharkey et al. (Both cis- and trans-HONO are expected to be formed.) Fulle et al. [127] report a high pressure limit in agreement with Forster et al. [118]. Pagsberg et al. [253] report low pressure values in SF_6 that are compatible (i.e. the ratio of collision efficiencies is about a factor of two.) with the recommendation. A study by Zabarnick [366] is noted. The error limits encompass the differences with the IUPAC [15] recommendation. (Table: 06-2, Note: 06-2) Back to table

C4. OH + NO_2. This reaction has been the subject of detailed study. There are two product channels, one to $HONO_2$ (nitric acid) and the other to HOONO (pernitrous acid). (There are at least two conformers of HOONO, cis-cis and trans-perp, but they are thought to be equilibrated under atmospheric conditions.) Golden and Smith [133] concluded that there were two pathways and they offered parameters in the format of this recommendation that were given in the note in JPL 02-25 [289]. Experiments by Hippler and co-workers [118, 127] up to about 100 bar at 300 K and the finding of a double exponential decay of OH at 430 K and 100 bar implicate a second pathway [145]. Nizkorodov and Wennberg [243] report 5% HOONO at 253K and 20 Torr of an N_2/He buffer gas. Bean et al. [28] and Pollack et al. [274] report on the spectroscopy of the HOONO conformer. Donahue et al. [102] support the finding of two pathways in an analysis of isotopic effects. Golden et al. [132] have performed RRKM/master-equation calculations on a new ab initio surface to yield the parameters recommended herein. The low pressure limit and the high pressure limiting rate constants and their temperature dependences are from a fit to the data of Hippler etal. [145], Anastasi and Smith [5], Wine et al. [357], Donahue et al. [103], Dransfield et al. [104], Brown et al. [45] and D'Ottone et al. [85]. (Brown et al. report that O_2 is about 30% less efficient than N_2 as a collider and suggest that air might therefore have a total efficiency of 0.94 relative to N_2) Data from Anderson et al. [8], Howard and Evenson [153], Burrows et al. [52], and Erler et al. [108] are in essential agreement. Data of Forster et al [118] and Fulle et al. [127] are acknowledged to be about 30% too high [145]. Burkholder et al. [48] and Dransfield et al. [104] have searched for the isomer HOONO and have been unable to identify it. The description of the reaction between HO and NO_2, as consisting of two product channels, requires that the data obtained at lower than 300 K represent the sum of the two pathways. Thus the fate of HOONO has to be included in atmospheric models. If this fate involves rapid loss due to reaction or photolysis, the effect of the second pathway is the diminution of the $HONO_2$ forming rate constant. Evaluation of data, taking into account both pathways, indicates that the contribution of the HOONO forming reaction can be from 5 to 15% under atmospheric conditions. The equilibrium constant is given in Table 3-1. (Table: 06-2, Note: 06-2) Back to table

C5. HO_2 + NO_2. Christensen et al. [66] report rate constants 219< T/K <298 and 45<P/torr<200. They show that methanol, present in most other studies confounds the results by forming bound complexes with HO_2. They also suggest that some measurements yielded low rate constants as a result of perturbations to the NO_2/N_2O_4 equilibrium. The parameters recommended are those from this study incorporating the results of Kurylo and Ouellette [187, 188] and Sander and Peterson [291]. The recommended k_o (300 K) is consistent with Howard [152]. Other studies by Simonaitis and Heicklen [308] and Cox and Patrick [82] are in reasonable agreement with the recommendation, as is the value of Christensen et al. [67]. (Table: 06-2, Note: 06-2) Back to table

C6. NO_2 + NO_3. Data with N_2 as the bath gas from Kircher et al.[178], Smith et al.[311], Burrows et al.[51], Wallington et al. [342] and Orlando et al. [249] ranging from 236 to 358 K were used to obtain k_o, k_∞, n and m. Values from Croce de Cobos et al. [83] are excluded due to arguments given by Orlando et al. [249], who point out that a reanalysis of these data using better values for the rate constant for $NO_3 + NO \rightarrow 2NO_2$ yields a negative value for $NO_2 + NO_3 + M$. The study of Fowles et al. [120] is noted, but not used. Johnston et al. [163] have reviewed this reaction. Hahn et al. [138] have studied this reaction between 300 and 400 K at pressures from 30 to 900 bar. Their suggested parameterization yields values indistinguishable from those in this recommendation under most atmospheric conditions. (There are deviations of 30 to 50% at pressures less than a mbar and greater than 5 bar.)

A study of the reverse reaction has been carried out by Cantrell et al. [55]. These data are in excellent agreement with those obtained by Connell and Johnston [73] and Viggiano et al. [335]. The equilibrium constant recommended in Table 3 is the one given in Cantrell et al. [55], who computed it from the ratio of the rate constant of Orlando et al [249] and their rate constants for the reverse reaction. (Table: 02-25, Note: 02-25) Back to table

C7. NO_3 + M. Johnston et al. [163] and Davidson et al. [91] have suggested significant thermal decomposition of NO_3. This has been disputed by Russell et al. [285]. Davis et al. [93] claim that the barrier to thermal dissociation is 47.3 kcal mol^{-1}. This would seem to rule out such a process in the atmosphere. (Table: 94-26, Note: 94-26) Back to table

D1. HO + CO. This recommendation takes into account the fact that the reaction proceeds via two channels, a chemical activation process directly to H + CO_2 and an association to yield HOCO. In the presence of O_2, the HOCO intermediate is converted to HO_2 + CO_2 (DeMore [95], Miyoshi et al. [227]). Miyoshi et al. report a

rate constant for the reaction of HOCO with O_2 of ~1.5×10^{-12} cm^3 $molecule^{-1}$ s^{-1} at 298 K)). Therefore, for atmospheric purposes, the products can be taken to be HO_2 and CO_2. The parameters are taken directly from Senosiain et al. [301] who performed master equation calculations on a theoretical surface. Pressure and temperature dependence of data from McCabe et al. [219] and Hynes et al. [158] are well represented by these parameters. In contrast with the previous evaluation where the rate constant increased with pressure, in this evaluation, it is shown to increase with number density. This reaction has been studied often by many workers. In general the results are in keeping with the current recommendation. Values have been reported by Dreier and Wolfrum [105], Husain et al. [157], Ravishankara and Thompson [279], Paraskevopoulos and Irwin [259], Hofzumahaus and Stuhl [149]. The results of Jonah et al. [165] are too high and were not included. An increase in k with pressure has been observed by a large number of investigators (Overend and Paraskevopoulos [251], Perry et al. [268], Chan et al. [61], Biermann et al. [31], Cox et al. [78], Butler et al. [53], Paraskevop and Irwin [258, 259], DeMore [95], Hofzumahaus and Stuhl [149], Hynes et al. [158]), and McCabe et al., [219]. In addition, Niki et al. [242] have measured k relative to OH + C_2H_4 in one atmosphere of air by following CO_2 production using FTIR. Previous controversy regarding the effect of small amounts of O_2 (Biermann et al. [31]) has been resolved and is attributed to secondary reactions (DeMore [95], Hofzumahaus and Stuhl [149],). The results of Butler et al. [53] have to be re-evaluated in the light of refinements in the rate coefficient for the OH + H_2O_2 reaction. The corrected rate coefficient is in approximate agreement with the recommended value. Currently, there are no indications to suggest that the presence of O_2 has any effect on the rate coefficient other than as a third body. Beno et al. [30] observe an enhancement of k with water vapor, which is in conflict with the flash photolysis studies; e.g., Ravishankara and Thompson [279], Paraskevopoulos and Irwin [259], Hynes et al. [158], and McCabe et al. [219]. Water is not expected to significantly change the rate coefficient for the reaction in the atmosphere and it is not expected to alter the products of the reaction.

Important: To calculate rate constants for the reaction OH + CO $\xrightarrow{M}$ HOCO, use the standard expression for termolecular reactions, $k_f([M\},T)$, given in the Introduction (section 2.1). The Arrhenius parameters for the reaction HOCO + $O_2 \rightarrow HO_2 + CO_2$ are given in Table 1-1. To calculate rate constants for the reaction OH + CO $\xrightarrow{M}$ H + CO_2 , use the expression for chemical activation reactions, $k_f^{ca}([M],T)$, given in the Introduction (section 2.1). (Table: 06-2, Note: 06-2) Back to table

D2. $CH_3 + O_2$. *The temperature dependence of the high pressure limit is positive. There has been a sign error in the last several versions of this recommendation!* Data from Kaiser [168] are fit to the NASA format. This ranges of this study were 3<P/torr<11000 and 264<T/K<370. The rate constant was measured relative to the reaction $CH_3 + Cl_2 \rightarrow CH_3Cl + Cl$. [$k/cm^3molecule^{-1}s^{-1}$ = 1.61E-12exp(-530/RT)] The recommended values are in good agreement with those from Selzer and Bayes [300]. These workers determined the rate constants as a function of pressure in N_2, Ar, O_2, and He. Plumb and Ryan [273] report a value in He which is consistent within error limits with the work of Selzer and Bayes. Pilling and Smith [270] have measured this process in Ar (32–490 Torr). Cobos et al. [69] have made measurements in Ar and N_2 from 0.25 to 150 atmospheres. They report parameters somewhat different than recommended here. The work of Laguna and Baughcum [189] seems to be in the fall–off region. Results of Pratt and Wood [276] in Ar are consistent with this recommendation, although the measurements are indirect. The suggested value accommodates the values of Keiffer et al., [175], who measured the process in Ar between 20 and 600 Torr and in the range 334<T/K<582. Data of van den Bergh and Callear [334], Hochanadel et al. [148], Basco et al. [24], Washida and Bayes [353], Laufer and Bass [192], and Washida [352] are also considered. A theoretical study by Zhu et al. [372] is in reasonable agreement with the recommendation. (Table: 06-2, Note: 06-2) Back to table

D3. $C_2H_5 + O_2$. Kaiser et al. [171] extract from a relative rate study: $k_\infty = (9.2 \pm 0.9) \times 10^{-12}$ cm^3 $molecule^{-1}s^{-1}$ and $k_o = (6.5 \pm 2.0) \times 10^{-29}$ cm^6 $molecule^{-2}s^{-1}$ in He at 298 K and pressures between 3 and 1500 Torr. k_∞ has been calculated by Wagner et al. [338], Miller and Klippenstein [225], and Sheng et al. [306] with k_∞ (300K)= 8,10,and 4×10^{-12} cm^3 $molecule^{-1}s^{-1}$, respectively. Although all cite some small temperature dependence, the values are stated to hold above 300K. The Kaiser et al. [171], extrapolation to the low-pressure limit is difficult due to the complex potential energy surface, but agrees with a Patrick and Golden–type calculation [265] using ΔH_o^0 = 32.4 kcal mol^{-1}. The recommended values use the calculated temperature dependence and a 2.5 times higher rate constant for air as the bath gas, in line with suggestions in Kaiser et al. [169]. (Table: 06-2, Note: 06-2) Back to table

D4. OH + C_2H_2. The rate constant for this complex process has been examined by Smith et al. [312] in the temperature range from 228 to 1400 K, and in the pressure range 1 to 760 Torr. Their analysis, which is cast in similar terms to those used here, is the source of the rate constants and temperature dependences at both limits.

The negative value of m reflects the fact that their analysis includes a 1.2 kcal/mol barrier for the addition of OH to C_2H_2. The data analyzed include those of Pastrana and Carr [264], Perry et al. [268], Michael et al. [224], and Perry and Williamson [269]. Other data of Wilson and Westenberg [356], Breen and Glass [40], Smith and Zellner [315], and Davis et al. [92] were not included. Studies by Liu et al. [206] and Lai et al. [190] are in general agreement with the recommendation. Calculations of k_o via the methods of Patrick and Golden [265] yield values compatible with those of Smith et al. [312]. A study by Sørensen et al. [316] at 298 K and pressures from 25 to 8000 torr of bath gas suggests k_0/cm^{6}molecule^{-2}s^{-1} = 2.92E-30, k_∞/cm^{3}molecule^{-1}s^{-1}. = 9.69E-13 and F_c = 0.6. No difference was found between air, N_2/O_2 mixtures or O_2 as the bath gas. These values yield rate constants as a function of pressure at 298K in agreement with this recommendation, so the recommended values are unchanged from JPL 02-25. Earlier, Fulle et al. [125] reported a high pressure limiting rate constant of 2E-12 cm^{3}molecule^{-1}s^{-1}, which is the basis for the IUPAC [15] recommendation. A theoretical study by Senosiain et al. [302] is in essential agreement with this recommendation. (Table: 06-2, Note: 06-2) Back to table

D5. OH + C_2H_4. A study by Vakhtin et al. [331] at 296K in N_2 between 2.85 × 10^{16} and 3.25 × 10^{18} molecules cm^{-3} and individual points 96K, 1.9 x 10^{16} molecules cm^{-3}; 110K, 2.65 × 10^{16} molecules cm^{-3}; and 165K and 3.5 × 10^{16} molecules cm^{-3}, as well as data of Tully [328], Davis et al. [92], Howard [151], Greiner [135], Morris et al. [231], and Overend and Paraskevopoulos [250] in helium, Atkinson et al. [12] in argon, and Lloyd et al. [207] and Cox [75] and Klein et al. [181] in nitrogen/oxygen mixtures, have been considered in the evaluation. This well–studied reaction is considerably more complex than most others in this table. The parameters recommended here fit the same curve proposed by Klein et al. [181] at 298 K. Kuo and Lee [185] report very strong temperature dependence for the low-pressure limit (n=4). Calculations of the type in Patrick and Golden [265] as described in Vakhtin et al. [331] yield n = 4.2, although they use a somewhat low value for energy transfer by nitrogen. The high-pressure limit temperature dependence has been determined by several workers. Zellner and Lorenz [370] report a value equivalent to m = +0.8 over the range (296<T/K<524) at about 1 atmosphere. A value of m = +2.0 fits the data (540<T/K<670) of Diau and Lee [98]. (Table: 06-2, Note: 06-2) Back to table

D6. CH_3O + NO. This reaction proceeds via a complex potential energy surface that includes both chemical activation and direct abstraction routes [59] to the disproportionation products CH_2O and HNO as well as the combination to form CH_3NO. The chemical activation process would have inverse pressure dependence and the direct abstraction would be pressure independent. The recommended values take into account the results of Frost and Smith [123] in Ar and CF_4 and of Caralp et al. [59] in He and Ar. In both of these references the disproportionation process is subtracted from total loss of CH_3O with a pressure independent, temperature dependent value. At 300K below one torr the disproportionation process dominates. Temperature dependences are from the higher temperature results. The low pressure rate constant is consistent with the measurements of McCaulley et al. [221] and Da le et al. [86] in helium. Studies by Ohmori et al. [245] and Dobé et al. [101] are in general agreement with respect to both the addition and bimolecular pathways. (See the note in Table 1-1 for the bimolecular pathway.) (Table: 06-2, Note: 06-2) Back to table

D7. CH_3O + NO_2. The recommended values are from the work mostly in Ar of Wollenhaupt and Crowley [361]. Agreement is good with earlier work at 298 K from the study of Frost and Smith [122] in Ar (corrected by Frost and Smith [124] and that of Biggs et al [32] and Martinez et al. [217] in He. Low pressure results agree within a factor of two with the measurements of McCaulley et al. [220] in He. A minor bimolecular (chemical activation) pathway is also observed. (See Table 1-1.) (Table: 02-25, Note: 06-2) Back to table

D8. C_2H_5O + NO. High-pressure data at 298 K in Ar from Frost and Smith [123] and in He between 286 and 388K at pressures from 30 to 500 torr, from Fitschen et al. [114]. Low-pressure measurements in He are from Daele et el. [87]. He experiments were scaled to N_2 by dividing by a factor of 2.5. Ar data were taken as equivalent to N_2 or air. The data were fit by subtracting an assumed pressure independent value of 1E-11 from the measured rate constants to account for the route to form HNO and CH_3CHO. The low pressure value agrees with theory. The bimolecular channel with an estimated rate of about 10^{-11} needs to be verified by direct studies. The temperature dependence of the low pressure limit is estimated and that of the high pressure limit is taken from Fitschen et al. [114]. (The high pressure rate expression in Fitschen et al. seems to be in error.) (Table: 06-2, Note: 06-2) Back to table

D9. C_2H_5O + NO_2. High-pressure rate constant at 298 K from Frost and Smith [122]. Other values estimated from similar reactions. (Table: 06-2, Note: JPL92-20) Back to table

D10. CH_3O_2 + NO_2. Golden [131] has re-evaluated the data for this reaction. The recommended parameters are from a fit to Percival [267] and temperature- and pressure-dependent data in Sander and Watson [293] and Ravishankara et al. [277]. The temperature dependence of the high pressure rate constant is a little high, but results from the statistical fit to the data. The values recommended herein, were taken with the data in a study

of the reverse reaction by Zabel et al. [367] to compute the value of the equilibrium constant in Table 3. Destriau and Troe [97] have fit the above data with k_∞ independent of temperature and $F_c = 0.36$. Bridier et al. [43] are in good agreement with this recommendation at one atmosphere and 298 K. (Table: 06-2, Note: 06-2) Back to table

D11. $C_2H_5O_2 + NO_2$. The only experimental study is that of Elfers et al. [106] who measured the rate constant relative to the $C_2H_5O_2 + NO$ reaction between 10 and 1000 mbar. Elfers et al. used a value of $k = 8.9 \times 10^{-12}$ cm^3 $molecule^{-1}$ s^{-1} for the reference reaction. By comparison the recommended rate constant for the reference reaction from Table 1-1 of this evaluation is 1.1×10^{-11} cm^3 $molecule^{-1}$ s^{-1} at 254 K. There are three data points. An evaluation of the Elfers et al. work by Destriau and Troe [97] cast the data in the format used in the IUPAC evaluation [16]. The parameters in Table 2 are adjusted to agree with the data corrected for the change in the reference reaction, using the simpler formula employed in this recommendation. (Table: 02-25, Note: 02-25) Back to table

D12. $CH_3C(O)O_2 + NO_2$. The recommended parameters are from the data of Bridier et al. [42], who report in the format represented here, but using $F_c = 0.3$. Their values are: $k_o^{300} = (2.7 \pm 1.5) \times 10^{-28}$, $k_\infty^{300} = (12.1 \pm 2.0) \times 10^{-12}$, with n = 7.1 ± 1.7 and m= 0.9 ± 0.15. Studies of the decomposition of $CH_3C(O)O_2NO_2$ [PAN] by Roberts and Bertman [284], Grosjean et al. [136], and Orlando et al. [248] are in accord with those of Bridier et al. [42]. In the Roberts and Bertman [284] study it was shown that PAN decomposition yields only peroxyacetyl radical and NO_2; no methyl nitrate. Studies by Seefeld et al. [297] and Sehested et al. [299] of the relative rates of $CH_3C(O)O_2$ with NO and NO_2 are confirmatory. A study by von Ahsen et al. [337] involving matrix isolation of the products of PAN decomposition, suggests a minor pathway due to O-O bond fission. (Table: 06-2, Note: 06-2) Back to table

D13. $CH_3CH_2C(O)O_2 + NO_2$. This reaction, forming peroxypropionyl nitrate (PPN), has been studied in the reverse direction by Schurath and Wipprecht [296], Mineshos and Glavas [226], Grosjean et al. [136] and Kirchner et al. [179]. Group additivity considerations indicate that the equilibrium constant for both PAN and PPN will be the same (both sides of the equilibrium for PPN differ from those for PAN by the group C-(C)(CO)$(H)_2$.) Therefore, the recommended value for the association reaction is taken from the decomposition studies multiplied by the same equilibrium constant as for PAN. The resulting values are very similar to those for $CH_3C(O)O_2 + NO_2$ forming peroxyacetyl nitrate (PAN). Conservative error limits are estimated. (Table: 02-25, Note: 06-2) Back to table

D14. $CH_3C(O)CH_2 + O_2$. Cox et al. [81] reported a value of $k = (1.5+/- 0.3) \times 10^{-12}$ cm^3 $molecule^{-1}s^{-1}$ at 298 K and 1 atm of SF_6 in which a pulse radiolysis study was modeled. This should be close to the high-pressure limit, but Cox et al point out that it is a bit low. (Using group additivity to calculate the entropy change yields about $10^{14.3}$ s^{-1} for the decomposition A-factor. This compares with almost 10^{15} s^{-1} for $C_2H_5O_2$ decomposition.) (Table: 02-25, Note: 02-25) Back to table

E1. $F + O_2$. Values are taken from a study by Campuzano-Jost et al. [54], with experiments from 100 to 420K at pressures of He, Ar and N_2 from 1 to 1000 bar. (They used $F_c = 0.54(T/300)^{-0.09}$, but the results are essentially the same with $F_c = 0.6$.) A study by Pagsberg et al. [257] reports k_o in argon = 4.38×10^{-33} $(T/300)^{-1.2}$. There is also good agreement with earlier values of Smith and Wrigley [313], Smith and Wrigley [314], Shamonina and Kotov [303], Arutyunov et al. [10], Wallington and Nielsen [348], Wallington et al. [347] and Ellerman et al. [107]. The values are slightly lower than the values of Chen et al. [64] and Chegodaev et al. [63]. Lyman and Holland [211] report a slightly lower value in Ar at 298K. Campuzano-Jost et al. [54] and Pagsberg et al. [257], also determined the equilibrium constant and thus $\Delta H_{f,298}(FO_2) = 6.13 \pm 0.5$ kcal mol^{-1}. See $F + O_2$ in Table 3-1. (Table: 06-2, Note: 06-2) Back to table

E2. F + NO. A study by Pagsberg et al [254], taking into account data from Zetzsch [371], Skolnik et al. [309], Kim et al. [177], Pagsberg et al. [256] and Wallington et al. [345], reports rate constants for this reaction in several bath gases. Re-evaluating the data and converting to the form used in this compilation yields the recommended parameters. (Table: 06-2, Note: 06-2) Back to table

E3. $F + NO_2$. Fasano and Nogar [111] studied this reaction in N_2 at 300K. Pagsberg et al. [255] studied the reaction in SF_6 and Zetzsch [371] studied it in He. The results from Fasano and Nogar [111] and Pagsberg et al. [255] were used to determine both the high and low pressure limits at 300 K. Treatment of the data for this system requires knowledge of the relative stabilities of FNO_2 and FONO. Patrick and Golden [265] assumed that the difference between these would be the same as between the $ClNO_2$ isomers. Theoretical work by Dixon and Christie [100], Lee and Rice [196] and Amos et al. [4] indicates that FNO_2 is 35–40 kcal mol^{-1} more stable than FONO, and therefore the measured rate refers to FNO_2 formation. The value of n = 2 is from Patrick and Golden, but consistent with Pagsberg et al. [255] who made a few measurements at 341K. The value of m is a

rough estimate from similar reactions, but is also consistent with Pagsberg et al. [255]. (Table: 06-2, Note: 06-2) Back to table

E4. FO + NO_2. Low pressure limit from strong collision calculation and $\beta = 0.33$. T dependence from resultant $\langle\Delta E\rangle = 0.523$ kcal mol^{-1}, high-pressure limit and T dependence estimated. A theoretical study by Rayez and Destriau [281] indicates that the product is the single isomer $FONO_2$. Bedzhanyan et al. [29] report a value extracted from a complex mixture of bath gases. (Table: 06-2, Note: 94-26) Back to table

E5. CF_3 + O_2. Caralp et al. [57] have measured the rate constant in N_2 between 1 and 10 Torr. This supersedes the value from Caralp and Lesclaux [56]. Kaiser et al. [172] have extended the pressure range to 580 Torr measuring the reaction relative to the reaction of CF_3 with Cl_2. Breheny et al. [41] report values at 295 K from 2-110 torr and they make a cogent argument for lowering the value of the rate constant used by Kaiser et al for their reference reaction by about 50%. This has the effect of lowering the Kaiser values. Each study recommends different parameters, but the data are well represented by the currently recommended values. Data of Ryan and Plumb [287] are in general agreement. Forst and Caralp [116] have examined this reaction theoretically. (Table: 06-2, Note: 06-2) Back to table

E6. CF_3O + NO_2. Fockenberg et al. [115] report values in nitrogen with 250<T/K<302 and 7<p/mbar<107. They report large error limits. Their values, including two sigma errors, using the previous format are: $k_0 = (3.1 \pm 3.0)\times10^{-28}$; n = (2.0 ± 2.0); $k_\infty = (1.5 \pm 0.5)\times10^{-28}$; m = (2.8±2.0). These were used in JPL 02-25. Here the data has been fit forcing m =1, as values as large as m =2.8 are not justifiable. The reaction products agree with those reported by Chen et al. [65], who used photolysis of CF_3NO to prepare CF_3O_2 and subsequently CF_3O in 700 Torr of air at 297 ± 2 K. They considered two product channels: (a) CF_3ONO_2 obtained via three–body recombination and (b) CF_2O + FNO_2 obtained via fluorine transfer. Both products were observed and found to be thermally stable in their reactor. They report $k_a/(k_a+k_b) > 90\%$ and $k_b/(k_a+k_b) < 10\%$, thus the formation of CF_3ONO_2 is the dominant channel at 700 Torr and 297 K. (Table: 06-2, Note: 06-2) Back to Table

E7. CF_3O_2 + NO_2. The data is from experiments in O_2 of Caralp et al. [58], who suggest a somewhat different fitting procedure than used here. A statistical best fit to the data yields a value of m= 5.7, but the values recommended here fit the data just about as well. Destriau and Troe [97] use yet a different fitting procedure that does not represent the data quite as well as that recommended here. Reverse rate data are given by Köppenkastrop and Zabel [183]. (Table: 06-2, Note: 06-2) Back to table

E8. CF_3O + CO. Values taken from Turnipseed et al. [329]. The numbers were obtained for Ar as the bath gas and are assumed to hold for N_2 as well. The temperature dependence of the high-pressure rate constant was determined over the range 233<T/K<332 in SF_6. No temperature dependence of the low-pressure-limiting rate constant was reported. The value in the table is an estimate. Wallington and Ball [343] report values in good agreement with Turnipseed et al. [329]. (Table: 06-2, Note: 06-2) Back to table

E9. CF_3O + M. The activation energy for thermal decomposition of CF_3O to CF_2O + F has been reported to be 31 kcal mol^{-1} by Kennedy and Levy [176]. Thermochemical data yield $\Delta H^o(298) = 23$ kcal mol^{-1}. This implies an intrinsic barrier of about 8 kcal mol^{-1} to elimination of F from CF_3O. Electronic structure calculations by Li and Francisco [204] support this observation. Adopting the A-factor for unimolecular dissociation, $A = 3 \times 10^{14}$ s^{-1} and E = 31 kcal mol^{-1} from Kennedy and Levy, k_∞ (298 K) is about $6 \times 10^{-9} s^{-1}$. This corresponds to a lifetime of about 6 years; therefore, thermal decomposition of CF_3O is unimportant throughout the atmosphere. (Table: 94-26, Note: 94-26) Back to table

F1. Cl + O_2. Nicovich et al. [237] measured the rate constant at 181<T/K< 200 and 15<p/torr<40 in O_2. They reported $k_o = (9 \pm 3)\ 10^{-33}$ cm^6 $molecule^{-2}s^{-1}$ at T = 187 ± 6 K in O_2. The recommended low pressure limiting parameters are from fitting their data over the entire range and assuming the same value for N_2 as the bath gas. The value from the calculation at 300 K (i.e., 2.2×10^{-33} cm^6 $molecules^{-2}$ s^{-1}) compares with an older value of Nicholas and Norrish [235] of 1.7×10^{-33} in an N_2 + O_2 mixture. Baer et al. [19] report a value in O_2 of $k_o = (1.6)\ 10^{-33}(T/300)^{-2.9}$ cm^6 $molecule^{-2}s^{-1}$ in good agreement with the value recommended here. They also report a value in N_2 of $k_o = (1.4)\ 10^{-33}(T/300)^{-3.9}$ cm^6 $molecule^{-2}s^{-1}$. A theoretical study by Zhu and Lin [376] suggests $k_o = (1.26)\ 10^{-16}T^{-6.22}\exp(-943/T)$ cm^6 $molecule^{-2}s^{-1}$ in O_2 (2.0×10^{-33}) at 300K with $k_\infty = (1.8)\ 10^{-10}s^{-1}$, which is adopted here. The Nicovich et al [237] data is so far from the high pressure limit, that the difference in values for the high pressure rate constant can't be evaluated easily. Baer et al [19] suggest $k_\infty = 2.7\times 10^{-11}$ s^{-1}, but the data suggest a higher value. (Table: 06-2, Note: 06-2) Back to table

F2. Cl + NO. Low-pressure limit and temperature dependence is from re-evaluation of data from Lee et al. [194]. Clark et al. [68] and Ashmore and Spencer [11] also have data in agreement with the recommendation. (Table: 06-2, Note: 06-2) Back to table

F3. Cl + NO_2. Low-pressure limit at 300 K from Leu [202] and Ravishankara et al. [278]. The latter study extended the data to 200 Torr in He. A turbulent flow study by Seeley et al. [298] extended the results to 250

Torr of Ar and the high-pressure limit was chosen to fit these two studies after taking into account differences in collisional efficiencies of the bath gases. Leu [202] confirms the observation of Niki et al. [241] that both ClONO and $ClNO_2$ are formed, with the former dominating. This has been explained by Chang et al. [62], with detailed calculations in Patrick and Golden [265]. The temperature dependence is as predicted in Patrick and Golden [265] and is the same as Leu's results in He. Ravishankara et al. [278] report a few data points in N_2 that may suggest a somewhat higher temperature dependence. The temperature dependence of the high-pressure limit is estimated. The uncertainty limits are estimated. (Table: 06-2, Note: 06-2) Back to table

F4. Cl + CO. From Nicovich et al. [238], who measured the process in N_2 for $185 \leq T/K \leq 260$. Hewitt et al. [144] report a value at one atmosphere and 298 K with ^{13}CO in agreement with Nicovich et al. [238]. (Table: 06-2, Note: 06-2) Back to table

F5. Cl + C_2H_2. The recommended values are a statistical fit to the work of Kaiser [167] in air. Kaiser and Wallington [166] extends the pressure range at 296K to 0.3–6000 Torr. The data are in reasonable agreement with earlier measurements of Brunning and Stief [46] and Wallington et al. [340], although the derived temperature dependence is less than obtained by Brunning and Stief [46]. These values are compatible with earlier studies of Poulet et al. [275], Atkinson and Aschmann [13], Lee and Rowland [193] and Wallington et al. [349]. Using FTIR, Zhu et al. [377] reported branching of 16% and 84% to the trans and cis adduct isomers, respectively, at 700 Torr N_2 and 295 K. (Table: 06-2, Note: 06-2) Back to table

F6. Cl + C_2H_4. Values at 300 K are from a relative rate study by Wallington et al. [340]. A relative rate study by Kaiser and Wallington [166] extends the pressure range to 0.3–6000 Torr and is compatible with earlier studies. Temperature dependence of k_o is taken from Kaiser and Wallington [170]. The temperature dependence of k_∞ is estimated. Values are in reasonable agreement with studies by Maricq et al. [214], Lee and Rowland [193], Iyer et al. [161], Atkinson and Aschmann [13], Atkinson and Aschmann [14] and Wallington et al. [350]. A study in He by Stutz et al. [320] is noted, as is a comment on it by Kaiser and Wallington [170]. Knyasev et al. [182] have done an extensive experimental and theoretical analysis. Their values agree with this recommendation. (Table: 97-4, Note: 02-25) Back to table

F7. Cl + C_2Cl_4. Recommendation is from the flash-photolysis study of Nicovich et al. [240] done at 231–390 K in 3–700 Torr N_2. A study by Thuner et al. [322] is in agreement. (Table: 97-4, Note: 02-25) Back to table

F8. ClO + NO_2. The low-pressure-limit recommendation and uncertainties are based on temperature-dependent values from Zahniser et al. [368], Lee et al. [198], Birks et al. [35], Leu et al. [202], Wallington and Cox [344], Cox et al. [76] and Molina et al. [228]. All of these data were collected in N_2 bath gas, except for several points from Lee et al. [198] collected in O_2.

The high-pressure-limit recommendation is based on the RRKM calculations of Smith and Golden [133]. There are several pressure-dependent data sets in the literature, such as Percival et al. [266], Handwerk and Zellner [139], Dasch et al. [90] and Cox and Lewis [80]; however, they are too disparate to extract unambiguous values. These data are all reproduced within two-sigma error limits by the current recommendation. However, the value of m = 1.9 is somewhat large. If m = 1 is chosen the computed rate constant is lower by about 20% at 180K and pressures above 500 torr. (Table: 06-2, Note: 06-2) Back to table

F9. OClO + NO_3. Friedl et al. [121], studied this system at $1 \leq P/Torr \leq 5$ for helium and $220 \leq T/K \leq 298$. They deduced values for the rate constant consistent with their data of $ko \approx 10^{-31}$ and $k\infty \approx 10^{-11}$. They also suggest a value for the equilibrium constant: $K/cm^3\ molecule^{-1} = 1 \times 10^{-28} \exp(9300/T)$. Boyd et al. [39] raised the question of possible heterogeneous effects in this system. Parthiban et al. [263] in a theoretical study, support the finding of Friedl et al. [121] of the species O_2ClONO_2, but suggest a very different equilibrium constant. (See Table 3-1). (Table: 94-26, Note: 06-2) Back to table

F10. ClO + ClO. The recommendation is based on a simultaneous fit to data from Bloss et al. (183–245 K) [38], (which supersedes earlier work of Sander et al. (194–247 K) [290]), Nickolaisen et al. (260–390 K) [236] and Trolier et al. (200–263 K) [327]. The latter data have been corrected for the effect of Cl_2 as third body, as suggested by Nickolaisen et al. With this adjustment all the data are in reasonable agreement. Error limits are from the statistical fit. Golden [130] has performed RRKM and master equation calculations using the potential energy surface in Zhu and Lin [373] and concluded that while a channel to form ClOClO might obtain, the best representation of the data remains as recommended in JPL 02-25. [The value of m = 2.4 is somewhat high, but since the recommended parameters fit data taken over the range of pressure and temperature obtaining in the atmosphere, they have not been altered.] The k_o value for N_2 is not in accord with a Patrick and Golden–type calculation [265]. This may be due to uncertainty in the ClOOCl thermochemistry, which is based on the equilibrium constants reported by Nickolaisen et al. and Cox and Hayman [79] (See Table 3.). It has been suggested [326] that the "radical-complex' mechanism may apply here. Other previous rate constant measurements, such as those of Hayman et al. [142], Cox and Derwent [77], Basco and Hunt [23], Walker

[339], and Johnston et al. [164], range from 1–5 × 10^{-32} cm^6 s^{-1}, with N_2 or O_2 as third bodies. The major dimerization product is chlorine peroxide (Birk et al. [34], DeMore and Tschuikow-Roux [96], Slanina and Uhlik [310], Stanton et al. [317] and Lee et al. [197]). (Table: 02-25, Note: 06-2) Back to table

F11. ClO + OClO. Data are from Burkholder et al. [49], who measured the rate constant in N_2 at 200 ≤ T/K ≤ 260 and densities from (1.1–10.9) × 10^{18} molecules cm^{-3}. They also measured the equilibrium constant. (See Table 3) Parr et al. [261] also report a value for the rate constant in reasonable agreement with the recommendation. Zhu and Lin [375] report an ab initio study of this system. Their parameters are somewhat different from those herein, but they fit the data equally well. Green et al. [134] report a value in He that is consistent with the values recommended herein. (Table: 06-2, Note: 06-2) Back to table

F12. O + OClO. The recommendation is based on data of Colussi et al. [72] and Colussi [71], who measured the pressure dependence between 248 and 312 K in Ar. They interpret the intercept of their k vs [M] curves as a zero-pressure rate constant of (1.6 ± 0.4) × 10^{-13} cm^3 $molecule^{-1}$ s^{-1} with a negative activation energy corresponding to a chemical activation channel producing ClO + O_2. A low pressure study by Gleason et al. [129], as well as a theoretical study by Zhu and Lin [374], suggests a direct abstraction with a positive activation energy. (Zhu and Lin [374] point out that sym-ClO_3 has a positive barrier for dissociation to ClO + O_2.) The recommended values are fit to the data after subtracting the abstraction channel. See Table 1-1. (Table: 06-2, Note: 06-2) Back to table

F13. CH_2Cl + O_2. Measured by Fenter et al. [112] over the range 298 ≤ T/K ≤ 448 and 1 ≤ P/Torr ≤ 760 in nitrogen. Two different techniques were employed: laser photolysis/photoionization mass spectrometry in the range 1–10 Torr and laser photolysis/UV absorption for the range 20–760 Torr. A study by Bilde et al. [33] in N_2 relative to the reaction $CH_2Cl + Cl_2 \rightarrow CH_2Cl_2 + Cl$ is in excellent agreement. Error limits transposed to the current format. (Table: 06-2, Note: 06-2) Back to table

F14. $CHCl_2$ + O_2. Measured by Fenter et al. [112] over the range 298 ≤ T/K ≤ 383 and 1 ≤ P/Torr ≤ 760 in nitrogen. Two different techniques were employed: laser photolysis/photoionization mass spectrometry in the range1–10 Torr and laser photolysis/UV absorption for the range 20–760 Torr. A study by Nottingham et al. [244], in He, is in agreement. Error limits transposed to the current format. Back to table

F15. CCl_3 + O_2. The recommendation incorporates studies by Fenter et al. [113], Danis et al. [89] and Luther et al. [210]. (Their data above 100 bar are affected by diffusion.) Experimental data of Ryan and Plumb [288] have been considered in the evaluation. A study by Nottingham et al. [244], in He, is in agreement. Forst and Caralp [116] have examined this reaction theoretically. A Patrick and Golden–type calculation using the thermochemistry of Russell et al. [286] yields $k_0^{300} = 1.5 \times 10^{-30}$, with β = 0.3. A value of $k_\infty^{300} = 5 \times 10^{-12}$ has been reported by Cooper et al. [74]. The value of the rate constants recommended here vary slightly from those of Luther et al., (who report $k_\infty^{300} = 5.2 \times 10^{-12}$; m = 1.4 and $k_0^{300} = 1.5 \times 10^{-30}$; n = -6.3; $F_c = 0.35 \times (T/300)^{-0.35}$ using the IUPAC formula) but yield an overall rate constant within their error limits. (Table: 06-2, Note: 06-2) Back to table

F16. $CFCl_2$ + O_2. Values for both low- and high-pressure limits at 300 K are from Caralp and Lesclaux [56]. Forst and Caralp [116] have examined this reaction theoretically. Temperature dependences are rough estimates based on their calculations and similar reactions. (Table: 06-2, Note: 06-2) Back to table

F17. CF_2Cl + O_2. Forst and Caralp [116] have examined this reaction theoretically. Temperature dependences are rough estimates based on their calculations and similar reactions. (Table: 06-2, Note: 06-2) Back to table

F18. CCl_3O_2 + NO_2. Statistical fit (constrained to m=1) to experiments in O_2 of Caralp et al. [58], who suggest a somewhat different fitting procedure, but the values recommended here fit the data as well. Destriau and Troe [97] use yet a different fitting procedure that does not represent the data quite as well as that recommended herein. Reverse rate data are given by Köppenkastrop and Zabel [183]. (Table: 06-2, Note: 06-2) Back to table

F19. $CFCl_2O_2$ + NO_2. Statistical fit to experiments in O_2 of Caralp et al. [58] with constraint that m=1. Caralp et al. [58] suggest a different fitting procedure, but the values recommended here fit the data as well. Destriau and Troe [97] use yet a different fitting procedure that does not represent the data quite as well as that recommended herein. Reverse rate data are given by Köppenkastrop and Zabel [183]. (Table: 06-2, Note: 06-2) Back to table

F20. CF_2ClO_2 + NO_2. A study by Xiong and Carr [364] of the reverse reaction, combined with the equilibrium constant, which was computed from correcting the study by Wu and Carr [363] of the forward reaction in a bath gas consisting of 80% CF_2ClBr + 20% O_2 for N_2 bath gas. (The study by Wu and Carr [363] supersedes the earlier work of Moore and Carr [229].) Xiong and Carr [364] report their parameterization differently than in this recommendation, but the values herein reproduce their results to a few percent. Reverse rate data are

also given by Köppenkastrop and Zabel [183] and in a theoretical study by Forst and Caralp [117]. (Table: 06-2, Note: 06-2) Back to table

G1. $Br+NO_2$. The recommended values are from a study by Kreutter et al. [184]. They regarded the product as $BrNO_2$. Their k_o value in He agrees with the measurement of Mellouki et al. [222] at 300 K. Broske and Zabel [44] and Orlando and Burkholder [246] have shown that cis-BrONO is the major product in their studies. Orlando and Burkholder [246] suggest that isomerization to $BrNO_2$ is heterogeneous. Lee [195] calculated structure, frequencies and energetics for $BrNO_2$, cis-BrONO and trans-BrONO. A Patrick-and-Golden-type calculation using the Lee [195] results yields k_o(strong collision) ≈ 1.2, 2.5 and 2.1 in units of $1x10^{-31}cm^6$ $molecule^{-2}s^{-1}$ for trans-BrONO, cis-BrONO and $BrNO_2$, respectively. The sum, $5.9x10^{-31}$, multiplied by a collision efficiency in N_2 of 0.3 is a factor of about 2.5 lower than the observed k_o value. Also, the relative yield of $BrNO_2$ is somewhat too high since Orlando and Burkholder [246] measure BrONO > 75%. Kreutter et al. [184] report an equilibrium constant, which, if cis-BrONO is assumed to be the product, suggests bond strengths for the BrONO compounds that are about 4 kcal $mole^{-1}$ higher than the Lee [195] calculation. Computing k_o with these new values yields k_o ≈ 4.5 and 6.4 in units of $1x10^{-31}$ for trans-BrONO and cis-BrONO respectively. When the sum of the rate constants for the three channels is multiplied by the collision efficiency (0.3), the result is 3.9E-31 and the yield of BrONO is 85%. (Table: 06-2, Note: 06-2) Back to table

G2. $BrO + NO_2$. Values from a study by Thorn et al. [321] that is in excellent agreement with Sander et al. [292] are recommended. Error limits are from a reanalysis of the data. Danis et al. [88] give slightly lower values for the low-pressure-limiting rate constant and a smaller temperature dependence as well. This latter study may be hampered by heterogeneous effects, but can be accommodated within the error limits recommended. A theoretical study by Rayez and Destriau [281] suggests that the bond-dissociation energy in $BrONO_2$ is 8.5 kcal mol^{-1} higher than in $ClONO_2$, thus rationalizing the relative values of the low-pressure-limiting rate constants for these two processes. A more detailed theoretical study by Parthiban and Lee [262], as well as a study by Orlando and Tyndall [247], who measured $BrONO_2$ decomposition and thus an equilibrium constant, both determine only 1.6 kcal mol^{-1} for the above difference. A theoretical study by Zou et al. [378] agrees with the latter figure. A Patrick and Golden [265] type calculation, even with the stronger bond of Rayez and Destriau [281] yields a value for the low pressure limiting rate constant that is less than observed. Lessar et al. [200] calculate a potential energy surface for BrOONO. They find that the BrO – ONO bond strength is of the order of 7 kcal mol^{-1}, which is too weak to have any effect on the overall rate of $BrO + NO_2$. *The temperature dependence of the high pressure rate constant seems large. The data can be fit quite well with* $k_\infty = 8 \times 10^{-12}(T/300)^{-1}$. (Table: 06-2, Note: 06-2) Back to table

H1. I + NO. Evaluation taken from IUPAC [160]. The data are from van den Bergh et al. [332] and Basco and Hunt [22]. Error limits transposed to the current format. The heat of formation of INO is given as 120.0±0.3 kJ/mole by Forte et al. [119]. (Table: 06-2, Note: 06-2) Back to table

H2. $I + NO_2$. Evaluation taken from IUPAC [160]. The data are from van den Bergh et al. [332], Mellouki et al. [222], Buben et al. [47] and van den Bergh and Troe [333]. IUPAC uses $F_c = 0.63$, which is the same as the universal value adopted here of $F_c = 0.6$. (No evidence of possible isomers [INO_2 or IONO] is reported.) Error limits transposed to the current format. (Table: 06-2, Note: 06-2) Back to table

H3. $IO + NO_2$. Data from Daykin and Wine [94], Hölscher and Zellner [150], Allan and Plane [3] and Jenkin and Cox [162]. Two more studies at lower pressures are available, Larin et al. [191], and Maguin et al. [212]. These do not agree very well with the above four studies and have higher experimental errors. The recommended k_o and k_∞ also agree with a theoretical study by Rayez and Destriau [281]. (Table: 06-2, Note: 06-2) Back to table

I1. HS + NO. Data and analysis are from the work of Black et al. [36]. The temperature dependence of k_o has been adjusted to give a better fit than in JPL 02-25. The temperature dependence of k_∞ has been estimated. (Table: 06-2, Note: 06-2) Back to table

I2. CH_3S + NO. The recommended values are fit to the study by Balla et al. [20]. The temperature range was 295 to 453K and pressures of N_2 from 1.5 to 300 torr. The change in the high pressure limiting rate coefficient and its temperature dependence reflect a better fit to the data. (Table: 06-2, Note: 06-2) Back to table

I3. $O + SO_2$. Naidoo et al. [233] studied this spin forbidden reaction in Ar over the temperature range 290<T/K<840 and pressure range 100<P/mbar<880. They fit the data very well using the IUPAC [15] format with $k_o = 9.5x10^{-23}T^{-3}exp(-2400/T)$ $cm^6molecule^{-2}s^{-1}$, $k_\infty = 6.1x10^{-13}exp(-850/T)$ $cm^3molecule^{-1}s^{-1}$ and F_c = 0.558exp(-T/316)+0.442exp(-T/7442). The recommended values transpose the rate constants to the form used in this evaluation and are used with the standard value of F_c =0.6. These parameters don't fit the higher temperatures as well as the values derived by Naidoo et al. [233], missing the values at 840K by about 50% and those at 699K by about 20%. Values at 289, 399 and 581K are fit quite well and are adequate for atmospheric

conditions. Earlier values are reported by Atkinson and Pitts [18] and M ller et al. [232] (Table: 06-2, Note: 06-2) Back to table

I4. OH + SO_2. Values of the rate constant as a function of pressure and temperature are from Blitz et al. [37]. They used a five parameter fit to the data, allowing Fc to be temperature dependent. The values of k_0 and k_∞ have been adjusted in the Table to accommodate Fc = 0.6. Blitz et al. [37] determined the high pressure limit from the reaction of OH(v=1) with SO_2. Their low pressure value was taken by re-evaluating the data of Wine et al. [359] in various bath gases at pressures up to 150 torr and temperatures between 260 K and 420 K, through the use of a master equation. The data of Paraskevopoulos et al. [260] in the same pressure range, is equally well fit. Lower pressure data from at 298 K from Leu [201] and Lee et al. [199] are well accommodated by the recommendation herein. Earlier data listed in Baulch et al. [27], Baulch et al. [26] and Atkinson et al. [15] are noted. Blitz et al [37] have calculated the entropy and measured a third law heat of formation for $HOSO_2$ (373±6kJ/mol). See also Li and McKee [203]. (Table: 06-2, Note: 06-2) Back to table

I5. CH_3SCH_2 + O_2. Wallington et al. [346] have employed a pulse radiolysis technique, obtaining k = (5.7 ± 0.4)×10^{-12} cm^3 $molecule^{-1}$ s^{-1} in 992 mbar of SF_6 at room temperature. A theoretical study by Resende and De Alemeida [282] yields a heat of formation of the product, $CH_3SCH_2O_2$, as 6.51 kcal mol^{-1}. (Table: 94-26, Note: 06-2) Back to table

I6. SO_3 + NH_3. Recommendation is from Lovejoy [208]. This study covered 20-80 Torr from 280 – 340 K. An earlier study by Lovejoy and Hanson [209], who studied this reaction from 10–400 Torr N_2 at 295 K is in agreement. Lovejoy and Hanson [209] observed that any incipient adduct rapidly becomes sulfamic acid (H_3NSO_3) which clusters efficiently with itself and sulfuric acid. The observed sulfamic acid dimerization rate constant exceeds 5 × 10^{-11} cm^3 $molecule^{-1}$ s^{-1}. Measurements of Shen et al. [305] made at 1–2 Torr He are much higher than those of Lovejoy and Hanson [209] or Lovejoy [208]. Error limits have been adjusted to take into account the fact that the exponent of the temperature dependence of the low pressure rate constant is unusually large. Lovejoy [208] also reports an equilibrium constant and heat of formation of sulfamic acid of -24±1 kcal mol^{-1}. (Table: 06-2, Note: 06-2) Back to table

I7. HO + CS_2. The data is from Hynes et al. [reaction 38 in Table 3-1] and Murrells et al. [reaction 32 in Table 3-1]. The value m = 1 is constrained. The adduct reacts slowly with O_2. (See Table 1-1.) (Table: 06-2, Note: 06-2) Back to table

I8. Cl + CS_2. The data is from Nicovich et al. [239]. Wallington et al. [341] have also studied this system. The value m = 0 is constrained. Nicovich et al. [239] confirm that the reaction proceeds via reversible adduct formation as suggested by Martin et al. [216]. The much larger rate constant values determined by Martin et al. may possibly be attributed to reactive impurities in the CS_2 sample. Nicovich et al. set an upper limit on the rate constant for the adduct (CS_2Cl) reacting with O_2 of 2.5 x 10^{-16} cm^3 $molecule^{-1}$ s^{-1} at room temperature. Wang and Phillips [351] have performed a theoretical study of the adduct. (Table: 06-2, Note: 06-2) Back to table

I9. Cl + $(CH_3)_2S$. If the HCl yield at 297K from Stickel et al. [318] is used as a measure of the abstraction reaction, the rate constant would be 1.64 x 10^{-10} cm^3 $molecule^{-1}$ s^{-1}. Using this value the complete data set from Stickel et al. [318] can be fit with form used in Table 2 with the addition of a term for the abstraction in the form k_{abs}=1.64x10^{-10}*$(T/300)^a$. The value of "a" obtained in this manner is almost zero, so the data is fit with: k_0= 4 x 10^{-28}*$(T/300)^{-7.0}$ and k_∞= 2 x 10^{-10} $(T/300)^{-1}$ along with the temperature independent value of k_{abs}. On the other hand, a study by Diaz-de-Mera et al. [99] performed in the temperature range 259<T/K<364 and in helium at pressures of 0.5<p/torr<1 reports a value k_{abs} = (2.0±1.2) x 10^{-10}exp[-(332±173)/T], which yields 6.6 x 10^{-11} cm^3 $molecule^{-1}$ s^{-1} at room temperature. Several studies, both experimental by Urbanski and Wine [330] and theoretical by Resende and De Almeida [283] make it clear that at higher pressures an adduct Cl-$S(CH_3)_2$ is formed and this adduct does not yield CH_3 radicals or the products of the abstraction pathway. (Table: 06-2, Note: 06-2) Back to table

I10 Br + $(CH_3)_2S$. Wine et al. [358] data for the adduct formation in N_2 at 25<P/torr<600 and 263<T/K<310 can be evaluated in the NASA format. This leads to the values recommended. Studies by Ingham et al. [159] and Nakano et al. [234] are in agreement. Nakano et al. [234] is also in agreement with the value of the equilibrium constant. However, Maurer et al. [218] find a value at 300K and 1 bar total pressure of a mixture of 5% O_2 and 95% N_2, only 2% as high as the value computed from the recommended parameters. This latter value is supported by Ballesteros et al. [21]. (Table: 06-2, Note: 06-2) Back to table

J1. Na + O_2. A study by Plane and Rajasekhar [272] finds k_o = (2.9 ± 0.7) × 10^{-30} cm^6 $molecule^{-2}$ s^{-1}at 300 K with n = 1.30 ± .04. They also estimate k_∞ to be about 6 × 10^{-10} cm^3 $molecule^{-1}$ s^{-1} with a small positive temperature dependence. Another study by Helmer and Plane [143] yields k_o = (3.1 ± 0.2) × 10^{-30} cm^6 $molecule^{-2}$ s^{-1} at 300 K with n = 1.52 ± 0.27. The recommended values are taken from these studies. They are consistent with values measured by Marshall et al. [215] at 600 K and those measured by Vinckier et al. [336] at higher

temperature. The k_o value is about 60% higher than that of Silver et al. [307]. (Table: 06-2, Note: 06-2) Back to table

J2. NaO + O_2. Ager and Howard [1] have measured the low- pressure limit at room temperature in several bath gases. Their value in N_2 is used in the recommendation. They performed a Troe calculation, as per Patrick and Golden [265], to obtain collision efficiency and temperature dependence. They obtained a high-pressure-limit rate constant by use of a simple model. The temperature dependence is estimated. (Table: 06-2, Note: 06-2) Back to table

J3. NaO + CO_2. Ager and Howard [1] have measured the rate constant for this process in the "fall–off" regime. Their lowest pressures are very close to the low-pressure limit. The temperature dependence is an estimate. Ager and Howard calculate the high-pressure rate constant from a simple model. (Table: 06-2, Note: 06-2) Back to table

J4. NaOH + CO_2. Ager and Howard [2] have measured the low-pressure-limiting rate constant. The temperature dependence is an estimate. Ager and Howard have calculated the high-pressure limit using a simple model. (Table: 06-2, Note: 06-2) Back to table

2.8 References .

1. Ager, J. W., III and C. J. Howard, 1986, Geophys. Res. Lett., **13**, 1395-1398.
2. Ager, J. W., III and C. J. Howard, 1987, J. Chem. Phys., **87**, 921-925.
3. Allan, B. J., and J. M. C. Plane, 2002, J. Phys. Chem. A, **106**, 8634-8641.
4. Amos, R. D., C. W. Murray and N. C. Handy, 1993, Chem. Phys. Lett., **202**, 489-494.
5. Anastasi, C. and I. W. M. Smith, 1976, J. Chem. Soc. Faraday Trans. 2, **72**, 1459-1468.
6. Anastasi, C. and I. W. M. Smith, 1978, J. Chem. Soc. Faraday Trans. 2, **74**, 1056.
7. Anderson, J. G. and F. Kaufman, 1972, Chem. Phys. Lett., **16**, 375-379.
8. Anderson, J. G., J. J. Margitan and F. Kaufman, 1974, J. Chem. Phys., **60**, 3310.
9. Anderson, S. M., D. Hulsebusch and Mauersberger, 1997, J. Chem. Phys., **107**, 5385-5392.
10. Arutyunov, V. S., L. S. Popov and A. M. Chaikin, 1976, Kinet. Katal., **17**, 286.
11. Ashmore, P. G. and M. S. Spencer, 1959, Trans. Faraday Soc., **55**, 1868.
12. Atkinson, D. B. and M. A. Smith, 1994, J. Phys. Chem., **98**, 5797-5800.
13. Atkinson, R. and S. M. Aschmann, 1985, Int. J. Chem. Kinet., **17**, 33-41.
14. Atkinson, R. and S. M. Aschmann, 1987, Int. J. Chem. Kinet., **19**, 1097-1105.
15. Atkinson, R., D. L. Baulch, R. A. Cox, J. N. Crowley, J. Hampson, R. F., R. G. Hynes, M. E. Jenkin, J. A. Kerr, M. J. Rossi and J. Troe. Web Version, 2004.
16. Atkinson, R., D. L. Baulch, R. A. Cox, J. Hampson, R. F., J. A. Kerr, M. J. Rossi and J. Troe, 1997, J. Phys. Chem. Ref. Data, **26**, 1329-1499.
17. Atkinson, R., D. A. Hansen and J. Pitts, J. N., 1975, J. Chem. Phys., **62**, 3284-3288.
18. Atkinson, R. and J. J. N. Pitts, 1978, Int. J. Chem. Kinet., **10**, 1081.
19. Baer, S., H. Hippler, R. Rahn, M. Siefke, N. Seitzinger and J. Troe, 1991, J. Chem. Phys., **95**, 6463-6470.
20. Balla, R. J., H. H. Nelson and J. R. McDonald, 1986, Chem. Phys., **109**, 101.
21. Ballesteros, B., N. R. Jensen, and J. Hjorth, 2002, J. Atmos. Chem., **43**, 135-150.
22. Basco, N. and J. E. Hunt, 1978, Int. J. Chem Kinet., **10**, 733-743.
23. Basco, N. and J. E. Hunt, 1979, Int. J. Chem. Kinet., **11**, 649-664.
24. Basco, N., D. G. L. James and F. C. James, 1972, Int. J. Chem. Kinet., **4**, 129.
25. Bates, R. W., D. M. Golden, R. K. Hanson and C. T. Bowman, 2001, Phys. Chem. Chem. Phys., **3**, 2337-2342.
26. Baulch, D. L., R. A. Cox, P. J. Crutzen, R. F. Hampson, Jr., J. A. Kerr, J. Troe and R. T. Watson, 1982, J. Phys. Chem. Ref. Data, **11**, 327-496.
27. Baulch, D. L., R. A. Cox, R. F. Hampson, Jr., J. A. Kerr, J. Troe and R. T. Watson, 1980, J. Phys. Chem. Ref. Data, **9**, 295-471.
28. Bean, B. D., A. K. Mollner, S. A. Nizkorodov, G. Nair, M. Okumura, S. P. Sander, K. A. Peterson and J. S. Francisco, 2003, Journal of Physical Chemistry A, **107**, 6974-6985.
29. Bedzhanyan, Y. R., E. M. Markin and Y. M. Gershenzon, 1993, Kinetics and Catalysis, **34**, 190-193.
30. Beno, M. F., C. D. Jonah and W. A. Mulac, 1985, Int. J. Chem. Kinet., **17**, 1091-1101.
31. Biermann, H. W., C. Zetzsch and F. Stuhl, 1978, Ber. Bunsenges Phys. Chem., **82**, 633.
32. Biggs, P., C. E. Canosa-Mas, J. M. Fracheboud, D. E. Shallcross, R. P. Wayne and F. Caralp, 1993, J. Chem. Soc. Faraday Trans., **89**, 4163-4169.
33. Bilde, M., J. Sehested, O. J. Nielsen, T. J. Wallington, R. J. Meagher, M. E. McIntosh, C. A. Piety, J. M. Nicovich and P. H. Wine, 1997, J. Phys.Chem. A, **101**, 8035-8041.
34. Birk, M., R. R. Friedl, E. A. Cohen, H. M. Pickett and S. P. Sander, 1989, J. Chem. Phys., **91**, 6588-6597.
35. Birks, J. W., B. Shoemaker, T. J. Leck, R. A. Borders and L. J. Hart, 1977, J. Chem. Phys., **66**, 4591-4599.
36. Black, G., R. Patrick, L. E. Jusinski and T. G. Slanger, 1984, J. Chem. Phys., **80**, 4065.
37. Blitz, M. A., K. J. Hughes and M. J. Pilling, 2003, J. Phys. Chem. A, **101**, 1971-1978.
38. Bloss, W. J., S. L. Nickolaisen, R. J. Salawitch, R. R. Friedl and S. P. Sander, 2001, J. Phys. Chem. A, **105**, 11226-11239.
39. Boyd, A. A., G. Marston and R. P. Wayne, 1996, J. Phys. Chem., **100**, 130-137.
40. Breen, J. E. and G. P. Glass, 1971, Int. J. Chem. Kinet., **3**, 145.
41. Breheny, C., G. Hancock, and C. Morrell, 2001, Zeitshrift fur Physikal. Chemie, **215**, 305-317.
42. Bridier, I., F. Caralp, H. Loirat, R. Lesclaux, B. Veyret, K. H. Becker, A. Reimer and F. Zabel, 1991, J. Phys. Chem., **95**, 3594-3600.
43. Bridier, I., R. Lesclaux and B. Veyret, 1992, Chem. Phys. Lett., **191**, 259-263.
44. Broske, R. and F. Zabel, 1998, J. Phys.Chem. A, **102**, 8626-8631.
45. Brown, S. S., R. K. Talukdar and A. R. Ravishankara, 1999, Chem. Phys. Lett., **299**, 277-284.
46. Brunning, J. and L. J. Stief, 1985, J. Chem. Phys., **83**, 1005-1009.
47. Buben, S. N., I. K. Larin, N. A. Messineva and E. M. Trofimova, 1990, Kinetika i Kataliz, **31**, 973.
48. Burkholder, J. B., P. D. Hammer and C. J. Howard, 1987, J. Phys. Chem., **91**, 2136-2144.

49. Burkholder, J. B., R. L. Mauldin, R. J. Yokelson, S. Solomon and A. R. Ravishankara, 1993, J. Phys. Chem., **97**, 7597-7605.
50. Burkholder, J. B. and A. R. Ravishankara, 2000, J. Phys. Chem. A, **104**, 6752-6757.
51. Burrows, J. P., G. S. Tyndall and G. K. Moortgat, 1985, J. Phys. Chem., **89**, 4848-4856.
52. Burrows, J. P., T. J. Wallington and R. P. Wayne, 1983, J. Chem. Soc. Faraday Trans. 2, **79**, 111-122.
53. Butler, R., I. J. Solomon and A. Snelson, 1978, Chem. Phys. Lett., **54**, 19.
54. Campuzano-Jost, P., A. E. Croce, H. Hippler, M. Siefke, and J. Troe, 1995, J. Chem. Phys., **102**, 5317-5326.
55. Cantrell, C. A., R. E. Shetter, J. G. Calvert, G. S. Tyndall and J. J. Orlando, 1993, J. Phys. Chem., **97**, 9141-9148.
56. Caralp, F. and R. Lesclaux, 1983, Chem. Phys. Lett., **102**, 54-58.
57. Caralp, F., R. Lesclaux and A. M. Dognon, 1986, Chem. Phys. Lett., **129**, 433-438.
58. Caralp, F., R. Lesclaux, M. T. Rayez, J.-C. Rayez and W. Forst, 1988, J. Chem. Soc. Faraday Trans. 2, **84**, 569-585.
59. Caralp, F., M-T. Rayez, W. Forst, N. Gomez, B. Delcroix, D. Fitschen and P. Devolder, 1998, J. Chem. Soc., Faraday Trans., **94**, 3321-3330.
60. Carleton, K. J., W. J. Kessler and W. J. Marinelli, 1993, J. Phys. Chem., **97**, 6412-6417.
61. Chan, W. H., W. M. Uselman, J. G. Calvert and J. H. Shaw, 1977, Chem. Phys. Lett., **45**, 240.
62. Chang, J. S., A. C. Baldwin and D. M. Golden, 1979, Chem. Phys., **71**, 2021.
63. Chegodaev, P. P. and B. I. Tubikov, 1973, Dokl. Akad. Nauk. SSSR, **210**, 647-649.
64. Chen, H. L., D. W. Trainor, R. E. Center and W. T. Fyfe, 1977, J. Chem. Phys., **66**, 5513.
65. Chen, J., V. Young, T. Zhu and H. Niki, 1993, J. Phys. Chem., **97**, 11696-11698.
66. Christensen, L. E., M. Okumura, S. P. Sander, R. R. Friedl, C. E. Miller and J. J. Sloan, 2004, J. Phys. Chem. A, **108**, 80-91.
67. Christensen, L. E., M. Okumura, S. P. Sander, R. J. Salawitch, G. C. Toon, B. Sen, J.-F. Blavier and K. W. Jucks, 2002, Geophys. Res. Let., **29**, 1029/2001GL014525.
68. Clark, T. C., M. A. A. Clyne and D. H. Stedman, 1966, Trans. Faraday Soc., **62**, 3354.
69. Cobos, C. J., H. Hippler, K. Luther, A. R. Ravishankara and J. Troe, 1985, J. Phys. Chem., **89**, 4332-4338.
70. Cobos, C. J., H. Hippler and J. Troe, 1985, J. Phys. Chem., **89**, 342-349.
71. Colussi, A. J., 1990, J. Phys. Chem., **94**, 8922-8926.
72. Colussi, A. J., S. P. Sander and R. R. Friedl, 1992, J. Phys.Chem., **96**, 4442-4445.
73. Connell, P. S. and H. S. Johnston, 1979, Geophys. Res. Lett., **6**, 553-556.
74. Cooper, R., J. B. Cumming, S. Gordon and W. A. Mulac, 1980, Radiat. Phys. Chem., **16**, 169.
75. Cox, R. A., 1975, Int. J. Chem. Kinet. Symp., **1**, 379.
76. Cox, R. A., J. P. Burrows and G. B. Coker, 1984, Int. J. Chem. Kinet., **16**, 445-67.
77. Cox, R. A. and R. G. Derwent, 1979, J. Chem. Soc. Far. Trans. 1, **75**, 1635-1647.
78. Cox, R. A., R. G. Derwent and P. M. Holt, 1976, J. Chem. Soc. Faraday Trans. 1, **72**, 2031.
79. Cox, R. A. and G. D. Hayman, 1988, Nature, **332**, 796-800.
80. Cox, R. A. and R. Lewis, 1979, J. Chem. Soc. Faraday Trans. 1, **75**, 2649-2661.
81. Cox, R. A., J. Munk, O. J. Nielsen, P. Pagsberg and E. Ratajczak, 1990, Chem. Phys. Lett., **173**, 206-210.
82. Cox, R. A. and R. Patrick, 1979, Int. J. Chem. Kinet., **11**, 635-648.
83. Croce de Cobos, A. E., H. Hippler and J. Troe, 1984, J. Phys. Chem., **88**, 5083-5086.
84. Croce de Cobos, A. E. and J. Troe, 1984, Int. J. Chem. Kinet., **16**, 1519-1530.
85. D'Ottone, L., P. Campuzano-Jost, D. Bauer and A. J. Hynes, 2001, J. Phys. Chem. A, **105**, 10538-10543.
86. Daele, V., G. Laverdet, G. Le Bras and G. Poulet, 1995, J. Phys. Chem., **99**, 1470-1477.
87. Daele, V., A. Ray, I. Vassali, G. Poulet and G. Le Bras, 1995, Int. J. Chem. Kinet., **27**, 1121-1133.
88. Danis, F., F. Caralp, J. Masanet and R. Lesclaux, 1990, Chem. Phys. Lett., **167**, 450.
89. Danis, F., F. Caralp, M. Rayez and R. Lesclaux, 1991, J. Phys. Chem., **95**, 7300-7307.
90. Dasch, W., K.-H. Sternberg and R. N. Schindler, 1981, Ber. Bunsenges. Phys. Chem., **85**, 611-615.
91. Davidson, J. A., C. A. Cantrell, R. E. Shetter, A. H. McDaniel and J. G. Calvert, 1990, J. Geophys. Res., **95**, 13963-13969.
92. Davis, D. D., S. Fischer, R. Schiff, R. T. Watson and W. Bollinger, 1975, J. Chem. Phys., **63**, 1707.
93. Davis, H. F., B. Kim, H. S. Johnston and Y. T. Lee, 1993, J. Phys. Chem., **97**, 2172-2180.
94. Daykin, E. P. and P. H. Wine, 1990, J. Phys. Chem., **94**, 4528-4535.
95. DeMore, W. B., 1984, Int. J. Chem. Kinet., **16**, 1187-1200.
96. DeMore, W. B. and E. Tschuikow-Roux, 1990, J. Phys. Chem., **94**, 5856-5860.
97. Destriau, M. and J. Troe, 1990, Int. J. Chem. Kinet., **22**, 915-934.
98. Diau, E. W.-G. and Y.-P. Lee, 1992, J. Chem. Phys., **96**, 377-386.
99. Diaz-de-Mera, Y., A. Aranda, D. Rodriguez, R. López, B. Cabañas and E. Martinez, 2002, J. Phys. Chem. A, **106**, 8627-8633.

100. Dixon, D. A. and K. O. Christie, 1992, J. Phys. Chem., **95**, 1018-1021.
101. Dobe, S., G. Lendvay, I. Szilagyi and T. Berces, 1994, Int. J. Chem. Kinet., **26**, 887-901.
102. Donahue, N., 2001, personal communication.
103. Donahue, N. M., M. K. Dubey, R. Mohrschladt, K. Demerjian and J. G. Anderson, 1997, J. Geophys. Res., **102**, 6159-6168.
104. Dransfield, T. J., K. K. Perkins, N. M. Donahue, J. G. Anderson, M. M. Sprengnether and K. Demerjian, 1999, Geophys. Res. Lett., **26**, 687-690.
105. Dreier, T. and J. Wolfrum. In *18th International Symposium on Combustion*; The Combustion Institute, 1980; pp 801-809.
106. Elfers, G., F. Zabel and K. H. Becker, 1990, chem. Phys. Lett., **168**, 14-19.
107. Ellerman, T., J. Sehested, O. J. Nielson, P. Pagsberg, T. J. Wallington, 1994, Chem. Phys. Lett., **218**, 287-294.
108. Erler, K., D. Field, R. Zellner and I. W. M. Smith, 1977, Ber. Bunsenges. Phys. Chem., **81**, 22.
109. Estupiñán, E. G., J. M. Nicovich, J. Li, D. M. Cunnold, and P. H. Wine, 2002, J. Phys. Chem. A, **106**, 5880-5890.
110. Fagerstrom, K., A. Lund, G. Mahmound, J. T. Jodkowski and E. Ratajczak, 1994, Chem. Phys. Lett., **224**, 43-50.
111. Fasano, D. M. and N. S. Nogar, 1983, J. Chem. Phys., **78**, 6688-6694.
112. Fenter, F. F., P. D. Lightfoot, F. Caralp, R. Lesclaux, J. T. Niranen and D. Gutman, 1993, J. Phys. Chem., **97**, 4695-4703.
113. Fenter, F. F., P. D. Lightfoot, J. T. Niranen and D. Gutman, 1993, J. Phys. Chem., **97**, 5313-5320.
114. Fitschen, C., A. Frenzel, K. Imrik, and P. Devolder, 1999, Int. J. Chem. Kinet., **31**, 860-866.
115. Fockenberg, C., H. Somnitz, G. Bednarek and R. Zellner, 1997, Ber. Bunsenges. Phys. Chem., **101**, 1411-1420.
116. Forst, W., and F. Caralp, 1991, J. Chem. Soc., Faraday Trans., **87**, 2307-2315.
117. Forst, W., and F. Caralp, 1992, J. Phys. Chem., **96**, 6291-6298.
118. Forster, R., M. Frost, D. Fulle, H. F. Hamann, H. Hippler, Schlepegreli and J. Troe, 1995, J. Chem. Phys., **103**, 2949-2958.
119. Forte, E., H. Hippler and H. van den Bergh, 1981, Int. J. Chem. Kinet., **13**, 1227-1233.
120. Fowles, M., D. N. Mitchell, J. W. L. Morgan and R. P. Wayne, 1982, J. Chem. Soc. Faraday Trans. 2, **78**, 1239-1248.
121. Friedl, R. R., S. P. Sander and Y. L. Yung, 1992, J. Phys. Chem., **96**, 7490-7493.
122. Frost, M. J. and I. W. M. Smith, 1990, J. Chem. Soc. Farad. Trans., **86**, 1751-1756.
123. Frost, M. J. and I. W. M. Smith, 1990, J. Chem. Soc. Farad. Trans., **86**, 1757-1762.
124. Frost, M. J. and I. W. M. Smith, 1993, J. Chem. Soc. Faraday Trans, **89**, 4251.
125. Fulle, D., H. F. Hamann, H. Hippler and C. P. J nsch, 1997, Ber. Bunsenges. Phys. Chem., **101**, 1433-1442.
126. Fulle, D., H. F. Hamann, H. Hippler and J. Troe, 1996, J. Chem. Phys., **105**, 1001-1006.
127. Fulle, D. H., H. F. Hamann, H. Hippler and J. Troe, 1998, J. Chem. Phys., **108**, 5391-5397.
128. Gaedtke, H. K., H. Hippler, K. Luther, and J. Troe. "14th International Symposium On Combustion", 1973, Pittsburgh, PA, 295-303.
129. Gleason, J. F., F. L. Nesbitt and L. J. Stief, 1994, J. Phys. Chem., **98**, 126-131.
130. Golden, D. M., 2003, Int. J. Chem. Kinet., **35**, 206-211.
131. Golden, D. M., 2005, Int. J. Chem. Kinet., Accepted.
132. Golden, D. M., J. R. Barker, and L. L. Lohr, 2003, J. Phys. Chem. A, **107**, 11057-11071.
133. Golden, D. M. and J. P. Smith, 2000, J. Phys. Chem. A, **104**, 3991-3997.
134. Green, T. J., M. Islam, P. Guest, K. Hickson, C. E. Canosa-Mas, and R. P. Wayne, 2003, Phys. Chem. Chem. Phys., **5**, 5409-5418.
135. Greiner, N. R., 1970, J. Chem. Phys., **53**, 1284-1285.
136. Grosjean, D., E. Grosjean and E. L. Williams, 1994, J. Air and Waste Manage. Assoc., **44**, 391-396.
137. Gross, A. and G. D. Billing, 1997, Chem. Phys., **217**, 1-18.
138. Hahn, J., K. Luther and J. Troe, 2000, Phys. Chem. Chem. Phys., **2**, 5098-5104.
139. Handwerk, V. and R. Zellner, 1984, Ber. Bunsenges. Phys. Chem., **88**, 405.
140. Harris, G. W. and R. P. Wayne, 1975, J. Chem. Soc. Faraday Trans. 1, **71**, 610.
141. Hathorn, B. C. and R. A. Marcus, 2000, J. Chem. Phys., **113**, 9497-9509.
142. Hayman, G. D., J. M. Davies and R. A. Cox, 1986, Geophys. Res. Lett., **13**, 1347-1350.
143. Helmer, M. and J. M. C. Plane, 1993, J. Geophys. Res., **98**, 23207-23222.
144. Hewitt, A. D., K. M. Brahan, G. D. Boone, and S. A. Hewitt, 1996, Int. J. Chem. Kinet., **28**, 763-771.
145. Hippler, H., S. Nasterlack and F. Striebel, 2002, Phys. Chem. Chem. Phys., **4**, 2959-2964.
146. Hippler, H., R. Rahn and J. Troe, 1990, J. Chem. Phys., **93**, 6560.
147. Hippler, H., M. Siefke, H. Stark and J. Troe, 1999, Phys. Chem. Chem. Phys., **1**, 57-61.
148. Hochanadel, C. J., J. A. Ghormley, J. W. Boyle and P. J. Ogren, 1977, J. Phys. Chem., **81**, 3-7.
149. Hofzumahaus, A. and F. Stuhl, 1984, Ber. Bunsenges Phys. Chem., **88**, 557-561.

150. Hölscher, D. and R. Zellner, 2002, Phys. Chem. Chem. Phys., **4**, 1839-1845.
151. Howard, C. J., 1976, J. Chem. Phys., **65**, 4771.
152. Howard, C. J., 1977, J. Chem. Phys., **67**, 5258.
153. Howard, C. J. and K. M. Evenson, 1974, J. Chem. Phys., **61**, 1943.
154. Hsu, K. J., S. M. Anderson, J. L. Durant and F. Kaufman, 1989, J. Phys. Chem., **93**, 1018.
155. Hsu, K. J., J. L. Durant and F. Kaufman, 1987, J. Phys. Chem., **91**, 1895-1899.
156. Huie, R. E., J. T. Herron and D. D. Davis, 1972, J. Phys. Chem., **76**, 2653-2658.
157. Husain, D., J. M. C. Plane and N. K. H. Slater, 1981, J. Chem. Soc. Faraday Trans. 2, **77**, 1949-1962.
158. Hynes, A. J., P. H. Wine and A. R. Ravishankara, 1986, J. Geophys. Res., **91**, 815-820.
159. Ingham, T., D. Bauer, R. Sander, P. J. Crutzen and J. N. Crowley, 1999, J. Phys. Chem. A, **103**, 7199-7209.
160. IUPAC, 1992, J. Phys. Chem. Ref. Data, **21**, 1125-1568.
161. Iyer, R. S., P. J. Rogers and F. S. Rowland, 1983, J. Phys. Chem., **87**, 3799.
162. Jenkin, M. E. and R. A. Cox, 1985, J. Phys. Chem., **89**, 192-199.
163. Johnston, H. S., C. A. Cantrell and J. G. Calvert, 1986, J. Geophys. Res., **91**, 5159-5172.
164. Johnston, H. S., E. D. Morris, Jr. and J. Van den Bogaerde, 1969, J. Am. Chem. Soc., **91**, 7712-7727.
165. Jonah, C. D., W. A. Mulac and P. Zeglinski, 1984, J. Phys. Chem., **88**, 4100-4104.
166. Kaiser, E. W. and T. J. Wallington, 1996, J. Phys. Chem., **100**, 4111-4119.
167. Kaiser, E. W., 1992, Int. J. Chem. Kinet., **24**, 179-189.
168. Kaiser, E. W., 1993, J. Phys. Chem., **97**, 11681-11688.
169. Kaiser, E. W., I. M. Lorkovic and T. J. Wallington, 1990, J. Phys. Chem., **94**, 3352-3354.
170. Kaiser, E. W. and T. J. Wallington, 1998, J. Phys. Chem. A, **102**, 6054-6055.
171. Kaiser, E. W., T. J. Wallington and J. M. Andino, 1990, Chem. Phys. Lett., **168**, 309.
172. Kaiser, E. W., T. J. Wallington and M. D. Hurley, 1995, Int. J. Chem. Kinet., **27**, 205-218.
173. Kajimoto, O. and R. J. Cvetanovic, 1976, J. Chem. Phys., **64**, 1005.
174. Kaye, J. A., 1986, J. Geophys. Res., **91**, 7865-7874.
175. Keiffer, M., M. J. Pilling and M. J. C. Smith, 1987, J. Phys. Chem., **91**, 6028-6034.
176. Kennedy, R. C. and J. B. Levy, 1972, J. Phys. Chem., **76**, 3480-3488.
177. Kim, P., D. I. MacLean and W. G. Valence, 1980, J. Phys. Chem., **84**, 1806.
178. Kircher, C. C., J. J. Margitan and S. P. Sander, 1984, J. Phys. Chem., **88**, 4370-4375.
179. Kirchner, F., A. Mayer-Figge, F. Zabel and K. H. Becker, 1999, Int. J. Chem. Kin., **31**, 127-144.
180. Klais, O., P. C. Anderson and M. J. Kurylo, 1980, Int. J. Chem. Kinet., **12**, 469-490.
181. Klein, T., I. Barnes, K. H. Becker, E. H. Fink and F. Zabel, 1984, J. Phys. Chem., **88**, 5020-5025.
182. Knyazev, V. D., I. J. Kalinovski and I. R. Slagle, 1999, J. Phys. Chem. A, **103**, 3216-3221.
183. KÖppenkastrop, D. and F. Zabel, 1991, Int. J. Chem. Kinet., **23**, 1-15.
184. Kreutter, K. D., J. M. Nicovich and P. H. Wine, 1991, J. Phys. Chem., **95**, 4020.
185. Kuo, C. H. and Y.-P. Lee, 1991, J. Phys. Chem., **95**, 1253.
186. Kurylo, M. J., 1972, J. Phys. Chem., **76**, 3518.
187. Kurylo, M. J. and P. A. Ouellette, 1986, J. Phys. Chem., **90**, 441-444.
188. Kurylo, M. J. and P. A. Ouellette, 1987, J. Phys. Chem., **91**, 3365-3368.
189. Laguna, G. A. and S. L. Baughcum, 1982, Chem. Phys. Lett., **88**, 568-71.
190. Lai, L.-H., Y.-C. Hsu and Y.-P. Lee, 1992, J. Chem. Phys., **97**, 3092-3099.
191. Larin, I. K., D. V. Nevozhai, A. I. Spasskii, and E. M. Trofimova, 1998, Kinetics and Catalysis, **39**, 666-672.
192. Laufer, A. H. and A. M. Bass, 1975, Int. J. Chem. Kinet., **7**, 639.
193. Lee, F. S. C. and F. S. Rowland, 1977, J. Phys. Chem., **81**, 86-87.
194. Lee, J. H., J. V. Michael, W. A. Payne, Jr. and L. J. Stief, 1978, J. Chem. Phys., **68**, 5410-5413.
195. Lee, T. J., 1996, J. Phys. Chem., **100**, 19847-19852.
196. Lee, T. J. and J. E. Rice, 1992, J. Chem. Phys., **97**, 4223-4232.
197. Lee, T. J., C. M. Rohlfing and J. E. Rice, 1992, J. Chem. Phys., **97**, 6593-6605.
198. Lee, Y.-P., R. M. Stimpfle, R. A. Perry, J. A. Mucha, K. M. Evenson, D. A. Jennings and C. J. Howard, 1982, Int. J. Chem. Kinet., **14**, 711-732.
199. Lee, Y.-Y., W. C. Kao and Y.-P. Lee, 1990, J. Phys. Chem., **94**, 4535.
200. Lesar, A., S. Prebil, M. M hlha ser and M. Hodo cek, 2002, Chem. Phys. Lett., **368**, 399-407.
201. Leu, M. T., 1982, J. Phys. Chem., **86**, 4558.
202. Leu, M. T., 1984, Int. J. Chem. Kinet., **16**, 1311-1320.
203. Li, W.-K., and M. L. McKee, 1997, J. Phys. Chem. A, **101**, 9778-9782.
204. Li, Z. and J. S. Francisco, 1989, J. Am. Chem. Soc., **111**, 5660-5667.
205. Lin, C. L. and M. T. Leu, 1982, Int. J. Chem. Kinet., **14**, 417.
206. Liu, A., W. A. Mulac and C. D. Jonah, 1988, J. Phys. Chem., **92**, 5942-5945.
207. Lloyd, A. C., K. R. Darnall, A. M. Winer and J. N. Pitts, Jr., 1976, J. Phys. Chem., **80**, 789.

208. Lovejoy, E. R., 1997, J. Phys. Chem. A, **101**, 4950-4953.
209. Lovejoy, E. R. and D. R. Hanson, 1996, J. Phys. Chem., **100**, 4459-4465.
210. Luther, K., K. Oum and J. Troe, 2001, J. Phys.Chem. A, **105**, 5535-5541.
211. Lyman, J. and R. Holland, 1988, J. Phys. Chem., **92**, 7232-7241.
212. Maguin, F., G. Laverdet, G. Le Bras and G. Poulet, 1992, J. Phys. Chem., **96**, 1775-1780.
213. Maric, D. and J. P. Burrows, 1992, J.Photochem. Photobiol. A: Chem., **66**, 291-312.
214. Maricq, M. M., J. J. Szente and E. W. Kaiser, 1993, J. Phys. Chem., **97**, 7970-7977.
215. Marshall, P., A. S. Narayan and A. Fontijn, 1990, J. Phys. Chem., **94**, 2998.
216. Martin, D., J. L. Jourdain and G. Le Bras, 1985, Int. J. Chem. Kinet., **17**, 1247.
217. Martinez, E., J. Albaladejo, E. Jiménez, A. Notario, and Y. Diaz de Mera, 2000, Chem. Phys. Lett., **329**, 191-.
218. Maurer, T., I. Barnes, and K. H. Becker, 1999, Int. J. Chem. Kinet., **31**, 883-893.
219. McCabe, D. C., T. Gierczak, R. K. Talukdar and A. R. Ravishankara, 2001, Geophys. Res. Lett., **28**, 3135-3138.
220. McCaulley, J. A., S. M. Anderson, J. B. Jeffries and F. Kaufman, 1985, Chem Phys. Lett., **115**, 180.
221. McCaulley, J. A., A. M. Moyle, M. F. Golde, S. M. Anderson and F. Kaufman, 1990, J. Chem Soc. Farad. Trans., **86**, 4001-4009.
222. Mellouki, A., G. Laverdet, J. L. Jourdain and G. Poulet, 1989, Int. J. Chem. Kinet., **21**, 1161.
223. Michael, J. V., M.-C. Su, J. W. Sutherland, J. J. Carroll and A. F. Wagner, 2002, J. Phys. Chem. A, **106**, 5297-5313.
224. Michael, J. V., D. F. Nava, R. P. Borkowski, W. A. Payne and L. J. Stief, 1980, J. Chem. Phys., **73**, 6108.
225. Miller, J. A., and S. J. Klippenstein, 2001, Int. J. Chem. Kinet., **33**, 654-668.
226. Mineshos, G. and S. Glavas, 1991, React. Kinet. Catal. Lett., **45**, 305-312.
227. Miyoshi, A., H. Matsui and N. Washida, 1994, J. Chem. Phys., **100**, 3532-3539.
228. Molina, M. J., L. T. Molina and T. Ishiwata, 1980, J. Phys. Chem., **84**, 3100-3104.
229. Moore, S. B. and R. W. Carr, 1990, J. Phys. Chem., **94**, 1393.
230. Morley, C. and I. W. M. Smith, 1972, J. Chem. Soc. Faraday Trans., **68**, 1016.
231. Morris, E. D., D. H. Stedman and H. Niki, 1971, J. Am. Chem. Soc., **93**, 3570.
232. M ller, M. A., R. A. Yetter, and F. L. Dryer, 2000, Int. J. Chem. Kinet., **32**, 317-339.
233. Naidoo, J., A. Goumri, and P. Marshall. Proceedings of the Combustion Institute, 2005; Vol. 30; pp 1219-1225.
234. Nakano, Y., M. Goto, S. Hashimoto, M. Kawasaki, and T. J. Wallington, 2001, J. Phys. Chem. A, **105**, 11045-11050.
235. Nicholas, J. E. and R. G. W. Norrish, 1968, Proc. Roy. Soc. A, **307**, 391.
236. Nickolaisen, S. L., R. R. Friedl and S. P. Sander, 1994, J. Phys. Chem., **98**, 155-169.
237. Nicovich, J. M., K. D. Kreutter, C. J. Shackelford and P. H. Wine, 1991, Chem. Phys. Lett., **179**, 367-373.
238. Nicovich, J. M., K. D. Kreutter and P. H. Wine, 1990, J. Chem. Phys., **92**, 3539-3544.
239. Nicovich, J. M. and P. H. Wine, 1990, Int. J. Chem. Kinet., **22**, 379-397.
240. Nicovoch, J. M., S. Wang, M. L. McKee and P. H. Wine, 1996, J. Phys. Chem., **100**, 680-688.
241. Niki, H., P. D. Maker, C. M. Savage and L. P. Breitenbach, 1978, Chem. Phys. Lett., **59**, 78.
242. Niki, H., P. D. Maker, C. M. Savage and L. P. Breitenbach, 1984, J. Phys. Chem., **88**, 2116-2119.
243. Nizkorodov, S. A. and P. O. Wennberg, 2002, J. Phys. Chem. A, in press.
244. Nottingham, W. C., R. N. Rudolph, K. P. Andrews, J. H. Moore and J. A. Tossell, 1994, Int. J. Chem. Kinet., **26**, 749-756.
245. Ohmori, K., K. Yamasaki and H. Matsui, 1993, Bull. Chem. Soc. Jpn., **66**, 51-56.
246. Orlando, J. J. and J. B. Burkholder, 2000, J. Phys.Chem. A, **104**, 2048-2053.
247. Orlando, J. J. and G. S. Tyndall, 1996, J. Phys. Chem., **100**, 19398-19405.
248. Orlando, J. J., G. S. Tyndall and J. G. Calvert, 1992, Atmos. Environ., **26A**, 3111-3118.
249. Orlando, J. J., G. S. Tyndall, C. A. Cantrell and J. G. Calvert, 1991, J. Chem. Soc. Far. Trans., **87**, 2345-2349.
250. Overend, R. P. and G. Paraskevopoulos, 1977, J. Chem. Phys., **67**, 674.
251. Overend, R. P. and G. Paraskevopoulos, 1977, Chem. Phys. Lett., **49**, 109.
252. Overend, R. P., G. Paraskevopoulos and C. Black, 1976, J. Chem. Phys., **64**, 4149.
253. Pagsberg, P., E. Bjergbakke, E. Ratajczak and A. Sillesen, 1997, Chem. Phys. Lett., **272**, 383-390.
254. Pagsberg, P., A. Sillesen, J. T. Jodowski and E. Ratajczak, 1996, Chem. Phys. Lett., **249**, 358-364.
255. Pagsberg, p., A. Sillesen, J. T. Jodowski and E. Ratajczak, 1996, Chem. Phys. Lett., **252**, 165-171.
256. Pagsberg, P., B. Sztuba, E. Ratajczak and A. Sillesen, 1991, Acta Chem. Scand., **45**, 329.
257. Pagsberg, P. B., E. Ratajczak, A. Sillesen and J. T. Jodkowski, 1987, Chem. Phys. Lett., **141**, 88-94.
258. Paraskevopoulos, G. and R. S. Irwin. XV Informal Conference on Photochemistry, 1982, Stanford, CA,
259. Paraskevopoulos, G. and R. S. Irwin, 1984, J. Chem. Phys., **80**, 259-266.
260. Paraskevopoulos, G., D. L. Singleton and R. S. Irwin, 1983, Chem. Phys. Lett., **100**, 83-87.
261. Parr, A. D., R. P. Wayne, G. D. Hayman, M. E. Jenkin and R. A. Cox, 1990, Geophys. Res. Lett., **17**, 2357-2360.
262. Parthiban, P. and T. Lee, 1998, J. Chem. Phys., **109**, 525-530.

263. Parthiban, S., T. J. Lee, S. Guha, and J. S. Francisco, 2003, J. Amer. Chem. Soc., **125**, 10446-10458.
264. Pastrana, A. V. and R. W. Carr, Jr., 1974, Int. J. Chem. Kinet., **6**, 587.
265. Patrick, R. and D. M. Golden, 1983, Int. J. Chem. Kinet., **15**, 1189-1227.
266. Percival, C. J., G. D. Smith, L. T. Molina and M. J. Molina, 1997, J. Phys. Chem. A, **101**, 8830-8833.
267. Percival, D. T. R.-D., A. Bacak, A. Bardwell. In *International Gas Kinetics Symposium*; Bristol, UK, 2004.
268. Perry, R. A., R. Atkinson and J. N. Pitts, Jr., 1977, J. Chem. Phys., **67**, 5577.
269. Perry, R. A. and D. Williamson, 1982, Chem. Phys. Lett., **93**, 331-334.
270. Pilling, M. J. and M. J. C. Smith, 1985, J. Phys. Chem., **89**, 4713-4720.
271. Pirraglia, A. N., J. V. Michael, J. W. Sutherland and R. B. Klemm, 1989, J. Phys. Chem., **93**, 282-291.
272. Plane, J. M. C. and B. Rajasekhar, 1989, J. Phys. Chem., **93**, 3135-3140.
273. Plumb, I. C. and K. R. Ryan, 1982, Int. J. Chem. Kinet., **14**, 861-874.
274. Pollack, I. B., I. M. Konen, E. X. J. Li, and M. I. Lester, 2003, J. Chem. Phys., **119**, 9981-9984.
275. Poulet, G., J. Barassin, G. Le Bras and J. Combourieu, 1973, Bull. Soc. Chim. Fr., **1**, 1.
276. Pratt, G. L. and S. W. Wood, 1984, J. Chem. Soc. Faraday Trans. 1, **80**, 3419-3427.
277. Ravishankara, A. R., F. L. Eisele and P. H. Wine, 1980, J. Chem. Phys., **73**, 3743.
278. Ravishankara, A. R., G. J. Smith and D. D. Davis, 1988, Int. J. Chem. Kinet., **20**, 811-814.
279. Ravishankara, A. R. and R. L. Thompson, 1983, Chem. Phys. Lett., **99**, 377.
280. Rawlins, W. T., G. E. Caledonia and R. A. Armstrong, 1987, J. Chem. Phys., **87**, 5209-5213.
281. Rayez, M. T. and M. Destriau, 1993, Chem. Phys. Lett., **206**, 278-284.
282. Resende, S. M. and W. B. D. Alemeida, 1999, J. Phys. Chem. A, **103**, 4191-4195.
283. Resende, S. M. and W. B. D. Almeida, 1997, J. Phys. Chem. A, **101**, 9738-9744.
284. Roberts, J. M. and S. B. Bertman, 1992, Int. J. Chem. Kinet., **24**, 297-307.
285. Russell, A. G., G. R. Cass and J. H. Seinfeld, 1986, Environ. Sci. Technol., **20**, 1167-1172.
286. Russell, J. J., J. A. Setula, D. Gutman, F. Danis, F.Caralp, P. D. Lightfoot, R. Lesclaux, C. F. Melius and S. M. Senkan, 1990, J. Phys. Chem., **94**, 3277-3283.
287. Ryan, K. R. and I. C. Plumb, 1982, J. Phys. Chem., **86**, 4678-4683.
288. Ryan, K. R. and I. C. Plumb, 1984, Int. J. Chem. Kinet., **16**, 591-602.
289. Sander, S. P., B. J. Finlayson-Pitts, R. R. Friedl, D. M. Golden, R. E. Huie, C. E. Kolb, M. J. Kurylo, M. J. Molina, G. K. Moortgat, V. L. Orkin and A. R. Ravishankara "Chemical Kinetics and Photochemical Data for Use in Atmospheric Studies, Evaluation Number 14," JPL Publication 02-25, Jet Propulsion Laboratory, Pasadena, 2002.
290. Sander, S. P., R. P. Friedl and Y. L. Yung, 1989, Science, **245**, 1095-1098.
291. Sander, S. P. and M. Peterson, 1984, J. Phys. Chem., **88**, 1566-1571.
292. Sander, S. P., G. W. Ray and R. T. Watson, 1981, J. Phys. Chem., **85**, 199.
293. Sander, S. P. and R. T. Watson, 1980, J. Phys. Chem., **84**, 1664.
294. Savarino, J. and M. Thiemens, 1999, J. Phys. Chem. A, **103**, 9221-9229.
295. Schieferstein, M., K. Kohse-HÖinghaus and F. Stuhl, 1983, Ber. Bunsenges. Phys. Chem., **87**, 361-366.
296. Schurath, U. and V. Wipprecht. 1st European Symposium on Physico-Chemical Behavior of Atmospheric Pollutants, 1979, Ispra, 157-166.
297. Seefeld, S., D. J. Kinnison and J. A. Kerr, 1997, J. Phys. Chem. A, **101**, 55-59.
298. Seeley, J. V., J. T. Jayne and M. J. Molina, 1996, J. Phys. Chem., **100**, 4019-4025.
299. Sehested, J., L. K. Christensen, T. Mogelberg, O. J. Nielsen, T. J. Wallington, A. Guschin, J. J. Orlando and G. S. Tyndall, 1998, J. Phys. Chem. A, **102**, 1779-1789.
300. Selzer, E. A. and K. D. Bayes, 1983, J. Phys. Chem., **87**, 392-394.
301. Senosiain, J. P., C. B. Musgrave and D. M. Golden, 2003, Int. J. Chem. Kinet., **35**, 464-474.
302. Senosiain, J. P., S. J. Klippenstein and J. A. Miller, 2005, J. Phys. Chem. A, submitted.
303. Shamonina, N. F. and A. G. Kotov, 1979, Kinet. i Kataliz., **20**, 233.
304. Sharkey, P., I. R. Sims, I. W. M. Smith, P. Bocherl and B. R. Rowe, 1994, J. Chem. Soc. Far. Trans., **90**, 3609-3616.
305. Shen, G., M. Suto and L. C. Lee, 1990, J. Geophys. Res., **95**, 13981-13984.
306. Sheng, C. Y., J. W. Bozzelli, A. M. Dean, and A. Y. Chang, 2002, J. Phys. Chem. A, **106**, 7276-7293.
307. Silver, J. A., M. S. Zahniser, A. C. Stanton and C. E. Kolb. In *20th International Symposium on Combustion* Pittsburgh, PA, 1984; pp 605-612.
308. Simonaitis, R. and J. Heicklen, 1978, Int. J. Chem. Kinet., **10**, 67-87.
309. Skolnik, E. D., M. G. Veysey, M. G. Ahmed and W. E. Jones, 1975, Can. J. Chem., **53**, 3188.
310. Slanina, Z. and F. Uhlik, 1991, Chem. Phys. Lett., **182**, 51-56.
311. Smith, C. A., A. R. Ravishankara and P. H. Wine, 1985, J. Phys. Chem., **89**, 1423-1427.
312. Smith, G. P., P. W. Fairchild and D. R. Crosley, 1984, J. Chem. Phys., **81**, 2667.
313. Smith, I. W. M. and D. J. Wrigley, 1980, Chem. Phys. Lett., **70**, 481.

314. Smith, I. W. M. and D. J. Wrigley, 1981, Chem. Phys., **63**, 321.
315. Smith, I. W. M. and R. Zellner, 1973, J. Chem. Soc. Faraday Trans. 2, **69**, 1617.
316. Sørensen, M., E. W. Kaiser, M. D. Hurley, T. J. Wallington and O. J. Nielsen, 2003, Int. J. Chem. Kinet., **35**, 191-197.
317. Stanton, J. F., C. M. L. Rittby, R. J. Bartlett and D. W. Toohey, 1991, J. Phys. Chem., **95**, 2107-2110.
318. Stickel, R. E., J. M. Nicovich, S. Wang, Z. Zhao and P. H. Wine, 1992, J. Phys. Chem., **96**, 9875-9883.
319. Stuhl, F. and H. Niki, 1972, J. Chem. Phys., **57**, 3677-3679.
320. Stutz, J., M. J. Ezell and B. J. Finlayson-Pitts, 1997, J. Phys. Chem. A, **101**, 9187-9190.
321. Thorn, R. P., E. P. Daykin and P. H. Wine, 1993, Int J. Chem. Kinet., **25**, 521-537.
322. Thuner, L. P., I. Barnes, K. H. Becker, T. J. Wallington, L. K. Christensen, J. J. Orlando and B. Ramacher, 1999, J. Phys.Chem. A, **103**, 8657-8663.
323. Trainor, D. W. and C. W. von Rosenberg, Jr., 1974, J. Chem. Phys., **61**, 1010-1015.
324. Troe, J., 1977, J. Chem. Phys., **66**, 4745.
325. Troe, J., 2001, Proc. Combust. inst., **28**, 1463-1469.
326. Troe, J., 2004, Chem. Rev., **104**, 4565-4576.
327. Trolier, M., R. L. Mauldin, III and A. R. Ravishankara, 1990, J. Phys. Chem., **94**, 4896-4907.
328. Tully, F. P., 1983, Chem. Phys. Lett., **96**, 148-153.
329. Turnipseed, A. A., S. B. Barone, N. R. Jensen, D. R. Hanson, C. J. Howard and A. R. Ravishankara, 1995, J. Phys. Chem., **99**, 6000-6009.
330. Urbanski, S. P. and P. H. Wine, 1999, J. Phys. Chem. A, **103**, 10935-10944.
331. Vakhtin, A. B., J. E. Murphy and S. R. Leone, 2003, J. Phys. Chem. A., **107**, 10055-10062.
332. Van den Bergh, H., N. Benoit-Guyot and J. Troe, 1977, Int. J. Chem Kinet., **9**, 223-234.
333. Van den Bergh, H. and J. Troe, 1976, J. Chem. Phys., **64**, 736-742.
334. Van den Bergh, H. E. and A. B. Callear, 1971, Trans. Faraday Soc., **67**, 2017.
335. Viggiano, A. A., J. A. Davidson, F. C. Fehsenfeld and E. E. Ferguson, 1981, J. Chem. Phys., **74**, 6113-6125.
336. Vinckier, C., A. Dumoulin and S. DeJaegere, 1991, J. Chem. Soc. Faraday Trans., **87**, 1075-1081.
337. von Ahsen, S., H. Wilner and J. S. Francisco, 2004, J. Chem. Phys., **121**, 2048-2057.
338. Wagner, A. F., I. R. Slagle, D. Sarzynski and D. Gutman, 1990, J. Phys. Chem., **94**, 1853-1864.
339. Walker, R. W. In *Ph.D. Thesis*; Queen Mary College University of London, 1972.
340. Wallington, T. J., J. M. Andino, I. M. Lorkovic, E. W. Kaiser and G. Marston, 1990, J. Phys. Chem., **94**, 3644-3648.
341. Wallington, T. J., J. M. Andino, A. R. Potts and P. H. Wine, 1991, Chem. Phys. Lett., **176**, 103-108.
342. Wallington, T. J., R. Atkinson, A. M. Winer and J. N. Pitts, Jr., 1987, Int. J. Chem. Kinet., **19**, 243-249.
343. Wallington, T. J. and J. C. Ball, 1995, J. Phys. Chem., **99**, 3201-3205.
344. Wallington, T. J. and R. A. Cox, 1986, J. Chem. Soc. Faraday Trans. 2, **82**, 275-289.
345. Wallington, T. J., T. Ellerman, O. J. Nielsen and J. Sehested, 1994, J. Phys. Chem., **98**, 2346.
346. Wallington, T. J., T. Ellermann and O. J. Nielsen, 1993, J. Phys. Chem., **97**, 8442-8449.
347. Wallington, T. J., M. M. Mariq, T. Ellerman and O. J. Nielsen, 1992, J. Phys. Chem., **96**, 982-986.
348. Wallington, T. J. and O. J. Nielsen, 1991, Int. J. Chem. Kinet., **23**, 785-798.
349. Wallington, T. J., L. M. Skewes and W. O. Siegl, 1988, J. Photochem. Photobiol. A, **45**, 167.
350. Wallington, T. J., L. M. Skewes, W. O. Siegl, C. H. Wu, S. M. Japar, 1988, Int. J. Chem. Kinet., **20**, 867-875.
351. Wang, D., and D. L. Phillips, 2002, Chem. Phys. Lett., **362**, 205-209.
352. Washida, N., 1980, J. Chem. Phys., **73**, 1665.
353. Washida, N. and K. D. Bayes, 1976, Int. J. Chem. Kinet., **8**, 777.
354. Westenberg, A. A. and N. de Haas, 1972, J. Chem. Phys., **57**, 5375-5378.
355. Whytock, D. A., J. V. Michael and W. A. Payne, 1976, Chem. Phys. Lett., **42**, 466-471.
356. Wilson, W. E. and A. A. Westenberg. In *11th Symposium on Combustion*; The Combustion Institute, Pittsburgh, 1967; pp 1143.
357. Wine, P. H., N. M. Kreutter and A. R. Ravishankara, 1979, J. Phys. Chem., **83**, 3191.
358. Wine, P. H., J. M. Nicovich, R. E. Stickel, Z. Zhao, C. J. Shackelford, K. D. Kreutter, E. P. Daykin and S. Wang *The Tropospheric Chemistry of Ozone in the Polar Regions*; Springer-Verlag: Berlin, 1993; Vol. 17.
359. Wine, P. H., R. J. Thompson, A. R. Ravishankara, D. H. Semmes, C. A. Gump, A. Torabi and J. M. Nicovich, 1984, J. Phys. Chem., **88**, 2095.
360. Wolf, S., M. Bitter, D. Krankowsky and K. Mauersberger, 2000, J. Chem. Phys., **113**, 2684-2686.
361. Wollenhaupt, M. and J. N. Crowley, 2000, J. Phys. Chem. A, **104**, 6429-6438.
362. Wong, W. D. and D. Davis, 1974, Int. J. Chem. Kinet., **6**, 401.
363. Wu, F. and R. W. Carr, 1991, Int. J. Chem. Kinet., **23**, 701-715.
364. Xiong, J. Q. and R. W. Carr, 1994, J. Phys. Chem., **98**, 9811-9822.
365. Yarwood, G., J. W. Sutherland, M. A. Wickramaaratchi and R. B. Klemm, 1991, J. Phys. Chem., **95**, 8771-8775.

366. Zabarnick, S., 1993, Chem Phys., **171**, 265-273.
367. Zabel, F., A. Reimer, K. H. Becker and E. H. Fink, 1989, J. Phys. Chem., **93**, 5500-5507.
368. Zahniser, M. S., J. Chang and F. Kaufman, 1977, J. Chem. Phys., **67**, 997-1003.
369. Zellner, R., F. Ewig, R. Paschke and G. Wagner, 1988, J. Phys. Chem., **92**, 4184-4190.
370. Zellner, R. and K. Lorenz, 1984, J. Phys. Chem., **88**, 984-989.
371. Zetzsch, C. European Symposium on Combustion, 1973, 35.
372. Zhu, R., C.-C. Hsu and M. C. Lin, 2001, J. Chem. Phys., **115**, 195-203.
373. Zhu, R. S., and M. C. Lin, 2003, J. Chem. Phys., **118**, 4094-4106.
374. Zhu, R. S. and M. C. Lin, 2002, J. Phys. Chem., A, **106**, 8386-8390.
375. Zhu, R. S. and M. C. Lin, 2003, J. Chem. Phys., **118**, 8645-8655.
376. Zhu, R. S. and M. C. Lin, 2003, J. Chem. Phys., **119**, 2075-2082.
377. Zhu, T., G. Yarwood, J. Chen and H. Niki, 1994, J. Phys. Chem., **98**, 5065-5067.
378. Zou, P., A. Derecskei-Kovacs and S. W. North, 2003, J. Phys. Chem. A, **107**, 888-896.

SECTION 3. EQUILIBRIUM CONSTANTS

Table of Contents

SECTION 3. EQUILIBRIUM CONSTANTS 3-1
3.1 Format 3-1
3.2 Definitions 3-1
3.3 Notes to Table 3 3-3
3.4 References 3-6

Tables

Table 3-1. Equilibrium Constants 3-2

3.1 Format

Some of the three-body reactions in Table 2 form products that are thermally unstable at atmospheric temperatures. In such cases the thermal decomposition reaction may compete with other loss processes, such as photodissociation or radical attack. Table 3 lists the equilibrium constants, K(T), for several reactions which may fall into this category. The table has three column entries, the first two being the parameters A and B which can be used to express K(T):

$$K(T)/cm^3\ molecule^{-1} = A\ \exp(B/T)\ (200 < T < 300\ K)$$

The third column entry in Table 3 is the calculated value of K at 298 K.

The data sources for K(T) are described in the individual notes to Table 3.

3.2 Definitions

When values of the heats of formation and entropies of all species are known at the temperature T, we note that:

$$\log_{10}\left[K(T)\ /\ cm^3 molecule^{-1}\right] = \frac{\Delta S_T^o}{2.303R} - \frac{\Delta H_T^o}{2.303RT} + \log_{10}(T) - 21.87$$

Where the superscript "o" refers to a standard state of one atmosphere. In some cases K values were calculated from this equation, using thermochemical data. In other cases the K values were calculated directly from kinetic data for the forward and reverse reactions. When available, JANAF values were used for the equilibrium constants. The following equations were then used to calculate the parameters A and B:

$$B/^\circ K = 2.303\left[\frac{(300\times 200)}{(300\text{-}200)}\right]\log_{10}\left(\frac{K_{200}}{K_{300}}\right) = 1382\log_{10}\left(\frac{K_{200}}{K_{300}}\right)$$

$$\log_{10}(A) = \log_{10}(K(T)) - \frac{B}{2.303\ T}$$

The relationships between the parameters A and B and the quantities ΔS^o(298 K) and ΔH^o(298 K) are:

$$A = \frac{eR'T}{N_{av}}\exp\left(\frac{\Delta S^o}{R}\right) = 3.7\text{x}10^{-22}T\exp\left(\frac{\Delta S^o}{R}\right)$$

where $R' = 82.1\ cm^3\ atm\ mole^{-1}K^{-1}$, and $N_{av} = 6.02 \times 10^{23}$ molecule mole^{-1} and

$$B/^\circ K = -\left[\frac{\Delta H^o + RT}{R}\right]$$

Table 3-1. Equilibrium Constants

Reaction	A/cm^3 molecule^{-1}	B/°K	K_{eq}(298 K)	f(298 K)[a]	g	Note
$HO + NO_2 \rightarrow HOONO$	3.9×10^{-27}	10125	2.2×10^{-12}	2	-400	1
$HO_2 + NO_2 \rightarrow HO_2NO_2$	2.1×10^{-27}	10900	1.6×10^{-11}	1.3	100	2
$NO + NO_2 \rightarrow N_2O_3$	3.3×10^{-27}	4667	2.1×10^{-20}	2	100	3
$NO_2 + NO_2 \rightarrow N_2O_4$	5.9×10^{-29}	6643	2.8×10^{-19}	1.4	100	4
$NO_2 + NO_3 \rightarrow N_2O_5$	2.7×10^{-27}	11000	2.9×10^{-11}	1.2	100	5
$CH_3O_2 + NO_2 \rightarrow 3CH_3O_2NO_2$	9.5×10^{-29}	11234	2.2×10^{-12}	1.3	500	6
$CH_3C(O)O_2 + NO_2 \rightarrow CH_3C(O)O_2NO_2$	9.0×10^{-29}	14000	2.3×10^{-8}	1.2	200	7
$CH_3CH_2C(O)O_2 + NO_2 \rightarrow CH_3CH_2C(O)O_2NO_2$	9.0×10^{-29}	14000	2.3×10^{-8}	10	800	8
$CH_3C(O)CH_2 + O_2 \rightarrow CH_3C(O)CH_2O_2$	7×10^{-27}	13000	6×10^{-8}	10	800	9
$F + O_2 \rightarrow FOO$	4.5×10^{-25}	6118	3.7×10^{-16}	1.5	300	10
$Cl + O_2 \rightarrow ClOO$	6.6×10^{-25}	2502	2.9×10^{-21}	1.7	100	11
$Cl + CO \rightarrow ClCO$	3.5×10^{-25}	3730	9.6×10^{-20}	1.2	200	12
$ClO + O_2 \rightarrow ClO{\cdot}O_2$	2.9×10^{-26}	<3700	$<7.2\times10^{-21}$			13
$ClO + ClO \rightarrow Cl_2O_2$	9.3×10^{-28}	8835	7.0×10^{-15}	1.2	300	14
$ClO + OClO \rightarrow Cl_2O_3$	1.6×10^{-27}	7155	4.3×10^{-17}	1.3	300	15
$OClO + NO_3 \rightarrow O_2ClONO_2$	6.6×10^{-29}	3971	4.0×10^{-23}	5.5	500	16
$OH + CS_2 \rightarrow CS_2OH$	4.5×10^{-25}	5140	1.4×10^{-17}	1.4	300	17
$CH_3S + O_2 \rightarrow CH_3SO_2$	1.8×10^{-27}	5545	2.2×10^{-19}	1.4	300	18
$Cl + CS_2 \rightarrow Cl\text{---}CS_2$	1.8×10^{-25}	4982	3.3×10^{-18}	1.3	150	19
$Br+CH_3SCH_3\rightarrow Br\text{---}(CH_3)_2S$	3.4×10^{-25}	3021	4.6×10^{-15}	1.2	100	20

K/cm^3 molecule^{-1} = A exp (B/T) [200 < T/K < 300] – shaded areas indicate changes or additions since JPL02-25

a f(298 K) is the uncertainty factor at 298 K, and g is a measure of the uncertainty in the quantity B. To calculate the uncertainty at temperatures other than 298 K, use the expression:

$$f(T) = f(298\ K)\exp\left[g\left(\frac{1}{T} - \frac{1}{298}\right)\right]$$

3.3 Notes to Table 3

JPL Publication numbers for the most recent revision of the table entry and note are given at the end of each note.

1. $HO + NO_2$. This value is for the HOONO product channel. Using the data from Hippler et al. [37], Golden et al. [30] performed a third law analysis using structures and frequencies from an ab initio quantum calculation at the QCISD(T)/cc-pVDZ level to extract the heat of formation of cis-cis HOONO at 0K of -9.28 kJ mol^{-1}. The value at 298K is -15.7 kJ $mole^{-1}$. (A small error in the entropy of HOONO caused Golden et al. [29] to suggest – 8.60 kJ $mole^{-1}$.) The data covers 430<T/K<475 with 30% uncertainties. The error limits reflect the fact that the uncertainty is greater at 298 K than in the temperature range where the data were taken. NEW ENTRY Back to table

2. $HO_2 + NO_2$. The value was obtained by combining the expression from Table 2-1 for the rate constant of the reaction as written with that from an average of the expressions from Graham et al. [33] and Zabel [72] for the reverse reaction. Values for the entropy and heat of formation of pernitric acid may be extracted. These values are: S(298 K) = 71.7 cal $mole^{-1}$ K^{-1} and ΔH_f(298 K) = –12.9 kcal $mole^{-1}$. If the entropy is calculated from the frequencies and moments of inertia given by Chen and Hamilton [16], the value becomes 71.0 and the heat is –13.1. The values in the Appendix to this report reflect these results. A study of the thermal decomposition of HO_2NO_2 by Gierczak et al. [27] combined with values for the association reaction are in agreement. (Table: JPL06, Note: JPL06) Back to table

3. $NO + NO_2$. The data are from JANAF [41] and Chao et al. [14]. This process is included because a measurement of the rate constant by Smith and Yarwood [63] and Markwalder et al. [44] shows that it is too slow to be an important process in most atmospheric and laboratory systems. (Table: 94-26, Note: 94-26) Back to table

4. $NO_2 + NO_2$. The data are from JANAF [41] and Vosper [68], Chao et al. [15] and Amoruso et al. [1]. Rate data for this process are reported by Brunning et al. [7], Borrell et al. [4] Gozel et al. [31] and Markwalder et al. [44]. A direct study by Harwood and Jones [35] at low temperatures is in agreement with the recommendation. Re-evaluation of the data suggests slightly different error limits than recommended in JPL 02-25. Estupiñán et al. [23], Wollenhaupt and Crowley [71] and Tuchler et al. [65] deduce values that are in essential agreement, within uncertainties, with the recommendation. (Table: 02-25, Note: 02-25) Back to table

5. $NO_2 + NO_3$. The recommendation is from Cantrell et al. [12]. They report rate constants for the decomposition reaction, which they combine with the rate constants of Orlando et al. [53] to obtain the equilibrium constant. Agreement is quite good with the data of Burrows et al. [9] and Cantrell et al. [11] and the room temperature data of Tuazon et al. [64] Perner et al. [56] and Hjorth et al. [38]. An evaluation by Pritchard [59] is also in excellent agreement with the recommendation. Pritchard [59] examined the data of Cantrell et al. [11], Burrows et al. [9], Graham and Johnston [32], Wangberg et al [69], Schott and Davidson [60], and the room temperature data of Tuazon et al. [64], Perner et al. [56] and Hjorth et al. [38]. He also included the values given by Smith et al. [62], and Kircher et al. [42], who combined data on the forward reaction, tabulated in Table 2-1, with decomposition data of by Connell and Johnston [18] and Viggiano et al. [67]. The Pritchard [59] result was used as the basis for the value in JPL 00-3, but some uncertainties in the entropies of NO_3 and N_2O_5 justify the reversion to the JPL 97-4 recommendations. In JPL 02-25, the values of the parameters were inadvertently left unchanged from those in JPL 00-3. The differences are very small. The one sigma error limits are better described with f(298) = 1.2. (Table: JPL06, Note: JPL06) Back to table

6. $CH_3O_2 + NO_2$. Zabel et al. [73] have measured k(dissociation) as a function of pressure (10<P/torr<800) and temperature (253<T/K<272). Bahta et al. [3] have measured k(dissociation) at 263 K. Using the values of k(recombination) suggested in this evaluation, (Table-2) Golden [28] has re-evaluated the equilibrium constant. Bridier et al. [6] measure an equilibrium constant in good agreement with this recommendation, reducing the uncertainty even further. (Table: JPL06, Note: JPL06) Back to table

7. $CH_3C(O)O_2 + NO_2$. The recommendation is derived from measurements of the rate constants in both directions by Bridier et al. [5]. These authors used the values of the rate constants at 298K and a calculated value of the entropy change to get a third law value of the equilibrium constant. Their value of the enthalpy is exactly reproduced in a theoretical study by Miller et al. [46]. (Table: JPL06, Note: JPL06) Back to table

8. $CH_3CH_2C(O)O_2 + NO_2$. Assumed to be the same as for PAN (Note 7). Both sides of the of the reaction differ from PAN by the group C–(C)(CO)$(H)_2$. Error limits are estimated and expanded from those for PAN. (Table: 02-25, Note: 02-25) Back to table

9. $CH_3C(O)CH_2 + O_2$. Estimated values of the entropy and enthalpy changes for the reaction are: $\Delta S = -33$ e.u. and $\Delta H = -26$ kcal/mole. The entropy is from group additivity and the enthalpy from group additivity for the hydroperoxide followed by assuming that the O–H bond dissociation energy is 88 kcal/mole. Error limits are estimated from the uncertainties in this procedure. (Table: 02-25, Note: 02-25) Back to table

10. $F + O_2$. Taken from Campuzano-Jost et al. [10]. There is good agreement with data from Pagsberg et al. [54]. This corresponds to a value for $\Delta H_{f,298}(FO_2) = 6.13 \pm 0.5$ kcal mol^{-1}. There are several modern theoretical computations [21, 24, 25]of this value, ranging from 6 to 9 kcal mol^{-1}. (Table: JPL06, Note: JPL06) Back to table

11. $Cl + O_2$. Data are from Baer et al. [2], Nicovich et al. [50] and Mauldin et al. [45]. Zhu and Lin [75] have reported structure and frequency calculations and a heat of formation for ClOO. Using known thermochemistry for Cl and O_2 and entropy values for ClOO computed from, $\Delta H_{f,0}$ (ClOO) = 23.85 ± 0.1 kcal mole^{-1} is obtained by the third law method from the individual data points of the Nicovich et al. [50] data. The Baer et al. [2] paper reports only one value at each temperature and only graphically, but yields essentially the same value as Nicovich et al [50]. The third law value from Mauldin et al. [45] is less stable by 0.4 kcal mole^{-1}. Earlier values, both experimental and theoretical, of the structural parameters of ClOO are referenced in [75]. $S°_{298}$ (ClOO) = 64.6 cal mole^{-1} K^{-1} and $\Delta H_{f,298}$ (ClOO) = 23.5 ± 0.5 kcal mole^{-1} are recommended. (Table: JPL06, Note: JPL06) Back to table

12. Cl + CO. From fitting the data of Nicovich et al. [51] who measured both k and K between 185 and 260 K in N_2. They report $\Delta H_{f,298}$ (ClCO) = –5.2 ± 0.6 kcal mole^{-1}. (Table: JPL06, Note: JPL06) Back to table

13. $ClO + O_2$. DeMore [20] reports $K < 4 \times 10^{-18}$ cm^3 molecule^{-1} at 197 K. His temperature dependence of the equilibrium constant is estimated using $S°_{298}$ ($ClO{\cdot}O_2$) = 73 cal mol^{-1}K^{-1} and $\Delta H°_{298}$ <7.7 kcal mol^{-1}. A higher value of K has been proposed by Prasad [57], but it requires S°($ClO{\cdot}O_2$) to be about 83 cal mol^{-1} K^{-1}, which seems unreasonably high. Carter and Andrews [13] found no experimental evidence for $ClO{\cdot}O_2$ in matrix experiments. Prasad and Lee [58] discuss these issues and question the validity of the upper limit reported by DeMore. (Table: 92-20, Note: 94-26) Back to table

14. ClO + ClO. The value is from a third-law calculation based on the data from Cox and Hayman [19] (except for the two lowest temperature points) and Nickolaisen et al.[49]. The entropy of ClOOCl, the value of which is 71.9cal mol^{-1} K^{-1} at 300 K, is calculated from structures and frequencies calculated by Zhu and Lin [74]. The heat of formation at 300 K is $\Delta H°_{f,300}$ = 30.4 kcal mol^{-1}. A study of branching ratios of ClO + ClO channels in $Cl_2/O_2/O_3$ mixtures by Horowitz et al. [39] also finds the equilibrium constant in O_2 at 285 K to be in agreement with the recommendation. Avallone and Toohey used K = 1.99E-30Texp(8854/T) derived from *in situ* experiments. (Table: JPL06, Note: JPL06) Back to table

15. ClO + OClO. Data are from Burkholder et al. [8], Hayman and Cox [36] and Green et al. [34]. The best van't Hoff fit to all the data (except for the lowest temperature point of) yields K/cm^3 molecule^{-1} = 2.5x10^{-25}exp(5850/T) for {232<T/K<298}. A calculation of the entropy and heat capacity from the structure and frequencies of ClOCl(O)O reported by Zhu and Lin [76] allows a "3rd Law" fit that yields the recommended parameters. The 95% error limits encompass all the data. From the 3rd Law calculations $S°_{298}$ (Cl_2O_3)=78.7 cal mol^{-1} K^{-1} and $\Delta H_{f,0}(Cl_2O_3)$ =33.6 kcal mol^{-1} and $\Delta H_{f,298}(Cl_2O_3)$ =32.4 kcal mol^{-1}. (This compares to a calculated value of $\Delta H_{f,0}(Cl_2O_3)$ =32.3 from [76] and 32.9 from a theoretical calculation by Sicre and Cobos [61]. Burkholder et al. [8] claim that treating the lowest vibration as a free internal rotation increases the entropy of ClOCl(O)O by almost 9 cal mol^{-1} K^{-1}. This value, repeated by Green et al. [34], is not correct. Clark and Francisco [17] calculated structure and frequencies and conclude that $S°_{298}$ (Cl_2O_3)=78.5 cal mol^{-1} K^{-1} in close agreement with the above, but they conclude that $\Delta H_{f,0}(Cl_2O_3)$ =36.9 kcal mol^{-1} by fitting the data of [8] and [36] including the lowest temperature point. Li et al. [43] have also reported theoretical calculations for

ClOCl(O)O. Their structure and frequencies are in general agreement with [76] and [17], but their energetics are quite different. (Table: JPL06, Note: JPL06) Back to table

16. OClO + NO_3. Theoretical calculations of Parthiban et al. [55]. This value replaces the value in 02-25 that was deduced by Friedl et al. [26]. Uncertainties are based on ±1 kcal $mole^{-1}$ uncertainty in calculated heat of formation. (Table: JPL06, Note: JPL06) Back to table

17. OH + CS_2. Fit to the data of Murrells et al. [47], Hynes et al. [40] and Diau and Lee [22] between 246 and 318 K. Re-analysis of errors led to lower value of g than in JPL-02-25. (Table: JPL06, Note: JPL06) Back to table

18. CH_3S + O_2. Turnipseed et al. [66] report the equilibrium constant for $216 \leq T/K \leq 258$. From a third law analysis using $\Delta S°_{237} = -36.8 \pm 2.6$ eu, they obtain $\Delta H°_{237} = -11.5 \pm 0.9$ kcal/mole. (Table: 94-26, Note: 94-26) Back to table

19. Cl + CS_2. Fit to the data of Nicovich et al. [52] between 193 and 258 K. NEW ENTRY Back to table

20. Br + CH_3SCH_3. Second Law fit to data of Wine et al. [70] and Nakano et al. [48]. This corresponds to a bond dissociation energy in the adduct of 13.84 kcal $mole^{-1}$. NEW ENTRY Back to table

3.4 References

1. Amoruso, A., L. Crescentini, G. Fiocco and M. Volpe, 1993, J. Geophys. Res., 98, 16857-16863.
2. Baer, S., H. Hippler, R. Rahn, M. Siefke, N. Seitzinger and J. Troe, 1991, J. Chem. Phys., 95, 6463-6470.
3. Bahta, A., R. Simonaitis and J. Heicklen, 1982, J. Phys. Chem., 86, 1849.
4. Borrell, P., C. J. Cobos and K. Luther, 1988, J. Phys. Chem., 92, 4377-4384.
5. Bridier, I., F. Caralp, H. Loirat, R. Lesclaux, B. Veyret, K. H. Becker, A. Reimer and F. Zabel, 1991, J. Phys. Chem., 95, 3594-3600.
6. Bridier, I., R. Lesclaux and B. Veyret, 1992, Chem. Phys. Lett., 191, 259-263.
7. Brunning, J., M. J. Frost and I. W. M. Smith, 1988, Int. J. Chem. Kinetics, 20, 957.
8. Burkholder, J. B., R. L. Mauldin, R. J. Yokelson, S. Solomon and A. R. Ravishankara, 1993, J. Phys. Chem., 97, 7597-7605.
9. Burrows, J. P., G. S. Tyndall and G. K. Moortgat, 1985, Chem. Phys. Lett., 119, 193-198.
10. Campuzano-Jost, P., A. E. Croce, H. Hippler, M. Siefke, and J. Troe, 1995, J. Chem. Phys., 102, 5317-5326.
11. Cantrell, C. A., J. A. Davidson, A. H. McDaniel, R. E. Shetter and J. G. Calvert, 1988, J. Chem. Phys., 88, 4997-5006.
12. Cantrell, C. A., R. E. Shetter, J. G. Calvert, G. S. Tyndall and J. J. Orlando, 1993, J. Phys. Chem., 97, 9141-9148.
13. Carter, R. O. and L. Andrews, 1981, J. Phys. Chem., 85, 2351.
14. Chao, J., R. C. Wilhoit and B. J. Zwolinski, 1974, Thermochim. Acta, 10, 359-360.
15. Chao, J., R. C. Wilhoit and B. J. Zwolinski, 1974, Thermochim. Acta, 10, 361-371.
16. Chen, Z. and T. P. Hamilton, 1996, J. Phys. Chem., 100, 15731-15734.
17. Clark, J. and J. S. Francisco, 1997, J. Phys. Chem. A, 101, 7145-7153.
18. Connell, P. S. and H. S. Johnston, 1979, Geophys. Res. Lett., 6, 553-556.
19. Cox, R. A. and G. D. Hayman, 1988, Nature, 332, 796-800.
20. DeMore, W. B., 1990, Geophys. Res. Lett., 17, 2353-2355.
21. Denis, P. A., and O. N. Ventura, 2004, Chem. Phys. Lett., 385, 292-297.
22. Diau, E. W.-G. and Y.-P. Lee, 1991, J. Phys. Chem., 95, 7726-7732.
23. Estupiñán, E. G., J. M. Nicovich and P. H. Wine, 2001, J. Phys. Chem. A, 105, 9697-9703.
24. Feller, D. and D. A. Dixon, 2003, J. Phys. Chem. A, 107, 9641-9651.
25. Francisco, J. S., Y. Zhao, W. A. Lester, Jr., and I. H. Williams, 1992, J. Chem. Phys., 96, 2861-2867.
26. Friedl, R. R., S. P. Sander and Y. L. Yung, 1992, J. Phys. Chem., 96, 7490-7493.
27. Gierczak, T., E. Jimenez, V. Riffault, J. B. Burkholder, and A. R. Ravishankara, 2005, J. Phys. Chem. A, 109, 586-596.
28. Golden, D. M., 2005, Int. J. Chem. Kinet., Accepted.
29. Golden, D. M., J. R. Barker and L. L. Lohr, 2004, J. Phys. Chem. A, 108, 8552.
30. Golden, D. M., J. R. Barker, and L. L. Lohr, 2003, J. Phys. Chem. A, 107, 11057-11071.
31. Gozel, P., B. Calpani and H. van den Bergh, 1984, Isrl. J. Chem., 24, 210.
32. Graham, R. A. and H. S. Johnston, 1978, J. Phys. Chem., 82, 254-268.
33. Graham, R. A., A. M. Winer and J. N. Pitts, Jr., 1977, Chem. Phys. Lett., 51, 215.
34. Green, T. J., M. Islam, P. Guest, K. Hickson, C. E. Canosa-Mas, and R. P. Wayne, 2003, Phys. Chem. Chem. Phys., 5, 5409-5418.
35. Harwood, M. H. and R. L. Jones, 1994, J. Geophys. Res., 99, 22955-22964.
36. Hayman, G. D. and R. A. Cox, 1989, Chem. Phys. Lett., 155, 1-7.
37. Hippler, H., S. Nasterlack and F. Striebel, 2002, Phys. Chem. Chem. Phys., 4, 2959-2964.
38. Hjorth, J., J. Nothholt and G. Restelli, 1992, Int. J. Chem. Kinet., 24, 51-65.
39. Horowitz, A., J. N. Crowley and G. K. Moortgat, 1994, J. Phys. Chem., 98, 11924-11930.
40. Hynes, A. J., P. H. Wine and J. M. Nicovich, 1988, J. Phys. Chem., 92, 3846-3852.
41. JANAF *Thermochemical Tables*, Third ed.; National Bureau of Standards, 1985.
42. Kircher, C. C., J. J. Margitan and S. P. Sander, 1984, J. Phys. Chem., 88, 4370-4375.
43. Li, Q., S. Lu, Y. Xie, P. V. R. Schleyer and H. F. Schaefer, III, 2003, Int. J. Quantum Chem., 95, 731-757.
44. Markwalder, B., P. Gozel and H. van den Bergh, 1992, J. Chem. Phys., 97, 5472-5479.
45. Mauldin, R. L., III, J. B. Burkholder and A. R. Ravishankara, 1992, J. Phys. Chem., 96, 2582-2588.
46. Miller, C. E., J. I. Lynton, D. M. Keevil and J. S. Franscisco, 1999, J. Phys. Chem. A, 103, 11451-11459.
47. Murrells, T. P., E. R. Lovejoy and A. R. Ravishankara, 1990, J. Phys. Chem., 94, 2381-2386.

48. Nakano, Y., M. Goto, S. Hashimoto, M. Kawasaki, and T. J. Wallington, 2001, J. Phys. Chem. A, 105, 11045-11050.
49. Nickolaisen, S. L., R. R. Friedl and S. P. Sander, 1994, J. Phys. Chem., 98, 155-169.
50. Nicovich, J. M., K. D. Kreutter, C. J. Shackelford and P. H. Wine, 1991, Chem. Phys. Lett., 179, 367-373.
51. Nicovich, J. M., K. D. Kreutter and P. H. Wine, 1990, J. Chem. Phys., 92, 3539-3544.
52. Nicovich, J. M. and P. H. Wine, 1990, Int. J. Chem. Kinet., 22, 379-397.
53. Orlando, J. J., G. S. Tyndall, C. A. Cantrell and J. G. Calvert, 1991, J. Chem. Soc. Far. Trans., 87, 2345-2349.
54. Pagsberg, P. B., E. Ratajczak, A. Sillesen and J. T. Jodkowski, 1987, Chem. Phys. Lett., 141, 88-94.
55. Parthiban, S., T. J. Lee, S. Guha, and J. S. Francisco, 2003, J. Amer. Chem. Soc., 125, 10446-10458.
56. Perner, D., A. Schmeltekopf, R. H. Winkler, H. S. Johnston, J. G. Calvert, C. A. Cantrell and W. R. Stockwell, 1985, J. Geophys. Res., 90, 3807-3812.
57. Prasad, S. S., 1980, Nature, 285, 152.
58. Prasad, S. S. and T. J. Lee, 1994, J. Geophys. Res., 99, 8225-8230.
59. Pritchard, H. O., 1994, Int. J. Chem. Kinet., 26, 61-72.
60. Schott, G. and N. Davidson, 1958, J. Amer. Chem. Soc., 80, 1841-1853.
61. Sicre, J. E. a. C. J. C., 2003, J. Molec. Structure, 620, 215-226.
62. Smith, C. A., A. R. Ravishankara and P. H. Wine, 1985, J. Phys. Chem., 89, 1423-1427.
63. Smith, I. W. M. and G. Yarwood, 1986, Chem. Phys. Lett., 130, 24-28.
64. Tuazon, E. C., E. Sanhueza, R. Atkinson, W. P. L. Carter, A. M. Winer and J. N. Pitts, Jr., 1984, J. Phys. Chem., 88, 3095-3098.
65. Tuchler, M. F., K. L. Schmidt, and M. Morgan, 2005, Chem. Phys. Lett., 401, 393-399.
66. Turnipseed, A. A., S. B. Baron and A. R. Ravishankara, 1992, J. Phys. Chem., 96, 7502-7505.
67. Viggiano, A. A., J. A. Davidson, F. C. Fehsenfeld and E. E. Ferguson, 1981, J. Chem. Phys., 74, 6113-6125.
68. Vosper, A. J., 1970, J. Chem. Soc. A, 1970, 625.
69. Wangberg, I., T. Etzkorn, I. Barnes, U. Platt and K. H. Becker, 1997, J. Phys. Chem. A, 101, 9694-9698.
70. Wine, P. H., J. M. Nicovich, R. E. Stickel, Z. Zhao, C. J. Shackelford, K. D. Kreutter, E. P. Daykin and S. Wang *The Tropospheric Chemistry of Ozone in the Polar Regions*; Springer-Verlag: Berlin, 1993; Vol. 17.
71. Wollenhaupt, M. and J. N. Crowley, 2000, J. Phys. Chem. A, 104, 6429-6438.
72. Zabel, F., 1995, Zeitschrift fur Physikalische Chemie, 188, 119-142.
73. Zabel, F., A. Reimer, K. H. Becker and E. H. Fink, 1989, J. Phys. Chem., 93, 5500-5507.
74. Zhu, R. S., and M. C. Lin, 2003, J. Chem. Phys., 118, 4094-4106.
75. Zhu, R. S. and M. C. Lin, 2003, J. Chem. Phys., 119, 2075-2082.
76. Zhu, R. S. and M. C. Lin, 2003, J. Chem. Phys., 118, 8645-8655.

SECTION 4. PHOTOCHEMICAL DATA

Table of Contents

SECTION 4. PHOTOCHEMICAL DATA 4-1
4.1 Format and Error Estimates 4-4
4.2 Halocarbon Absorption Cross Sections and Quantum Yields 4-5
4.3 Web Access to Recommended Data in Text and Graphical Formats 4-5
4.4 References 4-214

Tables

Table 4-1. Photochemical Reactions 4-6
Table 4-2. Combined Uncertainties for Cross Sections and Quantum Yields 4-9
Table 4-3. Absorption Cross Sections of O_2 Between 205 and 240 nm 4-10
Table 4-4. Summary of O_3 Cross Section Measurements 4-11
Table 4-5. Absorption Cross Sections of O_3 at 218 and 293-298 K 4-15
Table 4-6. Parameters for the Calculation of $O(^1D)$ Quantum Yields 4-17
Table 4-7. Absorption Cross Sections of HO_2 4-18
Table 4-8. Absorption Cross Sections of H_2O Vapor 4-18
Table 4-9. Absorption Cross Sections of H_2O_2 Vapor 4-19
Table 4-10. Mathematical Expression for Absorption Cross Sections of H_2O_2 as a Function of Temperature 4-19
Table 4-11. Summary of NO_2 Cross Section Measurements 4-20
Table 4-12. Absorption Cross Sections of NO_2 at 220 and 294 K 4-23
Table 4-13. Quantum Yields for NO_2 Photolysis 4-24
Table 4-14. Summary of NO_3 Cross Section Measurements 4-25
Table 4-15. Absorption Cross Sections of NO_3 at 298 K 4-28
Table 4-16. Quantum yields (multiplied by 1000) for the product channels $NO + O_2$ and $NO_2 + O(^3P)$ in the photolysis of NO_3 at 298, 230 and 190 K 4-30
Table 4-17. Summary of N_2O Cross Section Measurements 4-31
Table 4-18. Absorption Cross Sections of N_2O at 298 K 4-32
Table 4-19. Mathematical Expression for Absorption Cross Sections of N_2O as a Function of Temperature 4-32
Table 4-20. Absorption Cross Sections of N_2O_4 at 220 K 4-33
Table 4-21. Absorption cross sections N_2O_5 at 195-300 K and temperature coefficients 4-35
Table 4-22. Quantum Yields from Photolysis of N_2O_5 4-36
Table 4-23. Summary of HONO Cross Section Measurements 4-36
Table 4-24. Absorption Cross Sections of HONO at 298 K 4-38
Table 4-25. Absorption Cross Sections at 298 K and Temperature Coefficients of HNO_3 Vapor 4-40
Table 4-26. Absorption Cross Sections of HO_2NO_2 at 296-298 K 4-41
Table 4-27. Quantum Yields of HO_2NO_2 4-42
Table 4-28. Photodissociation Band Strengths and Quantum Yields for Several Overtone and Combination Bands of HO_2NO_2 4-42
Table 4-29. Summary of CH_2O Cross Section Measurements 4-42
Table 4-30. Absorption Cross Sections of CH_2O at 298 K and Temperature Coefficients Averaged over 1-nm Intervals 4-45
Table 4-31. Absorption Cross Sections of CH_2O at 298 K and Temperature Coefficients Averaged over Intervals Used in Atmospheric Modeling 4-46
Table 4-32. Quantum Yields for Photolysis of CH_2O at 296-300 K 4-47
Table 4-33. Absorption Cross Sections of CH_3CHO at 298-300 K 4-49
Table 4-34. Recommended Quantum Yields for the Photolysis of CH_3CHO at 1 bar Total Pressure 4-50
Table 4-35. Absorption Cross Sections C_2H_5CHO at 298-300 K 4-51
Table 4-36. Absorption Cross Sections of CH_3O_2, $C_2H_5O_2$, and $CH_3C(O)O_2$ 4-52
Table 4-37. Absorption Cross Sections of CH_3OOH 4-53
Table 4-38. Absorption Cross Sections of $HOCH_2OOH$ 4-54
Table 4-39. Absorption Cross Sections of $CH_3C(O)O_2NO_2$ at 298 K, Temperature Coefficients B 4-55
Table 4-40. Absorption Cross Sections of $C_2H_5C(O)O_2NO_2$ at 296 K and Temperature Coefficients B 4-56
Table 4-41. Absorption Cross Sections of CH_2=CHCHO at 298 K 4-57
Table 4-42. Absorption Cross Sections of CH_2=C(CH_3)CHO at 298 K 4-58
Table 4-43. Absorption Cross Sections of CH_3(O)CH=CH_2 at 298 K 4-60
Table 4-44. Absorption Cross Sections of $HOCH_2CHO$ at 298 K 4-61
Table 4-45. Absorption Cross Sections of $CH_3C(O)CH_3$ at 298 K and Temperature Coefficients 4-64

Table 4-46. Quantum Yields for the Photolysis of Acetone 4-66
Table 4-47. Absorption Cross Sections of $CH_3C(O)CH_2OH$ at 298 K 4-67
Table 4-48. Absorption Cross Sections of CHOCHO at 296 K 4-69
Table 4-49. Absolute Quantum Yields in the Photolysis of CHOCHO 4-70
Table 4-50. Absorption Cross Sections of $CH_3COC(O)H$ at 295-298 K 4-71
Table 4-51. Absorption Cross Sections of HC(O)OH and $(HC(O)OH)_2$ at 302 K 4-74
Table 4-52. Absorption Cross Sections of $CH_3C(O)OH$ and $(CH_3C(O)OH)_2$ at 298 K 4-75
Table 4-53. Absorption Cross Sections $CH_3C(O)OOH$ at 298 K 4-76
Table 4-54. Absorption Cross Sections of $CH_3C(O)C(O)OH$ at 298 K 4-77
Table 4-55. Absorption Cross Sections of $HC(O)OCH_3$ at 297-298 K 4-78
Table 4-56. Absorption Cross Sections of $HC(O)OC_2H_5$ at 297 K 4-78
Table 4-57. Absorption Cross Sections of FO_2 at 295 K 4-79
Table 4-58. Absorption Cross Sections of F_2O at 273 K 4-79
Table 4-59. Absorption Cross Sections of F_2O_2 at 193-195 and 273 K 4-80
Table 4-60. Absorption Cross Sections of FNO at 298 K 4-81
Table 4-61. Absorption Cross Sections of COF_2 at 298 K 4-82
Table 4-62. Absorption Cross Sections of COHF at 298 K 4-82
Table 4-63. Absorption Cross Sections CF_3OOCF_3 at 298 K. 4-83
Table 4-64. Absorption Cross Sections $CF_3O_3CF_3$ at 298 K. 4-84
Table 4-65. Absorption Cross Sections of CF_3CHO at 298 K 4-85
Table 4-66. Absorption Cross Sections of $CF_3C(O)F$ at 298 K 4-86
Table 4-67. Absorption Cross Sections of $CF_3C(O)Cl$ at 296-298 K 4-86
Table 4-68. Absorption Cross Sections of $CF_3(O)O_2NO_2$ at 298 K 4-87
Table 4-69. Absorption Cross Sections of CF_3CH_2CHO at 298 K 4-88
Table 4-70. Absorption Cross Sections of $CF_3C(O)OH$ at 296 K 4-89
Table 4-71. Absorption Cross Sections of $CH_3C(O)F$ at 296 K 4-89
Table 4-72. Absorption Cross Sections of $CH_2=CHCF_3$ at 295 K 4-90
Table 4-73. Absorption Cross Sections of $CH_2=CFCF_3$ at 295 K 4-90
Table 4-74. Absorption Cross Sections of $CF_2=CF_2$ at 295-298 4-91
Table 4-75. Absorption Cross Sections of $CF_2=CFCF_3$ at 295-298 K 4-92
Table 4-76. Absorption Cross Sections of Cl_2 at 298 4-93
Table 4-77. Absorption Cross Sections of ClO at 298 K 4-94
Table 4-78. Absorption Cross Sections of ClO at the band heads of the v′,v″ = 1,0 to 21,0 bands 4-95
Table 4-79. Absorption Cross Sections of ClOO 4-95
Table 4-80. Summary of Previous Measurements of OClO Cross Sections 4-96
Table 4-81. Absorption Cross Sections of OClO at 204 K (averages over 1-nm intervals) 4-97
Table 4-82. Absorption Cross Sections of OClO at the a(21) to a(3) Band Peaks at 213-293 K 4-98
Table 4-83. Absorption Cross Sections of OClO at the Band Peaks (after Wahner et al. [830]) 4-99
Table 4-84. Absorption Cross Sections of Cl_2O 4-101
Table 4-85. Absorption Cross Sections of ClOOCl at 195-265 K 4-102
Table 4-86. Absorption cross sections Cl_2O_3 at 220-260 K 4-103
Table 4-87. Absorption Cross Sections of Cl_2O_4 at 298 K 4-104
Table 4-88. Absorption Cross Sections of Cl_2O_6 at 298 K 4-105
Table 4-89. Absorption Cross Sections of Cl_2O_7 at 298 K 4-105
Table 4-90. Absorption Cross Sections of $ClClO_2$ at 298 K 4-106
Table 4-91. Absorption Cross Sections of HCl and DCl at 298 K 4-107
Table 4-92. Absorption Cross Sections of HOCl 4-108
Table 4-93. Absorption Cross Sections of ClNO 4-109
Table 4-94. Absorption Cross Sections of $ClNO_2$ at 298 K 4-110
Table 4-95. Absorption Cross Sections of ClONO at 231 K 4-110
Table 4-96. Absorption Cross Sections and Temperature Coefficients of $ClONO_2$ 4-111
Table 4-97. Absorption Cross Sections of CCl_4 at 295–298 K 4-114
Table 4-98. Absorption Cross Sections of CH_3OCl 4-114
Table 4-99. Absorption Cross Sections of $CHCl_3$ at 295–298 K 4-115
Table 4-100. Absorption Cross Sections of CH_2Cl_2 at 295–298 K 4-116
Table 4-101. Absorption Cross Sections of CH_3Cl at 295–298 K 4-117
Table4-102. Absorption Cross Sections of CH_3CCl_3 at 295–298 K 4-118
Table 4-103. Absorption Cross Sections of CH_3CH_2Cl at 298 K 4-118
Table 4-104. Absorption Cross Sections of $CH_3CHClCH_3$ at 295 K 4-118
Table 4-105. Absorption Cross Sections of $COCl_2$ at 294-298 K 4-120
Table 4-106. Absorption Cross Sections of COHCl at 298 K 4-121

Table 4-107. Absorption Cross Sections of COFCl at 296-298 K 4-123
Table 4-108. Absorption Cross Sections of $CFCl_3$ at 295–298 K 4-124
Table 4-109. Absorption Cross Sections of CF_2Cl_2 at 295–298 K 4-125
Table 4-110. Absorption Cross Sections of CF_3Cl at 295 K 4-125
Table 4-111. Absorption Cross Sections of $CF_2ClCFCl_2$ at 295–298 K 4-126
Table 4-112. Absorption Cross Sections of CF_2ClCF_2Cl at 295 K 4-127
Table 4-113. Absorption Cross Sections of CF_3CF_2Cl at 295–298 K 4-129
Table 4-114. Absorption Cross Sections of $CHFCl_2$ at 295–298 K 4-130
Table 4-115. Absorption Cross Sections of CHF_2Cl at 295–298 K 4-131
Table 4-116. Absorption Cross Sections of CH_2FCl at 298 K 4-131
Table 4-117. Absorption Cross Sections of CF_3CHCl_2 at 295 K 4-133
Table 4-118. Absorption Cross Sections of CF_3CHFCl at 295 K 4-134
Table 4-119. Absorption Cross Sections of CF_3CH_2Cl at 298 K 4-134
Table 4-120. Absorption Cross Sections of CH_3CFCl_2 at 295–298 K 4-135
Table 4-121. Absorption Cross Sections of CH_3CF_2Cl at 295–298 K 4-136
Table 4-122. Absorption Cross Sections of CH_2ClCHO at 298 K 4-137
Table 4-123. Absorption Cross Sections of $CHCl_2CHO$ at 298 K 4-138
Table4-124. Absorption Cross Sections of CF_2ClCHO at 298 K and Temperature Coefficients 4-139
Table 4-125. Absorption Cross Sections of $CFCl_2CHO$ at 298 K and Temperature Coefficients 4-139
Table 4-126. Absorption Cross Sections of CCl_3CHO at 298 K and Temperature Coefficients 4-140
Table 4-127. Absorption Cross Sections of $CH_3C(O)Cl$ at 295-298 K 4-141
Table 4-128. Absorption Cross Sections of $CH_2ClC(O)Cl$ at 298 K 4-142
Table 4-129. Absorption Cross Sections of $CHCl_2C(O)Cl$ at 298 K 4-142
Table 4-130. Absorption Cross Sections of $CCl_3C(O)Cl$ at 295 K 4-143
Table 4-131. Absorption Cross Sections of $CF_3CF_2CHCl_2$ and CF_2ClCF_2CFCl at 298 K 4-144
Table 4-132. Absorption Cross Sections of $CH_3C(O)CH_2Cl$ at 296 K 4-145
Table 4-133. Summary of Cross Section Measurements of Br_2 4-146
Table 4-134. Absorption Cross Sections of Br_2 at 298 K 4-147
Table 4-135. Summary of Cross Section Measurements of HBr 4-147
Table 4-136. Absorption Cross Sections of HBr at 296-298 K 4-148
Table 4-137. Summary of Cross Section Measurements of BrO 4-148
Table 4-138. Absorption Cross Sections at the Vibrational Band Peaks in the A ← X Spectrum of BrO (0.4 nm resolution) 4-149
Table 4-139. Absorption Cross Sections of BrO at 298 K 4-150
Table 4-140. Peak Absorption Cross Sections of OBrO at 298 K 4-152
Table 4-141. Absorption Cross Sections of OBrO at 298 K 4-153
Table 4-142. Absorption Cross Sections of Br_2O at 298 K 4-154
Table 4-143. Absorption Cross Sections of HOBr 4-155
Table 4-144. Absorption cross sections of BrNO at 298 K 4-157
Table 4-145. Absorption Cross Sections of BrONO at 253 K 4-157
Table 4-146. Absorption Cross Sections of $BrONO_2$ at 296 K and Temperature Coefficients 4-159
Table 4-147. Absorption Cross Sections of BrCl at 298 K 4-161
Table 4-148. Absorption Cross Sections of BrOCl at 298 K 4-161
Table 4-149. Absorption Cross Sections of CH_3Br at 295–296 K 4-162
Table 4-150. Absorption Cross Sections of CH_2Br_2 at 295–298 K 4-164
Table 4-151. Absorption Cross Sections of $CHBr_3$ at 295–296 K 4-165
Table 4-152. Absorption Cross Sections of CH_2BrCH_2Br at 295 K 4-166
Table 4-153. Absorption Cross Sections of C_2H_5Br at 295 K 4-166
Table 4-154. Absorption Cross Sections of $COBr_2$ at 298 K 4-167
Table 4-155. Absorption Cross Sections of COHBr at 298 K 4-168
Table 4-156. Absorption Cross Sections of CH_2ClBr at 295 K 4-169
Table 4-157. Absorption Cross Sections of $CHClBr_2$ at 296 K 4-170
Table 4-158. Absorption Cross Sections of $CHCl_2Br$ at 298 K 4-171
Table 4-159. Absorption Cross Sections of CCl_3Br at 298 K 4-171
Table 4-160. Absorption Cross Sections of CHF_2Br at 298 K 4-172
Table 4-161. Absorption Cross Sections of CF_2Br_2 at 295–296 K 4-174
Table 4-162. Absorption Cross Sections of CF_2ClBr at 295–298 K 4-177
Table 4-163. Absorption Cross Sections of CF_3Br at 295–298 K 4-179
Table 4-164. Absorption Cross Sections of $CH_2=CHBr$ at 295 K 4-179
Table 4-165. Absorption Cross Sections of $CHBr=CF_2$ at 295 K 4-180
Table 4-166. Absorption cross sections of $CFBr=CF_2$ at 295 K 4-180

Table 4-167. Absorption Cross Sections of CH_2=$CBrCF_3$ at 295 K 4-181
Table 4-168. Absorption Cross Sections of CF_3CH_2Br at 295 K 4-181
Table 4-169. Absorption Cross Sections of $CF_3CHClBr$ at 295–298 K 4-182
Table 4-170. Absorption Cross Sections of CF_3CHFBr at 295 K 4-183
Table 4-171. Absorption Cross Sections of CF_2BrCF_2Br at 296 K 4-184
Table 4-172. Absorption Cross Sections of CF_3CF_2Br at 298 K 4-185
Table 4-173. Absorption Cross Sections of $CH_3CH_2CH_2Br$ and $CH_3CHBrCH_3$ at 295 K 4-185
Table 4-174. Absorption Cross Sections of $CH_3C(O)CH_2Br$ at 296 K 4-186
Table 4-175. Absorption Cross Sections of I_2 at 295 K 4-188
Table 4-176. Cross Sections at the Maxima and Minima of I_2 at 295 K 4-189
Table 4-177. Summary of Cross Section Measurements of IO 4-190
Table 4-178. Absorption Cross Sections of IO at 298 K 4-191
Table 4-179. Absorption Cross Sections of OIO at 295 K 4-193
Table 4-180. Absorption Cross Sections of HI at 298 K 4-195
Table 4-181. Absorption Cross Sections HOI at 295-298 K 4-196
Table 4-182. Absorption Cross Sections of ICl at 298 K 4-197
Table 4-183. Absorption Cross Sections of IBr at 298 K 4-198
Table 4-184. Absorption Cross Sections of INO at 298 K 4-198
Table 4-185. Absorption Cross Sections of IONO at 298 K 4-199
Table 4-186. Absorption Cross Sections of $IONO_2$ at 298 K 4-199
Table 4-187. Absorption Cross Sections of CH_3I at 296–298 K and Temperature Coefficients 4-201
Table 4-188. Absorption Cross Sections of CH_2I_2 at 298 K 4-202
Table 4-189. Absorption Cross Sections of C_2H_5I at 298 K and Temperature Coefficients 4-203
Table 4-190. Absorption Cross Sections of CH_3CHI_2 at 298 K 4-203
Table 4-191. Absorption Cross Sections of C_3H_7I at 298 K and Temperature Coefficients 4-205
Table 4-192. Absorption Cross Sections of $(CH_3)_3CI$ at 298 K 4-206
Table 4-193. Absorption Cross Sections of CF_3I at 295-300 K 4-208
Table 4-194. Absorption Cross Sections of CF_2I_2 at 294 K 4-210
Table 4-195. Absorption Cross Sections of C_2F_5I at 323 K 4-210
Table 4-196. Absorption Cross Sections of 1-C_3F_7I at 295–298 K 4-211
Table 4-197. Absorption Cross Sections of CH_2ICl at 298 K and Temperature Coefficients 4-212
Table 4-198. Absorption Cross Sections of CH_2BrI at 298 K and Temperature Coefficients 4-212

Figures

Figure 4-1. Absorption Spectrum of NO_3 4-31
Figure 4-2. Absorption Spectrum of ClO 4-94
Figure 4-3. Absorption Spectrum of OClO at 204 K (after Wahner et al. [830]) 4-99
Figure 4-4. Absorption Spectrum of BrO (after Wahner et al. [829]) 4-151
Figure 4-5. Absorption spectrum of OBrO (after Knight et al. [413]) 4-154

4.1 Format and Error Estimates

In Table 4-1 we present a list of photochemical reactions considered to be of stratospheric interest. The absorption cross sections of O_2 and O_3 largely determine the extent of penetration of solar radiation into the stratosphere and troposphere. Some comments and references to these cross sections are presented in the text, but only a sample of the data is listed here. (See, for example, WMO Report No. 11 [1]; WMO Report No. 16 [851]) The photodissociation of NO in the O_2 Schumann-Runge band spectral range is another important process requiring special treatment and is not discussed in this evaluation (see, for example, Frederick and Hudson [250]; Allen and Frederick [12]; WMO Report No. 11 [1], and Minschwaner and Siskind [531]).

For some other species having highly structured spectra, such as CS_2 and SO_2, some comments are given in the text, but the photochemical data are not presented. The species CH_2O, NO_2, NO_3, ClO, BrO, and OClO also have complicated spectra, but in view of their importance for atmospheric chemistry a sample of the data is presented in the evaluation; for more detailed information on their high-resolution spectra and temperature dependence, the reader is referred to the original literature.

Table 4-2 gives recommended reliability factors for some of the more important photochemical reactions. These factors represent the combined uncertainty in cross sections and quantum yields, taking into consideration the atmospherically important wavelength regions, and they refer to the total dissociation rate regardless of product identity. The exception is $O(^1D)$ production from photolysis of O_3: the reliability factor applies to the quantum yield at the indicated wavelengths.

The error estimates are not rigorous numbers resulting from a detailed error propagation analysis of statistical manipulations of the different sets of literature values; they merely represent a consensus among the panel members as to the reliability of the data for atmospheric photodissociation calculations, taking into account the difficulty of the measurements, the agreement among the results reported by various groups, etc.

The absorption cross sections are defined by the following expression of Beer's Law:

$$I = I_o \exp(-\sigma n l),$$

where I_o and I are the incident and transmitted light intensity, respectively; σ is the absorption cross section in cm^2 $molecule^{-1}$; n is the concentration in molecule cm^{-3}; and l is the pathlength in cm. The cross sections are room temperature values at the specific wavelengths listed in the table, and the expected photodissociation quantum yields are unity, unless otherwise stated.

4.2 Halocarbon Absorption Cross Sections and Quantum Yields

The primary process in the photodissociation of chlorinated hydrocarbons is well established: absorption of ultraviolet radiation in the lowest frequency band is interpreted as an n–σ* transition involving excitation to a repulsive electronic state (antibonding in C–Cl), which dissociates by breaking the carbon-chlorine bond (Majer and Simons [468]). As expected, chlorofluoromethanes, which are a particular type of chlorinated hydrocarbons, behave in this fashion (Sandorfy [706]). Hence, quantum yield for photodissociation is expected to be unity for these compounds. There are several studies that show specifically that this is the case for CF_2Cl_2, $CFCl_3$, and CCl_4. These studies, which were reviewed in CODATA [177], also indicate that at shorter wavelengths, two halogen atoms can be released simultaneously in the primary process.

4.3 Web Access to Recommended Data in Text and Graphical Formats

The tables of recommended cross sections from this evaluation can be downloaded from the spectral atlas of the Max-Planck Institute for Chemistry at: http://www.atmosphere.mpg.de/enid/2295

Table 4-1. Photochemical Reactions

O_x Photochemistry

A1. $O_2 + h\nu \rightarrow O + O$

A2. $O_3 + h\nu \rightarrow O_2 + O$

$O_3 + h\nu \rightarrow O_2 + O(^1D)$

HO_x Photochemistry

B1. $HO_2 + h\nu \rightarrow$ products

B2. $H_2O + h\nu \rightarrow H + OH$

B3. $H_2O_2 + h\nu \rightarrow OH + OH$

NO_x Photochemistry

C1. $NO_2 + h\nu \rightarrow NO + O$

C2. $NO_3 + h\nu \rightarrow NO_2 + O$

$NO_3 + h\nu \rightarrow NO + O_2$

C3. $N_2O + h\nu \rightarrow N_2 + O(^1D)$

C4. $N_2O_4 + h\nu \rightarrow$ products

C5. $N_2O_5 + h\nu \rightarrow$ products

$NH_3 + h\nu \rightarrow NH_2 + H$ (1)

C6. $HONO + h\nu \rightarrow OH + NO$

C7. $HNO_3 + h\nu \rightarrow OH + NO_2$

C8. $HO_2NO_2 + h\nu \rightarrow$ products

Organic Photochemistry

$CO + h\nu \rightarrow C + O$ (1)

$CO_2 + h\nu \rightarrow CO + O$ (1)

$CH_4 + h\nu \rightarrow$ products (2)

D1. $CH_2O + h\nu \rightarrow$ products

D2. $CH_3CHO + h\nu \rightarrow$ products

D3. $C_2H_5CHO\ h\nu \rightarrow$ products

D4. $CH_3O_2 + h\nu \rightarrow$ products

D5. $C_2H_5O_2 + h\nu \rightarrow$ products

D6. $CH_3C(O)O_2 + h\nu \rightarrow$ products

D7. $CH_3OOH + h\nu \rightarrow$ products

D8. $HOCH_2OOH + h\nu \rightarrow$ products

D9 $CH_3C(O)O_2NO_2 + h\nu \rightarrow$ products

D10. $C_2H_5C(O)O_2NO_2 + h\nu \rightarrow$ products

D11. $CH_2{=}CHCHO + h\nu \rightarrow$ products

D12. $CH_2C(CH_3)CHO + h\nu \rightarrow$ products

D13. $CH_3C(O)CH{=}CH_2 + h\nu \rightarrow$ products

D14. $HOCH_2CHO + h\nu \rightarrow$ products

D15. $CH_3C(O)CH_3 + h\nu \rightarrow$ products

D16. $CH_3C(O)CH_2OH + h\nu \rightarrow$ products

D17. $CHOCHO + h\nu \rightarrow$ products

D18. $CH_3C(O)C(O)H + h\nu \rightarrow$ products

D19. $HC(O)OH + h\nu \rightarrow$ products

$(HC(O)OH)_2 + h\nu \rightarrow$ products

D20. $CH_3C(O)OH + h\nu \rightarrow$ products

D21. $CH_3C(O)OOH + h\nu \rightarrow$ products

D22. $C_2H_5C(O)OH + h\nu \rightarrow$ products

D23. $CH_3C(O)C(O)OH + h\nu \rightarrow$ products

D24. $HC(O)OCH_3 + h\nu \rightarrow$ products

D25. $HC(O)OC_2H_5 + h\nu \rightarrow$ products

D26. $HCN + h\nu \rightarrow$ products

D27. $CH_3CN + h\nu \rightarrow$ products

FO_x Photochemistry

E1. $HF + h\nu \rightarrow H + F$

E2. $FO_2 + h\nu \rightarrow$ products

E3. $F_2O + h\nu \rightarrow$ products

E4. $F_2O_2 + h\nu \rightarrow$ products

E5. $FNO + h\nu \rightarrow F + NO$

E6. $CF_4 + h\nu \rightarrow$ products

E7. $C_2F_6 + h\nu \rightarrow$ products

E8. $CF_2O + h\nu \rightarrow$ products

E9. $COHF + h\nu \rightarrow$ products

E10. $CF_3OH + h\nu \rightarrow$ products

E11. $CF_3OOCF_3 + h\nu \rightarrow$ products

E12. $CF_3OCF_3 + h\nu \rightarrow$ products

E13. $CF_3CHO + h\nu \rightarrow$ products

E14. $CF_3C(O)F + h\nu \rightarrow$ products

E15. $CF_3C(O)Cl + h\nu \rightarrow$ products

E16. $CF_3C(O)O_2NO_2 + h\nu \rightarrow$ products

E17. $CF_3CH_2CHO + h\nu \rightarrow$ products

E18. $CF_3C(O)OH + h\nu \rightarrow$ products

E19. $CH_3C(O)F + h\nu \rightarrow$ products

E20. $CH_2{=}CHCF_3 + h\nu \rightarrow$ products

E21. $CH_2{=}CFCF_3 + h\nu \rightarrow$ products

E22. $CF_2{=}CF_2 + h\nu \rightarrow$ products

E23. $CF_2{=}CFCF_3 + h\nu \rightarrow$ products

ClO_x Photochemistry

F1. $Cl_2 + h\nu \rightarrow Cl + Cl$

F2. $ClO + h\nu \rightarrow Cl + O$

F3. $ClOO + h\nu \rightarrow$ products

F4. $OClO + h\nu \rightarrow O + ClO$

F5. $ClO_3 + h\nu \rightarrow$ products

F6. $Cl_2O + h\nu \rightarrow$ products

F7. $ClOOCl + h\nu \rightarrow$ products

F8. $ClClO_2 + h\nu \rightarrow$ products

F9. $Cl_2O_3 + h\nu \rightarrow$ products

F10. $Cl_2O_4 + h\nu \rightarrow$ products

F11. $Cl_2O_6 + h\nu \rightarrow$ products

F12. $Cl_2O_7 + h\nu \rightarrow$ products

F13. $HCl + h\nu \rightarrow H + Cl$

$DCl + h\nu \rightarrow$ products

F14. $HOCl + h\nu \rightarrow$ products

F15. $ClNO + h\nu \rightarrow Cl + NO$

F16. $ClNO_2 + h\nu \rightarrow$ products

F17. $ClONO + h\nu \rightarrow$ products

F18. $ClONO_2 + h\nu \rightarrow$ products

F19. $CCl_4 + h\nu \rightarrow$ products

F20. $CH_3OCl + h\nu \rightarrow$ products

F21. $CHCl_3 + h\nu \rightarrow$ products

F22. $CH_2Cl_2 + h\nu \rightarrow$ products

F23. $CH_3Cl + h\nu \rightarrow$ products
F24. $CH_3CCl_3 + h\nu \rightarrow$ products
F25. $CH_3CH_2Cl + h\nu \rightarrow$ products
F26. $CH_3CHClCH_3 + h\nu \rightarrow$ products
F27. $CH_2ClCH_2Cl + h\nu \rightarrow$ products
F28. $CH_2ClCH_2CH_2Cl + h\nu \rightarrow$ products
F29. $CH_2Cl(CH_2)_2CH_2Cl + h\nu \rightarrow$ products
F30. $CCl_2O + h\nu \rightarrow$ products
F31. $COHCl + h\nu \rightarrow$ products
F32. $CClFO + h\nu \rightarrow$ products
F33. $CFCl_3$ (CFC-11) $+ h\nu \rightarrow$ products
F34. CF_2Cl_2 (CFC-12) $+ h\nu \rightarrow$ products
F35. CF_3Cl (CFC-13) $+ h\nu \rightarrow$ products
F36. $CF_2ClCFCl_2$ (CFC-113) $+ h\nu \rightarrow$ products
F37. CF_2ClCF_2Cl (CFC-114) $+ h\nu \rightarrow$ products
F38. CF_3CF_2Cl (CFC-115)$+ h\nu \rightarrow$ products
F39. $CHFCl_2$ (HCFC-21) $+ h\nu \rightarrow$ products
F40. CHF_2Cl (HCFC-22) $+ h\nu \rightarrow$ products
F41. CH_2FCl (HCFC-31) $+ h\nu \rightarrow$ products
F42. CF_3CHCl_2 (HCFC-123) $+ h\nu \rightarrow$ products
F43. CF_3CHFCl (HCFC-124) $+ h\nu \rightarrow$ products
F44. CF_3CH_2Cl (HCFC-133) $+ h\nu \rightarrow$ products
F45. CH_3CFCl_2 (HCFC-141b) $+ h\nu \rightarrow$ products
F46. CH_3CF_2Cl (HCFC-142b) $+ h\nu \rightarrow$ products
F47. $CH_2ClCHO + h\nu \rightarrow$ products
F48. $CHCl_2CHO + h\nu \rightarrow$ products
F49. $CF_2ClCHO + h\nu \rightarrow$ products
F50. $CFCl_2CHO + h\nu \rightarrow$ products
F51. $CCl_3CHO + h\nu \rightarrow$ products
F52. $CH_3C(O)Cl + h\nu \rightarrow$ products
F53. $CH_2ClC(O)Cl + h\nu \rightarrow$ products
F54. $CHCl_2C(O)Cl + h\nu \rightarrow$ products
F55. $CCl_3C(O)Cl + h\nu \rightarrow$ products
F56. $CF_3CF_2CHCl_2$ (HCFC-225ca) $+ h\nu \rightarrow$ products
F57. CF_2ClCF_2CHFCl (HCFC-225cb) $+ h\nu \rightarrow$ products
F58. $CH_3C(O)CH_2Cl + h\nu \rightarrow$ products

BrO_x Photochemistry

G1. $Br_2 + h\nu \rightarrow$ products
G2. $HBr + h\nu \rightarrow$ products
G3. $BrO + h\nu \rightarrow$ products
G4. $OBrO + h\nu \rightarrow$ products
G5. $Br_2O + h\nu \rightarrow$ products
G6. $HOBr + h\nu \rightarrow$ products
G7. $BrNO + h\nu \rightarrow$ products
G8. $BrNO + h\nu \rightarrow$ products
G9. $BrONO_2 + h\nu \rightarrow$ products
G10. $BrCl + h\nu \rightarrow Br + Cl$
G11. $BrOCl + h\nu \rightarrow$ products
G12. $CH_3Br + h\nu \rightarrow$ products
G13. $CH_2Br_2 + h\nu \rightarrow$ Products
G14. $CHBr_3 + h\nu \rightarrow$ Products
G15. $CH_2BrCH_2Br + h\nu \rightarrow$ Products
G16. $C_2H_5Br + h\nu \rightarrow$ Products
G17. $COBr_2 + h\nu \rightarrow$ products
G18. $COHBr + h\nu \rightarrow$ products
G19. CH_2ClBr (Halon-1011) $+ h\nu \rightarrow$ Products
G20. $CHClBr_2$ (Halon-1012) $+ h\nu \rightarrow$ Products
G21. $CHCl_2Br$ (Halon-1021) $+ h\nu \rightarrow$ Products
G22. CCl_3Br (Halon-1031) $+ h\nu \rightarrow$ Products
G23. CHF_2Br (Halon-1201) $+ h\nu \rightarrow$ Products
G24. CF_2Br_2 (Halon-1202) $+ h\nu \rightarrow$ Products
G25. CF_2ClBr (Halon-1211) $+ h\nu \rightarrow$ Products
G26. CF_3Br (Halon-1301) $+ h\nu \rightarrow$ Products
G27. $CH_2{=}CHBr + h\nu \rightarrow$ Products
G28. $CHBr{=}CF_2 + h\nu \rightarrow$ Products
G29. $CFBr{=}CF_2 + h\nu \rightarrow$ Products
G30. $CH_2{=}CBrCF_3 + h\nu \rightarrow$ Products
G31. CF_3CH_2Br (Halon-2301) $+ h\nu \rightarrow$ Products
G32. $CF_3CHClBr$ (Halon-2311) $+ h\nu \rightarrow$ Products
G33. CF_3CHFBr (Halon-2401) $+ h\nu \rightarrow$ Products
G34. CF_2BrCF_2Br (Halon-2402) $+ h\nu \rightarrow$ Products
G35. CF_3CF_2Br (Halon-2501) $+ h\nu \rightarrow$ Products
G36. $CH_3CH_2CH_2Br + h\nu \rightarrow$ Products
G37. $CH_3CHBrCH_3 + h\nu \rightarrow$ Products
G38. $CH_3C(O)CH_2Br + h\nu \rightarrow$ products

IO_x Photochemistry

H1. $I_2 + h\nu \rightarrow 2\ I$
H2. $IO + h\nu \rightarrow I + O(^3P), O(^1D)$
H3. $OIO + h\nu \rightarrow$ products
H4. $HI + h\nu \rightarrow$ products
H5. $HOI + h\nu \rightarrow OH + I$
H6. $ICl + h\nu \rightarrow I + Cl$
H7. $IBr + h\nu \rightarrow I + Br$
H8. $INO + h\nu \rightarrow I + NO$
H9. $IONO + h\nu \rightarrow I + NO_2$
H10. $IONO_2 + h\nu \rightarrow$ products
H11. $CH_3I + h\nu \rightarrow CH_3 + I$
H12. $CH_2I_2 + h\nu \rightarrow CH_2I + I$
H13. $C_2H_5I + h\nu \rightarrow C_2H_5 + I$
H14. $CH_3CHI_2 + h\nu \rightarrow$ Products
H15. $CH_3CH_2CH_2I + h\nu \rightarrow$ Products
H16. $CH_3CHICH_3 + h\nu \rightarrow$ Products
H17. $C_4H_9I + h\nu \rightarrow C_4H_9 + I$
H18. $(CH_3)_2CHCH_2I + h\nu \rightarrow (CH_3)_2CCH_2 + I$
H19. $(CH_3)_3CI + h\nu \rightarrow (CH_3)_3C + I$
H20. $C_5H_{11}I + h\nu \rightarrow C_5H_{11} + I$
H21. $CF_3I + h\nu \rightarrow CF_3 + I$
H22. $CF_2I_2 + h\nu \rightarrow$ products
H23. $C_2F_5I + h\nu \rightarrow C_2F_5 + I$
H24. $C_3F_7I + h\nu \rightarrow C_3F_7 + I$
H25. $C_4F_9I + h\nu \rightarrow C_4F_9 + I$
H26. $C_6F_{13}I + h\nu \rightarrow C_6F_{13} + I$
H27. $CH_2ICl + h\nu \rightarrow CH_2Cl + I$
H28. $CH_2BrI + h\nu \rightarrow$ products
H29. $CF_2BrCF_2I + h\nu \rightarrow$ products

SO_x Photochemistry

I1. $SO_2 + h\nu \rightarrow SO + O$

$H_2S + h\nu \rightarrow HS + H$ (1)

I2. $CS_2 + h\nu \rightarrow CS + S$

I3. $OCS + h\nu \rightarrow CO + S$

I4. $SF_6 + h\nu \rightarrow$ products

Metal Photochemistry

J1. $NaOH\ h\nu \rightarrow Na + OH$

J2. $NaCl + h\nu \rightarrow Na + Cl$

---

(1) Hudson and Kieffer [351].

(2) Turco [787].

(3) Shaded entries indicate changes to the recommendation and/or the note since JPL 02-25.

(4) Shaded, bold indicate new entries, not previously evaluated

Table 4-1. Combined Uncertainties for Cross Sections and Quantum Yields

Species	Uncertainty	Notes
O_2 (Schumann-Runge bands)	1.2	
O_2 (Continua)	1.2	
O_3 (Cross Sections Only)	1.1	
$O_3 \rightarrow O(^1D)$, λ >310 nm	1.3	
$O_3 \rightarrow O(^1D)$, 290 < λ < 310 nm	1.2	
H_2O_2	1.3	
NO_2	1.2	
NO_3	1.5	
N_2O	1.2	
N_2O_5	2.0	
HNO_3	1.3	
HO_2NO_2	2.0	
CH_2O	1.4	
CH_3OOH	1.5	
$CH_3C(O)O_2NO_2$	1.3	λ < 300 nm
$CH_3C(O)O_2NO_2$	2.0	$\lambda \geq$ 300 nm
HCl	1.1	
HOCl	1.4	
ClOOCl	1.5	λ < 300 nm
ClOOCl	3.0	$\lambda \geq$ 300 nm
Cl_2O_3	1.5	λ < 300 nm
Cl_2O_3	3.0	$\lambda \geq$ 300 nm
$ClONO_2$	1.3	
CCl_4	1.1	
CCl_3F	1.1	
CCl_2F_2	1.1	
CH_3Cl	1.1	
CF_2O	2.0	
CF_3Br	1.3	
CF_2ClBr	2.0	
CF_2Br_2	2.0	
$C_2F_4Br_2$	2.0	
HOBr	2.0	λ < 350 nm
HOBr	10	$\lambda \geq$ 350 nm
$BrONO_2$	1.4	

A1. $O_2 + h\nu \rightarrow O + O$. The photodissociation of molecular oxygen in the stratosphere is due primarily to absorption of solar radiation in the 200–220 nm wavelength region, i.e., within the Herzberg continuum. The 185–200-nm region—the O_2 Schumann-Runge band spectral range—is also very important, since solar radiation penetrates efficiently into the stratosphere at those wavelengths.

Frederick and Mentall [251] Herman and Mentall [327] and Anderson and Hall [20, 21] estimated O_2 absorption cross sections from balloon measurements of solar irradiance in the stratosphere. These authors find the cross sections in the 200–210 nm range to be ~35% smaller than the smallest of the older laboratory results, which are those of Shardanand and Prasad Rao [727]. The more recent laboratory studies (Johnston et al. [389]; Cheung et al. [165, 166], Jenouvrier et al. [378]) confirm the lower values obtained from solar irradiance measurements. The recommended absorption cross section values between 205 and 240 nm are listed in Table 4-2; they are taken from Yoshino et al. [859] and are based on the latter set of laboratory measurements. Amoruso et al. [17] have also carried out cross section measurements in this wavelength range (the Herzberg continuum); their values are ~15% lower than those reported by Yoshino et al.

Table 4-2. Absorption Cross Sections of O_2 Between 205 and 240 nm

λ (nm)	$10^{24}\ \sigma$ (cm^2)	λ (nm)	$10^{24}\ \sigma$ (cm^2)
205	7.35	223	3.89
206	7.13	224	3.67
207	7.05	225	3.45
208	6.86	226	3.21
209	6.68	227	2.98
210	6.51	228	2.77
211	6.24	229	2.63
212	6.05	230	2.43
213	5.89	231	2.25
214	5.72	232	2.10
215	5.59	233	1.94
216	5.35	234	1.78
217	5.13	235	1.63
218	4.88	236	1.48
219	4.64	237	1.34
220	4.46	238	1.22
221	4.26	239	1.10
222	4.09	240	1.01

The studies of the penetration of solar radiation in the atmosphere in the Schumann-Runge wavelength region were based originally on laboratory measurements of cross sections that were affected by instrumental parameters due to insufficient spectral resolution. Yoshino et al. [870] reported high resolution O_2 cross section measurements at 300 K, between 179 and 202 nm, obtaining the first set of results, which is independent of the instrument width. Additional studies at other temperatures, wavelengths, and isotopic compositions have been carried out by Yoshino et al. [861, 864-866, 869], Lewis et al. [441, 442], Cheung et al. [164], and Chiu et al. [169]. More recently, Yoshino et al. [860] reported cross sections of the Schumann-Runge bands in the window region between the rotational lines for wavelengths between 180 and 195 nm; these measurements supersede their earlier ones. Minschwaner et al. [530] have fit temperature-dependent O_2 cross sections between 175 and 204 nm with polynomial expressions, providing accurate means of determining the Schumann-Runge band cross sections with a model that incorporates the most recent laboratory data. Coquart et al. [183] have reported Herzberg continuum absorption cross sections in the wavelength region 196–205 nm of the Schumann-Runge bands.

For parameterizations of the O_2 absorption in the Schumann-Runge bands used in atmospheric modeling calculations, see, e.g., the review in WMO Report No. 16 [851]. More recent work by Murtagh [567], Nicolet and Kennes, [585] and Minschwaner et al. [530] incorporates results of the later laboratory measurements into efficient schemes for computing broad-band transmission and photolysis rates. Transmission values obtained by Murtagh [567] agree well with the WMO [851] recommendations, although the high-resolution calculations of Minschwaner and Salawitch differ with the WMO values by as much as 10–20% at some wavelengths.

In view of the quality of the high-resolution laboratory measurements, the primary source of uncertainty in modeling O_2 photolysis in the Schumann-Runge bands (other than the issue of absolute solar irradiance) has shifted to the choice of broadband parameterization.

A2. $O_3 + h\nu \rightarrow O + O_2$. The O_3 absorption cross-sections in the 200-790 nm region can be separated into four systems: the Hartley band (200-300 nm), the Huggins bands (300-370 nm), the Chappuis band (370-790 nm), and the Wulf bands extending towards longer wavelengths. The Hartley band is the strongest band and peaks around 255 nm. Although its overall shape is very smooth, there is residual vibrational structure in the region 250-260 nm. The Huggins band consists of a series of individual peaks, and is marked with a drastic change of absorption cross-sections (over more than five orders of magnitude) and strong temperature dependence. The Chappuis band is composed of a vibrational band progression superimposed on a continuous absorption in the visible region and is about thousand times weaker than the Hartley band. The very weak near-infrared part of the Chappuis band is clearly structured and corresponds to a different electronic transition (called the "Wulf bands").

For the three main bands in the region 200-790 nm, there have been many different measurements of the absorption spectrum and cross-sections at various experimental (temperature and pressure) and instrumental conditions (resolution) during the last century as shown in the following survey. The available measurements can be organized into three groups: (A) measurements of absolute cross-sections at single wavelengths (e.g. at the Hg resonance line at 253.65 nm), (B) measurements of absolute cross-sections over broad spectral regions (typically covering a few hundred nm), and (C) measurements of relative O_3 absorption spectra over broad spectral regions that have been scaled to absolute spectra using results from other studies (Type A or B).

Table 4-4. Summary of O_3 Cross Section Measurements

Reference	Spectral Range, nm	Type	Resolution, nm	Temperature, K
Ny and Choong, 1933 [592]	213-353	B	0.05	298
Vassy and Vassy, 1948 [811]	450-601	A	not stated	291,231,193,168
Vigroux, 1953 [818]	230-793 245-345	B	0.05	291 181-393
Inn and Tanaka, 1953 [365]	200-350 400-750	B	~0.05 0.5	300
Tanaka et al., 1953 [772]	105-220	B	0.5	300
Hearn, 1961 [323]	253.7-577.0	A	0.01-0.09	295
DeMore and Raper, 1964 [211]	210-300	B	0.2	77, 273
Vigroux, 1967 [819]	304-341	B	0.05	291
Griggs, 1968 [304]	200-360 450-850	B	0.1 0.5	303
Vigroux, 1969 [820]	230-270	B	0.1	291
Simons et al., 1973 [736]	300-370	B	0.4	195,300,333
Astholz et al. 1982 [27]	210-320	B	3	300,500,720,900
McPeters and Bass, 1982 [511]	300-310	C	0.02	229,245,295
Daumont et al., 1983 [202]	310-350	B	0.012	223,294
Brion et al., 1983 [95]	310-350	B	0.012	223,294
Brion et al., 1984 [96]	310-350	B	0.012	223,294
Freeman et al., 1984 [252]	250-350	C*	0.002	195
Bass and Paur, 1985 [54]	230-350	C*	<0.025	200,298
Paur and Bass, 1985 [628]	245-340	C*	<0.025	203,218,228,243,273,298
Freeman et al., 1985 [253]	281-335	A	0.003	195,228,293
Molina and Molina, 1986 [542]	185-350	B	0.07	226,263,298
Mauersberger et. al., 1986 [500]	253.7	A	not stated	297.5
Mauersberger et. al., 1987 [501]	253.7	A	not stated	297.5
Barnes and Mauersberger, 1987 [40]	237.7	A,C	not stated	195,221,237,253,273, 297,318,335,351
Yoshino et al., 1988 [867]	238.2-344.4	A	0.13-0.003	195,228,295
Malicet et al., 1989 [469]	253.36	A	not stated	229,295
Cacciani et al., 1989 [130]	339-355	B	0.012	220,293
Amoruso et al., 1990 [15]	590-610	B	0.05	230,299
Daumont et al. 1992 [201]	195-345	B*	0.01	295
Anderson and Mauersberger, 1992 [23]	543.5-632.8	A	not stated	295
Reference	Spectral Range,	Type	Resolution,	Temperature,

Reference	Spectral Range, nm	Type	Resolution, nm	Temperature, K
	nm		nm	K
Anderson et al., 1993 [22]	750-975	A	not stated	295
Brion et al., 1993 [94];	195-345 300-345	B*	0.01	218,228,243,295 273
Yoshino et al., 1993 [862]	185-254	A,B	0.13-0.003	195,228,295
Burkholder and Talukdar, 1994 [117]	407-763	C*	0.2	220,240,260,280,298
Brion et al., 1998 [93]	345-830 515-650	B*	0.01	295 218
Burrows et al., 1999 [123]	231-794	B*	0.2 - 0.4	202,221,241,273,293
Voigt et al., 2001 [825]	230-850	C*	5 cm^{-1}	203,223,246,280,293
Bogumil et al., 2001[81]	230-2400	C*	0.17-1.44	203,293
Bogumil et al., 2003 [82]	230-1070	C*	0.2-0.4	203,223,243,273,293

Earlier reviews on the measured absorption cross-sections were presented by Inn and Tanaka, 1958 [366], Ackermann, 1971 [4], Hudson, 1974 [350], Nicolet, 1981 [584], Brion et al., 1985 [97], Steinfeld et al., 1987 [751] and the WMO Report No. 16 [851], which was the basis for the previous JPL-97-4 evaluation. Orphal, 2003 [612, 614] has recently critically reviewed the available laboratory measurements up to 2003, and the current JPL evaluation is partly based on his review. Relevant for his evaluation are the measurements of type B and C, particularly those studies whose data were digitally available and marked with an asterisk*. Unfortunately, the recommended data set for the JPL-97-4 evaluation of Molina and Molina, 1986 [542] was not considered in his review.

In the Hartley and Huggins bands (about 240-325 nm) there is generally very good agreement (better than 2-3%) between the data measured at room temperature (293-300 K) by Bass and Paur, 1985 [54] and Paur and Bass, 1985 [628], Molina and Molina, 1986 [542], the Reims-team (Daumont et al. 1992 [201], Brion et al., 1993 [94], Malicet et al., 1995 [470] and Brion et al. 1998 [93]), Yoshino et al., 1993 [862], and the Bremen-team (Burrows et al., 1999 [123], Voigt et al., 2001 [825] and Bogumil et al., 2003 [82]). The older data by Ny and Choong, 1933 [592], Inn and Tanaka, 1953 [365] and Vigroux 1953 [818] are about 8% larger than the data of Molina and Molina, 1986 [542]. The vibration structure between 240 and 270 nm was observed in most studies, except those of Inn and Tanaka, 1953 [365], DeMore and Raper, 1964 [211] and Astholz et al. 1982 [27], who used lower resolution instruments.

A comparison of the O_3 cross-sections at the Hg-line wavelength 253.7 nm was performed by Orphal [612, 614] involving 13 absolute measurements and provided a mean value of $(114.1 \pm 0.9) \times 10^{-19}$ cm^2 $molecule^{-1}$. It has to be noted that the data of Bass and Paur, 1985 [54] and Paur and Bass, 1985 [628] are normalized to the absolute value 114.7×10^{-19} cm^2 $molecule^{-1}$ at 253.7 nm and 295 K measured by Hearn, 1961 [323]. In the range 230-260 nm, the data of the Reims-team (Daumont-Brion-Malicet-Brion) are generally lower (up to 2.5%) than the data of Molina and Molina, 1986 [542], Bass and Paur, 1985 [54] and the Bremen-team (Burrows-Voigt-Bogumil). Furthermore, the data of Voigt et al., 2001 [825] show a strong baseline shift below 255 nm and in the range 310-320 nm; in addition, the spectra are very noisy in the Hartley band maximum. The data of Bogumil et al. 2001 [81] and 2003 [82] contain periodic artefacts of the order of 0.5–1.0% in the range 240-270 nm and a straylight feature around 305 nm in the order of 2%.

Below 225 nm the room temperature cross-sections of Molina and Molina, 1986 [542], DeMore and Raper, 1964 [211] and the Reims-team (Daumont-Brion-Malicet) agree within 1-2%, but are 2-5% larger than the measurements of Yoshino et al., 1993 [862]. Other reported values measured by Ny and Choong, 1933 [592], Inn and Tanaka, 1953 [365], Astholz et al. 1982 [27] and Griggs, 1968 [304] differ up to 15%.

In the Huggins bands (310-350 nm) the studies differ in spectral resolution, which is mostly relevant only to atmospheric remote sensing. At wavelengths larger than 310 nm the vibrational structure becomes pronounced. In the range 310-340 nm, the agreement between the different studies is rather good (about 2%) for the data of Bass and Paur, 1985 [54], the Reims-team (Daumont-Brion-Malicet-Brion) and Burrows et al. 1999 [123], although important differences (up to 13%) due to wavelength shifts and spectral resolution are noticed by Orphal, 2003 [612, 614]. The data of Bass and Paur, 1985 [54] and of Reims-team (Daumont-Brion-Malicet-Brion) show wavelength shift of more than 0.02 nm. The data of Voigt et al., 2001 [825] and Bogumil et al., 2003 [82] contain systematic baseline drifts. Above 312 nm, the data of Molina and Molina, 1986 [542], which are listed every 0.5 nm up to 350 nm, occasionally miss the maxima and minima of the peaks. The reported values by Cacciani et al., 1989 [130] are typically 5-8% lower than the values of Molina and Molina, 1986 [542] in the range 339-355 nm.

The O_3 absorption cross-sections in the 350-450 nm region between the Huggins and Chappuis bands are very small and the available measurements of absolute values scatter significantly. They have been measured by Brion et al., 1998 [93] and the Bremen team (Burrows-Voigt-Bogumil). At the minimum near 378 nm, the reported absolute cross-sections at 298 K vary between 5×10^{-23} cm^2 $molecule^{-1}$ of Voigt et al. [825] and 5×10^{-24} cm^2 $molecule^{-1}$ of Brion et al., 1998 [93].

Absorption cross-section measurements of the Chappuis band of O_3 in the wavelength range 450-750 nm have been reported by Burkholder and Talukdar, 1994 [117], Brion et al., 1998 [93], the Bremen team (Burrows-Voigt-Bogumil) and at single wavelengths by Hearn, 1961 [323] and Anderson and Mauersberger, 1992 [23]. At the peak of the Chappuis band near 602 nm, the values agree within a few %, although the data of the Bremen-team (Burrows-Voigt-Bogumil) are consistently larger than those of Brion et al., 1998 [93] (by 2%) and Burkholder and Talukdar, 1994 [117] (by 4%) (the latter data are calibrated using the measurements of Anderson and Mauersberger, 1992 [23]). Note that there are pronounced deviations of data from Burkholder and Talukdar, 1994 [117] in the region 425-490 nm. The older values of Vassy and Vassy, 1948 [811], Vigroux, 1953 [818], Inn and Tanaka, 1953 [365], Griggs, 1968 [304] and Amoruso et al., 1990 [15] deviate up to 20%. Absorption cross-sections in the Wulf band region (>750 nm) have been reported by Anderson et al., 1993 [22] and Bogumil et al., 2003 [82].

The temperature dependence of the O_3 cross-sections has also been studied by several of the groups mentioned above, and tabulated in the survey. In his critical review, Orphal, 2003 [612, 614] calculated and compared the integrated cross-sections for 5 temperatures in the range 203 to 295 K in the different spectral regions of the O_3 spectrum. At all temperatures the agreement of the integrated cross-sections in the Hartley band is better than 2%, and less good agreement in the Chappuis band (4%). In particular, the integrated cross-sections of Burkholder and Talukdar, 1994 [117] lie systematically below the other measurements by about 3%, and the data of Burrows et al., 1999 [123] are always higher by 2%. In the Huggins bands and the blue tail of the Chappuis band the integrated cross-sections scatter by several percent (up to 5%), indicating systematic differences between the available data. The Hartley-band integrated cross-sections remain constant in the temperature range 203-293 K, within the experimental uncertainties. The integrated cross-sections in the Huggins bands decrease by more than 30% between 298 K and 203 K., and the differential cross sections of the bands increase significantly.

In the Hartley band most studies report a slight (0.9-1.6%) increase of the cross-section below 260 nm between room temperature and low temperatures 202-298 K, while Yoshino et al., 1993 [862] concluded that the temperature effect is negligible. Above 260 nm the cross-section decreases significantly at lower temperatures. This effect is due to the changing populations of the various vibrational and rotational quantum states of ozone, and has been analysed by Simons et al., 1973 [736]. The cross-section values are not linearly proportional to the temperature; instead the effect is larger at the maxima than it is at the minima of the spectral features.

The absorption cross-sections in the Huggins bands (310-350 nm) of O_3 decrease strongly with decreasing temperatures. Additionally, they depend on instrumental line shape and differences in wavelength calibration so that discrepancies up to 20% at the lowest temperatures are observed between the various studies. Comparison of the spectra obtained in the temperature range 220-229 K show good agreement (~3% at 325 nm, ~ 5% at 340 nm) with the data of Bass and Paur, 1985 [54], Molina and Molina, 1986 [542], the Brion team (Daumont-Brion-Malicet-Brion), and Burrows et al., 1999 [123]. The data of Voigt et al., 2001 [825] and Bogumil et al., 2003 [82] display sudden baseline jumps and are consistently lower than the other cited data sets. Voigt et al., 2001 [825] observed in the region 335-380 nm the presence of “hot bands”, which disappear with decreasing temperature, and “cold bands”, which become more pronounced at lower temperatures.

In the Chappuis band, the available cross-sections agree in showing a very small increase (1%) with decreasing temperature in the wavelength range 550-560 nm. However there is strong disagreement in the relative temperature dependence of the cross-sections in the wings (400-550 nm and 650-790 nm) of the Chappuis band. Burkholder and Talukdar, 1994 [117] report a decrease from 4% at 520 nm to 40% at 420 nm between 298 and 220 K., while Burrows et al. 1999 [123] observe a decrease at 420 nm to 70% at 221 K, and Bogumil et al., 2003 [82] a decrease of 20% at 223 K. These discrepancies could be due to baseline problems in the different measurements. It was also noted by the Bremen-team (Burrows-Voigt-Bogumil) that in the wings the differential cross-sections increase up to 10% between 298 and 203 K. In addition, the band structures between 400 and 500 nm shift toward shorter wavelengths with decreasing temperature.

Three different models have been proposed to reproduce the temperature-dependence of the O_3 cross-sections in the entire ultraviolet and visible regions within the experimental uncertainties. The first model was developed for the Hartley band by Adler-Golden [9] and uses an exponential function. The second model, developed by Bass and Paur 1985 [54], uses a quadratic polynomial to be applied in the Hartley and Huggins bands. The third model of Voigt et al., 2001 [825] uses a double exponential function. The accuracy of the

models was checked by Orphal, 2003 [612, 614], who concluded that the experimental data are better reproduced using a quadratic polynomial.

The pressure dependence of the O_3 absorption cross-sections was investigated by Hearn, 1961 [323] in the Hartley band, and by Voigt et al., 2001 [825] in the entire spectral region 240-790 nm. Both groups did not find experimental or theoretical support for pressure dependence, although Voigt et al., 2001 [825] proposed that temperature variations of the cross-sections around 400 nm might be due to the formation of a weakly bounded O_2-O_3 complex.

The recommended absorption cross sections are listed in Table 4-4, averaged over atmospheric intervals at 218 K and at room temperature (293-298 K). It has to be noted that cross sections are listed over 500 cm^{-1} intervals in the region 185-300 nm, over 1 nm intervals in the region 300 to 321 nm, over 2 nm intervals in the region 321.5 to 326.5 nm, and over 5 nm intervals in the region 330-825 nm. The 218 K values, measured by the Reims-team (Daumont-Brion-Malicet-Brion), are only listed for the range 196 to 340 nm. The room temperature data were selected for the range 185-233 nm from the data of Molina and Molina, 1986 [542], for the range 323-310 nm from Burrows et al. 1999 [123], and for the range 310-825 nm from the Reims team (Daumont-Brion-Malicet-Brion).

Table 4-5. Absorption Cross Sections of O_3 at 218 and 293-298 K

λ (nm)	10^{20} σ (cm^2) 218 K	293-298 K	λ (nm)	10^{20} σ (cm^2) 293-298 K
185.185–186.916		62.2	412.5–417.5	0.00295
186.916–188.679		57.6	417.5–422.5	0.00393
188.679–190.476		52.6	422.5–427.5	0.00656
190.476–192.308		47.7	427.5–432.5	0.00697
192.308–194.175		42.9	432.5–437.5	0.00882
194.175–196.078		38.5	437.5–442.5	0.0137
196.078–198.020	34.4	34.9	442.5–447.5	0.0165
198.020–200.000	32.0	32.4	447.5–452.5	0.0185
200.000–202.020	31.2	31.5	452.5–457.5	0.0218
202.020–204.082	32.4	32.6	457.5–462.5	0.0366
204.082–206.186	36.2	36.3	462.5–467.5	0.0367
206.186–208.333	43.2	43.3	467.5–472.5	0.0410
208.333–210.526	54.2	53.9	472.5–477.5	0.0481
210.526–212.766	69.6	69.3	477.5–482.5	0.0754
212.766–215.054	90.6	90.3	482.5–487.5	0.0813
215.054–217.391	119	118	487.5–492.5	0.0816
217.391–219.780	155	154	492.5–497.5	0.0908
219.780–222.222	201	199	497.5–502.5	0.121
222.222–224.719	256	255	502.5–507.5	0.160
224.719–227.273	323	322	507.5–512.5	0.158
227.273–229.885	403	401	512.5–517.5	0.166
229.885–232.558	492	490	517.5–522.5	0.183
232.558–235.294	589	590	522.5–527.5	0.219
235.294–238.095	692	693	527.5–532.5	0.267
238.095–240.964	799	802	532.5–537.5	0.287
240.964–243.902	905	908	537.5–542.5	0.295
243.902–246.914	995	1001	542.5–547.5	0.319
246.914–250.000	1074	1080	547.5–552.5	0.337
250.000–253.165	1116	1125	552.5–557.5	0.358
253.165–256.410	1136	1148	557.5–562.5	0.398
256.410–259.740	1105	1122	562.5–567.5	0.439
259.740–263.158	1047	1064	567.5–572.5	0.467
263.158–266.667	952	968	572.5–577.5	0.481
266.667–270.270	823	840	577.5–582.5	0.464
270.270–273.973	681	698	582.5–587.5	0.446
273.973–277.778	531	547	587.5–592.5	0.447
277.778–281.690	391	406	592.5–597.5	0.476
281.690–285.714	271	282	597.5–602.5	0.513
285.714–289.855	175	184	602.5–607.5	0.514
289.855–294.118	105	113	607.5–612.5	0.478
294.118–298.507	59.4	65.1	612.5–617.5	0.438
298.507-299.5	40.7	45.2	617.5–622.5	0.406
299.5-300.5	35.1	39.2	622.5–627.5	0.382
300.5-301.5	30.5	34.3	627.5–632.5	0.356
301.5-302.5	26.9	30.3	632.5–637.5	0.327
302.5-303.5	22.9	26.2	637.5–642.5	0.297
303.5-304.5	20.6	23.4	642.5–647.5	0.271
304.5-305.5	17.3	20.1	647.5–652.5	0.251
305.5-306.5	15.6	17.9	652.5–657.5	0.231
306.5-307.5	13.3	15.5	657.5–662.5	0.210
307.5-308.5	11.5	13.5	662.5–667.5	0.190
308.5-309.5	10.4	12.2	667.5–672.5	0.170
309.5-310.5	8.50	10.2	672.5–677.5	0.151
310.5-311.5	7.76	9.24	677.5–682.5	0.137

λ (nm)	10^{20} σ (cm^2) 218 K	293-298 K	λ (nm)	10^{20} σ (cm^2) 293-298 K
311.5-312.5	6.53	7.95	682.5–687.5	0.126
312.5-313.5	5.62	6.91	687.5–692.5	0.113
313.5-314.5	5.05	6.25	692.5–697.5	0.0989
314.5-315.5	4.08	5.19	697.5–702.5	0.0868
315.5-316.5	3.82	4.77	702.5-707.5	0.0784
316.5-317.5	3.11	4.02	707.5-712.5	0.0731
317.5-318.5	2.94	3.72	712.5-717.5	0.0696
318.5-319.5	2.11	2.89	717.5-722.5	0.0622
319.5-320.5	2.41	2.99	722.5-727.5	0.0543
320.5-321.5	1.43	2.10	727.5-732.5	0.0478
321.5-323.5	1.57	2.05	732.5-737.5	0.0442
323.5-325.5	1.02	1.41	737.5-742.5	0.0432
325.5-327.5	0.658	1.01	742.5-747.5	0.0447
327.5–332.5	0.483	0.697	747.5-752.5	0.0425
332.5–337.5	0.204	0.320	752.5-757.5	0.0338
337.5–342.5	0.0797	0.146	757.5-762.5	0.0286
342.5–347.5		0.0779	762.5-767.5	0.0262
347.5–352.5		0.0306	767.5-772.5	0.0260
352.5–357.5		0.0136	772.5-777.5	0.0294
357.5–362.5		0.00694	777.5-782.5	0.0318
362.5–367.5		0.00305	782.5-787.5	0.0262
367.5–372.5		0.00130	787.5-792.5	0.0208
372.5–377.5		0.000850	792.5-797.5	0.0173
377.5–382.5		0.000572	797.5-802.5	0.0157
382.5–387.5		0.000542	802.5-807.5	0.0156
387.5–392.5		0.000668	807.5-812.5	0.0186
392.5–397.5		0.000956	812.5-817.5	0.0221
397.5–402.5		0.00115	817.5-822.5	0.0206
402.5–407.5		0.00158	822.5-827.5	0.0145
407.5–412.5		0.00258		

Note:
T = 218 K, 196.078-342.5 nm, Reims team (1992-1995) (Daumont et al. 1992 [201], Brion et al., 1993 [94], Malicet et al., 1995 [470]),
T = 298 K, 185.185-232.558 nm, Molina and Molina, 1986 [542],
T = 293 K, 232.558-309.5 nm, Burrows et al. [123],
T = 295 K, 309.5-827.5 nm, Reims team (1992-1998) (Daumont et al. 1992 [201], Brion et al., 1993 [94], Malicet et al., 1995 [470], Brion et al. [93].

The recommendation for the $O(^1D)$ quantum yield from ozone photolysis as a function of wavelength and temperature is given by the expression,

$$\Phi(\lambda,T) = \left(\frac{q_1}{q_1+q_2}\right) \times A_1 \times \exp\left\{-\left(\frac{X_1-\lambda}{\omega_1}\right)^4\right\} + \left(\frac{q_2}{q_1+q_2}\right) \times A_2 \times \left(\frac{T}{300}\right)^2 \times \exp\left\{-\left(\frac{X_2-\lambda}{\omega_2}\right)^2\right\}$$
$$+ A_3 \times \left(\frac{T}{300}\right)^{1.5} \times \exp\left\{-\left(\frac{X_3-\lambda}{\omega_3}\right)^2\right\} + c$$

where $q_i = \exp\left(-\frac{\nu_i}{RT}\right)$ and X_{1-3}, A_{1-3}, ω_{1-3}, ν_{1-2} and c are best-fit parameters given in Table 4, λ is in nm, T is in K, and R = 0.695 (cm^{-1}/K). The parameter c is assumed to be temperature and wavelength independent.
This expression is valid only for the wavelength range 306–328 nm and temperature range 200–320 K.

Table 4-6. Parameters for the Calculation of $O(^1D)$ Quantum Yields

Parameter	i = 1	i = 2	i = 3
X_i (nm)	304.225	314.957	310.737
ω_i (nm)	5.576	6.601	2.187
A_i	0.8036	8.9061	0.1192
ν_i (cm^{-1})	0	825.518	–
c	0.0765	–	–

At room temperature (298 K) the uncertainties of the quantum yield values calculated with the above expression are estimated to be ±10 % (1σ) for $\Phi(\lambda, 298\ K) \geq 0.4$, while the uncertainties are estimated to be ±0.04 for $\Phi(\lambda, 298\ K) < 0.4$. At temperatures other than room temperature, the uncertainties are estimated to be ± 15 % for $\Phi(\lambda, T) \geq 0.4$ and ± 0.06 for $\Phi(\lambda, T) < 0.4$.

In the wavelength range 329–340 nm we recommend the value of $\Phi(O^1D) = 0.08 \pm 0.04$, independent of temperature. For $\lambda > 340$ nm, the quantum yield may be non-zero but no recommendation is made. For $\lambda < 306$ nm. the recommended quantum yield is 0.90, independent of temperature.

The recommendation for the temperature and wavelength dependences of the quantum yield for $O(^1D)$ production, $\Phi(O^1D)$, is taken from the review of Matsumi et al. [496]. Matsumi et al. derived the recommended values using the following procedure: The measured $O(^1D)$ quantum yields at 298 K between 306 and 328 nm from eight studies (Talukdar et al. [769], Takahashi et al. [762], Ball et al. [37], Armerding et al. [24], Bauer et al. [57], Brock and Watson [98], Trolier and Wiesenfeld [785] and Smith et al. [743], were normalized using $\Phi(O^1D) = 0.79$ at 308 nm. This value was derived from the studies listed in Table 1 of Matsumi et al. [496]. The resulting renormalized data were averaged. The wavelength dependence quantum yield data at various temperatures reported by Talukdar et al. [767, 769], Takahashi et al. [762], Hancock and Hofzumahaus [308] (this includes all the data from the Oxford group), Bauer et al. [57] and Smith et al. [743] were normalized to the value at 308 nm given above. These normalized data were used to obtain the best-fit parameters for eqn. 4-1 for the wavelength range 306–328 nm and temperature range 200–320 K. Because of the large number of studies upon which the 298 K evaluation is based, the averaged 298 K data were given a larger weight in the fitting procedure than the data at other temperatures.

The major differences between this recommendation and that of JPL 00-3 [703] are: (1) inclusion of more recent data from Smith et al., Hancock and Hofzumahaus, and Bauer et al., (2) selective deletion of data from the previous data from some of the groups, especially the use of data from Bauer et al. [57] which superseded the data of Silvente et al. [730] from the same group, (3) correcting for small differences in the absorption cross sections of ozone used by various groups, and (4) the normalization of all data to the selected value at 308 nm.

B1. $HO_2 + h\nu \rightarrow OH + H$. The absorption cross sections of the hydroperoxyl radical, HO_2, in the 190–260 nm region have been measured at room temperature by Paukert and Johnston [627], Hochanadel et al. [336], Cox and Burrows [187], McAdam et al. [505], Kurylo et al. [424], Moortgat et al. [559], Dagaut and Kurylo [200], Lightfoot and Jemi-Alade [450], who measured the cross sections up to 777 K, Crowley et al. [198], Maricq and Szente [482], Roehl et al. [677] and Sander et al. [704] at 227.5 nm. The absorption cross sections have been evaluated in earlier reviews by Lightfoot et al. [449] and Wallington et al. [832] who noted significant discrepancies in both the shapes of the spectra and the absolute magnitudes of the cross section values, particularly around 200 nm. The published ultraviolet absorption spectra have recently been reevaluated by Tyndall et al. [790]. Herein, the spectra were fitted to an analytical equation suggested by Maric et al. [479]:

$$\sigma = \frac{\sigma_{med}}{\left(1 - \frac{b}{\nu}\right)} \exp^{-a\left[\ln\left(\frac{\nu - b}{\nu_{med} - b}\right)\right]^2}$$

where $\sigma_{med} = 1.84 \times 10^{-18}$ cm^2 $molecule^{-1}$, a = 4.91, b = 30612 cm^{-1} and ν_{med}= 50260 cm^{-1}. Absolute cross sections were based on relative measurements of absorption cross sections of HO_2, CH_3O_2 and $C_2H_5O_2$ at 240 nm taken under identical conditions, combined with independent calibrations by Crowley et al. [198]. Table 4-7 lists the recommended cross sections, which are taken from the review by Tyndall et al. [790].

Lee [438] has detected $O(^1D)$ as a primary photodissociation product at 193 and at 248 nm, with a quantum yield that is about 15 times larger at the longer wavelength. The absolute quantum yield for $O(^1D)$ production has not been reported yet.

Photolysis of HO_2 in the stratosphere and troposphere is slow and can be neglected, but the UV absorption cross sections are important in laboratory studies of reaction kinetics.

Table 4-7. Absorption Cross Sections of HO_2

λ (nm)	$10^{20}\sigma$ (cm^2)
190	368
195	402
200	423
205	427
210	415
215	385
220	341
225	288
230	230
235	173
240	122
245	79.7
250	48.0
255	26.3
260	12.9

B2. $H_2O + h\nu \rightarrow H + OH$. Water vapor has a continuum absorption spectrum at wavelengths longer than 145 nm, with a maximum around 165 nm, the cross sections falling off rapidly toward longer wavelengths; the photodissociation threshold occurs at 246 nm. Below 69 nm the spectrum is also a continuum, and between 69 and 145 nm it consists of diffuse bands. In the atmosphere water vapor is photodissociated mainly by the solar Lyman alpha line (121.6 nm).

The absorption cross sections and the photochemistry of water vapor were reviewed by Hudson [349, 350], by Hudson and Kiefer [351], by Calvert and Pitts [136], and by Okabe [597].

The recommended absorption cross sections are taken from the review by Hudson and Kiefer [351] and are listed in Table 4-8 between 175 and 190 nm. At these wavelengths the quantum yield for production of H and OH is unity. At shorter wavelengths H_2 and O are also formed as primary products. Stief et al. [754] report a quantum yield of 0.11 for this process between 105 and 145 nm.

Table 4-8. Absorption Cross Sections of H_2O Vapor

λ(nm)	$10^{20}\sigma$ (cm^2)
175.5	262.8
177.5	185.4
180.0	78.1
182.5	23.0
185.0	5.5
186.0	3.1
187.5	1.6
189.3	0.7

B3. $H_2O_2 + h\nu \rightarrow OH + OH$. The recommended 298 K absorption cross section values, listed in Table 4-9, are the mean of the data of Lin et al. [455], Molina and Molina [539], Nicovich and Wine [586], and Vaghjiani and Ravishankara [799]. Molina and Molina [539] supersedes the earlier results of Molina et al. [546]. Nicovich and Wine measured the cross sections at $\lambda \pm 230$ relative to the values at 202.6, $\sigma = 4.32 \times 10^{-19}$ cm^2, and at 228.8 nm, $\sigma = 1.86 \times 10^{-19}$ cm^2. The values are within 2% of the recommended value.

Table 4-9. Absorption Cross Sections of H_2O_2 Vapor

λ (nm)	$10^{20}\sigma$ (cm^2)		λ (nm)	$10^{20}\sigma$ (cm^2)	
	298 K	355 K		298 K	355 K
190	67.2		270	3.3	3.5
195	56.4		275	2.6	2.8
200	47.5		280	2.0	2.2
205	40.8		285	1.5	1.6
210	35.7		290	1.2	1.3
215	30.7		295	0.90	1.0
220	25.8		300	0.68	0.79
225	21.7		305	0.51	0.58
230	18.2	18.4	310	0.39	0.46
235	15.0	15.2	315	0.29	0.36
240	12.4	12.6	320	0.22	0.27
245	10.2	10.8	325	0.16	0.21
250	8.3	8.5	330	0.13	0.17
255	6.7	6.9	335	0.10	0.13
260	5.3	5.5	340	0.07	0.10
265	4.2	4.4	345	0.05	0.06
			350	0.04	0.05

Nicovich and Wine have measured the temperature dependence of these cross sections. They expressed the measured cross sections as the sum of two components: σ_1, due to absorption from H_2O_2, which has the O–O stretch excited; and σ_0, due to absorption by ground state molecules. For atmospheric calculations the expression given in Table 4-10 may be used. The photodissociation quantum yield is believed to be unity. At and above 248 nm, the major photodissociation process is that leading to OH, i.e., the quantum yield for OH production is 2 (Vaghjiani and Ravishankara [800] and Vaghjiani et al. [801]). At 193 nm this quantum yield decreases to about 1.5 (Vaghjiani et al. [801]; Schiffman et al. [709]), and the quantum yield for O-atom production increases to about 0.16 (Vaghjiani et al. [801]).

Table 4-10. Mathematical Expression for Absorption Cross Sections of H_2O_2 as a Function of Temperature

$$10^{21}\,\sigma(\lambda,T) = \chi \sum_{n=0}^{7} A_n \lambda^n + (1-\chi) \sum_{n=0}^{4} B_n \lambda^n$$

Where T: temperature K; λ: nm; $\chi = (1 + \exp(-1265/T))^{-1}$

$A_0 = 6.4761 \times 10^4$	$B_0 = 6.8123 \times 10^3$
$A_1 = -9.2170972 \times 10^2$	$B_1 = -5.1351 \times 10^1$
$A_2 = 4.535649$	$B_2 = 1.1522 \times 10^{-1}$
$A_3 = -4.4589016 \times 10^{-3}$	$B_3 = -3.0493 \times 10^{-5}$
$A_4 = -4.035101 \times 10^{-5}$	$B_4 = -1.0924 \times 10^{-7}$
$A_5 = 1.6878206 \times 10^{-7}$	
$A_6 = -2.652014 \times 10^{-10}$	
$A_7 = 1.5534675 \times 10^{-13}$	

Range 260–350 nm; 200–400 K

C1. $NO_2 + h\nu \rightarrow NO + O\,(^3P)$. The NO_2 spectrum in the 200-800 nm region can be separated into two principal systems: the D-X band system below 250 nm, and the broad B-X and A-X band systems between 300 and 800 nm, with a maximum around 400 nm; due to interactions the forbidden C-X transition can also contribute to the visible spectrum. There is enormous spectral fine structure superimposed on the broad visible system. Due to the complexity of the electronic states of NO_2, it is impossible to predict its spectrum from molecular quantum theory within experimental accuracy. The absorption spectrum and cross sections of NO_2 have been measured at various resolutions during the last century as shown in the following survey.

Table 4-11. Summary of NO_2 Cross Section Measurements

Study	Range / nm	Type	Resolution / nm	Temperature / K
Holmes and Daniels, 1934 [337]	265-436	B	1	298
Dixon, 1940 [217]	400-700	A	1.5 and 4.0	295
Hall and Blacet, 1952 [307]	240-500	A	0.2-0.5	298
Nakayama et al., 1959 [571]	108-270	A	0.02	300
Jones and Bayes, 1973 [394]	297-579	B	0.2	300
Johnston and Graham, 1974 [387]	190-420	A	1.3	294
Bass et al., 1976 [53]	185-410	B	0.015-0.04	298,235
Harker et al., 1977 [311]	375-420	B	0.1	296
Hicks et al., 1979 [330]	425-450 at single λ	B	0.04	235,298
Schneider et al.,1987 [714]	200-700	A	0.04	298
Leroy et al., 1987 [440]	427-450	B	0.04	235,298
Koffend et al., 1987 [416]	391- 414/ intervals	B	0.005	251,300
Calvert et al., 1987 [135]	404.7	B	1.6	223,273,298,325,347, 370,406 496,566
Davidson et al., 1988 [204]	264-649	A	1.5 0.3-2.6 cm^{-1}	233,243,253,263,273,298 and higher up to 397
Corcoran et al., 1992 [184]	450-650/ intervals	A,B	0.075/0.003	295,573,673
Amoruso et al., 1993 [16]	440-460	B	0.134	220,298
Harwood and Jones, 1994 [314]	313-568	A	0.54	213,225,233,243,253, 263,273,298
Mérienne et al., 1995 [523]	300-500	A	0.01-0.015	293
Coquart et al., 1995 [182]	400-500	B	0.01	220,240,293
Vandaele et al., 1996 [806]	380-830	A	2.0 cm^{-1}	294
Frost et al. [254]	370-497	A	0.5 - 0.5 cm^{-1}	220
Jenouvrier et al., 1996 [377]	200-300	B	0.01	293
Mihalcea et al., 1996 [527]	395,670	B	0.001	296-774
Harder et al., 1997 [310]	350-585(294K) 350-560(low T)	A	0.15 cm^{-1}	217,230.2,238.6,293.8
Yoshino et al., 1997 [863]	360-470	B	0.14 cm^{-1}	298.5
Mérienne et al., 1997 [521]	200-400	A	0.05	220
Vandaele et al., 1998 [807]	238-1000	A	2.0 cm^{-1}	220,294
Burrows et al., 1998 [122]	231-794	C	0.2 - 0.4	221,241,273,293
Orphal et al., 1998 [615]	667-1111	B	0.012 cm^{-1}	298
Gierczak et al., 1999 [270]	413.4	B	1	259,298,323,348,385
Voigt et al., 2002 [826]	250-800	A	0.5-1.0 cm^{-1}	223,246,260,280,293
Vandaele et al., 2002 [804]	385-925	A	0.05-0.1 cm^{-1}	220,240,294
Bogumil et al., 2003 [82]	230-1070	C	0.2-0.4	203,223,243,273,293
Nizkorodov et al., 2004 [588]	415-525	B	0.06 cm^{-1}	215,230,250,273,298

The available studies can be organized into three groups: *type A*, measurements of *absolute* cross sections over broad spectral regions (typically covering a few hundred nm); *type B*, measurements of *absolute* cross sections at selected wavelengths or narrow spectral ranges; and *type C* measurements of *relative* NO_2 absorption spectra over broad spectral regions (typically a few hundred nm) that have been scaled to absolute spectra using results from other studies.

In the earlier years, the NO_2 ultraviolet-visible absorption cross section measurements were limited to lower spectral resolution. However since 1992 several sets of high-resolution measurements and their temperature and pressure dependence have been measured by several groups, mainly aimed at improving the accuracy of atmospheric measurements, in particular for the atmospheric remote sensing of NO_2. However laboratory measurements have been obtained at spectral resolutions that are limited by instrumental techniques.

The previous recommendations (JPL-97-04) [212] for the absorption cross sections of nitrogen dioxide were based on the work of Bass et al. [53], Schneider et al. [714] and by Davidson et al. [204]. Although at room temperature the agreement between these three sets of measurements is good (within 5% between 305 and 345 nm and within 10% at the longer wavelengths), serious non-uniform wavelength miscalibrations have

become apparent in the wavelength range 400-500 nm in the spectrum by Schneider et al. [714]. At the shorter wavelengths and at temperatures below 298 K the agreement is poor between the three sets of data. A possible cause for the discrepancies is the presence of N_2O_4, which is the weakly bound NO_2 dimer in equilibrium with the monomer, the ratio of the two species being pressure and temperature dependent. The corrections were needed to account for the presence of this species below 400 nm, especially in the near UV around 200 nm, where it absorbs strongly.

Kirmse et al. [409] analysed the spectra reported between 1976 and 1995 and concatenated selected (and corrected) cross sections to create a "new standard" spectrum in the range 300-708 nm at a resolution of 0.05 nm, and another spectrum extending to 908 nm at a lower resolution of 1 nm. This high resolution "new standard" spectrum consisted of the Mérienne et al. (1995) [523] cross sections from 300 to 500 nm, the Corcoran et al. [184] cross sections from 500 to 600 nm, and the Schneider et al. [714] cross sections from 600 to 710 nm. A critical review and evaluation of the cross section studies has been recently performed by Orphal (2002) [613] and Orphal (2003) [614], covering most studies published since 1995. In his evaluation Orphal [613, 614] considered baseline problems, wavelength calibration and integrated cross sections (after convolution of high-resolution cross sections of 0.1 nm or better). In addition, Vandaele et al. (2003) [805] derived temperature- and pressure-dependent parameters from high-resolution spectral data obtained since 1995. The current JPL (2006) evaluation is taken from the recommendations of Orphal (2003) [614] and Vandaele et al. (2003) [805].

At room temperature (295 ± 3 K) there is excellent agreement (better than 2-3%) between the absolute cross sections over the wavelength range covered by the measurements of Mérienne et al. (1995) [523], Coquart et al. [182], Vandaele et al. (1996) [806], Jenouvrier et al. [377], Yoshino et al. [863], Mérienne et al. (1997) [521], Vandaele et al. (1998) [807], Bogumil et al. [82] and Nizkorodov et al. [588]. Many of these studies differ in spectral resolution but this is much more relevant to atmospheric remote sensing. The cross sections of Harwood and Jones [314] are 6-8% below most of the other studies, while the data of Harder et al. [310] are slightly but systematically higher than the data of Vandaele et al. (1998) [807] (i.e. 2-5%) and show a systematic baseline drift of up to 10% at the lowest temperature.

The newest high-pressure cross-sections data of Vandaele et al. (2002) [804] and Vandaele et al. (2003) [805] are nearly 4% smaller than the Vandaele et al. (1996) [806] and Vandaele et al. (1998) [807] data. The cross sections of Burrows et al. [122] are about 6-8% lower than most recent high-resolution studies (Mérienne-95, Mérienne-97, Harder, Vandaele-96, Vandaele-98). The data of Voigt et al. [826] show several artificial peaks (probably Xenon lamp stray light) of a few percent and baseline shifts up to 10% (partly due to residual N_2O_4 absorption) at lower temperatures. The spectra of Bogumil et al. [82] were scaled to absolute values using the integrated cross section of Vandaele et al. (1998) [807].

The temperature effect on the NO_2 absorption cross sections has been studied by only a few research teams, as can be seen in the survey. The variation of the absorption consists mainly in an increase of the differential absorption cross sections with decreasing temperature. In his analysis of the temperature dependence of the cross sections in the 300-700 nm region, Orphal (2003) [614] observed a tilt in the baseline with decreasing temperature in the data of Davidson et al. [204], Burrows et al. [122], Bogumil et al. [82], but less pronounced in the data of Harwood and Jones [314], Harder et al. [310], and Vandaele et al. (2002) [804]. This is due to a change in the thermal population of the lower vibrational and rotational states, causing large discrepancies in the relative change and the absolute magnitude of the absorption cross sections. The comparison of the high-resolution absolute cross sections at temperatures below ambient reveals significant discrepancies in absolute magnitude of cross sections due to spectral resolution, baseline differences and possible wavelength calibration. For the temperatures 242 ± 2 and 220 ± 3 K, the overall agreement is within 15% in the region 350-500 nm, however outside this range the discrepancies are much larger. The integrated cross-sections for the range 400-500 nm were calculated by Orphal (2003) [614] to be $(4.50 \pm 0.10) \times 10^{-17}$ cm^2 $molecule^{-1}$ nm and are independent of temperature, as recently shown by Nizkorodov et al. [588] for the temperature range 215-298 K.

Orphal (2003) [614] and Vandaele et al. (2003) [805] compared the spectra after degrading the high-resolution spectra to a lower resolution. At 220 K the best agreement (within 1.6%) is obtained between the data of Coquart et al. [182], Mérienne et al. (1997) [521] and Vandaele et al. (1998) [807]. The data of Harder et al. [310] differ by 3.7% from the Vandaele et al. (1998) [807] data below 500 nm, but seem to contain more noise at larger wavelengths. The data of Voigt et al. [826] show larger disagreement, different at every temperature set. At 223 K their data are 22% lower than the Vandaele et al. (1998) [807] values.

The temperature dependence of the NO_2 cross sections in the entire ultraviolet and visible regions can be reproduced within the experimental uncertainties using analytical expressions at least at low and moderate spectral resolutions (i.e. 0.05 nm and less). Linear functions were proposed by Davidson et al. [204], Kirmse et al. [409] and Vandaele et al. (2002) [804], a quadratic polynomial by Burrows et al. [122] and a double exponential function by Voigt et al. [826]. For the high-resolution spectra Nizkorodov et al. [588] concluded that a linear temperature dependence is not valid, and a successful parameterisation needs further work.

The NO_2 cross sections are varying as a function of total pressure but these effects are only observed at high spectral resolution, i.e. better than 0.01 nm, as investigated by Harder et al. [310], Wennberg et al. [844], Vandaele et al. (1998) [807], Voigt et al. [826], Vandaele et al. (2002) [804], Nizkorodov et al. [588], using NO_2/N_2 (or air) mixtures at total pressures up to 1 atm. Nizkorodov et al. [588] showed that a simple Lorentzian broadening model, with linear dependence of the Lorentz width on pressure, provides an adequate description of the pressure broadening effects in NO_2.

The current recommendation is based on the data of Vandaele et al. (1998) [807]. Table 4- 12 displays cross sections for 294 and 220 K averaged over atmospheric intervals.

A number of studies of quantum yields of NO_2 photolysis for the atmospherically important 300–470 nm region have been reported: Jones and Bayes [394] for the wavelength range 295-445 nm and at selected wavelengths 492 nm, 546 nm and 579 nm; Gaedtke and Troe [259] in the range 313-416 nm; Harker et al. [311] for the range 375-420 nm at 1 nm intervals; Davenport [203] for the range 390-420 nm at 223 and 300 K; Gardner et al. [262] for the range 334-404 nm at 298 K, and at 404 nm at 273 and 370 K; and Roehl et al. [682] in the range 388-411nm at 248 and 298 K. In the range 360-398 nm the φ_1-values show a wide scatter, with differences as much as 60%, especially due to the data of Harker et al. [311]. Although Gardner et al. [262] obtained values of φ between 0.89 ± 0.05 and 0.97 ± 0.06 in the range 379-397 nm, they made a critical assessment of the quantum yield data and recommended that φ is near unity at wavelength up to and slightly beyond the dissociation limit of $\lambda_0 = 397.95$ nm (Jost et al., 1996; [395]) and then rapidly decreases to near zero at 424 nm. However Roehl et al. [682] determined $\varphi = (0.93 \pm 0.10)$ in the range 388-398 nm at 298 K, and $\varphi = (0.90 \pm 0.10)$ at 248 K. Troe [783] made a critical reanalysis of the quantum yield data of Gardner et al. [262] and Roehl et al. [682] below λ_0, and concluded that certain secondary reactions were not correctly accounted for, and recommended corrections for both data sets. The recommended quantum yield values listed in Table 4-13 are based on the data of Roehl et al. [682] corrected by Troe [783].

Table 4-12. Absorption Cross Sections of NO_2 at 220 and 294 K

λ (nm)	220 K x 10^{20}(cm^2)	294 K x 10^{20}(cm^2)	λ (nm)	220 K x 10^{20}(cm^2)	294 K x 10^{20}(cm^2)
240.964–243.902	4.14	5.77	442.5–447.5	47.9	48.8
243.902–246.914	0.961	2.79	447.5–452.5	49.3	49.8
246.914–250.000	0.859	1.62	452.5–457.5	40.6	41.6
250.000–253.165	0.191	0.998	457.5–462.5	43.5	43.6
253.165–256.410	0.496	1.05	462.5–467.5	41.5	41.4
256.410–259.740	0.872	1.28	467.5–472.5	32.7	33.7
259.740–263.158	1.26	1.58	472.5–477.5	38.8	38.7
263.158–266.667	1.77	2.05	477.5–482.5	33.4	33.7
266.667–270.270	2.36	2.64	482.5–487.5	24.0	25.4
270.270–273.973	3.03	3.24	487.5–492.5	30.9	30.8
273.973–277.778	3.94	4.07	492.5–497.5	29.4	29.4
277.778–281.690	5.16	5.21	497.5–502.5	16.7	18.2
281.690–285.714	6.29	6.23	502.5–507.5	24.4	24.3
285.714–289.855	7.72	7.59	507.5–512.5	22.8	23.1
289.855–294.118	9.64	9.51	512.5–517.5	14.8	16.0
294.118–298.507	11.6	11.5	517.5–522.5	17.7	16.1
298.507–303.030	13.2	13.2	522.5–527.5	17.5	17.9
303.030–307.692	16.0	16.1	527.5–532.5	14.9	15.3
307.692–312.5	18.5	18.8	532.5–537.5	9.71	10.6
312.5–317.5	20.8	21.6	537.5–542.5	10.3	10.8
317.5–322.5	24.2	25.3	542.5–547.5	12.6	12.7
322.5–327.5	27.2	28.7	547.5–552.5	10.4	11.0
327.5–332.5	29.4	31.7	552.5–557.5	7.40	7.97
332.5–337.5	33.0	35.8	557.5–562.5	5.56	6.05
337.5–342.5	37.0	40.2	562.5–567.5	8.62	8.70
342.5–347.5	38.6	41.8	567.5–572.5	8.25	8.48
347.5–352.5	43.5	46.2	572.5–577.5	4.12	4.71
352.5–357.5	47.7	49.7	577.5–582.5	4.11	4.47
357.5–362.5	49.2	50.9	582.5–587.5	4.60	4.69
362.5–367.5	53.7	54.9	587.5–592.5	5.14	5.39
367.5–372.5	55.2	56.1	592.5–597.5	3.82	4.08
372.5–377.5	58.4	59.0	597.5–602.5	3.71	3.95
377.5–382.5	58.5	59.3	602.5–607.5	1.56	1.85
382.5–387.5	59.2	60.1	607.5–612.5	2.38	2.54
387.5–392.5	62.4	63.0	612.5–617.5	3.47	3.53
392.5–397.5	58.5	59.7	617.5–622.5	2.39	2.57
397.5–402.5	64.0	64.4	622.5–627.5	1.77	1.96
402.5–407.5	57.0	58.2	627.5–632.5	1.00	1.21
407.5–412.5	61.8	62.4	632.5–637.5	1.23	1.33
412.5–417.5	58.3	59.1	637.5–642.5	1.48	1.53
417.5–422.5	59.3	59.9	642.5–647.5	1.86	1.92
422.5–427.5	56.0	57.0	647.5–652.5	1.24	1.35
427.5–432.5	53.7	54.4	652.5–657.5	0.755	0.873
432.5–437.5	55.5	55.9	657.5–662.5	0.508	0.566
437.5–442.5	47.5	48.8			

Note:
Integrated cross sections after Vandaele et al., 1998 [807].

Table 4-13. Quantum Yields for NO_2 Photolysis

λ, nm	Φ at 298 K	Φ at 248 K
300-398	1.00	1.00
399	0.95	0.94
400	0.88	0.86
401	0.75	0.69
402	0.62	0.56
403	0.53	0.44
404	0.44	0.34
405	0.37	0.28
406	0.30	0.22
407	0.26	0.18
408	0.22	0.14
409	0.18	0.12
410	0.15	0.10
411	0.13	0.08
412	0.11	0.07
413	0.09	0.06
414	0.08	0.04
415	0.06	0.03
416	0.05	0.02
417	0.04	0.02
418	0.03	0.02
419	0.02	0.01
420	0.02	0.01
422	0.01	0.01

Note:
after Troe et al. [783]

C2. $NO_3 + h\nu \rightarrow NO + O_2$ (1)
$NO_3 + h\nu \rightarrow NO_2 + O(^3P)$ (2)

The absorption spectrum of NO_3 shows about 20 diffuse bands between 400 and 700 nm. The most intense features, the 0-0 and 1-0 bands of the symmetric N-O stretching vibration in the excited state, are at 662 and 623 nm, with absorption cross sections of $\geq 2 \times 10^{-17}$ and $\geq 1.5 \times 10^{-17}$ cm^2 $molecule^{-1}$, respectively. The absorption cross section of the 0-0 band at 662 nm is of special interest, since it is used to monitor NO_3 both in the laboratory and in the atmosphere.

The absorption cross sections of NO_3 have been the subject of many laboratory studies in the last decades. Although agreement existed on the positions of the absorption features, estimates of the absolute cross sections varied by up to a factor of nearly two. The various studies and the cross sections measured at the 662-nm peak are listed in the following survey:

Table 4-14. Summary of NO_3 Cross Section Measurements

Reference	Year	NO_3 source Technique	Tempe-rature (K)	Wavelength range (nm)	Resolu-tion (nm)	σ(662 nm) (10^{-17} cm^2)
1) Schott and Davidson [716]	1958	N_2O_5 Shock pyrolysis	600, 650, 825, 1025	366-652	3.6	1.15 ± 0.4 [1)]
2) Johnston and Graham [387]	1974	$N_2O_5 + O_3$ Equilibrium constant calculation	295	450-680	0.7	0.347 (±50%) 1.48 [2)]
3) Graham and Johnston [296]	1978	$N_2O_5 + O_3$ Modulated photolysis	298	400-704	0.83	1.708
4) Mitchell et al. [534]	1980	$NO_2 + O_3$ Differential photomultiplier	294 ± 4	498-671	0.05	1.21 ± 0.20
5) Marinelli et al. [487]	1982	$NO_2 + O_3$ Tunable dye laser	296	654-671	0.05	1.90
6) Ravishankara and Wine [660]	1983	$F + HNO_3$ Discharge flow, dye laser	298	565-673	0.05	1.78 ± 0.23
7) Cox et al. [185]	1984	$Cl + ClONO_2$ Modulated photolysis, diode array spectrometer	296	662	0.4	1.63± 0.15
8) Burrows et al. [125]	1985	$F + HNO_3$, $Cl + HNO_3$ Modulated photolysis	298	615-670	1	1.85 ± 0.56
9) Ravishankara and Mauldin [658]	1986	$F + HNO_3$ Discharge flow, dye laser	298	652.5-672.5	0.05	1.90 ± 0.22
			240			2.31 ± 0.23
			220			2.71 ± 0.27
10) Sander [700]	1986	$Cl + ClONO_2$ Flash photolysis, diode array spectrometer	298	220-700	~0.4	2.28 ± 0.12 2.28 ± 0.34 [3)]
			250			2.62 ± 0.13
		$F + HNO_3$ Discharge flow	230			2.70 ±0.14
			298			1.83 ± 0.27
11) Canosa-Mas et al. [149]	1987	$F + HNO_3$ Discharge flow	296 ± 3	662	1.1	2.23 ± 0.35
12) Cantrell et al. [151]	1987	$NO_2 + O_3$ Fourier transform spectroscopy	348	662	0.22 (5 cm^{-1})	2.06 ± 0.27
			323			2.13 ± 0.22
			298			2.02 ± 0.20
			271			2.08 ± 0.18
			253			1.84 ± 0.43
			232			2.22 ± 0.33
			215			2.02 ± 0.24
			215-348			2.06 ± 0.32 (average)
13)Yokelson et al. [858]	1994	$Cl + ClONO_2$ Flash photolysis, diode array spectrometer	298	440-720	~0.1	2.23 ± 0.09
			258			2.49 ± 0.13
			230			2.76 ± 0.13
			200			2.99 ± 0.14
14) W ngberg et al. [836]	1997	$N_2O_5 \leftrightarrow NO_3 + NO_3$ Differential optical absorption spectroscopy	279.6-294.2	603-682	0.42	scaled to 2.10 [4)]
15) Orphal et al. [616]	2003	$N_2O_5 + O_3$ Fourier transform spectroscopy	294	465-794	0.6 cm^{-1} (0.026 nm at 662 nm)	2.18

[1)] Estimate for 300 K by Wayne et al. [840] from the data of Schott and Davidson [716].
[2)] Improvement by Graham and Johnston [296] using their more actual kinetic data.
[3)] The overall uncertainty (± 15%) includes the uncertainty of the absorbance measurement (± 5%) and the uncertainty of $\sigma(ClONO_2)$ (± 10%). The value for σ(662 nm) obtained by the flash photolysis method is preferred by Sander [700] over that obtained by the discharge flow method.
[4)] Recommendation by Wayne et al. [840].

It is apparent from the above compilation that there are significant differences between the reported absorption cross sections for the strong 0-0 band near 662 nm. The previous JPL recommendation derived a value of $(2.00 \pm 0.25)x10^{-17}$ cm^2 $molecule^{-1}$, which is the average of the results of references Nr. 5, 6, and 8-12 in Table 4-14. The recommendation of Wayne et al. [840] averaged the data of the more recent studies, references Nr. 9-12, and resulted in the higher value of $(2.10 \pm 0.20)x10^{-17}$ cm^2 $molecule^{-1}$. Higher values for the absorption cross section at 662 nm (see Table 4-14) were obtained in two most recent studies of Yokelson et al. [858] and Orphal et al. [616]. We averaged the results of Sander [700] and Yokelson et al. [858] to derive a new recommendation at 662 nm of $(2.25 \pm 0.15)x10^{-17}$ cm^2 $molecule^{-1}$ (the results of Cantrell et al. [151] have not been included; see the next paragraph concerning the temperature dependence). To obtain the recommended absorption cross sections listed in Table 4-15, we normalized the data of Sander [700] to this peak value (which actually is a reduction by only 1.3%).

Measurements of the temperature dependence of the absorption spectrum indicated an increase of the absorption cross sections with decreasing temperature. At the 662-nm peak an increase by 42% between 298 and 220 K was observed by Ravishankara and Mauldin [658], by 17% between 298 and 230 K by Sander [700], and increases by 34% between 298 and 200 K and 24% between 298 and 230 K by Yokelson et al. [858]. The results of Cantrell et al. [151], who reported temperature-independent cross sections averagin around $2.06x10^{-17}$ cm^2 $molecule^{-1}$ at T = 210-348 K, are in disagreement with these findings. A linear interpolation of the cross sections measured at 662 nm between 200 and 298 K, $\sigma(662\ nm, T) = (4.56 - 0.00787\ T)x10^{-17}$ cm^2 $molecule^{-1}$, was derived by Yokelson et al. [858].

A similar empirical relation, $\sigma(662\ nm, T) = (4.59 - 0.00\ 837\ T)x10^{-17}$ cm^2 $molecule^{-1}$, based on the data of Sander [700], normalized to $\sigma(662\ nm) = 2.1 \times 10^{-17}$ cm^2 $molecule^{-1}$, was given in the IUPAC 2003 recommendation. Orphal et al. [616] explained the temperature effect as resulting from changing populations of the vibrational levels of NO_3 and derived a formula for the cross section ratio as function of temperature:

$$\sigma(T)/\sigma(298K) = \{1 - \exp(-1096.4/T) - 2\ \exp(-529.5/T)\} / \{1 - \exp(-1096.4/298.0) - 2\ \exp(-529.5/298.0)\}$$

where the values of 1096.4 K^{-1} and 529.5 K^{-1} are the vibrational energies of 762 cm^{-1} and 368 cm^{-1} divided by the Boltzmann constant. Considering the absorption cross section ratio $\sigma(T)/\sigma(298\ K)$ as a function of reciprocal temperature, there is excellent agreement between the curves calculated by the Orphal model and the empirical relation of Yokelson et al. [858].

The quantum yields φ_1 and φ_2 have been measured by Graham and Johnston [296], and at higher spectral resolution by Magnotta and Johnston [467], who report the product of the cross section times the quantum yield in the 400-to-630-nm range. The total quantum yield value, $\varphi_1 + \varphi_2$, computed from the results of this latter study and the cross sections of Graham and Johnston [296], is about 1.5 for $\lambda < 585$ nm, based on the nearly constant yield of the major product $O(^3P)$, and a quantum yield for the NO production φ_1 near zero. Because systematic errors seems to exist in these data, Wayne et al. [840] in their review normalize φ_2 quantum yields to unity at $\lambda < 585$ nm. The quantum yield for the NO production φ_1 rises from zero at 585 nm to a maximum of $\varphi_1 = 0.35$ at 595 nm, where $\varphi_2 = 0.65$. At longer wavelengths both quantum yields φ_1 and φ_2 decrease to become zero at $\lambda = 640$ nm. Orlando et al. [611] measured the $O(^3P)$ and NO quantum yields in the photolysis of NO_3 between 570 and 635 nm, confirm qualitatively the previous measurements by Johnston and coworkers, but provide more accurate data for both channels. The $O(^3P)$ quantum yield was found to be unity in the range 570 to 585 to decrease to 0.1 at 635 nm. They observed anomalously low $O(^3P)$ yields in the region of the strong absorption band near 623 nm. Quantum yield of NO were < 0.10 at 580 nm, and 0.20 ± 0.10 near 590 nm. The shapes of the φ_1 and φ_2 curves are similar to those recommended in the review of Wayne et al. [840].

In a molecular beam study, Davis et al. [208] investigated the photodissociation processes of NO_3 in the range 532-662 nm, and determined a very sharp threshold for the dissociation of internally cold NO_3 into NO_2 and $O(^3P)$ at a wavelength of 587 nm. At shorter wavelengths, e.g., 585 nm, the NO + O_2 yield has dropped to values smaller than 0.05. At excitation energies just below this threshold, i.e., $\lambda = 588$ nm, a large quantum yield (0.70 ± 0.10) for a concerted three-center rearrangement was observed, resulting in NO + $O_2(^3\Sigma_g^-, {}^1\Delta)$. The yield of this NO + O_2 process decreases at longer wavelengths to zero at 613 nm. At $\lambda > 588$ nm the O + NO_2 channel arises from vibrational excitation of the ground electronic state of NO_3. These results imply that for thermally equilibrated NO_3, the branching ratios for dissociation of both channels (1) and (2) will strongly depend on the temperature, especially near the threshold wavelength.

Johnston et al. [385] have reanalyzed the available laboratory data relevant to NO_3 photolysis, including quantum yield for NO and NO_2 formation, fluorescence, and threshold energies from the molecular beam experiments. Their model reproduces the wavelength-dependent quantum yield values for $\varphi(O + NO_2)$, $\varphi(NO + O_2)$ and Φ(fluorescence) for three temperatures: 190, 230 and 298 K. At 298 K the calculated $\varphi(O + NO_2)$ quantum yields agree reasonably well with those obtained by Orlando et al. [611], but

show some systematic offset in the range 605-620 nm. The calculated $\varphi(NO + O_2)$ product yield agree with those observed by Magnotta and Johnston [467] within experimental scatter.

The recommended quantum yields are taken from the work of Johnston et al. [385] and are listed in Table 4-16 for the range 685 to 640 nm at three temperatures 190, 230 and 298 K. For $\lambda < 585$ nm, $\varphi(O + NO_2) = 1$, and $\varphi(NO + O_2) = 0$; at $\lambda > 640$ nm, $\varphi(O + NO_2)$ and $\varphi(NO + O_2)$ are zero.

Photodissiociation rates have been calculated by Johnston et al. [385] for overhead sun in the stratosphere:

$$J_1(NO + O_2) = 0.0201\ s^{-1}$$

$$J_2(NO_2 + O) = 0.156\ s^{-1}$$

The spectroscopy of NO_3 has been reviewed by Wayne et al. [840].

Table 4-15. Absorption Cross Sections of NO_3 at 298 K

λ (nm)	10^{20} σ (cm^2)	λ (nm)	10^{20} σ (cm^2)	λ (nm)	10^{20} σ (cm^2)	λ (nm)	10^{20} σ (cm^2)	λ (nm)	10^{20} σ (cm^2)
403	2	461	41	519	165	577	362	635	154
404	0	462	42	520	180	578	354	636	181
405	3	463	43	521	196	579	347	637	222
406	2	464	51	522	206	580	358	638	217
407	1	465	54	523	189	581	380	639	169
408	3	466	58	524	176	582	351	640	132
409	0	467	61	525	169	583	314	641	108
410	1	468	60	526	175	584	302	642	99
411	2	469	62	527	193	585	310	643	104
412	5	470	63	528	225	586	355	644	102
413	5	471	66	529	257	587	446	645	92
414	2	472	69	530	239	588	540	646	80
415	6	473	66	531	224	589	656	647	75
416	7	474	66	532	216	590	638	648	66
417	8	475	73	533	209	591	583	649	58
418	5	476	84	534	218	592	548	650	53
419	9	477	83	535	247	593	490	651	59
420	9	478	78	536	275	594	449	652	65
421	9	479	78	537	276	595	460	653	76
422	10	480	75	538	251	596	495	654	88
423	12	481	76	539	219	597	467	655	105
424	10	482	76	540	225	598	393	656	142
425	8	483	77	541	219	599	333	657	184
426	15	484	83	542	201	600	296	658	260
427	15	485	88	543	180	601	307	659	436
428	13	486	98	544	183	602	355	660	798
429	12	487	99	545	210	603	408	661	1551
430	18	488	102	546	260	604	468	662	2250
431	14	489	103	547	312	605	467	663	1869
432	16	490	111	548	320	606	355	664	1210
433	19	491	106	549	290	607	258	665	794
434	20	492	107	550	265	608	198	666	532
435	17	493	109	551	261	609	184	667	326
436	16	494	109	552	264	610	189	668	203
437	20	495	113	553	271	611	204	669	134
438	23	496	129	554	298	612	239	670	102
439	22	497	130	555	334	613	282	671	85
440	21	498	128	556	349	614	273	672	81
441	20	499	125	557	352	615	242	673	69
442	23	500	121	558	376	616	224	674	55
443	19	501	118	559	399	617	226	675	51
444	21	502	118	560	355	618	256	676	52
445	22	503	119	561	320	619	274	677	63
446	26	504	135	562	311	620	350	678	80
447	31	505	137	563	300	621	562	679	84
448	26	506	143	564	291	622	1090	680	74
449	30	507	137	565	292	623	1578	681	57
450	31	508	136	566	305	624	1291	682	42
451	33	509	145	567	301	625	898	683	33
452	36	510	162	568	305	626	783	684	28
453	34	511	186	569	310	627	806	685	19
454	38	512	189	570	299	628	789	686	17
455	38	513	172	571	296	629	748	687	13
456	38	514	169	572	294	630	724	688	13
457	42	515	170	573	298	631	518	689	13

λ (nm)	10^{20} σ (cm^2)	λ (nm)	10^{20} σ (cm^2)	λ (nm)	10^{20} σ (cm^2)	λ (nm)	10^{20} σ (cm^2)	λ (nm)	10^{20} σ (cm^2)
458	39	516	167	574	306	632	350	690	11
459	45	517	160	575	330	633	233	691	8
460	42	518	154	576	350	634	176		

Note:
403-691 nm, data of Sander [700] normalized to 2.25×10^{-17} cm^2 $molecule^{-1}$ at 662 nm.

Table 4-16. Quantum yields (multiplied by 1000) for the product channels $NO + O_2$ and $NO_2 + O(^3P)$ in the photolysis of NO_3 at 298, 230 and 190 K

λ nm	φ(NO)			φ(NO_2)		
	298 K	230 K	190 K	298 K	230 K	190 K
585	0.0	0.0	0.0	983.0	996.0	999.0
586	15.2	26.4	37.9	967.0	970.0	961.0
587	39.1	66.7	94.4	943.0	930.0	905.0
588	97.1	161.0	221.0	885.0	836.0	779.0
589	128.0	209.0	283.0	854.0	788.0	716.0
590	190.0	300.0	397.0	793.0	696.0	602.0
591	220.0	343.0	448.0	763.0	653.0	551.0
592	249.0	383.0	495.0	734.0	614.0	505.0
593	303.0	455.0	575.0	680.0	542.0	424.0
594	328.0	487.0	610.0	654.0	510.0	390.0
595	359.0	517.0	630.0	608.0	453.0	332.0
596	357.0	501.0	598.0	587.0	429.0	307.0
597	318.0	430.0	493.0	567.0	406.0	285.0
598	323.0	421.0	468.0	531.0	367.0	249.0
599	314.0	396.0	429.0	509.0	345.0	229.0
600	291.0	346.0	355.0	472.0	307.0	196.0
601	296.0	338.0	335.0	438.0	275.0	170.0
602	291.0	322.0	310.0	415.0	254.0	153.0
603	283.0	294.0	267.0	371.0	215.0	123.0
604	280.0	282.0	249.0	351.0	198.0	111.0
605	264.0	253.0	213.0	323.0	176.0	94.4
606	271.0	251.0	205.0	296.0	155.0	80.0
607	268.0	243.0	194.0	280.0	143.0	71.9
608	250.0	217.0	167.0	259.0	128.0	62.1
609	248.0	208.0	155.0	238.0	113.0	53.0
610	236.0	193.0	140.0	226.0	105.0	48.1
611	205.0	159.0	111.0	210.0	94.7	42.2
612	200.0	150.0	101.0	193.0	84.0	36.2
613	190.0	138.0	90.6	181.0	77.3	32.6
614	166.0	114.0	71.2	166.0	68.4	28.0
615	166.0	110.0	66.1	147.0	58.3	22.9
616	160.0	102.0	59.7	137.0	52.7	20.2
617	141.0	85.5	47.5	124.0	46.5	17.3
618	143.0	83.5	44.8	108.0	38.6	13.8
619	139.0	78.4	40.9	99.3	34.6	12.1
620	131.0	71.5	36.0	89.7	30.3	10.2
621	127.0	66.0	32.0	76.9	24.8	8.03
622	122.0	61.9	29.2	70.4	22.1	6.99
623	117.0	57.6	26.5	64.3	19.7	6.07
624	106.0	49.6	21.9	55.2	16.2	4.8
625	98.5	44.5	19.0	48.7	13.8	3.94
626	92.3	40.6	16.8	44.2	12.2	3.39
627	84.8	36.0	14.5	39.3	10.5	2.83
628	73.9	29.9	11.5	33.9	8.67	2.26
629	69.9	27.4	10.2	29.4	7.23	1.81
630	64.9	24.7	9.01	26.4	6.29	1.53
631	57.8	21.3	7.52	23.6	5.45	1.29
632	50.8	17.8	6.02	19.5	4.29	0.969
633	46.6	15.9	5.23	17.7	3.8	0.838
634	42.6	14.2	4.54	16.1	3.36	0.724
635	37.3	12.0	3.73	14.6	2.97	0.624
636	32.3	9.86	2.93	11.9	2.3	0.462
637	29.4	8.7	2.52	10.7	2.02	0.396
638	26.6	7.66	2.16	9.57	1.77	0.338
639	23.5	6.53	1.78	8.56	1.54	0.288
640	20.3	5.38	1.41	7.15	1.24	0.224

[a] From Johnston et al. [385].

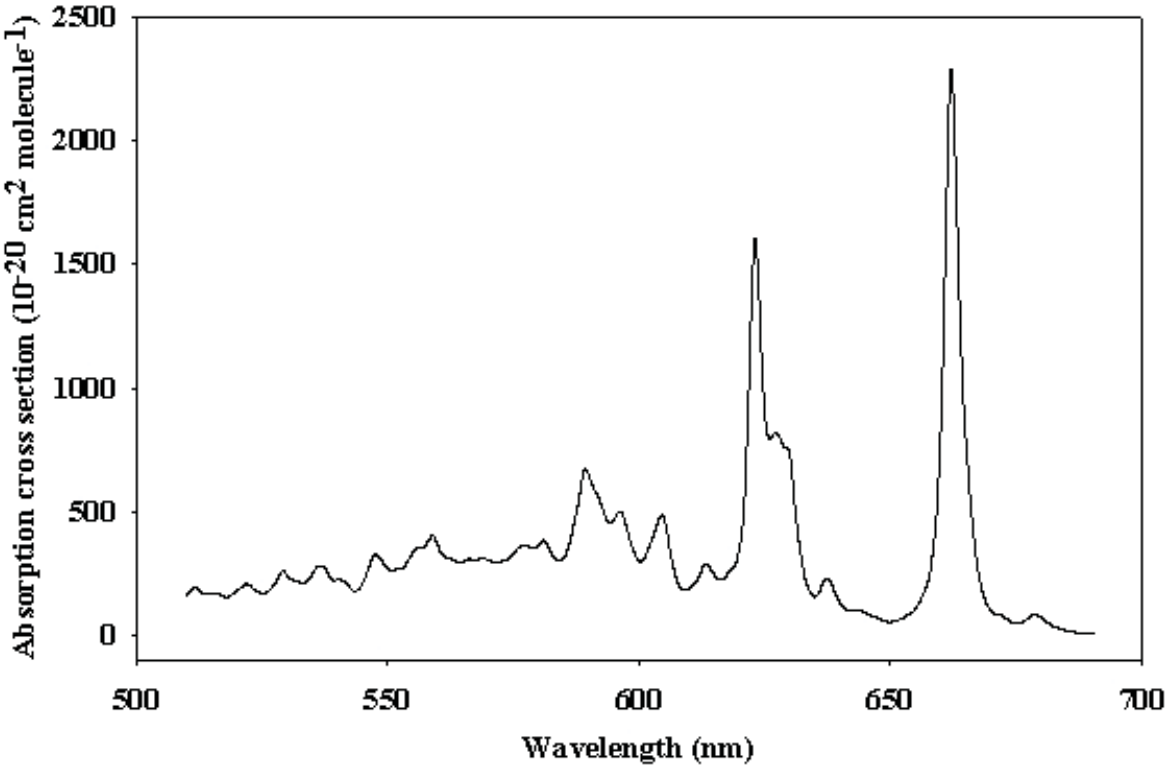

Figure 4-1. Absorption Spectrum of NO_3

C3. $N_2O + h\nu \rightarrow N_2 + O(^1D)$
$N_2O + h\nu \rightarrow N_2 + O(^3P)$
$N_2O + h\nu \rightarrow N(^4S) + NO(^2\Pi)$. Absorption cross sections of nitrous oxide NO_2 were measured in the VUV and UV spectral region between 108 and 315 nm and at temperatures between 194 and 302 K as shown in this survey:

Table 4-17. Summary of N_2O Cross Section Measurements

Reference	Year	Temperature (K)	Wavelength range (nm)	Spectral resolution (nm)
Romand and Mayence [685]	1949	291	139-231	not indicated
Zelikoff et al. [875]	1953	298	108-210	0.085
Zelikoff and Aschenbrand [874]	1954	298	184.9	not indicated
Thompson et al. [778]	1963	298	190-240	not indicated
Bates and Hays [55]	1967	298	190-315	not indicated
Johnston and Selwyn [390]	1975	298	210-300	not indicated
Selwyn et al. [722]	1977	194, 225, 243, 263, 302	173-240	0.7, 0.075
Hubrich and Stuhl [346]	1980	208, 298	160-235	0.3
Selwyn and Johnston [723]	1981	150-500	172-197	0.003, 0.05, 0.07
Yoshino et al. [868]	1984	295-299	169.6-222.6	0.0006
Mérienne et al. [522]	1990	220, 240, 296	200-240	0.02
Cantrell et al. [152]	1997	298, 353	184.9	<0.2
Creasy et al. [196]	2000	298	184.9	not indicated
von Hessberg et al. [828]	2004	233, 283	180-218	0.7, 1.1

The spectrum shows a broad absorption band between 160 and 260 nm with the maximum around 182 nm (σ_{max} = (1.24-1.47) × 10^{-19} cm^2 molecule^{-1}) and a stronger but smaller band between 137 and 160 nm with the maximum around 145 nm (σ_{max} = (5-6)) × 10^{-18} cm^2 molecule^{-1}). There is good agreement between the results of Selwyn et al. [722] and Hubrich and Stuhl [346] in the region of the broad absorption band. The agreement within this band is about 15%, around the 182 nm maximum better than 5%, with the data of Selwyn et al. [722] being somewhat larger than those of Hubrich and Stuhl [346]. The results of Mérienne et al. [522] for the region 220-240 nm are in excellent agreement (≤ 5%) with those of Selwyn et al. [722]. The

results of Cantrell et al. [152] and Creasy et al. [196] at 184.9 nm are in excellent agreement with the results of Selwyn et al. [722]. The high-resolution absorption curve reported by Yoshino et al. [868], showing vibrational structure around the maximum, lies very close to the absorption curve reported by Hubrich and Stuhl [346]. At wavelengths above 250 nm, there are large discrepancies between the results of Bates and Hayes [55] and those of Johnston and Selwyn [390]. Recommended cross sections are listed in Table 4-18. They are based on the room temperature results at 160, 165 and 170 nm of Hubrich and Stuhl [346] and the room temperature results between 173-240 nm of Selwyn et al. [722].

The temperature dependence of the absorption cross section in the atmospherically relevant wavelength region has been measured by Selwyn et al. [722], Hubrich and Stuhl [346], and Mérienne et al. [522] (see survey above). Their results are in excellent agreement. Absorption cross section decrease with decreasing temperature. Selwyn et al. [722] fitted their data with the expression shown in Table 4-19. Isotopomer specific cross sections for $^{14}N^{14}NO$, $^{15}N^{14}NO$, $^{14}N^{15}NO$, $^{15}N^{15}NO$ over the wavelength range 181-218 nm and at 233 and 283 K have been measured by von Hessberg et al. [828]; there is a slight decrease of the absorption cross sections of $^{14}N^{15}NO$ and $^{15}N^{5}NO$ as compared to those of $^{14}N^{14}NO$ and $^{15}N^{14}NO$, and again a decrease with decreasing temperature.

Quantum yield for photodissociation is unity, and products are almost exclusively N_2 and $O(^1D)$ (Zelikoff and Aschenbrand [874], Paraskevopoulos and Cvetanovic [621], Preston and Barr [645], Simonaitis et al. [735]). Yield of $N(^4S)$ and $NO(^2\Pi)$ is less than 1% (Greenblatt and Ravishankara [302]. The yield of $O(^3P)$ at 193 nm is reported to be 0.005±0.002 Nishida et al. [587].

Table 4-18. Absorption Cross Sections of N_2O at 298 K

λ (nm)	$10^{20}\sigma$ (cm^2)	λ (nm)	$10^{20}\sigma$ (cm^2)	λ (nm)	$10^{20}\sigma$ (cm^2)	λ (nm)	$10^{20}\sigma$ (cm^2)
160	4.30	188	12.5	206	1.65	224	0.0375
165	5.61	189	11.7	207	1.38	225	0.0303
170	8.30	190	11.1	208	1.16	226	0.0239
173	11.3	191	10.4	209	0.980	227	0.0190
174	11.9	192	9.75	210	0.755	228	0.0151
175	12.6	193	8.95	211	0.619	229	0.0120
176	13.4	194	8.11	212	0.518	230	0.00955
177	14.0	195	7.57	213	0.421	231	0.00760
178	13.9	196	6.82	214	0.342	232	0.00605
179	14.4	197	6.10	215	0.276	233	0.00478
180	14.6	198	5.35	216	0.223	234	0.00360
181	14.6	199	4.70	217	0.179	235	0.00301
182	14.7	200	4.09	218	0.142	236	0.00240
183	14.6	201	3.58	219	0.115	237	0.00191
184	14.4	202	3.09	220	0.0922	238	0.00152
185	14.3	203	2.67	221	0.0739	239	0.00123
186	13.6	204	2.30	222	0.0588	240	0.00101
187	13.1	205	1.95	223	0.0474		

Note:
160-170 nm, Hubrich and Stuhl [346],
173-240 nm, Selwyn et al. [722].

Table 4-19. Mathematical Expression for Absorption Cross Sections of N_2O as a Function of Temperature

$$\ln(\sigma(\lambda,T)) = \sum_{n=0}^{4} A_n \lambda^n + (T-300)\exp\left(\sum_{n=0}^{3} B_n \lambda^n\right)$$

Where T: temperature K; λ: nm;

$A_0 = 68.21023$ $B_0 = 123.4014$
$A_1 = -4.071805$ $B_1 = -2.116255$
$A_2 = 4.301146 \times 10^{-2}$ $B_2 = 1.111572 \times 10^{-2}$
$A_3 = -1.777846 \times 10^{-4}$ $B_3 = -1.881058 \times 10^{-5}$
$A_4 = 2.520672 \times 10^{-7}$

Ranges of applicability: 173 nm < λ < 240 nm; 194 K < T < 302 K

Several groups have investigated the isotopic fractionation of N_2O resulting from photolysis in the UV. Fractionation factors have been measured by several groups following photolysis at several wavelengths in the 193–213 nm range: Turatti et al. [786] employed high resolution FTIR spectroscopy; Röckmann et al. [675] used a modified isotope ratio mass spectrometric technique; and Rahn et al. [648] utilized conventional isotope ratio mass spectrometry. Zhang et al. [879] employed a low-resolution FTIR technique with N_2O photolysis at 213 nm, and Röckmann et al. [676] utilized a broadband photolysis source centered around 200 nm and simulating stratospheric actinic fluxes. The results are in reasonably good agreement, and indicate that the fractionation factors increase with photolysis wavelength from 193 to 213 nm. Furthermore, the fractionation factors show a clear dependence on the position of the ^{15}N atom, in agreement with the theoretical zero point energy model of Yung and Miller [872]; however, the Yung and Miller calculations underestimate the laboratory results by about a factor of two. A more detailed Hermite propagation model achieves better agreement with experimental enrichment factors (Johnson et al., [381]). Analysis of the isotopic composition of stratospheric air samples yields results that are in qualitative agreement with the laboratory results, confirming that photolysis is the predominant sink for N_2O [303, 676]. On the other hand, the fractionation factors measured in the atmospheric samples are smaller than those reported from the laboratory studies, indicating the influence of atmospheric diffusion and mixing [676].

C4. $N_2O_4 + h\nu \rightarrow 2\ NO_2$. The absorption cross sections of N_2O_4 have been derived from absorption measurements in NO_2-N_2O_4 mixtures. Data have been reported at 273 K and 265-405 nm by Holmes and Daniels [337]; at 300 K and 197 nm by Nakayama et al. [571]; at 298 K and 240-390 nm by Hall and Blacet [307] (as listed by Johnston and Graham [387]); at 273 K and 185-390 nm by Bass et al. [53]; at 298 K and 198-230 nm by Schneider et al. [714]; at 213, 225, 233, 243, and 253 K and 320-405 nm by Harwood et al. [314]; at 220 K and 200-390 nm by Mérienne et al. [521]; and at 220 K and 250-455 nm by Vandaele et al. [807]. The absorption spectrum of N_2O_4 exhibits an absorption band between 300 and 400 nm with the maximum at ~340 nm and a second, less pronounced maximum near ~265 nm followed by a sharp increase of the cross sections to another maximum in the region of ~190 nm. In the region 185-360 nm, there is good agreement between the various results as far as the shape of the absorption curve is concerned, with the exception that the spectrum reported by Bass et al. [53] is very noisy. In the region below 240 nm, there is good agreement between the absorption cross sections of Bass et al. [53] and Schneider et al. [714], whereas those reported by Mérienne et al. [521] are lower by ~30%. In the region between 250 and 300 nm, the results of Vandaele et al. [807] are systematically lower than the results of Mérienne et al. [521] by a factor ~0.85, whereas the results of Bass et al. [53] are higher by ~ 30%. In the region of the absorption band at 300-380 nm, there is good agreement between the results of Hall and Blacet [307], the low-temperature (213 and 224 K) data of Harwood et al. [314], and the results of Vandaele et al [807], the absorption cross sections for the maximum at 340 nm agreeing within 5%. The absorption curves reported by of Bass et al. [53] and Mérienne et al. [521] show higher values than the aforementioned ones, the differences for the absorption maximum being about 25% and 15%, respectively. As a recommendation we list in Table 4-20 the averages over 2-nm intervals of the high-resolution (0.01-0.03 nm) spectrum between 252 and 390 nm measured by Vandaele et al. [807].

Table 4-20. Absorption Cross Sections of N_2O_4 at 220 K

λ (nm)	$10^{20}\ \sigma$ (cm^2)	λ (nm)	$10^{20}\ \sigma$ (cm^2)	λ (nm)	$10^{20}\ \sigma$ (cm^2)	λ (nm)	$10^{20}\ \sigma$ (cm^2)
252	64.8	288	27.5	324	47.5	360	26.8
254	65.1	290	25.0	326	51.9	362	22.5
256	64.7	292	22.9	328	55.9	364	18.7
258	64.8	294	21.0	330	59.7	366	15.4
260	64.3	296	19.5	332	63.0	368	12.5
262	63.2	298	18.5	334	65.7	370	10.0
264	61.8	300	17.9	336	67.3	372	8.13
266	60.0	302	18.0	338	68.1	374	6.50
268	57.9	304	18.5	340	68.1	376	5.33
270	55.2	306	19.3	342	66.8	378	4.24
272	52.3	308	20.8	344	64.4	380	3.52
274	49.3	310	22.9	346	61.3	382	2.93
276	46.2	312	25.3	348	57.3	384	2.47
278	43.0	314	28.3	350	52.5	386	2.16
280	39.7	316	31.9	352	47.3	388	1.89
282	36.4	318	35.3	354	42.1	390	1.78

λ (nm)	10^{20} σ (cm^2)	λ (nm)	10^{20} σ (cm^2)	λ (nm)	10^{20} σ (cm^2)	λ (nm)	10^{20} σ (cm^2)
284	33.3	320	39.1	356	36.9		
286	30.3	322	43.2	358	31.7		

Note:
nm, Vandaele et al. [807].

C5. $N_2O_5 + h\nu \rightarrow NO_3 + NO_2$
$N_2O_5 + h\nu \rightarrow NO_3 + NO + O(^3P)$
$N_2O_5 + h\nu \rightarrow NO_3 + NO_2^*$. The absorption cross sections of dinitrogen pentoxide, N_2O_5 have been measured at 273 K and 265 and 280 nm by Holmes and Daniels [337] and at 280-380 nm by Jones and Wulf [393]; at room temperature and 210-290 nm by Johnston and Graham [387]; at 205-380 nm by Graham [295]; at 200-360 nm by Johnston et al. [384]; and at 208-398 nm by Harwood et al. [313]. The temperature dependence has been studied at 225 to 295 K and 290-380 nm by Yao et al. [856], at 273 and 295 K and 280-380 nm by Harwood et al. [316], and at 233-295 K and 240-420 nm by Harwood et al. [315]. Measurements in the far UV between 152 and 240 nm have been carried out at 195 K by Osborne et al. [617]. The absorption spectrum of N_2O_5 exhibits an absorption maximum at 160 nm and continuously decreasing absorption cross sections with increasing wavelength up to 420 nm.

The room temperature values of Yao et al. [856] and Harwood et al. [313, 315, 316] are in good agreement at wavelengths above 250 nm (within 10% in the region 250-280 nm and above 310 nm, and within 20% at ~290-310 nm). Below 250 nm, the cross sections reported by Yao et al. [856], which have been recommended in the 1997 evaluation, are systematically higher by up to a factor of ~2 at 208 nm than those reported by Harwood et al. [313]. A possible reason for this discrepancy could be contributions to the measured absorption from HNO_3 impurities as argued by Harwood et al. [313] who used N_2O_5 samples containing less than 1% HNO_3 impurities. This explanation was confirmed by the results of Osborne et al. [617], who also used thoroughly purified N_2O_5 samples and reported absorption cross sections (at 195 K indeed, but there is no temperature dependence at wavelengths smaller than 250 nm, see below) in excellent agreement with those of Harwood et al. [313] at 210-240 nm.

The recommended absorption cross sections listed in Table 4-21 are the mean of the data of Yao et al. [856] and Osborne [617] at 200-208 nm; the mean of the data of Yao et al. [856], Osborne et al. [617] (two data sets from different measurements), and Harwood et al. [313] at 210-240 nm; the data of Harwood et al. [313] at 242-398 nm, and the data of Harwood et al. [315] at 400-420 nm.

Temperature dependence of the absorption cross sections becomes significant at wavelengths above 280 nm. As observed in good agreement by Harwood et al. [313] and Yao et al. [856] the cross sections decrease with decreasing temperature, and the effect increases with increasing wavelength. The temperature coefficients A and B of a parameterization according to $\log_{10}(\sigma) = A + 1000B/T$ for T = 233-295 K, derived by Harwood et al. [315], are listed also in Table 4-21.

There are several studies on the primary photolysis products of N_2O_5: Swanson et al. [760] have measured the quantum yield for NO_3 production $\varphi_{248}(NO_3) = 0.89 \pm 0.15$ at 248 nm and $\varphi_{350}(NO_3) = 0.84 \pm 0.09$ at 350 nm, obtaining thus a value close to unity, which is consistent with the observations of Burrows et al. [124] for photolysis at 254 nm ($\varphi_{254}(NO_3) = 0.80$). Barker et al. [39] report a quantum yield for $O(^3P)$ production at 290 nm of less than 0.1, and 0.8 ± 0.2 for NO_3. For $O(^3P)$-atom production Margitan (private communication, 1985) measured a quantum yield value of 0.35 ± 0.10 at 266 nm, and Ravishankara et al. [662] report $\varphi(O^3P)$ values of 0.72 ± 0.09, 0.38 ± 0.08, 0.21 ± 0.03 and 0.15 ± 0.03 at 248, 266, 287, and 289 nm, respectively, with a quantum yield near unity for NO_3 production ($\varphi(NO_3) = 0.96 \pm 0.13$) at 248 nm. Quantum yields for NO_3 production were measured by Harwood et al. [313] at 248, 308 and 352.5 nm: $\varphi_{248}(NO_3) = 0.64 \pm 0.20$, $\varphi_{308}(NO_3) = 0.96 \pm 0.15$ and $\varphi_{352.5}(NO_3) = 1.03 \pm 0.15$.

Table 4-22 summarizes the above results. It appears, then, that NO_3 is produced with unity quantum yield at wavelengths above 300 nm, but that, based on the results by Harwood et al. [313], ($\varphi(NO_3)$ at $\lambda < 300$ nm is not well established. At e.g. 248 nm, the values vary between "near unity" and 0.64 ± 0.20. The $O(^3P)$-atom, and hence the NO yield, increases at shorter wavelengths, with a consequent decrease in the NO_2 yield.

The study of Oh et al. [595] indicates that, besides NO_3, the primary photolysis products are a wavelength-dependent mixture of NO_2, NO_2* and NO + O, where NO_2* represents one or more excited electronic states, most likely the $^2B_1$ state.

Table 4-21. Absorption cross sections N_2O_5 at 195-300 K and temperature coefficients

λ (nm)	10^{20} σ (cm^2)	A (cm^2)	B (cm^2 K^{-1})	λ (nm)	10^{20} σ (cm^2)	A (cm^2)	B (cm^2 K^{-1})	λ (nm)	10^{20} σ (cm^2)	A (cm^2)	B (cm^2 K^{-1})
200	910			270	16.2	-18.42	-0.104	340	0.368	-18.77	-0.492
202	842			272	14.9			342	0.328		
204	771			274	13.7			344	0.293		
206	682			276	12.4			346	0.262		
208	585			278	11.4			348	0.234		
210	445			280	10.5	-18.59	-0.112	350	0.210	-18.71	-0.583
212	381			282	9.59			352	0.188		
214	322			284	8.74			354	0.167		
216	267			286	7.94			356	0.149		
218	220			288	7.20			358	0.133		
220	181			290	6.52	-18.72	-0.135	360	0.120	-18.31	-0.770
222	151			292	5.88			362	0.107		
224	129			294	5.29			364	0.0958		
226	113			296	4.75			366	0.0852		
228	98.4			298	4.26			368	0.0763		
230	88.2			300	3.81	-18.84	-0.170	370	0.0685	-18.14	-0.885
232	80.5			302	3.40			372	0.0613		
234	74.0			304	3.03			374	0.0545		
236	69.2			306	2.70			376	0.0484		
238	64.6			308	2.40			378	0.0431		
240	59.8			310	2.13	-18.90	-0.226	380	0.0383	-18.01	-0.992
242	53.1			312	1.90			382	0.0341		
244	49.3			314	1.68			384	0.0305		
246	45.6			316	1.49			386	0.0273		
248	41.9			318	1.33			388	0.0242		
250	38.6			320	1.18	-18.93	-0.294	390	0.0215	-18.42	-0.949
252	35.5			322	1.05			392	0.0193		
254	32.6			324	0.930			394	0.0172		
256	29.9			326	0.826			396	0.0150		
258	27.5			328	0.735			398	0.0134		
260	25.2	-18.27	-0.091	330	0.654	-18.87	-0.388	400	0.014	-18.59	-0.966
262	23.1			332	0.582			410	0.009	-18.13	-1.160
264	21.1			334	0.518			420	0.005		
266	19.4			336	0.462						
268	17.8			338	0.412						

Note:
Absorption cross sections:
200-208 nm, mean of the data of Yao et al. [856] and Osborne et al. [617],
210-240 nm, mean of the data of Yao et al. [856], Osborne et al. [617] (two data sets), and Harwood et al. [313]
242-398 nm, data of Harwood et al. [313],
400-420 nm, data of Harwood et al. [315].
Temperature coefficients: 260-410 nm, Harwood et al. [315],
$\log_{10}(\sigma) = A + 1000B/T$ (T = 233-295 K). See text for a discussion of this parameterization.

Table 4-22. Quantum Yields from Photolysis of N_2O_5

λ (nm)	φ(NO_3)	φ(O^3P)	Reference
248	0.89 ± 0.15		Swanson et al. [760]
	0.96 ± 0.13	0.72 ± 0.09	Ravishankara et al. [662]
	0.64 ± 0.20		Harwood et al. [313]
254	0.80		Burrows et al. [124]
266		0.35 ±0.10	Margitan (private communication, 1985)
		0.38 ± 0.08	Ravishankara et al. [662]
287		0.21 ± 0.03	Ravishankara et al. [662]
289		0.15 ± 0.03	Ravishankara et al. [662]
290	0.8 ± 0.2	< 0.1	Barker et al. [39]
308	0.96 ± 0.15		Harwood et al. [313]
350	0.84 ± 0.09		Swanson et al. [760]
352.5	1.03 ± 0.15		Harwood et al. [313]

C6. HONO + hν → OH + NO

HONO + hν → H + NO_2. The absorption spectrum of HONO shows a structured absorption band between 300 and 400 nm, corresponding to vibrational progressions in the $A\,^1A'' \leftarrow X\,^1A'$ transition, with the highest peak near 354 nm. Below 270 nm there is a strong and broad absorption band with the maximum near 205 nm.

The absorption cross sections over the near-UV band have been measured at room temperature as shown in the following survey (the cross sections of the strongest vibrational band at 354 nm are given in the last column):

Table 4-23. Summary of HONO Cross Section Measurements

Reference	Year	Wavelength Range nm	Resolution nm	σ (354 nm) 10^{-19} cm^2
Johnston and Graham [387]	1974	300-399	0.87	1.23
Cox and Derwent [189]	1976	200-394	< 0.1	5.60
Perner [687]	1977	310-388	0.6	5.52
Stockwell and Calvert [755]	1978	310-396	< 1	4.96
Platt et al. [636]	1980	336-376	0.8	4.7
Vasudev [812]	1990	310-393	Not given	(4.97)*
Bongartz et al. [84]	1991	300-400	0.1 (λ<375 nm) 0.8 (λ<375 nm)	6.42**
Bongartz et al. [83]	1994	300-400	0.1 (λ<375 nm) 0.8 (λ>375 nm)	5.49**
Febo et al. [236]	1996	50-380	1	4.97**
Pagsberg et al. [618]	1997	348-376	0.06	5.02
Brust et al. [107]	2000	323-394	0.5	3.89
Stutz et al. [756]	2000	291-404	0.061±0.003	5.22
Wang and Zhang [835]	2000	352.2, 354.2, 357.0	< 0.1	4.89

* Normalized to the spectrum of Stockwell and Calvert [755].

** Bongartz et al. [83] corrected their 1991 results by a factor of 0.855.

There is good agreement between the various data sets as far as the peak positions are concerned. Discrepancies in the peak heights, generally, are a consequence of the different spectral resolutions used in the measurements. Stutz et al. [756] normalized the earlier cross section data to a resolution of 1 nm, which shows an agreement of better than 10% between their results and those of Bongartz et al. [83], Pagsberg et al. [618] and Vasudev [812]. The older measurements of Stockwell and Calvert [755] are in reasonable agreement with the more recent ones, whereas the data of Cox and Derwent [189] are higher by ~26% (presumably uncorrected NO_2 absorption) and those of Johnston and Graham [387] are smaller by 70% (presumably non equilibrium state of the $NO/NO_2/H_2O$ mixture during the measurements). The disagreement with the recent measurements of Brust et al. [107], whose results are smaller by ~25%, could not be explained.

Measurements in the region of the UV band have been carried out at 200-300 nm by Cox and Derwent [189] (resolution <0.1 nm) and at 184-274 nm by Kenner et al. [405] (resolution 0.38 nm). The reported spectra are in quantitative agreement over the wavelength range 220-270 nm. The sharp peak at 215 nm observed by Cox and Derwent [189], however, could not reproduced by Kenner et al. [405], who bring forward a number of arguments for the correctness of their results.

As recommended absorption cross sections, listed in Table 4-24, we choose for the region 184-274 nm the data of Kenner et al. [405] at 2-nm intervals (read from the plot given in their paper). The recommended absorption cross sections for the region 296-396 nm are based on the measurements of Stutz et al. [756]: for the regions 296-325 nm and 371-396 nm, we take the averages over 1-nm intervals of their high-resolution spectrum, and for the highly structured region 326-370 nm the averages over 0.5 nm intervals.

The quantum yield for OH radical production from the photolysis of HONO at 365 ± 5 nm was determined by Cox and Derwent [189] as (0.92 ± 0.16). The quantum yield for OH(A) production from the laser photolysis at 193 nm was measured as 1.8×10^{-5} by Kenner et al. [405]. Wollenhaupt et al. [852] determined an upper limit of 0.01 for the quantum yield of H-atom formation by the photolysis at 351 nm, using resonance fluorescence at 121.6 nm. The H + NO_2 (X $^2A_1$, A $^2B_2$, B $^2B_1$, C $^2A_2$) product channels in the photodissociation of HONO at 193.3 nm were recently examined by Amaral et al. [14], and branching ratios of the NO_2 electronic states estimated: X $^2A_1$: A $^2B_2$: B $^2B_1$: C $^2A_2$ $\approx$ 0.13 : 0.21 : 0.66.

Table 4-24. Absorption Cross Sections of HONO at 298 K

λ (nm)	10^{20} σ (cm^2)	λ (nm)	10^{20} σ (cm^2)	λ (nm)	10^{20} σ (cm^2)	λ (nm)	10^{20} σ (cm^2)
184	85.0	296	0.326	335.5	6.55	360.0	6.87
186	95.0	297	0.565	336.0	5.33	360.5	6.32
188	106	298	0.517	336.5	4.36	361.0	6.05
190	124	299	0.429	337.0	4.23	361.5	5.95
192	143	300	0.617	337.5	5.13	362.0	5.98
194	162	301	0.690	338.0	9.38	362.5	6.35
196	179	302	0.579	338.5	16.52	363.0	7.39
198	196	303	0.925	339.0	14.32	363.5	9.22
200	210	304	1.04	339.5	9.96	364.0	11.49
202	219	305	1.57	340.0	7.79	364.5	12.71
204	223	306	1.29	340.5	8.51	365.0	12.82
205	224	307	0.916	341.0	16.13	365.5	13.19
206	223	308	1.45	341.5	31.52	366.0	14.84
208	220	309	2.01	342.0	29.40	366.5	18.43
210	213	310	1.51	342.5	18.47	367.0	25.08
212	204	311	2.07	343.0	11.43	367.5	35.18
214	193	312	2.42	343.5	8.29	368.0	43.56
216	179	313	2.25	344.0	7.59	368.5	41.37
218	164	314	3.35	344.5	8.18	369.0	31.45
220	150	315	2.54	345.0	8.77	369.5	21.72
222	135	316	1.61	345.5	9.10	370	15.05
224	121	317	3.21	346.0	9.64	370	9.49
226	108	318	4.49	346.5	8.87	372	7.96
228	94.5	319	3.19	347.0	7.80	373	6.30
230	84.5	320	4.66	347.5	7.06	374	4.59
232	74.0	321	5.96	348.0	6.63	375	3.55
234	66.0	322	4.05	348.5	6.26	376	3.36
236	58.0	323	4.56	349.0	6.00	377	3.66
238	50.0	324	5.89	349.5	6.47	378	4.33
240	43.0	325	4.05	350.0	9.06	379	5.66
242	37.0	326	2.65	350.5	14.95	380	7.21
244	32.0	326.5	3.55	351.0	16.94	381	9.13
246	27.5	327.0	6.44	351.5	14.07	382	12.44
248	23.5	327.5	10.26	352.0	12.42	383	17.03
250	20.0	328.0	9.22	352.5	12.81	384	19.47
252	17.0	328.5	6.38	353.0	16.34	385	16.09
254	14.5	329.0	5.20	353.5	28.49	386	10.52
256	12.3	329.5	6.12	354.0	48.73	387	6.59
258	10.3	330.0	9.92	354.5	44.34	388	4.30
260	8.6	330.5	15.06	355.0	27.64	389	2.81
262	7.3	331.0	14.32	355.5	16.40	390	1.71
264	6.2	331.5	9.88	356.0	11.13	391	0.992
266	5.3	332.0	6.94	356.5	9.35	392	0.731
268	4.3	332.5	6.00	357.0	9.45	393	0.597
270	3.7	333.0	6.31	357.5	10.08	394	0.528
272	3.0	333.5	7.11	358.0	9.84	395	0.403
274	2.5	334.0	8.35	358.5	9.02	396	0.237
-	-	334.5	8.37	359.0	8.37		
-	-	335.0	7.71	359.5	7.67		

Note:
184-274 nm, Kenner et al. [405],
296-396 nm, Stutz et al. [756].

C7. $HNO_3 + h\nu \rightarrow OH + NO_2$ (1)
$HNO_3 + h\nu \rightarrow HONO + O(^3P)$ (2)
$HNO_3 + h\nu \rightarrow H + NO_3$ (3)
$HNO_3 + h\nu \rightarrow OH + NO_2^*(1^2B_2)$ (4)
$HNO_3 + h\nu \rightarrow HONO + O(^1D)$ (5)
$HNO_3 + h\nu \rightarrow HONO\ (a^3A) + O(^3P)$ (6)

The absorption spectrum of nitric acid shows a strong absorption band between 150 and 240 nm with the maximum near 183 nm and a second one, appearing as a shoulder above 240 nm on the long-wavelength wing of the strong band. The recommended absorption cross sections and their temperature dependence for the region 192-350 nm, listed in Table 4-25, are taken from the work of Burkholder et al. [119]. The temperature effect is very important for estimates of atmospheric photodissociation. The results of Burkholder et al. [119] agree well (within 10% above 200 nm) with those of Rattigan et al. [649, 650] measured at room temperature, whereas these latter authors report significantly smaller values at 239 K (smaller by 15-30% at 220-330 nm and smaller by ~50% at 330 nm). The recommended absorption cross sections at room temperature are in very good agreement (≤ 15% up to 310 nm) with the data of Molina and Molina [539]. These data are also in good agreement with the values reported by Biaume [68] and Johnston and Graham [386], except at the long wavelength ends. Okabe [598] has measured the cross sections in the 110–190 nm range and his results are 20–30% lower than those of Burkholder et al. [119], Biaume [68], and of Johnston and Graham [386] around 185–190 nm. Suto and Lee [758] have measured the cross sections between 105 and 210 nm, and their results are higher by 10-20% than those of Burkholder et al. [119], of Biaume [68], and of Johnston and Graham [386] around 185–190 nm, but show excellent agreement with the results of Molina and Molina [539] above 185 nm and with the results of Burkholder et al. [119] above 189 nm.

Johnston et al. [384] measured a quantum yield value of ~1 for the OH + NO_2 channel in the 200–315 nm range, using end product analysis. The quantum yield for O-atom production at 266 nm has been measured to be 0.03, and that for H-atom production ≤ 0.002, by Margitan and Watson [475], who looked directly for these products using atomic resonance fluorescence. Jolly et al. [391] measured a quantum yield for OH production of 0.89 ± 0.08 at 222 nm. Turnipseed et al. [789] have measured a quantum yield of (0.95 ± 0.09) for OH production at 248, (0.90 ± 0.11) at 222 nm, however, at 193 nm they reported φ(OH) be only 0.33 ± 0.06. They also measured the quantum yield for production of O-atoms [$O(^3P) + O(^1D)$] to be about 0.031 ± 0.01, 0.20 ± 0.03 and 0.81 ±0.13 at 248, 222 and 193 nm. Both $O(^3P)$ and $O(^1D)$ were observed at 222 and 193 nm, but only $O(^3P)$ was detected at 248 nm. Moreover, 40% of the O atoms formed at both 193 and 222 nm were $O(^1D)$ atoms, giving a $O(^1D)$ yield of 0.28 ± 0.07 at 193 nm. Turnipseed et al. [789] measured upper limits for $H(^2S)$ quantum yields: ≤ 0.002 at 238 nm, ≤ 0.01 at 222 nm, and ≤ 0.012 at 193 nm. Schiffman et al. [709] reported a larger quantum yield for OH production of 0.47 ± 0.06 at 193 nm, and some lower yield 0.75 ± 0.10 at 248 nm. Thus, it appears from these studies that HONO is a major photolysis product at 193 nm.

Felder et al. [240] reported the yield for (OH + NO_2) to be φ(OH) = 0.6 ± 0.1 and for (O + HONO) to be φ(HONO) = 0.4 ± 0.1 in the photolysis of HNO_3 at 193 nm using molecular beam/photofragment translational spectroscopy. Also Myers et al. [570] used this technique to measure the primary processes in the photolysis at 193 nm from the different photofragment ions, and found evidence of the participation of all channels (1) to (6), expect process (4). They determined the branching ratio (OH + NO_2)/(O+HONO) = 0.50 ± 0.05. They obtained φ(OH) = 0.33 ± 0.04 in excellent agreement with the value obtained by Turnipseed et al. [789]. The $\varphi(O)_{total}$ = 0.67 ± 0.04 is lower than the 0.81 ± 0.13 value measured by Turnipseed et al. [789], but the latter authors included the contribution of the secondary dissociation of NO_2 produced in channel (1). The primary yield of $O(^1D)$ formation = $\varphi(O^1D)$ = 0.54 ±0.04 is much larger than the $\varphi O(^1D)$ yield of 0.28 ± 0.07 measured by Turnipseed et al. [789], and remains unexplained. In a similar experiment using LIF and REMPI –TOF, Li et al. [444] found evidence for channel (2) with a yield of about 0.06.

Recent studies by Donaldson et al. [219], Zhang et al. [878] and Brown et al. [102] have indicated that photodissociation of HNO_3 by excitation of the vibrational overtones $3\nu_{O\text{-}H}$ (~983 nm), $4\nu_{O\text{-}H}$ (~755 nm) and $5\nu_{O\text{-}H}$ (~618 nm) in the near IR and visible occurs in the atmosphere providing an additional OH source. The band strengths (integrated absorption cross sections in cm^2 $molecule^{-1}$ cm^{-1}) of 2.63×10^{-20} for $3\nu_{O\text{-}H}$ and 2.37×10^{-21} for $4\nu_{O\text{-}H}$ transitions have been measured by Donaldson et al. [219], while Zhang et al. [878] obtained band strengths of $(2.9 \pm 0.7) \times 10^{-20}$ for $3\nu_{O\text{-}H}$ and $(2.8 \pm 1.0) \times 10^{-21}$ for $4\nu_{O\text{-}H}$ transitions. Brown et al. [102] measured the band strengths for $4\nu_{O\text{-}H}$ as $(2.25 \pm 0.15) \times 10^{-21}$ at 296 K and $(2.25 \pm 0.15) \times 10^{-21}$ at 251 K, and for 5 $\nu_{O\text{-}H}$ as $(2.57 \pm 0.15) \times 10^{-22}$ at 296 K and $(2.41 \pm 0.35) \times 10^{-21}$ at 251 K. Although the contributions of enhanced production of OH of photolysis due to overtone absorption is small, the current values are larger than those previously estimated by Donaldson et al. [218].

Table 4-25. Absorption Cross Sections at 298 K and Temperature Coefficients of HNO_3 Vapor

λ (nm)	$10^{20}\sigma$ (cm^2)	10^3 B (K^{-1})	λ (nm)	$10^{20}\sigma$ (cm^2)	10^3 B (K^{-1})	λ (nm)	$10^{20}\sigma$ (cm^2)	10^3 B (K^{-1})
192	1225	0	246	2.06	1.61	300	0.263	3.10
194	1095	0	248	2.00	1.44	302	0.208	3.24
196	940	1.70	250	1.97	1.34	304	0.167	3.52
198	770	1.65	252	1.96	1.23	306	0.133	3.77
200	588	1.66	254	1.95	1.18	308	0.105	3.91
202	447	1.69	256	1.95	1.14	310	0.0814	4.23
204	328	1.74	258	1.93	1.12	312	0.0628	4.70
206	231	1.77	260	1.91	1.14	314	0.0468	5.15
208	156	1.85	262	1.87	1.14	316	0.0362	5.25
210	104	1.97	264	1.83	1.18	318	0.0271	5.74
212	67.5	2.08	266	1.77	1.22	320	0.0197	6.45
214	43.9	2.17	268	1.70	1.25	322	0.0154	6.70
216	29.2	2.17	270	1.62	1.45	324	0.0108	7.16
218	20.0	2.21	272	1.53	1.49	326	0.00820	7.55
220	14.9	2.15	274	1.44	1.56	328	0.00613	8.16
222	11.8	2.06	276	1.33	1.64	330	0.00431	9.75
224	9.61	1.96	278	1.23	1.69	332	0.00319	9.93
226	8.02	1.84	280	1.12	1.78	334	0.00243	9.60
228	6.82	1.78	282	1.01	1.87	336	0.00196	10.5
230	5.75	1.80	284	0.909	1.94	338	0.00142	10.8
232	4.87	1.86	286	0.807	2.04	340	0.00103	11.8
234	4.14	1.90	288	0.709	2.15	342	0.00086	11.8
236	3.36	1.97	290	0.615	2.27	344	0.00069	9.30
238	2.93	1.97	292	0.532	2.38	346	0.00050	12.1
240	2.58	1.97	294	0.453	2.52	348	0.00042	11.9
242	2.34	1.88	296	0.381	2.70	350	0.00042	9.30
244	2.16	1.75	298	0.316	2.92			

Note:
192-350 nm, absorption cross sections σ and temperature coefficients B
($\sigma(\lambda, T) = \sigma(\lambda, 298) \exp(B(\lambda)(T - 298))$; T in K) of Burkholder et al. [119].

C8. $HO_2NO_2 + h\nu \rightarrow HO_2 + NO_2$ (1)
$HO_2NO_2 + h\nu \rightarrow OH + NO_3$ (2)
$HO_2NO_2 + h\nu \rightarrow O(^3P) + HNO_3$ (3)
$HO_2NO_2 + h\nu \rightarrow H + NO_2 + O_2$ (4)
$HO_2NO_2 + h\nu \rightarrow OH + NO_2 + O$ (5)
$HO_2NO_2 + h\nu \rightarrow HO_2 + NO + O(^3P)$ (6)
$HO_2NO_2 + h\nu \rightarrow H + O(^3P) + NO_3$ (7)

There are six studies of the UV spectrum of HO_2NO_2 vapor: at 269 K and 190-330 nm by Cox and Patrick [191], at 284 K and 195-265 nm by Morel et al. [561]; at room temperature and 200-290 nm by Graham et al. [297]; at 298 K and 190-330 nm by Molina and Molina [539]; at 253, 273, and 298 K and 210-329 nm by Singer et al. [737]; and at 273, 296, 318, and 343 K and 220-350 nm by Knight et al. [414]. There is very good agreement (within 5%) between the results of Molina and Molina [539] and Singer et al. [737] at 210-290 nm, which provided the basis for the earlier recommendation; discrepancies (~15-60%) appear in the critical wavelength range for atmospheric photodissociation ($\lambda \geq 290$ nm). The agreement between the data of Graham et al. [297] and Morel et al. [561] with those of Molina and Molina [539] is only within 30% up to 255 and 280 nm, respectively, and the data of Cox and Patrick [191] diverge from those of Molina and Molina [539]. The recent study of Knight et al. [414] over the wavelength range 220-350 nm used the data of Molina and Molina [539] and Singer et al. [737] in the 250-270-nm region for calibration and yielded reliable data for the long-wavelength region. The recommended absorption cross sections, listed in Table 4-26, are the data of Molina and Molina [539] at 190-205 nm, the mean of the data of Molina and Molina [539] and Singer et al. [737] at 210-275 nm, and the data of Knight et al. [414] at 280-350 nm.

In contrast to the measurements of Singer et al. [737], who found no temperature dependence between 253 and 298 K, Knight et al. [414] observed a temperature dependence between 273 and 343 K, i.e., an increase of the absorption cross sections with increasing temperature. An empirical parameterization of the measured temperature dependence by a simple two component absorption model is (T in K):

$$\sigma(T, \lambda) = \sigma_0(\lambda)/Q + \sigma_1(\lambda)\ (1-1/Q),$$

where the partition function is given by $Q = 1 + \exp(-\Delta E/(0.69T))$ with $\Delta E = 988\ cm^{-1}$ (O-O stretching vibration).

MacLeod et al. [464] measured the quantum yield of OH radicals in the photolysis of HO_2NO_2 at 248 nm as $\varphi_{248}(OH) = 0.34 \pm 0.16$ (channels 2 and 5), relative to the OH yield in the photolysis of H_2O_2. Roehl et al. [679] determined the quantum yield of NO_2 in the photolysis at 248 nm (relative to the NO_2 yield in the photolysis of HNO_3) as $\varphi_{248}(NO_2) = 0.56 \pm 0.17$ (channels 1,4 and 5). Recently Jimenez et al. [380] measured the yield of OH and HO_2 (arising from channels 1 and 6) at 193 and 248 nm (relative to the photolysis of H_2O_2), and the yield of NO_3 (relative to the photolysis of $ClONO_2$) at 193, 248 and 308 nm over a pressure range 10 to 84 Torr. Jimenez et al. [380] obtained: $\varphi_{193}(OH) = 0.21 \pm 0.12$, $\varphi_{248}(OH) = 0.085 \pm 0.08$, $\varphi_{193}(HO_2) = 0.56 \pm 0.02$, $\varphi_{248}(HO_2) = 0.89 \pm 0.26$, $\varphi_{193}(NO_3) = 0.35 \pm 0.03$, $\varphi_{248}(NO_3) = 0.08 \pm 0.03$ and $\varphi_{308}(NO_3) = 0.05 \pm 0.02$. These latest results indicate that at 248 nm the yields of OH and NO_3 are nearly identical as 0.08, assuming that only channel (2) contributes to OH and NO_3. This lower yield is not in agreement with the earlier results of MacLeod et al. [464] and Roehl et al. [679] at 248 nm. The high HO_2 yield (0.89 ± 0.26) measured at 248 nm by Jimenez et al. [380] overlaps within the experimental uncertainties with the NO_2 yield (0.56 ± 0.17) of Roehl et al. [679], assuming that the HO_2 arises from channel (1). It cannot however not be excluded that the difference in NO_2 yields reflects the contribution of channel (6). The recommended quantum yields are summarized in Table 4-27. The values below 200 nm are taken from Jimenez et al. [380]. The values above 200 nm represent an average between the results of Jimenez et al., Roehl et al. and MacLeod et al..The uncertainties on the recommended quantum yields are ± 0.2.

Recent studies, e.g., Wennberg et al. [845], Salawitch et al. [698] and Evans et al. [231], have indicated that photodissociation of HO_2NO_2 by excitation of the vibrational overtones $3\nu_1$ and $4\nu_1$ in the near IR and visible (at ~991 and 763 nm, respectively) occurs in the atmosphere providing an additional HO_x source. The band strengths (= integrated absorption cross sections) (all in cm^2 $molecule^{-1}$ cm^{-1}) $(3.8 \pm 1.1) \times 10^{-20}$ for $3\nu_1$ and $(3.0 \pm 1.8) \times 10^{-21}$ for $4\nu_1$ have been measured by Zhang et al. [877], and later $(3.3 \pm 0.7) \times 10^{-20}$ for $3\nu_1$ by Roehl et al. [680]. The latter group also measured absolute integrated band strengths and photodissociation quantum yields for 3 dissociative bands in the infrared region: $2\nu_1 + \nu_3$ (8242 cm^{-1}), $2\nu_1$ (6900 cm^{-1}) and $\nu_1 + 2\nu_3$(6252 cm^{-1}) as a function of temperature. The temperature-dependent cross sections and dissociation quantum yields are summarized in Table 4-27.

Table 4-26. Absorption Cross Sections of HO_2NO_2 at 296-298 K

λ (nm)	10^{20} σ (cm^2)	λ (nm)	10^{20} σ (cm^2)	λ (nm)	10^{20} σ (cm^2)	λ (nm)	10^{20} σ (cm^2)
190	1010	260	28.50	300	1.52	328	0.110
195	816	265	23.00	302	1.28	330	0.0926
200	563	270	18.05	304	1.05	332	0.0788
205	367	275	13.40	306	0.853	334	0.0650
210	239	280	9.29	308	0.702	336	0.0540
215	161	282	8.11	310	0.551	338	0.0456
220	117.5	284	6.93	312	0.465	340	0.0372
225	93.50	286	5.86	314	0.380	342	0.0320
230	79.20	288	4.91	316	0.313	344	0.0268
235	68.25	290	3.95	318	0.265	346	0.0228
240	58.10	292	3.37	320	0.216	348	0.0198
245	48.95	294	2.78	322	0.184	350	0.0168
250	41.25	296	2.30	324	0.152		
255	35.00	298	1.91	326	0.128		

Note:
190-205 nm, Molina and Molina [539],
10-275 nm, mean of the data of Molina and Molina [539] and Singer et al. [737],
280-350 nm, Knight et al. [414].

Table 4-27. Quantum Yields of HO_2NO_2

λ (nm)	Φ (OH)	Φ(NO_3)	Φ(HO_2)	Φ(NO_2)
<200	0.3	0.3	0.7	0.7
>200	0.2	0.2	0.8	0.8

Table 4-28. Photodissociation Band Strengths and Quantum Yields for Several Overtone and Combination Bands of HO_2NO_2

Band	Band center (cm^{-1})	$\int \sigma_{diss}\, \varphi_v\, d\nu$ Band strength cm^2 $molecule^{-1}$ cm^{-1}	Quantum yield
$4\nu_1$	13105	3.0×10^{-21} (b)	1
$3\nu_1$	10090	3.3×10^{-20}	1
$2\nu_1 + \nu_3$	8240	1.21×10^{-21}	0.76
$2\nu_1$	6900	4.09×10^{-18} exp(-826.5/T) (195 K > T > 224 K	0.14
$\nu_1 + 2\nu_3$	6250	1.87×10^{-19} exp(-1410.7/T) (195 K > T > 240 K)	0.02

Note:
a) Data from Roehl et al. [680]; b) from Zhang et al. [877].

PHOTOCHEM-D-Carbonyls

D1. $CH_2O + h\nu \rightarrow H + HCO$ ϕ_1
$CH_2O + h\nu \rightarrow H_2 + CO$ ϕ_2
$CH_2O + h\nu \rightarrow H + H + CO$ ϕ_3. The measurement of absorption spectra of formaldehyde at temperatures between 222 and 353 K have been the subject of many studies in the last four decades as shown in the following survey:

Table 4-29. Summary of CH_2O Cross Section Measurements

Reference	Year	Temperature (K)	Wavelength range (nm)	Resolution (nm)	Medium
McMillan [140]	1966	348	202-374	1	air
Bass et al. [52]	1980	223, 296	258-360	0.05	air
Moortgat et al.[555]	1980	285	215-370	0.5	air
Cantrell et al. [150]	1990	223, 233, 243, 253,263, 273, 283, 293, 296	300-358	1 cm^{-1} (~0.011)	vacuum
Rogers [683]	1990	296	235-365	0.04	vacuum
Meller and Moortgat [517]	2000	223, 298	224-373	~0.025	air
Bogumil et al. [82]	2003	293	247-400	0.25	air
Pope et al. [639]	2005	263, 294	313-320	0.1 cm^{-1} (~0.001)	air/vacuum
Pope et al. [640]	2005	294	308-320	0.1 cm^{-1}	air/vacuum

The UV absorption spectrum of formaldehyde displays a highly structured absorption band (of the $^1A_2 - X^1A_1$ transition) between 240 and 380 nm. An overview of the measurements up to the year 2000, including description of the techniques and experimental details of CH_2O generation and absorption measurements as well as comparison of the various results, is given by Meller and Moortgat [517]. Low resolution spectra were obtained by Mc Millan [140], and Moortgat et al. [555], whereas medium-resolution measurements were reported by Bass et al. [52], Rogers [683], and Bogumil et al. [82]. The spectrum reported by Cantrell et al. [150] was measured with the highest resolution (0.011 nm) for the 300-358-nm region using Fourier transform spectroscopy. Meller and Moortgat [517] provided a high-resolution spectrum in the complete UV

absorption band (224-373 nm) using diode array spectroscopy. Recently, a very high resolution spectrum (close to the Doppler limit of 0.07 cm^{-1}) of CH_2O was measured by Pope et al. [639, 640] in the range 308-320 nm using cavity ring-down spectroscopy (CRDS).

In general, the agreement between the medium and higher resolution data is good, whereby the data of Bass et al. [52] and Rogers [683] are consistently lower than the Meller and Moortgat [517] data. The contours of the spectral features measured by Bogumil et al. [82] obtained with the SCIAMACHY pre-flight satellite instrument, agree with the data of Meller and Moortgat [517]. Also, after convolution with lower-resolution instrument functions, the very high-resolution CH_2O spectrum measured by Pope et al. [639, 640] is in excellent agreement with the spectra obtained by Cantrell et al. [150] and Meller and Moortgat [517]. The low resolution absorption cross sections reported by Chen and Zhu [160, 161] and Chen et al. [162] for the 280-330-nm region at 5- and 10-nm intervals and measured for the calibration of photolysis measurements of some other carbonyl compounds deviate substantially up to 50% from those reported by Meller and Moortgat [517].

The high-resolution absorption cross sections obtained by Meller and Moortgat [517] are recommended for the wavelength range 225-375 nm of the absorption band. They are ~5-10% larger than the previously recommended cross sections of Cantrell et al. [150]. Cross sections averaged over 1-nm intervals are listed in Table 4-30, and over intervals used in atmospheric modeling in Table 4-31.

The temperature dependence of the absorption cross sections has been studied by Bass et al. [52], Moortgat et al. [555], Cantrell et al. [150], Meller and Moortgat [517], and Pope et al. [639, 640] (see above). Temperature effects are the strongest at the maximum of the absorption bands, where the lower temperatures result in larger absorptions. This effect is reversed in the wings of the absorption bands, where higher temperatures result in a higher absorption. A temperature sensitivity coefficient, Γ, allowing the calculation of the UV absorption spectrum at temperatures between 223 and 323 K and in the wavelength range 250-356 nm was derived by Meller and Moortgat [517]. Γ is defined by the equation

$$\sigma(\lambda, T) = \sigma(\lambda, 298\ K) + \Gamma(T - 298\ K)$$

Values of Γ averaged over 1-nm intervals and intervals used in atmospheric modeling are listed in Table 4-30 and Table 4-31, respectively.

VUV absorption cross sections for the wavelength region 60-185 nm have been obtained by Gentieu and Mentall [265], Mentall et al. [520], and Glicker and Stief [285] using optical methods and by Cooper et al. [180] for the region 6-261 nm using (e, e) dipole spectroscopy.

In earlier studies quantum yields have been measured by McQuigg et al. [512], Calvert et al. [133] who established a general trend of increasing radical yield with decreasing wavelength in the range 290-360 nm. More precise wavelength dependent quantum yield studies using monochromatic light sources were performed by Lewis et al. [443], Marling [488], Horowitz and Calvert [338], Clark et al. [173], Moortgat et al. [558] and Tang et al. [774] using radical scavengers. Moortgat and Warneck [560] and Moortgat et al. [555, 557] measured the yields of CO and H_2 from the photolysis of CH_2O in air (thus giving respectively $\varphi_1 + \varphi_2$ and φ_2) as a function of wavelength and pressure at 300 and 220 K. They showed that the yield of CO was essential unity for $290 < \lambda < 330$ nm at all pressures with no systematic temperature effect. For $\lambda > 330$ nm, both temperature and pressure have a significant effect on ϕ_2 but a negligible effect on ϕ_1. Also the total CO yield decreased at $\lambda < 290$ nm to 0.76 at 240 nm. An evaluation of the quantum yields was performed by Calvert et al. [132] based on the results of previous studies, similar to the JPL-recommendation given by DeMore et al. [213], but including algorithms for estimating the pressure and temperature dependence of ϕ_2.

Smith et al. [744] measured relative quantum yields for the production of radical products H and HCO (φ_1) using NO-chemical amplification and subsequent detection of NO_2 with chemical ionization mass spectrometry. These authors measured the quantum yields in the range 269 to 339 nm with sufficient resolution (0.62 nm, fwhm) to observe structure in the wavelength dependence, which previously had not been reported, and which is believed to provide evidence for a complicated competition among the various dissociation pathways 1, 2 and 3. The ϕ_1 yields, normalized to 0.753 at 303.75 nm based on the JPL-1997 recommendation [213], agreed qualitatively with the previous determinations reported by Horowitz and Calvert [338] and Moortgat et al. [557]. However at $\lambda > 320$ nm the reported ϕ_1 yields (measured at 50 mbar) by Smith et al. [744] are somewhat larger than the values recommended by DeMore et al. [213], resulting in a larger (~ 8%) overall rate of radical production. Pope et al. [639, 640] simultaneously measured HCO radical and CH_2O absorption cross sections using CRDS, from which HCO-quantum yields were calculated. This work showed that HCO yields in the region 308-319 nm vary with the vibrational level of the $^1A_2$ state of CH_2O and with the pressure of the bath gas.

The recommended quantum yields for photolysis of CH_2O are listed in Table 4-32, and are based on a fitting of the data for channel 1 (H + HCO) involving the data of Lewis et al. [443], Marling [488], Horowitz and Calvert [338], Clark et al. [173], Tang et al. [774], Moortgat et al. [557] and Smith et al. [744]. The parameters of the fitting expression

$\phi_1(\lambda) = a_0 + a_1\lambda + a_2\lambda^2 + a_3\lambda^3 + a_4\lambda^4$ (valid for the wavelength range $250 > \lambda > 338$ nm)

are $a_o = 717.057373$ $a_1 = -9.4955377$ $a_2 = 0.04665398$ $a_3 = -1.0065325 \times 10^{-4}$ $a_4 = 8.03898 \times 10^{-8}$

$\phi_2(\lambda)$ was optimized using the quantum data for CO (giving $\phi_{tot} = \phi_1 + \phi_2$) from Moortgat et al. [557] and the relation $\phi_2 = \phi_{tot} - \phi_1$.

The pressure and temperature dependence of ϕ_2 is based on the algorithm cited in Calvert et al. [132] and limited for values $\lambda > 330$ nm. The pressure dependence of ϕ_2 is represented in Stern-Volmer form

$$\phi_2(\lambda, p, T) = [(1/(1 - \phi_1(\lambda)) + \alpha(\lambda,T) \times P]^{-1}$$

where $\alpha(\lambda,T)$ is the quenching coefficient at pressure P, whose values at 300 K can be estimated directly from ϕ_1 and ϕ_2 (see Table 4-32 for quantum yields at atmospheric pressure P_{atm} and 300 K)**:**

$$\alpha(\lambda, 300) = 1/P_{atm}\ [\ 1/\phi_2(\lambda, P_{atm}, 300) - 1/(1 - \phi_1(\lambda))]$$

At temperatures T between 220 and 300 K the quenching coefficient $\alpha(\lambda, T)$ can be interpolated from

$$\alpha(\lambda, T) = \alpha(\lambda, 300)\ \{\ 1 + 0.05\ (\lambda - 329)\ [(T - 80)/80]\ \}$$

Table 4-30. Absorption Cross Sections of CH_2O at 298 K and Temperature Coefficients Averaged over 1-nm Intervals

λ (nm)	10^{20} σ (cm^2)	10^{24} Γ ($cm^2 \cdot K^{-1}$)	λ (nm)	10^{20} σ (cm^2)	$10^{24} \cdot$Γ ($cm^2 \cdot K^{-1}$)	λ (nm)	10^{20} σ (cm^2)	$10^{24} \cdot$Γ ($cm^2 \cdot K^{-1}$)
226	0.0179		276	2.59	-2.040	326	6.87	-5.640
227	0.0169		277	1.57	1.933	327	4.37	5.440
228	0.0177		278	1.03	1.427	328	1.22	5.067
229	0.0190		279	2.45	-2.547	329	3.12	-3.347
230	0.0205		280	2.34	-0.680	330	3.86	-2.173
231	0.0330		281	1.56	0.560	331	1.41	3.907
232	0.0335		282	0.972	0.809	332	0.346	1.792
233	0.0262		283	0.720	0.005	333	0.214	0.429
234	0.0325		284	4.27	-8.720	334	0.159	-0.228
235	0.0363		285	4.05	-1.800	335	0.0966	-0.005
236	0.0539		286	2.09	1.587	336	0.126	0.325
237	0.0771		287	1.15	0.760	337	0.383	0.329
238	0.0569		288	3.17	-4.707	338	1.92	1.600
239	0.0682		289	3.22	-1.213	339	5.50	-6.587
240	0.0782		290	1.17	1.707	340	3.15	5.520
241	0.0775		291	1.84	-1.160	341	0.978	5.863
242	0.123		292	0.796	1.155	342	0.504	1.216
243	0.159		293	3.11	-4.907	343	1.92	-2.987
244	0.109		294	7.15	-10.213	344	1.27	0.187
245	0.131		295	4.06	3.827	345	0.436	2.765
246	0.163		296	2.48	2.120	346	0.119	0.541
247	0.151		297	1.36	1.387	347	0.0441	-0.281
248	0.234		298	4.22	-4.933	348	0.0757	-0.664
249	0.318		299	3.17	1.480	349	0.0378	-0.560
250	0.257	0.203	300	0.963	4.267	350	0.0360	-0.728
251	0.204	0.177	301	1.63	-2.573	351	0.0894	-0.121
252	0.337	-0.072	302	0.852	-2.325	352	0.731	0.368
253	0.289	0.101	303	3.02	-3.600	353	2.28	-5.320
254	0.342	0.137	304	7.23	-4.827	354	1.65	0.600
255	0.450	0.272	305	4.74	4.173	355	0.696	2.456
256	0.629	0.169	306	4.29	0.320	356	0.148	-0.388
257	0.443	0.880	307	1.78	3.187	357	0.0344	
258	0.307	0.681	308	1.38	0.333	358	0.0186	
259	0.618	0.084	309	3.26	-3.867	359	0.0111	
260	0.604	0.447	310	1.74	2.360	360	0.0087	
261	0.660	0.093	311	0.461	0.075	361	0.0100	
262	0.602	0.635	312	1.19	-1.227	362	0.0211	
263	1.08	-0.813	313	0.902	-1.439	363	0.0141	
264	0.947	0.580	314	5.65	0.720	364	0.0094	
265	0.530	1.004	315	5.56	2.587	365	0.0088	
266	0.538	0.431	316	2.54	4.760	366	0.0085	
267	1.36	-0.880	317	5.79	-2.467	367	0.0091	
268	1.24	-0.120	318	3.15	3.307	368	0.0143	
269	0.990	1.116	319	0.975	2.532	369	0.0297	
270	0.960	0.748	320	1.19	0.240	370	0.0636	
271	1.94	-1.307	321	1.60	-2.187	371	0.0572	
272	1.43	1.000	322	0.721	0.149	372	0.0197	
273	0.810	1.228	323	0.327	0.389	373	0.0113	
274	0.657	0.871	324	0.861	-0.456	374	0.0091	
275	2.15	-2.733	325	1.54	2.213	375	0.0087	

Note: Absorption cross sections σ: 226-375 nm, Meller and Moortgat [517].
Temperature coefficients Γ: 250-356 nm, Meller and Moortgat [517],
$\sigma(\lambda, T) = \sigma(\lambda, 298\ K) + \Gamma(T - 298\ K)$ for the temperature range 223 -323 K.

Table 4-31. Absorption Cross Sections of CH_2O at 298 K and Temperature Coefficients Averaged over Intervals Used in Atmospheric Modeling

λ (nm)	λ range (nm)	10^{20} σ (cm^2) T = 298 K	10^{20} σ (cm^2) T = 223 K	10^{24} Γ (cm^2 K^{-1})
226.0	224.7 – 227.3	0.0166		
228.6	227.3 – 229.9	0.0181		
231.2	229.9 – 232.6	0.0303		
233.9	232.6 - 235.3	0.0313		
236.7	235.3 – 238.1	0.0625		
239.5	238.2 – 241.0	0.0704		
242.4	241.0 – 243.9	0.126		
245.4	243.9 – 246.9	0.139		
248.5	246.9 – 250.0	0.254		
251.6	250.0 – 253.2	0.270	0.2650	0.720
254.8	253.2 – 256.4	0.449	0.4350	1.77
258.1	256.4 – 259.7	0.478	0.4380	5.35
261.4	259.7 – 263.2	0.698	0.6870	1.45
264.9	263.2 – 266.7	0.736	0.6980	5.00
268.5	266.7 – 270.3	1.13	1.1100	2.80
272.1	270.3 – 274.0	1.30	1.2700	3.87
275.9	274.0 – 277.8	1.84	1.8900	-5.73
279.7	277.8 – 281.7	1.86	1.8900	-3.60
283.7	281.7 – 285.7	2.55	2.7200	-22.3
287.7	285.7 – 289.9	2.33	2.3800	-7.47
292.0	289.9 – 294.1	2.66	2.9300	-34.9
296.3	294.1 – 298.5	3.28	3.2300	5.73
300.8	298.5 – 303.0	1.60	1.5800	2.80
305.4	303.0 – 307.7	4.42	4.4300	-1.73
310.1	307.7 – 312.5	1.63	1.6700	-5.47
315	312.5 – 317.5	4.09	4.0300	8.40
320	317.5 – 322.5	1.53	1.4700	8.13
325	322.5 – 327.5	2.79	2.7600	3.87
330	327.5 – 332.5	1.99	1.9100	10.5
335	332.5 – 337.5	0.196	0.1830	1.71
340	337.5 – 342.5	2.390	2.2800	15.2
345	342.5 – 347.5	0.758	0.7550	0.480
350	347.5 – 352.5	0.194	0.2200	-3.40
355	352.5 – 357.5	0.961		
360	357.5 – 362.5	0.0139		
365	362.5 – 367.5	0.0010		
370	367.5 – 372.5	0.0369		

Note:
Absorption cross sections σ: 224.7-372.5 nm, Meller and Moortgat [517].
Temperature coefficients Γ: Meller and Moortgat [517]
$\sigma(\lambda, T) = \sigma(\lambda, 298\ K) + \Gamma(T - 298\ K)$ for the temperature range 223 -323 K

Table 4-32. Quantum Yields for Photolysis of CH_2O at 296-300 K

λ (nm)	Φ_1	Φ_2	λ (nm)	Φ_1	Φ_2	λ (nm)	Φ_1	Φ_2
250	0.317	0.483	288	0.669	0.291	326	0.463	0.537
251	0.311	0.489	289	0.680	0.284	327	0.435	0.565
252	0.307	0.493	290	0.690	0.278	328	0.406	0.594
253	0.304	0.496	291	0.700	0.272	329	0.375	0.625
254	0.303	0.497	292	0.710	0.266	330	0.343	0.657
255	0.303	0.497	293	0.718	0.262	331	0.310	0.690
256	0.305	0.495	294	0.726	0.259	332	0.276	0.714
257	0.307	0.493	295	0.734	0.256	333	0.240	0.740
258	0.311	0.489	296	0.740	0.255	334	0.203	0.737
259	0.316	0.484	297	0.746	0.254	335	0.165	0.735
260	0.322	0.478	298	0.751	0.249	336	0.126	0.724
261	0.329	0.471	299	0.755	0.245	337	0.085	0.695
262	0.337	0.468	300	0.758	0.242	338	0.043	0.687
263	0.346	0.464	301	0.761	0.239	339	0.0	0.665
264	0.355	0.460	302	0.762	0.238	340		0.650
265	0.366	0.454	303	0.762	0.238	341		0.620
266	0.377	0.448	304	0.762	0.238	342		0.590
267	0.388	0.442	305	0.760	0.240	343		0.560
268	0.400	0.435	306	0.758	0.242	344		0.530
269	0.413	0.427	307	0.754	0.246	345		0.500
270	0.425	0.420	308	0.749	0.251	346		0.480
271	0.439	0.411	309	0.744	0.256	347		0.450
272	0.452	0.403	310	0.737	0.263	348		0.430
273	0.466	0.394	311	0.729	0.271	349		0.400
274	0.480	0.385	312	0.720	0.280	350		0.380
275	0.494	0.376	313	0.709	0.291	351		0.350
276	0.508	0.367	314	0.698	0.302	352		0.320
277	0.623	0.357	315	0.685	0.315	353		0.280
278	0.537	0.358	316	0.671	0.329	354		0.250
279	0.551	0.349	317	0.656	0.344	355		0.220
280	0.565	0.342	318	0.639	0.361	356		0.180
281	0.579	0.334	319	0.622	0.378	357		0.160
282	0.593	0.327	320	0.603	0.397	358		0.130
283	0.607	0.320	321	0.583	0.417	359		0.009
284	0.620	0.313	322	0.561	0.439	360		0.004
285	0.633	0.307	323	0.539	0.461	361		0.0
286	0.645	0.302	324	0.515	0.485			
287	0.657	0.296	325	0.489	0.511			

Note:
The recommended quantum yields for photolysis of CH_2O are based on a fitting of the data for channel 1 (H + HCO) involving the data of Lewis et al. [443], Marling [488], Horowitz and Calvert [338], Clark et al. [173], Tang et al. [774], Moortgat et al. [557] and Smith et al. [744], and the data for channel 2 (H_2 + CO) from Moortgat et al. [557]; see also text.

D2. $CH_3CHO + h\nu \rightarrow CH_3 + HCO$ ϕ_1
$CH_3CHO + h\nu \rightarrow CH_4 + CO$ ϕ_2
$CH_3CHO + h\nu \rightarrow CH_3CO + H$ ϕ_3. The absorption spectrum of acetaldehyde has been measured at room temperature and 200-345 nm by McMillan [140]; at 221-345 nm by Meyrahn et al. [525]; at 197-362 nm by Schneider and Moortgat [687]; at 235-360 nm by Libuda et al. [445, 447]; at 202-365 nm by Martinez et al. [492]; and at 240-350 nm by Lim o-Vieira et al. [453]. Absorption cross-sections at 5 nm wavelength intervals in the range 290-355 nm were reported by Weaver et al. [842]. The UV spectrum shows an absorption band between 200 and 350 nm with resolved vibrational structure (~12 maxima or shoulders) above 260 nm. The agreement between the various results is very good, mostly 5% and better, except for the results of Meyrahn et al. [525], which are appreciably lower (10%) in the structured features around the absorption maximum. Our recommendation is based on the data of Libuda et al. [445, 447] (1-nm averages of 0.6 nm-resolution data) and Martinez et al. [492] (4-nm averages of 0.5 nm-resolution data at 202-278 nm and 1-nm averages at 280-360 nm), for which the agreement is within 5% between 255 and 325 nm. The preferred values in Table 4-33 are the results of Martinez et al. [492] for the region 202-238 nm and the mean of the results of Martinez et al. [492] and Libuda et al. [445, 447] for the region 280-360 nm.

Measurements in the VUV were carried out at 150-180 nm by Lake and Harrison [429]; at 118-189 nm by Lucazeau and Sandorfy [462]; at 120-180 nm by Brint et al. [91]; and at 113-200 nm by Lim o-Vieira et al. [453].

Quantum yield measurements have been reported by Calvert and Pitts [138], and Weaver et al. [842] at isolated wavelengths. Quantum yields of CO, CH_4 and CO_2 were determined in the photolysis of trace concentrations of CH_3CHO in air and N_2 in the spectral range 247-327 nm at 1 atmospheric pressure by Meyrahn et al. [525], which allowed the determination of ($\varphi_1 + \varphi_2$), φ_2, and φ_3, respectively. Product pressure-dependence was also investigated by Meyrahn [524] at 270, 303.4 and 313 nm. Horowitz et al. [340] and Horowitz and Calvert [339] measured the quantum yields of formation CO, CH_4 and H_2 at 290, 300, 313, 320 and 332 nm in the photolysis of CH_3CHO at various added pressures O_2, CO_2, from which φ_1 and φ_2 were derived. There seems to be evidence by Meyrahn et al. [524, 525] and Horowitz et al. [340] that some CO_2 is formed from secondary reactions of the CH_3CO radical, produced in channel (3). The quantum yield φ_3 was estimated as 0.025 at 300 nm, decreasing to zero at 320 nm. Both Meyrahn et al. [524, 525] and Horowitz et al. [339, 340] observed a pressure dependence of the products, from which Stern-Vollmer quenching coefficients were derived. These data were summarized by Calvert et al. [132] based on the results of previous studies.

Quantum yield recommendations are shown in Table 4-34 for atmospheric pressure, and are based on the evaluation by Atkinson and Lloyd [32] and on the measurements by Horowitz and Calvert [339], Meyrahn et al. [525] and Meyrahn [524]. A similar evaluation was performed by Calvert et al. [132].

Table 4-33. Absorption Cross Sections of CH_3CHO at 298-300 K

λ (nm)	10^{20} σ (cm^2)	λ (nm)	10^{20} σ (cm^2)	λ (nm)	10^{20} σ (cm^2)	λ (nm)	10^{20} σ (cm^2)
202	0.056	286	4.41	312	2.52	338	0.212
206	0.053	287	4.56	313	2.47	339	0.206
210	0.049	288	4.69	314	2.38	340	0.135
214	0.048	289	4.74	315	2.20	341	0.0664
218	0.052	290	4.86	316	2.07	342	0.0416
222	0.065	291	4.75	317	2.08	343	0.0305
226	0.096	292	4.66	318	1.98	344	0.0267
230	0.151	293	4.51	319	1.84	345	0.0210
234	0.241	294	4.31	320	1.70	346	0.0199
238	0.375	295	4.26	321	1.48	347	0.0149
242	0.639	296	4.24	322	1.38	348	0.0159
246	0.887	297	4.37	323	1.23	349	0.0664
250	1.18	298	4.41	324	1.06	350	0.00774
254	1.57	299	4.26	325	1.15	351	0.00695
258	2.03	300	4.15	326	1.09	352	0.00497
262	2.45	301	3.97	327	0.808	353	0.00552
266	3.06	302	3.87	328	0.715	354	0.00436
270	3.38	303	3.70	329	0.741	355	0.00500
274	4.03	304	3.46	330	0.699	356	0.00518
278	4.15	305	3.43	331	0.560	357	0.00345
280	4.48	306	3.41	332	0.496	358	0.00428
281	4.65	307	3.36	333	0.420	359	0.00207
282	4.66	308	3.31	334	0.333	360	0.00275
283	4.70	309	3.11	335	0.350		
284	4.58	310	2.92	336	0.227		
285	4.46	311	2.73	337	0.219		

Note:
202-238 nm, Martinez et al. [492],
240-360 nm, mean of Martinez et al. [492] and Libuda et al. [445, 447].

Table 4-34. Recommended Quantum Yields for the Photolysis of CH_3CHO at 1 bar Total Pressure

λ (nm)	Φ_1	Φ_2	λ (nm)	Φ_1
256	0.29	0.48	296	0.47
258	0.30	0.47	298	0.45
260	0.31	0.45	300	0.43
262	0.32	0.43	302	0.40
264	0.34	0.40	304	0.38
266	0.36	0.37	306	0.35
268	0.38	0.33	308	0.31
270	0.41	0.29	310	0.28
272	0.44	0.25	312	0.24
274	0.48	0.20	314	0.19
276	0.53	0.16	316	0.15
278	0.56	0.09	318	0.12
280	0.58	0.06	320	0.10
282	0.59	0.04	322	0.07
284	0.59	0.03	324	0.05
286	0.58	0.02	326	0.03
288	0.56	0.01	328	0.02
290	0.54	0.01	330	0.01
292	0.52	0.005	332	0
294	0.50	0		

D3. $C_2H_5CHO + h\nu \rightarrow C_2H_5 + CHO$ ϕ_1
$C_2H_5CHO + h\nu \rightarrow C_2H_6 + CO$ ϕ_2
$C_2H_5CHO + h\nu \rightarrow C_2H_4 + HCHO$ ϕ_3
$C_2H_5CHO + h\nu \rightarrow CH_3 + CH_2CHO$ ϕ_4. The absorption spectrum of propionaldehyde has been measured and room temperature at 118-190 nm by Lucazeau and Sandorfy [462], at 220-342 nm by McMillan [145], and at 262-365 nm by Martinez et al. [492]. The spectrum shows an absorption band between 200 and 360 nm with structured features (~9 maxima or shoulders) above 260 nm. Absorption cross sections have also been measured at isolated wavelengths by Blacet and Crane [76] in the range 187-313 nm, by Heicklen et al. [325] in the range 293-325 nm, and by Chen and Zhu [160] in the range 280-330 nm. The agreement between the results of the data Martinez et al. [492] and McMillan [140] is excellent, i.e., ≤ 5%, between 238 and 322 nm; at smaller wavelengths the differences increase to ~30%, at larger wavelengths up to nearly 50%. Three of the four data points reported by Heicklen et al. [325] fit well to the just mentioned absorption curves, the value reported for 293 nm however is lower by 20%. The cross sections measured at 5-nm intervals by Chen and Zhu [160] agree to within 10% with those reported by Martinez et al. [492], except the data at 285 and 330 nm which are 20% and 30% larger. The recommended absorption cross sections listed in Table 4-35 are those of Martinez et al. [492], which are the 4-nm averages of the 0.5 nm-resolution data at 202-278 nm and 1-nm averages at 280-360 nm.

Quantum yield measurements have been performed by Heicklen et al. [325] and recently by Chen and Zhu [160]. Heicklen et al. [325] investigated the laser photolysis at 298 K (at 294, 302, 312 and 325 nm) and the steady state photolysis at 263 and 298 K (at 254, 312 and 334 nm) of C_2H_5CHO in the presence of O_2. They measured the quantum yield of the HO_2 and $C_2H_5O_2$ radicals by UV absorption, yielding φ_1. From the determination of the products yields CO and C_2H_6, they derived $\varphi_1 = \varphi(CO) - \varphi(C_2H_6)$ and $\varphi_2 = \varphi(C_2H_6)$. A Stern-Volmer type pressure dependence of the quantum yields was observed at all wavelengths, giving lower quantum yields at higher pressures. At atmospheric pressure φ_1 = 0.22, 0.89, 0.85, 0.50, 0.26 and 0.15 were derived at 254, 294, 302, 313, 325 and 334 nm, respectively; at 254 nm Heicklen et al. [325] reported φ_2 = 0.33, but φ_2 = 0 at other larger wavelengths. The contribution of other primary processes (φ_3 and φ_4) was found to increase at λ < 265 nm from earlier studies cited in Calvert and Pitts [143].

Chen and Zhu [160] measured the yield of HCO radicals (= φ_1) in the wavelength range 280-330 nm using time-resolved cavity ring-down spectroscopy at 613.8 nm. The HCO yields were 0.85 ± 0.06 at 280 nm, 1.01 ± 0.07 at 285 nm, 0.95 ± 0.06 at 290 nm, 0.98 ± 0.06 at 295 nm, 0.92 ± 0.06 at 300 nm, 0.95 ± 0.08 at 305 nm, 0.98 ± 0.11 at 310 nm, 0.91 ± 0.05 at 315 nm, 1.08 ± 0.07 at 320 nm, 1.07 ± 0.14 at 325 nm, and 0.84 ±

0.08 at 330 nm. These values are quoted for zero-pressure, but the authors did not observe any pressure dependence upon addition of 400 Torr N_2.

Both quantum yield studies by Heicklen et al. [325] and Chen and Zhu [160] are only in agreement in the narrow wavelength range 290-305 nm. At $\lambda > 305$ nm, the data of Chen and Zhu do not show the decrease of φ_1 observed by Heicklen et al [325]. Because of the divergence of both data sets, no recommendation can be given.

Table 4-35. Absorption Cross Sections C_2H_5CHO at 298-300 K

λ (nm)	$10^{20}\ \sigma$ (cm^2)	λ (nm)	$10^{20}\ \sigma$ (cm^2)	λ (nm)	$10^{20}\ \sigma$ (cm^2)	λ (nm)	$10^{20}\ \sigma$ (cm^2)
202	0.049	285	5.86	310	3.60	335	0.325
206	0.049	286	5.82	311	3.53	336	0.280
210	0.057	287	5.72	312	3.50	337	0.230
214	0.069	288	5.59	313	3.32	338	0.185
218	0.080	289	5.52	314	3.06	339	0.166
222	0.091	290	5.56	315	2.77	340	0.155
226	0.115	291	5.68	316	2.43	341	0.119
230	0.163	292	5.81	317	2.18	342	0.076
234	0.257	293	5.88	318	2.00	343	0.045
238	0.407	294	5.80	319	1.86	344	0.031
242	0.622	295	5.57	320	1.83	345	0.025
246	0.909	296	5.37	321	1.78	346	0.019
250	1.29	297	5.16	322	1.66	347	0.016
254	1.75	298	5.02	323	1.58	348	0.014
258	2.25	299	5.02	324	1.49	349	0.013
262	2.88	300	5.04	325	1.30	350	0.010
266	3.43	301	5.09	326	1.13	351	0.008
270	4.12	302	5.07	327	0.996	352	0.007
274	4.59	303	4.94	328	0.828	353	0.005
278	5.17	304	4.69	329	0.685	354	0.004
280	5.16	305	4.32	330	0.575	355	0.002
281	5.21	306	4.04	331	0.494	356	0.001
282	5.35	307	3.81	332	0.466	357	0.001
283	5.57	308	3.65	333	0.430		
284	5.78	309	3.62	334	0.373		

Note:
202-357 nm, Martinez et al. [492].

D4. $CH_3O_2 + h\nu \rightarrow$ Products. The absorption cross sections of the methylperoxy radical, CH_3O_2, in the 195–310-nm region have been measured at room temperature by Parkes et al. [624], Hochanadel et al. [335], Parkes [623], Anastasi et al. [18], Kan et al. [402], Cox and Tyndall [193, 194] at 250 nm only; Adachi et al. [7], Sander and Watson [705] at 250 nm only; Pilling and Smith [635] at 254 nm only, Kurylo et al. [424], McAdam et al. [505], Jenkin et al. [374], Wallington et al. [831], Moortgat et al. [559], Dagaut and Kurylo [200], Simon et al. [731], Jenkin and Cox [373], Lightfoot and Jemi-Alade [450] who measured the cross sections up to 777 K., Maricq and Wallington [485], Wallington et al. [833], Roehl et al. [677], and Fahr et al. [233]. The absorption cross sections have been evaluated in earlier reviews by Lightfoot et al. [449] and Wallington et al. [832], who noted significant discrepancies in the both the shapes of the spectra and the absolute magnitude of the cross section values. The ultraviolet absorption spectra have recently been reevaluated by Tyndall et al. [790], who fitted the absorption spectra to a semilogarithmic Gaussian distribution function suggested by Lightfoot et al. [449] and Maric et al. [479] using:

$$\sigma = \sigma_{max} \exp^{-a\left[\ln\left(\frac{\lambda_{max}}{\lambda}\right)\right]^2}$$

Screening of the data suggested that most spectra published before 1987 did not constrain the shape of the spectrum very well as indicated by the large relative uncertainty of the width parameter a. The shape was determined by averaging the individual fitting parameters from McAdam et al. [505], Moortgat et al. [559], Simon et al. [731], Lightfoot and Jemi-Alade [450], Jenkin and Cox [373] and Maricq and Wallington [485], which were judged to be most reliable by Tyndall et al. [790]. Absolute cross sections were based on relative measurements of absorption cross sections of CH_3O_2 and $C_2H_5O_2$ at 240 nm taken under identical conditions

(Wallington et al. [832], Maricq and Wallington [485], Fenter et al. [242] and Roehl et al. [677]), combined with independent calibrations by Dagaut and Kurylo [200], Simon et al. [731] and Lightfoot and Jemi-Alade [450]. The fitting parameters are: $\sigma_{max} = 4.26 \times 10^{-18}$ cm^2 molecule^{-1}; a = 44.4; λ_{max} = 237.3 nm. Table 4-36 lists the recommended cross sections, which are taken from the review by Tyndall et al. [790].

Photolysis of CH_3O_2 in the stratosphere and troposphere is slow and can be neglected, but the UV absorption cross sections are important in laboratory studies of reaction kinetics.

Table 4-36. Absorption Cross Sections of CH_3O_2, $C_2H_5O_2$, and $CH_3C(O)O_2$

λ (nm)	10^{20} σ (cm^2)		
	CH_3O_2	$C_2H_5O_2$	$CH_3C(O)O_2$
195.0			389
200.0			564
205.0	165		665
210.0	219	195	656
215.0	276	257	564
220.0	330	319	451
225.0	376	374	366
230.0	408	418	326
235.0	424	444	319
240.0	424	452	326
245.0	407	440	330
250.0	378	412	322
255.0	339	372	300
260.0	294	324	268
265.0	248	273	229
270.0	203	222	187
275.0	162	176	147
280.0	126	136	111
285.0	96.1	102	81.2
290.0	71.5	74.6	57.3
295.0	52.0	53.3	
300.0		37.3	

D5. $C_2H_5O_2 + h\nu \rightarrow$ Products. The absorption cross sections of the ethylperoxy radical, $C_2H_5O_2$, in the 200–310-nm region have been measured at room temperature by Adachi et al. [6], Anastasi et al. [19], Cattell et al. [155], Wallington et al. [832], Bauer et al. [56], Maricq and Wallington [485], Fenter et al. [242], and Munk et al. [566]. The absorption cross sections have been evaluated in earlier reviews by Lightfoot et al. [449] and Wallington et al. [832], who noted significant discrepancies in the both the shapes of the spectra and the absolute magnitude of the cross section values. The ultraviolet absorption spectra have recently been reevaluated by Tyndall et al. [790], who fitted the absorption spectra to a semilogarithmic Gaussian distribution function suggested by Lightfoot et al. [449] and Maric et al. [479] using:

$$\sigma = \sigma_{max} \exp^{-a\left[\ln\left(\frac{\lambda_{max}}{\lambda}\right)\right]^2}$$

The shape was determined by averaging the individual fitting parameters from Wallington et al. [832], Bauer et al. [56], Maricq and Wallington [485] and Fenter et al. [242], which were judged to be most reliable by Tyndall et al. [790]. Absolute cross sections were based on relative measurements of absorption cross sections of CH_3O_2 and $C_2H_5O_2$ at 240 nm taken under identical conditions (Wallington et al. [832], Maricq and Wallington [485], Fenter et al. [242] and Roehl et al. [677]), combined with independent calibrations. The fitting parameters are $\sigma_{max} = 4.52 \times 10^{-18}$ cm^2 molecule^{-1}; a = 49.0; λ_{max} = 239.4 nm. Table 4-36 lists the recommended cross sections, which are taken from the review by Tyndall et al. [790].

Photolysis of $C_2H_5O_2$ in the stratosphere and troposphere is slow and can be neglected, but the UV absorption cross sections are important in laboratory studies of reaction kinetics.

D6. $CH_3C(O)O_2 + h\nu \rightarrow$ Products. The UV absorption spectrum of the acetylperoxy radical, $CH_3C(O)O_2$, exhibits two absorption maxima in the 185–285 nm region: a strong band near 207 nm, and a feature at 245 nm that is weaker by a factor of 2. The absorption cross sections have been measured at room temperature by Addison et al. [8], Basco and Parmer [50], Moortgat et al. [559], Maricq and Szente [484], and Roehl et al. [677]. The absorption cross sections have been evaluated in earlier reviews by Lightfoot et al. [449] and

Wallington et al. [832], who noted significant discrepancies in the both the shapes of the spectra and the absolute magnitude of the cross section values. The ultraviolet absorption spectra have recently been reevaluated by Tyndall et al. [790], who fitted the absorption spectra to the sum of two Gaussian-shaped absorption bands:

$$\sigma = \sigma_{\max 1} \exp^{-a_1\left[\ln\left(\frac{\lambda_{\max 1}}{\lambda}\right)\right]^2} + \sigma_{\max 2} \exp^{-a_2\left[\ln\left(\frac{\lambda_{\max 2}}{\lambda}\right)\right]^2}$$

The shape was determined by averaging the individual fitting parameters from Maricq and Szente [484] and Roehl et al. [677], which were judged to be the most reliable to date; the data by Maricq and Szente [484] were adjusted for their overcorrection for the contribution of CH_3O_2. Absolute cross sections were based on relative measurements of absorption cross sections of $C_2H_5O_2$ at 240 nm taken under identical conditions. The fitting parameters are
$\sigma_{max1} = 6.29 \times 10^{-18}$ cm^2 molecule^{-1}; $\lambda_{max1} = 206.0$ nm; $a_1 = 168.0$; $\sigma_{max2} = 3.26 \times 10^{-18}$ cm^2 molecule^{-1}; $\lambda_{max2} = 246.1$ nm; $a_2 = 64.2$. Table 4-36 lists the recommended cross sections, which are taken from the review by Tyndall et al. [790]

Photolysis of $CH_3C(O)O_2$ in the stratosphere and troposphere is slow and can be neglected, but the UV absorption cross sections are important in laboratory studies of reaction kinetics.

D7. $CH_3OOH + h\nu \rightarrow CH_3O + OH$. Vaghjiani and Ravishankara [799] measured the cross sections of CH_3OOH by monitoring the CH_3OOH concentration via trapping and titration. These results are recommended and are listed in Table 4-37. The earlier results of Molina and Arguello [547] are consistently 40% higher than the values shown in Table 4-37; this difference is believed to be due to difficulty in trapping CH_3OOH and measuring its concentration. CH_3OOH dissociates upon light absorption to give CH_3O with unit quantum yield (Vaghjiani and Ravishankara, [800]); these authors also observed some production of H and O atoms at shorter wavelengths (i.e., 193 nm). Thelen et al. [777] report unit quantum yield for OH production at 248 and 193 nm, in agreement with the results of Vaghjiani and Ravishankara [799].

Table 4-37. Absorption Cross Sections of CH_3OOH

λ (nm)	$10^{20}\ \sigma$ (cm^2)	λ (nm)	$10^{20}\ \sigma$ (cm^2)
210	31.2	290	0.691
215	20.9	295	0.551
220	15.4	300	0.413
225	12.2	305	0.313
230	9.62	310	0.239
235	7.61	315	0.182
240	6.05	320	0.137
245	4.88	325	0.105
250	3.98	330	0.079
255	3.23	335	0.061
260	2.56	340	0.047
265	2.11	345	0.035
270	1.70	350	0.027
275	1.39	355	0.021
280	1.09	360	0.016
285	0.863	365	0.012

D8. $HOCH_2OOH + h\nu \rightarrow HOCH_2O + OH$. The UV absorption spectrum of hydroxymethyl hydroperoxide, $HOCH_2OOH$, was measured at 298 K by Bauerle and Moortgat [59] in the range 205 to 360 nm. The cross sections are listed in Table 4-38. This photolysis is assumed to occur with unity quantum yield at wavelengths larger than 290 nm, in analogy with CH_3OOH.

Table 4-38. Absorption Cross Sections of $HOCH_2OOH$

λ (nm)	10^{20} σ (cm^2)	λ (nm)	10^{20} σ (cm^2)
205	26.9	285	0.75
210	22.6	290	0.63
215	18.7	295	0.51
220	15.5	300	0.40
225	12.5	305	0.29
230	10.1	310	0.22
235	7.89	315	0.18
240	5.98	320	0.13
245	4.68	325	0.10
250	3.78	330	0.073
255	2.88	335	0.059
260	2.31	340	0.045
265	1.81	345	0.036
270	1.48	350	0.028
275	1.21	355	0.022
280	0.93	360	0.017

D9. $CH_3C(O)O_2NO_2 + h\nu \rightarrow CH_3C(O)O_2 + NO_2$ φ_1
$CH_3C(O)O_2NO_2 + h\nu \rightarrow CH_3C(O)O + NO_3$ φ_2. The absorption cross sections of $CH_3C(O)O_2NO_2$ (peroxyacetyl nitrate, PAN) have been measured at room temperature and 220-450 nm by Stephens [752]; at 200-300 nm by Senum et al. [726]; at 210-250 nm by Basco and Parmar [51]; at 219-325 nm by Libuda and Zabel [446]; and at 250, 273, and 298 K and 196-350 nm by Talukdar et al. [766]. The five studies are in reasonable to good agreement over their range of overlap. The data of Talukdar et al. [766] and Libuda and Zabel [446] agree within 10% below 300 nm. The data of Stephens [752] are somewhat higher (up to 20%), those of Basco and Parmar [51] higher by up to about 45%, and those of Senum et al. [726] are smaller (within 20% and more beyond 280 nm) than the data of Talukdar et al. [766]. Libuda and Zabel [446] carried out simultaneous IR studies that showed that the measured cross sections need to be corrected for impurities that are transparent in the UV but contribute to the sample pressure in the absorption cell. These corrections are on the order of 20%. The recommended absorption cross section listed in Table 4-39 are those of Talukdar et al. [766] because of the good agreement with Libuda and Zabel [446] and the wider spectral coverage and temperature range of their study. The uncertainties in the reported cross sections are probably quite large (on the order of a factor of 2), decreasing to about 30% at shorter wavelengths.

A wavelength-dependent systematic decrease of the absorption cross sections with decreasing temperature was observed by Talukdar et al. [766]. The temperature dependence was parameterized to the expression

$$\ln \sigma(\lambda, T) = \ln \sigma(\lambda, 298K) + B(\lambda)(T-298)$$

to derive the temperature coefficients B(λ) which are also listed in Table 4-39.

Quantum yields for the production of NO_2 and NO_3 in the photolysis at 248 nm were reported by Mazely et al. [503, 504]: $\varphi(NO_2, 248\ nm) = 0.83 \pm 0.09$ and $\varphi(NO_3, 248\ nm) = 0.3 \pm 0.1$. The NO_3 quantum yield was obtained relative to the unity NO_3 quantum yield in the photolysis of N_2O_5 at 248 nm. However, this latter quantum yield was remeasured to be 0.8 ± 0.1 by Harwood et al. [313], so that the $\varphi(NO_3, 248\ nm)$ should be rescaled to 0.24. Quantum yields for the production of NO_3 in the photolysis of $CH_3C(O)O_2NO_2$ at 248 and 308 nm were recently measured by Harwood et al. [317]: $\varphi(NO_3, 248\ nm) = 0.19 \pm 0.04$ and $\varphi(NO_3, 308\ nm) = 0.41 \pm 0.10$. Assuming that only both product channels are produced and $\varphi_1 + \varphi_2 = 1$, it can be recommended that $\varphi_1 = 0.6$ and $\varphi_2 = 0.4$ at $\lambda > 300$ nm.

Table 4-39. Absorption Cross Sections of $CH_3C(O)O_2NO_2$ at 298 K, Temperature Coefficients B

λ (nm)	10^{20} σ (cm^2)	10^3 B (K^{-1})	λ (nm)	10^{20} σ (cm^2)	10^3 B (K^{-1})	λ (nm)	10^{20} σ (cm^2)	10^3 B (K^{-1})
196	429	2.02	248	14.6	3.64	300	0.189	8.44
198	398	1.73	250	12.9	3.76	302	0.152	8.61
200	361	1.36	252	11.4	3.87	304	0.125	8.76
202	325	1.07	254	10.0	3.98	306	0.0998	8.87
204	292	0.86	256	8.86	4.10	308	0.0816	9.01
206	261	0.75	258	7.80	4.23	310	0.0666	9.13
208	226	0.71	260	6.85	4.38	312	0.0538	9.30
210	196	0.75	262	6.01	4.53	314	0.0462	9.46
212	168	0.84	264	5.23	4.68	316	0.0363	9.57
214	143	0.97	266	4.54	4.82	318	0.0300	9.75
216	122	1.12	268	3.94	4.97	320	0.0252	10.0
218	104	1.29	270	3.37	5.14	322	0.0199	10.2
220	89.7	1.47	272	2.87	5.34	324	0.0166	10.4
222	77.7	1.64	274	2.45	5.55	326	0.0140	10.6
224	67.6	1.81	276	2.07	5.76	328	0.0117	10.7
226	59.3	1.98	278	1.74	5.98	330	0.0106	10.9
228	52.0	2.14	280	1.46	6.20	332	0.00857	11.2
230	45.8	2.30	282	1.21	6.43	334	0.00676	11.5
232	40.4	2.46	284	1.01	6.67	336	0.00615	11.7
234	35.5	2.63	286	0.810	6.90	338	0.00526	11.9
236	31.4	2.80	288	0.648	7.15	340	0.00502	12.2
238	27.9	2.96	290	0.537	7.39	342	0.00360	12.4
240	24.4	3.11	292	0.447	7.63	344	0.00241	12.5
242	21.5	3.25	294	0.369	7.86	346	0.00231	
244	18.8	3.39	296	0.297	8.08	348	0.00247	
246	16.6	3.52	298	0.245	8.27	350	0.00165	

Note:
Absorption cross sections σ: 196-350 nm, Talukdar et al. [766].
Temperature coefficients B: 250-298 K, Talukdar et al. [766] ($\ln \sigma(\lambda, T) = \ln \sigma(\lambda, 298\ K) + B(T-298)$).

D10. $C_2H_5C(O)O_2NO_2 + h\nu \rightarrow C_2H_5C(O)O_2 + NO_2$ φ_1
$C_2H_5C(O)O_2NO_2 + h\nu \rightarrow C_2H_5C(O)O + NO_3$ φ_2. The absorption cross sections of $C_2H_5C(O)O_2NO_2$ (peroxypropionyl nitrate, PPN) have been measured at room temperature and 200-300 nm by Senum et al. [726] and at 253, 273, and 296 K and 210-340 nm by Harwood et al. [317]. The absorption spectrum shows an exponential decrease of the cross sections with increasing wavelength. The absorption cross sections reported by Harwood et al. [317] are larger than those reported by Senum et al. [726] over the common wavelength range, larger by ~10% at 210 nm up to ~30% at 300 nm. A wavelength-dependent systematic decrease of the absorption cross sections with decreasing temperature was observed by Harwood et al. [317]. The temperature dependence was parameterized to the expression $\ln \sigma(\lambda, T) = \ln \sigma(\lambda, 296\ K) + B(\lambda)(T-296)$ to derive the temperature coefficients $B(\lambda)$. We recommend the results of Harwood et al. [317], which are listed in Table 4-40.

Quantum yields for the production of NO_3 in the photolysis of $C_2H_5C(O)O_2NO_2$ at 248 and 308 nm were measured also by Harwood et al. [317]: $\varphi_2(248\ nm) = 0.22 \pm 0.04$ and $\varphi_2(308\ nm) = 0.39 \pm 0.04$.

Table 4-40. Absorption Cross Sections of $C_2H_5C(O)O_2NO_2$ at 296 K and Temperature Coefficients B

λ (nm)	10^{20} σ (cm^2)	10^3 B (K^{-1})	λ (nm)	10^{20} σ (cm^2)	10^3 B (K^{-1})	λ (nm)	10^{20} σ (cm^2)	10^3 B (K^{-1})
210	174	1.22	254	9.27	3.25	298	0.325	10.3
212	154	1.20	256	8.23	3.47	300	0.273	10.8
214	135	1.19	258	7.28	3.69	302	0.228	11.2
216	115	1.20	260	6.44	3.92	304	0.192	11.7
218	99.9	1.21	262	5.66	4.17	306	0.162	12.2
220	86.1	1.24	264	4.96	4.42	308	0.136	12.6
222	74.7	1.27	266	4.35	4.69	310	0.114	13.2
224	64.8	1.32	268	3.80	4.96	312	0.0962	13.6
226	56.9	1.37	270	3.31	5.25	314	0.0835	14.2
228	49.6	1.44	272	2.87	5.54	316	0.0689	14.7
230	43.6	1.52	274	2.48	5.85	318	0.0571	15.2
232	38.3	1.60	276	2.14	6.17	320	0.0491	15.8
234	33.6	1.70	278	1.84	6.49	322	0.0443	16.3
236	29.5	1.81	280	1.57	6.83	324	0.0354	16.9
238	25.8	1.93	282	1.33	7.18	326	0.0282	17.5
2400	22.6	2.06	284	1.12	7.54	328	0.0242	18.1
242	19.8	2.20	286	0.940	7.91	330	0.0206	18.7
244	17.4	2.35	288	0.790	8.29	332	0.0174	19.3
246	15.3	2.51	290	0.662	8.68	334	0.0146	19.9
248	13.5	2.68	292	0.551	9.08	336	0.0107	20.5
250	11.9	2.86	294	0.462	9.49	338	0.0090	21.2
252	10.5	3.05	296	0.389	9.91	340	0.0066	21.8

Note:
Absorption cross sections σ: 210-340 nm, Harwood et al. [317].
Temperature coefficients B: 253-296 K, Harwood et al. [317] ($\ln \sigma(\lambda, T) = \ln \sigma(\lambda, 298\ K) + B(T-298)$).

D11. $CH_2{=}CHCHO + h\nu \rightarrow CH_2{=}CH + CHO$ φ_1
$CH_2{=}CHCHO + h\nu \rightarrow C_2H_4 + CO$ φ_2
$CH_2{=}CHCHO + h\nu \rightarrow CH_2{=}CHCO + H$ φ_3. The absorption cross sections of acrolein (propenal) have been measured at room temperature and 227-380 nm by Gardner et al. [261] and at 192-431 nm by Magneron et al. [466]. The spectrum displays a broad absorption band between 250 and 400 nm, which is structured at wavelengths above 360 nm. The results of both teams agree to within 10% between 298 and 370 nm (with a few exceptions at 352, 360, 362 and 368 nm). Below 298 nm the differences increase up to ~40% with decreasing wavelength, above 368 nm the differences increase up to ~100% with increasing wavelength. Our preferred values listed in Table 4-41 are the 2-nm averages of the high-resolution data of Magneron et al. [466].

The photodecomposition was studied by Gardner et al. [261] at 313 and 334 nm in the pressure range 26-760 Torr air, who found that the photolysis is very inefficient at both wavelengths at high pressures but increases at low pressure. At 313 nm the quantum yield for photodissociation Φ_d of acrolein was $\Phi_d = 0.0065$ at 1 atm and 0.081 at 26 Torr. The pressure dependence was described by

$1/(\Phi_d - 0.004) = 0.086 + 1.613 \times 10^{-17}$ [M] (for $8 \times 10^{17} < M < 2.6 \times 10^{19}$ molecule cm^{-3}).

The dominant observed products were CO and C_2H_4. Magneron et al. [466] used broad-band photolysis (275-380 nm) of dilute mixtures of acrolein in air, but did not observe any products using long-path FTIR spectroscopy. An effective quantum yield for photolysis $\Phi_{eff} \leq 0.005$ nm was measured in the outdoor smog chamber.

Table 4-41. Absorption Cross Sections of CH_2=CHCHO at 298 K

λ (nm)	10^{20} σ (cm^2)	λ (nm)	10^{20} σ (cm^2)	λ (nm)	10^{20} σ (cm^2)	λ (nm)	10^{20} σ (cm^2)
282	0.84	310	3.59	338	5.46	366	3.74
284	0.97	312	3.92	340	5.31	368	3.82
286	1.08	314	4.15	342	5.10	370	2.17
288	1.23	316	4.21	344	5.12	372	1.58
290	1.46	318	4.47	346	5.30	374	1.14
292	1.62	320	4.65	348	5.17	376	1.14
294	1.80	322	5.08	350	5.94	378	1.24
296	1.97	324	5.17	352	5.79	380	1.10
298	2.18	326	5.34	354	4.18	382	0.84
300	2.47	328	5.20	356	3.63	384	0.79
302	2.70	330	5.31	358	3.28	386	1.18
304	2.85	332	5.44	360	3.92	388	0.49
306	3.09	334	5.80	362	3.72	390	0.25
308	3.29	336	6.24	364	2.86		

Note:
282-390 nm, Magneron et al. [466].

D12. $CH_2=C(CH_3)CHO + h\nu \rightarrow CH_2=CCH_3 + CHO$ Φ_1
$CH_2=C(CH_3)CHO + h\nu \rightarrow C_3H_6 + CO$ Φ_2
$CH_2=C(CH_3)CHO + h\nu \rightarrow H + CH_2=C(CH_3)CO$ Φ_3. The absorption cross sections of methacrolein (2-methylpropenal, MACR) have been measured at room temperature and 237-391 nm by Meller (see Röth et al. [687]) and Raber and Moortgat [646]; and at 214 and 250-395 nm by Gierczak et al. [271]. Both teams used diode array spectroscopy. A detailed vibrational-electronic analysis was reported by Birge et al. [71]. The spectrum exhibits a broad absorption band between 250 and 390 nm with vibrational structure above 310 nm. The results of both teams are in very good agreement in the region 261-351 nm where the agreement is between ~1 and 10%. Below 260 nm, the differences increase to nearly 100% at 250 nm, where the results of Gierczak et al. [271] are always larger than those of Meller [687] and Raber and Moortgat [646]. The peaks in the structured region above 328 nm reported by Meller [687] and Raber and Moortgat [646] are always higher due to the better resolution (0.07 nm) than those measured by Gierczak et al. [271] at a resolution of 0.5 nm. At the maximum, Raber and Moortgat [646] measured $\sigma = 7.64 \times 10^{-20}$ cm^2 $molecule^{-1}$ at 330.7 nm, while Gierczak et al. [271] measured $\sigma = 7.2 \times 10^{-20}$ cm^2 $molecule^{-1}$ at 331 nm. The latter group also reported $\sigma = (2.21 \pm 0.11) \times 10^{-17}$ cm^2 $molecule^{-1}$ at 213.86 nm (Zn lamp source). The 1-nm averages of both teams generally (with a few exceptions) are within 20% up to 376 nm. Above 380 nm, the results of Gierczak et al. [271] become larger with increasing wavelength up to nearly 80% than the results of Meller (see Röth et al. [687]) and Raber and Moortgat [646]. A wavelength shift of ~1 nm to longer wavelengths can be observed above 340 nm in the absorption curve of Gierczak et al. [271] as compared to that reported by Meller (see Röth et al. [687]) and Raber and Moortgat [646]. The recommended absorption cross sections listed in Table 4-42 are those of Gierczak et al. [271].

Overall quantum yields were measured by Raber and Moortgat [646] using broad band photolysis in the wavelength range 275-380 nm, and determination of the products by FTIR spectroscopy (CO, CO_2, HCHO, C_2H_4, C_3H_6, C_2H_2). An upper limit of 0.05 was reported at 760 Torr. Gierczak et al. [271] determined overall quantum yields at 308 nm $\Phi = 0.008 \pm 0.001$ and $\Phi = 0.005 \pm 0.001$ at 25 and 650 Torr total pressure, respectively, and at 351 nm $\Phi = 0.005 \pm 0.002$ and $\Phi = 0.003 \pm 0.001$ at 25 and 650 Torr, respectively. Endproducts were analyzed by GC and GC-MS. Both studies indicate a very low quantum yield for dissociation of methacrolein, and a value $\Phi < 0.01$ is recommended at $\lambda > 308$ nm.

Table 4-42. Absorption Cross Sections of $CH_2=C(CH_3)CHO$ at 298 K

λ (nm)	10^{20} σ (cm^2)	λ (nm)	10^{20} σ (cm^2)	λ (nm)	10^{20} σ (cm^2)	λ (nm)	10^{20} σ (cm^2)
250	0.207	287	1.67	324	6.58	361	4.28
251	0.194	288	1.79	325	6.74	362	3.61
252	0.187	289	1.90	326	6.73	363	2.86
253	0.180	290	2.03	327	6.68	364	2.68
254	0.179	291	2.16	328	6.83	365	2.33
255	0.177	292	2.28	329	7.07	366	1.92
256	0.180	293	2.39	330	7.15	367	1.62
257	0.180	294	2.52	331	7.16	368	1.40
258	0.186	295	2.68	332	7.03	369	1.31
259	0.193	296	2.85	333	6.69	370	1.42
260	0.201	297	2.99	334	6.41	371	1.67
261	0.211	298	3.13	335	6.08	372	1.53
262	0.224	299	3.26	336	5.97	373	1.43
263	0.241	300	3.44	337	6.25	374	1.08
264	0.263	301	3.61	338	6.38	375	0.977
265	0.283	302	3.76	339	6.37	376	1.00
266	0.305	303	3.91	340	6.24	377	1.07
267	0.333	304	4.04	341	6.02	378	1.35
268	0.363	305	4.19	342	5.98	379	2.18
269	0.398	306	4.40	343	6.58	380	1.30
270	0.436	307	4.58	344	6.79	381	0.984
271	0.479	308	4.71	345	6.53	382	0.555
272	0.520	309	4.81	346	6.11	383	0.456
273	0.567	310	4.92	347	5.63	384	0.364
274	0.616	311	5.13	348	5.22	385	0.331
275	0.673	312	5.35	349	4.55	386	0.246
276	0.732	313	5.50	350	4.16	387	0.205
277	0.793	314	5.61	351	3.85	388	0.181
278	0.863	315	5.70	352	3.89	389	0.161
279	0.936	316	5.87	353	4.35	390	0.147
280	1.01	317	6.04	354	4.31	391	0.156
281	1.09	318	6.19	355	4.14	392	0.159
282	1.18	319	6.28	356	3.62	393	0.153
283	1.26	320	6.27	357	3.53	394	0.149
284	1.35	321	6.18	358	3.46	395	0.123
285	1.45	322	6.21	359	3.81		
286	1.56	323	6.34	360	5.05		

Note:
250-395 nm, Gierczak et al. [271].

D13. $CH_3C(O)CH=CH_2 + h\nu \rightarrow CH_3\text{-}CH=CH_2 + CO$
$CH_3C(O)CH=CH_2 + h\nu \rightarrow CH=CH_2 + CH_3C(O)$
$CH_3C(O)CH=CH_2 + h\nu \rightarrow CH=CH_2C(O) + CH_3$. The absorption cross sections of methyl vinyl ketone (MVK) have been measured at room temperature and 240-398 nm by Schneider and Moortgat (see Röth et al. [687]); at 235-400 nm by Raber and Moortgat [646]; and at 216.86 nm and 250-395 nm by Gierzcak et al. [271]. A detailed vibrational-electronic analysis was reported by Birge et al. [71]. The spectrum displays some weak vibrational band structure, which is superimposed on the continuum envelope. The data of Schneider and Moortgat (see Röth et al. [687]) and Raber and Moortgat [646] are somewhat lower around the maximum at 334 nm (agreement within ~10% between 290 and 365 nm), and higher by up to 50% and lower by up to ~60% in the short- and long-wavelength tails, respectively, than the results of Gierczak et al. [271]. The latter group reported $\sigma = (6.6 \pm 0.04) \times 10^{-17}$ cm^2 $molecule^{-1}$ at 213.86 nm (Zn lamp source). They also determined the spectrum at reduced temperatures (range 250-298 K), and observed a small increase of < 2% at 250 K. We recommend the data of Gierzcak et al. [271] measured at 1-nm intervals as listed in Table 4-43.

Product quantum yields were measured by Raber and Moortgat [646], who monitored the products (major CO, C_3H_6 and HCHO; minor CO_2, HCOOH, CH_3OH, CH_3COOH) by FTIR using broadband photolysis in the range 275-380 nm. They quote $\Phi = 0.05$ at 760 Torr, increasing to $\Phi = 0.12$ at 54 Torr. Gierczak et al. [271] measured quantum yields at 308, 337 and 351 nm, by monitoring the disappearance of MVK at 25 and 650 Torr. At 308 nm they observed $\Phi = 0.16$ at 25 Torr and $\Phi = 0.04$ at 760 Torr; at 337 nm $\Phi = 0.04$ at 25 Torr and $\Phi = 0.01$ at 760 Torr; and at 351 nm $\Phi = 0.01$ independent of pressure. The data were fitted to the following empirical expression, taking into account the Stern-Volmer type pressure-dependence, which is our recommendation.

$$\Phi(\lambda,P) = \exp[-0.055\,(\lambda - 308)] \;/\; (5.5 + 9.2 \times 10^{-19}\,[M]),$$

where λ is in nm and [M] in molecule cm^{-3}.

Table 4-43. Absorption Cross Sections of $CH_3(O)CH{=}CH_2$ at 298 K

λ (nm)	10^{20} σ (cm^2)	λ (nm)	10^{20} σ (cm^2)	λ (nm)	10^{20} σ (cm^2)	λ (nm)	10^{20} σ (cm^2)
250	0.241	287	2.03	324	6.88	361	3.60
251	0.241	288	2.15	325	6.95	362	3.49
252	0.224	289	2.29	326	7.02	363	3.36
253	0.241	290	2.43	327	7.09	364	3.29
254	0.241	291	2.55	328	7.16	365	3.03
255	0.258	292	2.67	329	7.23	366	2.77
256	0.275	293	2.81	330	7.28	367	2.50
257	0.275	294	2.93	331	7.30	368	2.20
258	0.293	295	3.08	332	7.26	369	2.01
259	0.310	296	3.24	333	7.18	370	1.88
260	0.327	297	3.39	334	7.04	371	1.74
261	0.361	298	3.56	335	6.94	372	1.58
262	0.379	299	3.70	336	6.85	373	1.48
263	0.396	300	3.87	337	6.70	374	1.39
264	0.430	301	4.05	338	6.56	375	1.31
265	0.465	302	4.20	339	6.47	376	1.26
266	0.499	303	4.35	340	6.44	377	1.24
267	0.534	304	4.51	341	6.42	378	1.21
268	0.568	305	4.66	342	6.35	379	1.21
269	0.620	306	4.82	343	6.35	380	1.05
270	0.654	307	4.96	344	6.30	381	0.981
271	0.706	308	5.13	345	6.23	382	0.912
272	0.757	309	5.30	346	6.14	383	0.878
273	0.809	310	5.44	347	6.08	384	0.929
274	0.878	311	5.58	348	5.77	385	0.757
275	0.929	312	5.73	349	5.47	386	0.637
276	0.998	313	5.87	350	5.20	387	0.534
277	1.08	314	6.02	351	4.94	388	0.448
278	1.15	315	6.14	352	4.72	389	0.396
279	1.24	316	6.28	353	4.53	390	0.344
280	1.33	317	6.42	354	4.32	391	0.310
281	1.41	318	6.54	355	4.15	392	0.293
282	1.50	319	6.63	356	4.03	393	0.275
283	1.60	320	6.70	357	3.94	394	0.241
284	1.70	321	6.76	358	3.89	395	0.207
285	1.81	322	6.83	359	3.89		
286	1.91	323	6.85	360	3.68		

Note:
250-395 nm, Gierzcak et al. [271].

D14. $HOCH_2CHO + h\nu \rightarrow CH_2OH + HCO$ φ_1
$HOCH_2CHO + h\nu \rightarrow CH_3OH + CO$ φ_2
$HOCH_2CHO + h\nu \rightarrow OH + CH_2CHO$ φ_3
$HOCH_2CHO + h\nu \rightarrow HOCH_2CO + H$ φ_4. The absorption cross sections of $HOCH_2CHO$ (glycolaldehyde, hydroxyacetaldehyde) have been measured at room temperature and 205-335 nm by Bacher et al. [33]; and at 210-330 nm by Magneron et al. [465]. The spectrum consists of a strong absorption below 220 nm and a weaker absorption band centered near 280 nm with evidence of vibrational progressions. The measurements performed by Magneron et al. [465] were done at two different laboratories and are nearly identical, but reveal significant differences as compared to the spectrum measured by Bacher et al. [33], being about 20% at the maximum. The cross sections of Magneron et al. [465] are therefore recommended and are listed in Table 4-44.

The broad band photolysis (285 ± 25 nm) of glycolaldehyde in air performed by Bacher et al. [33] revealed an overall quantum yield $\Phi > 0.5$, relative to the quantum yield ($\Phi = 0.3$) of removal of acetone. Product studies by FTIR suggests that channel (1) is the major photolysis channel (65-80%), while channel (2) accounts to 15-20%, and channel (3) contributes up to 15%. The formation of channel (4) was suggested to produce $HOCH_2CO$ as a source for OH radicals, whose presence was indirectly invoked due the formation of glyoxal. Magneron et al. [465] also photolysed glycolaldehyde (broadband lamps 275-380 nm) and measured products by FTIR (CO, CO_2, HCHO and CH_3OH). They observed direct evidence for OH production via channel (3) using OH-scavenger and OH-tracer species, and performed additional photolysis experiments where glycolaldehyde was used an OH source to measure rate constants for OH with a series of dienes. The contribution of channel (2) was estimated to 10%, and that of channels (1) + (2) to 90%. No evidence was found for channel (4).

Based on the combined product studies we recommend quantum yields: $\varphi_1 = 0.70$, $\varphi_2 = 0.15$ and $\varphi_3 = 0.15$

Table 4-44. Absorption Cross Sections of $HOCH_2CHO$ at 298 K

λ (nm)	10^{20} σ (cm^2)	λ (nm)	10^{20} σ (cm^2)	λ (nm)	10^{20} σ (cm^2)	λ (nm)	10^{20} σ (cm^2)
212	8.24	242	1.48	272	6.62	302	3.26
214	4.85	244	1.77	274	6.90	304	2.69
216	2.97	246	2.10	276	6.91	306	2.29
218	1.68	248	2.41	278	6.88	308	1.89
220	0.904	250	2.76	280	6.85	310	1.57
222	0.569	252	3.19	282	6.93	312	1. 30
224	0.334	254	3.58	284	6.60	314	0.95
226	0.262	256	3.97	286	6.38	316	0.72
228	0.284	258	4.45	288	6.09	318	0.55
230	0.425	260	4.89	290	5.89	320	0.42
232	0.489	262	5.21	292	5.49	322	0.31
234	0.672	264	5.53	294	4.90	324	0.23
236	0.845	272	5.99	296	4.52	326	0.16
238	1.03	274	6.25	298	4.13	328	0.12
240	1.25	270	6.41	300	3.77	330	0.096

Note:
212-330 nm, Magneron et al. [465].

D15. $CH_3C(O)CH_3 + h\nu \rightarrow CH_3C(O) + CH_3$ ($\lambda_{threshold} > 338$ nm) φ_1
$CH_3C(O)CH_3 + h\nu \rightarrow 2\ CH_3 + CO$ ($\lambda_{threshold} > 299$ nm) φ_2. The absorption spectrum of acetone has been measured at room temperature and 159-203 nm by Lake and Harrison [429]; at 200-300 nm by McMillan [139, 510]; at 220-368 nm by Meyrahn et al. [524, 526]; at 196-366 nm by Schneider and Moortgat (see Röth et al. [687]); at 253.7 nm and 260-360 nm by Hynes et al. [355]; at 202-335 nm by Martinez et al. [492]; at 215–349 nm by Gierczak et al. [269]; at 220-346 nm by Wollenhaupt et al. [852]; and at 240-350 nm by Yujing and Mellouki [871]. Cross sections have been determined at isolated wavelengths: at 193 nm (also for $CD_3C(O)CD_3$) by Braun et al. [87] and Seki and Okabe [720]; at 216.51 nm by Krasnoperov and Mehta [421]; and at 184.9 nm (also for $CD_3C(O)CD_3$) by Gierczak et al. [272].

The spectrum below 200 nm is highly structured in the regions 160-170 nm and 180-195 nm. A broad absorption band was observed between 210 and 340 nm for which high-resolution measurements give evidence for the existence of two bands with maxima at about 273 and 278 nm. The results of the various research teams are in excellent agreement, i.e., ≤ 8% in the 240-320-nm region of the absorption band. The

measured absorption cross-sections for the maxima vary between 5.2×10^{-20} and 4.8×10^{-20} cm^2 molecule^{-1}. In the tails of the absorption band, the various data sets become more and more divergent with decreasing wavelength up to about 50% at 220 nm and with increasing wavelength up to more than 100% at 340 nm. The data measured by Meyrahn et al. [524, 526] are systematically higher than the other studies at wavelengths larger than 320 nm. Our recommendation for the region of the absorption band is based on the recent results of Martinez et al. [492], Gierczak et al. [269], Wollenhaupt et al. [852] and Yujing and Mellouki [871], which agree within 2.5% in the region of the absorption maximum and within 50% in the short- and long-wavelength tails.

The temperature dependence has been studied at 300-340 nm and 261-362 K by Hynes et al. [355]; at 215-349 nm and 235-298 K by Gierczak et al. [269]; and (also for $CD_3C(O)CD_3$) at 184.9 nm and 222-296 K by Gierczak et al. [272]. The absorption spectrum shows modest temperature dependence in the long-wavelength tail of the absorption band above 270 nm, with the cross sections decreasing with decreasing temperature. At shorter wavelengths the spectrum is essentially independent of temperature, the cross section changes by < 5% between 298 and 235 K. Gierczak et al. [269] parameterized the temperature dependent cross sections by a quadratic expression $\sigma(\lambda, T) = \sigma(\lambda, 298\ K)[1 + c_1(\lambda)T + c_2(\lambda)T^2]$, which later was superseded by Burkholder [109] by a cubic expression $\sigma(\lambda, T) = \sigma(\lambda, 298\ K)[1 + A(\lambda)T + B_2(\lambda)T^2 + C(\lambda)T^3]$. In Table 4-45 are listed the recommended absorption cross sections at 298 K taken from the work of Gierczak et al. [269] and the temperature coefficients A, B, and C of the cubic fit derived by Burkholder [109].

The absorption cross section of $CH_3C(O)CH_3$ at 184.9 nm decreases very slightly with decreasing temperature from 296 to 222 K leading to an average value of $(2.98 \pm 0.10) \times 10^{-18}$ cm^2 molecule^{-1}, whereas that of $CD_3C(O)CD_3$ increases noticeably from 3.91×10^{-18} cm^2 molecule^{-1} (average of six results) at 295 K to 4.61×10^{-18} cm^2 molecule^{-1} at 232 K, as reported by Gierczak et al. [272].

Gardner et al. [263] measured the acetone loss ($-\Phi_{AC}$) and formation of products CO_2, CO, CH_3OH and HCHO of the photolysis of dilute acetone-air mixtures at 4 wavelengths in the range 279-313 nm, 25-745 Torr and 271-301 K. At pressures larger than 300 Torr, they observed a near constant quantum yield $-\Phi_{AC} \approx \varphi_{CO2} = \varphi_1 = 0.077$ in the range 279-313 nm, to increase slightly at lower pressures. Meyrahn et al. [524, 526] measured the quantum yields of CO and CO_2 in the photolysis of dilute mixtures of acetone in air at nine wavelengths in the range 250-330 nm. At 1 atm, φ_{CO2} decreased from 1.59 at 250 nm to 0.11 at 310 nm, to increase again to 0.27 at 330 nm; the Φ_{CO} decreased from 0.45 at 250 nm to 0.02 at 310 nm and increased again to 0.09 at 330 nm. The quantum yield φ_{CO2} being larger than unity was explained by the participation of secondary reactions. The same authors also measured the quantum yield of peroxyacetyl nitrate φ_{PAN} (which is a direct measure of φ_1) of acetone /air/NO_2 mixtures to decrease from ~0.78 at 250-260 nm to 0.03 at 230-330 nm. Meyrahn et al. [524, 526] observed φ_{CO2} to increase at lower pressures (Stern-Volmer mechanism) at 330 nm. Emrich and Warneck [229, 230] also determined the φ_{PAN} of acetone /air/NO_2 mixtures at six wavelengths in the range 280-330 nm and the total pressure range 10 to 760 Torr. At 760 Torr, φ_{PAN} decreased from 1.00 at 280 nm to 0.06 at 320 nm, and increased again to 0.13 at 330 nm. These authors also observed Stern-Volmer type pressure dependence at all wavelengths. The results were explained in terms of the rate of photodissociation from the excited singlet $^1[AC]^*$ state of acetone and the competing intersystem crossing to the triplet $^3[AC]^*$, both relative to that of pressure quenching, as a function of energy above the dissociation threshold. It was proposed that

$$^1[AC]^* \rightarrow 2\ CH_3 + CO \text{ and } ^3[AC]^* \rightarrow CH_3C(O) + CH_3.$$

Gierczak et al. [269] determined $-\Phi_{AC}$ and φ_{CO2} in the laser photolysis of acetone at nine wavelengths in the range 248-337 nm as a function of pressure (25 to 760 Torr air) and temperature in the range 195-298 K. At $\lambda > 270$ nm Φ displayed a Stern-Volmer type pressure dependence, and the zero pressure quantum yield was found to increase at decreasing wavelength, to reach unity near 290 nm. The quantum yields were found to be temperature independent at 308 nm. Their results at 298 K were nearly identical to those of Emrich and Warneck [229]. Gierczak et al. [269] presented an algorithm for the quantum yield based on the parameterization of their own data. Warneck [838] evaluated the results of Gierczak et al. [269] and Emrich and Warneck [229] of the quantum yields for the dissociation of acetone Φ_{diss} to derive an expression for the dependence of Φ_{diss} on wavelength and pressure.

Aloisio and Francisco [13] measured the quantum yield of acetone photodissociation at 248 and 308 nm in the presence and absence of water vapor. At 248 nm the apparent quantum yield Φ_{eff} decreased from unity to 0.73 ± 0.07 in the presence of 9 Torr H_2O, and at 308 nm Φ_{eff} was reduced from 0.28 ± 0.07 to 0.06 ± 0.04.

Recently Blitz et al. [77, 78] measured the pressure and temperature (218-295 K) dependent quantum yields of acetone between 279 and 327.5 nm. These authors used a spectroscopic technique to detect the CH_3CO radical based on the detection of the OH radical formed by the reaction

$$CH_3CO + O_2 \rightarrow CH_3COO_2^* \rightarrow OH + \text{“other products”}.$$

They observed "classical" Stern-Volmer behavior at $\lambda < 302$ nm, but at $\lambda > 302$ nm an extended form of the Stern-Volmer expression was necessary for pressures below 15 Torr to fit their data, reflecting the dissociation and quenching from both $^1[AC]^*$ and $^3[AC]^*$ excited states (Arnold et al. [25]). These authors established the total quantum yield $\Phi_{TOTAL}(\lambda, p, T) = \varphi_{CH3CO}(\lambda, p, T) + \varphi_{CO}(\lambda, T) = \varphi_1 + \varphi_2$.

At the limit pressure p = 0 Blitz et al. [77, 78] determined at 248 nm and 295 K, $\Phi_{TOTAL} = 1$, $\varphi_{CH3CO} = 0.65$ and $\varphi_{CO} = 0.35$. At $\lambda < 310$ nm and 1 atm, there was very good agreement with the data of Gierczak et al. [269] and Emrich and Warneck [229]; however at $\lambda > 310$ nm, the measured quantum yields were significantly smaller, the time-resolved studies of Blitz et al. [77, 78] being more direct and sensitive than previous studies. The T-dependence of Φ_{TOTAL} is small below 295 nm, but quite striking at longer wavelengths: the ratio of the quantum yields at 295 and 218 K, Φ_{TOTAL} (295 K) / Φ_{TOTAL} (218 K) ≈ 4 and ≈ 20 at 310 nm and 322.5 nm, respectively.

The major difference in the study of Blitz et al, [77, 78] is that the OH radicals are detected before undergoing secondary reactions, so that the OH yields represent the CH_3CO radicals produced. The quantum yield determined by the other previous studies (Gierczak et al. [269] and Emrich and Warneck [229]) were based upon the removal of CH_3COCH_3, which is affected by the additional loss by reaction with the OH radicals which are produced in the decomposition of CH_3CO.

The quantum yield data of Blitz et al. [77, 78] are recommended in the current evaluation. The optimized parameterization of the quantum yields for the range 279-327.5 nm, temperature 218 to 295 K and pressure up to 1000 mbar, is given by the following expressions:

$$\Phi_{TOTAL}(\lambda, [M], T) = \varphi_{CH3CO}(\lambda, [M], T) + \varphi_{CO}(\lambda, T)$$

For λ = 279-327.5 nm

$$\varphi_{CO}(\lambda, T) = 1 / (1 + A_0)$$

where $A_0 = [a_0 / (1 - a_0)] \exp[b_0 \{\lambda - 248\}]$

$$a_0 = (0.350 \pm 0.003)\,(T/295)^{(-1.28 \pm 0.03)}$$

$$b_0 = (0.068 \pm 0.002)\,(T/295)^{(-2.65 \pm 0.20)}$$

For λ = 279-302 nm

$$\varphi_{CH3CO}(\lambda, [M], T) = \{1 - \varphi_{CO}(\lambda, T)\} / \{1 + A_1[M]\}$$

where $A_1 = a_1 \exp[-b_1 \{(10^7/\lambda) - 33113\}]$

$$a_1 = (1.600 \pm 0.032) \times 10^{-19}\,(T/295)^{(-2.38 \pm 0.08)}$$

$$b_1 = (0.55 \pm 0.02) \times 10^{-3}\,(T/295)^{(-3.19 \pm 0.13)}$$

For λ = 302-327.5 nm,

$$\varphi_{CH3CO}(\lambda, [M], T) = \{(1 + A_4[M] + A_3) / [(1 + A_2[M] + A_3)(1 + A_4[M])]\}\,\{1 - \varphi_{CO}(\lambda, T)\}$$

where $A_2 = a_2 \exp[-b_2 \{(10^7/\lambda) - 30488\}]$

$$a_2 = (1.62 \pm 0.06) \times 10^{-17}\,(T/295)^{(-10.03 \pm 0.20)}$$

$$b_2 = (1.79 \pm 0.02) \times 10^{-3}\,(T/295)^{(-1.364 \pm 0.036)}$$

$A_3 = a_3 \exp[-b_3 \{(10^7/\lambda) - c_3\}^2]$

$$a_3 = (26.29 \pm 0.88)\,(T/295)^{(-6.59 \pm 0.23)}$$

$$b_3 = (5.72 \pm 0.20) \times 10^{-7}\,(T/295)^{(-2.93 \pm 0.09)}$$

$$c_3 = (30006 \pm 41)\,(T/295)^{(-0.064 \pm 0.004)}$$

$A_4 = a_4 \exp[-b_4 \{(10^7/\lambda) - 30488\}]$

$$a_4 = (1.67 \pm 0.14) \times 10^{-15}\,(T/295)^{(-7.25 \pm 0.54)}$$

$$b_4 = (2.08 \pm 0.02) \times 10^{-3}\,(T/295)^{(-1.16 \pm 0.15)}$$

In all cases [M] is in molecule cm^{-3}, λ in nm and T in K.

These equations have been used to calculate the quantum yields in the region 279-327 nm at 218, 248, 273 and 295 K, as displayed in Table 4-46**.**

Table 4-45. Absorption Cross Sections of $CH_3C(O)CH_3$ at 298 K and Temperature Coefficients

λ (nm)	10^{20} σ (cm^2)	10^3 A (K^{-1})	10^5 B (K^{-2})	10^8 C (K^{-3})	λ (nm)	10^{20} σ (cm^2)	10^3 A (K^{-1})	10^5 B (K^{-2})	10^8 C (K^{-3})
215	0.167	-10.46	8.346	-16.43	283	4.71	1.137	-1.350	3.272
216	0.180	-9.192	7.357	-14.51	284	4.62	0.8530	-1.158	2.943
217	0.196	-6.233	5.039	-10.01	285	4.54	0.6518	-1.023	2.714
218	0.212	-3.190	2.651	-5.359	286	4.44	0.4907	-0.9154	2.531
219	0.228	-1.002	0.9314	-2.003	287	4.36	0.3190	-0.7992	2.332
220	0.246	0.4104	-0.1807	0.1679	288	4.28	0.1109	-0.6586	2.092
221	0.270	1.567	-1.090	1.936	289	4.15	-0.1230	-0.5036	1.833
222	0.294	2.962	-2.183	4.058	290	4.06	-0.3698	-0.3426	1.568
223	0.318	4.839	-3.651	6.909	291	3.95	-0.6430	-0.1615	1.265
224	0.346	6.940	-5.293	10.09	292	3.82	-0.9625	0.05796	0.8847
225	0.380	8.598	-6.588	12.60	293	3.71	-1.316	0.306	0.4472
226	0.419	9.380	-7.200	13.79	294	3.57	-1.650	0.535	0.0477
227	0.456	9.551	-7.336	14.06	295	3.42	-1.905	0.699	-0.2168
228	0.492	9.705	-7.462	14.31	296	3.26	-2.084	0.796	-0.3430
229	0.535	10.08	-7.761	14.89	297	3.11	-2.234	0.867	-0.4086
230	0.584	10.41	-8.023	15.41	298	2.98	-2.391	0.942	-0.4824
231	0.637	10.39	-8.002	15.36	299	2.82	-2.590	1.055	-0.6387
232	0.693	10.01	-7.707	14.79	300	2.67	-2.915	1.277	-1.020
233	0.750	9.534	-7.332	14.06	301	2.58	-3.421	1.649	-1.709
234	0.815	9.138	-7.022	13.46	302	2.45	-4.008	2.091	-2.543
235	0.885	8.851	-6.799	13.02	303	2.30	-4.508	2.465	-3.248
236	0.956	8.638	-6.634	12.70	304	2.18	-4.858	2.715	-3.699
237	1.03	8.471	-6.504	12.45	305	2.05	-5.120	2.880	-3.959
238	1.11	8.318	-6.385	12.22	306	1.89	-5.433	3.062	-4.219
239	1.21	8.125	-6.235	11.93	307	1.75	-6.010	3.429	-4.805
240	1.30	7.861	-6.031	11.53	308	1.61	-6.986	4.096	-5.954
241	1.40	7.554	-5.793	11.07	309	1.49	-8.135	4.899	-7.370
242	1.50	7.268	-5.571	10.64	310	1.36	-8.897	5.415	-8.255
243	1.60	7.035	-5.390	10.29	311	1.24	-8.923	5.378	-8.097
244	1.72	6.838	-5.237	9.994	312	1.14	-8.494	5.001	-7.305
245	1.83	6.649	-5.093	9.718	313	1.06	-8.228	4.754	-6.772
246	1.95	6.472	-4.960	9.464	314	0.944	-8.445	4.881	-6.959
247	2.07	6.326	-4.850	9.256	315	0.837	-8.966	5.240	-7.592
248	2.20	6.210	-4.763	9.091	316	0.760	-9.409	5.528	-8.076
249	2.33	6.099	-4.680	8.936	317	0.684	-9.584	5.588	-8.085
250	2.47	5.972	-4.587	8.763	318	0.598	-9.736	5.596	-7.946
251	2.60	5.832	-4.486	8.576	319	0.523	-10.39	5.958	-8.433
252	2.74	5.697	-4.389	8.399	320	0.455	-11.80	6.869	-9.933
253	2.87	5.581	-4.306	8.249	321	0.411	-13.48	7.962	-11.75
254	3.01	5.483	-4.235	8.120	322	0.348	-14.59	8.600	-12.67
255	3.15	5.385	-4.164	7.989	323	0.294	-14.98	8.670	-12.47
256	3.30	5.261	-4.075	7.825	324	0.248	-15.39	8.743	-12.27
257	3.44	5.101	-3.961	7.620	325	0.210	-16.28	9.187	-12.77
258	3.57	4.932	-3.843	7.410	326	0.174	-17.09	9.588	-13.21
259	3.69	4.802	-3.756	7.262	327	0.141	-17.21	9.471	-12.68
260	3.81	4.746	-3.723	7.215	328	0.113	-16.92	9.048	-11.58
261	3.94	4.744	-3.730	7.239	329	0.0913	-16.66	8.672	-10.62
262	4.07	4.734	-3.729	7.246	330	0.0740	-15.94	7.979	-9.099
263	4.20	4.651	-3.674	7.155	331	0.0586	-13.93	6.340	-5.829
264	4.32	4.482	-3.559	6.956	332	0.0465	-10.93	3.969	-1.214
265	4.41	4.271	-3.416	6.712	333	0.0375	-8.186	1.847	2.840
266	4.49	4.087	-3.296	6.513	334	0.0311	-6.530	0.6289	5.067
267	4.56	3.983	-3.234	6.420	335	0.0248	-5.692	0.1022	5.880

λ (nm)	10^{20} σ (cm^2)	10^3 A (K^{-1})	10^5 B (K^{-2})	10^8 C (K^{-3})	λ (nm)	10^{20} σ (cm^2)	10^3 A (K^{-1})	10^5 B (K^{-2})	10^8 C (K^{-3})
268	4.64	3.969	-3.235	6.440	336	0.0199	-4.656	-0.5382	6.860
269	4.72	4.009	-3.273	6.524	337	0.0162	-2.090	-2.355	10.09
270	4.79	4.025	-3.294	6.577	338	0.0135	3.113	-6.237	17.33
271	4.87	3.935	-3.240	6.494	339	0.0113	11.01	-12.26	28.77
272	4.91	3.704	-3.085	6.231	340	00912	20.02	-19.22	42.15
273	4.94	3.378	-2.861	5.845	341	00729	27.20	-24.83	53.03
274	4.94	3.061	-2.645	5.473	342	00583	29.63	-26.80	56.96
275	4.94	2.854	-2.508	5.243	343	00494	25.97	-24.04	51.78
276	4.93	2.790	-2.474	5.201	344	00365	16.35	-16.63	37.55
277	4.92	2.816	-2.505	5.276	345	0.00301	3.774	-6.858	18.72
278	4.94	2.820	-2.518	5.316	346	0.00235	-2.414	-1.987	9.304
279	4.92	2.692	-2.433	5.175	347	0.00158	7.880	-9.888	24.53
280	4.91	2.389	-2.222	4.803	348	0.00111	29.52	-26.61	56.78
281	4.86	1.963	-1.922	4.272	349	0.00107	41.03	-35.51	73.95
282	4.79	1.517	-1.612	3.726					

Note:
215-349 nm, Gierczak et al. [269], parameterization of the temperature dependence revised by J. Burkholder (2005) [109]: $\sigma(T, \lambda) = \sigma(298\ K, \lambda)\ (1 + A\ T + B\ T^2 + C\ T^3)$ for T = 235-298 K.

Table 4-46. Quantum Yields for the Photolysis of Acetone

λ (nm)	218 K	248 K	273 K	295 K
279	0.680	0.579	0.571	0.617
280	0.663	0.558	0.551	0.597
281	0.644	0.536	0.530	0.578
282	0.621	0.513	0.509	0.559
283	0.594	0.489	0.489	0.540
284	0.565	0.465	0.468	0.521
285	0.534	0.441	0.448	0.502
286	0.500	0.417	0.427	0.483
287	0.465	0.393	0.407	0.464
288	0.430	0.369	0.388	0.446
289	0.394	0.345	0.368	0.428
290	0.359	0.322	0.350	0.411
291	0.324	0.300	0.331	0.394
292	0.291	0.279	0.314	0.377
293	0.260	0.258	0.297	0.361
294	0.231	0.239	0.280	0.345
295	0.205	0.221	0.264	0.330
296	0.180	0.203	0.249	0.315
297	0.158	0.187	0.235	0.301
298	0.138	0.172	0.221	0.287
299	0.121	0.158	0.208	0.274
300	0.105	0.144	0.195	0.261
301	0.0915	0.132	0.183	0.249
302	0.0794	0.121	0.125	0.237
303	0.0735	0.101	0.105	0.213
304	0.0557	0.0810	0.0873	0.184
305	0.0421	0.0646	0.0728	0.159
306	0.0317	0.0514	0.0608	0.137
307	0.0239	0.0409	0.0508	0.119
308	0.0180	0.0325	0.0426	0.103
309	0.0135	0.0258	0.0358	0.0887
310	0.0101	0.0205	0.0301	0.0769
311	0.00762	0.0164	0.0255	0.0669
312	0.00574	0.0131	0.0216	0.0584
313	0.00433	0.0105	0.0184	0.0511
314	0.00328	0.00842	0.0158	0.0449
315	0.00249	0.00679	0.0136	0.0396
316	0.00190	0.00550	0.0117	0.0350
317	0.00145	0.00447	0.0101	0.0311
318	0.00111	0.00365	0.00882	0.0278
319	0.000858	0.00299	0.00771	0.0248
320	0.000664	0.00246	0.00676	0.0223
321	0.000515	0.00204	0.00595	0.0201
322	0.000400	0.00169	0.00526	0.0181
323	0.000312	0.00141	0.00466	0.0164
324	0.000244	0.00117	0.00414	0.0149
325	0.000191	0.000983	0.00369	0.0135
326	0.000149	0.000826	0.00329	0.0124
327	0.000117	0.000696	0.00295	0.0113

D16. $CH_3C(O)CH_2OH + h\nu \rightarrow CH_3C(O) + CH_2OH$

$CH_3C(O)CH_2OH + h\nu \rightarrow HOCH_2C(O) + CH_3$. The absorption cross sections of $CH_3C(O)CH_2OH$ (hydroxyacetone, acetol) have been measured at room temperature and 235-340 nm by Orlando et al. [610]. The spectrum shows an absorption band with the maximum at 266 nm. In Table 4-47 are listed the averages over 1-nm intervals of the spectrum recorded at medium resolution of ~0.6 nm.

Quantum yields for removal of hydroxyacetone were estimated by Orlando et al. [610] to be 0.65 ± 0.25 for the wavelength range 240-420 nm, and < 0.6 for wavelengths larger than 290 nm.

Table 4-47. Absorption Cross Sections of $CH_3C(O)CH_2OH$ at 298 K

λ (nm)	10^{20} σ (cm^2)	λ (nm)	10^{20} σ (cm^2)	λ (nm)	10^{20} σ (cm^2)	λ (nm)	10^{20} σ (cm^2)
236	2.13	262	6.61	288	3.34	314	0.177
237	2.29	263	6.68	289	3.11	315	0.157
238	2.43	264	6.72	290	2.87	316	0.142
239	2.59	265	6.74	291	2.66	317	0.133
240	2.78	266	6.74	292	2.45	318	0.117
241	2.94	267	6.74	293	2.26	319	0.104
242	3.14	268	6.71	294	2.06	320	0.095
243	3.34	269	6.67	295	1.87	321	0.087
244	3.55	270	6.61	296	1.69	322	0.078
245	3.74	271	6.53	297	1.52	323	0.072
246	3.95	272	6.42	298	1.36	324	0.067
247	4.14	273	6.30	299	1.22	325	0.063
248	4.34	274	6.18	300	1.08	326	0.065
249	4.56	275	6.05	301	0.961	327	0.057
250	4.76	276	5.90	302	0.843	328	0.051
251	4.98	277	5.73	303	0.743	329	0.051
252	5.18	278	5.54	304	0.652	330	0.046
253	5.36	279	5.33	305	0.569	331	0.041
254	5.54	280	5.12	306	0.493	332	0.037
255	5.72	281	4.91	307	0.431	333	0.036
256	5.89	282	4.69	308	0.379	334	0.037
257	6.06	283	4.48	309	0.331	335	0.035
258	6.19	284	4.27	310	0.287	336	0.031
259	6.30	285	4.05	311	0.249		
260	6.41	286	3.82	312	0.219		
261	6.50	287	3.58	313	0.192		

Note:
236-236 nm, Orlando et al. [610].

D17. CHOCHO + hν → HCO + HCO (1)
CHOCHO + hν → H_2 + 2 CO (2)
CHOCHO + hν → HCHO + CO (3)
CHOCHO + hν → H + CO + HCO (4). The absorption spectrum of glyoxal has been measured at room temperature and 230-460 nm by Plum et al. [638]; at isolated wavelengths at 308 nm by Langford and Moore [432], at 193, 248, 308, and 351 nm by Zhu et al. [883], and between 290 and 420 nm at 10-nm intervals by Chen and Zhu [161]. Measurements at medium resolution were carried out with a diode-array spectrometer at 210-450 nm (resolution 0.6 nm) by Orlando and Tyndall [608], and at 210-480 nm (resolution 0.25 nm by Horowitz et al. [341], and measurements at high resolution using cavity ring-down spectroscopy in the narrow range 436-442 nm by Zhu and Johnston [882], and using a Fourier Transform spectrometer at 250-526 nm (resolution 1 cm^{-1} at 250-268 nm, 0.06 cm^{-1} at 368-526 nm) by Volkamer et al. [827]. The absorption spectrum exhibits two absorption bands in the region above 220 nm, a weak band with evidence of vibrational structure in the UV at 220-350 nm and a strong and highly structured band in the near UV and visible above 360 nm, with a maximum at 455 nm**.**

The data of Horowitz et al. [341] and Orlando and Tyndall [608] are in very good agreement, i.e., to better than 10% between 240 and 440 nm. The results of Chen and Zhu [161] agree to within 10% with those of Horowitz et al. [341] and Orlando and Tyndall [608] in the 290-310 nm region and at 330, 340, 400, and 420 nm, within 15% at 320, 370, and 390 nm, 20% at 360 and 410 nm, 35% at 380 nm, and 45% at 350 nm. The data of Plum et al. [638] agree to within 25% with these recent data except for the minimum near 350 nm and the region below 260 nm, where considerably lower absorption cross-section were observed by Plum et al. [638]. The absorption cross sections reported by Zhu et al. [883] at the excimer laser wavelengths 248, 308, and 351 nm also agree very well with the data of Horowitz et al. [341] and Orlando and Tyndall [608], and the strong absorption feature below 200 nm, indicated by the 193-nm measurement of Zhu et al. [883] ($\sigma = 4.8 \times 10^{-19}$ cm^2 $molecule^{-1}$), was also observed by Orlando and Tyndall [608].

The cross sections reported by Volkamer et al. [827] are in all spectral ranges roughly 10% larger than those reported by Horowitz et al. [341] and Orlando and Tyndall [608] (where comparison is possible), and this difference seems systematic. The UV spectrum reported by Volkamer et al. [827] is consistent with IR-spectral parameters, for which glyoxal photolysis is not a problem, and which were obtained by simultaneous recording of UV and IR spectra in identical glyoxal fillings of the absorption cell. As recommended room temperature absorption cross sections for glyoxal we choose the averages over 1-nm intervals (rounded to three significant figures) of the high-resolution spectrum of Volkamer et al. [827], which are listed in Table 4-48.

Calvert and Pitts [137] summarized the quantum yield data before 1966. Based on the work of Calvert and Layne [134] and Parmenter [625] it was established that channel (3) was the dominant photolysis channel (yield 0.84 to 0.6 in the range 254 to 435 nm) with little evidence for the radical channel (1). At 313 nm Plum et al. [638] measured a HCHO yield of 0.13 for wavelengths larger than 325 nm, but reported an "effective quantum yield" of $\phi_{eff} = 0.029$, based on measured outdoor relative photolysis rates compared to NO_2, $J_{CHOCHO}/J_{NO2} = 0.008 \pm 0.005$. Langford and Moore [432] determined HCO directly by resonance absorption and deduced total HCO yields of 0.8 ± 0.4 ($\Phi_1 \approx 0.4$) at 305 nm, and estimated quantum yields for the other two channels. Using cavity ring-down spectroscopy, Zhu et al. [883] found HCO yields of 1.5 ($\Phi_1 \approx 0.75$) at 351 nm, 069 ($\Phi_1 \approx 0.35$) at 308 nm, 0.52 ($\Phi_1 \approx 0.26$) at 248 nm and 0.42 ($\Phi_1 \approx 0.21$) at 193 nm. In a later study Chen and Zhu [161] determined zero pressure HCO yields $\phi_0(\lambda)$ at 10 nm intervals, to increase from 0.50 ± 0.01 at 290 nm to a maximum of 2.01 ± 0.08 at 390 nm and to drop to $0.74 \pm 0.08 \pm 400$ nm, 0.56 ± 0.04 at 410 nm and 0.48 ± 0.03 at 420 nm. HCO quantum yields were found independent of nitrogen buffer gas (10-400 Torr) in the 290-370 nm region, but decreased with increasing pressure in the 380-420 nm region. They deduced HCO quantum yields at 760 Torr N_2 to be 0.49 at 380 nm, 0.54 nm at 390 nm, 0.32 at 400 nm, 0.22 at 410 nm and 0.14 at 420 nm.

Tadić et al. [761] photolysed glyoxal with fluorescent broad-band lamps, overlapping selectively with one of the absorption bands of glyoxal, and determined the products CO, HCHO and HCOOH. Using 275-380 nm irradiation, the overall quantum yield was $\Phi_T = 0.97 \pm 0.05$ independent of pressure. The absolute quantum yields obtained with 390-470 nm radiation, covering the second absorption band of glyoxal, showed dependency on total pressure, ranging form $\Phi_T = 0.12$ at 100 Torr to $\Phi_T = 0.04$ at 700 Torr and which can be expressed as a Stern-Volmer equation $1/\Phi_T = 6.80 + [251.8 \times 10^{-4} \times P\ (\text{Torr})]$.

By combining the product yields with the literature data mentioned above, the quantum yields for channels (1), (2) and (3) were deduced, as summarized in Table 4-49. The product quantum yields indicate that dissociation into 2 HCO radicals is the most important pathway under atmospheric conditions. The mean photolysis rate was measured under solar radiation in the EUPHORE outdoor chamber to be $J_{obs} = 1.04 \pm 0.10 \times 10^{-4}\ s^{-1}$, corresponding to a mean effective quantum yield $\phi_{eff} = 0.035 \pm 0.007$ [554], [553]. Although glyoxal has a very low effective quantum yield, photolysis remains an important removal path in the atmosphere.

Table 4-48. Absorption Cross Sections of CHOCHO at 296 K

λ (nm)	10^{20} σ (cm^2)	λ (nm)	10^{20} σ (cm^2)	λ (nm)	10^{20} σ (cm^2)	λ (nm)	10^{20} σ (cm^2)	λ (nm)	10^{20} σ (cm^2)
250	1.73	306	3.22	362	0.706	418	7.87	474	0.108
251	1.52	307	3.20	363	0.639	419	9.13	475	0.159
252	1.48	308	3.15	364	0.680	420	5.60	476	0.155
253	1.55	309	3.12	365	0.665	421	7.19	477	0.181
254	1.60	310	3.10	366	0.743	422	6.99	478	0.255
255	1.67	311	3.22	367	0.860	423	13.0	479	0.142
256	1.62	312	3.34	368	1.01	424	8.24	480	0.074
257	1.81	313	3.39	369	1.06	425	10.4	481	0.070
258	1.82	314	3.23	370	1.14	426	16.4	482	0.065
259	1.85	315	2.80	371	1.18	427	16.1	483	0.053
260	1.83	316	2.65	372	1.14	428	21.4	484	0.071
261	1.96	317	2.46	373	1.21	429	6.50	485	0.050
262	2.03	318	2.21	374	1.35	430	7.03	486	0.041
263	2.14	319	1.93	375	1.33	431	6.52	487	0.056
264	2.18	320	1.85	376	1.38	432	6.08	488	0.070
265	2.26	321	1.89	377	1.47	433	5.66	489	0.042
266	2.33	322	1.77	378	1.61	434	6.81	490	0.045
267	2.37	323	1.72	379	1.53	435	7.66	491	0.041
268	2.36	324	1.68	380	1.93	436	13.2	492	0.039
269	2.48	325	1.60	381	2.46	437	9.19	493	0.040
270	2.51	326	1.61	382	2.02	438	13.8	494	0.041
271	2.61	327	1.70	383	2.07	439	12.1	495	0.042
272	2.72	328	1.94	384	1.94	440	25.9	496	0.045
273	2.81	329	1.86	385	1.89	441	13.1	497	0.033
274	2.92	330	1.69	386	1.83	442	9.01	498	0.035
275	3.00	331	1.13	387	2.29	443	11.1	499	0.032
276	3.06	332	1.05	388	3.00	444	13.5	500	0.033
277	3.09	333	0.966	389	3.21	445	15.1	501	0.038
278	3.08	334	0.919	390	3.48	446	7.82	502	0.031
279	3.09	335	0.737	391	3.92	447	3.73	503	0.042
280	3.13	336	0.630	392	3.80	448	4.14	504	0.034
281	3.22	337	0.589	393	2.85	449	5.53	505	0.035
282	3.32	338	0.647	394	3.15	450	8.68	506	0.046
283	3.45	339	0.585	395	3.86	451	13.8	507	0.042
284	3.57	340	0.553	396	3.68	452	15.9	508	0.037
285	3.67	341	0.563	397	3.36	453	30.4	509	0.030
286	3.80	342	0.510	398	4.32	454	26.9	510	0.023
287	3.79	343	0.499	399	4.35	455	52.0	511	0.023
288	3.81	344	0.649	400	3.87	456	15.7	512	0.030
289	3.80	345	0.624	401	4.46	457	2.66	513	0.023
290	3.73	346	0.733	402	5.84	458	2.20	514	0.030
291	3.64	347	0.631	403	7.16	459	0.902	515	0.053
292	3.65	348	0.604	404	6.24	460	1.20	516	0.035
293	3.68	349	0.415	405	4.49	461	0.883	517	0.051
294	3.73	350	0.391	406	4.48	462	0.588	518	0.102
295	3.81	351	0.395	407	4.07	463	0.322	519	0.065
296	3.82	352	0.423	408	3.44	464	0.339	520	0.100
297	3.92	353	0.415	409	4.01	465	0.330	521	0.169
298	4.07	354	0.403	410	5.66	466	0.416	522	0.037
299	4.12	355	0.422	411	7.22	467	0.522	523	0.011
300	4.04	356	0.443	412	7.41	468	0.149	524	0.007
301	3.91	357	0.431	413	10.8	469	0.091	525	0.004
302	3.78	358	0.471	414	10.1	470	0.076	526	0.000
303	3.57	359	0.503	415	10.2	471	0.086		
304	3.35	360	0.546	416	6.07	472	0.092		

λ (nm)	10^{20} σ (cm^2)	λ (nm)	10^{20} σ (cm^2)	λ (nm)	10^{20} σ (cm^2)	λ (nm)	10^{20} σ (cm^2)	λ (nm)	10^{20} σ (cm^2)
305	3.24	361	0.627	417	6.83	473	0.110		

Note:
250-526 nm, data of Volkamer et al. [827].

Table 4-49. Absolute Quantum Yields in the Photolysis of CHOCHO

λ (nm)	Φ_{tot}	Φ_1	Φ_2	Φ_3	λ (nm)	Φ_{tot}	Φ_1	Φ_2	Φ_3
225	1.0	0.241	0.560	0.199	**340**	0.978	0.648	0.051	0.279
230	1.0	0.246	0.535	0.219	**345**	0.856	0.616	0.036	0.204
235	1.0	0.251	0.504	0.245	**350**	0.691	0.520	0.021	0.150
240	1.0	0.256	0.475	0.269	**355**	0.540	0.424	0.008	0.108
245	1.0	0.261	0.448	0.291	**360**	0.404	0.332	0.0	0.072
250	1.0	0.266	0.420	0.314	**365**	0.293	0.253		0.040
255	1.0	0.271	0.395	0.334	**370**	0.213	0.191		0.022
260	1.0	0.278	0.370	0.352	**375**	0.156	0.142		0.014
265	1.0	0.286	0.345	0.369	**380**	0.115	0.104		0.011
270	1.0	0.293	0.320	0.387	**385**	0.085	0.077		0.008
275	1.0	0.301	0.295	0.404	**390**	0.064	0.057		0.007
280	1.0	0.310	0.270	0.420	**395**	0.048	0.043		0.005
285	1.0	0.320	0.250	0.430	**400**	0.037	0.033		0.004
290	1.0	0.330	0.230	0.440	**405**	0.029	0.026		0.003
295	1.0	0.343	0.206	0.451	**410**	0.022	0.020		0.002
300	1.0	0.357	0.186	0.457	**415**	0.017	0.016		0.001
305	1.0	0.374	0.166	0.460	**420**	0.013	0.013		0.0
310	1.0	0.396	0.146	0.458	**425**	0.010	0.010		
315	1.0	0.423	0.125	0.452	**430**	0.008	0.008		
320	1.0	0.457	0.110	0.433	**435**	0.006	0.006		
325	1.0	0.497	0.095	0.408	**440**	0.003	0.003		
330	1.0	0.541	0.080	0.379	**445**	0.001	0.001		
335	0.995	0.593	0.065	0.337					

D18. $CH_3C(O)C(O)H + h\nu \rightarrow CH_3CO + HCO$ (1)
$CH_3C(O)C(O)H + h\nu \rightarrow CH_4 + 2\ CO$ (2)
$CH_3C(O)C(O)H + h\nu \rightarrow CH_3CHO + CO$ (3). The absorption spectrum of methylglyoxal has been measured at room temperature and 230-470 nm by Plum et al. [638]; at 218-494 nm by Meller et al. [518]; and absorption cross-sections in 10 nm intervals at 290-440 nm by Chen et al. [159]. Measurements have been reported by Staffelbach et al. [749] at 248, 273, and 298 K and 205-474 nm, and by Kyle and Orchard [428] at 387 K and 436 nm. The absorption spectrum exhibits two absorption bands, a slightly structured band between 225 and 335 nm and a stronger band between 335 and 475 nm, which is highly structured in the region above 410 nm. A steep increase of the absorption cross sections was observed at shorter wavelengths going from 225 to 200 nm by Staffelbach et al. [749].

The room temperature values of Meller et al. [518] (measured at a spectral resolution of 0.07 nm) and Staffelbach et al. [749] (measured at a resolution of 0.125 nm) are in good agreement above 230 nm: in the weaker absorption band the data of Meller et al. [518] are higher by up to 10-15% than the data of Staffelbach et al. [749]. In the strong absorption band up to 400 nm, the data of Staffelbach et al. [749] are higher by up to ~10% than the data of Meller et al. [518], and at higher wavelengths the peak values reported by Meller et al. [518] are higher (due to the higher resolution used in their study) than those measured by Staffelbach et al. [749]. The data points of Chen et al. [159] determined at 10-nm intervals fit well to the absorption curves of Meller et al. [518] and Staffelbach et al. [749], except for the points at 380 and 400 nm were the differences are about 20%. The cross sections reported earlier by Plum et al. [638] are approximately only the half of the cross sections reported Meller et al. [518] and Staffelbach et al. [749]. The preferred absorption cross sections listed in Table 4-50 are the data points at 1-nm intervals selected from the data of Staffelbach et al. [749] at 200-218 nm and the averages over 1-nm intervals of the high-resolution data of Meller et al. [518] at 236-493 nm. For the region 219-235 nm, the mean of the values of Meller et al. [518] and Staffelbach et al. [749] have been chosen.

The temperature dependence of the absorption cross sections is not significant, only minor changes of the order of 10% were observed in the spectrum between 298 and 248 K by Staffelbach et al. [749]. The largest changes occur in the structured region between 410 and 450 nm, where the fine structure becomes more pronounced at lower temperatures.

Quantum yields have been measured by Staffelbach et al. [749] from the determination of products after photolysis of dilute mixtures of methylglyoxal in air using a Xe arc equipped with different band pass filters to isolate several regions of the spectrum. The observed products (CO, CO_2, HCHO, CH_3COOH, CH_3COOOH, CH_3OH and HCOOH,) let to the conclusion that only channel (1) is important in the photolysis range 240-480 nm. The quantum yields were derived by modeling the products, using a number of secondary radical reactions. At 760 Torr, the ϕ_1 yields were: 0.005 for the wavelength region 410-418 nm, 0.055 for 355-480 nm, 0.07 for 280-240 nm and 0.14 for 240-420 nm. Raber and Moortgat [646] irradiated methylglyoxal in air at different total pressures using two types of broad-band lamps and determined the products (CO, CO_2, HCHO, CH_3OOH, CH_3OH, HCOOH, CH_3CHO, CH_3COOH, CH_3COOOH and $CH_3COCOOH$). Quantum yield derived by modeling the products of the photolysis in the 275-380 nm region varied from 0.94 ± 0.04 at 54 Torr to 0.64 ± 0.03 at 760 Torr, and in the 390-470 nm region from 0.41 ± 0.04 to 0.23 ± 0.02.

Koch and Moortgat [415] determined the quantum yields of CO, HCHO and CH_3CHO formation at 298 K as a function of wavelength (260-440 nm) and pressure of synthetic air (30-900 Torr) using "broad" monochromatic light, with an optical resolution of 8.5 nm. For photolysis in the short wavelength band (260-320 nm), the overall quantum yield was found to be unity, independent of wavelength and pressure. The analysis of the data gave evidence that channel (1) is the predominant photolysis path. In the long-wavelength band (380-440 nm) ϕ_{CO} showed Stern-Volmer pressure dependence, but in addition, ϕ_{HCHO} increased with methylglyoxal pressure, which was attributed to the reaction of excited methylglyoxal with ground state methylglyoxal.

The quantum yield of channel (1) in the wavelength range 250-500 nm was expressed as:

$$1/\phi(\lambda) = 1/\phi_0(\lambda) + P(\text{Torr}) / k(\lambda)$$

where $\phi_0(\lambda) = 1$ for $\lambda < 380$ nm

$\phi_0(\lambda) = (8.15 \pm 0.7)\ 10^{-9}\ [\exp(7131 \pm 267) / \lambda]$ for $\lambda > 380$ nm

$k(\lambda) = (7.34 \pm 0.1)\ 10^{-9}\ [\exp(8793 \pm 300) / \lambda]$

Chen et al. [749] photolysed methylglyoxal in N_2 in the range 290-440 nm at 10 nm intervals using a tunable dye laser, and measured the yield of HCO radicals using cavity ring-down spectroscopy. The yield of HCO radicals was calibrated against HCO produced in the photolysis or HCHO or Cl_2/HCHO mixtures. The yield of HCO radicals were unity in the range 320-360 nm, but decreased slightly at shorter wavelengths to 0.82 ± 0.06 at 290 nm, and strongly at $\lambda \geq 370$ nm to 0.17 ± 0.02 at 440 nm. They observed a weak dependence of the HCO yield on the methylglyoxal partial pressure. The HCO yields were independent of 10-400 Torr N_2-pressure between 290 to 370 nm, but showed a Stern-Volmer pressure dependence at $\lambda \geq 380$ nm in the form

$$1/\phi(\lambda) = 1/\phi_0(\lambda) + k_Q(\lambda)\ P(\text{Torr}),$$

where $\phi_0(\lambda) = (3.63 \pm 0.32)\ 10^{-7}\ [\exp(5693 \pm 533) / \lambda]$

and $k_Q(\lambda) = (1.93 \pm 0.24) \times 10^4\ [\exp(-(5639 \pm 497) / \lambda]$

Both sets of zero pressure quantum yields $\phi_0(\lambda)$ are in good agreement at $\lambda \leq 420$ nm, but quantum yields at 760 Torr from Chen et al. [159] (extrapolated to higher pressures) and Koch and Moortgat [415] deviate by a factor 4 at $\lambda \geq 420$ nm. The data of Chen et al. [159] are recommended, since they were measured directly. Additional measurements are needed to establish the quantum yields in the long wavelength tail of the spectrum at atmospheric relevant pressures.

Table 4-50. Absorption Cross Sections of $CH_3COC(O)H$ at 295-298 K

λ (nm)	$10^{20}\ \sigma$ (cm^2)	λ (nm)	$10^{20}\ \sigma$ (cm^2)	λ (nm)	$10^{20}\ \sigma$ (cm^2)	λ (nm)	$10^{20}\ \sigma$ (cm^2)	λ (nm)	$10^{20}\ \sigma$ (cm^2)
200	33.8	259	3.25	318	1.82	377	2.10	436	11.1
201	30.6	260	3.29	319	1.68	378	2.18	437	10.0
202	27.0	261	3.33	320	1.50	379	2.30	438	10.6
203	23.0	262	3.36	321	1.34	380	2.42	439	11.0
204	18.6	263	3.42	322	1.22	381	2.54	440	9.94
205	15.3	264	3.49	323	1.14	382	2.70	441	10.4
206	12.1	265	3.59	324	1.01	383	2.88	442	10.2
207	10.0	266	3.73	325	0.924	384	3.03	443	10.2

λ (nm)	10^{20} σ (cm^2)	λ (nm)	10^{20} σ (cm^2)	λ (nm)	10^{20} σ (cm^2)	λ (nm)	10^{20} σ (cm^2)	λ (nm)	10^{20} σ (cm^2)
208	8.52	267	3.87	326	0.848	385	3.20	444	11.2
209	7.43	268	4.02	327	0.774	386	3.39	445	9.62
210	6.34	269	4.13	328	0.716	387	3.61	446	8.91
211	5.58	270	4.20	329	0.672	388	3.71	447	9.84
212	4.73	271	4.22	330	0.647	389	3.88	448	9.19
213	4.16	272	4.23	331	0.620	390	4.03	449	10.1
214	3.57	273	4.27	332	0.608	391	4.22	450	8.68
215	3.08	274	4.31	333	0.525	392	4.31	451	6.35
216	2.65	275	4.37	334	0.531	393	4.47	452	6.33
217	2.33	276	4.49	335	0.495	394	4.57	453	6.08
218	2.10	277	4.64	336	0.455	395	4.67	454	4.47
219	1.46	278	4.77	337	0.407	396	4.87	455	3.69
220	1.45	279	4.87	338	0.362	397	5.08	456	3.09
221	1.44	280	4.92	339	0.346	398	5.26	457	2.47
222	1.43	281	4.93	340	0.322	399	5.46	458	1.81
223	1.44	282	4.90	341	0.300	400	5.62	459	1.28
224	1.43	283	4.83	342	0.289	401	5.90	460	0.914
225	1.44	284	4.76	343	0.288	402	6.07	461	0.795
226	1.46	285	4.70	344	0.289	403	6.36	462	0.643
227	1.48	286	4.66	345	0.295	404	6.55	463	0.480
228	1.51	287	4.65	346	0.308	405	6.92	464	0.332
229	1.53	288	4.73	347	0.325	406	7.20	465	0.268
230	1.60	289	4.84	348	0.339	407	7.59	466	0.228
231	1.61	290	4.92	349	0.362	408	7.95	467	0.188
232	1.65	291	4.90	350	0.385	409	8.12	468	0.160
233	1.67	292	4.81	351	0.424	410	8.52	469	0.133
234	1.75	293	4.70	352	0.463	411	8.64	470	0.108
235	1.83	294	4.57	353	0.492	412	9.07	471	0.0998
236	1.86	295	4.37	354	0.523	413	9.38	472	0.0897
237	1.93	296	4.17	355	0.556	414	9.62	473	0.0776
238	1.96	297	4.00	356	0.597	415	9.69	474	0.0680
239	2.00	298	3.88	357	0.635	416	9.72	475	0.0627
240	2.07	299	3.76	358	0.676	417	10.0	476	0.0561
241	2.14	300	3.69	359	0.720	418	10.1	477	0.0515
242	2.19	301	3.70	360	0.765	419	10.1	478	0.0483
243	2.23	302	3.74	361	0.816	420	10.2	479	0.0462
244	2.27	303	3.74	362	0.872	421	10.3	480	0.0392
245	2.30	304	3.62	363	0.933	422	10.5	481	0.0366
246	2.33	305	3.38	364	1.00	423	10.5	482	0.0315
247	2.38	306	3.15	365	1.08	424	10.2	483	0.0278
248	2.46	307	2.92	366	1.15	425	10.3	484	0.0271
249	2.57	308	2.71	367	1.23	426	10.0	485	0.0243
250	2.64	309	2.52	368	1.31	427	9.84	486	0.0217
251	2.68	310	2.34	369	1.40	428	10.0	487	0.0186
252	2.71	311	2.18	370	1.47	429	9.94	488	0.0181
253	2.73	312	2.06	371	1.55	430	10.4	489	0.0170
254	2.76	313	1.97	372	1.64	431	10.5	490	0.0174
255	2.82	314	1.90	373	1.73	432	9.79	491	0.0162
256	2.93	315	1.86	374	1.81	433	10.6	492	0.0161
257	3.06	316	1.86	375	1.90	434	10.5	493	0.0138
258	3.17	317	1.87	376	2.02	435	10.8		

Note:
200-218 nm, Staffelbach et al. [749],
219-235 nm, mean of Meller et al. [518] and Staffelbach et al. [749],
219-493 nm, Meller et al. [518].

D19. $HC(O)OH + h\nu \rightarrow HCO + OH$ (1)
$HC(O)OH + h\nu \rightarrow H + COOH$ (2)
$HC(O)OH + h\nu \rightarrow HCOO + H$ (3)
$HC(O)OH + h\nu \rightarrow H_2 + CO_2$ (4)
$HC(O)OH + h\nu \rightarrow H_2O + CO$ (5)

$(HC(O)OH)_2 + h\nu \rightarrow HCO + OH + HCOOH$ (6)
$(HC(O)OH)_2 + h\nu \rightarrow CO + H_2O + HCOOH$ (7)
$(HC(O)OH)_2 + h\nu \rightarrow H_2 + CO_2 + HCOOH$ (8). The absorption cross sections of formic acid at its dimer have been measured at 300 K and three pressures (35.2, 16.4, and 2.45 Torr) in the region 200-249 nm by McMillan [141]; at 302 K and 29 pressures (0.5-22 Torr) in the region 195–250 nm by Singleton et al. [738]; in connection with quantum yield measurements at 222 nm and 298 K by Jolly et al. [392]; and at 296 and 356.2 K by Singleton et al. [740]. The absorption spectrum of the dimer shows a broad maximum near 205 nm and a monotonic decrease in intensity with increasing wavelength. The absorption maximum of the monomer seems to appear at larger wavelengths near 215 nm and is only one third as intense as that of the dimer. The decrease in cross sections with increasing wavelength is more rapid for the dimer than for the monomer, resulting in monomer values higher by up to a factor 10 at 250 nm. The three absorption curves reported by Mc Millan [141] have been derived assuming monomers only in spite of undefined amounts of monomer and dimer contributions. They lie between those reported by Singleton et al. [738] for the monomer and the dimer. The recommended absorption cross sections are listed in Table 4-51, taken from the data of Singleton et al [738] measured at a resolution of 1 nm.

Earlier studies reported yields of final products CO, CO_2, H_2, H_2O (Calvert and Pitts [147]) and favoured molecular elimination paths (4) and (5) in the range 220-260 nm, which were difficult to distinguish between primary photolytic products and subsequent secondary free-radical reactions, originating from both monomer and dimer. Jolly et al. [392] determined the quantum yield of OH formation via path (3) at 222 nm for the monomer to be $\phi_{3,M} = 1.05 \pm 0.14$ and essentially $\phi_{3,D}$ = zero for the dimer. In a follow-up study Singleton et al. [740] redetermined the OH-quantum yields at 222 nm at two temperatures: $\phi_{3,M}(OH) = 0.704 \pm 0.048$ at 298 K and 0.771 ± 0.030 at 356.2 K for the monomer, and $\phi_{3,D}(OH) = 0.153 \pm 0.028$ at 298 K for the dimer (the OH yield for the dimer at elevated temperatures was assumed to be zero). Photodissociation into the other radical channels (2) and (3) is minor, and has been discussed by He and Fang [322]. Photodissociation quantum yields for the dimer were determined by Singleton et al. [739] to be $\phi_{6,D} = 0.15$, $\phi_{7,D} = 0.81$ an $\phi_{8,D} = 0.04$.

Table 4-51. Absorption Cross Sections of HC(O)OH and $(HC(O)OH)_2$ at 302 K

λ (nm)	10^{20} σ (cm^2) monomer	dimer	λ (nm)	10^{20} σ (cm^2) monomer	dimer
195	9.18	27.4	223	11.9	17.0
196	9.96	29.1	224	11.3	15.5
197	9.57	30.8	225	10.9	14.1
198	10.0	32.2	226	9.87	12.7
199	10.7	33.3	227	10.4	11.3
200	10.7	34.6	228	9.24	10.1
201	11.5	35.4	229	9.15	8.87
202	11.9	36.2	230	8.12	7.78
203	12.5	36.7	231	7.18	6.77
204	12.5	37.3	232	7.07	5.87
205	13.8	37.4	233	6.44	5.01
206	13.6	37.4	234	6.68	4.26
207	13.7	37.2	235	5.24	3.58
208	13.6	36.9	236	5.40	2.95
209	14.1	36.2	237	4.10	2.46
210	14.4	35.5	238	4.32	2.03
211	14.2	34.6	239	3.58	1.63
212	13.6	33.6	240	3.79	1.31
213	14.3	32.4	241	2.79	1.02
214	14.9	31.0	242	2.83	0.795
215	15.0	29.4	243	1.98	0.659
216	13.7	28.1	244	2.10	0.490
217	13.6	26.7	245	1.73	0.337
218	13.4	25.1	246	1.79	0.267
219	13.5	23.4	247	1.18	0.190
220	12.9	21.8	248	1.23	0.134
221	11.6	20.2	249	0.855	0.093
222	12.4	18.6	250	0.861	0.072

Note:
199-250 nm, Singleton et al. [738].

D20. $CH_3C(O)OH + h\nu \rightarrow CH_4 + CO_2$ (1)
$CH_3C(O)OH + h\nu \rightarrow CH_3CO + OH$ (2)
$CH_3C(O)OH + h\nu \rightarrow CH_3 + COOH$ (3)
$CH_3C(O)OH + h\nu \rightarrow CH_3COO + H$ (4). The absorption cross sections of acetic acid at its dimer have been measured at 300 K and four pressures (12.9, 11.0, 8.3, and 3.6 Torr) in the region 200-241 nm by McMillan [146]; at 270 K and pressures of 0.15-1.5 Torr and at 298, 325, and 345 K and pressures of 0.12-3.6 Torr in the region 210-245 nm by Orlando and Tyndall [609]; and in connection with quantum yield measurements at 222 nm and 298 and 356.2 K by Singleton et al. [740]. The monomer spectrum reported by Orlando and Tyndall [609] displays a broad maximum near 207 nm and a monotonic decrease in intensity with increasing wavelength. The absorption maximum for the dimer appears at shorter wavelength below 205 nm and is twice as intense as that of the monomer. The decrease in cross sections with increasing wavelength is more rapid for the dimer than for the monomer, resulting in monomer values higher by up to a factor 6 than the dimer values at 240 nm. The four absorption curves reported by Calvert and Pitts [146] have been derived assuming monomers only in spite of undefined amounts of monomer and dimer contributions. The absorption curve for the highest pressure is close to the dimer curve reported by Orlando and Tyndall [609], and the other curves are shifted to lower absorption cross sections with decreasing temperature, but do not correspond with the monomer curve reported by Orlando and Tyndall [609]. The recommended absorption cross sections are listed in Table 4-52 at 2-nm intervals reported by Orlando and Tyndall [609] (measurements at 0.6-nm resolution).

Earlier studies reported yields of final products CO, CO_2, CH_4, and C_2H_6 (Calvert and Pitts [146]) and proposed molecular elimination path (1) and radical reactions (2) to (4) originating from the monomer. Hunnicutt et al. [354] photolysed acetic acid at 218 nm and determined channel (2) to be the dominant

photochemical path using photofragment laser fluorescence. Singleton et al. [740] determined the OH-quantum yield at 222 nm at two temperatures: $\phi_{2,M}(OH)$ = 0.546 ± 0.097 at 298 K, and 0.692 ± 0.024 at 356.2 K for the monomer, and $\phi_{2,D}(OH)$ = 0.038 ± 0.026 at 298 K for the dimer ($\phi_{2,D}(OH)$ = 0 assumed for the dimer at elevated temperatures).

Table 4-52. Absorption Cross Sections of $CH_3C(O)OH$ and $(CH_3C(O)OH)_2$ at 298 K

λ (nm)	10^{20} σ (cm^2) monomer	dimer	λ (nm)	10^{20} σ (cm^2) monomer	dimer
210	15.1	23.4	228	6.00	3.60
212	14.7	20.9	230	5.09	2.45
214	13.5	18.4	232	4.20	1.71
216	12.5	15.8	234	3.44	1.11
218	11.7	13.2	236	2.71	0.65
220	10.5	10.9	238	2.11	0.45
222	9.33	8.54	240	1.64	0.27
224	8.19	6.68	242	1.19	
226	7.17	4.95	244	0.89	

Note:
210-244 nm, Orlando and Tyndall [609].

D21. $CH_3C(O)OOH + h\nu \rightarrow$ Products. The absorption cross sections of peracetic acid have been measured at 248 and 298 K and 205-340 nm by Orlando and Tyndall [609]. The absorption cross sections decrease in a monotonic, pseudo-exponential fashion with increasing wavelength. The spectrum recorded at 248 K shows an apparently faster fall-off with increasing wavelengths than that recorded at room temperature. In Table 4-53 are listed the data at 2-nm intervals reported by Orlando and Tyndall [609] (measurements at 0.6-nm resolution).

Table 4-53. Absorption Cross Sections $CH_3C(O)OOH$ at 298 K

λ (nm)	10^{20} σ (cm^2)	λ (nm)	10^{20} σ (cm^2)	λ (nm)	10^{20} σ (cm^2)	λ (nm)	10^{20} σ (cm^2)
210	38.1	244	4.31	278	0.574	312	0.045
212	33.1	246	3.82	280	0.506	314	0.044
214	29.5	248	3.41	282	0.444	316	0.040
216	25.4	250	3.05	284	0.386	318	0.035
218	21.7	252	2.71	286	0.334	320	0.025
220	18.9	254	2.42	288	0.297	322	0.020
222	16.0	256	2.16	290	0.256	324	0.020
224	13.9	258	1.93	292	0.226	326	0.017
226	12.0	260	1.71	294	0.193	328	0.014
228	10.5	262	1.53	296	0.170	330	0.009
230	9.10	264	1.35	298	0.141	332	0.011
232	8.01	266	1.21	300	0.123	334	0.011
234	7.03	268	1.06	302	0.107	336	0.009
236	6.31	270	0.945	304	0.094	338	0.009
238	5.61	272	0.835	306	0.078	340	0.006
240	5.03	274	0.742	308	0.069		
242	4.83	276	0.651	310	0.062		

Note:
Orlando and Tyndall [609].

D22. $C_2H_5C(O)OH + h\nu \rightarrow$ Products. Absorption cross sections for propionic acid and its dimer have been measured at 298 and 356.2 K and 222 nm by Singleton et al. [740]. At 298 K, $\sigma = 12.2 \times 10^{-20}$ cm^2 $molecule^{-1}$, and at 356.2 K, $\sigma = 10.6 \times 10^{-20}$ cm^2 $molecule^{-1}$ for the monomer. For the dimer at 298 K, $\sigma = 10.6 \times 10^{-20}$ cm^2 $molecule^{-1}$, and at 356.2 K , $\sigma = 25.6 \times 10^{-20}$ cm^2 $molecule^{-1}$ (obtained by an extrapolation procedure).

Quantum yields for the formation of OH radicals at 222 nm have been also measured by Singleton et al. [740]: For the monomer, $\Phi = 0.148 \pm 0.90$ and 0.341 ± 0.014 for the monomer at 297.6 and 375.0 K, respectively. For the dimer, $\Phi = 0.018 \pm 0.06$ at 297.6 K ($\Phi = 0$ assumed for the dimer at elevated temperatures).

D23. $CH_3C(O)C(O)OH + h\nu \rightarrow CH_3CHO + CO_2$ (1)
$CH_3C(O)C(O)OH + h\nu \rightarrow CH_3CO + COOH$ (2)
$CH_3C(O)C(O)OH + h\nu \rightarrow CH_3COOH + CO$ (3)
$CH_3C(O)C(O)OH + h\nu \rightarrow CH_3CO + CO + OH$ (4). The absorption cross sections of pyruvic acid have been measured at room temperature and at high resolution (diode array spectrometer) between 250 and 410 nm by Horowitz et al. [341] and between 290 and 380 nm by Mellouki and Mu [519]. The absorption spectrum of pyruvic acid, reported as a plot of relative absorbances vs. wavelength, was also measured at 358 K and 250-400 nm by Yamamoto and Back [855]. The value $\sigma = 3.82 \times 10^{-20}$ cm^2 $molecule^{-1}$ for the absorption maximum at 350 nm given by Yamamoto and Back [855] was used by Horowitz et al. [341] to normalize the relative spectrum. The general shapes of the three spectra are quite similar to each other. The spectrum obtained by Yamamoto and Back [855], however, is shifted to the red and the cross sections below 300 nm are considerably higher as compared with the spectrum reported by Horowitz et al. [341], differences which in part can be ascribed to the effect of temperature. The cross sections measured by Mellouki and Mu [519] are systematically higher than those obtained by Horowitz et al. [341]. This difference reaches a factor two for wavelengths below 295 nm and is ~20-30% between 305 and 370 nm. These discrepancies can be attributed to the difficulties in handling the pyruvic acid sample and measurement of the concentrations. The recommended absorption cross sections listed in Table 4-54 are 1-nm averages of the high-resolution data of Horowitz et al. [341] at 252-285 nm, the mean of the data of Horowitz et al. [341] and Mellouki and Mu [519] (both 1-nm averages) at 290-380 nm, and the data of Horowitz et al. [341] at 385-399 nm.

Vesley and Leermakers [816] reported quantum yields of CO_2 of 1.02 ± 0.06 and of CH_3CHO of 0.6 by the photolysis at 366 nm. Yamamoto and Back [855] measured quantum yields of CO_2 of 0.9 ± 0.1 and CH_3CHO of 0.45 at 366 nm and 340 K, but the CH_3CHO yields were more variable at 320 and 345 nm. Berges and Warneck [67] measured the quantum yields for the products CH_3CHO, CO_2 and CH_3COOH in the 350 nm decomposition to be 0.48 ± 0.01, 1.27 ± 0.18 and 0.14, respectively. In the presence of NO_2, the quantum yield of CH_3CHO was reduced to 0.30 ± 0.04 and PAN was formed with a quantum yield of 0.15 ± 0.02. Berges and Warneck [67] established the quantum yields for the photolysis channels: $\phi_1 = 0.48 \pm 0.01$

and $\phi_2 = 0.39 \pm 0.10$. Mellouki and Mu [519] used a laser flash photolysis system at 355 nm to photolyse pyruvic acid, and observed the formation of OH originating via channel (4) with a quantum yield of $\phi_4 = 0.05 \pm 0.03$. Effective quantum yields were obtained in an outdoor photoreactor to be $\phi_{eff} = 0.43 \pm 0.07$ as reported by Moortgat [553]. The analysis of the products CH_3CHO, CO, CH_3COOH by Winterhalter et al. [850] are consistent with the data of Berges and Warneck [67], and lead to a quantum yield of channel (3) $\phi_3 = 0.08 \pm 0.03$.

Table 4-54. Absorption Cross Sections of $CH_3C(O)C(O)OH$ at 298 K

λ (nm)	10^{20} σ (cm^2)	λ (nm)	10^{20} σ (cm^2)	λ (nm)	10^{20} σ (cm^2)	λ (nm)	10^{20} σ (cm^2)	λ (nm)	10^{20} σ (cm^2)
252	1.54	280	0.118	312	1.34	340	3.93	368	3.16
253	1.55	281	0.101	313	1.42	341	3.94	369	3.52
254	1.61	282	0.093	314	1.49	342	4.19	370	3.26
255	1.56	283	0.098	315	1.57	343	4.24	371	2.87
256	1.52	284	0.104	316	1.69	344	4.17	372	2.04
257	1.41	285	0.113	317	1.83	345	4.26	373	1.76
258	1.25	290	0.302	318	1.94	346	4.46	374	1.68
259	1.07	291	0.323	319	2.05	347	4.58	375	1.22
260	0.908	292	0.370	320	2.17	348	4.73	376	1.09
261	0.801	293	0.409	321	2.31	349	4.92	377	0.950
262	0.737	294	0.439	322	2.41	350	4.98	378	0.842
263	0.718	295	0.470	323	2.50	351	4.79	379	0.688
264	0.718	296	0.491	324	2.54	352	4.63	380	0.521
265	0.700	297	0.519	325	2.60	353	4.54	385	0.097
266	0.651	298	0.548	326	2.72	354	4.47	386	0.084
267	0.566	299	0.594	327	2.78	355	4.13	387	0.077
268	0.470	300	0.639	328	2.84	356	3.89	388	0.066
269	0.367	301	0.678	329	2.98	357	3.66	389	0.056
270	0.278	302	0.724	330	3.15	358	3.41	390	0.047
271	0.224	303	0.775	331	3.35	359	3.22	391	0.034
272	0.195	304	0.822	332	3.66	360	3.44	392	0.031
273	0.185	305	0.898	333	3.87	361	3.59	393	0.026
274	0.182	306	0.977	334	3.91	362	3.37	394	0.015
275	0.188	307	1.04	335	3.96	363	3.01	395	0.011
276	0.189	308	1.13	336	4.02	364	2.85	396	0.006
277	0.180	309	1.21	337	4.02	365	2.86	397	0.002
278	0.164	310	1.22	338	3.99	366	2.80	398	0.002
279	0.139	311	1.27	339	3.956	367	2.88	399	<0.001

Note:
252-285 nm, Horowitz et al. [341],
290-380 nm, mean of the data of Horowitz et al. [341] and Mellouki and Mu [519],
385-399 nm, Horowitz et al. [341].

D24. $HC(O)OCH_3 + h\nu \rightarrow$ Products. The absorption cross sections of methyl formate have been measured at room temperature and 201-260 nm by McMillan [142] and at 211-260 nm by Vésine and Mellouki [815]. The spectrum exhibits a structured absorption band with the maximum near 215 nm. There is very good agreement, i.e., ≤ 10%, between the results of both studies. As a recommendation we list in Table 4-55 the data of McMillan [142] at 202-210 nm (read from a plot) and the data of Vésine and Mellouki [815] at 211-260 nm, which are averages over 1- and 2-nm intervals in the ranges 211-230 and 230-260 nm, respectively, of the high-resolution (0.04 nm) spectrum.

Table 4-55. Absorption Cross Sections of $HC(O)OCH_3$ at 297-298 K

λ (nm)	10^{20} σ (cm^2)	λ (nm)	10^{20} σ (cm^2)	λ (nm)	10^{20} σ (cm^2)	λ (nm)	10^{20} σ (cm^2)
202	16.2	213	20.3	224	16.8	240	3.56
203	17.0	214	21.2	225	15.7	242	2.65
204	17.9	215	21.1	226	14.0	244	1.65
205	18.2	216	20.3	227	12.5	246	1.24
206	18.7	217	19.3	228	12.4	248	0.770
207	18.9	218	19.7	229	12.3	250	0.480
208	19.1	219	20.0	230	11.3	252	0.301
209	19.5	220	19.2	232	8.36	254	0.162
210	20.4	221	17.9	234	7.48	256	0.0717
211	20.4	222	16.7	236	6.11	258	0.0455
212	20.1	223	16.6	238	4.15	260	0.0281

Note:
202-210 nm, McMillan [142],
211-260 nm, Vésine and Mellouki [815].

D25. $HC(O)OC_2H_5 + h\nu \rightarrow$ Products. The absorption cross sections of ethyl formate have been measured at room temperature and 201-260 nm by McMillan [142] and at 211-260 nm by Vésine and Mellouki [815]. The spectrum exhibits a structured absorption band with the maximum near 215 nm. The agreement between the data of both studies is within ~15%, where the data of Vésine and Mellouki [815] are always lower than the data of McMillan [142] in the range 211-236 nm. An explanation for the discrepancy could not be found by Vésine and Mellouki [815]. As a recommendation we list in Table 4-56 the data of Vésine and Mellouki [815] at 211-260 nm, which are averages over 1- and 2-nm intervals in the ranges 211-230 and 230-260 nm, respectively, of the high-resolution (0.04 nm) spectrum.

Table 4-56. Absorption Cross Sections of $HC(O)OC_2H_5$ at 297 K

λ (nm)	10^{20} σ (cm^2)	λ (nm)	10^{20} σ (cm^2)	λ (nm)	10^{20} σ (cm^2)	λ (nm)	10^{20} σ (cm^2)
211	18.6	220	17.8	229	11.2	246	1.47
212	18.6	221	17.1	230	11.0	248	1.04
213	18.3	222	15.9	232	9.03	250	0.665
214	18.5	223	15.1	234	7.21	252	0.405
215	19.0	224	15.0	236	6.50	254	0.251
216	18.9	225	14.9	238	4.96	256	0.119
217	18.1	226	14.0	240	3.67	258	0.0611
218	17.5	227	12.6	242	3.00	260	0.0391
219	17.6	228	11.5	244	2.18		

Note:
211-260 nm, Vésine and Mellouki [815].

D26. $HCN + h\nu \rightarrow$ Products. Herzberg and Innes [329] have studied the spectroscopy of hydrogen cyanide, HCN, that starts absorbing weakly at $\lambda < 190$ nm.

The solar photodissociation rate for this molecule is rather small, even in the upper stratosphere; estimates of this rate would require additional studies of the absorption cross sections and quantum yields in the 200-nm region.

D27. $CH_3CN + h\nu \rightarrow$ Products. McElcheran et al. [506] have reported the spectrum of acetonitrile or methyl cyanide, CH_3CN; the first absorption band appears at $\lambda < 220$ nm. More recently, Suto and Lee [759] and Zetzsch [876] have measured the cross sections around 200 nm; solar photodissociation is unimportant compared to reaction with OH radicals.

PHOTOCHEM-E

E1. $FO_2 + h\nu \rightarrow F + O_2$. After two earlier studies with FO_2 in liquid argon at 87 K by Chegodaev and Tupikov [158] and Matchuk et al. [494], the absorption spectrum of the fluoroperoxy radical in the gas phase has been measured at room temperature and 206-250 nm by Pagsberg et al. [620]; at 186–276 nm by Maricq and Szente [481]; at 215-254 nm by Ellermann et al. [228]; and a single value for $\lambda = 215$ nm has been reported by Lyman and Holland [463]. The results of Maricq and Szente [481], Ellermann et al. [228], and Lyman and Holland [463] are in excellent agreement, whereas the cross sections reported by Pagsberg et al. [620] are

larger by a factor of 1.4-1.8 between 206 and 245 nm, and larger by a factor 3 at 250 nm. As a recommendation we list the absorption cross sections reported by Maricq and Szente [481] in Table 4-57.

Table 4-57. Absorption Cross Sections of FO_2 at 295 K

λ (nm)	10^{20} σ (cm^2)	λ (nm)	10^{20} σ (cm^2)	λ (nm)	10^{20} σ (cm^2)
185.9	950	214.2	1150	242.5	139
188.5	1050	216.8	1050	245.1	112
191.1	1130	219.4	933.	247.6	82
193.6	1180	221.9	796	250.2	60
196.2	1200	224.5	677	252.8	51
198.8	1260	227.1	558	255.3	43
201.4	1310	229.6	451	257.9	36
203.9	1330	232.2	368	260.5	32
206.5	1350	234.8	289	263.1	26
209.1	1300	237.4	233	265.6	20
211.6	1240	239.9	173		

Note: 185.9-265.6 nm, Maricq and Szente [481].

E2. $F_2O + h\nu \rightarrow F_2 + O$

$F_2O + h\nu \rightarrow F + FO$. The absorption spectrum of fluorine oxide has been measured at 273 K and 210-546 nm by Glissmann and Schuhmacher [286]. Their data are listed in Table 4-58.

Table 4-58. Absorption Cross Sections of F_2O at 273 K

λ (nm)	10^{20} σ (cm^2)	λ (nm)	10^{20} σ (cm^2)	λ (nm)	10^{20} σ (cm^2)	λ (nm)	10^{20} σ (cm^2)
210.2	4.88	239.9	0.65	296.7	0.12	404.0	0.020
211.4	3.39	244.7	0.50	302.7	0.12	421.0	0.023
213.7	3.06	248.2	0.37	313.1	0.11	428.0	0.021
216.5	2.73	253.7	0.27	334.0	0.087	435.8	0.018
218.1	2.60	257.6	0.21	350.0	0.072	445.0	0.017
221.0	2.21	265.5	0.15	365.0	0.064	458.0	0.015
223.6	1.95	270.0	0.13	378.0	0.055	471.5	0.012
225.3	1.76	275.9	0.12	380.0	0.044	491.6	0.0091
229.5	1.30	280.6	0.12	387.0	0.033	513.5	0.0052
234.5	1.14	289.3	0.12	395.0	0.023	546.0	0.0052
237.8	0.78	292.5	0.12	399.0	0.020		

Note:
210-546 nm, Glissmamm and Schuhmacher [286].

E3. $F_2O_2 + h\nu \rightarrow$ Products. The absorption cross sections of dioxygen difluoride in the gas phase have been measured at 273 K and 220-522.5 nm by Brodersen et al. [99], 193 K and 197-260 nm by Chegodaev and Tupikov [158], at 195 K and 350-600 nm by Matchuk et al. [494], and at 298 K and 215 nm by Lyman and Holland [463]. A measurement with liquid F_2O_2 in liquid freon at 77 K and 200-480 nm has been reported by Kirshenbaum and Streng [410]. The absorption spectrum shows the long-wavelength wing of an absorption band, whose maximum is somewhere below 200 nm, and a weak shoulder at ~250-300 nm. A hump around 405 nm observed by Brodersen et al. [99] did not appear in the spectra reported by Matchuk et al. [494] and Kirshenbaum and Streng [410]. There is good agreement at 220-250 nm (within 10-15%) between the data of Brodersen et al. [99] and Chegodaev and Tupikov [158]. The 250-360-nm region of the absorption curve reported by Brodersen et al. [99] connects well the absorptions curves reported by Chegodaev and Tupikov [158] and Matchuk et al. [494]. We therefore list as recommended values in Table 4-59 the results of Chegodaev and Tupikov [158] at 200-250 nm, those of Brodersen et al. [99] at 260-360 nm, and the data of Matchuk et al. [494] for the 370-600 nm region.

Table 4-59. Absorption Cross Sections of F_2O_2 at 193-195 and 273 K

λ (nm)	10^{20} σ (cm^2)	λ (nm)	10^{20} σ (cm^2)	λ (nm)	10^{20} σ (cm^2)
200	700	340	10.9	480	0.34
210	325	350	7.54	490	0.27
220	208	360	5.90	500	0.24
230	145	370	5.15	510	0.22
240	107	380	4.50	520	0.20
250	87.9	390	3.77	530	0.19
260	98.2	400	3.06	540	0.17
270	86.7	410	2.46	550	0.15
280	72.5	420	1.97	560	0.13
290	60.6	430	1.57	570	0.11
300	44.7	440	1.25	580	0.09
310	32.4	450	0.96	590	0.07
320	22.3	460	0.69	600	0.04
330	15.4	470	0.47		

Note:
200-250 nm (193 K), Chegodaev and Tupikov [158],
260-360 nm (273 K), Brodersen et al. [99],
370-600 nm (195 K), Matchuk et al. [494].

E4. $HF + h\nu \rightarrow H + F$. The ultraviolet absorption spectrum of HF has been measured at 289.5, 326, 373, and 438 K and 153-182 nm by Safary et al. [696] and Safary [695]; at room temperature and 107-145 nm by Nee et al. [575]; and, applying electron energy-loss spectroscopy, at 298 K and 8-155 nm by Carnovale et al. [153], and 30-200 nm by Hitchcock et al. [333]. There is no absorption at $\lambda > 180$ nm, so that photodissociation of HF should be unimportant in the stratosphere.

E5. $FNO + h\nu \rightarrow F + NO$. The absorption cross sections of nitrosyl fluoride have been measured at room temperature and 180-350 nm by Burley et al. [121], who report their results in graphical form as well as in tabular form at 1-nm intervals. The spectrum shows vibronic structure at wavelengths longer than 250 nm. The cross section values are listed in Table 4-60 at 2-nm intervals for the continuous part of the absorption curve and at 1-nm intervals for the structured part ($\lambda > 260$ nm). Two single values at 310.5 nm (strongest vibrational peak) and 195 K measured by Johnston and Bertin [383] and at 298 K measured by Pagsberg et al. [619] fit well to the absorption curve reported by Burley et al. [121]. The quantum yield for decomposition is expected to be unity (Brandon et al. [85], Reid et al. [670]).

Table 4-60. Absorption Cross Sections of FNO at 298 K

λ (nm)	10^{20} σ (cm^2)	λ (nm)	10^{20} σ (cm^2)	λ (nm)	10^{20} σ (cm^2)	λ (nm)	10^{20} σ (cm^2)
180	52.4	246	1.65	286	5.17	319	21.4
182	51.7	248	1.41	287	5.78	320	15.2
184	50.7	250	1.54	288	10.4	321	35.6
186	49.4	252	1.25	289	16.6	322	40.2
188	47.5	254	1.23	290	17.0	323	25.5
190	45.1	256	1.36	291	11.3	324	17.8
192	42.7	258	1.58	292	11.9	325	14.3
194	40.0	260	1.30	293	18.1	326	12.1
196	37.3	261	1.45	294	7.11	327	9.40
198	33.8	262	1.64	295	6.75	328	9.39
200	30.5	263	1.85	296	9.15	329	12.4
202	27.7	264	2.03	297	14.1	330	12.9
204	24.8	265	2.67	298	22.0	331	11.3
206	22.2	266	1.96	299	23.1	332	13.0
208	19.9	267	1.99	300	15.6	333	18.9
210	17.6	268	2.10	301	23.1	334	19.3
212	15.8	269	2.66	302	25.4	335	16.1
214	13.9	270	2.81	303	10.4	336	13.1
216	12.3	271	3.06	304	8.85	337	10.8
218	10.7	272	4.47	305	10.4	338	8.96
220	9.35	273	4.30	306	11.8	339	7.13
222	8.32	274	3.97	307	15.6	340	5.65
224	7.22	275	3.77	308	32.2	341	4.61
226	6.30	276	4.24	309	21.8	342	3.81
228	5.44	277	4.44	310	15.5	343	3.17
230	4.68	278	3.41	311	54.2	344	2.68
232	4.10	279	5.03	312	31.6	345	2.30
234	3.52	280	8.26	313	16.0	346	1.96
236	3.09	281	10.1	314	12.3	347	1.72
238	2.76	282	7.58	315	11.7	348	1.48
240	2.25	283	6.59	316	11.0	349	1.30
242	2.08	284	7.26	317	13.0	350	1.18
244	1.74	285	7.45	318	25.5		

Note:
180-350 nm, Burley et al. [121]

E6. $CF_4 + h\nu \rightarrow$ products. See note E7.

E7. $C_2F_6 + h\nu \rightarrow$ products. CF_4 and C_2F_6 do not absorb in the ultraviolet at wavelengths longer than 105 and 120 nm, respectively (Sauvageau et al. [707, 708]; Inn, [364]); therefore, they are not expected to photodissociate until they reach the mesosphere.

E8. $COF_2 + h\nu \rightarrow COF + F$. The absorption cross-sections of COF_2 (carbonyl difluoride, difluorophosgene) have been measured at room temperature and 185-226 nm by Chou et al. [170]; at 186-224 nm by Molina and Molina [540]; and at 199-232 nm by Nölle et al. [590]. This wavelength region covers the long-wavelength wing of an absorption band. The high-resolution spectrum reported by Nölle et al. [590] is highly structured. Comparison of values averaged over the 500-cm^{-1} intervals used for atmospheric modeling shows that the data of Nölle et al. [590] are somewhat higher than those of Molina and Molina [540] with differences between 1.5 and 22%. The data of Chou et al. [170] are in good agreement with the data of Molina and Molina [540] at 186-197 nm, but disagreement becomes steadily larger with increasing wavelength by up to more than 200%. We follow our earlier recommendation of 1997 and list in Table 4-61 the 500-cm^{-1} averages of Molina and Molina [540] for the range 186-199 nm and those of Nölle et al. [590] at larger wavelengths.

The COF + F quantum yields were determined at 193 nm using an excimer laser, and at 210 and 220 nm using a Hg medium pressure lamp by Nölle et al. [591]. The "apparent" quantum yields for pure COF_2, $\Phi' = 0.47 \pm 0.03$, 0.57 ± 0.05, and 0.11 ± 0.02 were obtained at 193, 210 and 220 nm, respectively. In the case of

the laser photolysis at 193 nm, where high concentrations of COF are formed, the self-reaction of the COF photodissociation product regenerates COF_2 via COF + COF → COF_2 + CO. Under the assumption that all COF radicals quantitatively react in this way, hence the quantum yield becomes $\Phi_{193} = 0.94 \pm 0.06$. The quantum yields at 210 and 220 nm obtained with the lamp are the "true" values. A quantum yield of 0.26 at 206 nm reported by Molina and Molina [540] is considered to be too low by Nölle et al. [591].

Table 4-61. Absorption Cross Sections of COF_2 at 298 K

λ (nm)	10^{20} σ (cm^2)	λ (nm)	10^{20} σ (cm^2)	λ (nm)	10^{20} σ (cm^2)
186.0	5.5	199.0	1.6	213.9	0.188
187.8	4.8	201.0	1.32	216.2	0.120
189.6	4.2	203.1	0.987	218.6	0.077
191.4	3.7	205.1	0.754	221.0	0.046
193.2	3.1	207.3	0.508	223.5	0.032
195.1	2.6	209.4	0.392	226.0	0.021
197.0	2.1	211.6	0.272	228.6	0.015

Note:
186-199 nm, Molina and Molina [540],
201-229 nm, Nölle et al. [590].

E9. COHF + hν → HF + CO
COHF + hν → H + FCO
COHF + hν → F + HCO. The absorption spectrum of COHF (formyl fluoride) has been measured at room temperature and 195-255 nm by Giddings and Innes [268]; at 194-267 nm by Meller (see Röth et al. [687]); and at 220-267 nm by Rattigan et al. [653]. The latter authors found the absorption cross-sections to be independent of temperature in the range 233-318 K. The high-resolution measurements show the long-wavelength wing of a highly structured absorption band. The absorption cross-sections measured using conventional methods by Giddings and Innes [268] are larger by nearly a factor two than the high-resolution (0.016 nm) data obtained by Meller (see Röth et al. [687]) using diode array spectrometry. The cross-sections measured by Rattigan et al. [653] at a resolution of 1.2 nm lie between the latter two data sets in the range 220-230 nm and nearer to the data of Giddings and Innes [268] at 230-245 nm. In Table 4-62 we recommend the averages over 1-nm intervals of the high-resolution data of Meller (see Röth et al. [687]).

Table 4-62. Absorption Cross Sections of COHF at 298 K

λ (nm)	10^{20} σ (cm^2)	λ (nm)	10^{20} σ (cm^2)	λ (nm)	10^{20} σ (cm^2)	λ (nm)	10^{20} σ (cm^2)
200	8.28	217	7.38	234	2.98	251	0.151
201	9.75	218	7.97	235	2.04	252	0.241
202	8.30	219	6.28	236	2.28	253	0.213
203	7.55	220	6.85	237	1.24	254	0.071
204	8.52	221	5.70	238	1.71	255	0.123
205	10.15	222	6.07	239	1.75	256	0.0674
206	8.28	223	6.58	240	1.55	257	0.0520
207	7.41	224	4.94	241	0.967	258	0.0382
208	8.44	225	5.33	242	1.19	259	0.0446
209	9.55	226	4.00	243	0.575	260	0.0427
210	7.76	227	4.65	244	0.765	261	0.0232
211	7.36	228	4.43	245	0.675	262	0.0153
212	7.92	229	4.61	246	0.719	263	0.0156
213	8.56	230	3.57	247	0.412	264	0.0170
214	9.22	231	2.55	248	0.484	265	0.0126
215	7.67	232	3.16	249	0.279	266	0.0118
216	6.51	233	3.09	250	0.210		

Note:
200-266 nm, Meller (see Röth et al. [687]).

E10. CF3OH + hν → Products. An upper limit of 10^{-21} cm^2 has been determined experimentally by Molina and Molina [544] for the absorption cross sections of CF_3OH in the 185–300-nm wavelength range. This upper

limit is in agreement with estimates based on similarities between CF_3OH and CH_3OH, as well as with quantum chemistry calculations, as reported by Schneider et al. [715].

E11. $CF_3OOCF_3 + h\nu \rightarrow 2\ CF_3O$. The absorption spectrum of hexafluorodimethyl peroxide has been measured at room temperature and 200-263 nm by Meller and Moortgat [515]. The spectrum shows a part of a broad absorption band originating near 265 nm and increasing cross sections with decreasing wavelengths. Absorption cross sections averaged over 1-nm intervals of the medium-resolution (0.2 nm) results of Meller and Moortgat [515] are listed in Table 4-63.

Table 4-63. Absorption Cross Sections CF_3OOCF_3 at 298 K.

λ (nm)	$10^{20}\ \sigma$ (cm^2)	λ (nm)	$10^{20}\ \sigma$ (cm^2)	λ (nm)	$10^{20}\ \sigma$ (cm^2)	λ (nm)	$10^{20}\ \sigma$ (cm^2)
200	3.61	216	1.25	232	0.501	248	0.204
201	3.37	217	1.18	233	0.462	249	0.195
202	3.13	218	1.10	234	0.433	250	0.183
203	2.92	219	1.04	235	0.408	251	0.174
204	2.73	220	0.983	236	0.380	252	0.166
205	2.53	221	0.926	237	0.361	253	0.157
206	2.35	222	0.869	238	0.339	254	0.147
207	2.20	223	0.822	239	0.323	255	0.138
208	2.06	224	0.778	240	0.303	256	0.132
209	1.94	225	0.737	241	0.288	257	0.125
210	1.80	226	0.693	242	0.274	258	0.119
211	1.69	227	0.654	243	0.263	259	0.112
212	1.61	228	0.614	244	0.246	260	0.107
213	1.51	229	0.584	245	0.240	261	0.101
214	1.42	230	0.555	246	0.227	262	0.096
215	1.33	231	0.525	247	0.214	263	0.091

Note:
200-263 nm, Meller and Moortgat [515].

E12. $CF_3O_3CF_3 + h\nu \rightarrow$ Products. The absorption spectrum of hexafluorodimethyl trioxide has been measured at room temperature and 200-312 nm by Meller and Moortgat [515]. The spectrum shows a part of a broad absorption band originating near 312 nm and increasing cross sections with decreasing wavelengths. Absorption cross sections averaged over 1-nm intervals of the medium-resolution (0.2 nm) results of Meller and Moortgat [515] are listed in Table 4-64.

Table 4-64. Absorption Cross Sections $CF_3O_3CF_3$ at 298 K.

λ (nm)	10^{20} σ (cm^2)	λ (nm)	10^{20} σ (cm^2)	λ (nm)	10^{20} σ (cm^2)	λ (nm)	10^{20} σ (cm^2)
200	46.9	229	20.3	258	4.26	287	0.565
201	45.5	230	19.5	259	3.99	288	0.526
202	44.2	231	18.8	260	3.73	289	0.491
203	42.8	232	18.0	261	3.51	290	0.458
204	41.4	233	17.2	262	3.28	291	0.427
205	40.2	234	16.5	263	3.07	292	0.400
206	39.0	235	15.7	264	2.86	293	0.373
207	37.9	236	15.0	265	2.67	294	0.347
208	37.0	237	14.3	266	2.50	295	0.325
209	36.1	238	13.7	267	2.33	296	0.302
210	35.2	239	13.0	268	2.17	297	0.281
211	34.4	240	12.3	269	2.03	298	0.262
212	33.6	241	11.7	270	1.89	299	0.244
213	32.8	242	11.1	271	1.76	300	0.228
214	32.1	243	10.5	272	1.64	301	0.213
215	31.3	244	10.0	273	1.53	302	0.197
216	30.5	245	9.46	274	1.43	303	0.185
217	29.8	246	8.95	275	1.33	304	0.174
218	29.0	247	8.45	276	1.24	305	0.164
219	28.2	248	7.95	277	1.15	306	0.154
220	27.4	249	7.48	278	1.07	307	0.143
221	26.7	250	7.04	279	0.999	308	0.133
222	25.9	251	6.64	280	0.929	309	0.122
223	25.1	252	6.25	281	0.860	310	0.112
224	24.3	253	5.87	282	0.800	311	0.106
225	23.5	254	5.52	283	0.748	312	0.096
226	22.7	255	5.18	284	0.699		
227	21.9	256	4.86	285	0.653		
228	21.1	257	4.56	286	0.608		

Note:
200-312 nm, Meller and Moortgat [515].

E13. $CF_3CHO + h\nu \rightarrow$ Products. The absorption cross sections of CF_3CHO (trifluoroacetaldehyde) have been measured at room temperature and at 118-182 and 250-357 nm by Lucazeau and Sandorfy [462]; at 229-364 nm by Meller et al. [514]; at 230-400 nm by Francisco and Williams [249]; and at 200-400 nm by Sellev g et al. [721]. The absorption spectrum exhibits an absorption band in the near UV between 227 and ~360 nm, which is slightly structured at wavelength above 250 nm and has the maximum at 301 nm. The absorption cross sections reported by Francisco and Williams [249], Meller et al. [514], and Sellev g et al. [721] are in good agreement, generally 10% and better, in the wavelength region between 245 and 354 nm, where the data of Sellev g et al. [721] generally are the largest, those of Francisco and Williams [249] the smallest. Large discrepancies appear in the long and short wavelength wings of the absorption band, where the cross sections of Sellev g et al. [721] are smaller than those of Francisco and Williams [249] and larger than those of Meller et al. [514]. The data of Lucazeau and Sandorfy [462], which are given as a plot only, are appreciably smaller than those reported by the other three teams, in the maximum even lower by ~30%. As a recommendation are listed in Table 4-65 the data of Sellev g et al. [721] for the range 210-360 nm recorded at 1-nm intervals.

Effective quantum yields were obtained in an outdoor photoreactor to be $\Phi_{eff} < 0.02$ as reported by Sellev g et al. [721].

Table 4-65. Absorption Cross Sections of CF_3CHO at 298 K

λ (nm)	10^{20} σ (cm^2)	λ (nm)	10^{20} σ (cm^2)	λ (nm)	10^{20} σ (cm^2)	λ (nm)	10^{20} σ (cm^2)
210	0.197	248	0.311	286	2.63	324	2.06
211	0.192	249	0.339	287	2.67	325	1.90
212	0.179	250	0.369	288	2.73	326	1.72
213	0.172	251	0.400	289	2.79	327	1.64
214	0.159	252	0.433	290	2.86	328	1.62
215	0.152	253	0.472	291	2.92	329	1.55
216	0.140	254	0.511	292	2.94	330	1.44
217	0.132	255	0.548	293	3.00	331	1.35
218	0.121	256	0.591	294	3.05	332	1.26
219	0.113	257	0.638	295	3.06	333	1.18
220	0.105	258	0.686	296	3.08	334	1.13
221	0.098	259	0.737	297	3.08	335	1.06
222	0.090	260	0.789	298	3.10	336	1.01
223	0.084	261	0.840	299	3.14	337	0.993
224	0.080	262	0.896	300	3.17	338	0.891
225	0.076	263	0.954	301	3.20	339	0.730
226	0.074	264	1.02	302	3.15	340	0.622
227	0.073	265	1.09	303	3.12	341	0.585
228	0.075	266	1.15	304	3.15	342	0.569
229	0.075	267	1.22	305	3.13	343	0.531
230	0.078	268	1.29	306	3.07	344	0.471
231	0.081	269	1.35	307	3.03	345	0.425
232	0.086	270	1.42	308	2.97	346	0.385
233	0.091	271	1.50	309	2.95	347	0.337
234	0.097	272	1.58	310	2.92	348	0.310
235	0.104	273	1.66	311	2.92	349	0.286
236	0.112	274	1.74	312	2.91	350	0.246
237	0.121	275	1.82	313	2.78	351	0.235
238	0.131	276	1.89	314	2.67	352	0.232
239	0.142	277	1.96	315	2.65	353	0.162
240	0.155	278	2.03	316	2.62	354	0.096
241	0.169	279	2.11	317	2.52	355	0.071
242	0.184	280	2.19	318	2.42	356	0.058
243	0.201	281	2.28	319	2.33	357	0.050
244	0.220	282	2.35	320	2.25	358	0.044
245	0.240	283	2.42	321	2.19	359	0.042
246	0.262	284	2.50	322	2.13	360	0.038
247	0.285	285	2.57	323	2.08		

Note:
210-360 nm, Sellev g et al. [721].

E14. $CF_3C(O)F + h\nu \rightarrow$ Products. The absorption spectrum of $CF_3C(O)F$ (trifluoroacetyl fluoride) has been measured at room temperature and 200-281 nm by Meller [513] and 200-295 nm by Rattigan et al. [656]. These two studies are in agreement concerning the peak cross sections in this spectral region. However, the position of the absorption maximum observed by Rattigan et al. [656] is shifted by ~3 nm to longer wavelengths as compared to that observed by Meller [513]. The cross-sections agree within 0-13% up to 260 nm and then differ by 20-30% in the wing of the absorption band. As a recommendation we list in Table 4-66 the mean of the data (5-nm averages of high-resolution results) reported by Meller [513] and Rattigan et al. [656] at 200-275 nm and the value of Rattigan et al. [656] at 280 nm.

Table 4-66. Absorption Cross Sections of $CF_3C(O)F$ at 298 K

λ (nm)	10^{20} σ (cm^2)	λ (nm)	10^{20} σ (cm^2)	λ (nm)	10^{20} σ (cm^2)	λ (nm)	10^{20} σ (cm^2)
200	10.1	225	11.1	250	1.12	275	0.0036
205	12.2	230	8.67	255	0.492	280	0.0010
210	13.5	235	6.17	260	0.185		
215	13.8	240	3.93	265	0.0526		
220	12.9	245	2.21	270	0.0122		

Note:
200-275 nm, mean of Meller [513] and Rattigan et al. [656],
280 nm, Rattigan et al. [656]

E15. $CF_3C(O)Cl + h\nu \rightarrow$ Products. The absorption cross sections of $CF_3C(O)Cl$ (trifluoroacetyl chloride) have been measured at room temperature and 190-342 nm by Maricq and Szente [483]; at 233, 253 and 296 K and 220-330 nm by Rattigan et al. [656]; and at 223, 248, 273, and 298 K and 200-329 nm by Meller and Moortgat [516]. An absorption band was observed between 215 and 330 nm with the maximum around 254-255 nm and a strong increase of the absorption cross sections between 215 and 190 nm. The room temperature data of Rattigan et al. [656] and Meller and Moortgat [516] are in excellent agreement around the absorption maximum; the agreement is better than 5% between 240 and 315 nm. The data of Rattigan et al. [656] are smaller by nearly 70% than the data of Meller and Moortgat [516] around the absorption minimum at 215 nm, and become progressively smaller by up to 33% in the wing of the absorption band above 320 nm. Maricq and Szente [483] report an absorption maximum of 6.6×10^{-20} cm^2 $molecule^{-1}$ at ~255 nm compared to 6.8×10^{-20} cm^2 $molecule^{-1}$ and 6.7×10^{-20} cm^2 $molecule^{-1}$ observed by Rattigan et al. [656] and Meller and Moortgat [516], respectively. As a recommendation we list in Table 4-67 the mean of the data (5-nm averages of high-resolution results) reported by Rattigan et al. [656] and Meller and Moortgat [516] for the region 205-325 nm.

Both temperature studies show a decrease of the absorption cross sections with decreasing temperature from room temperature to 223 or 233 K in the wavelength regions below ~215 nm and above 255 nm. For the region between 215 and 255 nm, a very slight decrease of the absorption cross sections with decreasing temperature was observed by Rattigan et al. [656], whereas Meller and Moortgat [516] report nearly equal values for temperatures of 223–298 K and sometimes a slight increase of the cross sections between 248 and 223 K.

Table 4-67. Absorption Cross Sections of $CF_3C(O)Cl$ at 296-298 K

λ (nm)	10^{20} σ (cm^2)	λ (nm)	10^{20} σ (cm^2)	λ (nm)	10^{20} σ (cm^2)	λ (nm)	10^{20} σ (cm^2)
205	14.1	240	5.16	275	4.12	310	0.0756
215	1.38	250	6.57	285	2.12	320	0.00756
220	1.48	255	6.75	290	1.36	325	0.00233
225	2.10	260	6.55	295	0.794		
230	3.13	265	5.94	300	0.416		
235	4.17	270	5.08	305	0.194		

Note:
205-325 nm, mean of Rattigan et al. [656] and Meller and Moortgat [516].

E16. $CF_3C(O)O_2NO_2 + h\nu \rightarrow CF_3C(O)O_2 + NO_2$ φ_1
$CF_3C(O)O_2NO_2 + h\nu \rightarrow CF_3C(O)O + NO_3$ φ_2. The absorption cross sections of $CF_3C(O)O_2NO_2$ (trifluoroperoxyacetyl nitrate, FPAN) have been measured at room temperature and 227-305 nm by Libuda and Zabel [446]. Values averaged over 5-nm intervals of their medium-resolution (0.6 nm) data, which were reported with uncertainties of about 10% below 290 nm and of 15-45% at 295-305 nm, are listed in Table 4-68.

Table 4-68. Absorption Cross Sections of $CF_3(O)O_2NO_2$ at 298 K

λ (nm)	10^{20} σ (cm^2)	λ (nm)	10^{20} σ (cm^2)	λ (nm)	10^{20} σ (cm^2)
230	70.0	260	11.8	290	0.87
240	44.9	270	5.46	300	0.33
245	32.5	275	3.56	305	0.20
250	23.9	280	2.21		
255	17.0	285	1.40		

Note:
230-305 nm, Libuda and Zabel [446].

E17. $CF_3CH_2CHO + h\nu \rightarrow$ Products. The absorption spectrum of CF_3CH_2CHO (3,3,3-trifluoropropionaldehyde) has been measured at room temperature and 200-400 nm by Sellev g et al. [721]. The spectrum exhibits a slightly structured absorption band between 220 and 343 nm (the data reported for the wavelength region above 343 nm show large noise effects). The recommendation is taken from these results. In Table 4-69 the results of Sellev g et al. [721] are given for the wavelength region 200-343 nm.

Effective quantum yields were obtained in an outdoor photoreactor to be $\Phi_{eff} < 0.04$ as reported by Sellev g et al. [721].

Table 4-69. Absorption Cross Sections of CF_3CH_2CHO at 298 K

λ (nm)	10^{20} σ (cm^2)	λ (nm)	10^{20} σ (cm^2)	λ (nm)	10^{20} σ (cm^2)	λ (nm)	10^{20} σ (cm^2)
200	0.939	236	0.309	272	2.43	308	3.04
201	0.825	237	0.324	273	2.58	309	3.07
202	0.732	238	0.344	274	2.72	310	3.13
203	0.668	239	0.362	275	2.83	311	3.15
204	0.611	240	0.377	276	2.89	312	3.04
205	0.542	241	0.395	277	2.92	313	2.83
206	0.483	242	0.422	278	2.94	314	2.56
207	0.432	243	0.443	279	2.98	315	2.30
208	0.397	244	0.474	280	3.07	316	2.11
209	0.367	245	0.513	281	3.22	317	1.97
210	0.334	246	0.552	282	3.37	318	1.93
211	0.311	247	0.593	283	3.49	319	1.93
212	0.309	248	0.629	284	3.55	320	1.92
213	0.298	249	0.671	285	3.54	321	1.95
214	0.285	250	0.728	286	3.53	322	1.97
215	0.273	251	0.788	287	3.51	323	1.93
216	0.267	252	0.842	288	3.51	324	1.79
217	0.266	253	0.904	289	3.59	325	1.59
218	0.263	254	0.963	290	3.69	326	1.32
219	0.263	255	1.01	291	3.80	327	1.09
220	0.270	256	1.08	292	3.85	328	0.938
221	0.266	257	1.15	293	3.81	329	0.818
222	0.265	258	1.25	294	3.76	330	0.757
223	0.266	259	1.34	295	3.72	331	0.740
224	0.256	260	1.40	296	3.65	332	0.742
225	0.270	261	1.48	297	3.62	333	0.718
226	0.268	262	1.53	298	3.61	334	0.717
227	0.270	263	1.61	299	3.67	335	0.706
228	0.269	264	1.71	300	3.75	336	0.673
229	0.273	265	1.84	301	3.76	337	0.607
230	0.272	266	1.96	302	3.67	338	0.506
231	0.281	267	2.06	303	3.53	339	0.390
232	0.288	268	2.13	304	3.37	340	0.277
233	0.298	269	2.17	305	3.21	341	0.206
234	0.300	270	2.22	306	3.11	342	0.138
235	0.307	271	2.30	307	3.06	343	0.103

Note:
200-343 nm, Sellev g et al. [721].

E18. $CF_3C(O)OH + h\nu \rightarrow$ Products. The absorption cross sections of $CF_3C(O)OH$ (trifluoroacetic acid) have been measured at room temperature and 200-280 nm by Rattigan et al. [656]. The spectrum exhibits a single absorption band with a broad maximum near 215 nm, extending out to approximately 275 nm. In Table 4-70 are listed the averages over 5-nm intervals of the spectrum recorded at a resolution of 1.2 nm (diode-array spectrometer) by Rattigan et al. [656].

Table 4-70. Absorption Cross Sections of $CF_3C(O)OH$ at 296 K

λ (nm)	$10^{20}\ \sigma$ (cm^2)	λ (nm)	$10^{20}\ \sigma$ (cm^2)
200	5.20	245	1.69
205	6.48	250	0.870
210	7.23	255	0.390
215	7.59	260	0.155
220	7.76	265	0.050
225	7.21	270	0.013
230	6.03	275	0.006
235	4.46	280	0.000
240	2.89		

Note:
200-280 nm, Rattigan et al. [656].

E19. $CH_3C(O)F + h\nu \rightarrow$ Products. The absorption cross-sections of $CH_3C(O)F$ (acetyl fluoride) have been measured at room temperature and 200-310 nm by Rattigan et al. [656]. The spectrum exhibits a part of an absorption band with the maximum near 206 nm. In Table 4-71 are listed the averages over 5-nm intervals of the spectrum recorded at a resolution of 1.2 nm (diode-array spectrometer) by Rattigan et al. [656].

Table 4-71. Absorption Cross Sections of $CH_3C(O)F$ at 296 K

λ (nm)	$10^{20}\ \sigma$ (cm^2)	λ (nm)	$10^{20}\ \sigma$ (cm^2)	λ (nm)	$10^{20}\ \sigma$ (cm^2)	λ (nm)	$10^{20}\ \sigma$ (cm^2)
200	11.3	230	3.83	260	0.158	290	0.008
205	12.2	235	2.19	265	0.120	295	0.004
210	12.0	240	1.14	270	0.090	300	0.002
215	10.5	245	0.566	275	0.056	305	0.001
220	8.35	250	0.311	280	0.029	310	0.000
225	5.97	255	0.206	285	0.016		

Note:
200-310 nm, Rattigan et al. [656].

E20. $CH_2=CHCF_3 + h\nu \rightarrow$ Products. The absorption spectrum of $CH_2=CHCF_3$ (3,3,3-trifluoro-1-propene) has been measured at room temperature and 164-205 nm by Orkin et al. [601]. Their data recorded at 0.5-nm increments and selected at 1-nm intervals, are listed in Table 4-72.

Table 4-72. Absorption Cross Sections of $CH_2=CHCF_3$ at 295 K

λ (nm)	10^{20} σ (cm^2)	λ (nm)	10^{20} σ (cm^2)	λ (nm)	10^{20} σ (cm^2)
164	3569	178	168	192	0.681
165	3377	179	114	193	0.453
166	3146	180	77.7	194	0.298
167	2874	181	53.9	195	0.204
168	2538	182	36.5	196	0.131
169	2184	183	25.0	197	0.0872
170	1814	184	16.8	198	0.0581
171	1481	185	11.3	199	0.0404
172	1165	186	7.74	200	0.0278
173	899	187	5.22	201	0.0185
174	660	188	3.49	202	0.0129
175	475	189	2.32	203	0.00945
176	340	190	1.52	204	0.00669
177	240	191	1.02	205	0.00456

Note:
164-205 nm, Orkin et al. [601].

E21. $CH_2=CFCF_3 + h\nu \rightarrow$ Products. The absorption spectrum of $CH_2=CFCF_3$ (1,1,1,2-tetrafluoropropene) has been measured at room temperature and 164-186 nm by Orkin et al. [601]. Their data, recorded at 0.5-nm increments and selected at 1-nm intervals, are listed in Table 4-73.

Table 4-73. Absorption Cross Sections of $CH_2=CFCF_3$ at 295 K

λ (nm)	10^{20} σ (cm^2)	λ (nm)	10^{20} σ (cm^2)
164	3773	176	1130
165	3732	177	840
166	3730	178	600
167	3695	179	408
168	3594	180	273
169	3418	181	185
170	3176	182	124
171	2877	183	82.4
172	2535	184	55.5
173	2178	185	38.1
174	1802	186	26.2
175	1445		

Note:
164-186 nm, Orkin et al. [601].

E22. $CF_2=CF_2 + h\nu \rightarrow$ Products. The absorption spectrum of $CF_2=CF_2$ (tetrafluoroethylene) has been measured at room temperature and 185-209 nm by Sharpe et al. [728]; at 164–220 nm by Orkin et al. [601]; and at 115–320 nm by Eden et al. [227]. The spectrum shows a structured absorption band with five maxima and one shoulder between 170 and 220 nm (highest maximum near 189 nm). The results of Orkin et al. [601] and Eden et al. [227] agree within 10% at 164-182 nm, within 20% at 182-200 nm, and within 10% at 203-205 nm. Above 200 nm, a linear decrease of log σ is reported by Orkin et al. [601], whereas Eden et al. [227] reported a very noisy spectrum deviating from that of Orkin et al. [601]. The absorption curve reported by Sharpe et al. [728] shows a shift by 1-2 nm to shorter wavelengths. As recommended absorption cross sections are listed in Table 4-74, the mean of the data of Orkin et al. [601] and Eden et al. [227] for the region 164-205 nm, and the data of Orkin et al. [601] at 206-220 nm (selected at 1-nm intervals from the data reported at 0.5- and 0.1 nm-intervals, respectively).

Table 4-74. Absorption Cross Sections of CF_2=CF_2 at 295-298

λ (nm)	10^{20} σ (cm^2)	λ (nm)	10^{20} σ (cm^2)	λ (nm)	10^{20} σ (cm^2)	λ (nm)	10^{20} σ (cm^2)
164	335	179	341	194	423	209	0.429
165	324	180	362	195	387	210	0.257
166	300	181	432	196	263	211	0.162
167	272	182	521	197	169	212	0.0998
168	243	183	559	198	108	213	0.0633
169	227	184	485	199	64.0	214	0.0392
170	238	185	442	200	39.9	215	0.0249
171	268	186	491	201	23.8	216	0.0160
172	286	187	596	202	14.5	217	0.0105
173	281	188	682	203	8.74	218	0.00668
174	289	189	671	204	5.73	219	0.00443
175	327	190	507	205	3.23	220	0.00288
176	372	191	417	206	1.99		
177	390	192	399	207	1.17		
178	376	193	410	208	0.713		

Note:
164-205 nm, mean of the data of Orkin et al. [601] and Eden et al. [227],
206-220 nm, data of Orkin et al. [601].

E23. CF_2=$CFCF_3$ + hν → Products. The absorption spectrum of CF_2=$CFCF_3$ (hexafluoropropene) has been measured at room temperature and 185-209 nm by Sharpe et al. [728]; at 164–222 nm by Orkin et al. [601]; and at 115–330 nm by Eden et al. [226]. The spectrum shows an absorption band between 140 and 220 nm with two maxima at 155 and 158.5 nm ($\sigma \approx 3 \times 10^{-17}$ cm^2 $molecule^{-1}$) and two shoulders near 166 and 180 nm. In the region 164-200 nm, there is agreement within 15% between the result of Orkin et al. [601] and Eden et al. [226]; in the region 185-200 nm, the agreement between the results of the three teams is within 25%. Above 200 nm, a linear decrease of log σ is reported by Orkin et al. [601], whereas Eden et al. [226] reported a very noisy spectrum deviating from that of Orkin et al. [601]. As recommended absorption cross sections are listed in Table 4-75, the mean of the data of Orkin et al. [601] and Eden et al. [226] for the region 164-199 nm, and the data of Orkin et al. [601] at 200-222 nm (selected at 1-nm intervals from the data reported at 0.5- and 0.1 nm-intervals, respectively).

Table 4-75. Absorption Cross Sections of CF_2=$CFCF_3$ at 295-298 K

λ (nm)	10^{20} σ (cm^2)	λ (nm)	10^{20} σ (cm^2)	λ (nm)	10^{20} σ (cm^2)	λ (nm)	10^{20} σ (cm^2)
164	2290	179	929	194	97.8	209	0.585
165	2210	180	912	195	73.3	210	0.396
166	2130	181	880	196	54.7	211	0.269
167	2040	182	835	197	40.4	212	0.184
168	1920	183	779	198	29.7	213	0.125
169	1760	184	708	199	22.3	214	0.0838
170	1570	185	629	200	16.2	215	0.0564
171	1380	186	550	201	11.6	216	0.0381
172	1210	187	472	202	8.17	217	0.0261
173	1080	188	391	203	5.70	218	0.0177
174	995	189	321	204	3.95	219	0.0119
175	946	190	259	205	2.70	220	0.00795
176	930	191	207	206	1.85	221	0.00533
177	928	192	163	207	1.28	222	0.00354
178	931	193	127	208	0.866		

Note:
164-199 nm, mean of the data of Orkin et al. [601] and Eden et al. [226],
200-222 nm, data of Orkin et al. [601].

PHOTOCHEM-F-TOTAL CHLORINE

F1. $Cl_2 + h\nu \rightarrow Cl + Cl$. The recommended absorption cross sections are taken from the work of Maric et al. [477], who studied the absorption spectrum in the range 200-550 nm using a spectral resolution of 0.2 nm at 298 K. These authors also measured banded features in the range 476-496 nm at 0.04 nm resolution. The absorption cross sections can be calculated in the range 250-550 nm at various temperatures with the expression derived from their study and previous investigations, given at the bottom of Table 4-76. For convenience, some room temperature values are also listed in the table. Ganske et al. [260] have also measured the cross sections at room temperature, and the agreement with the recommended values is excellent. These two sets of data also agree well with the earlier recommendation, which was based on the work of Seery and Britton [719], which is in turn in good agreement with the results reported by Gibson and Bayliss [266], Fergusson et al. [243], and Burkholder and Bair [110]. At wavelengths larger than 250 nm, the absorption cross sections measured at room temperature by Hubinger and Nee [344] are in excellent agreement with the values of Maric et al. [477]. However, in the range 200-250 nm the cross sections deviate considerably between both groups. Room temperature cross sections have also been obtained by Roxlo and Mandl [692] for the range 170-214 nm. The low resolution absorption cross sections reported by Chen and Zhu [160, 161] and Chen et al. [162] for the 300-420-nm region at 5- and 10-nm intervals and measured for the calibration of quantum yield measurements of some carbonyl compounds deviate up to ~30% from those reported by Maric et al. [477].

The estimated atmospheric photodissociation rate is only weakly affected by the temperature dependency of the cross sections. Chininin [167] measured an upper limit of 5% for the branching ratio for excited atomic $Cl^*(^2P_{1/2})$ at 351 nm, in agreement with earlier studies by Bush et al. [128] and Park et al. [622], who determined an upper limit for Cl* formation of 0.01 in the photolysis of Cl_2 at 347.1 nm, and 308 and 340-355 nm, respectively.

Table 4-76. Absorption Cross Sections of Cl_2 at 298

λ (nm)	10^{20} σ (cm^2)	λ (nm)	10^{20} σ (cm^2)	λ (nm)	10^{20} σ (cm^2)
260	0.198	360	13.22	460	0.258
270	0.824	370	8.41	470	0.162
280	2.58	380	5.00	480	0.0957
290	6.22	390	2.94	490	0.0534
300	11.92	400	1.84	500	0.0283
310	18.50	410	1.28	510	0.0142
320	23.71	420	0.956	520	0.00681
330	25.55	430	0.732	530	0.00313
340	23.51	440	0.546	540	0.00137
350	18.77	450	0.387	550	0.00058

.

$$\sigma = 10^{-20}\alpha^{0.5}\left\{27.3\exp\left(-99.0\alpha\left(\ln\left(\frac{329.5}{\lambda}\right)\right)^2\right)+0.932\exp\left(-91.5\alpha\left(\ln\left(\frac{406.5}{\lambda}\right)\right)^2\right)\right\}$$

where α = tanh (402.7/T); λ in nm, 250 < λ < 550 nm, and T in K; 300 K > T > 195 K.

F2. ClO + hν → Cl + O. The UV absorption spectrum of chlorine monoxide, ClO, shown in Figure 4-2, is partly composed of a continuum absorption band from 210 nm to the maximum near 265 nm, and a characterized banded structure of a strong A $^2\Pi_{3/2} \leftarrow$ X $^2\Pi_{3/2}$ transition, superposing a weak A $^2\Pi_{1/2} \leftarrow$ X $^2\Pi_{1/2}$ system, ranging from 265 nm to 315 nm. The cross sections have been reviewed by Watson [839]. The more recent measurements yield results in reasonable agreement with the earlier ones, (1) Mandelman and Nicholls [473] in the 250–310 nm region; (2) Wine et al. [849] around 283 nm; (3) Rigaud et al. [672] in the 272-324 nm range; (4) Jourdain et al. [397] in the 272-320 nm range; (5) Barton et al. [44] in the 274-306 nm range at 315 K, (6) Lang et al. [431] at 253.7 and 257.7 nm; (7) Sander and Friedl [702] at 275.2 nm, at 220, 298, and 400 K; (8) Trolier et al. [784] in the 270–310-nm region and 200-263 K temperature range; and (9) Simon et al. [732] between 240 and 310 nm. The peak cross section at the maximum of the continuum (near 265 nm) is 5.2×10^{-18} cm^2 $molecule^{-1}$, based on the average of studies 4, 7-9 and Johnston et al. [388]. At 257.7 nm an average value of $(4.86 \pm 0.04) \times 10^{-18}$ cm^2 $molecule^{-1}$ was calculated from the data of the studies 1,6-9. It should be noted that the cross sections on the structured part are extremely dependent on instrument resolution. Figure 4-2 shows a spectrum of ClO based on the data of Sander and Friedl [702]. The recommended absorption cross sections listed in Table 4-77 are the averages over 1-nm intervals of the continuous and banded spectrum measured at a resolution of 0.3 nm by Sander and Friedl [702]. In Table 4-78 are compared the absorption cross sections for the band heads of the v',v" = 1,0 to 21,0 bands measured at various spectral resolutions.

The cross sections of the continuum are independent of temperature (Trolier et al. [784]), while the structured part is extremely temperature dependent. The bands sharpen and grow with a decrease in temperature. Sander and Friedl [702] measured the temperature dependence at the peak of the 12-0 sub-band in the range 220-400K. Clyne and Coxon [175] determined the following relationship for the 11-0 sub-band relative to the 298 K value for the temperature range 294-240 K:

$$\sigma_{294} / \sigma_T = 1 + 0.0036\ (T\text{-}294K).$$

Recently, Maric and Burrows [476] performed a detailed analysis of the ClO spectrum and developed an analytical approach, which allows the calculation of the UV absorption spectrum for any temperature and spectral resolution.

The calculations of Coxon et al. [195] and Langhoff et al. [434] indicate that photodecomposition of ClO accounts for at most 2 to 3% of the total destruction rate of ClO in the stratosphere, which occurs predominantly by reaction with oxygen atoms and nitric oxide.

The photodissociation of thermal ClO radicals in the wavelength range 237<λ<270 nm was studied by Schmidt et al. [711] using REMPI. Cl ($^2P_{3/2,1/2}$) and O(^{1}D) were formed with unity quantum yield. The cut-off excitation wavelength for O(^{1}D) was determined to be 263.4 nm.

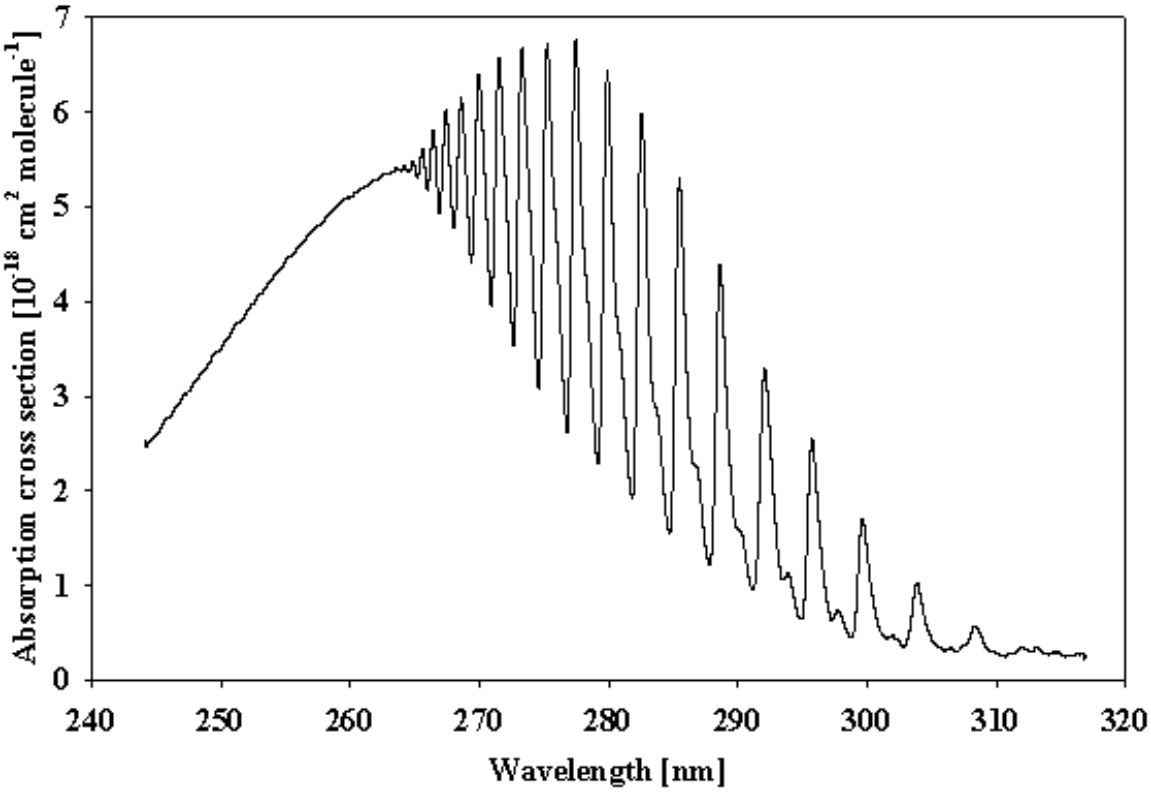

Figure 4-2. Absorption Spectrum of ClO

Table 4-77. Absorption Cross Sections of ClO at 298 K

λ (nm)	10^{20} σ (cm^2)	λ (nm)	10^{20} σ (cm^2)	λ (nm)	10^{20} σ (cm^2)	λ (nm)	10^{20} σ (cm^2)
245	260	263	536	281	329	299	74.8
246	279	264	540	282	311	300	133
247	297	265	541	283	445	301	56.6
248	315	266	549	284	245	302	45.2
249	333	267	546	285	292	303	44.9
250	352	268	529	286	362	304	87.8
251	371	269	529	287	200	305	45.5
252	388	270	575	288	197	306	33.2
253	407	271	489	289	337	307	33.1
254	425	272	532	290	165	308	47.7
255	442	273	515	291	111	309	41.9
256	457	274	470	292	270	310	28.7
257	473	275	507	293	161	311	27.3
258	486	276	456	294	102	312	33.1
259	500	277	418	295	94.5	313	32.5
260	511	278	501	296	206	314	28.9
261	520	279	283	297	83.1	315	27.8
262	529	280	538	298	65.1	316	26.8

Note:
Sander and Friedl [702]: Averages over 1-nm intervals of the continuous and banded spectrum measured at a resolution of 0.3 nm.

Table 4-78. Absorption Cross Sections of ClO at the band heads of the v′,v″ = 1,0 to 21,0 bands

Band	λ (nm)	10^{20} σ (cm^2)	λ (nm)	10^{20} σ (cm^2)	λ (nm)	10^{20} σ (cm^2)	λ (nm)	10^{20} σ (cm^2)	λ (nm)	10^{20} σ (cm^2)
v',v"	Trolier et al. resol. 0.6 nm		Sander, Friedl res. 0.3(0.18) nm		Simon et al. res. 0.3(0.03) nm		Mandelman resol. 0.22 nm		Jourdain et al. resol. 0.015 nm	
1,0			312.1	35					312.5	26
2,0	307.7	22	308.3	58	307.9	39	307.8	47	307.9	67
3,0	303.4	64	303.9	103	303.5	86	303.4	104	303.5	133
4,0	299.4	128	299.6	171	299.0	163	299.3	207	299.3	236
5,0	295.4	202	295.7	253	295.4	255	295.4	315	295.4	326
6,0	292.1	286	292.1	330	292.0	338 (400)	292.0	382	291.8	395
7,0	288.7	365	288.6	438	288.4	448 (502)	288.4	516	288.4	504
8,0	286.0	455	285.5	530	285.2	542	285.2	627	285.2	594
9,0	282.6	508	282.6	598	282.3	608	282.2	667	282.2	641
10,0	280.1	555	279.9	645	279.8	655	279.6	688	279.6	686
11,0	277.7	571	277.4	668	277.2	679	277.2	680	277.2	727
12,0	275.5	587	275.3	671 (836)	275.1	681	275.0	634	275.1	733
13,0	273.6	576	273.3	668					272.9	711
14,0	271.8	571	271.5	656						
15,0	269.9	556	270.0	640						
16,0	268.7	545	268.6	615						
17,0			267.4	603						
18,0			266.5	579						
19,0			265.6	562						
20,0			264.9	549						
21,0			264.2	543						

F3. ClOO + hν → ClO + O. Johnston et al. [388] measured the absorption cross sections of the ClOO radical using a molecular modulation technique that required interpretation of a complex kinetic scheme. More recently, Mauldin et al. [502] reported cross section measurements in the range from 220 to 280 nm, and Baer et al. [34] from 240 to 300 nm. These two studies are in agreement, yielding cross section values that are more than twice as large as the older Johnston et al. [388] values. The recommended cross sections are listed in Table 4-79, and are taken from the work of Mauldin et al. [502].

Table 4-79. Absorption Cross Sections of ClOO

λ (nm)	10^{20} σ (cm^2)	λ (nm)	10^{20} σ (cm^2)
220	611	252	2630
222	670	254	2370
224	747	256	2120
226	951	258	1890
228	1100	260	1610
230	1400	262	1370
232	1650	264	1120
234	1960	266	905
236	2240	268	725
238	2520	270	596
240	2730	272	435
242	2910	274	344
244	2960	276	282
246	2980	278	210
248	2950	280	200

λ (nm)	10^{20} σ (cm^2)	λ (nm)	10^{20} σ (cm^2)
250	2800		

F4. $OClO + h\nu \rightarrow O(^3P) + ClO$
$OClO + h\nu \rightarrow Cl + O_2\ (^3\Sigma_g^-,\ ^1\Delta_g)$
$OClO + h\nu \rightarrow ClOO$ The spectrum of OClO (chlorine dioxide) is characterized by a series of well-developed progressions of bands extending from ~280 to 480 nm, corresponding to the A ($^2A_2$) (i,j,k) ← X ($^2B_1$) (0,0,0) vibronic transitions. The spectroscopy of this molecule has been studied extensively, and the quantum yield for photodissociation appears to be unity throughout the above wavelength range. See for example, the review by Watson [839]. Birks et al. [73] have estimated a half-life against atmospheric photodissociation of OClO of a few seconds. The measurement of absorption spectra at temperatures between 200 and 378 K has been the subject of many studies as shown in the following survey:

Table 4-80. Summary of Previous Measurements of OClO Cross Sections

Reference	Year	Temperature K	Wavelength Range nm	Resolution nm
Martin and Gareis [490]	1956	298	263-414	Not given
Knauth et al. [411]	1979	333	270-440	0.3-1
Wahner et al. [830]	1987	204, 296, 378	242-477	0.25
Hubinger and Nee [343]	1994	298	240-477	Not given
Frost et al. [255]	1996	200	390-454	0.0015-0.0021
Marston et al. [489]	1998	298	275-400	0.05
Kromminga et al. [423]	2003	213, 233, 253	312.5-440.5	0.01-0.02
Bogumil et al. [82]	2003	293	290-460	0.25

Absorption cross sections at 10-nm intervals for the region 270-440 nm and at 333 K have been reported by Knauth et al. [411], and for the 351.5-nm maximum at room temperature by Clyne and Coxon [175] and Basco and Dogra [46]. The absorption cross sections of Wahner et al. [830] obtained at a resolution of 0.25 nm and at 204, 296, and 378 K have been used by Hubinger and Nee [343], Frost et al. [255] and Marston et al. [489] for the calibration of their relative spectra. The values at the peaks of the main vibrational bands a(0) to a(26) (i.e., A ($^2A_2$) (i,0,0) ← X ($^2B_1$) (0,0,0), i = 0 to 26) reported by Wahner et al. [830] have been selected as recommended absorption cross sections of OClO in the four foregoing JPL reports. Most recently, Kromminga et al. [423] reported high- and medium-resolution absorption spectra at five temperatures between 213 and 293 K obtained by using Fourier-transform spectroscopy, which has the advantage of accurate wavelength calibration. There is a clear wavelength shift (~0.2-0.5 nm) between the spectra of Kromminga et al. [423] and Wahner et al. [830], which cannot be explained by the shift between measurements in air and in vacuum. The absorption cross sections for the band peaks a(3) to a(26) reported by Kromminga et al. [423] are smaller by 5-10% than those reported by Wahner et al. [830]. A decrease of the temperature causes a sharpening of the vibrational bands and an increase of the peak cross sections as observed between 293 and 213 K by Kromminga et al. [423] and between 378 and 200 K by Wahner at al. [830].

The recommended absorption cross sections of OClO are listed in Table 4-81, and represent the averages over 1-nm intervals of the spectrum measured at medium resolution (0.25 nm) by Wahner et al. [830]. In Table 4-82 are listed the a(16) to a(3) band peaks at 213, 233, 253, 273, and 293 K recorded in the medium-resolution (0.2-0.4 nm) spectra by Kromminga et al. [423]. The values for the a(17) to a(23) bands at 293 K are the results of Bogumil et al. [82], who have measured the OClO spectrum at medium resolution (0.24-0.44 nm) with the SCIAMACHY pre-flight satellite instrument and have scaled the absorption cross sections to those measured by Kromminga et al. [423]. In addition, the peak cross sections determined by Wahner et al. [830] are listed in Table 4-83. Figure 4-3 shows the spectrum of OClO at 204 K based on the data of Wahner et al. [830].

VUV absorption cross sections have been measured at 148-183 nm by Basco and Morse [49], at 50-207 nm by Flesch et al. [246], at 127-183 nm by Hubinger and Nee [343], and at 115-191 nm by Marston et al. [489].

The photochemistry of OClO is extremely complex, with several electronic excited states involved in the photodissociation dynamics. Several channels have been observed at wavelengths important in the stratosphere, including O + ClO, Cl + O_2 and isomerization to ClOO. Colussi [178] measured the quantum

yield for chlorine atom production to be less than 0.01, and for oxygen atom production to be unity (within experimental error), both at 308 nm. Vaida et al. [802] and Ruhl et al. [693] reported chlorine atom production at 362 nm; and Bishenden et al. [74, 75] measured the quantum yield for this process to be 0.15 ± 0.10 around that same wavelength. In contrast, Lawrence et al. [437] report a quantum yield for Cl-atom production in the 359–368-nm region of less than 5×10^{-4}. This conclusion is supported by photofragment studies of Davis and Lee [209] between 350 and 475 nm, who report Cl yields <0.2% in the wavelength range 350-370 nm, rising to a maximum of 3.9 ± 0.8% near 404 nm. In a later study Davis and Lee [207] report a substantial yield of $O_2(^1\Delta_g)$ and show that the branching ratio between O + ClO, and Cl + O_2 depends on the OClO(A $^2A_2$) excited state vibrational mode. Delmdahl et al. [210] measured the yield of nascent Cl atoms to be below 3.6% in the photolysis in the 365-450 nm range. At λ < 365 nm, there was a sharp increase of the Cl yield, which was attributed to the photolysis of vibrationally excited ClO (v≥4).

The recommendation is to use a quantum yield value of unity for the production of $O(^3P)$ atoms in the range 270-480 nm. An upper limit for the Cl yield can be set at 0.04 in the range 365-450 nm. While accurate absorption cross section values are valuable for atmospheric measurements of OClO levels, the identity of the photodissociation products is only of minor importance in the context of atmospheric processes.

Table 4-81. Absorption Cross Sections of OClO at 204 K (averages over 1-nm intervals)

λ (nm)	10^{20} σ (cm^2)	λ (nm)	10^{20} σ (cm^2)	λ (nm)	10^{20} σ (cm^2)	λ (nm)	10^{20} σ (cm^2)
247	35.6	304	96.1	361	477	418	107
248	34.4	305	276	362	173	419	75.1
249	33.7	306	328	363	179	420	81.4
250	34.6	307	190	364	207	421	323
251	34.3	308	116	365	361	422	151
252	34.6	309	85.4	366	403	423	50.0
253	34.1	310	168	367	625	424	23.8
254	34.9	311	511	368	919	425	23.3
255	34.3	312	338	369	903	426	14.5
256	34.8	313	174	370	268	427	43.8
257	34.8	314	107	371	107	428	99.5
258	35.1	315	94.2	372	180	429	46.9
259	35.0	316	239	373	170	430	44.3
260	35.8	317	686	374	364	431	23.3
261	36.5	318	360	375	376	432	47.0
262	37.5	319	176	376	554	433	173
263	38.2	320	114	377	718	434	69.6
264	38.0	321	125	378	881	435	24.6
265	38.8	322	279	379	278	436	11.2
266	39.9	323	873	380	92.4	437	7.68
267	40.4	324	443	381	135	438	9.09
268	42.3	325	192	382	148	439	5.13
269	44.6	326	121	383	266	440	12.5
270	44.3	327	147	384	298	441	47.8
271	45.7	328	221	385	440	442	23.2
272	49.9	329	838	386	345	443	14.7
273	49.1	330	782	387	762	444	7.59
274	48.1	331	285	388	591	445	3.96
275	54.8	332	155	389	173	446	46.8
276	58.3	333	147	390	71.4	447	55.2
277	52.5	334	208	391	123	448	18.4
278	54.3	335	355	392	109	449	7.17
279	67.4	336	1090	393	203	450	6.96
280	67.2	337	782	394	270	451	4.50
281	58.3	338	266	395	285	452	1.66
282	65.4	339	155	396	275	453	3.57
283	82.4	340	167	397	370	454	0.907
284	77.6	341	250	398	653	455	13.3
285	67.2	342	414	399	225	456	9.70
286	77.7	343	925	400	70.1	457	4.76

λ (nm)	10^{20} σ (cm^2)	λ (nm)	10^{20} σ (cm^2)	λ (nm)	10^{20} σ (cm^2)	λ (nm)	10^{20} σ (cm^2)
287	100	344	1090	401	45.6	458	4.25
288	93.7	345	388	402	96.9	459	3.98
289	79.4	346	176	403	56.3	460	1.84
290	90.5	347	161	404	196	461	17.1
291	127	348	258	405	194	462	17.9
292	116	349	320	406	185	463	11.8
293	90.9	350	581	407	160	464	10.0
294	94.1	351	1100	408	158	465	4.01
295	147	352	993	409	493	466	1.40
296	172	353	330	410	210	467	2.53
297	122	354	164	411	71.6	468	10.1
298	92.0	355	190	412	34.0	469	15.0
299	106	356	276	413	46.8	470	7.69
300	226	357	343	414	44.6	471	6.14
301	222	358	597	415	30.0	472	3.18
302	143	359	830	416	164		
303	94.3	360	1210	417	100		

Note:
246.5-472.5 nm, Wahner et al. [830].

Table 4-82. Absorption Cross Sections of OClO at the a(21) to a(3) Band Peaks at 213-293 K

band peak	λ (nm)	10^{20} σ (cm^2)	λ (nm)	10^{20} σ (cm2)	λ (nm)	10^{20} σ (cm^2)	λ (nm)	10^{20} σ (cm^2)	λ (nm)	10^{20} σ (cm^2)
	T = 213 K		T = 233 K		T = 253 K		T = 273 K		T = 293 K	
a(21)									292.05	79.32
a(20)									295.79	107.60
a(19)									300.96	171.03
a(18)									306.12	273.85
a(17)									311.58	391.16
a(16)									316.86	528.84
a(15)	322.96	846.62	322.96	812.45	323.02	786.75	323.02	756.88	323.02	707.16
a(14)	329.49	1054.25	329.49	1011.91	329.55	984.42	329.55	945.36	329.55	892.88
a(13)	336.41	1224.61	336.41	1181.30	336.41	1148.79	336.48	1098.73	336.48	1044.48
a(12)	343.77	1313.77	343.77	1269.99	343.77	1243.47	343.77	1189.35	343.77	1134.36
a(11)	351.53	1328.23	351.53	1289.25	351.53	1265.01	351.53	1212.13	351.53	1164.23
a(10)	359.73	1280.34	359.73	1243.39	359.73	1220.29	359.73	1171.14	359.73	1127.62
a(9)	368.39	1187.04	368.39	1153.33	368.39	1128.23	368.39	1083.63	368.47	1045.41
a(8)	377.56	1048.31	377.56	1019.56	377.56	992.21	377.56	951.69	377.65	916.95
a(7)	387.29	869.95	387.29	849.00	387.29	818.37	387.29	783.53	387.38	750.49
a(6)	397.90	696.60	397.99	683.65	397.90	661.61	397.99	643.31	397.99	619.46
a(5)	408.82	523.40	408.82	518.32	408.82	488.85	408.92	473.08	408.92	452.82
a(4)	420.56	350.83	420.45	350.30	420.45	319.18	420.45	317.13	420.45	301.27
a(3)	432.88	220.71	432.99	197.98	432.99	174.81	432.99	194.21	432.99	189.51

Note:
292-317 nm, Bogumil et al. [82],
323-433 nm, Kromminga et al. [423].

Table 4-83. Absorption Cross Sections of OClO at the Band Peaks (after Wahner et al. [830])

λ(nm)	10^{20} σ(cm^2)		
	204 K	296 K	378 K
475.53		13	
461.15	17	17	16
446.41	94	69	57
432.81	220	166	134
420.58	393	304	250
408.83	578	479	378
397.76	821	670	547
387.37	1046	844	698
377.44	1212	992	808
368.30	1365	1136	920
359.73	1454	1219	984
351.30	1531	1275	989
343.44	1507	1230	938
336.08	1441	1139	864
329.22	1243	974	746
322.78	1009	791	628
317.21	771	618	516
311.53	542	435	390
305.99	393	312	291
300.87	256	219	216
296.42	190	160	167
291.77	138	114	130
287.80	105	86	105
283.51	089	72	90
279.64	073	60	79
275.74	059	46	
272.93	053	33	

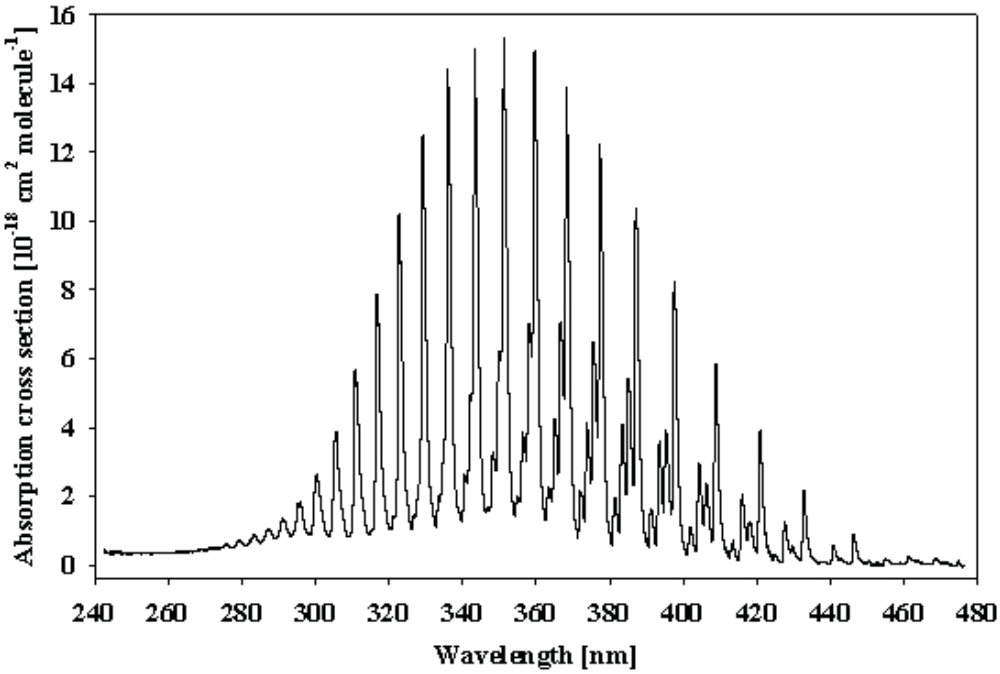

Figure 4-3. Absorption Spectrum of OClO at 204 K (after Wahner et al. [830])

F5. $ClO_3 + h\nu \rightarrow$ Products. The JPL-83 to JPL-90 recommendations for the absorption cross sections of the ClO_3 radical were based on the work of Goodeve and Richardson [288]. Lopez and Sicre [461], however, have shown that the spectrum reported by Goodeve and Richardson is most likely that of Cl_2O_6. Thermochemical estimates by Colussi et al. [179] further corroborate this assignment.

Grothe and Willner [305], [306] have reported the UV and IR spectra of ClO_3 trapped in a neon matrix following thermal decomposition of Cl_2O_4 or $FOClO_3$. By monitoring the amount of ClO formed as a photolysis product of ClO_3, they determined the absorption cross sections in the range 250-500 nm. The spectrum showing a highly structured absorption band around 320 nm ($\sigma \approx 3 \times 10^{-18}$ cm^2 molecule^{-1}) and a second band around 425 nm ($\sigma \approx 2.5 \times 10^{-18}$ cm^2 molecule^{-1}) is depicted in the review article of Wayne et al. [841]. A broad absorption spectrum between 280 and 450 nm peaking at ≈300 nm ($\sigma \approx 1.8 \times 10^{-17}$ cm^2 molecule^{-1}) was recorded for ClO_3 formed by radiolysis of aqueous solutions of chlorate ions.

For the absorption cross sections of ClO_3 in the gas phase no recommendation can be given at present.

F6. $Cl_2O + h\nu \rightarrow Cl + ClO$
$Cl_2O + h\nu \rightarrow Cl_2 + O(^3P)$
$Cl_2O + h\nu \rightarrow Cl_2 + O(^1D)$
$Cl_2O + h\nu \rightarrow O + 2Cl$. The absorption spectra of dichlorine monoxide have been measured at room temperature and 230-620 nm by Goodeve and Wallace [291], at 220-650 nm by Finkelnburg et al. [244], at 234-331 nm by Martin and Gareis [490], at 180-640 nm by Lin [454], at 200-450 nm by Molina and Molina [537], at 236-320 nm by Simon et al. [732], and at 190-399 nm by Smith et al. [742]. Johnsson et al. [382] measured the absorption spectrum at 210-350 nm of Cl_2O in Ar matrices and reported the absorption cross section at 260 nm for the gas phase. Measurements at 298 and 333 K and between 200 and 500 nm have been carried out by Knauth et al. [411]. The spectrum exhibits three absorption bands in the UV and visible regions: an asymmetrical band between ~220-380 nm with the maximum near 255 nm and a shoulder near 290 nm, and two weak bands at ~380-500 nm and ~500-650 nm with the maxima near 420 nm and 550 nm, respectively. The absorption cross sections measured by Lin et al. [454], Molina and Molina [537], Knauth et al. [411], and Smith et al. [742] are in very good agreement, i.e., within 10%, in the UV absorption band between 200 and ~350nm. The values reported by Molina and Molina [537] and Knauth et al. [411] are somewhat larger than those reported by Lin [454], which again are larger than those reported by Smith et al. [742]. The discrepancies between the various data sets become larger in the region of the absorption minimum, whereas above ~400 nm the agreement is again very good. The spectrum measured by Simon et al. [732] has been normalized to the data of Lin [454]. The earlier data reported by Goodeve and Wallace [291], Finkelnburg et al. [244], and Martin and Gareis [490] deviate substantially from the more recent results. VUV absorption cross sections have been reported by Nee [574] for the 150 –200 nm wavelength region, and by Motte-Tollet et al. [564] for the 128-190 nm region.

The recommended absorption cross sections for Cl_2O listed in Table 4-84 are based on the four spectra showing good agreement as outlined above: they are the mean of the data of Lin [454], Molina and Molina [537], Knauth et al. [411], and Smith et al. [742] at 200-350 nm; the mean of the data of Lin [454], Molina and Molina [537], and Knauth et al. [411], at 360-450 nm; the mean of the data of Lin [454] and Knauth et al. [411] at 460-500 nm; and the data of Lin [454] at 510-640 nm. Sander and Friedl [702] have measured the quantum yield for production of O-atoms to be 0.25 ± 0.05, using a broadband photolysis source extending from 180 nm to beyond 400 nm. The main photolysis products are Cl and ClO. Using a molecular beam technique, Nelson et al. [578] found Cl + ClO to be the only primary photodissociation channel at 308 nm, a major channel at 248 nm, and a minor channel at 193 nm. At 248 nm a fraction of the photoproduct ClO underwent spontaneous photodissociation. These authors find evidence that the dissociation in three atoms 2 Cl + O takes place at 193 nm, and that some $O(^1D)$ atoms are generated as well. More recently, Nickolaisen et al. [582] reported that broadband photolysis at wavelengths beyond 300 nm results in pressure-dependent ClO quantum yields, which was explained by the rapid intercrossing between two metastable states. These states undergo competitive dissociation to ClO + Cl and collisional relaxation to the ground states. Furthermore, these authors detected a transient absorption spectrum, which they assigned to a long-lived metastable triplet state of Cl_2O. However Moore et al. [550] estimated the lifetime of this metastable excited state to be much shorter. Chichinin [167] and Tanaka et al. [773], also found evidence of ground state ($^2P_{3/2}$) and spin-orbit excited ($^2P_{1/2}$) atomic chlorine products.

The implication is that the photodecomposition quantum yield is less than unity at atmospherically relevant wavelengths, in spite of the continuous nature of the absorption spectrum. Additional experimental work is needed to corroborate this interpretation.

Table 4-84. Absorption Cross Sections of Cl_2O

λ (nm)	10^{20} σ (cm^2)	λ (nm)	10^{20} σ (cm^2)	λ (nm)	10^{20} σ (cm^2)
200	67.7	350	1.84	500	0.218
210	22.4	360	0.893	510	0.210
220	8.42	370	0.493	520	0.214
230	26.5	380	0.446	530	0.237
240	101	390	0.575	540	0.256
250	184	400	0.829	550	0.256
260	186	410	1.08	560	0.222
270	144	420	1.25	570	0.203
280	121	430	1.23	580	0.176
290	98.9	440	1.10	590	0.149
300	68.1	450	0.848	600	0.122
310	38.6	460	0.625	610	0.0956
320	18.7	470	0.446	620	0.0688
330	8.59	480	0.313	630	0.0344
340	3.90	490	0.247	640	0.0153

Note:
200-350 nm, mean of the data of Lin [454], Molina and Molina [537], Knauth et al. [411], and Smith et al. [742],
360-450 nm, mean of the data of Lin [454], Molina and Molina [537], and Knauth et al. [411],
460-500 nm, mean of the data of Lin [454] and Knauth et al. [411],
510-640 nm, data of Lin [454].

F7. $ClOOCl + h\nu \rightarrow Cl + ClOO$

$ClOOCl + h\nu \rightarrow ClO + ClO$. The absorption cross sections of ClOOCl have been measured at low temperatures: at 265 K and 220-360 nm by Cox and Hayman [190] (1), at 250 K and 211-426 nm by Burkholder et al. [115] (2), at 235 K and 210-290 nm by Permien et al. [630] (3), at 206 K and 190-400 nm by DeMore and Tschuikow-Roux [214] (4), at 230 K and 204-380 nm by Vogt and Schindler [823] (5), at 195 K and 200-400 nm by Huder and DeMore [348] (6), and at 183-245 K and 210 nm by Bloss et al. [79] (7). Recently, a theoretical photoabsorption spectrum of ClOOCl has been reported by Toniolo et al. [780]. The absorption spectrum shows decreasing cross sections between 190 and 220 nm, an absorption band above 220 nm with the maximum near 245 nm and $\sigma \approx (6.3\text{-}6.8) \times 10^{-18}$ cm^2 $molecule^{-1}$, and decreasing cross sections for wavelengths up to 450 nm. There is good agreement between the results of (1) to (6) in the region of the absorption band, agreement within 15% up to ~260 nm and about 30% up to ~290 nm. Larger discrepancies occur in the tail above 300 nm, where the spectrum is weak, which may be attributed to uncertainties in the spectral subtraction of impurities such as Cl_2O, Cl_2, and Cl_2O_2. A measurement at 210 nm over the temperature range 183-245 K by Bloss et al. [79] resulted in $\sigma = (2.94 \pm 0.86) \times 10^{-18}$ cm^2 $molecule^{-1}$, which is larger by ~25% than the values of (4) and (6). The absorption spectra reported and assigned to ClOOCl by Molina and Molina [543] and Basco and Hunt [48] differ significantly from the rest of the results.

The recommended absorption cross sections listed in Table 4-85 are unchanged from JPL02-25. They are based on the data of DeMore and Tschuikow-Roux at 190-200 nm, and the mean of the data of Cox and Hayman [190], DeMore and Tschuikow-Roux [214], Permien et al. [630], and Burkholder et al. [115] for the wavelength range 200-360 nm. Data at wavelengths greater than 360 nm were obtained from a linear extrapolation of the logarithm of the cross sections, using the expression, $\log (10^{20}\ \sigma(cm^2) = 7.589 - 0.01915\ \lambda(nm)$. For $\lambda > 360$ nm the extrapolated data are considered to be more reliable than experimental measurements because of the very small dimer cross sections in this region.

The absorption studies also indicate that only one stable species is produced in the recombination reaction of ClO with itself, and that this species is dichlorine peroxide, ClOOCl, rather than ClOClO, or $ClClO_2$. Using submillimeter wave spectroscopy, Birk et al. [72] have further established the structure of the recombination product to be ClOOCl. These observations are in agreement with the results of quantum mechanical calculations (McGrath et al. [508, 509]; Jensen and Odershede [379]; Stanton et al. [750]).

Molina et al. [548] reported a quantum yield of approximately unity (1.03 ± 0.12) for the Cl + ClOO pathway from a flash photolysis study at 308 nm, in which the yield of Cl atoms was measured using time-resolved atomic resonance fluorescence. These results are in agreement with the steady-state photolysis study of Cox and Hayman [190]. In a molecular beam/flash-photolysis study Moore et al. [551] measured the relative Cl:ClO product yields from which the branching ratio for both photolysis channels ClOO + Cl and ClO +

ClO was derived: at 248 nm they obtained 0.88 ± 0.07 and 0.12 ± 0.07 respectively, and at 308 nm, 0.90 ± 0.1 and 0.10 ± 0.01. Kalekin and Morokuma [401] studied the photodissociation dynamics and predict the synchronous and sequential formation of 2Cl + O_2 at 308 nm, and three possible fragmentation routes at 248 nm: 2Cl + O_2, Cl + O(^{3}P) + ClO, and 2Cl + 2 O(^{3}P). Similar theoretical calculations were performed by Toniolo et al. [779] for 264, 325 and 406 nm excitation energies, and predict 2Cl + O_2 at all wavelengths with a small yield of 2ClO at the shortest wavelength. Recently Plenge et al. [637] measured the primary products from photolysis of ClO dimer at 250 and 308 nm, using photoionisation mass spectrometry. At both wavelengths exclusively formation of 2Cl + O_2 is observed, corresponding to a primary Cl-quantum yield near unity; at 250 nm $\varphi_{Cl} \geq 0.98$ and at 308 nm $\varphi_{Cl} \geq 0.90$. At both photolysis wavelengths the pathway leading to ClO is not observed, corresponding to $\varphi_{ClO} \leq 0.02$ at 250 nm and $\varphi_{ClO} \leq 0.10$ at 308 nm.

A quantum yield of $\varphi_{Cl} = 1.0$ (± 0.1) is recommended throughout the range at wavelengths below 300 nm, while $\varphi_{Cl} = 0.9$ (± 0.1) is recommended at $\lambda > 300$ nm.

Table 4-85. Absorption Cross Sections of ClOOCl at 195-265 K

λ (nm)	$10^{20}\sigma$(cm^2)	λ (nm)	$10^{20}\sigma$(cm^2)	λ (nm)	$10^{20}\sigma$(cm^2)	λ (nm)	$10^{20}\sigma$(cm^2)
190	565.0	256	505.4	322	23.4	388	1.4
192	526.0	258	463.1	324	21.4	390	1.3
194	489.0	260	422.0	326	19.2	392	1.2
196	450.0	262	381.4	328	17.8	394	1.1
198	413.0	264	344.6	330	16.7	396	1.0
200	383.5	266	311.6	332	15.6	398	0.92
202	352.9	268	283.3	334	14.4	400	0.85
204	325.3	270	258.4	336	13.3	402	0.78
206	298.6	272	237.3	338	13.1	404	0.71
208	274.6	274	218.3	340	12.1	406	0.65
210	251.3	276	201.6	342	11.5	408	0.60
212	231.7	278	186.4	344	10.9	410	0.54
214	217.0	280	172.5	346	10.1	412	0.50
216	207.6	282	159.6	348	9.0	414	0.46
218	206.1	284	147.3	350	8.2	416	0.42
220	212.1	286	136.1	352	7.9	418	0.38
222	227.1	288	125.2	354	6.8	420	0.35
224	249.4	290	114.6	356	6.1	422	0.32
226	280.2	292	104.6	358	5.8	424	0.29
228	319.5	294	95.4	360	5.5	426	0.27
230	365.0	296	87.1	362	4.5	428	0.25
232	415.4	298	79.0	364	4.1	430	0.23
234	467.5	300	72.2	366	3.8	432	0.21
236	517.5	302	65.8	368	3.5	434	0.19
238	563.0	304	59.9	370	3.2	436	0.17
240	600.3	306	54.1	372	2.9	438	0.16
242	625.7	308	48.6	374	2.7	440	0.15
244	639.4	310	43.3	376	2.4	442	0.13
246	642.6	312	38.5	378	2.2	444	0.12
248	631.5	314	34.6	380	2.1	446	0.11
250	609.3	316	30.7	382	1.9	448	0.10
252	580.1	318	28.0	384	1.7	450	0.09
254	544.5	320	25.6	386	1.6		

Note:

190-200nm, DeMore and Tschuikow-Roux [214],
200-360 nm, mean of Cox and Hayman [190], Burkholder et al. [115], Permien et al. [630] and DeMore and Tschuikow-Roux [214],
362-450 nm, extrapolation log (10^{20} σ(cm^2) = 7.589 - 0.01915 λ(nm)

F8. $Cl_2O_3 + h\nu \rightarrow$ Products. The absorption cross sections of Cl_2O_3 have been measured at 293 K and 257.7 nm by Lipscomb et al. [457], at 233 K and 220-335 nm by Hayman and Cox [321], at 200-260 K and 220-320 nm by Burkholder et al. [113], at 223 K and 220-330 nm by Harwood et al. [318], and recently at room temperature and 201-320 nm by Green et al. [301]. Although the shape of the spectrum measured by the different group is in agreement, the cross sections are significantly different. Hayman and Cox [318] report the largest values, whereas the new data of Green et al. [301] are the lowest of all measurements. Particularly the spectrum of Green et al. [301] matches the shape of the spectrum measured by Burkholder et al. [113] more closely that it does those of Harwood et al. [318] or Hayman and Cox [318]. In addition, Burkholder et al. [113] and Green et al. [301] observed no long-wavelength tail in the region 300-450 nm, such as is observed by Harwood et al. [318] and Hayman and Cox [318]. At the maximum of the spectrum the values differ by 30%. Table 4-86 lists the recommended values. These are derived by averaging the spectra of Hayman and Cox [321], Burkholder et al. [113], Harwood et al. [318], and Green et al. [301]. Additional work is needed, particularly in the spectral region beyond 300 nm.

Table 4-86. Absorption cross sections Cl_2O_3 at 220-260 K

λ (nm)	$10^{20}\ \sigma$ (cm^2)	λ (nm)	$10^{20}\ \sigma$ (cm^2)	λ (nm)	$10^{20}\ \sigma$ (cm^2)
220	1145	255	1443	290	763
225	1113	260	1596	295	566
230	1060	265	1661	300	417
235	1028	270	1614	305	294
240	1044	275	1464	310	212
245	1127	280	1239	315	159
250	1271	285	995	320	132

Note:
220-320 nm, mean of the data of Hayman and Cox [321], Burkholder et al. [113], Harwood et al. [318], and Green et al. [301].

F9. $Cl_2O_4 + h\nu \rightarrow$ Products. The absorption cross sections of Cl_2O_4 (dichlorine tetraoxide, chlorine perchlorate) have been measured at room temperature and 200-310 nm by Lopez and Sicre [460] and at 200-350 nm by Green et al. [300]. The absorption spectrum exhibits a weak band between 303 and 350 nm with the maximum at 327 nm, a stronger band between 212 and 303 nm with the maximum at 233 nm, and a further increase of the absorption cross sections below 212 nm. The absorption cross sections reported by Lopez and Sicre [460] and Green et al. [300], who applied a similar method of preparing Cl_2O_4, are in very good agreement in the region ~215-250 nm. Discrepancies are obvious below 215 nm, where the values of Lopez and Sicre [460] become larger by up to a factor ~1.7 at 200 nm than the values of Green et al. [300], and in the region of the weak absorption band, which has not been observed by Lopez and Sicre [460]. We follow the arguments of Green et al. [300] concerning their confidence in the accuracy of their measurements and recommend their results. Green et al. [300] report cross sections, which are the averages over 1-nm intervals of the data obtained at a resolution of 0.34 nm. We select the data for even wavelengths, which are listed in Table 4-87.

Table 4-87. Absorption Cross Sections of Cl_2O_4 at 298 K

λ (nm)	10^{20} σ (cm^2)	λ (nm)	10^{20} σ (cm2)	λ (nm)	10^{20} σ (cm^2)	λ (nm)	10^{20} σ (cm^2)
200	96.81	238	84.94	276	9.95	314	1.35
202	87.88	240	80.97	278	8.38	316	1.49
204	77.84	242	76.05	280	6.98	318	1.62
206	73.24	244	70.95	282	5.76	320	1.74
208	67.51	246	65.17	284	4.70	322	1.83
210	64.62	248	59.53	286	3.79	324	1.91
212	61.79	250	53.84	288	3.03	326	1.96
214	61.74	252	48.55	290	2.40	328	1.98
216	63.46	254	43.30	292	1.89	330	1.96
218	66.58	256	38.52	294	1.50	332	1.92
220	70.82	258	34.33	296	1.21	334	1.85
222	74.95	260	30.28	298	1.01	336	1.75
224	79.70	262	26.63	300	0.88	338	1.63
226	83.84	264	23.55	302	0.83	340	1.50
228	87.21	266	20.58	304	0.83	342	1.36
230	89.19	268	17.97	306	0.88	344	1.23
232	90.06	270	15.81	308	0.97	346	1.11
234	89.67	272	13.62	310	1.08	348	1.02
236	87.86	274	11.77	312	1.21	350	0.98

Note:
200-350 nm, Green et al. [300].

F10. $Cl_2O_6 + h\nu \rightarrow$ Products. The absorption cross sections for Cl_2O_6 (chlorine hexoxide, chloryl perchlorate) have been measured at room temperature and 200-386 nm by Lopez and Sicre [461], at 268 nm by Jansen et al. [369], and at 200-450 nm by Green et al. [300]. A spectrum measured by Goodeve and Richardson [288] and originally attributed to ClO_3, was shown by Lopez and Sicre [461] to be most likely that of Cl_2O_6. The cross sections measured by Lopez and Sicre [461] are several times larger than those reported by Goodeve and Richardson [288], but the shape of the spectrum is similar. There is excellent agreement between the data of Lopez and Sicre [461] and Green et al. [300] at wavelengths between 210 and 310 nm; the data of Green et al. [300] are smaller by ~10% than those of Lopez and Sicre [461] at 200 nm, and become increasingly larger at wavelengths above 320 nm by up to a factor ~ 3 at 380 nm. The absorption curve reported by Green et al. [300] shows a logarithmic decrease at wavelengths 300-390 nm. We recommend the most recent data of Green et al. [300] who report cross sections, which are the averages over 1-nm intervals of the data obtained at a resolution of 0.34 nm. We select the data for even wavelengths, which are listed in Table 4-88.

Table 4-88. Absorption Cross Sections of Cl_2O_6 at 298 K

λ (nm)	10^{20} σ (cm^2)	λ (nm)	10^{20} σ (cm^2)	λ (nm)	10^{20} σ (cm^2)	λ (nm)	10^{20} σ (cm^2)
200	1104	248	1085	296	1173	344	195
202	1135	250	1111	298	1115	346	180
204	1161	252	1142	300	1056	348	167
206	1208	254	1177	302	997	350	153
208	1233	256	1217	304	939	352	141
210	1254	258	1256	306	880	354	130
212	1261	260	1297	308	822	356	121
214	1266	262	1337	310	767	358	111
216	1260	264	1375	312	714	360	103
218	1245	266	1410	314	664	362	96
220	1230	268	1440	316	615	364	89
222	1207	270	1466	318	569	366	81
224	1182	272	1485	320	526	368	75
226	1156	274	1496	322	485	370	71
228	1132	276	1500	324	447	372	66
230	1108	278	1497	326	412	374	61
232	1086	280	1488	328	380	376	57
234	1066	282	1469	330	350	378	52
236	1052	284	1444	332	322	380	49
238	1042	286	1411	334	296	382	46
240	1039	288	1373	336	271	384	43
242	1041	290	1329	338	251	386	40
244	1049	292	1281	340	231	388	37
246	1065	294	1229	342	212	390	36

Note:
200-390 nm, Green et al. [300].

F11. $Cl_2O_7 + h\nu \rightarrow$ Products. The absorption cross sections of chlorine heptoxide have been measured at room temperature and 222-302 nm by Goodeve and Windsor [292] and at 180-310 nm by Lin [454]. There is agreement between the two data sets only near 290 nm. The cross sections reported by Goodeve and Windsor [292] become larger at shorter wavelengths than those reported by Lin [454], larger by up to a factor of more than 4 at 225 nm, and smaller at longer wavelengths by up to a factor ~3 at 300 nm. In Table 4-89 are listed the absorption cross sections of Cl_2O_7 measured by Lin [454].

Table 4-89. Absorption Cross Sections of Cl_2O_7 at 298 K

λ (nm)	10^{20} σ (cm^2)	λ (nm)	10^{20} σ (cm^2)	λ (nm)	10^{20} σ (cm^2)
180	1188	225	79.7	270	3.77
185	908.5	230	61.0	275	2.57
190	674.7	235	45.6	280	1.70
195	475.3	240	34.6	285	1.20
200	322	245	24.7	290	0.705
205	231	250	17.5	295	0.521
210	169	255	12.0	300	0.368
215	132	260	7.74	305	0.203
220	102	265	5.37	310	0.104

Note:
180-310 nm. Lin [454].

F12. $ClClO_2 + h\nu \rightarrow$ Products. The absorption cross sections of chloryl chloride have been measured in the gas phase at room temperature and 220-390 nm with a spectral resolution of 0.4 - 1 nm (and in noble gas matrices at low temperatures) by M ller and Willner [565], and reinvestigated using the same spectrometer between 180 and 390 nm by Jacobs et al. [367]. The spectrum exhibits two absorption maxima at 226 nm ($\sigma = 1.38 \times 10^{-17}$ cm^2 $molecule^{-1}$) and 296 nm ($\sigma = 1.51 \times 10^{-17}$ cm^2 $molecule^{-1}$), two minima at 192 and 261 nm, and a decrease of the cross sections above 300 nm. Absorption cross sections at 5-nm intervals as listed by M ller and Willner [565] are given in Table 4-90. Photolysis experiments of matrix isolated $ClClO_2$ suggest it to

absorb in the visible region, nevertheless cross section between 500 and 800 nm is estimated to be below 10^{-20} cm^2 $molecule^{-1}$.

Table 4-90. Absorption Cross Sections of $ClClO_2$ at 298 K

λ (nm)	10^{20} σ (cm^2)	λ (nm)	10^{20} σ (cm^2)	λ (nm)	10^{20} σ (cm^2)	λ (nm)	10^{20} σ (cm^2)
220	920	265	550	310	1120	355	50
225	1160	270	660	315	870	360	40
230	1270	275	830	320	630	365	40
235	1210	280	1050	325	430	370	30
240	1060	285	1260	330	280	375	30
245	880	290	1430	335	190	380	20
250	720	295	1500	340	120	385	20
255	590	300	1470	345	80	390	20
260	530	305	1330	350	60		

Note: M ller and Willner [565]

F13. $HCl + h\nu \rightarrow H + Cl$ ($^2P_{3/2}$ and $^2P_{1/2}$).

$DCl + h\nu \rightarrow D + Cl$. The absorption cross sections of HCl have been measured at room temperature and 139-207 nm by Romand and Vodar [686] and Romand [684], at 140-200 nm by Myer and Samson [568], at 140-220 nm by Inn [363], at 170-215 nm by Roxlo and Mandl [692], at 132-185 nm by Nee et al. [577], and at 120-230 nm (also for DCl) by Bahou et al. [36] and Cheng et al. [163]. Single absorption cross sections have been measured for 121.6 nm by Vatsa and Volpp [814], for 193 nm by Mo et al. [535], and for 135 nm by Hanf et al. [309]. Absorption cross sections obtained by dipole (e,e) spectroscopy have been reported for the region 8-40 eV (155-31 nm) by Daviel et al. [206]. The spectrum exhibits a broad absorption band between 135 and 230 nm, corresponding to the $A\ ^1\Pi \leftarrow X\ ^1\Sigma^+$ transition, with the maximum at ~154 nm for HCl and ~156 nm for DCl. There is good agreement within the experimental uncertainties among the recent data of Bahou et al. [36] / Cheng et al. [163] with those of Nee et al. [577], and Inn [363]. The values of Bahou et al. [36] / Cheng et al. [163] generally are larger than those of Nee et al. [577], larger by less than 10% at 132-170 nm and larger by less than 25% above 170 nm. Also the values of Bahou et al. [36] / Cheng et al. [163] generally are slightly smaller, by less than 10%, than those of Inn [363] except for the region above 210 nm. The absorption curve of Inn [363], who measured the cross sections at 2.5- nm intervals, seem to have shoulders near 147.5 nm and 160 nm around the distinct maximum at ~155 nm. This is in contrast to the results of Bahou et al. [36] / Cheng et al. [163] obtained at a resolution of 0.1 nm and those of Nee et al. [577] obtained at a resolution of 0.05 nm: their absorption curves show a smooth and continuous behavior around absorption maximum. As recommended absorption cross sections for HCl and DCl we choose the most recent results of Bahou et al. [36] / Cheng et al. [163]. In Table 4-91 are listed averages over 2.5- and 5-nm intervals of their data measured at 0.1-nm resolution as reported by Bahou et al. [36].

Photodissociation of HCl was studied by Matsumi et al. [497-499, 782] and the branching fraction Cl ($^2P_{1/2}$) / (Cl ($^2P_{1/2}$) + Cl ($^2P_{3/2}$)) determined to be 0.33 ± 0.05 at 193 nm and 0.45-0.47 (± 0.04) at 157 nm; Lambert et al. [430] measured branching fractions between 0.47 and 0.33 for eight wavelengths between 193 and 235 nm for HCl; Zhang et al. [880] obtained 0.41 ± 0.01 at 193.3 nm; Regan et al. [668] obtained values between 0.42 and 0.48 for 5 wavelengths in the range 201-210 nm, and Regan et al. [667] values between 0.41 to 0.53 for selected rovibrational states at 235 nm. The latter 4 studies and the results from Liyanage et al. [458] are in good agreement with calculations of Alexander et al. [11].

Table 4-91. Absorption Cross Sections of HCl and DCl at 298 K

λ (nm)	10^{20} σ (cm^2)		λ (nm)	10^{20} σ (cm^2)	
	HCl	DCl		HCl	DCl
135.0	123	45.5	**175.0**	106	87.1
137.5	152	75.9	**177.5**	79.6	58.9
140.0	205	120	**180.0**	58.9	38.5
142.5	238	184	**182.5**	42.3	23.9
145.0	279	248	**185.0**	29.4	14.5
147.5	311	308	**187.5**	20.3	8.80
150.0	334	364	**190.0**	13.8	4.93
152.5	342	393	**195.0**	5.96	1.67
155.0	343	415	**200.0**	2.39	0.485
157.5	327	407	**205.0**	0.903	0.136
160.0	306	367	**210.0**	0.310	0.040
162.5	273	321	**215.0**	0.101	0.011
165.0	240	267	**220.0**	0.030	0.0027
167.5	199	211	**225.0**	0.010	
170.0	163	166	**230.0**	0.0034	
172.5	136	119			

Note:
135-230 nm, Bahou et al. [36]

F14. $HOCl + h\nu \rightarrow OH + Cl$

$HOCl + h\nu \rightarrow HCl + O(^3P)$. The absorption spectrum of HOCl exhibits an intensive singlet-singlet absorption in the near-UV region with a strong maximum near 240 nm (mostly the $2\ ^1A' \leftarrow 1\ ^1A'$ transition), and a weak shoulder near 300 nm (arising from the $1\ ^1A'' \leftarrow 1\ ^1A'$ transition). The absorption cross sections of HOCl vapor have been measured by several groups. Molina and Molina [537] and Knauth et al. [411] produced this species using equilibrium mixtures with Cl_2O and H_2O; their results provided the basis for the earlier recommendation. More recently, Mishalanie et al. [533] and Permien et al. [630] used a dynamic source to generate the HOCl vapor. The cross section values reported by Molina and Molina [537], Mishalanie et al. [533], and Permien et al. [630] are in reasonable agreement between 250 and 330 nm. In this wavelength range, the values reported by Knauth et al. [411] are significantly smaller, e.g., a factor of 4 at 280 nm. Beyond 340 nm, the cross sections of Mishalanie et al. are much smaller than those obtained by the other three groups. At 365 nm, the discrepancy is about an order of magnitude.

Burkholder [108] has remeasured the absorption spectrum of HOCl over the wavelength range 200 to 380 nm, following photolysis of equilibrium mixtures of Cl_2O-H_2O-HOCl. The obtained spectrum displays two absorption maxima at 242 and 304 nm, and is in excellent agreement with the work of Knauth et al. [411], but in poor agreement with the measurements of Mishalanie et al. [533] and Permien et al. [630]. The discrepancies can be attributed mostly to difficulties in correcting the measured absorptions for the presence of Cl_2 and Cl_2O. In the study by Burkholder [108], several control experiments were carried out in order to check the internal consistency of the data. Moreover, Barnes et al. [42] examined the near-UV spectrum of HOCl by monitoring the OH fragments resulting from photodissociation, and revealed a third weak band centered at 387 nm extending down to 480 nm, arising from a weak singlet-triplet transition (Minaev [529]). The recommended cross sections up to 420 nm, calculated from an analytical expression provided by Barnes et al. [42] and based on the values of Burkholder [108] and Barnes et al. [42], are listed in Table 4-92. The work by Jungkamp et al. [400] yields cross section values in excellent agreement with this recommendation for wavelengths < 350 nm.

Molina et al. [549] observed production of OH radicals in the laser photolysis of HOCl around 310 nm, and Butler and Phillips [129] found no evidence for O-atom production at 308 nm, placing an upper limit of ~0.02 for the primary quantum yield for the HCl + O channel. Vogt and Schindler [824] used broadband photolysis in the 290–390 nm wavelength range, determining a quantum yield for OH production of >0.95. Schindler et al. [710] measured the quantum yield for atomic Cl as 1.00 ± 0.05 at 308 nm. These authors also determined the probability P to generate $Cl^*(^2P_{1/2})$ relative to Cl $(^2P_{3/2})$, P = 0.035 ± 0.02 at 308 nm, and P = 0.35 ± 0.02 at 235 nm, in agreement with P = 0.30 ± 0.07 at 236 nm reported by Bell et al. [65]. Fujiwara and Ishiwata [256] determined the relative yield of $OH(^2\Pi_{3/2})$ / $OH(^2\Pi_{1/2})$ to be 2.0 at 266 nm and 1.5 at 355 nm.

Table 4-92. Absorption Cross Sections of HOCl

λ (nm)	10^{20} σ (cm^2)	λ (nm)	10^{20} σ (cm^2)	λ (nm)	10^{20} σ (cm^2)
200	7.18	274	5.26	348	1.55
202	6.39	276	4.94	350	1.43
204	5.81	278	4.74	352	1.33
206	5.46	280	4.64	354	1.24
208	5.37	282	4.62	356	1.17
210	5.54	284	4.68	358	1.11
212	5.98	286	4.79	360	1.06
214	6.68	288	4.95	362	1.02
216	7.63	290	5.13	364	0.985
218	8.81	292	5.33	366	0.951
220	10.2	294	5.52	368	0.919
222	11.6	296	5.71	370	0.888
224	13.2	298	5.86	372	0.855
226	14.7	300	5.99	374	0.822
228	16.2	302	6.08	376	0.786
230	17.5	304	6.12	378	0.748
232	18.7	306	6.12	380	0.708
234	19.6	308	6.07	382	0.667
236	20.2	310	5.97	384	0.624
238	20.5	312	5.84	386	0.580
240	20.6	314	5.66	388	0.535
242	20.3	316	5.45	390	0.491
244	19.8	318	5.21	392	0.447
246	19.0	320	4.95	394	0.405
248	18.1	322	4.67	396	0.364
250	17.0	324	4.38	398	0.325
252	15.8	326	4.09	400	0.288
254	14.6	328	3.79	402	0.254
256	13.3	330	3.50	404	0.222
258	12.1	332	3.21	406	0.194
260	10.9	334	2.94	406	0.168
262	9.73	336	2.68	410	0.144
264	8.68	338	2.44	412	0.124
266	7.75	340	2.22	414	0.105
268	6.94	342	2.02	416	0.089
270	6.25	344	1.84	418	0.075
272	5.69	346	1.69	420	0.063

F15. $ClNO + h\nu \rightarrow Cl + NO$. Nitrosyl chloride has a continuous absorption extending beyond 650 nm. There is good agreement between the work of Martin and Gareis [490] for the 240-to-420-nm wavelength region, of Ballash and Armstrong [38] for the 185 to 540 nm region, of Illies and Takacs [360] for the 190-to-400-nm region, and of Tyndall et al. [792] for the 190-to-350-nm region except around 230 nm, where the values of Ballash and Armstrong are larger by almost a factor of two. Roehl et al. [681] measured the absorption cross sections between 350 and 650 nm at several temperatures between 223 and 343 K. Their room temperature results agree to within 15% with those of Martin and Gareis [490], Ballash and Amstrong [38], and Tyndall et al. [792]. Table 4-93 lists the recommended cross sections: these are taken from the work of Tyndall et al. [792] between 190 and 350 nm (unchanged from the previous recommendation), and from Roehl et al. [681] beyond 350 nm.

The quantum yield for the primary photolytic process has been reviewed by Calvert and Pitts [136]. It is unity over the entire visible and near-ultraviolet bands. Chichinin [167] found evidence of ground state ($^2P_{3/2}$) and excited ($^2P_{1/2}$) atomic chlorine products and measured a relative quantum yield $Cl(^2P_{1/2})/ (Cl(^2P_{1/2}) + Cl(^2P_{3/2}))$ to be 0.88 ± 0.12 at 248 nm and 0.90 ± 0.10 at 351 nm; Felder and Morley [239] obtained 0.80 at 248 nm; Skorokhodov et al. [741] obtained 0.48 ± 0.03 at 212 nm, 0.30 at 235 nm., and 0.52 ± 0.03 at 248 nm.

Table 4-93. Absorption Cross Sections of ClNO

λ (nm)	10^{20} σ (cm^2)	λ (nm)	10^{20} σ (cm^2)	λ (nm)	10^{20} σ (cm^2)	λ (nm)	10^{20} σ (cm^2)
190	4320	246	45.2	302	10.3	370	11.0
192	5340	248	37.7	304	10.5	375	9.95
194	6150	250	31.7	306	10.8	380	8.86
196	6480	252	27.4	308	11.1	385	7.82
198	6310	254	23.7	310	11.5	390	6.86
200	5860	256	21.3	312	11.9	395	5.97
202	5250	258	19.0	314	12.2	400	5.13
204	4540	260	17.5	316	12.5	405	4.40
206	3840	262	16.5	318	13.0	410	3.83
208	3210	264	15.3	320	13.4	415	3.38
210	2630	266	14.4	322	13.6	420	2.89
212	2180	268	13.6	324	14.0	425	2.45
214	1760	270	12.9	326	14.3	430	2.21
216	1400	272	12.3	328	14.6	435	2.20
218	1110	274	11.8	330	14.7	440	2.20
220	896	276	11.3	332	14.9	445	2.07
222	707	278	10.7	334	15.1	450	1.87
224	552	280	10.6	336	15.3	455	1.79
226	436	282	10.2	338	15.3	460	1.95
228	339	284	9.99	340	15.2	465	2.25
230	266	286	9.84	342	15.3	470	2.50
232	212	288	9.71	344	15.1	475	2.61
234	164	290	9.64	346	15.1	480	2.53
236	120	292	9.63	348	14.9	485	2.33
238	101	294	9.69	350	14.2	490	2.07
240	82.5	296	9.71	355	13.6	495	1.78
242	67.2	298	9.89	360	12.9	500	1.50
244	55.2	300	10.0	365	12.0		

F16 $ClNO_2 + h\nu \rightarrow Cl + NO_2$

$ClNO_2 + h\nu \rightarrow ClNO + O$. The absorption cross sections of nitryl chloride, $ClNO_2$, have been measured between 230 and 330 nm by Martin and Gareis [490], between 185 and 400 nm by Illies and Takacs [360], between 270 and 370 nm by Nelson and Johnston [580], by Ganske et al. [260] between 200 and 370 nm, and between 190 and 450 nm by Furlan et al. [258]. The absorption spectrum starts at ~400 nm and shows three broad bands, a weak band at ~300 nm and two stronger bands at ~215 nm and below 185 nm. In the range 220-280 nm weak, but distinct vibrational structure has been observed by Furlan et al. [258]. A major source of discrepancies in the data results from the presence of impurities. Table 4-94 lists the recommended values, which are the mean values of the data of Illies and Takacs [360] (as listed in the paper) and of Furlan et al. [258] (5-nm averages of their high-resolution data).

Nelson and Johnston [580] report a value of 0.93 ± 0.15 for the quantum yield for production of chlorine atoms; they also report a negligible quantum yield for the production of oxygen atoms (< 0.02). Carter et al. [154] reported at 235 nm the formation of NO_2 in the electronic ground state (yield 0.15 ± 0.05) and in the excited state (yield 0.85 ± 0.05).

Table 4-94. Absorption Cross Sections of $ClNO_2$ at 298 K

λ (nm)	10^{20} σ (cm^2)	λ (nm)	10^{20} σ (cm^2)
195	1060	280	20.7
200	445	290	16.3
205	310	300	14.1
210	321	310	12.1
215	339	320	9.40
220	325	330	6.79
225	279	340	4.62
230	221	350	3.05
235	169	360	1.86
240	132	370	1.12
250	90.9	380	0.772
260	58.7	390	0.475
270	33.7	400	0.327

F17. ClONO + hν → Products. Measurements in the near-ultraviolet of the cross sections of chlorine nitrite (ClONO) have been made by Molina and Molina [536]. Their results are listed in Table 4-95. The characteristics of the spectrum and the instability of ClONO strongly suggest that the quantum yield for decomposition is unity. The Cl–O bond strength is only about 20 kcal $mole^{-1}$, so that chlorine atoms are likely photolysis products.

Table 4-95. Absorption Cross Sections of ClONO at 231 K

λ (nm)	10^{20} σ (cm^2)	λ (nm)	10^{20} σ (cm^2)
235	215.0	320	80.3
240	176.0	325	75.4
245	137.0	330	58.7
250	106.0	335	57.7
255	65.0	340	43.7
260	64.6	345	35.7
265	69.3	350	26.9
270	90.3	355	22.9
275	110.0	360	16.1
280	132.0	365	11.3
285	144.0	370	9.0
290	144.0	375	6.9
295	142.0	380	4.1
300	129.0	385	3.3
305	114.0	390	2.2
310	105.0	395	1.5
315	98.1	400	0.6

F18. $ClONO_2$ + hν → Cl + NO_3
$ClONO_2$ + hν → ClO+ NO_2
$ClONO_2$ + hν → $O(^3P)$ + ClONO. The recommended cross sections are taken from the work of Burkholder et al. [118]; the values are listed in Table 4-96, together with the parameters needed to compute their temperature dependency. These values are in very good agreement with those reported by Molina and Molina [538], which provided the basis for the previous recommendation, and which supersedes the earlier work of Rowland et al. [689].

Several groups have investigated the identity of the primary photolytic fragments. Smith et al. [745] report O + ClONO as the most likely products, using endproduct analysis and steady-state photolysis. The results of Chang et al. [157], who employed the very low-pressure photolysis (VLPPh) technique, indicate that the products are Cl + NO_3, with a quantum yield of 1.0 ± 0.2. Adler-Golden and Wiesenfeld [10], using a flash photolysis atomic absorption technique, find O-atoms to be the predominant photolysis product and report a quantum yield for Cl-atom production of less than 4%. Marinelli and Johnston [486] report a quantum yield

for NO_3 production at 249 nm between 0.45 and 0.85, with a most likely value of 0.55; they monitored NO_3 by tunable dye-laser absorption at 662 nm. Margitan [474] used atomic resonance fluorescence detection of O- and Cl-atoms and found the quantum yield at 266 nm and at 355 nm to be 0.9 ± 0.1 for Cl-atom production and ~0.1 for O-atom production, with no discernible difference at the two wavelengths. These results were confirmed by Knauth and Schindler [412], who used end-product analysis to infer the quantum yields from photolysis studies at 265 and 313 nm. Burrows et al. [126] report also Cl and NO_3 as the photolysis products at 254 nm, with a quantum yield of unity within experimental error, and a O atom quantum yield of 0.24. In contrast, Nikolaisen et al. [583] using broadband photolysis found that at $\lambda > 200$ nm the relative branching ratios are 0.61 ± 0.20 for the channel ClO + NO_2 and 0.39 ± 0.20 for the channel Cl + NO_3; in the $\lambda > 300$ nm region the quantum yields are found to be 0.44 ± 0.08 for production of ClO and NO_2 and 0.56 ± 0.08 for production of Cl and NO_3. Minton et al. [532], Nelson et al. [579], and Moore et al. [552] made the first direct measurements of ClO and obtained comparable yields for the Cl + NO_3 and the ClO + NO_2 channels, using a molecular beam technique: at 193, they obtained respectively 0.64 ± 0.08 and 0.36 ± 0.08, at 248 nm 0.54 ± 0.08 and 0.46 ± 0.08, and at 308 nm 0.67 ± 0.06 and 0.33 ± 0.06. These authors found no evidence for channel O + ClONO, and placed an upper limit for this channel of 0.04. Tyndall et al. [791] observed quantum yields of 0.80 ± 0.08 and 0.28 ± 0.12 for Cl and ClO at 308 nm using resonance fluorescence detection methods, and reported a very small $O(^3P)$ yield ≤ 0.05. Ravishankara [657], Goldfarb et al. [287] and Yokelson et al. [857] have studied the photodissociation of $ClONO_2$ at 193, 222, 248 and 308 nm, using both atomic resonance fluorescence and time-resolved absorption methods. They found that Cl and ClO are the two major dissociation products at 222, 248 and 308 nm, whereas at 193 nm, the quantum yield of O atoms became larger than the yield of ClO. At 193, 222, 248 and 308 nm, the yield of Cl was 0.53 ± 0.10, 0.46 ± 0.10, 0.41 ± 0.13 and 0.64 ± 0.20, respectively; the O-atom yield 0.73 ± 0.08, 0.17 ± 0.08, <0.10 and <0.05; and the ClO yield 0.29 ± 0.20, 0.64 ± 0.20, 0.39 ± 0.19 and 0.37 ± 0.19. The yield of NO_3 was also determined by Yokelson et al. [857] as 0.93 ± 0.24 at 352.5 nm, 0.67 ± 0.09 at 308 nm, 0.60 ± 0.09 at 248 nm, and 0.18 ± 0.04 at 193 nm. In addition, they measured the Cl atom yield as 0.73 ± 0.14 at 308 nm, 0.60 ± 0.12 at 248 nm and 0.45 ± 0.08 at 193 nm, and the O atom yield as <0.4 at 248 nm and < 0.9 at 193 nm. Recently, Zou et al. [886] determined absolute quantum yields for the Cl and ClO channels at 235 nm to be 0.42 ± 0.1 and 0.58 ± 0.1, respectively, using molecular beam techniques and TOFMS/REMPI. The recommended quantum yield values for production of Cl + NO_3 (ϕ_1) and ClO + NO_2 (ϕ_2) are given at the bottom of Table 4-96 and are based on the work of Nelson et al. [579], Moore et al. [552], Nickolaisen et al. [583], and Ravishankara [657]. For wavelengths shorter than 308 nm the value of ϕ_1 is 0.6, and for ϕ_2 it is 0.4. For longer wavelengths ϕ_1 increases linearly to 0.9 at 350 nm, with the corresponding decrease in ϕ_2 to 0.1. There is no evidence for production of O + ClONO in the more recent work; the production of O-atoms reported in some of the earlier studies might have resulted from decomposition of excited NO_3. Zou et al. [886] determined the quantum yield of spontaneous decomposition of NO_3 into NO_2 + O to be 0.20, and into NO + O_2 to be 0.006.

Recent work by Nickolaisen et al. [583] indicates that the photodissociation quantum yield is less than unity at wavelengths longer than about 330 nm, because of the formation of a long-lived intermediate that might be quenched under atmospheric conditions (a situation analogous to that of Cl_2O). Additional work is needed to address these issues, which have potentially important atmospheric consequences.

Table 4-96. Absorption Cross Sections and Temperature Coefficients of $ClONO_2$

$\sigma(\lambda, T) = \sigma(\lambda, 296)\ (1 + A1\ (T - 296) + A2\ (T - 296)2)$; T in K

λ (nm)	$10^{20}\sigma(\lambda, 296)$ (cm^2)	A1*) (K^{-1})	A2*) (K^{-1})	λ (nm)	$10^{20}\sigma(\lambda, 296)$ (cm^2)	A1*) (K^{-1})	A2*) (K^{-1})
196	310	9.90 (–5)	–8.38 (–6)	316	1.07	5.07 (–3)	1.56 (–5)
198	294	6.72 (–5)	–8.03 (–6)	318	0.947	5.24 (–3)	1.69 (–5)
200	282	–5.34 (–6)	–7.64 (–6)	320	0.831	5.40 (–3)	1.84 (–5)
202	277	–1.19 (–4)	–7.45 (–6)	322	0.731	5.55 (–3)	2.00 (–5)
204	280	–2.60 (–4)	–7.50 (–6)	324	0.647	5.68 (–3)	2.18 (–5)
206	288	–4.12 (–4)	–7.73 (–6)	326	0.578	5.80 (–3)	2.36 (–5)
208	300	–5.62 (–4)	–8.05 (–6)	328	0.518	5.88 (–3)	2.54 (–5)
210	314	–6.96 (–4)	–8.41 (–6)	330	0.466	5.92 (–3)	2.70 (–5)
212	329	–8.04 (–4)	–8.75 (–6)	332	0.420	5.92 (–3)	2.84 (–5)
214	339	–8.74 (–4)	–9.04 (–6)	334	0.382	5.88 (–3)	2.96 (–5)
216	345	–9.03 (–4)	–9.24 (–6)	336	0.351	5.80 (–3)	3.05 (–5)
218	341	–8.86 (–4)	–9.35 (–6)	338	0.326	5.68 (–3)	3.10 (–5)
220	332	–8.28 (–4)	–9.38 (–6)	340	0.302	5.51 (–3)	3.11 (–5)
222	314	–7.31 (–4)	–9.34 (–6)	342	0.282	5.32 (–3)	3.08 (–5)

λ (nm)	$10^{20}\sigma(\lambda, 296)$ (cm^2)	A1*) (K^{-1})	A2*) (K^{-1})	λ (nm)	$10^{20}\sigma(\lambda, 296)$ (cm^2)	A1*) (K^{-1})	A2*) (K^{-1})
224	291	–6.04 (–4)	–9.24 (–6)	344	0.264	5.07 (–3)	2.96 (–5)
226	264	–4.53 (–4)	–9.06 (–6)	346	0.252	4.76 (–3)	2.74 (–5)
228	235	–2.88 (–4)	–8.77 (–6)	348	0.243	4.39 (–3)	2.42 (–5)
230	208	–1.13 (–4)	–8.33 (–6)	350	0.229	4.02 (–3)	2.07 (–5)
232	182	6.18 (–5)	–7.74 (–6)	352	0.218	3.68 (–3)	1.76 (–5)
234	158	2.27 (–4)	–7.10 (–6)	354	0.212	3.40 (–3)	1.50 (–5)
236	138	3.72 (–4)	–6.52 (–6)	356	0.205	3.15 (–3)	1.27 (–5)
238	120	4.91 (–4)	–6.14 (–6)	358	0.203	2.92 (–3)	1.06 (–5)
240	105	5.86 (–4)	–5.98 (–6)	360	0.200	2.70 (–3)	8.59 (–6)
242	91.9	6.64 (–4)	–6.04 (–6)	362	0.190	2.47 (–3)	6.38 (–6)
244	81.2	7.33 (–4)	–6.27 (–6)	364	0.184	2.22 (–3)	3.66 (–6)
246	71.6	8.03 (–4)	–6.51 (–6)	366	0.175	1.93 (–3)	2.42 (–7)
248	62.4	8.85 (–4)	–6.59 (–6)	368	0.166	1.62 (–3)	–3.62 (–6)
250	56.0	9.84 (–4)	–6.40 (–6)	370	0.159	1.33 (–3)	–7.40 (–6)
252	50.2	1.10 (–3)	–5.93 (–6)	372	0.151	1.07 (–3)	–1.07 (–5)
254	45.3	1.22 (–3)	–5.33 (–6)	374	0.144	8.60 (–4)	–1.33 (–5)
256	41.0	1.33 (–3)	–4.73 (–6)	376	0.138	6.73 (–4)	–1.54 (–5)
258	37.2	1.44 (–3)	–4.22 (–6)	378	0.129	5.01 (–4)	–1.74 (–5)
260	33.8	1.53 (–3)	–3.79 (–6)	380	0.121	3.53 (–4)	–1.91 (–5)
262	30.6	1.62 (–3)	–3.37 (–6)	382	0.115	2.54 (–4)	–2.05 (–5)
264	27.8	1.70 (–3)	–2.94 (–6)	384	0.108	2.25 (–4)	–2.11 (–5)
266	25.2	1.78 (–3)	–2.48 (–6)	386	0.103	2.62 (–4)	–2.11 (–5)
268	22.7	1.86 (–3)	–2.00 (–6)	388	0.0970	3.33 (–4)	–2.08 (–5)
270	20.5	1.94 (–3)	–1.50 (–6)	390	0.0909	4.10 (–4)	–2.05 (–5)
272	18.5	2.02 (–3)	–1.01 (–6)	392	0.0849	5.04 (–4)	–2.02 (–5)
274	16.6	2.11 (–3)	–4.84 (–7)	394	0.0780	6.62 (–4)	–1.94 (–5)
276	14.9	2.20 (–3)**	9.02 (–8)	396	0.0740	8.95 (–4)	–1.79 (–5)
278	13.3	2.29 (–3)	6.72 (–7)	398	0.0710	1.14 (–3)	–1.61 (–5)
280	11.9	2.38 (–3)	1.21 (–6)	400	0.0638	1.38 (–3)	–1.42 (–5)
282	10.5	2.47 (–3)	1.72 (–6)	402	0.0599	1.63 (–3)	–1.20 (–5)
284	9.35	2.56 (–3)	2.21 (–6)	404	0.0568	1.96 (–3)	–8.97 (–6)
286	8.26	2.66 (–3)	2.68 (–6)	406	0.0513	2.36 (–3)	–5.15 (–6)
288	7.24	2.75 (–3)	3.09 (–6)	408	0.0481	2.84 (–3)	–6.64 (–7)
290	6.41	2.84 (–3)	3.41 (–6)	410	0.0444	3.38 (–3)	4.47 (–6)
292	5.50	2.95 (–3)	3.74 (–6)	412	0.0413	3.96 (–3)	1.00 (–5)
294	4.67	3.08 (–3)	4.27 (–6)	414	0.0373	4.56 (–3)	1.60 (–5)
296	4.09	3.25 (–3)	5.13 (–6)	416	0.0356	5.22 (–3)	2.28 (–5)
298	3.57	3.45 (–3)	6.23 (–6)	418	0.0317	5.96 (–3)	3.07 (–5)
300	3.13	3.64 (–3)	7.36 (–6)	420	0.0316	6.70 (–3)	3.87 (–5)
302	2.74	3.83 (–3)	8.38 (–6)	422	0.0275	7.30 (–3)	4.58 (–5)
304	2.39	4.01 (–3)	9.30 (–6)	424	0.0242	7.82 (–3)	5.22 (–5)
306	2.09	4.18 (–3)	1.02 (–5)	426	0.0222	8.41 (–3)	5.95 (–5)
308	1.83	4.36 (–3)	1.11 (–5)	428	0.0207	9.11 (–3)	6.79 (–5)
310	1.60	4.53 (–3)	1.20 (–5)	430	0.0189	9.72 (–3)	7.52 (–5)
312	1.40	4.71 (–3)	1.30 (–5)	432	0.0188	9.96 (–3)	7.81 (–5)
314	1.22	4.89 (–3)	1.42 (–5)				

Notes:

*) (-n) means $x10^{-n}$.

**) Value corrected for an obvious misprint.

Quantum yields:

$$ClONO_2 + h\nu \rightarrow Cl + NO_3$$

$\phi_1 = 0.6$ ($\lambda < 308$ nm)

$\phi_1 = 7.143 \times 10^{-3}\ \lambda\ (nm) - 1.60$ (308 nm $< \lambda <$ 364 nm)

$\phi_1 = 1.0$ ($\lambda > 364$ nm)

$$ClONO_2 + h\nu \rightarrow ClO + NO_2$$

$$\phi_2 = 1 - \phi_1$$

F19. $CCl_4 + h\nu \rightarrow$ Products. The absorption cross sections of CCl_4 have been measured at room temperature and 110–200 nm by Russell et al. [694] and Causley and Russell [156]; at 204–250 nm by Gordus and Bernstein [293]; at 186–226 nm by Rowland and Molina [688]; at 170–230 nm by Roxlo and Mandl [692]; and at 160–275 nm by Hubrich and Stuhl [346]; at 105-210 nm by Ibuki et al. [357]; and at 135 and 195 nm by Hanf et al. [309]; at 297–477 K and 250 nm by Currie et al. [199], at 279 and 296 K and 190–252 nm by Vanlaethem-Meurée et al. [808]; at 225–295 K and 174–250 nm by Simon et al. [734]; and at 220–300 K and 186–240 nm by Prahlad and Kumar [644]. The room temperature data agree within 10% between 190 and 235 nm and within 20% and 40% at 240 and 250 nm (except the value at 250 nm reported by Currie et al [199], which is lower than the half of the other values). The absorption curve based on the data (reported at 0.5-nm intervals) of Prahlad and Kumar [644] shows wiggles over the whole range 186–240 nm obviously due to experimental uncertainties. In the range 180–186 nm, the values reported by Hubrich and Stuhl [346] are higher by up to 25% than those reported by Simon et al. [734], and the value at 186 nm reported by Prahlad and Kumar [644] is lower by 18% than the value of Simon et al. [734]. In the maximum near 176 nm, the absorption cross section is 1.01×10^{-17} cm^2, as reported by Hubrich and Stuhl [346] and Simon et al. [734], whereas the plotted spectrum reported by Roxlo and Mandl [692] shows a lower value of $\sim 7 \times 10^{-18}$ cm^2. For a wavelength of 313 nm, an absorption cross section of $\leq 3.7 \times 10^{-26}$ cm^2 was derived by Rebbert and Ausloos [663] from the C_2H_5Cl yield in the photolysis of CCl_4-C_2H_6 mixtures. The preferred absorption cross sections at room temperature, listed in Table 4-97, are the mean of the values reported by Hubrich and Stuhl [346] and Simon et al. [734] at 174–192 nm, the values of Simon et al. [734] at 194–250 nm, and the data of Hubrich and Stuhl [346] at 255–275 nm. Absorption cross sections obtained by using synchrotron radiation as a tunable photoexcitation source have been reported for the region 4.9-200 nm by Ho [334] and for the region 50-200 nm by Seccombe et al. [718]. Cross sections for the region 6.4-225 nm were obtained by dipole (e,e) spectroscopy by Burton et al. [127].

The temperature dependence of the absorption cross sections becomes significant at wavelengths above 205 nm, where the cross sections decrease with decreasing temperature between 300 and 210 K as observed in good agreement by Simon et al. [734] and Prahlad and Kumar [644]. Simon et al. [734] parameterized the cross sections and the temperature dependence by the polynomial expansion

$$\log_{10} \sigma(\lambda, T) = \sum A_n \lambda^n + (T - 273) \times \sum B_n \lambda^n$$

and reported smoothed values for T = 210, 230, 250, 270, and 295 K, every 2 nm, and at wavelengths corresponding to the wavenumber intervals generally used in stratospheric photodissociation calculations. The parameters An and Bn for the ranges T = 210–300 K and = 194–250 nm are as follows:

$A_0 = -37.104$	$B_0 = 1.0739$
$A_1 = -5.8218 \times 10^{-1}$	$B_1 = -1.6275 \times 10^{-2}$
$A_2 = 9.9974 \times 10^{-3}$	$B_2 = 8.8141 \times 10^{-5}$
$A_3 = -4.6765 \times 10^{-5}$	$B_3 = -1.9811 \times 10^{-7}$
$A_4 = 6.8501 \times 10^{-8}$	$B_4 = 1.5022 \times 10^{-10}$

Quantum yields ≥ 0.9 and ~0.75 for the photodissociative processes $CCl_4 + h\nu \rightarrow CCl_3 + Cl$ at 213.9 nm and $CCl_4 + h\nu \rightarrow CCl_2 + 2Cl$ at 163.3 nm, respectively, were derived from the gas-phase photolysis of CCl_4 in the presence of HCl, HBr, and C_2H_6 by Rebbert and Ausloos [663]. A quantum yield for $Cl^*(^2P_{1/2})$ atom formation in the broad band photolysis of CCl_4, $\Phi(Cl^*) = 0.78 \pm 0.27$, was reported by Clark and Husain [174]. Photolysis of CCl_4 after pulsed laser excitation at 193 and 135 nm resulted in the quantum yields $\Phi(Cl) = 1.1 \pm 0.05$ and $\Phi(Cl^*) = 0.4 \pm 0.02$ (thus $\Phi(Cl + Cl^*) = 1.5 \pm 0.1$) at 193 nm and $\Phi(Cl) = 1.5 \pm 0.07$ and $\Phi(Cl^*) = 0.4 \pm 0.02$ (thus $\Phi(Cl + Cl^*) = 1.9 \pm 0.1$) at 135 nm as reported by Hanf et al. [309].

Table 4-97. Absorption Cross Sections of CCl_4 at 295–298 K

λ (nm)	10^{20} σ (cm^2)	λ (nm)	10^{20} σ (cm^2)	λ (nm)	10^{20} σ (cm^2)
174	956	204	61.0	234	2.20
176	1010	206	57.0	236	1.60
178	982.5	208	52.5	238	1.16
180	806	210	46.9	240	0.830
182	647	212	41.0	242	0.590
184	478.5	214	34.5	244	0.413
186	338.5	216	27.8	246	0.290
188	227	218	22.1	248	0.210
190	145.5	220	17.5	250	0.148
192	99.6	222	13.6	255	0.0661
194	76.7	224	10.2	260	0.0253
196	69.5	226	7.60	265	0.0126
198	68.0	228	5.65	270	0.00610
200	66.0	230	4.28	275	0.00239
202	63.8	232	3.04		

Notes:

174–192 nm: mean of Hubrich and Stuhl [346] and Simon et al. [734]
194–250 nm: Simon et al. [734]
255–275 nm: Hubrich and Stuhl [346].

F20. $CH_3OCl + h\nu \rightarrow CH_3O + Cl$

$CH_3OCl + h\nu \rightarrow CH_2O + HCl$. The absorption cross sections of CH_3OCl have been determined by Crowley et al. [197] in the wavelength range 400-460 nm and by Jungkamp et al. [400] in the range 230-400 nm. The preferred cross sections, listed in Table 4-98, are the mean of the values reported by these two groups. The agreement between the two sets of measurements is excellent at wavelengths longer than 250 nm; at the maximum near 230 nm the results of Jungkamp et al. [400] are about 15% smaller.

Schindler et al. [710] measured the quantum yield $\varphi = 0.95 \pm 0.05$ for the product channel $Cl + CH_3O$ at 308 nm. They also determined an upper limit of < 0.01 for HCl at 248 nm and the ratio $Cl^*(^2P_{1/2})/ Cl(^2P_{1/2})$ following photolysis at 235 and 238 nm to be 1.45 ± 0.05. Krisch et al. [422] used photofragment translational spectroscopy to confirm photodissociation of CH_3OCl at 248 nm resulted in cleavage of only the O-Cl bond and the formation of Cl and CH_3O.

Table 4-98. Absorption Cross Sections of CH_3OCl

λ (nm)	10^{20} σ (cm^2)	λ (nm)	10^{20} σ (cm^2)	λ (nm)	10^{20} σ (cm^2)
230	14.9	290	1.32	350	0.662
232	15.4	292	1.34	352	0.611
234	15.7	294	1.35	354	0.574
236	15.9	296	1.37	356	0.529
238	15.8	298	1.40	358	0.482
240	15.5	300	1.43	360	0.445
242	14.9	302	1.45	362	0.411
244	14.2	304	1.47	364	0.389
246	13.2	306	1.48	366	0.356
248	12.2	308	1.49	368	0.331
250	11.1	310	1.49	370	0.298
252	9.96	312	1.48	372	0.273
254	8.86	314	1.47	374	0.246
256	7.77	316	1.46	376	0.225
258	6.80	318	1.43	378	0.209
260	5.87	320	1.41	380	0.202
262	5.05	322	1.37	382	0.186
264	4.31	324	1.33	384	0.17
266	3.69	326	1.30	386	0.16
268	3.16	328	1.24	388	0.15
270	2.71	330	1.20	390	0.13

λ (nm)	10^{20} σ (cm^2)	λ (nm)	10^{20} σ (cm^2)	λ (nm)	10^{20} σ (cm^2)
272	2.35	332	1.14	392	0.14
274	2.06	334	1.09	394	0.13
276	1.83	336	1.04		
278	1.64	338	0.980		
280	1.53	340	0.918		
282	1.42	342	0.875		
284	1.37	344	0.822		
286	1.33	346	0.760		
288	1.32	348	0.709		

F21. $CHCl_3 + h\nu \rightarrow$ Products. The absorption cross sections of $CHCl_3$ have been measured at room temperature and in the far UV region at 113–182 nm by Lucazeau and Sandorfy [462]; at the Lyman-α line at 121.6 nm by Brownsword et al. [104]; and at 110–200 nm by Russell et al. [694]; at room temperature and 222.7 nm by Gordus and Bernstein [293]; at 160–255 nm by Hubrich and Stuhl [346]; at 279 and 296 K and 190–230 nm by Vanlaethem-Meurée et al. [808]; and at 225–295 K and 174–240 nm by Simon et al. [734]. The room temperature data of Vanlaethem- Meurée et al. [808] and Simon et al. [734] are identical at 190–210 nm and increasingly deviate up to ~15% at 212–240 nm. The data of Hubrich and Stuhl [346] and Simon et al. [734] agree to within 10% between 180 and 234 nm. The discrepancy increases to ~25% in the long-wavelength tail with the values of Hubrich and Stuhl [346] being larger than those of Simon et al. [734]. In the region of the absorption maximum at ~176 nm, there is the largest spread: a cross section of $\sim 5 \times 10^{-18}$ cm^2 was measured by Simon et al. [734] compared with 3.7×10^{-18} cm^2 reported by Hubrich and Stuhl [346] and $<2 \times 10^{-18}$ cm^2 given in a plot by Lucazeau and Sandorfy [462]. We therefore recommend absorption cross sections only for the region above 180 nm. The values, listed in Table 4-99, are the mean of the values reported by Hubrich and Stuhl [346] and Simon et al. [734] for the range 180–240 nm. For the range 242–256 nm, these have been extrapolated ($\log \sigma = -1.2277 - 0.0844\,\lambda$) (in italics).

The temperature dependence of the absorption cross sections becomes significant at wavelengths above 194 nm, where the cross sections decrease with decreasing temperature between 295 and 210 K. Simon et al. [734] parameterized the cross sections and the temperature dependence by the polynomial expansion,

$$\log_{10} \sigma(\lambda, T) = \sum A_n \lambda^n + (T - 273) \times \sum B_n \lambda^n$$

and reported smoothed values for T = 210, 230, 250, 270, and 295 K, every 2 nm, and at wavelengths corresponding to the wavenumber intervals generally used in stratospheric photodissociation calculations. The parameters A_n and B_n for the ranges T = 210–300 K and λ = 190–240 nm are as follows:

$A_0 = 269.80$ $\quad$ $B_0 = 3.7973$
$A_1 = -6.0908$ $\quad$ $B_1 = -7.0913 \times 10^{-2}$
$A_2 = 4.7830 \times 10^{-2}$ $\quad$ $B_2 = 4.9397 \times 10^{-4}$
$A_3 = -1.6427 \times 10^{-4}$ $\quad$ $B_3 = -1.5226 \times 10^{-6}$
$A_4 = 2.0682 \times 10^{-7}$ $\quad$ $B_4 = 1.7555 \times 10^{-9}$

Quantum yields for H atom formation have been measured in the far UV by Brownsword et al. [104], [103]: $\Phi(H) = 0.23 \pm 0.03$ and 0.13 at 121.6 and 157.6 nm, respectively, whereas H atoms could not be detected in the photolysis at 193.3 nm.

Table 4-99. Absorption Cross Sections of $CHCl_3$ at 295–298 K

λ (nm)	10^{20} σ (cm^2)	λ (nm)	10^{20} σ (cm^2)	λ (nm)	10^{20} σ (cm^2)
180	372	206	20.7	232	0.158
182	317	208	15.1	234	0.107
184	248	210	10.7	236	0.0730
186	186	212	7.48	238	0.0503
188	144	214	5.24	240	0.0347
190	113	216	3.60	*242*	*0.0223*
192	89.9	218	2.48	*244*	*0.0151*
194	76.1	220	1.69	*246*	*0.01023*
196	64.2	222	1.13	*248*	*0.00694*
198	53.0	224	0.750	*250*	*0.00470*
200	42.6	226	0.503	*252*	*0.00319*
202	34.4	228	0.342	*254*	*0.00216*
204	27.2	230	0.234	*256*	*0.00147*

Note:

180–240 nm: mean of Hubrich and Stuhl [346] and Simon et al. [734]
242–256 nm: extrapolation of mean of Hubrich and Stuhl [346] and Simon et al. [734] data.

F22. $CH_2Cl_2 + h\nu \rightarrow$ Products. The absorption cross sections of CH_2Cl_2 have been measured at room temperature and 110–200 nm by Russell et al. [694]; at the Lyman-α line at 121.6 nm by Brownsword et al. [104]; at 213 nm by Gordus and Bernstein [293], at 160–255 nm by Hubrich and Stuhl [346]; at 279 and 296 K and 176–216 nm by Vanlaethem-Meurée et al. [808]; and at 225–295 K and 176–220 nm by Simon et al. [734]. The room temperature data of Vanlaethem-Meurée et al. [808] and Simon et al. [734] are nearly identical. The cross sections of Hubrich and Stuhl [346] are up to 12% larger than those of Simon et al. [734] in the 176–206 nm wavelength range, increasing to 50% in the 185–220 nm range. The preferred absorption cross sections, listed in Table 4-100, are the mean of the values reported by Hubrich and Stuhl [346] and Simon et al. [734] at 176–220 nm. For wavelengths above 220 nm, the average of their data at 200–210 nm has been extrapolated ($\log \sigma = -2.1337 - 0.08439\ \lambda$) (in italics) at wavelengths up to 256 nm. The measured values of Hubrich and Stuhl [346] are smaller by up to 7% below 230 nm and become larger by up to 50% between 235 and 255 nm than the extrapolated values.

The temperature dependence of the absorption cross sections becomes significant at wavelengths above 190 nm, where the cross sections decrease with decreasing temperature between 295 and 210 K. Simon et al. [734] parameterized the cross sections and the temperature dependence by the polynomial expansion

$$\log_{10} \sigma(\lambda, T) = \sum A_n \lambda^n + (T - 273) \times \sum B_n \lambda^n$$

and reported smoothed values for T = 210, 230, 250, 270, and 295 K, every 2 nm, and at wavelengths corresponding to the wavenumber intervals generally used in stratospheric photodissociation calculations. The parameters A_n and B_n for the ranges T = 210–300 K and
λ = 176–220 nm are as follows:

$A_0 = -1431.8$	$B_0 = -3.1171$
$A_1 = 27.395$	$B_1 = 6.7874 \times 10^{-2}$
$A_2 = -1.9807 \times 10^{-1}$	$B_2 = -5.5000 \times 10^{-4}$
$A_3 = 6.3468 \times 10^{-4}$	$B_3 = 1.9649 \times 10^{-6}$
$A_4 = -7.6298 \times 10^{-7}$	$B_4 = -2.6101 \times 10^{-9}$

Quantum yields for H atom formation have been measured in the far UV by Brownsword et al. [104], [103]: Φ(H) = 0.28 ± 0.03, 0.23, and 0.002 ± 0.001 at 121.6, 157.6, and 193.3 nm, respectively.

Table 4-100. Absorption Cross Sections of CH_2Cl_2 at 295–298 K

λ (nm)	10^{20} σ (cm^2)	λ (nm)	10^{20} σ (cm^2)	λ (nm)	10^{20} σ (cm^2)
176	186	204	4.41	*232*	*0.0194*
178	182	206	3.07	*234*	*0.0132*
180	173	208	2.13	*236*	*0.00892*
182	156	210	1.45	*238*	*0.00605*
184	135	212	0.978	*240*	*0.00410*
186	110	214	0.651	*242*	*0.00278*
188	84.2	216	0.435	*244*	*0.00188*
190	61.0	218	0.291	*246*	*0.00128*
192	43.9	220	0.190	*248*	*0.000866*
194	30.5	*222*	*0.135*	*250*	*0.000587*
196	20.6	*224*	*0.0918*	*252*	*0.000398*
198	14.1	*226*	*0.0623*	*254*	*0.000270*
200	9.48	*228*	*0.0422*	*256*	*0.000183*
202	6.40	*230*	*0.0286*		

Note:

176–220 nm: mean of Hubrich and Stuhl [346] and Simon et al. [734]
222–256 nm: extrapolation of mean of Hubrich and Stuhl [346] and Simon et al. [734] data.

F23. $CH_3Cl + h\nu \rightarrow$ Products. The absorption cross sections of CH_3Cl have been measured at room temperature and 110–200 nm by Russell et al. [694]; at the Lyman-α line at 121.6 nm by Brownsword et al. [104]; at 171.2 nm by Felps et al. [241]; and at 174–220 nm by Robbins [673]; at 208 and 298 K and 158–235 nm by Hubrich et al. [347]; at 255, 279, and 296 K and 186–216 nm by Vanlaethem-Meurée et al. [808]; and at 225–295 K and 174–216 nm by Simon et al. [734]. The room temperature data generally agree within 10% in the

wavelength range 174–216 nm, those of Vanlaethem-Meurée et al. [808] and Simon et al. [734] are nearly identical. The value at 171 nm of Felps et al. [103] is smaller by ~15% than that of Hubrich et al. [347]. The preferred absorption cross sections, listed in Table 4-101, are the mean of the values reported by Robbins [673], Hubrich et al. [347], and Simon et al. [734] at 174–184 nm, the mean of the values reported by Robbins [673], Hubrich et al. [347], Vanlaethem-Meurée et al. [808], and Simon et al. [734] at 186–216 nm, and the mean of the values reported by Robbins [673] and Hubrich et al. [347] at 218–220 nm. The values for the wavelength range 222–236 nm have been taken from an interpolation (at 2-nm intervals) of the 200–235-nm data of Hubrich et al. [347] ($\log \sigma = -0.24164 - 0.09743\ \lambda$).

The temperature dependence of the absorption cross sections becomes significant at wavelengths above 194 nm, where the cross sections decrease with decreasing temperature between 295 and 210 K. There is very good agreement between the low-temperature values at 250–255 K of Vanlaethem-Meurée et al. [808] and Simon et al. [734]. The latter authors parameterized the cross sections and the temperature dependence by the polynomial expansion $\log_{10} \sigma(\lambda, T) = \Sigma A_n \lambda^n + (T - 273) \times \Sigma B_n \lambda^n$ and reported smoothed values for T = 210, 230, 250, 270, and 295 K, every 2 nm, and at wavelengths corresponding to the wavenumber intervals generally used in stratospheric photodissociation calculations. The parameters A_n and B_n for the ranges T = 210–300 K and λ = 174–216 nm are as follows:

$A_0 = -299.80$ $\quad B_0 = -7.1727$

$A_1 = 5.1047$ $\quad B_1 = 1.4837 \times 10^{-1}$

$A_2 = -3.3630 \times 10^{-2}$ $\quad B_2 = -1.1463 \times 10^{-3}$

$A_3 = 9.5805 \times 10^{-5}$ $\quad B_3 = 3.9188 \times 10^{-6}$

$A_4 = -1.0135 \times 10^{-7}$ $\quad B_4 = -4.9994 \times 10^{-9}$

Note: There was a typographical error in the value for A_3 in JPL02-25 that has been corrected in this evaluation.

Quantum yields for H atom formation have been measured in the far UV by Brownsword et al. [104], [103]: $\Phi(H) = 0.53 \pm 0.05$ 0.29, 0.012 ± 0.006 at 121.6, 157.6, and 193.3 nm, respectively.

Table 4-101. Absorption Cross Sections of CH_3Cl at 295–298 K

λ (nm)	$10^{20}\ \sigma$ (cm^2)	λ (nm)	$10^{20}\ \sigma$ (cm^2)	λ (nm)	$10^{20}\ \sigma$ (cm^2)
174	110	196	3.96	218	0.0345
176	93.9	198	2.68	220	0.0220
178	78.2	200	1.77	*222*	*0.0135*
180	63.6	202	1.13	*224*	*0.00859*
182	46.5	204	0.731	*226*	*0.00549*
184	35.0	206	0.482	*228*	*0.00350*
186	25.8	208	0.313	*230*	*0.00224*
188	18.4	210	0.200	*232*	*0.00143*
190	12.8	212	0.127	*234*	*0.000911*
192	8.84	214	0.0860	*236*	*0.000582*
194	5.83	216	0.0534		

Note:
174–184 nm: mean of Robbins [673], Hubrich et al. [347], and Simon et al. [734]
186–216 nm: mean of Robbins [673], Hubrich et al. [347], Vanlaethem-Meurée et al. [808] and Simon et al. [734]
218–220 nm: mean of Robbins [673] and Hubrich et al. [347]
222–236 nm: extrapolation of Hubrich et al. [347] data.

F24. $CH_3CCl_3 + h\nu \rightarrow$ Products. The absorption cross sections of CH_3CCl_3 have been measured at room temperature and 147 nm by Salomon et al. [699], and at 160–255 nm by Hubrich and Stuhl [346], who corrected (< 10.7%) the absorption cross sections in the range 170–190 nm for the concentration and absorption cross sections of a 1,4-dioxane stabilizer present during the experiments. Measurements at 220–295 K and 182–240 nm were carried out by Vanlaethem-Meurée et al. [810] and at 223–333 K and 160 240 nm by Nayak et al. [573]. The latter authors also measured the absorption cross sections in the liquid phase at 235–260 nm and used a wavelength-shift procedure to convert the liquid-phase data into gas-phase data. The agreement of the room temperature data is within 20% at 165–205 nm (at 160 nm, the value reported by Nayak et al. [573] is larger by 50% than that reported by Hubrich and Stuhl [346]). Between 210 and 240 nm, the data of Vanlaethem-Meurée et al. [810] and Nayak et al. [573] are within 15%, whereas those of Hubrich and Stuhl [346] are larger by 100–150%. The preferred absorption cross sections, listed in Table 4-102, are the mean of the values reported by Hubrich and Stuhl [346] and Nayak et al. [573] at 170–180 nm, the mean of the values reported by Vanlaethem-Meurée et al. [810], Hubrich and Stuhl [346], and

Nayak et al. [573] at 185–205 nm, and the mean of the values reported by Vanlaethem-Meurée et al. [810] and Nayak et al. [573] at 210–240 nm. For wavelengths above 240 nm, the average of their data at 220–240 nm has been extrapolated ($\log \sigma = -1.59792 - 0.08066\ \lambda$) at wavelengths up to 255 nm. The measured values of Hubrich and Stuhl [346] are larger by up to ~140% at 250 nm and smaller by ~80% at 255 nm than the recommended values.

The temperature dependence of the absorption cross sections becomes significant at wavelengths above 210 nm, where the cross sections decrease with decreasing temperature, as observed in good agreement at 333–223 K by Nayak et al. [573] and at 295–210 K by Vanlaethem-Meurée et al. [810]. The latter authors parameterized the cross sections and the temperature dependence by the polynomial expansion $\log_{10} \sigma(\lambda, T) = \sum A_n \lambda^n + (T - 273) \times \sum B_n \lambda^n$ and reported smoothed values for T = 210, 230, 250, 270, and 295 K, every 2 nm, and at wavelengths corresponding to the wavenumber intervals generally used in stratospheric photodissociation calculations. The parameters A_n and B_n for the ranges T = 210–300 K and λ = 182–240 nm reported by Gillotay and Simon [281] are as follows:

$A_0 = 341.085191$ $\quad B_0 = -1.660090$
$A_1 = -7.273362$ $\quad B_1 = 3.079969 \times 10^{-2}$
$A_2 = 5.498387 \times 10^{-2}$ $\quad B_2 = -2.106719 \times 10^{-4}$
$A_3 = -1.827552 \times 10^{-4}$ $\quad B_3 = 6.264984 \times 10^{-7}$
$A_4 = 2.238640 \times 10^{-7}$ $\quad B_4 = -6.781342 \times 10^{-10}$

Table4-102. Absorption Cross Sections of CH_3CCl_3 at 295–298 K

λ (nm)	$10^{20}\ \sigma$ (cm^2)	λ (nm)	$10^{20}\ \sigma$ (cm^2)	λ (nm)	$10^{20}\ \sigma$ (cm^2)
170	406	200	92.1	230	0.717
175	424	205	52.0	235	0.276
180	404	210	25.5	240	0.111
185	301	215	10.9	*245*	*0.0437*
190	212	220	4.47	*250*	*0.0173*
195	147	225	1.82	*255*	*0.00682*

Note:
170–180 nm: mean of Hubrich and Stuhl [346] and Nayak et al. [573]
185–205 nm: mean of Vanlaethem-Meurée et al. [810], Hubrich and Stuhl [346] and Nayak et al. [573]
210–240 nm: mean of Vanlaethem-Meurée et al. [810] and Nayak et al. [573]
245–255 nm: extrapolation of mean of Vanlaethem-Meurée et al. [810] and Nayak et al. [573] data.

F25. $CH_3CH_2Cl + h\nu \rightarrow$ Products. The absorption cross sections of CH_3CH_2Cl have been measured at room temperature and 147 nm by Ichimura et al. [358] and at 160–240 nm by Hubrich and Stuhl [346]. The data of Hubrich and Stuhl [346] are listed in Table 4-103.

Table 4-103. Absorption Cross Sections of CH_3CH_2Cl at 298 K

λ (nm)	$10^{20}\ \sigma$ (cm^2)	λ (nm)	$10^{20}\ \sigma$ (cm^2)	λ (nm)	$10^{20}\ \sigma$ (cm^2)
160	189.0	190	6.85	220	0.0127
165	110.0	195	2.56	225	0.00463
170	70.5	200	1.17	230	0.00117
175	44.4	205	0.375	235	0.000395
180	30.4	210	0.147	240	0.000156
185	13.6	215	0.0433		

Note:
160–240 nm, Hubrich and Stuhl [346].

F26. $CH_3CHClCH_3 + h\nu \rightarrow$ Products. In a compilation of ultraviolet absorption cross sections of halocarbons by Gillotay and Simon [278] results are reported (erroneously) for $CH_3CH_2ClCH_3$, which presumably should be $CH_3CHClCH_3$. The data are listed in Table 4-104.

Table 4-104. Absorption Cross Sections of $CH_3CHClCH_3$ at 295 K

λ (nm)	$10^{20}\ \sigma$ (cm^2)	λ (nm)	$10^{20}\ \sigma$ (cm^2)	λ (nm)	$10^{20}\ \sigma$ (cm^2)
170	31.7	192	4.67	214	0.0965
172	27.0	194	3.49	216	0.0652
174	24.3	196	2.58	218	0.0444
176	22.1	198	1.88	220	0.0308
178	20.3	200	1.34	222	0.0212

λ (nm)	10^{20} σ (cm^2)	λ (nm)	10^{20} σ (cm^2)	λ (nm)	10^{20} σ (cm^2)
180	18.0	202	0.954	224	0.0144
182	15.0	204	0.671	226	0.0107
184	12.2	206	0.463	228	0.00752
186	9.99	208	0.311	230	0.00580
188	7.93	210	0.214		
190	6.06	212	0.144		

Note:

170–230 nm, Gillotay and Simon [278].

F27. $CH_2ClCH_2Cl + h\nu \rightarrow$ Products.

F28. $CH_2ClCH_2CH_2Cl + h\nu \rightarrow$ Products.

F29. $CH_2Cl(CH_2)_2CH_2Cl + h\nu \rightarrow$ Products. Absorption cross sections for these three dichloroalkanes at room temperature and 118–200 nm have been reported by Russell et al. [694].

F30. $COCl_2 + h\nu \rightarrow CO + Cl_2$
$COCl_2 + h\nu \rightarrow COCl + Cl$
$COCl_2 + h\nu \rightarrow CO + 2\ Cl$
$COCl_2 + h\nu \rightarrow CCl_2 + O$. The absorption cross-sections of $COCl_2$ (carbonyl dichloride, phosgene) have been measured at room temperature and 185-226 nm by Chou et al. [170], at 240-280 nm by Okabe [596], at 200-315 nm by Meller et al. [514], at 172-220 nm by J ger et al. [368], at some singular points between 147 and 254 nm by Okabe [599, 600], and Glicker and Okabe [284]; and at 210-295 K and 166-308 nm by Gillotay et al. [282]. The spectrum shows a weak absorption band between 215 and 310 nm with the maximum at ~235 nm and a strong absorption band below 200 nm with the maximum at ~174 nm. The room temperature values reported by the various teams are in very good agreement, generally within 10%; exceptions are the region of the absorption minimum and the region around 200 nm where the values of J ger at al. [368] are lower than those of Gillotay et al. [282] by up to 20%. Around the absorption minimum the values of Chou et al. [170] and Meller et al. [514] are between those of Gillotay et al. [282] and J ger et al. [368].

The preferred absorption cross-sections listed in Table 4-105 as averages over the 500-cm^{-1} intervals used for atmospheric modeling are the values of Gillotay et al. [282] at 168.10-173.15 nm, the mean of the values of Gillotay et al. [282] and J ger et al. [368] at 174.65-182.65 nm, the mean of the values of Chou et al. [170], Gillotay et al. [282], and J ger et al. [368] at 184.35-199.00 nm, the mean of the values of Chou et al. [170], Gillotay et al. [282], Meller et al. [514], and J ger et al. [368] at 201.01-218.59 nm, the mean of the values of Chou et al. [170], Gillotay et al. [282], and Meller et al. [514] at 221.00-226.00 nm, and the mean of the values of Gillotay et al. [282] and Meller et al. [514] at 228.58-305.36 nm.

The temperature dependence becomes significant only in the regions below 175 nm and above 250 nm as reported by Gillotay et al. [282]. The strong absorption band is shifted slightly to shorter wavelengths with deceasing temperature and becomes higher by nearly 20% between 295 and 210 K; in the region above 250 nm the absorption cross-sections become smaller with decreasing temperature, the differences increase up to about 80% at 305 nm.

Phosgene is a useful actinometer in the region 200-280 nm. The photodissociation processes $COCl_2 + h\nu \rightarrow COCl + Cl$ with subsequent decay of $COCl \rightarrow CO + Cl$, produces CO with unity quantum yield (see Okabe, [596], Wijnen, [847], Heicklen [324], Calvert and Pitts [136]).

Table 4-105. Absorption Cross Sections of $COCl_2$ at 294-298 K

λ (nm)	10^{20} σ (cm^2)	λ (nm)	10^{20} σ (cm^2)	λ (nm)	10^{20} σ (cm^2)	λ (nm)	10^{20} σ (cm^2)
168.10	301	193.25	68.8	223.47	12.6	264.92	2.68
170.95	433	195.15	52.1	226.00	13.0	268.50	1.85
173.15	493	197.05	40.6	228.58	13.2	272.12	1.17
174.65	509	199.00	31.7	231.23	13.4	275.88	0.689
176.20	475	201.01	25.7	233.93	13.5	279.74	0.370
177.80	427	203.05	20.7	236.69	13.0	283.70	0.182
179.40	369	205.14	17.2	239.53	12.4	287.78	0.0771
181.00	313	207.26	14.7	242.43	11.5	291.99	0.0298
182.65	261	209.43	13.0	245.41	10.4	296.32	0.0104
184.35	210	211.65	11.9	248.45	9.07	300.77	0.00323
186.05	178	213.89	11.4	251.59	7.75	305.36	0.000964
187.80	137	216.20	11.3	254.79	6.32		
189.60	112	218.59	11.5	258.08	5.02		
191.40	88.9	221.00	12.2	261.45	3.77		

Note:
168.10-173.15 nm, Gillotay et al. [282],
174.65-182.65 nm, mean of Gillotay et al. [282] and J ger et al. [368],
184.35-199.00 nm, mean of Chou et al. [170], Gillotay et al. [282], and J ger et al. [368],
201.01-218.59 nm, mean of Chou et al [170], Gillotay et al. [282], Meller et al. [514], and J ger et al. [368],
221.00-226.00 nm, mean of Chou et al. [170], Gillotay et al. [282], and Meller et al. [514],
228.58-305.36 nm, mean of Gillotay et al. [282] and Meller et al. [514].

F31. COHCl + hν → Products. The absorption spectrum of COHCl (formyl chloride) was measured at room temperature and 239-307 nm by Libuda et al. [448]. The absorption spectrum exhibits a highly structured absorption band with the maximum near 260 nm. In Table 4-106 are listed the averages over 1-nm intervals of the medium-resolution (0.7 nm) data of Libuda et al. [448].

Table 4-106. Absorption Cross Sections of COHCl at 298 K

λ (nm)	10^{20} σ (cm^2)	λ (nm)	10^{20} σ (cm^2)	λ (nm)	10^{20} σ (cm^2)	λ (nm)	10^{20} σ (cm^2)
240	2.76	257	3.92	274	3.53	291	0.624
241	3.36	258	5.03	275	2.30	292	0.605
242	3.41	259	4.45	276	3.28	293	0.342
243	3.32	260	5.46	277	2.38	294	0.431
244	3.03	261	5.09	278	2.09	295	0.303
245	3.53	262	4.66	279	1.89	296	0.275
246	4.01	263	4.54	280	2.22	297	0.184
247	4.64	264	4.03	281	1.06	298	0.165
248	4.44	265	3.83	282	1.98	299	0.178
249	4.27	266	4.72	283	1.36	300	0.0562
250	3.92	267	3.76	284	1.15	301	0.0912
251	4.38	268	4.83	285	1.51	302	0.0805
252	4.57	269	3.79	286	1.00	303	0.0319
253	4.98	270	3.34	287	0.784	304	0.0587
254	5.20	271	3.72	288	0.748	305	0.0275
255	4.59	272	2.68	289	0.880	306	0.0157
256	5.07	273	2.74	290	0.371	307	0.0131

Note:

240-307 nm, Libuda [448].

F32. $COFCl + h\nu \rightarrow COF + Cl$
$COFCl + h\nu \rightarrow COCl + F$
$COFCl + h\nu \rightarrow CO + F + Cl$. The absorption cross-sections of COFCl (carbonyl chlorofluoride, fluorochlorophosgene) have been measured at room temperature and 186-226 nm by Chou et al. [170] and Hermann et al. [328] and at 223, 248, 273, and 298 K and 200-262 nm by by Nölle et al. [589] [591]. The spectrum exhibits monotonically decreasing absorptions cross-sections with increasing wavelengths with a shoulder around 200 nm. The room temperature data of both teams are in excellent agreement in the common wavelength range with differences ≤6%. The preferred absorption cross-sections listed in Table 4-107, the averages over the 500-cm^{-1} intervals used for atmospheric modeling, are the data of Chou et al. [170] and Hermann et al. [328] at 186-199 nm, the mean of the data of Chou et al. [170], Hermann et al. [328] and Nölle et al. [589] [591] at 201 and 203.1 nm, and the data of Nölle et al. [589] [591] at wavelengths above 205 nm.

The study of the temperature dependence by Nölle et al. [589] [591] shows the following effects: a decrease of the absorption cross-section with decreasing temperature from 298 to 223 K was observed above 210 nm, where the difference between the 298- and 223-K values increases with increasing wavelength to about 40% at 260 nm. The reverse effect was observed below 210 nm, where the difference between the 298 and 223 K values increases with decreasing wavelength to about 18% at 201 nm.

The photolysis quantum yields of COFCl were determined at 193 nm using an excimer laser by Hermann et al. [328], at 210, 222.5 and 230 nm using an excimer pumped dye laser system, at 248 nm using an excimer laser, and at 210 nm using a Hg medium pressure lamp by Nölle et al. [591]. The relative distribution of the products CO and COF_2 was shown by Hermann et al. [328] to depend on the total pressure (range 10-to 900 mbar). The apparent quantum yields were taken as the quantum yields for the decomposition into COF + Cl and CO + F + Cl since the parent molecule cannot be reformed (as in the case of COF_2) and COCl is known to be unstable. The quantum yields are as follows:

λ in nm	193	210	222.5	230	248	254
Φ	0.98 ± 0.09	0.85 ± 0.25 (laser)	0.77 ± 0.33	0.71 ± 0.30	0.52 ± 0.14	0.90 ± 0.05 (Hg

lamp)

Table 4-107. Absorption Cross Sections of COFCl at 296-298 K

λ (nm)	10^{20} σ (cm^2)	λ (nm)	10^{20} σ (cm^2)	λ (nm)	10^{20} σ (cm^2)	λ (nm)	10^{20} σ (cm^2)
186.0	15.6	201.0	12.2	218.6	5.79	239.5	0.459
187.8	14.0	203.1	11.9	221.0	4.77	242.4	0.292
189.6	13.4	205.1	11.5	223.5	3.81	245.4	0.178
191.4	12.9	207.3	10.8	226.0	2.93	248.5	0.103
193.2	12.7	209.4	9.91	228.6	2.19	251.6	0.0635
195.1	12.5	211.6	8.96	231.2	1.57	254.8	0.0409
197.0	12.4	213.9	7.90	233.9	1.09	258.1	0.0279
199.0	12.3	216.2	6.84	236.7	0.724	261.4	0.0214

Note:
186.0-199.0 nm, Chou et al. [170] and Hermann et al. [328],
201.0 and 203.1 nm, mean of Chou et al. [170], Hermann et al. [328] and Nölle et al. [591],
205.1-261 4 nm, Nölle et al. [591].

F33. $CFCl_3$ (CFC-11) + hν → Products. The absorption cross sections of $CFCl_3$ have been measured at room temperature and 225 nm by Gordus and Bernstein [293], at 186–226 nm by Rowland and Molina [688], at 174–226 nm by Robbins and Stolarski [674], at 186–209 nm by Greene and Wayne [299]; at 213–296 K and 185–226 nm by Chou et al. [172]; at 208 and 298 K and 158–260 nm by Hubrich et al. [347] and Hubrich and Stuhl [346]; at 255, 279, and 296 K and 190–220 nm by Vanlaethem-Meurée et al. [809]; at 225–295 K and 174–230 nm by Simon et al. [734]; and at 220, 240, and 296 K and 200–238 nm by Mérienne et al. [522]. The room temperature data are in good agreement, generally within 10–15%. Absorption cross sections at 148–225 nm have also been derived from electron energy-loss measurements by Huebner et al. [353], which are up to 30% higher than the values obtained by optical measurements. The preferred absorption cross sections, listed in Table 4-108, are the values of Simon et al. [734] at 174–198 nm, the mean of the values reported by Simon et al. [734] and Mérienne et al. [522] at 200–230 nm, and the data of Hubrich and Stuhl [346] at 235–260 nm. Measurements in the far UV at 60–145 nm have been reported by Gilbert et al. [273], and at 120–200 nm by Doucet et al. [222].

The temperature dependence becomes significant at wavelengths above 185 nm, where the cross sections decrease with decreasing temperature between 296 and 210 K (Hubrich et al. [347] observed such a behavior only above 200 nm). Simon et al. [734] parameterized the temperature dependence of the cross sections by the polynomial expansion $\log_{10} \sigma(\lambda, T) = \Sigma A_n \lambda^n + (T - 273) \times \Sigma B_n \lambda^n$and reported smoothed values for T = 210, 230, 250, 270, and 295 K, every 2 nm, and at wavelengths corresponding to the wavenumber intervals generally used in stratospheric photo- dissociation calculations. Parameters A_n and B_n for the ranges T = 210–300 K and λ = 174–230 nm are as follows:

$A_0 = -84.611$ $B_0 = -5.7912$
$A_1 = 7.9551 \times 10^{-1}$ $B_1 = 1.1689 \times 10^{-1}$
$A_2 = -2.0550 \times 10^{-3}$ $B_2 = -8.8069 \times 10^{-4}$
$A_3 = -4.4812 \times 10^{-6}$ $B_3 = 2.9335 \times 10^{-6}$
$A_4 = 1.5838 \times 10^{-8}$ $B_4 = -3.6421 \times 10^{-9}$

A similar polynomial expansion, $\ln \sigma(\lambda, T) = \Sigma a_n (\lambda - 200)^n + (T - 296) \times \Sigma b_n(\lambda - 200)^n$, for the ranges T = 220–296 K and λ = 200–238 nm was used by Mérienne et al. [522] with the following parameters a_n and b_n:

$a_0 = -41.925548$ $b_0 = 3.58977 \times 10^{-4}$
$a_1 = -1.142857 \times 10^{-1}$ $b_1 = 3.02973 \times 10^{-4}$
$a_2 = -3.12034 \times 10^{-3}$ $b_2 = -1.13 \times 10^{-8}$
$a_3 = 3.6699 \times 10^{-5}$

A quantum yield for $Cl^*(^2P_{1/2})$ atom formation in the broad band photolysis of $CFCl_3$, Φ (Cl*) = 0.79 ± 0.27, was reported by Clark and Husain [174].

Table 4-108. Absorption Cross Sections of $CFCl_3$ at 295–298 K

λ (nm)	10^{20} σ (cm^2)	λ (nm)	10^{20} σ (cm^2)	λ (nm)	10^{20} σ (cm^2)
174	313.0	198	78.0	222	1.72
176	324.0	200	63.2	224	1.17
178	323.5	202	49.1	226	0.790
180	314.0	204	37.3	228	0.532
182	296.0	206	28.1	230	0.354
184	272.0	208	20.4	235	0.132
186	243.0	210	15.1	240	0.0470
188	213.0	212	10.7	245	0.0174
190	179.0	214	7.54	250	0.0066
192	154.0	216	5.25	255	0.0029
194	124.3	218	3.65	260	0.0015
196	99.1	220	2.51		

Note:

174–198 nm: Simon et al. [734]
200–230 nm: mean of Simon et al. [734] and Mérienne et al. [522]
235–260 nm: Hubrich and Stuhl [346].

F34. CF_2Cl_2 (CFC-12) + hν → Products. The absorption cross sections of CF_2Cl_2 have been measured at room temperature and 210 nm by Gordus and Bernstein [293], at 186–216 nm by Rowland and Molina [688], at 174–216 nm by Robbins and Stolarski [674], at 186–206 nm by Greene and Wayne [299]; at 234–442 K and 213.9 nm by Rebbert and Ausloos [664]; at 212, 252, and 296 K and 184–221 nm by Chou et al. [172]; at 208 and 298 K and 159–240 nm by Hubrich et al. [347]; at 255, 279, and 296 K and 190–216 nm by Vanlaethem-Meurée et al. [809]; at 225–295 K and 174–230 nm by Simon et al. [734]; and at 220, 240, and 296 K and 200–231 nm by Mérienne et al. [522]. The room temperature data are in good agreement, generally within 10–15%, except the data of Green and Wayne [299] above 195 nm and the data of Rowland and Molina [688] around 210 nm. Absorption cross sections at 148–218 nm have also been derived from electron energy-loss measurements by Huebner et al. [353], which agree within 10% with the data obtained by optical measurements around the absorption maximum and become higher than the optical data by up to 100% above 196 nm. The preferred absorption cross sections, listed in Table 4-109, are values of Hubrich et al. [347] at 170–172 nm, the mean of the values reported by Hubrich et al. [347] and Simon et al. [734] at 174–178 nm, the values of Simon et al. [734] at 180–198 nm, mean of the values reported by Simon et al. [734] and Mérienne et al. [522] at 200–226 nm, and the data of Mérienne et al. [522] at 228–230 nm. For the range 232–240 nm, absorption curve above 210 nm of Mérienne et al. [522] has been extrapolated ($\log \sigma = 2.1448 - 0.1061\ \lambda$). The measured values of Hubrich et al. [347] are lower by up to ~40% at 240 nm than the extrapolated values.

High-resolution absorption cross section measurements have been carried out by Seccombe et al. [717] between 50 and 150 nm, and by Limao-Vieira et al. [451] between 113 and 225 nm using a synchrotron radiation light source. The results of Limao-Vieira et al. [451] for the absorption band at 170–204 nm are in very good agreement with the recommendation in Table 4-109 (at wavelengths above 204 nm, noise effects become significant). The new cross section measurements for the far UV region from both recent studies significantly improve upon the earlier data of Gilbert et al. [273] for the wavelength range 60–135 nm and of Doucet et al. [222] for the wavelength range 120–200 nm.

The temperature dependence becomes significant at wavelengths above 186 nm, where the cross sections decrease with decreasing temperature between 296 and 210 K.A polynomial expansion, $\ln \sigma(\lambda, T) = \sum a_n (\lambda - 200)^n + (T - 296) \times \sum b_n(\lambda - 200)^n$, for the ranges T = 220–296 K and λ = 200–231 nm was used by Mérienne et al. [522] with the following parameters a_n and b_n:

$$a_0 = -43.8954569 \qquad b_0 = 4.8438 \times 10^{-3}$$
$$a_1 = -2.403597 \times 10^{-1} \qquad b_1 = 4.96145 \times 10^{-4}$$
$$a_2 = -4.2619 \times 10^{-4} \qquad b_2 = -5.6953 \times 10^{-6}$$
$$a_3 = 9.8743 \times 10^{-6}$$

Simon et al. [734] parameterized the temperature dependence of the cross sections by the polynomial expansion $\log_{10} \sigma(\lambda, T) = \sum A_n \lambda^n + (T - 273) \times \sum B_n \lambda^n$. **Note: The parameters reported by Simon et al. contain typographical error(s) that were reproduced in JPL02-25. The correct parameters are not known, and therefore the fitting parameters of Simon et al. are not given in this evaluation.**

A quantum yield for Cl*($^2P_{1/2}$) atom formation in the broad band photolysis of CF_2Cl_2, Φ(Cl*) = 0.75 ± 0.26, was reported by Clark and Husain [174].

Table 4-109. Absorption Cross Sections of CF_2Cl_2 at 295–298 K

λ (nm)	10^{20} σ (cm^2)	λ (nm)	10^{20} σ (cm^2)	λ (nm)	10^{20} σ (cm^2)
170	124.0	194	31.5	218	0.103
172	151.0	196	21.1	220	0.0624
174	168.0	198	13.9	222	0.0381
176	185.5	200	8.71	224	0.0233
178	189.5	202	5.42	226	0.0140
180	179.0	204	3.37	228	0.0090
182	160.0	206	2.06	230	0.0057
184	134.0	208	1.26	*232*	*0.0034*
186	107.0	210	0.762	*234*	*0.0021*
188	82.8	212	0.458	*236*	*0.0013*
190	63.2	214	0.274	*238*	*0.0008*
192	45.50	216	0.163	*240*	*0.0005*

Note:
170–172 nm, Hubrich et al. [347],
174–178 nm, the mean of Hubrich et al. [347] and Simon et al. [734],
180–198 nm, Simon et al. [734],
200–230 nm, mean of Simon et al. [734] and Mérienne et al. [522],
232–240 nm, extrapolation of Mérienne et al. [522] data.

F35. CF_3Cl (CFC-13) + hν → Products. The absorption cross sections of CF_3Cl have been measured at room temperature and 184–203 nm by Chou et al. [171]; at 255, 279, and 296 K and 172–200 nm by Vanlaethem-Meurée et al. [809]; at 208 and 298 K and 160–220 nm by Hubrich and Stuhl [346]; and at 225–295 K and 172–200 nm by Simon et al. [734]. The values of Vanlaethem-Meurée et al. [809] and Simon et al. [734] are identical, the room temperature values of Hubrich and Stuhl [346] deviate from the latter by up to about ±25%, and the data of Chou et al. [171] are always larger by about 15–30% in the region 185–200 nm. The recommended absorption cross sections for CF_3Cl, presented in Table 4-110, are taken from Simon et al. [734] for the range 172–200 nm. The values at 202–220 nm are obtained by extrapolation of the absorption curve above 200 nm (log σ = –5.048 – 0.0834 λ) of Simon et al. [734].

Measurements in the far UV at 65–130 nm have been reported by Gilbert et al. [273] and at 120–160 nm by Doucet et al. [222]. Measurements at the Lyman-α line at 121.6 nm have been carried out by Ravishankara et al. [659].

Temperature effects, if any, could not be detected by Vanlaethem-Meurée et al. [809] and Simon et al. [734], whereas Hubrich and Stuhl [346] report a decrease of the absorption cross sections between 298 and 208 K by 4% at160 nm to 74% at 205 nm. Simon et al. [734] parameterized the cross sections and the temperature dependence of the absorption cross sections by the polynomial expansion

$$\log_{10} \sigma(\lambda, T) = \sum A_n \lambda^n + (T - 273) \times \sum B_n \lambda^n \text{ (with all } B_n = 0),$$

and reported smoothed values for T = 295 K, every 2 nm, and at wavelengths corresponding to the wavenumber intervals generally used in stratospheric photodissociation calculations. The parameters A_n for the ranges T = 210–300 K and λ = 172–200 nm are:

$$A_0 = -1.55.88,\ A_1 = 2.0993,\ A_2 = -1.0486 \times 10^{-2},\ A_3 = 1.6718 \times 10^{-5}.$$

A quantum yield for Cl*($^2P_{1/2}$) atom formation in the broad band photolysis of CF_3Cl, Φ(Cl*) = 0.86 ± 0.29, was reported by Clark and Husain [174].

Table 4-110. Absorption Cross Sections of CF_3Cl at 295 K

λ (nm)	10^{20} σ (cm^2)	λ (nm)	10^{20} σ (cm^2)	λ (nm)	10^{20} σ (cm^2)
172	1.100	190	0.128	*206*	*0.00595*
174	0.970	192	0.0900	*208*	*0.00406*
176	0.825	194	0.0610	*210*	*0.00276*
178	0.681	196	0.0410	*212*	*0.00188*
180	0.542	198	0.0280	*214*	*0.00128*
182	0.425	200	0.0190	*216*	*0.000872*
184	0.326	200	0.0189	*218*	*0.000594*
186	0.244	202	*0.0128*	*220*	*0.000405*
188	0.175	204	*0.00874*		

Note:

172–200 nm, Simon et al. [734],
202–220 nm, extrapolation of Simon et al. [734] data.

F36. $CF_2ClCFCl_2$ (CFC-113) + hν → Products. The absorption cross sections of $CF_2ClCFCl_2$ have been measured at 298 K and 184–224 nm by Chou et al. [171]; at 208 and 298 K and 160–250 nm by Hubrich and Stuhl [346]; and at 225–295 K and 184–230 nm by Simon et al. [733]. The room temperature values agree within about 10% except in the region around 190 nm where the values of Hubrich and Stuhl [346] are smaller by up to 20% than the other values. The preferred absorption cross sections, listed in Table 4-111, are the values of Hubrich and Stuhl [346] at 175–180 nm, a value at 184 nm interpolated between those of Hubrich and Stuhl [346] at 180 nm and Simon et al. [733] at 186 nm, and the values of Simon et al. [733] at 186–230 nm. For the range 232–250 nm, the absorption curve of Simon et al. [733] above 230 nm has been extrapolated ($\log \sigma = -0.9860 - 0.0894\,\lambda$). The measured values of Hubrich and Stuhl [346] are larger than the extrapolated values by ~20–80% at 232–250 nm.

Measurements in the far UV at 110–200 nm have been carried out by Doucet et al. [223].

The temperature dependence becomes significant at wavelengths above 194 nm and below 170 nm, where the cross sections decrease with decreasing temperature. This was observed by Simon et al. [733] at 295–225 K and by Hubrich and Stuhl [346] at 298 and 208 K. Simon et al. [733] parameterized the temperature dependence of the cross sections by the polynomial expansion $\log_{10} \sigma(\lambda, T) = \sum A_n \lambda^n + (T - 273) \times \sum B_n \lambda^n$ and reported smoothed values for T = 210, 230, 250, 270, and 295 K, every 2 nm, and at wavelengths corresponding to the wavenumber intervals generally used in stratospheric photodissociation calculations. The parameters A_n and B_n for the ranges T = 210–300 K and λ = 182–230 nm are as follows:

$A_0 = -1087.9$ $\quad B_0 = 12.493$
$A_1 = 20.004$ $\quad B_1 = -2.3937 \times 10^{-1}$
$A_2 = -1.3920 \times 10^{-1}$ $\quad B_2 = 1.7142 \times 10^{-3}$
$A_3 = 4.2828 \times 10^{-4}$ $\quad B_3 = -5.4393 \times 10^{-6}$
$A_4 = -4.9384 \times 10^{-7}$ $\quad B_4 = 6.4548 \times 10^{-9}$.

Note: There was a typographical error in JPL02-25 for parameter B4 which has been corrected in this evaluation.

Table 4-111. Absorption Cross Sections of $CF_2ClCFCl_2$ at 295–298 K

λ (nm)	10^{20} σ (cm^2)	λ (nm)	10^{20} σ (cm^2)	λ (nm)	10^{20} σ (cm^2)
175	192	204	5.80	228	0.0410
180	155	206	4.00	230	0.0270
184	*123*	208	2.65	232	0.0188
186	104	210	1.80	234	0.0124
188	83.5	212	1.15	236	0.00824
190	64.5	214	0.760	238	0.00546
192	48.8	216	0.505	240	0.00361
194	36.0	218	0.318	242	0.00239
196	26.0	220	0.220	244	0.00159
198	18.3	222	0.145	246	0.00105
200	12.5	224	0.0950	248	0.000696
202	8.60	226	0.0630	250	0.000461

Note:
175–180 nm: Hubrich and Stuhl [346]
184 nm: interpolation: Hubrich and Stuhl and Simon et al.
186–230 nm: Simon et al. [733]
232–250 nm: extrapolation of Simon et al. [733] data.

F37. CF_2ClCF_2Cl (CFC-114) + hν → Products. The absorption cross sections of CF_2ClCF_2Cl have been measured at room temperature and 184–219 nm by Chou et al. [171]; at 208 and 298 K and 160–235 nm by Hubrich and Stuhl [346]; and at 225–295 K and 182–220 nm by Simon et al. [733]. The room temperature values of Simon et al. [733] and Chou et al. [171] agree within 5% except for a hump around 195 nm in the absorption curve reported by Chou et al. [171]. The values of Hubrich and Stuhl [346] are always larger than those of Simon et al. [733], around 190 nm by up to ~40% and between 200 and 220 nm up to ~50% with increasing

wavelength. The recommended absorption cross sections, listed in Table 4-112, are the values of Simon et al. [733] at 172–220 nm. For the range 222–235 nm, the absorption curve above 200 nm of Simon et al. [733] has been extrapolated ($\log \sigma = -1.8233 - 0.00913\ \lambda$). The measured values of Hubrich et al. [346] are larger by ~40% in that range than the extrapolated values.

Measurements at the Lyman-α line at 121.6 nm have been carried out by Ravishankara et al. [659]; and at 110–190 nm by Doucet et al. [223].

The temperature dependence has been observed at wavelengths above 190 nm, where Simon et al. [733] report decreasing cross sections with decreasing temperature 295–210 K. Hubrich and Stuhl [346] report for the range 160–210 nm and between 298 and 208 K a small decrease of the cross sections (generally <10%, except two data points). Simon et al. [733] parameterized the temperature dependence of the cross sections by the polynomial expansion $\log_{10} \sigma(\lambda, T) = \sum A_n \lambda^n + (T - 273) \times \sum B_n \lambda^n$ and reported smoothed values for T = 210, 230, 250, 270, and 295 K, every 2 nm, and at wavelengths corresponding to the wavenumber intervals generally used in stratospheric photodissociation calculations. The parameters A_n and B_n for the ranges T = 210–300 K, λ = 172–220 nm are as follows:

$A_0 = -160.50$	$B_0 = -1.5296$
$A_1 = 2.4807$	$B_1 = 3.5248 \times 10^{-2}$
$A_2 = -1.5202 \times 10^{-2}$	$B_2 = -2.9951 \times 10^{-4}$
$A_3 = 3.8412 \times 10^{-5}$	$B_3 = 1.1129 \times 10^{-6}$
$A_4 = -3.4373 \times 10^{-8}$	$B_4 = -1.5259 \times 10^{-9}$

Table 4-112. Absorption Cross Sections of CF_2ClCF_2Cl at 295 K

λ (nm)	$10^{20}\ \sigma$ (cm^2)	λ (nm)	$10^{20}\ \sigma$ (cm^2)	λ (nm)	$10^{20}\ \sigma$ (cm^2)
172	69.0	194	2.56	216	0.0290
174	55.0	196	1.75	218	0.0190
176	43.0	198	1.20	220	0.0122
178	34.0	200	0.800	*222*	*0.00809*
180	26.2	202	0.540	*224*	*0.00531*
182	19.8	204	0.370	*226*	*0.00349*
184	15.0	206	0.245	*228*	*0.00229*
186	11.0	208	0.160	*230*	*0.00151*
188	7.80	210	0.104	*232*	*0.00099*
190	5.35	212	0.0680	*234*	*0.00065*
192	3.70	214	0.0440	*235*	*0.00053*

Note:
172–220 nm: Simon et al. [733]
222–235 nm: extrapolation of Simon et al. [733] data.

F38. CF_3CF_2Cl (CFC-115) + hν $\rightarrow$ Products. The absorption cross sections of CF_3CF_2Cl have been measured at room temperature and 184–207 nm by Chou et al. [171]; at 208 and 298 K and 160–230 nm by Hubrich and Stuhl [346]; and at 225–295 K and 172–204 nm by Simon et al. [733]. The room temperature data of Simon et al. [733] and Hubrich and Stuhl [346] agree within ~20%, where Hubrich and Stuhl [346] report the larger values over the range 172–204 nm. The data of Chou et al. [171] are larger by up to more than 50% than those of Simon et al. [733]. The preferred absorption cross sections, listed in Table 4-113, are the mean of the values reported by Hubrich and Stuhl [346] and Simon et al. [733] at 172–204 nm. The mean of the values measured by Hubrich and Stuhl [346] and those obtained by extrapolating the absorption curve of Simon et al. [733] ($\log \sigma = -6.2191 - 0.0756\ \lambda$) were taken for the range 205–230 nm (the extrapolated values become larger by up to nearly 50% with increasing wavelength than the measured values of Hubrich and Stuhl [346]).

Measurements at the Lyman-α line at 121.6 nm have been carried out by Ravishankara et al. [659]; and at 120–175 nm by Doucet et al. [223].

Temperature effects, if any, could not be detected for this highly fluorinated species. Simon et al. [733] parameterized the absorption cross sections by the polynomial expansion

$\log_{10} \sigma(\lambda, T) = \sum A_n \lambda^n + (T - 273) \times \sum B_n \lambda^n$ (with all $B_n = 0$),

and reported smoothed values for T = 295 K, every 2 nm, and at wavelengths corresponding to the wavenumber intervals generally used in stratospheric photodissociation calculations. The parameters A_n for the ranges T = 210–300 K and λ = 172–204 nm are

$$A_0 = 5.8281,\ A_1 = -2.990 \times 10^{-1},\ A_2 = 1.3525 \times 10^{-3},\ A_3 = -2.6851 \times 10^{-6}.$$

Note: There were typographical errors in JPL02-25 for parameters A_1 and A_2 which have been corrected in the present evaluation.

Table 4-113. Absorption Cross Sections of CF_3CF_2Cl at 295–298 K

λ (nm)	10^{20} σ (cm^2)	λ (nm)	10^{20} σ (cm^2)	λ (nm)	10^{20} σ (cm^2)
172	5.50	188	0.403	204	0.0218
174	4.13	190	0.287	*205*	*0.0187*
176	3.08	192	0.203	*210*	*0.00700*
178	2.25	194	0.143	*215*	*0.00273*
180	1.58	196	0.0985	*220*	*0.00107*
182	1.13	198	0.0685	*225*	*0.00046*
184	0.790	200	0.0474	*230*	*0.00018*
186	0.563	202	0.0325		

Note:
172–204 nm: mean of Hubrich and Stuhl [346] and Simon et al. [733]
205–230 nm: mean of Hubrich and Stuhl [346] and extrapolated Simon et al. [733] data.

F39. $CHFCl_2$ (HCFC-21) + hν → Products. The absorption cross sections of $CHFCl_2$ have been measured at room temperature and 208 nm by Gordus and Bernstein [293]; at 174–222 nm by Robbins and Stolarski [674]; at 184–205 nm by and Green and Wayne [299]; and at 213.9 nm by Rebbert et al. [666]; at 208 and 298 K and 158–235 nm by Hubrich et al. [347]; and at 225–295 K and 174–222 nm by Simon et al. [734]. The results of these groups (except those of Green and Wayne [299] which deviate strongly) are in good agreement, generally within 15%, although the data of Hubrich et al. [347] show humps around 205 and 220 nm, where the agreement is only ~40%. The preferred absorption cross sections, listed in Table 4-114, are the values of Simon et al. [734] at 174–222 nm. For the range 224–236 nm, the absorption curve above 200 nm of Simon et al. [734] has been extrapolated ($\log \sigma = 0.9806 - 0.1014\,\lambda$). The measured values of Hubrich et al. [347] deviate from the extrapolated values by up to ~–20% and +50%.

Measurements in the far UV at 60–120 nm have been reported by Gilbert et al. [273], measurements at 120–200 nm by Doucet et al. [222], and a measurement at 147 nm by Rebbert et al. [666].

The temperature dependence becomes significant at wavelengths above 190 nm, where the cross sections decrease with decreasing temperature between 296 and 210 K. Simon et al. [734] parameterized the temperature dependence of the cross sections by the polynomial expansion

$$\log_{10} \sigma(\lambda, T) = \sum A_n \lambda^n + (T - 273) \times \sum B_n \lambda^n$$

and reported smoothed values for T = 210, 230, 250, 270, and 295 K, every 2 nm, and at wavelengths corresponding to the wavenumber intervals generally used in stratospheric photodissociation calculations. The parameters A_n and B_n for the ranges T = 210–300 K and λ = 174–222 nm are as follows:

$A_0 = -514.56$ $\quad$ $B_0 = -3.0577$
$A_1 = 8.7940$ $\quad$ $B_1 = 6.6539 \times 10^{-2}$
$A_2 = -5.6840 \times 10^{-2}$ $\quad$ $B_2 = -5.3964 \times 10^{-4}$
$A_3 = 1.5894 \times 10^{-4}$ $\quad$ $B_3 = 1.9322 \times 10^{-6}$
$A_4 = 1.6345 \times 10^{-7}$

Table 4-114. Absorption Cross Sections of $CHFCl_2$ at 295–298 K

λ (nm)	10^{20} σ (cm^2)	λ (nm)	10^{20} σ (cm^2)	λ (nm)	10^{20} σ (cm^2)
174	166.0	198	8.10	222	0.0319
176	164.5	200	5.24	*224*	*0.0195*
178	155.0	202	3.35	*225*	*0.0154*
180	138.0	204	2.12	*226*	*0.0122*
182	116.0	206	1.34	*228*	*0.00766*
184	92.4	208	0.836	*230*	*0.00480*
186	71.5	210	0.522	*232*	*0.00301*
188	53.2	212	0.325	*234*	*0.00189*
190	38.4	214	0.203	*235*	*0.00150*
192	26.9	216	0.127	*236*	*0.00119*
194	18.4	218	0.0797		
196	12.3	220	0.0503		

Note:
174–222 nm: Simon et al. [734]
224–236 nm: extrapolation of Simon et al. [734] data.

F40. CHF_2Cl (HCFC-22) + hν → Products. The absorption cross sections of CHF_2Cl have been measured at room temperature and 174–202 nm by Robbins and Stolarski [674] and at 181–194 nm by Green and Wayne [299]; at 208 K and 298 K and 158–220 nm by Hubrich et al. [347], and at 225–295 K and 174–204 nm by Simon et al. [734]. The results of Robbins and Stolarski [674], Hubrich et al. [347], and Simon et al. [734] are in good agreement generally within 15–20%, however those of Green and Wayne [299] deviate strongly. The preferred absorption cross sections, listed in Table 4-115, are the values of Hubrich et al. [347] at 170–172 nm and the values of Simon et al. [734] at 174–204 nm. For the range 206–220 nm, the absorption curve above 190 nm of Simon et al. [734] has been extrapolated ($\log \sigma = -4.1001 - 0.0870\ \lambda$). The measured values of Hubrich et al. [347] deviate from the extrapolated values by up to 20%.

Measurements in the far UV at 60–160 nm have been reported by Gilbert et al. [273], and measurements at 120–200 nm by Doucet et al. [222].

A weak temperature dependence has been observed above 190 nm, where the cross sections decrease with decreasing temperature between 296 and 210 K. Simon et al. [734] parameterized the cross sections and the temperature dependence by the polynomial expansion

$$\log_{10} \sigma(\lambda, T) = \sum A_n \lambda^n + (T - 273) \times \sum B_n \lambda^n$$

and reported smoothed values for T = 210, 230, 250, 270, and 295 K, every 2 nm, and at wavelengths corresponding to the wavenumber intervals generally used in stratospheric photodissociation calculations. The parameters A_n and B_n for the ranges T = 210–300 K and λ = 174–204 nm are as follows:

$A_0 = -106.029$ $\quad B_0 = -1.3399 \times 10^{-1}$
$A_1 = 1.5038$ $\quad B_1 = 2.7405 \times 10^{-3}$
$A_2 = -8.2476 \times 10^{-3}$ $\quad B_2 = -1.8028 \times 10^{-5}$
$A_3 = 1.4206 \times 10^{-5}$ $\quad B_3 = 3.8504 \times 10^{-8}$

Table 4-115. Absorption Cross Sections of CHF_2Cl at 295–298 K

λ (nm)	10^{20} σ (cm^2)	λ (nm)	10^{20} σ (cm^2)	λ (nm)	10^{20} σ (cm^2)
170	12.9	188	0.372	*206*	*0.00842*
172	9.79	190	0.245	*208*	*0.00636*
174	5.72	192	0.156	*210*	*0.00426*
176	4.04	194	0.103	*212*	*0.00285*
178	2.76	196	0.072	*214*	*0.00191*
180	1.91	198	0.048	*216*	*0.00128*
182	1.28	200	0.032	*218*	*0.00086*
184	0.842	202	0.0220	*220*	*0.00057*
186	0.576	204	0.0142		

Note:
170–172 nm: Hubrich et al. [347]
174–204 nm: Simon et al. [734]
206–220 nm: extrapolation of Simon et al. [734] data.

F41. CH_2FCl (HCFC-31) + hν → Products. The absorption cross sections of CH_2FCl have been measured at 208 and 298 K and 160–230 nm by Hubrich and Stuhl [346]. The room temperature data at 160–230 nm are listed in Table 4-116.

Measurements in the far UV at 60–120 nm have been reported by Gilbert et al. [273], and measurements at 120–200 nm by Doucet et al. [222].

Table 4-116. Absorption Cross Sections of CH_2FCl at 298 K

λ (nm)	10^{20} σ (cm^2)	λ (nm)	10^{20} σ (cm^2)	λ (nm)	10^{20} σ (cm^2)
160	47.9	185	4.20	210	0.0188
165	55.9	190	1.95	215	0.00560
170	43.0	195	0.544	220	0.00215
175	23.3	200	0.209	225	0.00049
180	12.5	205	0.069	230	0.00026

Note:
160–230 nm: Hubrich and Stuhl [346].

F42. CF_3CHCl_2 (HCFC-123) + hν → Products. The absorption cross sections of CF_3CHCl_2 have been measured at room temperature and 185–204 nm by Green and Wayne [299]; at 225–295 K and 170–250 nm by Gillotay and Simon [279]; at 203–295 K and 190–230 nm by Orlando et al. [607]; and at 223–333 K and 160–230 nm by Nayak et al. [572]. The agreement between the results of the latter three groups is within 25% in the region below 220 nm. The results of Green and Wayne [299] are very different below 200 nm. The preferred absorption cross sections at 295 K, listed in Table 4-117, are the mean of the values reported by Gillotay and Simon [279] and Nayak et al. [572] at 170–188 nm and the mean of the values reported by Gillotay and Simon [279], Orlando et al. [607], and Nayak et al. [572] at 190–230 nm. For the range 232–250 nm, the absorption curve above 210 nm of Orlando et al. [607] has been extrapolated ($\log \sigma = -3.1097 - 0.0794\,\lambda$).

The studies of the temperature dependence show a decrease of the absorption cross sections with decreasing temperature at wavelengths above 178–180 nm and below 170 nm. Between 170–180 nm, the reverse behavior was observed by Gillotay and Simon [279] and Nayak et al. [572]. An irregular temperature dependence was reported by Orlando et al. [607] for the range 210–230 nm, where the absorption curves show wiggles.

Various parameterized fits, i.e., polynomial expansions of the logarithm of the absorption cross section, have been proposed for the temperature dependence. Gillotay and Simon [279] parameterized the cross sections and the temperature dependence by the polynomial expansion $\log_{10} \sigma(\lambda, T) = \sum A_n \lambda^n + (T - 273) \times \sum B_n \lambda^n$ and reported smoothed values for T = 210, 230, 250, 270, and 295 K, every 2 nm, and at wavelengths corresponding to the wavenumber intervals generally used in stratospheric photodissociation calculations. The parameters A_n and B_n for the ranges T = 210–300 K and λ = 182–250 nm are as follows:

$A_0 = -513.996354$ $\quad B_0 = 1.757133$

$A_1 = 9.089141$ $\quad B_1 = -3.499205 \times 10^{-2}$

$A_2 = -6.136794 \times 10^{-2}$ $\quad B_2 = 2.593563 \times 10^{-4}$

$A_3 = 1.814826 \times 10^{-4}$ $\quad B_3 = -8.489357 \times 10^{-7}$

$A_4 = -1.999514 \times 10^{-7}$ $\quad B_4 = 1.037756 \times 10^{-9}$.

Nayak et al. [572] report sixth-order polynomial coefficients for the functions $\log_{10}(\sigma_T) = \sum C_n (\lambda - 170)^n$ at T = 223, 233, 253, 273, 295, 313, and 333 K and for the range 160–230 nm. The parameters C_n are as follows:

	223 K	273 K	295 K	333 K
C_0	–17.6732	–17.6773	–17.6792	–17.6722
C_1	1.70233×10^{-2}	1.3636×10^{-2}	1.19392×10^{-2}	9.07941×10^{-3}
C_2	-7.39366×10^{-4}	-4.98553×10^{-4}	-3.71661×10^{-4}	-1.29566×10^{-4}
C_3	-1.83761×10^{-4}	-1.70566×10^{-4}	-1.61218×10^{-4}	-1.56667×10^{-4}
C_4	7.80778×10^{-6}	6.73373×10^{-6}	6.03101×10^{-6}	5.56409×10^{-6}
C_5	-1.29836×10^{-7}	-1.02726×10^{-7}	-8.76762×10^{-8}	-7.77379×10^{-8}
C_6	8.05415×10^{-10}	5.66688×10^{-10}	4.61745×10^{-10}	3.93859×10^{-10}

A double expansion in terms of twelve parameters, $\ln \sigma(\lambda, T) = \sum (\sum a_{ij} (T-245.4)^{j-1}) (\lambda - 206.214)^{i-1}$, i = 1–4,
j = 1–3, T = 203–295 K, λ = 190–230 nm, was used by Orlando et al. [607]:

$a_{11} = -4.500 \times 10^{1}$	$a_{12} = 3.529 \times 10^{-3}$	$a_{13} = -4.181 \times 10^{-8}$
$a_{21} = -1.985 \times 10^{-1}$	$a_{22} = 6.826 \times 10^{-5}$	$a_{23} = 1.555 \times 10^{-6}$
$a_{31} = -2.802 \times 10^{-4}$	$a_{32} = -1.018 \times 10^{-5}$	$a_{33} = 4.037 \times 10^{-8}$
$a_{41} = 6.312 \times 10^{-5}$	$a_{42} = -3.055 \times 10^{-7}$	$a_{43} = -2.473 \times 10^{-9}$

Note: There was a typographical error in JPL02-25 for parameter a_{11} which has been corrected in this evaluation.

Table 4-117. Absorption Cross Sections of CF_3CHCl_2 at 295 K

λ (nm)	10^{20} σ (cm^2)	λ (nm)	10^{20} σ (cm^2)	λ (nm)	10^{20} σ (cm^2)
170	192	198	17.1	226	0.0880
172	207	200	11.9	228	0.0599
174	214	202	8.24	230	0.0451
176	213	204	5.70	*232*	*0.0295*
178	202	206	3.89	*234*	*0.0205*
180	184	208	2.67	*236*	*0.0142*
182	161	210	1.82	*238*	*0.0098*
184	135	212	1.23	*240*	*0.0068*
186	109	214	0.838	*242*	*0.0047*
188	85.5	216	0.573	*244*	*0.0033*
190	62.2	218	0.384	*246*	*0.0023*
192	46.4	220	0.266	*248*	*0.0016*
194	33.9	222	0.180	*250*	*0.0011*
196	24.2	224	0.124		

Note: 170–188 nm: mean of the values of Gillotay and Simon [279] and Nayak et al. [572]
190–230 nm: mean of the values of Gillotay and Simon [279], Orlando et al. [607], and Nayak et al. [572]
232–250 nm: extrapolation of Orlando et al. [607] data.

F43. CF_3CHFCl (HCFC-124) + hν → Products. The absorption cross sections of CF_3CHFCl have been measured at 203–295 K and 190–230 nm by Orlando et al. [607]; and at 210–295 K and 170–230 nm by Gillotay and Simon [280]. The agreement is better than 10% between 190 and 220 nm, whereas above 220 nm the values of Orlando et al. [607] become increasingly larger by up to 133% than those of Gillotay and Simon [280]. The preferred room temperature values, listed in Table 4-118, are the values of Gillotay and Simon [280] at 170–188 nm and 222–230 nm and the mean of the values reported by Gillotay and Simon [280] and Orlando et al. [607] at 190–220 nm.

The temperature dependence of the cross sections has been measured by both groups and a decrease of the absorption cross sections with decreasing temperature was observed at 170–230 nm by Gillotay and Simon [280] and at 190–215 nm by Orlando et al. [607]. An irregular temperature behavior was reported by Orlando et al. [607] for the range 215–230 nm, where the absorption curves show wiggles. Parameterized fits, i.e., polynomial expansions of the logarithm of the absorption cross section, have been derived. Gillotay and Simon [280] parameterized the cross sections and the temperature dependence by the polynomial expansion

$$\log_{10} \sigma(\lambda, T) = \sum A_n \lambda^n + (T - 273) \times \sum B_n \lambda^n$$

and reported smoothed values for T = 210, 230, 250, 270, and 295 K, every 2 nm, and at wavelengths corresponding to the wavenumber intervals generally used in stratospheric photodissociation calculations. The parameters A_n and B_n for the ranges T = 210–300 K and λ = 170–230 nm are as follows:

$A_0 = -101.230250$ $\quad B_0 = -5.795712 \times 10^{-2}$
$A_1 = 1.333519$ $\quad B_1 = 1.053901 \times 10^{-3}$
$A_2 = -6.888672 \times 10^{-3}$ $\quad B_2 = -6.530379 \times 10^{-6}$
$A_3 = 1.114172 \times 10^{-5}$ $\quad B_3 = 1.382056 \times 10^{-8}$

A double expansion in terms of twelve parameters, $\ln \sigma(\lambda, T) = \sum (\sum a_{ij} (T-251.7)^{j-1}) (\lambda - 206.214)^{i-1}$, i = 1–4, j = 1–3, T = 203–295 K, λ = 190–230 nm, was used by Orlando et al. [607]:

$a_{11} = -4.967 \times 10^{1}$ $\quad a_{12} = 6.562 \times 10^{-3}$ $\quad a_{13} = 1.735 \times 10^{-5}$
$a_{21} = -2.025 \times 10^{-1}$ $\quad a_{22} = 2.788 \times 10^{-4}$ $\quad a_{23} = -3.974 \times 10^{-6}$
$a_{31} = 6.839 \times 10^{-4}$ $\quad a_{32} = 5.523 \times 10^{-6}$ $\quad a_{33} = -3.092 \times 10^{-7}$
$a_{41} = 1.275 \times 10^{-4}$ $\quad a_{42} = -2.959 \times 10^{-7}$ $\quad a_{43} = -1.182 \times 10^{-8}$

Note: There was a typographical error in JPL02-25 for parameter a_{11} which has been corrected in this evaluation.

Table 4-118. Absorption Cross Sections of CF_3CHFCl at 295 K

λ (nm)	10^{20} σ (cm^2)	λ (nm)	10^{20} σ (cm^2)	λ (nm)	10^{20} σ (cm^2)
170	13.6	192	0.548	214	0.00859
172	11.1	194	0.387	216	0.00610
174	8.85	196	0.267	218	0.00431
176	6.93	198	0.185	220	0.00312
178	5.33	200	0.128	222	0.00214
180	4.03	202	0.0868	224	0.00153
182	3.00	204	0.0594	226	0.00111
184	2.20	206	0.0401	228	0.00082
186	1.60	208	0.0269	230	0.00061
188	1.14	210	0.0186		
190	0.772	212	0.0126		

Note:
170–188 nm, Gillotay and Simon [280],
190–220 nm, mean of the values of Gillotay and Simon [280] and Orlando et al. [607],
222–230 nm, Gillotay and Simon [280].

F44. CF_3CH_2Cl (HCFC-133) + hν → Products. The absorption cross sections of CF_3CH_2Cl have been measured at room temperature and 147 nm (σ = 1.35 × 10^{-17} cm^2) by Ichimura et al. [359], and 186–203 nm by Green and Wayne [299], and at 208 and 298 K and 160–245 nm by Hubrich and Stuhl [346]. There is no good agreement between the results at wavelengths above 180 nm. Table 4-119 gives the recommended room temperature data of Hubrich and Stuhl [346].

Table 4-119. Absorption Cross Sections of CF_3CH_2Cl at 298 K

λ (nm)	10^{20} σ (cm^2)	λ (nm)	10^{20} σ (cm^2)	λ (nm)	10^{20} σ (cm^2)
160	59.4	190	6.20	220	0.0887
165	64.6	195	2.95	225	0.0226
170	56.4	200	1.14	230	0.0147
175	37.3	205	0.598	235	0.00404
180	22.8	210	0.328	240	0.00181
185	11.6	215	0.169	245	0.00054

Note:
160–245 nm, Hubrich and Stuhl [346].

F45. CH_3CFCl_2 (HCFC-141b) + hν → Products. The absorption cross sections of CH_3CFCl_2 have been measured at 210–295 K and 170–240 nm by Gillotay and Simon [279]; at 203–295 K and 190–230 nm by Orlando et al. [607] (data of Orlando et al. reported by Gillotay and Simon [281]); at 203–295 K and 190–230 nm by Talukdar et al. [764]; and at room temperature and 190–240 nm by Fahr et al. [232], who investigated the spectrum both for the gas and liquid phases and used a wavelength-shift procedure to convert the liquid-phase data into gas-phase data. The agreement between the values reported by Gillotay and Simon [279] and Fahr et al. [232] for the 190–240-nm region is very good (1–10% up to 236 nm); the results of Orlando et al. [607] are also in good agreement with these, but only in the region 190–210 nm. The agreement of the results of Talukdar et al. [764] is not as good, their absorption cross sections become smaller below 210 nm by up to ~20% and become larger above 210 nm by up to about 70% than the above mentioned data. The preferred absorption cross sections, listed in Table 4-120, are the values of Gillotay and Simon [279] at 170–188 nm and the mean of the values reported by Gillotay and Simon [279] and Fahr et al. [232] at 190–240 nm.

A decrease of the absorption cross sections with decreasing temperature at wavelengths above 188 nm and below 172 nm and the reverse behavior between 172 and 188 nm was observed by Gillotay and Simon [279]. They parameterized the cross sections and the temperature dependence of the absorption cross sections using the polynomial expansion $\log_{10}$

$\sigma(\lambda, T) = \sum A_n \lambda^n + (T - 273) \times \sum B_n \lambda^n$. They derived the parameters

$A_0 = -682.913042$ $B_0 = 4.074747$
$A_1 = 12.122290$ $B_1 = -8.053899 \times 10^{-2}$
$A_2 = -8.187699 \times 10^{-2}$ $B_2 = 5.946552 \times 10^{-4}$
$A_3 = 2.437244 \times 10^{-4}$ $B_3 = -1.945048 \times 10^{-6}$
$A_4 = -2.719103 \times 10^{-7}$ $B_4 = 2.380143 \times 10^{-9}$

for the ranges 210–300 K and 172–240 nm and list smoothed values for T = 210, 230, 250, 270, and 295 K at 2-nm intervals and at wavelengths corresponding to the wavenumber intervals generally used in stratospheric photodissociation calculations. **Note: There were typographical errors in JPL02-25 for parameters B_0 and B_1 which have been corrected in this evaluation.**

A similar temperature behavior was observed by Orlando et al. [607] only between 190 and 210 nm, and by Talukdar et al. [764] only above 197 nm.

Table 4-120. Absorption Cross Sections of CH_3CFCl_2 at 295–298 K

λ (nm)	10^{20} σ (cm^2)	λ (nm)	10^{20} σ (cm^2)	λ (nm)	10^{20} σ (cm^2)
170	143.1	194	47.2	218	0.382
172	145.1	196	34.1	220	0.248
174	154.2	198	24.0	222	0.161
176	162.9	200	16.6	224	0.105
178	172.6	202	11.3	226	0.0680
180	172.3	204	7.56	228	0.0444
182	162.9	206	5.02	230	0.0290
184	146.4	208	3.30	232	0.0189
186	125.7	210	2.16	234	0.0123
188	103.6	212	1.40	236	0.00801
190	83.0	214	0.909	238	0.00518
192	63.6	216	0.589	240	0.00334

Note:
170–188 nm, Gillotay and Simon [279],
190–240 nm, mean of Gillotay and Simon [279] and Fahr et al. [232].

F46. CH_3CF_2Cl (HCFC-142b) + hν → Products. The absorption cross sections of CH_3CF_2Cl have been measured at room temperature and 120–180 nm by Doucet et al. [223]; at 184–210 nm by Green and Wayne [299]; at 298 and 208 K and 160–230 nm by Hubrich and Stuhl [346]; at 210–295 K and 170–230 nm by Gillotay and Simon [279]; at 203–295 K and 190–230 nm by Orlando et al. [607]; and at 223–333 K and 160–210 nm by Nayak et al. [572]. At wavelengths below 200 nm, the values of Hubrich and Stuhl [346] and Nayak et al. [572] are within 15%, those of Gillotay and Simon [279] and Orlando et al. [607] are lower than the latter by up to 30%. At wavelengths between 200 and 215 nm, the values of Gillotay and Simon [279], Orlando et al. [607], and Nayak et al [572] agree within 15%. Above 215 nm, the absorption curve reported by Orlando et [607] shows wiggles with deviations by up to 100% from the data of Gillotay and Simon [279]. Also the values reported for the range 205–230 nm by Hubrich and Stuhl [346] become increasingly large by up to 600% than those of Gillotay and Simon [279]. The results of Green and Wayne [299] are very different from all other data. The preferred room temperature absorption cross sections, listed in Table 4-121, are the mean of the values reported by Hubrich and Stuhl [346], Gillotay and Simon [279], and Nayak et al. [572] at 175–185 nm, the mean of the values reported by Gillotay and Simon [279], Orlando et al. [607], and Nayak et al. [572] at 190–210 nm, and the values reported by Gillotay and Simon [279] at 212–230 nm.

A decrease of the absorption cross sections with decreasing temperature was observed by Gillotay and Simon [279] and Nayak et al. [572] over the wavelength range 160–230 nm and by Orlando et al. [607] between 190 and 200 nm. An irregular temperature behavior was reported by Orlando et al. [607] for the range 215–230 nm, where the absorption curves for the various temperatures show several crossings. Various parameterized fits for the temperature dependence of the absorption cross sections have been offered. Gillotay and Simon [279] used the polynomial expansion

$$\log_{10} \sigma(\lambda, T) = \sum A_n \lambda^n + (T - 273) \times \sum B_n \lambda^n$$

and reported smoothed values for
T = 210, 230, 250, 270, and 295 K, every 2 nm, and at wavelengths corresponding to the wavenumber intervals generally used in stratospheric photodissociation calculations. Their parameters A_n and B_n for the ranges
T = 210–300 K and λ = 172–230 nm are as follows:

$A_0 = -328.092008$ $\quad B_0 = 4.289533 \times 10^{-1}$
$A_1 = 6.342799$ $\quad B_1 = -9.042817 \times 10^{-3}$
$A_2 = -4.810362 \times 10^{-2}$ $\quad B_2 = 7.018009 \times 10^{-5}$
$A_3 = 1.611991 \times 10^{-4}$ $\quad B_3 = -2.389065 \times 10^{-7}$
$A_4 = -2.042613 \times 10^{-7}$ $\quad B_4 = 3.039799 \times 10^{-10}$

Nayak et al. [572] report fourth-order polynomial coefficients $C_n(T)$ for the functions $\log_{10}(\sigma_T) = \sum C_n (\lambda - 160)^n$ at T = 223, 233, 253, 273, 295, 313, and 333 K and for the range 160–210 nm. The parameters C_n are as follows

	223 K	273 K	295 K	333 K
C_0	–18.2361	–18.2441	–18.2406	–18.1777
C_1	-1.26669×10^{-2}	-7.37889×10^{-3}	-6.48269×10^{-3}	-2.39647×10^{-2}
C_2	-2.32945×10^{-3}	-2.66537×10^{-3}	-2.80923×10^{-3}	-7.23910×10^{-4}
C_3	2.81933×10^{-5}	4.19193×10^{-5}	5.01979×10^{-5}	-1.08049×10^{-5}
C_4	-1.37963×10^{-7}	-2.88472×10^{-7}	-3.96860×10^{-7}	1.37618×10^{-7}

A double expansion in terms of twelve parameters,

$\ln \sigma(\lambda, T) = \sum (\sum a_{ij} (T-245.4)^{j-1}) (\lambda - 206.214)^{i-1}$, i = 1–4, j = 1–3, T = 203–295 K, λ = 190–230 nm,

was used by Orlando et al. [607]:

$a_{11} = -4.973 \times 10^{1}$	$a_{12} = 9.077 \times 10^{-3}$	$a_{13} = -4.651 \times 10^{-5}$
$a_{21} = -2.175 \times 10^{-1}$	$a_{22} = 4.712 \times 10^{-4}$	$a_{23} = -1.005 \times 10^{-5}$
$a_{31} = 4.133 \times 10^{-4}$	$a_{32} = -6.432 \times 10^{-5}$	$a_{33} = 1.141 \times 10^{-6}$
$a_{41} = 7.145 \times 10^{-5}$	$a_{42} = -5.396 \times 10^{-6}$	$a_{43} = 1.187 \times 10^{-7}$

Note: There was a typographical error in JPL02-25 for parameter a_{11} which has been corrected in this evaluation.

Quantum yields for Cl ($^2P_{3/2}$) and Cl*($^2P_{1/2}$) atom formation in the photolysis of CH_3CF_2Cl at 193.3 nm have been measured by Brownsword et al. [106] and quantum yields for H atom formation in the photolysis at 121.6 and 193.3 nm by Brownsword et al. [105]: Φ(Cl + Cl*) = 0.90 ± 0.17 with Φ(Cl) = 0.65 ± 0.12 and Φ(Cl*) = 0.25 ± 0.05 at 193.3 nm, and Φ(H) = 0.53 ± 0.12 and 0.06 ± 0.02 at 121.6 and 193.3 nm, respectively.

Table 4-121. Absorption Cross Sections of CH_3CF_2Cl at 295–298 K

λ (nm)	10^{20} σ (cm^2)	λ (nm)	10^{20} σ (cm^2)	λ (nm)	10^{20} σ (cm^2)
170	27.1	200	0.145	218	0.00243
175	14.0	202	0.0949	220	0.00145
180	6.38	204	0.0622	222	0.000845
185	2.73	206	0.0399	224	0.000484
190	1.02	208	0.0256	226	0.000271
192	0.706	210	0.0161	228	0.000148
194	0.482	212	0.0105	230	0.0000783
196	0.324	214	0.00652		
198	0.218	216	0.00401		

Note:
170–185 nm: mean of Gillotay and Simon [279], Hubrich and Stuhl [346], and Nayak et al. [572]
190–210 nm: mean of Gillotay and Simon [279], Orlando et al. [607], and Nayak et al. [572]
212–230 nm: Gillotay and Simon [279].

F47. $CH_2ClCHO + h\nu \rightarrow$ Products. The absorption spectrum of CH_2ClCHO (chloroacetaldehyde) has been measured at room temperature and 118-182 nm by Lucazeau and Sandorfy [462] and at 235–360 nm by Libuda [445] who report a slightly structured absorption band with the maximum around 290 nm. In Table 4-122 are listed the average absorption cross-sections over 1-nm intervals of the medium-resolution data (0.6 nm) of Libuda [445] for the range 240-357 nm.

Table 4-122. Absorption Cross Sections of CH_2ClCHO at 298 K

λ (nm)	10^{20} σ (cm^2)	λ (nm)	10^{20} σ (cm^2)	λ (nm)	10^{20} σ (cm^2)	λ (nm)	10^{20} σ (cm^2)
240	0.952	270	2.46	300	5.57	330	1.64
241	0.887	271	2.65	301	5.10	331	1.52
242	0.885	272	2.85	302	4.92	332	1.68
243	0.881	273	2.98	303	5.01	333	1.42
244	0.845	274	3.04	304	5.30	334	1.36
245	0.814	275	3.13	305	5.27	335	1.06
246	0.815	276	3.29	306	5.48	336	0.747
247	0.841	277	3.38	307	5.34	337	0.622
248	0.857	278	3.57	308	5.44	338	0.502
249	0.864	279	3.82	309	5.37	339	0.411
250	0.875	280	3.99	310	5.03	340	0.340
251	0.884	281	4.23	311	4.61	341	0.281
252	0.926	282	4.09	312	3.92	342	0.247
253	0.959	283	4.15	313	3.71	343	0.213
254	0.977	284	4.31	314	3.73	344	0.190
255	1.01	285	4.55	315	3.96	345	0.159
256	1.08	286	4.64	316	3.85	346	0.136
257	1.18	287	4.80	317	4.16	347	0.0977
258	1.23	288	4.99	318	3.84	348	0.0791
259	1.28	289	5.03	319	3.78	349	0.0623
260	1.33	290	5.20	320	3.84	350	0.0545
261	1.42	291	4.95	321	3.43	351	0.0558
262	1.53	292	4.94	322	3.26	352	0.0603
263	1.68	293	5.14	323	2.49	353	0.0633
264	1.84	294	5.48	324	2.11	354	0.0565
265	1.91	295	5.47	325	1.92	355	0.0377
266	1.98	296	5.64	326	1.87	356	0.0239
267	2.08	297	5.56	327	1.87	357	0.0123
268	2.23	298	5.75	328	1.70		
269	2.33	299	5.63	329	1.92		

Note:
240-357 nm, Libuda et al. [445].

F48. $CHCl_2CHO + h\nu \rightarrow$ Products. The absorption spectrum of $CHCl_2CHO$ (dichloroacetaldehyde) has been measured at room temperature and 118-182 nm by Lucazeau and Sandorfy [462] and at 253–360 nm by Libuda [445] who report an absorption band slightly structured around the maximum at about 300 nm. In Table 4-123 are listed the averages over 1-nm intervals of the medium-resolution data (0.6 nm) of Libuda [445] for the range 256-354 nm.

Table 4-123. Absorption Cross Sections of $CHCl_2CHO$ at 298 K

λ (nm)	10^{20} σ (cm^2)	λ (nm)	10^{20} σ (cm^2)	λ (nm)	10^{20} σ (cm^2)	λ (nm)	10^{20} σ (cm^2)
256	0.0462	281	3.66	306	5.76	331	1.47
257	0.0787	282	3.85	307	5.70	332	1.34
258	0.167	283	4.02	308	5.49	333	1.22
259	0.221	284	4.23	309	5.36	334	1.21
260	0.247	285	4.43	310	5.25	335	1.05
261	0.313	286	4.63	311	4.99	336	0.859
262	0.445	287	4.88	312	4.58	337	0.720
263	0.596	288	4.96	313	4.40	338	0.594
264	0.705	289	5.17	314	4.26	339	0.495
265	0.785	290	5.32	315	4.11	340	0.418
266	0.914	291	5.38	316	3.98	341	0.362
267	1.09	292	5.51	317	3.85	342	0.315
268	1.30	293	5.68	318	3.73	343	0.259
269	1.49	294	5.85	319	3.51	344	0.209
270	1.67	295	5.88	320	3.30	345	0.182
271	1.77	296	6.06	321	3.18	346	0.155
272	1.91	297	5.97	322	3.00	347	0.134
273	2.08	298	6.04	323	2.73	348	0.117
274	2.28	299	6.02	324	2.48	349	0.102
275	2.57	300	6.14	325	2.27	350	0.0844
276	2.74	301	5.94	326	2.14	351	0.0707
277	3.01	302	5.97	327	1.99	352	0.0697
278	3.14	303	5.93	328	1.80	353	0.0638
279	3.26	304	5.90	329	1.67		
280	3.48	305	5.77	330	1.58		

Note:
256-354 nm, Libuda et al. [445].

F49. $CF_2ClCHO + h\nu \rightarrow$ Products. The absorption spectrum of CF_2ClCHO (difluorochloroacetaldehyde) has been measured at room temperature and 235-355 nm by Libuda [445] and at 245-298 K and 235-370 nm by Rattigan et al. [655]. The spectrum displays an absorption band in that wavelength region with a maximum at 300 nm. The room temperature data are in very good agreement, within 3-10%, between 270 and 335 nm, where the data of Rattigan et al. [655] are always larger than those of Libuda [445]. Above 340 nm, the data of Rattigan et al. [655] become larger by up to 25% than the data of Libuda [445], and going from 265 to 235 nm, the data of Rattigan et al. [655] become increasingly larger by 15-~300% than the data of Libuda [445]. The preferred absorption cross-sections listed at 5-nm intervals in Table 4-124 are the mean values of the data of Libuda [445] (selected from 1-nm averages of medium-resolution (0.6 nm) data) and Rattigan et al. [655] (given as 5-nm averages of medium-resolution (0.6 nm) data) at 235-350 nm, and the data of Rattigan et al. [655] at 355-370 nm.

The temperature studies at several temperatures between 245 and 298 K show an increase of the absorption cross sections over the absorption band up to 340 nm and a decrease in the long-wavelength wing with decreasing temperature. A simple empirical relation for the temperature dependence between 245 and 298 K, $\ln \sigma(\lambda, T) = \ln \sigma(\lambda, 298K) + B(\lambda)\cdot(T-298)$, and temperature coefficients $B(\lambda)$ for λ = 235-370 nm at 5-nm intervals are given by Rattigan et al. [655]. These temperature coefficients B are also listed in Table 4-124.

Table4-124. Absorption Cross Sections of CF_2ClCHO at 298 K and Temperature Coefficients

λ (nm)	10^{20} σ (cm^2)	10^4 B (K^{-1})	λ (nm)	10^{20} σ (cm^2)	10^4 B (K^{-1})	λ (nm)	10^{20} σ (cm^2)	10^4 B (K^{-1})
235	0.120	-29.0	285	11.8	-10.2	335	4.64	-2.83
240	0.295	-17.9	290	13.7	-10.6	340	2.66	-2.84
245	0.584	-13.5	295	15.2	-9.54	345	1.46	14.0
250	1.07	-11.8	300	16.0	-10.4	350	0.670	37.3
255	1.78	-10.7	305	15.6	-7.09	355	0.148	68.1
260	2.78	-10.5	310	15.2	-9.73	360	0.036	75.8
265	4.09	-10.4	315	13.0	-8.32	365	0.012	52.9
270	5.75	-10.5	320	11.4	-7.71	370	0.003	63.1
275	7.67	-9.96	325	9.07	-5.02			
280	9.79	-10.6	330	6.38	-3.03			

Note:
Absorption cross-sections σ: 235-350 nm, mean of Libuda [445] and Rattigan et al. [655], 355-370 nm, Rattigan et al. [655].
Temperature coefficients B: 245-298 K, Rattigan et al. [655] ($\ln \sigma(\lambda, T) = \ln \sigma(\lambda, 298\ K) + B(T-298)$).

F50. $CFCl_2CHO + h\nu \rightarrow$ Products. The absorption spectrum of $CFCl_2CHO$ (fluorodichloroacetaldehyde) has been measured at room temperature and 235-355 nm by Libuda [445] and at 253-298 K and 235-370 nm by Rattigan et al. [655]. There is an absorption band in that wavelength region with a maximum near 296 nm. The data of Libuda [445] are larger by 10-30% than the data of Rattigan et al. [655] over the whole absorption band (except for a few points in the wings). The preferred absorption cross-sections listed at 5-nm intervals in Table 4-125 are the mean values of the data of Libuda [445] (selected from 1-nm averages of medium-resolution (0.6 nm) data) and Rattigan et al. [655] (given as 5-nm averages of medium-resolution (0.6 nm) data) at 235-355 nm, and the data of Rattigan et al. [655] at 355-370 nm.

The temperature studies at several temperatures between 253 and 298 K show an increase of the absorption cross sections around the absorption maximum at 260-305 nm and a decrease in the long- and short-wavelength wings with decreasing temperature. A simple empirical relation for the temperature dependence between 253 and 298 K, $\ln \sigma(\lambda, T) = \ln \sigma(\lambda, 298K) + B(\lambda)\cdot(T-298)$, and temperature coefficients $B(\lambda)$ for λ = 235-370 nm at 5-nm intervals are given by Rattigan et al. [655]. These temperature coefficients B are also listed in Table 4-125.

Table 4-125. Absorption Cross Sections of $CFCl_2CHO$ at 298 K and Temperature Coefficients

λ (nm)	10^{20} σ (cm^2)	10^4 B (K-1)	λ (nm)	10^{20} σ (cm^2)	10^4 B (K-1)	λ (nm)	10^{20} σ (cm^2)	10^4 B (K-1)
235	0.305	136.0	285	14.1	-7.82	335	2.50	24.60
240	0.599	87.0	290	15.3	-6.89	340	1.20	36.50
245	1.22	30.6	295	16.1	-6.41	345	0.616	58.10
250	1.91	6.41	300	15.7	-4.50	350	0.245	84.90
255	2.89	1.24	305	14.9	-2.93	355	0.067	92.80
260	4.21	-6.12	310	13.0	1.73	360	0.017	93.20
265	5.89	-7.55	315	10.9	2.70	365	0.007	103.2
270	7.84	-8.11	320	8.66	6.97	370	0.002	138.3
275	9.95	-8.28	325	5.97	12.2			
280	12.1	-8.04	330	4.11	15.6			

Note:
Absorption cross-sections σ: 235-355 nm, mean of Libuda [445] and Rattigan et al. [655], 360-370 nm, Rattigan et al. [655].
Temperature coefficients B: 253-298 K, Rattigan et al. [655] ($\ln \sigma(\lambda, T) = \ln \sigma(\lambda, 298\ K) + B(T-298)$).

F51. $CCl_3CHO + h\nu \rightarrow CCl_3 + CHO$
$CCl_3CHO + h\nu \rightarrow CCl_3CO + H$
$CCl_3CHO + h\nu \rightarrow Cl + CCl_2CHO$

$CCl_3CHO + h\nu \rightarrow CCl_3H + CO$. The absorption spectrum of CCl_3CHO (trichloroacetaldehyde, chloral) has been measured at room temperature and at 118-182 and 250-357 nm by Lucazeau and Sandorfy [462]; at 235-350 nm by Libuda [445]; at 243-298 K and 200-360 nm by Rattigan et al. [656], [655]; at 210-295 K and 166-348 nm by Gillotay et al. [282]; and at 200-360 nm by Talukdar et al. [770]. An absorption band was observed between 240 and 360 nm with the maximum near 290 nm and a stronger absorption feature at shorter wavelengths. Except for the data of Lucazeau and Sandorfy [462], the results for the region of the absorption band are in good agreement within the experimental uncertainties: Gillotay et al. [282] report the highest values, Libuda [445] the lowest, the agreement around the maximum is within 20%. For the data of Rattigan et al. [655] and Talukdar et al. [770] the agreement is even better than 10% around the absorption maximum. The data of the latter two teams are nearly identical above 300 nm, whereas those of Gillotay et al [282] become appreciably higher, the difference becoming greater than a factor of 2 with increasing wavelength up to 335 nm. There is no explanation for these differences. As recommended absorption cross-sections, listed in Table 4-126, we chose the results of Talukdar et al. [770] who report data at 2-nm increments measured at a resolution of 1 nm by using a diode array spectrometer.

The studies of the temperature dependence at 233-296 K by Rattigan et al. [656], [655]; at 210-295 K Gillotay et al. [282]; and at 240-360 K by Talukdar et al. [770] in agreement show that the absorption cross sections clearly decrease with decreasing temperature below ~260 nm and above ~290 nm. The temperature dependence of the absorption cross-sections was parameterized by the empirical relation,

$$\ln \sigma(\lambda, T) = \ln \sigma(\lambda, 298K) + B(\lambda)\cdot(T-298).$$

Rattigan et al. [655] derived temperature coefficients $B(\lambda)$ for T = 233-296 K and λ = 200-355 nm, Talukdar et al. [770] for T = 240-360 K and 200-344 nm. The temperature coefficients B of Talukdar et al. [770] are also listed in Table 4-126.

Quantum yields for the production of H, $O(^3P)$, and Cl atoms in the photolysis of CCl_3CHO at 193, 248, and 308 nm have been measured by Talukdar et al. [770]. The yields of H and O atoms were found to be small or below the detection limit, $\Phi(O(^3P))$ <0.02 and <0.01 at 248 and 308 nm, $\Phi(H) = 0.04 \pm 0.005$, <0.01, and <0.002 at 193, 248, and 308 nm. Despite of the major expected channel to be the production of CCl_3 + CHO, Cl atoms were found to be the primary photolysis products at 308 nm with $\Phi(Cl) = 1.3 \pm 0.3$.

Table 4-126. Absorption Cross Sections of CCl_3CHO at 298 K and Temperature Coefficients

λ (nm)	$10^{20}\ \sigma$ (cm^2)	10^4 B (K-1)	λ (nm)	$10^{20}\ \sigma$ (cm^2)	10^4 B (K-1)	λ (nm)	$10^{20}\ \sigma$ (cm^2)	10^4 B (K-1)
200	187	22.0	250	2.18	3.73	300	9.25	3.07
202	153	23.9	252	2.54	1.50	302	8.77	3.60
204	122	27.2	254	2.92	0.324	304	8.17	4.37
206	95.7	30.6	256	3.36	-0.569	306	7.50	5.25
208	73.8	34.1	258	3.84	-0.877	308	6.86	6.10
210	56.3	37.5	260	4.35	-1.23	310	6.18	6.91
212	42.6	40.9	262	4.90	-1.65	312	5.58	7.90
214	31.8	44.0	264	5.48	-1.62	314	4.98	9.30
216	23.8	47.2	266	6.07	-1.50	316	4.33	11.2
218	17.1	50.2	268	6.68	-1.41	318	3.68	13.2
220	13.1	52.9	270	7.28	-1.22	320	3.09	15.1
222	9.75	55.6	272	7.88	-1.07	322	2.51	16.7
224	7.24	57.6	274	8.46	-0.931	324	2.09	18.5
226	5.39	59.0	276	8.99	-0.584	326	1.76	21.1
228	4.06	60.4	278	9.49	-0.412	328	1.43	25.0
230	3.07	60.5	280	9.94	-0.481	330	1.12	30.3
232	2.39	59.5	282	10.3	-0.235	332	0.849	36.6
234	1.90	55.9	284	10.6	0.242	334	0.590	43.3
236	1.62	49.2	286	10.8	0.475	336	0.373	49.8
238	1.43	41.6	288	10.9	0.750	338	0.261	55.6
240	1.39	33.0	290	10.9	1.09	340	0.188	60.2
242	1.41	24.0	292	10.8	1.51	342	0.136	65.0
244	1.53	16.4	294	10.6	1.96	344	0.100	69.0
246	1.66	10.4	296	10.3	2.38			
248	1.91	6.50	298	9.92	2.71			

Note:

Absorption cross-sections σ: 200-344 nm, Talukdar et al. [770].
Temperature coefficients B: 240-360 K, Talukdar et al. [770] ($\ln \sigma(\lambda, T) = \ln \sigma(\lambda, 298\ K) + B(T-298)$).

F52. $CH_3C(O)Cl + h\nu \rightarrow$ Products. The absorption spectrum of $CH_3C(O)Cl$ (acetyl chloride) has been measured at room temperature and 233-300 nm by Libuda [445] and 190-341 nm by Maricq [480]. Both authors in agreement report an absorption band with a maximum of (1.15-1.17) × 10^{-19} cm^2 $molecule^{-1}$ in the 242-245-nm region. The band observed by Libuda [445], however, is narrower than that observed by Maricq [480] due to an obvious asymmetry on the short-wavelength wing and the maximum is shifted somewhat to larger wavelength. The data reported by Maricq [480] therefore become increasingly larger by up to ~50% between 242 and 233 nm than the data reported by Libuda [445]. Above 292 nm there are large differences between the data reported by both authors: the absorption curve reported by Libuda [445] shows a regular and continuous decrease with increasing wavelengths up to 302 nm, whereas the data of Maricq [480] show large variations obviously due to noise effects. As recommended absorption cross-sections we chose the 1-nm averages of the medium-resolution (0.5 nm) data of Maricq [480] for the region 191-292 nm and the 1-nm averages of the medium-resolution (0.6 nm) data of Libuda [445] for the region 293-302 nm as listed in Table 4-127.

Table 4-127. Absorption Cross Sections of $CH_3C(O)Cl$ at 295-298 K

λ (nm)	10^{20} σ (cm^2)	λ (nm)	10^{20} σ (cm^2)	λ (nm)	10^{20} σ (cm^2)	λ (nm)	10^{20} σ (cm^2)
191	34.7	219	5.95	247	11.0	275	1.98
192	26.3	220	6.28	248	10.9	276	1.90
193	23.6	221	6.57	249	10.6	277	1.67
194	20.5	222	6.93	250	10.4	278	1.42
195	17.1	223	7.15	251	10.1	279	1.24
196	14.1	224	7.53	252	9.76	280	1.12
197	11.4	225	7.99	253	9.51	281	0.959
198	9.08	226	8.23	254	9.17	282	0.781
199	7.53	227	8.59	255	8.77	283	0.653
200	6.37	228	8.98	256	8.36	284	0.479
201	5.17	229	9.27	257	8.03	285	0.391
202	4.34	230	9.61	258	7.67	286	0.389
203	3.83	231	9.93	259	7.27	287	0.327
204	3.54	232	10.1	260	6.86	288	0.307
205	3.45	233	10.3	261	6.55	289	0.267
206	3.28	234	10.5	262	6.20	290	0.213
207	3.12	235	10.7	263	5.79	291	0.200
208	3.16	236	10.9	264	5.40	292	0.173
209	3.35	237	11.2	265	5.11	293	0.129
210	3.48	238	11.3	266	4.76	294	0.103
211	3.72	239	11.3	267	4.39	295	0.0846
212	3.89	240	11.4	268	4.03	296	0.0716
213	4.06	241	11.5	269	3.70	297	0.0599
214	4.40	242	11.5	270	3.36	298	0.0500
215	4.68	243	11.4	271	3.06	299	0.0404
216	4.88	244	11.3	272	2.77	300	0.0336
217	5.14	245	11.2	273	2.49	301	0.0298
218	5.54	246	11.1	274	2.19	302	0.0265

Note:
191-292 nm, Maricq [480],
293-302 nm, Libuda [445].

F53. $CH_2ClC(O)Cl + h\nu \rightarrow$ Products. The absorption spectrum of $CH_2ClC(O)Cl$ (chloroacetyl chloride) has been measured at room temperature and 234-342 nm by Libuda [445]. The spectrum exhibits an absorption band with the maximum around 248 nm. Above 315 nm the data points show a somewhat irregular behavior. We therefore recommend the 1-nm averages of Libuda's [445] medium-resolution (0.6 nm) data for the region 235-316 nm, which are listed in Table 4-128.

Table 4-128. Absorption Cross Sections of $CH_2ClC(O)Cl$ at 298 K

λ (nm)	10^{20} σ (cm^2)	λ (nm)	10^{20} σ (cm^2)	λ (nm)	10^{20} σ (cm^2)	λ (nm)	10^{20} σ (cm^2)
235	9.50	256	11.2	277	4.00	298	0.409
236	10.0	257	11.0	278	3.71	299	0.353
237	10.4	258	10.7	279	3.41	300	0.300
238	11.0	259	10.4	280	3.15	301	0.248
239	11.5	260	10.0	281	2.89	302	0.199
240	11.8	261	9.67	282	2.65	303	0.170
241	12.0	262	9.32	283	2.43	304	0.157
242	12.3	263	8.94	284	2.21	305	0.131
243	12.5	264	8.55	285	2.03	306	0.113
244	12.7	265	8.16	286	1.85	307	0.0909
245	12.7	266	7.80	287	1.67	308	0.0809
246	12.7	267	7.41	288	1.50	309	0.0657
247	12.7	268	7.06	289	1.33	310	0.0547
248	12.8	269	6.72	290	1.17	311	0.0522
249	12.7	270	6.30	291	1.04	312	0.0419
250	12.5	271	5.90	292	0.918	313	0.0380
251	12.4	272	5.53	293	0.814	314	0.0311
252	12.3	273	5.23	294	0.717	315	0.0286
253	12.1	274	4.93	295	0.628	316	0.0214
254	11.8	275	4.61	296	0.546		
255	11.5	276	4.33	297	0.473		

Note:
235-316 nm, Libuda [445].

F54. $CHCl_2C(O)Cl + h\nu \rightarrow$ Products. The absorption spectrum of $CHCl_2C(O)Cl$ (dichloroacetyl chloride) has been measured at room temperature and 235-338 nm by Libuda [445] and 200-300 nm by Villenave et al. [821]. An absorption band with the maximum around 258 nm was observed in that wavelength region. The reported data are in very good agreement between 242 and 300 nm, where the data of Villenave et al. [821] are smaller by 1-10% than the data of Libuda [445]. At shorter wavelengths the absorption cross-sections reported by Libuda [445] become smaller by up to ~25% at 235 nm than those reported by Villenave et al. [821]. The latter authors observed a minimum near 232 nm and increasing cross-sections between 230 and 220 nm. At longer wavelengths the absorption curve reported by Libuda [445] shows a regular behavior up to 316 nm. In Table 4-129 are listed as a recommendation the absorption cross sections measured at 10-nm increments for 200-300 nm by Villenave et al. [821].

Table 4-129. Absorption Cross Sections of $CHCl_2C(O)Cl$ at 298 K

λ (nm)	10^{20} σ (cm^2)
220	21.7
230	13.2
240	15.7
250	20.0
256	20.9
260	20.8
270	17.1
280	10.5
290	4.7
300	1.4

Note:
220 -300 nm, Villenave et al. [821].

F55. $CCl_3C(O)Cl + h\nu \rightarrow$ Products. The absorption spectrum of $CCl_3C(O)Cl$ (trichloroacetyl chloride) has been measured at room temperature and 235-342 nm by Libuda [445] and 220-290 nm by Villenave et al. [821]; and at 210-295 K and 166-338 nm by Gillotay et al. [282]. An absorption band between 230 and 340 nm with a maximum of ~2.3×10^{-19} cm^2 $molecule^{-1}$ around 256 nm and a strong increase of the absorption cross-sections below 230 nm was observed in good agreement by Gillotay et al. [282] and Villenave et al. [821]. Gillotay et al. [282] report a second maximum of ~7.2×10^{-18} cm^2 $molecule^{-1}$ around 175 nm. The absorption curve reported by Libuda [445] is very shallow in the region 240-270 nm, it crosses the other two curves at ~245 nm and is higher by 30-40% at 235 nm and lower by 10-14% in the region of the maximum. In the wing of the absorption band above 290 nm the data reported by Libuda [445] become smaller by up to about 70% than the data reported by Gillotay et al. [282]. Since the data of Villenave et al. [821] and Gillotay et al. [282] are in good agreement, but Villenave et al. [821] measured absorption cross-sections at 10-nm increments only, we list in Table 4-130 the room temperature data of Gillotay et al. [282], which are averages over the 500-cm^{-1} and 5-nm intervals of the high-resolution spectrum (0.015 nm) generally used in stratospheric photodissociation calculations.

The temperature studies at 210-295 K by Gillotay et al. [282] show an increase of the absorption cross-sections with increasing temperature all over the observed wavelength region.

Table 4-130. Absorption Cross Sections of $CCl_3C(O)Cl$ at 295 K

λ (nm)	$10^{20}\ \sigma$ (cm^2)	λ (nm)	$10^{20}\ \sigma$ (cm^2)	λ (nm)	$10^{20}\ \sigma$ (cm^2)
166.7 – 169.5	671	204.1 - 206.2	231	256.4 - 259.7	22.6
169.5 - 172.4	699	206.2 - 208.3	194	259.7 - 263.2	22.3
172.4 - 173.9	712	208.3 - 210.5	160	263.2 - 266.7	21.1
173.9 - 175.4	716	210.5 - 212.8	129	266.7 - 270.3	19.1
175.4 - 177.0	717	212.8 - 215.0	102	270.3 - 274.0	16.6
177.0 - 178.6	714	215.0 - 217.4	78.9	274.0 - 277.8	13.7
178.6 - 180.2	706	217.4 - 219.8	59.5	277.8 - 281.7	10.7
180.2 - 181.8	694	219.8 - 222.2	44.0	281.7 - 285.7	8.14
181.8 - 183.5	677	222.2 - 224.7	31.8	285.7 - 289.9	5.86
183.5 - 185.2	655	224.7 - 227.3	25.8	289.9 - 294.1	4.03
185.2 - 186.9	630	227.3 - 229.9	21.9	294.1 - 298.5	2.67
186.9 - 188.7	599	229.9 - 232.6	19.5	298.5 - 303.0	1.68
188.7 - 190.5	567	232.6 - 235.3	18.3	303.0 - 307.7	0.921
190.5 - 192.3	528	235.3 - 238.1	17.9	307.7 - 312.5	0.605
192.3 - 194.2	487	238.1 - 241.0	18.1	312.5 - 317.5	0.339
194.2 - 196.1	445	241.0 - 243.9	18.7	317.5 - 322.5	0.188
196.1 - 198.0	402	243.9 - 246.9	19.7	322.5 - 327.5	0.104
198.0 - 200.0	358	246.9 - 250.0	20.9	327.5 - 332.5	0.0578
200.0 - 202.0	314	250.0 - 253.2	21.8	332.5 - 337.5	0.0326
202.0 - 204.1	272	253.2 - 256.4	22.3		

Note:
166.7-337.5 nm, Gillotay et al. [282].

F56. $CF_3CF_2CHCl_2$ (HCFC-225ca) + $h\nu \rightarrow$ Products.

F57. CF_2ClCF_2CHFCl (HCFC-225cb) + $h\nu \rightarrow$ Products. The absorption spectra of these compounds in the gaseous and liquid phases at 298 K have been measured by Braun et al. [86]. Table 4-131 lists the absorption cross sections for the gas phase taken from this work. The originally listed (0.5-nm intervals) absorption coefficients ε in (atm, 298 K)$^{-1}$ cm^{-1} ($\sigma = 4.06 \times 10^{-20}\ \varepsilon$) for both phases have been fitted with third-order polynomial expansions $\log_{10} \varepsilon = \sum a_n(\lambda - 160)^n$ with

$a_0 = 1.425$, $a_1 = 4.542 \times 10^{-2}$, $a_2 = -2.036 \times 10^{-3}$, $a_3 = 1.042 \times 10^{-5}$ for HCFC-225ca at 170–270 nm,

$a_0 = 1.677$, $a_1 = -2.175 \times 10^{-2}$, $a_2 = -1.484 \times 10^{-3}$, $a_3 = 1.147 \times 10^{-5}$ for HCFC-225cb at 165–250 nm.

Table 4-131. Absorption Cross Sections of $CF_3CF_2CHCl_2$ and CF_2ClCF_2CFCl at 298 K

λ (nm)	10^{20} σ (cm^2) $CF_3CF_2CHCl_2$ (HCFC-225ca)	CF_2ClCF_2CFCl (HCFC-225cb)	λ (nm)	10^{20} σ (cm^2) $CF_3CF_2CHCl_2$ (HCFC-225ca)	CF_2ClCF_2CFCl (HCFC-225cb)
160	268.7	187.9	202	11.58	0.479
162	236.8	173.3	204	8.185	0.369
164	207.6	154.8	206	5.802	0.291
166	189.0	135.1	208	4.084	0.254
168	181.4	113.2	210	2.903	0.250
170	182.7	91.35	212	2.042	
172	182.8	70.68	214	1.429	
174	189.0	54.73	216	1.05	
176	190.9	40.68	218	0.727	
178	187.9	30.04	220	0.463	
180	177.5	21.11	222	0.308	
182	161.1	14.90	224	0.209	
184	140.3	10.47	226	0.145	
186	118.3	7.308	228	0.0987	
188	96.51	5.075	230	0.0653	
190	74.30	3.492	232	0.0434	
192	57.08	2.412	234	0.0299	
194	42.83	1.661	236	0.0193	
196	31.75	1.165	238	0.0134	
198	23.22	0.873	239	0.0119	
200	16.24	0.633			

Note:
HCFC-225ca, 160–239 nm, Braun et al. [86],
HCFC-225cb, 160–210 nm, Braun et al. [86].

F58. $CH_3C(O)CH_2Cl + h\nu \rightarrow$ Products. The absorption cross sections of chloroacetone have been measured at 243-296 K and 210-370 nm by Burkholder et al. [111] at a resolution of 0.6 nm using a diode array spectrometer. The spectrum shows two absorption bands, a strong band with the maximum at ~223-224 nm and $\sigma = 3.35 \times 10^{-19}$ cm^2 $molecule^{-1}$ at room temperature and a weaker and broader one with the maximum at ~290-293 nm and $\sigma = 1.02 \times 10^{-19}$ cm^2 $molecule^{-1}$. The averages over 1-nm intervals of the medium-resolution absorption spectrum are listed in Table 4-132. A systematic decrease of the absorption cross-sections with decreasing temperature from 296 to 243 K was observed in the weaker absorption band above ~260 nm. Also a decrease of the absorption cross-sections is observed in the short-wavelength absorption band from the measurement made at 296, 273 to 243 K. However, the values obtained at 253 K are larger than those at 273 K below ~240 nm, and even larger than those at 296 K below ~230 nm.

Photodissociation quantum yields were measured by Burkholder et al. [111] as 0.5 ± 0.08 at 308 nm and 351 nm. At both wavelengths, the yields of CO and CO_2 were 0.50 and ~0.25, respectively, whereas the yield of HCOOH was measured as 0.25 and of HCl as 0.5.

Table 4-132. Absorption Cross Sections of $CH_3C(O)CH_2Cl$ at 296 K

λ (nm)	10^{20} σ (cm^2)	λ (nm)	10^{20} σ (cm^2)	λ (nm)	10^{20} σ (cm^2)	λ (nm)	10^{20} σ (cm^2)
210	22.0	248	3.36	286	9.89	324	2.58
211	23.0	249	3.11	287	9.98	325	2.37
212	24.3	250	2.96	288	10.00	326	2.16
213	25.5	251	2.90	289	10.10	327	1.95
214	26.4	252	2.92	290	10.20	328	1.73
215	27.5	253	3.00	291	10.20	329	1.52
216	28.9	254	3.10	292	10.20	330	1.33
217	30.1	255	3.24	293	10.20	331	1.14
218	30.9	256	3.39	294	10.10	332	0.979
219	31.7	257	3.56	295	10.00	333	0.832
220	32.4	258	3.75	296	9.89	334	0.707
221	32.8	259	3.97	297	9.77	335	0.598
222	33.2	260	4.19	298	9.66	336	0.506
223	33.5	261	4.40	299	9.54	337	0.427
224	33.5	262	4.63	300	9.41	338	0.361
225	33.0	263	4.86	301	9.25	339	0.302
226	32.3	264	5.12	302	9.04	340	0.2520
227	31.8	265	5.38	303	8.80	341	0.212
228	31.3	266	5.65	304	8.53	342	0.176
229	30.3	267	5.89	305	8.24	343	0.145
230	28.9	268	6.14	306	7.94	344	0.120
231	27.3	269	6.39	307	7.63	345	0.103
232	25.7	270	6.65	308	7.34	346	0.0887
233	24.0	271	6.93	309	7.06	347	0.0757
234	22.2	272	7.20	310	6.77	348	0.0642
235	20.3	273	7.47	311	6.50	349	0.0547
236	18.4	274	7.71	312	6.22	350	0.0458
237	16.5	275	7.94	313	5.93	351	0.0411
238	14.6	276	8.16	314	5.61	352	0.0328
239	12.7	277	8.37	315	5.28	353	0.0319
240	11.0	278	8.59	316	4.92	354	0.0220
241	9.50	279	8.82	317	4.57	355	0.0193
242	8.15	280	9.03	318	4.22	356	0.0138
243	6.93	281	9.23	319	3.89	357	0.0134
244	5.85	282	9.41	320	3.58	358	0.00917
245	4.95	283	9.56	321	3.30	359	0.0155
246	4.26	284	9.69	322	3.04	360	0.0128
247	3.74	285	9.80	323	2.80		

Note:
210-360 nm, Burkholder et al. [111].

G1. $Br_2 + h\nu \rightarrow 2\ Br$. The absorption spectrum of bromine has repeatedly been measured during the last century as shown in the following survey:

Table 4-133. Summary of Cross Section Measurements of Br_2

Reference	Year	Temperature, K	Wavelength Range, nm
Ribaud [671]	1919	289, 593, 893	356-608
Gray and Style [298]	1930	294	240-579
Acton et al. [5]	1936	293, 400, 531, 657, 767, 906	327.4-571.7
Seery and Britton [719]	1964	298	320-590
McMillan [144]	1966	298	200-599
Passchier et al. [626]	1967	298, 348, 423, 298, 573, 648, 713	200-750
Wen and Noyes [843]	1972	303	220-290
Hemenway et al. [326]	1979	296	556-616.3
Roxlo and Mandl [692]	1980	298	170-230
Röth et al. [687]	1991	294	315.2-512.4 504.0-552.6
Hubinger and Nee [345]	1995	295	190-600

The spectrum of Br_2 exhibits an absorption band between 190 and 300 nm with the maximum near 223 nm and another band between 300 and 600 nm, which is composed of three overlapping bands with the maxima at ~412, 480, and 549 nm. The results of the various research teams are in very good agreement in the region of the UV-visible absorption band. Discrepancies are observed above 550 nm, where the data of McMillan [144] and Hemenway et al. [326] are respectively up to 60% and 100% lower than the values measured by the other groups. Large discrepancies arise in the region of the absorption minimum between 230 and 340 nm due to a pressure-dependent component of the Br_2 vapor, possibly a Br_2-Br_2 collision dimer. A detailed discussion of the available absorption data of Br_2 and an evaluation is given by Maric et al. [478]. These authors fitted the most reliable data, i.e., those of Passchier et al. [626] and Wen and Noyes [843], to a four-band semi-logarithmic distribution function and derived a mathematical expression which allows the calculation of a smooth absorption curve for Br_2 in the wavelength region 200-650 nm:

$$\sigma(298\ K) = 1.06 \times 10^{-20}\ cm^2 \times \exp\{-52.3x[\ln(223.3\ nm/\lambda)]^2\}$$
$$+ 6.19 \times 10^{-19}\ cm^2 \times \exp\{-108.5[\ln(411.9\ nm/\lambda)]^2\}$$
$$+ 3.39 \times x10^{-19}\ cm^2 \times \exp\{-106.8[\ln(480.2\ nm/\lambda)]^2\}$$
$$+ 3.78 \times 10^{-20}\ cm^2 \times \exp\{-112.0[\ln(549.3\ nm/\lambda)]^2\}$$

The recommended absorption cross sections calculated from that expression are listed in Table 4-134. The results of Maric et al. [478] have been generally confirmed in a later study by Hubinger and Nee [345], who reported absorption cross sections for the wavelength range 190-600 nm; only the cross sections with values below 10^{-21} cm^2 $molecule^{-1}$, i.e., between 260 and 340 nm, are different from the recommended data of Maric et al. [478] and can only be considered as upper limits.

Studies of the temperature dependence at 293-906 K by Acton et al. [5] and at 298-713 K by Passchier et al. [626] show a decrease of the cross sections around the absorption maximum between ~380 and ~500 nm and an increase in the short- and long-wavelength tails with increasing temperature.

Photodissociation of Br_2 leads to the formation of Br atoms in the ground $Br(^2P_{3/2})$ and excited $Br^*(^2P_{1/2})$ state. A few studies have been performed to establish the relative quantum yields of (Br+Br) and (Br+Br*) at various wavelengths. Peterson and Smith [631] measured the yield of Br* atoms to increase from 0.4 to 0.89 in the range 444-510 nm, and to further decrease to ~ 0.4 at 530 nm. Lindeman and Wiesenfeld [456] observed the relative quantum yield (Br+Br*) to increase from 0.07 at 434 nm to 0.64 at 482 nm and then to decrease to 0.57 at 511 nm. Haugen et al. [320] determined the relative quantum yield (Br+Br*) to increase from 0.44 at 445 nm to 0.87 at 500 nm, followed by a decrease to 0.40 at 530 nm. Cooper et al. [181] measured the relative (Br+Br*) yield to be zero in the range 360 to 430 nm and to increase at longer wavelengths to 0.79 at 580 nm; at 260 nm they observed (Br+Br*) to be dominant. Jee at al. [370, 371] measured the relative yield of the photodissociation channel into (Br+Br*) at 234 nm to be unity and at 265 nm to be 0.96. Zaraga et al. [873] calculated the zero-pressure predissociation quantum yield from high-resolution spectroscopic studies of a banded region ($B\ ^3\Pi(0_u^+)$ state) overlapping a continuum at 588 nm to be near unity.

Table 4-134. Absorption Cross Sections of Br_2 at 298 K

λ (nm)	10^{20} σ (cm^2)	λ (nm)	10^{20} σ (cm^2)	λ (nm)	10^{20} σ (cm^2)	λ (nm)	10^{20} σ (cm^2)
200	0.562	315	0.0274	430	60.1	545	10.1
205	0.723	320	0.0626	435	57.1	550	8.68
210	0.870	325	0.141	440	54.0	555	7.47
215	0.983	330	0.300	445	51.2	560	6.43
220	1.05	335	0.602	450	48.8	565	5.54
225	1.06	340	1.14	455	46.8	570	4.77
230	1.01	345	2.05	460	45.2	575	4.09
235	0.925	350	3.49	465	44.0	580	3.50
240	0.808	355	5.63	470	42.8	585	2.98
245	0.676	360	8.66	475	41.6	590	2.52
250	0.544	365	12.7	480	40.3	595	2.11
255	0.422	370	17.8	485	38.6	600	1.76
260	0.316	375	23.9	490	36.6	605	1.45
265	0.229	380	30.7	495	34.3	610	1.19
270	0.161	385	37.9	500	31.8	615	0.958
275	0.110	390	45.1	505	29.0	620	0.767
280	0.0728	395	51.8	510	26.2	625	0.607
285	0.0472	400	57.4	515	23.4	630	0.475
290	0.0299	405	61.6	520	20.6	635	0.368
295	0.0187	410	64.2	525	18.0	640	0.282
300	0.0122	415	65.1	530	15.7	645	0.214
305	0.0100	420	64.5	535	13.6	650	0.161
310	0.0135	425	62.8	540	11.7		

Note: Cross sections calculated from the expression given by Maric et al. [478].

G2. HBr + hν → H + Br. The absorption cross sections of HBr have been repeatedly measured at room temperature and in the UV region as shown in the following survey:

Table 4-135. Summary of Cross Section Measurements of HBr

Reference	Year	Temperature, K	Wavelength Range, nm
Goodeve and Taylor [289]	1935	298	182-286
Romand [684]	1949	298	139-228
Huebert and Martin [352]	1968	297	170-230
Bridges and White [90]	1973	298	214
Okabe [596]	1977	296	240-270
Ravishankara et al. [661]	1979	298	184.9
Roxlo and Mandl [692]	1980	298	170-230
Okabe [600]	1983	296	184.9
Brion et al. [92]	1985	298	30-177
Nee et al. [576]	1986	298	105-238
Vaghjiani [798]	1993	296	193
Barone et al. [43]	1994	298	184.9,193.0

The spectrum exhibits a broad absorption band at wavelengths above 155 nm with the maximum near 178 nm and a large number of strong and sharp bands at shorter wavelengths down to 105 nm. The absorption cross sections near the maximum of the absorption band reported by Nee et al. [576] and Huebert and Martin [352] are in good agreement, whereas those reported by Romand [684] and Roxlo and Mandl [692] are lower: the absorption cross sections reported for the maximum are 2.4×10^{-18}, 2.7×10^{-18}, 2×10^{-18}, and 1.4×10^{-18} cm^2 $molecule^{-1}$, respectively. The results of Vaghjiani [798] and Barone et al. [43] for 193 nm fit well to the absorption curves reported by Nee et al. [576] and Huebert and Martin [352]. The cross section at 184.9 nm measured by Ravishankara et al. [661] and Barone et al. [43] lies between those reported by Nee et al. [576] and Huebert and Martin [352], that measured by Okabe [596] between those of Goodeve and Taylor [289] and Romand [684]. The recommended values, listed in Table 4-136, are derived as follows: the spectra of Goodeve and Taylor [289], Romand [684], Huebert and Martin [352], and Nee et al. [576] have been

normalized to the value $\sigma = 2.21 \times 10^{-18}$ cm^2 molecule^{-1} at 184.9 nm, which is the mean of the values reported by Okabe [596], Ravishankara et al. [661], and Barone et al. [43]; the normalized spectra have then been averaged, for 152-168 nm those of Romand [684] and Nee et al. [576], for 170-180 nm those of Romand [684], Huebert and Martin [352], and Nee et al. [576], and for 182-230 nm those of Goodeve and Taylor[289], Romand [684], Huebert and Martin [352], and Nee et al. [576].

The branching fraction for the formation of excited Br*($^2P_{3/2}$) atoms was determined by Regan et al. [669] in the wavelength range 201-253 nm to vary between 015 and 0.23. Baumfalk et al. [63] obtained a value for the branching fraction for Br* of 0.20 ± 0.03 at 243 nm, and a value of 0.18 ± 0.03 at 193 nm.

Table 4-136. Absorption Cross Sections of HBr at 296-298 K

λ (nm)	10^{20} σ (cm^2)	λ (nm)	10^{20} σ (cm^2)	λ (nm)	10^{20} σ (cm^2)	λ (nm)	10^{20} σ (cm^2)
152	139	172	233	192	181	212	54.8
154	124	174	240	194	168	214	45.7
156	138	176	244	196	154	216	38.8
158	148	178	244	198	140	218	33.0
160	161	180	242	200	125	220	28.0
162	176	182	233	202	111	222	22.9
164	189	184	225	204	98.1	224	18.2
166	201	186	217	206	85.5	226	14.4
168	211	188	206	208	74.7	228	11.7
170	225	190	194	210	64.4	230	9.32

Note:
Normalization of the data of Goodeve and Taylor [289], Romand [684], Huebert and Martin [352], and Nee et al. [576] to $\sigma = 2.21 \times 10^{-18}$ cm^2 molecule^{-1} at 184.9 nm and averaging:
152-168 nm, mean of Romand [684] and Nee et al. [576];
170-180 nm, mean of Romand [684], Huebert and Martin [352] and Nee et al. [576],
182-230 nm, mean of Goodeve and Taylor [289], Romand [684], Huebert and Martin [352] and Nee et al. [576].

G3. BrO + hν → Br + O. The BrO radical has a banded spectrum in the 290–380 nm range, which is attributed to the A $^2\Pi_{3/2} \leftarrow$ X $^2\Pi_{3/2}$ transition. The absorption spectrum has been measured in the region of this absorption band, and cross sections have been also determined for single absorption peaks, the strongest, the (7, 0) peak at 338.5 nm and the (11, 0) and (12, 0) peaks at 320.8 nm and 317.3 nm.

Table 4-137. Summary of Cross Section Measurements of BrO

Reference	Year	Temperature, K	Wavelength Range, nm	Resolution, nm
Clyne and Cruse [176]	1970	293	338.3	0.15
Basco and Dogra [45]	1971	298	320.8, 338.3	not given
Cox et al. [192]	1982	298	296-370	0.22
Wahner et al. [829]	1988	228, 243, 298	312-380	0.4
Sander and Friedl [702]	1989	220, 298	338.5	0.06-1.25
Orlando et al. [606]	1991	298	338.5	0.4
Laszlo et al [435]	1997	295	338.5	0.6
Gilles et al. [274]	1997	204, 222, 237, 252, 273, 298, 329, 369	338.5	0.5
Wheeler et al. [846]	1998	298	338, 317	4 cm^{-1}
Wilmouth et al. [848]	1999	298	317-388	1.0 cm^{-1}
Wilmouth et al. [848]	1999	228, 298	286-386	10 cm^{-1}
Fleischmann et al. [245]	2003	203, 223, 243, 273, 298	300-385	4 cm^{-1}

The measured cross sections are both temperature- and resolution-dependent, i.e., the peaks of the vibrational bands become higher and sharper with decreasing temperature and lower resolution. As an example, the spectrum measured by Wahner et al. [829] is shown in Figure 4-4. Wilmouth et al. [848] used their 10-cm^{-1} absorption spectra for an analysis of the results of Cox et al. [192], Wahner et al. [829], Orlando et al. [606], Laszlo et al.

[435], and Gilles et al. [274] at a common resolution of 0.40 nm (details of this procedure are described in the paper of Wilmouth et al. [848]).

The absorption cross sections for the peaks of the vibrational bands of the A ← X transition at 298 ± 2 and 228 ± 2 K obtained by this analysis are listed in Table 4-138. Averages over 0.5-nm intervals of the spectrum of Wilmouth et al. [848] are listed in Table 4-139.

Absorption cross sections for the rotational peaks of the (7,0) and (12,0) bands were measured at high-resolution (1.0 cm^{-1}) by Wilmouth et al. [848]: $\sigma = 2.17 \times 10^{-17}$ cm^2 $molecule^{-1}$ for the apex of the (7,0) band and $\sigma = 1.38 \times 10^{-17}$ cm^2 $molecule^{-1}$ for the apex of the (12,0) band.

The temperature dependence of the (7,0) absorption maximum (338 nm) is reported by Gilles et al. [274] for the range 204-388 K for a resolution of 0.5 nm by the following expression:

$$\sigma(T)_{338} = 3.29 - (5.58 \times 10^{-3}) \times T, \text{ in units of } 10^{-17}\ cm^2\ molecule^{-1}.$$

Table 4-138. Absorption Cross Sections at the Vibrational Band Peaks in the A ← X Spectrum of BrO (0.4 nm resolution)

v', v''	λ, nm	10^{20} σ, cm^2 $molecule^{-1}$	
		298 ± 2 K	228 ± 2 K
26, 0	286.46	107	88.3
25, 0	287.38	132	133
24, 0	288.45	145	175
23, 0	289.83	188	208
22, 0	291.40	188	267
21, 0	292.99	242	284
20, 0	294.88	295	348
19, 0	296.97	356	441
18, 0	299.30	447	541
17, 0	301.81	523	636
16, 0	304.54	601	728
15, 0	307.46	679	819
14, 0	310.54	772	932
13, 0	313.81	904	1090
12, 0	317.29	1190	1480
11, 0	321.20	1360	1670
10, 0	325.37	1260	1510
9, 0	329.56	1210	1430
8, 0	333.89	1250	1510
7, 0	338.69	1580	1970
6, 0	344.04	923	1060
5, 0	349.09	715	828
4, 0	355.02	723	864
3, 0	360.64	267	287
4, 1	364.32	126	95.4
2, 0	367.94	128	129
1, 0	374.69	74.5	77.3
2, 1	381.27	27.5	27.4
0, 0	286.46	22.5	
1, 1	287.38	9.86	

Note:
Wilmouth et al. [848]: The own data and data of Cox et al. [192], Wahner et al. [829], Orlando et al. [606], Laszlo et al. [435], Gilles et al. [274] were normalized to a common resolution of 0.40 nm and then averaged.

Table 4-139. Absorption Cross Sections of BrO at 298 K

λ (nm)	10^{20} σ (cm^2)	λ (nm)	10^{20} σ (cm^2)	λ (nm)	10^{20} σ (cm^2)	λ (nm)	10^{20} σ (cm^2)
286.5	104.8	311.5	453.1	336.5	258.7	361.5	226.6
287.0	106.5	312.0	294.8	337.0	222.1	362.0	182.9
287.5	128.8	312.5	203.7	337.5	202.0	362.5	145.2
288.0	95.04	313.0	197.3	338.0	201.8	363.0	119.9
288.5	147.7	313.5	723.9	338.5	1287.0	363.5	103.7
289.0	109.8	314.0	901.3	339.0	1296.0	364.0	113.3
289.5	126.4	314.5	650.8	339.5	734.4	364.5	122.2
290.0	183.8	315.0	443.2	340.0	444.8	365.0	99.15
290.5	133.1	315.5	310.9	340.5	303.1	365.5	87.15
291.0	133.5	316.0	231.7	341.0	243.1	366.0	86.23
291.5	188.6	316.5	173.7	341.5	217.5	366.5	91.26
292.0	157.2	317.0	721.1	342.0	235.0	367.0	105.0
292.5	128.3	317.5	1136.0	342.5	291.6	367.5	123.4
293.0	248.2	318.0	730.7	343.0	423.8	368.0	130.5
293.5	192.5	318.5	482.3	343.5	711.9	368.5	119.5
294.0	140.4	319.0	344.6	344.0	967.8	369.0	100.9
294.5	161.5	319.5	275.1	344.5	814.4	369.5	86.11
295.0	294.4	320.0	251.4	345.0	542.1	370.0	74.79
295.5	216.1	320.5	293.7	345.5	345.0	370.5	64.46
296.0	163.9	321.0	1138.0	346.0	225.9	371.0	53.91
296.5	152.9	321.5	1155.0	346.5	160.3	371.5	46.47
297.0	361.1	322.0	676.9	347.0	146.4	372.0	39.44
297.5	276.5	322.5	419.6	347.5	162.2	372.5	35.13
298.0	193.5	323.0	300.6	348.0	257.8	373.0	34.13
298.5	156.4	323.5	261.7	348.5	529.5	373.5	35.68
299.0	284.0	324.0	288.2	349.0	747.7	374.0	48.08
299.5	421.1	324.5	433.6	349.5	667.4	374.5	74.97
300.0	275.3	325.0	982.6	350.0	499.2	375.0	70.53
300.5	193.5	325.5	1283.0	350.5	363.4	375.5	51.46
301.0	180.1	326.0	837.6	351.0	272.4	376.0	35.44
301.5	350.9	326.5	494.8	351.5	215.3	376.5	30.47
302.0	502.3	327.0	312.0	352.0	181.9	377.0	27.46
302.5	318.4	327.5	231.1	352.5	165.9	377.5	25.66
303.0	217.4	328.0	223.5	353.0	162.8	378.0	25.61
303.5	195.9	328.5	343.1	353.5	163.2	378.5	21.82
304.0	274.0	329.0	789.1	354.0	179.5	379.0	18.60
304.5	609.6	329.5	1261.0	354.5	309.3	379.5	14.96
305.0	466.2	330.0	1058.0	355.0	789.4	380.0	12.28
305.5	298.4	330.5	706.2	355.5	498.6	380.5	13.03
306.0	221.1	331.0	453.4	356.0	276.2	381.0	19.55
306.5	209.7	331.5	295.9	356.5	166.2	381.5	20.93
307.0	407.2	332.0	203.1	357.0	119.9	382.0	16.76
307.5	703.1	332.5	164.7	357.5	111.1	382.5	9.049
308.0	518.3	333.0	259.8	358.0	115.3	383.0	3.059
308.5	343.6	333.5	952.8	358.5	123.6	383.5	4.924
309.0	227.6	334.0	1294.0	359.0	143.6	384.0	3.892
309.5	193.6	334.5	963.3	359.5	182.7	384.5	6.695
310.0	395.5	335.0	652.3	360.0	236.4	385.0	10.93
310.5	798.9	335.5	457.5	360.5	272.3		
311.0	659.2	336.0	338.8	361.0	264.4		

Note:
Wilmouth et al. [848]: Averages over 0.5-nm intervals of the high-resolution spectrum.

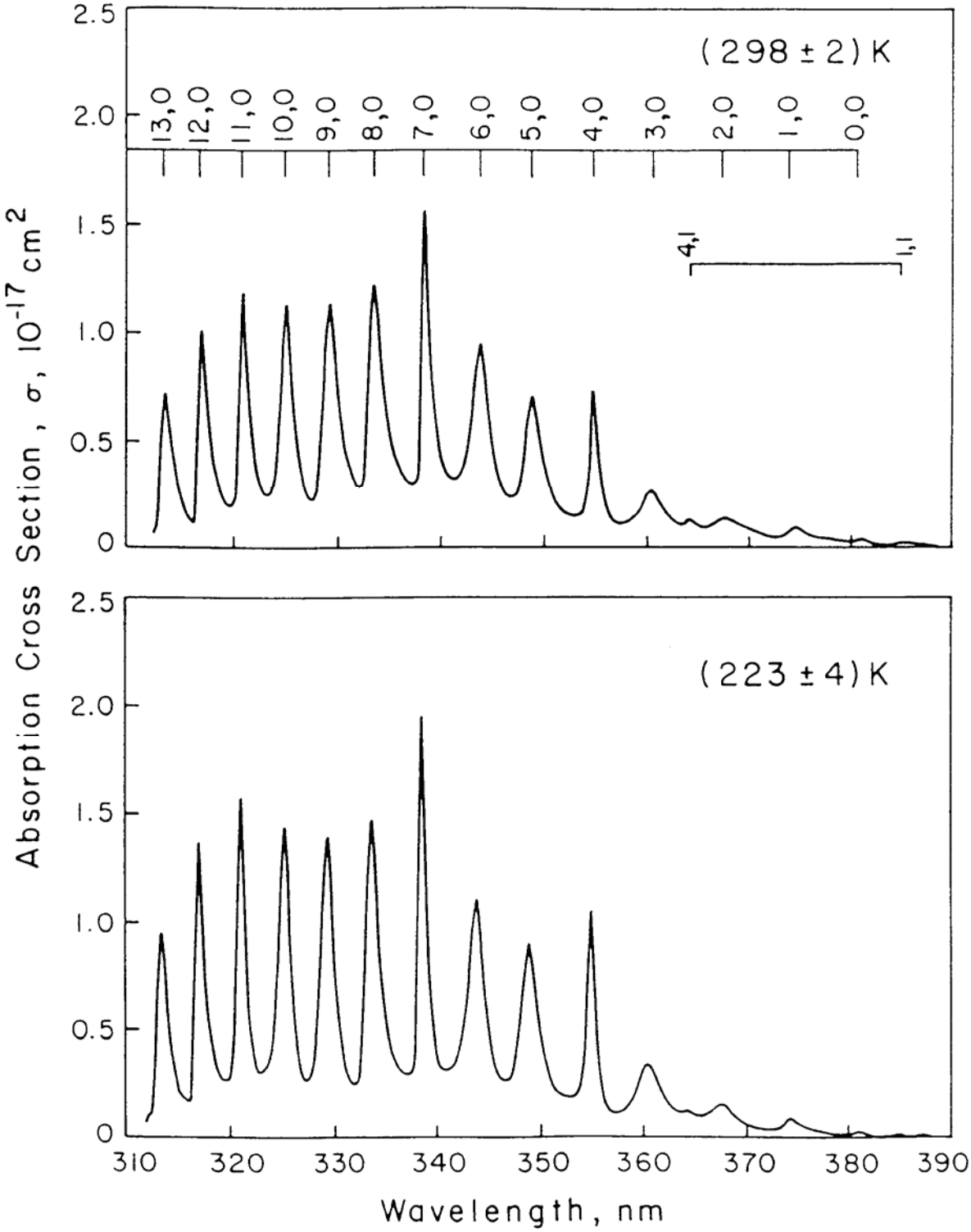

Figure 4-4. Absorption Spectrum of BrO (after Wahner et al. [829])

G4. $OBrO + h\nu \rightarrow BrO + O(^3P)$

$OBrO + h\nu \rightarrow Br + O_2$..The visible absorption spectrum of bromine dioxide has been measured in the 400-600-nm region at 273, 298, and 338 K by Rattigan et al. [651], at 298 K by Rowley et al. [690], at ~250 K by Miller et al. [528], and at 298 K by Knight et al. [413]. The spectrum shows a highly structured absorption band consisting of a progression of doublets with a maximum intensity near 500 nm and a progression of less intense bands between the doublets. The spectrum was identified as arising from the $C\ ^2A_2 \leftarrow X\ ^2B_1$ electronic transition by Miller et al. [528] who combined *ab initio* calculations of the lowest doublet electronic states of OBrO with Franck-Condon simulations. Whereas Rattigan et al. [651], Rowley et al. [690], and Miller et al. [528] observed only qualitative spectra, Knight et al. [413] were the first who measured the absorption cross sections. In Table 4-140 are listed the peak positions and corresponding absorption cross sections for the vibrational progressions (n,0,0)←(0,0,0) and (n,1,0)←(0,0,0). In Table 4-141 are listed the averages over 1-nm intervals of the spectrum measured at a resolution of 0.66 nm.

No quantum yields are available, but theoretical calculations by Vetter et al. [817] indicate that photodissociation occurs via $BrO + O(^3P)$ because of a large transition dipole moment for the $C\ ^2A_2 \leftarrow X\ ^2B_1$ transition. Photodissociation into $Br + O_2$ occurs via the 1^2B_2 state, which is less probably reached from the ground state, and therefore of minor importance.

Table 4-140. Peak Absorption Cross Sections of OBrO at 298 K

n	(n,0,0)←(0,0,0) λ (nm)	10^{20} σ (cm^2)	(n,1,0)←(0,0,0) λ (nm)	10^{20} σ (cm^2)
0	630.4		622.0	
1	606.1		598.4	
2	583.8		576.8	
3	563.4	1080	556.8	1350
4	544.4	1450	538.5	1740
5	527.1	1640	521.6	1910
6	510.7	1770	505.5	1960
7	495.5	1720	490.7	1760
8	481.2	1670	476.9	1510
9	468.2	1440	464.1	1260
10	455.8	1210	452.2	960
11	444.4	1020	440.8	720
12	433.7	790	430.4	490
13	423.5	570	420.6	310
14	414.1	400	411.0	220
15	405.1	260	402.3	130

Note:
Peak absorption cross sections, Knight et al. [413].

Table 4-141. Absorption Cross Sections of OBrO at 298 K

λ (nm)	10^{20} σ (cm^2)	λ (nm)	10^{20} σ (cm^2)	λ (nm)	10^{20} σ (cm^2)	λ (nm)	10^{20} σ (cm^2)
401	66.7	443	363	485	301	527	1530
402	112	444	834	486	463	528	1100
403	116	445	777	487	368	529	584
404	153	446	452	488	298	530	326
405	243	447	292	489	425	531	218
406	180	448	254	490	868	532	347
407	131	449	214	491	1580	533	547
408	113	450	180	492	993	534	361
409	105	451	323	493	641	535	344
410	128	452	854	494	583	536	539
411	201	453	672	495	1160	537	434
412	171	454	394	496	1430	538	1200
413	239	455	633	497	826	539	1500
414	380	456	1110	498	458	540	888
415	260	457	729	499	291	541	546
416	180	458	426	500	405	542	442
417	156	459	292	501	512	543	312
418	133	460	314	502	336	544	991
419	147	461	262	503	419	545	1230
420	269	462	213	504	483	546	716
421	274	463	399	505	1230	547	395
422	229	464	1100	506	1650	548	252
423	479	465	868	507	962	549	161
424	481	466	506	508	651	550	302
425	287	467	562	509	556	551	476
426	207	468	1230	510	1030	552	300
427	175	469	1020	511	1570	553	255
428	149	470	568	512	953	554	461
429	194	471	341	513	506	555	349
430	422	472	298	514	307	556	532
431	382	473	362	515	282	557	1250
432	274	474	239	516	532	558	870
433	577	475	286	517	433	559	472
434	661	476	563	518	303	560	350
435	392	477	1390	519	529	561	267
436	251	478	990	520	504	562	204
437	208	479	567	521	1390	563	791
438	179	480	577	522	1610	564	885
439	166	481	1260	523	921	565	504
440	363	482	1310	524	622	566	275
441	651	483	745	525	516	567	170
442	425	484	403	526	654	568	107

Note:
401-568 nm, Knight et al. [413] (columns 1, 3, 5, 7: center of interval).

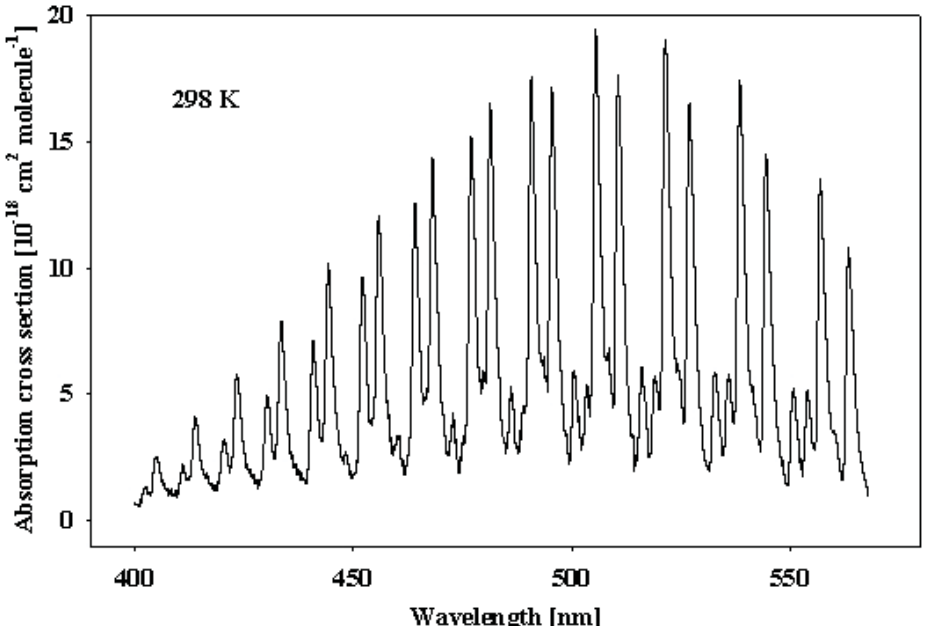

Figure 4-5. Absorption spectrum of OBrO (after Knight et al. [413])

G5. $Br_2O + h\nu \rightarrow$ Products. The absorption spectrum of dibromine monoxide has been measured at room temperature and 196-432 nm by Orlando and Burkholder [605], at 240-515 nm by Rattigan et al. [652], and at 208-444 nm by Deters et al. [215]. The spectrum exhibits a strong narrow absorption band below 220 nm with a maximum at 200 nm ($\sigma = 2 \times 10^{-17}$ cm^2 molecule^{-1}), a weaker and broader absorption band extending from 250 nm to about 450-470 nm with a maximum at 313 nm ($\sigma \approx (2.0\text{-}2.3) \times 10^{-18}$ cm^2 molecule^{-1}) and a shoulder near 350 nm ($\sigma = (1.74\text{-}1.95) \times 10^{-18}$ cm^2 molecule^{-1}), and two weak bands at 460-580 nm and 580-750 nm with maxima at ~520 nm ($\sigma \sim 4 \times 10^{-20}$ cm^2 molecule^{-1}) and ~665 nm ($\sigma \sim 6.2 \times 10^{-20}$ cm^2 molecule^{-1}). There is very good agreement between the various data sets in the wavelength region below 380 nm, where the data of Orlando and Burkholder [605] and Deters et al. [215] are nearly identical, and those of Rattigan et al. [652] are smaller by ~10% below 250 nm and above 290 nm and smaller by up to ~25% in the region of the absorption minimum near 270 nm. Large discrepancies between the three data sets are at wavelengths above 380 nm: The absorption cross sections reported by Orlando and Burkholder [605] and Deters et al. [215] rapidly decrease to values $\leq 1 \times 10^{-20}$ cm^2 molecule^{-1}, whereas the values reported by Rattigan et al. [652] show an exponential decrease at 400-470 nm followed by a new absorption band. The cutoff at 440 nm of the absorption curve reported by Orlando and Burkholder [605] is a result of the assumption that the absorbance of Br_2O is zero at 440 nm and beyond. The correction procedure used by Rattigan et al. [652] taking vibrational structure of the Br_2 spectrum into account resulted in appreciable absorption for Br_2O at wavelengths above 440 nm. The recommended cross sections listed in Table 4-142 are the data of Orlando and Burkholder [605] at 196 and 200 nm, the mean of the data of Orlando and Burkholder [605] and Deters et al. [215] at 210-230 nm, and the mean of the data of Orlando and Burkholder [605], Deters et al. [215], and Rattigan et al. [652] at 240-400 nm. No recommendation is given at wavelengths above 400 nm.

Table 4-142. Absorption Cross Sections of Br_2O at 298 K

λ (nm)	$10^{20}\,\sigma$ (cm^2)	λ (nm)	$10^{20}\,\sigma$ (cm^2)
196	1740	300	167
200	2000	310	220
210	1050	320	212
220	288	330	192
230	140	340	188
240	85.8	350	186
250	45.4	360	162
260	24.6	370	132
270	18.8	380	99.0
280	33.5	390	74.8
290	85.5	400	54.0

Note: 196, 200 nm, Orlando and Burkholder [605],
210-230 nm, mean of Orlando and Burkholder [605] and Deters et al. [215],
240-400 nm, mean of Orlando and Burkholder [605], Deters et al. [215] and Rattigan et al. [652].

G6. HOBr + hν → OH + Br

HOBr + hν → HBr + O(^{3}P). The absorption spectrum of HOBr has been measured by Orlando and Burkholder [605], Deters et al. [215], Benter et al. [66], Rattigan et al. [652], and Ingham et al. [361]. The spectra cluster has been measured in two groups. Orlando and Burkholder [605], Deters et al. [215], and Benter et al. [66] observe between 240 and 400 nm two absorption bands with maxima near 284 and 351 nm; the spectra agree reasonably well in their shape, but show a sharp decrease in cross section above 400 nm. In contrast, the cross sections reported by Rattigan et al. [652] and Ingham et al. [361] are roughly 50% larger between 300 and 400 nm.

In addition, the spectrum obtained by Rattigan et al. [652] shows a pronounced tail extending to 520 nm, whereas Ingham et al. [361] observe unambiguously a third weaker absorption band ranging to 550 nm with a maximum at 457 nm. These last two studies confirm the observations of Barnes et al. [41], who showed that laser photolysis of HOBr between 440–600 nm gives rise to OH fragments. The presence of a weak band beyond 400 nm is attributable to the presence of a forbidden transition from the ground electronic to a triplet state predicted by the *ab initio* calculations of Francisco et al. [248] and Minaev [529]. The differences in the spectral shapes are probably attributable to impurities such as Br_2O and Br_2, and/or the use of different Br_2O cross sections. However, the presence of impurities alone cannot explain the large difference in cross sections at the peak of the absorption bands.

The recommended absorption cross sections are listed in Table 4-143 over the range from 250 to 550 nm; below 250 nm the data are uncertain and no recommendation is given. The cross section values in the table are based on the latest study by Ingham et al. [361]. These authors generated HOBr in situ by laser photolytic production of OH in the presence of Br_2, and determined the HOBr spectrum using a gated diode camera shortly after the pulse, circumventing the problem associated with the presence of the strong absorbing impurity Br_2O, which was encountered in previous studies. The calibration of the absorption cross sections was made relative to the established cross sections of Br_2.

The data presented in Table 4-143 are computed with the following expression taken from Ingham et al. [361], which is based on a combination of three Gaussian fits, one for each absorption band:

$$\sigma(\lambda) = 24.77\exp\left\{-109.80\left[\ln\left(\frac{284.01}{\lambda}\right)\right]^2\right\} + 12.22\exp\left\{-93.63\left[\ln\left(\frac{350.57}{\lambda}\right)\right]^2\right\} + 2.283\exp\left\{-242.40\left[\ln\left(\frac{457.38}{\lambda}\right)\right]^2\right\}$$

$\sigma(\lambda)$: 10^{-20} cm^2 molecule^{-1}; $250 < \lambda < 550$ nm.

Benter et al. [66] measured quantum yields for HOBr photolysis at 261 and 363 nm (near the peaks of the second absorption bands). The observed quantum yield for Br formation at 363 nm was greater than 0.95, and a unity quantum yield into the product channel OH + Br is recommended. The other channel O + HBr was not observed. The laser photofragment study of Barnes et al. [41] claimed that OH was the major photolysis product at wavelengths beyond 400 nm. Lock et al. [459] found that at 490 and 510 nm OH and Br fragments are in their respective vibrational and spin-orbit ground states. The assumption of unit quantum yield of OH formation should be confirmed experimentally.

Table 4-143. Absorption Cross Sections of HOBr

λ (nm)	10^{20} σ (cm^2)	λ (nm)	10^{20} σ (cm^2)	λ (nm)	10^{20} σ (cm^2)
250	4.15	355	12.1	460	2.28
255	6.19	360	11.5	465	2.14
260	10.5	365	10.5	470	1.91
265	14.6	370	9.32	475	1.62
270	18.7	375	7.99	480	1.30
275	22.1	380	6.65	485	0.993
280	24.3	385	5.38	490	0.723
285	25.0	390	4.22	495	0.502
290	24.0	395	3.23	500	0.333
295	21.9	400	2.43	505	0.212
300	19.1	405	1.80	510	0.129
305	16.2	410	1.36	515	0.076
310	13.6	415	1.08	520	0.042
315	11.8	420	0.967	525	0.023
320	10.8	425	0.998	530	0.012
325	10.5	430	1.15	535	0.0059

λ (nm)	10^{20} σ (cm^2)	λ (nm)	10^{20} σ (cm^2)	λ (nm)	10^{20} σ (cm^2)
330	10.8	435	1.40	540	0.0029
335	11.3	440	1.68	545	0.0013
340	11.9	445	1.96	550	0.0006
345	12.3	450	2.18		
350	12.4	455	2.29		

Note:

250-550 nm, Ingham et al. [361]

G7. BrNO + hν → Br + NO. The absorption spectrum of nitrosyl bromide has been measured at room temperature and 275-550 nm by Eden et al. [225], at 200-800 nm by Houel and Van den Bergh [342] and at 189-300 nm by Uthman et al. [797], and single cross sections have been reported for 266 nm by Hippler et al. [332] and for 270 nm by Maloney and Palmer [471]. The spectrum exhibits three absorption bands between 200 and 800 nm: a strong absorption band between 190 and 290 nm with the maximum at ~213 nm, a weaker band between 290 and 600 nm with the maximum at 338 nm and a shoulder near 420 nm, and a still weaker band between 600 and 800 nm with the maximum at 708 nm. The results of the various research teams are (after correction of an error in the paper of Maloney and Palmer [471]) in very good agreement. In Table 4-144 are listed the results of Uthman et al. [797] for the UV absorption band at 189-300 nm and the cross sections at the maxima and the shoulder in the near UV and visible regions reported by Houel and Van den Bergh [342] (these authors as well as Eden et al. [225] only give plots of their measured spectra).

Table 4-144. Absorption cross sections of BrNO at 298 K

λ(nm)	10^{20} σ (cm^2)	λ(nm)	10^{20} σ (cm^2)
189	18.3	224	4740
193	39.0	230	2990
194	46.2	235	1920
197	166	240	1090
200	566	250	360
201	861	260	117
203	1690	270	40.1
205.5	2950	280	19.5
207	4340	290	16.8
210	6470	300	18.0
211	6910		
213	7270	338	31.0
216	7060	416	20.1
220	6070	708	2.94

Note:
189-300 nm, Uthman et al. [797],
338, 416, 708 nm, Houel and Van den Bergh [342].

G8. BrONO + hν → Products. The absorption spectrum of *cis*-BrONO (bromine nitrite) has been measured in the range 228 to 296 K and 200-365 nm by Burkholder and Orlando [114]. The spectrum exhibits a strong absorption band between 200 and 270 nm with the maximum at 228 nm and a broader and weaker band between 270 and 364 nm with the maximum at 316 nm. The relative shape of the BrONO spectrum was independent of the temperature within the uncertainties of the measurements. The results of Burkholder and Orlando [114] are listed in Table 4-145.

Table 4-145. Absorption Cross Sections of BrONO at 253 K

λ (nm)	10^{20} σ (cm^2)	λ (nm)	10^{20} σ (cm^2)	λ (nm)	10^{20} σ (cm^2)	λ (nm)	10^{20} σ (cm^2)
200	0	242	1070	284	247	326	400
202	116	244	874	286	262	328	394
204	221	246	720	288	277	330	387
206	358	248	602	290	293	332	382
208	496	250	514	292	310	334	375
210	687	252	446	294	331	336	364
212	822	254	391	296	350	338	350
214	107	256	345	298	366	340	332
216	128	258	306	300	377	342	308
218	161	260	273	302	386	344	284
220	194	262	244	304	393	346	263
222	224	264	221	306	400	348	248
224	252	266	205	308	407	350	233
226	263	268	196	310	413	352	214
228	271	270	192	312	415	354	195
230	262	272	191	314	413	356	176
232	239	274	194	316	409	358	157
234	217	276	200	318	406	360	138
236	186	278	211	320	406	362	123
238	155	280	223	322	406	364	117
240	124	282	235	324	405		

Note:
200-364 nm, Burkholder and Orlando [114].

G9. $BrONO_2 + h\nu \rightarrow Br + NO_3$
$BrONO_2 + h\nu \rightarrow BrO + NO_2$
$BrONO_2 + h\nu \rightarrow BrO + NO + O(^3P)$. The bromine nitrate cross sections have been measured at room temperature and 186-390 nm by Spencer and Rowland [748], at 220, 250, and 298 K and 200-500 nm by Burkholder et al. [116], and at 230 and 298 K and 210-500 nm by Deters et al. [216]. The results of Burkholder et al. [116] and Deters et al. [216] are nearly identical over the range of spectral overlap. The results of Spencer and Rowland [748] agree generally within 10% with those of Burkholder et al. [116] and Deters et al. [216] except for the region between 315 and 350 nm where the Spencer data are higher by 10-20%.

The temperature dependence of the absorption cross sections generally is small. Burkholder et al. [116] observed decreasing cross sections with decreasing temperature between 200 and 215 nm and between 230 and 500 nm and a slight increase between 215 and 230 nm.; the ratio $\sigma(220\ K)/\sigma(298\ K)$ has values of ~0.8 to 1.03 between 200-235 nm, a minimum of 0.90 at 260 nm, nearly constant values of ~0.95 between 290 and 370 nm, a minimum of ~0.87 at 430 nm, two maxima of ~ 0.98 around 440-450 nm, and rapidly decreases to ~0.5 at 500 nm. The measurements of Deters et al. [216] show a similar behavior of the $\sigma(230\ K)/\sigma(298\ K)$ vs. λ curve with the difference that all values lie below 1, i.e., the decrease of the cross sections with decreasing temperature is observed over the entire wavelength range 210 and 500 nm. As a recommendation we list in Table 4-146 the data of Burkholder et al. [116] for 296 K and the temperature coefficients A1 and A2 obtained from the parameterization of the temperature dependence by the relation

$$\sigma(\lambda,T) = \sigma(\lambda, 296\ K)\ [1 + A1\ (T - 296) + A2\ (T - 296)^2].$$

The quantum yields for NO_3 production were measured by Harwood et al. [313]: $\varphi(NO_3) = 0.28 \pm 0.09$ at 248 nm, 1.01 ± 0.35 at 305 nm and 0.92 ± 0.43 at 352.5 nm. The quantum yields for BrO and Br were also estimated at 248 nm to be $\varphi(BrO) \approx 0.5$ and $\varphi(Br) \approx 0.5$. Recently Soller et al. [746] investigated the production of Br, $O(^3P)$ and BrO from the photolysis of $BrONO_2$ in the wavelength range 248-355 nm. The quantum yield for the Br atom are 0.35 ± 0.08, 0.65 ± 0.14, $>0.62 \pm 0.11$, and 0.77 ± 0.19 at 248, 266, 308 and 355 nm, respectively. The values for the $O(^3P)$ atom quantum yields are 0.66 ± 0.15, 0.18 ± 0.04, $<0.13 \pm 0.03$, and <0.02 at 248, 266, 308 and 355 nm, respectively. The measured quantum yields for BrO are 0.37 ± 0.12 at 266 nm and 0.23 ± 0.08 at 355 nm. The measured quantum yields are summarized below.

Wavelength nm	NO_3	Br	BrO	$O(^3P)$
248	0.28 ± 0.09[a]	≈ 0.5[a] 0.35 ± 0.08[b]	≈ 0.5[a]	0.66 ± 0.15[b]
266		0.65 ± 0.14[b]	0.37 ± 0.12[b]	0.18 ± 0.04[b]
305	1.01 ± 0.35[a]			
308		$>0.62 \pm 0.11$[b]		$<0.13 \pm 0.03$[b]
352.5	0.92 ± 0.43[a]			
355		0.77 ± 0.19[b]	0.23 ± 0.08[b]	<0.02[b]

[a]Harwood et al. [313]
[b]Soller et al. [746]

A recommendation is only given for wavelengths above 300 nm, where total quantum yield Φ_{BrONO2} is unity, $\Phi_{Br+NO_3} = 0.85$ and $\Phi_{BrO+NO_2} = 0.15$. There is no recommendation for wavelengths below 300 nm.

Table 4-146. Absorption Cross Sections of $BrONO_2$ at 296 K and Temperature Coefficients

λ (nm)	10^{20} σ (cm^2)	10^3 A1 (K^{-1})	10^6 A2 (K^{-2})	λ (nm)	10^{20} σ (cm^2)	10^3 A1 (K^{-1})	10^6 A2 (K^{-2})	λ (nm)	10^{20} σ (cm^2)	10^3 A1 (K^{-1})	10^6 A2 (K^{-2})
200	680	0.852	-26.0	302	17.5	0.781	0.784	404	2.04	1.91	3.64
202	616	0.608	-26.1	304	16.6	0.870	1.88	406	1.95	1.86	2.63
204	552	0.308	-26.2	306	15.8	0.872	1.62	408	1.88	1.78	1.52
206	488	0.138	-23.7	308	15.0	0.772	-0.229	410	1.81	1.70	0.316
208	425	0.158	-17.5	310	14.2	0.660	-2.28	412	1.75	1.59	-0.981
210	361	0.184	-9.09	312	13.5	0.652	-1.95	414	1.69	1.49	-2.37
212	334	0.401	-2.61	314	12.8	0.643	-1.58	416	1.63	1.40	-2.60
214	307	0.657	5.03	316	12.1	0.652	-1.42	418	1.56	1.35	-1.54
216	286	0.882	11.2	318	11.6	0.684	-1.48	420	1.50	1.29	-0.381
218	272	1.05	15.3	320	11.0	0.719	-1.56	422	1.45	1.00	-2.34
220	258	1.24	19.7	322	10.5	0.719	-1.06	424	1.40	0.694	-4.43
222	247	1.19	19.7	324	10.1	0.720	-0.508	426	1.36	0.599	-4.31
224	236	1.12	19.6	326	9.64	0.743	0.087	428	1.33	0.734	-1.78
226	226	1.14	20.3	328	9.29	0.791	0.722	430	1.30	0.877	0.880
228	215	1.26	21.8	330	8.94	0.843	1.41	432	1.26	0.747	0.484
230	205	1.40	23.4	332	8.65	0.825	1.33	434	1.22	0.609	0.0625
232	193	1.40	23.1	334	8.36	0.806	1.25	436	1.18	0.519	0.0968
234	180	1.41	22.8	336	8.10	0.800	1.30	438	1.15	0.484	0.632
236	167	1.47	22.8	338	7.87	0.809	1.49	440	1.11	0.447	1.20
238	153	1.59	23.4	340	7.64	0.818	1.70	442	1.08	0.384	-0.388
240	139	1.73	24.0	342	7.45	0.898	2.52	444	1.05	0.318	-2.06
242	126	1.65	20.9	344	7.26	0.982	3.38	446	1.02	0.335	-1.82
244	113	1.56	17.2	346	7.07	0.991	3.48	448	0.974	0.446	0.568
246	101	1.62	15.5	348	6.86	0.918	2.75	450	0.930	0.567	3.18
248	90.0	1.88	16.8	350	6.66	0.842	1.98	452	0.892	0.739	4.40
250	79.5	2.22	18.5	352	6.48	0.942	2.83	454	0.853	0.926	5.74
252	71.7	2.24	17.4	354	6.30	1.05	3.74	456	0.816	1.09	6.94
254	64.0	2.27	16.0	356	6.11	1.08	4.10	458	0.779	1.23	8.00
256	57.5	2.30	14.9	358	5.90	1.03	3.87	460	0.743	1.39	9.16
258	52.3	2.32	14.6	360	5.69	0.969	3.62	462	0.707	1.32	5.99
260	47.1	2.36	14.1	362	5.48	1.02	4.08	464	0.670	1.24	2.46
262	43.8	2.38	14.4	364	5.27	1.08	4.57	466	0.635	1.39	1.87
264	40.5	2.40	14.7	366	5.07	1.13	5.16	468	0.600	1.83	4.74
266	37.9	2.38	14.6	368	4.86	1.18	5.87	470	0.566	2.32	7.95
268	35.8	2.31	14.0	370	4.66	1.24	6.63	472	0.524	2.72	10.9
270	33.8	2.22	13.4	372	4.46	1.29	6.93	474	0.482	3.18	14.4
272	32.5	2.19	13.6	374	4.26	1.35	7.25	476	0.447	3.75	17.9
274	31.2	2.16	13.8	376	4.07	1.44	7.74	478	0.418	4.45	21.4
276	30.0	2.10	13.7	378	3.88	1.54	8.41	480	0.390	5.24	25.4
278	28.9	2.01	13.2	380	3.69	1.66	9.15	482	0.344	5.92	36.6
280	27.9	1.91	12.7	382	3.51	1.60	8.15	484	0.298	6.80	51.2
282	27.0	1.85	12.5	384	3.32	1.54	7.04	486	0.269	7.91	61.2
284	26.1	1.78	12.3	386	3.16	1.62	7.02	488	0.256	9.11	63.1
286	25.1	1.66	11.2	388	3.02	1.85	8.28	490	0.243	10.4	65.2
288	24.2	1.46	9.01	390	2.88	2.11	9.67	492	0.231	11.7	70.6
290	23.2	1.24	6.66	392	2.74	2.16	9.74	494	0.220	13.2	76.5
292	22.2	1.01	4.11	394	2.60	2.22	9.83	496	0.198	14.5	85.0
294	21.2	0.758	1.31	396	2.47	2.21	9.05	498	0.167	16.0	98.6
296	20.2	0.636	-0.188	398	2.36	2.10	7.28	500	0.135	18.2	119
298	19.3	0.666	-0.197	400	2.25	1.98	5.34				
300	18.4	0.699	-0.207	402	2.15	1.95	4.53				

Note:

Absorption cross sections σ and temperature coefficients A1 and A2, 200-500 nm, Burkholder et al. [116] ($\sigma(\lambda,T) = \sigma(\lambda, 296\ K)\ [1 + A1\ (T - 296) + A2\ (T - 296)^2]$).

G10. BrCl + hν → Br + Cl. The absorption spectrum of bromine chloride has been measured at room temperature and 240-313 nm and 546 nm by Gray and Style [298], at 486-548 nm by Jost [396], at 220-510 nm by Seery and Britton [719], at 200-600 nm by Maric et al. [478], at 190-560 nm by Hubinger and Nee [345], and at 200-600 nm by Tellinghuisen [776]. The spectrum exhibits a small absorption band between 190 and 290 nm with the maximum at 230 nm ($\sigma \approx (6.0\text{-}7.2) \times 10^{-20}$ cm^2 molecule^{-1}) and a strong absorption band between 290 and 600 nm with the maximum at 375 nm ($\sigma \approx (3.9\text{-}4.1) \times 10^{-19}$ cm^2 molecule^{-1} and a shoulder near 470 nm. There is good agreement between the results of the six studies except for the values at 289 and 297 nm reported by Gray and Style [298] which are smaller by factors 2.5-6 and 2.5-4, respectively, than the rest of the results. The agreement is within 20% in the small absorption band around 230 nm between the results of Seery and Britton [719], Maric et al. [478], and Hubinger and Nee [345], where Seery and Britton [719] report the highest, Hubinger and Nee [345] the lowest values. Very good agreement within ~5-15% is in the strong absorption band around 375 nm, where Seery and Britton [719] and Tellinghuisen [776] report the highest, Hubinger and Nee [345] the lowest values. The discrepancies are larger, up to 50%, in the region of the absorption minimum around 290 nm, where Seery and Britton [719] and Hubinger and Nee [345] report the highest cross sections, Tellinghuisen [776] the lowest. Excellent agreement is to be observed in the long-wavelength tail above 450 nm between the data of Maric et al. [478] and Tellinghuisen [776], whereas those of Hubinger and Nee [345] are larger by 50% and more and those of Jost [396] are lower by ~20-40%. Maric et al. [478] fitted their data measured at a resolution of 0.2 nm to a three-band semi-logarithmic Gaussian distribution function and derived a mathematical expression which allows the calculation of a smooth absorption curve for BrCl in the wavelength region 200-600 nm:

$$\begin{aligned}\sigma(298\text{ K}) = {} & 6.52\text{x}10^{-20}\text{ cm}^2 \times \exp\{-54.1\,[\ln(227.6\text{ nm}/\lambda)]^2\} \\ & + 3.86\text{x}10^{-19}\text{ cm}^2 \times \exp\{-97.6\,[\ln(372.5\text{ nm}/\lambda)]^2\} \\ & + 9.99\text{x}10^{-20}\text{ cm}^2 \times \exp\{-66.9\,[\ln(442.4\text{ nm}/\lambda)]^2\}\end{aligned}$$

The recommended absorption cross sections calculated at 5-nm intervals from that expression are listed in Table 4.147.

The temperature dependence of the BrCl absorption cross sections has not been measured. A semiempirical expression based on the theory of Sulzer and Wieland [757], which describes the temperature and wavelength dependence of the absorption spectrum, was derived by Maric et al. [478]:

$$\begin{aligned}\sigma(T, \lambda) = {} & 7.34\text{x}10^{-20}\text{ cm}^2 \times \tanh^{0.5} \times \exp\{-68.6 \times \tanh \times [\ln(227.6\text{ nm}/\lambda)]^2\} \\ & + 4.35\text{x}10^{-19}\text{ cm}^2 \times \tanh^{0.5} \times \exp\{-123.6 \times \tanh \times [\ln(372.5\text{ nm}/\lambda)]^2\} \\ & + 1.12\text{x}10^{-19}\text{ cm}^2 \times \tanh^{0.5} \times \exp\{-84.8 \times \tanh \times [\ln(442.4\text{ nm}/l)]^2\}\end{aligned}$$

where λ is the wavelength in vacuum (200-600 nm), tanh = tanh ($hc\omega_e/2KT$) = tanh(318.8/T) (with ω_e = 443.1cm^{-1}), and T the temperature (195-300 K).

No quantum yield data are available, but is expected that BrCl photodissociates with unity quantum yield.

Table 4-147. Absorption Cross Sections of BrCl at 298 K

λ (nm)	10^{20} σ (cm^2)	λ (nm)	10^{20} σ (cm^2)	λ (nm)	10^{20} σ (cm^2)	λ (nm)	10^{20} σ (cm^2)
200	2.64	305	0.845	410	22.51	515	2.13
205	3.61	310	1.47	415	19.95	520	1.74
210	4.59	315	2.51	420	17.80	525	1.41
215	5.47	320	4.08	425	16.04	530	1.13
220	6.13	325	6.30	430	14.63	535	0.892
225	6.47	330	9.25	435	13.49	540	0.700
230	6.48	335	12.92	440	12.55	545	0.544
235	6.17	340	17.21	445	11.73	550	0.419
240	5.60	345	21.90	450	10.98	555	0.320
245	4.86	350	26.68	455	10.25	560	0.243
250	4.05	355	31.18	460	9.52	565	0.182
255	3.24	360	35.03	465	8.78	570	0.136
260	2.50	365	37.91	470	8.02	575	0.101
265	1.86	370	39.61	475	7.24	580	0.0739
270	1.35	375	40.04	480	6.47	585	0.0539
275	0.945	380	39.26	485	5.72	590	0.0390
280	0.653	385	37.45	490	4.99	595	0.0281
285	0.458	390	34.87	495	4.31	600	0.0200
290	0.357	395	31.82	500	3.68		
295	0.360	400	28.59	505	3.10		
300	0.504	405	25.43	510	2.59		

Note:
200-600 nm, Maric et al. [478]

G11. BrOCl + hν → Products. Absorption spectrum of bromine-chlorine monoxide has been measured at room temperature and 230-390 nm by Burkholder et al. [112]. Results are in Table 4-148.

Table 4-148. Absorption Cross Sections of BrOCl at 298 K

λ (nm)	10^{20} σ (cm^2)	λ (nm)	10^{20} σ (cm^2)	λ (nm)	10^{20} σ (cm^2)	λ (nm)	10^{20} σ (cm^2)
230	16.8	272	200	314	55.8	338	46.7
232	15.4	274	199	316	56.6	358	22.5
234	15.2	276	191	318	57.2	360	20.2
236	15.5	278	179	320	57.4	362	18.1
238	16.6	280	165	322	57.3	364	16.1
240	18.6	282	149	324	56.9	366	14.2
242	21.7	284	132	326	56.1	368	12.3
244	26.1	286	115	328	55.1	370	10.6
246	31.6	288	100	330	53.8	372	8.66
248	39.1	290	87.2	332	52.3	374	7.34
250	48.1	292	76.3	334	50.6	376	6.12
252	59.9	294	67.9	336	48.7	378	5.01
254	73.8	296	61.6	340	44.5	380	4.00
256	89.4	298	57.0	342	42.3	382	3.10
258	107	300	54.0	344	39.9	384	2.30
260	126	302	52.4	346	37.3	386	1.62
262	145	304	52.1	348	34.7	388	1.03
264	163	306	52.3	350	32.4	390	0.55
266	179	308	53.0	352	29.8		
268	192	310	53.9	354	27.2		
270	198	312	54.7	356	24.8		

Note:
230-390 nm, Burkholder et al. [112].

G12. $CH_3Br + h\nu \rightarrow$ Products**.** The absorption cross sections of CH_3Br have been measured at room temperature and 205–270 nm by Davidson [205]; at 204–260 nm by Gordus and Bernstein [293]; at 174–270 nm by Robbins [673]; at 200–260 nm by Uthman et al. [797]; at 190–290 nm by Molina et al. [545]; at 201.6 nm by Felps et al. [241]; at 180–264 nm by Man et al. [472]; and at 210–295 K and 180–280 nm by Gillotay and Simon [276]. Above 180 nm and below 270 nm, the room temperature values of Gordus and Bernstein [293], Robbins [673], Uthman et al. [797], Molina et al. [545], Gillotay and Simon [276], and the values of Davidson [205] above 210 nm are in very good agreement, i.e., generally within 10% and around the absorption maximum at 200–202 nm within 2%. The value at 202 nm of Felps et al. [241] is lower by ~10% than the rest of the data. The data of Man et al. [472], given as a plot in their paper, are lower by 20–30% over the whole absorption band than the above-mentioned agreeing data sets. The preferred absorption cross sections, listed in Table 4-149, are the values of Robbins [673] at 174–178 nm; the mean of the values reported by Gillotay and Simon [276] and Robbins [673] at 180–188 nm; the mean of the values reported by Gillotay and Simon [276], Uthman et al. [797], and Robbins [673] at 190–198 nm; the mean of the values reported by Gillotay and Simon [276], Molina et al. [545], Uthman et al. [797], and Robbins [673] at 200–260 nm; the mean of the values reported by Gillotay and Simon [276], Molina et al. [545], and Robbins [673] at 262–268 nm; the mean of the values reported by Gillotay and Simon [276] and Molina et al. [545] at 270–280 nm; and the data of Molina et al. [545] at 285–290 nm.

A slight temperature dependence was observed above 220 nm, where the absorption cross sections decrease with decreasing temperature 295–210 K. Gillotay and Simon [276] parameterized the cross sections and the temperature dependence by the polynomial expansion $\log_{10} \sigma(\lambda, T) = \sum A_n \lambda^n + (T - 273) \times \sum B_n \lambda^n$ and reported smoothed values for T = 210, 230, 250, 270, and 295 K, every 2 nm, and at wavelengths corresponding to the wavenumber intervals generally used in stratospheric photodissociation calculations. The parameters A_n and B_n for the ranges T = 210–300 K and λ = 200–280 nm are as follows:

$A_0 = 46.520$ $\quad$ $B_0 = 9.3408 \times 10^{-1}$

$A_1 = -1.4580$ $\quad$ $B_1 = -1.6887 \times 10^{-2}$

$A_2 = 1.1469 \times 10^{-2}$ $\quad$ $B_2 = 1.1487 \times 10^{-4}$

$A_3 = -3.7627 \times 10^{-5}$ $\quad$ $B_3 = -3.4881 \times 10^{-7}$

$A_4 = 4.3264 \times 10^{-8}$ $\quad$ $B_4 = 3.9945 \times 10^{-10}$

Quantum yields for Br and H atom formation in the photodissociation of CH_3Br were measured at 298 K by Talukdar et al. [771]. The quantum yields for Br atom formation were found to be close to unity, $\Phi(Br) = 1.05 \pm 0.11$, 1.10 ± 0.20, and 1.01 ± 0.16 at 193, 222, and 248 nm, respectively; the quantum yield for H atom formation in the photolysis at 193 nm was measured to be $\Phi(H) = 0.002 \pm 0.001$, whereas H atoms could not be detected in the photolysis at 222 and 248 nm. Broad band flash photolysis of CH_3Br produced $Br^*(^2P_{1/2})$ atoms with a quantum yield $\Phi(Br^*) = 0.15 \pm 0.12$ as reported by Ebenstein et al. [224].

Table 4-149. Absorption Cross Sections of CH_3Br at 295–296 K

λ (nm)	$10^{20}\sigma$ (cm^2)	λ (nm)	$10^{20}\sigma$ (cm^2)	λ (nm)	$10^{20}\sigma$ (cm^2)
174	533	212	59.9	250	0.921
176	1010	214	54.2	252	0.683
178	1280	216	47.9	254	0.484
180	44.6	218	42.3	256	0.340
182	19.8	220	36.6	258	0.240
184	21.0	222	31.1	260	0.162
186	27.8	224	26.6	262	0.115
188	35.2	226	22.2	264	0.0795
190	44.2	228	18.1	266	0.0551
192	53.8	230	14.7	268	0.0356
194	62.6	232	11.9	270	0.0246
196	69.7	234	9.41	272	0.0172
198	76.1	236	7.38	274	0.0114
200	79.0	238	5.73	276	0.00808
202	79.2	240	4.32	278	0.00553
204	78.0	242	3.27	280	0.00382
206	75.2	244	2.37	285	0.00110
208	70.4	246	1.81	290	0.00030
210	65.5	248	1.31		

Note:

174–178 nm, Robbins [673],
180–188 nm, mean of Gillotay and Simon [276] and Robbins [673],
190–198 nm, mean of Gillotay ad Simon [276], Uthman et al. [797], and Robbins [673],
200–260 nm, mean of Gillotay and Simon [276], Molina et al. [545], Uthman et al. [797] and Robbins [673],
262–268 nm, mean of Gillotay and Simon [276], Molina et al. [545], and Robbins [673],
270–280 nm, mean of Gillotay and Simon [276] and Molina et al. [545],
285–290 nm, Molina et al. [545].

G13. $CH_2Br_2 + h\nu \rightarrow CH_2Br + Br$. The absorption cross sections of CH_2Br_2 have been measured at room temperature and 200–300 nm by Molina et al. [545]; at 210–295 K and 174–290 nm by Gillotay et al. [281], [278]; and at 250–348 K and 215–300 nm by Mössinger et al. [563]. The results are in good agreement, at 200–255 nm within 10% and up to 275 nm within 30%. The preferred room temperature values, listed in Table 4-150, are the values of Gillotay et al. [281], [278] at 174–198 nm; the mean of the values reported by Molina et al. [545] and Gillotay et al. [281], [278] for the wavelength range 200–215 nm; the mean of the values reported by the three groups for the wavelength range 220–290 nm; and values of Mössinger et al. [563] at 295–300 nm.

Both studies of the temperature dependence show a decrease of the absorption cross sections with decreasing temperature at wavelength above ~235–239 nm, and the reverse behavior around the absorption maximum down to 207 nm. At lower wavelengths, Gillotay et al. [278, 281] report between 210 and 295 K a slight increase of σ at 175–189 nm and a slight decrease around the weaker absorption maximum at 198–201 nm. The latter group parameterized the cross sections and the temperature dependence by the polynomial expansion
$\log_{10} \sigma(\lambda, T) = \sum A_n \lambda^n + (T - 273) \times \sum B_n \lambda^n$ and report smoothed values for T = 210, 230, 250, 270, and 295 K, every 2 nm, and at wavelengths corresponding to the wavenumber intervals generally used in stratospheric photodissociation calculations. The parameters A_n and B_n for the ranges 210–290 nm and 210–300 K are as follows:

$A_0 = -70.211776$	$B_0 = 2.899280$
$A_1 = 1.940326 \times 10^{-1}$	$B_1 = -4.327724 \times 10^{-2}$
$A_2 = 2.726152 \times 10^{-3}$	$B_2 = 2.391599 \times 10^{-4}$
$A_3 = -1.695472 \times 10^{-5}$	$B_3 = -5.807506 \times 10^{-7}$
$A_4 = 2.500066 \times 10^{-8}$	$B_4 = 5.244883 \times 10^{-10}$

Mössinger et al. [563] list the temperature coefficients $B(\lambda)$ at 5-nm intervals for the ranges 215–300 nm and 250–348 K for the empirical relation $\ln \sigma(\lambda, T) = \ln \sigma(\lambda, 298K) + B(\lambda)x(T-298)$. Formulae used by Gillotay et al. [278, 281] and Mössinger et al. [563] produce cross sections that agree at 250 K within 5% in the range 215–265 nm and within 10% in the range 270–285 nm.

There are no quantum yield measurements, but it is expected that photolysis will rupture the C-Br bond with unity quantum yield.

Table 4-150. Absorption Cross Sections of CH_2Br_2 at 295–298 K

λ (nm)	10^{20} σ (cm^2)	λ (nm)	10^{20} σ (cm^2)	10^3 B (K^{-1})	λ (nm)	10^{20} σ (cm^2)	10^3 B (K^{-1})
174	1170.9	198	226.0		255	14.10	3.91
176	662.4	200	225.6		260	6.607	5.16
178	377.2	205	215.3		265	3.037	6.33
180	241.0	210	234.5		270	1.347	7.75
182	178.4	215	263.2	–2.02	275	0.590	8.74
184	154.4	220	272.0	–1.79	280	0.255	11.6
186	153.5	225	247.4	–1.50	285	0.114	13.8
188	166.1	230	195.8	–0.96	290	0.0499	15.3
190	187.0	235	138.9	–0.04	295	0.0210	16.5
192	209.3	240	88.60	0.71	300	0.0090	21.9
194	222.5	245	51.90	1.80			
196	228.3	250	28.03	2.70			

Note:
Absorption cross sections σ: 174–198 nm, Gillotay et al. [281], [278],
200–210 nm, mean of Molina et al. [545] and Gillotay et al. [281], [278],
215–290 nm, mean of Molina et al [545], Gillotay et al. [281], [278], and Mössinger et al. [563],
295–300 nm, Mössinger et al. [563].

Temperature coefficients B: 215–300 nm, Mössinger et al. [563].

G14. $CHBr_3 + h\nu \rightarrow CHBr_2 + Br$

$CHBr_3 + h\nu \rightarrow CHBr + Br_2$. The absorption cross sections of $CHBr_3$ have been measured at 240–295 K and 170–310 nm by Gillotay et al. [275] and at 256–296 K and 286–362 nm by Moortgat et al. [556]; the agreement in the overlap region is excellent. The recommended cross sections at room temperature, listed in Table 4-151, are the values of Gillotay et al. [275] for the range 170–284 nm; the mean of the values reported by Gillotay et al. [275] and Moortgat et al. [556] for the range 286–310 nm; and the values of Moortgat et al. [556] at 286–362 nm.

The studies of the temperature dependence show an increase of the absorption cross sections with decreasing temperature around the three absorption maxima at 178–189 nm, 194–208 nm, and 208–234 nm, and a decrease of the absorption cross sections below 179 nm, at 189–194 nm and above 235 nm. Gillotay et al. [275] parameterized the cross sections and the temperature dependence by the polynomial expansion

$$\log_{10} (\sigma(\lambda, T)) = \sum A_n \lambda^n + (T - 273) \times \sum B_n \lambda^n$$

and report smoothed values for T = 210, 230, 250, 270, and 295 K, every 2 nm, and at wavelengths corresponding to the wavenumber intervals generally used in stratospheric photodissociation calculations. The parameters A_n and B_n for the ranges 240–310 nm and 210–300 K are given by Gillotay and Simon [278]:

$A_0 = -110.2782$ $\quad B_0 = -1.5312 \times 10^{-1}$
$A_1 = 1.0281$ $\quad B_1 = 1.6109 \times 10^{-3}$
$A_2 = -3.6626 \times 10^{-3}$ $\quad B_2 = -5.8075 \times 10^{-6}$
$A_3 = 4.1226 \times 10^{-6}$ $\quad B_3 = 7.2893 \times 10^{-9}$

For wavelengths longer than 290 nm, the atmospherically important range, Moortgat et al. [556] give the expression

$$\sigma(\lambda,T) = \exp \{(0.06183 - 0.000241 \lambda) (273 - T) - (2.376 + 0.14757 \lambda)\} \quad (\lambda = 290–340 \text{ nm}, T = 210–300 \text{ K})$$

These two formulae produce continuous absorption curves for the range 240–340 nm also at low temperatures

At wavelengths longer than 290 nm, the cross sections are relatively small; the presence of impurities as well as optical artifacts arising, e.g., from adsorption of $CHBr_3$ on the cell windows, complicate the measurements. Hence, additional investigations of the spectrum would be useful.

The quantum yield for the formation of Br atoms were determined by Bayes et al. [64] between 266 and 324 nm. For 303 to 306 nm, the Br-atom quantum yield is unity within experimental error. At longer wavelengths, the quantum yields decreases to 0.76 at 324 nm, but the authors claim that the lower than unity values is the result of systematic and random errors and/or incorrect absorption cross sections. Support for unity quantum yield at λ > 300 nm comes from theoretical calculations by Peterson and Francisco [632], and is recommended for modeling in the troposphere. At 266 nm, the Br-atom quantum yield is 0.76 ± 0.03,

indicating that another photodissociation channel becomes important. Xu et al. [854] measured atomic Br and molecular Br_2 by TOF mass spectrometry from bromoform photolysis at 234 and 267 nm and report evidence for the formation of CHBr + Br_2. At 234 nm the $\varphi(Br) = 0.74$ and $\varphi(Br_2) = 0.26$, while at 267 nm $\varphi(Br) = 0.84$ and $\varphi(Br_2) = 0.16$.

It is recommended that the Br-atom quantum yield is unity at wavelengths above 300 nm.

Table 4-151. Absorption Cross Sections of $CHBr_3$ at 295–296 K

λ (nm)	$10^{20}\sigma$ (cm^2)	λ (nm)	$10^{20}\sigma$ (cm^2)	λ (nm)	$10^{20}\sigma$ (cm^2)
170	1603.8	236	323.9	302	0.534
172	1173.2	238	294.7	304	0.397
174	969.6	240	272.8	306	0.297
176	872.0	242	253.3	308	0.222
178	857.6	244	233.7	310	0.165
180	831.3	246	214.4	312	0.127
182	770.3	248	193.9	314	0.0952
184	683.3	250	174.1	316	0.0712
186	570.4	252	157.7	318	0.0529
188	470.8	254	136.1	320	0.0390
190	399.1	256	116.4	322	0.0289
192	360.2	258	98.6	324	0.0215
194	351.3	260	82.8	326	0.0162
196	366.1	262	68.9	328	0.0121
198	393.6	264	56.9	330	0.00916
200	416.4	266	46.7	332	0.00690
202	433.6	268	38.0	334	0.00525
204	440.6	270	30.8	336	0.00396
206	445.0	272	24.8	338	0.00307
208	451.4	274	19.8	340	0.00240
210	468.5	276	15.8	342	0.00176
212	493.4	278	12.5	344	0.00135
214	524.2	280	9.88	346	0.00102
216	553.5	282	7.77	348	0.00080
218	573.9	284	6.10	350	0.00064
220	582.6	286	4.79	352	0.00054
222	578.0	288	3.74	354	0.00046
224	557.8	290	2.89	356	0.00032
226	527.2	292	2.20	358	0.00024
228	486.8	294	1.69	360	0.00017
230	441.2	296	1.28	362	0.00013
232	397.4	298	0.956		
234	361.8	300	0.719		

Note:
170–284 nm, Gillotay et al. [275],
286–310 nm, mean of Gillotay et al. [275] and Moortgat et al. [556],
312–362 nm, Moortgat et al. [556].

G15. $CH_2BrCH_2Br + h\nu \rightarrow$ Products. Absorption cross sections of CH_2BrCH_2Br have been measured at room temperature and 190–270 nm by Uthman et al. [797]. Their data are listed in Table 4-152.

Table 4-152. Absorption Cross Sections of CH_2BrCH_2Br at 295 K

λ (nm)	10^{20} σ (cm^2)	λ (nm)	10^{20} σ (cm^2)	λ (nm)	10^{20} σ (cm^2)
190	230	218	170	246	9.3
192	250	220	150	248	7.1
194	270	222	130	250	5.9
196	290	224	110	252	4.4
198	300	226	89	254	4.0
200	310	228	75	256	2.8
202	310	230	62	258	2.1
204	300	232	50	260	1.9
206	290	234	41	262	1.7
208	280	236	32	264	1.4
210	260	238	26	266	1.1
212	230	240	20	268	0.9
214	210	242	16	270	0.7
216	190	244	11		

Note:
190–270 nm, Uthman et al. [797].

G16. $C_2H_5Br + h\nu \rightarrow$ Products. The absorption cross sections of C_2H_5Br have been measured at 295 K and 200–260 nm by Zhang et al. [881]. This wavelength range shows part of an absorption band with a maximum of ~ 6×10^{-19} cm^2 at ~200 nm. Estimated values at 5-nm intervals, read from a logarithmic plot, are presented in Table 4-153.

Table 4-153. Absorption Cross Sections of C_2H_5Br at 295 K

λ (nm)	10^{20} σ (cm^2)	λ (nm)	10^{20} σ (cm^2)	λ (nm)	10^{20} σ (cm^2)
200	61	225	24	250	1.1
205	60	230	15	255	0.5
210	54	235	8.3	260	0.2
215	45	240	4.3		
220	34	245	2.3		

Note:
200–260 nm, Zhang et al. [881], estimated values read from logarithmic plot.

G17. $COBr_2 + h\nu \rightarrow$ Products. The absorption cross-sections of $COBr_2$ (carbonyl dibromide, dibromophosgene) have been measured at room temperature and 235-353 nm by Libuda et al. [447] and Libuda [445]. The spectrum exhibits monotonically decreasing absorption cross-sections with increasing wavelength, the maximum obviously lies below 235 nm. As a recommendation are listed in Table 4-154 the averages over 1-nm intervals of the medium-resolution data (0.6 nm) for the range 240-331 nm where the absorption curve shows a regular behavior.

Table 4-154. Absorption Cross Sections of $COBr_2$ at 298 K

λ (nm)	10^{20} σ (cm^2)	λ (nm)	10^{20} σ (cm^2)	λ (nm)	10^{20} σ (cm^2)	λ (nm)	10^{20} σ (cm^2)
240	58.3	263	20.9	286	4.50	309	0.301
241	56.5	264	19.9	287	4.13	310	0.260
242	55.3	265	18.8	288	3.73	311	0.230
243	54.1	266	17.9	289	3.38	312	0.204
244	52.3	267	17.0	290	3.09	313	0.178
245	50.6	268	16.1	291	2.81	314	0.159
246	48.8	269	15.2	292	2.58	315	0.143
247	47.1	270	14.4	293	2.32	316	0.127
248	45.2	271	13.6	294	2.07	317	0.114
249	43.2	272	12.8	295	1.82	318	0.0995
250	41.3	273	12.0	296	1.62	319	0.0892
251	39.5	274	11.4	297	1.42	320	0.0789
252	37.7	275	10.7	298	1.26	321	0.0694
253	35.7	276	9.98	299	1.11	322	0.0633
254	33.7	277	9.24	300	0.971	323	0.0578
255	32.0	278	8.56	301	0.858	324	0.0528
256	30.4	279	7.99	302	0.750	325	0.0499
257	28.9	280	7.44	303	0.661	326	0.0449
258	27.4	281	6.91	304	0.578	327	0.0397
259	26.0	282	6.35	305	0.501	328	0.0336
260	24.5	283	5.81	306	0.437	329	0.0296
261	23.3	284	5.34	307	0.386	330	0.0264
262	22.1	285	4.92	308	0.331	331	0.0229

Note:
240-331 nm, Libuda et al. [447], Libuda [445].

G18. COHBr + hν → Products. The absorption spectrum of COHBr (formyl bromide) has been measured at room temperature and 240-340 nm by Libuda et al. [447] and Libuda [445]. The absorption spectrum exhibits a highly structured absorption band with the maximum near 268 nm. In Table 4-155 are listed the averages over 1-nm intervals of the medium-resolution (0.6 nm) data for the range 240-324 nm where the absorption curve shows a regular behavior.

Table 4-155. Absorption Cross Sections of COHBr at 298 K

λ (nm)	10^{20} σ (cm^2)	λ (nm)	10^{20} σ (cm^2)	λ (nm)	10^{20} σ (cm^2)	λ (nm)	10^{20} σ (cm^2)
240	18.7	262	32.4	284	21.7	306	2.77
241	20.1	263	29.9	285	20.1	307	2.43
242	19.4	264	31.1	286	19.1	308	2.12
243	19.8	265	29.9	287	17.5	309	1.90
244	19.1	266	32.5	288	17.3	310	1.65
245	20.0	267	31.6	289	14.9	311	1.51
246	22.6	268	33.8	290	15.5	312	1.34
247	22.6	269	30.9	291	12.7	313	1.13
248	23.6	270	31.9	292	13.3	314	1.01
249	22.5	271	30.9	293	11.1	315	0.801
250	22.3	272	29.6	294	10.8	316	0.687
251	24.0	273	31.4	295	9.79	317	0.613
252	25.0	274	29.3	296	9.08	318	0.611
253	27.1	275	31.5	297	8.03	319	0.576
254	26.9	276	28.5	298	7.35	320	0.522
255	27.5	277	29.1	299	5.97	321	0.476
256	27.5	278	26.8	300	5.86	322	0.424
257	26.9	279	25.6	301	5.25	323	0.363
258	28.8	280	25.1	302	4.47	324	0.308
259	28.9	281	23.2	303	4.38		
260	31.9	282	23.8	304	3.53		
261	30.1	283	22.0	305	3.18		

Note:
240-324 nm, Libuda [447].

G19. CH_2ClBr (Halon-1011) + hν → Products**.** The absorption cross sections of CH_2ClBr have been measured at room temperature and 210–260 nm by Cadman and Simons [131], and at 187–290 nm by Orkin et al. [603]. The data of Cadman and Simons [131], which are given only on a plot in their paper, are smaller by ≤20% than the data of Orkin et al. [603]. The recommended absorption cross sections, listed in Table 4-156, are the data of Orkin et al. [603].

Quantum yields for Br ($^2P_{3/2}$) and Br*($^2P_{1/2}$) atom formation in the photolysis of CH_2ClBr at 193–242 nm and 248–268 nm have been measured by Zou et al. [884] and McGivern et al. [507], respectively. Reported values are as follows:

	193 nm	234 nm	248.5 nm	261.5 nm	266.7 nm:
Φ(Br ($^2P_{3/2}$))	0.82 ± 0.10	0.80 ± 0.10	0.86 ± 0.10	0.84 ± 0.10	0.91 ± 0.10
Φ(Br*($^2P_{1/2}$))	0.18 ± 0.10	0.20 ± 0.10	0.14 ± 0.10	0.16 ± 0.10	0.09 ± 0.10

Table 4-156. Absorption Cross Sections of CH_2ClBr at 295 K

λ (nm)	10^{20} σ (cm^2)	λ (nm)	10^{20} σ (cm^2)	λ (nm)	10^{20} σ (cm^2)
187	151.1	222	57.4	258	1.45
188	126.4	224	50.5	260	1.09
190	104.6	226	44.1	262	0.807
192	100.5	228	38.2	264	0.596
194	104.7	230	32.8	266	0.440
196	111.8	232	28.0	268	0.322
198	119.4	234	23.6	270	0.235
200	124.7	236	19.7	272	0.170
202	127.1	238	16.3	274	0.123
204	126.3	240	13.4	276	0.089
206	122.5	242	10.8	278	0.064
208	116.3	244	8.73	280	0.046
210	108.4	246	6.94	282	0.033
212	99.6	248	5.46	284	0.024
214	90.5	250	4.24	286	0.0178
216	81.5	252	3.29	288	0.0129
218	72.9	254	2.52	290	0.0098
220	64.8	256	1.92		

Note:
187–290 nm, Orkin et al. [603].

G20. $CHClBr_2$ (Halon-1012) + hν → CH_2Cl + Br ($^2P_{3/2}$)
$CHClBr_2$ (Halon-1012) + hν → CH_2Cl + Br*($^2P_{1/2}$)
$CHClBr_2$ (Halon-1012) + hν → CH_2Br + Cl ($^2P_{3/2}$)
$CHClBr_2$ (Halon-1012) + hν → CH_2Br + Cl*($^2P_{1/2}$). The absorption cross sections of $CHClBr_2$ have been measured at room temperature and 106–200 nm by Ibuki et al. [356]; at 240, 261, and 296 K and 200–310 nm by Bilde et al. [69]; and at 295 K and 193.3 nm by Taketani et al. [763]. Two absorption bands are apparent above 200 nm, one maximizing near 206 nm and the other near 240 nm. Near the band maxima, the cross sections at 240 K are approximately higher by 10% than those at room temperature. A positive temperature dependence of the cross sections is evident in the long-wavelength tail of the spectrum, the room temperature cross section being about 15% higher at 270 nm than that obtained at 240 K. The recommended absorption cross sections, listed in Table 4-157, are the room temperature data of Bilde et al. [69] (originally listed at 1-nm intervals); values at 2-nm intervals are given for wavelengths above 212 nm, and values at 1-nm intervals are given or the region of the first absorption maximum (200–212 nm), where the absorption curve shows a somewhat irregular behavior. Taketani et al. [763] reported a value of 304 × 10^{20} cm^2 $molecule^{-1}$ at 193.3 nm.

Quantum yields for dissociation have been measured by Tzeng et al. [793] at 193 and 248 nm; by McGivern et al. [507] from 248 to 268 nm; by Zou et al, [884] between 193 and 242 nm; by Lee et al. [439] at 234 nm; and by Taketani et al. [763] at 193.3 nm. In the range 248-262 nm, $CHClBr_2$ undergoes C-Br bond rupture exclusively, whereas in the range 193-242 nm it predominantly dissociates via C-Br bond rupture, with a minor contribution from C-Cl bond rupture. The relative quantum yield for ground state Br($^2P_{3/2}$) varies from 0.80 to 0.90 in the range 193 to 267 nm, whereas the quantum yield for spin excited Br*($^2P_{1/2}$) ranges from 0.20 to 0.10.

Table 4-157. Absorption Cross Sections of $CHClBr_2$ at 296 K

λ (nm)	10^{20} σ (cm^2)	λ (nm)	10^{20} σ (cm^2)	λ (nm)	10^{20} σ (cm^2)
200	274.6	230	141.4	272	9.415
201	282.8	232	136.4	274	7.552
202	293.9	234	131.4	276	5.950
203	306.7	236	126.8	278	4.687
204	314.2	238	122.2	280	3.691
205	320.6	240	116.0	282	2.884
206	324.9	242	109.2	284	2.261
207	323.7	244	101.2	286	1.734
208	322.9	246	92.70	288	1.331
209	324.6	248	83.52	290	1.016
210	317.8	250	74.04	292	0.7907
211	306.2	252	64.83	294	0.6116
212	297.4	254	55.95	296	0.4583
214	279.4	256	47.67	298	0.3489
216	261.7	258	39.92	300	0.2692
218	234.9	260	33.35	302	0.2076
220	215.1	262	27.50	304	0.1588
222	199.1	264	22.50	306	0.1208
224	184.5	266	18.28	308	0.0945
226	165.3	268	14.78	310	0.0742
228	151.7	270	11.82		

Note:
200–310 nm, Bilde et al. [69]

G21. $CHCl_2Br$ (Halon-1021) + hν → Products. The absorption cross sections of $CHCl_2Br$ have been measured at room temperature and 106–200 nm by Ibuki [356]; at room temperature and 201–270 nm by Cadman and Simons [131]; and at 253, 273 and 298 K and 200–320 nm by Bilde et al. [69]. The data of Cadman and Simons [131], which are given only in a plot in their paper, agree between 200 and 260 nm within ≤15% with the room temperature data of Bilde et al. [69], the absorption maximum, however, is shifted to lower wavelengths. The recommended absorption cross sections, listed in Table 4-158, are those reported by Bilde et al. [69].

A decrease of the absorption cross sections with decreasing temperature was observed between 298 and 253 K over the whole spectrum. The cross section in the absorption maximum, which has been observed at 220 nm by Bilde et al. [69], is approximately 6% lower at 253 K than at room temperature. An increasingly positive temperature dependence was observed at longer wavelengths, the room temperature cross section at 320 nm becoming about four times larger than those at 253 K.

Table 4-158. Absorption Cross Sections of $CHCl_2Br$ at 298 K

λ (nm)	10^{20} σ (cm^2)	λ (nm)	10^{20} σ (cm^2)	λ (nm)	10^{20} σ (cm^2)
200	115.0	230	58.1	276	1.63
202	93.8	232	54.6	278	1.32
204	81.1	234	50.0	280	1.07
206	73.6	236	45.8	282	0.865
208	69.0	238	41.6	284	0.694
209	69.8	240	37.3	286	0.573
210	68.8	242	33.0	288	0.454
211	67.4	244	29.3	290	0.384
212	68.4	246	25.8	292	0.317
213	70.0	248	22.2	294	0.265
214	70.1	250	19.2	296	0.217
215	70.2	252	16.5	298	0.176
216	71.1	254	13.6	300	0.146
217	71.0	256	11.5	302	0.118
218	70.7	258	9.75	304	0.0962
219	71.3	260	8.19	306	0.0761
220	71.6	262	6.82	308	0.0617
221	70.6	264	5.61	310	0.0496
222	69.3	266	4.68	312	0.0395
223	68.7	268	3.74	314	0.0317
224	68.2	270	3.01	316	0.0259
226	65.2	272	2.48	318	0.0210
228	62.2	274	2.02	320	0.0171

Note:
200–320 nm, Bilde et al. [69].

G22. CCl_3Br (Halon-1031) + hν → CCl_3 + Br. The absorption cross sections of CCl_3Br have been measured at room temperature and 207–305 nm by Cadman and Simons [131], at 365 nm by Sidebottom et al. [729], at 170–230 nm by Roxlo and Mandl [692], at 105-198 nm by Ibuki et al. [357], and at 50-200 nm by Seccombe et al. [718]. The absorption spectrum shows a strong absorption band between 170 and 220 nm with the maximum near 185 nm and $\sigma \approx (1.1\text{-}1.4) \times 10^{-17}$ cm^2 $molecule^{-1}$ followed by a weak shoulder at 220-305 nm. The absorption cross sections for the wavelength region 235-305 nm listed in Table4-159 have been read at 5-nm intervals from a plot in the paper of Cadman and Simons [131], the value for 365 nm has been reported by Sidebottom et al. [729].

Product quantum yield were studied at 365 nm by Sidebottom et al. [729], showing evidence that Br + CCl_3 are the primary products, being pressure and temperature dependent. Quantum yields for Br*($^2P_{1/2}$) atom formation in the photolysis at 234 and 265 nm, Φ(Br*) = 0.31 ± 0.01 and 0.68 ± 0.02, respectively, were reported by Jung et al. [399].

Table 4-159. Absorption Cross Sections of CCl_3Br at 298 K

λ (nm)	10^{20} σ (cm^2)	λ (nm)	10^{20} σ (cm^2)
235	50	275	11
240	50	280	7.2
245	49	285	5.0
250	48	290	3.3
255	46	295	2.2
260	42	300	1.4
265	34	305	1.0
270	19	365	0.0077

Note:
235–305 nm, Cadman and Simons [131],
365 nm, Sidebottom et al. [729].

G23. CHF_2Br (Halon-1201) + hν → Products The absorption cross sections of CHF_2Br have been measured at room temperature and 207–255 nm by Davidson [205]; at 190–280 nm by Talukdar et al. [765]; and at 190–280 nm by Orkin and Kasimovskaya [602]. Gillotay et al. [281] carried out measurements at 210–295 K and

in the wavelength range 166–267 nm and report only smoothed values for T = 210, 230, 250, 270, and 295 K and at wavelengths corresponding to the wavenumber intervals generally used in stratospheric photodissociation calculations. The results of Davidson [205], Orkin and Kasimovskaya [602], and Gillotay et al. [281] are in excellent agreement at wavelengths below 240 nm; the values of Gillotay et al. [281] become increasingly smaller by up to about 40% at 260 nm, and those of Davidson [205] become smaller by up to about 30% at 250 nm than the values of Orkin and Kasimovskaya [602]. The results of Talukdar et al. [765], who report a plot on a logarithmic scale for measured values at 190–280 nm and extrapolated values up to 360 nm, appear to be in agreement with the results of Orkin and Kasimovskaya [602]. The preferred values, listed in Table 4-160, are the values of Gillotay et al. [281] at the centers of the 500-cm^{-1} intervals between 168 and 188 nm, and the values of Orkin and Kasimovskaya [602] at 190–280 nm.

With decreasing temperature 295–210 K, an increase of the absorption cross sections around the absorption maximum at 168–215 nm and a decrease at wavelengths above 215 nm was observed by Gillotay et al. [281] (the interpolation formula has not been reported for this molecule).

Table 4-160. Absorption Cross Sections of CHF_2Br at 298 K

λ (nm)	10^{20} σ (cm^2)	λ (nm)	10^{20} σ (cm^2)	λ (nm)	10^{20} σ (cm^2)
168.10	3.97	206	23.2	246	0.299
170.95	8.21	208	21.2	248	0.220
173.15	12.5	210	19.0	250	0.161
174.65	15.6	212	16.8	252	0.117
176.20	18.8	214	14.6	254	0.0849
177.80	21.9	216	12.6	256	0.0615
179.40	24.5	218	10.6	258	0.0444
181.00	26.6	220	8.85	260	0.0319
182.65	28.3	222	7.25	262	0.0230
184.35	29.6	224	5.88	264	0.0166
186.05	30.6	226	4.71	266	0.0121
187.80	31.4	228	3.73	268	0.0087
190	32.5	230	2.91	270	0.0063
192	32.4	232	2.24	272	0.0046
194	31.8	234	1.71	274	0.0034
196	31.0	236	1.30	276	0.0024
198	29.9	238	0.982	278	0.0018
200	28.6	240	0.735	280	0.0012
202	27.0	242	0.547		
204	25.2	244	0.405		

Note:
168–188 nm, Gillotay et al. [281],
190–280 nm, Orkin and Kasimovskaya [602].

G24. CF_2Br_2 (Halon-1202) + hν → Products. The absorption cross sections of CF_2Br_2 have been measured at room temperature and 215–290 nm by Davidson [205]; at 200–310 nm by Walton [834]; at 190–340 nm by Molina et al. [545]; at 190–320 nm by Orkin and Kasimovskaya [602]; at 210–295 K and 170–304 nm by Gillotay and Simon [277]; and at 210–296 K and 190–320 nm by Burkholder et al. [120]. The room temperature data, except those of Walton [834], are in good agreement, i.e., better than 10%, over their common wavelength range from 190 to 300 nm. In the absorption maximum around 226 nm, the older data of Davidson [205] and Molina et al. [545] are the highest and lowest, respectively, and the more recent data agree within 5% (the absorption maximum reported by Walton [834] is larger by ~50%). At wavelengths above 300 nm, the values of Orkin and Kasimovskaya [602] and Burkholder et al. [120] agree within 15%, whereas those of Molina et al. [545] become increasingly larger by up to ~200% at 320 nm (and larger by up to ~660% than the extrapolated values at 340 nm, see below). The preferred absorption cross sections, listed in Table 4-161, are the values of Gillotay and Simon [277] at 170–188 nm; the mean of the values reported by Gillotay and Simon [277], Orkin and Kasimovskaya [602], and Burkholder et al. [120] for the wavelength range 190–304 nm; and the mean of the values reported by the latter two groups for the range 306–320 nm. For wavelengths 322–340 nm, the mean of the values of Orkin and Kasimovskaya [602], and Burkholder et al. [120] for the range 306–320 nm have been extrapolated ($\log \sigma = 1.85109 - 0.07755\ \lambda$).

Measurements in the far UV were reported by Doucet et al. [221] for the wavelength range 60–220 nm and by Seccombe et al. [717] for the wavelength range 55–175 nm.

Both studies of the temperature dependence show an increase of the absorption cross sections in the two absorption bands around 190 and 226 nm with decreasing temperature 296–210 K and the reverse effect at wavelengths above 240 nm and below 177 nm. Gillotay and Simon [277] observed a regular temperature

behavior, i.e., an increase of the maximum absorption cross section at ~225 nm by ~0.09×10^{-18} cm^2 $molecule^{-1}$ per 20-K temperature decrease. Burkholder et al. [120] observed a less pronounced temperature behavior below 250 K (the maximum absorption cross sections agree within 1%), so that their maximum cross section at 210 K is 5% lower than that observed by Gillotay and Simon [277] (in contrast to the cross sections at room temperature which are nearly identical). Different parameterizations for the temperature dependence of the absorption cross section was proposed. Gillotay and Simon [277] give the polynomial expansion

$$\log_{10} \sigma(\lambda, T) = \sum A_n \lambda^n + (T - 273) \times \sum B_n \lambda^n$$

and report smoothed values for T = 210, 230, 250, 270, and 295 K, every 2 nm, and at wavelengths corresponding to the wavenumber intervals generally used in stratospheric photodissociation calculations. The parameters A_n and B_n for the ranges 222–304 nm and 210–300 K are as follows:

$A_0 = -206.2$	$B_0 = 1.0460 \times 10^{-1}$
$A_1 = 2.3726$	$B_1 = -1.4124 \times 10^{-3}$
$A_2 = -1.0527 \times 10^{-2}$	$B_2 = 6.9015 \times 10^{-6}$
$A_3 = 1.9239 \times 10^{-5}$	$B_3 = -1.5164 \times 10^{-8}$
$A_4 = -1.2242 \times 10^{-8}$	$B_4 = 1.3990 \times 10^{-11}$

Burkholder et al. [120] give the expansion

$$\ln \sigma(\lambda, T) = (\sum A_i (\lambda - 268.7998)^i) (1 + (296-T) \sum B_i (\lambda - 268.7998)^i)$$

and report the following parameters A_i and B_i for the ranges 235–260 nm and 210–296 K:

$A_0 = -44.42756$	$B_0 = 1.481886 \times 10^{-4}$
$A_1 = -1.464955 \times 10^{-1}$	$B_1 = 6.77182 \times 10^{-6}$
$A_2 = -5.692188 \times 10^{-4}$	$B_2 = 1.154347 \times 10^{-7}$
$A_3 = 1.155366 \times 10^{-5}$	$B_3 = -2.77145 \times 10^{-11}$
$A_4 = -1.399502 \times 10^{-7}$	$B_4 = -6.619515 \times 10^{-11}$

Burkholder et al. [120] also report a parameterization for cross sections extrapolated to 400 nm:

$$\ln \sigma(\lambda, T) = (\sum A_i (\lambda - 301.0104)^i) (1 + (296-T) \sum B_i (\lambda - 301.0104)^i)$$

and report the following parameters A_i and B_i for the ranges 260-400 nm and 210-296 K:

$A_0 = -49.50456$	$B_0 = 3.616315 \times 10^{-4}$
$A_1 = -1.633525 \times 10^{-1}$	$B_1 = 5.534952 \times 10^{-6}$
$A_2 = 5.170758 \times 10^{-6}$	$B_2 = -1.997903 \times 10^{-8}$
$A_3 = 4.332654 \times 10^{-6}$	$B_3 = -9.234512 \times 10^{-11}$
$A_4 = -3.899051 \times 10^{-8}$	$B_4 = 1.776346 \times 10^{-12}$

According to J. Burkholder (priv. comm.), there are several errors in the original Burkholder et al. publication [120]. In this paper, the parameterization equation is written in terms of $\log_{10}(\sigma(\lambda,T))$ but the correct expression should be given in terms of $\ln(\sigma(\lambda,T))$. In addition, the parameterization equation for extrapolated cross section data is incorrect. These errors were repeated in JPL02-25 but have been corrected in this evaluation.

The quantum yield for formation of CF_2O and Br_2 in the photolysis of CF_2Br_2 at 206, 248, and 302 nm, in the presence of O_2 has been measured to be unity by Molina and Molina [541], independent of pressure, in contrast to an earlier report by Walton [834] that the quantum yield at 265 nm decreases from unity when the system pressure is raised to 50 Torr of CO_2. Primary quantum yields for Br atom formation, $\Phi(Br) = 1.96 \pm 0.27$, 1.63 ± 0.19, and 1.01 ± 0.15, in the photodissociation of CF_2Br_2 at 193, 222, and 248 nm, respectively, were measured at 298 K by Talukdar et al. [771]. A quantum yield for CF_2 formation, $\Phi(CF_2) = 1.15 \pm 0.30$, in the 193-nm photolysis was reported by Talukdar et al. [768].

The transient CF_2Br was detected by molecular beam [420] and spectroscopic studies [294, 813] during photolysis at 248 nm, and confirm that the C-Br bond is broken.

Table 4-161. Absorption Cross Sections of CF_2Br_2 at 295–296 K

λ (nm)	10^{20} σ (cm^2)	λ (nm)	10^{20} σ (cm^2)	λ (nm)	10^{20} σ (cm^2)
170	124.5	228	253.4	286	0.336
172	78.1	230	244.7	288	0.245
174	55.3	232	230.2	290	0.178
176	49.5	234	211.9	292	0.128
178	60.3	236	191.6	294	0.0926
180	75.0	238	169.3	296	0.0672
182	86.6	240	147.3	298	0.0487
184	100.9	242	125.8	300	0.0352
186	111.8	244	106.0	302	0.0253
188	118.0	246	87.8	304	0.0183
190	115.9	248	72.0	306	0.0130
192	110.3	250	58.3	308	0.00919
194	101.6	252	46.5	310	0.00650
196	91.4	254	36.8	312	0.00456
198	82.1	256	28.9	314	0.00319
200	74.9	258	22.4	316	0.00222
202	71.7	260	17.3	318	0.00157
204	73.4	262	13.1	320	0.00105
206	80.7	264	9.90	*322*	*0.000759*
208	93.0	266	7.47	*324*	*0.000531*
210	110.0	268	5.59	*326*	*0.000371*
212	131.0	270	4.17	*328*	*0.000260*
214	154.9	272	3.08	*330*	*0.000182*
216	180.4	274	2.27	*332*	*0.000127*
218	204.7	276	1.66	*334*	*0.000089*
220	226.0	278	1.21	*336*	*0.000062*
222	244.2	280	0.888	*338*	*0.000044*
224	253.3	282	0.647	*340*	*0.000030*
226	256.8	284	0.470		

Note:
170 188 nm: Gillotay and Simon [277]
190–304 nm: mean of Gillotay and Simon [277], Orkin and Kasimovskaya [602], and Burkholder et al. [120]
306–320 nm: mean of Orkin and Kasimovskaya [602] and Burkholder et al. [120]
322–340 nm: extrapolation of mean of Orkin and Kasimovskaya [602], and Burkholder et al. [120] data.

G25. CF_2ClBr (Halon-1211) + hν → Products. The absorption cross sections of CF_2ClBr have been measured at room temperature and 191–307 nm by Giolando et al. [283]; at 190–330 nm by Molina et al. [545]; at 190–304 nm by Orkin and Kasimovskaya [602]; at 210–295 K and 170–302 nm by Gillotay and Simon [277]; and at 210–296 K and 190–320 nm by Burkholder et al. [120]. The agreement between the room temperature data of Orkin and Kasimovskaya [602], Gillotay and Simon [277], and Burkholder et al. [120] is very good in the region of the absorption band, i.e., within 10% over the range 190–240 nm and within 3% in the maximum at 205–206 nm, with one exception: Gillotay and Simon [277] observed a structure near the absorption maximum, different from the other observations, which resulted in values higher by about 10% at 200–202 nm. Molina et al. [545] reported values for the range 190–240 nm which are lower by 10–20% than the above mentioned data. The few data points (at 10-nm intervals) of Giolando et al. [283] fit well to the absorption curves reported by Orkin and Kasimovskaya [602], Gillotay and Simon [277], and Burkholder et al. [120]. The deviations between the various data sets increase at longer wavelengths to ≤30% at 300 nm and up to 55% at 320 nm. The preferred absorption cross sections at 295–298 K, listed in Table 4-162, are the values of Gillotay and Simon [277] at 170–188 nm; the mean of the values reported by Molina et al. [545], Gillotay and Simon [277], Burkholder et al. [120] and Orkin and Kasimovskaya [602] at 190–302 nm; the mean of the values reported by Molina et al. [545], Burkholder et al. [120], and Orkin and Kasimovskaya [602] at 304 nm; and the mean of the values reported by Molina et al. [545] and Burkholder et al. [120] at 306–320 nm.

Measurements in the far UV at 60–220 nm were reported by Doucet et al. [221].

Both studies of the temperature dependence show an increase of the absorption cross sections in the absorption band around 204–206 nm with decreasing temperature 296–210 K and the reverse effect at wavelengths above 233 nm and below 180 nm. Gillotay and Simon [277] observed a regular temperature behavior, i.e., an increase of the maximum absorption cross section by ~0.05×10^{-18} cm^2 $molecule^{-1}$ per 20 K temperature decrease. Burkholder et al. [120] observed a less pronounced temperature behavior (the maximum absorption cross sections agree within 2.5%), so that their maximum cross section at 210 K is lower by 15% than that observed by Gillotay and Simon [277] (in contrast to the cross sections at room temperature which are within 4%). Different parameterizations for the temperature dependence of the absorption cross section have been proposed. Gillotay and Simon [277] give the polynomial expansion

$$\log_{10} \sigma(\lambda, T) = \sum A_n \lambda^n + (T - 273) \times \sum B_n \lambda^n$$

and report smoothed values for T = 210, 230, 250, 270, and 295 K, every 2 nm, and at wavelengths corresponding to the wavenumber intervals generally used in stratospheric photodissociation calculations. The parameters A_n and B_n for the ranges 200–302 nm and 210–300 K are as follows:

$A_0 = -134.80$	$B_0 = 3.3070 \times 10^{-1}$
$A_1 = 1.7084$	$B_1 = -5.0957 \times 10^{-3}$
$A_2 = -9.1540 \times 10^{-3}$	$B_2 = 2.9361 \times 10^{-5}$
$A_3 = 2.1644 \times 10^{-5}$	$B_3 = -7.6198 \times 10^{-8}$
$A_4 = -1.9863 \times 10^{-8}$	$B_4 = 7.6825 \times 10^{-11}$

Burkholder et al. [120] give the expansion

$$\ln \sigma(\lambda, T) = (\sum A_i (\lambda - 259.8989)^i) (1 + (296-T) \sum B_i (\lambda - 259.8989)^i)$$

and report the following parameters A_i and B_i for the ranges 220–260 nm and 210–296 K:

$A_0 = -45.4087$	$B_0 = 1.528905 \times 10^{-4}$
$A_1 = -1.304811 \times 10^{-1}$	$B_1 = 6.024833 \times 10^{-6}$
$A_2 = -6.995443 \times 10^{-4}$	$B_2 = 1.030995 \times 10^{-7}$
$A_3 = 6.159709 \times 10^{-6}$	$B_3 = -6.387931 \times 10^{-11}$
$A_4 = -9.384074 \times 10^{-9}$	$B_4 = -3.718503 \times 10^{-11}$

Burkholder et al. [120] also report a parameterization for cross sections extrapolated to 400 nm:

$$\ln \sigma(\lambda, T) = (\sum A_i (\lambda - 292.2083)^i) (1 + (296-T) \sum B_i (\lambda - 292.2083)^i)$$

and report the following parameters A_i and B_i for the ranges 260-400 nm and 210-296 K:

$A_0 = -50.15428$	$B_0 = 3.778659 \times 10^{-4}$
$A_1 = -1.547025 \times 10^{-1}$	$B_1 = 6.338322 \times 10^{-6}$
$A_2 = -9.551083 \times 10^{-5}$	$B_2 = -1.294407 \times 10^{-8}$
$A_3 = 4.076334 \times 10^{-6}$	$B_3 = -2.430137 \times 10^{-10}$
$A_4 = -2.747685 \times 10^{-8}$	$B_4 = 2.234599 \times 10^{-12}$

According to J. Burkholder (priv. comm.), there are several errors in the original Burkholder et al. publication [120]. In this paper, the parameterization equation is written in terms of $\log_{10}(\sigma(\lambda,T))$ but the correct expression should be given in terms of $\ln(\sigma(\lambda,T))$. In addition, the parameterization equation for extrapolated cross section data is incorrect. These errors were repeated in JPL02-25 but have been corrected in this evaluation.

Quantum yields for Cl and Br atom formation in the photodissociation of CF_2ClBr at 193, 222, and 248 nm, $\Phi(Cl) = 1.03 \pm 0.14$, 0.27 ± 0.04, and 0.18 ± 003, $\Phi(Br) = 1.04 \pm 0.13$, 0.86 ± 0.11, and 0.75 ± 0.13, respectively, and a quantum yield for CF_2 formation in the 193-nm photolysis, $\Phi(CF_2) = 0.91 \pm 0.30$, were measured at 298 K by Talukdar et al. [768].

Table 4-162. Absorption Cross Sections of CF_2ClBr at 295–298 K

λ (nm)	10^{20} σ (cm^2)	λ (nm)	10^{20} σ (cm^2)	λ (nm)	10^{20} σ (cm^2)
170	323.0	222	68.3	274	0.250
172	234.2	224	60.4	276	0.184
174	176.0	226	52.7	278	0.135
176	120.9	228	45.7	280	0.0991
178	84.7	230	39.2	282	0.0724
180	58.1	232	33.8	284	0.0527
182	41.9	234	28.8	286	0.0385
184	35.0	236	24.4	288	0.0282
186	34.1	238	20.4	290	0.0205
188	38.9	240	16.9	292	0.0148
190	46.1	242	13.9	294	0.0106
192	57.0	244	11.4	296	0.00764
194	69.1	246	9.28	298	0.00544
196	81.4	248	7.50	300	0.00391
198	93.5	250	5.99	302	0.00279
200	106.0	252	4.76	304	0.00207
202	113.3	254	3.76	306	0.00161
204	117.4	256	2.94	308	0.00113
206	118.7	258	2.29	310	0.000803
208	117.7	260	1.76	312	0.000569
210	114.2	262	1.36	314	0.000403
212	108.5	264	1.03	316	0.000288
214	101.5	266	0.784	318	0.000213
216	93.6	268	0.593	320	0.000159
218	85.3	270	0.447		
220	76.8	272	0.336		

Note:
170–188 nm: Gillotay and Simon [277]
190–302 nm: mean of Molina et al. [545], Gillotay and Simon [277], Burkholder et al. [120], and Orkin and Kasimovskaya [602]
304 nm: mean of Molina et al. [545], Burkholder et al. [120], and Orkin and Kasimovskaya [602]
306–320 nm: mean of Molina et al. [545] and Burkholder et al. [120].

G26. CF_3Br (Halon-1301) + hν → CF_3 + Br. The absorption cross sections of CF_3Br have been measured at room temperature and 207–255 nm by Davidson [205]; at 170–230 nm by Roxlo and Mandl [692]; at 180–400 nm by Pence et al. [629]; at 190–300 nm by Molina et al. [545]; at 190–270 nm by Orkin and Kasimovskaya [602]; at 210–295 K and 168–280 nm by Gillotay and Simon [277]; and at 210–296 K and 190–285 nm by Burkholder et al. [120]. The agreement between the room temperature data is very good, i.e., 10% and better, in the region of the absorption band between 190 and 230 nm with the exception of the data of Davidson [205] below 210 nm and the whole data set of Roxlo and Mandl [692]. Pence et al. [629] report a plot of the absorbance (in arbitrary units) and give for 193 nm an absorption cross section smaller by one order of magnitude than the rest of the data for 193 nm. At wavelengths above 250 nm, Burkholder et al. [120] and Orkin and Kasimovskaya [602] measured higher values (up to ~ 35% at 270 nm) than those reported by Molina et al. [545] and Gillotay and Simon [277]. The preferred absorption cross sections at 295–298 K, listed in Table 4-163, are the values of Gillotay and Simon [277] at 168–188 nm, the mean of the values reported by Molina et al. [545], Gillotay and Simon [277], Burkholder et al. [120], and Orkin and Kasimovskaya [602] at 190–270 nm, the mean of the values reported by Molina et al. [545], Gillotay and Simon [277], and Burkholder et al. [120] at 272–280 nm, and the values of Molina et al. [545] at 295–300 nm.

Measurements in the far UV at 60–220 nm were reported by Doucet et al. [221].

Both studies of the temperature dependence show an increase of the absorption cross sections in the absorption band between 174 and 216 nm with decreasing temperature 296–210 K and the reverse effect at wavelengths above 218 nm and below 174 nm. Gillotay and Simon [277] observed a regular temperature behavior, i.e., an increase of the maximum absorption cross section by ~0.06×10^{-19} cm^2 $molecule^{-1}$ per 20 K temperature decrease. Burkholder et al. [120] observed a less pronounced temperature behavior (the maximum absorption cross sections agree within 2%), so that their maximum cross section at 210 K is lower by ~25% than that observed by Gillotay and Simon [277] (in contrast to the cross sections at room

temperature which are within 6%). Different parameterizations for the temperature dependence of the absorption cross section have been proposed. Gillotay and Simon [277] give the polynomial expansion

$$\log_{10} \sigma(\lambda, T) = \sum A_n \lambda^n + (T - 273) \times \sum B_n \lambda^n$$

and report smoothed values for T = 210, 230, 250, 270, and 295 K, every 2 nm, and at wavelengths corresponding to the wavenumber intervals generally used in stratospheric photodissociation calculations. The parameters A_n and B_n for the ranges 178–280 nm and 210–300 K are as follows:

$A_0 = 62.563$	$B_0 = -9.1755 \times 10^{-1}$
$A_1 = -2.0068$	$B_1 = 1.8575 \times 10^{-2}$
$A_2 = 1.6592 \times 10^{-2}$	$B_2 = -1.3857 \times 10^{-4}$
$A_3 = -5.6465 \times 10^{-5}$	$B_3 = 4.5066 \times 10^{-7}$
$A_4 = 6.7459 \times 10^{-8}$	$B_4 = -5.3803 \times 10^{-10}$

Burkholder et al. [120] give the expansion

$$\ln \sigma(\lambda, T) = (\sum A_i (\lambda - 242.2466)^i) (1 + (296-T) \sum B_i (\lambda - 242.266)^i)$$

and report the following parameters A_i and B_i for the ranges 214–285 nm and 210–296 K:

$A_0 = -46.70542$	$B_0 = 1.694026 \times 10^{-4}$
$A_1 = -1.55047 \times 10^{-1}$	$B_1 = 8.723247 \times 10^{-6}$
$A_2 = -1.020187 \times 10^{-3}$	$B_2 = 5.953165 \times 10^{-9}$
$A_3 = 2.246169 \times 10^{-5}$	$B_3 = -3.872168 \times 10^{-9}$
$A_4 = -1.300982 \times 10^{-7}$	$B_4 = -1.803325 \times 10^{-11}$

According to J. Burkholder (priv. comm.) there is a typographical error in the original Burkholder et al. publication [120]. In this paper, the parameterization equation is written in terms of $\log_{10} \sigma(\lambda, T)$ but the correct expression should be given in terms of $\ln \sigma(\lambda, T)$. This error was repeated in JPL02-25 but has been corrected in this evaluation.

Quantum yields for Br ($Br(^2P_{3/2} + Br^*(^2P_{1/2})$) atom formation in the photodissociation of CF_3Br at 193 and 222 nm, $\Phi(Br+Br^*) = 1.12 \pm 0.16$ and 0.92 ± 0.15, respectively, were measured at 298 K by Talukdar et al. [771]. A quantum yield for $Br^*(^2P_{1/2})$ atom formation at 193 nm, $\Phi(Br^*) = 0.56 \pm 0.05$, was reported by Pence et al. [629].

Table 4-163. Absorption Cross Sections of CF_3Br at 295–298 K

λ (nm)	10^{20} σ (cm^2)	λ (nm)	10^{20} σ (cm^2)	λ (nm)	10^{20} σ (cm^2)
168	0.517	210	12.1	252	0.107
170	0.696	212	11.4	254	0.0743
172	0.928	214	10.6	256	0.0516
174	1.22	216	9.71	258	0.0357
176	1.60	218	8.65	260	0.0248
178	2.05	220	7.56	262	0.0171
180	2.61	222	6.50	264	0.0118
182	3.26	224	5.47	266	0.00827
184	4.02	226	4.52	268	0.00580
186	4.88	228	3.69	270	0.00399
188	5.82	230	2.91	272	0.00271
190	6.56	232	2.32	274	0.00188
192	7.58	234	1.80	276	0.00129
194	8.63	236	1.39	278	0.00092
196	9.61	238	1.04	280	0.00064
198	10.5	240	0.766	285	0.00022
200	11.3	242	0.563	290	0.00008
202	11.9	244	0.414	295	0.00003
204	12.4	246	0.296	300	0.00001
206	12.5	248	0.212		
208	12.4	250	0.149		

Note:
170–188 nm: Gillotay and Simon [277]
190–270 nm: mean of Molina et al. [545], Gillotay and Simon [277], Burkholder et al. [120] and Orkin and Kasimovskaya [602]
272–280 nm: mean of Molina et al. [545] and Burkholder et al. [120]
285–300 nm: Molina et al. [545].

G27. CH_2=CHBr + hν → Products. The absorption spectrum of bromoethene (vinylbromide) has been measured at room temperature and 164 -254 nm by Orkin et al. [604]. The spectrum shows a very strong absorption band with the maximum at 192 nm, characteristic of the CH_2=CBr- group, and the absorption band of the CH_2=CH- group around 170 nm. Orkin et al. [604] recorded the spectrum at 0.5-nm increments. In Table 4-164 are listed their data selected at 2-nm intervals for the wavelength region 184-254 nm.

Table 4-164. Absorption Cross Sections of CH_2=CHBr at 295 K

λ (nm)	10^{20} σ (cm^2)	λ (nm)	10^{20} σ (cm^2)	λ (nm)	10^{20} σ (cm^2)
184	1970	208	306	232	18.2
186	2320	210	266	234	12.6
188	2710	212	232	236	8.47
190	3000	214	198	238	5.70
192	3160	216	166	240	3.69
194	2950	218	136	242	2.43
196	2470	220	109	244	1.58
198	1800	222	85.9	246	1.03
200	996	224	65.3	248	0.683
202	605	226	49.1	250	0.454
204	440	228	35.7	252	0.315
206	359	230	25.5	254	0.225

Note:
184-254 nm, Orkin et al. [604].

G28. CHBr=CF_2 + hν → Products. The absorption spectrum of 1-bromo-2,2-difluoroethene has been measured at room temperature and 164-266 nm by Orkin et al. [604]. The spectrum shows strong absorption bands between 164 and 190 nm, a weaker and less pronounced band between 190 and 210 nm (maximum 194 nm), and a still weaker band above 210 nm with the maximum near 220 nm. Orkin et al. [604] recorded the spectrum at 0.5-nm increments. In Table 4-165 are listed their data selected at 2-nm intervals for the wavelength region 184-266 nm.

Table 4-165. Absorption Cross Sections of $CHBr=CF_2$ at 295 K

λ (nm)	10^{20} σ (cm^2)	λ (nm)	10^{20} σ (cm^2)	λ (nm)	10^{20} σ (cm^2)	λ (nm)	10^{20} σ (cm^2)
184	2160	206	87.6	228	74.0	250	8.81
186	1020	208	70.1	230	68.2	252	6.51
188	670	210	63.4	232	61.3	254	4.75
190	635	212	63.5	234	53.7	256	3.49
192	671	214	66.7	236	45.9	258	2.54
194	703	216	71.1	238	38.8	260	1.86
196	610	218	75.8	240	31.7	262	1.37
198	471	220	79.3	242	25.5	264	1.04
200	306	222	80.7	244	20.1	266	0.796
202	193	224	80.6	246	15.4		
204	124	226	78.4	248	11.7		

Note:
184-266 nm, Orkin et al. [604].

G29. $CFBr=CF_2 + h\nu \rightarrow$ Products. The absorption spectrum of trifluorobromoethene has been measured at room temperature and 164-274 nm by Orkin et al. [604]. The spectrum shows strong absorption bands between 164 and 188 nm, a weaker and less pronounced band between 188 and 213 nm (maximum 194.5 nm), and a still weaker band above 213 nm with the maximum near 229 nm. Orkin et al. [604] recorded the spectrum at 0.5-nm increments. In Table 4-166 are listed their data selected at 2-nm intervals for the wavelength region 184-274 nm.

Table 4-166. Absorption cross sections of $CFBr=CF_2$ at 295 K

λ (nm)	10^{20} σ (cm^2)	λ (nm)	10^{20} σ (cm^2)	λ (nm)	10^{20} σ (cm^2)	λ (nm)	10^{20} σ (cm^2)
184	456	208	56.1	232	58.1	256	6.87
186	367	210	39.5	234	54.7	258	5.15
188	350	212	34.1	236	50.4	260	3.77
190	373	214	34.5	238	45.1	262	2.78
192	415	216	37.7	240	39.5	264	2.04
194	439	218	42.2	242	33.9	266	1.49
196	434	220	47.2	244	28.5	268	1.09
198	412	222	52.1	246	23.5	270	0.812
200	354	224	56.2	248	19.2	272	0.613
202	263	226	59.0	250	15.2	274	0.469
204	167	228	60.4	252	11.8		
206	95.1	230	60.0	254	9.03		

Note:
184-274 nm, Orkin et al. [604].

G30. $CH_2=CBrCF_3 + h\nu \rightarrow$ Products. The absorption spectrum of 2-bromo-3,3,3-trifluoro-1-propene has been measured at room temperature and 164-254 nm by Orkin et al. [604]. The spectrum shows a very strong absorption band above 174 nm with the maximum at 194 nm, characteristic of the $CH_2=CBr$- group. Orkin et al. [604] recorded the spectrum at 0.5–nm increments. In Table 4-167 are listed their data selected at 2-nm intervals for the wavelength region 184-252 nm.

Table 4-167. Absorption Cross Sections of CH_2=$CBrCF_3$ at 295 K

λ (nm)	10^{20} σ (cm^2)	λ (nm)	10^{20} σ (cm^2)	λ (nm)	10^{20} σ (cm^2)	λ (nm)	10^{20} σ (cm^2)
184	1370	202	1520	220	126	238	6.97
186	1700	204	1080	222	97.3	240	4.77
188	2040	206	774	224	73.1	242	3.26
190	2350	208	581	226	54.9	244	2.22
192	2590	210	440	228	40.1	246	1.50
194	2700	212	338	230	28.8	248	1.02
196	2620	214	263	232	20.5	250	0.705
198	2370	216	208	234	14.4	252	0.496
200	1980	218	162	236	10.2		

Note:
184-252 nm, Orkin et al. [604].

G31. CF_3CH_2Br (Halon-2301) + hν → Products. The absorption cross sections of CF_3CH_2Br have been measured at 295 K and 190–294 nm by Orkin and Kasimovskaya [602]. Their results are listed in Table 4-168.

Table 4-168. Absorption Cross Sections of CF_3CH_2Br at 295 K

λ (nm)	10^{20} σ (cm^2)	λ (nm)	10^{20} σ (cm^2)	λ (nm)	10^{20} σ (cm^2)
190	45.4	226	16.6	262	0.190
192	49.5	228	14.1	264	0.137
194	52.5	230	11.9	266	0.0983
196	54.4	232	9.85	268	0.0705
198	55.1	234	8.10	270	0.0504
200	54.7	236	6.58	272	0.0361
202	53.3	238	5.28	274	0.0258
204	51.2	240	4.20	276	0.0184
206	48.6	242	3.31	278	0.0132
208	45.7	244	2.58	280	0.0096
210	42.5	246	2.01	282	0.0069
212	39.1	248	1.53	284	0.0048
214	35.7	250	1.16	286	0.0034
216	32.2	252	0.876	288	0.0025
218	28.8	254	0.653	290	0.0018
220	25.5	256	0.484	292	0.0013
222	22.3	258	0.357	294	0.0011
224	19.4	260	0.261		

Note:
190–294 nm, Orkin and Kasimovskaya [602].

G32. $CF_3CHClBr$ (Halon-2311) + hν →. CF_3CHCl + Br

$CF_3CHClBr$ (Halon-2311) + hν →. CF_3CHBr + Cl. The absorption cross sections of $CF_3CHClBr$ have been measured at room temperature and 190–310 nm by Orkin and Kasimovskaya [602]; at 210–295 K and 170–290 nm by Gillotay et al. [281]; at 223–298 K and 200–310 nm by Bilde et al. [69]; and at 295 K and 193.3 nm by Taketani et al. [763]. The room temperature values are in good agreement within 5–15% at wavelengths below 280 nm, where Gillotay et al. [281], [278] report the lowest, Orkin and Kasimovskaya [602] the highest values. At wavelengths above 280 nm, the data of Bilde et al. [69] become increasingly higher (up to 100% at 310 nm) than those of Orkin and Kasimovskaya [602]. The preferred absorption cross sections, listed in Table 4-169, are the values of Gillotay et al. [281] at 170–188 nm; the mean of the values reported by Gillotay et al. [281] and Orkin and Kasimovskaya [602] at 190–198 nm; the mean of the values reported by the three groups at 200–290 nm; and the mean of the values reported by Orkin and Kasimovskaya [602] and Bilde et al. [69] at 292–310 nm. Taketani et al. [763] reported a value of 107×10^{-20} cm^2 $molecule^{-1}$ at 193.3 nm.

The study of the temperature dependence by Gillotay et al. [281] shows an increase of the absorption cross sections in the absorption band between 192 and 238 nm with decreasing temperature 295–210 K and the reverse effect at wavelengths above 238 nm and below 192 nm; the increase in the absorption maximum at ~202 nm is ~0.024×10^{-18} cm^2 $molecule^{-1}$ per 20 K temperature decrease, i.e., an increase by ~10% between 295 and 210 K. Bilde et al. [69] observed a less pronounced temperature behavior in the absorption band (the

maximum absorption cross sections agree within 3%) and a decrease of the absorption cross sections with decreasing temperature at wavelengths above 214 nm.

Gillotay and Simon [281] parameterized the cross sections and the temperature dependence of the absorption cross section by the polynomial expansion

$$\log_{10} \sigma(\lambda, T) = \sum A_n \lambda^n + (T - 273) \times \sum B_n \lambda^n$$

and report smoothed values for T = 210, 230, 250, 270, and 295 K, every 2 nm, and at wavelengths corresponding to the wavenumber intervals generally used in stratospheric photodissociation calculations. The parameters A_n and B_n for the ranges 190–290 nm and 210–300 K are as follows:

$A_0 = -127.157358$ $\quad B_0 = -7.959828 \times 10^{-2}$

$A_1 = 1.635435$ $\quad B_1 = 1.978026 \times 10^{-3}$

$A_2 = -9.002683 \times 10^{-3}$ $\quad B_2 = -1.627866 \times 10^{-5}$

$A_3 = 2.190678 \times 10^{-5}$ $\quad B_3 = 5.480744 \times 10^{-8}$

$A_4 = -2.062651 \times 10^{-8}$ $\quad B_4 = -6.480935 \times 10^{-11}$

Note: There was a typographical error in JPL02-25 for parameter A_4. The error has been corrected in the present evaluation.

Taketani et al. [763] reported the total yield of Cl atoms as 0.28 ± 0.02 in the photodissociation of $CF_3CHClBr$ at 193.3 nm, implying that the rupture of the C-Br bond should be dominant photodissociation channel.

Table 4-169. Absorption Cross Sections of $CF_3CHClBr$ at 295–298 K

λ (nm)	10^{20} σ (cm^2)	λ (nm)	10^{20} σ (cm^2)	λ (nm)	10^{20} σ (cm^2)
170	702.6	218	78.7	266	0.980
172	614.6	220	71.0	268	0.765
174	496.8	222	63.3	270	0.575
176	379.8	224	56.3	272	0.444
178	281.1	226	49.5	274	0.339
180	206.1	228	43.3	276	0.258
182	153.3	230	37.3	278	0.196
184	118.4	232	32.2	280	0.149
186	97.1	234	27.6	282	0.111
188	86.6	236	23.6	284	0.0818
190	93.4	238	20.0	286	0.0606
192	99.8	240	16.8	288	0.0448
194	107.1	242	14.0	290	0.0331
196	114.3	244	11.7	292	0.0263
198	119.7	246	9.51	294	0.0198
200	121.5	248	7.79	296	0.0147
202	123.0	250	6.38	298	0.0109
204	122.3	252	5.15	300	0.00808
206	119.7	254	4.13	302	0.00583
208	115.1	256	3.31	304	0.00450
210	109.0	258	2.63	306	0.00313
212	102.0	260	2.06	308	0.00235
214	94.6	262	1.61	310	0.00180
216	86.7	264	1.26		

Note:
170–188 nm, Gillotay et al. [281], [278],
190–198 nm, mean of Gillotay et al. [278, 281] and Orkin and Kasimovskaya [602],
200–290 nm, mean of Gillotay et al. [278, 281], Orkin and Kasimovskaya [602], and Bilde et al. [69],
292–310 nm, mean of Orkin and Kasimovskaya [602] and Bilde et al. [69].

G33. CF_3CHFBr (Halon-2401) + hν → Products. The absorption cross sections of CF_3CHFBr have been measured at 295 K and 190–280 nm by Orkin and Kasimovskaya [602]. Their results are listed in Table 4-170.

Table 4-170. Absorption Cross Sections of CF_3CHFBr at 295 K

λ (nm)	10^{20} σ (cm^2)	λ (nm)	10^{20} σ (cm^2)	λ (nm)	10^{20} σ (cm^2)
190	24.9	222	11.0	254	0.226
192	26.1	224	9.38	256	0.166
194	27.0	226	7.91	258	0.121
196	27.5	228	6.58	260	0.0873
198	27.7	230	5.42	262	0.0628
200	27.4	232	4.42	264	0.0450
202	26.9	234	3.53	266	0.0325
204	26.0	236	2.79	268	0.0235
206	24.8	238	2.19	270	0.0171
208	23.4	240	1.69	272	0.0124
210	21.9	242	1.30	274	0.0093
212	20.2	244	0.991	276	0.0069
214	18.3	246	0.736	278	0.0053
216	16.5	248	0.556	280	0.0040
218	14.6	250	0.416		
220	12.8	252	0.308		

Note:
190–280 nm, Orkin and Kasimovskaya [602].

G34. CF_2BrCF_2Br (Halon-2402) + hν → Products. The absorption cross sections of CF_2BrCF_2Br have been measured at room temperature and 195–320 nm by Molina et al. [545] and at 190–300 nm by Orkin and Kasimovskaya [602]; at 210–295 K and 170–280 nm by Gillotay et al. [281], and at 210–296 K and 190–320 nm by Burkholder et al. [120]. The room temperature data are in very good agreement, in the absorption band at 180–240 nm generally within 10%, in the absorption maximum at ~200 nm within 5%, and in the long-wavelength tail up to 310 nm within 15%. The preferred absorption cross sections at 295–298 K, listed in Table 4-171, are the values of Gillotay et al. [281] at 170–186 nm; the mean of the values reported by Molina et al. [545], Gillotay et al. [281], Burkholder et al. [120], and Orkin and Kasimovskaya [602] at 196–280 nm; the mean of the values reported by Molina et al. [545], Burkholder et al. [120], and Orkin and Kasimovskaya [602] at 282–300 nm; and the mean of the values reported by Molina et al. [545] and Burkholder et al. [120] at 302–320 nm. In the region around 190 nm, there is some uncertainty, because there is no continuous transition between the absorption curve of Gillotay et al. [281] and that obtained by averaging the data of Gillotay et al. [281], Burkholder et al. [120], and Orkin and Kasimovskaya [602]. We therefore smoothed the absorption curve between 186 and 196 nm and give estimated values for 188, 190, 192, and 194 nm.

The results of the two temperature studies are rather controversial. A regular, but weak decrease of the absorption cross sections at 194–280 nm with decreasing temperature 295 to 210 K and the reverse effect below 194 nm was observed by Gillotay et al. [281]; the decrease in the absorption maximum at ~200 nm is ~0.010×10^{-18} cm^2 $molecule^{-1}$ per 20-K temperature decrease, i.e., a decrease by ~4% between 295 and 210 K. Burkholder et al. [120] observed a strong increase over the whole absorption band (increase of the absorption maximum by 20%) with decreasing temperature 296–210 K, and the reverse effect above 230 nm. So, low-temperature data of these two groups are not comparable. Different parameterizations of the temperature dependence of the absorption cross section have been proposed. Gillotay and Simon [281] give the polynomial expansion

$$\log_{10} \sigma(\lambda, T) = \sum A_n \lambda^n + (T - 273) \times \sum B_n \lambda^n$$

and report smoothed values for T = 210, 230, 250, 270, and 295 K, every 2 nm, and at wavelengths corresponding to the wavenumber intervals generally used in stratospheric photodissociation calculations. The parameters A_n and B_n for the ranges 190–290 nm and 210–300 K are as follows:

$A_0 = 34.026000$	$B_0 = 4.010664 \times 10^{-1}$
$A_1 = -1.152616$	$B_1 = -8.358968 \times 10^{-3}$
$A_2 = 8.959798 \times 10^{-3}$	$B_2 = 6.415741 \times 10^{-5}$
$A_3 = -2.9089 \times 10^{-5}$	$B_3 = -2.157554 \times 10^{-7}$
$A_4 = 3.307212 \times 10^{-8}$	$B_4 = 2.691871 \times 10^{-10}$

Burkholder et al. [120] give the expansion

$$\ln \sigma(\lambda, T) = (\sum A_i (\lambda - 242.4015)^i)\ (1 + (296-T) \sum B_i (\lambda - 242.4015)^i)$$

and report the following parameters A_i and B_i for the ranges 190–320 nm and 210–296 K:

$A_0 = -43.69218$ $B_0 = 3.301341 \times 10^{-5}$
$A_1 = -1.124704 \times 10^{-1}$ $B_1 = 4.695917 \times 10^{-6}$
$A_2 = -1.213301 \times 10^{-3}$ $B_2 = 6.128629 \times 10^{-8}$
$A_3 = 5.275007 \times 10^{-6}$ $B_3 = -5.443107 \times 10^{-10}$
$A_4 = 6.936195 \times 10^{-8}$ $B_4 = -1.035596 \times 10^{-11}$

According to J. Burkholder (priv. comm.) there is a typographical error in the original Burkholder et al. publication [120]. In this paper, the parameterization equation is written in terms of $\log_{10} \sigma(\lambda, T)$ but the correct expression should be given in terms of $\ln \sigma(\lambda, T)$. This error was repeated in JPL02-25 but has been corrected in this evaluation.

Quantum yields for Br atom formation in the photodissociation of CF_2BrCF_2Br at 193, 233, and 266 nm, $\Phi(Br) = 1.9 \pm 0.1$, 1.9 ± 0.1, and 1.4 ± 0.1, respectively, were measured at room temperature by Zou et al. [885]. These values indicate bond breaking of both C–Br bonds in nearly all the CF_2BrCF_2Br molecules at 193 and 233 nm and in an appreciable fraction of the parent molecules still at 266 nm.

Table 4-171. Absorption Cross Sections of CF_2BrCF_2Br at 296 K

λ (nm)	10^{20} σ (cm^2)	λ (nm)	10^{20} σ (cm^2)	λ (nm)	10^{20} σ (cm^2)
170	50.9	222	59.6	274	0.112
172	56.4	224	52.6	276	0.0813
174	62.3	226	45.9	278	0.0592
176	68.5	228	39.7	280	0.0428
178	75.1	230	33.9	282	0.0300
180	81.8	232	28.8	284	0.0216
182	88.6	234	24.1	286	0.0152
184	95.3	236	19.9	288	0.0109
186	101.8	238	16.4	290	0.00784
188	*107.0*	240	13.2	292	0.00569
190	*112.0*	242	10.6	294	0.00410
192	*116.5*	244	8.45	296	0.00301
194	*120.0*	246	6.68	298	0.00219
196	122.3	248	5.25	300	0.00161
198	123.7	250	4.03	302	0.00124
200	124.3	252	3.12	304	0.00094
202	123.6	254	2.37	306	0.00071
204	120.3	256	1.78	308	0.00054
206	115.9	258	1.34	310	0.00042
208	110.4	260	0.973	312	0.00033
210	104.2	262	0.718	314	0.00026
212	97.4	264	0.529	316	0.00020
214	90.1	266	0.390	318	0.00016
216	82.4	268	0.287	320	0.00014
218	74.8	270	0.211		
220	67.0	272	0.154		

Note: 170–186 nm: Gillotay et al. [281]
188–194 nm: values estimated by smoothing the absorption curve
196–280 nm: mean of Molina et al. [545], Gillotay et al. [281], Burkholder et al. [120], and Orkin and Kasimovskaya [602]
282–300 nm: mean of Molina et al. [545], Burkholder et al. [120], and Orkin and Kasimovskaya [602]
302–320 nm: mean of Molina et al. [545] and Burkholder et al. [120].

G35. CF_3CF_2Br (Halon-2501) + hν → Products. Table 4-172 lists the absorption cross sections of CF_3CF_2Br measured at room temperature and reported at 5-nm intervals by Molina et al. [545]. The results of Zhang et al. [881], who report a plot on a logarithmic scale for measured values at 200–250 nm, are about 30% larger over that wavelength range than the results of Molina et al. [545]. Pence et al. [629] measured the absorption cross sections at 180–400 nm, report a plot of the absorbance (in arbitrary units) and give for 193 nm an absorption cross section smaller by ~ 40% than that reported by Molina et al. [545].

Broad band flash photolysis of CF_3CF_2Br produced $Br^*(^2P_{1/2})$ atoms with a quantum yield $\Phi(Br^*) = 0.48 \pm 0.02$ as reported by Ebenstein et al. [224]. A quantum yield for $Br^*(^2P_{1/2})$ atom formation at 193 nm, $\Phi(Br^*)$

= 0.16 ± 0.08, was reported by Pence et al. [629].

Table 4-172. Absorption Cross Sections of CF_3CF_2Br at 298 K

λ (nm)	10^{20} σ (cm^2)	λ (nm)	10^{20} σ (cm^2)	λ (nm)	10^{20} σ (cm^2)
190	18.1	230	3.83	270	0.0112
195	18.4	235	2.22	275	0.00505
200	18.1	240	1.20	280	0.00218
205	16.9	245	0.620	285	0.00100
210	14.8	250	0.305	290	0.00045
215	12.0	255	0.135	295	0.00020
220	8.94	260	0.0590	300	0.00009
225	6.13	265	0.0260		

Note:
190–300 nm, Molina et al. [545].

G36. $CH_3CH_2CH_2Br + h\nu \rightarrow$ Products.

G37. $CH_3CHBrCH_3 + h\nu \rightarrow$ Products. The absorption spectra of 1-bromopropane (n-propyl bromide) and 2-bromopropane (isopropyl bromide) have been measured at room temperature and 164-270 nm by Kozlov et al. [419]. The spectra show an absorption band above 180 nm with maxima at~201 nm for 1-bromopropane and ~209 nm for 2-bromopropane, respectively, and structured features below 180 nm characteristic of the C-Br band absorptions in bromoalkanes. In Table 4-173 are listed the absorption cross sections reported by Kozlov et al. [419] at 2-nm intervals over the stratospheric transparency window near 200 nm

Table 4-173. Absorption Cross Sections of $CH_3CH_2CH_2Br$ and $CH_3CHBrCH_3$ at 295 K

λ (nm)	10^{20} σ (cm^2)		λ (nm)	10^{20} σ (cm^2)	
	$CH_3CH_2CH_2Br$	$CH_3CHBrCH_3$		$CH_3CH_2CH_2Br$	$CH_3CHBrCH_3$
180	108.5	220.2	206	68.8	43.5
182	29.9	36.5	208	65.2	44.2
184	29.5	18.2	210	61.0	44.2
186	35.6	17.6	212	56.5	43.6
188	42.7	19.4	214	51.5	42.2
190	49.8	22.1	216	46.6	40.1
192	56.5	24.8	218	41.4	37.4
194	62.5	28.0	220	35.8	34.1
196	67.0	31.3	222	30.8	30.7
198	70.2	34.3	224	26.0	27.1
200	71.8	37.3	226	21.8	23.6
202	72.6	39.9	228	17.8	20.2
204	71.2	42.0	230	14.4	16.8

Note: 180-230 nm, Kozlov et al. [419].

G38. $CH_3C(O)CH_2Br + h\nu \rightarrow$ Products. The absorption cross sections of bromoacetone have been measured at 238-296 K and 210-370 nm by Burkholder et al. [111] at a resolution of .6 nm using a diode array spectrometer. The spectrum shows an absorption band above 255 nm with the maximum at ~299 nm of $\sigma = 1.15 \times 10^{-19}$ cm^2 $molecule^{-1}$ at room temperature and a rapid increase of the absorption cross sections below 255 nm to a second stronger band at or below 210 nm with $\sigma \leq 6 \times 10^{-19}$ cm^2 $molecule^{-1}$ at room temperature. The averages over 1-nm intervals of the medium-resolution absorption spectrum are listed in Table 4-174. A slight, but not systematic, decrease of the absorption cross-sections with decreasing temperature was observed only around the absorption minimum and in the long-wavelength wings of both absorption bands.

Photodissociation quantum yields were measured by Burkholder et al. [111] as 1.6 ± 0.25 at 308 nm and 1.0 ± 0.15 at 351 nm. At both wavelengths, the yields of CO and CO_2 were unity and ~0.5, respectively, whereas the yield of HCOOH was measured as 0.15 and that of HBr as ~0.15.

Table 4-174. Absorption Cross Sections of $CH_3C(O)CH_2Br$ at 296 K

λ (nm)	10^{20} σ (cm^2)	λ (nm)	10^{20} σ (cm^2)	λ (nm)	10^{20} σ (cm^2)	λ (nm)	10^{20} σ (cm^2)
210	59.2	248	6.40	286	9.78	324	5.55
211	58.0	249	6.07	287	9.98	325	5.20
212	57.5	250	5.77	288	10.2	326	4.87
213	56.2	251	5.49	289	10.4	327	4.55
214	53.2	252	5.25	290	10.6	328	4.24
215	50.7	253	5.14	291	10.8	329	3.94
216	48.4	254	4.98	292	11.0	330	3.64
217	46.2	255	4.88	293	11.1	331	3.35
218	43.9	256	4.76	294	11.2	332	3.06
219	41.8	257	4.68	295	11.3	333	2.77
220	39.7	258	4.62	296	11.4	334	2.51
221	37.5	259	4.66	297	11.4	335	2.26
222	35.6	260	4.70	298	11.5	336	2.02
223	33.9	261	4.76	299	11.5	337	1.80
224	32.0	262	4.72	300	11.5	338	1.60
225	30.1	263	4.79	301	11.4	339	1.41
226	28.5	264	4.91	302	11.4	340	1.24
227	26.8	265	5.01	303	11.3	341	1.09
228	25.2	266	5.12	304	11.2	342	0.955
229	23.7	267	5.39	305	11.1	343	0.831
230	22.1	268	5.44	306	11.1	344	0.724
231	20.7	269	5.57	307	10.9	345	0.627
232	19.4	270	5.77	308	10.7	346	0.545
233	18.1	271	6.03	309	10.4	347	0.473
234	16.9	272	6.25	310	10.2	348	0.408
235	15.7	273	6.48	311	9.89	349	0.351
236	14.7	274	6.68	312	9.62	350	0.303
237	13.6	275	6.90	313	9.36	351	0.259
238	12.6	276	7.16	314	9.10	352	0.223
239	11.7	277	7.45	315	8.82	353	0.190
240	10.9	278	7.74	316	8.52	354	0.164
241	10.2	279	8.00	317	8.19	355	0.140
242	9.47	280	8.25	318	7.83	356	0.120
243	8.80	281	8.50	319	7.45	357	0.108
244	8.18	282	8.75	320	7.06	358	0.0952
245	7.68	283	9.04	321	6.66	359	0.0838
246	7.22	284	9.29	322	6.28	360	0.0784
247	6.79	285	9.58	323	5.89		

Note:
210-360 nm, Burkholder et al. [111].

PHOTOCHEM-H- IODINE

H1. $I_2 + h\nu \rightarrow 2\ I$. The absorption cross sections of iodine have been measured at room temperature and 440-650 nm by Rabinowitch and Wood [647]; at 105-220 nm by Myer and Samson [569]; at 420-800 nm by Tellinghuisen [775]; at 170-230 nm by Roxlo and Mandl [692]; and at 182-750 nm by Saiz-Lopez et al. [697]. Measurements at single wavelengths (436 and 500 nm) were reported by Bauer et al. [58]. The rest of the measurements (from the years 1923 to 1966) have been carried out at elevated temperatures: at 321-673 K and 400-600 nm by Vogt and Koenigsberger [822]; at 353 K and 450-580 nm and at 613 K and 230-600 nm by Kort m and Friedheim [418]; at 423 to 1323 K and 360-740 nm by Sulzer and Wieland [757]; at 393 K and 600-800 nm by Mathieson and Rees [495]; and at 348 K and 400-650 nm by McMillan [144, 510].

The UV absorption spectrum of iodine shows strong absorption below 200 nm with maxima near 187-188 nm and 183 nm ($\sigma \approx (2\text{-}4) \times 10^{-17}$ cm^2 molecule^{-1}) and a rapid decrease of the cross sections down to $\sigma \approx 1 \times 10^{-20}$ cm^2 molecule^{-1} between 360 and 400 nm. The visible absorption spectrum shows a broad band between 400 and 650 nm, which is continuous below 500 nm, but shows pronounced rovibrational structure between 500 and 630 nm, which is due to the transition from the $X^1\Sigma$ ground state into the bound $B^3\Pi$ upper state. There is also a weaker underlying continuum in the structured region, due to the transition to the $^1\Pi$ repulsive state. The maximum is near 533 nm. At longer wavelengths above 650 nm, there is evidence for another weak absorption band.

The most recent room temperature results of Saiz-Lopez et al. [697] were obtained with a Fourier transform spectrometer at a resolution of 4 cm^{-1} (0.1 nm at 500 nm). The room temperature cross sections of Tellinghuisen [775], who recorded the spectrum with a continuum source of moderate resolution (~2.5 nm), are lower than those of Saiz-Lopez et al. [697] in the continuous region, i.e. lower within 30% at 420-450 nm and within 10% at 450-500 nm. Considering averages over 5-nm intervals of the high-resolution spectrum of Saiz-Lopez et al. [697] for the banded region, there is again good agreement (within 15%) with the results of Tellinghuisen [775]. Discrepancies between these two spectra appear above 600 nm: the results of Saiz-Lopez et al. [697] are larger by up to 35% than those of Tellinghuisen [775] at 600-670 nm; above 670 nm a more rapid decrease of the cross sections is observed by Saiz-Lopez et al. [697] compared to that observed by Tellinghuisen [775], where the cross sections of Saiz-Lopez et al [697] become lower by factors ~2 and ~20 at 710 and 740 nm, respectively. The cross sections obtained by Bauer et al. [58] $(1.41\pm0.05) \times 10^{-18}$ at 436 nm and $(2.25\pm0.09) \times 10^{-18}$ cm^2 molecule^{-1} at 500 nm are in close agreement with the integrated averages of Saiz-Lopez et al. [697]. The absorption curve reported by Rabinowitch and Wood [647] is different from those described above: it is shifted to lower wavelengths with the maximum at 500 nm and a hump near 550 nm.

It has to be noted that in the structured region the measurements of the cross sections have been found to be very dependent on the experimental conditions such as absolute I_2 concentrations and the bath gas pressure. The measurements of Saiz-Lopez et al. [697] were performed at high bath gas pressure and high resolution, so to better define the shape of the spectrum. As recommended absorption cross sections for iodine in the UV and visible regions, listed in Table 4-175, we take the averages over 5-nm intervals calculated from the reported values (at 1-nm intervals for the regions 182-500 nm and 640-750nm, and at 0.1-nm intervals at 500-640 nm) by Saiz-Lopez et al. [697]. In Table 4-176 are given the absorption cross sections for the maxima and minima in the banded region reported by Saiz-Lopez et al. [697].

The photodissociation quantum yields for the production of I atoms were obtained by Brewer and Tellinghuisen [88] by measuring the $I(^2P_{3/2})$ yield using the atomic fluorescence technique under condition of steady-state irradiation of I_2 at 12 wavelengths in the region 500-630 nm. The reported yields were determined relative to the purely dissociative continuum at 292 nm, where a unity quantum yield is assumed.

Table 4-175. Absorption Cross Sections of I_2 at 295 K

λ (nm)	10^{20} σ (cm^2)	λ (nm)	10^{20} σ (cm^2)	λ (nm)	10^{20} σ (cm^2)	λ (nm)	10^{20} σ (cm^2)
185	1853	315	15.1	445	25.8	575	96.6
190	2012	320	12.2	450	33.3	580	92.7
195	1226	325	10.5	455	44.0	585	74.1
200	732	330	7.79	460	57.1	590	65.8
205	519	335	6.18	465	72.2	595	59.4
210	418	340	4.71	470	89.7	600	47.4
215	352	345	4.08	475	109	605	43.3
220	302	350	2.58	480	131	610	40.8
225	290	355	1.94	485	155	615	34.4
230	225	360	1.24	490	179	620	30.5
235	197	365	1.02	495	204	625	28.2
240	169	370	0.659	500	228	630	28.0
245	147	375	0.823	505	254	635	22.6
250	128	380	1.14	510	277	640	23.6
255	110	385	1.01	515	297	645	22.8
260	97.1	390	0.925	520	309	650	21.6
265	84.2	395	1.11	525	319	655	20.7
270	72.9	400	2.93	530	326	660	19.0
275	63.1	405	3.89	535	320	665	17.3
280	54.4	410	4.43	540	306	670	17.7
285	45.9	415	5.44	545	281	675	15.9
290	38.9	420	5.96	550	265	680	14.9
295	32.4	425	8.32	555	237	685	13.9
300	27.4	430	13.5	560	191	690	12.8
305	23.1	435	15.7	565	155	695	10.9
310	18.1	440	20.3	570	130	700	10.3

Note:
185-700 nm, Saiz-Lopez et al. [697].

Table 4-176. Cross Sections at the Maxima and Minima of I_2 at 295 K

λ (nm) maximum	10^{20} σ (cm^2)	λ (nm) minimum	10^{20} σ (cm^2)	λ (nm) maximum	10^{20} σ (cm^2)	λ (nm) minimum	10^{20} σ (cm^2)
500.6	232.5	500.7	231.5	543.6	406.7	545.1	225.3
500.8	233.9	501.0	231.0	545.4	240.5	545.6	219.9
501.1	235.9	501.2	233.7	545.8	371.9	547.4	231.3
501.4	236.6	501.6	234.8	547.6	246.7	548.1	208.0
501.8	239.6	501.9	236.3	548.4	372.2	549.7	226.5
502.1	240.5	502.4	238.8	550.0	251.7	550.6	197.1
502.6	246.5	502.8	240.6	550.8	347.6	552.1	220.6
503.0	247.8	503.3	240.6	552.4	256.8	553.2	187.0
503.5	252.3	503.8	241.0	553.5	321.4	554.6	211.2
504.0	254.4	504.4	243.7	554.8	257.7	555.8	176.3
504.5	255.6	504.9	245.1	556.2	299.4	557.1	200.3
505.2	263.2	505.6	252.0	557.5	254.2	558.6	161.2
505.8	268.7	506.2	252.7	559.0	263.9	559.8	186.1
506.5	271.6	507.0	252.3	560.1	250.0	561.5	126.8
507.2	275.4	507.7	253.7	561.9	203.1	562.7	153.9
507.9	281.7	508.5	254.6	562.9	216.0	564.5	103.7
508.7	284.4	509.3	255.0	564.9	175.0	565.4	143.7
509.6	291.1	510.3	262.8	565.8	208.0	567.5	96.9
510.5	301.6	511.2	264.1	568.1	142.9	568.4	115.4
511.5	308.1	512.2	266.0	568.7	203.5	569.5	131.4
512.5	309.9	513.3	263.0	569.9	139.8	570.7	70.3
513.6	323.1	514.4	266.1	571.0	127.5	571.4	113.9
514.7	325.9	515.6	266.4	571.7	147.2	573.9	76.1
515.9	334.3	516.8	265.0	574.9	131.8	577.3	68.8
517.1	345.9	518.1	269.2	578.1	122.6	580.7	62.7
518.3	353.6	519.4	266.0	581.4	109.7	584.3	51.8
519.8	356.6	520.9	267.1	585.1	105.4	587.8	48.6
521.1	371.0	522.3	267.3	588.7	95.9	591.7	42.4
522.7	379.3	523.9	259.8	592.1	85.7	595.4	42.8
524.2	384.5	525.4	261.4	596.0	80.5	599.1	34.3
525.8	393.7	527.2	252.8	599.6	76.0	603.0	31.6
527.4	398.8	528.9	258.7	603.5	64.3	606.8	28.8
529.2	407.8	530.8	252.2	607.6	53.8	610.8	30.3
531.0	415.9	532.7	242.1	611.8	49.1	614.6	26.4
533.0	423.8	534.7	242.8	615.5	42.5	618.8	26.7
534.9	416.4	536.7	232.6	620.0	37.4	622.2	22.3
537.0	414.8	538.8	224.4	623.6	35.8	627.0	23.1
539.1	409.3	541.0	216.5	628.2	31.8	629.8	24.0
541.4	406.1	543.0	218.5				

Note:
500.6-629.8 nm, Saiz-Lopez et al [697].

H2. $IO + h\nu \rightarrow I + O(^3P)$

$IO + h\nu \rightarrow I + O(^1D)$. The absorption cross sections of iodine monoxide have been measured in the region of the A $^2\Pi_{3/2} \leftarrow$ X $^2\Pi_{3/2}$ electronic transition between 338 and 488 nm. The A –X band shows a smooth shoulder between 340 and 380 nm and some broad peaks superimposed on the continuum which maximizes around 400 nm. Pronounced vibrational structure is seen above 400 nm, the (7,0) to (0,0) and (3,1) to (1,1) bands could be assigned in the absorption spectra recorded at medium resolution. Of special interest (e.g., for the study of the reaction kinetics of IO) is the absorption cross section of the strongest vibrational peak (4,0) at 427.2 nm. The various studies (photolysis of N_2O/I_2, N_2O/CF_3I, and O_3/I_2 mixtures) and the corresponding (4,0) peak cross sections at room temperature are compiled in the following summary:

Table 4-177. Summary of Cross Section Measurements of IO

Reference	Year	Temperature, K	Wavelength Range, nm	Resolution, nm	σ(427.2 nm), 10^{-17} cm^2
Cox and Coker [188]	1983	303	415-470	0.27	3.1 (+2.0/-1.5)
Jenkin and Cox [372]	1985	303	426.9	0.27	2.2 ± 0.5
Sander [701]	1986	250, 273, 298, 317, 341, 373	427.2	0.17	3.1 ± 0.3
Stickel et al. [753]	1988	300	420-455 444.8-446.4	0.3 0.025	3.1 ± 0.6
Laszlo et al. [436]	1995	295	340-447	0.3	2.8 ± 0.5
Harwood et al [312]	1997	203, 220, 250, 338-488		0.14	3.6 ± 0.5*
		253, 275, 298, 323, 353, 373		0.44	3.0 ± 0.4
Atkinson et al. [28]	1999	295	444.48-447.83, 454.98-457.88	0.0013	
			445.04, 455.17	0.7	
Bloss et al. [15]	2001	220, 250, 273, 295, 325	342-455	1.13	1.9 ± 0.17

* Average value between 203 and 373 K (see text below)

At ambient temperature the general shape of the vibrational spectrum is similar for the spectra reported by Laszlo et al. [436], Harwood et al. [312] and Bloss et al. [80], however the difference in the size of the structural features depends on the resolution employed in the various studies. The absorption cross sections measured by Harwood et al. [312] at a resolution of 0.44 nm and scaled to 0.83 of the value obtained for the (4,0) maximum at high (0.14 nm) resolution generally (with exceptions for the region 350-415 nm, see below) are higher than those measured at a resolution of 0.3 nm by Lazlo et al [436] and of 1.13 nm by Bloss et al. [80]. The latter data are the lowest throughout the spectral region 340-465 nm; they are smaller than the values reported by Harwood et al. [312] by factors mostly of 1.5 in the continuous part of the spectrum and at the vibrational maxima, and smaller by factors up to 5 at the minima. Bloss et al. [80] attributed this difference to an underlying absorption due to the absorbing species I_2O_2, considered to be a product of the IO self-reaction.

The absorption curve reported by Laszlo et al. [436] is higher by a factor of ~1.2-1.5 at 350-370 nm and in the maxima of the 395-405-nm region than those reported by Harwood et al. [312], and is very similar to that curve in the region of the (6,0) to (4,0) maxima. The absorption cross section measured by Atkinson et al. [28] at an ultra-high resolution of 0.0013 nm for the (2,0) maximum is higher by a factor of nearly 5 than that measured by Harwood et al. [312], whereas the cross sections reported by Atkinson et al. [28] and Harwood et al. [312] for the (1,0) maximum are nearly the same.

The recommended cross sections were obtained by the following procedure: (1) the spectra of Harwood et al. [312] and Laszlo et al. [436] were degraded to the resolution of the spectrum of Bloss et al. [80] (1.13 nm), (2) the degraded spectra of Harwood et al. [312] were normalized to the (4,0) peak value of Bloss et al. [80], (3) the mean of the degraded and normalized spectra of Harwood et al. [312] and Laszlo et al. [436] and that of Bloss et al. [80] were calculated and averaged over 1 nm intervals. These values are listed in Table 4-178. The recent studies from Dillon et al. and Gómez Martin et al. are noted but were not considered in the present evaluation.

The temperature dependence of the absorption cross section of the (4,0) peak has been studied at 250-373 K by Sander [701]; at 203-373 K by Harwood et al. [312]; and at 220-325 K by Bloss et al. [80]. Sander [701] observed a significant increase of σ(427 nm) from $(2.1 \pm 0.1) \times 10^{-17}$ cm^2 molecule^{-1} at 373 K to $(5.3 \pm 0.5) \times 10^{-17}$ cm molecule^{-1} at 250 K upon flash photolysis of O_2/I_2 mixtures. Bloss et al. [80] observed a less pronounced increase of the absorption cross sections by approximately 40% (σ(T)/σ(295 K) ≈ 0.85 to 1.23) between 325 and 220 K (laser flash photolysis of O_2/I_2 mixtures). Harwood et al. [312], applying laser flash photolysis of N_2O/CF_3I, O_3/I_2, and N_2O/I_2 mixtures, measured absorption cross sections between $(3.1 \pm 0.4) \times 10^{-17}$ and $(3.9 \pm 0.1) \times 10^{-17}$ cm^2 molecule^{-1} independent of the temperature (203–373 K) and derived an average value of $(3.6 \pm 0.5) \times 10^{-17}$ cm^2 molecule^{-1} from the data obtained with the N_2O/CF_3I system.

The quantum yield for $O(^3P)$ formation following photolysis of IO at 355 nm was measured relative to NO_2 photolysis at the same wavelength and was determined as 0.91 ($^{+019}_{-0.26}$) by Ingham et al. [362]. The lifetime of the A $^2\Pi_{3/2}$ was observed to be < 20 ns by Turnipseed et al. [788], indicating that electronic collisional quenching cannot compete with the dissociation into $O(^3P)$ + I, thus confirming the results of Ingham et al. [362].

Table 4-178. Absorption Cross Sections of IO at 298 K

λ (nm)	10^{20} σ (cm^2)	λ (nm)	10^{20} σ (cm^2)	λ (nm)	10^{20} σ (cm^2)	λ (nm)	10^{20} σ (cm^2)
339	81.2	373	381	407	606	441	219
340	118	374	413	408	578	442	168
341	100	375	422	409	643	443	183
342	107	376	402	410	813	444	195
343	89	377	413	411	1010	445	957
344	96.2	378	435	412	976	446	805
345	86.2	379	463	413	786	447	392
346	126	380	504	414	589	448	214
347	112	381	548	415	568	449	269
348	108	382	472	416	414	450	156
349	142	383	435	417	460	451	96.9
350	160	384	523	418	734	452	102
351	154	385	560	419	1380	453	87.3
352	165	386	591	420	1200	454	100
353	163	387	603	421	681	455	457
354	181	388	580	422	365	456	441
355	185	389	598	423	253	457	213
356	194	390	622	424	204	458	132
357	207	391	620	425	205	459	183
358	223	392	617	426	302	460	123
359	230	393	642	427	2050	461	82.3
360	242	394	684	428	1370	462	51.9
361	247	395	694	429	543	463	53.6
362	242	396	709	430	309	464	38.2
363	241	397	701	431	208	465	43.4
364	268	398	654	432	173	466	118
365	273	399	671	433	166	467	134
366	291	400	671	434	177	468	67.2
367	313	401	700	435	653	469	24.2
368	326	402	765	436	1880	470	125
369	343	403	859	437	807	471	76.4
370	346	404	864	438	381		
371	339	405	787	439	249		

372	360	406	667	440	256

Note:
339-471 nm: see text

H3. $OIO + h\nu \rightarrow IO(^2\Pi) + O(^3P)$

$OIO + h\nu \rightarrow I(^2P_J) + O_2$. A qualitative absorption spectrum (optical densities vs. wavelengths) at 298 K and 476-667 nm was first reported by Himmelmann et al. [331], who observed a highly structured absorption band belonging to the A ($^2A_2$) (i,j,k) ← X ($^2B_1$) (0,0,0) vibronic transitions with vibrational progressions of the symmetric I-O stretch (i = 0-9) and the O-I-O bend (j = 0, 1, 2) in the upper electronic state. A first assessment indicated that the absorption cross section at 549.1 nm (in air, resolution of 0.3 nm) is larger than 2.5×10^{-17} cm^2 molecule^{-1} (see however Table 4-179). Absorption cross sections have been measured at room temperature and 514-573 nm at medium resolution of 1.13 nm by Cox et al. [186] and Bloss et al. [80], and at 558-578 nm at high resolution better than 0.006 nm (cavity ring-down spectroscopy) by Ashworth et al. [26]. The vibrational peaks at 562 and 568 nm recorded at high resolution are higher by a factor ~1.7 than those reported at medium resolution. As a recommendation (with a factor of 3 uncertainty) are listed in Table 4-179 the averages over 1-nm intervals of the data reported (at intervals of 0.22 and 0.23 nm) by Bloss et al. [80].

Photodissociation of OIO was studied at a laser wavelength of 532 nm by Ingham et al. [362]. O(^{3}P) atoms were not detected, which enabled the authors to place an upper limit to the quantum yield of $\Phi(O(^3P)) < 0.012$ (this assessment however is based on too high an absorption cross section of $(2.4 \pm 1.0) \times 10^{-17}$ cm^2 molecule^{-1} for OIO at 532 nm). Since photolysis to IO +O can be excluded, Ashworth et al. [26] implied that OIO must largely predissociate to I + O_2 via the upper $^2B_2$ state. Ingham et al. [362] detected I(^2P_J) atoms at very high laser fluence, presumably in a sequential two-photon process. An upper limit for the quantum yield, $\Phi(I(^2P_J)) < 0.15$, was determined.

Table 4-179. Absorption Cross Sections of OIO at 295 K

λ (nm)	10^{20} σ (cm^2)	λ (nm)	10^{20} σ (cm^2)	λ (nm)	10^{20} σ (cm^2)	λ (nm)	10^{20} σ (cm^2)
516	833	531	989	546	582	561	476
517	696	532	1012	547	513	562	769
518	565	533	779	548	665	563	709
519	599	534	636	549	1030	564	524
520	719	535	519	550	842	565	442
521	626	536	643	551	575	566	384
522	573	537	709	552	429	567	613
523	517	538	640	553	377	568	937
524	496	539	548	554	609	569	699
525	534	540	470	555	661	570	475
526	754	541	451	556	604	571	322
527	840	542	494	557	474	572	224
528	697	543	715	558	393		
529	626	544	817	559	373		
530	651	545	676	560	350		

Note:
516-572 nm, Bloss et al. [80].

H4. $HI + h\nu \rightarrow H + I(^2P_{3/2})$

$HI + h\nu \rightarrow H + I^*(^2P_{1/2})$. The absorption spectrum of hydrogen iodide has been measured at room temperature and 200-368 nm by Goodeve and Taylor [290]; at 149-159, 164-175, and 178-244 nm by Romand [684]; at 200-300 nm by Huebert and Martin [352]; at 192-313 nm by Ogilvie [593]; at 170-230 nm by Roxlo and Mandl [692]; at 198–341 nm by Campuzano-Jost and Crowley [148]; and at 195 K and 180-195 K by Huebert and Martin [352]. Single cross sections at room temperature and 254 nm and 147 nm were reported by Bridges and White [90] and Rebbert et al. [665], respectively. The spectrum shows, according to the most recent measurements by Campuzano-Jost and Crowley [148] and those of Huebert and Martin [352], Ogilvie [593], and Roxlo and Mandl [692], an absorption band between 185 and 375 nm with the maximum near 222 nm and a strong absorption peak at 176 nm. There is good agreement between the results of Campuzano-Jost and Crowley [148], Ogilvie [593], and Huebert and Martin [352]: the data reported by Huebert and Martin [352] and Campuzano-Jost and Crowley [148] are nearly identical around the absorption maximum up to ~275 nm; the data reported by Ogilvie [593] are slightly larger over the absorption band than those of the two former authors, where the agreement is better than 10% up to 290 nm and even better than 5% around the maximum from ~215 to 235 nm and in the wing between 255 and 285 nm. At wavelengths above ~280 nm, the three absorption curves are somewhat divergent: the cross sections reported by Huebert and Martin [352] become increasingly larger by up to 27%, those of Ogilvie [593] are smaller (within ~15%) than the cross sections reported by Campuzano-Jost and Crowley [148]. As a recommendation are listed in Table 4-180 the averages over 1-nm intervals of the high-resolution (0.08 nm) data of Campuzano-Jost and Crowley [148].

Martin and Willard [491] measured the quantum yield for H and I atoms in the photolysis at 184.9 and 253.7 nm to be near unity. The relative quantum yield for the formation of $I^*(^2P_{1/2}) = 0.47 \pm 0.03$ at 248 nm was determined by Brewer et al. [89]. Using a broadband flash photolysis, Donohue and Wiesenfeld [220] obtained a yield $I^*(^2P_{1/2}) = 0.10 \pm 0.05$. Recently a detailed study was performed by Langford et al. [433], measuring the branching ratio $I^*(^2P_{1/2}) / I(^2P_{3/2})$ at 24 different wavelengths in the range 200 to 303 nm, which they observed to increase from 0.2 near 208 nm to a maximum value of 1.7 near 252 nm, and to decrease again to 0.1 at 303 nm. In their paper, these authors review several similar studies performed previously and should be consulted for more detailed information.

Table 4-180. Absorption Cross Sections of HI at 298 K

λ (nm)	10^{20} σ (cm^2)	λ (nm)	10^{20} σ (cm^2)	λ (nm)	10^{20} σ (cm^2)	λ (nm)	10^{20} σ (cm^2)
199	59.7	235	71.9	271	16.1	307	1.29
200	61.1	236	70.6	272	15.1	308	1.19
201	62.4	237	69.2	273	14.2	309	1.10
202	63.7	238	67.6	274	13.3	310	1.01
203	65.0	239	66.2	275	12.5	311	0.929
204	66.4	240	64.6	276	11.7	312	0.852
205	67.7	241	62.9	277	10.9	313	0.781
206	69.0	242	61.3	278	10.2	314	0.715
207	70.3	243	59.6	279	9.57	315	0.653
208	71.5	244	57.9	280	8.94	316	0.596
209	72.7	245	56.1	281	8.36	317	0.544
210	73.8	246	54.2	282	7.81	318	0.495
211	74.8	247	52.5	283	7.30	319	0.450
212	75.9	248	50.7	284	6.82	320	0.409
213	76.9	249	48.8	285	6.37	321	0.371
214	77.7	250	47.0	286	5.94	322	0.336
215	78.4	251	45.2	287	5.55	323	0.303
216	79.1	252	43.5	288	5.18	324	0.274
217	79.7	253	41.7	289	4.83	325	0.247
218	80.2	254	39.9	290	4.51	326	0.223
219	80.5	255	38.2	291	4.21	327	0.200
220	80.8	256	36.5	292	3.92	328	0.180
221	80.9	257	34.8	293	3.66	329	0.162
222	81.0	258	33.2	294	3.41	330	0.145
223	80.9	259	31.6	295	3.18	331	0.130
224	80.7	260	30.0	296	2.96	332	0.116
225	80.4	261	28.5	297	2.76	333	0.104
226	80.0	262	27.1	298	2.57	334	0.0928
227	79.5	263	25.7	299	2.40	335	0.0828
228	78.9	264	24.3	300	2.23	336	0.0740
229	78.2	265	23.0	301	2.07	337	0.0660
230	77.4	266	21.7	302	1.92	338	0.0591
231	76.5	267	20.5	303	1.77	339	0.0528
232	75.5	268	19.4	304	1.64	340	0.0470
233	74.4	269	18.3	305	1.52		
234	73.2	270	17.2	306	1.40		

Note:
199-340 nm, Campuzano-Jost and Crowley [148].

H5. HOI + hν → OH + I. The absorption spectrum of hypoiodous acid has been measured at room temperature and 280-500 nm by Bauer et al. [58], and at 280-450 nm by Rowley et al. [691]. Two absorption bands of comparable intensity were observed, one between 280 and ~375 nm with the maximum near 340 nm, and another on between ~375 and 500 nm with the maximum near 404-410 nm. The spectra of Bauer et al. [58] and Rowley et al. [691] are in reasonable agreement. Differences comparing the results of Rowley et al. [691] with those of Bauer et al. [58] are: the absorption maxima are shifted by 2-3 nm to smaller wavelengths; the low-wavelength maximum is slightly higher (~3%), whereas the long-wavelength maximum is smaller by ~15%. As a recommendation are listed in Table 4-181 the mean of the values reported by Rowley et al. [691] and Bauer et al. [58].

Table 4-181. Absorption Cross Sections HOI at 295-298 K

λ (nm)	10^{20} σ (cm^2)	λ (nm)	10^{20} σ (cm^2)	λ (nm)	10^{20} σ (cm^2)	λ (nm)	10^{20} σ (cm^2)
280	0.077	332	36.1	384	20.8	436	11.9
282	0.121	334	37.6	386	22.1	438	10.6
284	0.186	336	38.5	388	23.4	440	9.30
286	0.281	338	39.1	390	24.8	442	8.10
288	0.417	340	39.2	392	26.1	444	7.03
290	0.608	342	38.9	394	27.3	446	6.05
292	0.867	344	38.2	396	28.4	448	5.17
294	1.22	346	37.1	398	29.4	450	4.40
296	1.68	348	35.6	400	30.1	452	3.72
298	2.27	350	33.9	402	30.6	454	3.13
300	3.02	352	32.0	404	30.9	456	2.61
302	3.95	354	30.1	406	30.9	458	2.17
304	5.09	356	28.0	408	30.7	460	1.79
306	6.44	358	26.0	410	30.2	462	1.47
308	8.03	360	24.1	412	29.5	464	1.20
310	9.85	362	22.4	414	28.5	466	0.973
312	11.9	364	20.8	416	27.4	468	0.785
314	14.2	366	19.5	418	26.1	470	0.632
316	16.6	368	18.5	420	24.7	472	0.505
318	19.2	370	17.8	422	23.1	474	0.402
320	21.9	372	17.4	424	21.5	476	0.318
322	24.6	374	17.3	426	19.9	478	0.250
324	27.3	376	17.5	428	18.2	480	0.196
326	29.9	378	18.0	430	16.6		
328	32.2	380	18.8	432	15.0		
330	34.3	382	19.7	434	13.4		

Note:
280-480 nm, mean of the data of Bauer et al. [58] and Rowley et al. [691].

H6. $ICl + h\nu \rightarrow I(^3P_{3/2}) + Cl(^3P_{3/2})$ (1)
$ICl + h\nu \rightarrow I(^3P_{3/2}) + Cl^*(^3P_{1/2})$ (2)
$ICl + h\nu \rightarrow I^*(^3P_{1/2}) + Cl(^3P_{3/2})$ (3)
$ICl + h\nu \rightarrow I^*(^3P_{1/2}) + Cl^*(^3P_{1/2})$ (4). The absorption spectrum of iodine chloride has been measured at room temperature and 380-570 nm by Gibson and Ramsperger [267], at 220-600 nm by Seery and Britton [719], and at 210-690 nm by Jenkin et al. [375]. Measurements at 293, 387, 489, and 685 K and 216.5-310.0 nm have been carried out by Binder [70]. The spectrum shows two absorption bands of nearly equal height, one between 220 and 350 nm with the maximum at ~240-244 nm, and one between 350 and 600 nm with the maximum near 470 nm. The latter band is asymmetric because of the overlap of two or three bands corresponding to the transitions $B\ ^3\Pi_{0+} \leftarrow X\ ^1\Sigma_{0+}$, $^1\Pi \leftarrow X\ ^1\Sigma_{0+}$, and $A\ ^3\Pi_i \leftarrow X\ ^1\Sigma_{0+}$ as shown by Seery and Britton [719] and Mashnin et al. [493]. The experimental data of Seery and Britton [719] and Jenkin et al. [375] are in excellent agreement in the region of the visible absorption band, but appreciably higher (by ~35% in the maximum) than the earlier data of Gibson and Ramsperger [267]. The UV maximum observed by Jenkin et al. [375] is higher by ~14% than those observed by Gibson and Ramsperger [267] and Seery and Britton [719]. The higher absorption cross sections observed by Seery and Britton [719] between the two absorption bands between 290 and 360 nm are certainly due to Cl_2 impurities as argued by Jenkin et al. [375] who used purified samples and subtracted possible Cl_2 contributions in their spectral analysis.

Jenkin et al. [375] give a plot of the absorption spectrum and two numerical values for the absorption maxima: 5.00×10^{-19} cm^2 molecule^{-1} at 244 nm and 4.20×10^{-19} cm^2 molecule^{-1} at 467 nm; further numerical data are no more available. We therefore list in Table 4-182 these values together with the absorption cross sections read at 10-nm intervals from Fig.5 of the paper of Jenkin et al. [375]. For the region between the absorption bands at 310-350 nm, values $<1\times10^{-20}$ cm^2 molecule^{-1} can only be read from the plot (linear scaling of the σ axis) of Jenkin et al. [375].

The temperature study of Binder [70] shows a decrease of the absorption cross sections in the UV band with increasing temperature: in the maximum at 240 nm from 4.40×10^{-19} cm^2 molecule^{-1} at 293 K to 3.53×10^{-19} cm^2 molecule^{-1} at 685 K.

The relative quantum yields Cl*/(Cl* + Cl) in the photodissociation of ICl have been measured by several groups. The work of Mashnin et al. [493] shows that at longer wavelengths (437-532 nm) the Cl*($^3P_{1/2}$) are produced from the channel (2, I +Cl*), with a relative quantum yield varying between 0.41 ± 0.02 and 0.79 ± 0.02. Ni and Flynn [581] measured Cl*/(Cl* + Cl) at 237 nm as 0.17 ± 0.04, while Chichinin [167] obtained 0.67 ± 0.05 at 248 nm, and Chichinin et al. [168] 0.55 ± 0.05 at 530 nm. Tonokura et al. [781] measured in the wavelength range 235-248 nm, the contribution of channels (1, I + Cl), (2, I + Cl*) and (3, I* + Cl) to be 0.2, 0.4 and 0.4, respectively. The branching ratio I*/I = 0.71 ± 0.27 was also determined by Tonokura et al. [781], and by Jung et al. [398] at 304 nm as I*/I = 0.43.

Table 4-182. Absorption Cross Sections of ICl at 298 K

λ (nm)	10^{20} σ (cm^2)	λ (nm)	10^{20} σ (cm^2)	λ (nm)	10^{20} σ (cm^2)
210	7.4	340	<1	480	41.8
220	21.3	350	<1	490	40.0
230	40.0	360	2.3	500	35.4
240	49.0	370	4.6	510	29.0
244	50.0	380	8.74	520	21.1
250	47.8	390	13.8	530	15.6
260	36.8	400	19.0	540	11.0
270	24.4	410	25.0	550	7.3
280	12.9	420	28.5	560	5.5
290	6.4	430	32.0	570	4.2
300	3.2	440	35.4	580	3.4
310	<1	450	38.8	590	2.9
320	<1	460	41.7	600	2.1
330	<1	470	42.0		

Note:
210-600 nm, Jenkin et al. [375].

H7. IBr + hν → I($^3P_{3/2}$) + Br($^3P_{3/2}$) (1)
IBr + hν → I($^3P_{3/2}$) + Br*($^3P_{1/2}$) (2)
IBr + hν → I*($^3P_{1/2}$) + Br($^3P_{3/2}$) (3)
IBr + hν → I*($^3P_{1/2}$) + Br*($^3P_{1/2}$) (4). The absorption spectrum of iodine bromide has been measured at room temperature and 220-600 nm by Seery and Britton [719]. The spectrum shows two absorption bands, a weak one between 220 and 350 nm with the maximum at ~270 nm, and a stronger one between 350 and 600 nm with the maximum at ~500 nm. The absorption cross sections reported by Seery and Britton [719] are listed in Table 4-183.

Absolute quantum yields for Br* formation upon IBr photodissociation were measured by Haugen et al. [319] in the range 450-530 nm. The quantum yields show a steady increase from 0.28 at 450 nm to reach a maximum of 0.73 near 500 nm. Relative Br*/(Br + Br*) quantum yields measured by Peterson and Smith [631] varying from ~0.3 at 444 nm to a maximum of unity near 520 nm, declining to ~0.1 at 670 nm, and of Wrede et al. [853] in the range 440-544 nm display a similar trend. Kim et al. [406] measured at 267 nm the relative quantum yields for the photolysis channels (1, I + Br), (2, I + Br*) and (3, I* + Br) to be respectively 0.23, 0.35 and 0.42.

Table 4-183. Absorption Cross Sections of IBr at 298 K

λ (nm)	10^{20} σ (cm^2)	λ (nm)	10^{20} σ (cm^2)	λ (nm)	10^{20} σ (cm^2)
220	3.59	350	1.45	480	111
230	5.70	360	1.52	490	120
240	10.2	370	2.37	500	122
250	16.7	380	4.17	510	116
260	21.4	390	6.96	520	103
270	23.1	400	12.0	530	85.8
280	21.1	410	20.5	540	67.5
290	16.8	420	31.7	550	52.3
300	12.4	430	44.8	560	36.6
310	7.95	440	58.7	570	27.2
320	5.39	450	71.9	580	19.9
330	3.36	460	85.2	590	14.6
340	2.14	470	98.5	600	11.3

Note:
220-600 nm, Seery and Britton [719].

H8. INO + hν → I + NO. The absorption cross sections of INO (nitrosyl iodide) have been measured at room temperature and 390-470 nm by Porter et al. [643], around 265 and 410 nm by van den Bergh and Troe [803], at 220-460 nm by Basco and Hunt [47], and at 223-300 nm and around 410 nm by Forte et al. [247]. The spectrum shows two absorption bands, a strong and asymmetric one in the UV between 220 and 300 nm with the maximum at 238 nm, and a second one, weaker by two orders of magnitude, between 355 and 470 nm with the maximum near 410 nm. The results for the UV band are in good agreement except for the region around 250 nm, where the absorption curve reported by Basco and Hunt [47] shows a hump and an absorption cross section larger by a factor of ~1.5 than that reported by Forte et al. [247]. The absorption curve in the near UV and visible reported by Porter et al. [643] is shifted to longer wavelengths by ~20 nm and the absorption cross sections are smaller by 50-30% at 400-430 nm compared to the results of Basco and Hunt [47].

As recommended absorption cross sections for the UV band we take the mean of the data of Basco and Hunt [47] and Forte et al. [247] at 223- 290 nm, and the data of Basco and Hunt [47] at 300 and 310 nm. For the absorption band in the near UV and visible we adopt the IUPAC (1982-2000) [61], [31], [30], [29] recommendations (which should be the mean of the data of Van den Berg and Troe [803], Basco and Hunt [47], and Forte et al. [247]), however after correcting the old errors for the values at 400 and 410 nm. The recommended cross sections are listed in Table 4-184.

Table 4-184. Absorption Cross Sections of INO at 298 K

λ (nm)	10^{20} σ (cm^2)	λ (nm)	10^{20} σ (cm^2)
223	225	360	45
230	1690	370	59
235	5640	380	65
238	6850	390	78
245	6000	400	92*
251	4880	410	110*
260	2270	420	100
270	1040	430	94
280	500	440	80
290	187	450	60
300	92	460	40
310	41		

Note:
223-290 nm, mean of Basco and Hunt [47] and Forte et al. [247],

300, 310 nm, Basco and Hunt [47],
360-460 nm, IUPAC-1982-2000 recommendations (* corrected) [61], [31], [30], [29].

H9. $IONO + h\nu \rightarrow I + NO_2$. The absorption cross sections of iodine nitrite have been measured at room temperature and 210-390 nm by Bröske [100]. The spectrum shows three broad bands with maxima of 4.20×10^{-18}, 9.6×10^{-19}, and 3.9×10^{-19} cm^2 $molecule^{-1}$ at 240, 282, and 342 nm, respectively. These values are only upper limits of the absorption cross sections assuming stoichiometric conversion of NO_2 to IONO in the photolysis of I_2 - NO_2 mixtures. The values listed in Table 4-185, which have to be considered as provisional, are taken from the IUPAC evaluation by Atkinson et al. [29].

Table 4-185. Absorption Cross Sections of IONO at 298 K

λ (nm)	10^{20} σ (cm^2)	λ (nm)	10^{20} σ (cm^2)	λ (nm)	10^{20} σ (cm^2)	λ (nm)	10^{20} σ (cm^2)
210	236	260	162	310	24.7	360	27.1
215	187	265	99.6	315	25.1	365	20.7
220	196	270	87.1	320	27.5	370	14.9
225	279	275	89.8	325	32.5	375	7.40
230	347	280	99.6	330	31.2	380	2.40
235	399	285	92.2	335	34.9	385	0.00
240	422	290	81.0	340	37.3	390	0.00
245	400	295	62.0	345	37.3		
250	330	300	37.3	350	29.8		
255	234	305	30.8	355	29.5		

Note:
210-390 m, Bröske [100], from IUPAC evaluation: Atkinson et al. [29].

H10. $IONO_2 + h\nu \rightarrow IO + NO_2$
$IONO_2 + h\nu \rightarrow I + NO$. The absorption cross sections of iodine nitrate produced in the gas phase by laser flash photolysis of $NO_2/CF_3I/N_2$ mixtures have been measured at room temperature in the spectral region 245-335 nm at a resolution of 1.67 nm and at 385-415 nm with a resolution of 0.55 nm by Mössinger et al. [562]. The cross sections for 335-385 nm, where absorption could not be recorded, were obtained by interpolation. The spectrum consists of a broad continuous absorption band. The cross sections averaged over 5-nm intervals are listed in Table 4-186.

Table 4-186. Absorption Cross Sections of $IONO_2$ at 298 K

λ (nm)	10^{20} σ (cm^2)	λ (nm)	10^{20} σ (cm^2)	λ (nm)	10^{20} σ (cm^2)	λ (nm)	10^{20} σ (cm^2)
245	1210	290	631	335	374	380	184
250	1170	295	577	340	360	385	153
255	1060	300	525	345	348	390	130
260	946	305	495	350	334	395	103
265	880	310	462	355	316	400	78.0
270	797	315	441	360	294	405	60.5
275	772	320	404	365	270	410	49.6
280	741	325	396	370	242	415	41.6
285	691	330	380	375	213		

Note:
245-415 nm, Mössinger et al. [562].

H11. $CH_3I + h\nu \rightarrow CH_3 + I(^2P_{3/2})$.
$CH_3I + h\nu \rightarrow CH_3 + I^*(^2P_{1/2})$. The absorption cross sections of CH_3I have been measured at room temperature and 147 nm by Rebbert et al. [665], at 200–360 nm by Porret and Goodeve [641], at 200–310 nm by Baughcum and Leone [60], at 180–400 nm by Pence et al. [629]; at 257.7 nm by Felps et al. [241], at 205–335 nm by Jenkin et al. [376], at 205–360 nm by Man et al. [472], and at 192–225 nm by Kwok and Phillips [427], who also measured the CH_3I spectrum in cyclohexane solution. Measurements were also carried out at 223–333 K and 160–330 nm by Fahr et al. [235]; at 243–333 K and 235–365 nm by Rattigan et al. [654]; and

at 210–298 K and 200–350 nm by Roehl et al. [678]. Fahr et al. [235] also measured the absorption cross sections at 330–400 nm for the liquid phase and used a wavelength-shift procedure to convert them into gas-phase values. The room temperature data for the absorption band at 210–305 nm are in reasonable to good agreement, whereby Rattigan et al. [654] report the lowest values and Fahr et al. [235] the highest values over the whole absorption band. The agreement generally is better than 15% except for the region around the absorption maximum where the spread is ~30%: Rattigan et al. [654] and Fahr et al. [235] report values of 1.07×10^{-18} cm^2 and 1.4×10^{-18} cm^2, respectively, for the maximum at ~260 nm, and the rest of the data ranges between 1.15×10^{-18} cm^2 and 1.22×10^{-18} cm^2. At wavelengths 305–330 nm, the agreement is still within 20%. At wavelengths below 210 nm, the few data points reported by Jenkin et al. [376] and Roehl et al. [678] and the absorption curve reported by Kwok and Phillips [426] obviously fit into the strong and highly structured band system observed by Fahr et al. [235] between 160 and 205 nm. The preferred room temperature absorption cross sections for the wavelength range above 210 nm, listed in Table 4-187, are the mean of the values reported by Jenkin et al. [376], Fahr et al. [235], and Roehl et al. [678] at 210–230 nm; the mean of the values reported by Jenkin et al. [376], Fahr et al. [235], Rattigan et al. [654], and Roehl et al. [678] at 235–330 nm; the mean of the values reported by Fahr et al. [235], Rattigan et al. [654], and Roehl et al. [678] at 335–350 nm; and the values of Rattigan et al. [654] at 355–365 nm. The data of Man et al. [472] are given only as a plot in their paper and have therefore not been included in the evaluation.

The three temperature studies are in qualitative agreement. An increase of the absorption cross sections in the absorption band at 210–270 nm with decreasing temperature 333–210 K has been observed. Very small temperature effects are reported by Rattigan et al. [654] for the temperature range 243–333 K, and by Fahr et al. [235] and Roehl et al. [678] for the range between room temperature and ~240–250 K and at 313–333 K. At wavelengths above 270 nm and below 210 nm, the absorption cross sections decrease with decreasing temperature. The low temperature absorption spectra observed by the three groups differ in the same manner as their room temperature spectra, i.e., Fahr et al. [235] report the highest and Rattigan et al. [654] the lowest values for the absorption band.

A simple analytical expression for the temperature dependence,

$$\sigma(\lambda, T) = \sigma(298\ \mathrm{K})\ (1 + a_1(T–298) + a_2(T–298)^2)$$

and the fitting parameters $a_1(\lambda)$ and $a_2(\lambda)$ for λ = 200–350 nm and T = 210– 298 K give Roehl et al. [678]. Another simple parameterization, $\ln \sigma(\lambda, T) = \ln \sigma(\lambda, 298\ \mathrm{K}) + B(T–298)$, and parameters $B(\lambda)$ for λ = 235–355 nm and T = 243–333 K report Rattigan et al. [654]. The parameters a_1, a_2, and B are listed also in Table 4-187.

Quantum yields for $I^*(^2P_{1/2})$ atom formation in the photolysis of CH_3I at several wavelengths between 222 and 333.5 nm have been reported: $\Phi(I^*) = 0.63 \pm 0.02$, 0.79 ± 0.02, 0.69 ± 0.02, and 0.43 ± 0.02 at 222, 266, 280, and ~305 nm by Uma and Das [794], [795], [796]; $\Phi(I^*) = 0.72 \pm 0.08$ at 248 nm by Gedanken [796], $\Phi(I^*) = 0.81 \pm 0.03$ and ~ 0.05 at 248 and 308 nm by Pence et al. [629], $\Phi(I^*) = 0.30$ at 304 nm by Kang et al. [403]; and $\Phi(I^*) = 0.47$, 0.77, and 0.92 at 325.8, 329.4, and 333.5 nm by Ogorzalek Loo et al. [594]. The latter authors report also quantum yields for CD_3I:

$\Phi(I^*)$:	0.66	0.59	0.83	0.91	0.90	0.57	0.80	0.92	>0.95	0.61	0.84
λ, nm:	312.6	314.4	317.0	319.8	322.9	324.5	327.8	330.5	333.8	336.2	339.3 3

Brewer et al. [89] report $\Phi(I^*) = 0.75 \pm 0.02$ at 248 nm for CD_3I.

Quantum yields for $I(^2P_{3/2})$ atom formation, $\Phi(I)$, can be derived from $\Phi(I) = 1 – \Phi(I^*)$.

Table 4-187. Absorption Cross Sections of CH_3I at 296–298 K and Temperature Coefficients

λ (nm)	10^{20} σ (cm^2)	10^3 $a_1(K^{-1})$	10^5 $a_2(K^{-2})$	10^3 $B(K^{-1})$	λ (nm)	10^{20} σ (cm^2)	10^3 $a_1(K^{-1})$	10^5 $a_2(K^{-2})$	10^3 $B(K^{-1})$
210	3.62	3.07	2.42		290	8.04	6.14	• 2.57	4.98
215	5.08	2.61	2.28		295	4.00	7.27	2.91	6.38
220	6.90	1.06	1.22		300	2.06	7.82	3.53	6.97
225	9.11	1.74	1.96		305	1.10	7.82	3.85	6.84
230	12.6	1.47	1.67		310	0.621	7.37	3.71	6.78
235	20.5	1.91	2.04	0.67	315	0.359	6.98	3.47	6.75
240	38.1	1.74	2.06	0.61	320	0.221	7.39	3.54	6.53
245	65.6	1.52	2.15	0.34	325	0.126	7.23	2.82	6.79
250	96.3	1.20	2.11	0.08	330	0.0684	8.93	3.74	7.82
255	117.7	0.890	1.95	–0.10	335	0.0388	10.88	4.88	9.34
260	119.7	0.882	1.93	–0.12	340	0.0212	11.30	4.46	10.95
265	102.9	1.21	2.00	0.10	345	0.0114	15.68	8.44	13.58
270	75.9	1.77	2.11	0.54	350	0.00609	15.94	8.22	16.83
275	49.6	2.52	2.12	1.33	355	0.00320			18.91
280	29.2	3.62	2.24	2.43	360	0.00190			17.28
285	15.6	4.84	2.38	3.74	365	0.00090			23.63

Note:
Absorption cross sections σ: 210–230 nm: mean of Jenkin et al. [376], Fahr et al. [235], and Roehl et al. [678],
235–330 nm: mean of Jenkin et al. [376], Fahr et al. [235], Rattigan et al. [654], and Roehl et al. [678],
335–350 nm: mean of Fahr et al. [235], Rattigan et al. [654], and Roehl et al. [678],
355–365 nm: Rattigan et al. [654].
Temperature coefficients a_1 and a_2: 210–298 K, Roehl et al. [678]:
$\sigma(\lambda, T) = \sigma(298\ K)\ [1 + a_1(T–298) + a_2(T–298)^2]$,
Temperature coefficients B: 243–333 K, Rattigan et al. [654]:
$\ln \sigma(\lambda, T) = \ln \sigma(\lambda, 298\ K) + B(T–298)$.

H12. $CH_2I_2 + h\nu \rightarrow CH_2I + I(^2P_{3/2})$.
$CH_2I_2 + h\nu \rightarrow CH_2I + I^*(^2P_{1/2})$. The absorption cross sections of CH_2I_2 have been measured at room temperature and 180–400 nm by Pence et al. [629], at 220–360 nm by Schmitt and Comes [712], at 200–360 nm by Baughcum and Leone [60], at 265–341 nm by Koffend and Leone [417]; and at 220–400 nm by Kwok and Phillips [425], who measured the spectrum also in methanol and cyclohexane. Measurements at 273 and 298 K and 205–380 nm have also been carried out by Roehl et al. [678]; and at 273, 298, and 348 K and 215–385 nm by Mössinger et al. [563]. There are absorption maxima at or below 215 nm, and around 250 and 290 nm. The room temperature data of the various teams (except those of Kwok and Phillips [425], which are presented only as a plot) are in very good agreement, i.e., generally within 5–10% between 230 and 380 nm, were the older data of Schmitt and Comes [712] and Koffend and Leone [417] for the prominent absorption band around 290 nm are higher than those of Roehl et al. [678] and Mössinger et al. [563]. The values of Kwok and Phillips [425] for the prominent absorption band around 290 nm are lower by 15–20% than the rest of the data. The preferred room temperature absorption cross sections, listed in Table 4-188, are the values of Roehl et al. [678] at 205–215 nm, the mean of the values reported by Roehl et al. [678] and Mössinger et al. [563] at 220–380 nm, which are very close, and the value of Mössinger et al. [563] at 385 nm.

Both temperature studies show, that decreasing the temperature from 298 or 348 K to 273 K causes a slight increase of the absorption cross sections between 275 and 300 nm (~2% in the maximum at 290 nm between 298 and 273 K) and a slight decrease outside this wavelength region. A simple empirical relation for the temperature dependence between 273 and 348 K, $\ln \sigma(\lambda, T) = \ln \sigma(\lambda, 298K) + B(\lambda)\cdot(T–298)$, and temperature coefficients $B(\lambda)$ for λ = 205–375 nm at 5-nm intervals are given by Mössinger et al. [563]. The temperature coefficients B are also listed in Table 4-188 (an erroneous B value at 305 nm has been corrected by Dr. Mössinger via a personal communication).

Quantum yields for $I^*(^2P_{1/2})$ atom formation in the photolysis of CH_2I_2 at 193, 248, and 308 nm, $\Phi(I^*)$ = ~0.05, 0.46 ± 0.04, and 0.25 ± 0.02, respectively, were reported by Pence et al. [629]. Quantum yields for $I(^2P_{3/2})$ atom formation, $\Phi(I)$, can be derived from $\Phi(I) = 1 – \Phi(I^*)$.

Table 4-188. Absorption Cross Sections of CH_2I_2 at 298 K

λ (nm)	10^{20} σ (cm^2)	10^3 B (K^{-1})	λ (nm)	10^{20} σ (cm^2)	10^3 B (K^{-1})
205	407.0		300	357.0	–0.37
210	404.0		305	338.5	–0.16
215	366.0	0.15	310	313.5	0.07
220	260.0	0.14	315	280.0	0.15
225	197.5	0.19	320	244.0	0.27
230	133.0	0.51	325	203.0	0.27
235	109.0	0.56	330	161.5	0.51
240	122.5	0.15	335	120.5	0.55
245	150.0	0.18	340	83.3	1.36
250	157.0	0.67	345	53.7	1.99
255	139.5	1.58	350	32.6	3.19
260	120.5	2.04	355	19.2	4.09
265	130.0	1.30	360	10.9	5.39
270	178.5	0.00	365	6.05	6.77
275	255.0	–0.71	370	3.45	8.25
280	328.5	–1.24	375	1.93	11.3
285	371.5	–1.21	380	1.17	
290	380.5	–0.94	385	0.769	
295	371.5	–0.58			

Note:
Absorption cross sections σ: 205–215 nm, Roehl et al. [678],
220–380 nm, mean of Roehl et al. [678] and Mössinger et al. [563],
385 nm, Mössinger et al. [563].
Temperature coefficients B: 273–348 K, Mössinger et al. [563]:
$\ln \sigma(\lambda, T) = \ln \sigma(\lambda, 298\ K) + B(T–298)$.

H13. $C_2H_5I + h\nu \rightarrow C_2H_5 + I(^2P_{3/2})$.
$C_2H_5I + h\nu \rightarrow C_2H_5 + I^*(^2P_{1/2})$. The absorption cross sections of C_2H_5I have been measured at room temperature and 147 nm ($\sigma = 1.48 \times 10^{-17}$ cm^2) by Rebbert et al. [665], at 205–360 nm by Porret and Goodeve [642]; at 223–298 K and 205–365 nm by Roehl et al. [678], at 243–333 K and 235–355 nm by Rattigan et al. [654], and at 323 K and 220–320 nm by Zhang et al. [881]. The room temperature data are in good agreement, the values of Roehl et al.[678] are higher by 5–15% at 235–325 nm and become increasingly higher up to 125% at 355 nm than the values of Rattigan et al. [654]. The latter authors found their data to agree within 10–15% with the plotted values of Porret and Goodeve [642]. The preferred absorption cross sections, listed in Table 4-189, are the mean of the values reported by Roehl et al. [678] and Rattigan et al. [654] in the common wavelength range 235–355 nm, and the data of Roehl et al. [678] at 215–230 nm.

The temperature studies of Roehl et al. [678] and Rattigan et al. [654] show, that decreasing the temperature in the range 333–223 K causes an increase of the absorption cross section in the absorption band at ~230–270 nm and a decrease at longer wavelengths. The differences between the low-temperature data of the two groups are comparable with those between the room temperature data. The data for 323 K, reported by Zhang et al. [881] as a plot on a logarithmic scale, are larger by 10–40% around the absorption maximum and up to more than 200% in the long-wavelength tail than the data for 313 and 333 K reported by Rattigan et al. [654]. A simple analytical expression for the temperature dependence,

$$\sigma(\lambda, T) = \sigma(298\ K)\ [1 + a_1(T–298) + a_2(T–298)^2],$$

and the fitting parameters $a_1(\lambda)$ and $a_2(\lambda)$ for λ = 205–365 nm and T = 223–298 K give Roehl et al. [678]. Another simple parameterization, $\ln \sigma(\lambda, T) = \ln \sigma(\lambda, 298\ K) + B(T–298)$, and parameters B(λ) for λ = 235–355 nm and T = 243–333 K is reported by Rattigan et al. [654]. The parameters a_1, a_2, and B are listed also in Table 4-189.

Quantum yields for $I^*(^2P_{1/2})$ atom formation in the photolysis of C_2H_5I at a few wavelengths between 222 and 305 nm have been reported: Φ(I*) = 0.57 ± 0.02, 0.72 (or 0.73) ± 0.02, 060 ± 0.02, and 0.39 ± 0.02 at 222, 266, 280, and ~305 nm by Uma and Das [794], [795], [796]; Φ(I*) = 0.78 ± 0.07 at 248 nm by Gedanken [264]; Φ(I*) = 0.68 ± 0.02 at 248 nm by Brewer et al. [89], Φ(I*) = 0.22 at 304 nm by Kang et al. [403]. Quantum yields for $I(^2P_{3/2})$ atom formation, Φ(I), can be derived from Φ(I) = 1 – Φ(I*).

At 147 nm, the overall process $C_2H_5I + h\nu \rightarrow C_2H_4 + H + I$ was observed with a quantum yield of 0.75 by Rebbert et al. [665].

Table 4-189. Absorption Cross Sections of C_2H_5I at 298 K and Temperature Coefficients

λ (nm)	10^{20} σ (cm^2)	10^3 $a_1(K^{-1})$	10^5 $a_2(K^{-2})$	10^3 $B(K^{-1})$	λ (nm)	10^{20} σ (cm^2)	10^3 $a_1(K^{-1})$	10^5 $a_2(K^{-2})$	10^3 $B(K^{-1})$
205	11.9	6.38	3.15		285	19.1	3.85	0.926	3.61
210	4.22	4.07	6.28		290	10.3	5.47	1.65	4.83
215	4.56	4.93	6.75		295	5.38	7.00	2.52	6.33
220	6.18	4.06	5.70		300	2.78	8.56	4.11	7.48
225	9.09	2.81	3.81		305	1.44	9.31	4.89	8.08
230	14.3	2.62	3.83		310	0.777	10.56	6.87	7.55
235	23.2	1.28	2.17	–0.27	315	0.416	10.83	6.81	7.92
240	41.7	0.876	1.96	–0.40	320	0.227	11.98	9.76	8.27
245	69.3	0.233	1.62	–0.62	325	0.127	12.98	11.3	8.81
250	99.3	–0.111	1.58	–0.79	330	0.0743	14.56	17.5	9.30
255	119.7	–1.03	0.606	–0.82	335	0.0403	18.81	24.6	10.20
260	121.8	–1.48	–0.0332	–0.75	340	0.0246	13.90	9.08	11.16
265	105.9	–1.09	1.2×10^{-6}	–0.44	345	0.0133	18.86	22.1	12.41
270	80.6	–0.538	–0.257	0.36	350	0.00840	20.19	20.1	11.28
275	54.4	0.770	0.0299	1.23	355	0.00488	–7.04	–40.5	12.20
280	33.5	2.01	0.110	2.36					

Note:
Absorption cross sections σ: 205–230 nm, Roehl et al. [678],
235–355 nm, mean of Roehl et al. [678] and Rattigan et al. [654].
Temperature coefficients a_1 and a_2: 223–298 K, Roehl et al. [678]:
$\sigma(\lambda, T) = \sigma(298\ K)\ [1 + a_1(T–298) + a_2(T–298)^2]$,
Temperature coefficients B: 243–333 K, Rattigan et al. [654]:
$\ln \sigma(\lambda, T) = \ln \sigma(\lambda, 298\ K) + B(T–298)$.

H14. $CH_3CHI_2 + h\nu \rightarrow$ Products. The absorption cross sections of CH_3CHI_2 have been measured at 298 K and 220–360 nm by Schmitt and Comes [712]. Their data are listed in Table 4-190.

Table 4-190. Absorption Cross Sections of CH_3CHI_2 at 298 K

λ (nm)	10^{20} σ (cm^2)	λ (nm)	10^{20} σ (cm^2)	λ (nm)	10^{20} σ (cm^2)
220	304	270	183	320	222
225	240	275	243	325	201
230	181	280	304	330	175
235	144	285	352	335	138
240	138	290	374	340	107
245	151	295	366	345	75.7
250	157	300	339	350	49.3
255	143	305	305	355	31.7
260	133	310	273	360	19.1
265	145	315	247		

Note:
220–360 nm, Schmitt and Comes [712].

H15. $CH_3CH_2CH_2I + h\nu \rightarrow$ Products.

H16. $CH_3CHICH_3 + h\nu \rightarrow$ Products. The absorption cross sections of 1-C_3H_7I have been measured at 223–298 K and 205–335 nm, those of 2-C_3H_7I at 223–298 K and 205–380 nm by Roehl et al. [678]. The absorption cross sections of 2-C_3H_7I in the gas phase and in cyclohexane solution have also been measured at room temperature and 235–305 nm by Phillips et al. [634]. The gas-phase data reported by Phillips et al. [634] and given as a plot in their paper are larger by 30–70% over the whole absorption band than the data of Roehl et al. [678]. Room temperature values at 147 nm for 1-C_3H_7I and 2-C_3H_7I have been reported by Rebbert et al. [665]. The recommended room temperature values for 1-C_3H_7I and 2-C_3H_7I, listed in Table 4-191, are taken from the paper of Roehl et al. [678].

Decreasing the temperature in the range 298–223 K causes an increase of the absorption cross sections around the absorption maximum, at 245–265 nm for 1-C_3H_7I and at 240–270 nm for 2-C_3H_7I, and a decrease

in the long-wavelength tail. Decrease of the absorption cross sections with decreasing temperature generally has been observed in the short-wavelength tail of the absorption band except for slight increases between 273 and 248 K in the case of 1-C_3H_7I and between 248 and 223 K in the case of 2-C_3H_7I. At wavelengths below the minimum (~210 nm), the absorption cross sections decrease with decreasing temperature between 298 and 223 K. The temperature dependence has been parameterized by the analytical expression

$$\sigma(\lambda, T) = \sigma(298\ K)\ [1 + a_1(T–298) + a_2(T–298)^2]$$

and the fitting parameters $a_1(\lambda)$ and $a_2(\lambda)$ for T = 223–298 K and λ = 205–335 nm (1-C_3H_7I) and λ = 205–380 nm (2-C_3H_7I) are reported by Roehl et al. [678]. These are listed also in Table 4-190.

Quantum yields for $I^*(^2P_{1/2})$ atom formation in the photolysis of C_3H_7I at a few wavelengths have been reported: $\Phi(I^*)$ = 0.54 ± 0.02, 0.66 ± 002, 0.56 ± 0.02, and 0.35 ± 0.02 at 222, 266, 280, and ~305 nm by Uma and Das [794], [796]; $\Phi(I^*)$ = 0.60 ± 0.02 at 248 nm by Brewer et al. [89], $\Phi(I^*)$ = 0.20 at 304 nm by Kang et al. [403] for 1-C_3H_7I; $\Phi(I^*)$ = 0.40 ± 0.02, 0.44 ± 0.03, and 0.19 ± 0.02 at 222, 266, and ~305 nm by Uma and Das [795], and $\Phi(I^*)$ = 0.26 ± 0.02 at 248 nm by Brewer et al. [89] for 2-C_3H_7I. Quantum yields for $I(^2P_{3/2})$ atom formation, $\Phi(I)$, can be derived from $\Phi(I) = 1 – \Phi(I^*)$.

At 147 nm, Rebbert et al. [665] observed the main overall processes

1-$C_3H_7I + h\nu \rightarrow C_3H_6 + H + I$ and

1-$C_3H_7I + h\nu \rightarrow CH_3 + C_2H_4 + I$

with quantum yields 0.38 and 0.47 and the processes

2-$C_3H_7I + h\nu \rightarrow C_3H_6 + H + I$ and

2-$C_3H_7I + h\nu \rightarrow CH_3 + C_2H_4 + I$

with quantum yields 0.80 and 0.07.

Table 4-191. Absorption Cross Sections of C_3H_7I at 298 K and Temperature Coefficients

λ (nm)	1-C_3H_7I			2-C_3H_7I		
	10^{20} σ (cm^2)	10^3 a_1 (K^{-1})	10^5 a_2 (K^{-2})	10^{20} σ (cm^2)	10^3 a_1 (K^{-1})	10^5 a_2 (K^{-2})
205	15.6	7.60	4.37	44.9	15.14	8.46
210	5.05	0.283	1.57	4.53	7.84	7.23
215	5.14	–1.49	–2.46	3.57	4.96	5.08
220	6.84	–1.59	–2.97	4.20	1.55	1.27
225	10.4	–0.891	–2.14	6.45	2.21	1.99
230	17.7	–0.375	–1.26	11.0	1.60	1.80
235	32.8	–0.311	–1.04	20.4	0.480	0.681
240	58.1	–0.611	–0.804	38.2	–0.333	0.121
245	91.9	–0.949	–0.609	66.7	–0.680	0.0947
250	124	–1.22	–0.611	102	–0.795	0.289
255	141	–1.55	–0.776	133	–0.966	0.570
260	136	–1.44	–0.867	148	–1.14	0.512
265	113	–1.02	–1.04	143	–0.589	0.824
270	82.2	–0.306	–1.16	120	–0.439,	0.281
275	53.4	0.524	–1.50	90.2	0.792	0.873
280	32.0	1.68	–1.66	61.4	1.65	0.466
285	18.1	3.08	–1.44	38.6	2.88	0.534
290	9.96	5.56	0.812	22.6	4.13	0.559
295	5.42	6.76	2.05	12.8	5.71	1.04
300	2.96	7.16	2.90,	6.94	7.20	1.93
305	1.63	6.90	3.20	3.73	8.19	2.33
310	0.945	7.10	4.01	2.04	8.75	2.81
315	0.532	5.59	2.78	1.09	8.49	2.25
320	0.301	3.68	0.0140	0.627	10.79	4.36
325	0.177	4.23	0.0238	0.348	9.54	2.76
330	0.110	11.40	12.3	0.202	10.99	5.94
335	0.0627	15.76	25.8	0.115	12.37	7.58
340				0.0688	13.69	12.2
345				0.0402	16.32	17.1
350				0.0253	18.50	24.7
355				0.0150	19.41	24.3
360				0.0105	18.61	13.9
365				0.00666	29.85	50.9
370				0.00479	37.24	76.8
375				0.00535	36.71	80.7
380				0.00530	22.00	40.0

Note:
Absorption cross sections σ: 205–380 nm, Roehl et al. [678],
Temperature coefficients a_1 and a_2: 223–298 K, Roehl et al. [678]:
$\sigma(\lambda, T) = \sigma(298\ K)\ [1 + a_1(T–298) + a_2(T–298)^2]$.

H17. $C_4H_9I + h\nu \rightarrow C_4H_9 + I(^2P_{3/2})$.
$C_4H_9I + h\nu \rightarrow C_4H_9 + I^*(^2P_{1/2})$.

H18. $(CH_3)_2CHCH_2I + h\nu \rightarrow (CH_3)_2CCH_2 + I(^2P_{3/2})$.
$(CH_3)_2CHCH_2I + h\nu \rightarrow (CH_3)_2CCH_2 + I^*(^2P_{1/2})$.

H19. $(CH_3)_3CI + h\nu \rightarrow (CH_3)_3C + I(^2P_{3/2})$.
$(CH_3)_3CI + h\nu \rightarrow (CH_3)_3C + I^*(^2P_{1/2})$. Absorption cross sections for *n*- and *iso*-C_4H_9I are not available. Absorption cross sections of *tert*-C_4H_9I have been measured at 323 K by Phillips et al. [634]. An absorptions band between 230 and 310 nm exhibits a maximum of ~2.1×10^{-18} cm^2 at ~268 nm. Estimated values at 5-nm intervals, read from a logarithmic plot, are presented in Table 4-192.

Quantum yields for $I^*(^2P_{1/2})$ atom formation in the photolysis of *n*-C_4H_9I at several wavelengths between 222 and 305 nm have been reported: $\Phi(I^*) = 0.51 \pm 0.02$, 0.64 ± 0.03, 0.50 ± 0.03, and 0.30 ± 0.02 at 222, 266, 280, and ~305 nm by Uma and Das [794], [796]; $\Phi(I^*) = 0.53 \pm 0.03$ at 248 nm by Brewer et al. [89], $\Phi(I^*) = 0.14$ at 304 nm by Kang et al. [403].

Quantum yields for $I^*(^2P_{1/2})$ atom formation in the photolysis of i*so*-C_4H_9I, $\Phi(I^*) = 0.71 \pm 0.01$, 0.56 ± 0.03, and 0.35 ± 0.02 at 266, 280, and ~305 nm, have been reported by Uma and Das [796], $\Phi(I^*) = 0.20 \pm 0.02$ at 248 nm by Brewer et al. [89].

Quantum yields for I atom formation in the photolysis of *tert*-C_4H_9I, $\Phi(I(^2P_{3/2})+I^*(^2P_{1/2})) = 0.93$ and 0.92 at 277 and 304 nm, have been reported by Kim et al. [408]. Quantum yields for $I^*(^2P_{1/2})$ atom formation, $\Phi(I^*(^2P_{1/2})) = 0.33 \pm 0.03$, 0.20 ± 0.03, and 0.12 ± 0.03, in the photolysis at 222, 266, and ~305 nm, have been reported by Uma and Das [795], $I^*(^2P_{1/2}) = 0.41 \pm 0.10$ and 0.03 ± 0.02 at 248 nm by Gedanken [264] and Brewer et al. [89], respectively.

Table 4-192. Absorption Cross Sections of $(CH_3)_3CI$ at 298 K

λ (nm)	10^{20} σ (cm^2)	λ (nm)	10^{20} σ (cm^2)	λ (nm)	10^{20} σ (cm^2)
235	28.5	265	209	295	54.0
240	42.5	270	211	300	34.0
245	64.8	275	186	305	21.5
250	98.0	280	150	310	14.0
255	140	285	116		
260	180	290	83.0		

Note:
235–310 nm, Phillips et al. [634], read from logarithmic plot.

H20. $C_5H_{11}I + h\nu \rightarrow C_5H_{11} + I(^2P_{3/2})$.
$C_5H_{11}I + h\nu \rightarrow C_5H_{11} + I^*(^2P_{1/2})$. Absorption cross sections for *n*-$C_5H_{11}I$ are not available. A quantum yield for $I^*(^2P_{1/2})$ atom formation in the photolysis of *n*-$C_5H_{11}I$ at 222 nm, $\Phi(I^*) = 0.50 \pm 0.03$, has been measured by Uma and Das [794].

H21. $CF_3I + h\nu \rightarrow CF_3 + I(^2P_{3/2})$
$CF_3I + h\nu \rightarrow CF_3 + I^*(^2P_{1/2})$. The absorption cross sections of CF_3I have been measured at room temperature and 170–230 nm by Roxlo and Mandl [692]; at room temperature and in shock waves at 625 and 1050 K and 220–360 nm by Brouwer and Troe [101]; at 200–298 K and 216–370 nm by Solomon et al. [747]; at 218–333 K and 160–350 nm by Fahr et al. [234]; at 243–333 K and 235–390 nm by Rattigan et al. [654], and at 205-325 nm (and in the VUV at 113-181 nm) by Lim o-Vieira et al. [452]. Measurements in the long-wavelength tail of the absorption band up to 455 nm and at temperatures up to ~4000 K were also carried out with hot molecules excited by IR laser pulses by Bagratashvili et al. [35] and Abel et al. [2, 3].

There is good agreement between the room temperature values above 200 nm, i.e., better than 20% around the absorption maximum at 265–270 nm and better than 15% below 255 nm and at 280–350 nm. Fahr et al. [234] report the highest absorption maximum of 7×10^{-19} cm^2, compared to 6.7×10^{-19}, 6.4×10^{-19}, 6.2×10^{-19}, and 5.9×10^{-19} cm^2 reported by Lim o-Vieira et al. [452], Solomon et al. [747], Brouwer and Troe [101], and Rattigan et al. [654], respectively. The long-wavelength data of Solomon et al. [747] become increasingly higher by up to ~70% than those of Rattigan et al. [654]. The new data of Lim o-Vieira et al. [452] confirm the JPL-97 recommendation between 230 and 310 nm better than the JPL-2002 recommendation, i.e., the absorption curve lies between those of Solomon et al. [747] and Fahr et al. [234], and the cross sections are higher than those of the JPL-2002 recommendation. In the wings (below 230 nm and above 310 nm) there are deviations from the rest of the result, i.e., the absorption curve shows an irregular behavior. We keep at the JPL-2002 recommendation, i.e., the preferred absorption cross sections, listed in Table 4-193 are the data of Fahr et al. [234] at 180–215 nm; the mean of the values reported by Brouwer and Troe [101], Solomon et al. [747], and Fahr et al. [234] at 220–230 nm; the mean of the values reported by Brouwer and Troe [101], Solomon et al. [747], Fahr et al. [234], and Rattigan et al. [654], at 235–310 nm; the mean of the values reported by Solomon et al. [747], Fahr et al. [234], and Rattigan et al. [654] at 315–350 nm; and the values of Rattigan et al. [654] at 355–385 nm.

Fahr et al. [234] and Lim o-Vieira et al. [452] observed in the short-wavelength region a band centered at about 171 nm with cross sections up to 3.6×10^{-17} and 7.4×10^{-17} cm^2, which shows vibrational structure, and a structured band with a maximum approaching values of ~1×10^{-16} cm^2 at or below 160 nm. The plotted spectrum at 170–230 nm reported by Roxlo and Mandl [692] is not in agreement with the results of Fahr et al. [234] and Lim o-Vieira et al. [452]. Four strong and structured bands are observed at still shorter wavelengths between 158 and 115 nm in the high-resolution spectrum reported by Lim o-Vieira et al. [452].

The temperature studies of Solomon et al. [747], Fahr et al. [234], and Rattigan et al. [654] agree in the observation, that the absorption cross sections increase in the region of the maximum (~240–280 nm) with decreasing temperature from 333 K or room temperature down to temperatures of 240–250 K; the ratios σ(298 K)/σ(~240 K) and σ(333 K)/σ(~240 K) around the maximum are ~0.9, the ratios σ(333 K)/σ(298 K) are ~1. Solomon et al. [747] observed a further increase of the cross sections down to 200 K, whereas Fahr at al. [234] observed a slight decrease between 253 and 218 K. A decrease of the absorption cross sections above 280 nm and between 333 and 200 K was observed by the three groups; the ratios σ(298 K)/σ(~240 K) increase from ~1.0 to ~1.9 at 280–340 nm, the ratios σ(333 K)/σ(298 K) are around 1.3. Thus, the temperature dependences reported by the three groups are compatible at least in the range 240–333 K.

Solomon et al. [747] and Rattigan et al. [654] fitted their spectra to the expression

$$\ln \sigma(\lambda, T) = \ln \sigma(\lambda, 298\ \mathrm{K}) + B(T–298)$$

and report the temperature coefficients $B(\lambda)$ for T = 200–298 K and λ = 216–344 nm (at 2-nm intervals) and for T = 243–333 K and λ = 235–390 nm (at 5-nm intervals), respectively. The temperature coefficients B reported by Solomon et al. [747] are nearly constantly larger by ~0.8×10^{-3} than those of Rattigan et al. [654] at 235–300 nm and become smaller by up to 1.75×10^{-3} between 315 and 345 nm. The B values reported by Rattigan et al. [654] for the ranges 235–385 nm and 243–333 K are listed also in Table 4-193.

Fahr et al. [234] gave fits for the long-wavelength tail using the expressions
$\sigma(\lambda) = \sigma_0(\lambda) \exp(–L/\lambda)$ for λ > 320 nm and $\sigma(T) = \sigma_0(T) \exp(–\theta/T)$ and reported values for the parameters $\sigma_0(\lambda)$ and L at T = 218, 235, 253, 273, 295, and 333 K and for $\sigma_0(T)$ and θ at 300, 310, 320, 330, 340, and 350 nm.

In the short-wavelength region at 160–180 nm, a decrease of the absorption cross sections with decreasing temperature 333–218 K has been observed by Fahr et al. [234].

Since CF_3I serves as model system for studying the dynamics of $I^*(^2P_{1/2})$ atom production by UV photolysis, there is a great number of studies which measure $I^*(^2P_{1/2})/I(^2P_{3/2})$ branching ratios and $I^*(^2P_{1/2})$ quantum yields from CF_3I photolysis in the wavelength region of the absorption band. The following quantum yields were reported for the range between 248 and 308 nm:

$\Phi(I^*) = 0.89 \pm 0.01$, 0.87 ± 0.04, and 0.88 at 248 nm by Brewer et al. [89], Gedanken et al. [264], and Felder [237], respectively;

$\Phi(I^*) = 0.89 \pm 0.05$, 0.79 ± 0.03 and 0.63 ± 0.02 at 266, 280, and ~305 nm by Kavita and Das [404];

$\Phi(I^*) = 0.87$ at 277 nm by Kim et al. [407]; $\Phi(I^*) = 0.69$ at 304 nm by Kang et al. [403];

$\Phi(I^*) = 0.21$ at 308 nm by Felder [238], and

$\Phi(I^*)$	0.99 ± 0.01	0.91 ± 0.01	0.89 ± 0.01	0.84 ± 0.01	0.81 ± 0.01	0.69 ± 0.01
λ (nm)	275	279	283	290	293	295
$\Phi(I^*)$	0.68 ± 0.01	0.63 ±0.02	0.61 ± 0.02	0.47 ± 0.01	0.41 ± 0.0	0.37 ± 0.01
λ (nm)	296	297	298	300	302	303

by Furlan et al. [257].

Quantum yields for $I(^2P_{3/2})$ atom formation, $\Phi(I)$, can be derived from $\Phi(I) = 1 - \Phi(I^*)$.

Table 4-193. Absorption Cross Sections of CF_3I at 295-300 K

λ (nm)	$10^{20}\ \sigma$ (cm^2)	10^3 B (K^{-1})	λ (nm)	$10^{20}\ \sigma$ (cm^2)	10^3 B (K^{-1})
180	3.11		285	33.4	0.55
185	0.75		290	22.7	1.65
190	0.28		295	14.3	2.98
195	0.16		300	8.6	4.22
200	0.15		305	5.06	5.61
205	0.19		310	2.82	6.84
210	0.34		315	1.62	7.68
215	0.68		320	0.905	8.27
220	1.52		325	0.485	8.74
225	2.88		330	0.262	9.25
230	5.03		335	0.142	9.92
235	8.21	0.16	340	0.0750	10.27
240	13.6	-0.16	345	0.0407	11.71
245	21.8	-0.52	350	0.0210	12.85
250	32.4	-0.86	355	0.0115	13.26
255	45.2	-1.17	360	0.0064	14.65
260	56.9	-1.37	365	0.0036	14.63
265	63.4	-1.43	370	0.002	15.49
270	63.1	-1.30	375	0.0011	17.14
275	56.1	-0.94	380	0.0007	17.66
280	45.1	-0.62	385	0.0004	19.71

Note: Absorption cross sections σ:
180–215 nm: Fahr et al. [234],
220–230 nm: mean of Brouwer and Troe [101], Solomon et al. [747], and Fahr et al.[234],
235–310 nm: mean of Brouwer and Troe [101], Solomon et al. [747], Fahr et al. [234], and Rattigan et al. [654],
315–350 nm: mean of Solomon et al. [747], Fahr et al. [234], and Rattigan et al. [654],
355–385 nm: Rattigan et al. [654].
Temperature coefficients B:
243–333 K, Rattigan et al. [654]: $\ln \sigma(\lambda, T) = \ln \sigma(\lambda, 298\ K) + B(T–298)$.

H22. $CF_2I_2 + h\nu \rightarrow CF_2I + I(^2P_{3/2})$
$CF_2I_2 + h\nu \rightarrow CF_2I + I^*(^2P_{1/2})$
$CF_2I_2 + h\nu \rightarrow CF_2 + I(^2P_{3/2}) + I(^2P_{3/2})$
$CF_2I_2 + h\nu \rightarrow CF_2 + I(^2P_{3/2}) + I^*(^2P_{1/2})$. The photodissociation of CF_2I_2 has been studied at room temperature and wavelengths 248, 308, 337, and 351 nm by Wannenmacher et al. [837] and Baum et al. [62]. These authors report also plots of the absorption spectrum at room temperature and between 190 and 420 nm, which suggest the presence of at least two overlapping transitions corresponding to the different dissociation processes. Numerical absorption data belonging to Wannenmacher et al. [837] and Baum et al. [62] were obtained via personal communication by Pfister and Huber [633]. The absorption cross sections listed in Table 4-194 are normalized to a

maximum value $\sigma = 2.929 \times 10^{-18}$ $cm^2 \cdot molecule^{-1}$ at 300 nm, which was derived from five different spectra and has an uncertainty of ±16%.

Table 4-194. Absorption Cross Sections of CF_2I_2 at 294 K

λ (nm)	10^{20} σ (cm^2)	λ (nm)	10^{20} σ (cm^2)	λ (nm)	10^{20} σ (cm^2)
190	3163	270	203.1	350	66.24
195	4616	275	215.7	355	57.76
200	4070	280	224.3	360	49.81
205	2285	285	236.4	365	41.51
210	837.0	290	259.5	370	33.92
215	238.1	295	281.9	375	26.85
220	75.78	300	292.9	380	18.90
225	36.39	305	288.5	385	13.60
230	29.50	310	266.7	390	9.892
235	35.51	315	235.6	395	6.713
240	47.34	320	198.6	400	4.240
245	66.07	325	163.9	405	3.356
250	89.21	330	135.5	410	1.943
255	118.0	335	111.6	415	1.413
260	150.1	340	91.33	420	0.7066
265	180.5	345	78.25		

Note:
190–420 nm, Wannenmacher et al. [837], Baum et al. [62], and Pfister and Huber [633].

H23. $C_2F_5I + h\nu \rightarrow C_2F_5 + I(^2P_{3/2})$.

$C_2F_5I + h\nu \rightarrow C_2F_5 + I^*(^2P_{1/2})$. The absorption cross sections of C_2F_5I were measured at 295 K and 268 nm ($\sigma = 6.39 \times 10^{-19}$ cm^2) by Pence et al. [629] and at 323 K and 220–320 nm by Zhang et al. [881]. The absorption band extending over the 220–320-nm range has a maximum of ~ 6.7×10^{-19} cm^2 at ~269 nm. Estimated values at 5-nm intervals, read from a logarithmic plot, are in Table 4-195.

Quantum yields for $I^*(^2P_{1/2})$ atom formation in the photolysis of C_2F_5I at 266, 288, and ~305 nm, Φ (I*) = 0.97 ± 0.03, 0.75 ± 0.03, and 0.83 ± 0.05, respectively, have been reported by Kavita and Das [404]. Quantum yields for $I(^2P_{3/2})$ atom formation, Φ (I), can be derived from Φ (I) = 1 – Φ (I*).

Table 4-195. Absorption Cross Sections of C_2F_5I at 323 K

λ (nm)	10^{20} σ (cm^2)	λ (nm)	10^{20} σ (cm^2)	λ (nm)	10^{20} σ (cm^2)
220	1.95	255	49.8	290	35.3
225	3.27	260	60.0	295	25.0
230	5.60	265	65.5	300	16.3
235	9.40	270	66.8	305	10.4
240	16.0	275	63.2	310	6.4
245	25.3	280	56.1	315	3.9
250	37.5	285	46.5	320	2.3

Note:
235–310 nm, Zhang et al. [881], read from logarithmic plot.

H24. $C_3F_7I + h\nu \rightarrow C_3F_7 + I(^2P_{3/2})$.

$C_3F_7I + h\nu \rightarrow C_3F_7 + I^*(^2P_{1/2})$. The absorption cross sections of 1-C_3F_7I have been measured at room temperature and 265–341 nm by Koffend and Leone [417] and at 180–400 nm by Pence et al. [629]. The latter authors report a plot of the absorbance (in arbitrary units), which shows an absorption band between ~220 and 340 nm with the maximum at ~268 nm, and absorption cross sections only for 248, 268, and 308 nm. The data for 268 and 308 nm are in good agreement with the corresponding data reported by Koffend and Leone [417]. The recommended absorption cross sections of 1-C_3F_7I, listed in Table 4-196, are the value for 248 nm reported by Pence et al. [629]; the mean of the values of Pence et al. [629] and Koffend and Leone [417] at 268 nm; and, for the range 270–340 nm, values obtained by interpolation and extrapolation at 5-nm intervals of the data reported at odd wavelength by Koffend and Leone [417].

Quantum yields for $I^*(^2P_{1/2})$ atom formation in the photolysis of C_3F_7I at 266, 288, and ~305 nm,

Φ(I*) = 0.83 ± 0.02, 0.89 ± 0.03, and 0.90 ± 0.05 for 1-C_3F_7I and

Φ(I*) = 0.83 ± 0.01, 0.80 ± 0.03, and 0.89 ± 0.02 for 2-C_3F_7I,

have been reported by Kavita and Das [404].

Quantum yields for $I(^2P_{3/2})$ atom formation, Φ(I), can be derived from Φ(I) = 1 – Φ(I*).

Table 4-196. Absorption Cross Sections of 1-C_3F_7I at 295–298 K

λ (nm)	10^{20} σ (cm^2)	λ (nm)	10^{20} σ (cm^2)	λ (nm)	10^{20} σ (cm^2)
248	31.0	290	43.7	320	3.3
268	77.3	295	31.8	325	2.0
270	77.0	300	21.3	330	1.2
275	74.0	305	14.2	335	0.70
280	66.5	310	9.2	340	0.42
285	56.2	315	5.5		

Note:
248 nm, Pence et al. [629],
268 nm, mean of Pence et al. [629] and Koffend and Leone [417]
270–340 nm, 5-nm inter- and extrapolation of Koffend and Leone [417] data.

H25. $C_4F_9I + h\nu \rightarrow C_4F_9 + I(^2P_{3/2})$.
$C_4F_9I + h\nu\ C_4F_9 + I^*(^2P_{1/2})$.

H26. $C_6F_{13}I + h\nu \rightarrow C_6F_{13} + I(^2P_{3/2})$.
$C_6F_{13}I + h\nu \rightarrow C_6F_{13} + I^*(^2P_{1/2})$. Absorption cross sections are not available for these perfluoroalkyl iodides.

Quantum yields for $I^*(^2P_{1/2})$ atom formation in the photolysis of both iodides at 266, 288, and ~305 nm. Φ(I*) = 0.75 ± 0.03, 0.80 ± 0.03, and 0.87 ± 0.02 for *n*-C_4F_9I and Φ(I*) = 0.82 ± 0.02, 0.74 ± 0.03, and 0.82 ± 0.01 for *n*-$C_6F_{13}I$, have been reported by Kavita and Das [404]. Quantum yields for $I(^2P_{3/2})$ atom formation, Φ(I), can be derived from Φ(I) = 1 – Φ(I*).

H27. $CH_2ICl + h\nu \rightarrow CH_2Cl + I$
$CH_2ICl + h\nu \rightarrow CH_2I + Cl$. The absorption cross sections of CH_2ICl have been measured at room temperature and 205–330 nm by Schmitt and Comes [713]; at 192–225 nm and 215–400 nm by Kwok and Phillips [427], [426], who also measured the CH_2ICl spectrum in cyclohexane solution. Measurements have also been carried out at 223–298 K and 205–355 nm by Roehl et al. [678] and at 243–333 K and 235–390 nm by Rattigan et al. [654]. The room temperature data of Roehl et al. [678] and Rattigan et al. [654] are in good agreement, where the values of Rattigan et al. [654] are lower by ≤10% between 240 and 345 nm. The older data of Schmitt and Comes [713] and the data of Kwok and Phillips [426] are higher with absorption maxima near 270 nm of 1.94×10^{-18} and 1.5×10^{-18} cm^2, respectively, compared to 1.35×10^{-18} and 1.21×10^{-18} cm^2 reported by the other two groups. The data of Kwok and Phillips [427] at 205 and 210 nm are lower by more than 80% than the data of Roehl et al. [678]. The preferred absorption cross sections, listed in Table 4-197, are the data of Roehl et al. [678] at 205–230 nm; the mean of the values reported by Roehl et al. [678] and Rattigan et al. [654] at 235–355 nm; and the data of Rattigan et al. [654] at 360–390 nm. The data of Schmitt and Comes [713] and Kwok and Phillips [427], [426] are given only as a plots in their papers and have therefore not been included in the evaluation.

Both temperature studies show an increase of the absorption cross sections around the absorption maximum (~250–285 nm) with decreasing temperature between 333 and 223 K and the reverse effect above 285 nm. The absorption maxima at ~250 K reported by the two groups agree within 15%. A simple analytical expression for the temperature dependence,

$$\sigma(\lambda, T) = \sigma(298\ K)\ [1 + a_1(T–298) + a_2(T–298)^2]$$

and the fitting parameters $a_1(\lambda)$ and $a_2(\lambda)$ for λ = 205–355 nm and T = 223– 298 K give Roehl et al. [678]. Another simple parameterization, $\ln \sigma(\lambda, T) = \ln \sigma(\lambda, 298\ K) + B(T–298)$, and parameters B(λ) for

λ = 235–390 nm and T = 243–333 K report Rattigan et al. [654]. The temperature coefficients a_1, a_2, and B are given also in Table 4-197.

The relative quantum yield of $I^*(^2P_{1/2})/(I(^2P_{3/2}) + I^*(^2P_{1/2}))$ has been determined by Senapati et al. [725] at 5 different wavelengths: 0.47 ± 0.02 at 222 nm, 0.51 ± 0.01 at 236 nm, 0.51 ± 0.02 at 266 nm, 0.55 ± 0.03 at 280 nm, and 0.38 ± 0.01 at 304 nm. Relative quantum yields of $Cl^*(^2P_{1/2})/(Cl(^2P_{3/2}) + Cl^*(^2P_{1/2}))$ were recently measured by Senapati and Das [724] at 4 different wavelengths: 0.44 at 222 nm, 0.44 at 266 nm, 0.30 at 280 nm, and 0.22 at 304 nm.

Table 4-197. Absorption Cross Sections of CH_2ICl at 298 K and Temperature Coefficients

λ (nm)	10^{20} σ (cm^2)	10^3 a_1(K^{-1})	10^5 a_2(K^{-2})	10^3 B(K^{-1})	λ (nm)	10^{20} σ (cm^2)	10^3 a_1(K^{-1})	10^5 a_2(K^{-2})	10^3 B(K^{-1})
205	132	–1.59	–3.83		300	25.9	2.38	–0.0473	2.56
210	42.1	8.47	3.76		305	16.7	3.13	0.394	3.08
215	11.1	6.12	4.30		310	10.9	3.13	0.303	3.50
220	7.50	0.232	0.129		315	7.16	2.74	–0.317	3.56
225	9.76	–0.0938	0.660		320	4.79	2.44	–0.533	3.46
230	14.9	–0.268	-1.4×10^{-6}		325	3.23	2.87	0.140	3.44
235	21.2	–0.512	–0.388	0.24	330	2.14	8.52	–4.21	3.72
240	32.1	–0.793	–0.664	0.12	335	1.40	2.02	–2.25	4.09
245	45.9	–0.929	–0.758	–0.02	340	0.906	5.20	4.54	4.87
250	63.3	–1.22	–1.13	–0.11	345	0.569	7.05	6.88	5.69
255	84.5	–1.25	–0.998	–0.28	350	0.350	9.12	11.7	6.88
260	106	–1.56	–1.14	–0.44	355	0.225	12.27	18.9	8.16
265	122	–1.05	–0.294	–0.55	360	0.133			9.01
270	128	–1.33	–0.593	–0.59	365	0.081			11.06
275	121	–1.07	–0.298	–0.47	370	0.048			11.47
280	104	–0.618	–0.309	–0.18	375	0.027			12.77
285	81.1	–0.326	–0.554	0.32	380	0.017			15.14
290	58.5	0.300	–0.711	0.99	385	0.008			19.12
295	39.9	1.55	–0.245	1.73	390	0.006			20.48

Note:
Absorption cross sections σ: 205–230 nm, Roehl et al. [678],
235–355 nm, mean of Roehl et al. [678] and Rattigan et al. [654],
360–390 nm, Rattigan et al. [654].
Temperature coefficients a_1 and a_2: 223–298 K, Roehl et al. [678]
($\sigma(\lambda, T) = \sigma(298\ K)\ [1 + a_1(T–298)+ a_2(T–298)2]$).
Temperature coefficients B: 243–333 K, Rattigan et al. [654]:
$\ln \sigma(\lambda, T) = \ln \sigma(\lambda, 298\ K) + B(T–298)$.

H28. $CH_2BrI + h\nu \rightarrow CH_2I + Br$.

$CH_2BrI + h\nu \rightarrow CH_2Br + I$. The absorption cross sections of CH_2BrI have been measured at room temperature and 180–360 nm by Man et al. [472]; and at 273, 298, and 348 K and 215–390 nm by Mössinger et al. [563]. The spectrum exhibits two absorption bands with maxima near 210 and 267 nm, which can be assigned to electronic transitions to repulsive states antibonding in C–Br and C–I, respectively. The results of the two studies are not in quantitative agreement: Mössinger et al. [563] report room temperature absorption cross sections of 5.7×10^{-18} and 2.3×10^{-18} cm^2 at 215 and 270 nm, whereas a plot in the paper of Man et al. [472] gives the larger values of ~1×10^{-17} and 3.5×10^{-18} cm^2, respectively. We recommend the data of Mössinger et al. [563], which are listed in Table 4-198.

The absorption cross sections increase with decreasing temperature around the band maxima and decrease in their long-wavelength tails at 220–240 nm and above 290 nm. The temperature dependence was parameterized by Mössinger et al. [563] by the empirical relation $\ln \sigma(\lambda, T) = \ln \sigma(\lambda, 298\ K) + B(T–298)$. The temperature coefficients B(λ) are listed also in Table 4-198 (an erroneous B value at 280 nm has been corrected by Dr. Mössinger via a personal communication).

Table 4-198. Absorption Cross Sections of CH_2BrI at 298 K and Temperature Coefficients

λ (nm)	10^{20} σ (cm^2)	10^3 B (K^{-1})	λ (nm)	10^{20} σ (cm^2)	10^3 B (K^{-1})	λ (nm)	10^{20} σ (cm^2)	10^3 B (K^{-1})
215	567	–2.16	275	214	–1.22	335	5.52	3.89
220	423	–0.12	280	184	–0.94	340	3.50	4.79
225	269	1.34	285	150	–0.53	345	2.24	5.74
230	155	2.06	290	110	0.10	350	1.41	6.73
235	97.9	2.05	295	82.5	0.63	355	0.817	9.47
240	80.9	1.01	300	60.6	1.03	360	0.498	11.5
245	93.7	0.00	305	42.9	1.13	365	0.303	11.6
250	125	–0.58	310	31.4	1.41	370	0.165	14.3
255	170	–1.16	315	23.1	1.52	375	0.098	17.4
260	207	–1.29	320	16.8	1.71	380	0.070	
265	228	–1.45	325	11.5	2.36	385	0.039	
270	229	–1.73	330	8.02	2.99	390	0.025	

Note:
Absorption cross sections σ: 205–380 nm, Mössinger et al. [563].
Temperature coefficients B: 273–348 K, Mössinger et al. [563]:
$\ln \sigma(\lambda, T) = \ln \sigma(\lambda, 298\ K) + B(T–298)$.

H29. $CF_2BrCF_2I + h\nu \rightarrow CF_2BrCF_2 + I$.
$CF_2BrCF_2I + h\nu \rightarrow CF_2ICF_2 + Br$. The absorption spectrum of CF_2BrCF_2I has been measured at room temperature and 190– 350 nm by Pence et al. [629]. The spectrum, reported as a plot (with arbitrary absorbance units), exhibits an absorption band with the maximum near 268 nm corresponding to the C–I bond and part of an absorption band with the maximum at or below 193 nm corresponding to the C–Br bond. A cross section $\sigma = 2.36 \times 10^{-18}\ cm^2$ and a quantum yield for $Br^*(^2P_{1/2})$ atom formation, $\Phi(Br^*) = 0.07 \pm 0.05$, at 193 nm have been reported.

4.4 References

1. *The Stratosphere 1981: Theory and Measurements*; National Aeronautics and Space Administration, 1982.
2. Abel, B., B. Herzog, H. Hippler and J. Troe, 1989, J. Chem. Phys., 91, 890-899, 900-905.
3. Abel, B., H. Hippler and J. Troe, 1992, J. Chem. Phys., 96, 8863-8871.
4. Ackermann, M. In *Mesospheric Models and Related Experiments*; G. Fiocco, Ed., 1971; pp 149-159.
5. Acton, A. P., R. G. Aickin and N. S. Bayliss, 1936, J. Chem. Phys., 4, 474-479.
6. Adachi, H., N. Basco and D. G. L. James, 1979, Int. J. Chem. Kinet., 11, 1211-1229.
7. Adachi, H., N. Basco and D. G. L. James, 1980, Int. J. Chem. Kinet., 12, 949-977.
8. Addison, M. C., J. P. Burrows, R. A. Cox and R. Patrick, 1980, Chem. Phys. Lett., 73, 283-287.
9. Adler-Golden, S. M., 1983, J. Quant. Spectrosc. Radiat. Transfer, 30, 175-185.
10. Adler-Golden, S. M. and J. R. Wiesenfeld, 1981, Chem. Phys. Lett., 82, 281-284.
11. Alexander, M. H., B. Pouilly and T. Duhoo, 1993, J. Chem. Phys., 99, 1752-1764.
12. Allen, M. and J. E. Frederick, 1982, J. Atmos. Sci., 39, 2066-2075.
13. Aloisio, S. and J. S. Francisco, 2000, Chem. Phys. Lett., 329, 179-184.
14. Amaral, G., K. Xu and J. Zhang, 2001, J. Phys. Chem., A, 105, 1465-1475.
15. Amoruso, A., M. Cacciani, A. di Sarra and G. Fiocco, 1990, J. Geophys. Res., 95, 20565.
16. Amoruso, A., L. Crescentini, G. Fiocco and M. Volpe, 1993, J. Geophys. Res., 98, 16857-16863.
17. Amoruso, A., L. Crescentini, M. Silvia Cola and G. Fiocco, 1996, J. Quant. Spectrosc. Radiat. Transfer, 56, 145- 152.
18. Anastasi, C., I. W. M. Smith and D. A. Parkes, 1978, J. Chem. Soc. Faraday Trans. 1, 74, 1693-1701.
19. Anastasi, C., D. J. Waddington and A. Woolley, 1983, J. Chem. Soc. Faraday Trans., 79, 505-516.
20. Anderson, G. P. and L. A. Hall, 1983, J. Geophys. Res., 88, 6801-6806.
21. Anderson, G. P. and L. A. Hall, 1986, J. Geophys. Res., 91, 14509-14514.
22. Anderson, M., P. Hupalo and K. Mauersberger, 1993, Geophys. Res. Lett., 20, 1579-1582.
23. Anderson, S. M. and K. Mauersberger, 1992, Geophys. Res. Lett., 19, 933-936.
24. Armerding, W., F. J. Comes and B. Schulke, 1995, J. Phys. Chem., 99, 3137-3143.
25. Arnold, S. R., M. P. Chipperfield, M. A. Blitz, D. E. Heard and M. J. Pilling, 2004, Geophys. Res. Lett., L07110, doi:10.1029/2003GL019099.
26. Ashworth, S. H., B. J. Allan and J. M. C. Plane, 2002, Geophys. Res. Lett., 29, 65-1 - 65-4.
27. Astholz, D. C., A. E. Croce and J. Troe, 1982, J. Phys. Chem., 86, 696-699.
28. Atkinson, D. B., J. W. Hudjens and A. J. Orr-Ewing, 1999, J. Phys. Chem. A, 103, 6173-6180.
29. Atkinson, R., D. L. Baulch, R. A. Cox, R. F. Hampson, Jr., J. A. Kerr, M. J. Rossi and J. Troe, 2000, J. Phys. Chem. Ref. Data, 29, 167-266.
30. Atkinson, R., D. L. Baulch, R. A. Cox, R. F. Hampson, J. A. Kerr, M. J. Rossi and J. Troe, 1997, J. Phys. Chem. Ref. Data, 26, 521-1011.
31. Atkinson, R., D. L. Baulch, R. A. Cox, R. F. Hampson, J. A. Kerr and J. Troe, 1992, J. Phys. Chem. Ref. Data, 21, 1125-1568.
32. Atkinson, R. and A. C. Lloyd, 1984, J. Phys. Chem. Ref. Data, 13, 315-444.
33. Bacher, C., G. S. Tyndall and J. J. Orlando, 2001, J. Atmos. Chem., 39, 171-189.
34. Baer, S., H. Hippler, R. Rahn, M. Siefke, N. Seitzinger and J. Troe, 1991, J. Chem. Phys., 95, 6463-6470.
35. Bagratashvili, V. N., S. I. Ionov, G. V. Mishakov and V. A. Semchishen, 1985, Chem. Phys. Lett., 115, 144-148.
36. Bahou, M., C.-Y. Chung, Y.-P. Lee, B. M. Cheng, Y. L. Yung and L. C. Lee, 2001, Astrophys. J., 559, L179-L182.
37. Ball, S. M., G. Hancock, S. E. Martin and J. C. Pinot de Moira, 1997, Chem. Phys. Lett., 264, 531-538.
38. Ballash, N. M. and D. A. Armstrong, 1974, Spectrochim Acta, 30A, 941-944.
39. Barker, J. R., L. Brouwer, R. Patrick, M. J. Rossi, P. L. Trevor and D. M. Golden, 1985, Int. J. Chem. Kinet., 17, 991-1006.
40. Barnes, J. and K. Mauersberger, 1987, J. Geophys. Res., 92, 14861-14864.
41. Barnes, R. J., M. Lock, J. Coleman and A. Sinha, 1996, J. Phys. Chem., 100, 453-457.
42. Barnes, R. J., A. Sinha and H. A. Michelsen, 1998, J. Phys. Chem. A, 102, 8855-8859.
43. Barone, S. B., A. A. Turnipseed, T. Gierczak and A. R. Ravishankara, 1994, J. Phys. Chem., 98, 11969-11977.
44. Barton, S. A., J. A. Coxon and U. K. Roychowdhury, 1984, Can. J. Phys., 62, 473-486.
45. Basco, N. and S. K. Dogra, 1971, Proc. Roy. Soc. A., 323, 417-429.
46. Basco, N. and S. K. Dogra, 1971, Proc. Roy. Soc. A., 323, 29-68.
47. Basco, N. and J. E. Hunt, 1978, Int. J. Chem Kinet., 10, 733-743.
48. Basco, N. and J. E. Hunt, 1979, Int. J. Chem. Kinet., 11, 649-664.
49. Basco, N. and R. D. Morse, 1974, Proc. Roy. Soc. London, A 336, 495-505.
50. Basco, N. and S. S. Parmar, 1985, Int. J. Chem. Kinet., 17, 891-900.
51. Basco, N. and S. S. Parmar, 1987, Int. J. Chem. Kinet., 19, 115-128.

52. Bass, A. M., L. C. Glasgow, C. Miller, J. P. Jesson and S. L. Filken, 1980, Planet. Space Sci. , 28, 675-679.
53. Bass, A. M., A. E. Ledford and A. H. Laufer, 1976, J. Res. Natl. Bur. Stand., 80A, 143-166.
54. Bass, A. M. and R. J. Paur. In *Atmospheric Ozone*; C. S. Zerefos and A. Ghazi, Eds., 1985; pp 606-610.
55. Bates, D. R. and P. B. Hays, 1967, Planet. Space Sci., 15, 189-197.
56. Bauer, D., J. N. Crowley and G. K. Moortgat, 1992, J. Photochem. and Photobiol., A65, 3530-3538.
57. Bauer, D., L. D'Ottone and A. J. Hynes, 2000, Phys. Chem. Chem. Phys., 2, 1421-1424.
58. Bauer, D., T. Ingham, S. A. Carl, G. K. Moortgat and J. N. Crowley, 1998, J. Phys. Chem., 102, 2857-2864.
59. Bauerle, S. and G. K. Moortgat, 1999, Chem. Phys. Lett., 309, 43-48.
60. Baughum, S. L. and S. R. Leone, 1980, J. Chem. Phys., 72, 6531-6545.
61. Baulch, D. L., R. A. Cox, P. J. Crutzen, R. F. Hampson, Jr., J. A. Kerr, J. Troe and R. T. Watson, 1982, J. Phys. Chem. Ref. Data, 11, 327-496.
62. Baum, G. P., P. Felder and R. J. Huber, 1993, J. Chem. Phys., 98, 1999-2010.
63. Baumfalk, R., U. Buck, C. Frischkorn, N. H. Nahler and L. H wel, 1999, J. Chem. Phys., 111, 2595-2605.
64. Bayes, K. D., D. W. Toohey, R. R. Friedl and S. P. Sander, 2003, J. Geophys. Res., 108, 4095, doi:10.29/2002JD002877.
65. Bell, A. J., S. A. Boggis, J. M. Dyke, J. R. Frey, R. Richter, N. Shaw and M. Tabrizchi, 1994, J. Chem. Soc. Faraday Trans., 90, 17-21.
66. Benter, T., C. Feldmann, U. Kirchner, M. Schmidt, S. Schmidt and R. N. Schindler, 1995, Ber. Bunsenges. Phys. Chem., 99, 1144-1147.
67. Berges, M. G. M. and P. Warneck, 1992, Ber. Bunsenges. Phys. Chem., 96, 413-416.
68. Biaume, F., 1973, J. Photochem., 2, 139-149.
69. Bilde, M., T. J. Wallington, G. Ferronato, J. J. Orlando, G. S. Tyndall, E. Estupinan and S. Haberkorn, 1998, J. Phys.Chem. A, 102, 1976-1986.
70. Binder, J. L., 1938, Phys. Rev., 54, 114-117.
71. Birge, R. R., W. C. Pringle and P. A. Leermakers, 1971, J. Am. Chem. Soc., 93, 6715-6726.
72. Birk, M., R. R. Friedl, E. A. Cohen, H. M. Pickett and S. P. Sander, 1989, J. Chem. Phys., 91, 6588-6597.
73. Birks, J. W., B. Shoemaker, T. J. Leck, R. A. Borders and L. J. Hart, 1977, J. Chem. Phys., 66, 4591-4599.
74. Bishenden, E., J. Haddock and D. J. Donaldson, 1991, J. Phys. Chem., 95, 2113-2115.
75. Bishenden, E., J. Haddock and D. J. Donaldson, 1992, J. Phys. Chem., 96, 6513.
76. Blacet, F. E. and R. A. Crane, 1954, J. Am. Chem. Soc., 76, 5337-5340.
77. Blitz, M. A., D. E. Heard, M. J. Pilling, S. R. Arnold and M. P. Chipperfield, 2004, Geophys. Res. Lett., 31, L09104, doi:10.1029/2004GL020182 (correction).
78. Blitz, M. A., D. E. Heard, M. J. Pilling, S. R. Arnold and M. P. Chipperfield, 2004, Geophys. Res. Lett., 31, L06111, doi:1029/2003GL018793.
79. Bloss, W. J., S. L. Nickolaisen, R. J. Salawitch, R. R. Friedl and S. P. Sander, 2001, J. Phys. Chem. A, 105, 11226-11239.
80. Bloss, W. J., D. M. Rowley, R. A. Cox and R. L. Jones, 2001, J. Phys. Chem. A, 105, 7840-7854.
81. Bogumil, K., J. Orphal, J. P. Burrows and J.-M. Flaud, 2001, Chem. Phys. Lett., 349, 241-248.
82. Bogumil, K., J. Orphal, T. Homann, S. Voigt, P. Spietz, O. C. Fleischmann, A. Vogel, M. Hartmann, H. Krominga, H. Bovensmann, J. Frerick and J. P. Burrows, 2003, J. Photochem. Photobiol. A.: Chem., 157, 167-184.
83. Bongartz, A., J. Kames, U. Schurath, C. George, P. Mirabel and J. L. Ponche, 1994, J. Atmos. Chem., 18, 149-169.
84. Bongartz, A., J. Kames, F. Welter and U. Schurath, 1991, J. Phys. Chem., 95, 1076-1082.
85. Brandon, J. T., S. A. Reid, D. C. Robie and H. Reisler, 1992, J. Chem. Phys., 97, 5246.
86. Braun, M., A. Fahr, R. Klein, M. J. Kurylo and R. E. Huie, 1991, J. Geophys. Res., 96, 13009-13015.
87. Braun, W., R. Klein, A. Fahr, H. Okabe and A. Mele, 1990, Chem. Phys. Lett., 166, 397-403.
88. Brewer, L. and J. Tellinghuisen, 1972, J. Chem. Phys., 56, 3929-3938.
89. Brewer, P., P. Das, G. Ondrey and R. Bersohn, 1983, J. Chem. Phys., 79, 720-723.
90. Bridges, L. and J. M. White, 1973, J. Phys. Chem., 77, 295-298.
91. Brint, P., L. O'Toole, C. A. Mayhew and W. Dussa, 1990, J. Chem. Soc. Faraday Trans., 86, 3349-3354.
92. Brion, C. E., Y. Iida, F. Carnovale and J. P. Thomson, 1985, Chem. Phys., 98, 327-339.
93. Brion, J., A. Chakir, J. Charbonnier, D. Daumont, C. Parisse and J. Malicet, 1998, J. Atmos. Chem., 30, 291-299.
94. Brion, J., A. Chakir, D. Daumont, J. Malicet and C. Parisse, 1993, Chem. Phys. Lett., 213, 610-612.
95. Brion, J., D. Daumont and J. Malicet, 1983, C. R. Acad. Sc. Paris, 297, 401-404.
96. Brion, J., D. Daumont and J. Malicet, 1984, J. Physique. Lett., 45, L57-L60.
97. Brion, J., D. Daumont, J. Malicet and P. Marché, 1985, J. Physique. Lett., 46, L105-L110.
98. Brock, J. C. and R. T. Watson, 1980, Chem. Phys., 46, 477-484.
99. Brodersen, P. H., P. Frisch and H.-J. Schumacher, 1937, Z. Phys. Chem. B, 37, 25-29.
100. Broske, R. Ph.D. Thesis, University of Wuppertal, Germany, 1999.

101. Brouwer, L. and J. Troe, 1981, Chem. Phys. Lett., 82, 1-4.
102. Brown, S. S., R. W. Wilson and A. R. Ravishankara, 2000, J. Phys. Chem., A, 104, 4963-4976.
103. Brownsword, R. A., M. Hillenkamp, T. Laurent, R. K. Vatsa, H.-R. Volpp and J. Wolfrum, 1997, J. Phys. Chem. A, 101, 5222-5227.
104. Brownsword, R. A., M. Hillenkamp, T. Laurent, R. K. Vatsa, H.-R. Volpp and J. Wolfrum, 1997, J. Chem. Phys., 106, 1359-1366.
105. Brownsword, R. A., M. Hillenkamp, T. Laurent, J. Wolfrum, H.-R. Volpp, R. K. Vatsa and H.-S. Yoo, 1997, J. Chem. Phys., 107, 779-785.
106. Brownsword, R. A., P. Schmiechen, H.-R. Volpp, H. P. Upadhyaya, Y. J. Jung and K.-H. Jung, 1999, J. Chem. Phys., 110, 11823-11829.
107. Brust, A. S., K. H. Becker, J. Kleffmann and P. Wiesen, 2000, Atmos. Environ., 34, 13-19.
108. Burkholder, J. B., 1993, J. Geophys. Res., 98, 2963-2974.
109. Burkholder, J. B., personal communication to the NASA JPL Panel.
110. Burkholder, J. B. and E. J. Bair, 1983, J. Phys. Chem., 87, 1859-1863.
111. Burkholder, J. B., M. K. Gilles, T. Gierczak and A. R. Ravishankara, 2002, Geophys. Res. Lett., 29, 1822, doi:10.1029/2002GL014712.
112. Burkholder, J. B., G. P. Knight and J. J. Orlando, 2000, J. Photochem. Photobiol. A: Chem., 134, 133-137.
113. Burkholder, J. B., R. L. Mauldin, R. J. Yokelson, S. Solomon and A. R. Ravishankara, 1993, J. Phys. Chem., 97, 7597-7605.
114. Burkholder, J. B. and J. J. Orlando, 2000, Chem. Phys. Lett., 317, 603-608.
115. Burkholder, J. B., J. J. Orlando and C. J. Howard, 1990, J. Phys. Chem., 94, 687-695.
116. Burkholder, J. B., A. R. Ravishankara and S. Solomon, 1995, J. Geophys. Res., 100, 16793-16800.
117. Burkholder, J. B. and R. K. Talukdar, 1994, Geophys. Res. Lett., 21, 581-584.
118. Burkholder, J. B., R. K. Talukdar and A. R. Ravishankara, 1994, Geophys. Res. Lett., 21, 585-588.
119. Burkholder, J. B., R. K. Talukdar, A. R. Ravishankara and S. Solomon, 1993, J. Geophys. Res., 98, 22937-22948.
120. Burkholder, J. B., R. R. Wilson, T. Gierczak, R. Talukdar, S. A. McKeen, J. J. Orlando, G. L. Vaghjiani and A. R. Ravishankara, 1991, J. Geophys. Res., 96, 5025-5043.
121. Burley, J. D., C. E. Miller and H. S. Johnston, 1993, J. Molec. Spec, 158, 377-391.
122. Burrows, J. P., A. Dehn, B. Deters, S. Himmelmann, A. Richter, S. Voigt and J. Orphal, 1998, J. Quant. Spectrosc. Radiat. Transfer, 60, 1025-1031.
123. Burrows, J. P., A. Richter, A. Dehn, B. Deters, S. Himmelmann, S. Voigt and J. Orphal, 1999, J. Quant. Spectrosc. Radiat. Transfer, 61, 509-517.
124. Burrows, J. P., G. S. Tyndall and G. K. Moortgat. 16th Informal Conf. on Photochemistry, 1984, Boston.
125. Burrows, J. P., G. S. Tyndall and G. K. Moortgat, 1985, J. Phys. Chem., 89, 4848-4856.
126. Burrows, J. P., G. S. Tyndall and G. K. Moortgat, 1988, J. Phys. Chem., 92, 4340-4348.
127. Burton, G. R., W. F. Chan, G. Cooper and C. E. Brion, 1994, Chem. Phys., 181, 147-172.
128. Bush, G. E., R. T. Mahoney, R. I. Morse and K. R. Wilson, 1969, J. Chem. Phys., 51, 449-450.
129. Butler, P. J. D. and L. F. Phillips, 1983, J. Phys. Chem., 87, 183-184.
130. Cacciani, M., A. D. di Sarra, G. Fiocco and A. Amoruso, 1989, J. Geophys. Res., 94, 8485-8490.
131. Cadman, P. and J. P. Simons, 1966, Trans. Faraday Soc., 62, 631-641.
132. Calvert, J. G., R. Atkinson, J. A. Kerr, S. Madronich, G. K. Moortgat, T. J. Wallington and Y. G. *The mechanisms of atmospheric oxidation of the alkenes*; Oxford University Press: New York - Oxford, 2000.
133. Calvert, J. G., J. A. Kerr, K. L. Demerjian and R. D. McQuigg, 1972, Science, 175, 751-752.
134. Calvert, J. G. and G. S. Layne, 1953, J. Am. Chem. Soc., 75, 856-859.
135. Calvert, J. G., S. Madronich, E. P. Gardner, J. A. Davidson, C. A. Cantrell and R. E. Shetter, 1987, J. Phys. Chem., 91, 6339-6341.
136. Calvert, J. G. and J. N. Pitts. In *Photochemistry*; John Wiley & Sons, Inc.: New York, 1966; pp 230-231.
137. Calvert, J. G. and J. N. Pitts *Photochemistry*; John Wiley & Sons, Inc.: New York, 1966.
138. Calvert, J. G. and J. N. Pitts Jr. In *Photochemistry*; John Wiley & Sons, Inc.: New York, 1966; pp 371.
139. Calvert, J. G. and J. N. Pitts Jr. In *Photochemistry*; John Wiley & Sons, Inc.: New York, 1966; pp 377.
140. Calvert, J. G. and J. N. Pitts Jr. In *Photochemistry*; John Wiley & Sons, Inc.: New York, 1966; pp 368.
141. Calvert, J. G. and J. N. Pitts Jr. In *Photochemistry*; John Wiley & Sons, Inc.: New York, 1966; pp 428.
142. Calvert, J. G. and J. N. Pitts Jr. In *Photochemistry*; John Wiley & Sons, Inc.: New York, 1966; pp 429.
143. Calvert, J. G. and J. N. Pitts Jr. In *Photochemistry*; John Wiley & Sons, Inc.: New York, 1966; pp 372.
144. Calvert, J. G. and J. N. Pitts Jr. In *Photochemistry*; John Wiley & Sons, Inc.: New York, 1966; pp 184.
145. Calvert, J. G. and J. N. Pitts Jr. In *Photochemistry*; John Wiley & Sons, Inc.: New York, 1966; pp 369.
146. Calvert, J. G. and J. N. Pitts Jr. In *Photochemistry*; John Wiley & Sons, Inc.: New York, 1966; pp 431.
147. Calvert, J. G. and J. N. Pitts Jr. In *Photochemistry*; John Wiley & Sons, Inc.: New York, 1966; pp 430.
148. Campuzano-Jost, P. and J. N. Crowley, 1999, J. Phys. Chem. A, 103, 2712-2719.
149. Canosa-Mas, C. E., M. Fowles, P. J. Houghton and R. P. Wayne, 1987, J. Chem. Soc. Faraday Trans. 2, 83, 1465-1474.

150. Cantrell, C. A., J. A. Davidson, A. H. McDaniel, R. E. Shetter and J. G. Calvert, 1990, J. Phys. Chem., 94, 3902-3908.
151. Cantrell, C. A., J. A. Davidson, R. E. Shetter, B. A. Anderson and J. G. Calvert, 1987, J. Phys. Chem., 91, 5858-5863.
152. Cantrell, C. A., A. Zimmer and G. S. Tyndall, 1997, Geophys. Res. Lett., 24, 2195-2198, 2687 (Erratum).
153. Carnovale, F., R. Tseng and C. E. Brion, 1981, J. Phys. B: Atom. Mol. Phys., 14, 4771-4785.
154. Carter, R. T., A. Hallou and R. J. Huber, 1999, Chem. Phys. Lett., 310, 166-172.
155. Cattell, F. C., J. Cavanagh, R. A. Cox and M. E. Jenkin, 1986, J. Chem. Soc. Faraday Trans. 2, 82, 1999-2018.
156. Causley, G. C. and B. R. Russell, 1977, J. Electron Spectrosc. Relat. Phenom., 11, 383-397.
157. Chang, J. S., J. R. Barker, J. E. Davenport and D. M. Golden, 1979, Chem. Phys. Lett., 60, 385-390.
158. Chegodaev, P. P. and B. I. Tubikov, 1973, Dokl. Akad. Nauk. SSSR, 210, 647-649.
159. Chen, Y., W. Wang and L. Zhu, 2000, J. Phys. Chem. A, 104, 11126-11131.
160. Chen, Y. and L. Zhu, 2001, J. Phys. Chem. A,, 105, 9689-9696.
161. Chen, Y. and L. Zhu, 2003, J. Chem. Phys. A,, 107, 4643-4651.
162. Chen, Y., L. Zhu and J. S. Francisco, 2002, J. Chem. Phys. A, 106, 7755-7763.
163. Cheng, B. M., C.-Y. Chung, M. Bahou, Y.-P. Lee and L. C. Lee, 2002, J. Chem. Phys., 117, 4293-4298.
164. Cheung, A. S. C., K. Yoshino, J. R. Esmond, S. S. L. Chiu, D. E. Freeman and W. H. Parkinson, 1990, J. Chem. Phys., 92, 842-849.
165. Cheung, A. S. C., K. Yoshino, W. H. Parkinson and D. E. Freeman, 1984, Geophys. Res. Lett., 11, 580-582.
166. Cheung, A. S. C., K. Yoshino, W. H. Parkinson, S. L. Guberman and D. E. Freeman, 1986, Planet. Space Sci., 34, 1007-1021.
167. Chichinin, A. I., 1993, Chem. Phys. Lett., 209, 459-463.
168. Chichinin, A. I., S. A. Chasovnikov and L. N. Krasnoperov, 1987, Chem.Phys.Lett., 138, 371-376.
169. Chiu, S. S. L., A. S. C. Cheung, K. Yoshino, J. R. Esmond, D. E. Freeman and W. H. Parkinson, 1990, J. Chem. Phys., 93, 5539-5543.
170. Chou, C. C., G. Crescentini, H. Vera-Ruiz, W. S. Smith and F. S. Rowland. "Stratospheric Photochemistry of CF_2O, CClFO, and CCl_2O"; 173rd American Chemical Society Meeting, 1977, New Orleans, LA.
171. Chou, C. C., R. J. Milstein, W. S. Smith, H. Vera-Ruiz, M. J. Molina and F. S. Rowland, 1978, J. Phys. Chem., 82, 1-7.
172. Chou, C. C., W. S. Smith, H. V. Ruiz, K. Moe, G. Crescentini, M. J. Molina and F. S. Rowland, 1977, J. Phys. Chem., 81, 286-290.
173. Clark, J. H., C. B. Moore and N. S. Nogar, 1978, J. Chem. Phys., 68, 1264-1271.
174. Clark, R. H. and D. Husain, 1984, J. Photochem., 24, 103-115.
175. Clyne, M. A. A. and J. A. Coxon, 1968, Proc. Roy. Soc. A, 303, 207-231.
176. Clyne, M. A. A. and H. W. Cruse, 1970, Trans. Faraday Soc., 66, 2214-2226.
177. CODATA, 1982, J. Phys. Chem. Ref. Data, 11, 327-496.
178. Colussi, A. J., 1990, J. Phys. Chem., 94, 8922-8926.
179. Colussi, A. J., S. P. Sander and R. R. Friedl, 1992, J. Phys.Chem., 96, 4442-4445.
180. Cooper, G., J. E. Anderson and C. E. Brion, 1996, Chem. Phys., 209, 61-77.
181. Cooper, M. J., E. Wrede, A. J. Orr-Ewing and M. N. R. Ashfold, 1998, J. Chem. Soc. Faraday Trans., 94, 2901-2907.
182. Coquart, B., A. Jenouvier and M. F. Merienne, 1995, J. Atm. Chem, 21, 251-261.
183. Coquart, B., M. F. Merienne and A. Jenouvrier, 1990, Planet. Space Sci., 38, 287.
184. Corcoran, T. C., E. J. Beiting and M. O. Mitchell, 1992, J. Molecular Spectroscopy, 154, 119-128.
185. Cox, R. A., R. A. Barton, E. Ljungstrum and D. W. Stocker, 1984, Chem. Phys. Lett., 108, 228-232.
186. Cox, R. A., W. J. Bloss, R. L. Jones and D. M. Rowley, 1999, Geophys. Res. Lett., 26, 1857-1860.
187. Cox, R. A. and J. P. Burrows, 1979, J. Phys. Chem., 83, 2560-2568.
188. Cox, R. A. and G. B. Coker, 1983, J. Phys. Chem., 87, 4478-4484.
189. Cox, R. A. and R. G. Derwent, 1976, J. Photochem., 52, 23-34.
190. Cox, R. A. and G. D. Hayman, 1988, Nature, 332, 796-800.
191. Cox, R. A. and R. Patrick, 1979, Int. J. Chem. Kinet., 11, 635-648.
192. Cox, R. A., D. W. Sheppard and M. P. Stevens, 1982, J. Photochem., 19, 189-207.
193. Cox, R. A. and G. Tyndall, 1979, Chem. Phys. Lett., 65, 357-360.
194. Cox, R. A. and G. S. Tyndall, 1980, J. Chem. Soc. Faraday Trans. 2, 76, 153-163.
195. Coxon, J. A., W. E. Jones and D. A. Ramsey. 12th International Symposium on Free Radicals, 1976, Laguna Beach, California.
196. Creasey, D. J., D. E. Heard and J. D. Lee, 2000, Geophys. Res. Lett., 27, 1651-1654.
197. Crowley, J. N., R. Helleis, R. Muller, G. K. Moortgat, P. J. Crutzen and J. J. Orlando, 1994, J. Geophys. Res., 99, 20683-20688.

198. Crowley, J. N., F. G. Simon, J. P. Burrows, G. K. Moortgat, M. E. Jenkin and R. A. Cox, 1991, J. Photochem. and Photobiol. A: Chem., 60, 1-10.
199. Currie, J., J. H. Sidebottom and J. Tedder, 1974, Int. J. Chem. Kinet., 6, 481-492.
200. Dagaut, P. and M. J. Kurylo, 1990, J. Photochem. and Photobiol. A:Chem., 51, 133-140.
201. Daumont, D., J. Brion, J. Charbonnier and J. Malicet, 1992, J. Atmos. Chem., 15, 145-155.
202. Daumont, D., J. Brion and J. Malicet, 1983, Planet. Space Sci., 31, 1229-1234.
203. Davenport, J. E. "Determination of NO_2 Photolysis Parameters for Stratospheric Modeling," FAA-EQ-78-14, Federal Aviation Administration, Washington, DC. 1978.
204. Davidson, J. A., C. A. Cantrell, A. H. McDaniel, R. E. Shetter, S. Madronich and J. G. Calvert, 1988, J. Geophys. Res., 93, 7105-7112.
205. Davidson, N., 1951, J. Am. Chem. Soc., 73, 467-468.
206. Daviel, S., Y. Iida, F. Carnovale and C. E. Brion, 1984, Chem. Phys., 83, 319-406.
207. Davis, F. H. and Y. T. Lee, 1996, J. Chem. Phys., 105, 8142-8163.
208. Davis, H. F., B. Kim, H. S. Johnston and Y.-T. Lee, 1993, J. Phys. Chem., 97, 2172-2180.
209. Davis, H. F. and Y. T. Lee, 1992, J. Phys. Chem., 96, 5681-5684.
210. Delmdahl, R. F., S. Ulrich and K.-H. Gericke, 1998, J. Phys. Chem. A,, 102, 7680-7685.
211. DeMore, W. B. and O. Raper, 1964, J. Phys. Chem., 68, 412-414.
212. DeMore, W. B., S. P. Sander, D. M. Golden, R. F. Hampson, M. J. Kurylo, C. J. Howard, A. R. Ravishankara, C. E. Kolb and M. J. Molina, 1997, JPL Publication 97-4, Evaluation 12.
213. DeMore, W. B., S. P. Sander, D. M. Golden, R. F. Hampson, M. J. Kurylo, C. J. Howard, A. R. Ravishankara, C. E. Kolb and M. J. Molina "Chemical Kinetics and Photochemical Data for Use in Stratospheric Modeling, Evaluation Number 12," JPL Publication 97-4, Jet Propulsion Laboratory, California Institute of Technology, Pasadena, CA, 1997.
214. DeMore, W. B. and E. Tschuikow-Roux, 1990, J. Phys. Chem., 94, 5856-5860.
215. Deters, B., J. P. Burrows, S. Himmelmann and C. Blindauer, 1996, Ann. Geophysicae, 14, 468-475.
216. Deters, B., J. P. Burrows and J. Orphal, 1998, J. Geophys. Res., 103, 3563-3570.
217. Dixon, J. K., 1940, J. Chem. Phys., 8, 157-160.
218. Donaldson, D. J., G. J. Frost, K. H. Rosenlof, A. F. Tuck and V. Vaida, 1997, Geophys. Res. Lett., 24, 2651-2654.
219. Donaldson, J., J. J. Orlando, S. Amann, G. S. Tyndall, R. J. Proos, B. R. Henry and V. Vaida, 1998, J. Phys. Chem., 102, 5171-5174.
220. Donohue, T. and J. R. Wiesenfeld, 1975, J. Chem. Phys., 63, 3130-3135.
221. Doucet, J., J. R. Gilbert, P. Sauvageau and C. Sandorfy, 1975, J. Chem. Phys., 62, 366-369.
222. Doucet, J., P. Sauvageau and C. Sandorfy, 1973, J. Chem. Phys., 58, 3708-3716.
223. Doucet, J., P. Sauvageau and C. Sandorfy, 1975, J. Chem. Phys., 62, 355-359.
224. Ebenstein, W. L., J. R. Wiesenfeld and G. L. Wolk, 1978, Chem. Phys. Lett., 53, 185-189.
225. Eden, C., H. Feilchenfeld and S. Manor, 1969, Anal. Chem, 41, 1150-1151.
226. Eden, S., P. Lim o-Vieira, S. V. Hoffmann and N. J. Mason, 2003, Chem. Phys. Lett., 379, 170-176.
227. Eden, S., P. Lim o-Vieira, P. A. Kendall, N. J. Mason, J. Delwich, M.-J. Hubin-Franskin, T. Tanaka, M. Kitajima, H. Tanaka, H. Cho and S. V. Hoffmann, 2004, Chem. Phys., 297, 257-269.
228. Ellerman, T., J. Sehested, O. J. Nielson, P. Pagsberg and T. J. Wallington, 1994, Chem. Phys. Lett., 218, 287-294.
229. Emrich, M. and P. Warneck, 2000, J. Phys. Chem. A, 104, 9436-9442.
230. Emrich, M. and P. Warneck, 2005, J. Phys. Chem. A, 109, 1752.
231. Evans, J. T., M. P. Chipperfield, H. Oelhaf, M. Stowasser and G. Wetzel, 2003, Geophys. Res. Lett., 29, 10.1029/2002GL016470, 27-21 - 27-24.
232. Fahr, A., W. Braun and M. J. Kurylo, 1993, J. Geophys. Res., 98, 20467-20472.
233. Fahr, A., A. H. Laufer, M. Kraus and R. Osman, 1997, J. Phys. Chem A, 101, 4879-4886.
234. Fahr, A., A. K. Nayak and R. E. Huie, 1995, Chem. Phys., 199, 275-284.
235. Fahr, A., A. K. Nayak and M. J. Kurylo, 1995, Chem. Phys., 197, 195-203.
236. Febo, A., C. Perrino and I. Allegrini, 1996, Atmos. Environ., 30, 3599-3609.
237. Felder, P., 1991, Chem. Phys., 155, 435-445.
238. Felder, P., 1992, Chem. Phys. Lett., 197, 425-432.
239. Felder, P. and G. P. Morley, 1994, Chem. Phys., 185, 145-151.
240. Felder, P., X. Yang and J. R. Huber, 1993, Chem. Phys. Lett., 215, 221-227.
241. Felps, W. S., K. Rupnik and S. P. McGlynn, 1991, J. Phys. Chem., 95, 639-656.
242. Fenter, F. F., V. Catoire, R. Lesclaux and P. D. Lightfoot, 1993, J. Phys. Chem., 97, 3530-3538.
243. Fergusson, W. C., L. Slotin and W. G. Style, 1936, Trans. Far. Soc., 32, 956-962.
244. Finkelnburg, W., H.-J. Schumacher and G. Stieger, 1931, Z. Phys. Chem., B15, 127-156.
245. Fleischmann, O. C., J. P. Burrows and J. Orphal, 2003, Photochem. Photobiol, A: Chem., 157, 127-136.
246. Flesch, R., E. R hl, K. Hottmann and H. Baumg rtel, 1993, J. Phys. Chem., 97, 837-844.
247. Forte, E., H. Hippler and H. van den Bergh, 1981, Int. J. Chem. Kinet., 13, 1227-1233.

248. Francisco, J. S., M. R. Hand and I. H. Williams, 1996, J. Phys. Chem., 100, 9250-9253.
249. Francisco, J. S. and I. H. Williams, 1992, Mol. Phys., 76, 1433-1441.
250. Frederick, J. E. and R. D. Hudson, 1979, J. Atmos. Sci., 36, 737-745.
251. Frederick, J. E. and J. E. Mentall, 1982, Geophys. Res. Lett., 9, 461-464.
252. Freeman, D. E., K. Yoshino, J. R. Esmond and W. H. Parkinson, 1984, Planet. Space Sci., 32, 239-248.
253. Freeman, D. E., K. Yoshino, J. R. Esmond and W. H. Parkinson. In *Atmospheric Ozone*; C. S. Zerefos and A. Ghazi, Eds., 1985; pp 622-624.
254. Frost, G. J., L. M. Goss and V. Vaida, 1996, J. Geophys. Res, 101, 3869-3877.
255. Frost, G. J., L. M. Goss and V. Vaida, 1996, J. Geophys. Res., 101, 3879-3884.
256. Fujiwara, H. and T. Ishiwata, 1998, J. Phys. Chem., 102, 3856-3859.
257. Furlan, A., T. Gejo and R. J. Huber, 1996, J. Phys. Chem., 100, 7956-7961.
258. Furlan, A., M. A. Haeberli and R. J. Huber, 2000, J. Phys. Chem. A, 104, 10392-10397.
259. Gaedtke, H. and J. Troe, 1975, Ber. Bunsenges. Phys. Chem., 79, 184-191.
260. Ganske, J. A., H. N. Berko and B. J. Finlayson-Pitts, 1992, J. Geophys. Res., 97, 7651-7656.
261. Gardner, E. P., P. D. Sperry and J. G. Calvert, 1987, J. Phys. Chem., 91, 1922-1930.
262. Gardner, E. P., P. D. Sperry and J. G. Calvert, 1987, J. Geophys. Res., 92, 6642-6652.
263. Gardner, E. P., R. D. Wijayaratne and J. G. Calvert, 1984, J. Phys. Chem., 88, 5069-5076.
264. Gedanken, A., 1987, Chem. Phys. Lett., 137, 462-466.
265. Gentieu, E. P. and J. E. Mentall, 1970, Science, 169, 681-683.
266. Gibson, G. E. and N. S. Bayliss, 1933, Phys. Rev., 44, 188-192.
267. Gibson, G. E. and H. C. Ramsperger, 1927, Phys. Rev., 30, 598-600.
268. Giddings, L. E., Jr. and K. K. Innes, 1961, J. Mol. Spectrosc., 6, 528-549.
269. Gierczak, T., J. B. Burkholder, S. Bauerle and A. R. Ravishankara, 1998, Chem. Phys., 231, 229-244.
270. Gierczak, T., J. B. Burkholder and A. R. Ravishankara, 1999, J. Phys. Chem. A, 103, 877-883.
271. Gierczak, T., J. B. Burkholder, R. K. Talukdar, A. Mellouki, S. B. Barone and A. R. Ravishankara, 1997, J. Photochem. Photobiol. A: Chem., 110, 1-10.
272. Gierczak, T., M. K. Gilles, S. Bauerle and A. R. Ravishankara, 2003, J. Phys. Chem. A, 107, 5014-5020.
273. Gilbert, R., P. Sauvageau and C. Sandorfy, 1974, J. Chem. Phys., 60, 4820-4824.
274. Gilles, M. K., A. A. Turnipseed, J. B. Burkholder and A. R. Ravishankara, 1997, J. Phys. Chem. A, 101, 5526-5534.
275. Gillotay, D., A. Jenouvrier, B. Coquart, M. F. Mérienne and P. C. Simon, 1989, Planet. Space Sci., 37, 1127-1140.
276. Gillotay, D. and P. C. Simon, 1988, Annales Geophysicae, 6, 211-215.
277. Gillotay, D. and P. C. Simon, 1989, J. Atmos. Chem., 8, 41-62.
278. Gillotay, D. and P. C. Simon, 1990, Aeronomica Acta A, A356, 1-173.
279. Gillotay, D. and P. C. Simon, 1991, J. Atmos. Chem., 12, 269-285.
280. Gillotay, D. and P. C. Simon, 1991, J. Atmos. Chem., 13, 289-299.
281. Gillotay, D., P. C. Simon and L. Dierickx, 1988, Aeronomica Acta, A335, 1-25.
282. Gillotay, D., P. C. Simon and L. Dierickx, 1993, Aeronomica Acta, A368, 1-15.
283. Giolando, D. M., G. B. Fazekas, W. D. Taylor and G. A. Takacs, 1980, J. Photochem., 14, 335-339.
284. Glicker, S. and H. Okabe, 1987, J. Phys. Chem., 91, 437-440.
285. Glicker, S. and L. J. Stief, 1971, J. Chem. Phys., 54, 2852-2857.
286. Glissmann, A. and H.-J. Schumacher, 1934, Z. Phys. Chem. B, 24, 328-334.
287. Goldfarb, L., A.-M. Schmoltner, M. K. Gilles, J. Burkholder and A. R. Ravishankara, 1997, J. Phys. Chem. A., 101, 6658-6666.
288. Goodeve, C. F. and F. D. Richardson, 1937, Trans. Faraday. Soc., 33, 453-457.
289. Goodeve, C. F. and A. W. C. Taylor, 1935, Proc. Roy. Soc. London, A 152, 221-230.
290. Goodeve, C. F. and A. W. C. Taylor, 1936, Proc. Roy. Soc. London, A 154, 181-187.
291. Goodeve, C. F. and J. I. Wallace, 1930, Trans. Faraday Soc., 26, 254-260.
292. Goodeve, C. F. and B. A. M. Windsor, 1936, Trans. Faraday Soc., 32, 1518-1519.
293. Gordus, A. A. and R. B. Bernstein, 1954, J. Chem. Phys., 22, 790-795.
294. Gosnell, R. R., A. J. Taylor and J. L. Lyman, 1991, J. Chem. Phys., 94, 5949-5953.
295. Graham, R. A. Photochemistry of NO_3 and the Kinetics of the N_2O_5-O_3 System, Ph. D. Thesis, University of California, Berkeley, CA, 1975.
296. Graham, R. A. and H. S. Johnston, 1978, J. Phys. Chem., 82, 254-268.
297. Graham, R. A., A. M. Winer and J. N. Pitts, Jr., 1978, Geophys. Res. Lett., 5, 909-911.
298. Gray, L. T. M. and D. W. G. Style, 1930, Proc. Roy. Soc. London, A 126, 603-612.
299. Green, R. G. and R. P. Wayne, 1976/77, J. Photochem., 6, 375-377.
300. Green, T. J., M. Islam, C. Canosa-Mas, G. Marston and R. P. Wayne, 2004, J. Photochem. Photobiol. A: Chem., 162, 353-370.
301. Green, T. J., M. Islam, P. Guest, K. Hickson, C. E. Canosa-Mas, and R. P. Wayne, 2003, Phys. Chem. Chem. Phys.,, 5, 5409-5418.

302. Greenblatt, G. D. and A. R. Ravishankara, 1990, J. Geophys. Res., 95, 3539-3547.
303. Griffith, D. W. T., G. C. Toon, B. Sen, J.-F. Blavier and R. A. Toth, 2000, Geophys. Res. Lett., 27, 2485-2488.
304. Griggs, M., 1968, J. Phys. Chem., 49, 857-859.
305. Grothe, H. and H. Willner, 1994, Angew. Chem., 106, 1581-1584.
306. Grothe, H. and H. Willner, personal communication to Wayne et al. (1995).
307. Hall, J., T. C. and F. E. Blacet, 1952, J. Chem. Phys., 20, 1745-1749.
308. Hancock, G. and A. Hofzumahaus "Experimental Study of the Altitude Dependence of the Tropospheric Ozone Photolysis Frequency, J(O(1D)) Between 0 and 12 km Height (ATOP)," ENV4-CT95-0158, EU R and D Programme Environment and Climate 1997.
309. Hanf, A., A. La ter and H.-R. Volpp, 2003, Chem. Phys. Lett., 368, 445-451.
310. Harder, J. W., J. W. Brault, P. V. Johnston and G. H. Mount, 1997, J. Geophys. Res., D102, 3681-3879.
311. Harker, A. B., W. Ho and J. J. Ratto, 1977, Chem. Phys. Lett., 50, 394-397.
312. Harwood, M. H., J. B. Burkholder, M. Hunter, R. W. Fox and A. R. Ravishankara, 1997, J. Phys. Chem. A, 101, 853-863.
313. Harwood, M. H., J. B. Burkholder and A. R. Ravishankara, 1998, J. Phys. Chem. A, 102, 1309-1317.
314. Harwood, M. H. and R. L. Jones, 1994, J. Geophys. Res., 99, 22955-22964.
315. Harwood, M. H., R. L. Jones, R. A. Cox, E. Lutman and O. V. Rattigan, 1993, J. Photochem. Photobiol. A: Chem., 73, 167-175.
316. Harwood, M. H., O. V. Rattigan, R. L. Jones and R. A. Cox, 1992, Proc. SPIE Int. Soc. Opt. Eng., 1715, 113-124.
317. Harwood, M. H., J. M. Roberts, G. J. Frost, A. R. Ravishankara and J. B. Burkholder, 2003, J. Phys. Chem. A, 107, 1148-1154.
318. Harwood, M. H., D. M. Rowley, R. A. Freshwater, R. A. Cox and R. L. Jones, 1995, J. Chem. Soc. Faraday Trans, 91, 3027-3032.
319. Haugen, H. K., E. Weitz and S. R. Leone, 1964, J. Chem. Phys., 83, 3402-3412.
320. Haugen, H. K., E. Weitz and S. R. Leone, 1985, J. Chem. Phys., 83, 3402-3412.
321. Hayman, G. D. and R. A. Cox, 1989, Chem. Phys. Lett., 155, 1-7.
322. He, H.-Y. and W.-H. Fang, 2003, J. Am. Chem. Soc., 125, 16139-16147.
323. Hearn, A. G., 1961, Proc. Phys. Soc. London, 78, 932-940.
324. Heicklen, J., 1965, J. Am. Chem. Soc., 87, 445-453.
325. Heicklen, J., J. Desai, A. Bahta, C. Harper and R. Simonaitis, 1986, J. Photochem., 34, 117-135.
326. Hemenway, C. P., T. G. Lindeman and J. R. Wiesenfeld, 1979, J. Chem. Phys., 70, 3560-3561.
327. Herman, J. R. and J. E. Mentall, 1982, J. Geophys. Res., 87, 8967-8975.
328. Hermann, M., A. Nölle and H. Heydtmann, 1994, Chem. Phys. Lett., 226, 559-562.
329. Herzberg, G. and K. K. Innes, 1957, Can. J. Phys., 35, 842-879.
330. Hicks, E., B. Leroy, P. Rigaud, J.-L. Joudain and G. Le Bras, 1979, J. Chem. Phys., 76, 693-698.
331. Himmelmann, S., J. Orphal, H. Bovensmann, A. Richter, A. Ladst tter-Weissenmayer and J. P. Burrows, 1996, Chem. Phys. Lett., 251, 330-334.
332. Hippler, H., S. Luu, H. Teitelbaum and J. Troe, 1978, Int. J. Chem. Kinet., 10, 155-169.
333. Hitchcock, A. P., G. R. J. Williams, C. E. Brion and P. W. Langhoff, 1984, Chem. Phys., 88, 65-80.
334. Ho, G. H., 1998, Chem. Phys., 226, 101-111.
335. Hochanadel, C. J., J. A. Ghormley, J. W. Boyle and P. J. Ogren, 1977, J. Phys. Chem., 81, 3-7.
336. Hochanadel, C. J., J. A. Ghormley and P. J. Ogren, 1972, J. Chem. Phys., 56, 4426-4432.
337. Holmes, H. H. and F. Daniels, 1934, J. Am. Chem. Soc., 56, 630-637.
338. Horowitz, A. and J. G. Calvert, 1978, Int. J. Chem. Kinet., 10, 805-819.
339. Horowitz, A. and J. G. Calvert, 1982, J. Phys. Chem., 86, 3105-3114.
340. Horowitz, A., C. J. Kershner and J. G. Calvert, 1982, J. Phys. Chem., 86, 3094-3104.
341. Horowitz, A., R. Meller and G. K. Moortgat, 2001, J. Photochem. Photobiol. A: Chem., 146, 19-27.
342. Houel, N. and H. Van den Bergh, 1977, Int. J. Chem. Kinet., 9, 867-874.
343. Hubinger, S. and J. B. Nee, 1994, Chem. Phys., 181, 247-257.
344. Hubinger, S. and J. B. Nee, 1995, J. Photochem. Photobiol. , 86, 1-7.
345. Hubinger, S. and J. B. Nee, 1995, J. Photochem. and Photobiol. A: Chem., 86, 1-7.
346. Hubrich, C. and F. Stuhl, 1980, J. Photochem., 12, 93-107.
347. Hubrich, C., C. Zetzsch and F. Stuhl, 1977, Ber. Bunsenges. Phys. Chem., 81, 437-442.
348. Huder, K. J. and W. B. DeMore, 1995, J. Phys. Chem., 99, 3905-3908.
349. Hudson, R. D., 1971, Reviews of Geophysics and Space Physics, 9, 305-399.
350. Hudson, R. D., 1974, Canad. J. Chem., 52, 1465-1478.
351. Hudson, R. D. and L. J. Kieffer. Absorption Cross Sections of Stratospheric Molecules. In *The Natural Stratosphere of 1974*; CIAP, 1975; Vol. Monograph 1; pp (5-156)-(5-194).
352. Huebert, B. J. and R. M. Martin, 1968, J. Phys. Chem., 72, 3046-3048.

353. Huebner, R. H., J. Bushnell, D. L., R. J. Celotta, S. R. Mielczarek and C. E. Kuyatt, 1975, Nature, 257, 376-378.
354. Hunnicutt, S. S., L. D. Waits and J. A. Guest, 1989, J. Phys. Chem., 93, 5188-5195.
355. Hynes, A. J., E. A. Kenyon, A. J. Pounds and P. H. Wine, 1992, Spectrochim. Acta, 48A, 1235-1242.
356. Ibuki, T., 1992, J. Chem. Phys., 96, 8793-8798.
357. Ibuki, T., N. Takahashi, A. Hiraya and K. Shobatake, 1986, J. Chem. Phys., 85, 5717-5722.
358. Ichimura, T., A. W. Kirk, G. Kramer and E. Tschuikow-Roux, 1976/1977, J. Photochem., 6, 77-90.
359. Ichimura, T., A. W. Kirk and E. Tschuikow-Roux, 1977, J. Phys. Chem., 81, 1153-1156.
360. Illies, A. J. and G. A. Takacs, 1976, J. Photochem., 6, 35-42.
361. Ingham, T., D. Bauer, J. Landgraf and J. N. Crowley, 1998, J. Phys. Chem. A, 102, 3293-3298.
362. Ingham, T., M. Cameron and J. N. Crowley, 2000, J. Phys. Chem. A, 104, 8001-8010.
363. Inn, E. C. Y., 1975, J. Atmos. Sci., 32, 2375-2377.
364. Inn, E. C. Y., 1980, J. Geophys. Res., 85, 7493-7494.
365. Inn, E. C. Y. and Y. Tanaka, 1953, J. Opt. Soc. Am., 43, 870-873.
366. Inn, E. C. Y. and Y. Tanaka, 1958, Adv. Chem. Ser., 21, 263-268.
367. Jacobs, J., M. Kronberg, H. S. P. M ller and H. Willner, 1994, J. Am. Chem. Soc., 116, 1106-1114.
368. J ger, M., H. Heydtmann and C. Zetzsch, 1996, Chem. Phys. Lett., 263, 817-821.
369. Jansen, M., G. Schatte, K. M. Tobias and H. Willner, 1988, Inorg. Chem., 27, 1703-1706.
370. Jee, Y.-J., Y.-S. Jung and K.-H. Jung, 2001, J. Chem. Phys., 115, 9739-9746.
371. Jee, Y.-J., M. S. Park, Y. S. Kim, Y.-S. Jung and K.-H. Jung, 1998, Chem. Phys. Lett., 287, 701-708.
372. Jenkin, M. E. and R. A. Cox, 1985, J. Phys. Chem., 89, 192-199.
373. Jenkin, M. E. and R. A. Cox, 1991, J. Phys. Chem., 95, 3229-3237.
374. Jenkin, M. E., R. A. Cox, G. Hayman and L. J. Whyte, 1988, J. Chem. Soc. Faraday Trans. 2, 84, 913-930.
375. Jenkin, M. E., R. A. Cox, A. Mellouki, G. Le Bras and G. Poulet, 1990, J. Phys. Chem., 94, 2927-2934.
376. Jenkin, M. E., T. P. Murrells, S. J. Shalliker and G. D. Hayman, 1993, J. Chem. Soc. Faraday Trans., 89, 433-446.
377. Jenouvrier, A., B. Coquart and M.-F. Mérienne, 1996, J. Atmos. Chem., 25, 21-32.
378. Jenouvrier, A., B. Coquart and M. F. Merienne, 1986, J. Quant. Spectros. Radiat. Transfer 36, 349-354.
379. Jensen, F. and J. Oddershede, 1990, J. Phys. Chem., 94, 2235-2237.
380. Jimenez, E., T. Gierczak, H. Stark, J. B. Burkholder and A. R. Ravishankara, 2005, Phys. Chem. Chem. Phys., 7, 342-348.
381. Johnson, M. S., G. D. Billing, A. Gruodis and M. H. M. Janssen, 2001, J. Phys. Chem. A, 105, 8672-8680.
382. Johnsson, K., A. Engdahl and B. Nelander, 1995, J. Phys. Chem., 99, 3965-3968.
383. Johnston, H. S. and H. J. Bertin, Jr., 1959, J. Mol. Spectrosc., 3, 683-696.
384. Johnston, H. S., S. Chang and G. Whitten, 1974, J. Phys. Chem., 78, 1-7.
385. Johnston, H. S., H. F. Davis and Y. T. Lee, 1996, J. Phys. Chem., 100, 4713-4723.
386. Johnston, H. S. and R. Graham, 1973, J. Phys. Chem., 77, 62-63.
387. Johnston, H. S. and R. Graham, 1974, Canad. J. Chem., 52, 1415-1423.
388. Johnston, H. S., E. D. Morris, Jr. and J. Van den Bogaerde, 1969, J. Am. Chem. Soc., 91, 7712-7727.
389. Johnston, H. S., M. Paige and F. Yao, 1984, J. Geophys. Res., 89, 661.
390. Johnston, H. S. and G. S. Selwyn, 1975, Geophys. Res. Lett., 2, 549-551.
391. Jolly, G. S., D. L. Singleton, D. J. McKenney and G. Paraskevopoulos, 1986, J. Chem. Phys., 84, 6662-6667.
392. Jolly, G. S., D. L. Singleton and G. Paraskevopoulos, 1987, J. Phys. Chem., 91, 3463-3465.
393. Jones, E. L. and O. R. Wulf, 1937, J. Chem. Phys., 5, 873-877.
394. Jones, I. T. N. and K. Bayes, 1973, J. Chem. Phys., 59, 4836-4844.
395. Jost, R., J. Nygard, A. Pasinski and A. Delon, 1996, J. Chem. Phys., 105, 1287-1290.
396. Jost, W., 1931, Z. Phys. Chem. A, 153, 143-152.
397. Jourdain, J. L., G. Le Bras, G. Poulet, J. Combourieu, P. Rigaud and B. LeRoy, 1978, Chem. Phys. Lett., 57, 109-112.
398. Jung, K.-W., T. S. Ahmadi and M. A. El-Sayed, 1997, J. Phys. Chem. A, 101, 6562-6567.
399. Jung, Y.-J., M. S. Park, Y. S. Kim, K.-H. Jung and H.-R. Volpp, 1999, J. Chem. Phys., 111, 4005-4012.
400. Jungkamp, T. P. W., U. Kirchner, M. Schmidt and R. N. Schindler, 1995, J. Photochem. Photobiol. A: Chemistry, 99, 1-6.
401. Kalekin, A. L. and K. Morokuma, 2000, J. Chem. Phys., 113, 5750-5762.
402. Kan, C. S., R. D. McQuigg, M. R. Whitbeck and J. G. Calvert, 1979, Int. J. Chem. Kinet., 11, 921-933.
403. Kang, W. K., K. W. Jung, D.-C. Kim and K.-H. Jung, 1996, J. Chem. Phys., 104, 5815-5820.
404. Kavita, K. and P. K. Das, 2000, J. Chem. Phys., 112, 8426-8431.
405. Kenner, R. D., F. Rohrer and F. Stuhl, 1986, J. Phys. Chem., 90, 2635-2639.
406. Kim, Y. S., Y. J. Jung and K.-H. Jung, 1997, J. Chem. Phys., 107, 3805-3812.
407. Kim, Y. S., W. K. Kang and K.-H. Jung, 1996, J. Chem. Phys., 105, 551-557.
408. Kim, Y. S., W. K. Kang, D.-C. Kim and K.-H. Jung, 1997, J. Phys. Chem. A, 101, 7576-7581.

409. Kirmse, B., A. Delon and R. Jost, 1997, J. Geophys. Res., D103, 16089-16098.
410. Kirshenbaum, A. D. and A. G. Streng, 1961, J. Chem. Phys., 35, 1440-1442.
411. Knauth, H. D., H. Alberti and H. Clausen, 1979, J. Phys. Chem., 83, 1604-1612.
412. Knauth, H. D. and R. N. Schindler, 1983, Z. Naturforsch., 38a, 893-895.
413. Knight, G. P., A. R. Ravishankara and J. B. Burkholder, 2000, J. Phys. Chem. A, 104, 11121-11125.
414. Knight, G. P., A. R. Ravishankara and J. B. Burkholder, 2002, Phys. Chem. Chem. Phys., 4, 1432-1437.
415. Koch, S. and G. K. Moortgat, 1998, J. Phys. Chem. A, 102, 9142-9153.
416. Koffend, J. B., J. S. Holloway, M. A. Kwok and R. F. Heidner III, 1987, J. Quant. Spectrosc. Radiat. Transfer, 37, 449-453.
417. Koffend, J. B. and S. R. Leone, 1981, Chem. Phys. Lett., 81, 136-141.
418. Kort m, G. and G. Friedheim, 1947, Z. Naturforsch., 2a, 20-27.
419. Kozlov, S. N., V. L. Orkin, R. E. Huie and M. J. Kurylo, 2003, J. Phys. Chem. A, 107, 1333-1338.
420. Krajnovich, D., Z. Zhang, L. Butler and Y. T. Lee, 1984, J. Chem. Phys., 88, 4561-4566.
421. Krasnoperov, L. N. and K. Mehta, 1999, J. Phys. Chem. A, 103, 8008-8020.
422. Krisch, M. J., L. R. McCunn, K. Takematsu, L. J. Butler, F. R. Blase and J. Shu, 2004, J. Phys. Chem., A, 108, 1650-1656.
423. Kromminga, J., J. Orphal, P. Spietz, S. Voigt and J. P. Burrows, 2003, J. Photochem. Photobiol. A: Chem., 157, 149-160.
424. Kurylo, M. J., T. J. Wallington and P. A. Ouellette, 1987, J. Photochem., 39, 201-215.
425. Kwok, W. M. and D. L. Phillips, 1996, J. Chem. Phys., 104, 2529-2540.
426. Kwok, W. M. and D. L. Phillips, 1997, Mol. Phys., 90, 315-326.
427. Kwok, W. M. and D. L. Phillips, 1997, Chem. Phys. Lett., 270, 506-516.
428. Kyle, E. and S. W. Orchard, 1977, J. Photochem., 7, 305-317.
429. Lake, J. S. and A. J. Harrison, 1959, J. Chem. Phys., 30, 361-362.
430. Lambert, H. M., P. J. Dagdigian and M. H. Alexander, 1998, J. Chem. Phys., 108, 4460-4466.
431. Lang, V. I., S. P. Sander and R. R. Friedl, 1988, J. Mol. Spectrosc., 132, 89-103.
432. Langford, A. O. and C. B. Moore, 1984, J. Chem. Phys., 80, 4211-4221.
433. Langford, S. R., P. M. Regan, A. J. Orr-Ewing and N. M. R. Ashfold, 1998, Chem. Phys., 231, 245-260.
434. Langhoff, S. R., L. Jaffe and J. O. Arnold, 1977, J. Quant. Spectrosc. Radiat. Transfer, 18, 227-235.
435. Laszlo, B., R. E. Huie, M. J. Kurylo and A. W. Miziolek, 1997, J. Geophys. Res., 102, 1523-1532.
436. Laszlo, B., M. J. Kurylo and R. E. Huie, 1995, J. Phys. Chem., 99, 11701-11707.
437. Lawrence, W. G., K. C. Clemitshaw and V. A. Apkarian, 1990, J. Geophys. Res., 95, 18591-18595.
438. Lee, L. C., 1982, J. Chem. Phys., 76, 4909-4915.
439. Lee, S.-H., Y.-J. Jung and K.-H. Jung, 2000, Chem. Phys., 260, 143-150.
440. Leroy, B., P. Rigaud and E. Hicks, 1987, Ann. Geophys. A., 5, 247-250.
441. Lewis, B. R., L. Berzins and J. H. Carver, 1986, J. Quant. Spectrosc. Radiat. Transfer, 36, 209-232.
442. Lewis, B. R., L. Berzins, J. H. Carver and S. T. Gibson, 1986, J. Quant. Spectrosc. Radiat. Transfer, 36, 187-207.
443. Lewis, R. S., K. Y. Tang and E. K. C. Lee, 1976, J. Chem. Phys., 65, 2910-2911.
444. Li, Q., R. T. Carter and J. R. Huber, 2001, Chem. Phys. Lett., 334, 39-46.
445. Libuda, H. G. Spektroskopische und kinetische Untersuchungen an halogenierten Carbonylverbindungen von atmosph rischem Interesse, PhD-Thesis, University of Wuppertal, Germany, 1992.
446. Libuda, H. G. and F. Zabel, 1995, Ber. Bunsenges. Phys. Chem., 99, 1205-1213.
447. Libuda, H. G., F. Zabel and K. H. Becker. "UV spectra of some organic chlorine and bromine compounds of atmospheric interest"; Kinetics and Mechanisms for the Reactions of Halogenated Organic Compounds in the Troposphere. STEP-HALOCSIDE/AFEAS WORKSHOP, 1991, Dublin, Ireland.
448. Libuda, H. G., F. Zabel, E. H. Fink and K. H. Becker, 1990, J. Phys. Chem., 94, 5860-5865.
449. Lightfoot, P. D., R. A. Cox, J. N. Crowley, M. Destriau, G. D. Hayman, M. E. Jenkin, G. K. Moortgat and F. Zabel, 1992, Atmos. Environ., 26A, 1805-1961.
450. Lightfoot, P. D. and A. A. Jemi-Alade, 1991, J. Photochem. and Photobiol. A: Chem., 59, 1-10.
451. Limao-Vieira, P., S. Eden, P. A. Kendall, N. J. Mason and S. V. Hoffmann, 2002, Chem. Phys. Lett., 364, 535-541.
452. Lim o-Vieira, P., S. Eden and N. J. Mason, 2003, Radiation Phys. Chem., 68, 187-192.
453. Lim o-Vieira, P., S. Eden, N. J. Mason and S. V. Hoffmann, 2003, Chem. Phys. Lett., 376, 737-747.
454. Lin, C. L., 1976, J. Chem. Eng. Data, 21, 411-413.
455. Lin, C. L., N. K. Rohatgi and W. B. DeMore, 1978, Geophys. Res. Lett., 5, 113-115.
456. Lindeman, T. G. and J. R. Wiesenfeld, 1979, J. Chem. Phys., 70, 2882-2888.
457. Lipscomb, F. J., R. G. W. Norrish and B. A. Thrush, 1956, Proc. Roy. Soc. London, A 233, 455-464.
458. Liyanage, R., Y.-A. Yang, S. Hashimoto, R. J. Gordon and R. W. Field, 1995, J. Chem. Phys., 103, 6811-6814.
459. Lock, M., R. J. Barmes and A. Sinha, 1996, J. Phys. Chem., 100, 7972-7980.
460. Lopez, M. I. and J. E. Sicre, 1988, J. Phys. Chem., 92, 563-564.

461. Lopez, M. I. and J. E. Sicre, 1990, J. Phys. Chem., 94, 3860-3863.
462. Lucazeau, G. and C. Sandorfy, 1970, J. Mol. Spectrosc., 35, 214-231.
463. Lyman, J. and R. Holland, 1988, J. Phys. Chem., 92, 7232-7241.
464. MacLeod, H., G. P. Smith and D. M. Golden, 1988, J. Geophys. Res., 93, 3813-3823.
465. Magneron, I., A. Mellouki, G. Le Bras, G. K. Moortgat, A. Horowitz and K. Wirtz, 2005, J. Phys. Chem. A, 109, 4552-4561.
466. Magneron, I., R. Thévenet, A. Mellouki, G. Le Bras, G. K. Moortgat and K. Wirtz, 2002, J. Phys. Chem. A, 106, 2526-2537.
467. Magnotta, F. and H. S. Johnston, 1980, Geophys. Res. Lett., 7, 769-772.
468. Majer, J. R. and J. P. Simons. Photochemical Processes in Halogenated Compounds. In *Advances in Photochemistry*; Interscience, 1964; Vol. 2; pp 137-181.
469. Malicet, J., J. Brion and D. Daumont, 1989, Chem. Phys. Lett., 158, 293-296.
470. Malicet, J., D. Daumont, J. Charbonnier, C. Parisse, A. Chakir and J. Brion, 1995, J. Atm. Chem, 21, 263-273.
471. Maloney, K. K. and H. B. Palmer, 1973, Int. J. Chem. Kinet., 5, 1023-1037.
472. Man, S.-Q., W. M. Kwok, D. L. Phillips and A. E. Johnson, 1996, J. Chem. Phys., 105, 5842-5857.
473. Mandelman, M. and R. W. Nicholls, 1977, J. Quant. Spectrosc. Radiat. Trans., 17, 483-491.
474. Margitan, J. J., 1983, J. Phys. Chem., 87, 674-679.
475. Margitan, J. J. and R. T. Watson, 1982, J. Phys. Chem., 86, 3819-3824.
476. Maric, D. and J. P. Burrows, 1999, J. Quant. Spectrosc. Radiat. Transfer, 62, 345-369.
477. Maric, D., J. P. Burrows, R. Meller and G. K. Moortgat, 1993, J. Photochem. Photobiol. A Chem., 70, 205-214.
478. Maric, D., J. P. Burrows and G. K. Moortgat, 1994, J. Photochem. Photobiol A: Chem., 83, 179-192.
479. Maric, D., J. N. Crowley and J. P. Burrows, 1997, J. Phys. Chem., 101, 2561-2567.
480. Maricq, M. M., personal communication to JPL subcommittee.
481. Maricq, M. M. and J. J. Szente, 1992, J. Phys. Chem., 96, 4925-4930.
482. Maricq, M. M. and J. J. Szente, 1994, J. Phys. Chem., 98, 2078-2082.
483. Maricq, M. M. and J. J. Szente, 1995, J. Phys. Chem., 99, 4554-4557.
484. Maricq, M. M. and J. J. Szente, 1996, J. Phys. Chem., 100, 4507-4513.
485. Maricq, M. M. and T. J. Wallington, 1992, J. Phys. Chem., 96, 982-986.
486. Marinelli, W. J. and H. S. Johnston, 1982, Chem. Phys. Lett., 93, 127-132.
487. Marinelli, W. J., D. M. Swanson and H. S. Johnston, 1982, J. Chem. Phys., 76, 2864-2870.
488. Marling, L., 1977, J. Chem. Phys., 66, 4200-4225.
489. Marston, G., I. C. Walker, N. J. Mason, J. M. Gingell, H. Zhao, K. L. Brown, F. Motte-Tollet, J. Delwiche and M. R. F. Siggel, 1998, J. Phys. B: Atom. Mol. Phys., 31, 3387-3405.
490. Martin, H. and R. Gareis, 1956, Z. Elektrochemie, 60, 959-964.
491. Martin, R. M. and J. E. Willard, 1964, J. Chem. Phys., 40, 2999-3007.
492. Martinez, R. D., A. A. Buitrago, N. W. Howell, C. H. Hearn and J. A. Joens, 1992, Atmos. Environ., 26A, 785-792.
493. Mashnin, T. S., A. V. Cheryshev and L. N. Krasnoperov, 1993, Chem. Phys. Lett., 207, 105-109.
494. Matchuk, N. M., V. I. Tupikov, A. I. Malkova and S. Y. Pshezhetskii, 1976, Opt. Spektrosk. (Opt. Spectrosc.), 40, 14-18 (17-19).
495. Mathieson, L. and A. L. G. Rees, 1956, J. Chem. Phys., 25, 753-761.
496. Matsumi, Y., F. J. Comes, G. Hancock, A. Hofzumahaus, A. J. Hynes, M. Kawasaki and A. R. Ravishankara, 2002, J. Geophys. Res., in press.
497. Matsumi, Y., P. K. Das and M. Kawasaki, 1990, J. Chem. Phys., 92, 1696-1701.
498. Matsumi, Y., P. K. Das and M. Kawasaki, 1992, J. Chem. Phys., 97, 5261.
499. Matsumi, Y., K. Tonokura, M. Kawasaki and T. Ibuki, 1990, J. Chem. Phys., 93, 7981-7985.
500. Mauersberger, K., J. Barnes, D. Hanson and J. Morton, 1986, Geophys. Res. Lett., 13, 671-673.
501. Mauersberger, K., D. Hanson, J. Barnes and J. Morton, 1987, J. Geophys. Res., 92, 8480-8482.
502. Mauldin, R. L., III, J. B. Burkholder and A. R. Ravishankara, 1992, J. Phys. Chem., 96, 2582-2588.
503. Mazely, T. L., R. R. Friedl and S. P. Sander, 1995, J. Phys. Chem., 99, 8162-8169.
504. Mazely, T. L., R. R. Friedl and S. P. Sander, 1997, J. Phys. Chem., 101, 7090-7097.
505. McAdam, K., B. Veyret and R. Lesclaux, 1987, Chem. Phys. Lett., 133, 39-44.
506. McElcheran, D. E., M. H. J. Wijnen and E. W. R. Steacie, 1958, Can. J. Chem., 36, 321-339.
507. McGivern, W. S., R. Li, P. Zou and S. W. North, 1999, J. Chem. Phys., 111, 5771-5779.
508. McGrath, M. P., K. C. Clemitshaw, F. S. Rowland and W. J. Hehre, 1988, Geophys. Res. Lett., 15, 883-886.
509. McGrath, M. P., K. C. Clemitshaw, F. S. Rowland and W. J. Hehre, 1990, J. Phys. Chem., 94, 6126-6132.
510. McMillan, V., personal communication.
511. McPeters, R. D. and A. M. Bass, 1982, Geophys. Res. Lett., 9, 227-230.
512. McQuigg, R. D. and J. G. Calvert, 1969, J. Am. Chem. Soc., 91, 1590-1599.

513. Meller, R., personal communication to NASA Data Panel.
514. Meller, R., D. Boglu and G. K. Moortgat. "UV spectra of several halogenated carbonyl compounds and FTIR studies of the degradation of CF_3COCl, HCFC-123 and HFC-143a"; Kinetics and Mechanisms for the Reactions of Halogenated Organic Compounds in the Troposphere. STEP-HALOCSIDE/AFEAS WORKSHOP, 1991, Dublin, Ireland.
515. Meller, R. and G. K. Moortgat, 1995, J. Photochem. Photobio. A: Chem., 86, 15-25.
516. Meller, R. and G. K. Moortgat, 1997, J. Photochem. Photobiol. A: Chem., 108, 105-116.
517. Meller, R. and G. K. Moortgat, 2000, J. Geophys. Res. D, 105, 7089-7101.
518. Meller, R., W. Raber, J. N. Crowley, M. E. Jenkin and G. K. Moortgat, 1991, J. Photochem. Photobiol., 62, 163-171.
519. Mellouki, A. and Y. Mu, 2003, J. Photochem. Photobiol. A: Chem., 157, 295-300.
520. Mentall, J. E., E. P. Gentieu, M. Krauss and D. Neumann, 1971, J. Chem. Phys., 55, 5471-5479.
521. Mérienne, M.-F., A. Jenouvrier, B. Coquart and J. P. Lux, 1997, J. Atmos. Chem., 27, 219-232.
522. Mérienne, M. F., B. Coquart and A. Jenouvrier, 1990, Planet. Space Sci., 38, 617-625.
523. Mérienne, M. F., A. Jenouvrier and B. Coquart, 1995, J. Atm. Chem, 20, 281-297.
524. Meyrahn, H. Bildungswege und Analytik des Peroxyacetylnitrats (PAN) in der Atmosph re, PhD-Thesis, Johann-Gutenberg-Universit t, 1984.
525. Meyrahn, H., G. K. Moortgat and P. Warneck, 1981, J. Photochem., 17, 138.
526. Meyrahn, H., J. Pauly, W. Schneider and P. Warneck, 1986, J. Atmos. Chem., 4, 277-291.
527. Mihalcea, R. M., D. S. Baer and R. K. Hanson, 1996, Appl. Optics, 35, 4059-4064.
528. Miller, C. E., S. L. Nickolaisen, J. S. Francisco and S. P. Sander, 1997, J. Chem. Phys., 107, 2300-2307.
529. Minaev, B. F., 1999, J. Phys. Chem. A, 103, 7294-7309.
530. Minschwaner, K., G. P. Anderson, L. A. Hall and K. Yoshino, 1992, J. Geophys. Res., 97, 10103-10108.
531. Minschwaner, K. and D. E. Siskind, 1993, J. Geophys. Res., 98, 20401-20412.
532. Minton, T. K., C. M. Nelson, T. A. Moore and M. Okumura, 1992, Science, 258, 1342-1345.
533. Mishalanie, E. A., J. C. Rutkowski, R. S. Hutte and J. W. Birks, 1986, J. Phys. Chem., 90, 5578-5584.
534. Mitchell, D. N., R. P. Wayne, P. J. Allen, R. P. Harrison and R. J. Twin, 1980, J. Chem. Soc. Faraday Trans. 2, 76, 785-793.
535. Mo, Y., K. Tonokura, Y. Matsumi, M. Kawasaki, T. Sato, T. Arikawa, P. T. A. Reilly, Y. Xie, Y. Yang, Y. Huang and R. J. Gordon, 1992, J. Chem. Phys., 97, 4815-4826.
536. Molina, L. T. and M. J. Molina, 1977, Geophys. Res. Lett., 4, 83-86.
537. Molina, L. T. and M. J. Molina, 1978, J. Phys. Chem., 82, 2410-2414.
538. Molina, L. T. and M. J. Molina, 1979, J. Photochem., 11, 139-144.
539. Molina, L. T. and M. J. Molina, 1981, J. Photochem., 15, 97-108.
540. Molina, L. T. and M. J. Molina. "Chemistry of fluorine in the stratosphere"; 182nd American Chemical Society National Meeting, 1982, New York.
541. Molina, L. T. and M. J. Molina, 1983, J. Phys. Chem., 87, 1306-1308.
542. Molina, L. T. and M. J. Molina, 1986, J. Geophys. Res., 91, 14501-14508.
543. Molina, L. T. and M. J. Molina, 1987, J. Phys. Chem., 91 433-436.
544. Molina, L. T. and M. J. Molina, 1996, Geophys. Res. Lett., 23, 563-565.
545. Molina, L. T., M. J. Molina and F. S. Rowland, 1982, J. Phys. Chem., 86, 2672-2676.
546. Molina, L. T., S. D. Schinke and M. J. Molina, 1977, Geophys. Res. Lett., 4, 580-582.
547. Molina, M. J. and G. Arguello, 1979, Geophys. Res. Lett., 6, 953-955.
548. Molina, M. J., A. J. Colussi, L. T. Molina, R. N. Schindler and T. L. Tso, 1990, Chem. Phys. Lett., 173, 310-315.
549. Molina, M. J., T. Ishiwata and L. T. Molina, 1980, J. Phys. Chem., 84, 821-826.
550. Moore, T. A., M. Okumura and T. K. Minton, 1997, J. Phys. Chem., 1-7, 3337-3338.
551. Moore, T. A., M. Okumura, J. W. Seale and T. K. Minton, 1999, J. Phys. Chem. A, 103, 1692-1695.
552. Moore, T. A., M. Okumura, M. Tagawa and T. K. Minton, 1995, Faraday Discuss, 100, 295-307.
553. Moortgat, G. K., 2001, Pure Appl. Chem., 73, 487-490.
554. Moortgat, G. K. "RADICAL: Evaluation of Radical Sources in Atmospheric Chemistry through Chamber and Laboratory Studies," ENVA-CT97-0419, EUR 20254 EN, 2002.
555. Moortgat, G. K., W. Klippel, K. H. MÖbus, W. Seiler and P. Warneck FAA-EE-80-47, Federal Aviation Administration, Washington, DC 1980.
556. Moortgat, G. K., R. Meller and W. Schneider. Temperature dependence (256-296K) of the absorption cross-sections of bromoform in the wavelength range 285-360 nm. In *The Tropospheric Chemistry of Ozone in the Polar Regions*; H. Niki and K. H. Becker, Eds.; Springer-Verlag: Berlin, 1993; pp 359-369.
557. Moortgat, G. K., W. Seiler and P. Warneck, 1983, J. Chem. Phys., 78, 1185-1190.
558. Moortgat, G. K., F. Slemr, W. Seiler and P. Warneck, 1978, Chem. Phys. Lett., 54, 444-447.
559. Moortgat, G. K., B. Veyret and R. Lesclaux, 1989, J. Phys. Chem., 93, 2362-2368.
560. Moortgat, G. K. and P. Warneck, 1979, J. Chem. Phys., 70, 3639-3651.

561. Morel, O., R. Simonaitis and J. Heicklen, 1980, Chem. Phys. Lett., 73, 38-42.
562. Mössinger, J. C., D. M. Rowley and R. A. Cox, 2002, Atmos. Chem. Phys., 2, 227-234.
563. Mossinger, J. C., D. E. Shallcross and R. A. Cox, 1998, J. Chem. Soc. Faraday Trans., 94, 1391-1396.
564. Motte-Tollet, F., M.-P. Ska, G. M. Marston, I. C. Walker, M. R. F. Siggel, J. M. Gingell, L. Kaminski, K. L. Brown and N. J. Mason, 1997, Chem. Phys. Lett., 275, 298-306.
565. M ller, H. S. P. and H. Willner, 1992, Ber. Bunsenges. Phys. Chem., 96, 427-431.
566. Munk, J., P. Pagsberg, E. Ratajczak and A. Sillesen, 1986, J. Phys. Chem. , 90, 2752-2757.
567. Murtagh, D. P., 1988, Planet. Space Sci., 36, 819-828.
568. Myer, J. A. and J. A. R. Samson, 1970, J. Chem. Phys., 52, 266-271.
569. Myer, J. A. and J. A. R. Samson, 1970, J. Chem. Phys., 52, 716-718.
570. Myers, T. L., N. R. Forde, B. Hu, D. C. Kitchen and L. J. Butler, 1997, J. Chem. Phys., 81, 5361-5373.
571. Nakayama, T., M. T. Kitamura and K. Watanabe, 1959, J. Chem. Phys., 30, 1180-1186.
572. Nayak, A. K., T. J. Buckley, M. J. Kurylo and A. Fahr, 1996, J. Geophys. Res., 101, 9055-9062.
573. Nayak, A. K., M. J. Kurylo and A. Fahr, 1995, J. Geophys. Res, 100, 11185-11189.
574. Nee, J. B., 1991, J. Quant. Spectrosc. Radiat. Transfer, 46, 55.
575. Nee, J. B., M. Suto and L. C. Lee, 1985, J. Phys. B: Atom. Mol. Phys., 18, L293-L294.
576. Nee, J. B., M. Suto and L. C. Lee, 1986, J. Chem. Phys., 85, 4919-4924.
577. Nee, J. B., M. Suto and L. C. Lee, 1986, J. Chem. Phys., 85, 719-724.
578. Nelson, C. M., T. A. Moore and M. Okumura, 1994, J. Chem. Phys., 100, 8055-8064.
579. Nelson, C. M., T. A. Moore, M. Okumura and T. K. Minton, 1996, Chem. Phys, 2248, 287-307.
580. Nelson, H. H. and H. S. Johnston, 1981, J. Phys. Chem., 85, 3891-3896.
581. Ni, C.-K. and G. W. Flynn, 1993, Chem. Phys. Lett., 210, 333-339.
582. Nickolaisen, S. L., C. E. Miller, S. P. Sander, M. R. Hand, I. H. Williams and J. S. Francisco, 1996, J. Chem. Phys., 104, 2857.
583. Nickolaisen, S. L., S. P. Sander and R. R. Friedl, 1996, J. Phys. Chem., 100, 10165-10178.
584. Nicolet, M., 1981, Planet. Space Sci., 29, 951-974.
585. Nicolet, M. and R. Kennes, 1989, Planet. Space Sci., 37, 459-491.
586. Nicovich, J. M. and P. H. Wine, 1988, J. Geophys. Res., 93, 2417.
587. Nishida, S., K. Takahashi, Y. Matsumi, N. Taniguchi and S. Hayashida, 2004, J. Phys. Chem. A., 108, 2451-2456.
588. Nizkorodov, S. A., S. P. Sander and L. R. Brown, 2004, J. Phys. Chem. A, 108, 4864-4872.
589. Nölle, A., H. Heydtmann, R. Meller and G. K. Moortgat, 1993, Geophys. Res. Lett., 20, 707-710.
590. Nölle, A., H. Heydtmann, R. Meller, W. Schneider and G. K. Moortgat, 1992, Geophys. Res. Lett., 19, 281-284.
591. Nölle, A., C. Krumscheid and H. Heydtmann, 1999, Chem. Phys. Lett., 299, 561-565.
592. Ny, T.-Z. and S.-P. Choong, 1933, Chinese J. Phys., 1, 38-54.
593. Ogilvie, J. F., 1971, Trans. Faraday Soc., 67, 2205-2215.
594. Ogorzalek Loo, R., H.-P. Haerri, G. E. Hall and P. L. Houston, 1989, J. Chem. Phys., 90, 4222-4236.
595. Oh, D., W. Sisk, A. Young and H. Johnston, 1986, J. Chem. Phys., 85, 7146-7158.
596. Okabe, H., 1977, J. Chem. Phys., 66, 2058-2062.
597. Okabe, H. In *Photochemistry of Small Molecules*; John Wiley and Sons Inc.: New York, 1978; pp 217.
598. Okabe, H., 1980, J. Chem. Phys., 72, 6642-6650.
599. Okabe, H., 1981, J. Chem. Phys., 75, 2772-2778.
600. Okabe, H., 1983, J. Chem. Phys., 78, 1312-1317.
601. Orkin, V. L., R. E. Huie and M. J. Kurylo, 1997, J. Phys. Chem. A, 101, 9118-9124.
602. Orkin, V. L. and E. E. Kasimovskaya, 1995, J. Atm. Chem, 21, 1-11.
603. Orkin, V. L., V. G. Khamaganov, A. G. Guschin, R. E. Huie and M. J. Kurylo, 1997, J. Phys. Chem. A, 101, 174-178.
604. Orkin, V. L., F. Louis, R. E. Huie and M. J. Kurylo, 2002, J. Phys. Chem. A, 106, 10195-10199.
605. Orlando, J. J. and J. B. Burkholder, 1995, J. Phys. Chem., 99, 1143-1150.
606. Orlando, J. J., J. B. Burkholder, A. M. R. P. Bopegedera and C. J. Howard, 1991, J. Mol. Spectrosc., 145, 278-289.
607. Orlando, J. J., J. B. Burkholder, S. A. McKeen and A. R. Ravishankara, 1991, J. Geophys. Res., 96, 5013-5023.
608. Orlando, J. J. and G. S. Tyndall, 2001, Int. J. Chem. Kinet., 33, 149-156.
609. Orlando, J. J. and G. S. Tyndall, 2003, J. Photochem. Photobiol. A: Photochem., 157, 161-166.
610. Orlando, J. J., G. S. Tyndall, J.-M. Fracheboud, E. G. Estupiñan, S. Haberkorn and A. Zimmer, 1999, Atmos. Environ., 33, 1621-1629.
611. Orlando, J. J., G. S. Tyndall, G. K. Moortgat and J. G. Calvert, 1993, J. Phys. Chem., 97, 10996-11000.
612. Orphal, J. "A Critical Review of the Absorption Cross-Sections of O_3 and NO_2 in the 240-790 nm Region, Part 1, Ozone," ESA Technical Note MO-TN-ESA-GO-0302, European Space Agency, ESA-ESTEC, Noordwijk, 2002.

613. Orphal, J. "A Critical Review of the Absorption Cross-Sections of O_3 and NO_2 in the 240-790 nm Region, Part 2, Nitrogen Dioxide," ESA Technical Note MO-TN-ESA-GO-0302, European Space Agency, ESA-ESTEC, Noordwijk, 2002.
614. Orphal, J., 2003, J. Photochem. Photobiol., A 157, 185-209.
615. Orphal, J., S. Dreher, S. Voigt, J. P. Burrows, R. Jost and A. Delon, 1998, J. Chem. Phys., 109, 10217-10221.
616. Orphal, J., C. E. Fellows and J.-M. Flaud, 2003, J. Geophys. Res., 108 (D3), 4077.
617. Osbourne, B. A., G. Marston, L. Kaminski, N. C. Jones, J. M. Gingell, N. J. Mason, I. C. Walker, J. Delwiche and M.-J. Hubin-Franskin, 2000, J. Quant. Spectrosc. Radiat. Transfer, 64, 67-74.
618. Pagsberg, P., E. Bjergbakke, E. Ratajczak and A. Sillesen, 1997, Chem. Phys. Lett., 272, 383-390.
619. Pagsberg, P., A. Sillesen, J. T. Jodowski and E. Ratajczak, 1996, Chem. Phys. Lett., 249, 358-364.
620. Pagsberg, P. B., E. Ratajczak, A. Sillesen and J. T. Jodkowski, 1987, Chem. Phys. Lett., 141, 88-94.
621. Paraskevopoulos, G. and R. J. Cvetanovic, 1969, J. Am. Chem. Soc., 91, 7572.
622. Park, J., Y. Lee and G. W. Flynn, 1991, Chem. Phys. Lett., 186, 441-449.
623. Parkes, D. A., 1977, Int. J. Chem. Kinet., 9, 451-469.
624. Parkes, D. A., D. M. Paul, C. P. Quinn and R. C. Robson, 1973, Chem. Phys. Lett., 23, 425-429.
625. Parmenter, C. S., 1964, J. Chem. Phys., 41, 658-665.
626. Passchier, A. A., J. D. Christian and N. W. Gregory, 1967, J. Phys. Chem., 71, 937-942.
627. Paukert, T. T. and H. S. Johnston, 1972, J. Chem. Phys., 56, 2824-2838.
628. Paur, R. J. and A. M. Bass. In *Atmospheric Ozone*; C. S. Zerefos and A. Ghazi, Eds., 1985; pp 610-616.
629. Pence, W., S. Baughum and S. Leone, 1981, J. Phys. Chem., 85, 3844-3851.
630. Permien, T., R. Vogt and R. N. Schindler. Mechanisms of Gas Phase-Liquid Phase Chemical Transformations. In *Air Pollution Report #17*; R. A. Cox, Ed.; Environmental Research Program of the CEC: Brussels, 1988.
631. Petersen, A. B. and I. W. M. Smith, 1978, Chem. Phys., 30, 407-413.
632. Peterson, K. A. and J. S. Francisco, 2002, J. Chem. Phys., 117, 6103-6107.
633. Pfister, R. and R. J. Huber, 2002, personal communication.
634. Phillips, D. L., A. B. Myers and J. J. Valentini, 1992, J. Phys. Chem., 96, 2039-2044.
635. Pilling, M. J. and M. J. C. Smith, 1985, J. Phys. Chem., 89, 4713-4720.
636. Platt, U., D. Perner, G. W. Harris, A. M. Winer and J. N. Pitts Jr., 1980, Nature, 285, 312-314.
637. Plenge, J., R. Flesch, S. K hl, B. Vogel, R. M ller, F. Stroh and E. R hl, 2004, J. Phys. Chem. A, 108, 4859-4863.
638. Plum, C. N., E. Sanhueza, R. Atkinson, W. P. L. Carter and J. N. J. Pitts, 1983, Environ. Sci. Technol., 17, 479-484.
639. Pope, F. D., C. A. Smith, N. M. R. Ashfold and A. J. Orr-Ewing, 2005, Phys. Chem. Chem. Phys., 7, 79-84.
640. Pope, F. D., C. A. Smith, P. R. Davis, D. E. Shallcross, M. N. R. Ashfold and A. J. Orr-Ewing, 2005, J. Chem. Soc., Faraday Disc, 130/4, 1-14.
641. Porret, D. and C. F. Goodeve, 1937, Trans. Faraday Soc., 33, 690-693.
642. Porret, D. and C. F. Goodeve, 1938, Proc. Roy. Soc. London A, 165, 31-42.
643. Porter, G., Z. G. Szabo and M. G. Townsend, 1962, Proc. Roy. Soc. London, A 270, 493-500.
644. Prahlad, V. and V. Kumar, 1995, J. Quant. Spectrosc. Radiat. Transfer, 54, 945-955.
645. Preston, K. F. and R. F. Barr, 1971, J. Chem. Phys., 54, 3347-3348.
646. Raber, W. H. and G. K. Moortgat. Photooxidation of selected carbonyl compounds in air: methyl ethyl ketone, methyl vinyl ketone, methacrolein, and methylglyoxal. In *Progress and Problems in Atmospheric Chemistry*; J. Barker, Ed.; World Scientific Publ. Co.: Singapore, 1996; pp 318-373.
647. Rabinowitch, E. and W. C. Wood, 1936, Trans. Faraday Soc., 32, 540-546.
648. Rahn, T., H. Zhang, M. Wahlen and G. A. Blake, 1998, Geophys. Res. Lett., 25, 4489-4492.
649. Rattigan, O., E. Lutman, R. L. Jones and R. A. Cox, 1992, Ber. Bunsenges. Phys. Chem., 96, 399-404.
650. Rattigan, O., E. Lutman, R. L. Jones, R. A. Cox, K. Clemitshaw and J. Williams, 1992, J. Photochem. Photobiol. A: Chem., 69, 125-126.
651. Rattigan, O. V., R. L. Jones and R. A. Cox, 1994, Chem. Phys. Lett., 230, 121-126.
652. Rattigan, O. V., D. J. Lary, R. L. Jones and R. A. Cox, 1996, J. Geophys. Res., 101, 23021-23033.
653. Rattigan, O. V., D. M. Rowley, O. Wild, R. L. Jones and R. A. Cox, 1994, J. Chem. Soc. Faraday Trans., 90, 1819-1829.
654. Rattigan, O. V., D. E. Shallcross and R. A. Cox, 1997, J. Chem. Soc. Soc. Faraday Trans., 93, 2839-2846.
655. Rattigan, O. V., O. Wild and R. A. Cox, 1998, J. Photochem. Photobiol. A: Chem., 112, 1-7.
656. Rattigan, O. V., O. Wild, R. L. Jones and R. A. Cox, 1993, J. Photochem. Photobiol. A: Chem., 73, 1-9.
657. Ravishankara, A. R., 1995, Faraday Discuss, 100, 335-336.
658. Ravishankara, A. R. and R. L. Mauldin, 1986, J. Geophys. Res., 91, 8709-8712.
659. Ravishankara, A. R., S. Solomon, A. A. Turnipseed and R. F. Warren, 1993, Science, 259, 194-199.
660. Ravishankara, A. R. and P. H. Wine, 1983, Chem. Phys. Lett., 101, 73-78.
661. Ravishankara, A. R., P. H. Wine and A. O. Langford, 1979, Chem. Phys. Lett., 63, 479-484.

662. Ravishankara, A. R., P. H. Wine, C. A. Smith, P. E. Barbone and A. Torabi, 1986, J. Geophys. Res., 91, 5355-5360.
663. Rebbert, R. E. and P. Ausloos, 1976/1977, J. Photochem., 6, 265-276.
664. Rebbert, R. E. and P. J. Ausloos, 1975, J. Photochem., 4, 419-434.
665. Rebbert, R. E., S. G. Lias and P. Ausloos, 1973, Int. J. Chem. Kinet., 5, 893-908.
666. Rebbert, R. E., S. G. Lias and P. Ausloos, 1978, J. Photochem., 8, 17-27.
667. Regan, P. M., D. Ascenzi, A. Brown, G. G. Balint-Kurti and A. J. Orr-Ewing, 2000, J. Chem. Phys., 112, 10259-10268.
668. Regan, P. M., S. R. Langford, D. Ascenzi, P. A. Cook, A. J. Orr-Ewing and M. N. R. Ashfold, 1999, Phys. Chem. Chem. Phys., 1, 3247-3251.
669. Regan, P. M., S. R. Langford, A. J. Orr-Ewing and M. N. R. Ashfold, 1999, J. Chem. Phys., 110, 281-288.
670. Reid, S. A., J. T. Brandon and H. Reisler, 1993, J. Phys. Chem., 97, 540-543.
671. Ribaud, M. G., 1919, Ann. Phys., 12, 107-226.
672. Rigaud, P., B. Leroy, G. Le Bras, G. Poulet, J. L. Jourdain and J. Combourieu, 1977, Chem. Phys. Lett., 46, 161-163.
673. Robbins, D. E., 1976, Geophys. Res. Lett., 3, 213-216. See also Erratum, GRL, 1976, Vol. 3, p. 757.
674. Robbins, D. E. and R. S. Stolarski, 1976, Geophys. Rev. Lett., 3, 603-606.
675. Röckmann, T. J., C. A. M. Brenninkmeijer, M. Wollenhaupt, J. N. Crowley and P. J. Crutzen, 2000, Geophys. Res. Lett., 27, 1399-1402.
676. Röckmann, T. J., J. Kaiser, C. A. M. Brenninkmeijer, J. N. Crowley, R. Borchers, W. A. Brand and P. J. Crutzen, 2001, J. Geophys. Res., 106, 10,403-10,410.
677. Roehl, C. M., D. Bauer and G. K. Moortgat, 1996, J. Phys. Chem., 100, 4038-4047.
678. Roehl, C. M., J. B. Burkholder, G. K. Moortgat, A. R. Ravishankara and P. J. Crutzen, 1997, J. Geophys. Res., 102, 12819-12829.
679. Roehl, C. M., T. L. Mazely, R. R. Friedl, Y. M. Li, J. S. Francisco and S. P. Sander, 2001, J. Phys. Chem. A, 105, 1592-1598.
680. Roehl, C. M., S. A. Nizkorodov, H. Zhang, G. A. Blake and P. O. Wennberg, 2002, J. Phys. Chem., A, 106, 3766-3772.
681. Roehl, C. M., J. J. Orlando and J. G. Calvert, 1992, J. Photochem. Photobiol. A: Chem., 69, 1-5.
682. Roehl, C. M., J. J. Orlando, G. S. Tyndall, R. E. Shetter, G. J. Vasquez, C. A. Cantrell and J. G. Calvert, 1994, J. Phys. Chem., 98, 7837-7843.
683. Rogers, J. D., 1990, J . Phys. Chem., 94, 4011-4015.
684. Romand, J., 1949, Ann. Phys. (Paris), 4, 529-590.
685. Romand, J. and J. Mayence, 1949, Compt. Rend. Acad. Sci. Paris, 228, 998-1000.
686. Romand, J. and B. Vodar, 1948, Compt. Rend. Acad. Sci. Paris, 226, 238-240.
687. Röth, E. P., R. Ruhnke, G. Moortgat, R. Meller and W. Schneider "UV/VIS-Absorption Cross Sections and Quantum Yields for Use in Photochemistry and Atmospheric Modeling," Forschungszentrum J lich Publication, Part 1 : Inorganic Substances (j l-3340), Part 2: Organic Substances (j l-3341), 1997.
688. Rowland, F. S. and M. J. Molina, 1975, Rev. Geophys. Space Phys., 13, 1-35.
689. Rowland, F. S., J. E. Spencer and M. J. Molina, 1976, J. Phys. Chem., 80, 2711-2713.
690. Rowley, D. M., M. H. Harwood, R. A. Freshwater and R. L. Jones, 1996, J. Phys. Chem., 100, 3020-3029.
691. Rowley, D. M., J. C. Mössinger, R. A. Cox and R. L. Jones, 1999, J. Atmos. Chem., 34, 137-151.
692. Roxlo, C. and A. Mandl, 1980, J. Appl. Phys., 51, 2969-2972.
693. Ruhl, E., A. Jefferson and V. Vaida, 1990, J. Phys. Chem., 94, 2990-2994.
694. Russell, B. R., L. O. Edwards and J. W. Raymonda, 1973, J. Am. Chem. Soc., 95, 2129-2133.
695. Safary, E., 1954, Ann. Phys. (Paris), 9, 203-254.
696. Safary, E., J. Romand and B. Vodar, 1951, J. Chem. Phys., 19, 379-380.
697. Saiz-Lopez, A., R. W. Saunders, D. M. Joseph, S. H. Ashworth and J. M. C. Plane, 2004, Atmos. Chem. Phys., 4, 1443-1450.
698. Salawitch, R. J., P. O. Wennberg, G. C. Toon, B. Sen and J.-F. Blavier, 2002, Geophys. Res. Lett., 29, 10.1029/2002GL015006, 9-1 - 9-4.
699. Salomon, D., A. W. Kirk and E. Tschuikow-Roux, 1977, J. Photochem., 7, 345-353.
700. Sander, S. P., 1986, J. Phys. Chem., 90, 4135-4142.
701. Sander, S. P., 1986, J. Phys. Chem., 90, 2194-2199.
702. Sander, S. P. and R. R. Friedl, 1989, J. Phys. Chem., 93, 4764-4771.
703. Sander, S. P., R. R. Friedl, W. B. DeMore, D. M. Golden, M. J. Kurylo, R. F. Hampson, R. E. Huie, G. K. Moortgat, A. R. Ravishankara, C. E. Kolb and M. J. Molina "Chemical Kinetics and Photochemical Data for Use in Stratospheric Modeling, Evaluation Number 13," JPL Publication 00-3, Jet Propulsion Laboratory, California Institute of Technology, Pasadena, CA, 2000.
704. Sander, S. P., M. Peterson, R. T. Watson and R. Patrick, 1982, J. Phys. Chem., 86, 1236-1240.
705. Sander, S. P. and R. T. Watson, 1981, J. Phys. Chem., 85, 2960-2964.
706. Sandorfy, C., 1976, Atmos. Environ., 10, 343-351.

707. Sauvageau, P., J. Doucet, R. Gilbert and C. Sandorfy, 1974, J. Chem. Phys., 61, 391-395.
708. Sauvageau, P., R. Gilbert, P. P. Berlow and C. Sandorfy, 1973, J. Chem. Phys., 59, 762-765.
709. Schiffman, A., D. D. Nelson, Jr. and D. J. Nesbitt, 1993, J. Chem. Phys., 98, 6935-6946.
710. Schindler, R., M. Liesner, S. Schmidt, U. Kirschner and T. Benter, 1997, J. Photochem. Photobiol. A: Chem., 107, 9-19.
711. Schmidt, S., T. Benter and R. N. Schindler, 1998, Chem. Phys. Lett., 282, 292-298.
712. Schmitt, G. and F. J. Comes, 1980, J. Photochem., 14, 107-123.
713. Schmitt, G. and F. J. Comes, 1987, J. Photochem. Photobiol. A, 41, 13-30.
714. Schneider, W., G. K. Moortgat, J. P. Burrows and G. Tyndall, 1987, J. Photochem. Photobiol., 40, 195-217.
715. Schneider, W. F., T. J. Wallington, K. Minschwaner and E. A. Stahlberg, 1995, Environ. Sci. Technol., 29, 247-250.
716. Schott, G. and N. Davidson, 1958, J. Amer. Chem. Soc., 80, 1841-1853.
717. Seccombe, D. P., R. Y. L. Chim, R. P. Tucket, H. W. Jochims and H. Baumgaertel, 2001, J. Chem. Phys., 114, 4058-4073.
718. Seccombe, D. P., R. P. Tuckett, H. Baumg rtel and H. W. Jochims, 1999, Phys. Chem. Chem. Phys., 1, 773-782.
719. Seery, D. J. and D. Britton, 1964, J. Phys. Chem., 68, 2263-2266.
720. Seki, K. and H. Okabe, 1992, J. Phys. Chem., 96, 3345-3349.
721. Sellev g, S. R., T. Kelly, H. Sidebottom and C. J. Nielsen, 2004, Phys. Chem. Chem. Phys., 6, 1243-1252.
722. Selwyn, G., J. Podolske and H. S. Johnston, 1977, Geophys. Res. Lett., 4, 427-430.
723. Selwyn, G. S. and H. S. Johnston, 1981, J. Chem. Phys., 74, 3791-3803.
724. Senapati, D. and P. K. Das, 2004, Chem.Phys. Lett., 393, 535-538.
725. Senapati, D., K. Kavita and P. K. Das, 2002, J. Phys. Chem. A, 106, 8479-8482.
726. Senum, G. I., Y.-N. Lee and J. S. Gaffney, 1984, J. Phys. Chem., 88, 1269-1270.
727. Shardanand and A. D. P. Rao, 1977, J. Quant. Spectrosc. Radiat. Transfer, 17, 433-439.
728. Sharpe, S., B. Hartnett, H. S. Sethi and D. S. Sethi, 1987, J. Photochem., 38, 1-13.
729. Sidebottom, H. W., J. M. Tedder and J. C. Walton, 1969, Trans. Faraday Soc., 65, 755-762.
730. Silvente, E., R. C. Richter, M. Zheng, E. S. Saltzman and A. J. Hynes, 1997, Chem. Phys. Lett., 264, 309-315.
731. Simon, F.-G., W. Schneider and G. K. Moortgat, 1990, Int. J. Chem. Kinet., 22, 791-813.
732. Simon, F. G., W. Schneider, G. K. Moortgat and J. P. Burrows, 1990, J. Photochem. Photobiol., A55, 1-23.
733. Simon, P. C., D. Gillotay, N. Vanlaethem-Meurée and J. Wisemberg, 1988, Annales Geophysicae, 6, 239-248.
734. Simon, P. C., D. Gillotay, N. Vanlaethem-Meurée and J. Wisemberg, 1988, J. Atmos. Chem., 7, 107-135.
735. Simonaitis, R., R. I. Greenberg and J. Heicklen, 1972, Int. J. Chem. Kinet., 4, 497-512.
736. Simons, J. W., R. J. Paur, H. A. Webster III and E. J. Blair, 1973, J. Phys. Chem., 59, 1203-1208.
737. Singer, R. J., J. N. Crowley, J. P. Burrows, W. Schneider and G. K. Moortgat, 1989, J. Photochem. Photobiol., 48, 17-32.
738. Singleton, D. L., G. Paraskevopoulos and R. S. Irwin, 1987, J. Photochem., 37, 209-216.
739. Singleton, D. L., G. Paraskevopoulos and R. S. Irwin, 1989, Res. Chem. Intermediates, 12, 1-12.
740. Singleton, D. L., G. Paraskevopoulos and R. S. Irwin, 1990, J. Phys. Chem., 94, 695-699.
741. Skorokhodov, V., Y. Sato, K. Suto, Y. Matsumi and M. Kawasaki, 1996, J. Phys. Chem., 100, 12321-12328.
742. Smith, F.-G., F. M. G. Tablas, L. T. Molina and M. J. Molina, 2001, J. Phys. Chem. A, 105, 8658-8664.
743. Smith, G. D., L. T. Molina and M. J. Molina, 2000, J. Phys.Chem. A, 104, 8916-8921.
744. Smith, G. D., L. T. Molina and M. J. Molina, 2002, J. Phys. Chem. A, 106, 1233-1240.
745. Smith, W. S., C. C. Chou and F. S. Rowland, 1977, Geophys. Res. Lett., 4, 517-519.
746. Soller, R., J. M. Nicovich and P. H. Wine, 2002, J. Phys. Chem. A, 106, 8378-8385.
747. Solomon, S., J. B. Burkholder, A. R. Ravishankara and R. R. Garcia, 1994, J. Geophys. Res., 99, 20929-20935.
748. Spencer, J. E. and F. S. Rowland, 1978, J. Phys. Chem., 82, 7-10.
749. Staffelbach, T. A., J. J. Orlando, G. S. Tyndall and J. G. Calvert, 1995, J. Geophys. Res., 100, 14189-14198.
750. Stanton, J. F., C. M. L. Rittby, R. J. Bartlett and D. W. Toohey, 1991, J. Phys. Chem., 95, 2107-2110.
751. Steinfeld, J. I., S. M. Adler-Golden and J. W. Gallagher, 1987, J. Phys. Chem. Ref. Data, 16, 911-951.
752. Stephens, E. R., 1969, Adv. Environ. Sci. Technol., 1, 119-146.
753. Stickel, R. E., A. J. Hynes, J. D. Bradshaw, W. L. Chameides and D. D. Davis, 1988, J. Phys. Chem., 92, 1862-1864.
754. Stief, L. J., W. A. Payne and R. B. Klemm, 1975, J. Chem. Phys., 62, 4000-4008.
755. Stockwell, W. R. and J. G. Calvert, 1978, J. Photochem., 8, 193-203.
756. Stutz, J., E. S. Kim, U. Platt, P. Bruno, C. Perrino and A. Febo, 2000, J. Geophys. Res., 105, 14585-14592.

757. Sulzer, P. and K. Wieland, 1952, Helv. Phys. Acta, 25, 653-676.
758. Suto, M. and L. C. Lee, 1984, J. Chem. Phys., 81, 1294-1297.
759. Suto, M. and L. C. Lee, 1985, J. Geophys. Res., 90, 13037-13040.
760. Swanson, D., B. Kan and H. S. Johnston, 1984, J. Phys. Chem., 88, 3115-3118.
761. Tadic, J., G. K. Moortgat and K. Wirtz, 2005, J. Photochem. Photobiol. A: Chem., 177, 116-124.
762. Takahashi, K., Y. Matsumi and M. Kawasaki, 1996, J. Phys. Chem., 100, 4084-4089.
763. Taketani, F., K. Takahashi and Y. Matsumi, 2005, J. Phys. Chem. A, 109, 2855-2860.
764. Talukdar, R., A. Mellouki, T. Gierczak, J. B. Burkholder, S. A. McKeen and A. R. Ravishankara, 1991, J. Phys. Chem., 95, 5815-5821.
765. Talukdar, R., A. Mellouki, T. Gierczak, J. B. Burkholder, S. A. McKeen and A. R. Ravishankara, 1991, Science, 252, 693-695.
766. Talukdar, R. K., J. B. Burkholder, A.-M. Schmoltner, J. M. Roberts, R. Wilson and A. R. Ravishankara, 1995, J. Geophys. Res., 100, 14163-14173.
767. Talukdar, R. K., M. K. Gilles, F. Battin-Leclerc, A. R. Ravishankara, J.-M. Fracheboud, J. J. Orlando and G. S. Tyndall, 1997, Geophys. Res. Lett., 24, 1091-1094.
768. Talukdar, R. K., M. Hunter, R. F. Warren, J. B. Burkholder and A. R. Ravishankara, 1996, Chem. Phys. Lett., 262, 669-674.
769. Talukdar, R. K., C. A. Longfellow, M. K. Gilles and A. R. Ravishankara, 1998, Geophys. Res. lett., 25, 143-146.
770. Talukdar, R. K., A. Mellouki, J. B. Burkholder, M. K. Gilles, G. Le Bras and A. R. Ravishankara, 2001, J. Phys. Chem. A, 105, 5188-5196.
771. Talukdar, R. K., G. L. Vashjiani and A. R. Ravishankara, 1992, J. Chem. Phys., 96, 8194-8201.
772. Tanaka, Y., E. C. Y. Inn and K. Watanabe, 1953, J, Chem. Phys., 21, 1651-1653.
773. Tanaka, Y., M. Kawasaki, Y. Matsumi, H. Fujiwara, T. Ishiwata, L. J. Rogers, R. N. Dixon and M. N. R. Ashfold, 1998, J. Chem. Phys., 109, 1315-1325.
774. Tang, K. Y., P. W. Fairchild and E. K. C. Lee, 1979, J. Phys. Chem., 83, 569-573.
775. Tellinghuisen, J., 1973, J. Chem. Phys., 58, 2821-2834.
776. Tellinghuisen, J., 2003, J. Phys. Chem. A, 107, 753-775.
777. Thelen, M.-A., P. Felder and J. R. Huber, 1993, Chem. Phys. Lett., 213, 275-281.
778. Thompson, B. A., P. Harteck and J. Reeves, R. R., 1963, J. Geophys. Res., 68, 6431-6436.
779. Toniolo, A., G. Granucci, S. Inglese and M. Persico, 2001, Phys. Chem. Chem. Phys., 3, 4266-4279.
780. Toniolo, A., M. Persico and D. Pitea, 2000, J. Phys. Chem. A, 104, 7278-7283.
781. Tonokura, K., Y. Matsumi, M. Kawasaki, H. L. Kim, S. Yabushita, S. Fujimura and K. Saito, 1993, J. Chem. Phys., 99, 3461-3467.
782. Tonokura, K., Y. Matsumi, M. Kawasaki, S. Tasaki and R. Bersohn, 1992, J. Chem. Phys., 97, 8210-8215.
783. Troe, J., 2000, Z. Phys. Chem., 214, 573-581.
784. Trolier, M., R. L. Mauldin, III and A. R. Ravishankara, 1990, J. Phys. Chem., 94, 4896-4907.
785. Trolier, M. and J. R. Wiesenfeld, 1988, J. Geophys. Res., 93, 7119-7124.
786. Turatti, F., D. W. T. Griffith, S. R. Wilson, M. B. Esler, T. Rahn, H. Zhang and G. A. Blake, 2000, Geophys. Res. Lett., 27, 2489-2492.
787. Turco, R. P., 1975, Geophys. Surveys, 2, 153-192.
788. Turnipseed, A. A., M. K. Gilles, J. B. Burkholder and A. R. Ravishankara, 1995, Chem. Phys. Lett., 242, 427-434.
789. Turnipseed, A. A., G. L. Vaghjiani, J. E. Thompson and A. R. Ravishankara, 1992, J. Chem. Phys., 96, 5887-5895.
790. Tyndall, G. S., R. A. Cox, C. Granier, R. Lesclaux, G. K. Moortgat, M. J. Pilling, A. R. Ravishankara and T. J. Wallington, 2001, J. Geophys. Res., 106, 12157-12182.
791. Tyndall, G. S., C. S. Kegley-Owen, J. J. Orlando and J. G. Calvert, 1997, J. Chem. Soc. Faraday Trans., 93, 2675-2682.
792. Tyndall, G. S., K. M. Stedman, W. Schneider, J. P. Burrows and G. K. Moortgat, 1987, J. Photochem., 36, 133-139.
793. Tzeng, W. B., Y. R. Lee and S. M. Lin, 1994, Chem. Phys. Lett., 227, 467-471.
794. Uma, S. and P. K. Das, 1994, Can. J. Chem., 72, 865-869.
795. Uma, S. and P. K. Das, 1995, Chem. Phys. Lett., 241, 335-338.
796. Uma, S. and P. K. Das, 1996, J. Chem. Phys., 104, 4470-4474.
797. Uthman, A. P., P. J. Demlein, T. D. Allston, M. C. Withiam, M. J. McClements and G. A. Takacs, 1978, J. Phys. Chem., 82, 2252-2257.
798. Vaghjiani, G., 1993, J. Chem. Phys., 99, 5936-5943.
799. Vaghjiani, G. L. and A. R. Ravishankara, 1989, J. Geophys. Res., 94, 3487-3492.
800. Vaghjiani, G. L. and A. R. Ravishankara, 1990, J. Chem. Phys., 92, 996-1003.
801. Vaghjiani, G. L., A. A. Turnipseed, R. F. Warren and A. R. Ravishankara, 1992, J. Chem. Phys., 96, 5878.
802. Vaida, V., S. Solomon, E. C. Richards, E. Ruhl and A. Jefferson, 1989, Nature, 342, 405-408.

803. Van den Bergh, H. and J. Troe, 1976, J. Chem. Phys., 64, 736-742.
804. Vandaele, A. C., C. Hermans, S. Fally, M. Carleer, R. Colin, M.-F. Mérienne, A. Jenouvrier and B. Coquart, 2002, J. Geophys. Res., D 107, 4384.
805. Vandaele, A. C., C. Hermans, S. Fally, M. Carleer and M.-F. Merienne, 2003, J. Quant. Spectrosc. Radiat. Transfer, 76, 373-391.
806. Vandaele, A. C., C. Hermans, P. C. Simon, M. Van Roozendael, J. M. Guilmot, M. Carleer and R. Colin, 1966, J. Atmos. Chem., 25, 289-305.
807. Vandaele, A. C., D. Hermans, P. C. Simon, M. Carleer, R. Colin, S. Fally, M.-F. Meriénne, A. Jenouvrier and B. Coquart, 1998, J. Quant. Spectrosc. Radiat. Transfer, 59, 171-184.
808. Vanlaethem-Meurée, N., J. Wisemberg and P. C. Simon, 1978, Bull. Acad. Roy. Belgique Cl. Sci., 64, 31.
809. Vanlaethem-Meurée, N., J. Wisemberg and P. C. Simon, 1978, Bull. Acad. Roy. Belgique Cl. Sci., 64, 42.
810. Vanlaethem-Meurée, N., J. Wisemberg and P. C. Simon, 1979, Geophys. Res. Lett., 6, 451-454.
811. Vassy, A. and E. Vassy, 1948, J. Chem. Phys., 16, 1163-1164.
812. Vasudev, R., 1990, Geophys. Res. Lett., 17, 2153-2155.
813. Vatsa, R. K., A. Kumar, P. D. Naik, K. V. S. Rama Rao and J. P. Mittal, 1993, Chem. Phys. Lett., 207, 75-80.
814. Vatsa, R. K. and H.-R. Volpp, 2001, Chem. Phys. Lett., 340, 289-295.
815. Vésine, E. and A. Mellouki, 1997, J. Chim. Phys. Physico-Chim. Biol., 94, 1634-1641.
816. Vesley, G. F. and P. A. Leermakers, 1964, J. Phys. Chem., 68, 2364-2366.
817. Vetter, R., T. Ritschel and L. Zulicke, 2003, J. Phys. Chem., A, 107, 1405-1412.
818. Vigroux, E., 1953, Ann. Phys., 8, 709-762.
819. Vigroux, E., 1967, C. R. Acad. Sc. Paris, 264, 1290-1291.
820. Vigroux, E., 1969, Ann. Geophys., 25, 169-172.
821. Villenave, E., I. Morozov and R. Lesclaux, 2000, J. Phys. Chem. A, 104, 9933-9940.
822. Vogt, K. and J. Koenigsberger, 1923, Z. Physik, 13, 292-310.
823. Vogt, R. and R. N. Schindler. Air Pollution Report 34, 1990; pp 167-171.
824. Vogt, R. and R. N. Schindler, 1992, J. Photochem. Photobiol. A: Chem., 66, 133-140.
825. Voigt, S., J. Orphal, K. Bogumil and J. P. Burrows, 2001, J. Photochem. Photobiol. A, 143, 1-9.
826. Voigt, S., J. Orphal and J. P. Burrows, 2002, J. Photochem. Photobiol. A: Chem., 149, 1-7.
827. Volkamer, R., P. Spietz, J. P. Burrows and U. Platt, 2005, J. Photochem. Photobiol. A: Chem., 172, 35-36.
828. von Hessberg, P., J. Kaiser, M. B. Enghoff, C. A. McLinden, S. L. Sorensen, T. Rockmann and M. S. Johnson, 2004, Atmos. Chem. Phys., 4, 1237-1253.
829. Wahner, A., A. R. Ravishankara, S. P. Sander and R. R. Friedl, 1988, Chem. Phys. Lett., 152, 507-512.
830. Wahner, A., G. S. Tyndall and A. R. Ravishankara, 1987, J. Phys. Chem., 91, 2734-2738.
831. Wallington, T. J., P. Dagaut and M. J. Kurylo, 1988, J. Photochem. Photobiol. A: Chemistry, 42, 173-185.
832. Wallington, T. J., P. Dagaut and M. J. Kurylo, 1992, Chem. Rev., 92, 667-710.
833. Wallington, T. J., M. M. Mariq, T. Ellerman and O. J. Nielsen, 1992, J. Phys. Chem., 96, 982-986.
834. Walton, J. C., 1972, J. Chem. Soc. Farad. Trans., 68, 1559-1565.
835. Wang, L. and J. Zhang, 2000, Environ. Sci. Technol., 34, 4221-4227.
836. Wangberg, I., T. Etzkorn, I. Barnes, U. Platt and K. H. Becker, 1997, J. Phys. Chem. A, 101, 9694-9698.
837. Wannenmacher, E. A. J., P. Felder and R. J. Huber, 1991, J. Chem. Phys., 95, 986-997.
838. Warneck, P., 2001, Atmos. Environ., 35, 5773-5777.
839. Watson, R. T., 1977, J. Phys. Chem. Ref. Data, 6, 871-917.
840. Wayne, R. P., I. Barnes, J. P. Burrows, C. E. Canosa-Mas, J. Hjorth, G. Le Bras, G. K. Moortgat, D. Perner, G. Poulet, G. Restelli and H. Sidebottom, 1991, Atmos. Environ., 25A, 1-203.
841. Wayne, R. P., G. Poulet, P. Biggs, J. P. Burrows, R. A. Cox, P. J. Crutzen, G. D. Hayman, M. E. Jenkin, G. Le Bras, G. K. Moorgat, U. Platt and R. N. Schindler, 1995, Atmos. Environ., 29, 2675-2881.
842. Weaver, J., J. Meagher and J. Heicklen, 1976, J. Photochem., 6, 111-126.
843. Wen, W. Y. and R. M. Noyes, 1972, J. Phys. Chem., 76, 1017-1018.
844. Wennberg, P. O., J. W. Brault, T. F. Hanisco, R. J. Salawitch and G. H. Mount, 1997, J. Geophys. Res., D102, 8887-8898.
845. Wennberg, P. O., R. J. Salawitch, D. J. Donaldson, T. F. Hanisco, E. J. Lanzendorf, K. K. Perkins, S. A. Lloyd, V. Vaida, R. S. Gao, E. J. Hintsa, R. C. Cohen, W. H. Swartz, T. L. Kusterer and D. E. Anderson, 1999, Geophys. Res. Lett., 26, 1373-1376.
846. Wheeler, M. D., S. M. Newman, T. Ishiwata, M. Kawasaki and A. J. Orr-Ewing, 1998, Chem. Phys. Lett., 285, 346-351.
847. Wijnen, M. H., 1961, J. Am. Chem. Soc., 83, 3014-3017.
848. Wilmouth, D. M., T. F. Hanisco, N. M. Donahue and J. G. Anderson, 1999, J. Phys. Chem A, 103, 8935-8945.
849. Wine, P. H., A. R. Ravishankara, D. L. Philen, D. D. Davis and R. T. Watson, 1977, Chem. Phys. Lett., 50, 101-106.

850. Winterhalter, R., N. R. Jensen, I. Magneron, K. Wirtz, A. Mellouki, Y. Mu, J. Tadic, A. Horowitz, G. K. Moortgat and J. Hjorth. "Proceedings of the EUROTRAC-2 Symposium 2000", 2001, Springer, Berlin.
851. WMO *Atmospheric Ozone: 1985*; National Aeronautics and Space Administration: Geneva, 1986.
852. Wollenhaupt, M., S. A. Carl, A. Horowitz and J. N. Crowley, 2000, J. Phys. Chem., A, 104, 2695-2705.
853. Wrede, E., S. Laubach, S. Schulenburg, A. Brown, E. R. Wouters, A. J. Orr-Ewing and N. M. R. Ashfold, 2001, J. Chem. Phys., 114, 2629-2646.
854. Xu, D., J. S. Francisco, J. Huang and W. M. Jackson, 2002, J. Chem. Phys., 117, 2578-2585.
855. Yamamoto, S. and R. A. Back, 1985, Can. J. Chem., 63, 549-554.
856. Yao, F., I. Wilson and H. Johnston, 1982, J. Phys. Chem., 86, 3611-3615.
857. Yokelson, R. J., J. Burkholder, R. W. Fox and A. R. Ravishankara, 1997, J. Phys. Chem. A, 101, 6667-6678.
858. Yokelson, R. J., J. B. Burkholder, R. W. Fox, R. K. Talukdar and A. R. Ravishankara, 1994, J. Phys. Chem., 98, 13144-13150.
859. Yoshino, K., A. S. C. Cheung, J. R. Esmond, W. H. Parkinson, D. E. Freeman, S. L. Guberman, A. Jenouvrier, B. Coquart and M. F. Merienne, 1988, Planet. Space Sci., 36, 1469-1475.
860. Yoshino, K., J. R. Esmond, A. S.-C. Cheung, D. E. Freeman and W. H. Parkinson, 1992, Planet. Space Sci., 40, 185-192.
861. Yoshino, K., J. R. Esmond, A. S. C. Cheung, D. E. Freeman and W. H. Parkinson, 1990, J. Geophys. Res., 95, 11743.
862. Yoshino, K., J. R. Esmond, D. E. Freeman and W. H. Parkinson, 1993, J. Geophys. Res., 98, 5205-5211.
863. Yoshino, K., J. R. Esmond and W. H. Parkinson, 1997, Chem. Phys., 221, 169-174.
864. Yoshino, K., D. E. Freeman, J. R. Esmond, R. S. Friedman and W. H. Parkinson, 1988, Planet. Space Sci., 36, 1201-1210.
865. Yoshino, K., D. E. Freeman, J. R. Esmond, R. S. Friedman and W. H. Parkinson, 1989, Planet. Space Sci., 37, 419-426.
866. Yoshino, K., D. E. Freeman, J. R. Esmond and W. H. Parkinson, 1987, Planet. Space Sci., 35, 1067-1075.
867. Yoshino, K., D. E. Freeman, J. R. Esmond and W. H. Parkinson, 1988, Planet. Space Sci., 36, 395-398.
868. Yoshino, K., D. E. Freeman and W. H. Parkinson, 1984, Planet. Space Sci., 32, 1219-1222.
869. Yoshino, K., D. E. Freeman and W. H. Parkinson, 1984, J. Phys. Chem. Ref. Data, 13, 207-227.
870. Yoshino, K., D. F. Freeman, J. R. Esmond and W. H. Parkinson, 1983, Planet. Space Sci., 31, 339-353
871. Yujing, M. and A. Mellouki, 2000, J. Photochem. Photobiol. A: Chem., 134, 31-36.
872. Yung, Y. L. and C. E. Miller, 1997, Science, 278, 1778-1780.
873. Zaraga, F., N. S. Nogar and C. B. Moore, 1976, J. Mol. Spectrosc., 63, 564-571.
874. Zelikoff, M. and L. M. Aschenbrand, 1954, J. Chem. Phys., 22 1685-1687.
875. Zelikoff, M., K. Watanabe and E. C. Y. Inn, 1953, J. Chem. Phys., 21, 1643-1647.
876. Zetzsch, C. In *Proceedings of the International Ozone Symposium 1988*; R. Bojkov and P. Fabian, Eds.; Deepak: Hampton, VA, 1989.
877. Zhang, H., C. M. Roehl, S. P. Sander and P. O. Wennberg, 2000, J. Geophys. Res., D 105, 14593-14598.
878. Zhang, H., C. M. Roehl, S. P. Sander and P. O. Wennberg, 2000, J. Geophys. Res., 105, 14593-14598.
879. Zhang, H., P. O. Wennberg, V. H. Wu and G. A. Blake, 2000, Geophys. Res. Lett., 27, 2481-2484.
880. Zhang, J., M. Dulligan and C. Wittig, 1997, J. Chem. Phys., 107, 1403-1405.
881. Zhang, L., W. Fuss and K. L. Kompa, 1990, Chem. Phys., 144, 289-297.
882. Zhu, L. and G. Johnston, 1995, J. Phys. Chem., 99, 15114-15119.
883. Zhu, L., D. Kellis and C.-F. Ding, 1996, Chem. Phys. Lett., 257, 487-491.
884. Zou, P., W. S. McGivern and S. W. North, 2000, Phys. Chem. Chem. Phys., 2, 3785-3790.
885. Zou, P., W. S. McGivern, O. Sokhabi, A. G. Suits and S. W. North, 2000, J. Chem. Phys., 113, 7149-7157.
886. Zou, P., J. Park, B. A. Schmitz, T. Nguyen and S. W. North, 2002, J. Phys. Chem. A, 106, 1004-1010.

SECTION 5. HETEROGENEOUS CHEMISTRY

Table of Contents

SECTION 5. HETEROGENEOUS CHEMISTRY 5-1
5.1 Introduction 5-1
5.2 Surface Types—Acid/Water, Liquids and Solids 5-2
5.3 Surface Types—Soot and Alumina 5-2
5.4 Surface Types—Solid Alkali Halide Salts and Aqueous Salt Solutions 5-3
5.5 Surface Composition and Morphology 5-4
5.6 Surface Porosity 5-4
5.7 Temperature Dependences of Parameters 5-5
5.8 Solubility Limitations 5-5
5.9 Data Organization 5-5
5.10 Parameter Definitions 5-5
5.11 Mass Accommodation Coefficients for Surfaces Other Than Soot 5-9
5.12 Notes to Table 5-1 5-12
5.13 Gas/Surface Reaction Probabilities for Surfaces Other Than Soot 5-21
5.14 Notes to Table 5-2 5-26
5.15 Soot Surface Uptake Coefficients 5-50
5.16 Notes to Table 5-3 5-50
5.17 Henry's Law Constants for Pure Water 5-53
5.18 Notes to Table 5-4 5-56
5.19 Ion-Specific Schumpe Parameters 5-61
5.20 Henry's Law Constants for Acids 5-62
5.21 Notes to Table 5-6 5-63
5.22 References 5-66

Tables

Table 5-1. Mass Accommodation Coefficients (α) for Surfaces Other Than Soot 5-9
Table 5-2. Gas/Surface Reaction Probabilities (γ) for Surfaces Other Than Soot 5-21
Table 5-3. Soot Surface Uptake Coefficients 5-50
Table 5-4. Henry's Law Constants for Pure Water 5-53
Table 5-5. Ion-Specific Schumpe Parameters 5-61
Table 5-6. Henry's Law Constants for Acids 5-62

Figures

Figure 5-1. Recommended reactive uptake coefficients as a function of temperature for key stratospheric heterogeneous processes on sulfuric acid aerosols. 5-9

5.1 Introduction

We have evaluated and tabulated the currently available information on heterogeneous stratospheric processes. In addition, because of the increasing level of interest in tropospheric processes with a direct bearing on the fluxes of reactive species into the stratosphere, such as heterogeneous loss processes for partially oxidized degradation products of hydrohalocarbons and heterogeneous contrail and cloud processing of exhaust species from aircraft, we have included kinetic data for selected heterogeneous interactions relevant to modeling cloud droplet and aqueous aerosol chemistry in the free troposphere. However, both stratospheric and tropospheric heterogeneous chemistry are relatively new and rapidly developing fields, and further results can be expected to change our quantitative and even our qualitative understanding on a regular basis. The complexity is compounded by the difficulty of characterizing the chemical and physical properties of atmospheric heterogeneous surfaces and then reproducing suitable simulations in the laboratory [288]. New and/or updated heterogeneous kinetics evaluations in this document have focused on processes on liquid water, on water ice, on alumina, and on solid alkali halide salts and and their aqueous solutions. Uptake studies of volatile organic species (VOCs) on water ice surfaces have not been included in this evaluation. Several groups have investigated the interaction of small oxygenated organic compounds (alcohols, aldehydes, acids, and ketones) with ice surfaces, measuring equilibrium uptakes at

temperatures relevant to the upper troposphere (see e.g., review by Abbatt [5]). The amounts taken up are relatively small compared to inorganic acids. The uptake process is fully reversible on the time scale of the experiments, and thus has little consequences for upper tropospheric chemistry. A few important uptake processes occurring on liquid sulfuric acid surfaces have also been added or updated. The compilation of Henry's law parameters for pure water has been extended and a procedure for estimating the effective Henry's law parameters for aqueous salt solutions has been added.

5.2 Surface Types—Acid/Water, Liquids and Solids

To a first approximation there are three major types of surfaces believed to be present at significant levels in the stratosphere. They are: (1) Type I polar stratospheric clouds (PSCs), nominally composed of nitric acid trihydrate ($HNO_3 \cdot 3H_2O$); (2) crystals of relatively pure water ice, designated as Type II PSCs because they form at lower temperatures than Type I and are believed to be nucleated by Type I (similar surfaces may form as contrails behind high-altitude aircraft under some stratospheric conditions); and (3) sulfuric acid aerosol, which is nominally a liquid phase surface generally composed of 60–80 weight percent H_2SO_4 and, concomitantly, 40–20 weight percent H_2O. While PSCs, as their name suggests, are formed primarily in the cold winter stratosphere at high latitudes, sulfuric acid aerosol is present year round at all latitudes and may influence stratospheric chemistry on a global basis, particularly after large injections of volcanic sulfur episodically increase their abundance and surface area. There is also increasing evidence that ternary $H_2SO_4/HNO_3/H_2O$ liquid solutions may play a significant role in PSC formation.

In addition to the major stratospheric surface types noted above, several other types of heterogeneous surfaces are found in the stratosphere and may play a significant role in some stratospheric processes. For instance, laboratory work has indicated that nitric acid dihydrate (NAD) may play an important role in the nucleation of Type I PSCs (Worsnop et al. [481], Fox et al. [150]) and that mixtures of solid nitric acid hydrates and sulfuric acid tetrahydrate (SAT) (Molina et al. [336], Zhang et al. [502]) and/or a more complex sulfuric acid/nitric acid hydrate (Fox et al. [150]) may also be key to understanding Type I PSC nucleation and evolution. Analyses of the range of atmospheric conditions possible in the polar stratosphere have also led to interest in solid SAT surfaces and possibly other forms of frozen sulfuric acid aerosols (Toon et al. [446], Middlebrook et al. [327]), as well as liquid sulfuric acid aerosols significantly more dilute than the 60–80 weight percent normally present at lower latitudes (Wolff and Mulvaney [479], Hofmann and Oltmans [222], Toon et al. [446]).

In the free troposphere the heterogeneous surfaces of interest include liquid or solid water (cloud droplets, contrails), and aqueous sulfate solutions. Uptake data are compiled for liquid water for several reasons. First this surface is one asymptote of the aqueous acid aerosol continuum; second, the interactions of some trace species with liquid water and water ice (Type II PSC) surfaces are often similar, and third, the uptake of some trace species by liquid water surfaces in the troposphere can play a key role in understanding their tropospheric chemical lifetimes and thus, the fraction that may be transported into the stratosphere.

5.3 Surface Types—Soot and Alumina

Aircraft at cruise altitudes and rocket exhausts contribute small but measurable amounts of carbonaceous "soot" (Pueschel et al. [362]) and aluminized solid propellant rocket exhausts and spacecraft debris produce increasing levels of alumina (Al_2O_3) and similar metal oxide particles (Zolensky et al. [505]) in the stratosphere and upper troposphere. Soot lofted above from surface combustion sources may also be present in the upper troposphere, and to a lesser extent in the lower stratosphere. Alumina from rocket exhausts is generally emitted as liquid droplets from the rocket nozzle and deposited in the alpha or metastable gamma phases as it quickly solidifies in the exhaust plume. "Soot" refers to a material that is a combination of elemental and organic carbon, with proportions varying depending on the source material and the combustion conditions. In studies of soot directed to understanding the interaction with atmospheric gases, two types of soot have been used: carbon blacks having relatively small hydrogen and oxygen contents (e.g. Degussa FW2, Cabot Monarch 1000, ground charcoal and spark-generated soot) and organic combustion soots having higher hydrogen, oxygen and nitrogen content (e.g. soots from the combustion of n-hexane, methane, propane, decane, ethylene, acetylene, toluene, stearic candles). In the case of organic combustion soots, even different fuels used to generate the soot have been reported to affect the chemistry; for example, the yields of HONO from the reaction of NO_2 with acetylene, toluene, ethylene and decane soots were observed to vary with the fuel used [19, 162].

Polycyclic aromatic hydrocarbons (PAH) and oxygenated polycyclic aromatic compounds (O-PAC) are major constituents of soots formed from the combustion of liquid fuels [14-16, 71, 146, 172, 418]. The bulk composition of soot can have varying amounts of C, H, and O. For example, Chughtai et al. [91] report that the

composition (in weight %) of *n*-hexane soot varies from 87 to 92 % C, 1.2 to 1.6 % H, and 11 to 6% oxygen. Stadler and Rossi [424] showed that the elemental composition of the soot as well as its surface area depended on whether the flame was rich or lean; in the case of the rich flame giving a grey-colored soot, the composition (weight %) was 97.3% C, 0.83% H, 1.65% O, and 0.20% N while the lean flame gave a black soot comprised of 96.4% C, 0.19% H, 3.2% O, and 0.27% N.

The functional groups on the soot surface are expected to be important in terms of the uptake and reaction of gases on the surface. XPS studies of *n*-hexane soot show surface carbon and oxygen, although the specific nature of the bonding could not be determined (Akhter et al. [16]). The surface functional groups on soot vary, depending on the fuel composition, method of generation and the post-treatment of the soot. For example, Degussa FW2 carbon black, which has been used in a number of studies of uptake and reactions of gases on soots, is post-treated with NO_2 by the manufacturer and Cabot Monarch 1000 is post-treated with aqueous HNO_3. There may be sufficient NO and NO_2 concentrations generated under some conditions during the formation of soots by spark generators that these may also have been reacted with these gases prior to collection and uptake studies. Studies of a number of gases interacting with soot surfaces suggest there are at least two and likely more, types of reactive surface sites; one type reacts very rapidly, e.g. with O_3, while others react more slowly. The first type may be most relevant to the reactions of soot particles in exhaust plumes from combustion sources, while the latter is most relevant to soot diluted in air.

Fourier transform infrared (FTIR), Raman and electron paramagentic resonance (EPR) spectroscopic studies of n-hexane soot show C–O functionalities assigned to anhydrides and aryl ethers, alkyl ketones, as well as =C–H, highly substituted aromatics and conjugated carbonyl-aromatic groups [14, 418]. Kirchner et al. [277] measured the FTIR spectra of soots from the combustion of diesel fuel and *n*-hexane (described as "flame deposited") and soots collected from a commercial spark generator in Ar, from the emissions of a diesel automobile and Degussa FW2 soot (described as "filter deposited"). In all cases, absorption peaks due to –C–C–, –C=C–, –C–O, aromatic –C=O, and carboxylic –C=O groups (both aromatic and aliphatic) were observed. However, the flame-deposited soot showed bands due to substituted aromatics while the filter-collected samples did not. The filter-deposited samples had bands due to aliphatic –C–H groups that were not observed for the flame-deposited soots. Only the spark-generated soot showed bands due to both –C=C–H and to –O–H.

For soot formed from the combustion of liquid fuels, the location in the flame at which the soot is collected also changes the surface enough to alter its reactions. For example, Akhter et al. [14] showed that the functional groups as well as particle size depend on the height of collection of soot from the base of the flame. Such changes appear to also alter the reactions of soot; for example, Gerecke et al. [162] measured HONO and NO yields from the reaction of NO_2 with ethylene soot and found that the HONO yield decreased with distance from the bottom of the flame that the soot was collected from, while the yield of NO increased. Kirchner et al. [277] reported much stronger infrared absorption bands due to substituted aromatics in soot samples collected from the combustion of *n*-hexane near the bottom of the flame compared to the top; in addition, absorption bands due to the –O–H group were only observed in samples collected at the bottom of the flame.

Not only can the surface groups directly affect its interaction with gases, but they determine the hygroscopic properties of the soot surface. Chughtai et al. [97, 100] have shown that the hydration of soot surfaces depends on the fuel composition (particularly sulfur and trace metal content) and combustion conditions, as well as the extent of surface oxidation. A highly hygroscopic surface holding significant amounts of water may behave differently than a "dry" surface with respect to the interaction with gases; for example, black carbon suspended in aqueous solutions with ozone and irradiated to generate OH has been shown to help assist in the initiation of bulk solution phase OH chemistry [244]. There are also free radical sites on soot surfaces whose EPR signals are strongly affected by the adsorption of paramagnetic species such as NO_2 (e.g. see Chughtai et al. [91]). These unpaired electrons in soot may contribute to the surface reactivity.

The *International Steering Committee for Black Carbon Reference Materials* (http://www.du.edu/~dwismith/bcsteer.html) has issued preliminary recommendations for representative black carbon reference materials. They recommend that soot formed from the combustion of saturated hydrocarbons, preferably *n*-hexane, be used for soot black carbon. For aerosol black carbon, they recommend the use of Urban Dust Reference Material (SRM) 1649a, which is a sample collected in Washington, D.C. in a baghouse in 1976–1977. However, for studies of the uptake and reactions of gases in the atmosphere with combustion-generated soots, organic combustion generated soots, particularly *n*-hexane soot, appear to be the most reasonable surrogate.

5.4 Surface Types—Solid Alkali Halide Salts and Aqueous Salt Solutions

Some modeling studies also suggest that certain types of major volcanic eruptions transport significant levels of sodium chloride and associated alkali halide salts into the stratosphere (Michelangeli et al. [326]), so studies of stratospheric trace species interacting with solid NaCl or similar alkali halide salts, as well as salt solutions, have also been included. Sea salt aerosols are, of course, much more abundant in the troposphere, and have their largest influence on the chemistry of the marine boundary layer.

The heterogeneous chemistry of salt surfaces is very complex. For example; the uptake and reaction of gases with NaCl and NaBr have been shown to be very sensitive to the presence of small amounts of strongly adsorbed water (SAW) on the salt surface. Because water is not taken up on the 100 crystal surface of NaCl at room temperature, the SAW is thought to be concentrated at steps and edges where one water molecule can interact with two ions, resulting in a larger enthalpy of adsorption. This means that powders of salt, which have a larger surface-to-volume than single crystals, also have more SAW because of the relatively larger numbers of steps and edges. In addition, the amount of SAW on sprayed films is affected by the solvent used, with more SAW when water is used as the solvent. This SAW plays a key role in facilitating the reorganization of the surface during the reaction; thus, it appears to mobilize the product ions and allow them to recrystallize into 3-D microcrystallites of product on the surface, exposing fresh salt and allowing the reaction to continue well beyond the point that the surface would normally passivate. While the overall features of this process are reasonably well understood, the exact nature of the SAW and the molecular level interactions and processes are not. The overall effect, however, is a time-dependent uptake coefficient.

5.5 Surface Composition and Morphology

The detailed composition and morphology of each surface type are uncertain and probably subject to a significant range of natural variability. Certain chemical and physical properties of these surfaces, such as their ability to absorb and/or solvate HCl and HNO_3, are known to be strongly dependent on their detailed chemical composition. Moreover, most heterogeneous processes studied under laboratory conditions (and in some cases proceeding under stratospheric conditions) can change the chemical composition of the surface in ways that significantly affect the kinetic or thermodynamic processes of interest. Thus, a careful analysis of the time-dependent nature of the active surface is required in the evaluation of measured uptake kinetics experiments. Experimental techniques which allow the measurement of mass accommodation or surface reaction kinetics with high time resolution and/or with low trace gas fluxes are often more credible in establishing that measured kinetic parameters are not seriously compromised by surface saturation or changing surface chemical composition.

The relevant kinetic uptake parameters: mass accommodation coefficients and surface reaction probabilities, are separately documented for relevant atmospheric trace gas species for the major and, where available, the minor stratospheric and upper tropospheric surfaces noted above. Since these parameters can vary significantly with surface composition (e.g., the H_2SO_4/H_2O ratio for sulfate aerosol or the HNO_3/H_2O ratio for Type I PSC) the dependence of these parameters on surface composition is reviewed where sufficient data are available. Due to its chemical and morphological complexity, uptake values for soot are documented in a separate table.

5.6 Surface Porosity

The experimental techniques utilized to measure mass accommodation, heterogeneous reaction, and other uptake coefficients generally require knowledge of the surface area under study. For solid surfaces, and most particularly for water and acid ice surfaces formed *in situ*, the determination of how the molecular scale ice surface differs from the geometrical surface of the supporting substrate is not easy. Keyser, Leu, and coworkers have investigated the structure of water and nitric acid ice films prepared under conditions similar to those used in their flow reactor for uptake studies [272, 273, 275]. They have demonstrated that ice films grown *in situ* from the vapor can have a considerably larger available surface than that represented by the geometry of the substrate; they have also developed a simple model to attempt to correct measured uptake rates for this effect [274, 275]. This model predicts that correction factors are largest for small uptake coefficients and thick films. The application of the model to experimental uptake data remains controversial (Keyser et al. [274], Hanson and Ravishakara [205], Kolb et al. [288]). Some experimenters prefer to attempt growing ice surfaces as smooth as possible and to demonstrate that their measured uptake coefficients are only weakly dependent on surface thickness (Hanson and Ravishankara [204]).

Similar issues arise for uptake experiments performed on powered, fused and single crystal salt or oxide surfaces (Fenter et al. [137]; Hanning-Lee et al. [187]). There are two issues here. First, the molecular level (BET) surface area that is commonly measured by determining the mass of a gas such as N_2 adsorbed by a given sample mass is for many atmospheric solids, larger than the geometric surface area. However, determining the BET surface

area of porous materials does not necessarily reflect the available surface area for molecules larger than that used in the BET measurement. Second, many experimental studies have used samples consisting of multiple layers of particles in order to increase the amount of gas that is taken up and hence improve the accuracy of the measurement. However, there is considerable uncertainty in how to accurately assess the fraction of the total sample that is available for reaction. When recommendations are made for uptake coefficients on solid alkali salts in this assessment, the values have generally been obtained using at least two different sample types (e.g., powders, single crystals and spray-deposited films) and/or two different techniques (e.g., flow tubes and Knudsen cells).

The issue of surface area available for uptake is also important for interpreting uptake measurements on soot and soot surrogate surfaces. The degree to which measured uptake parameters must be corrected for porosity effects will remain in some doubt until a method is devised for accurately determining the effective surface area for the surfaces actually used in uptake studies.

Some studies evaluated in this review assume that the effective ice or salt surface area is the geometrical area, but more recent studies on solid surfaces generally attempt to assess the available surface area by employing BET measurements and porosity models. However, uncertainty in true reactive surface area for heterogeneous uptake on solids is often the dominate systematic error in reporting uptake coefficient values for these systems and makes evaluation of these data across laboratories and techniques difficult.

5.7 Temperature Dependences of Parameters

A number of laboratory studies have shown that mass accommodation coefficients and, to some extent, surface reaction probabilities can be temperature dependent. While these dependencies have not been characterized for many systems of interest, temperature effects on kinetic data are noted where available. More work that fully separates heterogeneous kinetic temperature effects from temperature controlled surface composition is obviously needed.

5.8 Solubility Limitations

The uptake of certain trace gases by atmospherically relevant surfaces is usually governed by solubility limitations rather than kinetic processes. In these cases properly analyzed data can yield measurements of trace gas solubility parameters relevant to stratospheric conditions. In general, such parameters can be strongly dependent on both condensed phase composition and temperature. Such parameters may be very important in stratospheric models, since they can govern the availability of a reactant for a bimolecular heterogeneous process (e.g., the concentration of HCl available for the HCl + $ClONO_2$ reaction on sulfuric acid aerosols) or the gas/condensed phase partitioning of a heterogeneous reaction product (e.g., the HNO_3 formed by the reaction of N_2O_5 on sulfuric acid aerosols). Surface saturation limitations have also been observed in experimental uptake studies on solid surfaces, including water and water/acid ice surfaces.

5.9 Data Organization

Data for trace-gas heterogeneous interactions with relevant condensed-phase surfaces are tabulated in Tables 5-1 through 5-5. These are organized into:

Table 5-1—Mass Accommodation Coefficients for Surfaces Other Than Soot

Table 5-2—Surface Reaction Probabilities for Surfaces Other Than Soot

Table 5-3—Soot-Surface Uptake Coefficients

Table 5-4—Solubility Data for Pure Water

Table 5-5—Ion Specific Schumpe Parameters

Table 5-6—Solubility Data for Acids

5.10 Parameter Definitions

Mass accommodation coefficients (α), represent the probability of reversible uptake of a gaseous species colliding with the condensed surface of interest. For liquid surfaces this process is associated with interfacial (gas-to-liquid) transport and is generally followed by bulk liquid phase solvation. Examples include: simple surface absorption, absorption followed by ionic dissociation and solvation (e.g., $HCl + nH_2O \leftrightarrow H^+(aq) + Cl^-(aq)$), and

absorption followed by a reversible chemical reaction with a condensed phase substituent (e.g., $SO_2 + H_2O \leftrightarrow H^+ + HSO_3^-$ or $CH_2O + H_2O \leftrightarrow CH_2(OH)_2$).

The term "sticking coefficient" is often used for mass accommodation on solid surfaces where physisorption or chemisorption takes the place of true interfacial mass transport.

Processes involving liquid surfaces are subject to Henry's law, which limits the fractional uptake of a gas phase species into a liquid. The distribution of a substance between the gas and liquid phase is controlled, at equilibrium, by the Henry's Law constant for that substance, which relates the concentration of the substance in solution to the partial pressure of the substance in the gas phase:

$$H = [\text{solution}]/P(\text{gas})$$

This is a limiting law, strictly valid only at the limit of zero concentration. For most gasses at concentrations of interest, deviations from this law are not significant. The value of the Henry's Law constant, *H*, depends strongly upon temperature. For a typical gas, it decreases with increasing temperature at lower temperatures. At higher temperatures, typically well above 298 K, the value will increase with temperature. Over limited temperature ranges, the value is well represented by a linear relationship between the logarithm of *H* and the reciprocal of temperature.

$$\text{Ln}(H) = A + B/T$$

For a number of gasses, the experimental data are sufficient to display the expected curvature in a plot of Ln *H* vs. 1/T. In this review, where sufficient data are available, we have represented these results by the three-parameter equation

$$\text{Ln}(H) = A + B/T + C\ \text{Ln}(T)$$

If the gas phase species is simply solvated, a physical Henry's law constraint holds; if the gas phase species reacts with a condensed phase substituent, as in the sulfur dioxide or formaldehyde hydrolysis cases noted above, a "chemically modified" or "effective" Henry's law constraint holds (Clegg and Brimblecombe [101], Schwartz [403], Watson et al. [469]). Henry's law constants relate the equilibrium concentration of a species in the gas phase to the concentration of the same species in a liquid phase, and they have, in this report, units of M atm^{-1}.

The solubility of a gas also depends upon the presence of other substances in the solution. The best known effect is that of an added salt. In most cases, the addition of a salt to the solution results in a lowering of the solubility of the gas. This effect is usually described by the Sechenov equation:

$$\text{Log}(c^o/c) = \text{Log}(H^o/H) = K_S\, c_S$$

which relates the relates the ratio of the concentrations of gas dissolved for a given pressure in the absence, c^o, and presence, c, of a given concentration of salt, c_S. The proportionality constant is the Sechenov coefficient, K_S. The Sechenov coefficient is specific to both the gas and the specific salt. Thus, in general, one needs a new value for any particular gas-salt combination, a tremendous amount of data. For this reason, models have been developed to extend measurements of K_S to systems for which no measurements have been made. Schumpe and co-workers [398, 472] developed the particular procedure adopted in this review. It assumes that K_S is composed of ion- and gas-specific constants:

$$K_S = \Sigma\, (h_i + h_G)\, n_i$$

Where h_i is the ion-specific constant, h_G is the gas-specific constant, and n_i is the ion index. For a mixed electrolyte solution,

$$\text{Log}(H^o/H) = \Sigma\, (h_i + h_G)\, c_i$$

The small temperature dependence of K_S is assumed to lie completely in h_G. Thus

$$h_G = h_{G,0} + h_T\, (T - 298.15\ \text{K})$$

Weisenberger and Schumpe [472] analyzed 892 Sechenov constants for various gases in salt solutions over the temperature range 273 K to 363 K. They derived an optimum set of h_i, $h_{G,0}$, and h_T parameters for a diverse set of ions and gases. Values for O_2 and H^+ were set to zero to make the set unique. The standard deviation in the predicted Sechenov constants is 0.026. We have included their values for the ion-specific parameters in Table 5--5.

Available gas-specific constants, $h_{G,0}$ and h_T, are included in Table 5-4, along with the Henry's law constants for pure water. In Table 5-4, we present those "salting out" parameters included in the optimum set derived by Weisenberger and Schumpe, along with some parameters derived from other studies. In the latter cases, the ion parameters are considered fixed and we solve for the gas-specific parameters.

Available Henry's law parameters for sulfuric acid/water, and in a few cases, sulfuric acid/nitric acid/water solutions are presented in Table 5-6. Effective Henry's law constants are designated H*, while simple physical Henry's law constants are represented by H. Effective Henry's law constants are also employed to represent decreased trace gas solubilities in moderate ionic strength acid solutions via a Sechenov coefficient formulation which relates H* to the concentration of the acid [233]. Available Henry's law constants for reactive upper tropospheric/stratospheric species in binary sulfuric acid/water solutions, and for a few cases of ternary sulfuric acid/nitric acid/water solutions, are tabulated as a function of acid weight percent and temperature. It is presently unclear whether "surface solubility" effects govern the uptake on nominally solid water ice or HNO_3/H_2O ice surfaces in a manner analogous to bulk solubility effects for liquid substrates and no solubility parameters for these "ice" systems are presented.

For some trace species on some surfaces, experimental data suggest that mass accommodation coefficients untainted by experimental saturation limitations have been obtained. These are tabulated in Table 5-1. In other cases experimental data can be shown to be subject to Henry's law constraints, and Henry's law constants, or at least their upper limits, can be determined. Some experimental data sets are insufficient to determine if measured "uptake" coefficients are true mass accommodation coefficients or if the measurement values are lower limits compromised by saturation effects. These are currently tabulated, with suitable caveats, in Table 5-1.

Surface reaction probabilities (γ) are kinetic values for generally irreversible reactive uptake of trace gas species on condensed surfaces. The rates of such processes may not be limited by Henry's law constraints; however, the fate of the uptake reaction products may be subject to saturation limitations. For example, N_2O_5 has been shown to react with sulfuric acid aerosol surfaces. However, if the H_2SO_4/H_2O ratio is too high, the product HNO_3 will be insoluble, and a large fraction will be expelled back into the gas phase. Surface reaction probabilities for substantially irreversible processes are presented in Table 5-2. Reaction products are identified where known.

Surface reaction probabilities on crystalline and non-ice amorphous solid surfaces, such as alumina and alkali salts are particularly susceptible to surface saturation effects, especially when exposed to the relatively high trace gas concentrations sometimes employed in laboratory experiments. In the case of gaseous HNO_3 reacting with NaCl for example, there is a rapid initial uptake of HNO_3 and formation of nitrate on the surface, followed by a decrease to a relatively constant (but slowly declining) value. When they are available, we tabulate the initial uptake coefficient, γ_0, in Table 5-2, since that value often sets the upper limit for atmospheric uptake. In the corresponding note we may also site the reactive uptake coefficient appropriate to longer time exposure when the uptake appears to have reached an approximate steady-state, γ_{ss}.

The total experimental uptake coefficient measured in laboratory heterogeneous kinetic experiments are also often represented by the symbol γ. In those cases where surface and/or bulk reaction dominate the uptake, the total uptake coefficient (γ_{total}) and reactive uptake coefficient (γ_{rxn}) may well be identical. More formally, for cases where bulk liquid phase reaction is facile and there are no gas phase diffusion constraints, the total uptake coefficient for aerosol or cloud droplets can be approximated in terms of γ_{rxn} and γ_{sol} as [288]:

$$\frac{1}{\gamma_{total}} = \frac{1}{\alpha} + \frac{1}{\gamma_{sol} + \gamma_{rxn}}$$

where

$$\gamma_{sol} = \frac{8HRT}{\pi^{1/2}\bar{c}}\left(\frac{D}{t}\right)^{1/2}$$

and

$$\gamma_{rxn} = \frac{4HRT}{\bar{c}}\left(Dk_{rxn}\right)^{1/2}$$

where t is the time integrated exposure of the trace gas to the liquid surface, R is the gas constant, D is the liquid phase diffusion coefficient, and $\bar{c}$ is the mean trace gas molecular speed. In the limit of low solubility or long exposure time γ_{sol} becomes negligible and

$$\frac{1}{\gamma_{total}} = \frac{1}{\alpha} + \frac{1}{\gamma_{rxn}}$$

Discussion of how to use this approach to model chemical reactions in liquid stratospheric aerosols can be found in Hanson et al. [210] and Kolb et al. [288]. Note that these formulations are approximate. In cases where separate terms are competitive, more rigorous solution of the kinetic differential equations may be appropriate.

For solid surfaces, bulk diffusion is generally too slow to allow bulk solubility or bulk kinetic processes to dominate uptake. For solids, reactive uptake is driven by chemisorption/chemical reaction at the interface, a process that can also influence trace gas uptake on liquids. For liquids, surface reaction (γ_{surf}) occurs in parallel, rather than in series with mass accommodation, thus:

$$\gamma_{total} = \gamma_{surf} + \left[\frac{1}{\alpha} + \frac{1}{\gamma_{sol} + \gamma_{rxn}}\right]^{-1}$$

Examples where this more complex situation holds for liquid surfaces can be found in Hu et al. [226] and Jayne et al. [249]. In such cases γ may be significantly larger than α.

Uptake of gases on soot may occur due to three different processes: (1) physisorption (e.g. SO_2 or HNO_3 at room temperature and low nitric acid pressures); (2) reaction with the surface (e.g. NO_2), and (3) catalytic decomposition/reactions of the gas on the surface. All three processes may occur in parallel, and the relative contributions of each of these three may vary during the course of the reaction as the surface "ages." As discussed above, there are different types of reactive sites on soot, leading in some cases to a rapid initial uptake followed by a slower uptake; these are often characterized as reactions on "fresh" and "aged" surfaces respectively. Another complexity is that in some cases the geometric surface areas were used to calculate the uptake coefficients from the experimental data while in others, the available reactive surface area was estimated and used.

Because of these complexities with soot heterogeneous chemistry, uptake coefficients for soot interactions with gases have been broken out into a separate Table 5-3 rather than being included with the other surfaces in Table 5-1 and Table 5-2. When the uncertainty is more than an order of magnitude, a recommendation is not given in Table 5-3 and the range of reported values is given in the Notes. In most cases, the available reactive surface area rather than the geometric areas have been used in obtaining the uptake coefficients; in those cases where the geometric area was used but a higher available surface area was involved in the measured uptake, the uptake coefficient is given as an upper limit. Data are most commonly available for room temperature or there are very limited data at lower temperatures characteristic of the upper troposphere.

The data in Table 5-1 and Table 5-2 for uptake on non-soot surfaces are organized by trace gas species, since some systematic variation may be expected for surface accommodation or reaction as the surface composition and/or phase is varied. Data presented for one surface may be judged for "reasonableness" by comparing with data for a "similar" surface. In some cases it is not yet clear if surface uptake is truly reversible (accommodation) or irreversibly reactive in nature. In such cases the available uptake coefficients are generally tabulated in Table 5-1 as accommodation coefficients, a judgment that will be subject to change if more definitive data become available.

Where a specific evaluated value for an accommodation coefficient or reaction probability has been obtained, an estimated uncertainty factor is also tabulated. However, when the data evaluation yielded only a lower or upper limit, no uncertainty factor can be reliably estimated and none is presented.

Description of and reference citations to many of the laboratory techniques used to obtain the data in the following tables can be found in Kolb et al. [288].

Reactions of N_2O_5, $ClONO_2$, HOCl and $BrONO_2$ on/in sulfuric acid are generally dependent on the species' Henry's law solubility and liquid phase diffusion coefficient in the liquid acid as well as the surface and/or liquid phase reaction rate parameters. All of these processes are generally functions of the acid composition and temperature (Hanson et al. [210], Robinson et al. [376] Shi et al. [414]. Thus, these reactions' reactive uptake

coefficients must be represented by a complex phenomenological or empirical models that defy simple entry into Table 5-2. The notes in Table 5-2 for these reactions discuss and present the models adopted.

To aid in visualizing the resulting reactive uptake parameters the results for several reactions have been plotted in Figure 5.1 as a function of temperature for a background pressure of 50 mbar and background water vapor and HCl mixing ratios of 5 ppmv and 2 ppbv, respectively. These calculations are presented for monodisperse background sulfate aerosol particles with a radius of 1×10^{-5} cm (0.1 μm).

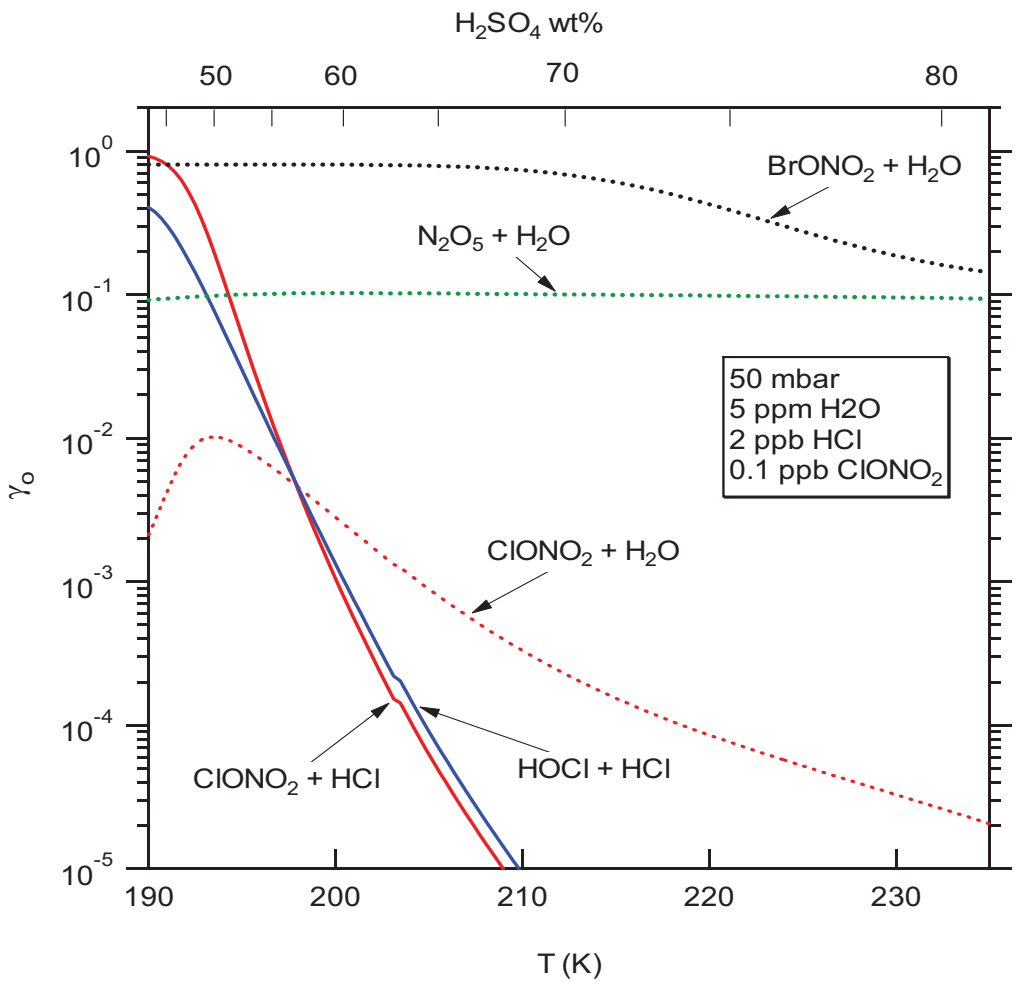

Figure 5-1. Recommended reactive uptake coefficients as a function of temperature for key stratospheric heterogeneous processes on sulfuric acid aerosols. For $ClONO_2$ and HOCl species, the aerosol radius used in the calculation is 10^{-5} cm, a typical value in the stratosphere. Because the current uptake models for N_2O_5 and $BrONO_2$ hydrolysis do not provide the information about the reacto-diffusive length (ℓ), the aerosol radius used in the calculation is assumed to be much larger than their reacto-diffusive length (i.e. ℓ for N_2O_5 and $BrONO_2$ are set to zero.)

5.11 Mass Accommodation Coefficients for Surfaces Other Than Soot

Table 5-1. Mass Accommodation Coefficients (α) for Surfaces Other Than Soot

Gaseous Species	Surface Type	Surface Composition	T(K)	α	Uncertainty Factor	Notes
O	Water Ice Sulfuric Acid	$H_2O(s)$ $H_2SO_4 \cdot nH_2O(l)$ (97 wt.% H_2SO_4)	See Note 298	See Note See Note		1 2

Gaseous Species	Surface Type	Surface Composition	T(K)	α	Uncertainty Factor	Notes
O_3	Water Ice	$H_2O(s)$	195–262	>0.04		3
	Liquid Water	$H_2O(l)$	275-300	≥1 × 10^{-2}*		4
	Nitric Acid Ice	$HNO_3 \cdot 3H_2O(s)$	195	2.5 × 10^{-4}‡	3	3
	Sulfuric Acid	$H_2SO_4 \cdot nH_2O(l)$ (50–98 wt.% H_2SO_4)	193–295	See Note		5
OH	Water Ice	$H_2O(s)$	205–253	>0.1		6
	Liquid Water	$H_2O(l)$	275-300	≥1 × 10^{-2}*		7
HO_2	Liquid Water	$H_2O(l)$	275	> 0.02		8
	Aqueous Salts	$NH_4HSO_4(aq)$ and $LiNO_3(aq)$	293	> 0.2		8
H_2O	Water Ice	$H_2O(s)$	200	0.5	2	9
	Liquid Water	$H_2O(l)$	250-290	≥0.1*		10
	Liquid Nitric Acid	$HNO_3 \cdot nH_2O(l)$	278	>0.3		11
	Nitric Acid Ice	$HNO_3 \cdot 3H_2O(s)$	197	See Note		12
	Sulfuric Acid	$H_2SO_4 \cdot nH_2O$ (96 wt.% H_2SO_4)	298	> 2 × 10^{-3}‡		13
		(50 wt.% H_2SO_4)	250-280	0.5	1.3	13
		(70 wt.% H_2SO_4)	250-295	0.6	1.3	13
		(82 wt.% H_2SO_4)	270-300	0.85	1.3	13
	Sodium Chloride	NaCl(s)	~298	See Note		14
		NaCl(aq)	~299	See Note		15
H_2O_2	Liquid Water	$H_2O(l)$	273	0.18*	2	16
	Sulfuric Acid	$H_2SO_4 \cdot nH_2O(l)$ (96 wt.% H_2SO_4)	298	> 8 × 10^{-4}‡		17
NO	Water Ice	$H_2O(s)$	195	See Note		18
	Sulfuric Acid	$H_2SO_4 \cdot nH_2O$		See Note		
		(70 wt.% H_2SO_4)	193–243	See Note		19
		(97 wt.% H_2SO_4)	298	See Note		19
NO_2	Water Ice	$H_2O(s)$	195	See Note		21
NO_3	Liquid Water	$H_2O(l)$	273	See Note		20
HONO	Water Ice	$H_2O(s)$	180–200	See Note		22
HNO_3	Water Ice	$H_2O(s)$	200	See Note	3	23
	Liquid Water	$H_2O(l)$	250-300	≥0.05*		24
	Nitric Acid Ice	$HNO_3 \cdot 3H_2O(s)$	191–200	0.4	2	25
	Liquid Nitric Acid	$HNO_3 \cdot nH_2O(l)$	278	0.6	2	26
	Sulfuric Acid	$H_2SO_4 \cdot nH_2O(l)$				
		(57.7 wt.% H_2SO_4)	191–200	>0.3		27
		(73 wt.% H_2SO_4)	283	0.1	2	27
		(75 wt.% H_2SO_4)	230	>2 × 10^{-3}		27
		(97 wt.% H_2SO_4)	295	>2.4 × 10^{-3}		27
	Sulfuric Acid Tetrahydrate	$H_2SO_4 \cdot 4\ H_2O(s)$	~192	>0.02*		27
HO_2NO_2	Water Ice	$H_2O(s)$	[a]200	0.1‡	3	28
	Sulfuric Acid	$H_2SO_4 \cdot nH_2O(l)$ (97 wt.% H_2SO_4)	298	See Note		29
NH_3	Liquid Water	$H_2O(l)$	260-300	≥0.05*		30
CO_2	Liquid Water	$H_2O(l)$	290-300	≥5 x 10^{-5}		31
CH_3OH	Liquid Water	$H_2O(l)$	260–291	0.12–0.02*	2	32
CH_3CH_2OH	Liquid Water	$H_2O(l)$	260–292	≥2 x 10^{-2}*		33
$CH_3CH_2CH_2OH$	Liquid Water	$H_2O(l)$	260–291	0.08–0.02*	2	34
$CH_3CH(OH)CH_3$	Liquid Water	$H_2O(l)$	260–291	0.10–0.02*	2	34
$HOCH_2CH_2OH$	Liquid Water	$H_2O(l)$	260–291	0.13–0.04*	2	35
CH_3O_2	Sodium Chloride	NaCl(s)	296	>4 × 10^{-3}		36
CH_3OOH	Liquid Water	$H_2O(l)$	260-282	≥7 x 10^{-3}*		37
CH_2O	Liquid Water	$H_2O(l)$	260–270	0.04	3	38
	Sulfuric Acid	$H_2O \cdot mHNO_3 \cdot nH_2O(l)$	235–300	0.04	3	38
CH_3CHO	Liquid Water	$H_2O(l)$	267	>0.03*		39
CH(O)CH(O)	Liquid Water	$H_2O(l)$	260-285	≥1 x 10^{-2}*		40
$CH_3C(O)CH_3$	Liquid Water	$H_2O(l)$	260–292	≥2 x 10^{-2}*		41
$CH_3C(O)CHO$	Liquid Water	$H_2O(l)$	260-293	≥1 x 10^{-4}*		42
$CH_3OC(O)OCH_3$	Liquid Water	$H_2O(l)$	270-278	≥2 x 10^{-2}*		43
HC(O)OH	Liquid Water	$H_2O(l)$	260–291	0.10–0.02*	2	44
$CH_3C(O)OH$	Liquid Water	$H_2O(l)$	258-292	≥2 x 10^{-2}*		45
Cl_2	Water Ice	$H_2O(s)$	200	See Note		46
OClO	Water Ice	$H_2O(s)$	100,189, 200	See Note		47

Gaseous Species	Surface Type	Surface Composition	T(K)	α	Uncertainty Factor	Notes
HCl	Water Ice	$H_2O(s)$	191– 211	0.3	3	48
	Liquid Water	$H_2O(l)$	260-295	≥0.05*		49
	Nitric Acid Ice	$HNO_3 \cdot 3H_2O(s)$	191– 211	0.3	3	50
	Sulfuric Acid	$H_2SO_4 \cdot nH_2O(l)$	283	0.15*	2	51
		(n≥8, ≤40 wt.% H_2SO_4)	218	>0.005*		51
		(n<8, >40 wt.% H_2SO_4)	†	†	†	51
	Sulfuric Acid Tetrahydrate	$H_2SO_4 \cdot 4H_2O(s)$	192–201	See Note		52
$ClONO_2$	Liquid Water	$H_2O(l)$	260-280	≥0.05*		53
CCl_2O	Liquid Water	$H_2O(l)$	260–290	See Note		54
CCl_3CClO	Liquid Water	$H_2O(l)$	260–290	See Note		54
HBr	Water Ice	$H_2O(s)$	200	> 0.2		55
	Liquid Water	$H_2O(l)$	260-295	≥0.05*		56
	Nitric Acid Ice	$HNO_3 \cdot 3H_2O(s)$	200	> 0.3		55
HOBr	Water Ice	$H_2O(s)$	190–239	See Note		57
	Liquid Water	$H_2O(l)$	298	0.6	1.5	58
	Sulfuric Acid	H_2SO_4 in $H_2O(l)$ (58 wt.% H_2SO_4)	228	>0.05‡		59
$BrONO_2$	Liquid Water	$H_2O(l)$	260-280	≥0.03*		60
	Sulfuric Acid	H_2SO_4 in $H_2O(l)$ (45-83 wt.% H_2SO_4)	230-300	0.8	1.5	61
$CHBr_3$	Water Ice	$H_2O(l)$	220	See Note		62
	Sulfuric Acid	$H_2SO_4 \cdot nH_2O(l)$ (97 wt.% H_2SO_4)	220	$>3 \times 10^{-3}$‡		62
BrCl	Liquid Water	$H_2O(l)$	270-285	≥0.15*		63
I_2	Liquid Water	$H_2O(l)$	270-293	≥0.01*		64
HI	Liquid Water	$H_2O(l)$	260-280	≥0.05*		65
HOI	Sulfuric Acid	$H_2SO_4 \cdot nH_2O(l)$				66
		(40 wt.% H_2SO_4)	195	0.07	3	
		(40 wt.% H_2SO_4)	205	0.03	3	
		(40 wt.% H_2SO_4)	212	0.04	3	
		(50 wt.% H_2SO_4)	222–224	0.02	3	
		(70 wt.% H_2SO_4)	230–232	0.02	3	
		(70 wt.% H_2SO_4)	252	0.02	3	
HF	Water Ice	$H_2O(s)$	200	See Note		67
	Nitric Acid Ice	$HNO_3 \cdot 3H_2O(s)$	200	See Note		67
CF_2O	Water Ice	$H_2O(s)$	192	See Note		68
	Liquid Water	$H_2O(l)$	260–290	See Note		54
	Nitric Acid Ice	$HNO_3 \cdot 3H_2O(s)$	192	See Note		68
	Sulfuric Acid	$H_2SO_4 \cdot nH_2O(l)$	215–230			
		(40 wt.% H_2SO_4)		$>3 \times 10^{-6}$‡		68
		(60 wt.% H_2SO_4)		$>6 \times 10^{-5}$‡		68
CF_3CFO	Liquid Water	$H_2O(l)$	260–290	See Note		54
CF_3COOH	Liquid Water	$H_2O(l)$	263–288	0.2–0.1*	2	69
CF_3CClO	Liquid Water	$H_2O(l)$	260–290	See Note		54
SO_2	Liquid Water	$H_2O(l)$	260–298	≥0.12*	2	70
	Sulfuric Acid	$H_2SO_4 \cdot nH_2O(l)$ (97 wt.% H_2SO_4)	298	See Note		71
H_2S	Liquid Water	$H_2O(l)$	260-298	≥0.05*		72
H_2SO_4	Sulfuric Acid	$H_2SO_4 \cdot nH_2O(l)$ (50–98 wt.% H_2SO_4)	200–300	0.7	1.4	73
$CH_3S(O)CH_3$	Liquid Water	$H_2O(l)$	262–281	0.16–0.08*	2	74
$CH_3S(O_2)CH_3$	Liquid Water	$H_2O(l)$	262–281	0.27–0.08*	2	74
$CH_3S(O_2)OH$	Liquid Water	$H_2O(l)$	260-283	≥0.1*		74

* Varies with T, see Notes

No data—all measurements; limited by HCl solubility

May be affected by surface saturation

γ_o is an experimental initial reactive uptake coefficient, indicating a reactive uptake that decreases with measurement time.

5.12 Notes to Table 5-1

1. O on $H_2O(s)$. Murray and Plane [346] measured the uptake of O atoms on water ice at temperatures relevant to the upper mesosphere (112 -151 K), where noctilucent clouds are present. Their results indicate that in the absence of oxygen molecules the uptake coefficient α is small (7×10^{-6}). They recommend the following expression: $\alpha = 7 \times 10^{-6} + 1.5 \times 10^{-10}$ exp (11.4 kJ/mol/RT), with an uncertainty of ± 24%. Back to Table

2. O on $H_2SO_4 \bullet nH_2O$. Knudsen cell experiment of Baldwin and Golden [34] measured an uptake coefficient limit of $<10^{-6}$, this result probably cannot be equated with an accommodation coefficient due to surface saturation. Back to Table

3. O_3 on $H_2O(s)$ and $HNO_3 \bullet nH_2O$. Undoped ice surfaces saturate too quickly for reliable measurements. When ice is doped with Na_2SO_3 to chemically remove absorbed O_3 the apparent α increases to 1×10^{-2} (0.1M) or up to 4×10^{-2} (1M) (Dlugokencky and Ravishankara [122]). Limit of $\gamma < 10^{-6}$ for undoped ice is consistent with earlier measurement by Leu [294] of $\geq 1 \times 10^{-4}$ and with $< 6 \times 10^{-5}$ obtained by Kenner et al. [271]. Dlugokencky and Ravishankara also measured the tabulated value of an uptake coefficient for O_3 on a NAT "like" surface, but the data were difficult to reproduce and the surfaces were not well characterized. Kenner et al. also measured a lower limit for an uptake coefficient of 8×10^{-5} on NAT at 183 K, but this measurement is also certainly limited by surface saturation. Back to Table

4. O_3 on $H_2O(l)$. Utter et al. [453] used a wetted wall flow tube technique with various chemical scavengers to measure a lower limit for α of 2×10^{-3}. The stopped flow measurement technique using an SO_3^{2-} scavenger (Tang and Lee [437]) is subject to saturation effects, so their quoted α of 5.3×10^{-4} is also taken as a lower limit. Using a droplet train flow reactor Hu et al. [226] measured a value of ~0.1 at 277 K with I^- as a reactive scavenger, consistent with a more extensive droplet train flow reactor measurement by Magi et al. [314] yielding a value of ≥0.1 also using I^- as a reactive scavenger. Schurath et al. [399] used a coaxial flow liquid jet to obtain a value of 4.5×10^{-3} at 298 K, probably limited by surface saturation although they also used I^-as a reactive scavenger. M ller and Heal [344] obtained a value of 4×10^{-2} at 293 K in a wetted wall flow tube with $S_2O_3^{2-}$ as a reactive scavenger. Sch tze and Herrmann [400] measured a lower limit of 2×10^{-2} at 298 K using a suspended droplet flow reactor method that also employed I^- as a reactive scavenger. It is highly likely that the mass accommodation coefficent for ozone on liquid water is ≥0.01 between ~275 and 300 K and may be significantly higher, although it is possible that interfacial reactions with near surface I^- bias some mass accommodation evaluations high because surface reactive uptake occurs in parallel with mass accommodation. Molecular dynamic simulations of O_3 uptake on water by Roeselováet al. [380] indicate a mass accommodation coefficent of order 0.1. Back to Table

5. O_3 on $H_2SO_4 \bullet nH_2O$. Flow tube measurements (Dlugokencky and Ravishankara [122]) of an uptake coefficient limit of $<10^{-6}$ on both 50 and 97 wt.% H_2SO_4 surfaces are consistent with earlier, but probably less quantitative, static systems measurements of Olszyna et al. [350] and aerosol chamber measurements of Harker and Ho [211], who report uptake coefficients of the order 10^{-8} or less for a variety of sulfuric acid concentrations and temperatures. In these earlier experiments, doping the H_2SO_4 with Ni^{2+}, Cr^{2+}, Al^{3+}, Fe^{3+}, and NH_4^+ (Olszyna et al. [350]) or Al_2O_3 or Fe_2O_3 (Harker and Ho [211]) did not significantly increase measured O_3 loss. An upper limit of 1×10^{-6} was also reported by Baldwin and Golden [33] for 97 wt.% H_2SO_4 at 295 K. Il'in et al. [236] performed static tube reactor measurements on 98 wt.% sulfuric acid at 239, 258, 273 K measuring uptake coefficients between 1.2 and 1.75×10^{-6}. Although these measurements are slightly larger than the limits in the other studies, uptake values this small are extremely hard to quantify and these measurements are not seen to be in serious disagreement with other studies finding slightly lower upper limits. All measurements are subject to solubility limitations and probably do not reflect true limits on mass accommodation. Back to Table

6. OH on $H_2O(s)$. Cooper and Abbatt [104] analyzed uptake rates in a wall-coated flow tube to determine an initial $\gamma \sim 0.1$ over the temperature range of 205 – 230 K. Uptake coefficients decreased at longer exposure times, indicating surface saturation. These data indicate that α is at least 0.1 and possibly much larger. This is confirmed by an earlier experiment using a coated insert/flow tube technique by Gershenzon et al. [166], which yielded $\alpha > 0.4$ at 253 K. Back to Table

7. OH on $H_2O(l)$. A lower limit of α on pure water of 3.5×10^{-3} at 275 K was determined by Hanson et al. [194]) using a liquid-wall flow tube. Takami et al. [435] using a gas/liquid impinging flow technique obtained a pure water value near pH 7 at 293 K of $(4.2 \pm 2.8) \times 10^{-3}$ while values 2 to 3 times higher where

obtained for acid (pH=1) and basic (pH=10-13) aqueous solutions; a value of $(1.1 \pm 0.4) \times 10^{-2}$ was obtained when benzoic acid was added as a radical scavenger. Takami et al. also observed that uptake for pure water solutions decreased with gas/liquid contact times, indicating a saturation limitation and explaining the higher uptake values observed for solutions with H^+, OH^-, or benzoic acid reactive scavengers. Based on these experimental results a value of $\alpha \geq 0.1$ is suggested. This recommendation is consistent with molecular dynamics calculations by Roeselováet al. [380, 381] who first published simulation values at room temperature 0.2 to 0.3, but later reported a value of 0.83 at 300 K using revised intermolecular potentials. Back to Table

8. HO_2 on $H_2O(l)$. Determination of α in liquid-wall flow tube (Hanson et al. [194]) is dependent on gas-phase diffusion corrections; measured limit (α >0.02) is consistent with $\alpha = 1$. In the aqueous salt aerosol measurements of Mozurkewich et al. [340], HO_2 was chemically scavenged by Cu^{++} from added $CuSO_4$ to avoid Henry's law constraints; the measured limit of >0.2 is also consistent with $\alpha = 1$. Back to Table

9. H_2O on $H_2O(s)$. Measurements are available from Leu [293] giving 0.3 (+0.7, –0.1) at 200 K and Haynes et al. [215] (1.06 ± 0.1 to 0.65 ± 0.08) from 20 to 185 K. Brown et al. [66] used molecular beam reflection techniques to measure a value of $\alpha = 0.99 \pm 0.03$ between 85 and 150 K and optical interference methods to obtain $\alpha = 0.97 \pm 0.10$ between 97 and 145 K. Back to Table

10. H_2O on $H_2O(l)$. Because the uptake of water vapor on liquid water is a fundamental process and plays an extremely important role in cloud physics, it has been the subject of over 40 published experimental studies spanning over eight decades. Many of these studies were reviewed by Marek and Staub [316], who note values of α deduced from these experiments range from ~0.001 to 1.0, with experiments involving growing water drops tending to higher values. Recently several new experiments have been published supporting values nearer the higher end of the range. Shaw and Lamb [413] used an electrodynamic droplet levilation cell to make simultaneous ice nucleation/water droplet evaporation rate observations to deduce a range of $0.04 < \alpha < 0.1$, at ~237K. Li et al. [300] used a droplet train flow reactor to measure the uptake of small excesses of $H_2{}^{17}O$ on water droplets that were in equilibrium with the surrounding normal water vapor, deducing a value of 0.17±0.03 at 280K which increased to 0.32±0.04 at 258K. Winkler et al. [477] used precise Mie scattering analyses of the growth of freshly nucleated droplets in an expansion chamber to deduce $0.4<\alpha<1.0$ over a temperature range of 250 to 290 K. Given the precision of these latter two experiments, it seems clear that mass accommodation values of water vapor on liquid water for temperatures below 290 K must exceed 0.1. The Li et al. and Winkler et al. experiments are further discussed in Davidovits et al. [112] which notes that the differences in their deduced values may reflect the different state of the water surface in equilibrium versus supersaturated vapor regimes. Back to Table

11. H_2O on $HNO_3/H_2O(l)$. Rudolf and Wagner[390] used aerosol expansion chamber techniques to illustrate that on liquid water/nitric acid aerosols α is greater than 0.3 and is consistent with 1.0 at 278 K. Experiments are similar to those at Winkler et al. [477]; supersaturated vapor may lead to a larger value of α than found for near equibrium conditions. Back to Table

12. H_2O on $HNO_3 \bullet nH_2O(s)$. Middlebrook et al. [328] measured an uptake coefficient of 0.002 for water vapor co-depositing with nitric acid over NAT at 197 K. Back to Table

13. H_2O on $H_2SO_4 \bullet nH_2O$. Baldwin and Golden [33] using a Knudsen cell measured $\alpha \sim 2 \times 10^{-3}$ at 96 wt.%, which is strongly affected by surface saturation (see Note for H_2O_2 on $H_2SO_4 \bullet nH_2O$). Gershenzon et al. [163] used a droplet train flow reactor to measure the uptake of $H_2{}^{17}O$ on 50 wt.% sulfuric acid from 250 to 278 K, on 70 wt.% from 250 to 295 K, and on 82 wt.% from 272 to 298 K. Measured mass accommodation coefficients range from 0.4 to 0.9, increasing with acid wt.% and decreasing temperature. Back to Table

14. H_2O on NaCl(s). Fenter et al. [135] used Knudsen cell/mass spectrometry methods to measure $\gamma < 2 \times 10^4$ for $H_2O(g)$ uptake on NaCl powders, an observation confirmed by Beichert and Finlayson-Pitts [53], who found $\gamma < 1 \times 10^{-5}$. However, Dai et al. [107] used FTIR spectroscopy on NaCl crystallite films at 240 and 296 K to determine that a water adlayer does adhere to dry salt and that a small fraction of surface sites (<1%) cause H_2O dissociation. It is likely that the measurements of Fenter et al. and Beichert and Finlayson-Pitts were affected by surface saturation. Back to Table

15. H_2O on NaCl(aq). Fung et al. [155] used Mie resonance scattering techniques to quantify aqueous NaCl droplet growth (5.8 to 7.8 µm), yielding fitted values of $\alpha > 0.5$ and consistent with 1.0. Such droplet growth measurements require modeling of heat and mass transfer and may not correspond to atmospheric conditions near vapor/liquid equilibrium. Back to Table

16. H_2O_2 on $H_2O(l)$. Measured accommodation coefficient (Worsnop et al. [483]) has a strong negative temperature dependence over the measured range of 260–292 K, with $\alpha = 0.3$ at 260 K decreasing to 0.1 at 292 K. Back to Table

17. H_2O_2 on $H_2SO_4 \bullet nH_2O$. Knudsen cell uptake measurements are subject to surface saturation, thus uptake coefficient value of 7.8×10^{-4} quoted by Baldwin and Golden [33] is almost certainly a lower limit for α. This effect is probably also responsible for the lack of measured uptake ($\gamma < 10^{-6}$) for NO, NO_2, SO_2, Cl_2, and other species reported in this reference and Baldwin and Golden [34]. Back to Table

18. NO on $H_2O(s)$. NO data (Leu [294], Saastad et al. [391]) subject to same concerns as NO_2. See Note for NO_2 on $H_2O(s)$. Back to Table

19. NO on $H_2SO_4 \bullet nH_2O$. See Notes for H_2O_2 on $H_2SO_4 \bullet nH_2SO_4$ and NO_2 on $H_2SO_4 \bullet nH_2O$. NO is subject to the same concerns as NO_2 for both reported measurements (Saastad et al. [391]; Baldwin and Golden [33]). Back to Table

20. NO_2 on $H_2O(s)$. In the absence of a chemical sink, Leu [294] measured no sustained uptake of NO_2 on ice yielding an apparent $\alpha \leq 1 \times 10^{-4}$. Saastad et al. [391] measured a lower limit of 5×10^{-5} for temperatures between 193 and 243 K. However these values are probably influenced by surface saturation. Back to Table

21. NO_3 on $H_2O(l)$. Rudich et al. [388] analyzed uptake on KI solutions as a function of $[I^-]$ at 273 K. This work suggested that $\alpha > 0.04$, but this result may be biased due to reactive uptake by interfacial I^-. Back to Table

22. HONO on $H_2O(s)$. Fenter and Rossi [137] measured reversible uptake on water ice between 180 and 200 K using a Knudsen cell technique. An initial uptake coefficient of 1×10^{-3} suggests that α equals or exceeds this value. Chu et al. [86] used a cylindrical flow reactor to measure the uptake coefficient as a function of temperature, obtaining values ranging from 3.7×10^{-3} at 178 K to 6.4×10^{-4} at 200 K, in good agreement with the results of Fenter and Rossi. On the other hand, Chu et al. report significantly lower values after correction for the effects of surface porosity, i.e. 1.4×10^{-4} at 178 K and 1.3×10^{-5} at 200 K (see Keyser et al. [275]). Back to Table

23. HNO_3 on $H_2O(s)$. Leu [293] reports $\alpha = 0.3$ (+0.7, -0.1). Some additional uncertainty is introduced by effective ice surface area in fast-flow measurement (see Keyser et al. [275]). Hanson [191] measured an uptake coefficient of > 0.3 at 191.5 and 200 K. Aguzzi and Rossi [12] measured an uptake coefficient of 0.3 over the temperature range from 180 to 190 K, the value decreasing at T >195 with an exponential temperature dependence of -(3400 ± 500)/T. They attributed this change to an increasing evaporation rate, concluding that the accommodation coefficient most likely remains large. Abbatt [4] measured equilibrium uptake values at 208 – 248 K on the order of 1 to 3 x 10^{14} molecule cm^{-2}. Zondlo et al. [506] report the formation of a supercooled H_2O/HNO_3 liquid layer at 185 K, forming NAT or NAD only after decreasing the relative humidity below the ice frost point. Hynes et al. [235] measured uptake coefficients as a function of temperature decreasing from 0.03 at 215 K to 0.006 at 235 K. Hudson et al. [229] report initial uptake coefficients ranging from 0.007 at 209 K to 0.003 at 220 K. It appears, thus, that the uptake coefficient is large below 200 K and decreases rapidly as the temperature increases. Back to Table

24. HNO_3 on $H_2O(l)$. Measurements using a droplet train flow reactor show that α has a strong negative temperature dependence varying from 0.19 ± 0.02 at 268 K to 0.07 ± 0.02 at 293 K (Van Doren et al. [456]). Ponche et al. [357] measured a very consistent mass accommodation coefficient of 0.05 ± 0.01 at 297 K using the same technique. Sch tze and Herrmann [400] measured a lower limit of 3 x 10^{-2} at 298 K using a suspended droplet flow reactor method, consistent with the droplet train flow reactor measurements. Back to Table

25. HNO_3 on $HNO_3 \bullet nH_2O(s)$. Hanson [191] measured uptake coefficients of >0.3 and >0.2 on NAT surfaces at 191 K and 200 K, respectively. Middlebrook et al. [328] measured an uptake coefficient of 0.7 on NAT at 197 K under conditions where both nitric acid and water vapor were co-depositing. Back to Table

26. HNO_3 on $HNO_3 \bullet nH_2O(l)$. Rudolf and Wagner [390] used aerosol expansion chamber techniques to deduce that α for HNO_3 on 278 K H_2O/HNO_3 droplets is > 0.3 and probably close to 1. The consistency of this value with smaller (~0.2) values measured for uptake on pure water by Van Doren et al. [456] is unclear, since the mechanism of co-condensation is unknown and the composition of the surface in the aerosol expansion chamber experiments may be kinetically controlled and has not been well determined. Back to Table

27. HNO_3 on $H_2SO_4 \bullet nH_2O$ and $H_2SO_4 \bullet 4H_2O(s)$. Initial uptake at 73 wt.% H_2SO_4 allows a measurement of $\alpha = 0.11 \pm 0.01$ at 283 K (Van Doren et al. [456]). This value is expected to increase at lower temperatures,

in a manner similar to $H_2O(1)$ uptake (Van Doren et al. [455]). Total HNO_3 uptake is subject to Henry's law solubility constraints, even at stratospheric temperatures (Reihs et al. [365]). Solubility limitations also affected the earlier "sticking coefficient" measurements of Tolbert et al. [443] for 75 wt.% H_2SO_4 at 230 K. Hanson [191] measured an uptake coefficient of >0.3 for frozen 57.7 wt.% sulfuric acid at 191.5 and 200 K. Baldwin and Golden [33] reported a lower limit of 2.4×10^{-4} on 97 wt.% H_2SO_4 at 295 K, also reflecting solubility limits. Iraci et al. [240] monitored nitric acid trihydrate growth on sulfuric acid tetrahydrate with infrared techniques, measuring HNO_3 uptake coefficient limits of >0.03 at 192.5 K and >0.08 at 192 K. These measurements involved co-deposition of water vapor. Back to Table

28. HO_2NO_2 on $H_2O(s)$. Li et al. [302] measured an uptake coefficient of 0.15 ±0.10; uptake may be limited by surface saturation. Back to Table

29. HO_2NO_2 on $H_2SO_4 \bullet nH_2O(l)$. Baldwin and Golden [33] measured $\gamma = 2.7 \times 10^{-5,}$ which is probably solubility limited; see Note for H_2O_2 on $H_2SO_4 \bullet nH_2O$. Back to Table

30. NH_3 on $H_2O(l)$. Ponche et al. [357] used a droplet train technique to obtain $\alpha = (9.7 \pm 0.9) \times 10^{-2}$ at 290 K, and Bongartz et al.[62] used a liquid jet technique to obtain $\alpha = 4.0\ (+3.0, -0.05) \times 10^{-2}$ at the same temperature. These experiments where extended to other temperatures by Carstens et al. [80], demonstrating a negative temperature dependence. Ammonia uptake on liquid water as a function of both pH and temperature was investigated by Shi et al. [415] using a droplet train apparatus, yielding values that also demonstrated negative temperature dependence, varying between 0.08 at 290 K to 0.35 at 260 K. The data from these four studies are all in reasonable agreement and a temperature dependent data plot with a non-linear least squares fit to all of these measurements has been published by Worsnop et al. [482]. Earlier levitated droplet evaporation experiments [438] on NH_4Cl obtained a larger evaporation coefficient of $\alpha = 0.29 \pm 0.03$, which is discounted because of the indirect nature of the experiment. Back to Table

31. CO_2 on $H_2O(l)$. Noyes et al. [348] used a dynamic stirring technique to monitor pressure decreases in a closed cylinder. They inferred $\alpha = (5.5 \pm 0.5) \times 10^{-8}$ at 293 K. This technique is uncalibrated against more widely used procedures and probably suffers from severe surface saturation effects. Schurath et al. [399] employed a coaxial jet flow technique to measure a 298K value of α of $1\text{-}2 \times 10^{-4}$, noting that its low Henry's law solubility in water made the measurement very difficult. For this reason the measurement probably also suffered from surface saturation even at their shortest gas/liquid contact times, so this value is most likely a lower limit. Boniface et al. [63] used a bubble train reactor to study the uptake by water as a function of pH. At high pH the reaction of CO_2 with OH^- partially relieves surface saturation allowing determination that the uptake coefficient, and therefore α, is $\geq 1 \times 10^{-5}$, consistent with the value measured by Schurath et al. and completely inconsistent with the much lower value obtained by Noyes et al. [348]. Back to Table

32. CH_3OH on $H_2O(l)$. Jayne et al. [246] measured uptake from 260–291 K and derived accommodation coefficients fitting $\alpha/(1-\alpha) = \exp(-\Delta G_{obs}/RT)$, where $\Delta G_{obs} = -8.0$ kcal/mol + 34.9 cal mol^{-1} K^{-1} T(K). Back to Table

33. CH_3CH_2OH on $H_2O(l)$. Jayne et al. [246] measured uptake from 260–291 K with a droplet train flow reactor and derived mass accommodation coefficients fitting $\alpha/(1-\alpha) = \exp(-\Delta G_{obs}/RT)$, where $\Delta G_{obs} = -11.0$ kcal/mol + 46.2 cal mol^{-1} K^{-1} T(K). Similar, but somewhat larger values were reported for chloro-, bromo-, and iodo-ethanols. Shi et al. [416] used the same technique to measure the uptake of both normal and deuterated ethanol over the temperature range of 263-291 K as a function of pH. Normal ethanol uptake was not dependent on pH, while the uptake of the deuterated species was enhanced by surface isotopic exchange, especially at high and low pH. The mass accommodation values obtained for normal ethanol obtained by Shi et al. ranged from 0.128±0.023 at 263 K to 0.057±0.005 are consistent, within experimental error, with the lowest temperature value measured by Jayne et al., but are significantly higher above ~275 K. Katrib et al. [269] also used the droplet train technique to measure the ethanol mass accommodation coefficient between ~266 and 281 K, obtaining lower values than those measured by Shi et al., [416] but agreeing with the higher temperature data of Jayne et al. [246]. Katrib et al. obtained mass accommodation coefficients fitting $\alpha/(1-\alpha) = \exp(-\Delta G_{obs}/RT)$, where $\Delta G_{obs} = -(5.6 \pm 1.5)$ kcal/mol + (27.4 ± 5.5) cal mol^{-1} K^{-1} T(K). While the data of Shi et al. and Katrib et al. are off-set by about a factor of three, the negative temperature dependencies measure by the two groups are very similar. The differences between the three data sets are difficult to explain, given that all three used essentially the experimental same technique; the recommended lower limit is consistent with the lower values measured by Katrib et al. [269]. Back to Table

34. $CH_3CH_2CH_2OH$ and $CH_3CH(OH)CH_3$ on $H_2O(l)$. Jayne et al. [246] measured uptake coefficients between 260 and 291 K and derived accommodation coefficients fitting $\alpha/(1-\alpha) = \exp(-\Delta G_{obs}/RT)$, where $\Delta G_{obs} = -9.2$ kcal mol^{-1} + 40.9 cal mol^{-1} K^{-1} T(K) for 1-propanol and –9.1 kcal mol^{-1} + 43.0 cal mol^{-1} K^{-1} T(K) for 2-propanol. Similar data for t-butanol were also reported. Back to Table

35. $HOCH_2CH_2OH$ on $H_2O(l)$. Jayne et al. [246] measured uptake coefficients for ethylene gycol between 260 and 291 K and derived accommodation coefficients fitting $\alpha/(1-\alpha) = \exp(-\Delta G_{obs}/RT)$, where $\Delta G_{obs} = -5.3$ kcal mol^{-1} + 24.5 cal mol^{-1} K^{-1} T(K). Back to Table

36. CH_3O_2 on NaCl(s). Gershenzon et al. [165] measured the uptake of CH_3O_2 on crystalline NaCl(s) in a central rod flow apparatus. They determined a value of $\gamma = (4 \pm 1) \times 10^{-3}$ at 296 K, suggesting that $\alpha \geq 4 \times 10^{-3}$. Back to Table

37. CH_3OOH on $H_2O(l)$. Magi et al. [314] used a droplet train flow reactor to measure α over a temperature range of 261-281 K, showing a negative temperature dependence with values ranging from 9.2×10^{-3} at 281 to 20.8×10^{-3} at 261 K. Allowing for measurement uncertainty produces a recommendation that $\alpha \geq 7 \times 10^{-3}$ from 260 to 282 K. Back to Table

38. CH_2O on $H_2O(l)$ and $H_2SO_4 \bullet mHNO_3 \bullet nH_2O(l)$. Jayne et al.[249] report uptake measurements for 0 – 85 wt.% H_2SO_4 and 0 – 54 wt.% HNO_3 over a temperature range of 241–300 K. Measured uptake coefficients vary from 0.0027–0.027, increasing with H^+ activity (Jayne et al ([249]; Tolbert et al., [441]), and with increasing pH above 7 (Jayne et al., [247]). Reversible uptake is solubility limited through reactions to form $H_2C(OH)_2$ and CH_3O^+. A model of uptake kinetics (Jayne et al., [249]) is consistent with $\gamma = 0.04 \pm 0.01$ for all compositions. A chemisorbed surface complex dominates uptake at 10 – 20 wt.% H_2SO_4, and CH_3O^+ formation dominates above 20 wt.% (Tolbert et al., [441]; Jayne et al. [249], Iraci and Tolbert [241]). Low temperature (197–214 K) uptake studies by Iraci and Tolbert [241] confirm that uptake is solubility limited for uptake coefficients in the 10^{-3} to 10^{-2} range even at low temperatures. These chemical mechanisms allow γ to greatly exceed α for strong acidic and basic solutions. A full uptake model for acid solutions is presented in Jayne et al. [249], and for basic solutions in Jayne et al. [247]. XPS surface analysis by Fairbrother and Somorjai [132] failed to see CH_3O^+ surface species reported by Jayne et al.; however, their sensitivity of 1% of surface coverage is too poor to see the predicted amounts of the surface species. Back to Table

39. CH_3CHO on $H_2O(l)$. Jayne et al. [247] measured a lower accommodation coefficient limit of > 0.03 at 267 K. Uptake can be limited by Henry's law and hydrolysis kinetics effects—see reference. Back to Table

40. CH(O)CH(O) on H_2O (l). Schweitzer et al. [406] used a droplet train flow reactor to investigate the uptake of glyoxyl by water droplets over a temperature range of 263-283 K; measured uptake was near their detection limit. They reported an average α over their experimental temperature range of $2.3\ (+1.1/-0.7) \times 10^{-2}$. Back to Table

41. $CH_3C(O)CH_3$ on $H_2O(l)$. Duan et al. [125] measured uptake between 260 and 285 K, deriving $\alpha = 0.066$ at the lower temperature and 0.013 at the higher, with several values measured in between. Measured values fit $\alpha/(1-\alpha) = \exp(-\Delta G_{obs}/RT)$, where $\Delta G_{obs} = -12.7$ kcal/mol + 53.6 cal mol^{-1} K^{-1} T(K). Sch tze, M. and H. Herrmann [401] used a single suspended droplet flow reactor to measure the uptake of acetone and several larger carbonyl compounds at 293 K; their value for acetone of $\alpha = 5.4(+4.5/-2.6) \times 10^{-3}$ agrees well with the values of Duan et al. extrapolated to 293 K. Back to Table

42. $CH_3C(O)CHO$ on $H_2O(l)$. Sch tze and Herrmann [401] used a single suspended droplet flow reactor to measure the uptake of 2-oxypropynal at 293 K, their value of $\alpha = (1.5 \pm 0.5) \times 10^{-4}$ is lower than those measured for acetone and acetaldehyde. Back to Table

43. $CH_3OC(O)OCH_3$ on $H_2O(l)$. Katrib et al. [268] measured the uptake of dimethyl carbonate on pure water and 0.1M aqueous NaOH over a temperature range of 270-278 K using a droplet train flow reactor. Uptake was not obviously dependent on $[OH^-]$ and displayed a negative temperature dependence with individual measurements varying from $(11 \pm 2) \times 10^{-2}$ at 270 K to $(1.2 \pm 0.9) \times 10^{-2}$ at 276 K. Although the data are fairly noisy the authors derived a mass accommodation coefficient fitting of $\alpha/(1-\alpha) = \exp(-\Delta G_{obs}/RT)$, where $\Delta G_{obs} = -(26 \pm 9)$kcal mol^{-1} + (99±35) cal mol^{-1} K^{-1} T(K). Similar mass accommodation data for diethyl carbonate are also presented. Back to Table

44. HC(O)OH on $H_2O(l)$. Jayne et al. [246] measured uptake coefficients for formic acid between 260 and 291 K and derived accommodation coefficients fitting $\alpha/(1 - \alpha) = \exp(-\Delta G_{obs}/RT)$, where $\Delta G_{obs} = -7.9$ kcal mol^{-1} + 34.9 cal mol^{-1} K^{-1} T(K). Back to Table

45. $CH_3C(O)OH$ on $H_2O(l)$. Jayne et al. [246] using a droplet train flow reactor measured uptake coefficients for acetic acid between 260 and 291 K and derived a mass accommodation coefficient fitting $\alpha/(1-\alpha) = \exp(-\Delta G_{obs}/RT)$, where $\Delta G_{obs} = -8.1$ kcal mol^{-1} + 34.9 cal mol^{-1} K^{-1} T(K). Shi et al. [416] used the same technique to measure the uptake of both normal and deuterated acetic acid at 258 K and pH=7. They obtained α= 0.19 (± 0.03) for normal acetic acid, while the uptake coefficient of the deuterated species was enhanced by surface isotopic exchange, equaling 0.96 (± 0.21). Back to Table

46. Cl_2 on $H_2O(s)$. Measurement of Leu [293] yielded a limit of $<1 \times 10^{-4}$ for Cl_2 and is subject to same concern as NO_2 (see note). A similar limit of $<5 \times 10^{-5}$ has been measured by Kenner et al. [271], which is also probably limited by surface saturation. Back to Table

47. OClO + $H_2O(s)$. Brown et al. [67] and Graham et al. [177] used complementary ultra high-vacuum (UHV) and coated-wall flow tube techniques to show sub-monolayer reversible absorption of OClO on water ice at 100 K (UHV) and 189 and 200 K (flow tube). No kinetic data are available at stratospheric temperatures but the mass accommodation coefficient for 100 K ice surfaces is near unity, with values of 0.8 ± 0.2 reported for amorphous ice and 0.6 ±0.2 for crystalline ice [177]. Back to Table

48. HCl on $H_2O(s)$. Leu [293] (0.4; +0.6, –0.2) and Hanson and Ravishankara, [202] ($\alpha \geq 0.3$) are in reasonable agreement at stratospheric ice temperatures. More recently, a great deal of experimental effort (Abbatt et al. [6], Koehler et al. [286], Chu et al. [89], Graham and Roberts [175], Graham and Roberts [176]; Rieley et al. [369]) has gone into understanding the uptake of HCl by ice surfaces. Rieley et al. measured $\alpha = 0.95 \pm 0.05$ at 80–120 K. Water ice at stratospheric temperatures can take up a large fraction of a monolayer even at HCl partial pressures typical of the stratosphere. Both the thermodynamic and spectroscopic properties of this absorbed HCl indicate that it has dissociated to ions, forms ionic hydrates, and is highly reactive. These experimental results contrast with initial theoretical calculations that predicted undissociated HCl hydrogen bonded to the ice surface and a very small adsorption probability at stratospheric temperatures (Kroes and Clary [289]); more recent simulations result in higher adsorption energies and theoretical accommodation coefficients of one for 190-K surfaces (Wang and Clary [466]). Recent molecular dynamics calculations by Gertner and Hynes [168] also show that ionic absorption is thermodynamically favorable by about 5 kcal/mole. At HCl partial pressures significantly above those typical of the stratosphere, a liquid surface layer forms on the ice, greatly enhancing the total amount of HCl that the surface can absorb. Back to Table

49. HCl on $H_2O(1)$. Recommendation is based on Van Doren et al. [455] and Schweitzer et al. [409]. Using a droplet train flow reactor, Van Doren et al. [455] measured α's decrease from 0.18 ± 0.02 at 274 K to 0.064 ± 0.01 at 294 K, demonstrating strong negative temperature dependence. Schweitzer et al. [409] used the same technique over a temperature range of 262 to 281 K obtaining values decreasing from 0.24 to 0.13 that agree very well with the Van Doren et al. data. Tang and Munkelwitz [438] have measured a larger (0.45 ±0.4) HCl evaporation coefficient for an aqueous NH_4Cl droplet at 299 K. Back to Table

50. HCl on $HNO_3 \cdot nH_2O$. There was previously severe disagreement between Hanson and Ravishankara [202] ($\alpha \geq 0.3$) for NAT (54 wt.% HNO_3), and Leu and coworkers (Moore et al. [337], Leu et al. [295]). However, subsequent experiments at lower HCl concentrations by Leu and coworkers (Chu et al. [89]) as well as Abbatt and Molina [8] are generally consistent with Hanson and Ravishankara. In particular, Abbatt and Molina [8] report a large uptake coefficient ($\alpha > 0.2$). The measurements of Hanson and Ravishankara are consistent with $\alpha = 1$. The experiments at stratospherically representative HCl concentrations show that HNO_3-rich NAT surfaces adsorb significantly less HCl than H_2O-rich surfaces. Back to Table

51. HCl on $H_2SO_4 \cdot nH_2O$. Measurements by Watson et al. [469] at 284 K show $\alpha = 0.15 \pm 0.01$ independent of n for $n \geq 8$. Experimental uptake and, therefore, apparent α falls off for $n \leq 8$ ($\geq$40 wt.% H_2SO_4). This behavior is also observed at stratospheric temperature (218 K) by Hanson and Ravishankara [202]. More recent measurements by Robinson et al. [377] extend mass accommodation measurements to lower temperatures, yielding significantly higher values. Solubility constraints also controlled earlier low temperature uptake measurements of Tolbert et al. [443]. A review of the most recent solubility data is presented in Table 5-6. Back to Table

52. HCl on $H_2SO_4 \cdot 4H_2O(s)$. Uptake is a strong function of temperature and water vapor partial pressure (relative humidity) (Zhang et al. [502]), both of which affect adsorbed surface water. Back to Table

53. $ClONO_2$ on $H_2O(1)$. Dieber et al. [119] used a droplet train apparatus to measure the uptake of $ClONO_2$ on NaBr aqueous solutions to deduce the mass accommodation coefficient of 0.108±0.011 at 274.5 K. This value may be affected by the reaction with interfacial Br^-. Back to Table

54. Halocarbonyls on $H_2O(l)$. Uptake is limited by Henry's law solubility and hydrolysis rate constants (De Bruyn et al. [114, 116] and Georg et al. [159, 161]. Back to Table

55. HBr on $H_2O(s)$ and $HNO_3 \bullet nH_2O$. Hanson and Ravishankara [201, 203] have reported large uptake coefficients for HBr on 200-K ice and NAT. Lower limits of >0.3 and >0.2 for ice are reported in the two referenced publications, respectively, and a limit of >0.3 is reported for NAT. No surface saturation was observed, leading to the supposition that HBr, like HCl, dissociates to ions on ice surfaces at stratospheric temperatures. Abbatt [1] measured an uptake coefficient lower limit of >0.03 on water ice at 228 K consistent with Hanson and Ravishankara. Rieley et al. [369] measured an α of 1.0 ± 0.05 for water ice at 80–120 K. Fl ckiger et al. [148] report α values of ~0.2 at 210 K, increasing to ~0.3 at 190 K, while Percival et al. [355] measured an α of 0.03 ± 0.005 for water ice at T > 212 K, and α > 0.1 at T< 212 K, attributing the apparent increase in the uptake coefficient to an increase in the surface area of the ice. More definitive experiments will need to be carried out to resolve the discrepancy. Hudson et al. [228] report α = 0.61 ± 0.06 at 140 K, and α = 0.24 ± 0.05 at 100 K, for HBr pressures ranging from 3×10^{-8} to 1.4×10^{-7} Torr. Equilibrium HBr coverages for ice are reported by Chu and Heron [88] at 188 and 195 K, and by Chu and Chu [84] at 180–220 K. The latter authors also report the formation of various solid HBr hydrates. Back to Table

56. HBr on $H_2O(1)$. Schweitzer et al. [409] used the droplet train flow reactor technique over a temperature range of 262 to 281 K obtaining values decreasing from 0.16 to 0.0.68. Li et al. [301] and Zhang et al. [494] used the same technique to measure higher values of 0.14±0.02 at 283 K and 0.21± 0.3 at 273 K, respectively. Given the good agreement between the two groups for HCl mass accommodation coefficients on water, there is no obvious reason for the discrepancy of a factor of 2-3 for HBr. Back to Table

57. HOBr on $H_2O(s)$. Abbatt [1] measured an uptake coefficient for water ice of 2×10^{-3} at 228 K. Chu and Chu [84] report an uptake coefficient corrected for porosity effects in the range 0.11 to 0.007 at 190–218 K, with an exponential temperature dependence of (3809 ± 76)/T, and in the range 2×10^{-3} to 6×10^{-4} at 223-239 K, with an exponential temperature dependence of (4658 ± 456)/T. Chaix et al. [81] measured the uptake coefficient as a function of temperature on three different types of water-ice, obtaining values ranging from ~0.3 at 185 K to ~0.03 at 205 K, with an exponential temperature dependence of (4900 ± 500)/T. Mössinger et al. [338] report an uptake coefficient value of 0.003 at 227 K increasing to 0.040 at 205 K. The four sets of results are in reasonable agreement with each other, and the temperature dependence of the uptake coefficient is attributed predominantly to changes in the evaporation rate. The results indicate that the uptake of HOBr on ice cannot be explained with Langmuir-type adsorption isotherms and that the process is not reversible, possibly involving the formation of hydrates. Using a common precursor model, Fl ckiger and Rossi [147] have estimated accommodation coefficients α which are considerably larger than the measured uptake coefficients, with α values ranging from 0.18 at 215 K to 0.46 at 190 K. Back to Table

58. HOBr on $H_2O(l)$. See Note on HOBr + KBr and NaBr in reactive uptake table. Back to Table

59. HOBr on $H_2SO_4 \bullet nH_2O(l)$. Abbatt [1] measured an uptake coefficient of 0.06 ± 0.02 by measuring HOBr gas phase loss at 228 K. This result may well be a lower limit due to surface saturation effects. Back to Table

60. $BrONO_2$ on $H_2O(1)$. Dieber et al. [119] used a droplet train apparatus to measure the uptake of $BrONO_2$ on NaBr aqueous solutions to deduce the mass accommodation coefficient of 0.063±0.021 at 274.5 K. This value may be affected by the reaction with interfacial Br^-. Back to Table

61. $BrONO_2$ on $H_2SO_4 \bullet nH_2O$. Hanson [188] modeled wetted-wall flow reactor data and aerosol flow reactor data to estimate α = 0.80 over a wide range of temperatures and acid concentrations. Back to Table

62. $CHBr_3$ on $H_2O(s)$ and $H_2SO_4 \bullet nH_2O(l)$. Hanson and Ravishankara [203] investigated the uptake of bromoform on ice and 58 wt.% sulfuric acid at 220 K. No uptake on ice was observed, with a measured uptake coefficient of $<6 \times 10^{-5}$. Reversible uptake by the sulfuric acid surface was observed with an initial uptake coefficient of $>3 \times 10^{-3}$; both measurements are probably limited by surface saturation. Back to Table

63. BrCl on $H_2O(1)$. Katrib et al. [267] used a droplet train flow reactor to measure the uptake of BrCl as a function of NaOH concentration over the temperature range of 270-285 K. Data were too noisy to assign a clear temperature dependence, but an average over measurements at 270, 274, 280 and 285 K for higher

[NaOH} where reactive scavenging relieved solubility constraints yielded $\alpha = 0.33 \pm 0.18$. The recommended lower limit is consistent with this value. Back to Table

64. I_2 on $H_2O(1)$. Takami et al. [436] used the impinging flow techique to investigate the uptake of I_2 at 293 K as a function of pH. While solubility constraints prevented a clear measure of mass accommodation, they modeled high pH data where solubility constraints were relaxed by reactive scavenging by OH^- to determine that $\alpha \geq 0.1$. Back to Table

65. HI on $H_2O(1)$. Schweitzer et al. [409] used the droplet train flow reactor technique over a temperature range of 262 to 281 K, obtaining values decreasing from 0.19 to 0.079. Zhang et al. [494] used the same technique to obtain a value of 0.17 ± 0.02 at 273 K, which is a little less than a factor of two higher than indicated by the Schweitzer et al. measurements for that temperature. Back to Table

66. HOI on $H_2SO_4 \bullet nH_2O$. Knudsen cell studies by Allanic and Rossi [24] measured uptake at several temperatures for 40, 50, and 70 acid wt.%. Time dependent studies show no sign of saturation, so uptake coefficients should correspond to mass accommodation coefficients. Some acid concentration data in the table have been averaged for similar temperatures and rounded to one significant figure. An uncertainty factor of three has been assigned due to the relatively small number of temperature/concentration points studied and a lack of confirming studies from other laboratories. The authors note evidence of HOI disproportionation to form I_2, however, this second order reaction is unlikely to occur under atmospheric conditions. Back to Table

67. HF on $H_2O(s)$ and $HNO_3 \bullet nH_2O(s)$. Hanson and Ravishankara [201] attempted to measure the uptake of HF by 200 K water ice and NAT surfaces but were unable to observe measurable adsorption. They surmise that, unlike HCl and HBr, HF does not dissociate to ions on ice or NAT surfaces at 200 K. Lack of measurable uptake is probably due to surface saturation. Back to Table

68. CF_2O on $H_2O(s)$, $HNO_3 \bullet nH_2O$ and $H_2SO_4 \bullet nH_2O$. Uptake coefficient measurements by Hanson and Ravishankara [199] on stratospheric surfaces are probably subject to surface and/or bulk saturation effects and may not represent accommodation coefficient measurements, particularly the lower limits of $>3 \times 10^{-6}$ reported for water and nitric acid ices. Back to Table

69. CF_3COOH on $H_2O(l)$. Hu et al. [227] measured mass accommodation coefficients for five haloacetic acids, including trifluoroacetic acid (TFA); the others were mono-, di-, trichloro-, and chlorodifluoro-acetic acids. All displayed negative temperature dependence and values for α of about 0.1 at 273 K. Back to Table

70. SO_2 on $H_2O(1)$. Using a droplet train flow reactor Worsnop et al.measured an α of 0.11 ± 0.02 with no significant temperature variation over a temperature range of 260–292 K (Worsnop et al. [483]). Ponche et al. [357] measured 0.13 ± 0.01 at 298 K, in agreement with the earlier measurement. Shimono and Koda [417] estimated an α of 0.2 at 293.5 K from analysis of pH-dependent uptake coefficients in a liquid impingement technique. Schurath et al. [399] used a coaxial flow liquid jet to obtain a value of 0.1 at 298 K. Boniface et al. [63] performed more extensive droplet train flow reactor measurements at high pH to relieve solubility constraints, obtaining a negative temperature dependence with α values ranging from 0.43 ± 0.4 at 264 K to 0.175 ± 0.015 at 291 K, their data can be fit to $\alpha/(1-\alpha) = \exp(-\Delta G_{obs}/RT)$, where $\Delta G_{obs} = -(7.6 \pm 0.6)$ kcal/mol + (29.2 ± 2.1) cal mol^{-1} K^{-1} T(K). Donaldson et al. [123] have used second harmonic generation spectroscopy to detect a chemisorbed SO_2 surface species which was predicted from earlier uptake measurements by Jayne et al. [245]; this surface complex may play a role in SO_2 heterogeneous reactions on aqueous surfaces. Back to Table

71. SO_2 on $H_2SO_4 \bullet nH_2O$. See Note for H_2O_2 on $H_2SO_4 \bullet nH_2O$. Back to Table

72. H_2S on $H_2O(1)$. Boniface et al. [63] performed droplet train flow reactor measurements over at 260-298 K at high pH to relieve solubility constraints, measured uptake coefficients were consistent with $\alpha \geq 0.05$. Back to Table

73. H_2SO_4 on $H_2SO_4 \bullet nH_2O$. Poschl et al. [358] measured $0.43 < \alpha < 1.0$ for 73–98 wt.% H_2SO_4 at 303 K in a wetted wall flow tube. Lower temperatures and acid concentrations would be expected to lead to larger values of α. As discussed in Poschl et al. [358] this contradicts an indirect measurement of $0.02 < \alpha < 0.09$ at 42.5 wt.% at 298 K by Van Dingenen and Raes [454] in a photochemical aerosol reactor. The Poschl et al. [358] result is consistent with room temperature α values very near that measured for $(NH_4)_2SO_4$ particles in an aerosol flow reactor by Jefferson et al. [250]. Back to Table

74. $CH_3S(O)CH_3$, $CH_3S(O_2)CH_3$ and $CH_3S(O_2)OH$ on $H_2O(l)$. De Bruyn et al. [115] measured uptake over the temperature range ~262–281 K and derived accommodation coefficients fitting $\alpha / (1 - \alpha) = \exp(-\Delta G_{obs}/RT)$, where ΔG_{obs} =

- –0.12 kcal molecule^{-1} + 23.1 cal molecule^{-1} K^{-1} T(K) for dimethylsulfoxide
- –10.7 kcal molecule^{-1} + 43.0 cal molecule^{-1} K^{-1} T(K) for dimethylsulfone
- –3.50 kcal molecule^{-1} + 16.7 cal molecule^{-1} K^{-1} T(K) for methanesulfonic acid.

Schweitzer et al. [406] used a droplet train flow reactor to investigate the uptake of $CH_3S(O_2)OH$ by water over a temperature range of 262-281 K, obtaining mass accommodation coefficient values decreasing from 0.17 to 0.11, in excellent agreement with those obtained by De Bruyn et al. [115]. Back to Table

5.13 Gas/Surface Reaction Probabilities for Surfaces Other Than Soot

Table 5-2. Gas/Surface Reaction Probabilities (γ) for Surfaces Other Than Soot

Gaseous Species	Surface Type	Surface Composition	T(K)	γ	Uncertainty Factor	Notes
O_3 + Surface → Products						
O_3	Alumina	$Al_2O_3(s)$	210–300	$\gamma_o<2\times10^{-4}$		1
	Sodium Chloride	NaCl(s)	223-300	$\gamma_o<10^{-4}$		2
		NaCl(aq)	298	$\gamma_o<10^{-4}$		2
	Sodium Bromide	NaBr(s)	300	$\gamma_o<10^{-4}$		3
		NaBr(aq)	298	See Note		3
	Potaassium Bromide	KBr(s)	300	$\gamma_o<10^{-4}$		3
	Sea Salt	See Note	300	$\gamma_o<2 \times 10^{-2}$		4
OH + Surface →Products						
OH	Water Ice	$H_2O(s)$	205–230	>0.01		5
	Hydrochloric Acid	$HCl \cdot nH_2O(l)$	220	>0.2		6
	Nitric Acid Ice	$HNO_3 \cdot 3HzO(s)$	200–228	>0.2		7
	Sulfuric Acid	$H_2SO_4 \cdot nH_2O(l)$	200–298	>0.2		7
	Sodium Chloride	NaCl(s)	245–300	$\gamma_o\sim10^{-2}$	3	8
		NaCl(aq)	298	See Note		9
	Alumina	$Al_2O_3(s)$	250-300	$\gamma_o<0.1$		10
HO_2 + Surface →Products						
	Water Ice	$H_2O(s)$	223	0.025	3	11
	Sulfuric Acid	$H_2SO4 \cdot nH_2O(l)$				11
		(28 wt.%)	275	>0.07		
		(55 wt.%)	223	>0.05		
		(80–96 wt.%)	243	>0.2		
	Sodium Chloride	NaCl(s)	245-300	See Note		12
	Potassium Chloride	KCl(s)	295	See Note		12
H_2O + Surface →Products						
H_2O	Alumina	αAl_2O_3	295-300	$\gamma_o<0.2$		13
$2NO_2 + H_2O(l) \rightarrow HONO + HNO_3$						
NO_2	Liquid Water	$H_2O(l)$	270-295	$<1 \times 10^{-3}$		14
	Sulfuric Acid	$H_2SO_4 \cdot nH_2O$ (40–98 wt.%)	250–325	5×10^{-7}	3	15
		γAl_2O_3	298	$\gamma_o <1\times10^{-7}$		16
		αAl_2O_3	298	$\gamma_o <5\times10^{-5}$		16
$2NO_2$ (N_2O_4) + MX →Products						
NO_2/N_2O_4	Sodium Chloride	NaCl(s)	298	See Note		17
		NaCl(aq)	298	$<1 \times 10^{-4}$		17
	Sodium Bromide	NaBr(s)	298	See Note		18
	Sea Salt	See Note for O_3 + Sea Salt	298	See Note		19
$NO_3 + H_2O \rightarrow HNO_3 + OH$						
NO_3	Water Ice	$H_2O(s)$	170–200	$<10^{-3}$		20
	Liquid Water	$H_2O(l)$	273	2×10^{-4}	20	21
NO_3 + NaX →Products						
NO_3	Sodium Chloride	NaCl(s)	293	$\gamma_o <6\times10^{-2}$		22
		NaCl(aq)	273-293	See Note		22
	Sodium Bromide	NaBr(s)	293	$\gamma_o=0.2\pm0.1$	2	23
		NaBr(aq)	273	See Note		23
	Sodium Iodide	NaI(aq)	273	See Note		23
$N_2O_5 + H_2O \rightarrow 2HNO_3$						
N_2O_5	Water Ice	$H_2O(s)$	188–195	0.02	2	24
	Liquid Water	$H_2O(l)$	260–295	See Note	See Note	25
	Nitric Acid Ice	$HNO_3 \cdot 3H_2O(s)$	200	4×10^{-4}	3	26
	Sulfuric Acid	$H_2SO_4 \cdot nH_2O(l)$	195–300	See Note*	See Note	27
	Sulfuric Acid Monohydrate	$H_2SO_4 \cdot H_2O(s)$	200–300	See Note	3	28
	Sulfuric Acid Tetrahydrate	$H_2SO_4 \cdot 4H_2O(s)$	195–207	0.006	2	29
	Ternary Acid	$H_2SO_4 \cdot nHNO_3 \cdot nH_2O(l)$	195–218	See Note		27

Gaseous Species	Surface Type	Surface Composition	T(K)	γ	Uncertainty Factor	Notes
$N_2O_5 + HCl \rightarrow ClNO_2 + HNO_3$						
N_2O_5	Water Ice Nitric Acid Ice Sulfuric Acid Monohydrate	$H_2O(s) \cdot HCl(s)$ $HNO_3 \cdot 3H_2O(s) \cdot HCl(s)$ $H_2SO_4 \cdot H_2O(s)$	190–220 200 195	0.03 0.003 $<1 \times 10^{-4}$	See Note 2	30 31 32
$N_2O_5 + HBr \rightarrow BrNO_2 + HNO_3$						
N_2O_5	Water Ice Nitric Acid Ice	H_2O $HNO_3 \cdot 3H_2O(s)$	180–200 200	See Note 0.005	 10	33 34
$N_2O_5 + MX \rightarrow$ Products						
N_2O_5	Sodium Chloride Potassium Bromide Sodium Bromide Sodium Iodide Sea Salt	NaCl(s) NaCl(aq) KBr(s) NaBr(aq) NaI(aq) See Note for O_3 _ Sea Salt	295 262-291 298 270-277 262-278 295	$\gamma_o < 5\times10^{-3}$ $\gamma_o < 0.05$ $\gamma_o < 5\times10^{-3}$ $\gamma_o < 0.05$ $\gamma_o < 0.05$ See Note		35 35 36 36 36 37
$HONO + H_2O \rightarrow$ Products						
HONO	Liquid Water	$H_2O(l)$	245-295	0.03	5	38
$HONO + H_2SO_4 \rightarrow$ Products						
HONO	Sulfuric Acid	$H_2SO_4 \cdot nH_2O(l)$	180–200	See Note		39
$HONO + HCl \rightarrow ClNO + H_2O$						
HONO	Water Ice Sulfuric Acid	$H_2O(s)$ $H_2SO_4 \cdot nH_2O(l)$	180–200	0.05 See Note	3 See Note	40 41
$HONO + NaCl \rightarrow$ Products						
HONO	Sodium Chloride	NaCl(s)	~300	$<1 \times 10^{-4}$		42
$HNO_3 + NaX(s) \rightarrow HX + NaNO_3$						
HNO_3	Sodium Chloride Sodium Bromide Potassium Bromide Sea Salt	NaCl(s) NaCl(aq) NaBr(s) KBr(s) See Note for O_3 + Sea Salt	295–298 298 298 298 298	$\gamma_o = 2\times10^{-3}$ $\gamma_o > 0.1$ $\gamma_o < 3\times10^{-2}$ $\gamma_o < 3\times10^{-2}$ $\gamma_o > 0.1$	2	43 43 44 44 45
$HNO_3 + Al_2O_3(s) \rightarrow$ Products						
Al_2O_3	Alumina	αAl_2O_3	295-300	$\gamma_o < 0.2$		46
$HO_2NO_2 + HCl \rightarrow$ Products						
HO_2NO_2	Sulfuric Acid	$H_2SO_4 \cdot nH_2O$ (50–75 wt.%)	200–225	$<1 \times 10^{-4}$		47
$NH_3 + H_2SO_4 \rightarrow NH_4HSO_4$						
NH_3	Sulfuric Acid	$H_2SO_4 \cdot nH_2O$ < 50 wt.% 50-70 wt.%	 260-300 260-300	 See Note 1.0	 1.2	48
$H_2CO + Al_2O_3 \rightarrow$ Products						
H_2CO	Alumina	Al_2O_3	290-300	$\gamma_o < 2\times10^{-5}$		49
$CH_3OH + Al_2O_3 \rightarrow$ Products						
CH_3OH	Alumina	Al_2O_3	290-300	$\gamma_o < 3\times10^{-4}$		49
$CH_3COOH + Al_2O_3 \rightarrow$ Products						
CH_3COOH	Alumina	Al_2O_3	290-300	$\gamma_o < 1\times10^{-2}$		49
$CH_3CHO + Al_2O_3 \rightarrow$ Products						
CH_3CHO	Alumina	Al_2O_3	290-300	$\gamma_o < 6\times10^{-5}$		49
$CH_3CH_2CHO + Al_2O_3 \rightarrow$ Products						
CH_3CH_2CHO	Alumina	Al_2O_3	290-300	$\gamma_o < 9\times10^{-5}$		49
$CH_3C(O)CH_3 + Al_2O_3 \rightarrow$ Products						
$CH_3C(O)CH_3$	Alumina	Al_2O_3	290-300	$\gamma_o < 4\times10^{-5}$		49
$CH_3C(O)O_2 + H_2O \rightarrow CH_3C(O)OH + HO_2$						

Gaseous Species	Surface Type	Surface Composition	T(K)	γ	Uncertainty Factor	Notes
$CH_3C(O)O_2$	Liquid Water	$H_2O(l)$	225	4×10^{-3}	3	50
	Sulfuric Acid	$H_2SO_4 \cdot nH_2O$				50
		(84 wt.% H_2SO_4)	246	3×10^{-3}	3	
		(51 wt.% H_2SO_4)	223	1×10^{-3}	3	
		(71 wt.% H_2SO_4)	298	1×10^{-3}	3	
$CH_3C(O)O_2NO_2$ + HCl, Cl, ClO, and OClO → Products						
$CH_3C(O)O_2NO_2$	Sulfuric Acid	H2SO4 • nH2O (40–70 wt.%)	200–225	$<1 \times 10^{-4}$		51
Cl + Surface →Products						
Cl	Sulfuric Acid	$H_2SO_4 \cdot nH_2O(l)$	221–296	2×10^{-4}	10	52
Cl_2 + HBr →BrCl + HCl						
Cl_2/HBr	Water Ice	$H_2O(s)$	200	>0.2		53
Cl2 + MX →Products						
Cl_2	Sodium Chloride	NaCl(s)	298	$\gamma_o < 1 \times 10^{-3}$		54
	Sodium Bromide	NaBr(s)	298	0.02		55
				γ_o <0.2; See Note		
		NaBr(aq)	263-293	γ_o <0.3		55
	Sodium Iodide	NaI(aq)	263-293	γ_o <0.3		55
	Potassium Bromide	KBr(s)	298	0.02		56
	Sea Salt	See Note for O_3 + Sea Salt	298	$<\gamma_o$ <0.2; See Note		57
ClO + Surface →Products						
ClO	Water Ice	$H_2O(s)$	190	See Note		58
	Nitric Acid Ice	$HNO_3 \cdot 3H_2O(s)$	183	See Note		58
	Sulfuric Acid	$H_2SO_4 \cdot nH_2O(l)$ (60 to 95 wt.% H_2SO_4)	221–296	See Note		59
HCl + HNO_3 → Products						
HCl + HNO_3	Sulfuric Acid	$H_2SO_4 \cdot mHNO_3 \cdot nH_2O(l)$		See Note	See Note	60
HOCl + HCl →Cl_2 + H_2O						
HOCl/HCl	Water Ice	$H_2O(s) \cdot HCl(s)$	195–200	0.2	2	61
	Nitric Acid Ice	$HNO_3 \cdot 3H_2O(s) \cdot HCl(s)$	195–200	0.1	2	61
	Sulfuric Acid	$H_2SO_4 \cdot nH_2O(l)$	198–209	See Note	See Note	62
HOCl + HBr → BrCl + H_2O						
HOCl/HBr	Water Ice	$H_2O(s)$	189–220	See Note		63
	Sulfuric Acid	$H_2SO_4 \cdot nH_2O(l)$	228	See Note	See Note	64
HOCl + KBr →Products						
HOCl	Potassium Bromide	KBr(s)	300	$\gamma_o > 5 \times 10^{-3}$		65
ClNO + Surface →Products						
ClNO	Sodium Chloride	NaCl(s)	298	$<1 \times 10^{-5}$		66
	Liquid Water	$H_2O(l)$	270-295	$\geq 4 \times 10^{-3}$*		67
$ClNO_2$ + H_2O →Products HCl + HNO_3						
$ClNO_2$	Liquid Water	$H_2O(l)$	275-295	4×10^{-6}	2	68
$ClNO_2$ + MX →Products						
$ClNO_2$	Potassium Bromides	KBr(s)	300	1×10^{-4}	2	69
	Sodium Chloride	NaCl(aq)	291	See Note		69
	Sodium Bromide	NaBr(aq)	275-293	See Note		69
	Sodium Iodide	NaI(aq)	275-293	See Note		69
$ClONO_2$ + H_2O →HOCl + HNO_3						
$ClONO_2$	Water Ice	$H_2O(s)$	180–200	0.3	3	70
	Liquid Water	$H_2O(l)$	270-290	2.5×10^{-2}	4	71
	Nitric Acid Ice	$HNO_3 \cdot 3H_2O(s)$	200–202	0.004	3	72
	Sulfuric Acid	$H_2SO_4 \cdot nH_2O(l)$	200–265	See Note*	See Note	73
	Sulfuric Acid Monohydrate	$H_2SO_4 \cdot H_2O(s)$	195	$<1 \times 10^{-3}$		74
	Sulfuric Acid Tetrahydrate	$H_2SO_4 \cdot 4H_2O(s)$	196–206	See Note		74
$ClONO_2$ + HCl →Cl_2 + HNO_3						

Gaseous Species	Surface Type	Surface Composition	T(K)	γ	Uncertainty Factor	Notes
$ClONO_2/HCl$	Water Ice	$H_2O(s)$	180–200	0.3	3	75
	Nitric Acid Ice	$HNO_3 \cdot 3H_2O \cdot HCl$	185–210	0.2	2	76
	Sulfuric Acid	$H_2SO_4 \cdot nH_2O(l) \cdot HCl(l)$	195–235	See Note	See Note	77
	Sulfuric Acid Monohydrate	$H_2SO_4 \cdot H_2O(s)$	195	$<1 \times 10^{-4}$		78
	Sulfuric Acid Tetrahydrate	$H_2SO_4 \cdot 4H_2O(s)$	195–206	See Note		78
	Alumina	Al_2O_3	180–200	0.3	3	79
$ClONO_2 + MX \rightarrow$ Products						
$ClONO_2$	Sodium Chloride	NaCl(s)	295	0.005		80
				$<\gamma_o<0.2$		
		NaCl(aq)	272-280	See Note		80
	Potassium Bromide	KBr(s)	298	>0.1		81
	Sodium Bromide	NaBr(aq)	272-280	See Note		81
	Sea Salt	See Note for O_3 + Sea Salt	298	>0.1		82
$ClONO_2 + HBr \rightarrow BrCl + HNO_3$						
$ClONO_2/HBr$	Water Ice	$H_2O(s) \cdot HBr(s)$	200	>0.3		83
	Nitric Acid Ice	$HNO_3 \cdot 3H_2O(s) \cdot HBr(s)$	200	>0.3		83
$ClONO_2 + HF \rightarrow$ Products						
$ClONO_2/HF$	Water Ice	$H_2O(s) \cdot HF(s)$	200	See Note		84
	Nitric Acid Ice	$H_2O(s) \cdot HNO_3(s) \cdot HF(s)$	200	See Note		84
$CF_xCl_y + Al_2O_3 \rightarrow$ Products						
CCl_4	Alumina	$Al_2O_3(s)$	120–300	1×10^{-5}	10	85
$CFCl_3$	Alumina	$Al_2O_3(s)$	120–300	1×10^{-5}	10	85
CF_2Cl_2	Alumina	$Al_2O_3(s)$	120–300	1×10^{-5}	10	85
CF_3Cl	Alumina	$Al_2O_3(s)$	120–300	1×10^{-5}	10	85
$BrCl + MX \rightarrow$ Products						
BrCl	Sodium Chloride	NaCl(s)	298	See Note		86
	Potassium Bromide	KBr(s)	298	See Note		86
	Sodium Iodide	NaI(aq)	273-288	See Note		86
$Br_2 + MX \rightarrow$ Products						
Br_2	Sodium Chloride	NaCl(s)	298	See Note		87
	Potassium Bromide	KBr(s)	298	See Note		87
	Sodium Iodide	NaI(aq)	263-293	$\gamma_o<0.5$		87
$2BrO \rightarrow Br_2 + O_2$						
BrO	Water Ice	$H_2O(s)$	213	See Note		88
	Sulfuric Acid	$H_2SO_4 \cdot nH_2O$				
		(60 wt.% H_2SO_4)	213	See Note		88
		(70 wt.% H_2SO_4)	213	See Note		88
	Aqueous Sodium Chloride	NaCl(aq) (23 wt.% NaCl)	53	See Note		88
$HOBr + HCl \rightarrow BrCl + H_2O$						
HOBr/HCl	Water Ice	$H_2O(s) \cdot HBr(s)$	180–228	0.3	3	89
	Sulfuric Acid	$H_2SO_4 \cdot nH_2O$ (60–69 wt.% H_2SO_4)	198–218	See Note		90
$HOBr + HBr \rightarrow Br_2 + H_2O$						
HOBr/HBr	Water Ice	$H_2O(s) \cdot HBr(s)$	180-228	>0.1		91
	Sulfuric Acid	$H_2SO_4 \cdot nH_2O$	228	See Note		91
$HOBr + MX \rightarrow$ Products						
HOBr	Sodium Chloride	NaCl(s)	298	$\gamma_o<10^{-2}$		92
	Alkali Bromides	NaCl(aq)	298	$\gamma_o>0.2$		92
	Potassium Bromide	KBr(s)	298	$\gamma_o \leq 0.2$		93
	Sodium Bromide	NaBr(s)	250	See Note		93
		NaBr(aq)	298	$\gamma_o = 0.6$	1.5	93
$BrNO_2 + H_2O \rightarrow$ Products						
$BrNO_2$	Liquid Water	$H_2O(l)$	275-300	2×10^{-6}	2	94
$BrNO_2 + MX \rightarrow$ Products						

Gaseous Species	Surface Type	Surface Composition	T(K)	γ	Uncertainty Factor	Notes
$BrNO_2$	Potassium Chloride Sodium Chloride Potassium Bromide Sodium Bromide Sodium Iodide	KCL(s) NaCl(aq) KBr(s) NaBr(aq) NaI(aq)	298 277-293 298 277-293 262-278	See Note γ_o >10^{-6} γ_o >0.1 See Note See Note		95 95 96 96 96
$BrONO_2 + H_2O \rightarrow HOBr + HNO_3$						
$BrONO_2$	Water Ice Liquid Water Sulfuric Acid	$H_2O(s)$ $H_2O(l)$ $H_2SO_4 \cdot nH_2O$	190–200 270-280 210–300	>0.2 3 x 10^{-2} See Note	4	97 98 99
$BrONO_2 + HCl \rightarrow BrCl + HNO_3$						
$BrONO_2$/HCl	Water Ice Sulfuric Acid	$H_2O(s)$ $H_2SO_4 \cdot nH_2O$	200 229	See Note 0.9	2	97 99
$BrONO_2$ + HBrl						
$BrONO_2$/HBr	Water Ice_	$H_2O(s)$	180-210	γ_o >0.1		100
$BrONO_2$ + MX → Products						
$BrONO_2$	Sodium Chloride Potassium Bromide Sodium Bromide	NaCl(s) NaCl(aq) KBr(s) NaBr(aq)	298 278-280 298 272-280	γ_o>0.2 See Note γ_o>0.2 See Note		101 101 102 102
$CF_2Br_2 + Al_2O_3 \rightarrow$ Products						
CF_2Br_2	Alumina	Al_2O_3	210, 315	2×10^{-5}	10	85
$CF_3OH + H_2O \rightarrow$ Products						
CF_3OH	Water Ice Sulfuric Acid	$H_2O(l)$ $H_2SO_4 \cdot nH_2O$ (40 wt.% H_2SO_4) 45 wt.% H_2SO_4) (50 wt.% H_2SO_4) (50 wt.% H_2SO_4)	274 210–250 210–250 210–250 210–250	>0.01 0.07 0.04 0.01 0.001	 3 3 3 3	103 103 103 103 103
$SO_2 + O_3 \rightarrow$ Products						
SO_2/O_3		Al_2O_3	See Note	See Note		104
$SO_2 + H_2O_2$, O_3, HONO, NO_2 and $HNO_3 \rightarrow$ Products						
SO_2/H_2O_2, etc.	Sulfuric Acid	$H_2SO_4 \cdot nH_2O$ (20–60 wt.% H_2SO_4)	293	See Note		105
$SO_2 + Al_2O_3 \rightarrow$ Products						
SO_2	Alumina	Al_2O_3	295-300	<4 x 10^{-4}		106
SO_2 + MX → Products						
SO_2	Sodium Chloride Sea Salt	NaCl(s) See Note for O_3 + Sea Salt	298 298	γ_o <1x10^{-4} γ_o <0.1		107 107
$SO_3 + H_2O \rightarrow$ Products						
SO_3	Sulfuric Acid	$H_2SO_4 \cdot nH_2O$ (78–92 wt.% H_2SO_4)	300	1.0	+0.0, –0.3	108

*γ is temperature dependent

5.14 Notes to Table 5-2

1. $O_3 + Al_2O_3(s)$. Very low ozone decomposition efficiencies for reaction on coarse (3 µm dia.) and fine (0.1 µm dia., partially hydroxylated) γ-alumina and coarse (3 µm dia.) α-alumina were measured in flowing and static systems by Hanning-Lee et al. [187] at temperatures ranging between 212 and 473 K. Based on measured BET surface areas, γs ranged from 2×10^{-11} to 4×10^{-10} over the 212 to 298 K temperature range. γs for γ-alumina at lower temperatures exceeded those for α-alumina. Results are roughly consistent with earlier, unpublished flow tube data from L. F. Keyser and from fluidized bed reactor studies of Alebić-Juretić et al. [20]. Note that γs based on geometric surface particle surface areas would be significantly (10^4–10^7) larger. Additional fluidized bed reactor studies by Alebić-Juretić et al. [21] demonstrated that room temperature uptake are initially first order in O_3, but change to a slower second order reaction at longer exposure times. Klimvskii et al. [282] reported an initial uptake coefficient (γ_o) of 1×10^{-4} on a γ-alumina surface at 293K assuming a geometric surface area, BET surface correction presumably would have yielded a lower value. Michel et al. [324, 325] reported Knudsen cell uptake studies at 296K on α-alumina particles that yielded γ_o values of $(8\pm5) \times 10^{-5}$ and $(1.4 \pm 0.3) \times 10^{-4}$ after BET surface area corrections. Sullivan et al. [429] used a coated wall flow reactor to obtain 298K γ_o values of 7×10^{-6} to $1{,}6 \times 10^{-5}$ for α-alumina powder films exposed to no more than $[O_3]$ of 10^{13} cm^{-3} after BET surface area correction. Higher $[O_3]$ yielded lower apparent γ_os. Usher et al. [452] demonstrated the pretreatment of α-alumina with HNO_3 vapor reduced O_3 Knudsen cell γ_o values by ~70%. Back to Table

2. O_3 + NaCl. The reaction of O_3 with NaCl is slow. Il'in et al. [236] measured the loss of O_3 in a coated reactor over the temperature range 223 - 305 K, and found the same uptake coefficients, $\gamma \sim 10^{-6}$, independent of temperature, for NaCl and NH_4NO_3 and $(NH_4)_2SO_4$, suggesting that even the small uptake is not due to reaction with the chloride. Alebić-Juretić [20] did not observe any uptake on NaCl powders using a fluidized bed reactor but did not report an upper limit to the uptake coefficient. Akimoto and coworkers [332, 394], reported an upper limit of $\gamma_o < 1 \times 10^{-5}$ on NaCl. When the NaCl was mixed with 0.5 - 1% w:w $FeCl_3$, γ_0 increased to 3×10^{-2} and production of gaseous Cl_2 was observed with yields from 25 - 50% of the ozone taken up. With 0.1 % $FeCl_3$, no production of Cl_2 was observed but the initial uptake coefficient was still 3×10^{-2}. These experiments were carried out with a Knudsen cell using multiple salt layers and the measured initial uptake coefficients were converted to the reported values using the pore diffusion model of Keyser et al. [274, 275].

   Abbatt and Waschewsky [10] followed O_3 in a flow tube containing deliquesced 1 - 5 µm NaCl particles (75% RH); no significant loss was observed on unbuffered particles or particles buffered at pH of 7.2. An upper limit of $\gamma_o < 1 \times 10^{-4}$ was derived from these measurements. Back to Table

3. O_3 + NaBr and KBr. Mochida et al. [332] did not observe any uptake of O_3 on NaBr or KBr powders, from which they derived an upper limit of $\gamma < 1 \times 10^{-5}$. Hirokawa et al. [218] reported production of gas phase Br_2 from the reaction of O_3 with NaBr only when water vapor was added so that the salt was near deliquescence.

   Uptake of O_3 and production of gas phase Br_2 has been observed for deliquesced NaBr salt on a glass surface [29]. Production of Br_2 has also been measured by Hunt et al. [231] in the reaction of O_3 with deliquesced NaBr particles in the dark in an aerosol chamber; the production of Br_2 exceeded that from known aqueous phase chemistry by about an order of magnitude, suggesting that a surface reaction of O_3 with bromide at the air-solution interface was occurring with a reaction probability of
   $\gamma_0 = (1.9 \pm 0.8) \times 10^{-6}$ (2 σ). Back to Table

4. O_3 + sea salt. Akimoto and coworkers [332, 394], reported uptake coefficients for O_3 on synthetic and natural sea salt powders of $\sim 1 \times 10^{-3}$ using a Knudsen cell with multiple salt layers. Similar uptake coefficients were reported for the hydrates of $MgBr_2$ and $CaBr_2$. These are the initial uptake coefficients after correction for the available surface area using the pore diffusion model of Keyser et al. [274, 275]. The measured values before this correction was applied were about a factor of 20 larger. Given the uncertainty associated with these corrections, the final values derived have a large uncertainty associated with them as well. When $FeCl_3$ was added to synthetic sea salt (Fe/Na weight ratio of 1%), the uptake coefficient increased by an order of magnitude to $(3.2 \pm 1.1) \times 10^{-2}$. Br_2 was the gas phase product, with variable yields up to 100% of the O_3 lost. The enhanced reactivity of sea salt compared to NaCl and NaBr is due to the significant amounts of surface-adsorbed water (SAW) present on sea salt; the component of sea salt present in

the second highest concentration is magnesium chloride which forms a stable hydrate and is quite hygroscopic. Reactions with powders of $MgCl_2 \cdot 6H_2O$ and sea salt are often observed to be similar to reaction with aqueous salt solutions (see note on SO_2 uptake). The formation of Br_2 is favored over Cl_2 by a number of factors: (1) surface segregation of bromide ions [170, 171, 490] in mixed solid crystals of NaCl and NaBr; (2) higher solubility of NaBr which increases its concentration in the surface layer as a mixture of NaCl and NaBr crystallizes; (3) faster oxidation of Br^- compared to Cl^-; [143, 181, 182, 384], (4) solution phase chemistry of chloride and bromide ion mixtures that favors the production of gas phase bromine compounds; [143, 384], (5) enhanced interfacial bromide ion concentrations compared to chloride ions at the air-water interface of aqueous solutions of mixed salts [253, 254]. Back to Table

5. OH + H_2O(s). Cooper and Abbatt [104] measured initial irreversible OH uptake coefficients of ~ 0.1 for water ice between 205–230 K; these decayed to $\gamma = 0.03 \pm 0.02$ after repeated exposure to OH. Self-reaction to form H_2O or H_2O_2 was indicated by the lack of observable gas phase products despite observation of first-order OH loss. Back to Table

6. OH + HCl • nH_2O(l). Cooper and Abbatt [104] demonstrated significant enhancement of OH uptake (to $\gamma > 0.2$) after HCl doping of 220 K ice surfaces sufficient to melt the surface layer. It is unclear whether OH is lost to self-reaction or reaction with hydrated Cl^- ions. Back to Table

7. OH + $HNO_3 \cdot 3H_2O$. Cooper and Abbatt [104] measured $\gamma > 0.2$ for nitric acid-doped ice surfaces under conditions suitable for NAT formation at 200 and 228 K. Increase over pure ice uptake rates is probably due to $HNO_3 + OH \rightarrow H_2O + NO_3$ reaction. Back to Table

8. OH + $H_2SO_4 \cdot nH_2O$. Lower limits of 0.2 for uptake coefficients on 45–65 wt.% H_2SO_4 between 220 and 230 K and for 96 wt.% H_2SO_4 at 230 and 298 K by Cooper and Abbatt [104] are consistent with a lower limit of 0.07 on 28 wt.% H_2SO_4 at 275 K in similar experiments by Hanson et al. [194] and a probable surface saturated value of $(4.9 \pm 0.5) \times 10^{-4}$ from Knudsen cell measurements by Baldwin and Golden [34] and an estimate of $\gamma = 1$ on ~96 wt.% H_2SO_4 at 298 K by Gerhenzon et al. [166] using a coated insert flow tube technique. Uptake is probably reactive with $OH + HSO_4^- \rightarrow H_2O + SO_4^-$ the hypothesized process. Back to Table

9. OH + NaCl. Ivanov et al. [242] measured the uptake of OH on NaCl and on NH_4NO_3 over the temperature range from 245 - 340 K using a fast flow discharge reactor with a coated rod along the axis and EPR detection of OH. The initial values of the uptake coefficient approached 10^{-2}. The OH was generated from the reaction of H atoms with excess NO_2; it is not clear whether NO_2 might have also reacted with the salt surface. Given that the uptake coefficients were similar for NaCl and NH_4NO_3, the uptake likely does not reflect oxidation of the chloride. The pseudo-steady state value, γ_{ss}, was measured to be 4×10^{-3} at 298 K and the temperature dependence was described by $\gamma_{ss} = (1.2 \pm 0.7) \times 10^{-5} \exp[(1750 \pm 200)/T]$.

   Aerosol chamber studies by Finlayson-Pitts and coworkers showed that there was no Cl_2 production from NaCl particles when OH was generated by reaction of $O(^1D)$ from photolysis of O_3 at relative humidities below the deliquescence point of NaCl; above the deliquescence point, however, a rapid reaction of OH with Cl^- at the interface to generate gas phase Cl_2 is observed [283, 352]. Because the mechanism is uncertain, and clearly must involve multiple steps, a unique value of the reaction probability for this interface reaction could not be obtained. Back to Table

10. OH on Al_2O_3(s). Measured value is from flow tube experiment with native oxide on aluminum as the active surface. An uptake coefficient of 0.04 ± 0.02 independent of temperature over the range of 253–348 K was recommended by (Gershenzon et al. based on three measured values ranging unsystematically from 0.02 to 0.06 at 253, 298 and 348 K [166]). Back to Table

11. HO_2 + H_2O(s) and $H_2SO_4 \cdot nH_2O$(l). Uptake of HO_2 on ice and super-cooled 55 wt.% sulfuric acid at 223 K has been demonstrated to be limited by HO_2 surface saturation by Cooper and Abbatt [104]. They argue that self-reaction, presumably $2HO_2 \rightarrow H_2O_2 + O_2$ is limiting measured uptake coefficients of 0.025 ± 0.005 for ice and 0.055 ± 0.020 for 55 wt.% H_2SO_4. However, Gershenzon et al. [165] measured $\gamma > 0.2$ for 80 and 96 wt.% H_2SO_4 at 243 K and Hanson et al. [194] measured a lower limit for 28 wt.% H_2SO_4 at 275 K of 0.07. However, large gas phase diffusion corrections mean this value is consistent with $\gamma = 1$. Back to Table

12. HO_2 + NaCl(s) and KCl(s). Gershenzon and coworkers [165, 366] used a combination of matrix isolation EPR and gas phase EPR with a fast flow tube to measure the uptake of HO_2 on NaCl from 245 - 335 K. Early studies by Gershenzon et al. [165] measured values of $\gamma = 1.8 \times 10^{-2}$ for KCl and 1.6×10^{-2} for NaCl, both at

295 K, supplementing an even earlier value of $\gamma \sim 8 \times 10^{-3}$ measured by Gershenzon and Purmal [167]. In later studies on NaCl [366] the uptake was reported to remain constant for at least 30 min, so this is likely to be a steady-state value, $\gamma_{ss} = 1.2 \times 10^{-2}$ at 295 K. The temperature dependence is given by $\gamma_{ss} = (5.7 \pm 3.6) \times 10^{-5} \exp[(1560 \pm 140)/T]$. Above 330 K, the uptake coefficient was significantly smaller than expected from this temperature dependence. The data are indistinguishable, within experimental error, from the uptake of HO_2 on NH_4NO_3, suggesting that the uptake of HO_2 likely involves recombination on the surface rather than oxidation of the chloride. The surface recombination was interpreted in terms of a combined Eley-Rideal and Langmuir-Hinshelwood mechanism. The addition of small amounts of water vapor decreased the uptake coefficient for HO_2; the authors attributed this to water adsorption on the active sites. Another possibility is formation of HO_2-H_2O complexes whose uptake and recombination on the surface is not as fast as for uncomplexed HO_2. Back to Table

13. H_2O (g) + Al_2O_3 (s). Isotopic thermal programmed desorption studies at 300K by Elam et al. [129] show that H_2O dissociatively absorbs on α-alumina surfaces and that initial uptake coefficient (γ_o) is ~0.1. Pre-hydroxylation or long term exposure to water vapor decreases the H_2O uptake coefficient nearly exponentially. Al Albadeleh et al. [18] used FTIR techniques to study water vapor uptake at 296K on α-alumina crystal 0001 surfaces as a function of relative humidity (RH). Below 10% RH uptake is dissociative, but molecular absorption dominates uptake between 10 and 70% RH. FTIR spectra of water absorbed on both α-alumina and γ-alumina powder surfaces are similar to those on 0001 crystal surfaces. Goodman et al. [173] used FTIR to show that α-alumina surfaces saturated with HNO_3 vapor has the same water absorption isotherm as untreated samples at 296 K. Back to Table

14. NO_2 + H_2O(1). Value for γ of $(6.3 \pm 0.7) \times 10^{-4}$ at 273 K (Tang and Lee, [437]) was achieved by chemical consumption of NO_2 by SO_3^{2-}; their stopped-flow measurement was probably still affected by surface saturation, leading to the measurement of a lower limit. Ponche et al. [357] measured an uptake coefficient of $(1.5 \pm 0.6) \times 10^{-3}$ at 298 K, which was also probably subject to saturation limitations. Mertes and Wahner [323] used a liquid jet technique to measure a lower limit of $\gamma \geq 2 \times 10^{-4}$ at 278 K, and they observed partial conversion of the absorbed NO_2 to HONO. Msibi et al. [342] used a cylindrical/annular flow reactor to derive $\gamma = (8.7 \pm 0.6) \times 10^{-5}$ on pH = 7 deionized water surfaces and $(4.2 \pm 0.9) \times 10^{-4}$ on pH = 9.3 wet ascorbate surfaces; it seems likely that these results are also subject to surface saturation given the gas/surface interaction times involved in the experiment. Harrison and Collins [212] performed aerosol flow reactor experiments on deliquescent sodium chloride and ammonium sulfate droplets at 279 K obtaining reactive uptake coefficients in the range of $(2.8\text{-}10) \times 10^{-4}$, probably with some surface saturation constraints. Cheung et al. [82] used a droplet train flow reactor to show that the reactive uptake coefficient for NO_2 at number densities between 10^{13} and 10^{16} on pure water at 273 K is $<5 \times 10^{-4}$, contradicting many of the earlier experiments. Cheung et al. also used a bubble train reactor to demonstrate that the reactive uptake of NO_2 is second order, so that experimental uptake coefficients will be dependent on gas phase NO_2 concentrations. Data are consistent with a reactive uptake coefficient of $<1 \times 10^{-3}$ for 270–295 K and a liquid-phase second-order hydrolysis of NO_2 to HONO and HNO_3 which depends on temperature and pH. However, the interplay between accommodation, possible surface reaction, and bulk reaction may be complex. Back to Table

15. NO_2 + $H_2SO_4 \bullet nH_2O$. Kleffman et al. [281] performed bubble tube reactor uptake measurements for 0–98 wt.% acid at 298 K and for 44.6 and 56.1 wt.% from 250–325 K. At 298 K, measured uptake coefficients varied between 6 and 3×10^{-7} with a minimum near 70 wt.%. Most measurements at 44.6 and 56.1 wt.% overlapped within their error limits and showed little temperature dependence although there is evidence that uptake increases at the lowest temperatures. The data can all be captured with a recommended value of 5×10^{-7} with an uncertainty factor of three.

    This recommendation is consistent with earlier upper limits of 1×10^{-6} by Baldwin and Golden [33] for 96 wt.% at 295 K and 5×10^{-6} for 70 wt.% between 193 and 243 K by Saastad et al. [391]. Kleffman et al. [281] conclude that their uptake measurements are mass accommodation limited; however, it is not clear that their values are not influenced by bulk or surface reaction of two NO_2 with H_2O to form HONO and HNO_3 at lower acid wt.% values and the formation of nitrosyl sulfuric acid at higher acid concentrations. Kleffman et. al. [281] did perform separate static wetted wall reactor studies showing the formation of gas phase HONO at acid concentrations below 60 wt.%. It is more likely that reactive uptake is a controlling factor and the measured uptakes are solubility and/or reaction rate limited. Thus, the mass accommodation coefficient may be much larger than the recommended uptake values. Back to Table

16. NO_2 on Al_2O_3. Miller and Grassian [330] observed NO_2 absorbed reactively on γ-alumina using FTIR and UV spectroscopy to observe surface nitrite and nitrate. Underwood et al. [448-450] report Knudsen cell studies measuring γ_o values on γ-alumina particles of 2×10^{-8}, 2.0×10^{-8}, and 2.2×10^{-8} at 298K based on BET surface area corrections and either KML [272] or linear mass dependent (LMD) corrections for porosity, with the KML and LMD corrections leading to very similar values [448]. They also report larger γ_o values for α-alumina of 9.3×10^{-6} and 9.1×10^{-6} [448, 450]. Underwood et al. [450] also suggest a final "multiple collision" that would raise the γ_o values for γ-alumina by factor of 1,1 and α-alumina by 9.4. This proposed correction is not included in the recommended upper limits. Börensen et al. [64] report diffuse reflectance FTIR measurements of uptake on γ-alumina showing that the reaction order is 1.86±0.1 in NO_2. They report BET corrected γ_o values varying linearly from 7.3×10^{-10} to 1.3×10^{-8} as $[NO_2]$ was increased from 2.5×10^{13} to 8.5×10^{14}. Back to Table

17. NO_2/N_2O_4 + NaCl. Schroeder and Urone reported that NO_2 at Torr concentrations reacted with NaCl to form ClNO [397]. Subsequently, Finlayson-Pitts [142] showed that the reaction contined at ppm concentrations of NO_2 and estimated a lower limit to the uptake coefficient for NO_2 of 5×10^{-8}, assuming the reaction was first order in NO_2. Winkler et al. [478] used XPS to follow the increase in nitrate during the reaction of NO_2 with NaCl and reported that the rate was proportional to the square of the NaCl surface sites and the square root of NO_2. Vogt and Finlayson-Pitts [460-462] used diffuse reflectance Fourier transform infrared spectrometry (DRIFTS) to follow the formation of nitrate and showed that the reaction was second order in NO_2; assuming that N_2O_4 was the reactant, the uptake coefficient was measured to be $(1.3 \pm 0.6) \times 10^{-4}$ (1 σ). Peters and Ewing [356] followed the formation of nitrate on single crystal NaCl(100) and also found the reaction was second order in NO_2. Assuming that N_2O_4 is the reactant, the uptake coefficient was $(1.3 \pm 0.3) \times 10^{-6}$, two orders of magnitude less than reported by Vogt and Finlayson-Pitts. However, in the presence of 9.5 mbar water vapor, the uptake coefficient increased by a factor of about 100. It is likely that the difference is that their single crystals did not hold significant amounts of surface adsorbed water, whereas the powders used by Vogt and Finlayson-Pitts are known to hold significant amounts of SAW [53] which enhances the reactivity through mobilization of the nitrate ions and exposure of fresh NaCl during the reaction. Caloz et al. [72] measured using a Knudsen cell an upper limit of $<10^{-7}$ for uptake of NO_2 on NaCl and $< 2 \times 10^{-7}$ for uptake on KBr, with the reaction being first order in NO_2. Yoshitake [485] also used DRIFTS to study this reaction and reported that for "dry" NaCl, the reaction was second order in NO_2 with an uptake coefficient assuming the reactant is N_2O_4 of $(4 \pm 2) \times 10^{-5}$. However, if the NaCl had been pretreated with water vapor, the uptake was first order in NO_2 with $\gamma = (1.5 \pm 0.2) \times 10^{-8}$. Karlsson and Ljungstrom [266] generated NaCl particles and measured the loss of chloride and formation of nitrate using ion chromatography on particles collected on filters; they obtained a lower limit for the reaction probability of 3×10^{-4}. Surprisingly, the conversion of to nitrate decreased as the relative humidity increased from 9 to 79%. These reactions are sufficiently slow that they are unlikely to be important in the atmosphere.

    Abbatt and Waschewsky [10] measured the loss of NO_2 in a flow tube containing deliquesced 1 - 5 μm NaCl particles (75% RH); no significant loss was observed on unbuffered particles or particles buffered at pH of 7.2 or having pH of 0.3 using HCl. An upper limit of $\gamma_o < 1 \times 10^{-4}$ for the uptake of NO_2 was derived from these measurements. Back to Table

18. NO_2 + NaBr(s). Vogt et al. [459] used diffuse reflectance infrared spectroscopy to study NO_2 + NaBr(s) at 298 K. The reaction was determined to be approximately second order in NO_2. Assuming that adsorbed N_2O_4 is the reactant leads to $\gamma = 2\ (+4, -1.3) \times 10^{-4}$. Back to Table

19. NO_2/N_2O_4 + sea salt. Sverdrup and Kuhlman [430] measured the uptake of NO_2 on artificial sea salt using the NO_2 loss measured in a flow tube lined with the salt. The uptake coefficient was reported to increase from 10^{-7} to 10^{-6} as the relative humidity increased from 44% to 88%. Langer et al. [291] used diffuse reflectance Fourier transform infrared spectrometry to follow nitrate formation on synthetic sea salt and found the reaction was approximately second order (1.8 ± 0.2) in NO_2 in He carrier gas but approximately first order (1.2 ± 0.2) in NO_2 in air. Assuming that N_2O_4 was the reactant in He, $\gamma_{ss} = 1 \times 10^{-4}$, and assuming NO_2 is the reactant in air, $\gamma_{ss} = 1 \times 10^{-8}$. These reactions are sufficiently slow that they are unlikely to be important in the atmosphere. Back to Table

20. NO_3 on H_2O(s). Fenter and Rossi [138] measured an upper limit for γ of 10^{-3} over the range from 170 to 200 K. Back to Table

21. $NO_3 + H_2O(l)$. Rudich et al. [388, 389] used wetted-wall flow tube techniques to measure uptake coefficients for NO_3 on pure water and aqueous NaCl, NaBr, NaI, and $NaNO_2$ solutions. These studies were extended to other aqueous solutions by Imamura et al. [238]. Uptake on pure water was consistent with reaction of NO_3 to produce HNO_3 and OH. Uptake coefficients with solutions containing I^-, Cl^-, Br^-, NO_2^- and other anions were larger and scaled with anion concentration, indicating electon transfer reactions to produce NO_3^-. The γ of $(2.0 \pm 1.0 \times 10^{-4})$ at 273 K determined for pure water by Rudich et al. is significantly lower than the lower limit of 2.5×10^{-3} quoted by Mihelcic et al. [329]. A detailed analysis of uptake coefficients for KI aqueous solutions indicated that the NO_3 mass accommodation coefficient is >0.04 [388]. Back to Table

22. NO_3 + NaCl. Recommended value for the initial uptake coefficient on solid NaCl is based on work of Seisel et al. [410, 411] Gershenzon and coworkers [164] and Gratpanche and Sawerysyn [178]. Seisel et al. [410, 411] used a Knudsen cell with mass spectrometric and laser-induced fluorescence detection of the NO_3. Salt powders from 60 - 630 μm in size were used, as well as spray-deposited samples; no dependence on the sample mass for powders or between powders and the spray-deposited samples was observed so no corrections for diffusion into underlying layers were applied. They obtained values for γ_0 of $(4.9 \pm 3) \times 10^{-2}$ and $(4.6 \pm 4) \times 10^{-2}$ (1 σ), respectively. Gershenzon and coworkers used flow reactors with ESR and MS detection and measured the loss of NO_3 on an axially located rod coated with salt; they interpret their results, and the associated value of γ_0 derived from their data based on a multi-step mechanism involving adsorption and then reaction of NO_3 on the salt. The value for γ_0 is sensitive to several unknown parameters in the model, and they give a range from $(0.2 - 3.9) \times 10^{-2}$. Gratpanche and Sawerysyn [178] used a flow tube coated with NaCl and ESR detection of NO_3, and reported a value of $(1.7 \pm 1.2) \times 10^{-2}$ (1 σ); on very dry NaCl, no uptake was observed, again indicating the importance of small amounts of water for the reaction. Gershenzon et al. [164] reported that the uptake coefficient decreased by about a factor of 20 over about half an hour, suggesting that the steady state value of γ_{ss} is approximately 1.5×10^{-3}. Zelenov et al. [491, 492] reported that the uptake coefficient for NO_3 on NaCl (and NaBr; see next note) [491, 492] could be fit by a time-dependent term and a time-independent term: $\gamma(t) = \gamma_0 \exp(-t/\tau) + \gamma_{ss}$. They observed that γ_{ss} depends on the type of salt, as well as the NO_3 and water concentrations, while γ_0 depended only on the type of salt and NO_3 concentration. They concluded that the products are chemisorbed Cl atoms. No temperature dependence has been observed over the temperature range 258 - 301 K by Gratpanche and Sawerysyn, [178] consistent with only an ~ 10% change in the uptake coefficient from 293 to 373 K observed by Gershenzon et al. [164].

    The uptake of NO_3 on aqueous solutions of NaCl has been measured at 273 K by Rudich et al. [389] and at 293 K by Thomas et al. [439]. NO_3 reacts in solutions with the halide ions. The measured uptake coefficients varied from $(0.8 - 6) \times 10^{-3}$ for solutions of activity ranging from 0.008 to 0.45 at 273 K [389] and was reported to be $> 2 \times 10^{-3}$ on 0.1 M NaCl at 293 K [439]. Back to Table

23. NO_3 + NaBr and NaI. See note for NO_3 + NaCl. Recommended value of γ_0 for the reaction with solid NaBr is based on reported values of 0.16 ± 0.08, [410] 0.20 ± 0.10, [411] a range of 0.1 to 0.3 [164] and 0.11 ± 0.06 [178] (all errors cited are 1 σ). Gershenzon et al. [164] observed a decrease of about a factor of two with time, suggesting that γ_{ss} ~ 0.05. Gratpanche and Sawerysyn [178] found a slight negative temperature dependence, $\gamma_0 = (1.6^{+1.8}_{-0.9} \times 10^{-3}) \exp[(1210 \pm 200)/T]$ over the range from 243 - 293 K. Gershenzon et al. [164] also reported a small (30%) decrease in γ_0 from 293 to 373 K. Zelenov et al. [491, 492] reported that the uptake coefficient for NO_3 on NaBr (and NaCl; see preceding note) could be fit by a time-dependent term and a time-independent term: $\gamma(t) = \gamma_0 \exp(-t/\tau) + \gamma_{ss}$. They observed that γ_{ss} depends on the type of salt, as well as the NO_3 and water concentrations, while γ_0 depended only on the type of salt and NO_3 concentration. They concluded that the products are gas phase bromine atoms in agreement with the observations of the branching ratio as well as the mass balance by Seisel et al. [410, 411].

    Rudich et al. [388] measured the uptake of NO_3 on aqueous KI solutions; NO_3 is taken up and reacts with I^- in solution. Uptake coefficients increased with the concentration of I^-, ranging from $\gamma = 0.9 \times 10^{-3}$ at 5×10^{-6} M KaI to 3.2×10^{-3} at a concentration of 8×10^{-5} M. Back to Table

24. $N_2O_5 + H_2O(s)$. Leu [293] and Hanson and Ravishankara [200] measured nearly identical values of 0.028 (±0.011) and 0.024 (±30%) in the 195–202 K range on relatively thick ice films in coated wall flow tubes. Quinlan et al. [363] measured a maximum value for γ on ice surfaces at 188 K of 0.03 in a Knudsen cell reactor. The average of these three studies is 0.027 with a standard deviation of 0.003. Hanson and Ravishankara [202, 204] presented new and re-analyzed data as a function of ice thickness, with a value of ~0.008 for the thinnest ice sample, rising to 0.024 for the thickest. From these data there would appear to be

no strong dependence on temperature, at least over the 188–195 K range. It is unclear whether the measured dependence on ice film thickness is due to added porosity surface area in the thicker films or decreased ice film integrity in thinner films. The error estimate in the table is driven by the possible systematic error due to unresolved film thickness effects rather than the small statistical error among the "thick film" values from the three groups.

Zondlo et al. [506] report the formation of a supercooled H_2O/HNO_3 liquid layer at 185 K as a reaction product, forming NAT or NAD only after decreasing the relative humidity below the ice frost point. This effect is similar to that resulting from the interaction of gaseous HNO_3 or $ClONO_2$ with the ice surface. These authors measured $\gamma = (7 \pm 3) \times 10^{-4}$ at 185 K for the reaction of N_2O_5 with this supercooled liquid layer. Back to Table

25. $N_2O_5 + H_2O(l)$. Reaction on liquid water has a negative temperature dependence. Van Doren et al. [455] measured γs of 0.057 ± 0.003 at 271 K and 0.036 ± 0.004 at 282 K using a droplet train uptake technique. George et al. [160] also used a droplet train technique to measure s of $(3.0 \pm 0.2) \times 10^{-2}$ (262 K), $(2.9 \pm 1.2) \times 10^{-2}$ (267 K), $(2.0 \pm 0.2) \times 10^{-2}$ (273 K), $(1.6 \pm 0.8) \times 10^{-2}$ (276 K), and $(1.3 \pm 0.8) \times 10^{-2}$ (277 K) on pure water, while Schweitzer et al. [407] used the same approach for pure water and salt solutions between 262 and 278 K, obtaining similar results. Mozurkewich and Calvert [339] studied uptake on $NH_3/H_2SO_4/H_2O$ aerosols in a flow reactor. For their most water-rich aerosols (RH = 76%) they measured γs of 0.10 ±0.02 at 274 and 0.039 ±0.012 at 293 K. However, similar studies by Hu and Abbatt [225] on $(NH_3)_2SO_4$ aerosols at 297 K showed that uptake rises with decreasing relative humidity (RH); their 94% RH results agree very well with the temperature trend measured by Van Doren et al., Msibi et al. [341] measured a smaller γ of 2.5×10^{-3} for water adsorbed on a denuder flow tube well under 66–96% relative humidity conditions at room temperature. $N_2O_5 + H_2O(l)$. Sch tze and Herrmann [400] measured a γ of 2×10^{-2} at 298 K using a single suspended droplet flow reactor method 0.0011 (+.0012/ 0.0006) that was almost certainly constrained by nitrate build-up in the droplet's surface layer. Mental and co-workers [465] and [322] studied N_2O_5 uptake on deliquescent salt particles from 291 to 298 K in an aerosol chamber; for sodium sulfate particles γ was in the range of 0.2 to 0.4, while sodium nitrate particles demonstrated uptakes more than an order of magnitude lower, demonstrating the negative influence of nitrate on the reaction rate. Behnke et al. [50] also used an aerosl chamber to study uptake on deliquescent NaCl particles, measuring γ=0.032±0.02 for 76-94% relative humidity with some contribution from the reaction of N_2O_5 with Cl^-.

The higher γ values of Van Doren et al., Mozurkewhich and Calvert, and Hu and Abbatt are quite consistent when temperature and RH effects are factored in. The lower values from the Louis Pasteur (George et al.; Schweitzer et al.) and Birmingham (Msibi et al.) groups appear to have much less pronounced temperature dependence and are inconsistent with the other measurements. The aerosol chamber measurements at low nitrate loadings are generally consistent with the higher range of values. The same function used to fit the N_2O_5 uptake on sulfuric acid as a function of temperature and concentration, discussed in below, has been extended to the Van Doren et al. and Hu and Abbatt data for pure water and very high RH aerosols. See note on $N_2O_5 + H_2SO$ on H_2O for the functional fit and its error discussion. Back to Table

26. $N_2O_5 + HNO_3 \cdot 3H_2O(s)$. Hanson and Ravishankara [198] have measured γ = 0.0006 (± 30%) near 200 K. They presented re-analyzed and additional data as a function of ice thickness (Hanson and Ravishankara [202]; [204]), deriving a value of 3×10^{-4} for the thinnest NAT covered ice layer, with values up to three times higher for thicker NAT-covered ice layers. As in the case of uptake on water ice this may be due to increased surface area from porosity in the thicker films, or less integrity in the thinner films. The uncertainty listed in Table A-1 is driven by this observed effect. All of the Hanson et al. data are in very poor agreement with the γ = 0.015 ± 0.006 reported by Quinlan et al. [363] from their Knudsen cell measurements; this measurement may have been biased by formation of a super-cooled aqueous nitric acid surface and is judged to be unreliable. Back to Table

27. $N_2O_5 + H_2SO_4 \cdot nH_2O(l)$. This reaction has been intensively studied between 195 and 296 K for a wide range of H_2SO_4 wt.% values using four complementary experimental techniques. Data are available from aerosol flow tube studies (Fried et al. [154], Hanson and Lovejoy [195], Hu and Abbatt [225], and Hallquist et al. [184]), coated wall flow tube studies (Hanson and Ravishankara [198], Zhang et al. [497]), a stirred Knudsen cell (Manion et al. [315]) and droplet train studies (Van Doren et al. [455], Robinson et al. [376]). All studies have yielded γs between ~0.05 and 0.20 with modest dependence on surface H_2SO_4 wt.% and temperature. The Knudsen cell studies, aerosol flow tube studies at higher N_2O_5 exposure and the ternary $H_2SO_4/HNO_3/H_2O$ studies of Zhang et al. [497] all illustrate that significant levels of HNO_3 in the

H_2SO_4/H_2O solutions will reduce γ measurably; this fact explains some of the scatter in aerosol flow tube studies and the surface saturation evident in the Knudsen cell studies. The effect of 5.0×10^{-7} Torr HNO_3 on γ as a function of temperature at two water vapor concentrations are plotted in Zhang et al. [497]; the decrease in γ is greatest at low temperatures, approaching a factor of 2–5 between 200 and 195 K.

Experimental data on sulfuric acid surfaces between 40 and 80 wt.% sulfuric acid deemed to be free of saturation effects, plus the pure water uptake data of Van Doren et al. [455] and high relative humidity ammonium sulfate aerosol uptake data of Hu and Abbatt [225] were all fit to a polynomial expression to yield a single model describing γ for N_2O_5 uptake valid between 0 and 80 wt.% H_2SO_4 and 180 to 300 K (Robinson et al. [376]). The form of this function is: $\gamma_o = \exp(k_o + k_1/T + k_2/T^2)$, where T is the temperature in K. The parameters k_o, k_1, and k_2 obtained from the best-fit are:

$$k_o = -25.5265 - 0.133188wt + 0.00930846wt^2 - 9.0194\times10^{-5}wt^3$$

$$k_1 = 9283.76 + 115.345wt - 5.19258wt^2 + 0.0483464wt^3$$

$$k_2 = -851801 - 22191.2wt + 766.916\,wt^2 - 6.85427wt^3$$

where wt is the weight percentage of H_2SO_4.

The overall error of applying the uptake function provided here consists of two components. One is the standard deviation of the model-calculated value with respect to measured data, σ_m, which is given by

$$\sigma_m = \sqrt{\frac{\sum_{i=1}^{N}\left(1-\frac{\gamma_i}{\gamma_{\text{model}}}\right)^2}{N-1}}\,.$$

The other is the standard deviation of relative experimental measurement error from the mean, σ_d, which is given by

$$\sigma_d = \sqrt{\frac{\sum_{i=l}^{N}\left(\frac{\Delta\gamma_i}{\gamma_i}\right)^2}{N(N-1)}}\,.$$

The overall error is

$$\sigma = \sqrt{\sigma_m^2 + \sigma_d^2}\,.$$

(These formulations are also applied below in the error estimation for the $ClONO_2 + H_2O$ and HCl, $BrONO_2 + H_2O$, and HOCl + HCl reaction system. For N_2O_5, the error is estimated to be 15% (one sigma), with σ_m=14.7% and σ_d=2.9%). Back to Table

28. $N_2O_5 + H_2SO_4 \bullet H_2O(s)$. Zhang et al. [498] used coated flow tube techniques to measure the uptake of N_2O_5 on solid sulfuric acid monohydrate over a temperature range of 200 to 225 K. The measurement values of γ were significantly higher at 200 K ($\gamma \sim 1 \times 10^{-3}$) than at 225 K ($\gamma \sim 10^{-4}$) and were well fit by $\log \gamma = [4.78 - 0.0386T(K)]$. Acid-rich $H_2SO_4 \bullet H_2O$ surfaces had a lower γ than water rich surfaces ($\log \gamma = [0.162 - 0.789 \times \log p_{H2O}]$ where p_{H2O} is their experimental water vapor partial pressure). Back to Table

29. $N_2O_5 + H_2SO_4 \bullet 4H_2O(s)$. Hanson and Ravishankara [205] studied N_2O_5 uptake by frozen 57.5 and 60 wt.% H_2SO_4 as a function of temperature and relative humidity. The 57.5 wt.% surface was not sensitive to relative humidity and was slightly more reactive (γ = 0.008 vs 0.005) at 205 K than at 195 K. Reaction probabilities on the 60 wt.% surface dropped off with temperature and relative humidity. Back to Table

30. N_2O_5 + HCl on $H_2O(s)$. Leu [294] measured $\gamma = 0.028 \pm 0.011$ at 195 K, while Tolbert et al. [442] measured a lower limit of 1×10^{-3} at 185 K. These experiments were done at high HCl levels probably leading to a liquid water/acid surface solution (Abbatt et al. [6]). Seisel et al. [412] measured $\gamma \sim 0.03$ at 200 K using a Knudsen flow reactor with a range of HCl flows. The uptake coefficient at low HCl flows is only slightly enhanced compared to the uptake on a pure ice surface. Back to Table

31. N_2O_5 + HCl on $HNO_3 \cdot 3H_2O(s)$. Hanson and Ravishankara [198] measured $\gamma = 0.0032$ (±30%) near 200 K. Back to Table

32. N_2O_5 + HCl on $H_2SO_4 \cdot H_2O(s)$. Zhang et al. [498] saw no increase in N_2O_5 uptake on sulfuric acid monohydrate at 195 K upon exposure to HCl, setting $\gamma < 10^{-4}$. Back to Table

33. N_2O_5 + HBr on $H_2O(s)$. Seisel et al. [412] report γ values ranging from ~3×10^{-3} to 0.1, depending on the HBr concentrations employed; the measurements were conducted at 180 and 200 K. These authors report Br_2 and HONO in 80% yield as products with respect to N_2O_5 taken up, generated presumably by the secondary reaction of the primary product $BrNO_2$ with HBr. Back to Table

34. N_2O_5 + HBr on $HNO_3 \cdot 3H_2O(s)$. This reaction, yielding γ ~0.005, was investigated on NAT surfaces near 200 K by Hanson and Ravishankara [201]. Under some conditions a much higher reaction coefficient of ~0.04 was observed. Back to Table

35. N_2O_5 + NaCl. The uptake of N_2O_5 on solid NaCl has been studied using Knudsen cells [136, 220], flow reactors [297, 306], annular reactors [341] and diffusion tubes [285]. The reaction has two possible channels if there is water available on the surface: $N_2O_5 + NaCl \rightarrow ClNO_2 + NaNO_3$ (1) and $N_2O_5 + H_2O/NaCl \rightarrow 2\ HNO_3$ (2). The presence of the two channels is supported by measured yields of $ClNO_2$ (relative to N_2O_5 lost) that vary from 60 - 100% [136, 220, 285, 306] and by the observation of gaseous HCl as a reaction product [220]. Because hydrolysis on the surface occurs in addition to the reaction with Cl^-, the net uptake coefficient for N_2O_5 is particularly sensitive to the presence of surface-adsorbed water (SAW), with higher values for powders where there are more steps and edges that hold SAW. For example, Leu et al. [297] measured an upper limit of $\gamma < 1.0 \times 10^{-4}$ for salt powders that had been heated overnight in a vacuum, but ~ 4.5×10^{-4} for samples that were only pumped on for about an hour. Fenter et al. [136] reported a preferred value for the uptake coefficient of $(5 \pm 2) \times 10^{-4}$; however, the measured values varied from 2×10^{-3} for monodisperse powders (after correction for pore diffusion by factors of ~ 5 to 30) to $< 1.0 \times 10^{-4}$ for a polished window face. Hoffman et al. [220] report a steady state value of $\gamma_{ss} = 3 \times 10^{-3}$ based on Knudsen cell studies of powders using less than a layer of salt where corrections to the available surface area due to diffusion into the salt are not necessary; the branching ratio for reaction (1) was measured to be 0.73 ± 0.28 (2σ). Stewart and Cox [428] measured the uptake of N_2O_5 on NaCl particles in a flow tube; after correction for diffusion/particle size effects, an uptake coefficient of 3×10^{-2} was derived at relative humidities 30% and above.

The uptake of N_2O_5 on NaCl solutions or aqueous particles has been measured by a number of techniques [50, 51, 158, 341, 407, 493]. The reported values of γ range from 1.5×10^{-2} to 5.0×10^{-2}. Zetzsch and coworkers [50, 51, 493], used an aerosol chamber to measure the uptake of N_2O_5 on deliquesced NaCl particles from 71 - 94% RH, and obtained a value of $\gamma = 3.2 \times 10^{-2}$. Behnke et al. [50], measured $ClNO_2$ in a yield of 66 ± 7% from aerosol particle experiments; in a wetted wall flow tube, the yield was observed to increase to 100% at concentrations of NaCl of 1 M and above. They proposed a mechanism involving a competition between the reaction of NO_2^+ with water to form HNO_3 or with Cl^- to form $ClNO_2$. George et al. [158] used a droplet train and measured the formation of NO_3^- in the droplets; the value of γ decreased from 0.039 ± 0.013 at 263 K to 0.014 ± 0.008 at 278 K.

Schweitzer et al. [407] used a droplet train apparatus to measure the uptake of N_2O_5 on water and on solutions of NaCl, NaBr and NaI with concentrations ranging from 0.1 to 1 M over a temperature range from 262 to 278 K. Within experimental error, all of the uptake coefficients were the same, with an average value of $\gamma = 0.018 \pm 0.003$. For 1 M NaCl, the $ClNO_2$ yield was 100%. Back to Table

36. N_2O_5 + KBr, NaBr, NaI. Fenter et al. [136] and Koch et al. [285] measured the uptake coefficient for N_2O_5 on KBr at ambient temperature using a Knudsen cell and molecular diffusion tube respectively. The Knudsen cell experiments gave a value of $(4 \pm 2) \times 10^{-3}$ after correction (by factors of 6-16) for pore diffusion, and the molecular diffusion tube a value of $(2.5 \pm 1) \times 10^{-3}$. In the Knudsen cell studies, the uptake coefficient was larger for powders and a depolished window face (both 4×10^{-3}) than for a polished window face ($< 1 \times 10^{-4}$), similar to the observations for the NaCl reaction (see note 10); this again suggests the importance of surface-adsorbed water and possibly surface defects created by roughening (which, however, also hold water) for the reaction. The initial product of the reaction is $BrNO_2$, identified by Finlayson-Pitts et al. [145] by FTIR but this can react further with the salt to generate Br_2, the product observed by Fenter et al. [136].

Schweitzer et al. [407] used a droplet train apparatus to measure the uptake of N_2O_5 on water and on solutions of NaBr and NaI, as well as NaCl, with concentrations ranging from 0.1 to 1 M over a temperature range from 262 to 278 K. Within experimental error, all of the uptake coefficients were the same, with an average value of $\gamma = 0.018 \pm 0.003$. For the NaBr reaction, the gas phase products were $BrNO_2$, Br_2 and HONO. For the NaI reaction, the only gas phase product observed was I_2. Back to Table

37. N_2O_5 + sea salt. The uptake of N_2O_5 on synthetic sea salt was measured to be $\gamma = (3.4 \pm 0.8) \times 10^{-2}$ (2 σ) by Hoffman et al. [220]. This will be an upper limit as 1-2 layers of salt were used and no correction was made for diffusion into the bottom layer. However, it is clear that the reaction is at least an order of magnitude faster than that for NaCl; the yield of $ClNO_2$ is 100%. Stewart and Cox [428] measured the uptake of N_2O_5 on submicron synthetic sea salt aerosols in a flow tube; after correction for diffusion/particle size effects, a value of $\gamma = 2.5 \times 10^{-2}$ was derived, independent of relative humidity above 30%. Back to Table

38. HONO + H_2O(l). Bongartz et al. [61] present uptake measurements by two independent techniques, the liquid jet technique of Schurath and co-workers and the droplet train/flow tube technique of Mirabel and co-workers (Ponche et al. [357]). With a surface temperature of ~245 K the droplet train techniques yielded $0.045<\gamma<0.09$, while the liquid jet operating with a surface temperature of 297 K obtained $0.03 < \gamma < 0.15$. Mertes and Wahner [323] used a liquid jet technique to measure $4 \times 10^{-3} < \gamma < 4 \times 10^{-2}$ at 278 K. Harrison and Collins [212] performed aerosol flow reactor experiments on deliquescent sodium chloride and ammonium sulfate droplets at 279 K obtaining reactive uptake coefficients of 0.0028±0.0015 and 0.0028±0.0006, for 85% relative humidity conditions, respectively; these measurements are probably subject to significant surface saturation. Since HONO uptake by liquid water probably involves hydrolysis, an increase in Henry's law solubility with decreasing temperature may be offset by a decreasing hydrolysis rate constant, leaving the uptake coefficient's temperature trend uncertain. Measured uptake coefficients will not correspond to the mass accommodation coefficient. Back to Table

39. HONO + $H_2SO_4 \bullet nH_2O$(l). Zhang et al. [500] measured uptake coefficients for HONO on sulfuric acid that increased from $(1.6 \pm 0.1) \times 10^{-2}$ for 65.3 wt.% H_2SO_4 (214 K) to $(9.1 \pm 1.6) \times 10^{-2}$ for 73 wt.% H_2SO_4 (226 K). Fenter and Rossi [137] measured uptake coefficients rising from 1.8×10^{-4} for 55 wt.% H_2SO_4 (220 K) to 3.1×10^{-1} for 95 wt.% H_2SO_4 (220 K and 273 K). Baker et al. [31] measured much smaller uptake coefficients for 60 wt.% at 298 K. In general, the values measured by Zhang et al. [500] are a factor of 2 to 5 higher than those of Fenter et al. [137] for comparable acid concentrations. Since the reaction probably depends on both temperature and acid concentration and since the data scatter is high in both experiments, further independent data will be required to define γ as a function of acid concentration and temperature. These data are generally consistent with the effective Henry' law constant measurements of Becker et al. [49] who illustrate that HONO solubility decreases exponentially with H_2SO_4 concentration until ~53 wt.%, at which point reaction to form nitrosyl sulfuric acid increases H* dramatically as H_2SO_4 concentration increases. Baker et al. [31] invoke surface decomposition of HONO to explain their room temperature data, since they separately determine that the bulk second-order disproportionation rate for HONO is too slow to account for even their small uptake coefficients. It is possible that surface formation of nitrosyl sulfuric acid and not HONO disproportionation is responsible for much of their measured uptake. The Zhang et al. [500] and Fenter and Rossi [137] data have been combined and fit with a four-term polynomial as a function of acid wt.% (these data did not show an obvious temperature dependence):

$$\ln \gamma = a + b\,wt + c\,wt^2 + d\,wt^3$$

where wt is the H_2SO_4 wt.%, and

$$a = -155.7 \pm 29.7$$

$$b = 5.663 \pm 1.232$$

$$c = -0.07061 \pm 0.01679$$

$$d = 0.000297 \pm 0.000076$$

This parameterization should be used only within the 55–95-wt.-%-H_2SO_4 range and the 214-to-273-K temperature range. Back to Table

40. HONO + HCl + H_2O(s). Knudsen cell uptake studies for HONO/HCl co-deposited on ice (180–200 K) and for HONO on 0.1 to 10 m HCl frozen solutions (~190 K) by Fenter and Rossi [137] showed HONO uptake

coefficients in the 0.02 to 0.12 range as long as surface HCl concentrations significantly exceed HONO concentrations. ClNO was evolved quantitatively with HONO consumption. Back to Table

41. HONO + HCl on $H_2SO_4 \bullet nH_2O(l)$. Fenter and Rossi [137] saw no reaction for acid wt.% > 65. They measured $\gamma = 2.0 \pm 0.7 \times 10^{-3}$ for 60 wt.% acid saturated with HONO at 230 K. Zhang et al. [500] also measured the uptake of HCl after exposure to HONO, they observed HCl uptake with γs between 0.01–0.02 over an acid wt.% range of 60.8–71.3 (T = 207.9–222.6 K). The reaction was also studied by Longfellow et al. [307] using both HCl doped and HONO doped sulfuric acid aerosols. Their uptake measurements confirmed reaction at higher acid wt.%, but by using lower HONO partial pressures they measured smaller γs. The reverse reaction, ClNO hydrolysis, was also studied in a wetted wall flow reactor and in the aerosol flow reactor by Longfellow et al. [307] and in a Knudsen cell reactor by Fenter and Rossi [137]. Data show clear evidence of both surface and bulk kinetics for the forward reaction. Longfellow et al. [307] report k^{II} values for the bulk reaction (in units of 10^4 $M^{-1}s^{-1}$) for 50 wt.%: 81 at 250 K and 15 at 205 K; for 60 wt.%: 9.4 at 250 K, 6.9 at 230 K and 5.0 at 219 K; for 67 wt.%: 3.9 at 250 K; and for 70 wt.%: 5.8 at 269 K and 0.35 at 215 K. The reaction is clearly complex and will require a comprehensive model of both the surface and bulk processes to arrive at an appropriate parameterization for γ. Back to Table

42. HONO + NaCl(s). Diffuse reflectance experiments by Vogt and Finlayson-Pitt [461] on room temperature NaCl(s) and Knudsen cell uptake experiments by Fenter and Rossi on room temperature NaCl(s) and frozen 0.1 M NaCl aqueous solutions, all failed to show HONO uptake [137]. The latter results yield $\gamma < 1 \times 10^{-4}$. HONO + NaCl. Junkermann and Ibusuki [255] reported that HONO reacts with NaCl to form nitrite on the surface. However, subsequent studies [461] showed that the infrared bands assigned to NO_2^- were due to nitrate, likely from the reaction of gas phase NO_2 and perhaps HNO_3 present in the HONO. There is no evidence at the present time for a reaction between HONO and NaCl. Back to Table

43. HNO_3 + NaCl. Recommendation is based on an average of the values of Hoffman et al. [221], Ghosal and Hemminger [169], the data of Davies and Cox [113] as revised by Ghosal and Hemminger [169] using their model for surface reactivation, and the single crystal data of Leu et al. [297] Hoffman et al. [221] used less than a single layer of particles so that diffusion into the underlying layers is not a factor to obtain an initial value of $\gamma_0 = (2.3 \pm 1.9) \times 10^{-3}$ (2σ). This is consistent within the combined experimental errors with a value of $(1.3 \pm 0.6) \times 10^{-3}$ determined from the formation of nitrate on the surface of single crystal (100) NaCl by Ghosal and Hemminger [169], and with a value of 1.1×10^{-3} from application of the Ghosal and Hemminger model to the Davis and Cox data [113]. Ghosal and Hemminger suggest that the value could be as high as 5×10^{-3} for NaCl powders that have more steps and edges that hold SAW [170]. At longer reaction times, the steady-state value [221] is a factor of two smaller, $\gamma = 1 \times 10^{-3}$. The reaction is hypothesized to occur both on dry terraces, which saturate rapidly, and on steps and edges that hold surface-adsorbed water. The water acts to recrystallize the product $NaNO_3$ so that the surface does not passivate during the reaction at atmospherically relevant HNO_3 pressures. This model, developed and modified by several research groups [53, 113, 169, 221] brings together most of the seemingly disparate measurements of the reaction probability made using a variety of techniques including flow tubes [113], Knudsen cells [53, 135, 136, 221], and XPS studies of nitrate formation on single crystals [169, 170, 461]Laux, 1994 #2173}. The only gas phase product observed is HCl, with a yield that is within experimental error of 100%. The higher value of $(1.3 \pm 0.4) \times 10^{-2}$ of Leu et al. [297] was obtained by correcting even larger measured values using a pore diffusion model;[274, 275] the corrections were typically in the range of a factor of 4-6. On single crystal NaCl where such corrections were not necessary, Leu et al. [297] measured a value of $(2.4 \pm 0.6) \times 10^{-3}$. A value of $(4 \pm 1) \times 10^{-2}$ was measured using a molecular diffusion tube technique by Koch et al. [285]. The corrected value of $(8.7 \pm 1.4) \times 10^{-5}$ reported by Zangmeister and Pemberton [488, 489] using Raman spectroscopy to follow the nitrate formed on the surface is lower than the other values likely because a much higher HNO_3 concentration was used (~ 10^{18} cm^{-3}), which would lead to a larger coverage of the surface by the recrystallized $NaNO_3$ product and passivation of much of the NaCl surface.

Abbatt and Waschewsky [10] measured the loss of gas phase HNO_3 in a flow tube containing deliquesced 1 - 5 μm NaCl particles (75% RH) and obtained a lower limit to the uptake coefficient for HNO_3 of 0.2 on unbuffered NaCl. Guimbaud et al. [179] measured the uptake coefficient of HNO_3 on 70 nm supersaturated NaCl particles (deliquesced NaCl particles held at 55% RH) to be 0.50 ± 0.20; they concluded that this was the mass accommodation coefficient. Tolocka et al. [445] followed the reaction of HNO_3 with 100 - 220 nm NaCl particles at 80% RH using single particle MS to measure the Cl^-/NO_3^- ratio; the uptake coefficient for 100 nm particles was $(4.9 \pm 2.7) \times 10^{-3}$ and increased with droplet size. The combination of these studies

shows that the initial uptake of HNO_3 into solution is fast, with $\gamma_0 > 0.2$; as the solution becomes acidified, HCl is expelled as the gaseous product. Back to Table

44. HNO_3 + NaBr and KBr. Fenter et al. [135] reported that the value of γ for uptake of HNO_3 on NaCl, NaBr, KBr and KCl was the same, $(2.8 \pm 0.3) \times 10^{-2}$, independent of sample mass. Koch et al. [285] reported an uptake coefficient of HNO_3 on KBr of $(2 \pm 1) \times 10^{-2}$ using a molecular diffusion tube technique. As discussed in Note 7, integration of the results of an extensive series of studies in different laboratories using different techniques, uptake coefficients for HNO_3 on NaCl give a value for the HNO_3-NaCl reaction that is smaller than measured in the Fenter et al. [135] and Koch et al. [285] studies. These values for KBr may therefore be upper limits. Leu et al. [296] reported a value that is an order of magnitude smaller, $(2.8 \pm 0.5) \times 10^{-3}$ after applying large corrections (about an order of magnitude) for pore diffusion; the average uncorrected value using the geometric area was 0.027. Back to Table

45. HNO_3 + sea salt. The uptake coefficient for HNO_3 on synthetic sea salt [118] is much larger than that on NaCl, which is attributed to the very hygroscopic nature of sea salt due to such components as the magnesium chloride and its hydrates (see Note 4). De Haan and Finlayson-Pitts [118] reported initial uptake coefficients of γ_0 in the range of 0.07 to 0.75 and steady state values in the range of 0.03 to 0.25; these were measured using salt layers from 2 layers to 10^3 layers. The initial uptake on $MgCl_2 \bullet 6H_2O$ was ≥ 0.4 and the steady-state value > 0.1. At these high uptake values, the correction for diffusion into underlying layers is expected to be small. The large uptake coefficient on sea salt is consistent with the values measured for uptake on concentrated aqueous solutions of NaCl (see Note 7) and the high water content of the surface of sea salt (see Note 4). The yield of HCl was within experimental error of 100%. Back to Table

46. $HNO_3 + Al_2O_3$. Börensen et al. [64] used diffuse reflectance FTIR observations to show that HNO_3 reacts with surface hydroxyl groups on γ-alumina at 299 K to produce surface bonded nitrate, while Goodman et al. reported similar observations for α-alumina at 296 K [173]. Goodman et al. [173] also observed that higher relative humidity lead to higher HNO_3 uptake. They integrated their nitrate absorbance feature to yield a time averaged uptake coefficient of $(4\pm1) \times 10^{-8}$ [173]. Underwood et al. [447] report a liner mass dependent, BET corrected γ_o for α-alumina at 295 K of $(9.7\pm0.5) \times 10^{-5}$. Hanisch and Crowley also measured liner mass dependent γ_os on α-alumina (at 298 k) for four particle sizes, which yielded an average value of 0.133 ± 0.033 [186]. They argue that the lack of variance of γ_os on a large range of particle sizes and masses indicate that the BET correction to the geometrical surface area is not required. They also measured γ_o for an unpolished single crystal of $(1.6\pm1.4) \times 10^{-3}$ and smaller values on polished single crystals, showing the higher density of surface defect sites on small amorphous particle are critical for their high reactive active uptake coefficients. The recommendation is based on the Hanisch and Crowley data and analyses for particulate samples [186]. Back to Table

47. HO_2NO_2 + HCl on $H_2SO_4 \bullet nH_2O(l)$. Zhang et al. [501] performed wetted-wall flow-reactor studies with HCl and HO_2NO_2 partial pressures in the 10^{-6} to 10^{-7} Torr range. Using chemical ionization mass spectrometry (CIMS) to detect expected reaction products, no Cl_2 (using SF_4^- as an analyte ion) or HOCl (using F^-) was detected over a temperature range of 200–225 K and an acid concentration range of 50–70 wt.% H_2SO_4. An upper limit for the reactive uptake coefficient for HO_2NO_2 reacting with HCl of $\gamma < 1 \times 10^{-4}$ was deduced. Back to Table

48. $NH_3 + H_2SO_4 \bullet nH_2O$. Robbins and Cadle [372], Huntzicker et al. [232], McMurry et al. [320], and Daumer et al. [111] all studied NH_3 uptake by sulfuric acid aerosols in near room temperature flow reactors (T = 281–300 K). Uptake coefficients varied between 0.1 and 0.5. Rubel and Gentry [387] used levitated H_3PO_4 acid droplets to show that heterogeneous reaction does control the initial NH_3 uptake on strong acid solutions. Both Rubel and Gentry and D umer et al. also explored the effect of organic surface coatings. Swartz et al. [431] used a droplet train flow reactor to measure reactive uptake coefficients on 20 to 70 wt.% acid over a temperature range from 248 t0 288 K. Measured uptake coefficients varied from 1.0 at 55 wt.% and above to 0.3 at 20 wt.% and drop off smoothly to the pure water results reported by the same group, as well as other droplet train flow reactor and coaxial jet uptake studies [482]. Hanson and Kosciuch [189] used an aerosol flow reactor to measure reactive uptake coefficients at room temperature (287 to 297 K) from 15 to 65 wt.%. While the data have a fair amount of scatter, taken as a whole they are consistent with γ=1 over the whole range of acid concentrations. There is no obvious reason for the discrepancy between the 15 to ~45 wt.% results from Swartz et al. [431] and Hanson and Kosciuch [189], the two groups have discussed conceivable issues at length in print [482] and Hanson and Kosciuch [190]. Back to Table

49. VOCs on Al_2O_3. Carlos-Cueller et al. [76] and Li et al. [299] have reported Knudsen cell studies that determined γ_o values for oxygenated volatile organic compounds (VOCs) at 295 and 298 K, respectively. Carlos-Cueller [76] measured γ_os on α-alumina for formaldehyde, $(7.7\pm0.3) \times 10^{-5}$, methanol, $(1.0\pm0.7) \times 10^{-4}$, and acetic acid, $(2 \pm 1) \times 10^{-3}$ based on BET surface areas and the KML [272] correction for porosity; the reported value for the relatively "sticky" acetic acid may not require the full BET and porosity corrections and thus may be underestimated. Li et al. [299] measured BET corrected γ_os on α-alumina for acetaldehyde, 3.2×10^{-5}, propionaldehyde, 4.7×10^{-5}, and acetone, 2.0×10^{-5}. The recommended upper limits are factors higher than the measured values since all the measurements are from a single laboratory using a single experimental technique. BET may overcorrect. Back to Table

50. $CH_3C(O)O_2$ + $H_2O(l)$ and $H_2SO_4 \bullet nH_2O$. Villalta et al. [457] used wetted-wall flow tube techniques to measure $\gamma = 4.3 (+ 2.4 /–1.5) \times 10^{-3}$ for water at 274 ± 3K. They also measured uptake for 34 wt.% H_2SO_4 at 246 K ($\gamma = (2.7 \pm 1.5) \times 10^{-3}$), 51 wt.% at 273 K ($\gamma = (0.9 \pm 0.5) \times 10^{-3}$), and 71 wt.% at 298 K ($\gamma = (1.4 \pm 0.7) \times 10^{-3}$). They suggest that products subsequent to hydrolysis are HO_2 and $CH_3C(O)OH$. Back to Table

51. $CH_3C(O)O_2NO_2$ + HCl, Cl, ClO, and OClO on $H_2SO_4 \bullet nH_2O(l)$. Zhang and Leu [496] performed wetted wall flow reactor studies with Cl species partial pressures in the 10^{-6} to 10^{-7} Torr range and $CH_3C(O)O_2NO_2$ at 3×10^{-6} Torr after equilibrating the acid surfaces (42, 51, and 69 wt.% at 202 and 224 K) with $CH_3C(O)O_2NO_2$. Also uptake studies with 5×10^{-7} Torr $CH_3C(O)O_2NO_2$ were performed after exposing the acid surface to the Cl species. No Cl species or $CH_3C(O)O_2NO_2$ uptake enhancements were observed under either condition and an upper limit for the reactive uptake coefficient of $\gamma < 1 \times 10^{-4}$ of $CH_3C(O)O_2NO_2$ was deduced. No gas phase reaction products were observed using CIMS after 42 wt.% H_2SO_4at 210 K was exposed to $CH_3C(O)O_2NO_2$ and each Cl species for 20 minutes. Back to Table

52. Cl + $H_2SO_4 \bullet nH_2O(l)$. Measured reaction probability (Martin et al. [317]) varies between 3×10^{-5} and 7×10^{-4} as H_2O and T co-vary. Reaction product is claimed to be HCl. Back to Table

53. Cl_2+HBr + $H_2O(s)$. Hanson and Ravishankara [201] measured a reaction probability of > 0.2 on water ice near 200 K. BrCl was not detected, presumably due to rapid reaction with excess HBr. Back to Table

54. Cl_2 + NaCl. Mochida et al. [331] used salt powders and spray-deposited films of NaCl and reported an initial uptake coefficient of 1.0×10^{-3}. Aguzzi and Rossi [11] reported no measurable uptake of Cl_2 on NaCl. Back to Table

55. Cl_2 + NaBr and NaI. Mochida et al. [331] used salt powders and spray-deposited films to obtain a value for the initial uptake coefficient of 2×10^{-2}. The measured uptake coefficients for the salt powders were a factor of six larger, but application of the pore diffusion model of Keyser et al. [274, 275] gave this value, which is in agreement with that for a spray-deposited film. Br_2 was generated in a yield of 100%, within experimental error.

    Hu et al. [226] measured the uptake of Cl_2 on aqueous solutions of NaBr and NaI over the temperature range of 263 - 293 K using a droplet train flow reactor. Measured values of the uptake coefficients on NaBr solutions ranged from 0.16 at 263 K to 0.05 at 293 K, and there was evidence of a surface reaction between Cl_2 and Br^- at the air-particle interface. Similarly, the uptake coefficients for Cl_2 on NaI solutions ranged from 0.20 to 0.07 over the same temperature range, again with evidence for a contribution from an interface reaction. Back to Table

56. Cl_2 + KBr. Mochida et al. [331] used salt powders and spray-deposited films to obtain a value for the initial uptake coefficients. The value measured for salt powders was 0.176, but after correction for pore diffusion, this became 3.7×10^{-2}, similar to a value of 2.3×10^{-2} measured for spray-deposited films. Br_2 was generated in a yield of 100%, within experimental error. Aguzzi and Rossi [11] measured a similar value, 2.7×10^{-2}, using a Knudsen cell. Santschi and Rossi [395] reported an initial value of $\gamma_0 = 0.11$ for the uptake of Cl_2 on thin spray-deposited films of KBr that had not been extensively pumped on; this initial value was 4×10^{-2} for films that had been pumped on for hours. They attributed the difference to the removal of surface-adsorbed water (SAW) by extensive pumping. Back to Table

57. Cl_2 + sea salt. Mochida et al. [331] used a synthetic sea salt and a "natural" seasoning sea salt in Knudsen cell studies of the uptake of Cl_2. The synthetic sea salt value of $(2.2 \pm 0.3) \times 10^{-2}$ is the value reported after correction of the measured value of 0.138 using the pore diffusion model. For the "natural" seasoning salt, the measured value was 0.11 which after correction for diffusion into the underlying layers became (3.1 ±

1.1) × 10^{-2}. Br_2 was the major gas phase product, with small mass spectrometric signals also seen for BrCl. Back to Table

58. ClO + H_2O(s) and HNO_3 • nH_2O(s). Proposed reaction (Leu [294]) is 2 ClO → Cl_2 + O_2; reactive uptake may depend on ClO surface coverage, which in turn may depend on gas phase ClO concentrations. Kenner et al. [271] measured reaction probabilities of (8 ±2) × 10^{-5} for ice at 183 K which is far lower than the limit of >1 × 10^{-3} obtained by Leu [294]. Abbatt [3], using nearly the same low levels of ClO as Kenner et al., obtained $\gamma < 1 \times 10^{-5}$ at 213 K. The difference may lie in the level of ClO or other adsorbable reactive species present. The lower value of Abbatt is probably closer to the expected reactivity under stratospheric conditions. Kenner et al. also measured a reaction probability limit of < (8 ±4) × 10^{-5} for NAT at 183 K. Back to Table

59. ClO + H_2SO_4 • nH_2O. Measured reaction probability (Martin et al. [317]) varies between 2 × 10^{-5} and 2 × 10^{-4} as H_2O content is varied by changing wall temperature. Reaction product is claimed to be HCl, not Cl_2. Abbatt [3] measured $\gamma < 1 \times 10^{-5}$ for 60 and 70 wt.% H_2SO_4 at 213 K. Back to Table

60. HCl + HNO_3 on H_2SO_4• m HNO_3 • nH_2O(l). Two studies have noted HCl activation in concentrated ternary $H_2SO_4/HNO_3/H_2O$ solutions or ice slurries. Luick et al. [311] saw only gas phase HCl in 64.6 wt.% H_2SO_4/ 4.8 wt.% HNO_3 at 200 K, but saw a vapor phase Cl partitioning of 50% HCl and 50% $ClNO/ClNO_2$ for a 76.6/20.1 wt.% solution (an ice slurry) at 200 K. Cappa et al. [75] saw substantial yields of ClNO, $ClNO_2$, and Cl_2 at 273 K for a range of solution compositions; e.g. 32.6%, 9.8% and 44.4% respectively for a total HCl conversion of 86.9% in a 35% H_2SO_4 /45% HNO_3 solution and 20.2%, 6.9%, 27.9% for a 60/25 wt.% solution. While no kinetic coefficients or detailed mechanisms are available, these studies do show the potential for HCl activation in strong $H_2SO_4/HNO_3/H_2O$ solutions. Back to Table

61. HOCl + HCl + H_2O(s) and HNO_3 • $3H_2O$(s). Hanson and Ravishankara [202] and Abbatt and Molina [8] have investigated the HOCl + HCl reaction on water ice and NAT-like surfaces, and Chu et al. [90]; [85] studied the reaction on water ice. Product yield measurements support the identification of Cl_2 and H_2O as the sole products. The measured yield of product Cl_2 is 0.87 ±0.20 and was stated to be similar on both surfaces according to Abbatt and Molina. Within the accuracy of the experiments, the reaction probability does not depend on the gas phase HCl and HOCl densities. Only Abbatt and Molina investigated at more than one temperature, their data indicates that γ increases at lower temperatures. A plot of data from the three studies does show a weak temperature trend, with γ increasing about a factor of two as the temperature drops from 202 to 188 K. However, the data are too sparse to assign a definitive temperature dependence. The average of all three studies yields $\gamma = 0.26 \pm 0.08$ for data based on the geometrical area of the flow tube surfaces. Chu et al. [85] indicate that a porosity correction for their data would reduce their value bya factor of 3 to 4. The real uncertainty would appear to be dominated by systematic uncertainties in porosity corrections and a potential temperature dependence. Given the fact that any porosity correction must reduce the value, a central value of 0.2 is adopted with an uncertainty factor of 2. The high reaction probabilities measured for water ice indicate that this reaction may play a significant role in release of reactive chlorine from the HCl reservoir.

    Two studies (Hanson and Ravishankara [202]; Abbatt and Molina [8]) have measured the reaction probability of HOCl + HCl on NAT surfaces. These data show γ increases as the ambient water pressure increases and then reaches a plateau. At relatively high water pressure, the two studies averaged $\gamma = 0.135 \pm 0.049$, with no porosity correction. The reaction probability on water poor NAT-like surfaces falls off dramatically (a factor of 10). A recommendation of 0.1 with an uncertainty factor of 2 is shown in Table 5-2. Carslaw and Peter [78] have published a model of this reaction and its dependence on HCl uptake. Back to Table

62. HOCl + HCl + H_2SO_4 • nH_2O(l). This process has been studied in coated flow tubes over ~200–260 K by Zhang et al. [495], Hanson and Ravishankara [206], Donaldson et al. [124], and Hanson and Lovejoy [197]. Hanson and Lovejoy also made measurements in an aerosol flow tube from 251 to 276 K. A model of this and related sulfuric acid aerosol reactions tailored to stratospheric conditions has been published by Hanson et al. [210]. Zhang et al. held the water vapor partial pressure at 3.8 × 10^{-4} Torr and showed γ increased by a factor of 50 as the temperature was lowered from 209 to 198 K increasing the water mole fraction, showing that the reaction rate is strongly dependent on water activity.

    A detailed kinetic uptake model has been developed to fit the experimental data [414]. The formulation for γ is given as:

$$\frac{1}{\gamma} = \frac{1}{\alpha} + \frac{1}{\Gamma^{rxn}_{HOCl}}$$

where

$$\Gamma^{rxn}_{HOCl} = \frac{4H_{HOCl}RT}{\bar{c}}\left(D_{HOCl}k_{HOCl\ \ HCl}\right)^{1/2}$$

At the low temperatures of interest, α for HOCl was assumed to be unity consistent with the value for HCl measured at 240 K and below (Robinson et al. [377]). The individual formulations for H_{HOCl}, D_{HOCl} and $k_{HOCl\text{-}HCl}$ are given in Table A-4 in Shi et al. [414]. Reaction of HOCl with HCl is considered to be acid catalyzed. It is known that the reaction rate for HOCl + HCl in pure water is low (Donaldson et al. [124]). Experimental data noted above indicated that the reaction rate of HOCl + HCl increases with acidicity of H_2SO_4 solution. The data from the experimental studies noted above were fit to the model without bias. Using the same error analysis discussed in the note for N_2O_5 uptake on sulfuric acid, a detailed kinetic model yields a 33.4% error (one sigma fit to the available data set, with σ_m=33.3% and σ_d=3.0%).

In the cold stratosphere where T<190 K, the reaction of $ClONO_2$ + HCl is so fast that HCl is depleted which slows down the reaction of HOCl + HCl. As shown in Table A-4 in Shi et al., the effect of HCl depletion on the HOCl reactive uptake coefficient (due to reaction with $ClONO_2$ inside/on the surface of particles) is taken into account via the factor F_{HCl} (also see the note on chlorine nitrate/hydrochloric acid reactive uptake on sulfuric acid surfaces). Back to Table

63. HOCl + HBr on H_2O(s). Chu and Chu [85] measured γ at 189 K to be in the range from 0.06 to 0.38 for HBr partial pressures ranging from 1.1×10^{-7} to 6.6×10^{-5} Torr. At 220 K they measured γ in the range from 0.01 to 0.07 for HBr partial pressures in the range from 7.2×10^{-7} to 1.3×10^{-5} Torr. These γ values were estimated assuming the area of the ice surface to be equal to the geometric area of the cylindrical flow reactor; corrections for surface porosity effects range from a factor of 3 to 10 lower. Back to Table

64. HOCl + HBr on $H_2SO_4 . nH_2O$(l). Abbatt and Nowak [9] measured uptake of HOCl in the presence of excess HBr on a 69.3 wt.% sulfuric acid solution in a wetted wall flow reactor at 228 K. A second order bulk reaction rate constant, k^{II}, of 2×10^6 $M^{-1}s^{-1}$ was derived; this is a factor of ~10 faster than HOBr + HCl under the same conditions. Since HOCl and HBr have similar solubilities under stratospheric conditions, characterizing this reaction with a simple uptake coefficient is not appropriate. A full reaction/solubility/liquid phase diffusion model will require further data. Back to Table

65. HOCl + KBr. Rossi reported [384] studies of the uptake of HOCl in a Knudsen cell using KBr powders and spray-deposited thin films. Values for the initial uptake coefficients covered a wide range, from 5×10^{-3} to 0.2, due to changes in the surface from adsorbed reaction products. The major product initially was Br_2, and subsequently BrCl and HOBr, with much smaller amounts of BrOCl and Br_2O. The mechanism was interpreted as the formation of small amounts of HBr on the surface from hydrolysis of KBr, followed by the reaction of HOCl with adsorbed HBr to form BrCl which then reacts with KBr to form Br_2. Back to Table

66. ClNO + H_2O(l). Scheer et al. [396] used droplet train and wetted wall flow reactor measurements to determine reactive uptake coefficients for ClNO over a temperature range of 273-293 K. Measured values show a weak negative temperature dependence ranging from 0.12 at 273 K to 0.0058 at 293K. Thereaction was shown to be base catalyzed producing HONO. Back to Table

67. ClNO + NaCl(s). Using a Knudsen cell technique Beichart and Finlayson-Pitts [53] set upper limits of γ < ~10^{-5} for reactive uptake of ClNO on NaCl(s) powders at 298 K. Back to Table

68. $ClNO_2$ + H_2O(l). Behnke, George and co-workers have used droplet train and wetted wall flow reactor techniques to investigate the reactive uptake of $ClNO_2$ on aqueous solutions [50, 139, 158, 407]. Droplet train flow reactor experiments fron 268-279 K demonstrated that the reactive uptake coefficient on pure water is <1 x 10^{-5} [158]. Wetted wall flow reactor studies from 279 to 292 K on pure water and very low concentration sodium halide solutions all yielded reactive uptake coefficients in the 10^{-6} range, with typical values of (4.84±0.13) x 10^{-6} at 291 K [50], and 3.41 x 10^{-6} at 276.6 K, 4.27 x 10^{-6} at 282.2 K, and 4.48 x 10^{-6} at 287.4 K [139]. There is apparently no significant temperature dependence. Back to Table

69. $ClNO_2$ + KBr, NaBr, NaI and NaCl. Caloz et al. [74] measured the uptake of $ClNO_2$ on solid KBr at room temperature using a Knudsen cell and salt samples in the form of powders, spray-deposited films, polished

windows and depolished windows. The uptake coefficient increased with the number of layers of salt powders; correction of the uptake coefficients using the pore diffusion model gave initial uptake coefficients of (1.0 - 1.3) × 10^{-4}, in agreement with values measured for the spray-deposited film (1.0 × 10^{-4}) and depolished window (1.0 × 10^{-4}). The value for the polished window was an order of magnitude smaller, as expected since this has much less surface-adsorbed water (SAW) that assists in keeping the surface from becoming passivated. The yield of Br_2 relative to $ClNO_2$ lost was 0.55 ± 0.2. Using a diffusion tube method, Koch and Rossi [284] measured an uptake coefficient of 2.0 × 10^{-4}, in reasonable agreement with the Knudsen cell results.

The uptake of $ClNO_2$ on aqueous solutions of NaBr has been shown to increase with the concentration of NaBr. Frenzel et al. [152] measured the uptake of $ClNO_2$ on (0.5 - 5) × 10^{-3} M NaBr solutions from 275–291 K using a wetted wall flow tube apparatus; the values of γ increased from 1.2 × 10^{-5} to 4.0 × 10^{-5} over this range of NaBr concentrations. Schweitzer et al. [407] used a droplet train apparatus from 275 - 288 K; γ increased from 8.6 × 10^{-6} to 9.4 × 10^{-4} as the NaBr concentration increased from 10^{-4} to 1.0 M. The main product was Br_2, with traces of $BrNO_2$ and BrCl. In a subsequent study [408], they applied a wetted wall flow tube method from 275–293 K and reported uptake coefficients that were independent of temperature over this range, but again increased with the concentration of NaBr: γ increased from 7.1 × 10^{-6} at 10^{-4} M NaBr to 9.2 × 10^{-4} at 1.0 M. Fickert et al. [141] used a wetted wall flow tube at 274 K and measured an uptake coefficient of 1.1 × 10^{-5} for 10^{-4} M NaBr, increasing to 1.1 × 10^{-4} for 10^{-2} M NaBr. The major gas phase products were Br_2 and $BrNO_2$, with the yield of $BrNO_2$ decreasing as the initial bromide ion concentration in solution increased. The mass accommodation coefficient for $ClNO_2$ on aqueous solutions at 275 K was measured to be (9 ± 4) × 10^{-3}. A Knudsen cell study by Beichart and Finlayson-Pitts [53] found $\gamma < \sim 10^{-5}$ on NaCl powders at 298 K.

The uptake of $ClNO_2$ on solutions of NaI was studied by George et al. [158] and by Schweitzer et al. [407, 408]. The uptake coefficient increases with the concentration of NaI. For example, George et al. [158] reported that γ_0 increased from 1.1 × 10^{-3} to 6.6 × 10^{-3} as the iodide concentration increased from 10^{-3} M to 10^{-2} M at 280 K. This is consistent with the results of Schweitzer et al. [407, 408] who reported that γ_0 increased from 3.1 × 10^{-5} to 4.5 × 10^{-3} as the iodide concentration increased from 10^{-4} M to 10^{-2} M at 275 K.

The uptake of $ClNO_2$ on solutions of NaCl is much slower than on NaBr or NaI solutions. Behnke et al. [50] reported uptake of $ClNO_2$ at 291 K using a wetted wall flow tube, with uptake coefficients decreasing as the NaCl concentration increased. At 0.1 M NaCl, γ_0 = (3.1 ± 0.3) × 10^{-6} but at 4.6 M NaCl, the value was about an order of magnitude smaller, γ_0 = (0.27 ± 0.02) × 10^{-6}. They proposed that this was due to the common ion effect owing to the reversible hydrolysis of $ClNO_2$ to Cl^- + NO_2^+. Back to Table

70. $ClONO_2$ + H_2O(s). Measurement of γ = 0.3 (+0.7, –0.1) (Hanson and Ravishankara [198]) significantly exceeds previous measurements of Molina et al. [335], Tolbert et al. [444], Leu [293] and Moore et al. [337] but agrees reasonably well with subsequent measurements by Chu et al. [90] and Zhang et al. [497] when geometrical surface areas are assumed for analysis. Previous measurements were probably complicated by NAT formation on the surface (Hanson and Ravishankara [202]; Chu et al. [90]). Lower levels of $ClONO_2$ (g) used by Hanson and Ravishankara [198] minimized this surface saturation problem. Also, using lower $ClONO_2$ concentrations, Zhang et al. obtained a reaction probability of 0.08 ± 0.02 at 195 K, in fair agreement with the range of 0.03 to 0.13 measured by Chu et al. Subsequent Knudsen cell measurements at 180 and 200 K by Oppliger et al. [351] showed initial uptake γs in the 0.2 to 0.4 range. Measured reaction products were HNO_3 and HOCl. All of the HNO_3 and much of the HOCl is retained on the surface under polar stratospheric conditions (Hanson and Ravishankara [198, 202]). Hanson [192] deposited $ClONO_2$ on $H_2{}^{18}O$ enriched ice and detected $H^{18}OCl$ showing the Cl–ONO2 bond is broken at 191 K.

Data plots confirm a trend showing that at a high density of $ClONO_2$, the product HNO_3 covers the ice surface preventing the further reaction of $ClONO_2$ with H_2O molecules on the surface. Therefore, data obtained at high $ClONO_2$ densities (>10^{14} molecules/cm^3) are excluded from further evaluation. An experiment (Berland et al. [58]) using a laser-induced thermal desorption technique yielded a much lower value of $ClONO_2$ reaction probability at 190 K (about 3 orders of magnitude lower) after extrapolating the results obtained at temperatures of 140 K and below. We also exclude this point in the averaging of data since the physical characteristics of ice surfaces at these very low temperatures may not be very representative of those found at stratospheric temperatures. Selected data show no temperature dependence between T=180 and 200 K and averaged γ_o= 0.28 ± 0.25. Again, within the experimental accuracy, the Hanson and Ravishankara [202, 204] and Chu et al. [90] data show that uptake measurements are nearly

independent of ice substrate thickness. See Henson et al. [216] for discussion of a model which accounts for the effect of HNO_3 on the reaction $ClONO_2$ on water and nitric acid ice surfaces.

Zondlo et al. [506] report the formation of a supercooled H_2O/HNO_3 liquid layer at 185 K as a reaction product, forming NAT or NAD only after decreasing the relative humidity below the ice frost point. This effect is similar to that resulting from the interaction of gaseous HNO_3 or N_2O_5 with the ice surface. These authors measured $\gamma = (3 \pm 2) \times 10^{-3}$ at 185 K for the reaction of $ClONO_2$ with this supercooled liquid layer. Back to Table

71. $ClONO_2 + H_2O$. Deiber et al [119] used a droplet train rector to measure to uptake of $ClONO_2$ on pure water between 274 and 285 K. No apparent temperature dependence was observed with all three temperatures measured resulting in reactive uptake measurements near 0.025. Back to Table

72. $ClONO_2 + HNO_3 \bullet nH_2O(s)$. Hanson and Ravishankara [198] report a γ value of 0.006 at 201 K for the $ClONO_2$ reaction with the water on NAT ($HNO_3 \bullet nH_2O$). However, these authors present re-analyzed and additional data with $\gamma \approx 0.001$ at 191 K in Hanson and Ravishankara [202, 204]. Similar experiments (Moore et al. [337], Leu et al. [295]) report a larger value of 0.02 ±0.01 which falls very rapidly as slight excesses of H_2O above the 3/1 H_2O/HNO_3 ratio for NAT are removed. They measure γ of less than 1×10^{-6} for slightly water poor NAT surfaces. The inconsistency between Hanson and Ravishankara and the JPL group (Moore et al. [337]; Leu et al., [295]) has not been resolved. Abbatt and Molina [7] report γ values reaching 0.002 at 202 K and high RH. Hanson and Ravishankara [202] reported that γ for this reaction increases by a factor of 4 as the surface temperature increases from 191 to 211 K. However, Knudsen cell measurements at 185 K by Barone et al. [37] reported $\gamma = 0.004$ at a relative humidity (RH) of 100%, rising to 0.007 near RH = 120%, indicating a possible mild negative temperature dependence when high RH values from this and other studies are compared. Excluding the JPL data, the other data obtained at high RH (~90%) were averaged, assuming no temperature dependence, to yield $\gamma = 0.0043 \pm 0.0021$. The strong dependence on RH and the possible temperature dependence suggest that systematic error probably exceeds the calculated statistical error. Within the experimental accuracy, the data of Hanson and Ravishankara [202, 204] show that measured uptake coefficients are independent of ice substrate thickness. Barone et al. report very similar uptake coefficients for nitric acid dihydrate (NAD) as for NAT as a function of RH at 202 K. See Henson et al. [216] for discussion of a model which accounts for the effect of HNO_3 on the reaction of $ClONO_2$ on water and nitric acid ice surfaces. Back to Table

73. $ClONO_2 + H_2SO_4 \bullet nH_2O(l)$. Results from wetted-wall flow tube (Hanson and Ravishankara [207]) Knudsen cell reactor (Manion et al. [315]), aerosol flow tube (Hanson and Lovejoy [196]), and droplet train uptake (Robinson et al. [376]) experiments supplement older wetted-wall flow tube (Hanson and Ravishankara, [200]) and Knudsen cell measurements (Rossi et al. [386], Tolbert et al [443]). Although earlier Knudsen cell measurements probably suffered from surface saturation, more recent results compare well with those from other techniques. Saturation free results, available over a temperature range of 200–265 K and a H_2SO_4 concentration range of 39 to 75 wt.%, were fit to a phenomenological model developed by Robinson et al. [376]. Measured γ values depend strongly on H_2SO_4 concentration and vary modestly with temperature, with a trend to somewhat higher values for the 210–220 K temperature range. The temperature-dependent uptake model takes into account the temperature and composition dependence of the effective Henry's Law constant, liquid phase diffusion coefficient, and the liquid phase hydrolysis rate constant. The hydrolysis reaction was treated by modeling two reaction channels, a direct hydrolysis process dominating reaction at low H_2SO_4 concentrations with a reaction rate proportional to water activity and a proton-catalyzed reaction with a rate proportional to H^+ activity, which dominates at higher acid concentrations.

The data fit to the original Robinson et al. model have been supplemented by additional wetted-wall flow tube and aerosol flow tube data from Hanson [193] and aerosol flow tube data from Ball et al. [35]. A revised kinetic model (Shi et al. [414]) incorporating these data has been developed that is based on the earlier work of Robinson et al. [376]. In this model, γ is calculated using the expression

$$\frac{1}{\gamma} = \frac{1}{\alpha} + \frac{1}{\Gamma_b^{H_2O}}$$

where,

$$\Gamma_b^{H_2O} = \frac{4H_{ClONO_2}RT}{\bar{c}}\left(D_{ClONO_2}k_{hydr}\right)^{1/2}$$

The detailed parameterizations for H_{ClONO_2}, D_{ClONO_2}, and k_{hydr} are given in the Appendix in Shi et al. [414] As was the case for N_2O_5 hydrolysis k_{hydr} is seen to have a direct and an acid catalyzed channel. Using the same error analysis approach as in the note on N_2O_5 uptake, the model error is about 32.4% (one sigma), with σ_m=32.2% and σ_d=4.0%.

In the calculation of the chlorine activation (Cl_2 production) rate under stratospheric conditions, one needs to take into account the competition between the reactions of $ClONO_2 + H_2O$ and $ClONO_2 + HCl$. The presence of HCl will depress the reaction probability of $ClONO_2$ with H_2O. Back to Table

74. $ClONO_2 + H_2SO_4 \cdot H_2O(s)$ and $H_2SO_4 \cdot 4H_2O(s)$. Measurements by Hanson and Ravishankara [205] and Zhang et al. [495] demonstrate that the reaction probability on the tetrahydrate is a strong function of both temperature and relative humidity, both of which affect the level of adsorbed H_2O. Both groups covered the temperature range of 192–205 K. The reaction is slowest at higher temperatures and lower relative humidities. Zhang et al. [495] have parameterized their data in the form of $\log \gamma = a_1 + a_2 \log x + a_3 \log^2 x$; for 195 K and x = water partial pressure in Torr: $a_1 = 10.12$, $a_2 = 5.75$ and $a_3 = 0.62$; for a water partial pressure of 3.4×10^{-4} Torr and x = T(K) between 182 and 206: $a_1 = 318.67$, $a_2 = -3.13$ and $a_3 = 0.0076$. Zhang et al.[499] have also measured a low value of $\gamma \sim 2 \times 10^{-4}$ on sulfuric acid monohydrate at 195 K. Back to Table

75. $ClONO_2 + HCl + H_2O(s)$. Reaction probabilities of 0.27 (+0.73, –0.13) (Leu [293]) and 0.05 to 0.1 (Molina et al. [335]) were reported at 195 and 185 K, respectively. Abbatt and Molina [7] and Hanson and Ravishankara [200] report that a portion of the reaction may be due to $HOCl + HCl \rightarrow Cl_2 + H_2O$, with HOCl formed from $ClONO_2 + H_2O(s) \rightarrow HOCl + HNO_3(s)$. Hanson and Ravishankara [198] saw no enhancement of the $ClONO_2$ reaction probability when $H_2O(s)$ is doped with HCl. Their preferred value at 192 K is $\gamma = 0.3$, but this is consistent with $\gamma = 1$. Chu et al. [90] also report a value of 0.27 (±0.19) at 188 K, assuming no correction for porosity, but suggest the true value is 0.10 (±0.08). Using a Knudsen cell technique and looking at initial uptake, Oppliger et al. [351] measured $\gamma = 0.7$ at 180 K and 0.2 at 200 K with HCl in excess. Eliminating the Molina et al. points, which were taken at much higher $ClONO_2$ concentrations than the others, plots of the remaining data show no obvious bias when plotted as a function of reactant concentration or temperature (180–200 K). Their average value $\gamma = 0.26 \pm 0.06$. The Oppliger et al. data were presented for two HCl concentrations, differing by a factor of three. All points from both HCl concentrations were included since all the data were generally consistent with previous measurements, although the higher HCl concentrations did tend to produce modestly higher uptake coefficients. Until a fuller model is available, a single temperature independent value with a moderate uncertainty due to surface porosity seems appropriate. Back to Table

76. $ClONO_2 + HCl + HNO_3 \cdot 3H_2O$. Measurements by Hanson and Ravishankara [198, 202], Leu and co-workers in Moore et al. [337] and Leu et al. [295], and Abbatt and Molina [7] all report high γ values (>0.1) on NAT for temperatures between 192 and 202 K. Hanson and Ravishankara indicate that reaction probabilities on NAD are similar to those on NAT. The most recent NAT studies (Abbatt and Molina [7]) show a strong fall-off with relative humidity from $\gamma > 0.2$ at 90% RH to 0.002 at 20% RH, indicating the necessity of sufficient water to solvate reactants. Within the limited measurements, data plots show no indication that the reaction probability of $ClONO_2 + HCl$ depends on HCl and $ClONO_2$ gas phase concentrations or temperature between 191 and 202 K. Averaged data yield is $\gamma = 0.23 \pm 0.10$. Carslaw and Peter [78] have published a model of this reaction and its dependence on HCl uptake. Back to Table

77. $ClONO_2 + HCl + H_2SO_4 \cdot nH_2O(l)$. Early work by Tolbert et al. [443] and Hanson and Ravishankara [200] indicated that the presence of HCl had little effect on the reaction of $ClONO_2$ with concentrated sulfuric acid (>65 wt.% H_2SO_4). Subsequent realization that HCl would be more soluble, and therefore a more potent reactant, in the colder, more dilute sulfuric acid aerosols characteristic of the polar stratosphere led to additional investigations by Hanson and Ravishankara [207], Zhang et al. [495], Elrod et al. [131] and Hanson [193]. All these measurements show a strong dependence of reactivity on HCl solubility, which in turn depends on water activity. The solubility of HCl in a wide range of sulfuric acid solutions has been experimentally determined by a range of techniques that agree well with current thermodynamic models. See Robinson et al. [377] for a review. Hanson and Lovejoy [196] measured a reacto-diffusive length, ℓ, of only 0.009±0.005 μm for 60 wt.% H_2SO_4 in an aerosol flow reactor. (See Hanson et al. [210] for a definition of

ℓ.) This is a factor of four lower than the value for the hydrolysis reaction of $ClONO_2$ showing the significant enhancement of $ClONO_2$ uptake due to HCl.

The $ClONO_2$ + HCl reaction on sulfuric acid has been modeled in Shi et al. [414] using the same phenomenological model for $ClONO_2$ hydrolysis driven uptake by sulfuric acid. Since the effect of HCl on the $ClONO_2$ uptake is to increase the $ClONO_2$ pseudo-first-order reaction rate, the model of $ClONO_2$ uptake (see note on $ClONO_2$ uptake on sulfuric acid) should include the pseudo first order reaction rate, k_{HCl}. The formulation of k_{HCl} is found in the Appendix in Shi et al. [414]. It is likely that the $ClONO_2$ reaction with HCl, like the $ClONO_2$ hydrolysis reaction, is acid catalyzed via protonated $HClONO_2^+$, where Cl^+ is activated as in the case of HOCl + HCl. For the $ClONO_2$ + HCl reaction, there is also a surface reaction (Hanson [193]). Hanson proposed that Γ_s is linearly proportional to water activity; however, the calculated value of γ_o at 250 K and 60 wt.% H_2SO_4 using his formulation is 0.02 (here $\gamma_o \sim \Gamma_s$), which is contradictory to his aerosol flow reactor result, which yielded γ_o=0.0079 (here $\gamma_o \sim \Gamma_b$) (Hanson and Lovejoy [196]). In the model presented in the Shi et al. appendix, it is assumed that that Γ_s is linearly proportional to Henry's law constant of $ClONO_2$, rather than the water activity. The temperature dependence of Γ_s is determined, based on two measured values of Γ_s at 203 K (Hanson, [193]) and 250 K (Hanson and Lovejoy, [196]). The model yields a value of $\gamma_o \sim 0.011$ (here $\gamma_o \sim \Gamma_s$), which is close to the measured value.

In the stratosphere, when the reaction rate of $ClONO_2$ with HCl exceeds the flux of HCl to the particle surface, HCl is depleted. This, in turn, will depress the rate of both the $ClONO_2$ and HOCl + HCl reactions, and increase the $ClONO_2$ hydrolysis rate. Shi et al. [414] have proposed a model in which this effect is taken into account by including a factor F_{HCl} (see Table A–3 in Shi et al.). The formulation of F_{HCl} is based on scaling HCl reaction and accommodation fluxes. This flux correction is not exact (i.e. it does not rigorously calculate the HCl surface or bulk concentration) but provides a good approximation to the expected reduction in HCl + $ClONO_2$/HOCl reactivity and, just as importantly, the effective increase in $ClONO_2$ + H_2O reactivity when $p_{ClONO_2} > p_{HCl}$. This is particularly relevant during cold Cl activation events when HCl can be removed almost completely (i.e., see Jaegle et al. [243]).

Using the same error analysis approach as in the note on N_2O_5 uptake by sulfuric acid, the error of using the model in the Appendix is about 40.0% (one sigma), with σ_m=39.8% and σ_d=4.0% Back to Table

78. $ClONO_2$+HCl + $H_2SO_4 \cdot H_2O$(s) and $H_2SO_4 \cdot 4H_2O$(s). This reaction has been studied by Hanson and Ravishankara [205] and Zhang et al. [495]. The reaction probability is strongly dependent on the thermodynamic state of the SAT surface, which is controlled by the temperature and the water vapor partial pressure. At a water vapor pressure of 5.6×10^{-4} Torr the measured γ drops by over two orders of magnitude as the SAT surface temperature rises from 195 to 206 K. The results from the two groups are in qualitative agreement, but sample different H_2O and HCl partial pressures. Zhang et al. have parameterized their data as a function of water partial pressure (at 195 K) and temperature (both at an HCl partial pressure of 4 to 8×10^{-7} Torr) in the form $\log \gamma = a_1 + a_2 \log x + a_3 (\log x)^2$. For H_2O partial pressure, $a_1 = 5.25$, $a_2 = 1.91$, and $a_3 = 0.0$; for T(K), $a_1 = 175.74$, $a_2 = -1.59$, and $a_3 = 0.0035$. Care must be taken in extrapolating either data set to lower HCl concentrations. Zhang et al. [499] measured no enhancement of $ClONO_2$ uptake on sulfuric acid monohydrate at 195 K with $(2–8) \times 10^{-7}$ Torr of HCl present, implying $\gamma < 1 \times 10^{-4}$. Back to Table

79. $ClONO_2$ + HCl + Al_2O_3(s). Molina et al. [334] used flow tube techniques to measure $\gamma = 0.020 \pm 0.005$ on α–alumina at 195–230 K with stratospheric (5 ppmV) water vapor levels. Measured γ was independent of T and was affected very little by 5 ppbv HNO_3 vapor. The same γ was measured for a Pyrex surface, indicating the absorbed water and not the inorganic substrate hosted the reaction. Back to Table

80. $ClONO_2$ + NaCl. Timonen et al. [440] studied the uptake of $ClONO_2$ on NaCl powders at 296 K and 225 K using a flow tube. Complete deactivation of the surface was observed at 225 K but not at 296 K. The initial uptake coefficients, after correction (typically by an order of magnitude) using the pore diffusion model of Keyser et al. [274, 275] were $\gamma_0 = (4.6 \pm 3.1) \times 10^{-3}$ (1 σ) at 296 K and $\gamma_0 = (6.7 \pm 3.2) \times 10^{-3}$ (1 σ) at 225 K. Caloz et al. [73] used a Knudsen cell and found that the initial uptake coefficient was 0.23 ± 0.06, independent of the type of salt used (powders, single crystals, deposited salt films) and without applying a correction for pore diffusion since no mass dependence for γ was observed; in similar studies. Aguzzi and Rossi [11] measured a value of $\gamma_0 = 0.10 \pm 0.05$ for the uptake of $ClONO_2$ on NaCl and 0.27 ± 0.10 for uptake on the unreactive $NaNO_3$ and Na_2SO_4 salts. The Cl_2 yield was 100% for NaCl, in agreement with the earlier studies [73, 440] but 27 ± 7 % on the unreactive salts. Koch and Rossi [284] used a diffusion tube technique to measure a value of 0.1 for the uptake coefficient. Gebel and Finlayson-Pitts [156] used a

Knudsen cell and measured an initial value of $\gamma_0 = 0.14 \pm 0.11$ (2 σ) and a steady-state value of $\gamma = (3.9 \pm 1.8) \times 10^{-2}$, but concluded that approximately two layers of salt were sampled in these multi-layer experiments. The use of a single or sub-single layer of NaCl gave a steady state value corrected using the model of Hoffman et al. of $\gamma = (2.4 \pm 1.2) \times 10^{-2}$ [220]. The source of the very disparate results from the different groups and techniques is not clear. All studies agree that the yield of Cl_2 is 100%, consistent with $ClONO_2 + NaCl \rightarrow Cl_2 + NaNO_3$ as observed earlier [144], with small amounts of HOCl from hydrolysis of $ClONO_2$ on the surface being observed in the presence of water.

Deiber et al. [119] studied the uptake of $ClONO_2$ on water, NaCl and NaBr solutions using a droplet train flow reactor. The uptake coefficient was the same on water and 0.1 M NaCl, and Cl_2 was observed as the gas phase product. Back to Table

81. $ClONO_2$ + KBr and NaBr. Caloz et al. [73] and Aguzzi and Rossi [11] report a rapid uptake of $ClONO_2$ on KBr solid salts at room temperature, $\gamma_0 = 0.35 \pm 0.06$ and $\gamma_0 = 0.18 \pm 0.07$ respectively; corrections for pore diffusion were not applied but are not expected to be large at these high uptake coefficients (see Introduction). This is consistent with a value of 0.1 measured by Koch and Rossi [284] using a diffusion tube technique. The reaction products are BrCl, Br_2 and Cl_2. BrCl is the initial reaction product formed from $ClONO_2 + KBr \rightarrow BrCl + KNO_3$. Br_2 is generated in a secondary reaction of BrCl with KBr: $BrCl + KBr \rightarrow Br_2 + KCl$. Cl_2 is then formed as the surface KBr is converted to KCl, which then reacts with $ClONO_2$.

    Deiber et al. [119] studied the uptake of $ClONO_2$ on water, NaCl and NaBr solutions using a droplet train flow reactor. On NaBr, the uptake increased from 0.041 at 0.01 M NaBr to 0.073 at 1 M NaBr. From the dependence on the NaBr concentration, a value for the mass accommodation coefficient for $ClONO_2$ of 0.108 $\pm$ 0.033 (2 σ) was obtained. The gas phase products were BrCl and Br_2, the latter formed by secondary reactions of BrCl with Br^-. Back to Table

82. $ClONO_2$ + sea salt. Gebel and Finlayson-Pitts [156] reported a rapid reaction between $ClONO_2$ and synthetic sea salt, with initial values based on the geometric sample area of $\gamma_0 = 0.42$ and steady-state values of $\gamma = 0.16$ (2 σ). These were measured with multiple salt layers (3 - 236) but corrections for diffusion into underlying layers for such high uptake coefficients are relatively small, less than a factor of three. The yield of Cl_2 was 78 $\pm$ 13%; small amounts of HCl and HOCl were also observed as products. The recommended lower limit is based on these studies and the rapid uptake of other reactive species such as HNO_3 and N_2O_5. Back to Table

83. $ClONO_2$+HBr + $H_2O(s)$ and $HNO_3 \bullet nH_2O(s)$. This reaction was studied by Hanson and Ravishankara [201] on water ice and NAT near 200 K. A diffusion-limited reaction probability of >0.3 was observed. Allanic et al. [23] measured $\gamma = 0.56 \pm 0.11$ at 200 K on water ice, observing Cl_2 and Br_2 to be formed in yields of 100% and 66 to 80%, respectively, in the range 180 to 200 K. Back to Table

84. $ClONO_2$ + HF + $H_2O(s)$ and $HNO_3 \bullet nH_2O(s)$. Hanson and Ravishankara [201] were not able to observe this reaction on water ice and NAT surfaces near 200 K. Back to Table

85. $CF_xCl_{(4-x)}$ (x=0–3) and $CF_2Br_2 + Al_2O_3(s)$. Robinson et al. [374] reported dissociative uptake of CF_2Cl_2 and CF_2Br_2 on α-alumina surfaces at 210 and 315 K. Reaction probabilities of about 1×10^{-3} at 210 K were measured by monitoring the amounts of surface species bonded to the Al_2O_3 substrate. A re-analysis (Robinson et al. [375]) lowered this value by about a factor of 50. Moderate surface dosage with water vapor did not quench the reaction. In addition, Dai et al. [108] and Robinson et al. [373] studied dissociative chemisorption of CF_3Cl, CF_2Cl_2, $CFCl_3$, and CCl_4 on dehydroxylated γ-alumina powders. The obtained reactive uptake probabilities ranging from 0.4×10^{-5} for $CFCl_3$ to 1.0×10^{-5} for $CFCl_3$ over a temperature range of 120 to 300 K. HCl and halomethyl radicals were observed as desorption products. Loss of these products may point to somewhat higher γs, since they were measured by integrating halogen bound to Al_2O_3 substrates. Back to Table

86. BrCl + NaCl, KBr and NaI. The uptake of BrCl on solid NaCl and KBr using a Knudsen cell has been reported by Aquzzi and Rossi [11], yielding 298 K values of 6×10^{-2} for NaCl and 0.14 on KBr. An earlier preliminary study from the same group reported a value at γ>0.1 on KBr [73]. Insufficient data are available to make a recommendation.

    Katrib et al. [267] measured the uptake of BrCl on aqueous solutions of NaI over the temperature range from 273 to 288 K; the uptake coefficient increased from 0.37×10^{-2} to 0.7 as the I^- concentration increased from 1

$\times 10^{-4}$ to 0.5 M NaI. The complex dependence on the I^- concentration indicated that a surface reaction was occurring at the air-solution interface. Back to Table

87. Br_2 + NaCl, KBr and NaI. Only one report of the uptake of Br_2 on solid NaCl and KBr using a Knudsen cell is available [11] as part of a study of $BrONO_2$ uptake on salts. The uptake coefficient for Br_2 was 4 x 10^{-3} on NaCl and 3×10^{-3} on KBr. Insufficient data are available to make a recommendation.

    Hu et al. [226] measured the uptake of Br_2 on aqueous solutions of NaI using a droplet train flow reactor over the temperature range of 263 to 293 K. The measured uptake coefficients decreased from 0.33 at 263 K to 0.08 at 293 K, with evidence for a significant contribution from a reaction at the interface between Br_2 and I^-. Back to Table

88. BrO + H_2O(s), $H_2SO_4 \bullet nH_2O$(l) and NaCl(aq). Abbatt [3] used a coated flow tube technique to measure heterogeneous uptake on water ice, 60 and 70 wt.% H_2SO_4 at 213 K, and 23 wt.% aqueous NaCl at 253 K. He obtained γ(ice) = $(1.0 \pm 0.4) \times 10^{-3}$, γ (60 wt.% H_2SO_4) = $(7 \pm 2) \times 10^{-4}$, γ (70 wt.% H_2SO_4) = $(5 \pm 2) \times 10^{-4}$ and γ (23 wt.% NaCl) < 3×10^{-3}. He observed product Br_2, indicating BrO self-reaction on both water ice and sulfuric acid solutions. Since reaction rate will depend on BrO concentrations, no recommendation is made for an atmospheric rate. Back to Table

89. HOBr + HCl(s). Abbatt [1] measured γ = 0.25 (+0.10/-0.05) for this reaction on ice at 228 K. Chaix et al. [81] measured γ = 0.3 on ice from 180 to 195 K, dropping to ~0.15 at 205 K. The BrCl product was observed by mass spectrometry. Mossinger et al. [338] report a lower limit for γ of 0.1, under conditions with HCl concentration in excess of the HOBr concentration. No data on NAT surfaces is available. Back to Table

90. HOBr + HCl + $H_2SO_4 \bullet nH_2O$. For the sulfuric acid reaction, Abbatt [2] measured γs of ~ 0.1 to 0.2 for [HCl] > 1×10^{12} cm^{-3} over 68.8 wt.% H_2SO_4 at 228 K; yielding an estimated $k^{II}_{HCl+HOBr} = 1.4 \times 10^5$ M^{-1} s^{-1} with a factor of 2 uncertainty. Hanson and Ravishankara [208] also measured γ< = 0.2 [+0.2, – 0.1] for 60 wt.% H_2SO_4 at 210 K. However, both of these measurements were based on significant underestimation of the solubility of HOBr in the relevant sulfuric acid solutions. More recent measurements by Waschewsky and Abbatt [468] indicate that H for HOBr varies slightly with acidity between 60 to 70 wt.% H_2SO_4 and more strongly with temperature between 208 and 238 K. (For 59.7 wt.% H_2SO_4, H (M atm^{-1}) = 1.2×10^6 at 208 K and and 2.2×10^5 at 228 K.) The HOBr + HCl second order liquid phase rate constant, $k^{II}_{HCl+HOBr}$, varies between 2×10^5 and 3×10^8 ($M^{-1}s^{-1}$) between 213 and 238 K over the same composition range (60–70 wt.% H_2SO_4). Such a strong dependence on acid composition for the reaction rate of HOBr + HCl and the very small acid composition dependence for HOBr solubility in H_2SO_4 solution might be partially due to the formation of H_2OBr^+ in the acidic solution as discussed in their paper. However, this acid catalyzed reaction, i.e. H_2OBr^+ + HCl, alone does not completely account for measured reaction rates over the acid composition range studied.

    Using the Henry's Law data for HOBr reported by Waschewsky and Abbatt [468], the limiting reagent will vary depending on atmospheric temperature (H_2SO_4 wt.%) and the concentrations of HOBr and HCl. For stratospheric conditions where [HOBr] is 10 pptv and [HCl] 1ppbv, they predict dissolved HOBr will be in excess above 204 K and HCl in excess below 204 K for a H_2O vapor partial pressure of $3x10^{-7}$ atm. From their coated wall flow reactor uptake measurements, Waschewsky and Abbatt [468] derived expressions for $k^{II}_{HCl+HOBr}$ and predicted uptake coefficients. For temperature between 204 and 218 K where HOBr is likely to be in excess, they calculated HCl uptake coefficients, γ_{HCl}, which range between 7×10^{-5} and 9×10^{-5}. For temperatures in the 202–198 K range, where dissolved HCl is likely to be excess, the calculated uptake coefficients for HOBr, γ_{HOBr}, of ~1×10^{-2}. Hanson has reported Henry's law solubility data for 58-70 wt.% sulfuric acid and reactive uptake coefficients for HCl on HOBr doped sulfuric acid surfaces using a wetted wall flow reactor [188]. Hanson's reported that H_{HOBr} was independent of acid concentration at 250 K, however, the heat of solvation for HOBr derived is significantly lower (-12.5±3.7 versus -9±1 kcal/mol reported at lower temperatures by Waschewsky and Abbatt) that the values of H_{HOBr} based on Hanson's data are mush lower than the prior study's when extrapolated to their lower temperatures. Hanson's reported γ_{HCl} are strongly dependent on HOBr partial pressure and drop almost three orders of magnitude as the sulfuric acid concentration is raised from 58 t6 9.5 wt.%, possibly because HCl may be reacting with sulfuric acid at higher acid concentrations. The higher temperature $k^{II}_{HCl+HOBr}$ values computed by Hanson for his data disagree, when extraplated to lower temperatures with the vales reorted by Waschewsky and Abbatt as well as a prior lower temperature value reported by Hanson and Ravishankara [208], better agreement can be obtained if the solvation enthalpy reported by Hanson is used to adjust the H_{HOBr} values used in the earlier, lower temperature studies. Clearly, the HOBr + HCl reaction will be difficult to parameterize in a simple

manner. Potential inconsistencies in their $k^{II}_{HCl+HOBr}$ values, as discussed by Waschewsky and Abbatt [468] and Hanson [188] indicate that further measurements will be required before this reaction can be definitively modeled. Back to Table

91. HOBr + HBr + H_2O(s) and $H_2SO_4 \bullet nH_2O$. Abbatt [1] measured $\gamma = 0.12 \pm (0.03)$ on ice at 228 K. Chiax et al. [81] measured γ_o values ranging from 0.44 at 180 K to 0.15 at 205 K. The Br_2 product was observed by mass spectrometry. Abbatt [2] measured $\gamma = 0.25$ for [HBr] = 1×10^{12} cm^{-3} over 68.8 wt.% H_2SO_4 at 228 K; yielding an estimated $k_{II} > 5 \times 10^4$ M^{-1} s^{-1}. Back to Table

92. HOBr + NaCl. Mochida et al. [333] studied the uptake of HOBr on NaCl using multi-layer powders (10 - 500 μm) in a Knudsen cell at room temperature. After correction (by about an order of magnitude) for diffusion into the underlying layers, they obtained values for the initial uptake coefficient in the range of $(0.97 - 6.5) \times 10^{-3}$, with the corrected values decreasing with increasing concentrations of HOBr. They attributed this to competition between the reaction of HOBr with NaCl and a self-reaction of HOBr on the surface: 2 HOBr $\rightarrow$ Br_2 + H_2O + O_2. Their final value of $\leq 6.5 \times 10^{-3}$ is based on their extrapolation back to very low HOBr concentrations. Both Br_2 and BrCl were observed as products. Chu et al. [87] measured the uptake of HOBr on NaCl at 250 K over a range of RH from 1.5 to 22.5%. After correcting the measured loss of HOBr by a factor of ~ 30 for diffusion into the underlying salt layers using the pore diffusion model, they obtained a value $\gamma_o = 5 \times 10^{-5}$. The smaller value compared to the Knudsen cell results of Mochida et al. [333] may be due to the much lower temperature they used; BrCl was the only gas phase product observed.

Abbatt and Waschewsky [10] measured the uptake of HOBr on deliquesced 1 - 5 μm NaCl particles (75% RH); for particles at pH values of 0.3 and 7.2, a lower limit to the uptake coefficient of $\gamma_o > 0.2$ was measured. On unbuffered particles, the upper limit for the uptake coefficient was $\gamma_o < 1.5 \times 10^{-3}$ due to the limited availability of H^+ for the reaction between HOBr and Cl^- to form BrCl. Back to Table

93. HOBr + KBr and NaBr. Mochida et al. [333] studied the uptake of HOBr on solid KBr using multi-layer powders and spray-deposited films in a Knudsen cell. After correction (by factors of ~ 4-5) for diffusion into the underlying layers for the powders, they obtained values for the initial uptake coefficient in the range of $(1.3 - 8.4) \times 10^{-2}$, with the corrected values again decreasing with increasing concentrations of HOBr due to the self-reaction of HOBr on the surface: 2 HOBr $\rightarrow$ Br_2 + H_2O + O_2. On spray-deposited films where correction for diffusion into the underlying layers is not necessary, a value of 0.18 ± 0.04 was measured. The recommended upper limit is based on their extrapolation back to very low HOBr concentrations for the powders, and the spray-deposited film results. Br_2 was the only product observed.

Chu et al. [87] measured the uptake of HOBr on NaBr at 250 K in a flow tube at RH from 0.5 to 12 %. After correction by approximately an order of magnitude for diffusion of HOBr into the underlying salt layers using a pore diffusion model, a value for γ_0 of 2.5×10^{-3} was obtained; the smaller value may be due to the much lower temperature at which these studies were carried out. Again, Br_2 was the only product observed.

The uptake of HOBr on aqueous solutions of NaBr has been measured by Wachsmuth et al. [463] and by Fickert et al. [140] Wachsmuth et al. [463] report a rapid rate of uptake that is limited by mass accommodation; the mass accommodation coefficient was calculated to be 0.6 ± 0.2. This is consistent with the studies of Fickert et al. [140] who reported a lower limit for the mass accommodation coefficient of 1×10^{-2} at 274 K and observed that Br_2 was released at 100% yield at pH < 6.5. The yield of Br_2 decreased rapidly with pH at higher pH values due to the declining ratio of HOBr to BrO^-.

Fickert et al. [140] also measured the uptake of HOBr on aqueous solutions containing mixtures of NaCl and NaBr. BrCl was the major product at small Br^- concentrations while Br_2 dominated as the bromide ion concentration in solution increased. Back to Table

94. $BrNO_2$ + H_2O(l). Behnke, George and co-workers have used wetted wall flow reactor techniques to investigate the reactive uptake of $BrNO_2$ on aqueous solutions from 276 to 298 K [407] and [139]. Measured reactive uptake coefficients range from 1 to 3.5×10^{-6} with a small postive temperature dependence. Back to Table

95. $BrNO_2$ + KCl and NaCl. Caloz et al. [74] measured an uptake coefficient for $BrNO_2$ on KCl of 5×10^{-2}, but concluded that it was due only to reaction with a small bromide impurity in the KCl; as expected if this is the case, only Br_2 was generated in the reaction.

The uptake of $BrNO_2$ on aqueous solutions of 0.5 M NaCl has been measured using a droplet train flow reactor by Schweitzer et al. [407] from 277 - 293 K yielding $\gamma_0 \sim 1 \times 10^{-5}$. Frenzel et al. [152] used a wetted wall flow tube to obtain a lower limit for the uptake coefficient of 3.8×10^{-5} at 291 K. Back to Table

96. $BrNO_2$ + KBr, NaBr and NaI. Caloz et al. [74] used a Knudsen cell to study the uptake of $BrNO_2$ on solid KBr powders. The uptake was fast, $\gamma_0 \geq 0.3$, with production of Br_2 as the gas phase product.

On aqueous solutions of NaBr, the uptake coefficient increases as the concentration of NaBr increases [152, 407, 408]. For example, at 278 K, γ_0 increased from 8.6×10^{-6} to 1.1×10^{-4} as the NaBr concentration increased from 5×10^{-4} to 5×10^{-2}, but was independent of temperature over the range from 275 - 293 K [408]. The major gas phase product is Br_2, with smaller amounts of $BrNO_2$ and only at the smaller concentrations of NaBr [407, 408].

The uptake of $BrNO_2$ on aqueous NaI solutions has been determined using a droplet train flow reactor [407] and a wetted wall flow tube [408]; the uptake coefficient from 4.4×10^{-5} to 4.4×10^{-4} as the iodide concentration increased from 10^{-4}M to 5×10^{-3} M [408]. Back to Table

97. $BrONO_2$ and $BrONO_2$ + HCl + H_2O(s). Hanson and Ravishankara [204] investigated these reactions in an ice-coated flow reactor at 200 (±10) K. The reaction of $BrONO_2$ with H_2O(s) proceeded at a rate indistinguishable from the gas phase diffusion limit, implying that the reaction probability may be as high as one; the product BrNO(g) was observed. Allanic et al [22] used a Knudsen cell reactor to measure $BrONO_2$ uptake between 190-200 K. Values of initial γ's in the 0.2-0.3 range were observed. An average $\gamma = 0.26 \pm 0.05$ was obtained from all of the appropriate data from both experiments**.** Aguzzi and Rossi [13] studied the hydrolysis reaction on various types of ices, obtaining $\gamma = 0.34 \pm 0.03$ at 180 K and $\gamma = 0.15 \pm 0.01$ at 210 K. They observed HOBr as the main product and Br_2O as a secondary product. Hanson and Ravishankara [204] also codeposited HCl with $BrONO_2$ observing rapid production of BrCl. It is unclear whether BrCl is produced directly from $BrONO_2$ + HCl or via HOBr (from $BrONO_2$ hydrolysis) reacting with HCl. Back to Table

98 $BrONO_2$ + H_2O(l). Deiber et al. [119] used a droplet train rector to measure to uptake of $BrONO_2$ on pure water between 272 and 280 K. An apparent positive temperature dependence was observed with measured reactive uptake measurements ranging from 0.024±0.0008 at 272.5 K to 0.039±0.0012 at 279.7 K. Back to Table

99. $BrONO_2$ and BrONO2 + HCl + H_2SO_4•nH_2O(l). Hanson and co-workers used both coated flow tube and aerosol flow tube techniques to show that the reaction of $BrONO_2$ with 45–70 wt.% H_2SO_4 is extremely facile at temperatures from 210 to 298 K. Hanson and Ravishankara [208] measured γs of 0.5 (+0.5, –0.25) (45 wt.% H_2SO_4, 210 K, 0.4 (+0.6, –0.2) (60 wt.%, 210 K), and 0.3 (+0.7, –0.1) (70 wt.%, 220 K) in a coated-wall flow tube experiment. Hanson et al. [209], measured $\gamma \sim 0.8$ (20 to 40% error) for submicron aerosols at temperatures between 249 and 298 K and H_2SO_4 concentrations of 45 to 70 wt.%; there was a sharp fall off in γ for H_2SO_4 concentrations between 73 and 83 wt.%. Hanson also reported additional temperature dependent (230-295 K) coated flow reactor and room temperature (295-300 K) aerosol flow reactor studies extending measurements to higher acid wt.% values [188]. Hanson has analyzed these combined data sets, the data indicated that γ is a function of sulfuric acid concentration, but independent of temperature. After eliminating one previously reported anomalously low 83 wt.% data point Hanson has fit an empirical expression for measured γs for $BrONO_2$ + H_2O in the form of: $1/\gamma=1/\alpha +1/\gamma_{rxn}$, where $\gamma_{rxn} = \exp(a+b*wt.)$ and α=0.80, and a=29.2, b=–0.40 [188]. Using the same approach as detailed in the note for N_2O_5 uptake on sulfuric acid, the error for $BrONO_2$+ H_2O is 27.3% (one sigma), with γ_m=26.6% and γ_d=6.3%. Addition of excess HCl to 229 K, 40 and 60 wt.% H_2SO_4 aerosols caused an increase in γ to 1.0 and 0.9, respectively [209]. Back to Table

100. $BrONO_2$ + HBr. Aguzzi and Rossi [13] measured γ over the 180-210 K temperature range, with $\gamma = 0.3$ at 180 K and an activation energy of -1.2 ± 0.2 kcal/mol. Back to Table

101. $BrONO_2$ + NaCl. Aguzzi and Rossi [11] used a Knudsen cell and three types of NaCl samples (powders, spray-deposited and single crystal) to measure the uptake of $BrONO_2$ and obtained consistent results with $\gamma_0 = 0.31 \pm 0.12$. No correction for diffusion into the powders was made because of the high uptake coefficient (see Subsection 5.6). BrCl was the major product, 80 ± 20%, with smaller amounts (~ 10%) of Br_2 and some HCl. Rapid uptake of $BrONO_2$ of the same magnitude was observed on the unreactive salts $NaNO_3$ and Na_2SO_4, with a Br_2 yield of 45 ± 10%; this uptake and reaction was attributed to the self-reaction of $BrONO_2$ on the surface to generate Br_2O which decomposed to Br_2.

Deiber et al. [119] studied the uptake of $BrONO_2$ on water, NaCl and NaBr solutions using a droplet train apparatus from 272 - 280 K. The uptake coefficient was the same on water and 0.1 M NaCl, where BrCl was observed as the gas phase product. On NaBr, the uptake increased with the square root of the NaBr concentration, from which a value for the mass accommodation coefficient for $BrONO_2$ of 0.063 ± 0.021 (2 σ) was obtained. Back to Table

102. $BrONO_2$ + KBr and NaBr. Aguzzi and Rossi [11] used a Knudsen cell and three types of KBr samples (powders, spray-deposited and single crystal) to measure the uptake of $BrONO_2$ and obtained consistent results with $\gamma_0 = 0.33 \pm 0.12$. No correction for diffusion into the powders was made because of the high uptake coefficient (see Subsection 5.6). Br_2 was the major product, with its yield decreasing as the concentration of $BrONO_2$ increased; this was attributed to a competition between the reaction of $BrONO_2$ with KBr and the self-reaction of $BrONO_2$ on the surface.

    Deiber et al. [119] studied the uptake of $BrONO_2$ on water, NaCl and NaBr solutions using a droplet train flow reactor from 272 - 280 K. The uptake coefficient was the same on water and 0.1 M NaCl. On NaBr, the uptake increased with the square root of the NaBr concentration, from which a value for the mass accommodation coefficient for $BrONO_2$ of 0.063 ± 0.021 (2 σ) was obtained. The gas phase product on the NaBr solution was Br_2. Back to Table

103. $CF_3OH + H_2O + H_2O(l)$ and $H_2SO_4 \bullet nH_2O(l)$. Lovejoy et al. [310] used both wetted-wall and aerosol flow tube techniques to measure reactive uptake of CF_3OH on water at 274 K and 39–60 wt.% H_2SO_4 at various temperatures between 206 and 250 K. γ's showed a strong dependence on water activity. Aerosol uptake studies yielded reacto-diffusive lengths of > 0.4 µm for 40 wt.% H_2SO_4 and 1.0 µm for 50 wt.% H_2SO_4, both at 250 K. Recommended γ's were estimated by averaging bulk uptake measurements at similar H_2SO_4 concentrations and ignoring temperature effects on water activity. Back to Table

104. $O_3 + SO_2 + Al_2O_3(s)$. Usher et al. [452] present Knudsen cell data showing that pretreatment of α-alumina with SO_2 increases γ_o values for O_3 uptake by 30%; FTIR observations by the same group show that O_3 oxidized surface sulfite and bisulfite formed by SO_2 absorption to sulfate and bisulfate. Back to Table

105. $SO_2 + H_2O_2$, O_3, HONO, NO_2, $HNO_3 + H_2SO_4 . nH_2O(l)$. Rattigan et al. [364] used a bubble train reactor to measure the uptake of SO_2 in the presence of solvated oxidants at 293 K. For H_2O_2 the second order rate constant at 1 wt.% H_2SO_4 agreed well with previous bulk kinetics measurements and with previous droplet train/flow reactor measurements. Measurements at 20, 40, and 60 wt.% H_2SO_4 are the first reported for concentrated acid. Reaction rate data were fit to a two term (acid catalyzed and water catalyzed) bulk second order rate expression, which, in the limit of high acid activity ($a_{H^+} = \alpha_{H+}[H^+]$, where α_{H+} is the H^+ activity coefficient) reduces to: $k^{II}_{H_2O_2} = 8.3 \times 10^4 (\alpha_{H_2O} / a_{H^+})$, where α_{H_2O} is the water activity coefficient. Both α_{H+} and α_{H_2O} can be obtained from the sulfuric acid thermodynamic model of Carslaw et al. [77]. The high a_{H^+} approximation for $k^{II}_{H_2O_2}$ should be accurate to a factor of two between 40 and 70 wt.%.

    Uptake of SO_2 in the presence of solvated O_3 was measured for 1–70 wt.% acid; the Henry's law expression for O_3 was determined in separate experiments. Measured second order rates agree reasonably well with previous results measured below 18 wt.%. A three term fit for reaction with $SO_2(aq)$, HSO_3^-, and $SO_4^=$ was fit to the data: $k^{ii}_{O_3} = 6.6 \times 10^3 [SO_2(aq)] + 3.2 \times 10^5 [HSO_3^-] + 1 \times 10^9 [SO_4^=]$. This expression should be accurate to a factor of two between 20 and 70 wt.%.

    The HONO reaction was studied by adding nitrosyl sulfuric acid to 20, 40, 60, and 70 wt.% acid. Measured second order rate constants were moderately consistent with previous measurements below 10 wt.%. A $k^{II}_{HONO} = 142[H^+]$ was fit to the full data set; it should be accurate to a factor of two for acid concentrations between 10 and 70 wt.%.

    No enhanced SO_2 uptake was observed with added gas phase NO, NO_2, or with 20 wt.% HNO_3 added to 50–60 wt.% sulfuric acid. Back to Table

106. $SO_2 + Al_2O_3$. Goodman et al. [174] used FTIR observations of SO_2 absorption on α-alumina to show that surface bound sulfite and bisulfite products are produced, they integrated these surface feature absorbencies to estimate a γ_o of $(9.5 \pm 0.3) \times 10^{-5}$. Usher et al. [451] performed BET corrected room temperature studies on four α-alumina samples reporting and average γ_o of $(1.6 \pm 0.5) \times 10^{-4}$. FTIR studies of SO_2 uptake on commercial γ-alumina catalyst samples also show sulfite formation on non-hydroxylated surfaces [110, 265]. Back to Table

107. SO_2 + NaCl and sea salt. Gebel et al. [157] reported no measurable uptake of SO_2 on NaCl, yielding an upper limit of 1×10^{-4} for the uptake coefficient. The same was true for synthetic sea salt that had been heated while pumping. However, sea salt that had not been heated or pumped on extensively had a rapid uptake of SO_2, with initial uptake coefficients as large as 0.09. The time dependence of the uptake coefficient was consistent with uptake of SO_2 into a liquid layer, likely due to large amounts of water adsorbed on the hygroscopic components of sea salt such as magnesium hydrate. No gas phase products were observed but sulfite formation in the salt was seen by FTIR, indicating that uptake was due to dissolution of SO_2 into the water film on the salt surface. Back to Table

108. $SO_3 + H_2SO_4 . nH_2O(l)$. Jayne et al. [248] measured the uptake coefficient in a wetted wall-flow reactor at 300 K over a composition range of 78–92 H_2SO_4 wt.%. The measured γ was indistinguishable from 1.0. Higher water concentrations and lower temperatures probably tend to increase γ, so a value near 1.0 probably holds for all atmospheric conditions. Back to Table

5.15 Soot Surface Uptake Coefficients

Table 5-3. Soot Surface Uptake Coefficients

Gaseous Species	Uptake Coefficient (γ)	Notes
SO_2	See Note	1, 2
NH_3	0, See Note	1, 3
O_3	See Note	1, 4
HNO_3	See Note	1, 5
N_2O_5	See Note	1, 6
NO_2	See Note	1, 7
NO_3	See Note	1, 8
HO_2	See Note	1, 9
HO_2NO_2	See Note	1, 10
H_2O	See Note	1, 11

5.16 Notes to Table 5-3

1. See also the sections on soot under "Surface Types" and "Parameter Definitions" for a description of some of the factors affecting the uptake and reaction of gases on soot surfaces. In most cases, the available reactive surface area rather than the geometric areas have been used in obtaining the uptake coefficients; in those cases where the geometric area was used but a higher available surface area was involved in the measured uptake, the uptake coefficient is given as an upper limit. Most data are available at room temperature or there are very limited data at lower temperatures characteristic of the upper troposphere. Back to Table

2. SO_2 + soot. $\gamma \leq 3 \times 10^{-3}$ measured using Degussa FW2 carbon black by Rogaski et al. [382]. This is an upper limit since it is based on the geometric surface area. Koehler et al. [287] measured an average value of $(2 \pm 1) \times 10^{-3}$ over the first 10–30 s on n-hexane soot at –100° C (the initial uptake may be larger), but indicate that taking into account surface roughness would reduce this value. A number of studies [32, 91, 92, 103, 287, 303, 382] suggest that uptake is primarily due to physisorption on the surface; oxidation occurs in the presence of water, oxidants and metals. Back to Table

3. NH_3 + soot. Chughtai et al. [91] and Muenter and Koehler [343] measured the uptake of NH_3 on soot. Based on Muenter and Koehler [343] where conditions are closest to atmospheric, NH_3 is not taken up by soot particles at temperatures above 173 K. Back to Table

4. O_3 + soot. Many studies report a rapid, initial loss of O_3 followed by a slower loss that also occurs on aged soot or soot pre-exposed to ozone [96, 100, 121, 133, 134, 236, 262, 309, 382, 419, 422, 427]. Initial, rapid O_3 loss may be most applicable for soot as it comes out of aircraft exhaust, with $\gamma^{init} \sim 10^{-3}$ from most studies using both carbon black and organic combustion soots [133, 134, 236, 382, 427]. The second stage of the reaction is probably more applicable to soot dispersed in air; $\gamma^{aged} \sim 10^{-4}$–$10^{-6}$ using both carbon black and organic combustion soots [133, 134, 236, 262, 309, 359, 427], but in the range of 10^{-4} to 10^{-5} based on organic combustion soot data alone [236, 309]. A few studies have been carried out at temperatures below room temperature [96, 236, 262, 309]; given the wide ranges measured even at room temperature, these values generally fall in the same range. Il'in et al. [236] report a temperature dependence for the initial uptake on fresh soot of $\gamma^{fresh} = 1.9 \times 10^{-3}(\exp{-780/T})$ and for aged soots, $\gamma^{aged} = 1.8 \times 10^{-4}(\exp{-1000/T})$. Both physisorption and reaction of ozone with the surface appear to take place. The studies of Fendel et al. [133] suggest that lower particle growth in size below 40 ppb O_3 is due to less than a monolayer of O_3 on the surface. Stephens et al. [427] proposed a Langmuir-type reversible adsorption of O_3, followed by a slower reaction with the surface. Pöschl et al. [359] proposed a similar scheme for uptake of ozone on spark-generated graphite soot coated with benzo[*a*]pyrene. Initial reversible physisorption occurred with $\gamma \sim 10^{-3}$, and "apparent reaction probabilities" for O_3 with BaP on soot of $\gamma \sim 10^{-5}$–10^{-6} were reported. The presence of water inhibited the reaction, which was postulated to be due to competitive adsorption between water and ozone on the surface; this is in contrast to the report of Chughtai et al. [95] in which the rate of ozone loss increased with RH. Pöschl et al. [359] report Langmuir adsorption equilibrium constants for O_3 and H_2O, and a second order surface reaction rate constant for the O_3-BaP reaction of $(2.6 \pm 0.8) \times 10^{-17}$ cm^{-2} s^{-1}. Three possible paths have been proposed: (1) chemisorption of O_3; (2) catalytic decomposition of O_3: $2O_3 \rightarrow 3O_2$; (3) surface oxidation and formation of gas-phase carbon oxides. The studies of Fendel et al. [133] suggest

that lower particle growth in size below 40 ppb O_3 is due to less than a monolayer of O_3. Studies of Smith et al. [422] and Smith and Chughtai [419] suggest that catalytic decomposition occurs to some extent over the entire reaction sequence. CO_2 and H_2O are the major gas phase and surface oxidized functional groups on the surface such as carboxylic acids are observed [95-97, 121, 133, 262, 319, 419-421, 427]. Back to Table

5. HNO_3 + soot. Studies of the uptake of HNO_3 on soot have been carried out over a range of nitric acid pressures [83, 105, 120, 277, 309, 382, 385, 392, 393]. Measured values of γ at room temperature are typically in the range 10^{-1}–10^{-5}, with smaller uptake coefficients measured at longer reaction times. Saatthoff et al. [392] report an upper limit of 3×10^{-7} as a time-averaged value over two days. At lower concentrations characteristic of the atmosphere, uptake appears to be primarily due to physisorption while at higher concentrations, $> 2 \times 10^{12}$ molecule cm^{-3}, a surface reaction occurs. At 220 K, $\gamma \sim 0.1$ with irreversible uptake attributed to reaction with surface groups [83]. Reaction of HNO_3 at concentrations from $(1–9) \times 10^{12}$ molecule cm^{-3} with "grey" soot from a rich flame using hexane has been reported [393] to generate HONO as the major gaseous product with initial and steady-state reaction probabilities of $\gamma_o = 4.6 \times 10^{-3}$ and $\gamma_{ss} = 5.2 \times 10^{-4}$ respectively; reaction with "black" soot from a lean flame gave NO as the major gaseous product, with initial and steady-state reaction probabilities of $\gamma_o = 2.0 \times 10^{-2}$ and $\gamma_{ss} = 4.6 \times 10^{-3}$ respectively (based on geometric surface area of sample holder). The NO was hypothesized to result from secondary reactions of an initial HONO product. Back to Table

6. N_2O_5 + soot. Brouwer et al. [65], Longfellow et al. [309] and Saathoff et al. [392] studied the uptake of N_2O_5 at room temperature on a ground charcoal (carbon black) sample, on propane soot and on spark-generated graphite soot, respectively. Brouwer et al. and Longfellow et al. report uptake coefficients based on the geometric sample surface area, and therefore give upper limits. An upper limit of $\gamma \leq 0.02$ can be derived based on the larger value of 0.016 reported by Longfellow et al. As discussed below, much smaller values are reported by Saathoff et al.: 4×10^{-5} under dry conditions and 2×10^{-4} at 50% RH. Three possible reactions may occur: (1) Decomposition of N_2O_5 on the surface to generate $NO_2 + NO_3$; (2) reaction of N_2O_5 with the soot; (3) hydrolysis of N_2O_5 with water on the surface to generate HNO_3. The studies of Longfellow et al. support the decomposition reaction, with yields of NO_2 within experimental error of 100%; the generation of NO_3 on the surface followed by its decomposition to NO_2, may contribute to the observed production of NO_2. The studies of Brouwer et al. suggest that a redox reaction with the soot surface to generate NO occurs in parallel with hydrolysis of N_2O_5 to generate HNO_3. Saathoff et al. propose two independent, parallel reactions: (1) hydrolysis generating HNO_3, N_2O_5 + soot $\rightarrow$ 2 HNO_3 with $\gamma = (4 \pm 2) \times 10^{-5}$ under dry conditions (< 10 ppm H_2O) which increases to $(2 \pm 1) \times 10^{-4}$ at 50% RH. (2) decomposition to NO and NO_2: N_2O_5 + soot $\rightarrow$ NO + NO_2 + products, with $\gamma = (4 \pm 2) \times 10^{-6}$ under dry conditions. Back to Table

7. NO_2 + soot. A fast initial uptake of NO_2 is observed on fresh soots [17, 19, 27, 91, 94, 98, 99, 162, 257, 277, 308, 382, 424, 433, 434] with the initial uptake coefficient in studies involving both carbon blacks and organic combustion soots in the range of $\gamma^{init} \cong 10^{-1}$ to 10^{-4}. For longer reaction times on carbon black soots, $\gamma^{aged} \sim 10^{-4}$ based on studies by Kalberer et al. [258] and Ammann et al. [27, 28]. However, Kleffmann et al. [280] report a lower uptake coefficient of $\sim 10^{-7}$ on carbon black over the first 5 minutes of reaction and and Saathoff et al. [392] report an upper limit of $< 4 \times 10^{-8}$ averaged over 5 days under dry conditions (< 10 ppm H_2O) on spark-generated graphite. On organic combustion soots, γ^{aged} has been reported to be in the range of $\sim 10^{-4}$–10^{-6} [17, 28, 30, 308, 393, 424]. All studies were done at room temperature except those of Longfellow et al. [308] which were carried out at 262 K. The surface deactivates on continued exposure to NO_2, suggesting a maximum amount of HONO that can be formed per cm^2 of soot area or mg of soot; this has been reported to be in the range of 10^{16} to 10^{18} HONO per mg of soot [30, 162, 256, 257, 280, 424]. However, reactivation on heating of the surface, exposure to water vapor and/or with time after the exposure is stopped has been observed [162, 308, 424, 433, 434]. A small portion (~10-20%) of the NO_2 taken up appears to be chemisorbed to the surface [17, 30, 94, 256, 257, 277, 280, 424, 433, 434]. Infrared studies [17, 277, 421] show that surface C–ONO, C–N–NO_2, and C–NO_2 groups are formed. The remainder of NO_2 reacted appears as gaseous HONO and NO; Salgado and Rossi [393] report HONO as the major product for hexane soot from a flame at near stoichiometric ratio but NO as the major product for soot from an extremely lean flame. In addition, N_2O, CO, and CO_2 have been observed as products at higher temperatures [41, 42]. At lower NO_2 concentrations, the HONO yield can approach 100%; production of NO may be due to the bimolecular reaction of HONO on the surface at higher concentrations to give NO + NO_2 + H_2O. The HONO yield at 262 K appears to be smaller than at room temperature [308]. Formation of HONO is due to reaction with a reduced surface site and not to NO_2 surface-catalyzed hydrolysis. The formation of HONO from the

reaction of NO_2 with unspecified semi-volatile organics in diesel exhaust has been reported [180] and proposed to be a much larger source of HONO than the reaction with the soot itself. Back to Table

8. NO_3 + soot. Saathoff et al. [392] report an upper limit of $\gamma < 3 \times 10^{-4}$ on dry soot (< 10 ppm H_2O) and $\leq 10^{-3}$ at 50% RH based on measurements of NO_3 and N_2O_5. Back to Table

9. HO_2 + soot. Saathoff et al. [392] report an upper limit of $\gamma < 10^{-2}$ on dry soot (<10 ppm H_2O) based on the decay of HO_2NO_2 (in equilibrium with HO_2 and NO_2) in the presence and absence of soot. Back to Table

10. HO_2NO_2 + soot. Saathoff et al. [392] report an upper limit of $\gamma < 10^{-5}$ on dry soot (<10 ppm H_2O) based on the decay of HO_2NO_2 in the presence and absence of soot. Back to Table

11. H_2O + soot. Alcala–Jornod et al. [19] report an upper limit to the initial uptake coefficient of $\gamma < 2 \times 10^{-3}$, consistent with the earlier measurements of Rogaski et al. [382]. The uptake is most likely a reversible physisorption [19, 358] although based on water uptake isotherms, Chughtai et al. [91, 93, 97, 100] propose that at low relative humidities (< 25%) chemisorption occurs. While prior exposure of Degussa FW-2 to NO_2 and SO_2 was not found to increase the uptake coefficient for water, treatment with HNO_3 increased the measured uptake coefficient by a factor of 28 and with H_2SO_4 by a factor of 68 [382]. Water adsorption isotherms on soot have been measured in a number of studies, e.g. [91, 93, 95, 97, 100] and the amount of water taken up found to increase with the air/fuel ratio used to generate the soot, with the sulfur content, with aging and oxidation of the surface (e.g. by O_3) and with the presence of metals [91, 93, 95, 97, 100, 471]. Back to Table

5.17 Henry's Law Constants for Pure Water

Table 5-4. Henry's Law Constants for Pure Water

Substance	Temperature Range, K	H (298 K)[a]	*A*	*B*	*C*	Uncertainty Range[b]	100 x $h_{G,o}$ M^{-1}	1000 x h_T, $M^{-1}K^{-1}$	Note
O_2	273–348	1.27×10^{-3}	–161.6	8160	22.39	I	≡ 0	–0.334	1
O_3	273–333	1.03×10^{-2}	–14.08	2830		II	0.396	1.79	2
H	273–298	2.6×10^{-4}				IV			3
OH	298	39				III			4
HO_2	298	690				IV			5
H_2O_2	278–303	7.73×10^{4}	–13.27	7310		III			6
N_2	273–348	6.52×10^{-4}	–177.1	8640	24.71	I	–0.10	–0.605	7
NH_3	273–348	60.2	–9.84	4160		III	–4.81		8
NH_2Cl	293-313	87	-15.51	5960		IV			9
$NHCl_2$	293-313	29	-10.68	4180		IV			9
NCl_3	293-313	0.10	-16.17	4130		IV			9
NO	273–358	1.92×10^{-3}	–157.1	7950	21.298	II	0.60		10
NO_2	298	1.4×10^{-2}				III			11
NO_3	298	3.8×10^{-2}				IV			12
N_2O	273–313	2.42×10^{-2}	–148.1	8610	20.266	I	–0.85	–0.479	13
CO	278–323	9.81×10^{-4}	–178.0	8750	24.875	I			14
CO_2	273–353	3.38×10^{-2}	–145.1	8350	19.960	I	–1.72	–0.338	15
CH_4	273–328	1.41×10^{-3}	–194.7	9750	27.274	I	0.22	–0.524	16
C_2H_6	273–323	1.88×10^{-3}	–240.2	12420	33.744	I	1.20	–0.601	17
C_3H_8	273–348	1.51×10^{-3}	–281.1	14510	39.652	I	2.40	–0.702	18
n–C_4H_{10}	273–348	1.24×10^{-3}	–269.9	14330	37.734	I	2.97	–0.726	19
$CH_3CH(CH_3)CH_3$	278–318	9.18×10^{-4}	–360.6	18020	51.444	II			20
C_2H_4	288–348	5.96×10^{-3}	–154.6	8540	21.202	II	0.37		21
C_2H_2	273–343	4.14×10^{-2}	–145.8	7880	20.384	II	–1.59		22
CH_3F	273-313	6.15×10^{-2}	-9.478	1990		IV			23
CH_3Cl	273-313	0.127	-13.13	3270		III			23
CH_3Br	273-313	0.173	-12.16	3100		III			23
CH_3I	273-313	0.200	-13.52	3550		III			23
CH_2Cl_2	273-313	0.366	-14.68	4080		III			23
$CHCl_3$	273-313	0.255	-16.48	4510		II			23
$CHCl_2Br$	273-313	0.409	-18.32	5200		III			23
$CHClBr_2$	273-313	0.868	-18.67	5530		III			23
$CHBr_3$	273-313	1.76	-16.79	5170		III			23
CF_2Cl_2	273-313	3.09×10^{-3}	-17.41	3470		III			23
$CFCl_3$	273-313	1.07×10^{-2}	-15.74	3340		III			23

Substance	Temperature Range, K	H (298 K)[a]	*A*	*B*	*C*	Uncertainty Range[b]	100 x $h_{G,o}$ M^{-1}	1000 x h_T $M^{-1}K^{-1}$	Note
CCl_4	273-313	3.47×10^{-2}	–17.38	4180		II			23
CH_3OH	273–298	220	–12.08	5210		III			24
CH_3CH_2OH	273–298	200	–16.98	6630		III			25
n–C_3H_5OH	273–298	130	–20.16	7470		IV			26
iso–C_3H_5OH	273–298	130	–20.15	7450		IV			26
n–C_4H_9OH	273–298	127	–19.34	7210		IV			26
iso–C_4H_9OH	298	102				IV			26
sec–C_4H_9OH	273–298	110	–19.65	7260		IV			26
tert–C_4H_9OH	273–298	70	–23.63	8310		IV			26
CH_3OOH	277–293	300	–11.99	5280		IV			27
$HOCH_2OOH$	278–293	1.7×10^{6}	–18.79	9870		V			28
HCHO	288–318	3.23×10^{3}	–15.73	7100		IV	–240	69	29
CH_3CHO	273–313	12.9	–17.19	5890		IV	–3.0	–5.5	30
C_2H_5CHO	273–313	10.0	–12.20	4330		V	2.2	–4.0	31
C_3H_7CHO	283–318	9.6	–18.59	6220		V	8.7	–0.06	32
CH_3COCH_3	273–311	28.1	–13.62	5050		IV	–5.2	–2.9	33
$C_2H_5COCH_3$	273–298	18	–16.40	5740		IV	1.1	–0.9	34
$CH_3C(O)O_2$	274	<0.1				V			35
HC(O)OH	275–308	8.9×10^{3}	–11.40	6100		IV			36
$CH_3C(O)OH$	275–308	4.1×10^{3}	–12.50	6200		IV			37
$CH_3C(O)C(O)OH$	278-308	3.11×10^{5}	-4.417	5090		V	9.0		38
CH_3CN	273–303	52.8	–9.35	3970		III	–0.049		39
CH_3NO_2	293–323	34.6	–9.92	4010		IV			40
$C_2H_5NO_2$	293–323	21.7	–11.80	4430		IV			40
$C_3H_7NO_2$	293–323	13.1	–13.22	4710		IV			40
$CH_3CH(NO_2)CH_3$	293–323	8.42	–13.02	4520		IV			40
CH_3ONO_2	273–298	2.0	–15.20	4740		IV			41
$C_2H_5ONO_2$	273–298	1.59	–17.50	5360		IV			41
1–$C_3H_7ONO_2$	273–298	1.10	–18.31	5490		IV			41
2–$C_3H_7ONO_2$	273–298	0.791	–18.20	5360		IV			41
1–$C_4H_9ONO_2$	273–298	1.01	–19.40	5790		IV			41
2–$C_4H_9ONO_2$	273–298	0.648	–18.59	5410		IV			41
$CH_3C(O)O_2NO_2$	274–297	2.8	–18.15	5730		IV	–6.5		42
$O_2NOC_2H_4ONO_2$	293	640				IV			43
$HOC_2H_4ONO_2$	293	3.99×10^{4}				IV			43
$HOCH_2CH(ONO_2)CH_3$	293	7.3×10^{3}				IV			43
$CH_3CH(OH)CH_2ONO_2$	293	6.7×10^{3}				IV			43
$CH_3CH(ONO_2)CH_2ONO_2$	293	175				IV			43
$CH_3C(O)CH_2ONO_2$	293	1.01×10^{3}				IV			43

Substance	Temperature Range, K	H (298 K)[a]	*A*	*B*	*C*	Uncertainty Range[b]	100 x $h_{G,o}$ M^{-1}	1000 x h_T $M^{-1}K^{-1}$	Note
Cl	298	2.3				IV			44
Cl_2	283–383	9.29×10^{-2}	–134.4	7590	18.702	II			45
ClO	298	0.71				VI			46
Cl_2O	273–293	17	–3.23	1810		IV			47
ClO_2	383–333	1.01	–11.65	3470		II			48
HOCl		660	–13.2	5880		IV			49
Br_2	273–308	0.725	–15.05	4390		II			50
BrCl	279–299	0.98	–18.9	5630		III			51
HOBr	298	$>1.3\times10^{2}$				V			52
SO_2	278–383	1.36	–39.72	4250	4.525	II	–6.07	0.275	53
H_2S	273–323	0.102	–145.2	8120	20.296	III	–3.33		54
CS_2	274–305	0.062	–17.05	4250		IV	5.49	–4.65	55
COS	273–288	2.02×10^{-2}	–15.68	3510		IV			56
CH_3SH	298–368	0.39	–12.42	3420		V	0.3		57
C_2H_5SH	298–368	0.28	–13.82	3740		V			58
CH_3SCH_3	272–305	0.54	–12.19	3460		V	–3.1	–0.26	59
$CH_3S(O)CH_3$	298	9.9×10^{4}				V			60

a. $\ln H = A + B/T + C \ln(T)$ [M atm^{-1}]

b. Uncertainty Classes:

I—Better than 10%
II—10% to 50%
III—50% to 100%
IV—Factor of 2 to factor of 10
V—Factor of 10 to factor of 100
VI—Greater than a factor of 100

5.18 Notes to Table 5-4

Many of the data sets required various transformations to convert them to the units (mol L^{-1} atm^{-1}) and form (solubility instead of volatility) used in this Table. The transformations often involve either the mass or molar density of water, which in all cases was taken from [292].

1. O_2. The recommendation was taken from the studies of Benson [57] and Rettich [368]. The data show clear curvature in a plot of ln H v. 1/T. A two parameter fit gives A = –13.26 and B = 1950 K for the temperature range 273–285 K. The salt effect parameter $h_{G,o}$ is by definition, as zero (see text). The temperature dependent salt effect parameter is from the optimization of Weisenberger and Schumpe [472]. Back to Table

2. O_3. The recommendation of Rischbieter [371] was accepted and refitted. Salt effect parameters were obtained from the effect of NaCl, KCl, Na_2SO_4, and $Ca(NO_3)_2$ on H, combined with specific ion parameters. Back to Table

3. H. An average of estimates of the solubility of H based on two approaches: One is simply the assumption that the solubility of H is the same as the solubility of H_2. [353, 354]. The second assumes that the solubility of H is what would be expected for a rare gas atom of the same radius [379]. The average value from 273 K to 298 K is 2.6×10^{-4}, with very small variation with temperature. Above room temperature the solubility increases. Back to Table

4. OH. Calculated from the reduction potential of the OH radial, $E^o(OH/OH^-)$ = (1.90±0.02)V, derived from an equilibrium with Tl^+ [405]. Back to Table

5. HO_2. The recommendation was from a calculation by Schwartz [402] based on the gas phase constituents HO_2, H^+, and O_2^-. Thermodynamic values were updated to those in our Thermodynamic tables, to pK_a=(4.8±0.1), and to a reduction potential $E(O_2/O_2^-)$ = -(0.35±0.01)V. The reduction potential, referenced to one atmosphere O_2, is based primarily on equilibria reported by Meisel and Czapski, [321] corrected for a revised duroquinone potential [467]. Back to Table

6. H_2O_2. The data of Lind and Kok [304, 305], Hwang and Dasgupta [234], Yoshizumi et al. [486], and O'Sullivan et al. [349] are all in good agreement. The recommendation is from a two-parameter fit to all the results. Back to Table

7. N_2. The recommendation of Battino [41] was accepted and refitted to three-parameter equations. A two parameter fit gives A = 12.81 and B = 1625 K for the temperature range 273–293 K. Salt effect parameters taken from the optimization of Weisberger and Schumpe [472]. Back to Table

8. NH_3. Based on the recommendation by Edwards et al. [128], refit to a two-parameter equation. Over the temperature range 273–348 K, there appears to be little curvature in the data. The more recent data of Dasgupta and Dong [109] are in quite good agreement with this recommendation, whereas the results of Hales and Drewes [183] are somewhat higher and those of Shi and Davidovits [415] (an uptake study) are significantly lower. The Hales and Drewes paper also included studies of the effect of dissolved CO_2 on the solubility of NH_3. The solubility of NH_3 in solutions containing a wide variety of ions is discussed by Clegg and Brimblecombe [102]. Salt effect parameters taken from the optimization of Weisberger and Schumpe [472]. Back to Table

9. Chloramines. Derived from flashoff studies with glass sparging columns at 20°C and 40°C [224]. The data point for ammonia at 20°C is in exact agreement with the recommended value in this Table. Back to Table

10. NO. Three-parameter refit from the recommendation of Battino [39]. Two-parameter fit gives A = –12.27 and B = 1790 K for the temperature range 273–293 K. Salt effect parameters taken from the optimization of Weisberger and Schumpe [472]. Back to Table

11. NO_2. From analysis of studies of reactive dissolution of NO_2 by Schwartz and White [404]. Back to Table

12. NO_3. From the reduction potential $E^o(NO_3/NO_3^-)$ = (2.46±0.02)V, which is an average based on determinations of equilibria with Cl^- [70, 360]. This value is in good agreement with that calculated from the uptake of NO_3 into a wetted-wall flow reactor containing Cl^- [389]. It is in very poor agreement with the much higher value derived from a study of the uptake of NO_3 by a series of wetted denuders [439]. Back to Table

13. N_2O. Three-parameter refit to the recommendation of Battino [38]. Two parameter fit gives A = 13.40 and B = 2880 K for the temperature range 273–293 K. Salt effect parameters taken from the optimization of Weisberger and Schumpe [472]. Back to Table

14. CO. The recommendation is based on smoothed data from Rettich et al. [367] and refit to three-parameter equation. A two parameter fit gives A = –12.72 and B = 1720 K for the temperature range 273–293 K. Back to Table

15. CO_2. Refit to three- parameter equation from the recommendation of Wilhelm et al. [473]. Two parameter fit gives A = 12.49 and B = 2710 K for the temperature range 273–293 K. Salt effect parameters taken from the optimization of Weisberger and Schumpe [472]. Back to Table

16. CH_4. The recommendation is a three-parameter fit to the smoothed recommendation of Battino [48]. There is very good agreement with the more recent data of Ben-Naim and Battino [54]. A two parameter fit gives A = –13.45 and B = 2040 K for the temperature range 273–293 K. Salt effect parameters taken from the optimization of Weisberger and Schumpe [472]. Back to Table

17. C_2H_6. The recommendation is a three-parameter fit to the smoothed recommendation of Battino [40]. There is very good agreement with the more recent data of Ben-Naim and Battino [54]. Two parameter fit gives A = –15.95 and B = 2875 K for the temperature range 273–293 K. Salt effect parameters taken from the optimization of Weisberger and Schumpe [472]. Back to Table

18. C_3H_8. The recommendation is from a three-parameter fit to the smoothed recommendation of [47]. There is very good agreement with the more recent data of Ben-Naim and Battino [54]. A two parameter fit gives A = 17.52 and B = 3275 K for the temperature range 273–293 K. Salt effect parameters taken from the optimization of Weisberger and Schumpe [472]. Back to Table

19. n-C_4H_{10}. The recommendation is from a three-parameter fit to the smoothed recommendation of Battino [46]. There is very good agreement with the more recent data of Ben-Naim and Battino [54]. A two parameter fit gives A = –19.28 and B = 3740 K for the temperature range 273–288 K. Salt effect parameters taken from the optimization of Weisberger and Schumpe [472]. Back to Table

20. $CH_3CH(CH_3)CH_3$. The recommendation is from a three-parameter fit to the smoothed recommendation of Battino [45]. A two parameter fit gives A = 18.22 and B = 3340 K for the temperature range 278–293 K. Back to Table

21. C_2H_4. The recommendation is from a three-parameter fit to the smoothed recommendation of Wilhelm [473]. A two parameter fit gives A = –12.40 and B = 2170 K for the temperature range 288–313 K. Salt effect parameters taken from the optimization of Weisberger and Schumpe [472]. Back to Table

22. C_2H_2. The recommendation is from a three-parameter fit to the smoothed recommendation of Wilhelm [473]. The recommendation of Yaws et al. [484] generates identical results. A two parameter fit gives A = –10.12 and B = 2065 K for the temperature range 273–298 K. Back to Table

23. Halomethanes. A refit to the evaluation of Staudinger and Roberts [426]. Back to Table

24. CH_3OH. The recommendation is based on the two data points of Snider and Dawson [423]. The 298 K result of Butler et al. [69] and a calculation based on the NBS Thermodynamic tables, [464], are in very good agreement. The 298 K result of Altschuh et al. [26] is about 40% lower. Back to Table

25. C_2H_5OH. The recommendation is based on the two data points of Snider and Dawson [423]. The 298 K results of [69] and [383], and a calculation based on the NBS Thermodynamic tables, [464], are in very good agreement. The 298 K result of Altschuh [26] is about 50% lower. Back to Table

26. All of the recommendations for the C3–C4 alcohols are based on two data points each from Snider and Dawson [423]. Room temperature data from other studies ([68, 69], and [26]) typically support these results. Back to Table

27. CH_3OOH. The data of Lind and Kok [304, 305] and O'Sullivan et al. [349] are in excellent agreement and were fit to a two-parameter expression. Back to Table

28. $HOCH_2OOH$. The results of O'Sullivan [349] and Staffelback and Kok [425] are very close and were fit to obtain the recommended values. The results of Zhou and Lee [503] are much lower and were not included. Back to Table

29. HCHO. The recommended value is the apparent Henry's law constant and includes a contribution due to hydrolysis $H^* = H(1 + K_{hyd})$. Data from Betterton and Hoffmann [59] and Zhou and Mopper [504] are in substantial agreement and were fit to a two-parameter expression. Betterton and Hoffmann have calculated H = 2.5 M atm^{-1} at 298 K for the physical solubility. Salt effect parameters derived from data on the effect of seawater concentration (0 to 100%) on the measured H [504]. For these calculations, the seawater was assumed to be a solution of pure NaCl, with 35% salinity equal to 0.6 M. Back to Table

30. CH_3CHO. The recommended value is the apparent Henry's law constant and includes a contribution due to hydrolysis $H^* = H(1 + K_{hyd})$. The results of Snider and Dawson [423], Benkelberg et al. [56], and Betterton and Hoffmann [59] are in excellent agreement and have been fit to a two-parameter expression for the recommendation. The results of Zhou and Mopper [504] curve off at higher temperatures and were not included in the fit. (Note the similar situation for acetone.) Betterton and Hoffmann have calculated H = 4.8 M atm^{-1} at 298 K for the physical solubility. Salt effect parameters derived from data on the effect of seawater concentration (0 to 100%) on the measured H [504]. For these calculations, the seawater was assumed to be a solution of pure NaCl, with 35% salinity equal to 0.6 M. Back to Table

31. C_2H_5CHO. Results of Zhou and Mopper [504] and Snider and Dawson [423] agree only to within about a factor of two. The two points from the former were weighted by 3 and combined with the five points of the latter to generate the recommendation. Salt effect parameters derived from data on the effect of seawater concentration (0 to 100%) on the measured H [504]. For these calculations, the seawater was assumed to be a solution of pure NaCl, with 35% salinity equal to 0.6 M. Back to Table

32. C_3H_7CHO. The only results are from Zhou and Mopper [504], which have been fit to a two-parameter expression. Salt effect parameters derived from data on the effect of seawater concentration (0 to 100%) on the measured H [504]. For these calculations, the seawater was assumed to be a solution of pure NaCl, with 35% salinity equal to 0.6 M. Back to Table

33. CH_3COCH_3. The recommendation is from a fit to the data of Snider and Dawson [423] and Benkelberg et al. [56]. Room temperature data points of Hoff et al. [219], Burnett [68] and Vitenberg et al. [458] are in very good agreement. Results of Zhou and Mopper [504] are somewhat higher, particularly at room temperature and above. The situation is similar for acetaldehyde. Salt effect parameters derived from data on the effect of seawater concentration (0 to 100%) on the measured H [504]. For these calculations, the seawater was assumed to be a solution of pure NaCl, with 35% salinity equal to 0.6 M. The K_S values from this work are somewhat different than those obtained by Benkelberg et al. [56], 0.089 vs 0.17 at 298 K and 0.17 vs 0.085 at 273 K. The magnitude of this difference is not too great, but the two studies predict a different sign for h_T. Back to Table

34. $C_2H_5COCH_3$. The recommendation is from the two points of Snider and Dawson [423]. The room temperature points of Vitenberg et al. [458] and Rohrschneider [383] are in good agreement. The higher temperature data of Zhou and Mopper [504] are somewhat higher and those of Friant and Suffet [153] are lower than the recommendation. Salt effect parameters derived from data on the effect of seawater concentration (0 to 100%) on the measured H [504]. For these calculations, the seawater was assumed to be a solution of pure NaCl, with 35% salinity equal to 0.6 M. Back to Table

35. $CH_3C(O)O_2$. Villalta et al. [457] measured an upper limit for H of 0.1 M atm-1 in coated-wall flow tube uptake experiments on aqueous sodium ascorbate solutions. Back to Table

36. HC(O)OH. The results of Johnson et al. [252] are accepted. The 298 K result of Khan et al. [276] are about 75% lower. Back to Table

37. $CH_3C(O)OH$. The results of Johnson et al. [252] are accepted. A value calculated from the NBS Thermodynamic tables [464] is about a factor of two higher. Back to Table

38. $CH_3C(O)C(O)OH$. Taken from Khan et al. [276] Salt effect derived from effect of NaCl (k_s = 0.236 M^{-1}) and KCl (k_s = 0.235 M^{-1}) on partial pressure over 1.5 M solution of pyruvic acid at various salt concentrations. Much different values derived when other salts were used, suggesting complications due to specific interactions and, possibly, to the weakly buffered nature of the solution. Back to Table

39. CH_3CN. The values reported by Benkelberg [56], Snider and Dawson [423], Hamm et al. [185] are all in good agreement and have been fit to a two-parameter expression for the recommendation. The Hamm et al. paper includes a measurement with artificial seawater at 293 K. Salt effect derived from the effect of 0.6 mol L^{-1} NaCl on solubility at 293 K [56]. Back to Table

40. Nitroalkanes (CH_3NO_2, $C_2H_5NO_2$, $C_3H_7NO_2$, and $CH_3CH(NO_2)CH_3$). The recommended values are all taken from the work of Benes and Dohnal [55]. For nitromethane, the 298 K value from Rohrschneider [383] is about 30% higher. Back to Table

41. Alkyl nitrates (CH_3ONO_2, $C_2H_5ONO_2$, 1-$C_3H_7ONO_2$, 2-$C_3H_7ONO_2$, 1-$C_4H_9ONO_2$, 2-$C_4H_9ONO_2$). The recommended values are all taken from the work of Kames and Schurath [260]. The results of Luke et al. [312] are in very good agreement for 1-butyl and 2- butyl nitrates, but the values reported by Hauff [213] for 1- and 2-propyl and butyl nitrates by head-space chromatography are significantly (~50%) lower. Back to Table

42. $CH_3C(O)O_2NO_2$. The results of Kames and Schurath [260] and Frenzel et al. [151] are close, but somewhat higher (~60%) than the single temperature point of Holdren et al. [223]. The recommendation is a fit to the data of Kames and Schurath, and Frenzel et al. Frenzel et al., Kames and Schurath, and Holdren et al. also measured hydrolysis rate constants. $K_s = 0.0807\ M^{-1}$ for NaCl at 293.2 K based on solubility in artificial sea water (~0.7 M) [260]. Back to Table

43. Bifunctional alkyl nitrates. The recommended values (at 293 K) are taken from the work of Kames and Schurath [259]. Back to Table

44. Cl. $E^o(Cl/Cl^-) = (2.43\pm0.03)V$ from an analysis of the reaction of OH with Cl^-, yielding the equilibrium constant for $OH + Cl^- + H^+ \leftrightarrow H_2O + Cl$ ($K_{eq} = 1.1 \times 10^5\ M^{-2}$, corrected to a standard state of water at unit activity), [487] and the reduction potential $E^o(OH^-,H^+/H_2O) = (2.73\pm0.02)V$ [405]. Back to Table

45. Cl_2. Three-parameter refit to the recommendation of Battino [43]. Two parameter fit gives A = 9.38 and B = 2090 K for the temperature range 283–313 K. Back to Table

46. ClO. From the reduction potential $E(ClO/ClO^-) = (1.41\pm0.02)V$, which is based on an equilibrium with carbonate at high pH and ionic strength [230]. Due to the high ionic strength, 3 M, it was not possible to correct this value and obtain a reduction potential for the standard state. Thus, the derived Henry's Law constant must be considered uncertain. Back to Table

47. Cl_2O. Fit to recommendation of Wilhelm et al. [473]. Data appear somewhat uncertain. Back to Table

48. ClO_2. Two-parameter fit to the recommendation of Battino [42]. Back to Table

49. HOCl. Huthwelker et al. [233] analyzed the limited data for pure water from Blatchley et al. [60] and Holzwarth et al. [224] along with the more extensive data for uptake by sulfuric acid from Hanson and Ravishankara [206], along with thermodynamic information, and obtained a consistent expression for the solubility of HOCl. Back to Table

50. Br_2. The results of Kelley and Tartar [270] and Jenkins and King [251] agree well below about 313 K, and with the 298 K point of Hill et al. [217]. Recommendation based on a two-parameter fit to all data at and below 308 K. Back to Table

51. BrCl. The recommendation is from the study of Barlett and Margerum [36]. Back to Table

52 HOBr. The Henry's law constant was estimated to be more than twice that of HOCl based on a study of the effective Henry's law constant for free bromine from a stripping column [60]. Back to Table

53. SO_2. The recommendation of Battino [44] was accepted and refit to a three-parameter equation. The earlier recommendation of Edwards et al. [128] is slightly lower. A two parameter fit gives A = –9.53 and B = 2930 K for the temperature range 278–298 K. New value of $h_{SO2,0}$ from absorption equilibria studies in aqueous HCl and NaCl solutions [378]. Temperature dependence from the optimization of Weisberger and Schumpe [472]. Back to Table

54. H_2S. In the recommendation of Fogg [149], two expressions were given, representing the results above and below 283 K. The predicted values from these expressions were calculated, with the points at 283 K averaged, converted to the desired units, and then fit with the two- and three-parameter expressions. These are the recommended values. More recent results of Rinker and Sandall [370] and Munder et al. [345] are slightly lower; in these studies, the physical solubility of H_2S was determined through measurements involving aqueous solutions of glycols or amines, neutralized with HCl. The reported values of De Bruyn et al. [117] are significantly (~30%) lower. The earlier recommendation of Edwards et al. [128] is very close to the recommendation of Fogg [149] as is the recommendation of Yaws et al. [484]. The room temperature point calculated from the NBS Thermodynamic tables Wagman et al. [464] is also slightly lower. The work

of De Bruyn et al. [117] covered also a wide range of NaCl and $(NH_4)_2SO_4$ concentration and of pH. Salt effect parameters taken from the optimization of Weisberger and Schumpe [472]. Back to Table

55. CS_2. The recommendation is from a fit to data of Elliott [130], who also present data in 0.5 mol L^{-1} NaCl. The results of De Bruyn et al. [117] are significantly (50%) lower. The work of DeBruyn et al. covered also a wide range of NaCl and $(NH_4)_2SO_4$ concentration and of pH. Salt effect parameters derived from the ratio of the solubility of CS_2 in water and 0.5 M NaCl [130]. At 278 K, k_s = 0.184 M^{-1}, compared to 0.150 M^{-1} from the results of de Bruyn, et al. [117]. Note also De Bruyn et al. obtained K_s = 0.410 M^{-1} for $(NH_4)_2SO_4$, whereas these parameters would predict 0.261 M^{-1}. Back to Table

56. COS. The reviews by Wilhelm et al. [473] and Yaws et al. [484] result in identical results over the low temperature range (<303 K) and are combined to generate the recommendation. The results of De Bruyn et al. [117] are somewhat (~25%) lower at the lower temperature range. The work of De Bruyn et al. covered also a wide range of NaCl and $(NH_4)_2SO_4$ concentration and of pH. Back to Table

57. CH_3SH. The recommendation is based on the data of Przyjazny et al. [361]. Results of De Bruyn et al. [117] are about half the recommended value at 298 K. Similar low values were observed for other compounds in the work of De Bruyn et al. The work of De Bruyn et al. covered a wide range of pH and NaCl and $(NH_4)_2SO_4$ concentrations. At 298 K, De Bruyn et al. [117] obtained K_s = 0.314 M^{-1} for $(NH_4)_2SO_4$ and K_s = 0.143 M^{-1} for NaCl. From the latter, we calculate h_G = 0.003 M^{-1}; the values for $(NH_4)_2SO_4$ from this work have tended to be high. Back to Table

58. C_2H_5SH. The recommendation is based on the data of Przyjazny et al. [361]. The results of Vitenberg [458] are slightly lower than the extrapolated value at 293 K. Back to Table

59. CH_3SCH_3. The recommendation is based on the values of Dacey et al. [106]. The single temperature point of Wong and Wang [480] and the higher temperature results of Przyjazny et al. [361] are in good agreement. The results of De Bruyn et al. [117] are about 30% lower. The studies of Dacey et al. [106] and Wong and Wang [480] were also carried out with seawater. The work of De Bruyn et al. [117] covered also a wide range of NaCl and $(NH_4)_2SO_4$ concentration and of pH. Salt effect parameters based on the values of Dacey et al. [106] for Sargasso sea water from 0 to 29 C. The values for K_H obtained by Wong and Wang [480] for sea water from 18 to 44 C are in good agreement. Dacey et al. also measured K_H at 18 C for NaCl solutions up to 32%. For the 10 – 32% data, a value of K_s = 0.117 M^{-1} can be derived, in good agreement with the predicted value of 0.113 M^{-1}. The 278 K value of K_s = 0.180 M^{-1} obtained by De Bruyn et al. [117] is somewhat larger. Note also the de Bruyn, et al. obtained K_s = 0.332 M^{-1} for $(NH_4)_2SO_4$, whereas the recommended parameters would predict 0.223. Back to Table

60. $CH_3S(O)CH_3$. The recommendation is from Watts and Brimblecombe [470], cited by Allen et al. [25]. Back to Table

5.19 Ion-Specific Schumpe Parameters

Table 5-5. Ion-Specific Schumpe Parameters

Cation	h^c_i		Anion	h^a_i
H^+	0		OH^-	0.0839
Li^+	0.0754		HS^-	0.0851
Na^+	0.1143		F^-	0.092
K^+	0.0922		Cl^-	0.0318
Rb^+	0.0839		Br^-	0.0269
Cs^+	0.0759		I^-	0.0039
NH_4^+	0.0556		NO_2^-	0.0795
Mg^{2+}	0.1694		NO_3^-	0.0128
Ca^{2+}	0.1762		ClO_3^-	0.1348
Sr^{2+}	0.1881		BrO_3^-	0.1116
Ba^{2+}	0.2168		IO_3^-	0.0913
Mn^{2+}	0.1463		ClO_4^-	0.0492
Fe^{2+}	0.1523		IO_4^-	0.1464
Co^{2+}	0.168		CN^-	0.0679
Ni^{2+}	0.1654		SCN^-	0.0627
Cu^{2+}	0.1675		$HCrO_4^-$	0.0401
Zn^{2+}	0.1537		HCO_3^-	0.0549
Cd^{2+}	0.1869		CO_3^{2-}	0.1423
Al^{3+}	0.2174		HPO_4^{2-}	0.1499
Cr^{3+}	0.0648		SO_3^{2-}	0.127
Fe^{3+}	0.1161		SO_4^{2-}	0.1117
La^{3+}	0.2297		$S_2O_3^{2-}$	0.1149
Ce^{3+}	0.2406		PO_4^{3-}	0.2119
Th^{4+}	0.2709		$Fe(CN)_6^{4-}$	0.3574

The values in this table can be used to estimate the solubility of a gas in various mixed electrolyte solutions, even if these data have not been obtained experimentally for all of the ions. For example, the solubility of ozone in a solution of 0.8 M HCl and 1.2 M Na_2SO_4 at 273 K would be estimated as follows:

First, $H^o = 0.024$ M atm^{-1} at 273 K, from the Henry's Law Table; from the same Table, the gas-specific parameters for ozone are $h_{G,o} = 0.00396$ M^{-1} and $h_T = 1.79 \times 10^{-3}$ M^{-1} K^{-1}, thus:

$$k_G = 0.00396 + 1.79E\text{-}3(273 - 298) = -0.0408 \text{ M}^{-1}$$

The specific ion parameters from Table 5-4 are corrected by this value to calculate the change in the logarithm of the Henry's law constant

$\log (H^o/H^{273}) = 2 \times 1.2 \text{ M} \times (0.1143 - 0.0408) \text{ M}^{-1} + 1.2 \text{ M} \times 0.1117 - 0.0408) \text{ M}^{-1} +$

$0.8 \text{ M} \times (0 - 0.0408) \text{ M}^{-1} + 0.8 \text{ M} \times (0.0318 - 0.0408) \text{ M}^{-1} = 0.181$

Thus, $(H^o/H^{273}) = 1.517$

$H = 0.024 \text{ M atm}^{-1}/1.517 = 0.016 \text{ M atm}^{-1}$ for O_3 in this salt solution at 273 K.

5.20 Henry's Law Constants for Acids

Table 5-6. Henry's Law Constants for Acids

	T(K)	Wt.% H_2SO_4	H or H* (M/atm)	Notes
O_3 in $H_2SO_4 \cdot nH_2O(l)$	293	1–70	$Ln(H_o/H) = (4.08 \pm 0.2) \times 10^{-3} \times wt$ $H_o = 0.012$ M atm^{-1} wt is the H_2SO_4 wt.%	1
NO_2 in $H_2SO_4 \cdot nH_2O(l)$	203–343	39–68	See Note	2
HONO in $H_2SO_4 \cdot nH_2O(l)$	248–298	>60	$\ln H^* = a_1 + a_2 wt + a_3 wt^2 + (b_1 + b_2 wt)/T$ $a_1 = 26.1 \pm 9.4$, $a_2 = -1.095 \pm 0.21$, $a_3 = 0.00732 \pm 0.00121$ $b_1 = -5792 \pm 1610$, $b_2 = 181.3 \pm 24$	3
HNO_3 in $H_2SO_4 \cdot nH_2O(l)$	~195–300	0–80	See Note	4
HNO_3 and HCl in $H_2SO_4 \cdot nHNO_3 \cdot mH_2O(l)$	~195–300	0–80	See Note	4
HO_2NO_2 in $H_2SO_4 \cdot nH_2O(l)$	201–230	50–75	$\ln H = 3.69 - mH_2SO_4 \times (-0.25 + 65/T) - 8400 \times (1/T_o - 1/T)$ mH_2SO_4 is the molality of the H_2SO_4 solution, $T_o = 298.15$ K	5
CH_2O in $H_2SO_4 \cdot mHNO_3 \cdot nH_2O(l)$	240–300	10–85 also 8–40 wt.% HNO_3	See Note	6
CH_3OH in $H_2SO_4 \cdot nH_2O(l)$	197–223		See Note	7
$CH_3C(O)CH_3$ in $H_2SO_4 \cdot nH_2O(l)$	198–298	10–80	$\ln H^* = a1+a2\ wt+a3\ wt2 + (b1+b2\ wt+b3\ wt2)/T$ wt is the H2SO4 wt.%, $a1 = -21.438 \pm 4.31$, $a2 = -0.32163 \pm 0.207$, $a3 = 0.0072935 \pm 0.00235$ $b1 = 7292 \pm 1220$, $b2 = 33.524 \pm 53.42$, $b3 = -0.975 \pm 0.571$	8
$CH_3C(O)O_2NO_2$ in $H_2O(l)$, $H_2SO_4 \cdot nH_2O(l)$	199–295	0–75	$\ln H^* = 1.07 - mH_2SO_4 \times (0.69 - 152/T) - 5810 \times (1/T_o - 1/T)$, mH_2SO_4 = molality of the H_2SO_4 solution $T_o = 298.15$ K	9
CF_2O in $H_2SO_4 \cdot nH_2O(l)$	215–230	60	< 5	10
CF_3OH in $H_2SO_4 \cdot nH_2O(l)$	250	40 50	> 240 210	11
HOCl in $H_2SO_4 \cdot nH_2O(l)$	200–300	46–80	$H_{HOCl} = 1.91 \times 10^{-6} \times \exp(5862.4/T) \times \exp(-S_{HOCl} M_{H2SO4})$ M atm^{-1} where: $S_{HOCl} = 0.0776 + 59.18/T$ M^{-1}, $M_{H2SO4} = H_2SO_4$ molar conc	12
$ClONO_2$ in $H_2SO_4 \cdot nH_2O(l)$	200–265	40–75	$H_{ClONO2} = 1.6 \times 10^{-6} \times \exp(4710/T) \times \exp(-S_{HOCl} M_{H2SO4})$ M atm^{-1} where: $S_{ClONO2} = 0.306 + 24.0/T$ M^{-1}, $M_{H2SO4} = H_2SO_4$ molar conc.	13
HBr in $H_2SO_4 \cdot nH_2O \cdot H_2O(l)$ and $H_2SO_4 \cdot nHNO_3 \cdot mH_2O(l)$	200–240	40–72	$\ln H^* = a_1 + (b_1 + b_2 wt)/T$ $a_1 = -11.695 \pm 0.537$, $b_1 = 11{,}101 \pm 163$, $b_2 = -90.7 \pm 1.2$	14
SO_2 in H_2O (l), $H_2SO_4 \cdot nH_2O(l)$	193–242	0–97	$\ln H^* = a_1 + a_2 wt + a_3 wt^2 + (b_1 + b_2 wt + b_3 wt^2)/T$, where: wt is the H_2SO_4 wt.%, $a_1 = -10.778 \pm 2.07$, $a_2 = -0.11541 \pm 0.0827$, $a_3 = 0.0012506 \pm 0.000811$ $b_1 = 3310 \pm 578$, $b_2 = 30.581 \pm 22.2$, $b_3 = -0.35469 \pm 0.209$	15

5.21 Notes to Table 5-6

1. O_3 in $H_2SO_4 . nH_2O(l)$. Bubble train uptake measurements where performed by Rattigan et al. [364] at 293 K for 1–70 wt.% H_2SO_4. Recommended expression is a Sechenov coefficient formulation where H_o = 0.012 M atm^{-1} is the 293 K value of H for pure water fom Wilhelm et al. [473]. In the measurement, account was taken of the loss of O_3 due to reaction with H^+. Back to Table

2. NO_2 in $H_2SO_4 \bullet nH_2O(l)$. Langenberg et al. [290] present novel capillary gas chromatography measurements for 39, 59, and 68 wt.% H_2SO_4 over the temperature range of 203 to 243 K. However, NO_2 solubility must be derived from chromatographic waveforms which are contorted by much higher N_2O_4 solubility. The resulting values for H_{NO2} are in the 1 to 10^2 range, but show inconsistent trends with temperature and concentration, indicating possibly large systematic error. Back to Table

3. HONO in $H_2SO_4 . nH_2O(l)$. Becker et al. [49] measured HONO partial pressue, P_{HONO}, over bulk solutions in a temperature range of 248–298 K and a H_2SO_4 concentration range of 0–67 wt.%. Longfellow et al. [307] measured P_{HONO} in a wetted wall flow reactor over a temperature range of 218–295 K and an acid concentration range of 60–83 wt.%. Agreement between these two data sets is excellent. H* decreases from 0 wt.% to 53 wt.% due to physical solubility, then increases above 53 wt.% due to protonation and/or association with H_2SO_4 to make nitrosyl sulfuric acid. Becker et al. parameterize their data as a function of sulfuric acid wt.% and temperature. However, the Becker et al. parameterization is not able to fit the combined sets of Becker et al. [49] and Longfellow et al. [307] data, particularly at the lower temperatures and higher wt.% most relevant to the stratosphere. Therefore, the recommended functional form was used to fit the data for >60 wt.%. This function fits both sets of data very well. It is important to note that this function is only valid for H_2SO_4 concentrations near 60 wt.% and above. The parameterization in Becker et al. [49] should be used to calculate H for H_2SO_4 concentrations <60 wt.%. (Note that the units for H are mol/kg-bar in Becker et al. [49]. The density parameterization of Myhre et al. [347] was used to convert to M/atm units.) Back to Table

4. HNO_3 and HCl in $H_2SO_4 \bullet nH_2O(l)$ and $H_2SO_4 \bullet nHNO_3 \bullet mH_2O(l)$. Effective Henry's law coefficients, H^*, for HNO_3, and HCl in binary H_2SO_4/H_2O and ternary $H_2SO_4/HNO_3/H_2O$ solutions over the temperature range 195 to 300 K are required to model the composition and heterogeneous chemistry of stratospheric and upper tropospheric aerosols. Solubility data can be obtained from analysis of heterogeneous uptake experiments with the liquid phase diffusion coefficient estimated from acid solution viscosity (Williams and Long [476]). Solubilities can also be obtained from equilibrium or from vapor pressure data.

   Experimental solubility data for HNO_3 is provided by Van Doren et al. [456], Reihs et al. [365] and Zhang et al. [502]. Data for HCl solubility is provided by Watson et al. [469], Hanson and Ravishankara [202, 206], Zhang et al. [502], Williams and Golden [474], Abbatt [2], Elrod et al.[131] and Robinson et al. [377].

   These studies all show that trace species solubility in H_2SO_4/H_2O and $H_2SO_4/HNO_3/H_2O$ solutions is a strong function of water activity, which, in turn, depends on both temperature and acid concentrations. Prediction of HNO_3 and HCl H^* values for atmospheric compositions requires a sophisticated model. Comprehensive thermodynamic models of acid solutions for a range of atmospheric conditions have been published by Carslaw et al. [77], Tabazadeh et al. [432] and Luo et al. [313] and reviewed by Carslaw and Peter [79]. These models do an excellent job of reproducing the available experimental data, even for ternary $H_2SO_4/HNO_3/H_2O$ solutions (Elrod et al. [131]). These models and the Carslaw review should be consulted for plots/predictions of H^* for HNO_3 and HCl in strong acid solutions over the atmospheric temperature range. The most widely used model of Carslaw et al. [77] was revised in Massucci et al. [318]. Back to Table

5. HO_2NO_2 in $H_2SO_4 . nH_2O(l)$. Zhang et al. [501] performed wetted wall flow reactor studies using CIMS to detect HO_2NO_2 uptake over a temperature range of 201–230 K and an acid concentration range of 52.9–74 wt.% H_2SO_4. $HD_l^{1/2}$ values where determined for 52.9, 58.3/59.1, 66.4 and 73.8/74 wt.%, with 5 to 15 data points per temperature or temperature pair. All uptake appeared to be reversible with the variation in H strongly temperature dependent, but only moderately dependent on H_2SO_4 wt.%. D_l values were calculated from a cubic cell model to derive H. Uncertainties in measured H values were estimated by authors to be 25% for H $<1 \times 10^6$ M atm^{-1} and 50% for H $>1 \times 10^6$ M atm^{-1}. These data were parameterized by Leu and Zhang [298] in the Sechenov coefficient form adopted by Huthwelker for HOCl [233], and their formulation is recommended. Back to Table

6. CH_2O in $H_2SO_4 \bullet mHNO_3 \bullet nH_2O(l)$. The recommended Henry's Law relationship is:

$$H^* = H\left(1+K_2 a_{H_2O} + K_3 a_{H^+}\right)$$

where: $H = 3.4 \times 10^{-5} \exp -[(-0.0456 + 55.5/T)\ (0.46\ m_{H_2SO_4} + 0.13\ m_{HNO_3})]$ M atm^{-1}, T is the temperature in K, and $m_{H_2SO_4}$ and m_{HNO_3} are the respective acid molalities; $K_2 = \exp(4020/T–5.83)$ M^{-1}, $K_3 = 0.56 \exp[8.84–(T–260/T)]$ M^{-1}, and a_{H_2O} and a_{H+} are the water and H^+ activities which are obtained from a thermodynamic model of the solution, e.g. Carslaw et al. [77]. Valid for 10–85 wt.% H_2SO_4, 8–40 wt.% HNO_3, T = 240–300 K.

Knudsen cell studies by Tolbert et al. [441] and Iraci and Tolbert [241] and droplet train/flow reactor studies by Jayne et al. [249] all yield data showing that CH_2O is strongly absorbed by sulfuric acid solutions, and Jayne et al. also provide data for ternary acid solutions. The Jayne et al. [249] studies included H_2SO_4 concentrations from 10 to 85 wt.% and HNO_3 concentration between 8 and 40 wt.% with temperature variations from 241 to 300 K. These data were parameterized with three terms, representing physical CH_2O solubility, reversible hydrolysis to $CH_2(OH)_2$, important in more dilute solutions, and reversible formation of CH_3O^+, dominant at high acidities. The Jayne et al. [249] parameterization is recommended above. The H* data from Iraci and Tolbert [241] cover 49 to 95 wt.% H_2SO_4 and a temperature range of 197 to 214.5 K and are in fair agreement with extrapolation of H* expression from Jayne et al. [249] for concentrations below ~75 wt.%. However, the Iraci and Tolbert data are taken on such thin acid films that initial uptake slopes are difficult to determine accurately and the data scatter is large. While the Iraci and Tolbert data do indicate significantly larger H* values for H_2SO_4 concentrations above 75 wt.%, the data do not compel a reformulation of the Jayne et al. parameterization. Back to Table

7. CH_3OH in $H_2SO_4 \bullet nH_2O(l)$. H* data from Kane and Leu [263], taken over 40–85 wt.% H_2SO_4 and from 210–235 K, indicate soluble uptake below 65 wt.% and predominately reactive uptake to form methanesulfonic acid and dimethysulfate above 65 wt.%. Uptake decreased slightly with temperature below 65 wt.% and increases slightly with temperature above. Data yield $H^*k^{1/2}$ at high acid concentrations. Weakly temperature dependent γs of ~0.15 were measured for 65, 75, and 80 wt.%. However, Knudsen cell studies by Iraci et al. [239] at 45, 61 and 72 wt.% over a 197–223 K temperature range show only well behaved reversible uptake. They argue that low vapor pressures explain the lack of CH_3OH recovery for the short observation times used by Kane and Leu. They also cite three older literature studies on the reaction of methanol and ethanol at room temperature in sulfuric acid which report reaction rate constants much lower than those deduced by Kane and Leu [239]. Iraci et al. present the following parameterization of their data plus data for water:

$$\log H^* = A + 1000B/T$$

where $A = 7.00 + \log M_{H2O}$, $B = 0.000619\ m^2 + 0.00544\ m + 2.267$, M_{H2O} is the molarity of water in the solution (mol L^{-1}) and m is the molality of the H_2SO_4 (moles H_2SO_4 per kg H_2O).

Note that this parameterization is based only on the Iraci et al. data. A reanalysis of the Kane and Leu [263] results to provide additional data in the 40–72 wt.% range, and H^* values for higher wt.% should be undertaken to validate and extend the Iraci et al. data. Back to Table

8. $CH_3C(O)CH_3$ in $H_2SO_4 \bullet nH_2O(l)$. Duncan et al. [126, 127] used IR spectra of thin sulfuric acid films to establish that acetone is absorbed as the protonated species. Above 70 wt.% protonated acetone undergoes a self-condensation/dehydration reaction to form protonated mesityl oxide, which, in turn, reacts with an additional protonated acetone to form trimethyl benzene. Duncan et al. [127] measured reversible uptake and derived Henry's law constants for 70 wt.% H_2SO_4 at 180, 187 and 195 K and a value at 201 K for 76 wt.%. Kane et al. [264] measured uptake in a wetted wall flow reactor and derived H* parameters for 40, 50, 65, and 75 wt.% over a much wider temperature range than Duncan et al. [127]. Their data diverge above 80 wt.% which they attribute to reactive uptake as suggested by Duncan et al. [126, 127]. Klassen et al. [278] provide Knudsen cell uptake derived data for 48.7 to 78.3 H_2SO_4 wt.% between 210 and 240 K that are generally consistent with that of Kane et al. [264]. Imamura and Akiyoshi [237] report wetted wall flow reactor H* measurements at 230 K for 50 and 60 wt.%, 250 K for 60, 69 and 76 wt.%, and 270 K for 76 and 79 wt.%; their data diverges a factor of 2 to 4 from that of Kane et al. [264] and Klassen et al. [278].

Equally weighted data sets from Kane et al. [264] and Klassen et al. [278] were combined and fit to generate the recommended parameterization. Two points for the solubility of acetone in water at 298 K and 273 K (Benkelberg et al. [56]) were included to improve the extrapolation to low wt.% solutions.

The data points from Imamura and Akiyoshi [237] were not included because they were inconsistent with the other data and have a very different temperature dependence. The few data points from Duncan et al. [126, 127] are also inconsistent with the other data and were not included in the parameterization. Back to Table

9. $CH_3C(O)O_2NO_2$ in H_2O and $H_2SO_4 \cdot nH_2O(l)$. Zhang and Leu [496] performed wetted wall flow reactor studies using CIMS to detect $CH_3C(O)O_2NO_2$ uptake over a temperature range of 199 to 226 K. Uptake studies were performed at 46, 54, 59, and 72 wt.% H_2SO_4 to yield $H^*D_l^{1/2}$ values. D_l values were calculated from a cubic cell model to derive H*. Leu and Zhang [298] fit their data from Zhang and Leu [496], including water data from Kames and Schurath [260] and Kames et al. [261], using the Sechenov coefficient form adopted by Huthwelker for HOCl [233]. This formulation is recommended for both water and sulfuric acid solutions. Back to Table

10. CF_2O in $H_2SO_4 \cdot nH_2O(l)$. Hanson and Ravishankara [199] calculate an upper limit for H of CF_2O based on assumed solubility limit resulting in lack of measurable uptake into 60 wt.% H_2SO_4. Back to Table

11. CF_3OH in $H_2SO_4 \cdot nH_2O(l)$. Lovejoy et al. [310] determined reacto-diffusive lengths of > 0.4 µm and 1.0 µm for CF_3OH uptake at 250 K on 40 and 50 wt.% H_2SO_4 aerosols, respectively. This leads to H^* estimates of >240 and 210 M atm^{-1}, respectively. Back to Table

12. HOCl in $H_2SO_4 \cdot nH_2O(l)$. Recommendation is from the model of Shi et al. [414] which is based on wetted wall flow tube data from Hanson and Ravishankara [205] and Hanson and Lovejoy [197], and uptake by stirred and static solutions by Donaldson et al. [124]. This model incorporates newer, higher temperature data and replaces earlier recommended formulation by Huthwelker et al. [233]. Back to Table

13. $ClONO_2$ in $H_2SO_4 \cdot nH_2O(l)$. Recommendation is from the model of Shi et al. [414] who used a measurement of the hydrolysis reaction's reacto-diffusive length by Hanson and Lovejoy [196] on 60 wt.% H_2SO_4 at 250 K to derive the hydrolysis rate constant, k_{hyd}, and constrain H_{ClONO2} at 250 K. Shi et al. fit the $Hk^{1/2}$ dependence of the $ClONO_2$ uptake coefficients for a variety of $ClONO_2$ hydrolysis and $ClONO_2$ + HCl data to derive a parameterization for H as a function of wt.% and T. Back to Table

14. HBr in $H_2SO_4 \cdot mHNO_3 \cdot nH_2O(l)$. Experimental data for HBr solubility is provided by Williams et al. [475], Abbatt [2], Abbatt and Nowak [9], Kleffman et al. [279], and Behr et al. [52]. Data from time-dependent uptake measurements and from vapor pressure measurements is in good agreement after correcting for the fact that for some of the vapor pressure measurements the HBr concentration in solution was high enough to increase the acidity and thereby decrease the HBr solubility. By comparing pairs of data points with different HBr concentrations (from the same experiment), an average correction factor was obtained. The correction factor was used to correct the vapor pressure data of Williams et al. [475], Abbatt and Nowak [9] and Kleffmann et al. to zero effective HBr concentration. (This is different than the approach taken in Kleffmann et al. of using a "corrected" H_2SO_4 wt.%. However, the resulting parameterization is very similar to the one in Kleffmann et al. [279].) The time-dependent uptake data of Williams et al. [475] and Abbatt [2], and the molecular beam uptake data of Behr et al. [52] did not require correction. All of the experimental data have been fit to obtain the recommended parameterization as a function of H_2SO_4 wt.% and temperature.

    Agreement between this parameterization and the updated activity coefficient model of Massucci et al. [318] (and http://www.hpc1.uea.ac.uk/~e770/aim.html) is good for > 60 wt.%, but not very good at lower H_2SO_4 wt.%, particularly at low temperatures. Therefore, this parameterization is recommended for calculating HBr Henry's law solubilities.

    The only data for HBr solubilities in ternary solutions is from Kleffmann et al. [279]. The data do not agree well with the updated activity coefficient in Massucci et al. [279] or with the older activity coefficient model in Luo et al. [313]. Until further information becomes available, the recommendation is to use the parameterization for ternary solutions given in Kleffmann et al. [279]. Back to Table

15. SO_2 in $H_2SO_4 \cdot nH_2O(l)$. Room temperature vapor pressure measurements reviewed by Hayduk et al. [214] and bubble train reactor uptake measurements by Rattigan et al. [364] for 0–70 wt.% H_2SO_4 agree very well. Langenberg et al. [290] used a novel capillary gas chromatography technique to deduce H* values for 41–83 wt.% H_2SO_4 over a temperature range of 193–242 K. The recommended parameterization is a fair fit to the Rattigan et al. and Langenberg et al. data sets and allows reasonable extrapolation over the full range of atmospheric temperatures. Note that the Langenberg et al. [290] data is in mol/kg-bar units and was converted to mole/l units using the density parameterization of Myhre et al. [347]. Back to Table

5.22 References

1. Abbatt, J. P. D., 1994, Geophys. Res. Lett., **21**, 665-668.
2. Abbatt, J. P. D., 1995, J. Geophys. Res., **100**, 14009-14017.
3. Abbatt, J. P. D., 1996, Geophys. Res. Lett., **23**, 1681-1684.
4. Abbatt, J. P. D., 1997, Geophys. Res. Lett., **24**, 1479-1482.
5. Abbatt, J. P. D., 2003, Chem. Rev., **103**, 4783-4800.
6. Abbatt, J. P. D., K. D. Beyer, A. F. Fucaloro, J. R. McMahon, P. J. Wooldridge, R. Zhong and M. J. Molina, 1992, J. Geophys. Res., **97**, 15819-15826.
7. Abbatt, J. P. D. and M. J. Molina, 1992, J. Phys. Chem., **96**, 7674-7679.
8. Abbatt, J. P. D. and M. J. Molina, 1992, Geophys. Res. Lett., **19**, 461-464.
9. Abbatt, J. P. D. and J. B. Nowak, 1997, J. Phys. Chem. A, **101**, 2131-2137.
10. Abbatt, J. P. D. and G. C. G. Waschewsky *Heterogeneous Interactions of HOBr, HNO_3, O_3, and NO_2 with Deliquescent NaCl Aerosols at Room Temperature*, 1998; Vol. 102.
11. Aguzzi, A. and M. J. Rossi, 1999, Phys. Chem. Chem. Phys., **1**, 4337-4346.
12. Aguzzi, A. and M. J. Rossi, 2001, Phys. Chem. Chem. Phys., **3**, 3707-3716.
13. Aguzzi, A. and M. J. Rossi, 2002, J. Phys. Chem. A, **106**, 5891-5901.
14. Akhter, M. S., A. R. Chughtai and D. M. Smith, 1985, Appl. Spectrosc., **39**, 143-153.
15. Akhter, M. S., A. R. Chughtai and D. M. Smith, 1985, Appl. Spectrosc., **39**, 154-167.
16. Akhter, M. S., A. R. Chughtai and D. M. Smith, 1991, Appl. Spectrosc., **45**, 653-665.
17. Al-Abadleh, H. A. and V. H. Grassian, 2000, J. Phys. Chem. A, **104**, 11926-11933.
18. Al-Abedeleh, H. A. and V. H. Grassian, 2003, Langmuir, **19**, 6443-6457.
19. Alcala-Jornod, C., H. Van den Bergh and M. J. Rossi, 2000, Phys. Chem. Chem. Phys., **2**, 5584-5593.
20. Alebić-Juretić, A., T. Cvitas and L. Klasinc, 1992, Ber. Bunsenges Phys. Chem., **96**, 493-495.
21. Alebić-Juretić, A., T. Cvitas and L. Klasinc, 2000, Chemosphere, **41**, 667-670.
22. Allanic, A., R. Oppliger and M. J. Rossi, 1997, J. Geophys. Res., **102**, 23529-23541.
23. Allanic, A., R. Oppliger, H. Van den Bergh and M. J. Rossi, 2000, Zeitschrift fur Physikalische Chemie, **214**, 11, 1479-1500.
24. Allanic, A. and M. J. Rossi, 1999, J. Geophys. Res., **104**, 18,689-18,696.
25. Allen, H. C., D. E. Gragson and G. L. Richmond, 1999, J. Phys. Chem. B, **103**, 660-666.
26. Altschuh, J., R. Bruggemann, H. Santl, G. Eichinger and O. G. Piringer, 1999, Chemosphere, **39**, 1871-1887.
27. Ammann, M., M. Kalberer, D. T. Jost, L. Tobler, E. Rossler, D. Piguet, H. W. Gaggeler and U. Baltensperger, 1998, Nature, **395**, 157-160.
28. Ammann, M., M. Kalberer, K. Tabor, K. Tobler, C. Zellweger, E. Weingartner, S. Nyeki, Y. Parrat, F. Li, D. Piguet, E. Rossler, D. T. Jost, H. W. Gaggeler and U. Baltensperger. "Proc. 7th Euro. Symp. on Physico-Chem. Behav. of Atmos. Poll." 1996.
29. Anastasio, C. and M. Mozurkewich, 2002, J. Atmos. Chem., **41**, 135-162.
30. Arens, F., L. Gutzwiller, U. Baltensperger, H. Gaggeler and M. Ammann, 2001, Environ. Sci. Technol., **35**, 2191-2199.
31. Baker, J., S. F. M. Ashbourn and R. A. Cox, 1999, Phys. Chem. Chem. Phys., **1**, 683-690.
32. Baldwin, A. C., 1982, Int. J. Chem. Kin., **14**, 269-277.
33. Baldwin, A. C. and D. M. Golden, 1979, Science, **206**, 562.
34. Baldwin, A. C. and D. M. Golden, 1980, J. Geophys. Res., **85**, 2888-2889.
35. Ball, S. M., A. Fried, B. E. Henry and M. Mozurkewich, 1998, Geophys. Res. Lett., **25**, 3339-3342.
36. Barlett, W. P. and D. W. Margerum, 1999, Environ. Sce. Technol., **33**, 3410-3414.
37. Barone, S. B., M. A. Zondlo and M. A. Tolbert, 1997, J. Phys. Chem. A, **101**, 8643-8652.
38. Battino, R. Nitrous oxide in water. In *Oxides of Nitrogen*; C. L. Young, Ed.; Pergamon: Oxford, 1981; Vol. 8; pp 1-22.
39. Battino, R. Oxygen in water. In *Oxygen and Ozone*; R. Battino, Ed.; Pergamon: Oxford, 1981; Vol. 7; pp 1-5.
40. Battino, R. Ethane in water. In *Ethane*; W. Hayduk, Ed.; Pergamon: Oxford, 1982; Vol. 9; pp 1-26.
41. Battino, R. Nitrogen in water. In *Nitrogen and Air*; R. Battino, Ed.; Pergamon: Oxford, 1982; Vol. 10; pp 1-29.
42. Battino, R. Chlorine dioxide in water. In *Sulfur Dioxide, Chlorine, Fluorine and Chlorine Oxides*; C. L. Young, Ed.; Pergamon: Oxford, 1983; Vol. 12; pp 454-456.

43. Battino, R. Chlorine in water. In *Sulfur Dioxide, Chlorine, Fluorine and Chlorine Oxides*; C. L. Young, Ed.; Pergamon: Oxford, 1983; Vol. 12; pp 333-347.
44. Battino, R. Sulfur dioxide in water. In *Sulfur Dioxide, Chlorine, Fluorine and Chlorine Oxides*; C. L. Young, Ed.; Pergamon: Oxford, 1983; Vol. 12; pp 3-33.
45. Battino, R. 2-Methylpropane in water. In *Propane, Butane and 2-Methylpropane*; W. Hayduk, Ed.; Pergamon: Oxford, 1986; Vol. 24; pp 34-37.
46. Battino, R. Butane in water. In *Propane, Butane and 2-Methylpropane*; W. Hayduk, Ed.; Pergamon: Oxford, 1986; Vol. 24; pp 16-32.
47. Battino, R. Propane in water. In *Propane, Butane and 2-Methylpropane*; W. Hayduk, Ed.; Pergamon: Oxford, 1986; Vol. 24; pp 1-15.
48. Battino, R. Methane in water. In *Methane*; H. L. Clever and C. L. Young, Eds.; Pergamon: Oxford, 1987; Vol. 27/28; pp 1-44.
49. Becker, K. H., J. Kleffman, R. Kurtenbach and P. Wiesen, 1996, J. Phys. Chem., **100**, 14,984-14,990.
50. Behnke, W., C. George, V. Scheer and C. Zetsch, 1997, J. Geophys. Res., **102**, 3795-3804.
51. Behnke, W., H.-U. Kruger, V. Scheer and C. Zetzsch, 1991, J. Aerosol Sci., **22**, S609-S612.
52. Behr, P., J. R. Morris, M. D. Antman, B. R. Ringeisen, J. Splan and G. M. Nathanson, 2001, Geophys. Res. Lett., **28**, 1961-1964.
53. Beichert, P. and B. J. Finlayson-Pitts, 1996, J. Phys. Chem., **100**, 15218-15228.
54. Ben-Naim, A. and R. Battino, 1985, J. Sol. Chem., **14**, 245-253.
55. Benes, M. and V. Dohnal, 1999, J. Chem. Eng. Data, **44**, 1097-1102.
56. Benkelberg, H. J., S. Hamm and P. Warneck, 1995, J. Atmos. Chem., **20**, 17-34.
57. Benson, B. B., D. Krause and M. A. Peterson, 1979, J. Sol. Chem., **8**, 655-690.
58. Berland, B. S., M. A. Tolbert and S. M. George, 1997, J. Phys. Chem. A, **101**, 9954-9963.
59. Betterton, E. A. and M. R. Hoffmann, 1988, Environ. Sci. Technol., **22**, 1415-1418.
60. Blatchley, E. R., R. W. Johnson, J. E. Alleman and W. F. McCoy, 1991, Wat. Res., **26**, 99-106.
61. Bongartz, A., J. Kames, U. Schurath, C. George, P. Mirabel and J. L. Ponche, 1994, J. Atmos. Chem., **18**, 149-169.
62. Bongartz, A., S. Schweighoefer, C. Roose and U. Schurath, 1995, J. Atmos. Chem., **20**, 35-58.
63. Boniface, J., Q. Shi, Y. Q. Li, J. L. Chueng, O. V. Rattigan, P. Davidovits, D. R. Worsnop, J. T. Jayne and C. E. Kolb, 2000, J. Phys. Chem. A, **104**, 7502-7510.
64. Borensen, C., U. Kirchner, V. Scheer, R. Vogt and R. Zellner, 2000, J. Phys. Chem. A, **104**, 5036-5045.
65. Brouwer, L., M. J. Rossi and D. M. Golden, 1986, J. Phys. Chem., **90**, 4599-4603.
66. Brown, D. E., S. M. George, C. Huang, E. K. L. Wong, K. B. Rider, R. S. Smith and B. D. Kay, 1996, J. Phys. Chem., **100**, 4988-4995.
67. Brown, L. A., V. Vaida, D. R. Hanson, J. D. Graham and J. T. Roberts, 1996, J. Phys. Chem., **100**, 3121-3125.
68. Burnett, M. G., 1963, Anal. Chem., **35**, 1567-1570.
69. Butler, J. V. A., C. N. Ramchandani and D. W. Thomson, 1935, J. Chem. Soc., 280285.
70. Buxton, G. V., G. A. Salmon and J. Wang, 1999, Phys. Chem. Chem. Phys., **1**, 3589-3593.
71. Cachier, H. Carbonaceous Combustion Aerosols. In *Atmospheric Particles*; R. M. Harrison and R. VanGrieken, Eds.; Wiley: New York, 1998.
72. Caloz, F., F. F. Fenter, K. D. Tabor and M. J. Rossi, 1997, Rev. Sci. Instrum., **68**, 3172-3179.
73. Caloz, F., F. F. Fentner and M. J. Rossi, 1996, J. Phys. Chem., **100**, 7494-7501.
74. Caloz, F., S. Seisel, F. F. Fenter and M. J. Rossi, 1998, J. Phys. Chem. A, **102**, 7470-7479.
75. Cappa, C. D., S. E. Kuipers, J. M. Roberts, A. S. Gilbert and M. J. Elrod, 2000, J. Phys. Chem. A, **104**, 4449-4457.
76. Carlos-Cuellar, S., P. Li, A. P. Christensen, B. J. Krueger, C. Burrichter and V. H. Grassian, 2003, J. Phys. Chem. A, **107**, 4250-4261.
77. Carslaw, K. S., S. L. Clegg and P. Brimblecombe, 1995, J. Phys. Chem., **99**, 11,557-11,574.
78. Carslaw, K. S. and T. Peter, 1997, Geophys. Res. Lett., **24**, 1743-1746.
79. Carslaw, K. S., T. Peter and S. L. Clegg, 1997, Rev. Geophys., **35**, 125-154.
80. Carstens, T., C. Wunderlich and U. Schurath. "*Proceedings EUROTRAC Symposium ' 96*", 1996, Southhampton, U. K.
81. Chaix, L., A. Allanic and M. J. Rossi, 2000, J. Phys. Chem. A, **104**, 7268-7277.
82. Cheung, J. L., Y. Q. Li, J. Boniface, Q. Shi, P. Davidovits, D. Worsnop, J. T. Jayne and C. E. Kolb, 2000, J. Phys. Chem. A, **104**, 2655-2662.
83. Choi, W. and M. T. Leu, 1998, J. Phys. Chem A, **102**, 7618-7630.

84. Chu, L. and L. T. Chu, 1999, J. Phys. Chem. A, **103**, 8640-8649.
85. Chu, L. and L. T. Chu, 1999, J. Phys. Chem. A, **103**, 691-699.
86. Chu, L., G. Diao and L. T. Chu, 2000, J. Phys. Chem. A, **104**, 3150-3158.
87. Chu, L. T., G. Diao and L. Chu, 2002, J. Phys Chem. B, **106**, 5679-5688.
88. Chu, L. T. and J. W. Heron, 1995, Geophys. Res. Lett., **22**, 3211-3214.
89. Chu, L. T., M.-T. Leu and L. F. Keyser, 1993, J. Phys. Chem., **97**, 7779-7785.
90. Chu, L. T., M.-T. Leu and L. F. Keyser, 1993, J. Phys. Chem., **97**, 12798-12804.
91. Chughtai, A. R., M. M. O. Atteya, J. Kim, B. K. Konowalchuck and D. M. Smith, 1998, Carbon, **36**, 1573-1589.
92. Chughtai, A. R., M. E. Brooks and D. M. Smith, 1993, Aer. Sci. Tech., **19**, 121-132.
93. Chughtai, A. R., M. E. Brooks and D. M. Smith, 1996, J. Geophys. Res., **101**, 19505-19514.
94. Chughtai, A. R., S. A. Gordon and D. M. Smith, 1994, Carbon, **32**, 405-416.
95. Chughtai, A. R., J. M. Kim and D. M. Smith, 2002, J. Atmos. Chem., **43**, 21-43.
96. Chughtai, A. R., J. M. Kim and D. M. Smith, 2002, J. Atmos. Chem., **45**, 231-243.
97. Chughtai, A. R., N. J. Miller, D. M. Smith and J. R. Pitts, 1999, J. Atmos. Chem., **34**, 259-279.
98. Chughtai, A. R., W. F. Welch, M. S. Akhter and D. M. Smith, 1990, Appl. Spectrosc., **44**, 294-298.
99. Chughtai, A. R., W. F. Welch and D. M. Smith, 1990, Carbon, **28**, 411-421.
100. Chughtai, A. R., G. R. Williams, M. M. O. Atteya, N. J. Miller and D. M. Smith, 1999, Atmos. Environ., **33**, 2679-2687.
101. Clegg, S. L. and P. Brimblecombe, 1986, Atmos. Environ., **20**, 2483.
102. Clegg, S. L. and P. Brimblecombe, 1989, J. Phys. Chem., **93**, 7237-7248.
103. Cofer, W. R., D. R. Schryer and R. S. Rogowski, 1981, Atm. Environ., **15**, 1281-1286.
104. Cooper, P. L. and J. P. D. Abbatt, 1996, J. Phys. Chem., **100**, 2249-2254.
105. Cowin, J. P., personal comm.
106. Dacey, J. W. H., S. G. Wakeham and B. L. Howes, 1984, Geophys. Res. Lett., **11**, 991-994.
107. Dai, D. J., S. J. Peters and G. E. Ewing, 1995, J. Phys. Chem., **99**, 10,299-10,304.
108. Dai, Q., G. N. Robinson and A. Freedman, 1997, J. Phys. Chem., **101**, 4940-4946.
109. Dasgupta, P. K. and S. Dong, 1986, Atmos. Environ., **20**, 565-570.
110. Datta, A., R. G. Cavell, R. W. Tower and Z. M. George, 1985, J. Phys. Chem., **89**, 443-449.
111. Daumer, R. Nissner and D. Klockow, J. Aerosol Sci., **23**, 315-325.
112. Davidovits, P., D. R. Worsnop, J. T. Jayne, C. E. Kolb, P. Winkler, A. Vrtala, P. E. Wagner, M. Kulmula, K. E. J. Lehtinen, T. Vessala and M. Mozurkewich, 2004, Geophys. Res. Lett., **31**, L22111, doi: 10.1029/2004GRL020835.
113. Davies, J. A. and R. A. Cox, 1998, J. Phys. Chem. A, **102**, 7631-7642.
114. De Bruyn, W. J., S. X. Duan, X. Q. Shi, P. Davidovits, D. R. Worsnop, M. S. Zahniser and C. E. Kolb, 1992, Geophys. Res. Lett., **19**, 1939-1942.
115. De Bruyn, W. J., J. A. Shorter, P. Davidovits, D. R. Worsnop, M. S. Zahniser and C. E. Kolb, 1994, J. Geophys. Res., **99**, 16927-16932.
116. De Bruyn, W. J., J. A. Shorter, P. Davidovits, D. R. Worsnop, M. S. Zahniser and C. E. Kolb, 1995, Environ. Sci Technol., **29**, 1179-1185.
117. De Bruyn, W. J., E. Swartz, J. H. Hu, J. A. Shorter, P. Davidovits, D. R. Worsnop and M. S. Zahniser, 1995, J. Geophys. Res., **100**, 7245-7251.
118. DeHaan, D. O. and B. J. Finlayson-Pitts, 1997, J. Phys. Chem. A, **101**, 9993-9999.
119. Deiber, G., C. George, S. Le Calve, F. Schweitzer and P. Mirabel, 2004, Atmos. Chem. Phys., **4**, 1291-1299.
120. Disselkamp, R. S., M. A. Carpenter and J. P. Cowin, 2000, J. Atmos. Chem., **37**, 113-123.
121. Disselkamp, R. S., M. A. Carpenter, J. P. Cowin, C. M. Berkowitz, E. G. Chapman, R. A. Zaveri and N. S. Laulainen, 2000, J. Geophys. Res., **105**, 9767-9771.
122. Dlugokencky, E. J. and A. R. Ravishankara, 1992, Geophys. Res. Lett., **19**, 41-44.
123. Donaldson, D. J., J. A. Guest and M. C. Goh, 1995, J. Phys. Chem., **99**, 9313-9315.
124. Donaldson, D. J., A. R. Ravishankara and D. R. Hanson, 1997, J. Phys. Chem. A, **101**, 4717-4725.
125. Duan, S. X., J. T. Jayne, P. Davidovits, D. R. Worsnop, M. S. Zahniser and C. E. Kolb, 1993, J. Phys. Chem., **97**, 2284-2288.
126. Duncan, J. L., L. R. Schindler and J. T. Roberts, 1998, Geophys. Res. Lett., **25**, 631-634.
127. Duncan, J. L., L. R. Schindler and J. T. Roberts, 1999, J. Phys. Chem. B, **103**, 7247-7259.
128. Edwards, T. J., G. Maurer, J. Newman and J. M. Prausnitz, 1978, AIChE, **24**, 966-976.

129. Elam, J. W., C. E. Nelson, M. A. Cameron, M. A. Tolbert and S. M. George, 1998, J. Phys. Chem. B, **102**, 7008-7015.
130. Elliott, S., 1989, Atmos. Environ., **23**, 1977-1980.
131. Elrod, M. J., R. E. Koch, J. E. Kim and M. S. Molina, 1995, Faraday Discuss, **100**, 269-278.
132. Fairbrother, D. H. and G. Somorjai, 2000, J. Phys. Chem. B, **104**, 4649-4652.
133. Fendel, W., D. Matter, H. Burtscher and A. Schimdt-Ott, 1995, Atmos. Environ, **29**, 967-973.
134. Fendel, W. and A. Schmidt-Ott, 1993, J. Aerosol Sci., **24**, S317-S318.
135. Fenter, F. F., F. Caloz and M. J. Rossi, 1994, J. Phys. Chem., **98**, 9801-9810.
136. Fenter, F. F., F. Caloz and M. J. Rossi, 1996, J. Phys. Chem., **100**, 1008-1019.
137. Fenter, F. F. and M. J. Rossi, 1996, J. Phys. Chem., **100**, 13765-13775.
138. Fenter, F. F. and M. J. Rossi, 1997, J. Phys. Chem. A, **101**, 4110-4113.
139. Fenzel, A., V. Scheer, R. Sikorski, C. George, W. Behnke and C. Zetsch, 1998, J. Phys. Chem. A, **102**, 1329-1337.
140. Fickert, S., J. W. Adams and J. N. Crowley, 1999, J. Geophys. Res., **104**, 23719-23727.
141. Fickert, S., F. Helleis, J. W. Adams, G. K. Moortgat and J. N. Crowley, 1998, J. Phys. Chem. A, **102**, 10689-10696.
142. Finlayson-Pitts, B. J., 1983, Nature, **306**, 676-677.
143. Finlayson-Pitts, B. J., 2003, Chem Rev., **103**, 4801-4822.
144. Finlayson-Pitts, B. J., M. J. Ezell and J. N. Pitts, Jr., 1989, Nature, **337**, 241-244.
145. Finlayson-Pitts, B. J., F. E. Livingston and H. N. Berko, 1989, J. Phys. Chem., **93**, 4397-4400.
146. Finlayson-Pitts, B. J. and J. N. Pitts *Chemistry of the Upper and Lower Atmosphere: Theory, Experiments and Applications*; Academic: San Diego, 2000.
147. Fl ckiger, B. and M. J. Rossi, 2003, J. Phys. Chem. A, **107**, 4103-4115.
148. Fl ckiger, B., A. Thielmann, L. Gutzwiller and M. J. Rossi, 1998, Ber. Bunsenges. Phys. Chem., **102**, 915-928.
149. Fogg, P. G. T. Hydrogen sulfide in water. In *Hydrogen Sulfide, Deuterium Sulfide and Hydrogen Selenide*; P. G. T. Fogg and C. L. Young, Eds.; Pergamon: Oxford, 1988; Vol. 32; pp 1-19.
150. Fox, L. E., D. R. Worsnop, M. S. Zahniser and S. C. Wofsy, 1994, Science, **267**, 351-355.
151. Frenzel, A., S. Kutsuna, K. Takeuchi and T. Ibusuki, 2000, Atmos. Environ., **34**, 3641-3544.
152. Frenzel, A., V. Scheer, R. Sikorski, C. George, W. Behnke and C. Zetzsch, 1998, J. Phys. Chem. A, **102**, 1329-1337.
153. Friant, S. L. and I. H. Suffet, 1979, Anal. Chem., **51**, 21672176.
154. Fried, A., B. E. Henry, J. G. Calvert and M. Mozukewich, 1994, J. Geophys. Res., **99**, 3517-3532.
155. Fung, K. N., I. N. Tang and H. R. Munkelwitz, 1987, Appl. Optics, **26**, 1282-1287.
156. Gebel, M. E. and B. J. Finlayson-Pitts, 2001, J. Phys. Chem. A, **105**, 5178-5187.
157. Gebel, M. E., B. J. Finlayson-Pitts and J. S. Ganske, 2000, Geophys. Res. Lett., **27**, 887-890.
158. George, C., W. Behnke, V. Scheer, C. Zetsch, L. Magi, J. L. Ponche and P. Mirabel, 1995, Geophys. Res. Lett., **22**, 1505-1508.
159. George, C., J. Lagrange, P. Lagrange, P. Mirabel, C. Pallares and J. L. Ponche, 1994, J. Geophys. Res., **99**, 1255-1262.
160. George, C., J. L. Ponche, P. Mirabel, W. Behnke, V. Sheer and C. Zetzsch, 1994, J. Phys. Chem., **98**, 8780-8784.
161. George, C., J. Y. Saison, J. L. Ponche and P. Mirabel, 1994, J. Phys. Chem., **98**, 10857-10862.
162. Gerecke, A., A. Thielmann, L. Gutzwiller and M. J. Rossi, 1998, Geophys. Res. Lett., **25**, 2453-2456.
163. Gershenzon, M., P. Davidovits, L. R. Williams, Q. Shi, J. T. Jayne, C. E. Kolb and D. Worsnop, 2004, J. Phys. Chem. A, **106**, 1567-1573.
164. Gershenzon, M. Y., S. Il'in, N. G. Fedotov, Y. M. Gershenzon, E. V. Aparina and V. V. Zelenov, 1999, J. Atmos. Chem., **34**, 119-135.
165. Gershenzon, Y. M., V. M. Grigorieva, A. V. Ivanov and R. G. Remorov, 1995, Faraday Discuss, **100**, 83-100.
166. Gershenzon, Y. M., A. V. Ivanov, S. I. Kucheryavyi and V. B. Rozenshtein, 1986, Kinet. Katal., **27**, 1069-1074.
167. Gershenzon, Y. M. and A. P. Purmal, 1990, Russ. Chem. Rev., **59**, 1007-1023.
168. Gertner, B. J. and J. T. Hynes, 1996, Science, **271**, 1563-1566.
169. Ghosal, S. and J. C. Hemminger, 1999, J. Phys. Chem. A, **103**, 4777-4781.
170. Ghosal, S. and J. C. Hemminger, 2004, J. Phys. Chem. A, in press.
171. Ghosal, S., A. Shbeeb and J. C. Hemminger, 2000, Geophys. Res. Lett., **27**, 1879.

172. Goldberg, E. D. *Black Carbon in the Environment*; Wiley: New York, 1985.
173. Goodman, A. L., E. T. Bernard and V. H. Grassian, 2001, J. Phys. Chem. A, **105**, 6443-6457.
174. Goodman, A. L., P. Li, C. R. Usher and V. H. Grassian, 2002, J. Phys. Chem. A, **105**, 6109-6120.
175. Graham, J. D. and J. T. Roberts, 1994, J. Phys. Chem., **98**, 5974-5983.
176. Graham, J. D. and J. T. Roberts, 1995, Geophys. Res. Lett., **22**, 251-254.
177. Graham, J. D., J. T. Roberts, L. A. Brown and V. Vaida, 1996, J. Phys. Chem., **100**, 3115-3120.
178. Gratpanche, F. and J.-P. Sawerysyn, 1999, J. Chim. Phys., **96**, 213-231.
179. Guimbaud, C., F. Arens, L. Gutzwiller, H. W. G ggeler and M. Ammann, 2002, Atmos. Chem. Phys., **2**, 249-257.
180. Gutzwiller, L., F. Arens, U. Baltensperger, H. W. G ggeler and M. Ammann, 2002, Environ. Sci. Technol., **36**, 677-682.
181. Haag, W. R. and J. Hoigné, 1983, Environ. Sci. Technol., **17**, 261-267.
182. Haag, W. R. and J. Hoigné, 1983, Wat. Res., **17**, 1397-1402.
183. Hales, J. M. and D. R. Drewes, 1979, Atmos. Environ., **13**, 1133-1147.
184. Hallquist, M., D. J. Stewart, J. Baker and R. A. Cox, 2000, J. Phys. Chem. A, **104**, 3984.
185. Hamm, S., J. Hahn, G. Helas and P. Warneck, 1984, Geophys. Res. Let., **11**, 1207-1210.
186. Hanisch, F. and J. N. Crowley, 2001, J. Phys. Chem. A, **105**, 3096-3106.
187. Hanning-Lee, M. A., B. B. Brady, L. R. Martin and J. A. Syage, 1996, Geophys. Res. Lett., **23**, 1961-1964.
188. Hanson, D., 2003, J. Geophys. Res., **108**, doi: 10.1029/2002JD002519.
189. Hanson, D. and E. Kosciuch, 2003, J. Phys. Chem. A, **107**, 2199-2208.
190. Hanson, D. and E. Kosciuch, 2003, J. Phys. Chem. A, **108**, 5849-5851.
191. Hanson, D. R., 1992, Geophys. Res. Lett., **19**, 2063-2066.
192. Hanson, D. R., 1995, J. Phys. Chem., **99**, 13,059-13,061.
193. Hanson, D. R., 1998, J. Phys. Chem. A, **102**, 4794-4807.
194. Hanson, D. R., J. B. Burkholder, C. J. Howard and A. R. Ravishankara, 1992, J. Phys. Chem., **96**, 4979-4985.
195. Hanson, D. R. and E. R. Lovejoy, 1994, Geophys. Res. Lett., **21**, 2401-2404.
196. Hanson, D. R. and E. R. Lovejoy, 1995, Science, **267**, 1326-1329.
197. Hanson, D. R. and E. R. Lovejoy, 1996, J. Phys. Chem., **100**, 6397-6405.
198. Hanson, D. R. and A. R. Ravishankara, 1991, J. Geophys. Res., **96**, 5081-5090.
199. Hanson, D. R. and A. R. Ravishankara, 1991, Geophys. Res. Lett., **18**, 1699-1701.
200. Hanson, D. R. and A. R. Ravishankara, 1991, J. Geophys. Res., **96**, 17307-17314.
201. Hanson, D. R. and A. R. Ravishankara, 1992, J. Phys. Chem., **96**, 9441-9446.
202. Hanson, D. R. and A. R. Ravishankara, 1992, J. Phys. Chem., **96**, 2682-2691.
203. Hanson, D. R. and A. R. Ravishankara. In *The Tropospheric Chemistry of Ozone in the Polar Regions*; H. Niki and K. H. Becker, Eds.; NATO, 1993; pp 17281-17290.
204. Hanson, D. R. and A. R. Ravishankara, 1993, J. Phys. Chem., **97**, 2802-2803.
205. Hanson, D. R. and A. R. Ravishankara, 1993, J. Geophys. Res., **98**, 22931-22936.
206. Hanson, D. R. and A. R. Ravishankara, 1993, J. Phys. Chem., **97**, 12309-12319.
207. Hanson, D. R. and A. R. Ravishankara, 1994, J. Phys. Chem., **98**, 5728-5735.
208. Hanson, D. R. and A. R. Ravishankara, 1995, Geophys. Res. Lett., **22**, 385-388.
209. Hanson, D. R., A. R. Ravishankara and E. R. Lovejoy, 1996, J. Geophys. Res., **101**, 9063-9069.
210. Hanson, D. R., A. R. Ravishankara and S. Solomon, 1994, J. Geophys. Res., **99**, 3615-3629.
211. Harker, A. B. and W. W. Ho, 1979, Atmos. Environ., **13**, 1005-1010.
212. Harrison, R. M. and G. M. Collins, 1998, J. Atmos. Chem., **30**, 397-406.
213. Hauff, K., R. G. Fischer and K. Ballschmiter, 1998, Chemosphere, **37**, 2599-2615.
214. Hayduk, W., H. Asatani and B. C. Y. Lu, 1988, J. Chem. Eng. Data, **33**, 506-509.
215. Haynes, D. R., N. J. Tro and S. M. George, 1992, J. Phys. Chem., **96**, 8502-8509.
216. Henson, B. F., K. R. Wilson and J. M. Robinson, 1996, Geophys. Res. Lett., **23**, 1021-1024.
217. Hill, J. O., I. G. Worsley and L. G. Helper, 1968, J. Phys. Chem., **72**, 3695-3697.
218. Hirokawa, J., K. Onaka, Y. Kajii and H. Akimoto, 1998, Geophys. Res. Lett., **25**, 2449-2452.
219. Hoff, J. T., D. Mackay, R. Gillham and W. Y. Shiu, 1993, Environ. Sci. Tehcnol., **27**, 2174-2180.
220. Hoffman, R. C., M. E. Gebel, B. S. Fox and B. J. Finlayson-Pitts, 2003, Phys. Chem. Chem. Phys., **5**, 1780-1789.
221. Hoffman, R. C., M. Kaleuati and B. J. Finlayson-Pitts, 2003, J. Phys. Chem. A, **107**, 7818-7826.
222. Hofmann, D. J. and S. J. Oltmans, 1992, Geophys. Res. Lett., **22**, 2211-2214.
223. Holdren, M. W., C. W. Spicer and J. M. Hales, 1984, Atmos. Environ., **18**, 1171-1173.

224. Holzwarth, G., R. G. Balmer and L. Soni, 1984, Water Res., **18**, 1421-1427.
225. Hu, J. H. and J. P. D. Abbatt, 1997, J. Phys. Chem. A, **101**, 871-878.
226. Hu, J. H., Q. Shi, P. Davidovits, D. R. Worsnop, M. S. Zahniser and C. E. Kolb, 1995, J. Phys. Chem., **99**, 8768-8776.
227. Hu, J. H., J. A. Shorter, P. Davidovits, D. R. Worsnop, M. S. Zahniser and C. E. Kolb, 1993, J. Phys. Chem., **97**, 11037-11042.
228. Hudson, P. K., K. L. Foster, M. A. Tolbert, S. M. George, S. R. Carlo and V. H. Grassian, 2001, J. Phys. Chem. A, **105**, 694-702.
229. Hudson, P. K., J. E. Shilling, M. A. Tolbert and O. B. Toon, 2002, J. Phys. Chem. A, **106**, 9874-9882.
230. Huie, R. E., C. L. Clifton and P. Neta, 1991, Radiat. Phys. Chem., **38**, 477-481.
231. Hunt, S. W., M. Roesolová, W. Wang, L. M. Wingen, E. M. Knipping, D. J. Tobias, D. Dabdub and B. J. Finlayson-Pitts, 2004, J. Phys Chem. A, **108**, 11559-11572.
232. Huntzicker, J. J., R. A. Cary and C.-S. Ling, 1980, Environ. Sci. Technol., **14**, 819-824.
233. Huthwelker, T., T. Peter, B. P. Juo, S. L. Clegg, K. S. Carshlaw and P. Brimblecombe, 1995, J. Atmos. Chem., **21**, 81-95.
234. Hwang, H. and P. K. Dasgupta, 1985, Environ. Sci. Technol., **19**, 255-258.
235. Hynes, A. J., M. A. Fernandez and R. A. Cox, 2002, J. Geophys. Res.,, **107**, 4797.
236. Il'in, S. D., V. V. Selikhonovich, Y. M. Gershenson and V. B. Rozenshtein, 1991, Sov. J. Chem. Phys., **8**, 1858-1880.
237. Imamura, T. and H. Akiyoshi, 2000, Geophys. Res. Lett., **27**, 1419-1422.
238. Imamura, T., Y. Rudich, R. K. Talukdar, R. W. Fox and A. R. Ravishankara, 1997, J. Phys. Chem., **101**, 2316-2322.
239. Iraci, L. T., A. M. Essin and D. M. Golden, 2002, J. Phys. Chem. A, **106**, 4054-4060.
240. Iraci, L. T., A. M. Middlebrook, M. A. Wilson and M. A. Tolbert, 1994, Geophys. Res. Lett., **21**, 867-870.
241. Iraci, L. T. and M. A. Tolbert, 1997, J. Geophys. Res., **102**, 16,099-16,107.
242. Ivanov, A. V., Y. M. Gershenzon, F. Gratpanche, P. Devolder and J.-P. Saverysyn, 1996, Ann. Geophys., **14**, 659-664.
243. Jaegle, L., C. R. Webster, R. D. May, D. C. Scott, R. M. Stimpfle, D. W. Kohn, P. O. Wennberg, T. F. Hansico, R. C. Cohen, M. H. Proffitt, K. K. Kelly, J. Elkins, D. Baumgardner, J. E. Dye, J. C. Wilson, R. F. Pueschel, K. R. Chan, R. J. Salawitch, A. F. Tuck, S. J. Hovde and Y. L. Yung, 1997, J. Geophys. Res., **102**, 13,235-13,253.
244. Jans, U. and J. Hoigne, 2000, Atmos. Environ., **34**, 1069-1085.
245. Jayne, J. T., P. Davidovits, D. R. Worsnop, M. S. Zahniser and C. E. Kolb, 1990, J. Phys. Chem., **94**, 6041-6048.
246. Jayne, J. T., S. X. Duan, P. Davidovits, D. R. Worsnop, M. S. Zahniser and C. E. Kolb, 1991, J. Phys. Chem., **95**, 6329-6336.
247. Jayne, J. T., S. X. Duan, P. Davidovits, D. R. Worsnop, M. S. Zahniser and C. E. Kolb, 1992, J. Phys. Chem., **96**, 5452-5460.
248. Jayne, J. T., U. Poschl, Y. Chen, D. Dai, L. T. Molina, D. R. Worsnop, C. E. Kolb and M. J. Molina, 1997, J. Phys. Chem. A, **101**, 10,000-10,011.
249. Jayne, J. T., D. R. Worsnop, C. E. Kolb, E. Swartz and P. Davidovits, 1996, J. Phys. Chem., **100**, 8015-8022.
250. Jefferson, A., F. L. Eisele, P. J. Zieman, R. J. Weber, J. J. Marti and P. H. McMurry, 1997, J. Geophys. Res., **102**, 19,021-19,028.
251. Jenkins, J. and M. B. King, 1965, Chem. Engin. Sci., **20**, 921-922.
252. Johnson, B. J., E. A. Betterton and D. Craig, 1996, J. Atmos. Chem., **24**, 113-119.
253. Jungwirth, P. and D. Tobias, 2001, J. Phys. Chem. B., **105**, 10468-10472.
254. Jungwirth, P. and D. J. Tobias, 2002, J. Phys. Chem. B, **106**, 6361-6373.
255. Junkermann, W. and T. Ibusuki, 1992, Atmos. Environ., **26A**, 3099-3103.
256. Kalberer, M., M. Ammann, F. Arens, H. W. Gaggeler and U. Baltensperger, 1999, J. Geophys. Res., **104**, 13825-13832.
257. Kalberer, M., M. Ammann, H. W. Gaggeler and U. Baltensperger, 1999, Atmos. Environ., **33**, 2815-2822.
258. Kalberer, M., K. Tabor, M. Ammann, Y. Parrat, E. Weingartner, D. Piguet, E. Rossler, D. T. Jost, A. Turler, H. W. Gaggeler and U. Baltensperger, 1996, J. Phys. Chem., **100**, 15487-15493.
259. Kames, J. and U. Schurath, 1992, J. Atmos. Chem., **15**, 79-95.
260. Kames, J. and U. Schurath, 1995, J. Atmos. Chem., **21**, 151-164.
261. Kames, J., S. Schweighoefer and U. Schurath, 1991, J. Atmos. Chem., **12**, 169-180.

262. Kamm, S., O. Mohler, K.-H. Naumann, H. Saathoff and U. Schurath, 1999, Atmos. Environ., **33**, 4651-4661.
263. Kane, S. M. and M.-T. Leu, 2001, J. Phys. Chem. A, **105**, 1411-1415.
264. Kane, S. M., R. S. Timonen and M.-T. Leu, 1999, J. Phys. Chem. A, **103**, 9259-9265.
265. Karge, H. G. and I. G. Dalla Lana, 1984, J. Phys. Chem., **88**, 1538-1543.
266. Karlsson, R. and E. Ljungstrom, 1995, J. Aerosol Sci., **26**, 39-50.
267. Katrib, Y., G. Deiber, F. Schweitzer, P. Mirabel and C. George, 2001, J. Aerosol Sci., **32**, 893-911.
268. Katrib, Y., Y. Deiber, P. Mirabel, S. Le Calve, C. George, A. Mellouki and G. Le Bras, 2002, J. Atmos. Chem., **43**, 151-174.
269. Katrib, Y., P. Mirabel, S. Le Calve, G. Weck and E. Kochanski, 2002, J. Phys. Chem. B., **106**, 7237-7245.
270. Kelley, C. M. and H. V. Tartar, 1956, J. Amer. Chem. Soc., **78**, 5752-5756.
271. Kenner, R. D., I. C. Plumb and K. R. Ryan, 1993, Geophys. Res. Lett., **20**, 193-196.
272. Keyser, L. F. and M.-T. Leu, 1993, J. Colloid Interface Sci., **155**, 137-145.
273. Keyser, L. F. and M.-T. Leu, 1993, Micros. Res. Technol., **25**, 434-438.
274. Keyser, L. F., M.-T. Leu and S. B. Moore, 1993, J. Phys. Chem., **97**, 2800-2801.
275. Keyser, L. F., S. B. Moore and M. T. Leu, 1991, J. Phys. Chem., **95**, 5496-5502.
276. Khan, I., P. Brimblecombe and S. L. Clegg, 1995, J. Atmos. Chem., **22**, 285-302.
277. Kirchner, U., V. Scheer and R. Vogt, 2000, J. Phys. Chem. A, **104**, 8908-8915.
278. Klassen, J. K., J. Lynton, D. M. Golden and L. R. Williams, 1999, J. Geophys. Res., **104**, 26,355-26,361.
279. Kleffman, J., K. H. Becker, R. Broske, D. Rothe and P. Wiesen, 2000, J. Phys. Chem. A, **104**, 8489-8495.
280. Kleffman, J., K. H. Becker, M. Lackhoff and P. Wiesen, 1999, Phys. Chem. Chem. Phys., **1**, 5443-5450.
281. Kleffman, J., K. H. Becker and P. Wiesen, 1998, Atmos. Environ., **32**, 3129-3137.
282. Klimovskii, A. O., A. V. Bavin, V. S. Tkalich and A. A. Lisachenko, 1983, React. Kinet. Catal. Lett., **23**, 95-98.
283. Knipping, E. M., M. J. Lakin, K. L. Foster, P. Jungwirth, D. J. Tobias, R. B. Gerber, D. Dabdub and B. J. Finlayson-Pitts, 2000, Science, **288**, 301.
284. Koch, T. G. and M. J. Rossi, 1998, J. Phys. Chem. A, **102**, 9193-9201.
285. Koch, T. G., H. vandenBergh and M. J. Rossi, 1999, Phys. Chem. Chem. Phys., **1**, 2687-2694.
286. Koehler, B. G., L. S. McNeill, A. M. Middlebrook and M. A. Tolbert, 1993, J. Geophys. Res., **98**, 10563-10571.
287. Koehler, B. G., V. T. Nicholson, H. G. Roe and E. S. Whitney, 1999, J. Geophys. Res., **104**, 5507-5514.
288. Kolb, C. E., D. R. Worsnop, M. S. Zahniser, P. Davidovits, L. F. Keyser, M.-T. Leu, M. J. Molina, D. R. Hanson, A. R. Ravishankara, L. R. Williams and M. A. Tolbert. Progress and Problems in Atmospheric Chemistry. In *Adv. Phys. Chem. Series, 3*; J. R. Barker, Ed., 1994; pp 771-875.
289. Kroes, G.-J. and D. C. Clary, 1992, J. Phys. Chem., **96**, 7079-7088.
290. Langenberg, S., V. Proksch and U. Schurath, 1998, Atm. Environ., **32**, 3129-3137.
291. Langer, S., R. S. Pemberton and B. J. Finlayson-Pitts, 1997, J. Phys. Chem. A, **101**, 1277-1286.
292. Lemmon, E. W., M. O. McLinden and D. G. Friend. Thermophysical properties of fluid systems. In *NIST Chemistry WebBook; NIST Standard Reference Database No. 69*; W. G. Mallard and P. J. Linstrom, Eds.; National Institute of Standards and Technology: Gaithersburg, MD, 2000.
293. Leu, M.-T., 1988, Geophys. Res. Lett., **15**, 17-20.
294. Leu, M.-T., 1988, Geophys. Res. Lett., **15**, 851-854.
295. Leu, M.-T., S. B. Moore and L. F. Keyser, 1991, J. Phys. Chem., **95**, 7763-7771.
296. Leu, M.-T., R. S. Timonen and L. F. Keyser, 1997, J. Phys. Chem. A, **101**, 278-282.
297. Leu, M.-T., R. S. Timonen, L. F. Keyser and Y. L. Yung, 1995, J. Phys. Chem., **99**, 13203-13212.
298. Leu, M.-T. and R. Zhang, 1999, Geophys. Res. Lett., **26**, 1129-1132.
299. Li, P., K. A. Perreau, E. Covington, C. H. Song, G. R. Carmichael and V. H. Grassian, 2001, J. Geophys. Res., **106**, 5517-5529.
300. Li, Y. Q., P. Davidovits, Q. Shi, J. T. Jayne, C. E. Kolb and D. R. Worsnop, 2001, J. Phys. Chem. A, **105**, 10623-10634.
301. Li, Y. Q., H. Z. Zhang, P. Davidovits, J. T. Jayne, C. E. Kolb and D. R. Worsnop, 2002, J. Phys. Chem. A, **106**, 1220-1227.
302. Li, Z., R. R. Friedl, S. B. Moore and S. P. Sander, 1996, J. Geophys. Res., **101**, 6795-6802.
303. Liberti, A., D. Brocco and M. Possanzini, 1978, Atmos. Environ., **12**, 255-261.
304. Lind, J. A. and G. L. Kok, 1986, J. Goephys. Res., **91**, 7889-7895.
305. Lind, J. A. and G. L. Kok, 1994, J. Geophys. Res., **99**, 21119.
306. Livingston, F. E. and B. J. Finlayson-Pitts, 1991, Geophys. Res. Lett., **18**, 17-21.

307. Longfellow, C. A., T. Imamura, A. R. Ravishankara and D. R. Hanson, 1998, J. Phys. Chem. A, **102**, 3323-3332.
308. Longfellow, C. A., A. R. Ravishankara and D. R. Hanson, 1999, J. Geophys. Res., **104**, 13833.
309. Longfellow, C. A., A. R. Ravishankara and D. R. Hanson, 2000, J. Geophys. Res., **105**, 24,345-24,350.
310. Lovejoy, E. R., L. G. Huey and D. R. Hanson, 1995, J. Geophys. Res., **100**, 18,775-18,780.
311. Luick, T. J., R. W. Heckbert, K. Schultz and R. S. Disselkamp, 1999, J. Atmos. Chem., **32**, 315-325.
312. Luke, W. T., R. R. Dickerson and L. J. Nunnermacker, 1989, J. Geophys. Res., **94**, 14905-14921.
313. Luo, B., K. S. Carslaw, T. Peter and S. L. Clegg, 1995, Geophys. Res. Lett., **22**, 247-250.
314. Magi, L., F. Schweitzer, C. Pallares, S. Cherif, P. Mirabel and C. George, 1997, J. Phys. Chem. A, **4**, 4943-4948.
315. Manion, J. A., C. M. Fittschen, D. M. Golden, L. R. Williams and M. A. Tolbert, 1994, Israel J. Chem., **34**, 355-363.
316. Marek, R. and J. Straub, 2001, Int. J. Heat Mass Transfer, **44**, 39-53.
317. Martin, L. R., H. S. Judeikis and M. Wun, 1980, J. Geophys. Res., **85**, 5511-5518.
318. Massucci, M., S. L. Clegg and P. Brimblecombe, 1999, J. Phys. Chem. A, **103**, 4209-4226.
319. Mawhinney, D. B. and J. J. T. Yates, 2001, Carbon, **39**, 1167-1173.
320. McMurry, P. H., H. Takano and G. R. Anderson, 1983, Environ. Sci. Technol., **17**, 347-357.
321. Meisel, D. and G. Czapski, 1975, J. Phys. Chem., **79**, 1503-1509.
322. Mental, T. F., M. Sohn and A. Wahner, 2000, Phys. Chem. Chem. Phys., **2**, 5451-5457.
323. Mertes, S. and A. Wahner, 1995, J. Phys. Chem., **99**, 14000-14006.
324. Michel, A. E., C. R. Usher and V. H. Grassian, 2002, Geophys. Res. Lett., **29**, doi: 1029/2002/GL014896.
325. Michel, A. E., C. R. Usher and V. H. Grassian, 2003, Atmos. Environ., **37**, 3201-3211.
326. Michelangeli, D. V., M. Allen and Y. L. Yung, 1991, Geophys. Res. Lett., **18**, 673-676.
327. Middlebrook, A. M., L. T. Iraci, L. S. McNeil, B. G. Koehler, M. A. Wilson, O. W. Saastad and M. A. Tolbert, 1993, J. Geophys. Res., **98**, 20473-20481.
328. Middlebrook, A. M., B. G. Koehler, L. S. McNeill and M. A. Tolbert, 1992, Geophys. Res. Lett., **19**, 2417-2420.
329. Mihelcic, D., D. Klemp, P. Msgen, H. W. Ptz and A. Volz-Thomas, 1993, J. Atmos. Chem., **16**, 313-335.
330. Miller, T. M. and V. H. Grassian, 1998, Geophys. Res. Lett., **25**, 3835-3838.
331. Mochida, M., H. Akimoto, H. v. d. Bergh and M. J. Rossi, 1998, J. Phys. Chem. A, **102**, 4819-4828.
332. Mochida, M., J. Hirokawa and H. Akimoto, 2000, Geophys. Res. Lett., **27**, 2629-2632.
333. Mochida, M., J. Hirokawa, Y. Kajii and H. Akimoto, 1998, Geophys. Res. Lett., **25**, 3927-3930.
334. Molina, M. J., R. F. Meads, D. D. Spencer and L. T. Molina, 1997, Geophys. Res. Lett., **24**, 1619-1622.
335. Molina, M. J., T. L. Tso, L. T. Molina and F. C. Wang, 1987, Science, **238**, 1253-1259.
336. Molina, M. J., R. Zhang, P. J. Woolridge, J. R. McMahon, J. E. Kim, H. Y. Chang and K. D. Beyer, 1993, Science, **261**, 1418-1423.
337. Moore, S. B., L. F. Keyser, M. T. Leu, R. P. Turco and R. H. Smith, 1990, Nature, **345**, 333-335.
338. Mossinger, J. C., R. G. Hynes and R. A. Cox, 2002, J. Geophys. Res.,, **107**, 4740.
339. Mozurkewich, M. and J. Calvert, 1988, J. Geophys. Res., **93**, 15882-15896.
340. Mozurkewich, M., P. H. McMurray, A. Gupta and J. G. Calvert, 1987, J. Geophys. Res., **92**, 4163-4170.
341. Msibi, I. M., Y. Li, J. P. Shi and R. M. Harrison, 1994, J. Atmos. Chem., **18**, 291-300.
342. Msibi, I. M., J. P. Shi and R. M. Harrison, 1993, J. Atmos. Chem., 17339-17351.
343. Muenter, A. H. and B. G. Koehler, 2000, J. Phys. Chem. A, **104**, 8527-8534.
344. M ller, B. and M. R. Heal, 2002, Phys. Chem. Chem. Phys.,, **4**, 3365-3369.
345. Munder, B., H. Lidal and O. C. Sandall, 2000, J. Chem. Eng. Data, **45**, 1201-1204.
346. Murray, B. J. and M. C. Plane, 2003, Phys. Chem. Chem. Phys., **107**, 4129-4138.
347. Myhre, C. E. L., C. J. Nielsen and O. W. Saastad, 1998, J. Chem. Eng. Data, **43**, 617-622.
348. Noyes, R. M., M. B. Rubin and P. G. Bowers, 1996, J. Phys. Chem., **100**, 4167-4172.
349. O'Sullivan, D. W., M. Lee, B. C. Noone and B. G. Heikes, 1996, J. Phys. Chem., **100**, 3241-3247.
350. Olszyna, K., R. D. Cadle and R. G. dePena, 1979, J. Geophys. Res., **84**, 1771-1775.
351. Oppliger, R., A. Allanic and M. J. Rossi, 1997, J. Phys. Chem. A, **101**, 1903-1911.
352. Oum, K. W., M. J. Lakin, D. O. DeHaan, T. Brauers and B. J. Finlayson-Pitts, 1998, Science.
353. Parker, V. D., 1992, J. Am. Chem. Soc., **114**, 7458-7462.
354. Parker, V. D., 1992, Acta Chem. Scan., **45**, 692-694.
355. Percival, C. J., J. C. Mossinger and R. A. Cox, 1999, Phys. Chem. Chem. Phys., **1**, 4565-4570.
356. Peters, S. J. and G. E. Ewing, 1996, J. Phys. Chem., **100**, 14093-14102.
357. Ponche, J. L., C. George and P. Mirabel, 1993, J. Atmos. Chem., **16**, 1-21.

358. Poschl, U., M. Canagaratna, J. T. Jayne, L. T. Molina, D. R. Worsnop, C. E. Kolb and M. J. Molina, 1998, J. Phys. Chem. A, **102**, 10,082-10,089.
359. Pöschl, U., T. Letzel, C. Schauer and R. Niessner, 2001, J. Phys. Chem. A, **105**, 4029-4041.
360. Poskrebyshev, G. A., R. E. Huie and P. Neta, 2003, J. Phys. Chem. A, **107**, 1964-1970.
361. Przyjazny, A., W. Janicki, W. Chrzanowski and R. Staszewski, 1984, J. Chromatogr., **280**, 249-260.
362. Pueschel, R. F., D. F. Blake, A. G. Suetsinger, A. D. A. Hansen, S. Verma and K. Kato, 1992, Geophys. Res. Lett., **19**, 1659-1662.
363. Quinlan, M. A., C. M. Reihs, D. M. Golden and M. A. Tolbert, 1990, J. Phys. Chem., **94**, 3255-3260.
364. Rattigan, O. V., J. Boniface, E. Swartz, P. Davidovits, J. T. Jayne, C. E. Kolb and D. R. Worsnop, 2000, J. Geophys. Res., **105**, 29,065-29,078.
365. Reihs, C. M., D. M. Golden and M. A. Tolbert, 1990, J. Geophys. Res., **95**, 16,545-16,550.
366. Remorov, R. G., Y. M. Gershenzon, L. T. Molina and M. J. Molina, 2002, J. Phys. Chem. A, **106**, 4558-4565.
367. Rettich, T. R., R. Battino and E. Wilhelm, 1982, Ber. Bunsen. Phys. Chem., **86**, 1128-1132.
368. Rettich, T. R., R. Battino and E. Wilhelm, 2000, J. Chem. Themo., **32**, 1145-1156.
369. Rieley, H., H. D. Aslin and S. Haq, 1995, J. Chem. Soc. Faraday Trans., **91**, 2349-2351.
370. Rinker, E. B. and O. C. Sandall, 2000, Can. J. Chem. Eng., **78**, 232-236.
371. Rischbieter, E., H. Stein and A. Schumpe, 2000, J. Chem. Eng. Data, **45**, 338-340.
372. Robbins, R. C. and R. D. Cadle, 1958, J. Phys. Chem., **62**, 469-471.
373. Robinson, G. N., Q. Dai and A. Freedman, 1997, J. Phys. Chem., **101**, 4947-4953.
374. Robinson, G. N., A. Freedman, C. E. Kolb and D. R. Worsnop, 1994, Geophys. Res. Lett., **21**, 377-380.
375. Robinson, G. N., A. Freedman, C. E. Kolb and D. R. Worsnop, 1996, Geophys. Res. Lett., **23**, 317.
376. Robinson, G. N., D. R. Worsnop, J. T. Jayne, C. E. Kolb and P. Davidovits, 1997, J. Geophys. Res., **102**, 3583-3601.
377. Robinson, G. N., D. R. Worsnop, J. T. Jayne, C. E. Kolb, E. Swartz and P. Davidovits, 1998, J. Geophys. Res., **103**, 25371-25381.
378. Rodriguez-Sevilla, J., M. Alvarez, G. Liminana and M. C. Diaz, 2002, J. Chem. Engineer. Data, **47**, 1339-1345.
379. Roduner, E. and D. M. Bartels, 1992, Ber. Bunsenges. Phys. Chem., **96**, 1037-1042.
380. Roeselová, M., P. Jungwirth, D. J. Tobias and R. B. Gerber, 2003, J. Phys. Chem. B.,, **107**, 12690-12699.
381. Roeselová, M., J. Vieceli, L. X. Dang, B. C. Garrett and D. J. Tobias, 2004, J. Am. Chem. Soc.,, **126**, 16308-16309.
382. Rogaski, C. A., D. M. Golden and L. R. Williams, 1997, Geophys. Res. Lett., **24**, 381-384.
383. Rohrschneider, L., 1973, Anal. Chem., **45**, 1241-1247.
384. Rossi, M. J., 2003, Chem Rev., **103**, 4823-4882.
385. Rossi, M. J., F. F. Fenter, K. Tabor, F. Caloz and L. Gutzwiller. In *Heterogeneous and Liquid Phase Processes. Transport and Chemical Transformation of Pollutants in the Troposphere*; P. Warneck, Ed.; Springer-Verlag. Berlin, 1996; pp 213-220.
386. Rossi, M. J., R. Malhotra and D. M. Golden, 1987, Geophys. Res. Lett., **14**, 127-130.
387. Rubel, G. O. and J. W. Gentry, 1984, J. Aerosol Sci., **15**, 661-671.
388. Rudich, Y., R. K. Talukdar, T. Imamura, R. W. Fox and A. R. Ravishankara, 1996, Chem. Phys. Lett., **261**, 467-473.
389. Rudich, Y., R. K. Talukdar, A. R. Ravishankara and R. W. Fox, 1996, J. Geophys. Res., **101**, 21023-21031.
390. Rudolf, R. and P. E. Wagner, 1994, J. Aerosol Sci., **25**, 597-598.
391. Saastad, O. W., T. Ellerman and C. J. Nielson, 1993, Geophys. Res. Lett., **20**, 1191-1193.
392. Saathoff, H., K.-H. Naumann, N. Riemer, S. Kamm, O. Möhler, U. Schurath, H. Vogel and B. Vogel, 2001, Geophys. Res. Lett., **28**, 1957-1960.
393. Salgado-Muñoz, M. S. and M. J. Rossi, 2002, Phys. Chem. Chem. Phys., **4**, 5110-5118.
394. Sandanaga, Y., J. Hirokawa and H. Akimoto, 2001, Geophys. Res. Lett., **28**, 4433-4436.
395. Santschi, C. and M. J. Rossi, 2004, Phys. Chem. Chem. Phys., **6**, 3447-3460.
396. Scheer, V., A. Frenzel, W. Behnke, C. Zetsch, L. Magi, C. George and P. Mirabel, 1997, J. Phys. Chem. A, **101**, 9359-9366.
397. Schroeder, W. H. and P. Urone, 1974, Environ. Sci. Technol., **8**, 756-758.
398. Schumpe, A., 1993, Chem. Engineer. Sci., **48**, 153-158.
399. Schurath, U., A. Bongartz, J. Kames, C. Wunderlich and T. Carstens. In *Heterogeneous and Liquid Phase Processes. Transport and Chemical Transformation of Pollutants in the Troposphere*; P. Warneck, Ed.; Springer-Verlag: Berlin, 1996; Vol. 2; pp 182-189.

400. Sch tze, M. and H. Herrmann, 2002, Phys. Chem. Chem. Phys.,, **4**, 60-67.
401. Sch tze, M. and H. Herrmann, 2004, Phys. Chem. Chem. Phys., **6**, 965-971.
402. Schwartz, S. E., 1984, J. Geophys. Res., **89**, 11589-11598.
403. Schwartz, S. E., 1988, Atmos. Environ., **22**, 2331.
404. Schwartz, S. E. and W. H. White. In *Trace Atmospheric Species. Properties, Transformations and Fates*; S. E. Schwartz, Ed.; John Wiley & Sons: New York, 1983; Vol. 12; pp 1-116.
405. Schwarz, H. A. and R. W. Dodson, 1984, J. Phys. Chem., **88**, 3643-3647.
406. Schweitzer, F., L. Magi, P. Mirabel and C. George, 1998, J. Phys. Chem. A, **102**, 593-600.
407. Schweitzer, F., P. Mirabel and C. George, 1998, J. Phys. Chem. A, **102**, 3942-3952.
408. Schweitzer, F., P. Mirabel and C. George, 1999, J. Atmos. Chem., **34**, 101-117.
409. Schweitzer, F., P. Mirabel and C. George, 2000, J. Phys. Chem. A, **104**, 72-76.
410. Seisel, S., F. Caloz, F. F. Fenter, H. vandenBergh and M. J. Rossi, 1997, Geophys. Res. Lett., **24**, 2757-2760.
411. Seisel, S., B. Fluckiger, F. Caloz and M. J. Rossi, 1999, Phys. Chem. Chem. Phys., **1**, 2257-2266.
412. Seisel, S., B. Fluckiger and M. J. Rossi, 1998, Ber. Bunsenges. Phys. Chem., **102**, 811-820.
413. Shaw, R. A. and D. Lamb, 1999, J. Chem. Phys.,, **111**, 10659-10663.
414. Shi, Q., P. Davidovits, J. T. Jayne, C. E. Kolb and D. R. Worsnop, 2001, J. Geophys. Res., **106**, 24259-24274.
415. Shi, Q., P. Davidovits, J. T. Jayne, D. R. Worsnop and C. E. Kolb, 1999, J. Phys. Chem. A, **103**, 8812-8823.
416. Shi, Q., Y. Q. Li, P. Davidovits, J. T. Jayne, D. R. Worsnop, M. Mozurkewich and C. E. Kolb, 1999, J. Phys. Chem. B., **103**, 2418-2420.
417. Shimono, A. and S. Koda, 1996, J. Phys. Chem., **100**, 10,269-10,276.
418. Smith, D. M. and A. R. Chughtai, 1995, Colloids and Surfaces, **105**, 47-77.
419. Smith, D. M. and A. R. Chughtai, 1996, J. Geophys. Res., **101**, 19607-19620.
420. Smith, D. M. and A. R. Chughtai, 1997, J. Atmos. Chem., **26**, 77-91.
421. Smith, D. M., W. F. Welch, S. M. Graham, A. R. Chughtai, B. G. Wicke and K. A. Grady, 1988, Appl. Spectrosc., **42**, 674-680.
422. Smith, D. M., W. F. Welch, J. A. Jassim, A. R. Chughtai and D. H. Stedman, 1988, Appl. Spectros., **42**, 1473-1482.
423. Snider, J. R. and G. A. Dawson, 1985, J. Geophys. Res., **90**, 3797-3805.
424. Stadler, D. and M. J. Rossi, 2000, Phys. Chem. Chem. Phys., **2**, 5420-5429.
425. Staffelbach, T. A. and G. L. Kok, 1993, J. Geophys. Res., **98**, 12713-12717.
426. Staudinger, J. and P. V. Roberts, 2001, Chemosphere, **44**, 561-576.
427. Stephens, S., M. J. Rossi and D. M. Golden, 1986, Int. J. Chem. Kinetics, **18**, 1133-1149.
428. Stewart, D. J. and R. A. Cox, 2004, Atmos. Chem. Phys. Discuss., **4**, 569-590.
429. Sullivan, R. C., T. Thornberry and J. P. D. Abbatt, 2004, Atmos. Chem. Phys., **4**, 1301-1310.
430. Sverdrup, G. M. and M. R. Kuhlman. "Heterogeneous Nitrogen Oxide-Particle Reactions"; 14th International Colloquium on Atmospheric Pollution, 1980, Paris.
431. Swartz, E., Q. Shi, P. Davidovits, J. T. Jayne, D. Worsnop and C. E. Kolb, 1999, J. Phys. Chem. A, **103**, 8824-8833.
432. Tabazadeh, A., R. P. Turco and M. Z. Jacobson, 1994, J. Geophys. Res., **99**, 12,897-12,914.
433. Tabor, K., L. Gutzwiller and M. J. Rossi, 1993, Geophys. Res. Lett., **20**, 1431-1434.
434. Tabor, K., L. Gutzwiller and M. J. Rossi, 1994, J. Phys. Chem., **98**, 6172-7186.
435. Takami, A., S. Kato, A. Shimono and S. Koda, 1998, Chem. Phys.,, **231**, 215-227.
436. Takami, A., T. Kondo, A. Kado and S. Koda, 2001, J. Atmos. Chem., **39**, 139-153.
437. Tang, I. N. and J. H. Lee. In *The Chemistry of Acid Rain*; G. E. Gordon and R. W. Johnson, Eds.; Am. Chem. Soc. Symp. Series, 1987; pp 109-117.
438. Tang, I. N. and H. R. Munkelwitz, 1989, J. Colloid Interface Sci., **128**, 289-295.
439. Thomas, K., A. Volz-Thomas, D. Mihelcic, H. G. J. Smit and D. Kley, 1998, J. Atmos. Chem., **29**, 17-43.
440. Timonen, R. S., L. T. Chu, M.-T. Leu and L. F. Keyser, 1994, J. Phys. Chem., **98**, 9509-9517.
441. Tolbert, M. A., J. Praff, I. Jayaweera and M. J. Prather, 1993, J. Geophys. Res., **98**, 2957-2962.
442. Tolbert, M. A., M. J. Rossi and D. M. Golden, 1988, Science, **240**, 1018-1021.
443. Tolbert, M. A., M. J. Rossi and D. M. Golden, 1988, Geophys. Res. Lett., **15**, 847-850.
444. Tolbert, M. A., M. J. Rossi, R. Malhotra and D. M. Golden, 1987, Science, **238**, 1258-1260.
445. Tolocka, M., T. D. Saul and M. V. Johnston, 2004, J. Phys. Chem. A, **108**, 2659-2665.

446. Toon, O., E. Browell, B. Gray, L. Lait, J. Livingston, P. Newman, R. Russell, P. P., M. Schoeberl, G. Toon, W. Traub, F. P. J. Valero, H. Selkirk and J. Jordan, 1993, Science, **261**, 1136-1140.
447. Underwood, G. M., P. Li, H. A. Al-Abedeleh and V. H. Grassian, 2001, J. Phys. Chem. A, **105**, 6609-6620.
448. Underwood, G. M., P. Li, C. R. Usher and V. H. Grassian, 2000, J. Phys. Chem. A, **104**, 819-829.
449. Underwood, G. M., T. M. Miller and V. H. Grassian, 1999, J. Phys. Chem. A, **103**, 6184-6190.
450. Underwood, G. M., C. H. Song, M. Phadnis, G. R. Carmichael and V. H. Grassian, 2001, J. Geophys. Res., **106**, 18055-18066.
451. Usher, C. R., H. Al-Hosney, S. Carlos-Cuellar and V. H. Grassian, 2002, J. Geophys. Res., **107**, 4713.
452. Usher, C. R., A. E. Michel, D. Stec and V. H. Grassian, 2003, Atmos. Environ., **37**, 5337-5347.
453. Utter, R. G., J. B. Burkholder, C. J. Howard and A. R. Ravishankara, 1992, J. Phys. Chem., **96**, 4973-4978.
454. Van Dingenen, R. and F. Raes, 1991, Aerosol Sci. Technol., **15**, 93-106.
455. Van Doren, J. M., L. R. Watson, P. Davidovits, D. R. Worsnop, M. S. Zahniser and C. E. Kolb, 1990, J. Phys. Chem., **94**, 3265-3269.
456. Van Doren, J. M., L. R. Watson, P. Davidovits, D. R. Worsnop, M. S. Zahniser and C. E. Kolb, 1991, J. Phys. Chem., **95**, 1684-1689.
457. Villalta, P. W., E. R. Lovejoy and D. R. Hanson, 1996, Geophys. Res. Lett., **23**, 1765-1768.
458. Vitenberg, A. G., B. V. Ioffe, Z. S. Dimitrova and I. L. Butaeva, 1975, J. Chromatog., **112**, 319-327.
459. Vogt, R., C. Elliott, H. C. Allen, J. M. .Laux, J. C. Hemminger and B. J. Finlayson-Pitts, 1996, Atmos. Environ, **30**, 1729-1737.
460. Vogt, R. and B. Finlayson-Pitts, 1994, J. Phys. Chem., **98**, 3747-3755.
461. Vogt, R. and B. F. Finlayson-Pitts, 1994, Geophys. Res. Lett., **21**, 2291-2294.
462. Vogt, R. and B. J. Finlayson-Pitts, 1995, J. Phys. Chem., **99**, 13,052.
463. Wachsmuth, M., H. W. G ggeler, R. v. Glasow and M. Ammann, 2002, Atmos. Chem. Phys., **2**, 121-131.
464. Wagman, D. D., W. H. Evans, V. B. Parker, R. H. Schumm, I. Halow, S. M. Bailey, K. L. Churney and R. L. Nutall, 1982, J. Phys. Chem. Ref. Data, **11,** , Suppl. No. 1.
465. Wahner, A., T. F. Mental, M. Sohn and J. Stier, 1998, J. Geophys. Res., **103**, 31103-31112.
466. Wang, L. and D. C. Clary, 1996, J. Chem. Phys., **104**, 5663-5673.
467. Wardman, P., 1991, Free Rad. Res. Comm., **14**, 57-67.
468. Waschewsky, G. C. G. and J. P. D. Abbatt, 1999, J. Phys. Chem. A, **103**, 5312-5320.
469. Watson, L. R., J. M. V. Doren, P. Davidovits, D. R. Worsnop, M. S. Zahniser and C. E. Kolb, 1990, J. Geophys. Res., **95**, 5631-5638.
470. Watts, S. F. and P. Brimblecombe, 1987, Environ. Technol. Lett., **8**, 483-486.
471. Weingartner, E., H. Burtscher and U. Baltensperger, 1997, Atmos. Environ., **31**, 2311-2327.
472. Weisenberger, S. and A. Schumpe, 1996, AIChE Journal, **42**, 298-300.
473. Wilhelm, E., R. Battino and R. J. Wilcock, 1977, Chem. Rev., **77**, 219-262.
474. Williams, L. R. and D. M. Golden, 1993, Geophys. Res. Lett., **20**, 2227-2230.
475. Williams, L. R., D. M. Golden and D. L. Huestis, 1995, J. Geophys. Res., **100**, 7329-7335.
476. Williams, L. R. and F. S. Long, 1995, J. Phys. Chem., **99**, 3748-3751.
477. Winkler, P., A. Vrtala, P. E. Wagner, M. Kulmula, K. E. J. Lehtinen and T. Vesala, 2004, Phys. Rev. Lett., **93**, doi: 10.1103/Phys.Rev.Lett93.075701.
478. Winkler, T., J. Goschnick and H. J. Ache, 1991, J. Aerosol Sci., **22**, S605-S608.
479. Wolff, E. W. and R. Mulvaney, 1991, Geophys. Res. Lett., **18**, 1007-1010.
480. Wong, P. K. and Y. H. Wang, 1997, Chemosphere, **35**, 535-544.
481. Worsnop, D. R., L. E. Fox, M. S. Zahniser and S. C. Wofsy, 1993, Science, **259**, 71-74.
482. Worsnop, D. R., L. R. Williams, C. E. Kolb, M. Mozurkewich, M. Gershenzon and P. Davidovits, 2004, J. Phys. Chem. A, **108**, 5846-5848.
483. Worsnop, D. R., M. S. Zahniser, C. E. Kolb, J. A. Gardner, L. R. Watson, J. M. V. Doren, J. T. Jayne and P. Davidovits, 1989, J. Phys. Chem., **93**, 1159-1172.
484. Yaws, C. L., J. R. Hopper, X. Wang and A. K. Rathinsamy, 1999, Chem. Eng., 102-105.
485. Yoshitake, H., 2000, Atmos. Environ., **34**, 2571-2580.
486. Yoshizumi, K., K. Aoki, I. Nouchi, T. Okita, T. Kobayashi, S. Kamakura and M. Tajima, 1984, Atmos. Environ., **18**, 395-401.
487. Yu, X. Y. and J. R. Barker, 2003, J. Phys. Chem. A.
488. Zangmeister, C. D. and J. E. Pemberton, 2001, J. Phys. Chem. A, **105**, 3788-3795.
489. Zangmeister, C. D. and J. E. Pemberton, 2004, J. Phys. Chem. A, **108**, 236-236.
490. Zangmeister, C. D., J. A. Turner and J. E. Pemberton, 2001, Geophys. Res. Lett., **28**, 995.

491. Zelenov, V. V., E. V. Aparina, M. Y. Gershenzon, S. D. Il'in and Y. M. Gershenzon, 2003, Khim. Fiz., **22**, 58-70.
492. Zelenov, V. V., E. V. Aparina, M. Y. Gershenzon, S. D. Il'in and Y. M. Gershenzon, 2003, Khim. Fiz., **22**, 37-48.
493. Zetzsch, C. and W. Behnke, 1992, Ber. Bunsenges. Phys. Chem., **96**, 488-493.
494. Zhang, H. Z., Y. Q. Li, P. Davidovits, W. L. R., J. T. Jayne, C. E. Kolb and D. R. Worsnop, 2003, J. Phys. Chem. A, **107**, 6398-6407.
495. Zhang, R., J. T. Jayne and M. J. Molina, 1994, J. Phys. Chem., **98**, 867-874.
496. Zhang, R. and M.-T. Leu, 1997, J. Geophys. Res., **102**, 8837-8843.
497. Zhang, R., M.-T. Leu and L. F. Keyser, 1994, J. Phys. Chem., **98**, 13,563-13,574.
498. Zhang, R., M.-T. Leu and L. F. Keyser, 1995, Geophys. Res. Lett., **22**, 1493-1496.
499. Zhang, R., M.-T. Leu and L. F. Keyser, 1995, J. Geophys. Res., **100**, 18,845-18,854.
500. Zhang, R., M.-T. Leu and L. F. Keyser, 1996, J. Phys. Chem., **100**, 339-345.
501. Zhang, R., M.-T. Leu and L. F. Keyser, 1997, J. Phys. Chem. A, **101**, 3324-3330.
502. Zhang, R., P. J. Wooldridge and M. J. Molina, 1993, J. Phys. Chem., **97**, 8541-8548.
503. Zhou, X. and Y. N. Lee, 1992, J. Phys. Chem., **96**, 265-272.
504. Zhou, X. and K. Mopper, 1990, Environ. Sci. Technol., **24**, 1864-1869.
505. Zolensky, M. E., D. S. McKay and L. A. Kaczor, 1989, J. Geophys. Res., **94**, 1047-1056.
506. Zondlo, M. A., S. B. Barone and M. A. Tolbert, 1998, J. Phys. Chem. A, **102**, 5735-5748.

APPENDIX A. GAS-PHASE ENTROPY AND ENTHALPY VALUES FOR SELECTED SPECIES AT 298.15 K AND 100 KPA

SPECIES	ΔH_f(298 K) kJ mol^{-1}	ΔH_f(298 K) kcal mol^{-1}	S(298 K) J K^{-1} mol^{-1}	S(298 K) cal K^{-1} mol^{-1}	Reference[1-3]
H	217.998±0.006	52.103±.001	114.717±0.002	27.418±.0.001	[33]
H_2	0.00	0.00	130.680±0.003	31.233±0.001	[33]
$O(^3P)$	249.18±0.10	59.56±0.02	161.059±0.003	38.194±0.001	[33]
$O(^1D)$	438.05±0.1	104.70±0.03			[82]
O_2	0.00	0.00	205.152±0.005	49.033±0.001	[33]
$O_2(^1\Delta_g)$	94.29±0.01	22.54±0.01			[46]
$O_2(^1\Sigma_g^+)$	156.96±0.01	37.51±0.01			[46]
O_3	141.8±2	33.9±0.5	239.01	57.12	[43]
OH	37.28±0.29	8. 91±0.07	183.74	43.91	[105] [43, 102]
HO_2	13.4±2.1	3..2±0.5	229.1	54.76	[96] [43, 45]
HO_3	-4±20	-1±5			[115]
H_2O	-241.826±0.040	-57.798±0.010	188.835±0.010	45.133±.002	[33]
H_2O_2	-135.9±0.2	-32.5±0.05	234.5±0.1	56.05±0.02	[36]
$N(^4S)$	472.68±0.40	112.973±0.10	153.301±0.003	36.640±0.001	[33]
N_2	0.00	0.00	191.609±0.004	45.796±0.001	[33]
NH	357±1	85.3±0.3	181.25±0.04	43.32±0.01	[4]
NH_2	186±1	44.5±0.3	194.71±0.05	46.54±0.01	[4]
NH_3	-45.94±0.35	-10.98±0.08	192.77±0.05	46.07±0.01	[33]
NH_2OH	-40.2±9.2	-9.6±2.2	236.18	56.45	[5]
NH_2NO_2	-26±10	-6.2±3	268.54	64.18	[43]
NO	91.29±0.17	21.82±0.04	210.76	50.37	[5, 27]
N_2O	81.6±0.5	19.50±0.12	220.01	52.58	[43]
NO_2	34.19±0.5	8.17±0.1	240.17	57.40	[43]
NO_3	73.7±1.4	17.6±0.3	258.4±1.0	61.76±0.24	[1, 35]
N_2O_3	86.6±1	20.7±0.3	314.74	75.22	[43]
N_2O_4	11.1±1	2.65±0.25	340.45	81.37	[43]
N_2O_5	13.3±1.5	3.18±0.36	355.7±7	85.01±2	[43]
HNO	107.1±2.5	25.6±0.6			[5]
HONO	-78.45±0.8	-18.75±0.2	254.07	60.72	[43]
$HONO_2$	-134.3±0.5	-32.1±0.1	266.88±0.7	63.78±0.2	[36]
HO_2NO	-23.8	-5.7	274	65.6	[73], calc.
HO_2NO_2	-53.1±2.5	-12.7±0.6	294±3	70.3±0.7	[97]
C	716.68±0.45	171.29±0.11	158.100±0.001	37.787±0.001	[33]
CH	597.37±1.3	142.77±0.3	183.04	43.75	[43]
$CH_2(^3B_1)$	390.4±0.8	93.31±0.2	194.90	46.58	[103]
$CH_2(^1A_1)$	428.0±0.8	102.3±0.2			[49]
CH_3	146.65±0.29	35.05±0.07	193.96	46.36	[43, 103]
CH_4	-74.48±0.41	-17.80±0.10	186.38	44.55	[40, 94]
CN	440±5	105±1	202.64	48.43	[43]

SPECIES	ΔH_f(298 K) kJ mol^{-1}	ΔH_f(298 K) kcal mol^{-1}	S(298 K) J K^{-1} mol^{-1}	S(298 K) cal K^{-1} mol^{-1}	Reference[1-3]
HCN	132±4	31.5±1	201.82	48.24	[43]
C_2N_2	309.1±0.8	73.9±0.2	242.20	57.89	[43]
CH_2NH_2	149±8	35.6±2			[74], corr.
CH_3NH_2	-23.4±1.0	-5.6±0.3	242.89	58.05	[40, 91]
CH_2NO	157±4	37.5±1			[114], calc.
NH_2CO	-15.1±4	-3.6±1			[114], calc.
NCO	151±14	36±3	232.38	55.54	[86] corr ,[43]
HNCO	-104±12	- 24.8±2.8	237.97±0.8	56.9±0.2	[116] corr,[124]
CO	-110.53±0.17	-26.42±0.04	197.660±0.004	47.242±0.001	[33]
CO_2	-393.51±0.13	-94.05±0.03	213.785±0.010	51.096±0.002	[33]
HCO	44.15±0.43	10.55±0.10	224.34	53.62	[10] corr., [43]
CH_2O	-108.7±0.05	-25.98±0.01	218.76	52.28	[43]
trans-HOCO	-181.2±8	-43.3±2			[38], calc.
cis-HOCO	-173.2±8	-41.4±2			[38], calc.
HCOO	127	30	244.7	58.5	[129], calc.
C(O)OH	-193	-45	251.6	60.1	[129]
HC(O)OH	-378.8±0.5	-90.54±0.1	248.87	59.48	[43, 129]
CH_3O	17.15±3.8	4.1±0.9	232.86	55.655	[13, 43]
CH_3O_2	9.0±5.1	2.15±1.2			[57]
CH_2OH	-11.5±1.3	-2.75±0.31	244.170±0.018	58.358±0.004	[51]
CH_3OH	-201.0±0.6	-48.04±0.14	239.865	57.329	[43]
CH_3OOH	-139.0±8.1	-33.2±1.9			[57]
CH_2NO_2	147.3	35.2	272.48	65.12	[40]
CH_3NO_2	-74.3±0.6	-17.8±0.2	275.2	65.8	[40, 91]
CH_3ONO	-64.0	-15.3	284.3	67.95	[117]
CH_3ONO_2	-122.2±4.3	-29.2±1.1	301.9	72.15	[91, 117]
C_2H	565.3±2.9	135.1±0.7	209.73	50.13	[13, 43]
C_2H_2	227.4±0.8	54.35±0.2	200.93	48.02	[43]
C_2H_2OH	121±11	28.9±2.6			[42]
C_2H_3	299±5	71.5±.1			[118]
C_2H_4	52.4±0.5	12.52±0.12	219.316	52.418	[43]
C_2H_5	120.9±1.7	28.9±0.4	250.52	59.88	[13, 43]
C_2H_6	-83.85±0.29	-20.04±0.07	229.162	54.771	[43, 94]
CH_2CN	252.6±4	60.4±1.0			[63]
CH_3CN	74.04±0.37	17.70±0.09	245.12±0.8	58.59±0.2	[2, 124]
CH_2CO	-49.58±0.88	-11.85±0.21			[103]
CH_3CO	-10.0±1.2	-2.4±0.3			[13]
CH_2CHO	10.5±9.2	2.5±2.2			[13]
CH_3CHO	-166.1±0.5	-39.7±0.1	263.95	63.09	[40, 91]
CH_3CH_2O	-15.5±3.3	-3.7±0.8			[13]
$(CHO)_2$	-212±0.8	-50.7±0.2			[36]
C_2H_5O	-17.2	-4.1			[74]
$C_2H_5O_2$	-27.4±9.9	-6.6±2.4			[57]
C_2H_5OOH	-175.4±12.9	-41.9±3.1			[57]

SPECIES	ΔH_f(298 K) kJ mol^{-1}	ΔH_f(298 K) kcal mol^{-1}	S(298 K) J K^{-1} mol^{-1}	S(298 K) cal K^{-1} mol^{-1}	Reference[1-3]
CH_2CH_2OH	-31±7	-7.5±1.7			[42]
CH_3CHOH	-63.7±4	-15.2±1			[74]
C_2H_5OH	-234.8±0.5	-56.12±0.12	281.622	67.309	[43]
$CH_3C(O)O$	-190	-45	284.9	68.1	[129], calc.
$CH_2C(O)OH$	-252.3±12.6	-60.3±3.0	238.4	57.0	[125] [129]
$CH_3C(O)O$	-192.5	-46.0			[75], calc.
$CH_3C(O)OH$	-432.8±0.5	-103.4±0.1	332.67	79.51	[23, 91]
$CH_3C(O)O_2$	-154.4	-36.9			[75], calc.
$CH_3C(O)O_2NO_2$	-240.1	-57.4			[75], calc.
$HOCH_2COOH$	-583±10	-139±3	318.6±5.0	76.1±1.2	[37]
CH_3OCH_2	-13.0±4	-3.1±1			[74], corr.
CH_3OCH_3	-184.1±0.5	-44.0±0.1	267.34	63.90	[40, 91]
$CH_2(OH)CH_2OH$	-392.2±4.0	-93.7±1.0	303.81	72.61	[40, 91]
CH_3OOCH_3	-125.5±5.0	-30.0±1.2			[37]
$(HOCO)_2$	-731.8±2.0	-174.9±0.5	320.6±5.0	76.6±1.2	[37]
C_3H_5	166.1±4.3	39.7±1.0	248±15	59.3±3.6	[111]
C_3H_6	20.0±0.7	4.78±0.2	266.6	63.72	[22, 91]
n-C_3H_7	100±2	24±0.5			[118]
i-C_3H_7	86.6±2.0	20.7±0.5	281±5	67.2±1.2	[113]
i-$C_3H_7O_2$	-65.4±11.3	-15.6±2.7			[57]
C_3H_8	-104.68±0.50	-25.02±0.12	270.20	64.58	[21, 94]
C_2H_5CHO	-185.6±0.8	-44.4±0.2	304.51		[40, 91]
CH_3COCH_3	-217.1±0.7	-51.9±0.2	295.46	70.62	[40, 91]
F	79.38±0.30	18.94±0.07	158.751±0.004	37.942±0.001	[33]
F_2	0.00	0.00	202.791±0.005	48.468±0.001	[33]
HF	-273.30±0.70	-65.32±0.17	173.799±0.003	41.539±0.001	[33]
HOF	-98.3±4.2	-23.5±1.0	226.77±0.21	54.20±0.05	[27]
FO	109±10	26±3	216.40±0.3	51.72±0.07	[26]
FOF	24.5±2	5.86±0.5	247.46±0.4	59.14±0.1	[26]
OFO	380±20	90.8±5	251±1	60.0±0.3	[26], calc.
FOO	25.4±2	6.07±0.5	259.5±0.2	62.02±0.05	[26]
FOOF	19.2±2.0	4.59±0.5	277.2±0.2	66.25±0.05	[26]
FONO	67	16			[8], est
FNO	-65.7	-15.70	248.0	59.27	[117]
FNO_2	-79	-19.0	277.1	66.24	[117]
$FONO_2$	10±2	2.5±0.5	290	70	[27], est.
CF	244.1±10	58.3±2.4	213.03±0.04	50.92±0.01	[27, 43]
CHF	143.1±12	34.2±3.0	234.87	56.14	[43, 95]
CF_2	-184±8	-44.0±2	240.83±0.04	57.56±0.01	[27, 95]
CF_3	-465.7±2.1	-111.3±0.5	264.56	63.23	[43, 104]
CF_4	-933.20±0.75	-223.04±0.18	261.454	62.49	[33]
CHF_3	-692.9±2.1	-165.6±0.5	259.67	62.06	[43, 104]
CHF_2	-239±4	-57.1±1.0	258.50	61.78	[93]
CH_2F_2	-452.7±0.8	-108.2±0.2	246.59	58.94	[99]
CH_2F	-32±8	-7.6±2	236.52	56.53	[93]

SPECIES	ΔH_f(298 K) kJ mol^{-1}	ΔH_f(298 K) kcal mol^{-1}	S(298 K) J K^{-1} mol^{-1}	S(298 K) cal K^{-1} mol^{-1}	Reference[1-3]
CH_3F	-238±8	-56.8±2	222.78	53.246	[99], H est.
FCO	-161.2±8.1	-38.5±2.0			[55]
CHFO	-383±7	-91.6±1.7	246.82	58.99	[108],calc., [43]
CF_2O	-623.8±5.9	-149.1±1.4	258.97	61.89	[6], [43]
CF_3O	-635.1±7.1	-151.8±1.7			[34]
CF_2O_2	-427±6	-102±1.5			[59], calc.
CF_3O_2	-612.5±15.4	-146±4			[68]
CF_3OH	-908.8±3.8	-217.2±0.9			[7]
CF_3OOCF_3	-1434±11	-343±3			[108]
CF_3OF	-740.1±7.5	-176.9±1.8			[7]
CF3OCl	-734.7±4.2	-175.6±1.0			[7]
CH_2CH_2F	-59.4±8	-14.2±2	279.7	66.86	[78],[30], calc
CH_3CHF	-70.3±8	-16.8±2	274.0	65.48	[78], [31], calc
CH_3CH_2F	-277.4±4.2	-66.3±1	265.1	63.4	[71], est. [43]
CH_2FCH_2F	-432±25	-103.2±6			[53]
CH_2FCHF	235.5	56.28	293.3	70.11	[32]
CH_2FCHF_2	-665±4	-158.9±1			[62], corr
CHF_2CHF_2	-860±24	-205.6±5.7	320.3	76.6	[76], corr. [40]
CH_2CF_3	-517.1±5	-123.6±1.2	306.8	73.32	[30, 127]
CH_3CF_3	-745.6±1.7	-178.2±0.4	287.3	68.67	[28]
CHF_2CH_2	-277	-66.3	297.8	71.17	[30], calc.
CH_3CF_2	-302.5±8.4	-72.3±2	290.3	69.39	[92], [31], S calc
CH_3CHF_2	-500.1±6.3	-119.7±1.5	282.4	67.50	[28]
$CHFCF_3$	-697	-166.5	326.2	77.97	[32], H corr.
CH_2FCF_3	-896±8	-214.1±2	316.2	75.58	[28], H est.
CF_2CF_3	-891±5	-213±1.3			[128]
CHF_2CF_3	-1105±5	-264±1.1	333.7	79.76	[28]
C_2F_6	-1344.3±3.4	-321.3±0.8	331.8	79.30	[28, 104]
CF_3CO	-605±2	-144.6±0.4			[123] calc.
Cl	121.301±0.008	28.992±0.002	165.190±0.004	39.481±0.001	[33]
Cl_2	0.00	0.00	223.081±0.010	53.318±0.002	[33]
HCl	-92.31±0.10	-22.06±0.02	186.902±0.005	44.671±0.001	[33]
ClO	101.63±0.1	24.29±0.03	225.07±0.5	53.79±0.12	[27]
ClOO	98.0±4	23.4±1	269.32±0.5	64.37±0.1	[27]
ClOOH	0.8±4	0.2±1			[66], calc.
OClO	94.6±1.2	22.6±0.3	256.84±0.1	61.39±0.03	[27, 84]
ClO_3	194±12	46±3	270.75±0.5	64.71±0.1	[27]
ClClO	90±30	22±7	278.8±2.0	66.6±0.5	[27]
ClOCl	81.3±1.8	19.4±0.4			[44]
ClOOCl	127.6±2.9	30.5±0.7	301.0±5.0	71.9±1.2	[84]; Chase, 1998 #2979}
$ClClO_2$	154.2	36.9	294±2	70.3±0.5	[67],calc.,

SPECIES	ΔH_f(298 K) kJ mol^{-1}	ΔH_f(298 K) kcal mol^{-1}	S(298 K) J K^{-1} mol^{-1}	S(298 K) cal K^{-1} mol^{-1}	Reference[1-3]
					[27]
ClOClO	175.5	41.9	309±2	73.9±0.5	[67],calc., [27]
Cl_2O_3	150±6	35.8±1.5	390±20	94±5	[19]
HOCl	-74.8±1.2	-17.9±0.3	236.50±0.42	56.52±0.10	[27, 44]
ClNO	52.7±0.5	12.6±0.1	261.58	62.52	[43]
$ClNO_2$	12.5±1.0	3.0±0.3	272.23	65.06	[43]
cis-ClONO	64.4±6.3	15.4±1.5			[65], calc.
trans-ClONO	75.3±6.3	18.0±1.5			[65], calc.
ClO_2NO	102	24.3	316	75.5	[73], calc.
$ClONO_2$	22.9±2.0	5.5±0.5	302.38	72.27	[3]
O_2ClONO_2	92±17	22±4			[41], corr.
FCl	-55.70±0.31	-13.31±0.07	217.94	52.09	[43]
CHCl	326±8	78.0±2.0	234.88	56.85	[43, 95]
CCl_2	230±8	55.0±2.0	265.03	63.34	[43, 95]
CCl_3	71.1±2.5	17.0±0.6	303.24	72.47	[47]
CCl_3OH	-293±20	-70.0±5			[107], calc.
CCl_3O	-43.5±20	-10.4±5			[107], calc
CCl_3O_2	-20.9±8.9	-5.0±2.1			[57]
CCl_4	-95.6±2.5	-22.8±0.6	309.90	74.069	[72],[48, 99]
$CHCl_3$	-102.9±2.5	-24.6±0.6	295.51	70.63	[72],[99]
$CHCl_2$	89.0±3.0	21.3±0.7	280±7	66.9±2	[109]
$CHCl_2O_2$	-17±7	-4±2			[109]
CH_2Cl	117.3±3.1	28.0±0.7	271±7	64.5±2	[109]
CH_2ClO_2	-4±11	-1±3			[109]
CH_2Cl_2	-95.1±2.5	-22.8±0.6	270.31	64.606	[72],[99]
CH_3Cl	-81.9±0.6	-19.6±0.2	227.15	54.290	[72],[99]
ClCO	-24.9±4.2	-5.9±1.0	266.0	63.6	[27, 69]
CHClO	-164±20	-38±5	259.07	61.92	[43], H est,
CCl_2O	-220.9	-52.8	283.8	67.82	[117]
CH_2OCl	135.5±9.2	32.4±2.2	279.7	66.85	[18] calc.
CH_3OCl	-64.5±6.2	-15.4±1.5	272.8	65.19	[52] calc.
CH_2ClOCl	-92.3±10.3	-22.05±2.5	311.8	74.53	[52] calc.
$CHCl_2OCl$	-109.4±19.6	-26.1±3.6	339.1	81.04	[52] calc.
CCl_3OCl	-111.8±19.6	-26.7±4.7	357.2	85.37	[52] calc.
CHFCl	-61±10	-14.5±2.4			[119]
CH_2FCl	-264±8	-63.2±2	264.3	63.17	[29, 119], H est.
CFCl	31±13	7.4±3.2	259.032	61.91	[43, 95]
$CFCl_2$	-89.1±10.0	-21.3±2.4			[119]
$CFCl_3$	-285.3	-68.2	309.9	74.06	[29], corr.
CF_2Cl_2	-494.1	-118.1	300.7	71.87	[29], corr.
CF_3Cl	-709.2±2.9	-169.5±0.7	285.2	68.16	[29, 104]
$CHFCl_2$	-285±9	-68.1±2.1	293.0	70.04	[29], H est.
CHF_2Cl	-484.8	-115.6	280.8	67.11	[29], H est.
CF_2Cl	-279±8	-66.7±2			[80]
CFClO	-429±20	-103±5	276.70	66.13	[43]

SPECIES	ΔH_f(298 K) kJ mol^{-1}	ΔH_f(298 K) kcal mol^{-1}	S(298 K) J K^{-1} mol^{-1}	S(298 K) cal K^{-1} mol^{-1}	Reference[1-3]
$CH_2ClCOOH$	-427.6±1.0	-102.2±0.2	325.9±5.0	77.9±1.2	[37]
C_2H_3Cl	22±3	5.3±0.7			[72]
CH_3CHFCl	-313.4±2.6	-74.9±0.6			[58]
CH_2CF_2Cl	-318	-75.9	322.08	76.98	[88]
CH_3CF_2Cl	-536.2±5.2	-128.2±1.2	307.1	73.41	[58, 88]
C_2Cl_4	-18.8±4	-4.5±1	341.03	81.51	[43, 48]
1,1-$C_2H_2Cl_2$	2.4±2.0	0.6±0.5			[72]
Z-1,2-$C_2H_2Cl_2$	-3±2	-0.7±0.5			[72]
E-1,2-$C_2H_2Cl_2$	-0.5±2.0	-0.1±0.5			[72]
C_2HCl_3	-19.1±3.0	-4.6±0.7	325.20	77.72	[40, 89]
CH_2CCl_3	71.5±8	17.1±2			[100]
1,1,1-$C_2H_3Cl_3$	-144.6±2.0	-34.6±0.5	320.03	76.488	[72],[20, 58]
1,1,2-$C_2H_3Cl_3$	-148.0±4.0	-35.4±0.9			[72]
1,1,1,2-$C_2H_2Cl_4$	-152.3±2.4	-36.4±0.6			[72]
1,1,2,2-$C_2H_2Cl_4$	-156.7±3.5	-37.5±0.8			[72]
C_2HCl_5	-155.9±4.3	-37.3±1.0			[72]
CH_3CCl_2	42.5±1.7	10.2±0.4	288±5	68.8±1.1	[109]
$CH_3CCl_2O_2$	-69.7±4	-16.7±1			[56], corr.
1,1-$C_2H_4Cl_2$	-132.5±3.5	-31.7±0.8	305.05	72.908	[72],[20, 58]
$CHCl_2CH_2$	90.1±0.8	21.5±0.2			[112], calc.
1,2-$C_2H_4Cl_2$	-132.0±3.5	-31.5±0.8			[72]
CH_2CH_2Cl	93.0±2.4	22.2±0.6	271±7	64.8±2	[110]
CH_3CHCl	76.5±1.6	18.2±0.4	279±6	66.7±1.4	[109]
CH_3CH_2Cl	-112.1±0.7	-26.8±0.2	275.78	65.913	[72],[20]
C_2Cl_6	-142±4	-34.0±1	398.62	95.27	[43, 48]
Br	111.870±12	26.74±0.03	175.018±0.004	41.830±0.001	[33]
Br_2(g)	30.91±0.11	7.39±0.03	245.468±0.005	58.668±0.001	[33]
HBr	-36.29±0.16	-8.67±0.04	198.700±0.004	47.490±0.001	[33]
Br_2O	106.2±2.5	25.4±0.6			[44]
HOBr	-60.5±1.1	-14.5±0.3			[44]
BrO	126.2±1.7	30.2±0.4	232.97±0.1	55.681±0.023	[24, 126]
OBrO	163.9±4.4	39.2±1.1	271±2	64.8±0.5	[54],[24]
BrOO	108±40	26±10	289±3	69.1±0.7	[24]
BrO_3	221±50	53±12	285±2	68.1±0.5	[24], est.
BrOBr	107.6±3.5	25.7±0.8	290.8±2	69.50±0.48	[24]
BrBrO	168±20	40±5	313±2	74.8±0.5	[24], est.
BrNO	82.17±0.8	19.64±0.2	273.66±0.8	65.41±0.2	[124]
Z-BrONO	71.9	17.19			[64], calc.
E-BrONO	88.3	21.1			[64], calc.
$BrNO_2$	45.2	10.8			[64], calc.
$BrONO_2$	42.3±6.3	10.1±1.5			[87]
O $BrONO_2$	153.6±8	36.7±2			[90] calc.
O_2 $BrONO_2$	161.9±8	38.7±2			[90] calc.
BrF	-58.9±1.0	-14.08±0.3	228.985	54.729	[43]

SPECIES	ΔH_f(298 K) kJ mol^{-1}	ΔH_f(298 K) kcal mol^{-1}	S(298 K) J K^{-1} mol^{-1}	S(298 K) cal K^{-1} mol^{-1}	Reference[1-3]
BrCl	14.79±0.16	3.53±0.04	240.046	57.372	[43]
CH_2Br	169±4	40.4±1.0			[119]
$CHBr_3$	23.8±4.5	5.7±1.1	330.67	79.03	[15]calc.,[43]
$CHBr_2$	188±9	45.0±2.2			[119]
CBr_3	235±25	56±6	334.57	80.0	[43]
CH_2Br_2	-11.1±5.0	-2.7±1.2	294	70.23	[15],calc.
CH_3Br	-37.7±1.5	-9.02±0.36	245.85±0.25	58.76±0.06	[60]
CHBrCl	145±8	35±2			[112], calc.
CBr_2Cl	163±8	39±2			[112], calc.
$CBrCl_2$	124±8	30±2			[112], calc.
CH_2CH_2Br	135.6±6.7	32.4±1.6			[12]
CH_3CHBr	127±4	30.4±1			[79] corr.
CH_3CH_2Br	-61.5±1.0	-14.7±0.3	287.3±0.4	68.66±0.09	[58, 61]
CH_3CBr_2	140.2±5.4	33.5±1.3			[81]
CH_3CBr_2H	26.7±1.9	6.4±0.5			[58]
CF_3Br	-641.4±2.3	-153.3±0.5			[104]
CBr_4	83.9±3.4	20.0±0.8	358.06	85.6	[15],[43]
$CH_2BrCOOH$	-383.5±3.1	-91.7±0.7	337.0±5.0	80.5±1.2	[37]
I	106.76±0.04	25.52±0.01	180.787±0.004	43.209±0.001	[33]
I_2	62.42±0.08	14.92±0.02	260.687±0.005	62.306±0.001	[33]
HI	26.50±0.10	6.33±0.03	206.590±0.004	49.376±0.001	[33]
HOI	-69.6±5.4	-16.6±1.3	255.0±0.1	60.95±0.03	[14, 44]
IO	115.9±5.0	27.7±1.2	239.6±0.1	57.27±0.03	[11, 44]
OIO	77±15	18±4	279.9	66.9	[77], calc.
IOO	96.6±15	23±4	308.4	73.7	[77], calc.
IO_3	242±50	58±12	293±4	70.0±1.0	[25], est.
IOI	92.4±15	22.1±4	306.5	73.3	[77]
IIO	134.1±15	32.1±4	317.8	76.0	[77]
IOOI	156.8±15	37.5±4	337.0	80.5	[77], calc.
IIOO	103.0±15	24.6±4	339.9	81.2	[77], calc.
IOIO	124.2±15	29.7±4	349.7	83.6	[77], calc.
OIIO	224.0±15	53.5±4	356.3	85.2	[77], calc.
	68.4±10	16.3±2.4			[77], calc., corr.
ClOI	76.2±10	18.2±2.4			[77], calc., corr.
IClO	166.1±10	39.7±2.4			[77], calc., corr.
$ClIO_2$	10.7±10	2.6±2.4			[77], calc., corr.
ClOIO	107.1±10	25.6±2.4			[77], calc., corr.
ClOOI	125.7±10	30.0±2.4			[77], calc., corr.
IOClO	153.6±10	36.7±2.4			[77], calc., corr.

SPECIES	ΔH_f(298 K) kJ mol^{-1}	ΔH_f(298 K) kcal mol^{-1}	S(298 K) J K^{-1} mol^{-1}	S(298 K) cal K^{-1} mol^{-1}	Reference[1-3]
$IClO_2$	187.8±10	44.9±2.4			[77], calc., corr.
INO	121±4	29.0±1	282.8±4	67.6±1	[121]
INO_2	60.2±4	14.4±1	294±6	70.3±1.5	[121]
ICl	17.506±0.105	4.184±0.025	427.567	102.191	[27]
IBr	40.88±0.08	9.77±0.02	258.95	61.89	[27]
CH_3I	13.76±0.12	3.29±0.03	253.70±0.25	60.635±0.06	[60]
CH_2I_2	118.4±0.1	28.30±0.03	309.41±1.34	73.95±0.32	[60]
CF_3I	-586.2±2.1	-140.1±0.5	307.78	73.56	[43, 104]
CH_3CH_2I	-7.5±0.9	-1.79±0.2	295.52±0.42	70.63±0.10	[58, 61]
ICH_2CN	172.5±4.0	41.2±1.0			[63]
S	277.17±0.15	66.25±0.04	167.829±0.006	40.112±0.002	[33]
S_2	128.6±0.3	30.74±.07	228.167±0.010	54.533±0.003	[33]
HS	142.92±0.78	34.16±0.19	195.552	46.738	[70]
H_2S	-20.6±0.5	-4.92±0.12	205.81±0.05	49.19±0.01	[33]
SO	4.78±0.25	1.14±0.06	221.94	53.04	[43]
SO_2	-296.81±0.20	-70.94±0.05	248.223±0.050	59.327±0.012	[33]
SO_3	-395.9±0.7	-94.62±0.17	256.541	61.315	[43]
S_2O	-55.39±1.10	13.24±0.26	266.961	63.81	[70]
HSO	-6.1±2.9	-1.5±0.7			[9]
$HOSO_2$	-373±6	-89±1.5			[17]
HSNO	95.2±5	22.8±1			[16], corr., est error
H_2SO_4	-732.7±2	-175.1±0.5	311.3±1.5	74.40±0.36	[36]
CS	279.775±0.75	66.87±0.18	210.55	50.32	[43]
CS_2	116.7±1.0	27.9±0.2	237.882	56.855	[43]
CS_2OH	110.5±4.6	26.4±1.1	321±20	77±5	[83]
CH_3S	125.0±1.8	29.87±0.44			[85] corr.
CH_2SH	145.7±9.2	34.8±2.2			[101], corr.
$CH_2S(O)O$	-144.7±8.4	-34.6±2.0			[122], calc.
CH_3SH	-22.9±0.7	-5.47±0.17	255.14	60.98	[40, 91]
CH_2SO	-30±6	-7.2±1.4			[106]
CH_3SO	-70.3	-16.8			[98], calc.
$CH_3S(O)O$	-211±4	-50.4±1			[39] calc.
CH_3OSO	-230±4	-55±1			[39] calc.
CH_3SOO	76.1±5.4	18.2±1.3			[120], corr.
CH_3SH_2	136.8±5.9	32.7±1.4			[50]
CH_3SCH_3	-37.4±0.6	-8.94±0.2	285.96	68.35	[40, 91]
CH_3SSCH_3	-24.7±1.0	-5.9±0.3	336.80	80.50	[40, 91]
OCS	-141.7±2	-33.9±0.5	231.644	55.36	[43]
n-C_4H_{10}	-125.65±0.67	-30.03±0.16	309.91	74.07	[40, 94]
2(CH_3)-C_3H_7	-134.18±0.63	-32.07±0.15	295.50	70.63	[40, 94]
$(CH_3COO)_2$	-500±10	-120±3	390.7±6.0	93.4±1.4	[37]

Notes:

1. Error limits are estimates from the original references.
2. If two references are given for a substance, the first refers to the enthalpy value while the second to the entropy.
3. The terms “calc” and “est” indicate that the value is calculated or estimated. The term “corr” indicates that an enthalpy value has been adjusted to reflect the value chosen in this table for a reference substance.

A.1 References

1. Abramowitz, S. and M. W. Chase, 1991, Pure App. Chem., **63**, 1449-1454.
2. An, X. W. and M. Mansson, 1983, J. Chem. Thermo., **15**, 287-293.
3. Anderson, L. C. and D. W. Fahey, 1990, J. Phys. Chem., **94**, 644-652.
4. Anderson, W. R., 1989, J. Phys. Chem., **93**, 530-536.
5. Anderson, W. R., 1999, Comb. Flame, **117**, 394-403.
6. Asher, R. L., E. H. Appelman and B. Ruscic, 1996, Journal of Chemical Physics, **105**, 9781-9795.
7. Asher, R. L., E. H. Appelman, J. L. Tilson, M. Litorja, J. Berkowitz and B. Ruscic, 1997, Journal of Chemical Physics, **106**, 9111-9121.
8. Atkinson, R., D. L. Baulch, R. A. Cox, R. F. Hampson, J. A. Kerr, M. J. Rossi and J. Troe, 1997, J. Phys. Chem. Ref. Data, **26**, 521-1011.
9. Balucani, N., P. Casavecchia, D. Stranges and G. G. Volpi, 1993, Chem. Phys. Lett., **211**, 469-472.
10. Becerra, R., I. W. Carpenter and R. Walsh, 1997, J. Phys. Chem., **101**, 4185-4190.
11. Bedjanian, Y., G. Le Bras and G. Poulet, 1997, J. Phys. Chem. A, **101**, 4088-4096.
12. Bedjanian, Y., G. Poulet and G. Le Bras, 1999, J. Phys. Chem. A, **103**, 4026-4033.
13. Berkowitz, J., G. B. Ellison and D. Gutman, 1994, J. Phys. Chem., **98**, 2744-2765.
14. Berry, R. J., Y. Yuan, A. Misra and P. Marshall, 1998, J. Phys. Chem. A, **102**, 5182-5188.
15. Bickerton, J., M. E. M. da Piedade and G. Pilcher, 1984, J. Chem. Thermo., **16**, 661-668.
16. Black, G., R. Patrick, L. E. Jusinski and T. G. Slanger, 1984, J. Chem. Phys., **80**, 4065-4070.
17. Blitz, M. A., K. J. Hughes and M. J. Pilling, 2003, J. Phys. Chem. A, **101**, 1971-1978.
18. Bozzelli, J. W. and D. Jung, 2001, J. Phys. Chem. A, **105**, 3941-3946.
19. Burkholder, J. B., R. K. Talukdar, A. R. Ravishankara and S. Solomon, 1993, J. Geophys. Res., **98**, 22937-22948.
20. Chao, J., A. S. Rodgers, R. C. Wilhoit and B. J. Zwolinski, 1974, J. Phys. Chem. Ref. Data, **3**, 141-162.
21. Chao, J., R. C. Wilhoit and B. J. Zwolinski, 1973, J. Phys. Chem. Ref. Data, **2**, 427-437.
22. Chao, J. and B. J. Zwolinski, 1975, J. Phys. Chem. Ref. Data, **4**, 251-261.
23. Chao, J. and B. J. Zwolinski, 1978, J. Phys. Chem. Ref. Data, **7**, 363-377.
24. Chase, M. W., 1996, J. Phys. Chem. Ref. Data, **25**, 1069-1111.
25. Chase, M. W., 1996, J. Phys. Chem. Ref. Data, **25**, 1297-1340.
26. Chase, M. W., 1996, J. Phys. Chem. Ref. Data, **25**, 551-603.
27. Chase, M. W., 1998, J. Phys. Chem. Ref. Data, **Monograph 9**.
28. Chen, S. S., A. S. Rodgers, J. Chao, R. C. Wilhoit and B. J. Zwolinski, 1975, J. Phys. Chem. Ref. Data, **4**, 441-456.
29. Chen, S. S., R. C. Wilhoit and B. J. Zwolinski, 1976, J. Phys. Chem. Ref. Data, **5**, 571-580.
30. Chen, Y., A. Rauk and E. Tschuikow-Roux, 1990, J. Chem. Phys., **93**, 6620-6629.
31. Chen, Y., A. Rauk and E. Tschuikow-Roux, 1990, J. Chem. Phys., **93**, 1187-1195.
32. Chen, Y., A. Rauk and E. Tschuikow-Roux, 1991, J. Chem. Phys., **94**, 7299-7310.
33. Cox, J. D., D. D. Wagman and V. A. Medvedev *CODATA Key Values for Thermodynamics*; Hemisphere Publishing Corp.: New York, 1989.
34. Curtiss, L. A., K. Raghavachari, P. C. Redfern and J. A. Pople, 1997, J. Chem. Phys., **106**, 1063-1079.
35. Davis, H. F., B. Kim, H. S. Johnston and Y.-T. Lee, 1993, J. Phys. Chem., **97**, 2172-2180.
36. Dorofeeva, O., V. S. Iorish, V. P. Novikov and D. B. Neumann, 2003, J. Phys. Chem. Ref. Data, **32**, 879-901.
37. Dorofeeva, O., V. P. Novikov and D. B. Neumann, 2001, J. Phys. Chem. Ref. Data, **30**, 475-513.
38. Duncan, T. V. and C. E. Miller, 2000, J. Chem. Phys., **113**, 5138-5140.
39. Frank, A. J. and F. Turecek, 1999, J. Phys. Chem. A, **103**, 5348-5361.
40. Frenkel, M., G. J. Kabo, K. N. Marsh, G. N. Roganov and R. C. Wilhoit *Thermodynamics of organic compounds in the gas state*; Thermodynamics Research Center: College Station, TX, 1994; Vol. I.
41. Friedl, R. R., S. P. Sander and Y. L. Yung, 1992, J. Phys. Chem., **96**, 7490-7493.
42. Fulle, D., H. F. Hamann, H. Hippler and C. P. Jänsch, 1997, Ber. Bunsenges. Phys. Chem., **101**, 1433-1442.
43. Gurvich, L. V., I. V. Veyts and C. B. Alcock *Thermodynamic Properties of Individual Substances*, Fourth ed.; Hemisphere Publishing Corp.: New York, 1991; Vol. 2.
44. Hassanzadeh, P. and K. K. Irikura, 1997, J. Phys. Chem. A, **101**, 1580-1587.

45. Hills, A. J. and C. J. Howard, 1984, J. Chem. Phys., **81**, 4458-4465.
46. *Constants of Diatomic Molecules*; Huber, K. P. and G. Herzberg, Eds.; National Institute of Standards and Technology, 1998.
47. Hudgens, J. W., R. D. Johnson, R. S. Timonen, J. A. Seetula and D. Gutman, 1991, J. Phys. Chem., **95**, 4400-4405.
48. Huybrechts, G., M. Marmon and B. Van Mele, 1996, Int. J. Chem. Kinet., **28**, 27-36.
49. Jacox, M. E. *Vibrational and Electronic Energy Levels of Polyatomic Transient Molecules*; National Institute of Standards and Technology, 1998.
50. Jefferson, A., J. M. Nicovich and P. H. Wine, 1994, J. Phys. Chem., **98**, 7128-7135.
51. Johnson, R. D. and J. W. Hudgens, 1996, J. Phys. Chem., **100**, 19874-19890.
52. Jung, D., C. J. Chen and J. W. Bozzelli, 2000, J. Phys. Chem. A, **104**.
53. Kerr, J. A. and D. M. Timlin, 1971, Int. J. Chem. Kinet., **3**, 427-441.
54. Klemm, R. B., R. P. Thorn, L. J. Stief, T. J. Buckley and R. D. Johnson, 2001, J. Phys. Chem. A, **105**, 1638-1642.
55. Knyazev, V. D., A. Bencsura and I. R. Slagle, 1997, J. Phys. Chem. A, **101**, 849-852.
56. Knyazev, V. D., A. Bencsura and I. R. Slagle, 1998, J. Phys. Chem. A, **102**, 1760-1769.
57. Knyazev, V. D. and I. R. Slagle, 1998, J. Phys. Chem. A, **102**, 1770-1778.
58. Kolesov, V. P. and T. S. Papina, 1983, Russ. Chem. Rev., **52**, 425-439.
59. Kraka, E., Z. Konkoli, D. Cremer, J. Fowler and H. F. Schaefer, 1996, J. Amer. Chem. Soc., **118**, 10595-10608.
60. Kudchadker, S. A. and A. P. Kudchadker, 1975, J. Chem. Phys. Ref. Data, **4**, 457-470.
61. Kudchadker, S. A. and A. P. Kudchadker, 1979, J. Phys. Chem. Ref. Data, **8**, 519-526.
62. Lacher, J. R. and H. A. Skinner, 1968, J. Chem. Soc. A, 1034-1038.
63. Lafleur, R. D., B. Szatary and T. Baer, 2000, J. Phys. Chem. A, **104**, 1450-1455.
64. Lee, J. H., R. B. Timmons and L. J. Stief, 1976, J. Chem. Phys., **64**, 300-305.
65. Lee, T. J., 1994, J. Phys. Chem., **98**, 111-115.
66. Lee, T. J. and A. P. Rendell, 1993, J. Phys. Chem., **97**, 6999-7002.
67. Li, W. K. and C. Y. Ng, 1997, J. Phys. Chem. A, **101**, 113-115.
68. Lightfoot, P. D., R. A. Cox, J. N. Crowley, M. Destriau, G. D. Hayman, M. E. Jenkin, G. K. Moortgat and F. Zabel, 1992, Atmos. Environ., **26A**, 1805-1961.
69. Lim, K. P. and J. V. Michael, 1994, J. Phys. Chem., **98**, 211-215.
70. Lodders, K., 2004, J. Chem. Phys. Ref. Data, **33**, 357-367.
71. Luo, Y. R. and S. W. Benson, 1997, J. Phys. Chem. A, **101**, 3042-3044.
72. Manion, J. A., 2002, J. Phys. Chem. Ref. Data, **31**, 123-172.
73. McGrath, M. P. and F. S. Rowland, 1994, J. Phys. Chem., **98**, 1060-1067.
74. McMillen, D. F. and D. M. Golden, 1982, Ann. Rev. Phys. Chem., **33**, 493-532.
75. Miller, C. E., J. I. Lynton, D. M. Keevil and J. S. Franscisco, 1999, J. Phys. Chem. A, **103**, 11451-11459.
76. Millward, G. E., R. Hartig and E. Tschuikow-Roux, 1971, J. Phys. Chem., **75**, 3195-3201.
77. Misra, A. and P. Marshall, 1998, J. Phys. Chem. A, **102**, 9056-9060.
78. Miyokawa, K., S. Ozaki and T. Yano, 1996, Bull. Chem. Soc. Jpn., **69**, 869-873.
79. Miyokawa, K. and E. Tschuikow-Roux, 1990, J. Phys. Chem., **94**, 715-717.
80. Miyokawa, K. and E. Tschuikow-Roux, 1992, J. Phys. Chem., **96**, 7328-7331.
81. Miyokawa, K. and E. Tschuikow-Roux, 1999, Bull. Chem. Soc. Jpn., **72**, 1-5.
82. Moore, C. E. *Atomic Energy Levels*; NSRDS: Washington. DC, 1971; Vol. 1.
83. Murrells, T. P., E. R. Lovejoy and A. R. Ravishankara, 1990, J. Phys. Chem., **94**, 2381-2386.
84. Nickolaisen, S. L., R. R. Friedl and S. P. Sander, 1994, J. Phys. Chem., **98**, 155-169.
85. Nicovich, J. M., K. D. Kreutter, C. A. van Dijk and P. H. Wine, 1992, J. Phys. Chem., **96**, 2518-2528.
86. Okabe, H., 1970, J. Chem. Phys., **53**, 3507-3515.
87. Orlando, J. J. and G. S. Tyndall, 1996, J. Phys. Chem., **100**, 19398-19405.
88. Paddison, S. J., Y. H. Chen and E. Tschuikow-Roux, 1994, Can. J. Chem., **72**, 561-567.
89. Papina, T. S. and V. P. Kolesov, 1985, Russ. J. Phys. Chem., **59**, 1289-1292.
90. Parthiban, S. and T. J. Lee, 2000, J. Chem. Phys., **113**, 145-152.
91. Pedley, J. B. *Thermochemicsl Data and Structures of Organic Compounds*; Thermodynamics Data Center: College Station, TX, 1994.
92. Pickard, J. M. and A. S. Rodgers, 1977, J. Amer. Chem. Soc., **99**, 691-694.

93. Pickard, J. M. and A. S. Rodgers, 1983, Int. J. Chem. Kinet., **15**, 569-577.
94. Pittam, D. A. and G. Pilcher, 1972, J. Chem. Soc. Farad. Trans 1, **68**, 2224-2229.
95. Poutsma, J. C., J. A. Paulino and R. R. Squires, 1997, J. Phys. Chem. A, **101**, 5327-5336.
96. Ramond, T. M., S. J. Blanksby, S. Kato, V. M. Bierbaum, G. E. Davico, R. L. Schwartz, W. C. Lineberger and G. B. Ellison, 2002, J. Phys. Chem. A, **106**, 9641-9647.
97. Regimbal, J. M. and M. Mozurkewich, 1997, J. Phys. Chem. A, **101**, 8822-8820.
98. Resende, S. M. and F. R. Ornellas, 2003, Chem. Phys. Lett., **367**, 489-494.
99. Rodgers, A. S., J. Chao, R. C. Wilhoit and B. J. Zwolinski, 1974, J. Phys. Chem. Ref. Data, **3**, 117-140.
100. Rodgers, A. S. and P. Jerus, 1988, Int. J. Chem. Kinet., **20**, 565-575.
101. Ruscic, B. and J. Berkowitz, 1993, J. Chem. Phys., **98**, 2568-2579.
102. Ruscic, B., D. Feller, D. A. Dixon, K. A. Peterson, L. B. Harding, R. L. Asher and A. F. Wagner, 2001, J. Phys. Chem A, **105**, 1-4.
103. Ruscic, B., M. Litorja and R. L. Asher, 1999, J. Phys. Chem. A, **103**, 8625-8633.
104. Ruscic, B., J. V. Michael, P. C. Redfern, L. A. Curtiss and K. Raghavachri, 1998, J. Phys. Chem. A, **102**, 10889-10899.
105. Ruscic, B., A. F. Wagner, L. B. Harding, R. L. Asher, D. Feller, D. A. Dixon, K. A. Peterson, Y. Song, X. M. Qian, C. Y. Ng, J. B. Liu and W. W. Chen, 2002, J. Phys. Chem. A, **106**, 2727-2747.
106. Ruttink, P. J. A., P. C. Burgers, M. A. Trikoupis and J. K. Terlouw, 2001, Chem. Phys. Lett., **342**, 447-451.
107. Schneider, W. F., B. I. Nance and T. J. Wallington, 1995, J. Amer. Chem. Soc., **117**, 478-485.
108. Schneider, W. F. and T. J. Wallington, 1994, J. Phys. Chem., **98**, 7448-7451.
109. Seetula, J. A., 1996, J. Chem. Soc. Faraday Trans., **92**, 3069-3078.
110. Seetula, J. A., 1998, J. Chem. Soc. Faraday Trans., **94**, 891-898.
111. Seetula, J. A., 1999, Phys. Chem. Chem. Phys., **1**, 4727-4731.
112. Seetula, J. A., 2000, Phys. Chem. Chem. Phys., **2**, 3807-3812.
113. Seetula, J. A. and I. R. Slagel, 1997, J. Chem. Soc. Faraday Trans., **93**, 1709-1719.
114. Shapley, W. A. and G. B. Bacskay, 1999, J. Phys. Chem. A, **103**, 4505-4513.
115. Speranza, M., 1996, Inorg. Chem., **35**, 6140-6151.
116. Spiglanin, T. A., R. A. Pery and D. W. Chandler, 1986, J. Phys. Chem., **90**, 6184-6189.
117. Stull, D. R., E. F. Westrum and G. C. Sinke *The Chemical Thermodynamics of Organic Compounds*; John Wiley & Sons: New York, 1969.
118. Tsang, W. Heats of formation of organic free radicals by kinetic methods. In *Energetics of Free Radicals*; J. A. M. Simoes, A. Greenberg and J. F. Liebman, Eds.; Blackie Academic & Professional: London, 1996; pp 22-58.
119. Tschuikow-Roux, E. and S. Paddison, 1987, Int. J. Chem. Kinet., **19**, 15-24.
120. Turnipseed, A. A., S. B. Barone and A. R. Ravishankara, 1992, Journal of Physical Chemistry, **96**, 7502-7505.
121. Van den Bergh, H. and J. Troe, 1976, J. Chem. Phys., **64**, 736-742.
122. Ventura, O. N., M. Kieninger and P. A. Denis, 2003, J. Phys. Chem. A, **107**, 518-521.
123. Viskolcz, B. and T. Berces, 2000, Phys. Chem. Chem. Phys., **2**, 5430-6436.
124. Wagman, D. D., W. H. Evans, V. B. Parker, R. H. Schumm, I. Halow, S. M. Bailey, K. L. Churney and R. L. Nutall, 1982, J. Phys. Chem. Ref. Data, **11**, Suppl. No. 1.
125. Wenthold, P. G. and R. R. Squires, 1994, Journal of the American Chemical Society, **116**, 11890-11897.
126. Wilmouth, D. M., T. F. Hanisco, N. M. Donahue and J. G. Anderson, 1999, J. Phys. Chem A, **103**, 8935-8945.
127. Wu, E. C. and A. S. Rodgers, 1974, J. Phys. Chem., **78**, 2315-2317.
128. Wu, E. C. and A. S. Rodgers, 1976, J. Amer. Chem. Soc., **98**, 6112-6115.
129. Yu, D., A. Rauk and D. A. Armstrong, 1994, J. Chem. Soc. Perkin Trans 2, 2207-2215.